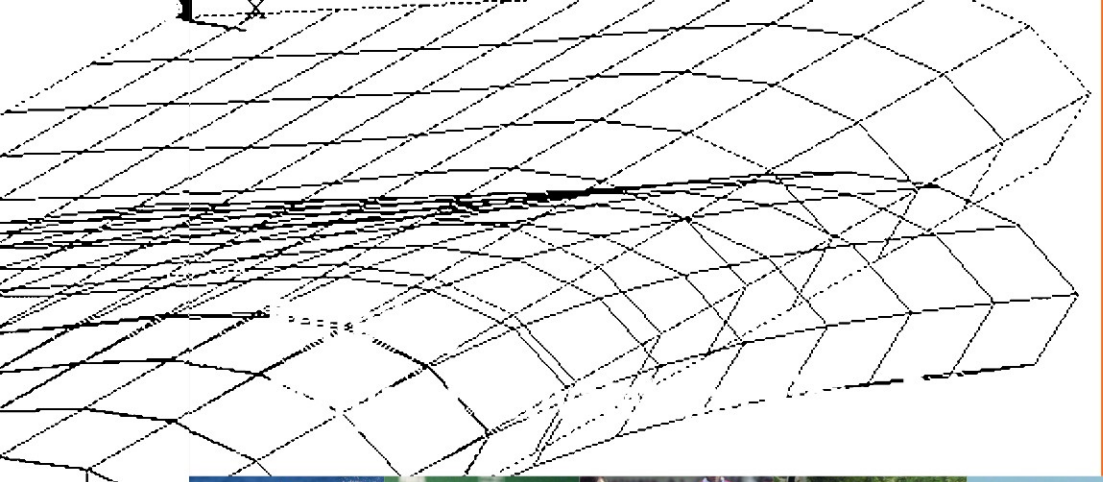

The Engineering of Sport 7

Volume 2

Springer

The Engineering of Sport 7

Vol. 2

Springer

Paris
Berlin
Heidelberg
New York
Hong Kong
Londres
Milan
Tokyo

Margaret Estivalet
Pierre Brisson

The Engineering of Sport 7

Vol. 2

Springer

Margaret Estivalet

ESTIA
Technopole Izarbel
64210 Bidart
France

Pierre Brisson

UTC, Centre de Transfert
66, avenue de Landshut
60200 Compiègne
France

ISBN-13 : 978-287-09412-5 Springer Paris Berlin Heidelberg New York

Cover design: Jean-François Montmarché

ISEA 2008, just before the summer olympic games!

What a fantastic opportunity to present a compilation of more than 160 articles talking about sports engineering, analysing the coefficients of friction between the balls and the rim and back-board for leather and synthetic basket balls, extracting the aerodynamic force data during real ski jumping flights, optimizing new prosthesis of the lower human leg, analysing the golf ball spin rate after impact, analysing the most common injury in sport climbing using eight fresh dozen cadaver fingers, describing the heat transfer in footwear using finite elements, measuring the aerodynamic performance of cycling time trial helmets, etc, …

What a challenge too to be honnest!

A huge diversity of articles, top level contributions to sports engineering.

Today the world is convinced sport is not only fun but economically a sector, a multi sector, which is not only growing if you only take into acccount the total turn over but is becoming one of the fast growing business.

Sport is not any more reserved for top sporters who want to maintain a certain level in some disciplines, it became a new philosophy of life, a new trend, a way to cope with aging population, with the reality of the society today.

Our every day life is concerned with sport or sport derived products or services, it is in our shoes, our suits, our car, our bike, at home, when we eat, when we drink, when we sleep, relax, when we look at TV for international events, when we listen, watch the news, for fun.The sports engineering community as it was noted two years ago keeps growing.

We have to admit it was a very difficult task to review all the contributions and to come down to 150 articles; It was very difficult too to allocate reviewers to contributions because a lot of articles were proposing not only scientific contributions but also engineering solutions and methodologies.

Some groups of articles could have been selected as a basis for a workshop in itself!

In front of such a diversity of contributions we have decided not to group the articles by families, by themas, by keywords, by branches, by sports, by subjects, by numbers of contributions but we decided to regroup it in two different volumes without any introduction which we thought would not bring anything to the readers, just proposing the articles in a natural order creating of course some surprises, but it was a choice!

Of course there is a table listing the articles with their authors and co-authors and the programme will indicate evey time the article number.

Complex to read? Difficult to apprehend? We thought it would give the best way to understand the complexity of sports engineering today; An article about football in a ball section of proceedings, in the shoes section, in the field surface section, in the injury section, in the training part, in the video group, in the sliding effect paragraph, in the referee point of view chapter, in the leather section may be, why not the aerodynamics or the finite elements analysis, may be in the professional sports section or the leisure, the TV business, the star system, …

So many possibilities, we just did it in the way we were convinced would be the most open!

What we wanted to do is to provide the readers with the best sports engineering contributions in 2008, before the biggest sports event on earth, the olympic games, in front of 5 billions telespectators who will enjoy the show and for many of them start again sporting, or just start a new sport, realising what they can do, discover a new passion, using in any case the brain storming of the world of engineering contributors to improve our every day life.
This is the magic of sport!

Margaret ESTIVALET & Pierre BRISSON

Contents

Measurement of the Forces on Ball in Flight Using Built-in Accelerometer (P138)

R., Koyanagi[1], Y., Ohgi[2]

Abstract: In this study, tri-axial accelerometer was installed in a ball to measure the aerodynamic forces during the ball's flight. The control experiments to validate were conducted besides the pitching experiment, to examine ball linear or angular velocity components independently. These were performed using a turntable and free fall test, respectively. The acceleration data of the throwing experiment showed a semi-sinusoidal wave pattern. On the other hand, this wave pattern was not observed in the acceleration data of both the rotational table experiment and free-fall experiment. It was revealed that the change of the orientation vectors of the gravitational acceleration and the translation acceleration on the sensor coordinate system caused the sinusoidal acceleration pattern.

Keywords: Accelerometer, aerodynamic force, flying ball, baseball.

1- Background

The measurement of the aerodynamic forces during the flight of the ball is one of the major topics in the fluid mechanics in sports. The wind tunnel test and the image analysis are mainly used to measure of the fluid forces. However, both of the methods have some difficulties. The experimental condition of the wind tunnel is different from the actual flying ball in the point that the ball is fixed. As for the image analysis, it is difficult to observe flying ball continuously. In this research, the author proposes a new methodology to measure the aerodynamic forces by the built-in accelerometer. To validate the acceleration components, controlled experiments in the laboratory were conducted in addition to the pitching experiment. The controlled experiments were described as follows, 1) Rotational table experiment, 2) Free fall experiment. The ball moves the gyration without translational acceleration in the rotational table experiment, and the ball moves the translational movement without rotational condition in the free fall experiment.

1. Room No. o206, 5322 Endo, Fujisawa, Kanagawa, JAPAN, 252-8520 - E-mail: lenonk@sfc.keio.ac.jp
2. Room No. o206, 5322 Endo, Fujisawa, Kanagawa, JAPAN, 252-8520, Associate Professor, Graduate School of Media and Governance, Keio Univ. - E-mail: ohgi@sfc.keio.ac.jp

2 Methods

2.1 Equipment

Figure 1 shows the wireless piezo-electric acceleration sensor, W988-H (Hitachi Metals Co. Ltd). The measurement range of this accelerometer is ±3g (±29.4 (m/s^2)). The sampling rate of the accelerometer is 200Hz. The measured acceleration data are transmitted to the receiver by wireless. The accelerometer was capsulated by the FRP (fiber-reinforced polymer) and subereous case. The diameter and mass of the sensor ball is similar to the baseball ball.

Figure 1 - Wireless accelerometer.

Figure 2 - Overview of the sensor baseball.

Table 1 - Comparison between baseball and experiment balls.

_	Baseball ball	Experimental ball
Mass (kg)	0.1417_0.1488	0.148
Radius (m)	No regulations	0.035±0.002
Circumference (m)	0.229-0.235	0.220±0.012

2.2 Experiments

2.2.1 Pitching experiment

The author conducted a real pitching experiment. A Subject performed ball pitching using the ball built-in wireless piezo-electric acceleration sensor. The closed up release point image was acquired using two high speed cameras (1000Hz). The synchronization between the high speed cameras and the accelerometer was accomplished by the contact switch. The distance of the ball's flight was about 17 (m). The subject pitched straight ball in this experiment.

2.2.2 Rotational table experiment

The sensor ball was rotated with a turntable and its acceleration was acquired. The author set the magnitude and the time of the angular velocity acting to the ball. The magnitude of the angular velocity increased from 2π (rad/s) to 10π (rad/s) by 1π (rad/s) (Fig. 3). Each angular velocity acted to the ball for five seconds. The z axis of the acceleration sensor was corresponding to the rotation axis and the author observed x axis of the accelerometer. In this experiment, the authors examined the acceleration of the rotating ball with no translational movement.

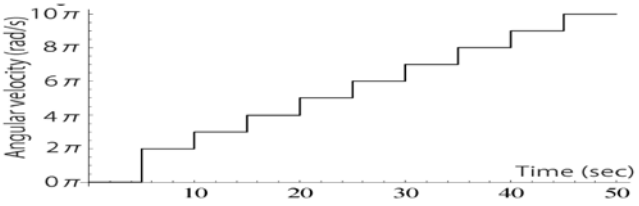

Figure 3 - The change of angular velocity in the rotational table experiment.

2.2.3 Free fall experiment

The sensor ball was dropped from 7.5 (m) height without rotation. This experiment was performed indoor condition avoiding the wind effect. The positive z axis of the accelerometer was corresponding in the direction of the fall.

3 Results

3.1 Pitching experiment

The acceleration data obtained in the pitching experiment had four components, such as the gravitational acceleration, the translational acceleration, the centrifugal acceleration and tangential acceleration [01]. Therefore, the equation can be rewritten as follows.

$$\mathbf{A} = \mathbf{a}_t + \mathbf{g} + \boldsymbol{\omega}_B \times (\boldsymbol{\omega}_B \times (-\mathbf{r}_S)) + \dot{\boldsymbol{\omega}}_B \times (-\mathbf{r}_S) \quad (1)$$

Where, **A** indicates measured acceleration by built-in accelerometer in the baseball, **g** indicates gravitational acceleration, $\mathbf{r}_s$ indicates distance vector of the ball's axis, $\mathbf{a}_t$ indicates translational acceleration acting on the accelerometer, and ω_B indicates angular velocity of the ball.

The sum of these four components is output. Gravitational acceleration, translational acceleration, centrifugal acceleration and tangential acceleration are output from the accelerometer.

Figure 4 shows the acceleration data acquired in the pitching experiment. Figure 5 shows its flight phase shown in Fig. 4.

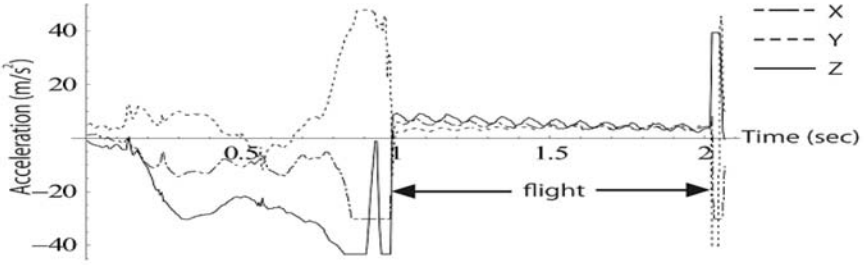

Figure 4 - The waveforms of the acceleration at the pitching experiment.

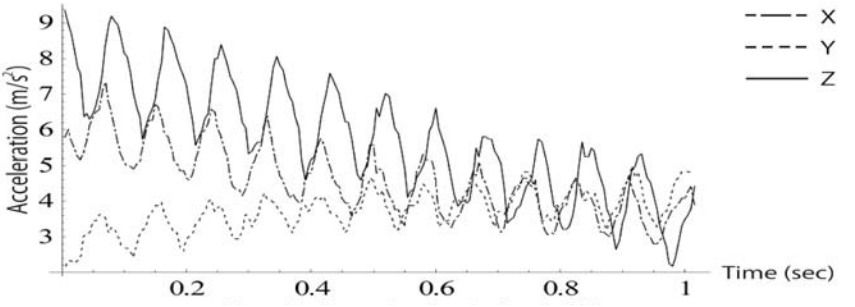

Figure 5 - the acceleration during the flight.

The FFT analysis was conducted to reveal the frequency characteristics of these wave patterns. Figure 6 shows the power spectrum of the acceleration shown in Fig. 5.

From Figure 6, the power spectrum of the acceleration data had its peak in sbout 15 (Hz) except DC component.

Therefore, the periodic change of the acceleration data in the pitching experiment was indicated.

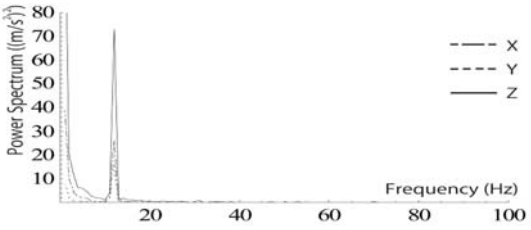

Figure 6 - The power spectrum of acceleration in Figure 5.

3.2 Rotational table experiment

In the rotation table experiment, $\mathbf{a}_t$ must be **0** because the translational movement doesn't exist on the ball. The author set that the observed acceleration axis is perpendicular with the direction of the gravitational acceleration. Therefore, the acceleration output by this experiment can be simplified as follows.

$$\mathbf{A} = \boldsymbol{\omega}_B \times (\boldsymbol{\omega}_B \times (-\mathbf{r}_S)) + \dot{\boldsymbol{\omega}}_B \times (-\mathbf{r}_S) \tag{2}$$

Figure 7 shows the x axis acceleration acquired by the rotation table experiment.

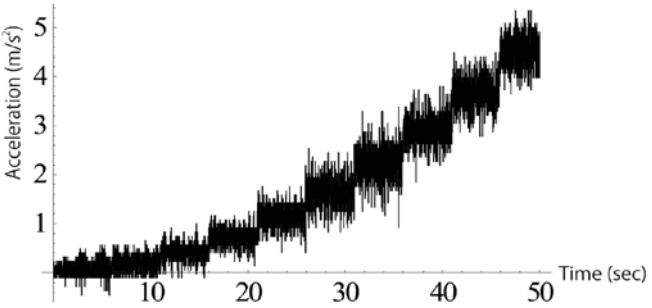

Figure 7 - The x-axis acceleration in rotational table experiment.

Figure 8 was the power spectrum of the acceleration shown in Figure 7 by FFT.

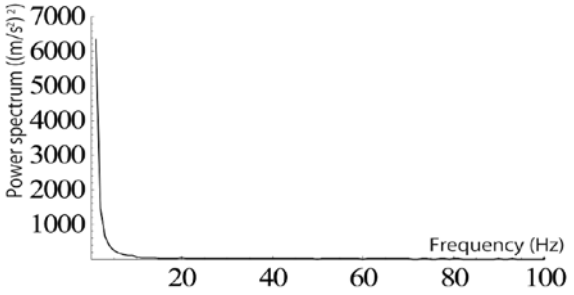

Figure 8 - The power spectrum of the x-axis acceleration in the turntable experiment

Figure 8 indicates no periodic change of the acceleration which was observed in the pitching experiment.

3.3 Free fall experiment

In the free fall experiment, the centrifugal and tangential acceleration must be 0 because the rotational movement doesn't exist on the ball. Therefore, the acceleration output by the free fall experiment can be simplified as follows.

$$\mathbf{A} = \mathbf{a}_t + \mathbf{g} \tag{3}$$

Under this configuration, the direction of the air drag is opposite to gravitational acceleration. When there is no air resistance, the absolute value of the acceleration signal must be 0 because of the counterbalancing acceleration by the free fall. Therefore, the change of the acceleration from zero is thought to be an air resistance.

Figure 9 shows the z-axis acceleration acquired in the free fall experiment. The waveform showed approximately zero when the ball was dropped off, and the acceleration decreased in proportion to the time squared.

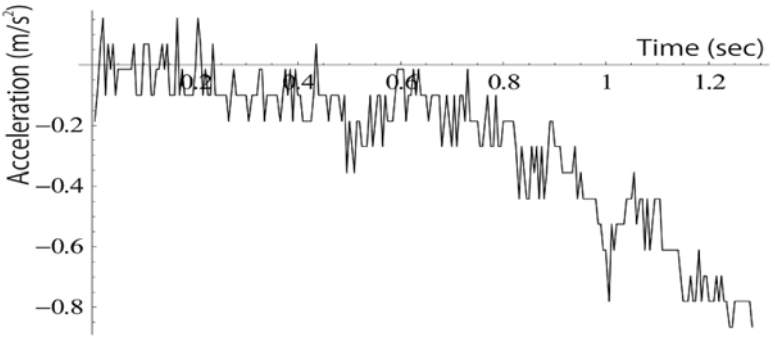

Figure 9 - Waveform example of the z-axis acceleration in the free-fall experiment.

The power spectrum was calculated for the comparison with the pitching experiment. Figure 10 shows the power spectrum of acceleration shown in Figure 9.

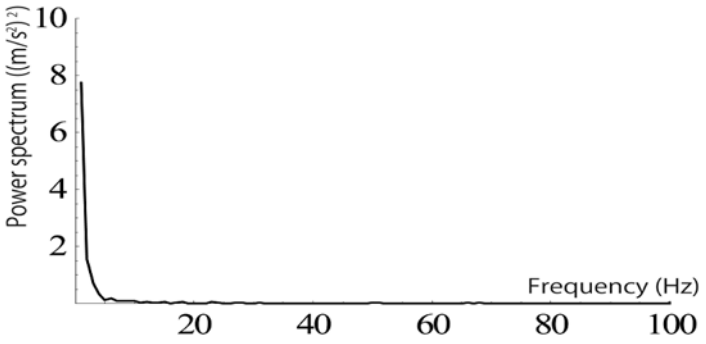

Figure 10 - The power spectrum of z-axis acceleration in the free fall experiment.

From Figure 9, no remarkable peak spectrum can be seen in the free fall experiment.

4- Discussion

The turntable experiment and free-fall experiment, no remarkable spectrum peak observed in the pitching experiment was observed on the FFT results. Therefore, when the ball flies with translational and rotational movement at the same time, the sinusoidal wave pattern appears. No external force except the aerodynamic forces and gravity influences the translational acceleration of the flying sensor ball. Therefore, the author

supposes that the aerodynamic forces which influence translational movement of the ball in the pitching experiment. When a global coordinate system was fixed on the ground, the direction of the aerodynamic forces and gravitational acceleration are constant with respect to the global coordinate system. On the other hand, the direction of the aerodynamic forces and gravitational acceleration on the sensor coordinate system rotate, because the acceleration sensor rotates itself during its flight phase. The centrifugal force depends on a radius between the center of rotation and the sensor and the angular velocity. Therefore, the direction of the centrifugal force on the global coordinate system always changes. And on the sensor coordinate system it is stable and pointing to the center of rotation. The gravity and the aerodynamic forces appear as the amplitude of the wave on the acceleration. On the contrary, the centrifugal force is output to the acceleration as the drift level of the wave.

The obtained acceleration in the pitching experiment showed the periodic change. It is thought that the periodic change of the acceleration waveform shows the influence of gravity and the aerodynamic forces on the ball. When a resultant vector of the aerodynamic forces and gravity have changed periodically, it was thought that one single cycle of the waves indicated one rotation of the ball in the pitching experiment. Therefore, the angular velocity could be estimated by measuring the time of one cycle.

For our future work, the authors would like to distinguish each acceleration component to estimate the rotational axis and the aerodynamics forces of the ball.

5- Conclusion

The acceleration time histories in the pitching experiment showed the sinusoidal curves. The periodic change of its magnitude was observed. According to different types of experiment, both the free fall experiment and the rotation table experiment, the author quantified translational and rotational effects. According to the result of the rotational table experiment and the free fall experiment, the acceleration component of each force in the pitching experiment was estimated. The gravity and the aerodynamic forces were indicated as the amplitude of the acceleration wave. On the contrary, the centrifugal force was indicated as the DC component of the acceleration wave.

6- Reference

[01] Ohta, K., Ohgi, Y., Kimura, H., and Hirotsu, N., (2005). Sports Data. Tokyo, Japan : Kyoritsu Shuppan Co.,Ltd. (In Japanese)

[02] Koyanagi, R., (2008). Estimation of physical parameters on flight ball using built-in accelerometer. Master's thesis of Graduate School of Media and Governance, Keio Univ.

An Experimental Study on Ski Jumping Styles (P140)

Shinichiro Ito[1], Kazuya Seo[2], Takeshi Asai[3]

Topics: Ski & other Winter Sports.

Abstract: A style of ski jumping has been changed from a parallel style to the present V-style. The glide ratio varies in jumping styles. The glide ratio and the pitching moment of different jumping styles were examined with wind tunnel experiments by using a replica of a human figure. Opening angle between skis, spacing of skis and a posture of the figure were defined as parameters. It was observed that the glide ratio of the V-style was higher than that of the parallel style at the same angle of attack. A stoop shouldered style was also effective to increase the glide ratio. Differences of the flow field among jumping styles were observed with cotton balls and a tuft method in a smoke wind tunnel. While strong but narrow band downwash was appeared in a wake of the parallel style, wide but weaker band downwash was seen in that of V-style.

Keywords: Ski Jumping, V-style, Posture, Glide Ratio, Flow Visualization.

1- Introduction

The V-style is a style of the present main current in the ski jumping. In the flight phase, the aerodynamic characteristics of the posture control jumping distance. The V-style posture used to be considered as a disordered form so that style points were marked off. However, there was an advantage of 4 meters or more in distance to compensate for the marked off points. That was how the V-style became the main current nowadays. A scientific research on the ski jumping started with wind tunnel experiments with a small size replica by Tani *et al* (1951). Based on the experimental results, they proposed a parallel style, the previously popular jumping style, in which a jumper's hands were placed on the side of the body. A jumping style before the parallel style was a parallel style with jumper's hands extended over the head. An average jumping distance had improved greatly because of their study. Experimental studies on ski jumping with a

1. Dept. of Mechanical Engineering, National Defense Academy, 1-10-20 Hashirimizu, Yokosuka,239-8686, Japan
E-mail: ito@nda.ac.jp
2. The Faculty of Education, Art and Science, Yamagata University, 1-4-12 Kojirakawa, Yamagata, 990-8560, Japan
E-mail: seo@e.yamagata-u.ac.jp
3. Dept. of Human Science, Tsukuba University, Tennodai, Tsukuba, 305-8577, Japan - E-mail: asai@taiiku.tsukuba.ac.jp

human body or a human sized dummy in a large wind tunnel has been a primary concern for the recent years to agree the Reynolds number to the reality. And flight simulation was conducted based on those experimental results. Watanabe (1993) investigated aerodynamic characteristics of opening angles of ski boards of the V-style in a large-scaled wind tunnel using a real human. Müller (1996) experimentally examined aerodynamical changes due to posture changes during the flight phase with a human in a large-scaled wind tunnel and compared with field measurement and with computer simulation. Seo *et al* (2004-1, 2), one of the authors, conducted experiments with a real human in a large-scaled wind tunnel. They examined aerodynamic characteristics and did the optimized calculations in order to extend flight distance by changing ski-opening angles of the V-style during the flight. They gave us some suggestion to fly further. Concerning the experiments in a large-scale wind tunnel, simplified and limited experiments were conducted because various parameters existed in the human body experiment after-mentioned. Therefore, we performed the aerodynamic experiments to acquire an optimal posture to fly further by investigating a lot of various styles and postures with a scaled figure. On the other hand, flow visualization helps to understand the flow field around a ski jumper and to improve the specification of drag and lift forces. Masunaga and Okamoto (1993) captured longitudinal vortices behind legs and skis on a parallel style by the disturbance of tuft with tuft grid experiment in a circulating water channel. These vortices showed the generation of lift and increase of drag. We also visualized air flow around a ski jumper to understand the flight phase.

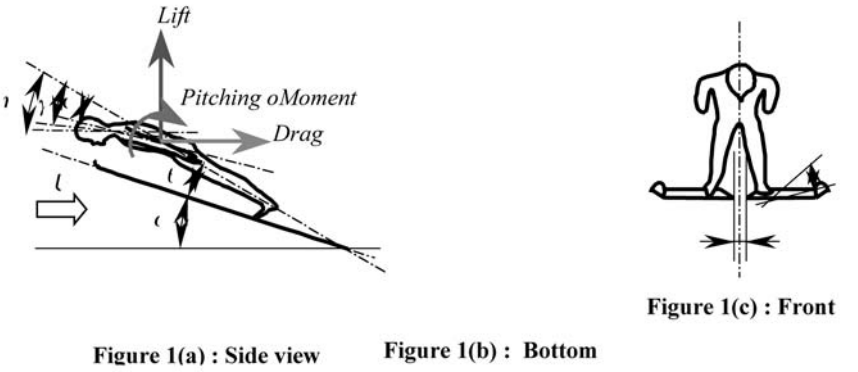

Figure 1 - Definitions of Variables concerning Ski Jumping.

Jumping distance is related to a height of a take-off ramp and glide ratio. Glide ratio (Reach/Height), also called as a lift-to-drag ratio, is an aviation term that refers to a distance which an aircraft moves forward for any given amount of lost altitude (the cotangent of the downward angle). Concerning ski-jumping games, the height of take-off ramps is fixed. Therefore, a posture which has high glide ratio is desirable for ski jumping. However, stability during flight phase is also required. A negative pitching moment initiates unbalance of the posture because raising up force of the upper body is necessary to maintain the posture during the flight in this case. Grasp of positive pitching moment is important to keep a stable flying posture. That is to say that it is

indispensable to ski jumping to choose an appropriate jumping posture with a high glide ratio and a positive pitching moment. Various jumping postures were tried on a figure of about 1/5 in scale and lift and drag characteristics were obtained using an advantage of modal test in this research. The air flow around the scaled figure was also visualized to understand the air flow during the flight phase.

2- Method

A scaled figure (L=259mm) was made based on the data of Daito Takahashi, a player in the Japan's Olympic team. This was a figure replica reproduced accurately with his ski size (250cm) and the binding position based on his height, weight (168cm, 61kg) and Body Mass Index (FIS regulation, 2007). In addition, we defined angle of attack α composed of skis and wind velocity U, inclination angle θ of skis and legs, thorax angle γ between the chest backbone and legs, abdominal angle (lower back bend angle) σ between the lower back and legs and head up angle η between the head and legs indicated in Figure 1(a), ski opening angle λ between each V shaped skis , spacing h of each ski indicated in Figure 1(b), arm angle μ between an arm and a trunk and dihedral angle δ of skis in Figure 1(c). Drag and lift forces were measured by a three component load cell. The back of the hand was arranged facing to the front so that ski jumpers might do so. All the experiments were conducted at a wind velocity of 20m/s, that is to say, on Reynolds' number Re=5.12 x 10^5 as wind velocity U * length of skis l/dynamic viscosity of air v. This was equivalent to 1/8-1/10 of the actual Reynolds number. Firstly, a parallel type was examined to check influences on front inclination angle: θ, opening angle μ of the arm, lower back bend angle: σ, thorax angle: γ and head-up angle: η. Secondary, we investigated the optimal opening angle μ of V-type referring to the most suitable angles obtained from the experiments with the parallel type above. Moreover, lift L, drag D, and pitching moment M were normalized by dynamic pressure, ski projection area S and ski length l. coefficient of lift C_L: $C_L = L/(1/2 \cdot \rho v^2 S)$, drag coefficient C_D: $C_D = D/(1/2 \cdot \rho v^2 S)$and moment coefficient C_M: $C_M = M/(1/2 \cdot \rho v^2 S l)$ were estimated by angle of attack α. In addition, in order to examine factors to generate aerodynamic characteristics of each parallel and V-style, the flow field was visualized in a wind tunnel with three methods; a smoke wind tunnel, a tuft, and a method with cotton balls. The experiments with a smoke method were conducted at Reynolds number $Re = 5.12 \times 10^4$. The other experiments were conducted at $Re = 5.12 \times 10^5$, defined by the characteristic length which was the ski length l.

3- Result and Discussion

3.1 Aerodynamic Specification

Both Figure 2 and 3 are the experimental data in the parallel style. Figure 2 shows the effect of posture angle by glide ratio at angle of attack α in a condition of h=1W where ski spacing is equal to ski width with forward inclination θ = 10°. The trunk becomes parallel to the ski by 10° with lower back bend angle σ=10°. In case of γ= 10°, where the

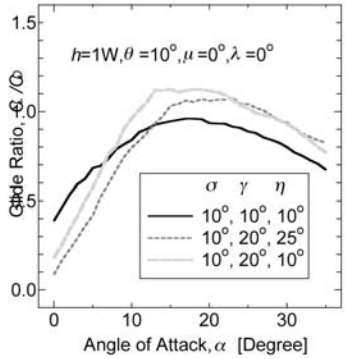

Figure 2 - Glide Ratio and Posture Angle.

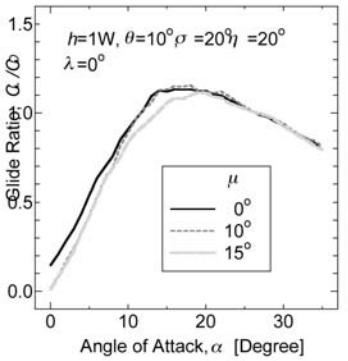

Figure 3 - Glide Ratio and Arm-Trunk Angle, μ.

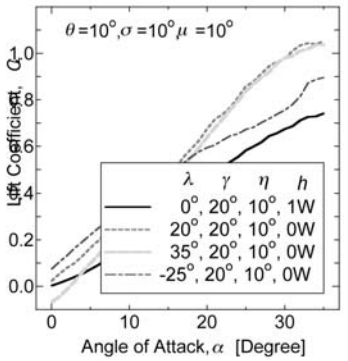

Figure 4 - Lift Coefficient and Ski Opening Angle, λ.

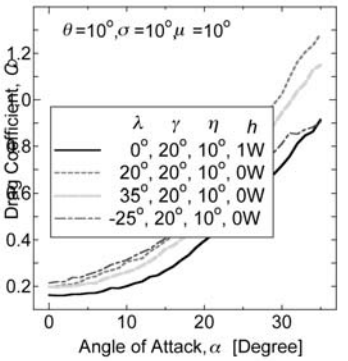

Figure 5 - Drag Coefficient and Ski Opening Angle, λ.

back bone becomes almost a straight line to the legs, glide ratio line draws a gentle curve and reaches to the maximum of 0.96 at about α=17°. In case of so-called stoop-shouldered posture with γ=20°, the glide ratio curve rises straight to the maximum point area. When the head-up angle is η=10°, glide ratio reaches to the maximum of 1.13 at α=13°. With the head-up angle of η=25°. The maximum of 1.07 is at about α=17°. This fact indicates that the stoop-shouldered posture generates higher glide ratio than the straighten posture. That is because the body and ski take an airfoil shape as a whole with the stoop-shouldered posture. The drag force decreases and the lift force increases because the flow separation area may decrease at the back corresponding to a suction surface of the wing. Consequently, the glide ratio increases relatively. The effect of arm-to-trunk angle is indicated in Figure 3. The maximum points of glide ratio are (α, *L/D*) = (14°, 1.13) and (15°-18°, 1.15) at each arm-to-trunk angle of μ=0°, μ=10°. The maximum glide ratio at μ=10° is slightly higher than the other. When μ = 15° where an arm is apart from the trunk, the glide ratio becomes lower than the two above. When the arm is close enough to the body, they are considered as part of the body, and the load of projection area is increased. This causes an effect of increasing the lift. On the other hand, when the arm is apart from the body to some degrees, the effect of increasing the

projection area is lost, and the arm no longer increases the lift. The glide ratio decreases consequently. Therefore, the arm should be placed nearby or on the body. Based on these results, the stoop posture at η =20° with the forward inclining angle of θ=10° and the arm opening angle of μ=10° was adopted for the following experiments in V-style posture.

Figure 4 indicates an effect of V-style ski-opening angle λ to the lift coefficient. C_L curves are compared in the following cases: parallel, λ = 0°, V-style in λ= 20°, λ=35° and the reverse V-style, -25°. With increasing angle of attack α, the lift coefficient C_L of jumping postures except for the reverse V-style, λ =-25°, increases monotonously. The angle of attack on the maximum of C_L shows more than $\alpha \geq$30°. In case of two dimensional wings, it is generally is less than 20°. Figure 4 shows each style does not to stall easily even in large angle of attack compared with those of two dimensional wings. The lift force coefficient of a V-style jumping posture and a reverse V-style jumping posture is larger than that of a parallel jumping posture (λ =0°) in the same angle of attack because the actual projection area increases. The coefficient of lift of a reverse V-style jumping posture is smaller than that of a V-style jumping posture in more than 18° of α. The lift gradient of V-style postures is larger than that of a reverse V shape posture. The curves of C_L gradient at λ = 20° and λ= 35° of V style is almost the same degree.

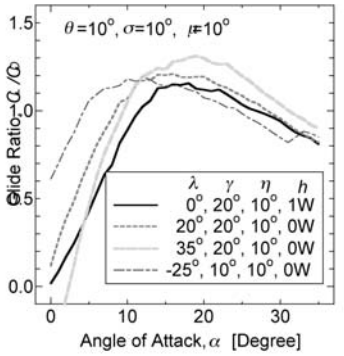

Figure 6 - Glide Ratio and Ski Opening Angle, λ.

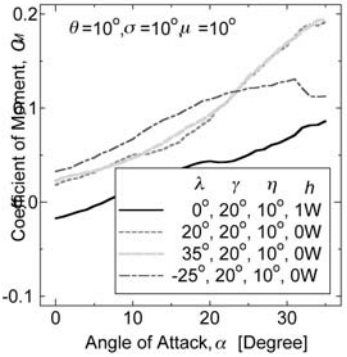

Figure 7 - Pitching Moment and Ski Opening Angle, λ.

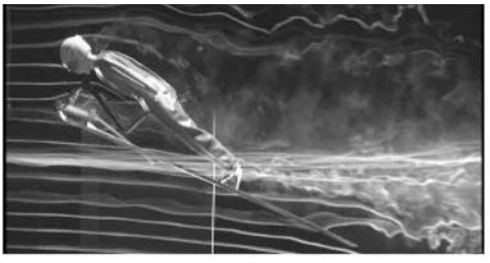

Figure 8 - Flow field around a ski jumper.

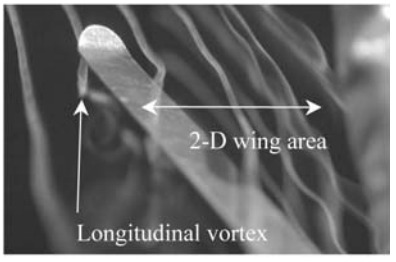

Figure 9 - Tip Vortex occurred at the tip of ski.

Similarly, Figure 5 indicates the consequence of opening angle of V-style of ski in the drag coefficient. C_D also becomes larger than that of a parallel style for that of a V-style as the projection area increases. With increasing angle of attack, the drag force coefficient also increases monotonously mostly like the lift coefficient. The drag coefficient of the reverse V-style posture, λ =-25°, indicates larger than that of the parallel posture, and the drag coefficient of the V-style posture is larger than that of a reverse V-style posture in more than 18° of α. And the drag coefficient of the V-style posture in λ=20° is indicated larger than that in λ=35°.

The relation among the V-style opening angle of ski on glide ratio is shown in Figure 6 based on these. The value of the maximum points in the glide ratio were (α, *L/D*) = (16°, 1.15), (16°, 1.21), (15°, 1.34), (13°, 1.18) respectively. They were found to become larger with increasing the V-style opening angle λ than parallel clearly. In case of the reverse V-style, λ=-25°, the glide ratio was more predominant than the other styles in low angle of attack, less than 10°. It was almost the same degree with parallel styles in more than 10° of angle of attack. A specific rise of glide ratio can be seen again in more than 30° of α in this reverse V-style. In the V-style jumping posture, the jumping at the angle attack from 13° to 25° is desirable because of its high value of the glide ratio.

The relation between the pitching moment coefficient C_M and the angle of attack α is shown in Figure 7. In case of the parallel style, an unstable state of negative C_M is seen when the angle of attack is less than 6°. This unstable state means a possibility for the ski jumper to fall or stall. The state turns to stable and tends to increase monotonously at more than 6° of angle of attack. The pitching moment coefficient is positive at any angle of attack in V-style and in reverse V-style. In this stable state where the pitching moment coefficient is positive, the ski jumper can maintain the forward inclined posture being well balanced in the air. In case of the reverse V-style at more than 30° of α, a sudden irregular change in C_M appears. It might be difficult for the jumper to keep his balance compared with the monotonous increase in C_M like with the other style.

3.2 Specification of the Flow Field

Figure 8 shows smoke streak lines in a smoke wind tunnel at V-style opening angle γ =35° and angle of attack α= 25° with the stoop-shouldered posture at γ=20°. It is seen that the flow line flows along the back of the replica without flow separation. It means that the jumper is not stalling. Obviously, the jumper?s posture also affects jumping distance besides ski styles. Mechanism of lift generation in airfoil is classified into two sorts, two-dimensional wing and three dimensional one., Flow separation causes a stall in 2-D wing. On the other hand, flow separation and three-dimensional longitudinal vortices generate lift forces in 3-D wing like a delta wing. Therefore, lift forces can be maintained even at high angle of attack in 3-D wing. Because of small aspect ratio of a jumper with skis, the occurrence of large tip vortex can be expected at the outer edge of skis. Although a wing stalls at less than angle of attack=20° in 2-D wing in general, a lift-curve of the parallel style (a solid line shown in Figure 4) indicates that stall does not occur even at angle of attack=35°. Therefore, the flow field around the jumper with skis as a whole is expected to be three dimensional. And the aspect of lift curve can be expected the generation of three-dimensional longitudinal tip vortices. Figure 9 visua-

lized the tip vortex and the streamlines in a V-style posture, where V-style ski-opening angle λ=35º, forward inclination θ =10º in a smoke wind tunnel. The longitudinal vortex occurs from the pointed end of the ski front, which circumvent from underneath to upside the ski board, but the flow around the other part of the ski was two-dimensional against the cross-section like 2-D wings.

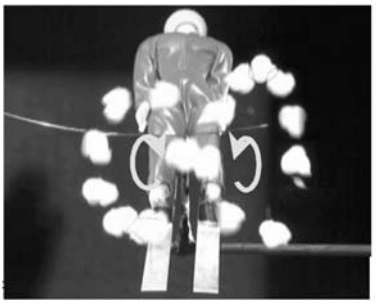

Figure 10 - Wake configuration of parallel style.

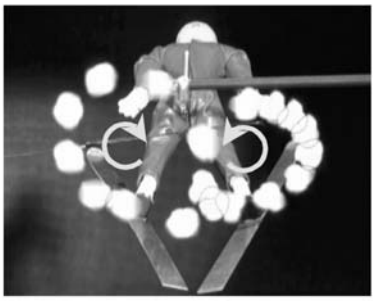

Figure 11 - Wake configuration of V-style.

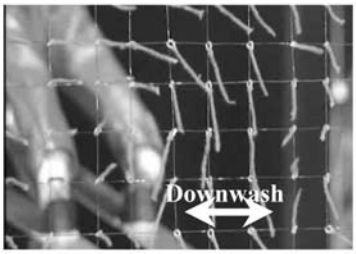

Figure 12 - Downwash flow of parallel style.

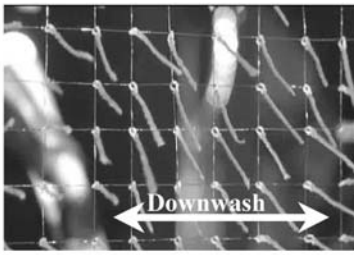

Figure 13 - Downwash flow of V-style.

Figure 14 - Actual picture of ski jumping (Reath, 2002).

Figure 10 and 11 show longitudinal vortices created into a slipstream visualized with cotton balls tied with a thin fishing line from upstream. They show cross-sectional views of the flow field behind the figure. Trajectories of the cotton balls form a bottom of a conic shape with an ellipse in cross-section in the parallel style in Figure 10. The left and right tip vortices are produced at the outer side edges of the parallel skis which have long

wing tips. On the other hand, Figure 11 shows circular trajectories with a conic bottom cross-section in the V-style. The three dimensional flow of the tip vortex is created at the point end of the ski front and circumvent outside from underneath to upside the ski board. The left and right tip vortices associate with each other and the flow appears as downwash right behind the figure replica. Strength and area of the downwash are visualized with a tuft method in Figure 12 and 13. Spacing of each tuft is 15mm. Figure 12 shows the aspect of downwash in the parallel style. Every tuft in two rows behind the replica faces downward as if pasted on the tuft mesh. It shows that narrow but strong downwash is generated in the parallel style. On the other hand, Figure 13 shows that tufts in four rows just inclined downward in the V-style. It means that the speed of downwash is less but the effective area is broader in the V-style. Considering downwash as a reaction of the momentum against the lift, the lift of ski jumping is generated by the downwash caused by three-dimensional tip vortex. With weaker downwash projected at broader area, skis seem to be more stable than with stronger downwash at narrower area. Although verification has not been done yet, the V-style seems to be more stable in rolling motion by downwash than the parallel style.

4- Comparison with actual jumping posture and experimental result

Looking at an actual jumping posture in flight, ski boards are inclined upward as shown in Figure 14. Figure 6 indicates that the maximum glide ratio of the V-style ranges at angle of attack to the ski of $13° \leq \alpha \leq 25°$, However, the angle of attack estimated from the actual picture is from 30° to 40°. Of course, it needs to take photography conditions into consideration, but it is necessary for ski jumpers to lean more forward by overcoming their fear to fall in order to achieve the theoretical optimal jumping distance.

5- Conclusion

The aerodynamic specification of the ski-jumping posture: lift, drag and pitching moment were investigated by conducting wind tunnel experiments. The relation between the flow field and postures was also examined by flow visualization. As a result, the following facts were confirmed.

1. Lift increases monotonously at any style with increasing the angle of attack up to at least 35°.
2. Drag also increases monotonously at any style with increasing the angle of attack up to at least 35°.
3. The advantage of a V-style against a parallel style was confirmed as high glide ratio.
4. The maximum glide ratio was obtained at the opening angle μ=35 ° in our experiments.
5. V-style ski-jumping form is easy to maintain the forward tilt posture with the positive pitching moment at any angle of attack
6. Stoop-shouldered posture increases glide ratio than straight posture because the stoop-shouldered posture creates less turbulence at the back of the skier.

7. Flow visualization around ski jumping indicated that the lift generation mechanism was three-dimensional.

6- References

[F1] FIS regulation, http://www.fis-ski.com/data/document/ausre-edition-2007.pdf
[MO1] Masunaga, K., Okamoto, H., Vortices downstream of a ski jumper, 162, In Fantasy of Flow, Ohmsha, Japan/ IOS Press, Amsterdam.
[MP1] Müller, W., Platzer, D. and Schmölzer, B., Dynamics of human flight on skis: Improvements in safety and fairness in ski jumping, Journal of Biomechanics, 29-8, pp.1061-1068, 1996.
[R1] Reath, P., Photograph Galleries - Home Page,
http://www.viewcalgary.com/peter/skiJump/Frames.html
http://www.viewcalgary.com/peter/skiJump/images/DSC_1607.jpg
[SW1] Seo, K., Watanabe, I., and Murakami, M., Aerodynamic force data for a V-style ski jumping flight, Sports Engineering 7-1, pp.31-40, 2004.
[SM1] Seo, K., Murakami, M. and Yoshida, K., Optimal flight technique for V-style ski jumping, Sports Engineering, 7-2, pp.97-106, 2004.
[TM1] Tani, I. and Mituisi, S.: Aerodynamics of Ski Jumping,. Kagaku 21, 117-122 , 1951.
[WW1] Watanabe, K. and Watanabe, I., Aerodynamics of ski-jumping-Effect of "V style" to distance, Proceedings of the International Society of Biomechanics XIVth Congress, 1452-1453. Paris; International Society of Biomechanics, 1993

Quantification of the Grip Difficulty of a Climbing Hold (P142)

Franz Konstantin Fuss[1], Günther Niegl[2]

Topics: Climbing and Mountaineering.

Abstract: The difficulty of a climbing hold was attempted to be quantified based on fractal dimensions. The difficulty was confined to the change of a single value, namely the inclination of the grip surface, by increasing the overhang of the wall. Sixteen climbers of different experience levels participated in this experiment and had to climb a route equipped with an instrumented hold repeatedly until they failed at a specific degree of overhang. The force-time signals served to calculate the Hausdorff dimension. Subsequently, the Hausdorff dimension was normalised to force and time by a power fit. The normalised Hausdorff dimension increases significantly with the difficulty of a climbing hold, which is – in this study – the inclination of the grip surface. Weaker climbers produced larger normalised Hausdorff dimensions. If the climber fails at the instrumented hold, the force-time signal shows smaller normalised Hausdorff dimensions. Fractal dimensions are a suitable tool to quantify the difficulty of a hold if applied with caution.

Keywords: sport climbing; instrumented climbing holds; perception; force analysis; Hausdorff dimension.

1- Introduction

The difficulty of a climbing route depends on the shape (difficulty to grip) and the sequence of holds (difficulty of movements), as well on the inclination of the wall. The difficulty to grip a climbing hold is related to the shape factor, which summarises the size, the curvatures, the surface texture, and the type of grip (crimp, open hand, pinch, finger pocket, etc.). The most difficult part of the route, the crux, decisively influences the grading. Route grading, however, requires extensive experience and is simply a matter of perception. Other than perception, no means for route grading are available. Different scales were developed in different countries and thus no uniform scale is avai-

1. Sports Engineering Research Team, Division of Bioengineering, Nanyang Technological University, Singapore
E-mail: mfkfuss@ntu.edu.sg
2. Department of Anthropology, Faculty of Life Sciences, University of Vienna, Vienna, Austria
E-mail: guenther.niegl@univie.ac.at

lable: e.g. UIAA scale (Union Internationale des Associations d'Alpinisme, International Mountaineering and Climbing Federation), Yosemite Decimal System (USA), UK scale, French scale, Australian scale, etc.

The performance of a climber can be quantified with instrumented holds and climbing walls (Fuss *et al.* 2003, 2003, Fuss and Niegl 2006a, 2007), based on mechanical parameters (Fuss *et al.* 2003, 2003, Fuss and Niegl 2006a) and fractal dimensions (Fuss and Niegl 2007). The more experienced a climber is, the smaller is the force applied to the hold, the shorter is the contact time, the larger is the coefficient of friction, and the smaller is the Hausdorff dimension of the force-time signal (Fuss *et al.* 2003, 2003, Fuss and Niegl 2006a, 2007). Fuss and Niegl (2007) applied fractal dimensions for the assessment of different grips and moves within an instrumented climbing route. The results roughly suggested that the Hausdorff dimension increases with the difficulty to grip a hold and to execute a move. The disadvantage of comparing different holds lies in the number of different variables related to the shape factor. A hold ideally suited for such a study should be capable of continuously changing a single shape parameter and thus the grip difficulty.

The aim of this study was to design an experiment, which allows for continuous change of one shape parameter of a climbing hold, to identify this fractal dimension which correlates best with the shape parameter, and to prove that the Hausdorff dimension increases with the difficulty to hold the grip.

2- Experimental

The hold used in this study was a sloper (figure 1) with a horizontal grip surface when mounted on a vertical wall. This hold was originally designed for a speed climbing experiment (Fuss and Niegl 2006b). The hold was mounted on a 3D piezoelectric force transducer (9327A, Kistler, Switzerland). The transducer was mounted on a bouldering wall (figures 1 & 2) which allowed for continuous change of the wall's inclination. Thus, the grip difficulty was confined to a single parameter, namely the inclination of the grip surface, by simply increasing the degree of wall overhang. The perceived degree of difficulty corresponded to the wall angle.

Sixteen climbers (12 males, 4 females; body mass: 49-91 kg; age 17-42 yrs) of different climbing age (1-22 yrs) and experience (UIAA red point RP 6+ - 10+) participated in this experiment. The participants had to climb the route – a boulder with defined hand- and foot-holds (figures 1 & 2) – repeatedly, with a 10 minute rest period after each climb. After each successful climb, we increased the angle in increments of 5°, until the climber failed 3 times at a specific wall angle. The climbers were instructed to place the fingers on the top surface of the hold without touching its lateral sides with any finger or thumb. The coordinate system of the force transducer was: x: parallel to the hold's surface, towards the climber, y: leftward, z: perpendicular to the surface, downward. The parameters analysed were: mean force (x-, y-, z-directions and resultant), maximal force, impulse, and the Hausdorff dimension of the force components and resultant, mean and maximal coefficient of friction, and contact time. The Hausdorff dimension was calculated according to the method described by Kulish *et al.* (2006).

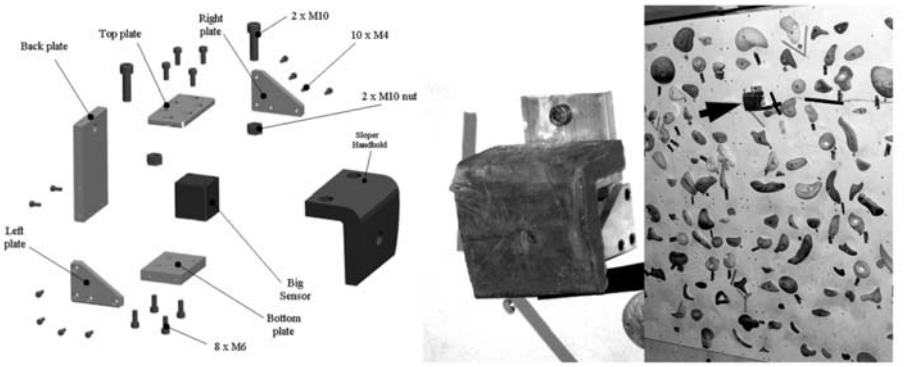

Figure 1 - instrumented sloper hold used in the experiment (exploded view and mounted on the wall).

Figure 2 - sequence of climbing moves (the arrow indicated the position of the instrumented hold).

3- Results

3.1 Experience of the climbers

The UIAA red-point value correlated well with the maximal inclination of the hold a climber was no longer able to grip (failure angle, figure 3). The correlation coefficient was $r = 0.7927$, and the difference between climbers of RP < 8 and > 8 was significant at $p = 0.00014$. The more difficult the hold (inclination angle), the more experience is required (red-point, RP) to successfully grip the hold. This result is mirrored in the coefficient of friction, which is expected to increase with the inclination angle (figure 4; linear correlation coefficient $r = 0.828$). The more experienced a climber is, the larger the coefficient of friction he can produce (Fuss *et al.* 2003, 2003, Fuss and Niegl 2006a).

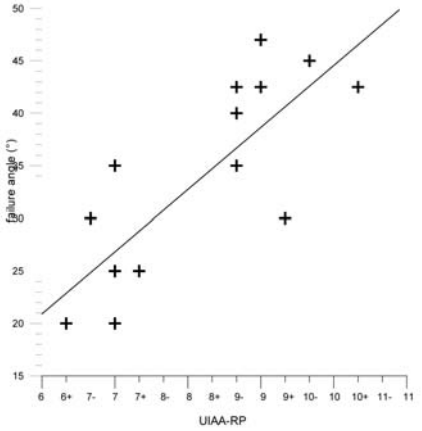

Figure 3 - failure angle against red-point value.

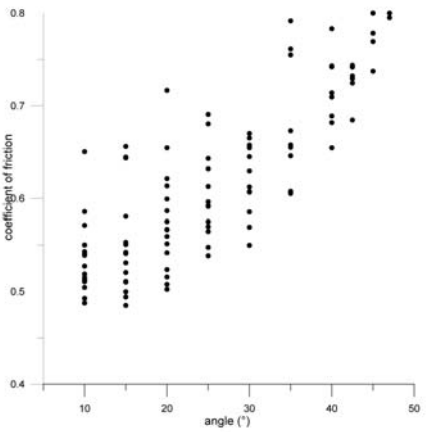

Figure 4 - coefficient of friction against wall angle.

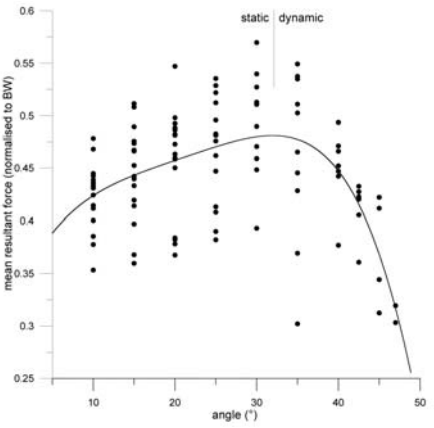

Figure 5 - mean resultant force against wall angle.

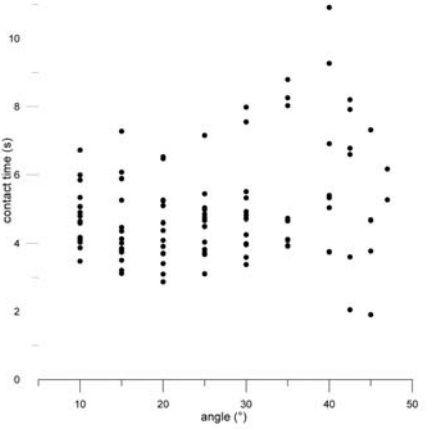

Figure 6 - contact time against wall angle.

3.2 Quantification of difficulty

3.2.1 Identification of suitable parameters

The Hausdorff dimension increases with the amplitude of a signal, with its length (duration), with the impulse (time integral of the amplitude), and with frequency and chaoticness. Thus, the mean load on a hold and the contact time influence the Hausdorff dimension. The relationship between Hausdorff dimension and amplitude, duration, and impulse follows a power law (Fuss, unpublished results).

The mean resultant force (normalised to the body weight) increases initially with the inclination angle, until an angle of ~32°, and drops again beyond that (figure 5). The normalised mean tangential and normal forces exhibit the same trend. The angle of ~32°

marks the transition from static move to dynamic. A dynamic move is required to grip the hold at higher angles. The decrease of the load beyond 32° comes from accelerating the centre of mass (COM) downward or decelerating upward, which reduces the gravitational force by the thus produced inertial force. A similar trend, although not that clear, is seen in the contact time (figure 6) and the impulse.

The Hausdorff dimension of the resultant force (figure 7) increases with the angle, however, the correlation coefficient is only 0.2596. It is even worse in the Hausdorff dimension of the normal force: r = 0.1035. The Hausdorff dimension of the tangential force, Hx, correlates far better with the inclination angle (figure 8): r = 0.6442. Thus, Hx is selected for representing the difficulty of gripping the hold.

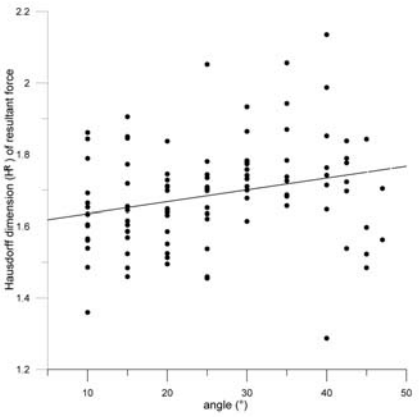

Figure 7 - Hausdorff dimension of resultant force against angle

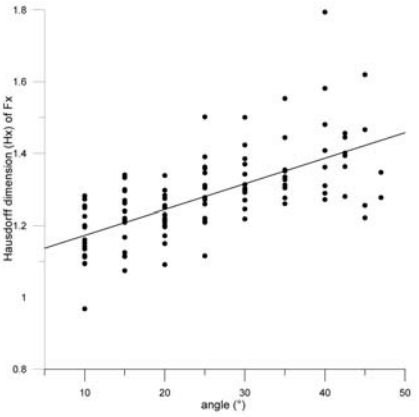

Figure 8 - Hausdorff dimension of tangential force against angle

3.2.2 Normalisation of the Hausdorff dimension

In order to make Hx independent of the amplitude (force) and the duration of the signal (contact time), as well as the impulse (time integral of the contact force; mean force Fx in x-direction times contact time), Hx was expressed as a power function of the impulse of Fx (figure 9) by applying a power fit. Subsequently, Hx was normalised to the power function: any normalised Hx above, on, or below the power fit is positive, zero, or negative respectively.

3.2.3 Correlation of normalised Hausdorff dimension and wall angle

Although the correlation between normalised Hx and angle (figure 10) is poor (r = 0.3815), the difference between different data groups of different angles is significant:

- 10°-15° and 40°-50°, p = 0.00013
- 10°-30° and 35°-50°, p = 0.00172
- 10°-25° and 30°-50°, p = 0.00457

The larger the wall angle, and thus the difficulty, the larger is the normalised Hausdorff dimension Hx.

The linear regression line (figure 10) of climbers of RP<8 has a steeper gradient compared to more experienced climbers (RP>8). This clearly explains the influence of experience, even if data of weaker climbers at higher angles is missing (figure 10).

The reason for the poor correlation might be related to the human factor, i.e. the personal climbing style and the performance at a specific hold. If a climber fails at, and slips off, a hold, then he has either misjudged the difficulty or he cannot exceed a specific difficulty level. Thus, it is expected that force-time signals of a failed grip show a smaller normalized Hausdorff dimension. This is indeed the case, when comparing the successful and failed attempts to grip the hold (figure 11). Examples of normalized Hx against angle are shown in figure 12.

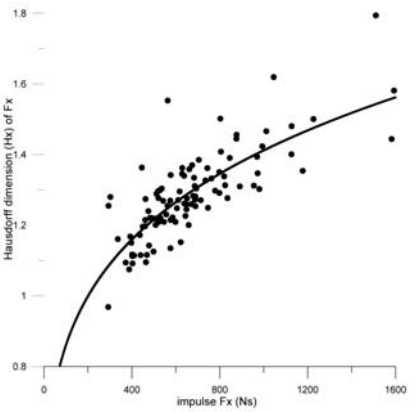

Figure 9 - Hausdorff dimension of tangential force against impulse

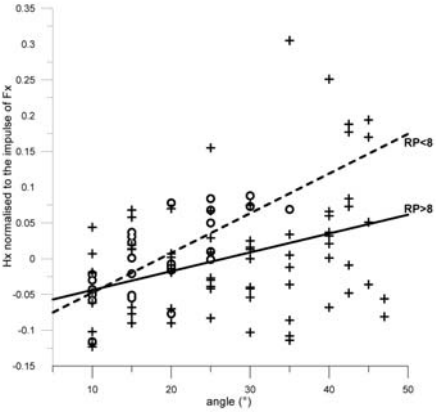

Figure 10 - normalised Hausdorff dimension of tangential force against angle (+: climbers of red-point >8; O: climbers of red-point <8)

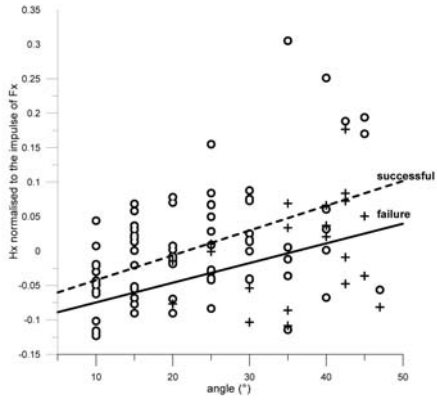

Figure 11 - Hausdorff dimension of tangential force against angle (+: failed attempts; O: successful attempts)

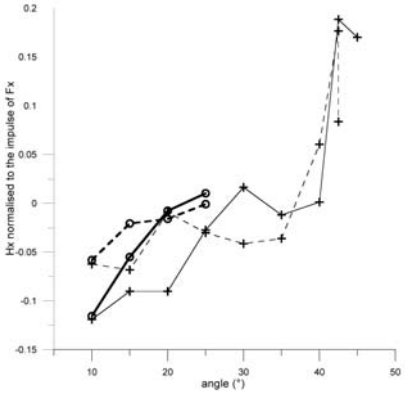

Figure 12 - normalised Hausdorff dimension of tangential force against angle (+ and O: better and weaker climbers)

4- Discussion

The results of this experiment prove indeed that the normalized Hausdorff dimension Hx increases with the inclination of the hold and thus with the difficulty. This study, however, does not necessarily provide a general solution for quantitative route grading. It is known from other studies (Fuss and Niegl, unpublished results), that the type of the hold, and the type of the grip has to remain the same, in order to quantify the difficulty of holds of the same type. This means, the hold should not be changed from a jug to a 2-finger pocket, nor should the grip be changed from crimp to pinch. Furthermore it was observed (Fuss and Niegl, unpublished results) that in two routes of different difficulty, by changing shape, rather than the location of the holds, the more difficult route forces the climber to shift the load from the hands to the feet. This resulted into smaller grip forces whereas the contact time increased in the more difficult route. Thus, the normalised Hausdorff dimension was unexpectedly smaller in the more difficult route, which suggests, that a climber tends to make a difficult route easier by changing and adjusting the climbing style. Or, in other words, a difficult route forces you to climb better and more economically.

5- Conclusion

The normalised Hausdorff dimension increases significantly with the difficulty of a climbing hold, which is – in this study – the inclination of the grip surface.

Weaker climbers produce larger normalised Hausdorff dimensions.

The force-time signal at a hold failed to grip shows smaller normalised Hausdorff dimensions.

Fractal dimensions are a suitable tool to quantify the difficulty of a hold if applied reasonably and with caution.

6- References

[FN1] Fuss F.K., Niegl G., Boey L.W., and Liu X. Mechanical parameters of handhold forces during sport climbing. In: Sports Dynamics, Discovery and Application, Eds: Subic A, Trivailo P, Alam F. RMIT University Press, Melbourne, Australia, pp. 283-288, 2003a.

[FN2] Fuss F.K., Niegl G., and Yap Y.H. Dynamics of sport climbing: influence of experience and training. In: Sports Dynamics, Discovery and Application, Eds: Subic A, Trivailo P, Alam F. RMIT University Press, Melbourne, Australia, pp. 24-29, 2003b.

[FN3] Fuss F.K., and Niegl G. Instrumented Climbing Holds and Dynamics of Sport Climbing. In: The Engineering of Sport 6, Vol. 1 – Developments for Sports, Eds: Moritz EF, Haake S. Springer, Munich, pp. 57-62, 2006a.

[FN4] Fuss F.K., and Niegl G. Dynamics of Speed Climbing. In: The Engineering of Sport 6, Vol. 1 – Developments for Sports, Eds: Moritz EF, Haake S; Springer, Munich, pp. 51-56, 2006b.

[FN5] Fuss F.K., and Niegl G. The Fully Instrumented Climbing Wall: Performance Analysis, Route Grading and Vector Diagrams – A Preliminary Study. In: The Impact of Technology on Sport II, Eds: Fuss FK, Subic A, Ujihashi S. Taylor and Francis Group, London, pp. 677-682, 2007

[KS1] Kulish V., Sourin A. and Sourina O. Human electroencephalograms seen as fractal time series: Mathematical analysis and visualization. Computers in Biology and Medicine, 36: 291–302, 2006.

Artificial Turf Development as Surface for Golf Practice (P143)

David Rosa, Nicolás Ortega, Mercedes Sanchis, Enrique Alcántara, Francisco Parra, Francisco Matey, Pedro Vera, Carlos Soler[1]

Topics: Golf.

Abstract: Demand for new golf courses is rising due to the increasing number of golfers, especially in coastal areas of South Europe with high sunshine and temperatures, but with very restrictive factors as water shortage. This factor has produced a growing interest in the introduction of artificial grass for golf courses. The aim of this study was the development of artificial turf for golf. At present, the behaviour of natural grass is considered as the reference for the development of artificial grass as a surface for golf courses. However, there is little information about its mechanical behaviour. The first step of this study was to generate a reference model of natural turf behaviour. Two discussion groups were conducted to identify and prioritize the requirements of the main zones of a golf course. After that, testing procedures and devices were developed for the study of the above-mentioned requirements. The tests carried out were rotational resistance, divot hole strength, ball roll, distance after bounce and angled ball rebound. The testing results were used to develop the proposed reference model in terms of reference values for the measured properties. After that, artificial turf samples (tee (14 samples),fairway (18), green (8)) were build using different carpets, sand size infill and different shock pads. The same tests were carried out on these samples. ANOVA statistical treatment was carried out on the obtained results. From the ANOVA, those artificial turf samples with the most similar behaviour to natural turf's behaviour were determined for each golf course area.

Keywords: golf, artificial turf, surface properties.

1- Introduction

Golf players' number is constantly rising around the world, especially in developed areas where there is golf tradition, being North America (52.39% of world participants) and Asia (37.39%) the areas with higher number of golfers (National Golf Foundation USA, 2004).

Instituto de Biomecánica de Valencia, Universidad Politécnica de Valencia- Edificio 9C - Camino de Vera s/n, E-46022 Valencia, Spain - E-mail: david.rosa, nicolas.ortega, mercedes.sanchis, enrique.alcantara, francisco.parra, francisco.matey, pedro.vera, carlos.soler@ibv.upv.es

In Europe, in spite of a lower number of golfers (5.9% of world participants), there is an important increasing in numbers of participants, particularly marked in those north European countries with the longest golf tradition and significant numbers of participants. In Southern Europe, despite the low tradition, the golf courses demand is increasing quickly, especially in coastal areas with high sunshine and temperatures, fuelled by North European tourist who want to enjoy golf practise all seasons. However, these areas present important restrictions as water shortage, which added to high maintenance costs of natural turf golf courses, has led to an increasing interest in the introduction of the artificial grass as golf course surface. As opposite of other sports in which artificial turf is being used for many years and there are several standards (FIFA 2006, UNE 2002), the artificial turf for golf is a new product and no references exist.

At present, natural turf behaviour is considered as the reference for the development of artificial grass as surface for golf courses. While numerous studies have been carried out on equipment construction or agronomical grass properties, there is little information about mechanical grass behaviour and their mechanical interaction with equipment. Despite this, some authors have worked on it with interesting results. An apparatus was developed for studying the impact of golf balls on natural turf and their application on the field (Haake, 1987, 1989, 1981). The playing characteristics of a wide range of golf greens have been studied by means of physical measurements complemented by a questionnaire survey (Baker *et al.* 1996). Joining together both grass knowledge and playing characteristics study, the changes in playing performance have been studied depending on sand type and rootzone amendments (Baker *et al.* 1999).

The aim of this study was to develop some artificial turf samples suitable for each golf course area according to the natural turf behaviour.

2. Methodology

The study has been conducted in phases. First, subjective requirements were determined by means of discussion groups and questionnaires with golf course users and managers. Secondly, test devices and procedures were developed from other sports' standards (FIFA 2006, UNE 2002) for studying the requirements determined in the previous phase. Tests were carried out on natural turf in order to obtain reference values of natural turf behaviour. Next, artificial turf samples were build and tested. Finally, test results were analyzed leading to the suitable artificial turf samples for each area according to the natural turf behaviour.

Surveys and tests were carried out in 5 golf courses, selected in different Spain areas (north, east, centre and south) to include in the model the different climatic areas.

The course ratings were between 72 and 72.5 for men, and between 72.8 and 75.1 for women. The courses slope were between 127 and 134 for men, and between 125 and 131 for women.

2.1 Identification of requirements

The study of requirements has been developed in two phases.

At first, two discussion groups were conducted to identify the requirements demanded. The first group conducted was formed by 7 professional golf players, and the second one was formed by 7 golf course professionals (greenkeepers and managers). The treatment of information was realized by means of an interpretive analysis. This analysis is based on a descriptive model in which the answers of the participants are summarized creating brief descriptions and offering, besides, the meaning of the obtained information. This model of analysis uses the recording audio of the session and the records of observation, to contrast the information with the context in which they have been expressed, participants roles, etc.

Next, a 63 items questionnaire was distributed in five golf courses to prioritize the requirements identified in the previous phase. In response, 96 valid surveys were obtained. Statistical descriptive analysis of data has been carried out with the statistical software SPSS 14.0.

2.2 Tests description and procedure

The test carried out, described in next paragraphs, were rotational resistance, divot hole strength, green speed, distance after bound and angled ball rebound. These tests were chosen because they are appropriated methods for studying the mechanical properties related to the obtained requirements. All tests on natural turf were realized in the morning, two hours after the irrigation with grass in wet conditions in June and July 2006. Test on artificial turf were carried out in laboratory in controlled conditions.

Urethane Elastomer™ covered 3-piece multicomponent golf balls were used in the tests of green speed, distance after bound and angled ball rebound.

Test results were analyzed by means of ANOVA ($p<0.05$) using the software SPSS 14.0.

2.2.1 Rotational resistance

Based on standards (FIFA 2006, UNE 2002), this test evaluates the surface grip measuring the torque required to rotate a loaded test foot with four golf studs in contact with the surface. This test was carried out on the Tee and Fairway.

The load applied with the apparatus was determined studying with a force plate the loads applied in each foot during the swing by five professional golf players. To simulate the forward foot load is 26 Kg and for the backward foot the test load is 8 kg. Drop height of the test disc is the same as FIFA (FIFA 2006), 60 ± 5 mm.

Five individual measurements were made on each zone with each load described.

2.2.2 Divot hole strength

A test apparatus was developed to study the horizontal force needed to break the turf cover with a horizontal displacement at controlled speed. Due to the difficulties to reproduce the head club speed during impact and to measure the force applied for making a divot hole, we were constrained to carry out the test with a reduced displacement speed.

The test is performed with a vertical force equal to 150 N and a constant horizontal displacement speed of 0.4 m/s.

The variable obtained from this test is CFD_{peak} (maximum traction capable of being supplied by the ground prior to break).

Nine individual measurements were carried out on the Fairway from each course.

2.2.3 Green speed or Stimpmeter

This test, described in UNE (UNE 2002) according to USGA recommendations (USGA 1993), measures the ball's capability of rolling on the Green area. This test was carried out as described in the mentioned standard.

2.2.4 Angled ball rebound

A ball is projected with a pneumatic cannon at a specified speed and angle onto the surface. A high speed camera records the rebound. Using the videos, the absolute, horizontal and vertical velocities are determined and the energy coefficients of restitution (absolute (COF ABS), horizontal (COF X) and vertical (COF Y)) are calculated from the ratio of the ball's velocity just after impact to the velocity just prior to impact. These coefficients are accepted as good indicators of ball behaviour after rebound.

Five measurements on each zone (Fairway and Green) were carried out at 14 m/s and an angle of 43º.

2.2.5 Distance after bounce

Using the same cannon as in 2.2.4, the ball is projected with different speed and angle, depending on the zone studied and it is measured the distance covered by the ball from the first bounce to the point where it stops.

Test specifications shown in table 1 were determined by means of test carried out with five professional golf players.

Table 1 - Distance after bounce test specifications.

ZONE	SPEED	ANGLE	SIMULATED CLUB
TEE to FAIRWAY	37 m/s	24 degrees	3 - Wood
FAIRWAY to GREEN	27 m/s	38 degrees	8 - Iron

2.3 Artificial Turf Samples

Initially, 60 artificial turf samples were considered using 16 carpets types, 2 sand size infill and 3 shock pads types. Due to the large number of samples, an orthogonal experiment design was made and as result, 40 samples were built and tested. From this samples, 14 were built for the Tee, 18 for the Fairway and 8 for the Green. The test carried on the samples were Angle ball rebound, Rotational Resistance and Divot hole Stregth.

3. Results

3.1 Golf course requirements

Both discussion groups considered that the course zones to be taken into account should be TEE, FAIRWAY and GREEN.

In the next paragraphs are described the main results by zones.

In the TEE, the mowing uniformity and height are considered very relevant aspects by the 79.2% and the 78.1% of the surveys participants respectively. About the surface properties, is considered very important the surface uniformity by the 86.3% of the participants. Finally, about the interaction between the player and the surface, the most relevant aspect for the 90.7% of the participants is the surface grip to avoid sliding during swing.

In the FAIRWAY, the grass relevant aspects are the mowing height and grass density for the 87.6% and the 88.6% of the participants. In opinion of the participants, a good drainage (84.4% of participants) and a smooth feel when removing divot holes (85.2% of participants) are the most relevant surface properties. About the interaction between the surface and the ball, the participants considered the rebound (77.6%) and ball roll after bounce (70.5%) very relevant for the game. The surface grip (79.1%), as in the TEE, is very relevant in the Fairway.

In the GREEN, the grass properties considered very relevant are grass density (87.1%), the mowing height (87.1%) and mowing uniformity (86%). A good drainage (88.1%) and surface uniformity (72%) are surface requirements very relevant and relevant respectively. The rebound (87.9%), a constant trajectory (87%) and green speed (84.8%) are the most relevant aspects related to the interaction between the surface and the ball.

This results has led to develop the tests described in the paragraph 2.2.

3.2 Tests results

From the Analysis of the variance (ANOVA) for natural turf results, two intervals of behaviour have been determined. The first one, more restrictive, comprises the rank from the 25^{th} percentile to the 75^{th} percentile. The second one, wider, comprises the rank from the fifth percentile to the 95^{th}. The aim of creating two intervals is, based on FIFA (FIFA 2006), to provide two criteria for developing different qualities in artificial surfaces, depending on the assigned use. To compare the behaviour of natural turf with artificial samples', in the figures 1 to 5 are shown the test results. The horizontal lines, represents the two mentioned intervals of natural turf results. The results represented by means of the Mean and the Standard Deviation, are the different artificial turf samples separated by golf course areas.

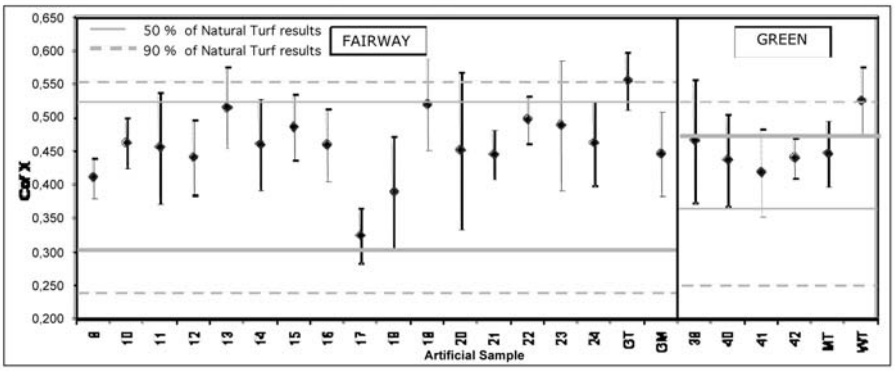

Figure 1 - Angle ball rebound. Horizontal Coefficient of restitution (COF X).

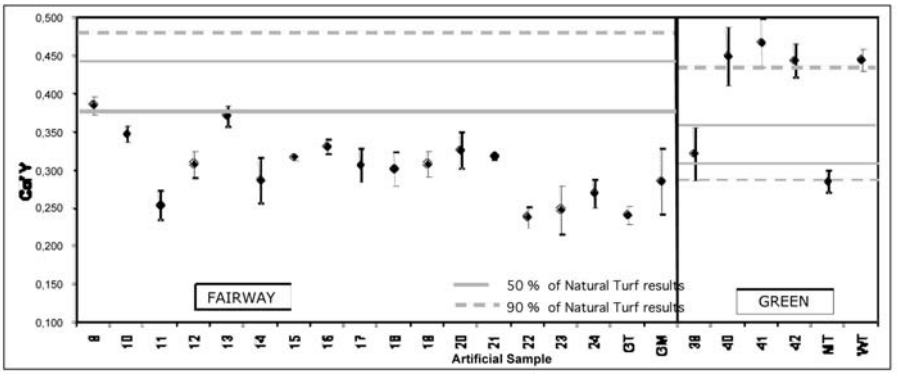

Figure 2 - Angle Ball Rebound. Vertical Coefficient of restitution (COF Y).

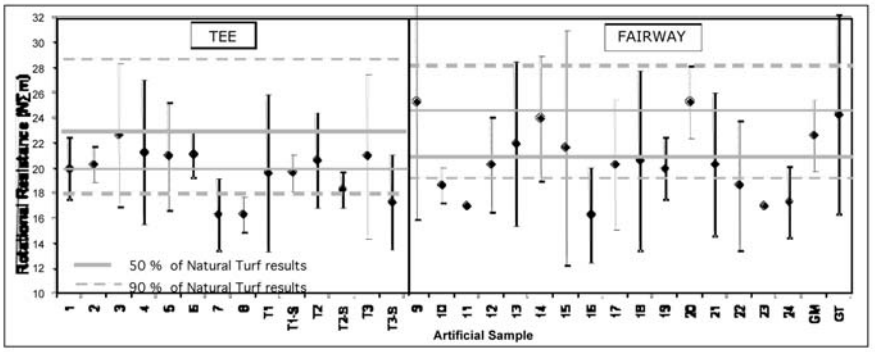

Figure 3 - Rotational Resistance. Foreward Foot.

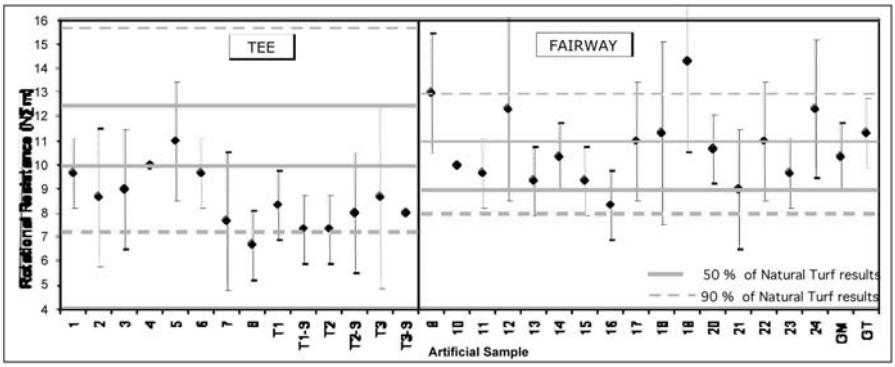

Figure 4 - Rotational Resistance. Backward Foot.

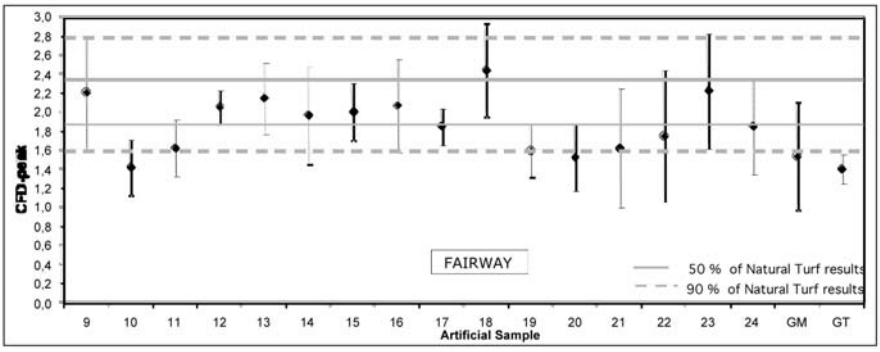

Figure 5 - Divot Hole Strength.

For determining the most suitable samples for each area, the results of artificial turf have been compared with natural turf results selecting those samples with the closer behaviour. The weight of each test in the global evaluation of each sample has been defined according to the surveys results.

4. Discussions and conclusions

As a result of this work, a first reference model of natural turf behaviour has been generated for developing artificial grass for golf. This model has been used to determine which artificial turf samples would be more suitable for each golf course area.

Once requirements identification was made by means of discussion groups and surveys, test procedures and devices were developed to measure the behaviour characteristics that results from the requirements. Test results have generated the proposed model. it consists of reference values for tests depending on the golf course area.

Obviously, the natural grass behaviour depends on many factors such as grass species and others that haven't been considered because this model is a first approach to natural turf behaviour.

In this first reference model, the number of golf courses and variables included are limited and more tests should be carried out to make the model more representative of the natural turf behaviour.

Although the number of test carried out on artificial turf samples was limited, the selected samples according to the results will be installed in a show golf facility, where more tests will be carried out and in order to study the surface properties evolution and their durability. The golfers opinion will be checked to study the users perception of the surface properties.

In the future, standards related to golf course surface behaviour should be developed to guarantee the quality of the surfaces installed. This work could be a first step for standards developing.

5. References

[BH1] Baker, S.W., Hind, P.D., Lodge, T.A., Hunt, J.A., Binns, D.J., A survey of golf greens in Great Britain. IV. Playing Quality. Journal of the Sports Turf Research Institute. 72, pp. 9-24, 1996.

[BM1] Baker, S.W., Mooney, S.J., Cook, A. The effects of sand type and rootzone amendments on golf green performance. III. Playing Quality. Journal of the Sports Turf Research Institute. 75, pp.27-35, 1999.

[F1] FIFA QUALITY CONCEPT. Handbook of Test Methods for Football Turf. 2006.

[H1] Haake, S.J. Technical note. An apparatus for measuring the physical properties of golf turf. Journal of the Sports Turf Research Institute. 63, pp.149-152, 1987.

[H2] Haake, S.J. Apparatus and test methods for measuring the impact of golf balls on turf and their application in the field. Ph.D Thesis, University of Aston, Birmingham, 203 pp., 1989.

[H3] Haake, S.J., The impact of golf balls on natural turf. II. Results and conclusions. Journal of the Sports Turf Research Institute, 67, pp 128-134, 1991.

[U1] UNE 41959-1: 2002 IN. Sport surfaces of natural turf. Part 1: Construction systems for sport surfaces of football, American football and golf. 2002.

[U2] USGA Recommendations for Putting Green Construction ,1993.

Shoe Signature Monitoring for Advanced Running Technique (P145)

Young, C[1], Fleming, P. R.[1], Dixon, S[2], Carré, M. J.[3]

Topics: Biomechanics; Innovation & Design; Performance Sports.
Abstract: An athlete and support team will utilise whatever tools are at their disposal to help 'measure' the athletic ability and develop it further. However, assessment of the athletic motion technique and propulsion mechanics is usually limited to a combination of indirect techniques (visual, high-speed video etc.) and may include some direct measurement of foot-surface contact forces or pressures in a controlled laboratory environment. The next logical step in research and development is to provide high quality information of the foot-surface interaction during the athlete's motion in training by the development of advanced instrumentation attached in some way. This information could provide enormous benefits to individuals to both enhance their performance and also provide unique feedback on their (more controlled) rehabilitation from injury. This paper describes findings to date from a current EPSRC/UK Sport funded study to evaluate, in the first instance, what and how appropriate feedback could be given to elite athletes and their coaches of their running characteristics. The research undertaken thus far has elicited the detailed user requirements from a series of interviews and workshops with elite coaches and athletes and sets out a framework for delivering appropriate technology directly tailored to both measure and enhance performance. The qualitative data is presented as a hierarchical graphical plot showing the six general dimensions (technique, footwear and surface, environment, performance, injury and cardiovascular). These are discussed in detail in turn, with regard to the instrumentation technology required for delivery, and with an emphasis on ideal processed data visualisation techniques required for relatively simple absorption and actions by the athlete and coaching team.
Keywords: gait analysis, instrumentation, coaching, rehabilitation, performance, perception.

1. Sport Technology Institute, Loughborough University, Loughborough, LE11 3QF - E-mail: p.r.fleming, c.young@lboro.ac.uk
2. School of Sport and Health Sciences, University of Exeter, Exeter, EX1 2LU - E-mail: s.j.dixon@exeter.ac.uk
3. Department of Mechanical Engineering, University of Sheffield, Mappin Street, Sheffield, S1 3JD, UK
E-mail: m.j.carre@sheffield.ac.uk

1- Introduction

During a typical training session, analysis of athlete technique is generally limited to visual observation. For more technical skills, such as long or high jump takeoff, there is an increasing use of video analysis. However, force technology has not become as widely or routinely applied to the analysis of sports technique in a coaching environment. From the early work of Cavanagh and LaFortune (1980) we learned that runners have differing ground contact styles. However, the application of force measurements to assess running foot strike patterns has not progressed greatly from this initial crude classification of runners as rearfoot, midfoot or forefoot strikers. The recent development of technology allows the quantification of pressure distribution across the shoe-surface or shoe-foot interface. Knowledge of variables such as peak pressure or impulse at specific foot locations and the timing of these events have improved our understanding of typical loading patterns during running (de Cock *et al.* 2005). Measurements of centre of pressure with pressure systems also provides simultaneous footprint and centre of pressure pathways, revealing different centre of pressure patterns with different foot strike patterns (Dixon, 2006). The ShoeSMART feasibility study aims to explore the potential of force/pressure systems to provide feedback to coaches to aid in the assessment of running technique.

Potential applications of in-shoe load measurements in sport relate to both the understanding of performance and the management of sports injury. The proposed ShoeSMART system aims to provide a novel and practical means of assessing foot strike patterns. Figure 1 illustrates a hierarchical diagram showing the factors identified as influencing running performance (Hay and Reid, 1988). This simplified model demonstrates that the underpinning factors key to performance are the forces and their respective duration of application during the surface contact and takeoff phases. Determination of the exact variables of interest to coaches and practitioners remains to be established and is the focus of the initial phase of the project, described in the current paper. In terms of applications within injury prevention and management, knowledge of the typical load distribution for an individual athlete may allow the detection of injury susceptibility and differences when technique is varied in response to factors such as fatigue or gait adjustment due to injury.

The overall aim of the ShoeSMART project is to evaluate the feasibility of an instrumented shoe (or insole/sock) to provide detailed quantitative data on the running characteristics of the user (without undue influence) to enhance performance and injury rehabilitation. The aim of the current phase of the project is to assess what information elite athletes and coaches believe they require regarding running characteristics. This information on athlete and coach perceived requirements will inform the future phases of the project, which will consider the technology available to provide appropriate information and the most suitable form of this feedback.

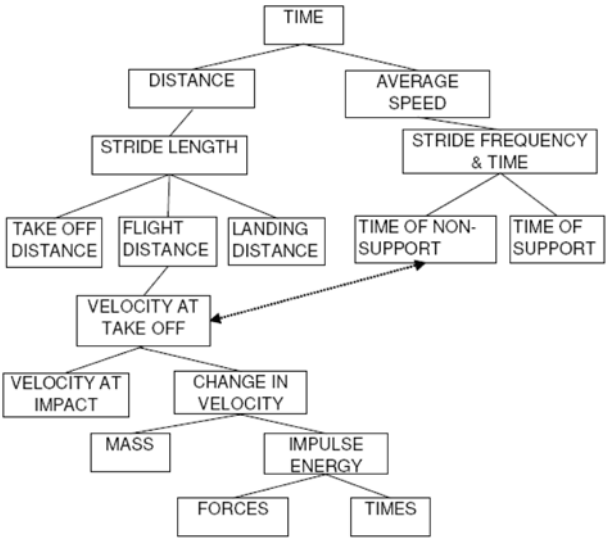

Figure 1 - Simplified Running Model (adapted from Hay & Reid, 1988).

2- Study Design

A previous study exploring players' perceptions of running technique from which a suitable methodology could be drawn was not identified in the literature. Previous methodologies used to investigate perceptions with sports equipment (Roberts *et al.*, 2001; Fleming *et al.*, 2005) have shown a propensity towards the use of surveys or interviews within a qualitative analytical framework as the primary data collection method. These methods were successful in identifying participants perceptions, opinions and preferences regarding their interaction with equipment, including aspects such as feel and performance.

It was identified that a subject led semi-structured interview was suitable for eliciting athlete perceptions, in that it permitted investigation of selected issues in depth and detail (Patton, 1987). Interviews were used to elicit subject led responses and minimise investigator expectations and/or bias, and were primarily individual (i.e. one investigator and one participant). In addition two group sessions were undertaken with one interviewer and between 4 and 6 participants. The objectives of the interviews were to elicit undiluted information that was rich in depth and detail from which selected themes could be chosen for further investigation. The approach facilitated the participants to lead the interview and ensured accuracy of matters significant to them and reduced the risk of investigator bias, through preconceptions.

Data were collected through one-on-one interviews and two group seminars. An interview guide was produced to aid the investigator and optimise the amount of data obtained from the athletes and coaches. It also provided a selection of unambiguous questions and ensured that a consistent approach was followed. Additionally, a series of leading questions were included at the end of the guide to help prompt athletes and

coaches that were having trouble articulating their responses. If required a note was made that these had been used and in particular which ones. Prior to the development of the interview guide several elite coaches and a performance analyst were consulted as to its design and content (including the prompts).

Patton (2002) raises the issues of sampling for qualitative methods. The quality of data can be influenced by the sample of people from which the data is collected. An approach known as 'purposeful sampling' was used to select the participants for this study. Purposeful sampling targets participants from which one can learn a great deal about issues of central importance to the purpose of the study. It was envisaged that elite athletes and coaches would provide a relatively high quality of response due to their higher level of skill/ability and better understanding of factors influencing their performance. Therefore, elite (national standard or better) athletes and coaches (trained an athlete to national standard or better) were selected. In order to evaluate the ability of each athlete their age, event, personal best and gender were recorded. Full ethical approval was obtained in accordance with the University requirements

During interviews there were several data quality issues of concern, including the participants misunderstanding what was being asked, the interviewer misinterpreting the responses and the preconceived attitudes and opinions of the interviewer influencing the participants responses (Cohen and Manion, 1980). For example, athlete terminology could differ from the investigator's, causing misunderstanding. Throughout these interviews a number of methods were employed to reduce the potential for bias. Prior to the interview phase, discussion with elite coaches and an expert performance analyst helped define athletes' terminology and to construct the interview guide. The interviewer had experience in interview techniques of this kind and was consistent and clear in questioning and probing using the interview guide.

Data analysis involved the organisation of raw data (quotes and statements) into a set of meaningful structured themes by means of inductive analysis. An inductive analysis involved obtaining categories and themes from the quotes rather than forcing them into pre-determined groups. The analysis followed the procedure developed by Scanlan *et al.*, (1989) which began with each interview transcript (produced from the notes of the interview) being read and analysed. This increased familiarity with the interview data and helped identify the emerging themes. To aid analysis the software package QSR-N6 NUD*IST (QSR International Pty Ltd, 2000) was used to identify and group each emergent theme. Once emergent themes had been identified, the next phase was to group them together into a hierarchical structure to develop the dimensions.

3- Findings

The themes that emerged as part of the inductive analysis of the participants responses were grouped together to form each of the dimensions. Each dimension was formed from a hierarchy of sub-themes derived from participant quotes. Throughout the process relationships between the dimensions were identified and a structured relationship model was produced (Figure 1) to illustrate each relationship.

A total of 28 athletes (age 18 to 31 years) and 5 coaches were interviewed individually with an additional 6 athletes (age 17 to 24) and 4 coaches via group interview. All participants were chosen as national standard or above, this was based on their personal best time for their main events. The personal best times were compared to the national rankings and entry standard to national competitions for the relevant ages groups and events. The interviews typically lasted 15 minuets and resulted in 10 pages of quotations from the participants. This differed for each subject with large variability in length and details between individuals.

Six general dimensions emerged from the inductive analysis of the responses. These were identified as: Technique, Footwear and Surface (or Equipment), Environment, Performance, Injury, and Cardiovascular. A structured relationship model was produce (Figure 1) to visually represent the hierarchical structure of two dimensions. It illustrates how the analysis progressed from athlete and coaches responses, through levels of clustering, to form the base themes, sub themes and into the eventual general dimensions. It was found that some quotes could be placed into more than one dimension, hence inter-dimensional relationships are also illustrated. Transcriptions of the interviews were used during the inductive analysis and consequently the dimensions, sub-themes and base themes are all derived from quotations; hence, unfamiliar terminology may be presented. However, clarification of some words is given to help the reader understand their meaning when it is not clear within the context of the statement. Quotations are used throughout this section to illustrate and reinforce points made within the text.

The interviews started with the open-ended question;

"*With improving technology we have the ability to measure many aspects of running. What information would you find beneficial to help you train and improve?*"

The first response was then probed from which the investigator elicited the following dimensions. Not all athletes mentioned aspects of each dimension, therefore, this is a combination of all participant responses. To fulfil the length requirements this section of the document is abridged and only includes analysis of two of the six dimensions (Technique and Performance).

3.1 Technique

Technique or 'running style' was formed from two sub-themes, cadence and kinematics. Cadence was further split into stride frequency and stride length. These base themes were identified by the participant as crucial aspects of running technique and indeed running speed as illustrated by the inter-dimensional link between the two. Many participants, identified monitoring cadence as an essential aspect of running technique.

"*Using a combination of stride length and frequency you can calculate the speed at which the athlete is running. Real time feedback of this would be very beneficial to training*" *[400 m Coach]*

Kinematics are commonly evaluated in the laboratory using high speed video analysis, force plates, pressure pads and other less common methods (e.g. goniometers). The sub-theme kinematics was split into three base themes of joint angles, foot contact type and foot contact duration. Joint angles were mentioned in relation to mainly the lower limbs (ankle and knee) and identified as potentially useful as a training aid.

"It would be useful to know how my knee and foot [ankle] joint angles were changing as I ran" [3000 m Runner]

The base theme of 'foot contact duration' was mentioned as another useful measure of running technique. It was generally mentioned that a shorter contact time was preferable.

"…it would be very useful to see how long my foot was in contact with the ground for. I am always trying to shorten the time but have no way of measuring it. I have to rely on how it feels and what my coach tells me" [100 m Runner]

The final base theme 'foot contact type' was commonly mentioned with quotes relating to midfoot, rearfoot and forefoot. Comments were also made relating to inversion (supination) and eversion (pronation) of the foot.

"I know I run on my heels [rearfoot] and my coach always tells me to run on my toes [forefoot]… when he is not about I don't have anyone reminding me to run on my toes so a device that could do that would be great." [5000 m Runner]

Foot contact type was also raised in relation between pressure distribution and force generation. Several participants identified that different foot contact types would result in difference kinetic properties during contact with the ground hence two inter-dimensional relationships are present.

3.2 Performance

The general dimension performance was the most commonly mentioned theme and consisted of five base themes. The five themes were; speed, duration, distance, force generation and pressure distribution. Most common in conventional training is a combination of distance and duration which in turn can be interpreted as speed. Consequently these three sub themes were often mentioned interchangeably by the participants.

Duration is generally measured with a simple stopwatch. This device is very common and in some form used by almost every athlete as a training aid. More advanced devices that can identify split times were mentioned as favourable and commonly used by coaches.

"I would say over 90 % of my training is dictated by using a stopwatch to analyse the performance of my athletes" [Middle Distance Coach]

Figure 2 - Structure Relationship Model of Two Dimensions.

Distance when running on the track or circuit does not need to be measured as it is already known. However, several athletes identify that a way of measuring distance accurately would be very useful for non-track training. Some athletes mentioned the use of GPS (e.g. Garmin Forerunner 305) and/or accelerometer systems (e.g. Polar RS800SD) as an existing method of measuring distance. However, some identify that the accuracy of these systems is limited for short runs with quick changes in speed.

"*When I'm out on a long run I don't know how far I have gone unless I run a circuit I'm familiar with. This makes it difficult to know how fast I'm running and if I'm trying had enough*" *[3000 m Runner]*

"*I have tried using both a GPS watch and foot pod system [accelerometer] to measure my distance and speed but I don't find it very useful for shorter distances… less than 400 m they are not very accurate especially when you change speed lots*" *[800 m Runner]*

Running speed was identified as a key characteristic of performance. It was the most commonly mentioned theme by athletes and coaches. A method that is capable of measuring running speed was seen as essential. The limitations of existing devices over shorter distances was highlighted. However, they were praised by longer distance runners.

"*A method by which it is possible to measure accurate running speeds over short distances would be a great advantage for my athletes. I could see how they run a race and break it down into small sections and identify areas for improvement*" *[400 m Coach]*

"*When I'm not on the track I used a Polar foot pod [accelerometer] to monitor my speed and distance. Its great when I start running too slow and I know and can pick-up the pace.*" *[1500 m Runner]*

Force generation and pressure distribution were identified by participants as indicators of performance. Some of the comments by the participants related to both kinematics and performance hence the inter-dimensional relationship between the two. Force generation was identified as a potentially useful way of assessing running.

"*It would be good to see how the amount of force I produced changed of the different phases [start, middle and end] of my race*" *[200 m Runner]*

"*I would like to compare the force production for each of my athletes and see how it changes as they get stronger and fitter and it could help identify areas they need to train harder.*" *[Sprints Coach]*

Pressure distribution of foot contact was also identified by athletes and coaches as a useful method of assessing running.

"*It would be interesting to see how the pressure is spread of [over] my foot and compare that with other people to see if I need to work on changing anything*" *[100 m Runner]*

"*I have athletes that have very unusual foot positions when running, I would love to see how this influences the pressure under their foot and see if I could identify a way to make them more efficient.*" *[Sprints Coach]*

4- Discussion

Within the dimension of technique, aspects of both cadence and kinematics may be provided by an instrumented shoe, although this system would likely require both acce-

lerometers and load transducers. Of the five base themes within the general dimension of performance, force and pressure distribution would most appropriately be provided by an instrumented shoe/sock/insole. Speed, duration and distance may be more appropriately provided by alternative technologies, such as GPS. This initial phase of the project has therefore revealed that, based on athlete and coach perception, there are key aspects of performance feedback that could be provided by an instrumented shoe system. It may be that the most suitable system will combine in-shoe load measurement, accelerometers and some form of GPS system.

Whilst this phase of the project has elicited detailed information from the athletes and coaches it does not give an indication of the relative importance of them. The next stage of the project will identify the importance of each theme, it is also aimed at identifying what level of accuracy is required by athletes and coaches, how intrusive they are prepared to have a system and what kind of feedback would be most useful (detailed vs. simple, visual vs. audio etc.). Once these details have been identified the project will investigate the feasibility of producing a device that is capable of measuring the required aspects of running.

5- Conclusions

The perceptions elicited within the paper have helped to direct and focus the ShoeSMART research project. The detailed feedback from the interviews with coaches and athletes has identified 6 general dimensions. This paper presents two of these themes in detail; techniques and performance. The next phase of research is to investigate via questionnaires to identify the relative importance of each theme to the athlete and coach. This information will then focus the wider project to produce a device capable of providing detailed feedback to the athlete and coach.

6- Acknowledgements

The authors would like to thank the athletes and coaches who gave up time in their busy schedules to be interviewed. Gratitude is also given to the EPSRC and UK Sport for funding the ongoing project.

7- References

[CM1] Cohen, L. and Manion, L. (1980). Research Methods in Education. London: Routledge.

[DD1] de Cock, A., de Clercq, D., Willems, T. and Witrouvuw, E. (2005) Temporal characteristics of foot roll-over duringbarefoot jogging: reference data for young adults. Gait and Posture 21, 432-439.

[DW1] de Cock, A., Willems, T., Witrouvuw, E., Varenterghem, J. and de Clercq, D. (2006) A functional foot type classification with cluster analysis based on plantar pressure distribution during jogging. Gait and Posture 23, 339- 347.

[D1] Dixon, S.J. (2006). Application of center of pressure data to indicate rearfoot inversion-eversion in shod running. Journal of the American Podiatric Medical Association, 96, 305-312.

[FY1] Fleming, P. R., Young, C., Dixon, N., Roberts, J. R & Jones, R. (2005). Human Perception of Artificial Surfaces for Field Hockey. (Dec 2005) Journal of Sports Engineering.
[HJ1] Hocknell, A., Jones, R. and Rothberg, S.J. (1996). Engineering 'feel' in the design of golf clubs. In The Engineering of Sport: Proceedings of the 1st International Conference on the Engineering of Sport (edited by S.J. Haake), pp. 333 - 337. Rotterdam: A.A. Balkema.
[HR1] Hay J.G. and Reid J.G. (1988) Anatomy, Mechanics, and Human Motion (2nd edition) Englewood Cliffs, NJ: Prentice Hall.
[P1] Patton, M.Q. (1990). Qualitative Evaluation and Research Methods. London: Sage.
[RJ1] Roberts. J. R, Jones. R, Harwood. C, Mitchell. S & Rothberg, S (2001) Human perceptions of sports equipment under playing conditions. Journal of Sports Science 19 pp 485-497.
[SR1] Scanlan, T.K., Ravizza, K. and Stein, G.L. (1989a). An in depth study of former elite Figure skaters: I. Introduction to the project. Journal of Sport and Exercise Psychology, 11, 54-64.
[SS1] Scanlan, T.K., Stein, G.L. and Ravizza, K. (1989b). An in depth study of former elite Figure skaters: II. Sources of enjoyment. Journal of Sport and Exercise Psychology, 11, 65-83.
[CL1] Cavanagh PR, Lafortune MR (1980). Ground reaction forces in distance running. Journal of Biomechanics 13.

Logarithmic Visco-elastic Impact Modelling of Golf Balls (P147)

Franz Konstantin Fuss[1]

Topics: Golf.

Abstract: The stress relaxation in golf balls follows the logarithmic law, based on which a logarithmic impact model was developed. The model allows the conversion of the stiffness measured at different deflection rates into the velocity-independent elasticity parameter, as well as the calculation of impact forces. The stiffness and the viscosity parameter were derived from compression and stress relaxation tests respectively. The softer, or less stiff, a ball is, the smaller is its viscosity constant. Wound balls are generally less viscous than solid core balls. The impact forces calculated from the model were compared to forces measured in impact tests at approximately 10 m/s. The logarithmic visco-elastic model predicts peak impact forces accurately. However, the measured impact forces were partially inconsistent with a high standard deviation. As a recommendation, golf balls should be graded with two compression numbers (instead of the conventional Atti or Riehle numbers), or with the gradient of the mean stiffness, in addition to the conventional compression numbers.

Keywords: golf ball; nonlinear viscoelasticity; stress relaxation; compression tests; impact modelling.

1- Introduction

The impact of a golf ball is usually modelled with linear models, consisting of 2- or 3-elements (springs and dashpot), e.g. Kelvin-Voight, Zener, Kelvin-3-element model (Ujihashi 1994, Lieberman and Johnson 1994, Cochran 2002). Even when assigning non-linear properties to the springs and dashpot, the models remain linear, or pseudo/quasi-linear, as the overall stiffness of the different models shows either a minimal value of >0 (Kelvin-Voight), or both minimum (>0) and maximum values (<∞; Zener and Kelvin-3-element models), which does not correspond to experimental results.

1. Sports Engineering Research Team, Division of Bioengineering, Nanyang Technological University, Singapore
E-mail: mfkfuss@ntu.edu.sg

The aim of this study is determine the elasticity and viscosity parameters of a logarithmic visco-elastic model from compression and stress relaxation tests, to calculate the impact force of different golf ball models, and to compare the force calculated to the force measured during impact.

2- Experimental

2.1 Testing

28 golf ball models (figure 1; 1-61 balls per model, mean=7.36) were subjected to stress relaxation tests at different constant deflections, and to compression tests at 5 different deflection rates (5, 16, 50, 160, 500 mm/min). The force-deflection curves served to calculate the stiffness, the Atti number, and the average gradient of the stiffness-deflection curve. A logarithmic fit was applied to the force-time curves of the stress relaxation tests and the viscosity parameter B was obtained from Eqn (1).

2.2 Impact model

The stress relaxation of golf balls follows the logarithmic law (Fuss 2007):

$$F = x_0 Ax - x_0 B_x \mathrm{LN}(t) \tag{1}$$

where F is the force, t the relaxation time, x_0 the constant deflection, A the velocity independent elasticity parameter, and B the viscosity parameter.

Thus, a logarithmic non-linear visco-elastic model was developed to model the impact of golf balls, the constitutive equation of which is (Fuss 2007):

$$\hat{F} = \hat{x}A + \hat{x}B(\gamma + \mathrm{LN}\ s) \tag{2}$$

where the caret (^) denotes the transformed parameter (after Laplace transform), and γ is the Euler-Mascheroni constant (0.577215665…).

From Eqn (2), the relationship between stiffness and deflection rate is calculated (Fuss 2007):

$$k_v = A_x - B_x \mathrm{LN}x_i + B_x \mathrm{LN}v \tag{3}$$

where v is the deflection rate, and k_v is the stiffness at a specific v and deflection x_i.

Eqn (3) serves to calculate the elasticity parameter A at a specific deflection; A is independent of the deflection rate:

$$A_x = k_v + B_x \mathrm{LN}x_i - B_x \mathrm{LN}v \tag{4}$$

A was calculated in 5 golf ball models (AD, TD, BF, 12 balls each, and 3 soft and hard RB; figure 1), from the stiffness at the 5 different compression rates, and the viscosity

parameter *B* (figure 2). As an object is stiffer during single-sided impact than during double-sided compression, parameter *A* (figure 3) was multiplied by 1.333 (Fuss 2007).

The impact was modelled from the equilibrium of inertial and contact force, the latter force results from Eqn (3):

$$s^2\hat{x}m - mv_0 + \hat{x}A + \hat{x}B(\gamma + \mathrm{LN}\ s) = 0 \tag{5}$$

Based on Eqn (4), the time-dependent behaviour of deflection, contact force, and velocity during impact is derived:

$$\hat{x} = v_0 \frac{1}{s^2 + \frac{A}{m} + \frac{B(\gamma + \mathrm{LN}\ s)}{m}} \tag{6}$$

$$\hat{F} = v_0 \frac{A + B(\tilde{a} + \mathrm{LN}\ s)}{s^2 + \frac{A}{m} + \frac{B(\gamma + \mathrm{LN}\ s)}{m}} \tag{7}$$

$$s\hat{x} = v_0 \frac{s}{s^2 + \frac{A}{m} + \frac{B(\gamma + \mathrm{LN}\ s)}{m}} \tag{8}$$

The velocity before impact v_0 is the common multiplier, and thus the deflection and velocity of the centre of mass, as well as the contact and inertial forces increase linearly with v_0.

Based on the parameters *A* (multiplied by 1.333 [Fuss 2007]) and *B*, both as functions of the displacement *x*, the peak impact force at different initial velocities (up to 50 m/s) is calculated numerically from Eqn. (7) by applying Piessen and Huysmans' (1984) routine for inverse Laplace transform, programmed in Matlab. In addition to the peak force, the displacement of the COM at the peak force (which is slightly smaller than the maximal displacement) was determined from Eqn. (6) as well as the time between initial contact and peak force. In addition, different magnitudes of *A* and *B* were combined to understand their influence on the coefficient of restitution. The initial and final velocity was obtained from solving Eqn. (8) numerically.

2.3 Measurement of impact force

The 5 different golf ball models (AD, TD, BF, 3 balls each, and 3 soft and hard RB), used for impact modeling, were dropped 4 times each from a height of 5.3 m on a portable force plate (Kistler, model 9286A). This drop height results in a velocity of approximately 10.2 m/s before impact. The weight, or gravitational force, of the ball is negligible compared to the peak impact forces and thus does not have to be included in Eq (5). The reaction forces were recorded at 10 kHz and the peak forces were determined by fitting a polynomial regression into the force data. The peak forces obtained from the model and the impact measurements were compared in order to validate the model.

3- Results

3.1 Stiffness and viscosity of golf balls

Figure 1 shows that the initial stiffness (expressed by the Atti number), correlates positively with the average gradient of the stiffness. Solid core tournament balls and range balls of better quality exhibit a smaller gradient than the low quality Chinese range balls (solid core) and the hybrid balls (larger solid core and less rubber windings). Wound tournament balls, although initially very soft, show a steep stiffness gradient and thus are far stiffer at larger deflections than solid core balls.

The viscosity parameter *B* (figure 2) seems to depend both on the stiffness and on the construction, and increases with deflection. Softer solid core balls are less viscous. In the wound ball (TD), although soft at small deflections and hard at higher deflections (figure 3), generally is less viscous than solid core balls. The elasticity parameter *A* (figure 3) is a function of the deflection as well.

3.2 Impact model

The increase of the peak force with impact speed (figure 4) mirrors the behaviour of the elasticity parameter *A* with deflection: compared to the solid core balls, TD is the softest (smallest impact force) at smaller impact velocities and deflections, but the hardest at higher impact velocities and deflections. The deflection (figure 5), however, is not influenced by the gradient of the stiffness (parameter A), but rather follows the initial stiffness, i.e., the stiffness at small deflections. The softer a ball initially is, the larger the deflection during impact. In general, the contact time drops with increasing impact speed.

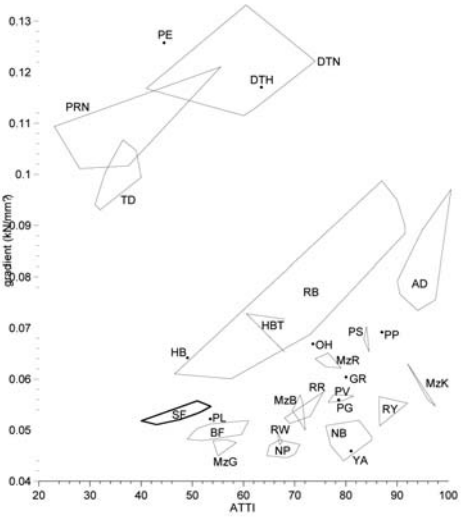

Figure 1 - average gradient of stiffness against Atti number (compression rate = 500 mm/min. *Solid core range balls:* RB: Chinese Range Balls, RW: white Korean Range Balls, RY: yellow Korean Range Balls, RR: Dura Range / Seoul Nassau Co. *Solid core tournament balls:* AD: Awesome Distance / Top-Flite / Spalding, BF: Buttery Feel / Top-Flite / Spalding, SF: HVC SoftFeel / Titleist / Acushnet, GR: Golden Ram / RAM Golf Corp., PG: Pinnacle Gold / Pinnacle / Acushnet, YA: Yakui, PS: Pro Special / Srixon, OH: Optima HP / PGF International, PL: Precept Lady / Precept / Bridgestone Golf, PP: Prostaff Platinum Pure Distance / Wilson, NP: Nike One Platinum / Nike, NB: Nike One Black / Nike, PV: Pro V1x / Titleist / Acushnet, MzK: T301 Black / Mizuno, MzR: D301 Red / Mizuno, MzB: C301 Blue / Mizuno, MzG: S301 Green / Mizuno. *Hybrid tournament balls:* HB: Hi Brid / Srixon, HBT: Hi Brid Tour / Srixon. *Wound tournament balls:* PE: Penfold Tradition / Penfold,

PRN: Professional 90 / Titleist / Acushnet, DTN: DT Wound 90 / Titleist / Acushnet, DTH: DT Wound 100 / Titleist / Acushnet, TD: TourDistance / Titleist / Acushnet).

3.3 Measurement of impact force

The impact forces measured at approximately 10 m/s (figure 7) match the calculated forces very closely. The force range (maximum force – minimum force) of the model BF was less consistent than in the other 4 models (table 1, figure 7).

Table 1 - maximum impact forces measured at impact velocity of 10 m/s.

Model	AD	RBh	BF	RBs	TD
Mean	2416	2304	1956	1767	1645
st. dev.	76.7	46.5	294.7	187.2	154.4
Minimum	2341	2248	1608	1534	1463
Maximum	2515	2362	2321	2074	1852

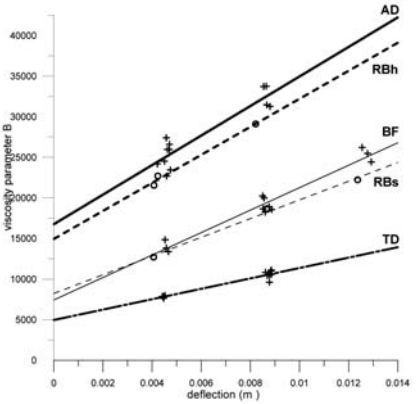

Figure 2 - viscosity parameter *B* against deflection (+: tournament balls, O: range balls)

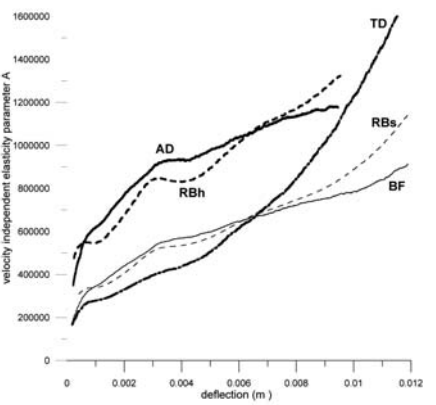

Figure 3 - elasticity parameter *A* against deflection (RBh and RBs: hard and soft Chinese range balls)

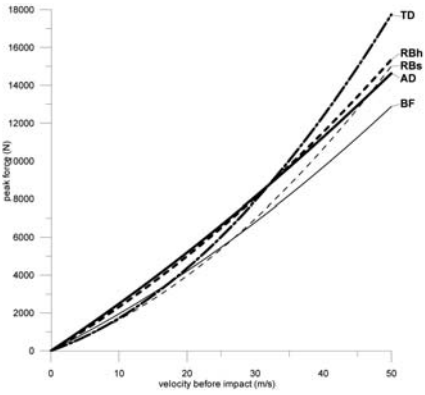

Figure 4 - impact peak force against impact velocity.

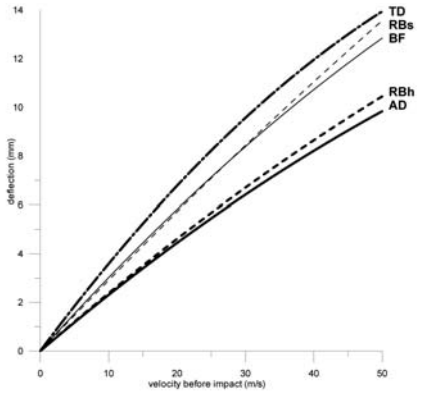

Figure 5 - deflection at peak force against impact velocity.

4- Discussion

The logarithmic visco-elastic model was successfully validated with impact tests at an impact velocity of approximately 10 m/s. The data obtained from impact tests, however, were partially inconsistent (figure 7): e.g. the standard deviation of the BF peak force was 15% of the mean, whereas the one of BRh was merely 2%. The measurement of impact forces at higher velocities will be considered as part of further research.

Interestingly, the viscosity parameter *B* seems to depend on the velocity-independent elasticity parameter *A*. Figure 2 shows, that harder solid-core balls have higher viscosity parameters. From Eq. (8) it becomes clear, that the coefficient of restitution (*COR*) remains unaffected by v_0. The *COR*, however, increases with *A* and decreases with *B*. Doubling both *A* and *B* results in almost the same *COR*, thereby cancelling the opposing effect of *A* and *B* on the *COR*.

The advantage of logarithmic visco-elastic model over spring-damper models is that the logarithmic model requires only 2 parameters for characterisation of the visco-elastic behaviour, namely the velocity-independent elasticity parameter *A* and the viscosity parameter *B* – both expressed as a function of the deflection. In contrast to that, spring-damper models capable of creep and stress relaxation, require a minimum of 3 elements (2 springs, 1 damper).

The Atti number, as well as comparable stiffness parameters like the Riehle number and the "deflection 130kg-10kg", is only valid in small deflections and thus misleading, with respect to grading of the ball's hardness. For instance, TD is softer than BF and AD at small deflections, but harder at large deflections (figure 3). Two stiffness values taken at two different deflections, or the intercept (initial hardness) and the mean gradient of the stiffness curve (figure 1), could be used for better characterization of the hardness, in addition to the viscosity parameter. The latter causes the increase of the stiffness with compression speed.

5- Conclusion

Golf balls should be graded with two compression numbers (instead of the conventional Atti or Riehle numbers), or with the gradient of the mean stiffness, in addition to the conventional compression numbers.

The softer, or less stiff, a ball is, the smaller is its viscosity constant. Wound balls are generally less viscous than solid core balls.

The logarithmic visco-elastic model predicts peak impact forces accurately, at least as smaller impact velocities (around 10 m/s).

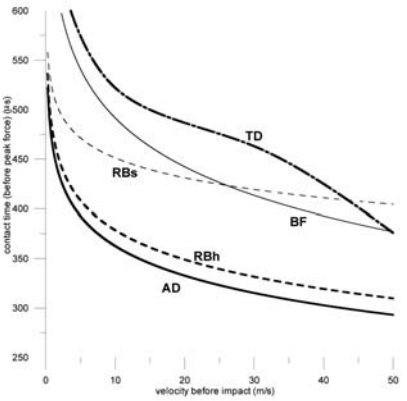

Figure 6: contact time against impact velocity

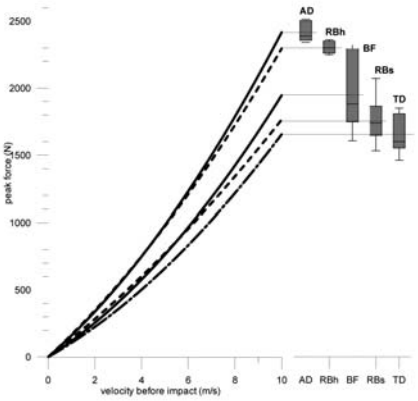

Figure 7: calculated and measured peak forces

Figure 6 - contact time against impact velocity

Figure 7 - calculated and measured peak forces

6- References

[C1] Cochran A. J. Development and use of one-dimensional models of a golf ball. Journal of Sports Sciences, 20: 635-641, 2002.

[F1] Fuss F. K. Non-Linear Viscoelastic Properties of Golf Balls. In: The Impact of Technology on Sport II, Eds: Fuss F. K., Subic A., Ujihashi S., Taylor and Francis Group, London, pp. 207-222, 2007.

[LJ1] Lieberman B. B. and Johnson S. H. An analytical model for ball barrier impact. Part 1: models for normal impact. In: Cochran A. J. and Farrally M. R. (Eds.) Science and Golf II. Spon, London, pp 309-314, 1994.

[PH1] Piessens R. and Huysmans R. Algorithm 619: Automatic numerical inversion of the Laplace transform. ACM Trans. Math. Softw., 10(3): 348–353, 1984.

[U1] Ujihashi S. Measurement of dynamic characteristics of golf balls and identification of their mechanical models. In: Cochran A.J. and Farrally M.R. (Eds.) Science and Golf II. Spon, London, pp 302-308, 1994.

Rowing Strategies in Cambridge Bumps Races (P148)

Matt Findlay, Dr Stephen Turnock[1]

Topics: Sailing/Water Sports; Modelling; Computer Application in Sports.
Abstract: 'Bumps' racing is a form of rowing with boats in a line astern which has evolved to allow a large number of crews to race simultaneously on narrow rivers. Boats line up with approximately 1.5 lengths between them and start simultaneously. A crew is successful if they manage to catch and 'bump' the crew ahead without being caught by the crew behind. This process can take as little as 30s or may require the crew to row the whole course which can take upwards of 10 minutes. The physiological demands of bumps racing are therefore unique as the crews do not know a priori how long the race will last. Selecting the appropriate race strategy and level of pacing is therefore both very important and difficult to do. In order to investigate different pacing strategies a multiple degree of freedom computational model of a rowing boat was used. This determines the boat velocity by balancing the force application by the athletes with drag components arising from the motion of the boat, oars and athletes. This velocity prediction program (VPP) is coupled with a physiological model of an athlete whereby the athlete's ability to deliver force is assumed to vary as a function of the work done during the current bout of exercise. The level of effort required from the crew is dictated by the coxswain in terms of stroke rate in accordance with measured data and dimensional scaling analysis. It is shown that different starting strategies are appropriate on different days of racing when the crew would have either a limited or good knowledge of the specific capabilities of the crews ahead and behind them. In addition an evaluation was made of the dynamic tactical options available to a crew and it is shown that when an attacking boat came within striking range, an aggressive rate change was tactically the most effective complement to an otherwise defensive strategy.
Keywords: Rowing; Decision Making; 'Bumps' Racing.

1- Introduction

Bumps racing is a form of rowing competition in which a number of boats chase each other in single file; each boat attempting to catch and touch ('bump') the boat in front without being caught by the boat behind. This form of racing is particularly suited to

1. Fluid-Structure Interactions Research Group, School of Engineering Sciences, University of Southampton, UK
Email: matt.findlay,srt@soton.ac.uk

stretches of river which are too narrow or not straight enough to permit more conventional side by side racing. In Cambridge racing takes place over four days and there are currently seven Lent and ten May divisions, each with 17 or 18 boats. The two events are independent of each other with the starting order based on the previous years finishing positions. Racing takes place in eight oared rowing shells in which 8 athletes each handle one oar to power the craft while steering is carried our by the coxswain ('cox') whose also makes tactical decisions and helps execute the crew's chosen race strategy.

Initially the boats are separated by 1.5 boat lengths, *L*, of clear water (approx 27m) and they begin racing simultaneously with the firing of a loud cannon. When two boats bump they pull into the side of the bank to allow other boats to continue racing and they then swap positions for the start of the next race. The boat behind them still has to continue racing and if lucky (or exceptionally skilful) it may catch the boat ahead of the bumping pair and therefore move up three (or even five) positions. This is known as an "over-bump". If a boat fails to bump the boat ahead and is not bumped by a boat behind they must row the full length of the course. This is known as "rowing over" and is a distance of approximately 2200m for the top half of the men's division.

After the four days of racing, the aim of the top crews is to be at the "head of the river," i.e. leading the first division. Lower crews cannot expect to achieve this, but can "win their blades" by bumping up every day. Figure 1 shows how the results of bumps racing are represented diagrammatically with the starting order of the boats shown on the left, the finishing order, after four days, on the right. The intermediate positions can be determined from the line joining the two.

The physiological demands of bumps racing are unusual because the athletes do not know in advance how long their race is going to last. For example if a crew is evenly matched with the crews ahead and behind (or if crews ahead and behind bump out) it may have to row-over which means rowing the entire length of the course – a process that can take over 10 minutes for the slower crews. This places a high emphasis on the endurance capabilities of the athletes.

On the other hand, when a crew behind is much stronger than the crew ahead they may take less than a minute to bump – hardly placing any emphasis on the aerobic capability of the crew, but generally requiring that the crew be extremely strong and skilful in order to rapidly accelerate the boat from rest.

Since the race is of an indefinite length the main strategy variable is pacing. The main variables influencing this strategy will be the crews own strengths and weaknesses, as well as the perceived abilities of the crews ahead and behind assessed in context of the course and weather conditions. If a crew counts among it's strengths a fast start and ability to deliver a large amount of force to the oar handle – even if only for a short period of time, they may choose a sprint style strategy with the aim of achieving a quick bump. On the other hand a crew that rates its endurance capabilities more highly might make a more conservative start and aim to settle into a good rhythm with a view to "rowing down" the boat ahead over a longer period of time.

On the first day of the bumps regatta a crew will have minimal knowledge of the specific capabilities of the crews around them whereas on days 2, 3 and 4 they will have an increasing awareness of other crew's capabilities based on results and eye-witness

accounts of other crew's strategy and performance. In addition, whether a crew bumps or not will also be determined by their ability to respond dynamically to the tactics of the crew ahead or behind. The athletes face backwards so can see and react to the tactics of the chasing crew however the crew rely on support from coaches on the river bank in order to gauge the distance between themselves and the crew ahead.

Typically this information is relayed from the coach via hooter or whistle using the following system:

- Sound 1 blast when you close within 1 length of the boat ahead,
- Sound 2 blasts when you close within half a length of the boat ahead
- Sound 3 blasts when you close within a canvas (approx 1.5m) of the boat ahead, and
- Hoot continuously once you have established an overlap with the boat ahead.

Tactical decisions are therefore executed by the cox at each of these points. The execution of a tactical decision represents an increase or decrease of rowing effort by the athletes. This can be expressed by a step change in stroke rate; upwards in the event of an increase in effort and vice versa. This research aims to investigate the relationships between a crew's specific capabilities, their choice of strategy and tactics (dynamic response to the behaviour of crews ahead and behind) and their performance in a bumps race. By characterising the dynamic tactics using two parameters we aim to find the most successful tactical approach given the modelling assumptions.

2- Modelling Assumptions

2.1 Overview

In order to reduce the size of the problem we choose to model only male athletes, competing from the start to 'top finish', a distance of 2200m for the first crew. The course is assumed to be one-dimensional i.e. a straight line, and boats bump as soon as an overlap is established between them. For those who know the River Cam, the location of bends is an important strategic consideration, however, in this work we concentrate on the relationship between crew pace and energy reserve.

It is assumed that each crew can be classified into one of two weight categories; light or heavy. The lightweight crew is assumed to be geometrically similar to the heavyweight crew and each athlete is assumed to have the following mass: 72kg (lightweights) and 90kg (heavyweights.) These values are selected based on approximate averages for international athletes in those weight categories.

It is assumed that all crews race in identical boats so that their equipment has the same weight and geometrical characteristics and is not specifically tailored to their weight.

2.2 Strategy

The crews row at a stroke rate which is dictated by the cox and assumed to be based on one of two possible strategic approaches to the race as follows:

1. Offensive. This is an aggressive and high risk strategy that aims to achieve the bump as quickly as possible. The risk is that if the bump is not achieved quickly the crew may burn out and be at risk of being bumped themselves. The crew set off at the maximum stroke rate and at all times use all of their available power to propel the boat.
2. Defensive. In this mode the crew aim to pace themselves (such that they would minimise their time to complete the full course) but react dynamically to the behaviours of the crew ahead and behind. This tactical behaviour is based on the system used by crews in reality, as detailed below.

When the distance between boats falls below one boat length, L, a step increase of A strokes per minute (SPM) is implemented. When the distance falls below $0.5L$ a step increase of B SPM is applied. It is assumed that when the distance between boats falls below 1.5m (Canvas) the stroke rate is always increased to the maximum possible.

In order to simplify the parameter search it is also assumed that the tactics are symmetrical – i.e. that the dynamic response to a chasing crew is the same as the dynamic response to a leading crew for the same distance between boats.

2.3 Velocity Prediction Program

The boat speed is determined as a function of the stroke rate using a velocity prediction program (VPP.) The VPP models the rowing system as a system of connected masses (boat and athletes) in order to determine the motion of the boat as a function of handle force and rower position. The VPP is implemented in Matlab using a fourth order Runge-Kutta solver for each time step.

The equations of motion are those described by Sanderson and Martindale, 1986, and the gate force is calculated as a function of handle force by applying the assumption of "no blade slip" following Brearley and de Mestre, 1996. The motion of the rower within the boat is assumed to be sinusoidal (Brearley and de Mestre, 1996) with amplitude proportional to the cube root of the mass of the athlete as per Lazauskas, 1997. The handle force is assumed to vary sinusoidally throughout the drive phase of the stroke and to be zero elsewhere as in Sanderson and Martindale, 1986.

Drag forces arising from hydrodynamic components are modelled using standard ship theory (Claughton *et al.* 1998) using skin friction plus a form factor in accordance with Scragg and Nelson, 1993, and wavemaking drag in accordance with Wellicome, 1967. Aerodynamic drag is modelled using data from Hoerner, 1965.

The stroke rate and rhythm (ratio of drive time to total stroke time) are assumed to be correlated in accordance with the observations of Lazauskas 1997, so that only one parameterisation is needed to define both. For the same reason, the peak handle force and stroke rate are also assumed to be correlated (Kleshnev 1996), with the relationship determined using dimensional analysis. It is therefore only necessary to prescribe the stroke rate in the VPP and the handle force and rhythm are calculated based on a dimensional scaling of a rower's performance.

2.4 Physiological Model

The athletes are able to row at a given rate only if it is within their physiological capabilities which are a function of their size and level of fatigue. This is determined by a physiological model of the athlete as a battery with a finite amount of energy available to expend during the course of the race.

The VPP calculates the work done by each athlete on the boat. After dividing by an efficiency value of 0.8 (Cabrera and Ruina, 2006, and Kleshnev, 1999) to account for losses at the blade, this information is used by the physiological model to determine the maximum handle force, F, (and therefore stroke rate) available to the athlete at any moment.

This initial amount of energy available to each athlete is assumed to be proportional to the mass$^{4/3}$ in keeping with scaling laws. The relationship between the athlete's ability to deliver force to the handle and the work done thus far is illustrated in Figure 2. The maximum handle force initially available to the athlete, F_{Max}, is determined by limiting the maximum allowable value of stroke rate to 48 SPM for heavyweights and 49.8 SPM for the lightweights. The values for heavyweights are chosen on the basis that this approaches the upper limit that excellent crews are capable of before rowing coordination deteriorates. The values for lightweights are based on appropriate scaling of the heavyweight values ($s \sim M^{-1/6}$).

It assumed that the ability to deliver a maximal handle force, *F*, is only impaired once the work done by the athlete reaches 70% of his total energy available. From this point onwards the maximal handle force that the athlete can deliver decreases linearly with work done. If the maximal handle force, *F*, is less than the force required by the current stroke rate (requested by the cox), the rate is reduced accordingly.

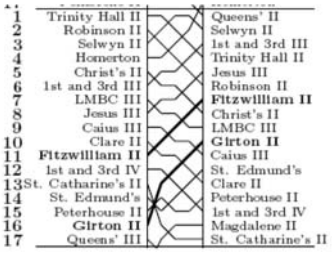

Figure 1 - Results for the men's 3rd division of the 2007 Lent Bumps, Cambridge.

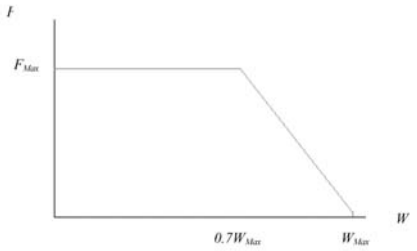

Figure 2 - Deterioration of athlete's ability to deliver force with work done, W.

3- Results

In strategy mode 1 (offensive), the cox requests a maximal rate which is equal to the maximal rate the athletes can supply. Initially this is 48 SPM for the heavyweights and 49.8 SPM for the lightweights. As the athletes become fatigued the handle force (and therefore consequently the rate and boat speed) drops in accordance with the physiological model.

In strategy mode 2 (defensive), the initial rate is chosen to optimise the time over the course but may be raised by the cox in accordance with the dynamic tactics discussed above and the capabilities of the athletes. By running the simulation in time- trial fashion for a range of initial stroke rates it was possible to determine the stroke rate for each crew that minimised that crew's time to complete the 2200m course. The optimal stroke rate is approximately 36.5 SPM rate for the lightweight crew (t=457.1s) and 37 SPM for the heavyweight crew (t=416.9s.)

It is of interest to observe the pacing that results in these course times and Figure 3, shows the performance of the heavyweight crew at their optimum stroke rate (37 SPM) and near their maximum stroke rate (45 SPM.)

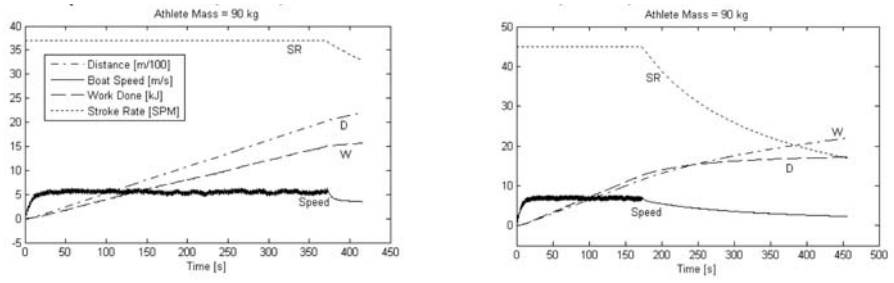

Figure 3 - Heavyweight crew time trial starting at 37 SPM (left) and at 45 SPM (right).

It can be seen that the optimal rate is just slightly higher than one that could be maintained at an even pace throughout the race; a phenomena that is observed in many sports and a result that adds credibility to the simple physiological model.

3.1 Bumps racing

The effectiveness of a given tactical approach can be investigated by fixing the constants *A* and *B* (*A*=2, *B*=4, for example) and running the simulation for 16 possible combinations of two boats racing under bumps conditions. Each boat may be either light- or heavyweight and use either strategy 1 or strategy 2.

The results can be used directly to determine which strategy (1 or 2) is most appropriate given knowledge of the boat ahead and behind a particular crew. If nothing is known about the characteristics (weight and strategy) of the crews ahead or behind the best strategic option can be determined from a probability analysis of the 16 possible combinations in which a particular crew could find themselves. This is scored as a win if the crew bumps before they are bumped; a draw if they neither bump, nor are bumped by the crew behind and a loss if they are bumped before they bump the crew ahead. An example of this type of analysis, for *A*=2, *B*=4, is shown in Table 1.

Since a crew is only concerned with whether it gains or looses a place for the next day's racing a weighting of 1 point for a win, 0 for a draw (row-over) and -1 for a loss has been assigned. The score is defined as the sum of the weightings.

This example shows that if crews choose to react dynamically by increasing the stroke rate by *A*=2 SPM at *L* and *B*=4 SPM at 0.5*L* of separation then strategy 2 is not the best

strategy to select at the beginning of the week when little is known of the opposition (this is true for both lightweight and heavyweight crews). More formally, each crew may rank the strategy as follows: *Ranking = score(strategy1) – score(strategy2)*. Thus a positive ranking indicates that strategy 1 is favoured for that crew and negative ranking favours strategy 2 for that crew. In the example above the ranking is 12 for both heavyweight and lightweight crews indicating a strong bias for strategy 1.

Using this ranking system it is possible to find the pair (*A*,*B*) representing the crew's tactical approach that gives the most favourable ranking for strategy 2. This is done by performing the above analysis for all possible pairs of (*A*,*B*) up to the maximum stroke rate with an assumed minimum step change of 2 SPM.

To limit the possible combinations to a workable number it was necessary to impose the constraint that all crews racing under strategy 2 use the same dynamic tactics *A*,*B*. Nevertheless it is still possible to show that such a system does indeed have a minima, located near the point *A*=6, *B*=8, as can be seen from the bar chart of results shown in Figure 4.

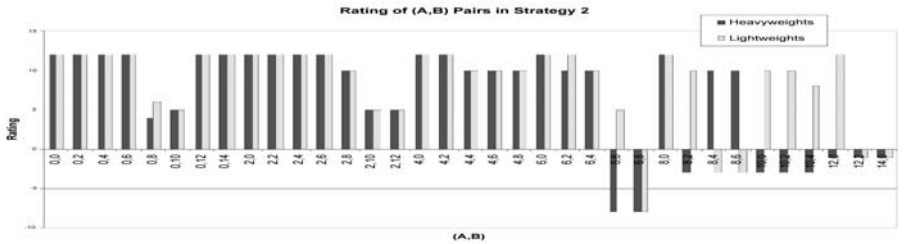

Figure 4 - Ranking of (A,B) pairs used tactically in strategy mode 2.

The results of this parameter search show that, as would be expected, strategy 1 is heavily favoured when the tactics for strategy 2 are fairly mild (*A* + *B* small.) As the tactical response becomes more aggressive the defensive strategy becomes more effective. In particular, for the lightweights, strategy 2 with tactics (6,8), (8,4), (8,6), (12,2) and (14,0) are more effective than strategy 1. Heavyweights using strategy 2 also benefit more from using tactics in this region.

Another notable feature of the results is that as parameter *A* increases in value towards the positive limit the difference between strategies 1 and 2 decreases. This is true in reality as strategy 2 begins to approximate strategy 1's 'straight to maximum stroke rate' approach, only delayed until within one boat length of the opposition rather than from the start.

There appears to be an optimum value for strategy 2 in the region of *A* = 6, *B*= 8. Of particular interest is the case of *A*=8, *B*=2, however, as it can be seen that the lightweights have better outcomes using strategy 1 (rating = 10) and the heavyweights have better outcomes using strategy 2 (rating = -3). The win loss table and pairs racing table are shown in Tables 2 and 3, respectively. Rows 1,6,11 and 16 in Table 3 show cases in which the lead and tail boats are identical. No bumps would be expected to occur in these situations. Rows 5, 14 and 15 of Table 3 show cases in which the boat behind failed to achieve a bump and the boat ahead 'rowed over'. This happened when a lightweight

crew chased a heavyweight crew and both were on the same strategy (cases 5 and 15), or when the heavyweight crew ahead was able to hold off a chasing lightweight crew on an attacking strategy.

It is therefore apparent that the reason that strategy 2 is effective for heavyweights but not for lightweights is because the tactical approach (8,2) is sufficient to allow the heavyweights to fend off an attacking boat behind, but not sufficient for the lightweights to do the same.

A particular example of this can be seen in Figure 5, below which is that of case 14; a heavyweight crew using strategy 2 to fend off an attack from a heavyweight crew behind using strategy 1.

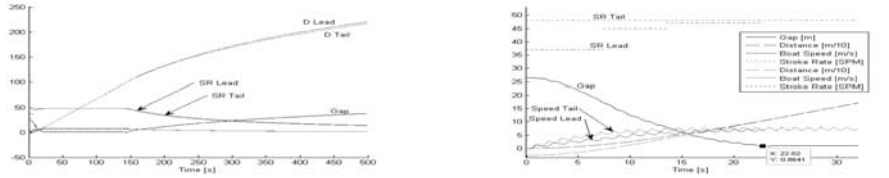

Figure 5 - Overview of case 14 (left) and detail of case 14 (right); holding off an attack

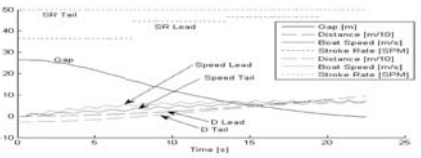

Figure 6 - Case 9; Unable to defend against an attacking crew

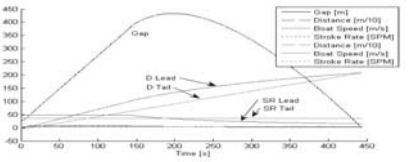

Figure 7 - Case7; Rowing down the heavyweight crew in front after 2083m

The initial raise of rating by 8 SPM by the leading boat can clearly be seen but is not enough and within 6s the crew are forced to raise the rate again as the opposition has now closed to within half a boat length. After another 9s the leading crew are forced to raise the rate to the maximum allowable when the chasing crew close to within a canvas and this is just sufficient to maintain a gap of 0.85m between the crews.

On the other hand, case 9 (Figure 6) shows a lightweight crew using an aggressive strategy chasing a lightweight crew using a defensive strategy. The tactical response (8,2) is not sufficiently aggressive for the leading crew to keep the attacking crew at bay and they are bumped after just 22 seconds of racing.

Case 7 (Figure 7) shows the hard fought battle between a lightweight crew who have paced themselves chasing a heavyweight crew that has gone off hard using strategy 1. In this case it can be seen that the lightweights rowed down their opposition after some 2083m of racing.

4- Concluding Remarks

The use of a simple physiological model has given an insight into why pacing is important in bumps racing. A crew who go off very hard (strategy 1) and fail to achieve a bump

are at a greater risk of being bumped themselves later in the race if followed by a crew who have paced themselves well using a defensive strategy. Nevertheless, to be effective, a defensive strategy must allow for aggressive implementation of rate changes at key tactical points or the crew will not be able to hold off an attacking boat. The best tactical approach appears to vary depending on the strength (weight) of the crew as illustrated by the case A=8, B=2, which represents an effective tactical approach for heavyweights but not for lightweight crews. In general, with the assumptions used in this research, the minimum step change of rating at 1 boat length of separation is approximately 6 SPM up from the optimal racing rate.

It has been shown that if a crew is aware of the characteristics of the boats ahead and behind them, they should be able to select an appropriate strategy to maximise their chances of a successful outcome. In addition, if a crew does not know the characteristics of the crews around them (as on the first day of racing) a combinatorial analysis can be undertaken to evaluate the effectiveness of different strategy options based on the current trend for tactical response (A,B values.). A limitation of the investigation is that all boats are assumed to use the same tactics when using strategy 2, however this does not affect the outcome that there are minimum values for the tactics in strategy 2 that make it an effective defence against crews using strategy 1.

A further enhancement of strategy 2 might be to start more aggressively and then throttle back to a more manageable pace once the initial threat from strategy 1 opponents has been dealt with. This might allow strategy 2 to be more effective with lower values of (A,B) and it would be interesting to investigate further this hybrid strategy approach. Empirical evidence suggests that a hybrid approach is probably closest to the approach used by the top crews in actual bumps racing.

Further limitations of the research arises from the fact that the non-dimensional coefficients were calculated using recorded performances of world class athletes who are not, in general, dimensionally similar to the athletes that compete in bumps races. However the variability and range of athletes competing in bumps races, coupled with the general lack of data regarding the performances of these athletes means that there is no greater benefit from using that data over the data based on Olympic race times. The conclusions remain the same (that there are situations in which a lighter crew can catch a heavier crew if they pace themselves well) and could possibly be strengthened on the basis that crew coordination will deteriorate more quickly with fatigue in college crews than in international crews and so the effect of fatiguing on boat speed may be enhanced in college crews due to this mechanism.

5- Acknowledgements

This work was carried out under the auspices of the Engineering Doctorate programme at the University of Southampton, with support from the Engineering and Physical Sciences Research Council (UK) and UK Sport.

Table 1 - Win-loss table for all possible starting combinations. Tactics are *A*=2; *B*=4.

Weight	Strategy	Wins	Losses	Draws	N	Score
72	1	8	6	2	16	2
90	1	12	2	2	16	10
72	2	2	12	2	16	-10
90	2	6	8	2	16	-2

Table 2 - Win-loss table for all possible starting combinations. Tactics are *A*=8; *B*=2.

Weight	Strategy	Wins	Losses	Draws	N	Score
72	1	7	7	2	16	0
90	1	8	4	4	16	4
72	2	2	12	2	16	-10
90	2	10	3	3	16	7

Table 3 - Outcome of pairs (one on one) bumps racing. Tactics are *A*=8, *B*=2.

	Boat Ahead		Boat Behind			
Case	Strategy	Weight	Strategy	Weight	Time (s)	Distance (m)
1	1	72	1	72	614.26	2200.00
2	1	72	1	90	77.36	503.92
3	1	72	2	72	389.59	1824.28
4	1	72	2	90	313.87	1642.71
5	1	90	1	72	504.49	2200.00
6	1	90	1	90	504.49	2200.00
7	1	90	2	72	443.67	2083.19
8	1	90	2	90	361.28	1894.70
9	2	72	1	72	21.63	88.55
10	2	72	1	90	18.31	70.42
11	2	72	2	72	463.47	2200.00
12	2	72	2	90	48.36	235.19
13	2	90	1	72	90.18	568.54
14	2	90	1	90	498.22	2200.00
15	2	90	2	72	420.57	2200.00
16	2	90	2	90	420.57	2200.00

6- References

[BM1] Brearley, M. N. and de Mestre, N. J. (1996). Modelling the Rowing Stroke and Increasing its Efficiency, Proceedings of the 3rd Conference on Maths and Computers in Sport, Bond University, pp. 35-46

[CR1] Cabrera, D. and Ruina, A., (2006). Propulsive Efficiency of Rowing Oars, Submitted to Journal of Applied Biomechanics

[CW1] Claughton, Wellicome and Shenoi (1998). Sailing Yacht Design: Theory. Addison Wesley Longman Limited

[H1] Hoerner, S. F. (1965). Fluid-dynamic drag. New York: S. F. Hoerner

[K1] Kleshnev, V. (1996). The Effects of Stroke Rate on Biomechanical Parameters and Efficiency of Rowing, In Abrantes, J.M.C.S (ed.) XIV Symposium on Biomechanics in Sports. Funchal, Madeira, Portugal. Proceedings, Lisboa, Edicoes FMH, c1996, pp321-324

[K2] Kleshnev, V. (1999). Propulsive Efficiency of Rowing, In Proceedings of the XVII International Symposium on Biomechanics in Sports, pp. 224 – 228. Edith Cowan University, Perth, Western Australia

[L1] Lazauskas, L. (1997). A Performance Prediction Model for Rowing Races, Technical Report: L9702, Dept. of Applied Mathematics, University of Adelaide, Adelaide, Australia
[SM1] Sanderson, B. and Martindale, W. (1986). Towards Optimizing Rowing Technique, Medicine and science in sports and exercise , 18(4) pp. 454-468
[SN1] Scragg, C. A. and B. D. Nelson. (1993). The Design of an Eight-Oared Rowing Shell. Marine Technology, Vol. 30, No. 2 pp.84-99.
[W1] Wellicome, J. F. (1967). Report on Resistance Experiments Carried Out On Three Racing Shells. National Physical Laboratory, Ship Division, Project 11.7. England.

Improvements to a Sailing VR Simulator Environment for Assessing and Improving Helm Performance (P149)

Thomas Spenkuch[1], Dr. Stephen Turnock[1], Dr. Matteo Scarponi[2], Prof. Ajit Shenoi[1]

Topics: Sailing/Water Sports; Performance Sports; Virtual reality; Computer application in Sports.

Abstract: The sailing simulator 'Robo-Race' is used to examine the effect on sailor performance of enhancing the realism of the simulation. For this purpose, the following two human interface device/display environments were evaluated. Firstly, a Basic Display Environment (BDE) which consists of two screens in conjunction with a joystick. Secondly the Advanced Display Environment (ADE) that consists of three projectors with an additional screen and a steering (or helm) wheel as interface device. A number of sailors who were divided according to their sailing skills and their experience with computer game interface devices had to deal with seven upwind races against two computer controlled America's Cup Class (ACC) yachts. The experiment shows that the combination of BDE/joystick limits their natural sailing behaviour. However, the combination of ADE/steering wheel significantly improved the sailors' efficiency. The ADE setup has been shown to enhance the realism of the simulation and allowed the sailors' to race opponents in a more realistic manner.

Keywords: Virtual reality; yacht racing; simulation; America's cup; decision making.

1- Introduction

Considerable progress has been made in enhancing the physical realism of Velocity Prediction Programs (VPPs) suitable for analysis of racing yacht performance since their first use by Kerwin in the 1970's (Kerwin at al., 1979). Similarly, the sensor capabilities (smaller mass, lower power consumption, and greater accuracy) have been enhanced rapidly and with a resultant increase in use in helping assess and improve actual racing yacht performance. While these tools and techniques will be further refined and computations speeded up, there is also a need to assess the performance of the yacht's helm and crew.

1. Fluid Structure Interactions Research Group, School of Engineering Sciences, University of Southampton, UK
Email: ts305@soton.ac.uk
2. Wolfson Unit for Marine Technology and Industrial Aerodynamics, University of southampton, UK
Email: ts305@soton.ac.uk

Robo-Race is a real-time MATLAB®-Simulink® based sailing race assessment tool, (Scarponi, 2008, Scarponi *et al.*, 2007). It is suitable for assessing both the effect of aero/hydrodynamic design changes and crucially the effect of tactical decisions made by the yacht crew. Advantage has been taken of various Simulink® toolboxes to allow fleet racing within a virtual reality environment which includes stochastic effects due to shifting winds, covering effects of other yachts and race rules. In these simulated regattas sailors can race against other yachts crewed by an Artificial Intelligence (AI) tactical decision making that has been captured using a combination of interviews and questionnaires designed to identify expertise level based response.

The aim of the present research is to examine the effect on sailor performance of enhancing the realism of the simulation through use of a wrap around visualisation of the racing course viewed by the helmsman/tactician. In particular, differences will be assessed between the use of standard joystick inputs and suitably instrumented steering wheel/joystick. Analysis will be based on ACC rule keel based yachts and will be presented as a series of case studies comparing performance against opponents with known/unknown race styles.

2- The Sail Simulator Robo-Race – An Overview

Robo-Race is a sailing simulator which takes into account the human factor with respect to strategic decisions during a fleet race. The simulator is designed in a way that one or more users (sailors) can interact with computer controlled yachts.

This setup provides the recording, analysis, and comparison of the sailors' behaviour, strategies, tactics, and decisionmaking process. Different models for the yacht-crew interaction have been designed and implemented for the helmsman and the sail tailers, as well as a 'routing engine' which solves problems of a strategical and a tactical nature, like collision avoidance and navigation in wind shifts. The simulator Robo-Race is a MATLAB®-Simulink® based tool which is built on the module 'Robo-Yacht' which provides the yacht 'physics engine' as well as behavioural models for the automatic crew.

A virtual reality environment supports the sailor with a visual real-time feedback of the race state and of his/her yacht within a virtual 3D world.

In order to simulate fleet races with N yachts, Robo-Race includes M Robo-Yachts which are controlled by the simulator and (N-M) human controlled yachts. In order to define a yacht-crew system the setup of the hull, rig and crew parameters for each Robo-Yacht are required. In addition, two further modules were implemented in order to enhance the realism of the simulation. Firstly, a weather module is used, which prescribes the spatial and temporal variation of the wind speed and direction. Secondly, a race scenario module has been implemented which deals with rule-based routing strategy and an additional library which achieves efficient race tactics and addresses conflicts between tactics and race strategy. An example is tacking onto an unfavoured beat to sail in clean air that is not in the wake of a leading yacht.

The yacht motion is modelled by a four degrees of freedom (DoF) model (surge, sway, yaw and roll) developed by Masuyama (1995) which has proven to perform well for tacking simulations in calm water as the obtained results were in good agreement with those of full scale experiments.

3- The Experiment – The Setup

In order to evaluate the performance of individual sailors, the methodology adopted is that of using a realistic sailing simulator. In order to evaluate the realism of the simulation two different display-input device-environments were set up to determine the effect on sailor performance through a systematic series of races. A basic human-computer interaction setup and then a more realistic interaction environment between sailor and computer were used.

The basic device-environment BDE setup consists of a joystick as the only input device and two flat screens (see Fig. 1).

The joystick deals with the following two tasks: firstly the adjustment of the default rudder angle given by the PIDcontroller and secondly the change of the viewpoint distance via zooming. The virtual environment and the onboard instruments are displayed the two flat screens.

An advanced device environment ADE is composed of an additional steering wheel (helm) which controls the rudder angle directly, whilst the joystick is still used for changing the viewpoint, a 17"flat screen is used for displaying the onboard instruments and three projectors for displaying the 3D sailing environment on a cluster of screens (see Fig. 2). In addition to the improvement of the visualisation of the simulation, a direct control of the sailing yacht by the sailor is implemented to ensure a direct relationship of the wheel motion to the rudder angle.

Figure 1 - Basic Display Environment, BDE showing instruments on laptop and VR on standard monitor.

Figure 2 - Advanced Display Environment, ADE, showing wheel and curved display panels for VR driven by three data projectors.

3.1 The Input Devices: Joystick and Steering Wheel

The joystick is designed as a controller device to alter the rudder angle and adjust the viewpoint. This human interface device is manufactured by Saitek® (model Cyborg Evo) and connected to the computer via a USB port. To transfer the input of the sailor to the sailing simulator, a Simulink® interface block is used. Clicking on buttons #5 and #6 adjust the rudder angle by coming up and bearing away by 0.2 degree per click which leads to a technically achievable rudder angle rate of 3.33 deg/sec. Clicking the front trigger starts an automatic tack, which is executed accordingly to a technique described in Scarponi *et al.*, (2007). The second task of the joystick is the viewpoint adjustment.

The stick has to be pushed forwards to zoom in on the racing area, while moving it backwards allows zooming out.

In addition to the joystick, a steering wheel with force feedback is connected to the computer via a USB interface. The steering wheel, model Xbox 360 Wireless Racing Wheel, is manufactured by Microsoft® and offers 270 degrees of steering rotation. The motion of the wheel is transferred to a Simulink® block which converts the motion directly as the desired rudder angle without using the PID-controller. The setup for the signal output of the steering wheel is designed in a way that a full steering rotation of the wheel corresponds to a rudder angle between -30 degrees and 30 degrees and that every desired rudder angle within this range is possible accordingly to the actual default wheel position controlled by the sailor.

3.2 The Onboard Instruments

In order to inform the sailor about the actual performance of the yacht and the sailing environment, a number of onboard instruments are available which display surge speed, apparent wind angle, wind speed, true wind speed and rudder angle.

Therefore, to determine the current state in real time, the onboard instrument variables are updated at every time step.

Furthermore, a virtual GPS screen is included in which the tracks of all participating yachts are displayed. In order to get a reasonable overview about the actual race state, the 'virtual GPS' window draws the tracks as solid lines on a white background which is supplemented by a dashed black line grid for a better orientation during the race (see Fig. 1 and Fig. 2).

3.3 The Virtual Reality – Basic and Advanced Display Environment

A Virtual Reality (VR) environment provides a 3D world where the yacht controlled by the sailor and those controlled by the computer are displayed. The sea surface is modelled as a calm blue surface to which a grey Cartesian grid is superimposed for positional information. Furthermore, in order to support the sailor with secondary visual navigation aids, the coastline is implemented as a comprehensive navigation support as well as the race mark as a limited navigation tool as it can only be seen from a certain distance. The objects within the VR are updated every time step to ensure a fluent and realistic simulation. MATLAB®'s VR toolbox is used as the interface between the Simulink® model and the Virtual Reality Modelling Language, (Scarponi *et al.*, 2007).

The 'Basic Display Environment' (BDE) consists of two flat screen monitors. Screen#1 (17 inches) collects the 'Onboard Instruments' (see section 3.2), whereas screen#2 (20 inches) deals with the display of the animation of the VR.

In order to enhance the realism of the simulation, the location of the flight simulator laboratory of the University of

Southampton is used. This 'Advanced Display Environment' (ADE) consists of three projectors which display the VR on three curved walls. In addition to this 12 m2 projection area, a 17 inches flat screen monitor is placed in front of the sailor to display the

onboard instrument support. The generated output data from the computer for the VR are split up by the Matrox® RT.X2 splitter and afterwards forwarded to the three projectors.

3.4 Test Sailor Matrix, Sailor Level, Computer Game and Interface Device Definition

In order to compare the performance and strategies of experts and those of novices and the influence of an advanced displaying environment, the following sailors and setups are made. Tables 1 and 2 show the sailors and the level definition which are used for the experiment phase of this project. Table 3 deals with sailor's background of the use of computer games (CG) use and the corresponding interface devices (ID).

Table 1 - Experiment Sailor Matrix.

Sailor Information				CG and ID Information	Simulator/Input Environment	
Sailor #	Gender	Age	Sailor Level	Sailor's Level	BDE/Joystick	ADE/Wheel
1	Male	20-30	Novice	Experienced	+	
2	Male	20-30	Experienced	Experienced	+	
3	Female	20-30	Expert	Novice	+	
4	Male	20-30	Experienced	Expert	+	+
5	Male	20-30	Expert	Experienced	+	+
6	Male	30-40	Novice	Expert		+
7	Female	20-30	Experienced	Novice		+
8	Male	20-30	Expert	Expert		+

Table 2 - Sailor Level Definition.

Novice	No experience in sailing races- leisure sailing instead. Limited or no tactical/technical capabilities
Experienced	Sailed national races. Experienced and good tactical and technical capabilities
Expert	Sailed international races. Very experienced and very good understanding of tactical/technical coherence

Table 3 - Computer Game and Interface Device Definition.

Novice	No experience in playing computer games
Experienced	Plays computer games rarely (max. twice a month) with different interface devices
Expert	Plays computer games often (at least twice a week) with different interface devices

4 - The Experiment – The Races

The task of the sailor consists in racing an upwind leg against two computer driven yachts with the finish occuring at the rounding of the mark (see Fig. 3). The distance between the starting point and upwind mark is 3/4 of a nautical mile (or 1389m). The three ACC yachts start in the same line with a lateral distance of 100 meters between each yacht. Therefore, the starting positions can be classified in three categories as the yacht at the right hand side has the best location (position 1) according to the imposed initial heading, followed by the yacht in the middle (position 2) and lastly the yacht on the left with the worst starting position (position 3). Furthermore, the history of the stochastic wind conditions remains the same for all races for the sake of comparability and repeatability of the experiments. The wind speed and wind angle vary about a value of 5 m/s and about ± 20º with an oscillatory pattern. The simulation is run twice as fast

as real-time in order to execute more races. The yacht performance is controlled by the parameter which affects the sail setup which consists of a Jib and Mainsail. The sail trim parameter of 1.0 stands for 100% sail drive force whereas the value of 0.9 denotes 90% of the maximum sail drive force (see Table 4) (Scarponi, 2008).

4.1 Systematic procedure for a Sail Race Session

An identical presentation is made at the beginning of every session to ensure that each sailor has the same pre-knowledge.

This contains an introduction to the sail simulator, an overview of the different input devices, environments, onboard instruments, and finally the task which is required. Two questions are posed to the sailor to determine his/her sailing background and computer game input device experience. Afterwards, a trial is run in order to familiarise the sailor with the simulator, input device, and environment. Before the first race the sailor are informed about the performance of his/her yacht relative to the computer driven yachts and his/her starting position. For subsequent races, in order to compare the performance against opponents with known/unknown yacht performances, the sailor is informed or not about his/her yacht performance relative to the others. Several questions are answered by the sailor before and during the races to elucidate his/her tactics and possible selection of yacht manoeuvres. After the session of seven races, the sailor has to complete a questionnaire which deals with the realism of the simulator, the usability of the input devices and suggestions for further improvements.

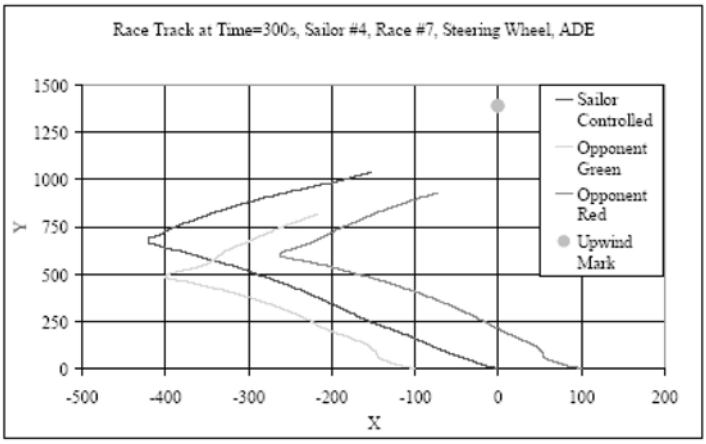

Figure 3 - Example of Race Tracks from Sailor #4, Race #7 using ADE/Steering Wheel, as the two computer controlled yachts respond to the wind shifts the pattern of wind variation can be seen in their course variation.

4.2 Set of Races

The sets of seven races with each sailor in both the BDE and ADE were carried out to determine.

- Improvement to the sailor's performance during the session based on experience with a specific input device. The first and last race of a session are made identical without the sailor's knowledge to ensure a natural and unprejudiced behaviour.
- Influence of the sailor's performance when enhancing the realism of the simulation by replacing the joystick through a wheel and the screen for the virtual reality by three projectors-wall environment.

The following table gives an overview about the race setup, where Opp=Opponents, C=centre, L=left, R=right (see Fig.3), and OI=onboard instruments.

Table 4 - Race Setup.

Race #	Description	Sailor	Opp 1	Opp 2	Sailor	Opp 1	Opp 2	OI
1	Basic Run	1	1	1	C	L	R	+
2	Different level of opponents	1	0.9	0.9	C	L	R	+
3	Different starting position	1	1	1	L	C	R	+
4	Basic Run without OI	1	1	1	C	L	R	-
5	2nd run without OI	1	0.9	0.9	C	L	R	-
6	Different level of opponents	0.9	1	0.9	C	L	R	+
7	Basic Run	1	1	1	C	L	R	+

5- Real Sailor vs. Two Computer Controlled Yachts

In order to determine the influence of the two different human interface device, the performance of the sailor-simulatorsystem is investigated. The interaction of the sailor with the interface device during a race session, and how it influences the implementation of the sailor's tactics as well as the rapidity with which a given sailor learns how to sail in the simulator environment are assessed with regard to the following:`(1) the elapsed race time in reaching the upwind mark; (2) the order of arrival at the upwind mark with consideration to the level of sailing expertise and computer game background of the sailor and the used interface device; and`(3) the number of input errors during the race session for the joystick setup and steering wheel setup. This is evaluated by counting the number of clicks on button #5 instead of button #6 and vice versa, and the selection of the wrong steering wheel rotation direction respectively. The influence of an improved display environment is assessed by analysing the interaction of the sailor with the BDE and the ADE respectively. This data analysis is based on the recorded observation of the sailor's behaviour during the races and the sailor's individual feedback recorded on the questionnaire.

5.1 Performance Improvement using the Joystick

Table 5 shows the results for the different parameters which are recorded and calculated in order to determine the sailor's performance using the joystick as the input device, ID. The race time achieved for reaching the upwind mark is used in order to determine the performance improvement of the sailor during the session.

Three out of the five sailors could defend or improve their starting position, whereas only sailor #4 was able to win the fleet race. For three sailors the performance improvements using the joystick is within the range of 8% to 12%. The great decline of the performance improvement of sailor #1 and #5 is based on a wrong tactical decision and

the resultant disadvantage in race #7 and a good performance in race #1 which explains the decline of -15% and -19%. It is worth pointing out that the novices in both categories have the lowest input error for race #1 which can be explained in their limited confidence in using the joystick due to the lack of knowledge of handling it or because of the insufficient knowledge of how to sail a race. Hence they used the PID-controller frequently which results in this low input error rate.

Just sailor #4 and #5 could reduce the number of wrong inputs, whereas a significant decrease was achieved by sailor #5 who halved his wrong inputs to 3. All other three sailors, experienced or novices increased their number of wrong inputs. It was observed that all seven sailors become more confident in using the simulator within the session which result in a more active behaviour and interaction which in turns ends in a more frequent use of the joystick and a greater probability in using the wrong input button. Sailor #4 and #5 who are experts and experienced in one of the categories and are able to base their decisions on their experience which in turns gave them more time to concentrate on clicking the right input device button instead of concentrating on the race. The other sailors were distracted either by the making the right decision within the race or by handling the joystick in the right way, which did not give them the chance of a more natural behaviour.

The trends for the joystick results are mixed and a uniform picture about the performance using the joystick cannot be drawn. Generally, all sailors struggled using this joystick setup associated with the PID-controller. This setup limited the sailors' way of sailing, like ducking behind another yacht or make spontaneous manoeuvres, and consequently their natural sailing behaviour was restricted by the simulator and the BDE.

Table 5 - Results for BDE/joystick.

Sailor #	Level of Sailing Skills	Level of CG and ID	Race Time/ Performance Improvement [%]	Position in Race #1 /Race Time [s]	Position in Race #7 /Race Time [s]	Wrong Input Race #1	Wrong Input Race #7
1	Novice	Experienced	-15.2	1 / 451.5	3 / 532.1	3	8
2	Experienced	Experienced	12.1	3 / 522.5	2 / 466.0	6	7
3	Expert	Novice	7.8	3 / 545.5	2 / 506.2	3	5
4	Experienced	Expert	11.3	3 / 479.9	1 / 431.1	9	7
5	Expert	Experienced	-19.3	3 / 493.1	2 / 611.1	6	3

5.2 Performance Improvement using the Wheel

Table 6 shows the results for the different parameters which are recorded and calculated in order to obtain the sailor's performance using the steering wheel as the ID. Three out of five sailors improve their starting position within the first race (race #1) and could win their race, whereas the other two sailors, sailor #7 and #8 had to adapt to the simulator setup within the first race which resulted in the loss of a position when arriving at the upwind mark. Furthermore, all five sailors are able to win the last race (race #7) and all sailors apart from sailor #6 could reduce their needed race time for reaching the upwind mark during the session by 6% to 21%. The exception of sailor #6 is based on a perfect performance in race #1 and the fact that the sailor tried to apply the new gathered race knowledge which resulted in a slightly worse higher race time of almost 5%.

Input errors made by the sailors are very limited and only occurred during the first two races. The novice in the category ID experience (sailor #7) struggled slightly in race #1 and #2 as she is used to dealing with a tiller which performs in the opposite direction to the steering wheel. Generally, all sailors adapted to the steering wheel quickly. It is also observed that during the first two races the sailors had to make small adjustments after the tack by turning the steering wheel slightly in the opposite direction. This phenomenon disappeared during the session as all sailors became confident with the ID which results in a good race time and performance. This observation and the fact that no wrong input could be recorded after the 2nd race yields to the conclusion that this ID is a straightforward and handy tool which supports the sailor in sailing the race accordingly to his/her natural behaviour as he/she is not distracted by the handling of the ID. Consequently, the sailors could race a more realistic race as they only focus on the race, their tactics, strategies and quick manoeuvres like ducking behind an opponent's yacht to avoid a collision. It is also worth pointing out that the race time for all races with the joystick setup is higher than for those with the steering wheel, (compare Tables. 5 and 6). The direct performance improvement of the sailor #4 and #5 using the joystick and the steering wheel is between 5% and 15%, whereas the value of 51% could be taken into account as this race of sailor #5 is based on a wrong tactical decision.

The trend for the steering wheel results without the support of the PID-controller is consistently positive. All sailors finished their races within a remarkable race time and were able to win race #7. Furthermore, four out of five sailors could improve their performance within the session. This setup allows the sailor to race the desired course and arranged tactic without a limitation caused by the ID. Consequently, the sailor's natural sailing behaviour is not only limited but also supported by this setup with the steering wheel.

Table 6 - Results for ADE/steering wheel.

Sailor #	Level of Sailing Skills	Level of CG and ID	Performance Improvement [%]	Position in Race #1 /Race Time [s]	Position in Race #7 /Race Time [s]	Comparison to Joystick Race #1	Comparison to Joystick Race #7
4	Experienced	Expert	8.4	1 / 443.2	1 / 408.8	8.3	5.4
5	Expert	Experienced	6.3	1 / 429.7	1 / 404.3	14.8	51.1
6	Novice	Expert	-4.5	1 / 408.6	1 / 427.8		
7	Experienced	Novice	16.8	3 / 516.5	1 / 442.1		
8	Expert	Expert	20.7	3 / 520.7	1 / 431.2		

5.3 Two Screen Environment vs. Three Projector/One Screen Environment

The comparison of the two different display environments is based on observations which have been made during the races and on the answers of the questionnaires. Generally, important differences of the sailor's use of the virtual reality could be observed between the BDE and ADE. The basic display environment is judged to be sufficient in supporting the sailor with the necessary information about the current performance of the yacht and the sailing environment. The sailor is more focused on the onboard instruments, especially on the virtual GPS than on the VR and consequently

the zoom in/out option is not frequently used. The screen which displays the VR attracts the attention of the sailor when events like rounding the mark or interaction with an opponent occur. A vital and active interaction between the VR and the sailor is not developed with the BDE which limits the realism of this setup compared to real life sailing.

The advance display environment achieves a much more positive feedback from the sailors as it supports the sailor with the necessary information about the actual state of the yacht and the race but also with a large display environment. The sailor is much more involved in the actual race which is expressed in an active body language, frequent head and eye movements.

Furthermore, jerkily body motions are observed when an opponent's yacht appears on the edge of the projection area which stands for a very vital and active interaction between the VR and the sailor. Consequently, the ADE attracts the sailor's attention more often as the BDE which in turn influences the sailor's use of the provided onboard instruments. In addition, the zooming is used more often, especially the zoom in option when rounding the mark or when interacting with another yacht. In these events the decision made by the sailor is exclusively based on the information delivered by the ADE. Compared to the BDE where the sailor focuses on the OI, the picture changing regarding the ADE, where the sailor focuses on the VR and uses the OI as a support information tool and found in real life sailing. The ADE is an important factor of enhancing the realism of the simulation and in supporting the natural behaviour of sailor.

Nevertheless, the sailors had problems to determine the position of their yacht relative to the other yachts using the VR, which forced them to make a crosscheck with the virtual GPS. This lack of orientation is caused by the distortion and the coarse grid within the VR and can be improved by the application of a finer superimposed grid.

6- Conclusion

The experiments show an important effect on sailor performance when enhancing the realism of the simulation. The improvement of the realism of the simulation was achieved by using two different display setups, the Basic Display Environment (BDE) and Advanced Display Environment (ADE).

In considering the joystick setup which uses the PID-controller no clear picture of the sailors' performance improvement can be drawn. This phenomenon was also observed by Andonian *et al.*, 2003. The results for the joystick show that the setup of the PID-controller and the adjustment of the rudder angle by clicking button#5 and #6 are neither practical nor effective. Furthermore this setup confuses the sailor and constrains his/her natural way of sailing which in turn limits the realism of the simulation. It was observed that even computer game and ID experienced sailors needed at least three races to reduce their input error whereas other sailors struggled with the correct input until the end of the session.

A completely different picture emerges when using the steering wheel with the direct control of the rudder angle. There is a clear improvement in the control of the yacht's motion. This allowed the user to sail the desired course and to apply the arranged tactic and strategy without a limitation caused by the ID, which in turn supports the sailor in his/her natural sailing behaviour.

An important change of the novices' race behaviour was observed during the sessions. Within the first races the novices adapt to the behaviour of their opponents and then developed their own tactics and strategies which they applied in the following races. They still made wrong tactical decisions due to the lack of specific sailing knowledge and experience, but a significant improvement of the general race performance was observed. Therefore, this simulator with the appropriate steering wheel/ADE setup could be used as a training tool.

The effect on the sailor's performance when enhancing the display environment is not measurable, but the observation made during the races and the feedback of the sailors about the realism of the setup is much more positive for the ADE than for the BDE. The improvement of the realism causes a more active and involved behaviour of the sailor within the races. The combination of the ADE and the steering wheel without the use of the PID-controller has shown to be the right choice to enhance the realism of the simulation which is proven by the results of the steering wheel/ADE runs and the feedback of the sailors who attended this study.

7- Acknowledgement

We would like to thank all the participated sailors for their support, time and patience with us. We would also like to thank Dr Kenji Takeda for his help and support to execute this experiment within the Flight Simulator Laboratory of the University of Southampton. The authors acknowledge the support of the School of Engineering Sciences and also MASTRUCT, Network of Excellence on Marine Structures financed by the European Union through the growth programme.

8- References

Andonian B., Rauch W., Bhise V., 2003, 'Driver Steering Performance Using Joystick vs. Steering Wheel Controls', SAE International, SAE World Congress.

Kerwin, J.E., Newman, J.N., 1979, 'A Summary of the H. Irving Pratt Ocean Race Handicapping Project', Proceedings of the 4th Chesapeake Sailing Yacht Symposium.

Masuyama Y., Kukasawa T., Sasagaw H., 1995, 'Tacking Simulations of Sailing Yachts – Numerical Integration of Equation of Motion and Application of Neural Network Technique', SNAME, Proceedings of the 12th Chesapeake Sailing Yacht Symposium, pp.117-131.

Scarponi M, 2008, 'Including Human Performance in the Dynamic Model of a Sailing Yacht: A Combined Ship Science – Behavioural Science Approch Towards a Winning Yacht-Sailor Combination', PhD Thesis, Università di Perugia.

Scarponi M., Shenoi, R.A., Turnock, S.R., Conti, P., 2007, 'Including Human Performance in the Dynamic Model of A Sailing Yacht: A MATLAB®-Simulink® Based Tool', The Modern Yacht, pp. 143-156.

The Behaviour of Recycled Rubber Shockpads for Synthetic Sports Pitches (P150)

P.R. Fleming, L.J. Anderson, M.A. Ansarifar[1]

Abstract: Shock-absorbing layers perform vital roles in the user comfort, safety and ball interaction characteristics of synthetic sports pitches. This layer typically comprises a porous composite of granulated recycled rubber bound in a polyurethane resin, mixed on site and compacted and cured to form a flat continuous pad upon which the synthetic carpet is laid. A lack of published scientific information regarding shockpad behaviour or design prompted research at Loughborough University. This research investigated fundamental behavioural aspects of in-situ shockpad layers, including: their design; construction; mechanical behaviour; and sought appropriate and novel test methods for their assessment in the laboratory and field. This paper provides a summary of these unique findings in relation to the effect of mix design variables, including binder content, bulk density, layer thickness and rubber size distribution. Data are presented for shockpad energy restitution, impact behaviour, and shockpad tensile strength. In addition, the effect of short pile and long pile carpet systems placed above to replicate whole pitch systems is presented. Conclusions are presented and include recommended requirements for the industry to incorporate changes in design and construction quality assurance.
Keywords: Synthetic Sports Pitch, Shockpad, Mechanical Properties, Rubber.

1- Introduction

Synthetic sports pitches are composite structures of several layers, often divided into the 'surface system' and the 'foundation'. The foundation generally comprises an engineered sequence of porous bound macadam (up to 65mm thick), overlying crushed rock (up to 300mm thick typically) and the natural soil. This provides a solid platform which should remain porous, stable and 'flat' for at least 25 years. The surface system comprises the sport specific (or multi-use) carpet (either filled or unfilled) overlying the shockpad. Typically the carpet may be expected under normal use to last 5-10 years, and the shockpad perhaps two carpet lifetimes. Each of the components of the system interacts to provide the aspects of performance required, typically ball rebound, adequate compression resistance/deformation for user movement and comfort, and safety charac-

1. Loughborough University, Loughborough, Leicestershire, LE11 3TU, England - E-mail : p.r.fleming@lboro.ac.uk

teristics related to foot-surface and possibly head and skin surface interactions dependent upon the sport which the pitch is intended (or multi-sport use). A previous review of shockpads for synthetic pitches (Anderson *et al.*, 2004) highlighted a dearth of published scientific investigation, and very little guidance from sports governing bodies or from industry construction guidelines to ensure consistent quality of shockpad layers. Some preliminary results were reported by Anderson *et al.* (2006) and showed the effect of some mix design variables, whilst an overview of all of the key findings is addressed herein.

In-situ (also called wetpour) shockpads comprise recycled rubber granule bound in a (thin) coating of polyurethane (typically 5-10% by weight), mixed on site and then spread and lightly compacted (in lanes typically 2-3m wide) to produce a porous and continuous layer of a specified thickness (set by the spreading and compaction plant). The shockpad binder is air cured and usually left for several days before the carpet and associated plant are permitted onto the surface. There are many aspects and variables regarding the design and construction that may be expected to affect the properties of the finished product, and these are set out in Table 1. The variables are numerous, but it became clear that from an engineering viewpoint the predominant ones to investigate in the laboratory included rubber size, binder content, and shockpad layer thickness, and bulk density. Rubber shape and size are both expected to affect the efficiency of coating of the binder due to differences in surface area. However, after observing the shredding process it was observed that it (ambient) produces a range of shapes and these are controlled largely by the mechanical process of cutting, and would be a similar distribution for a range of recycling plants using the same process. The shapes vary from approximately cubic to more elongated and the edges are not always neatly cut, dependent on the sharpness of the shredding blades. However, for consistency, only one source of shredded rubber was utilised for this work and each batch underwent the same level of processing.

The site variables, assuming a consistent source and supply of rubber and binder, were expected to primarily affect the binder coating efficiency, the compacted thickness, bulk density and to some extent the availability of cured binder-rubber contact. A programme of fieldwork on actual construction sites (Young, 2005), in particular retrieving undisturbed samples of cured shockpad, was utilised to evaluate typical binder content, particle sizes, layer thickness and bulk density. The feedback from the industry steering committee was that the sole acceptance criteria comprised tensile strength – used as an indirect measure of likely long-term durability. However, there were clear issues regarding the retrieval of truly undisturbed samples from site (the pad often sticks to the macadam layer beneath) and additionally the damage caused by cutting of the dog-bone shape samples for the tensile test rig without causing damage. Small dog-bone samples specified follow the principles for solid plastics and are arguably not suited to the voided structures of shockpads where the aspect ratio of sample width to maximum particle size may be as low as 4 (i.e. maximum rubber size of 6mm within a 25mm wide sample).

The literature review (Anderson, 2004) raised few key references, but that of Kim (1997), concluded that a binder content of 13% produced optimal pad tensile strength,

and larger size rubber shred produced a stronger pad than smaller rubber sizes. Conversely, Sobral *et al.* (2003) found smaller rubber sizes produced higher strengths. However, the rubber particle sizes investigated by both these researchers were in the range 0.1 to 3mm, which is smaller than those used to construct shockpads in the UK (usually 2-6mm or 2-8mm). The tensile test is used in the industry as a 'durability' quality indicator, and is a measure of the integrity of the rubber-binder interface under increasing tensile strain – but is clearly not representative of in-situ loading conditions. A shockpad under a carpet is expected to experience many repeated applications of force and resulting strains that are predominantly compressive from running and ball bounce, with components of induced shear and tension. The size of strains induced will depend on the loading from player motion, with braking/stopping, turning (and maintenance equipment) thought to provide greater magnitudes of horizontal forces and strains. The frictional restraint provided between the interfaces of carpet and shockpad, and shockpad and substrate will have a large effect on the size of the horizontal strains and it may be more applicable to think of cumulative damage under repeated applications of 'low' strain for durability than simply increasing the strain in the quasi-static tensile test. In addition, tensile strength gives no indication of the likely performance of a shockpad with regard to its play performance, such as the ball and athlete interaction characteristics, and its role in the composite structure of a surface system.

This paper summarises the key findings of the programme of laboratory work. Of the mix design variables identified as having a potential effect, see Table 1, this paper presents the findings for four variables; pad thickness, bulk density, binder content, and rubber particle size distribution. The effects on the characteristic behaviour were assessed through three main test methods, representing ball interaction, athlete interaction and durability via tensile strength.

Table 1 - Design and construction variables expected to affect recycled rubber in-situ shockpads.

Design Variables	Construction Variables
Rubber size	Raw materials consistency
Rubber particle size distribution	Rubber - Polyurethane mix efficiency
Rubber shape	Rate of construction
Binder type	Compaction applied
Binder Content	Cure environment and time
Layer thickness	
Bulk Density	

2- Effect of Design Variables on Shockpad Behaviour

2.1 Test Method

A 'standard' shockpad was created to provide a benchmark to assess the extent that the changes in design had on measured behaviour. The design variables are shown in Table 2, with the range of change investigated derived from measurements of installed shockpad samples during construction of several water-based hockey pitches and 3rd

generation football fields. Three samples of each shockpad were constructed to assess repeatability. The consistency of physical properties for these repeat samples was considered to be good, with variability in the range 0-5% for aspects such as density, binder content (i.e. 5% of binder %), size and thickness. This demonstrated a consistent method of hand construction (see section 2.2). A separate set of shockpads was produced as each variable was altered from the benchmark value, through the range selected, while all other variables remained constant. This produced fourteen combinations of shockpad design in total.

The 'performance' related tests carried out on each sample included one related to construction quality (tensile test), two for user comfort (Clegg Hammer and 'Berlin' artificial athlete test –for comparative purposes) and one for ball behaviour (simple standard vertical ball rebound test). The tensile test was carried out to the recognised industry standard BS EN 12230, with samples cut to a dumbbell shape 25 mm wide by 150 mm long and strained to failure at a rate of 50 mm/min. It is interesting to note that the industry has target values for tensile strength - dependent upon the sport – however the 'certification' of the surface systems for FIH or FIFA licenses allows shockpad samples to be hand made rather than sampled from site.

A portable impact device, the Clegg Hammer, was used to simulate the effect of athlete foot-surface interaction, in addition to the Berlin test. The device records the peak deceleration of an instrumented 2.25kg weight dropped from a height of 450mm, guided through a plastic tube onto the surface. Peak forces generated by the Clegg Hammer have been shown to be similar to that of an athlete heal strike, albeit over a shorter contact time. Useful correlations of the Clegg to the industry standard 'Berlin Artificial Athlete' have been published by Fleming *et al.* (2004) and the Clegg is easier and quicker to use, permitting more tests per pitch. Higher Clegg Impact Values indicate a harder (less shock absorbent) surface.

The ball-surface test comprised dropping a hockey ball from a height of 1.5m onto a shockpad and measuring the rebound height, as per FIH guidelines (FIH, 1999). The ratio of drop height to rebound height is used to determine rebound resilience (R.R). Low rebound resilience is a result of large energy losses during the ball impact.

Table 2 - Standard shockpad specifications, variables and ranges.

	Standard Shockpad	Variation Range
Binder Content	9 %	5, 12, 15 %
Bulk Density	550 kg/m^3	500, 600 kg/m^3
Rubber Size	2-6 mm	2-8mm
Rubber PSD	Standard 2-6mm	Fine and coarse side of the size envelope
Rubber Shape	Variable, not controlled	Variable, not controlled
Thickness	12mm	8, 15, 20mm

2.2 Shockpad Construction and Cure

The laboratory constructed shockpads were made from recycled truck tyre rubber granules, sieved into separate particle size ranges using mesh sieves, reconstituted to

form the required particle size distribution. The particles were washed and dried to remove residual dust. The total mass of rubber required for each shockpad was controlled for both binder mix design and target density for the required thickness. The rubber granulate and binder were mixed in the required proportions using a small bench-top mixer. The mix was carefully placed into moulds 900 mm by 300 mm in plan, to the required thickness, and lightly compacted by a cylindrical steel bar rolled across the surface until the required thickness and a flat surface was achieved. Curing was controlled for temperature and humidity at 22±3oC and 65±5%RH respectively in an environmental chamber. A pilot study refined the mixing and compaction method to create repeatable samples similar to industry standard, and additionally determined that for 14 days curing time was sufficient for a shockpad to reach a plateau in mechanical properties. Upon reaching 14 days curing time, the shockpads were removed from the moulds for testing.

2.3 Test Results

The key test results are presented in Table 3, the coefficient of variance (CoV) for each result is given as a bracketed number determined from the ratio of the standard deviation to the mean (in %). Each set of results is the average of repeat tests (i.e. 15 Clegg tests, 5 Berlin tests, 15 ball bounce tests and 5 tensile tests). This carefully measured data is unique and provides a benchmark of shockpad physical properties and useful measured performance related parameters for manufacturing companies, installers and test houses. Figures 1 to 3 show relationships to assist in gauging the *scale* of mix design variable changes on the measurements.

It is useful to consider the results in terms of mechanical properties, and to further classify these by aspects of compression behaviour (also termed impact resistance or shock absorbency), energy recovery (in relation to ball rebound), and durability (inferred from tensile strength). There are no current guidelines in industry standards or from the literature that assist in the decision as to whether the measured changes observed are in fact 'significant', in the sense that they may have a real impact on the players or in-game effects. However, from previous work by Young (2005), wherein he compared mechanical test data to player feedback across a range of 6 hockey surfaces, the following is considered a useful preliminary guide - a ball rebound of 3% (5cm), and a Force Reduction (Berlin) of 5%. In addition, the measured tensile strength values all fell below the industry recommended values (typically 100kPa to 120kPa). The relationship between the Clegg Impact data and the Berlin force reductions appears to be useful, albeit non-linear, though the Clegg appears a little more sensitive on thinner shockpads and less sensitive on the thicker shockpads.

Table 3 - Mechanical test results for shockpads with design variations. CoV given in brackets. (R.R = Rebound Resilience, CIV = Clegg Impact Value, FR = force reduction, T.S. = tensile strength).

Variable		C.I.V [g's]	F. R [%]	R.R [%]	T.S [kPa]
Binder Content	**5**	250.8 (2.6)	41.0 (0.32)	36.9 (1.9)	20.7 (42.0)
[%]	**9**	257.4 (1.3)	41.2 (0.03)	36.7 (0.4)	33.9 (25.0)
	12	227.6 (0.3)	42.6 (0.01)	36.4 (1.7)	45.1 (21.5)
	15	252.1 (7.7)	41.1 (0.07)	36.6 (1.9)	70.9 (12.0)
Bulk Density	**500**	290.3 (3.7)	40.5 (0.06)	36.2 (0.6)	26.8 (39.9)
[kg/m³]	**550**	257.4 (1.3)	41.2 (0.03)	36.7 (0.4)	33.9 (25.1)
	600	246.8 (3.3)	41.5 (0.35)	36.5 (0.4)	49.3 (20.5)
Rubber PSD	**Std.**	257.4 (3.4)	41.2 (0.03)	36.7 (0.4)	33.9 (8.5)
(2-6mm)	**Small**	229.7 (7.4)	41.1 (0.09)	35.7 (0.5)	38.9 (10.5)
	Large	225.3 (2.3)	56.1 (0.20)	35.9 (0.4)	34.0 (8.9)
Rubber PSD	**Std.**	268.8 (1.9)	38.5 (0.04)	36.5 (0.4)	40.3 (7.5)
(2-8mm)	**Small**	226.8 (9.3)	44.3 (0.53)	36.0 (0.5)	40.9 (7.2)
	Large	253.5 (1.3)	41.7 (0.25)	36.8 (0.5)	54.5 (7.1)
Thickness	**8**	> 444	30.9 (0.46)	32.3 (0.5)	20.8 (7.1)
	12	257.4 (1.3)	41.2 (0.03)	36.7 (0.4)	33.9 (25.0)
	15	154.7 (3.4)	50.7 (0.18)	36.5 (0.5)	46.4 (8.5)
	20	122.3 (4.1)	56.1 (0.04)	36.5 (0.5)	56.6 (6.0)
Binder type	**1**	257.4 (1.3)	41.2 (0.03)	36.7 (0.4)	33.9 (25.0)
	2	251.7 (6.4)	40.9 (0.29)	35.6 (0.9)	43.8 (16.0)
	3	241.0 (8.5)	42.3 (0.09)	35.9 (0.6)	39.7 (7.2)

In compression loading, the data showed that there was some influence of all the mix variables except binder content, although it is clear that some integrity is required and there is likely to be an acceptable lower limit. The largest effects were observed for changes in shockpad thickness, as might be expected with a rigid substrate beneath and for these dimensions which could be classed as thin (relative to the width/diameter of loading). Some change in compressive behaviour was observed for the variation in rubber size distribution, density and binder type, though these were small relative to the effects of thickness change (see Table 3). In practice, the thickness may change by several millimetres or more locally due to undulations on the surface on which the shockpad is laid.

The general effect, in compression, of the mix design changes once the carpet is laid on top of the shockpad is to reduce the variation to virtually negligible except for changes in thickness. The absolute effect of adding the carpet was a large change increase force reduction (or reduction in Clegg value) giving a better shock absorbency, by up to 25% for the thinnest shockpad, and around 10% for the thickest shockpad. However, the extra protection afforded by the carpet may be expected to reduce over time as the carpet wears, flattens and the infill compacts (depending on the maintenance efficacy of course).

The energy recovery (ball rebound resilience) showed very little change for all the mix design variations except thickness, although the maximum percentage reached a plateau. The energy losses are clearly greater for thinner shockpads, where it is expected that the hockey ball itself will deform and lose energy. With the (hockey) carpet added, however, the changes in rebound were negligible. The absolute change was around 5%, due to energy losses in the carpet fibres deforming – with relatively complex viscous elasto-plastic behaviour mechanism.

The shockpad durability, inferred from tensile strength, was affected by all the mix design variables, and thus may have a significant effect on shockpad life – or more importantly to the industry on pads passing the quality assurance tests specified in many sport standards. Binder content exhibited the greatest effect on tensile strength, with the strength increasing approximately linearly and a relatively constant standard deviation (hence the reduction of CoV in Table 3). The tensile strength also increased to a large degree with increased bulk density and thickness, which is a significant finding for site practice. There was a relatively small effect with decreasing particle size, but not significant with respect to the repeatability of the test. Tensile strength is reliant on sufficient binder being available at contact points to adhere the rubber particles together, thus density and binder content would be expected to affect the number and integrity of contact points in the cross-section of the shockpad. Reducing particle sizes within a distribution creates higher surface area, however, so it might be expected that an increase in the amount of binder would be required to sufficiently coat the rubber surface. This suggests an optimisation process whereby the combined effect of particle size, pad density and binder quantity would all affect tensile strength. The role of thickness is less easily explained, except that for the thinner layers the likelihood of zones of weakness initiating the tensile failure is considered to increase as there are less particles in the cross sectional area.

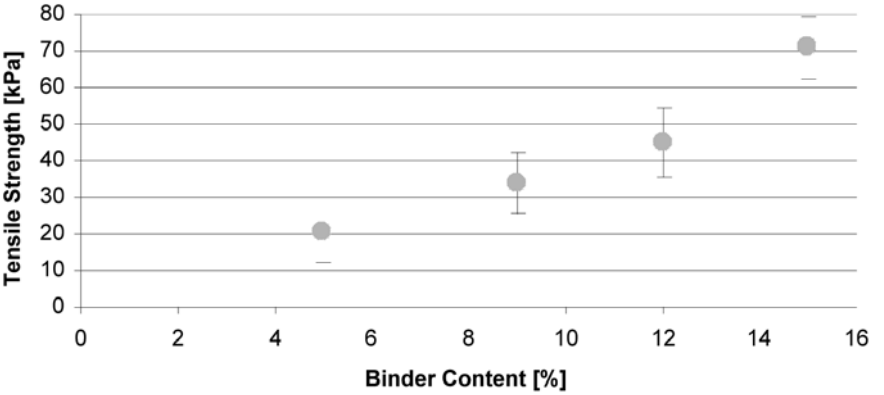

Figure 1 - The effect of binder content on tensile strength of shockpad with varying binder content. The error bars represent one standard deviation (n=5) and are indicative of sampling issues and low aspect ratio.

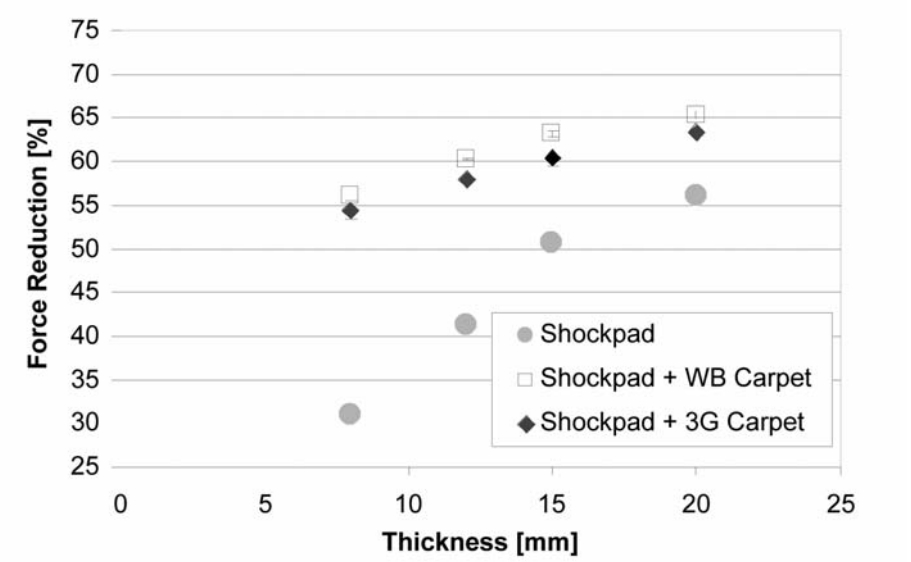

Figure 2 - The effect of shockpad thickness on the variation in the shockpad shock absorption (force reduction), and for the effect of a short pile hockey carpet (WB) and long pile football carpet (3G).

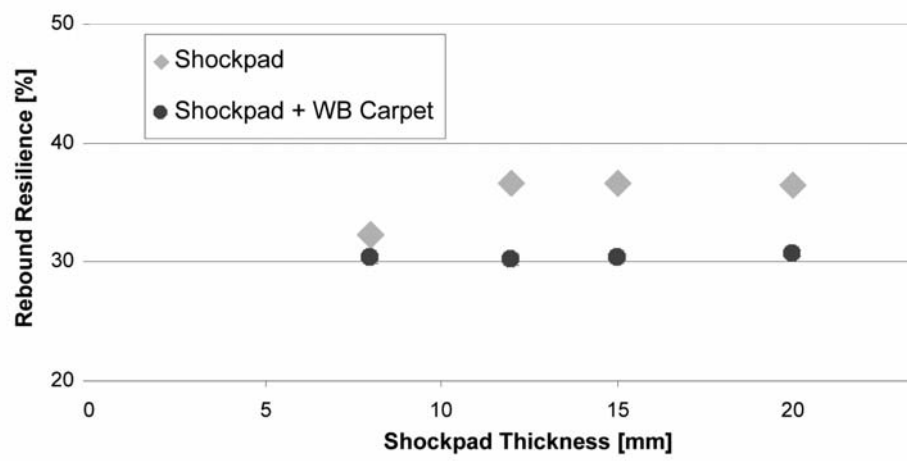

Figure 3 - Effect of shockpad thickness on ball rebound resilience, and for the effect of a short pile hockey carpet (WB).

3- Discussion

The overall findings are summarised in Table 4, providing a brief overview of the magnitude of mix design changes on the shockpad and shockpad-carpet combinations. It is observed from the findings that the rubber particle size and its packing density determines how the shockpad will behave in compression and unloading. The binder acts to hold the rubber particles together, and although this provides tensile restraint it may be

concluded that under the compressive loads applied its influence over shockpad behaviour is not nearly as significant compared to physical characteristics of the rubber, such as shape, packing density and (although not compare herein) the intrinsic compression behaviour of the rubber itself. Under the tensile test the binder content is clearly the primary variable, although (apparently as a function of the size of samples) the shockpad thickness also contributes as does the density of the composite structure. The density has little effect on the compression behaviour of the shockpad, as measured by the Berlin Athlete, although the Clegg data showed some effect. It is apparent then that if a tensile strength criterion is the primary measure used by the industry for quality assurance that the application of a greater compactive effort and binder content in a sample will effect a larger tensile strength result (without showing any appreciable change in play performance properties related to balls and athletes). The historical system of hand making shockpad samples on site to represent those made by machine is clearly flawed, in that manual compaction and even a small addition of binder will produce a sample strength perhaps far removed from that actually achieved on site. Furthermore, there are issues on site whereby the binder (especially on a warm day) remains mobile and may gravitate toward the base of the pad during all the stages of transporting the mix (usually via dumper), stockpiling the mix and time delays prior to spreading, and during the spreading and compacting of the mix. The cured pad often adheres to the underlying substrate to the extent that 'sampling' an in-situ shockpad by cutting and lifting renders appreciable damage and can be the source of poor quality samples that fail the tensile test. Laying in-situ onto trays that are removed and cured is a more pragmatic and reliable approach, but again may not fully replicate the site-wide process.

It is also interesting to contrast the loading and unloading behaviour of the shockpad. The Clegg Hammer and Berlin impacts are much higher in energy (similar to a Berlin Artificial Athlete) than the ball impacts, and therefore produce higher strains and deformations, and hence more hysteresis it is thought. Ball impacts strain only the upper shockpad surface, and beyond a certain thickness, 8mm in this case, are not influenced by the bulk of the shockpad or the substrate.

A model for the stages of deformation of the shockpad in loading and unloading has been suggested by Anderson (2007), that there are three clear stages of behaviour during compression. These were described as: the initial compression of the void space in the composite material, (void space can be estimated as around 45% for the 550 kg/m3 bulk density) which is relatively low resistance; an intermediate stage whereby the number of point contacts between rubber particles increases and some initial relatively low strain compression of the rubber occurs; and a third stage whereby at higher compression strains the rubber is providing increased resistance and reaching its limiting intrinsic material stiffness and with little void space remaining. It follows that under different energy (and shape) impactors the response of the composite system with its high porous structure will vary dependent on the stage of compression achieved. Furthermore, it may be postulated that the stiffness response may be anisotropic due to the nature of the construction process favouring vertical rather than horizontal volume changes during the low level tamping.

Table 4 - Summary of the effect of each mix design variable on player interactions, ball interactions and durability for shockpads and shockpad-carpet systems (SP=Shockpad).

	Player Interactions		Ball Interactions		Durability
	SP	SP & Carpet	SP	SP & Carpet	Tensile
Thickness	High	Med	Low	Low	High
Binder Content	None	None	None	None	High
Bulk Density	Low	None	None	None	Med
Rubber Size and Distribution	Low	None	None	None	Low
Binder Type	Low	None	None	None	Low

Shockpads are rarely used as the surface layer in pitch constructions, so the effect of the carpet and infill materials requires careful consideration. Third generation football and rugby pitches with a long carpet pile filled with rubber are not considered to be greatly affected by the shockpad until infill compaction has occurred (several years). Water-based hockey carpets (no infill) are more affected by the shockpad, especially after wear has occurred. It must be noted that the results of this testing do not indicate changes to the actual whole pitch performance. They only act to indicate that pitch performance may be affected by altering these variables and magnitude will depend on the carpet and infill materials used.

4- Conclusions & Recommendations

Notwithstanding this project there is little published literature or industry guidance with regard to shockpad mix design for synthetic playing surfaces. The key play performance indicators are player comfort and ball interaction, and durability of the site-constructed system is a key construction performance parameter. Altering the mix design variables in shockpads has been shown for some variables to effect the pad mechanical response to dynamic compression tests and energy recovery for ball impacts, and have large effects on tensile strength (inferring durability issues). The primary variables that can influence play performance were identified as shockpad thickness, and bulk density. The primary variables affecting tensile strength were binder content and shockpad thickness, with the optimum strength produced by a high binder content, high bulk density and small-dominated rubber particle sizes. The effect of combining the (new) carpet sample with the shockpad showed a reduced significance of the mix design variables, though it is interesting to postulate the effects of carpet wear and flattening with time whereby the shockpad performance may be more dominant within the surface system response.

The data can be used by manufacturing companies, pitch shockpad installers, and sport test houses to assist their understanding of shockpad design and behaviour, benchmark their products, and assess the likely effects of variations in site practice and the need for specific measurements during quality assurance. Whilst a simple means of assessing the binder content of a cured sample eludes the industry, field measures of thickness and density should be carried out at many positions to ensure consistency – with perhaps a simple device such as the Clegg Hammer utilised to provide a rapid assessment test of the combined compression properties. The Clegg Hammer is thought

to be particularly useful for refurbishment contracts where a carpet is lifted and the shockpad needs a rapid assessment to confirm its integrity prior to a new carpet being laid.

5- Acknowledgements

The authors are grateful for the financial support and advice of the technical steering committee, comprising Andy Shaw of Polytan (UK), Barry Stocker of Murfitts Industries Ltd, and Bob Allen of Aggregate Industries.

6- References

[A1] Anderson LJ, Fleming PR, Ansarifar A, (2004), Shock Absorbing Layers for Synthetic Sports Pitches In: The Engineering of Sport 5: Proceedings of the 5th International Conference on the Engineering of Sport (eds M. Hubbard, R.D. Mehta & J.M. Pallis) Vol. 2, ISEA, UK.

[A2] Anderson LJ, Fleming PR, Ansarifar A, (2006), Recent Advances in Understanding the Behaviour of Shockpads for Outdoor Synthetic Sports Pitches, Proceedings of the 6th International Conference on the Engineering of Sport, (eds E.F. Moritz & S.J. Haake) Vol. 3, Springer, New York.

[A3] Anderson, L. J., (2007), Elastomeric Shockpads for Outdoor Synthetic Sports Pitches, PhD thesis, Loughborough University

[F1] FIH (1999) Handbook of Performance Requirements for Outdoor Synthetic Hockey Pitches, International Hockey Federation. Brussels, Belgium

[F2] Fleming P, Young C, Dixon N, (2004) Performance Measurements on Synthetic Turf Hockey Pitches, The Engineering of Sport 5, ISEA, M. Hubbard, R. D. Mehta, and J.M Pallis (Eds), Vol 2, pp524-531. ISBN 0-9547861-1-4.

[K1] Kim, J.K. (1997) Experimental and Theoretical Studies on Crumb Rubber/Polyurethane Blend System, Korea Polymer Journal, 5(4), pp. 241-247

[S1] Sobral, M., Samagaio, A.J.B., Ferreira, J.M.F. and Labrincha, J.A. (2003) Mechanical and Acoustical Characteristics of Bound Rubber Granulate, Journal of Materials Processing Technology, 142(2), pp. 427-433

[Y1] Young, C., (2005), Mechanical and Perceived Behaviour of Synthetic Turf Field Hockey Pitches, PhD thesis, Loughborough University

Implementation of Knowledge Engineering Fundamentals in Exercise Science and Individualization (P151)

Hamed Zaribafzadeh[1], Reza Abedian Dehaghani[1]

Topics: Athletics, Modelling.

Abstract: The evolution of traditional sports training, to the concept of exercise science, is attracting an ever increasing attention. A systems approach to exercise science however, directs emphasis towards the concept of individualization.

Individualization, however, poses challenging problems, when faced with the wide range of non-systematic definitions. The individualized approach to training tends to encompass information regarding the athlete, the sport is question and the equipment available. The ensuing and ideally, optimized training program, is governed by what might be termed as expertise exhibited by the coaching team in utilizing the training principles.

A systematic implementation of the principles of training, however, requires a systems approach to both "Experience" and "Knowledge". The ability to extract useful hidden knowledge and to act on that knowledge is becoming increasingly important in today's competitive championship world. So, having a knowledge base along with a realistic decision making system could be considered a valuable asset and a useful tool for a coach.

In this paper, the mechanism of the application of Knowledge Engineering fundamentals to both coach experience and sports training knowledge is discussed. The approach could be advanced to form an Expert System capable of making decisions towards organization of an optimized time oriented training program which is backed by both experience and elements of exercise science.

Keywords: Knowledge Engineering, Fuzzy Logic, Exercise Science, Sports.

1- Introduction

The academic research area for developing models, methods, and basic technologies for representing and processing knowledge and for building intelligent knowledge-based systems, is called knowledge engineering (Kasabov 1996).

Knowledge engineering is the discipline of developing knowledge systems using sound and principled methods. Perhaps because it is a relatively new field, the term engi-

1. Biomedical Engineering Faculty, Amirkabir University of Technology (Tehran Polytechnic), Tehran, Iran
E-mail: hamedzaribaf, abediyan@gmail.com

neering is used to stress its relationship with other engineering disciplines and emphasize that the development of knowledge systems should follow established scientific method for the creation of complex artifacts. The treatment of different aspects of knowledge engineering shows an ingrained reliance on an engineering metaphor for the development of knowledge systems.

A knowledge system can be defined as a computer system that emulates the decision-making ability of a human to solve problems that are difficult enough to require significant human expertise for their solution. The knowledge model consists of individual quanta of knowledge that can be employed individually, in combination with others. The knowledge model contains representations of knowledge, used to assert new facts from the existing facts. The main goal for knowledge systems is to provide more effective and efficient use of knowledge. Also the reason to employ a knowledge system is because the user is not capable of performing some tasks without this knowledge. In most cases, the availability of the knowledge is the problem to be solved. Some experts exist that possess the knowledge, but these experts are hardly ever available. In a similar situation the expertise can be distributed among different experts and is therefore not accessible at a central location. The main problem here is not the complexity of the knowledge but merely the fact that some knowledge cannot be accessed in the support of some task. The users in this case are not experts in the task themselves but regularly require support from these experts.

Features looked for in such knowledge systems are availability and reliability. In other situations a knowledge system may be developed because there is the need to collate, archive and inspect the knowledge to improve the quality of the knowledge.

Features looked for in this type of knowledge system is consistency and quality. In either case it is not easy to enumerate the benefits in terms of direct financial benefits or savings.

It is believed that modeling will progressively become one of the most important principles in training [2]. In general terms, a model, a simulation of realty, made from specific elements of the phenomenon that we observe or investigate. It is also an isomorphous image, which we obtain through abstraction, a mental process of making generalizations from concrete examples.

Thus, an established model is an abstract representation of the actions that someone is interested in at a given time. When creating a model, it is important to set a hypothesis for its evaluation and results' analysis.

Developing a model is not a short process. On the contrary, a future model should rely on previous examples while eliminating errors, a process that may require a few years. The more effort and time you contribute to improving the model, the better it will be.

We see that in training program design process, the coach should decide on how achieving the training goal and all alterations that he or she must make to develop an individualized program, regarding different crucial factors. So considering training science as a knowledge base, there is a logical need to represent it in a way that show the way through which the coach makes decision.

Knowledge engineering has some tools which are picked by the experts in different field of men's knowledge to suit mainly the field itself together with the needs of modeling which in turns shows the importance of choosing the best tool to perform the so-called modeling.

Studies show that exercise science which is one of the fundamental areas in sport sciences is highly regarded as a platform to build the championship sports over or achieve a smoothly improving program for the athletes. Focusing on the very basic parameters of exercise science such as Volume and Intensity and other factors affecting them in turn shows the detailed viewpoint of this area over athlete training.

Researches on the two main categories providing the basics of exercise science which are "Reference books" and "experts" show that the experimental nature of these fields made them totally composed of linguistic rules. As it was declared before the nature of knowledge bases force us to pick certain tools from knowledge engineering toolbox to be applied to the under-study area.

One of the most powerful and fully known tools of knowledge engineering is "Fuzzy Inference System". This approach is totally adaptable to areas based on linguistic rules in case that they try to organize the system of rules as endless series of conditional simple rules. These rules are sometimes simply called "if-then" rules while being referred to as a means of organizing a set of linguistic rules.

In the following, we will show how Fuzzy Logic can be utilized to model exercise science parameters, for example Intensity, regarding its related crucial variables and linguistic rules that explain the relationships among them.

2- Method

Fuzzy logic has two different meanings. In a narrow sense, fuzzy logic is a logical system, which is an extension of multivalued logic. But in a wider sense, which is in predominant use today, fuzzy logic (FL) is almost synonymous with the theory of fuzzy sets, a theory which relates to classes of objects with unsharp boundaries in which membership is a matter of degree.

What is important to recognize is that, even in its narrow sense, the agenda of fuzzy logic is very different both in spirit and substance from the agendas of traditional multivalued logical systems.

The basic concept underlying FL is that of a linguistic variable, that is, a variable whose values are words rather than numbers.

In effect, much of FL may be viewed as a methodology for computing with words rather than numbers. Although words are inherently less precise than numbers, their use is closer to human intuition. Furthermore, computing with words exploits the tolerance for imprecision and thereby lowers the cost of solution.

As mentioned above, rules in exercise science are mainly linguistic. As a matter of fact, there is no exact boundary in different zones and phases. There are rules which define the relationships between crucial parameters that lead to a desired factor. In other words, there may be some overlaps that are the nature of so-called linguistic rules.

Intensity, as one the two basic elements in exercise science, is defined as the quality of work (Bompa and Carrera, 2005).

There are three main variables that intensity is related to; Load (%1RM), Speed of movement, and Rest interval. It means that by alternation of these three parameters, the amount intensity will change. Rest interval is also a function of load itself. So we can simply say that intensity is related to load, and speed of movement.

As can be seen in Table 1 (Bompa and Carrera, 2005, Bompa 1999), we can write five rules as follow :

If speed is slow and load is high then intensity is in zone one;

If speed is moderate and load is high then intensity is in zone two;

If speed is moderate and load is medium then intensity is in zone three;

If speed is fast and load medium then intensity is in zone four; and

If speed is moderate and load is low then intensity is in zone five.

Now considering speed and load as input space of fuzzy inference system, we should define membership functions; the curves that define how each point in the space is mapped to a membership value (or degree of membership) between 0 and 1.

Table 1 - Intensity zones and load and speed variation in strength training.

Intensity	1	2	3	4	5
Load (%1RM)	High (100-125)	High (90-100)	Medium (80-90)	Medium (50-80)	Low (30-50)
Speed	Slow	Moderate	Moderate	Fast	moderate

In this process we define a grading range for speed from 0 to 10. If speed is slow, the grade will be 0, and if it is fast it will be 10. It means that any grades between 0 and 10 tell us how fast the movement is done. In a similar way, the range of variation for load is 30 to 125 (%1RM) and that would 1 to 6 for intensity. We use a Gaussian function for speed and load membership functions, and a triangular function for intensity membership function (Figures 1 to 3). These modeling are done in Fuzzy Logic Toolbox environment of MATLAB.

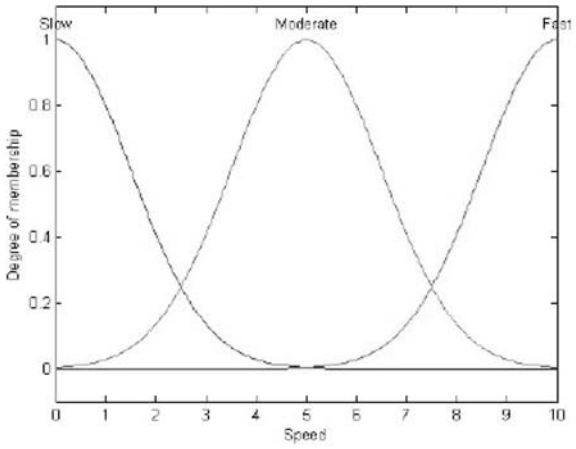

Figure 1 - Membership functions of Speed.

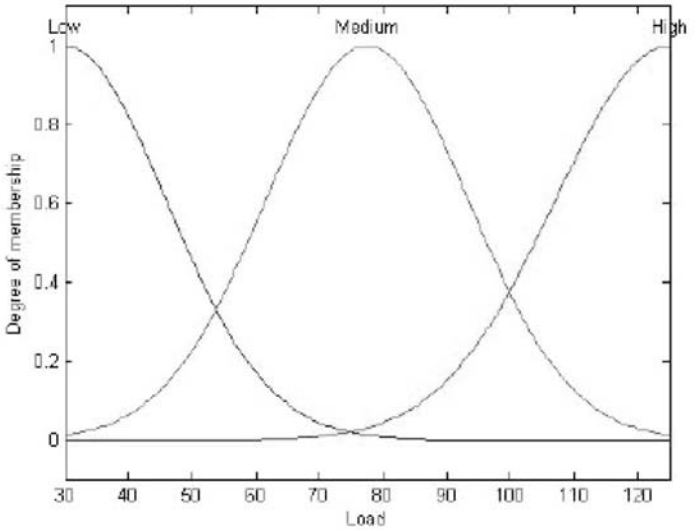

Figure 2 - Membership functions of Load.

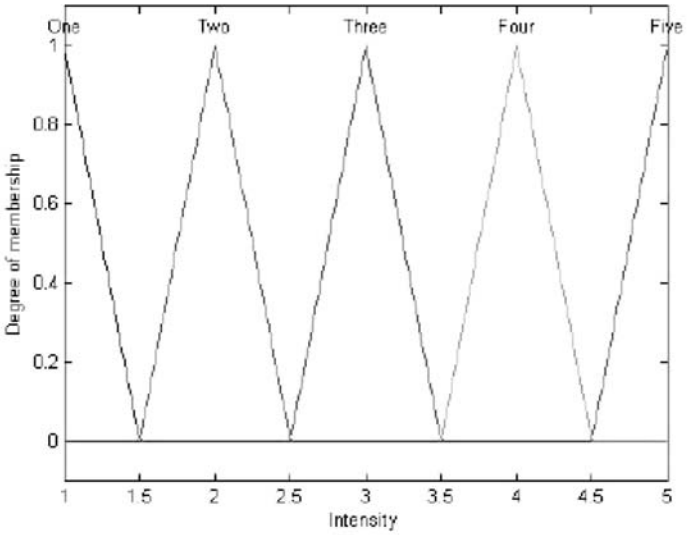

Figure 3 - Membership function of Intensity.

3- Results

With the help of fuzzy logic we mapped the input space (speed and load) to output space (intensity). In other words, all the five rules and the ranges of variable are considered at the same time and the result is a surface that depicts the interesting relationships among intensity, speed, and load (Figures 4). Now it is possible not only for a coach or expert, but also for every one to find out the amount of each of these three elements in respect of the other ones.

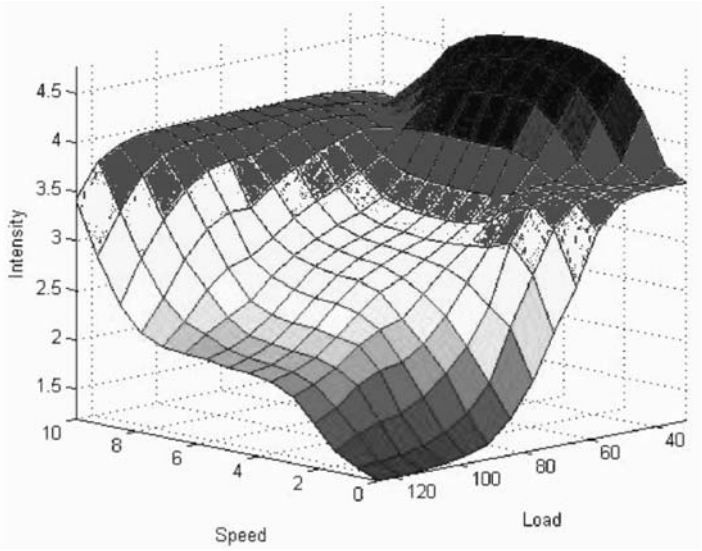

Figure 4 - Surface demonstration of intensity, load, and speed relationships.

5- Conclusions

This work has shown the mechanism of the implementation of Knowledge Engineering fundamentals to sports exercise science about one of the most challenging concepts, i.e. intensity. The approach could be advanced to build up an Expert System capable of making decisions towards organization of an optimized time oriented training program which is supported by both experience and elements of exercise science.

Although the most effective variables are taken into account, we believe that of course there are other variables influencing the model. Regarding these variables of may be lower or even higher importance, we would be able to find out how they affect the output space, such as intensity, and the level of importance for each new parameter could be understood, and this may lead us to crucial facts behind existing exercise science that can revolutionize the championship world.

6- Acknowledgement

We thank Dr. Bahraminejad and Mr. Komasi, the experts of National Olympic Academy of Islamic Republic of Iran, who helped us by their precious knowledge and experience in the field of exercise science.

7- References

[B1] Bompa T. O., Periodization: Theory and Methodology of Training, USA. Human Kinetics, 1999.

[BC1] Bompa T. O., Carrera M. C. Periodization Training for Sports, USA. Human Kinetics. 2005.

[K1] Kasabov N. K. Foundations of Neural Networks, Fuzzy Systems, and Knowledge Engineering, Cambridge, Massachusetts, London, England. The MIT Press, 1996.

Long-term Cushioning Properties of Running Shoes (P152)

Stefan Schwanitz, Stephan Odenwald[1]

Topics: Materials; Shoes; Testing, Benchmarking.
Abstract: In this report a test setup is presented that has been developed to generate a life cycle stress to the heel part of running shoes. The force-time-relationship has been derived from biomechanical investigations on ground reaction forces during running. By having investigated a range of 13 shoes it could be demonstrated that mechanical degradation leads to significant changes in the ability of sole materials to absorb energy. Furthermore an increased stiffness can be shown.
Keywords: Durability; Mechanical Testing; Running shoes.

1- Introduction

Currently running is one of the world's most popular sports. Several scientists have focused their work on the running movement and the resulting stress of the human body. Nigg (2001) claimed that shoe midsole hardness effects impact forces and shock attenuation properties. Impact forces were not directly connected to chronic or acute running injuries but to muscle activity, comfort and fatigue. Midsole material and mechanical properties differs among brand marketing concepts, proposed usage, quality level etc. (Heidenfelder & Odenwald 2006). But also mechanical aging of the shoe during its life cycle because of repeated deformation seems to have an influence on the cushioning behaviour of running footwear (Verdejo & Mills 2004-1). Verdejo & Mills (2004-2) presented a procedure to test midsole material samples of only 20x20x12 mm size. In literature there is no data about long-term behaviour of state of the art running footwear. The aim of this study was to create a machine based test design and to do an independent benchmark test on scientific level to obtain those data.

1. Chemnitz University of Technology, Institute of Mechanical and Polymer Engineering, Sports Equipment and Technology, Reichenhainer Str. 70, 09126 Chemnitz, Germany - E-mail: stefan.schwanitz,stephan.odenwald@mb.tu-chemnitz.de

2- Materials & Methods

2.1 – Test Setup

A hydraulic testing device (Zwick GmbH & Co. KG, Ulm/Germany) described by Heidenfelder & Odenwald (2005) has been used to transfer 240.000 load cycles to the heel part of running shoes. Load was applied perpendicular to a ground plate which the shoe was placed on. A heel-like shaped rigid stamp with a diameter of 50 mm constituted the contact zone between actuator and sole. Data collection regarding force and travel of the stamp was done at a frequency of 1000 Hz. The load-time profile has been derived from biomechanical investigations on ground reaction forces during running on concrete. Under controlled conditions (running velocity 3.4 – 3.6 m/s) it has been found that vertical ground reaction force rises during initial ground contact up to twice the runner's body weight independent of midsole material and design. Peak time was found to be varying according to shoe condition and has been set to 35 ms for the machine test. Stride frequency was approximately 1.4 Hz and total duration of the heel-ground contact phase has been 100 ms. Figure 1 shows the transfer of the biomechanical data into machine nominal value curve. One cycle lasted 700 ms and every sample was tested continuously for approximately 47 hours. This leads to a calculated theoretical running mileage of approximately 600 km. After a recovery period of 48 hours each shoe has been retested for 100 cycles. Results of that test were compared to those of the 100th cycle of the first period. The smaller the difference between new and aged property is the better the long term behaviour is rated.

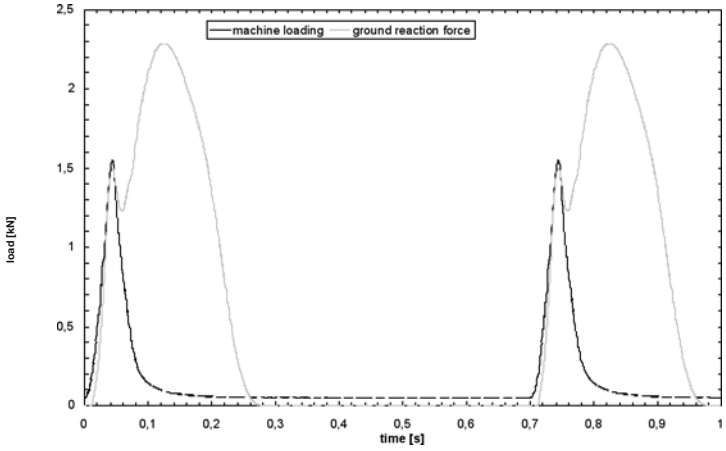

Figure 1 - Vertical GRF vs. load cycle.

2.2 Parameters

The height of the shoes in the tested area has been measured at the beginning of a cycle with a preload of 50 N (1). Furthermore sole height at peak load has been recorded and maximum deformation quantified (2). Calculations were done regarding the energy input (3), return (4) and loss (5) as being the shock attenuating properties. Stiffness of

the sole has been calculated as the increase of the load deformation curve in between 200-400 N (6) and 1000-1500 N (7) of loading.

$$height_{F=50} = def_0 \tag{1}$$

$$def_{\max} = height_{F=50} - height_{F=1550} \tag{2}$$

$$E_{input} = \int_{def_0}^{def_{\max}} F \ \Delta def \tag{3}$$

$$E_{return} = \int_{def_{\max}}^{def_0} F \ \Delta def \tag{4}$$

$$E_{loss} = E_{input} - E_{return} \tag{5}$$

$$stiffness^1 = \frac{400N - 200N}{def_{F=400N} - def_{F=200N}} \tag{6}$$

$$stiffness^2 = \frac{1500N - 1000N}{def_{F=1500N} - def_{F=1000N}} \tag{7}$$

2.3 Samples

This study involved 13 shoes (size UK 9, weight 353±16.8 g) produced by 9 different brands. All of them were mainly made of moulded EVA as midsole material. Eight out of those shoes had additional elements built in the rearfoot area: air chambers (n=2), silicon gel pads (n=3), TPU reinforcements (n=2) or EVA structure elements (n=1).

3- Results and Discussion

Fig. 2 is giving an example of the changed load-deformation behaviour of a new and aged shoe. Unloaded sole height is reduced to about -19.3 % ±3.2 as well as height of the sole under peak load (Fig. 3, -15.9 % ±2.3). The originally highest sample (height = 34.1 mm) showed the lowest loss in height (-13.8 %) and the second best result in maximum deformation (-14.9 %). Otherwise an only 30.4 mm high sample showed the best durability regarding maximum deformation (-14.8 %) while a comparable high shoe (30.3 mm) revealed the worst result in that category (-32.3 %).

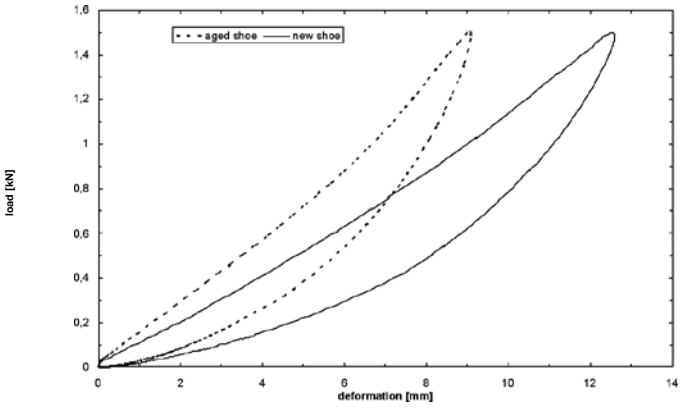

Figure 2 - Hysteresis of new vs. aged material.

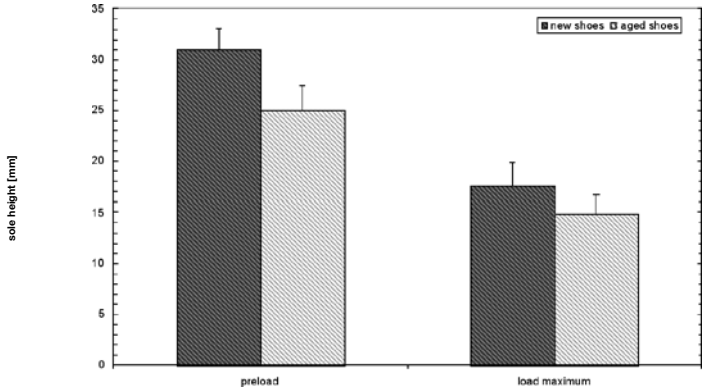

Figure 3 - Sole height (preloaded, load maximum) of new vs. aged material.

With the decreasing material height in the heel zone of the investigated running shoes due to the aging process the shock absorbing ability of the sole material is reduced (Fig. 4). Energy input diminished by -22.5 % ±5.7 and energy loss dropped about -22.3 % ±6.0. The second highest sample (34.0 mm) presented the least changes in these parameters (energy input: -13.8 %; energy loss: -13.7 %).

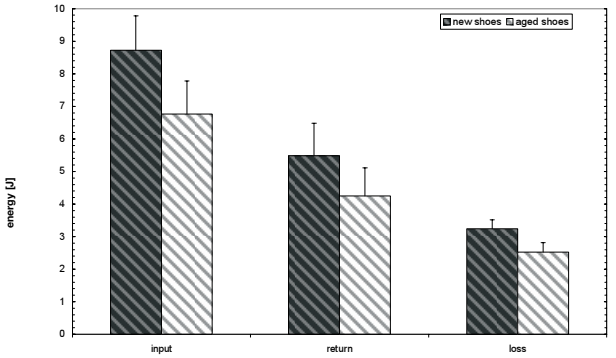

Figure 4 - Energy balance of new vs. aged material.

Fig. 5 shows the increased stiffness (stiffness[1]: 35.2 % ±15.3; stiffness[2]: 38.2 % ±9.6) of all tested samples. Material stiffness magnification in between 200-400 N differed from 9.3 % (highest sample) to 62.5 % (sample height when new 33.1 mm). Dynamic stiffness in the range of 1000-1500 N changed from 23.4 % (sample height 34.0 mm) up to 56.2 % (thinnest sample, height 26.6 mm).

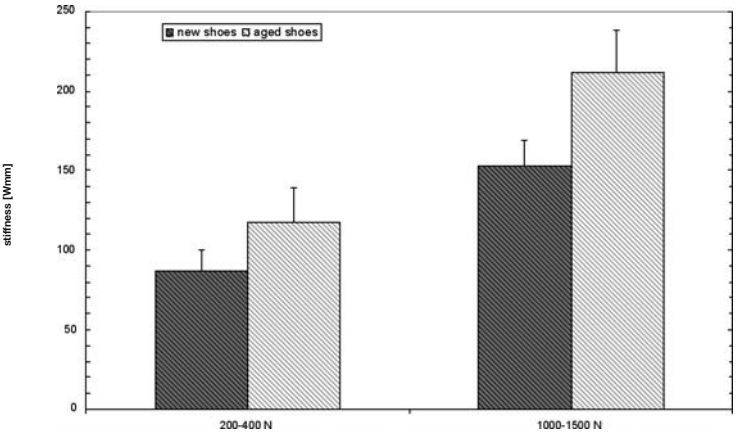

Figure 5 - Stiffness of new vs. aged material.

4- Conclusion

Mechanical degradation leads to significant ($p<0.001$ for all tested parameters) reduction in running shoe midsole materials shock absorbing function. An explanation of this is that due to collapsing air cells as a result of EVA overuse (Even-Tzur *et al.* 2006) material thickness in the loaded area is lowered. One tendency of the presented results is that higher samples were more resistant against aging than the flatter ones. Highly significant correlation ($p<0.001$) towards original sole height can be reported for the alteration of stiffness[2] ($r = .784$) and energy loss ($r = .781$).The much greater influencing factor seems to be the individual midsole material because of the obvious differences in changing of the characteristics of samples with comparatively identical height. There is no evidence for advantages or disadvantages regarding the long term behaviour of additional elements in the rearfoot area of running footwear.

The next step in future of material durability research in running needs to be a comparison of biomechanical aged footwear towards the machine degraded. That will give an evaluation of the test methodology. Furthermore proved biomechanical relevance of the reduced cushioning abilities would strengthen the mechanical aging approach.

5- References

[EW1] Even-Tzur N., Weisz E., Hirsch-Falk Y., Gefen A. Role of EVA viscoelastic properties in the protective performance of a sport shoe: Computational studies. In Bio-Medical Materials and Engineering, 16(5): 289-299, 2006.

[HO1] Heidenfelder J., Odenwald S. Mechanische Prüfung von Laufschuhen: In DIVERS-Vortragsreihe Wechselwirkung zwischen Materialtechnologie & Bewegungs-Analyse im Sport, Wien, 2005.

[HO2] Heidenfelder J.; Odenwald S. Parameter der dynamischen Materialprüfung an Laufschuhen: In: Polymerwerkstoffe 2006– Mikrostruktur, Morphologie und Bauteile, Halle/Saale, 2006.

[N1] Nigg B.M. The role of impact forces and foot pronation: A new paradigm. In Clinical Journal of Sport Medicine, 11(1): 2-9, 2001.

[VM1] Verdejo R., Mills N.J. Heel–shoe interactions and the durability of EVA foam running-shoe midsoles, In Journal of Biomechanics 37(9): 1379-1386, 2004.

[VM2] Verdejo R., Mills N.J. Simulating the effects of long distance running on shoe midsole foam, In Polymer Testing 23(5): 567-574, 2004.

An Analysis of the Interaction Between Slider Physique and Descent Time for the Bob Skeleton (P153)

James Roche[1], Dr. StephenTurnock[1], Dr. Sandy Wright[2]

Topics: Winter Sports; Sliding Sports; Olympic Games; Performance Sports.

Abstract: A single degree of freedom simulator has been developed to analyse the influence of athlete physique on descent time in the bob skeleton. A model of human proportions is used to predict frontal and total surface area of an athlete for a given weight and height. Empirical relationships are then used to estimate the viscous and pressure form components of drag as functions of sled speed. A parametric variation of athlete height and mass is used to evaluate the influence on descent time excluding the influence of the initial sprint time. The actual descent times for the top 15 male competitors at the 2007 St Moritz world championships are compared to the simulated descent time for each athlete based on their mass and height. The results demonstrate gains in aerodynamic performance are made from being taller for a given weight and also for increased overall weight. A final analysis shows the influence of the rule that attempts to equalise overall mass show an advantage for an athlete being lighter for a given height. A normalisation of the world championship race times so that start time is not taken into account shows a correlation between athlete experience and descent time.

Keywords: Wintersports, Bob Skeleton, Performance Analysis.

1- Introduction

The difference between first and second place in high level bob skeleton competition can be as little as 0.01 seconds over the course of two or more usually four, runs down the track with a duration of the order of one minute. With such small margins of victory the importance of equipment and athlete optimisation cannot be ignored. The race consists of an initial sprint phase, 15 metres into the sprint phase a photoelectric cell is triggered to start the timing system. The athlete then dives onto the sled and adopts a head first, prone position. The initial sprint time is recorded after 65 m from the sprint

1. Fluid Structure Interactions Research Group, School of Engineering Sciences, University of Southampton, UK
Email: jr403@soton.ac.uk, srt@soton.ac.uk
2. Wolfson Unit for Marine technology and Industrial Aerodynamics, University of Southampton, U.K.
Email: a.m.wright@soton.ac.uk

start (50 m from start timing gate).Once loaded, the main resistance forces acting on the sled and athlete system are the ice friction which increases during cornering and steering phases and aerodynamic drag which increases with athlete speed. Aerodynamic drag becomes the dominant drag force after the athlete is loaded onto the sled. A number of the nations that compete in the bob skeleton run talent identification programs which aim to find and develop athletes for high level competition. The current practice is to select athletes primarily for their sprint ability under the assumption that the other key elements of the descent can be subsequently taught. This paper attempts to analyze by the use of a one degree of freedom run simulator whether athlete physique significantly influences run time through a trade-off between aerodynamic drag and body mass. It also suggests that there may be an optimum physique for the descent phase that could be used in the future selection of athletes.

2- Methodology

The approach adopted was to concentrate solely on the influence of the likely aerodynamic drag variation due to body shape. To this end a one degree of freedom simulator was created that examines the acceleration in the sled's direction of motion. In this case the axis system is fixed at the combined sled-slider centre of gravity with the x-axis oriented along the longitudinal axis of the sled. The sled is constrained to pass along a predetermined path which may be approximated to a typical descent of an ice track with the local track gradient θ known at any *x*, as are the transverse orientation of the track, β and the local radius of curvature *r* during curved sections. The sprint phase of the descent is not modelled, instead the simulation begins with the athlete lying on the sled leaving the start block with a predetermined speed. The simulator was developed using MATLAB Simulink.

Equation (1) gives the single equation of motion solved based on this information, which assumes added mass effects are negligible in air,

$$\frac{d^2x}{dt^2} = g(\sin\theta - \mu\cos\theta\cos\beta) - \left(\frac{\mu}{r}\sin\beta + \frac{\rho C_D A}{2m}\right)\left(\frac{dx}{dt}\right)^2 \quad (1)$$

where *g* is the acceleration due to gravity, μ is the friction coefficient of ice, ρ is the density of air, *m*, the mass of the slider and sled, *CD* the drag coefficient found using a non-dimensional area *A*. This equation is valid in both straight descent and the banked and curved sections of track. The force components are discussed further by Larman *et al.* (2008). A backwards difference fourth order standard Runge-Kutta scheme is used to solve for the new value of acceleration and hence velocity and descent position x at a time step of *0.01s*.

2.1 The Track

The track geometry used for this simulation is a representation of the Olympia Bobrun in St. Moritz, Switzerland. This track is the only remaining natural bobsled track still in existence. Accurate track geometry is difficult to obtain for many bobsled tracks however it is made more difficult by the ever changing geometry of the Olympia Bobrun year on

year. Track data was obtained via publicly available track plans and satellite imagery. A cubic spline interpolation was used to determine position and local track characteristics such as gradient in between the sampled data points (Huffman 1995). The angle of sled inclination in the corners was calculated using data based on surveys by Bromley (1999) linking velocity and corner radius to sled inclination angle.

2.2 Aerodynamic drag of a sled and athlete combination

The aerodynamic drag (or resistance) of a body moving in a fluid flow can be found from a surface integration of normal surface pressure and tangential shear stress (skin friction). For bluff bodies the pressure component will be a function of the body frontal area whilst the skin friction drag is a function of the total surface area of the body and associated velocity distribution. In this work, as a parametric investigation was to be carried out, the ITTC 1957 skin friction correlation line (International Towing Tank Conference 2002) was used to predict skin friction. This is an appropriate empirical relationship used for scaling of ship models and is developed in Equation (2).

$$C_f = \frac{0.075}{(\log_{10} \mathrm{Re} - 2)^2} \tag{2}$$

Re is the slider height based Reynolds number using sled speed and the kinematic viscosity of air.

The bluff body assumption of completely separated flow for a given cross-sectional flow is moderated by the presence of curvature around the head and shoulders as well as the influence of the lower torso and legs/feet. A suitable value of nondimensional pressure drag coefficient was based on information from Hoerner (1965), Walpert (1989) and Bromley (1999) and was taken to be 0.38.

2.3 The human form

Dempster and Gaughran (1969) provide statistical data for the density and proportion of total body mass (male) contributed by each major body part as well as their size as a proportion of total height. By approximating the body as a series of attached cylinders and half cylinders the exposed surface area of each major body part can be determined. Figure 1 shows a representation of the simplified human form. The frontal area was taken as the sum of the end area of the torso (half cylinder) and the end area of the upper arms (half cylinders). The head was assumed not to protrude outside of the projected torso area. All athletes were assumed to use one sled of identical geometry.

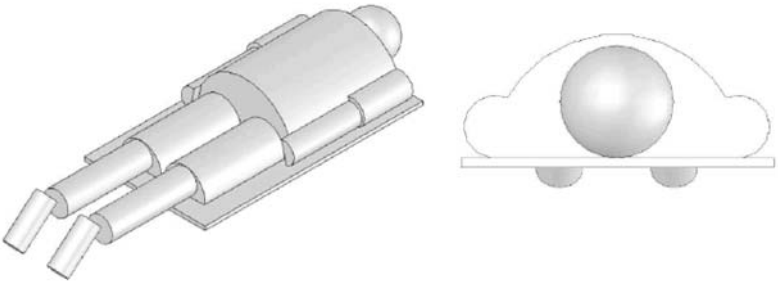

Figure 1 - Representation of the Athlete and Sled Using Simple Geometric Shapes.

3- Simulations

The human form model was used to generate CdA values for a range of speeds for an athlete of a given height and weight. Aerodynamic drag on the system was calculated by interpolating this data in the simulator for any given speed. The combined mass of the athlete and an assumed constant mass sled were used to give the overall mass in the simulator. A sequential variation of seven body masses for six athlete heights in a range from 60-90kg and 1.65-1.9m respectively were run. Each simulation had the same initial start speed of 8m/s and recorded 6 split times and a finish time.Data was also obtained for the top 15 male athletes at the 2007 St. Moritz world championship, based on height and weight data supplied by the FIBT athlete database (Federation Internationale de Bobsleigh et Tobogganning 2007).

3.1 Athlete Physique Variation

The effect of athlete physique on aerodynamic performance is discussed with respect to Figures 2 to 5. Figure 2 shows the effect of athlete height and weight on finish time for a parametric variation of athlete physiques. The results are presented as the difference between the individual descent time and the average for the range of 42 tested physiques. The results show that an optimum race time is achieved by an athlete who is taller and heavier than his competitors. For any given weight the taller athlete is faster and for any given height the heavier athlete is faster.

The improved performance of a heavier athlete suggests that the penalty paid in increased ice friction by this athlete does not outweigh the advantage he has by initially accelerating faster. Velocity plots for the run in Figure 4 show that the heavier athlete has a steadily increasing advantage for the majority of the run, however in the final uphill portion of the race this advantage is quickly eroded by the lighter athlete who does not decelerate as quickly through a combination of lower mass and aerodynamic drag. Figure 4 also shows the effect of the track geometry on the individual athletes with the highest absolute speed obtained in Martineau corner and the rapid acceleration seen before this point due to the track gradient being at its steepest between Bridge and Gunter-Sachs Corner (Larman *et al.* 2008).

The taller athlete being faster can be explained by the breakdown of drag into its component parts. For a typical skeleton athlete the total drag force is made up of approximately 20% viscous component and 80% pressure component. Consequently as athlete height is increased for a given weight the overall surface area increases while the projected frontal area decreases. This reduces the pressure component and increases the viscous drag component. However, as the viscous component makes up a smaller proportion of overall drag the reduction in the pressure component outweighs the increase in viscous drag and as such overall drag is reduced. Figure 3 shows the variation with speed of viscous, pressure and overall drag for a simulated athlete of mass 80kg and height 1.8m.

Figure 5 shows as a form of validation a comparison of the simulator performance with reference to the 2007 World championship winning runs. The simulator was configured with the athlete data (Height 1.8m, Mass 75kg) for the winning athlete and the start speed matched to the average start time for the athlete. The results show good correlation to the final descent times and to a lesser extent the final split time. There is however a fairly large variation in the middle three split times. There may be a number of reasons for this variation and could be due to the influence of accurate track geometry and precise placement of timing gates in the simulation.

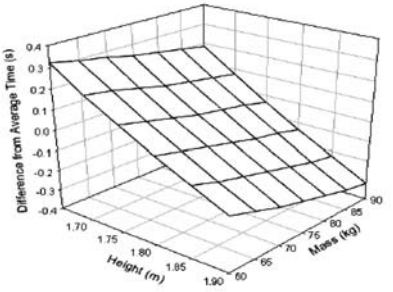

Figure 2 - Variation of Race Time with Athlete Mass and Height.

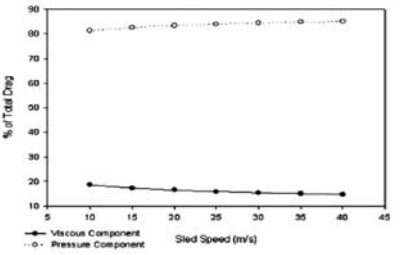

Figure 3 - Variation of Skin Friction Component with Speed: (Athlete: 80kg 1.8m).

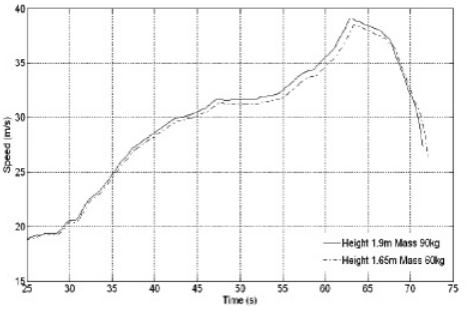

Figure 4 - Variation of Speed with Time for Two Extremes of Athlete Physique.

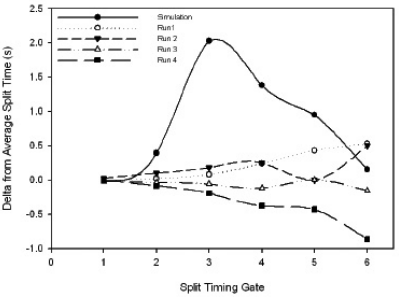

Figure 5 - Comparison of Split Times with 2007 World Championship Winning Runs.

The most likely source of error is considered to be from the method of simulating the start. By beginning the simulation with a velocity faster than a typical sprint the sled will necessarily take more speed into the initial part of the track which could cause the observed error. Another principal source of error is thought to be the approximations used in prediction of aerodynamic data.

Whilst an approximation of skeleton aerodynamics can be obtained by this method the physical flow around a skeleton slider is dominated by large regions of flow separation and re-circulation which cannot be accurately modelled in this manner. It is suggested that the surface area method used here under predicts drag values at lower Reynolds numbers and over predicts the drag for higher Reynolds numbers. Figure 9 shows the variation of Reynolds Number with *CdA* for a typical simulated descent. The model is however sufficiently accurate to model total descent time as the errors appear to average out over the course of the run.

Other factors including the ice friction model and accurate sled weight may also have contributed to overall model error.

3.2 World Championship Competitor Data

Figure 6 shows the simulated descent times for the top fifteen male competitors at the 2007 world championships. There is no obvious pattern to the data other than that most of the competitors fall under the average run time for the range of tested physiques displayed in Figure 2. The finish time data is affected by the individual start times of the athletes (Zanoletti 2006) and so the simulator was used to systematically analyze the effects of start time on finish time for a typical athlete. The results are shown in Figure 7. The difference between an individual athlete's average corrected race time and their simulated time with the influence of the start removed are shown in Figure 8. It is clear that the top four athletes all produce race times faster than their simulated time whilst much of the rest of the field do not. The only athlete outside the top four to go faster than his simulated time was the 12th placed athlete. Analysis of the results sheets show that he has a slower push starter than his competitors but appears to recover during the run through superior driving skills.

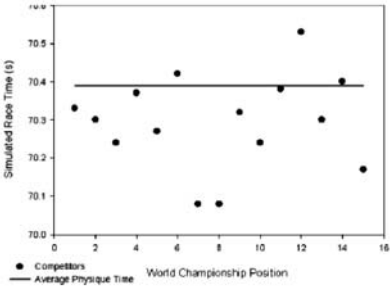

Figure 6 - Simulated Race Time for 2007 World Championship Top 15

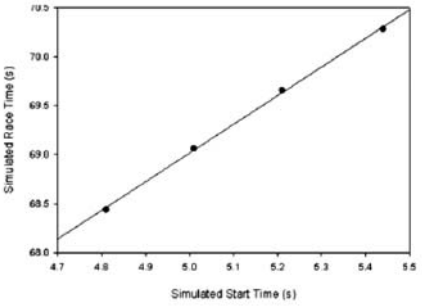

Figure 7 - Effect of Start Time on Simulated Final Descent Time

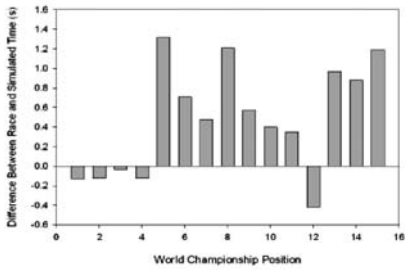

Figure 8 - Difference Between Simulated Time and Average Corrected Race Time for World Championship Top 15

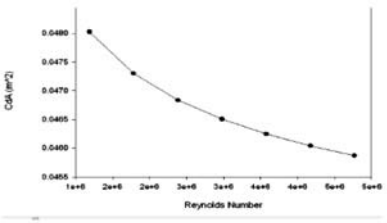

Figure 9 - Variation of CdA with Reynolds Number for a Typical Athlete

It is supposed that the lack of correlation between athlete physique and descent time in competition results is due to the significant variability in the driving skills of individual athletes. Steering errors can lead to time differences measured in seconds rather than tenths or hundredths of seconds. It is also true that the final race victory is often measured in hundredths of seconds and so the results are still significant.

3.3 Effect of Mass Equalisation Rule

The competition rules for Skeleton put in place restrictions on the maximum and minimum mass of the sled. The maximum sled mass is 43kg and the minimum 33kg (Federation Internationale de Bobsleigh et Toboganning 2007-08). This rule is intended to try and equalise the effect of athlete mass on overall descent time. The maximum combined mass for sled and athlete is 115kg. If an athlete is using the lightest sled available and still has a combined mass greater than 115kg he is still allowed to compete. To test the effectiveness of this rule the systematic athlete variation simulations were repeated with each athlete using the heaviest sled available to him. Figure 10 shows the results. A different optimum physique is shown compared to that found in Section 3.1.

The lightest and tallest physique results in the fastest descent time. The effect of weight equalisation is to benefit the lighter athlete who can place more mass in the sled without compromising aerodynamic drag. The smaller variation in overall mass over the range of physiques is now not enough to overcome the effects of aerodynamic gains made by the smaller athlete.

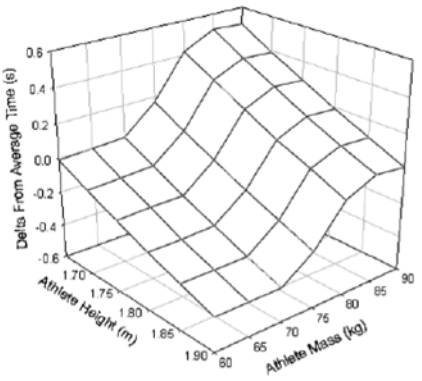

Figure 10 - Effect of Athlete Mass and Height on Descent Time for Mass Equalised Sleds.

A bob skeleton descent is made up of two components, the push start and the descent. Figure 7 shows the importance of a good start on final descent time. It should be noted that the physique required to descend fast may not match the ideal physique required to produce a fast push time (Sands 2005). As an example an athlete 1.90m tall and weighing 60kg is unlikely to possess the necessary sprinting power to produce a fast push start time.

4- Conclusions

A single degree of freedom simulator has been used to analyse the effect of athlete physique on descent time in the bob skeleton.

Data for a systematic variation of athlete physique has been obtained as well as data for the top 15 athletes at the 2007 World championships. The results have provided significant insight into factors affecting descent time in competition.

The principle findings are that for a constant sled weight, optimum descent times are recorded by athletes who are relatively heavy and tall compared to the average. This is due to a combination of faster acceleration provided by increased total mass and reduced frontal area relative to a smaller athlete of similar mass. However, for mass equalised sleds in accordance with F.I.B.T rule 10.10, optimum descent times are recorded by light but tall athletes relative to the average. This is due to weight equalisation negating the advantage of increased body mass. The lighter athlete has a smaller frontal area and lower aerodynamic drag for a similar overall mass. Although no direct correlation was seen between finish time at the 2007 world championships and simulated

finish times due to the simplicity of the model used the run simulator has proved a useful tool for estimating the effect of individual factors on overall descent time in bob skeleton.

This work would suggest that athlete physique for the descent phase should also be considered during talent identification programmes.

5- Acknowledgements

This work was carried out under the auspices of the Engineering Doctorate programme at the University of Southampton, with support from the Engineering and Physical Sciences Research Council (UK) and UK Sport.

6- References

Bromley, K. (1999). Factors Affecting Performance of Skeleton Bobsled. PhD Thesis, Mechanical Engineering, University of Nottingham.

Dempster, W. T., Gaughran, G.R.L (1969). Properties of Body Segments Based on Size and Weight American Journal of Anatomy 120: 33-54

Federation Internationale de Bobsleigh et Toboganning. (2007). Athlete information database from http://www.fibt.com.

Federation Internationale de Bobsleigh et Toboganning (2007-08). F.I.B.T International Skeleton Rules. 10.10: 21. Hoerner, S. F. (1965). Fluid-dynamic drag : practical information on aerodynamic drag and hydrodynamic resistance Brisk Town, N.J.

Huffman, R. K. (1995). Design and Construction of an Interactive Virtual Reality Bobsled Simulator. Mechanical Engineering. Davis, University of California. PhD Thesis.

International Towing Tank Conference (2002). ITTC - Recommended Procedures. ITTC.

Larman, R., Turnock, S. R., Hart, J, (2008). Mechanics of the bob skeleton and analysis of the variation in performance at the St Moritz World Championship of 2007. 7th International Sports Engineering Conference. June 2nd-6th, Biarritz, France

Sands, W. A., Smith, S.L, Kivi, M.R, McNeal, J.R, Doorman, J.C, Stone, M.H, Cormie, P. (2005). Anthropometric and Physical Abilities Profiles: US National Skeleton Team. Sports Biomechanics 4(2): 197-214.

Walpert, R. A., Kyle, Chester R. (1989). Aerodynamics of the Human Body in Sports. Journal of Biomechanics 22(10): 1096.

Zanoletti, C., A. La Torre, G. Merati, E. Rampinini, F.M. Impellizzeri (2006) Relationship Between Push Phase and Final Race Time in Skeleton Performance. The Journal of Strength and Conditioning Research 20(3): 579-583.

Determining Ground Reaction Forces Using a Pressure Distribution Measuring System (P156)

Alexander Kraus[1], Stephan Odenwald[2]

Topics: Measurement Systems, Shoes indicate major topics.

Abstract: In- shoe pressure measurement systems are intended to measure the dispersion of load between the foot and the shoe. This is achieved, for example, by using insoles which contain capacitive sensors dispersed over the sole of the foot. Based on the resulting pressure distribution data there is the option to calculate the interacting forces

In the present study the accuracy of the calculated forces is detected by means of a comparison with real ground reaction forces. For that it is used the Pedar® system by novel GmbH and a Kistler® force plate. Subject- matter is the deviation of the results measured with both systems depending on several factors, i.e. the surface texture, the number of active sensors in the measurement, the kind of load (static or dynamic) and fit of the Pedar® insoles to the shoe. The latter is analyzed in two ways, first by a comparison between barefoot and shoed measurement to reveal the proportion of error caused by the deformation of the Pedar® insoles in the foot rest, and second by comparing several insole geometries and its influence on the accuracy of the results.

Finally, reasons for inexact force measurements are summarized and rated.

Moreover, relevant literature regarding the validity of force values calculated by the Pedar® system is discussed and the corresponding data is critically reviewed and compared to the results of the present study.

As a result there are clear dependences between accuracy of the measurement system and the hardness of surface as well as the number of activated sensors. Dynamic measurements lead to a better congruity of data because the number of active sensors is less than with static loading. Furthermore the deformation of the Pedar® insoles contains a significant potential for failure.

Keywords: force; pressure; pedar; accuracy; jump.

1. Chemnitz University of Technology, Institute of Mechanical and Polymer Engineering, Sports Equipment and Technology, Reichenhainer Str. 70, 09126 Chemnitz, Germany - E-mail: alexander.kraus,stephan.odenwald@mb.tu-chemnitz.de

1- Introduction

In-shoe pressure measurement systems are intended to measure the dispersion of load between the foot and the shoe. This is achieved, for example, by using insoles which contain an array of capacitive sensors dispersed over the sole of the foot.

Based on the resulting pressure distribution data there is the option to calculate the interacting forces. But this is involved with inaccuracies in a considerable quantity.

In a review of relevant literature several authors observed Pedar was generating lower force-values than forces which were measured with a force-plate.

In this study the reasons for inexact measurements are compiled.

2- Materials & Methods

To get an overview of the factors that cause inaccuracies in estimating forces with Pedar the study was separated in three parts: Firstly a literature research to analyse the experiences with this problem up to now, secondly static tests to analyse the influence of surface hardness and of fit of the insoles and thirdly dynamic tests to determine how movement changes the precision of measurement.

2.1 Literature research

Literature, published between 1992 and 2006, was searched for keywords like "Pedar, distribution, force, accuracy, insole, jump" mainly in online search engines, e.g. scirus.com, scopus.com and ubka.uni-karlsruhe.de. The results of 15 studies were collected for which the pressure-distribution-measurement-system Pedar by Novel was used to calculate ground reaction forces (GFK) [BK1, CS1, DK1, HG1, PA1, WC1]. A comparison with force-plates was carried out in eight of these studies, six of which contain percentage information of inaccuracies [KS1, A1, HB1, BB1, FK1, BC1].

2.2 Static measurements

Pedar Insoles were loaded barefoot with the bodyweight of a test person on several surfaces, hard PVC coating and soft carpet. The measured parameter was the weight force of the test person.

In every measurement the test person had to ensure that the COP (centre of pressure) in the horizontal plane was located at the same position below the foot. The control and correction of the COP was possible by a live transmission of data.

The number of active sensors varied with the test person standing on one leg only or on both legs. Five trials where collected for each condition.

2.3 Dynamic measurements

Dynamic measurements were performed as Counter-Movement-Jumps on a Kistler force-plate with Ski-Jumping-Boots equipped with Pedar insoles. The sampling rate of the Kistler platform was 1000 Hz and the Pedar soles measured with 100 Hz which is the maximum sampling rate of the system due to activating the complete sensor matrix of each sole.

Afterwards, a comparison of values of both measurement systems was carried out.

The Pedar soles were calibrated with the original Novel calibration device. It is considered as the best calibration method for that system [HG1].

3- Results and Discussion

3.1 Literature research

Figure 1 shows differences between calculated and real ground-reaction-forces of six studies which contain information of inaccuracies. Brüggemann and Kersting (1997) [BK1] detected that Pedar generally generates lesser forces than the force-platform.

Two factors have been found in literature to be crucial in this regard, i.e. manner of measurement and time factors.

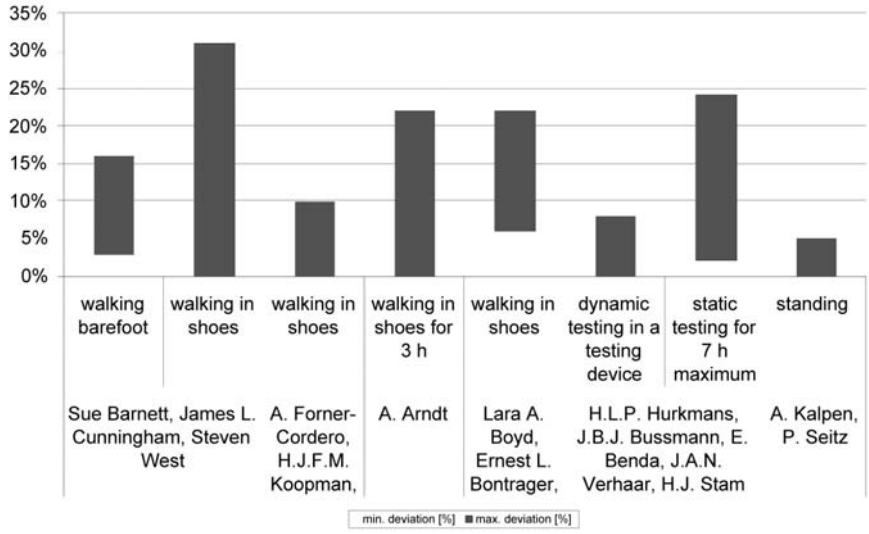

Figure 1 - Deviation of force values in studies.

Firstly, there are different accuracies for measurements in shoes or barefoot as well as differences between static and dynamic loading. The modulus of this deviation reaches up to 30 %. These maximum values mainly refer to measurements of walking in shoes. Studies of measuring of GRF while jumping were not found so far.

Secondly, the precision of measurements depends on the age of the Pedar soles [HG1] and on duration of the measurement [HB1]. According to Arndt *et al.* [A1], a creeping of the sensor material and an offset drift lead to errors of 4 % after the first 10 minutes and up to 26 % after 7 hours of testing.

3.2 Accuracy of static measurements

After calibration, the Pedar soles were put on the floor. The load of the test person's body weight was measured and the accuracy was compared between different surfaces. Afterwards the body weight was measured by putting the Pedar soles into leather shoes.

There is a noticeable difference between the average deviation for barefoot standing (2.6 %) and for standing in shoes (20.3 %). As surface, the hard PVC coating allows for more exact measurements (1 % deviation) than the soft carpet (3 %). It is obvious that the deformation of the insole causes higher deviation from real forces. The direction of measurement is perpendicular to the surface of the sensors. If they are deformed, which is more likely on a soft cushion of a shoe than on a hard floor, the direction differs from direction of the ground reaction force vector and leads to lower values.

Misfits of the insole cause inexact lower force values. If the Pedar soles are too large, compared to the shoe they will be deformed at the periphery. If they are too small, the force will be transmitted to the sensor soles and beyond.

The precision of measurements is higher when the test person stands barefoot only with one foot on a Pedar sole (0.1 % average deviation) than when standing with both feet (3 % average deviation). The same is true for in-shoe measurements: 35% deviation for two feet and 23.5 %. average deviation for one foot.

The sources of error will be analyzed in chapter 3.3.

3.3 Accuracy of dynamic measurements

Figure 2 shows the force over time for a Counter- Movement- Jump recorded with the Pedar insoles and the Kistler force-plate. Within the stance phase (around 5 s) there is a significant difference of approx. 20 % between both force values. Whereas both forces are almost the same in the phase of take off (around 6 s).

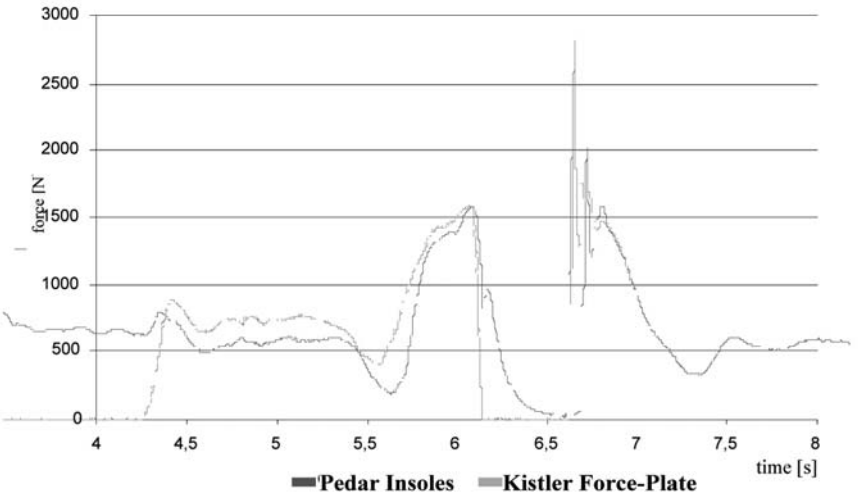

Figure 2 - force-time-diagram of a Counter-Movement-Jump in comparison of Pedar- and Kistler force values.

The difference between the quasi static stance phase and the dynamic take off phase is due to the different number of activated sensors. While the test person is standing, the whole foot presses on the insole and nearly all sensors are activated (see figure 3). However, during take off only the ball and toes set pressure to the insole (see figure 4) and, respectively, to a lower number of sensors.

A detailed look at one activated sensor at the side of the foot may serve as an explanation: Even though the foot covers only a part of this sensor, the whole area of the sensor is used for calculating the force that loads it. This calculation results a lower force. The error is added up with every sensor which is activated but not covered fully by the foot. The more sensors are activated, the more likely the error is higher.

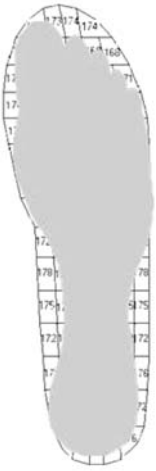

Figure 3 - Higher number of activated sensors in stance phase.

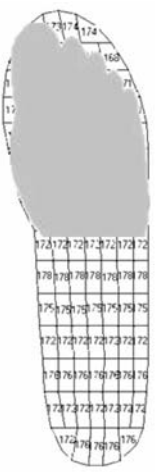

Figure 4 - Lower number of activated sensors in take-off-phase.

The different number of sensors involved in the measurement on one leg respectively two legs also accounts for the different accuracies of measurement as described in chapter 3.2.

The average error of all test jumps is 11 % difference from the values of the forceplate.

4- Summary

As a summary of the mentioned factors which cause differences between calculated forces and GRF, the following recommendations can be given to increase the accuracy:

- To increase precision of mobile force measurements with the pressure distribution measurement system Pedar by Novel it is necessary to be aware of some sources of errors:
- The insole of the shoe should be as flat and as hard as possible.
- It is important to consider the number of activated sensors involved in the measurement and which influence the quantity of errors.

- The insoles should be calibrated more often than the fabricator recommends, before every study, once a day.
- It is necessary to keep the fabricators recommendations for acclimatization after the Pedar soles are inserted into a shoe and the test person has put it on.

5- References

[A1] Arndt A.: Correction for sensor creep in the evaluation of long-term plantar pressure data. In: Journal of Biomechanics 36 (2003), S. 1813–1817.
[BC1] Barnett Sue, Cunningham James L., West Steven: A Comparison of vertical force and temporal parameters produced by an in-shoe pressure measuring system an a force platform. In: Clinical Biomechanics 16 (2001), S. 353-357.
[BB1] Boyd Lara A., Bontrager Ernest L., Mulroy Sara L., Perry Jacquelyn: The Reliability and Validity of the Novel Pedar System of In-Shoe Pressure Measurement During Free Ambulation. In: Gait & Posture (1997), S.165.
[BK1] Brüggemann Gert- Peter, Kersting Uwe: Erfassung der Druckverteilung unter dem Fuß. In: Medizin und Technik 7/8 (1997), S. 40-45.
[CS1] Chesnin Kenneth J, Selby-Silverstein Lisa, Besser Marcus P.: Comparison of an in-shoe pressure measurement device to a force plate: concurrent validity of center of pressure measurements. In: Gait & Posture 12 (2000), S. 128-132.
[DK1] DiLiberto F.E., Baumhauer J.F., Wilding G.E., Nawoczenski D.A: Alterations in plantar pressure with different walking boot designs. In: Foot Ankle Int 28 (2007), S. 55-60.
[FK1] Forner Cordero A., Koopman H.J.F.M., van der Helm F.C.T.: Use of pressure insoles to calculate the complete ground reaction forces. In: Journal of Biomechanics 36 (2004), S. 1427-1432.
[HG1] Hsiao Hongwai, Guan Jinhua, Weatherly Matthew: Accuracy and precision of two in-shoe pressure measurement systems. In: ERGONOMICS 45/8 (2002), S. 537-555.
[HB1] Hurkmans H.L.P., Bussmann J.B.J., Benda E., Verhaar J.A.N., Stam H.J.: Accuracy and repeatability of the Pedar Mobile system in long-term vertical force measurements. In: Gait & Posture 23 (2006), S. 118–125.
[KS1] Kalpen A., Seitz P.: Comparison between the force values measured with the Pedar system and Kistler platform. In: Gait & Posture 2 (1994), S. 238-239.
[PA1] Putti A.B., Arnold G.P., Cochrane L., Abboud R.J.: The Pedar in-shoe system: Repeatability and normal pressure values. In: Gait & Posture (2006).
[WC1] WU Ge, Chiangb Jin-Hsien: The effects of surface compliance on foot pressure in stance. In: Gait & Posture 4 (2006), S. 122-129.

Mechanics of the Bob Skeleton and Analysis of the Variation in Performance at the St Moritz World Championship of 2007 (P160)

Rachel Larman[1], Dr Stephen Turnock[1], Dr John Hart[2]

Topics: Winter Sports; Sliding Sports; Olympic Games; Performance Sports.

Abstract: The skeleton bobsled is a relatively new discipline of winter sports that competes in the winter Olympic Games. It is a sport with high speeds where fearless determination of the individual slider is required to achieve a winning margin which can be a 100th of a second. Skeleton bobsled requires the athlete to sprint, board a sled (weighing upto 43kg) and slide down a bobsleigh track with their chin just millimetres from the ice at speeds up to 130kmph in a head first position. This paper explores the basic physics that underlie the sport comprising the physics of ice friction, the aerodynamics of the slider, the dynamics of the descent of a curved track, control of direction and position on the track. The rules that govern the sport have a significant impact on the methods whereby performance can be improved and in effect determine the upper limits of achievable speeds. The relative differences in performance between the various competitors are analysed with respect to the published data for the male and female sliders who competed in the 2006/2007 World Championship in St Moritz. It is difficult to identify actual optimum body height and weight but interesting to note that the victors in both the men's and women's event were of similar size.

Keywords: Wintersports, Bob Skeleton, Performance Analysis.

1- Introduction

Skeleton bobsled is a sport involving one athlete (slider) and a sled. The sled, a complex construction enclosed in a thin casing atop two runners, is often referred to as the 'tea tray'. The athlete lies on the sled for the majority of the descent in a head first prone position. However the athlete boards the sled from a bent over pushing position, held through an initial sprint initiating the momentum of both sled and athlete, see Fig 1. Races consist of two or four runs down a track depending upon the competition event. The race winner is determined as the athlete with the shortest combined descent times of the track over the runs(FIBT 2007). All the tracks are different in geometry and length

1. Fluid Structure Interactions Research Group, University of Southampton, UK - Email: {r.larman,srt}@soton.ac.uk
2. Sports Engineering Research Group, Sheffield Hallam University, UK - Email: john.hart@shu.ac.uk

taking between fifty to seventy seconds to descend from start to finish. Athletes race one at a time within a set time period in an attempt to ensure that athletes experience comparative weather conditions.

The St Moritz track is built each year from scratch, following a basic plan, Fig 2. Wood and stones are used to give this track its basic form, before the ice is built up on top and shaped with carving to give the final shape. Tracks are kept at particular temperatures though localised refrigeration/freezing. Due to the length of the tracks the temperature can vary, this is can be due to the weather conditions. The sun can be an important factor in changing the surface and structure of the ice. This can significantly change the interaction between the track and sled. In these parts screens are used to prevent melting of the track surface. Track complexity can vary significantly and restrictions are in place to prevent the tracks from being too dangerous for the sliders. For example there is a limit of 5g for 2 seconds imposed on the athletes and the max gradient of 20%.

2- Background

The athlete starts the decent of the track with a sprint from the starting block, pushing and then boarding the sled. A single groove (spur) is cut into the ice for a finite distance, which the sled runner sits in, aiding initial directional stability off the start. The first split time at the start is taken fifteen meters from the starting block. Athletes can load before or after this first time line and this is dependant on numerous variables, the most significant being the geometry of the track governing the number of strides the athlete takes. The sprint by the athlete, wearing spikes, creates the forward motion whilst initiating significant backwards force. This is similar to running on tarmac or grass, and also to the way in which speed skaters initiate the start off the blocks (R W De-Boer, 1988, J M Wakling, 2001). The spikes allow the power to be translated into greater speed of the sled to stop the low frictional force causing the foot to slip and reducing the momentum stored at the end of the sprint (Carr, 1997).

Figure 1 - Two-handed push start, (Photographer J. Hart, Slider A. Schmid).

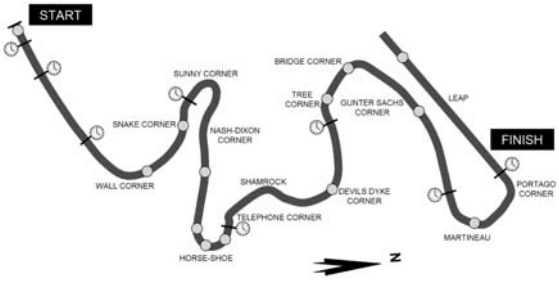

Figure 2 - St Moritz track layout (FIBT, 2007).

As the sled travels down the length of the track it accelerates and decelerates. This is caused not only by the differing gradient along the track, but also by entering and exiting corners which in turn induce different levels of 'g' force. The athlete is only allowed to ride the sled in a prone position during decent. However the athlete may leave the sled to move or push it if required, but must be lying on it at the finish line. Skiers talk of 'weighting' and 'unweighting' their skis; implying a pushing down to increase the friction and in turn increasing control levels or lessening the force between the skis and the snow to reduce the friction. Controlling this process at the correct times helps to perform accurate manoeuvres (Carr, 1997). This approach can be applied to the understanding of the skeleton-runner interaction with the ice. Force only needs to be applied by the athlete when trying to manoeuvre the sled; this assumes a well tuned and balanced sled set-up.

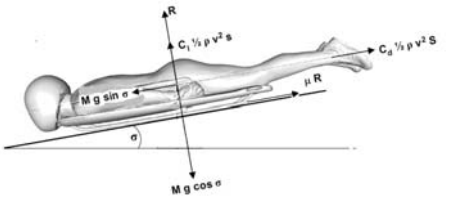

Figure 3 - Basic sled decent – the net reaction force is determined by the difference in aerodynamic lift and the normal gravitational force.

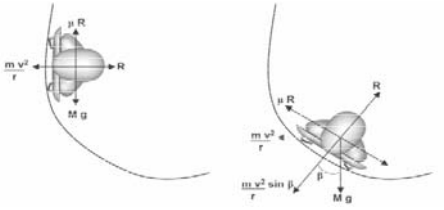

Figure 4 - Cornering sleds.

Figures 3 and 4 show schematically the basic forces that are applied to the sled and slider. in straight and curved track sections.

C_d – Non-dimensional coefficient of drag
C_l – Non-dimensional coefficient of lift
g – Gravitational acceleration, m/s^2
M – Mass, kg
R – Reaction force, N
r – Radius of curvature, m
S – Cross sectional area of slider and sled, m^2
v – Velocity, m/s
β – Angle between vertical and normal to sled, deg
μ – Coefficient of friction, between rail and ice
σ – Angle of track to horizontal, deg – arctan of gradient
ρ – Density, kg/m^3

The component of reaction force R in each situation is relative to the balance of forces shown, (Bromley 1999). In practice the forces are never completely in balance and the sled-slider combination will accelerate/decelerate as turns are entered, straights descended. The application of voluntary control forces by slider (toe-taps, adjusting head/shoulder/lower leg positions) or those imposed by track walls will adjust the orien-

tation of the sled relative to the track. The challenge is to minimise these as each control application will typically lose energy. A combination of good technique and sled design will ensure that the momentum achieved at the end of the start sprint is then added to by the gravitational potential energy released during the descent. Key areas are, therefore the losses due to ice-friction, application of control forces, and aerodynamic resistance, as well as selection of the best line.

Exercise in a cold climate requires the human physiological reactions to adapt to the surroundings. The adaptation to the cold exposure increases the metabolic requirements associated with muscular activity otherwise known as shivering. (Horvath, 1981). The athletes endure approximately sixty seconds of intense anaerobic exercise, a power sport in high pressure scenarios and cold climates. They are exposed to 5-6 g forces for split seconds several times through out the track. This is not the same as experienced in other forms of transport as the body is in a streamlined and rigid position – head on. Inertial forces are exerted on the slider with a change in direction, inertia causes a moving body to try and maintain the same speed and direction of travel, any change to this causes some amount of g-force. The human tolerance to acceleration is dependant on the magnitude, duration, and orientation of the g-force exerted on the body. The human body is flexible yet deformable and even vibrations at low g values can be damaging if they are at the resonant frequency of the organs or connecting tissue. G-tolerance is somewhat trainable and each individual varies. For example a slider and sled taking a corner of 50m radius at a speed of 40m/s would experiencing 3.26 g, Tracks have fifteen to twenty corners and the sled induces vibrations continuously on the athlete along with the varying g-forces. This is a demanding environment for the athletes to perform and make decisions, (Ainsworth 2004; Atkinson 2005).

3- Aim

It is interesting to pose the question whether there is an 'ideal' slider mass and height. An examination of the publicly available data (FIBT, 2007) for athletes shows that they exhibit a mix of shapes and sizes. Initial inspection of previous championship events shows that there is not any significant correlation between result and athlete shape/size characterised by height and mass. However, the sleds can be adjusted, within rule limitations, to suit the athletes. This could act to counteract differences in the size and shape of the athletes. Another influence that may mask the measures of simple body mass and height parameters is the distribution/variation in local shape, for instance whether top or bottom heavy, wide or narrow shoulders, arm to leg length ratios. These are all biomechanical factors that can affect the control, speed and aerodynamic properties of the performance. The aim of this work is consider the detailed information now published after each event, in this case focussing on the 2007 World Championship to see if there is a discernable optimum combination of height and mass.

4- Methodology

In order to investigate whether measures of athlete size and weight indicate the data available from the World Championships in 2007 held on the track in St Moritz were used.

These give detailed start time, split times during a run, the total descent time and overall position. Data was collected for all the male and female competitors at the world championships 2007 held in St Moritz. The data is assumed correct at the time of collection, and were collated from a number of sources, including personal websites, the general winter Olympics website and the International skeleton bobsled website, (FIBT, 2007). The data used include their position at the Championship, the personal best start time of the athletes and their height and weight. This information is used to determine the current performance, trends in size and shape and the importance of the starting time. It should be noted that the world championships held in St Moritz in late January 2007 were in relatively consistent weather conditions of minus 15 degrees Celsius with sporadic light snow.

5- Results

Figure 5 shows the wide range of heights and weights amongst the athletes, with weights from 53-96 kg, therefore, demanding a wide range of sled weights (maximum sled weight in the men's event is 43 kg and for the women the maximum sled weight is 35kg). The lengths of the sled can be varied, this could also be key for many athletes depending on their steering techniques, with their heights ranging from 1.54-1.96 m.

The winning athletes from both the women and men classes were of similar height and weight as shown in Table 1.

This makes the winning female much larger than the average female athlete, whilst the winning male is similar to the average male. Both athletes were sliding on different sleds, winning male on a Davenport and winning female on a Parker. The first three positions taken in the men's class were by athletes within the average height and weight bracket whilst the women's was led by 72.5 kg athlete followed by 54 kg athlete. This is a large range and indicates that particular sleds may suite specific athletes for them to achieve similar descent times. It is important to note the similarities between the winning female and male sliders, with 2cm difference in height and 3.5kgs in weight, making these athletes close in body geometry and the location of their centre of gravity.

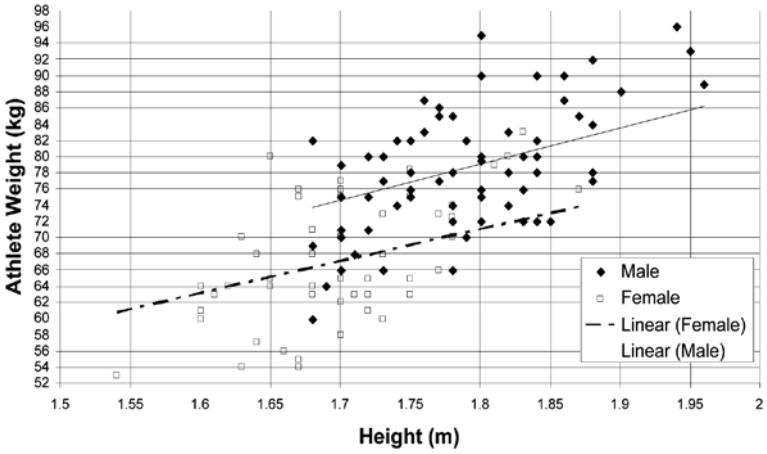

Figure 5 - Height and weight for male and female athletes.

Table 1 - Athlete particulars.

Athlete	Height	Weight	Sled
Winning Female	1.78 m	72.5 kg	Parker
Average – Female	1.67 m	61.7 kg	
Winning Male	1.8 m	76 kg	Davenport
Average – Male	1.8 m	78.7 kg	

5.1 Influence of start time

The push start times of the athletes varies significantly but does not always determine the finishing position (Fig. 6). The men are faster in the push start than the women, with only the slowest men and fastest women achieving similar start times. Those who had the fastest start times did not even come close to winning the event. The fastest female start time was achieved by a slider who finished 15th overall, whilst the winning female sliders' fastest start time was 15th in the rankings. In the men's event a similar pattern with observed with the fastest start time achieved by 5th placed athlete, whilst the winning male was 5th in the rankings for best start time achieved. The heaviest male achieved the 2nd fastest start time and finished 8th overall; this is good indication that there are benefits throughout the run for all shapes and sizes. The influence on weight on the start times had little correlation. One identifiable trend is that the lighter males have a faster start time. Figure 6 shows that the finishing separation time (time difference between fastest and slowest top 20) for the men was half that for the women. .

5.2 Influence of athlete height and weight

The main trend for the athletes separated by gender tends to converge as you go down the final positions ranking list. However as stated before the winners of the men's and women's competitions were similar in size. The weight of the athletes has a consistent trend throughout the results list for both the men and the women. There is currently a wide range of weight for the most successful athletes suggesting no current optimum weight. However, the weight of each competitor's sled is unknown but is presumably is as heavy as allowed by the rukes. Figure 7 shows the Body Mass Index (BMI kg/m^2) of each athlete with regards to position. This supports the existence of an optimum. The further away from a podium position the higher or lower the BMI. Fig. 8 shows no specific effect of height and weight individually with respect to final position.

6- Discussion

In examining the winners from the event there is an indication that an optimum size and shape exists for a given sled for the fastest descent phase. However the runners up and remaining competitors are drawn from a wide variety of heights and weights. This would indicate that it is the skill and consistency of the athlete that dominate performance. The effect of the start time appears to have a limited influence for this specific track. It would be interesting to investigate the trade-off between best physique for the initial sprint and the identified optimum BMI.

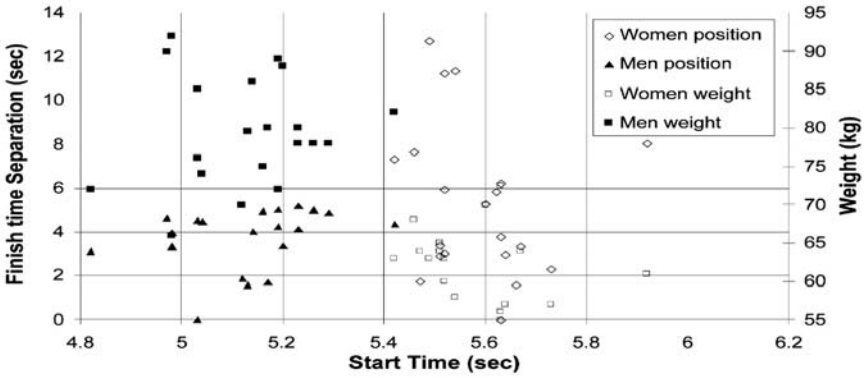

Figure 6 - Start time analysis with respect to finishing separation and athlete weight.

The human body is not a rigid object, so the location of its centre of gravity depends on the position of its limbs. The left and right sides are symmetrical, so the centre of gravity lies within the plane that divides the body into left and right halves. As a rule of thumb the plane passes approximately through your shoulder and hip joints and slightly in front of your ankle joints for a front to back split. The location of the centre of gravity in the vertical dimension is more difficult to estimate. The centre of gravity from top to bottom lies within a plane that passes horizontally through a body 25-50mm below the navel or about 150mm above the crotch. This plane is slightly more than half of standing (about 55-57%) height. For females this value tends to the lower end of the range due to the wider pelvic girdles and narrower shoulders on average with respect to men. A good sprinting technique in the upright plane demands an optimal mix of stride length, power, flexibility and frequency – a predominance of fast-twitch muscle fibres (Carr 1997; McGinnis 1999). Therefore having the supporting muscle group well trained for the sprint could alter the centre of gravity for the skeleton athlete. Other areas of training that could alter the centre of gravity in the vertical direction are the use of muscles in the upper body and this could be dependant on the steering technique and body position during sliding. It is to be expected that with a limited range of sled length and a wide range in heights of the athletes the centre of gravity location of the athletes when on the sled will vary significantly and alter the 'feel' of the sled..

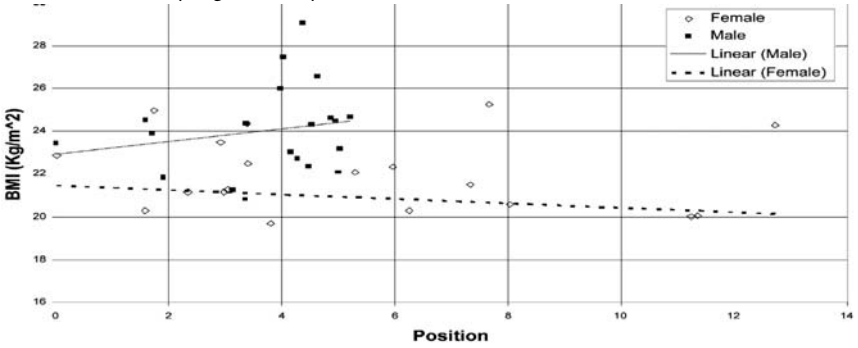

Figure 7 - BMI of athletes with respect to position.

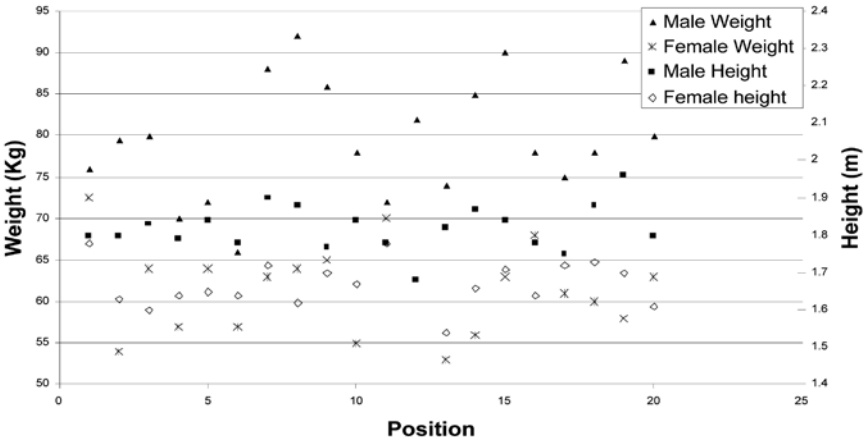

Figure 8 - Weight and height with respect to overall position.

7- Conclusions

At the St Moritz bob skeleton World Championship of 2007 the best combination of height and weight was similar for both the male and female disciplines. These are not only of similar values but also with different sled types. Many questions still remain from this ppreliminary analysis. However, treated in isolation from the skill of the athlete the descent time will be expected to be strongly influenced by the combined mass:of sled and slider and their resultant aerodynamic drag. It is clear for the track analysed that start time only made a small contribution to the overall performance. Tracks that are more dependent on the start time (and resulting momentum) would require an athlete who combines good sprinting ability as well as an optimum body mass index.

8- Acknowledgements

This work was carried out under the auspices of the Engineering Doctorate programme at the University of Southampton, with support from the Engineering and Physical Sciences Research Council (UK) and UK Sport.

9- References

[A1] Ainsworth, C. (2004). Built to Win. New Scientist: 50-53.

[A2] Atkinson, P. G. (2005). Analysis of Skeleton performance times. Research Institute for Sport and Exercise SciencesLiverpool John Moores University, Henry Cotton Campus, Webster Street, Liverpool L3 2ET.

[B1] Bromley, K. (1999). Factors affecting performance of Skeleton bobsled. PhD Thesis, University of Nottingham.

[C1] Carr, G. A. (1997). Mechanics of Sport: a practitioners guide, Human Kinetics.

[F1] FIBT (2007). F.I.B.T International Skeleton Rules, www.bobsleigh.com, accessed 28/2/08.

[F2] FIBT (2007). www.bobsleigh.com, www.bobsleigh.com, accessed 28/2/08.

[H1] Horvath, S. M. (1981) "Exercise in a cold climate." Exercise & Sports Science Reviews, Vol 9: 221-263
[WN1] J M Wakling, V. V. T., B M Nigg, P Stergiou (2001). "Muscle Activity in the leg is tuned in response to ground reaction forces." Journal applied physicol 91: 1307-1317.
[M1] McGinnis, P. M. (1999). Biomechanics of sport and exercise, Human Kinetics.
[BG1] R W de-Boer, G. J. C. E., H van-Gorkum, G De-Groot, G J Van-Ingen-Scheneau (1988). "A geometrical model of speed skating the curves." Journal of Biomechanics 21(6): 445-50.

Subjective Evaluation of Sport Equipment - Deriving Preference Values from Pairwise Comparison Matrices (P162)

Harald Böhm[1], Christian Krämer[1], Veit Senner[1]

Abstract: Design as well as usability of sport equipment is difficult to quantify by objective measurements. Subjective evaluations of different prototypes could be done by ranking the different alternatives in descending order. Discrimination of complex attributes such as design overburdens the testers. Designers routinely rank alternatives in a variety of settings using a staple of comparison, the pairwise comparison test (PCT). The advantage of this method is that it requires only a simple decision between two alternatives. The focus of this study is to use the PCT for the evaluation of sport equipment to establish this method in sports engineering. We also give insight regarding the procedural method, the underlying mathematical formulation as well as the interpretation of the results.
Two applications were performed: first, a ski design test on a total of 103 subjects on six to seven alternatives in different ski categories. Second, four different prototypes of anti-slip pads in snowboarding were evaluated with a total of 40 testers at three different skill levels. The strength of the PCT method in decisional effectiveness was existent; the results provide additional information by the ranking in a metric scale of the tested abilities. Because of these advantages the PCT method provides a useful tool for subjective evaluation of sport equipment.
Keywords: subjective evaluation, pairwise comparison, design, sport equipment, ranking.

1- Introduction

Design as well as usability of sport equipment is difficult to quantify by objective measurements. Subjective evaluations of different prototypes could be done by ranking the different alternatives in descending order. Discrimination of complex attributes such as design or usability overburdens the testers [MD1]. Therefore Designers routinely rank alternatives in a variety of settings using a staple of comparison, the pairwise comparison test (PCT) [D1]. The advantage of this method is that it requires only a simple decision between two alternatives. The focus of this study is to use the PCT method for the evaluation of sport equipment to establish this method in the field of sports engi-

1. Department of Sport Equipment and Materials, University of Technology Munich, Connollystr 32, 80339 Munich, Germany - E-mail: boehm, kraemer, senner@sp.tum.de

neering. We also give insight regarding the procedural method, the underlying mathematical formulation as well as the significance of the results.

Two different applications were presented: first, a ski design test (figure 1) and second, a test of a new safety anti slip pad in snowboarding (figure 2 and 3) which is ought to improve steering abilities when exiting the ski lift on a snowboard. In both examples quantitative measurements would be very challenging because they require sophisticated and expensive methods, e.g. for the steering abilities 3D motion analysis and calculation of mechanical stability with a computer model could be performed to quantify the mechanical stability of the subjects when exiting the ski lift. Further steering ability (usability, stability) as well as design (colors, shape of drawings, shape, haptics) are very complex attributes and the testers might be overburden to define a rank of all abilities so that the PCT method is especially suitable for the applications presented here.

2- Method

2.1 Subjects and material

In the ski design test a total of 103 testers were assigned to test 10 different ski categories from Allmountain, Allround to Multicondition. In each category 5 to 7 skis were tested by about 20 testers. The skis including their biding were aligned in pairs shown in figure 1. The test was performed indoors to simulate a typical showroom. The testers perform a PCT between two types according to the test protocol explained in section 2.2. In the test of the steering ability in snowboarding four different prototypes of anti-slip pads (figure 2 and 3) were tested by 40 snowboarders at different skill levels: beginners (n=15), advanced (n=19) and experts (n=6).

Figure 1- Design test setup for the pairwise comparison of skis.

2.2 Pairwise comparison protocol

The PCT method on n abilities (skis or anti slip pads) requires a number of n(n-1)/2 different combinations which must be tested by each tester. The detailed procedure is explained in the following exemplified on the test of the four different pads. The procedure can easily be transferred to the ski design test on a greater number of attributes.

The snowboarders had to perform a total of six pairwise comparison of four different anti slip pads (figure 3) according to the following procedure: AB; AC; AD; BC; BD; CD, this means that type of the first letter is compared to type of the second letter. Both the sequence of all six pairings and the sequence within every pairing were arranged randomly. Consecutive testing of the same pad (e.g.: BA followed by AC) was excluded. Each subject performed four trials per pairing, two frontside and than two backside turns or vice versa which led to 24 test runs altogether. After each trial the type of pad was changed. Immediately after the second backside or frontside trial of a pairing, subjects had to decide which pad provides better steering abilities.

Figure 2 - Free foot standing on the anti-slip pad with rim next to the binding. The front of the board is on the left side.

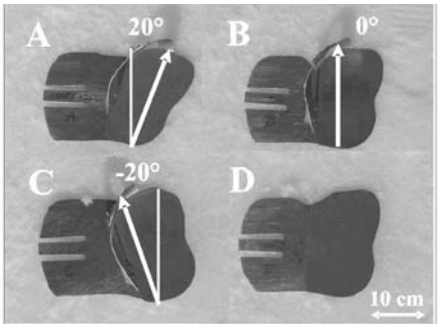

Figure 3 - Different anti-slip pads with varied rotational angle.

2.3 Data processing and statistics

The four competing alternatives A, B, C and D were evaluated by using a 4 × 4 square decision matrix of each tester (table1) , from which a set of preference values for the alternatives were derived [CW1]. The decision matrix of all testers for the backside turn is shown in table 2 and is normalized on the number of subjects in table 3. Transformation of normalized ranked data in table 3 to ratio scaled preferences z-values were calculated according to [H1] in table 4, based on the assumption of a standard normal distribution justified by the law of comparative judgement [T1]. The results, the scaled preference values were calculated as the average over the columns of table 4, and are shown below table 4. With this method any information about the absolute position of the alternatives A, B, C and D on the metric axis can be obtained, it only give information about the relative positions within each other. To compare the results between two different situations e.g. frontside and backside turns or two different groups e.g. beginners and advanced snowboarders or male and females subjects, the zero level was

set to the average value of the last preferred element and the scaled values were thereafter normalized on the most preferred element calculated within the group. The normalized values of the average values below table 4 are shown on the left side in figure 4.

Cochran's Q-test was used to test the inconsistency of the decision matrices (table 1) across the testers. Inconsistency was tested for all testers and for each experienced based sub-group for frontside and backside turns separately. The significance level · was set to 0.05.

Table 1 - PCT matrix of the first tester, "1"indicates in the second row of the first column that pad B is preferred to pad A.

ASR-Pads	A	B	C	D
A	-	0	1	0
B	1	-	1	0
C	0	0	-	0
D	1	1	1	-

Table 2 - Sum of the specific PCT matrices of all 19 testers.

ASR-Pads	A	B	C	D
A	-	7	10	8
B	12	-	10	5
C	9	9	-	8
D	11	14	11	-

Table 3 - Normalized PCT matrix of all testers is obtained by dividing the elements in table 3 by the number of testers (19).

ASR-Pads	A	B	C	D
A	0.5	0.37	0.53	0.42
B	0.63	0.5	0.53	0.26
C	0.47	0.47	0.5	0.42
D	0.58	0.74	0.58	0.5

Table 4 - replacement of the normalized PCT values by the corresponding z-values of the standard normal distribution.

ASR-Pads	A	B	C	D
A	0	-0.34	0.07	-0.20
B	0.34	0	0.07	-0.63
C	-0.07	-0.07	0	-0.20
D	0.20	0.63	0.20	0
average	0.12	0.06	0.08	-0.26

3- Results

3.1 Snowboard anti slip pad test

The test of inconsistency of the decision matrices of all 40 testers was significant for the backside (p=0.051) as well as for the frontside turn (p=0.008). This means that significantly different opinions exist among the testers in these situations. Testing of the inconsistency of the decision matrices of testers of different skill levels for the backside turns reveals that beginners and advanced were not significantly inconsistent (p=0.192) and (p=0.359) respectively. For the frontside turn the beginners and advanced were also not inconsistent (p=0.478) and (p=0.326) respectively. Whereas the six experts showed inconsistent results for backside (p=0.008) as well as for frontside turns (p=0.001). Since the preferences of all testers grouped together showed significant inconsistent opinions, so that the results of all testers were not convincing. Consistent preferences were for the most parts observed when different groups of skill levels were evaluated separately. The beginners and advanced snowboarders groups revealed consistent preferences for the backside as well as for the frontside turns. Whereas the group of six experts showed significantly inconsistent results for both, frontside and backside turns. Due to limited space only the results for the group of advanced snowboarders are shown in Fig. 4. During the backside turn A, C and B were close together on the first three places, and pad D without rim was the least preferred pad with a large difference of 85 % to the third preferred pad.

During the frontside turns pad B with a neutral 0° alignment was the most preferred, followed by pad C preferred 50% less than B. The least preferred pad was D.

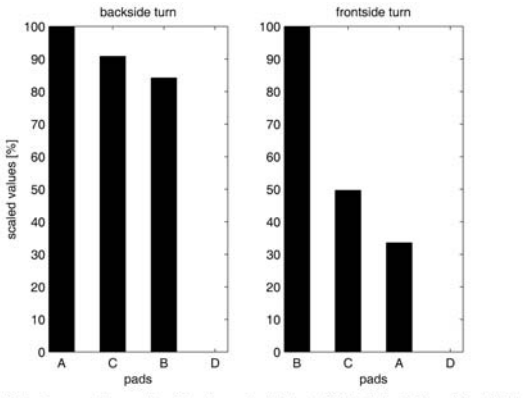

Figure 4 - Pairwise comparison results of the advanced subjects (n=19) for the backside and frontside turn.

3.2 Ski design test

From the large number of ski categories the results of two categories the Allmountain skis (n=5) and of the Multicondition skis (n=6) were shown in figure 5 to exemplify the typical outcome of the PCT method in the design test. The test of inconsistency of the decision matrices was not significant for the Allmountain (p=0.61) but for the Multicondition ski category (p=0.002). In the Allmountain ski category the design of the skis El and Ro were close together on the first place, the others were considerably less preferred. The testers of the Multicondition skis gave inconsistent preferences so that the results are not significant but ski type St was clearly the first followed by the others with more then 80% less preferences.

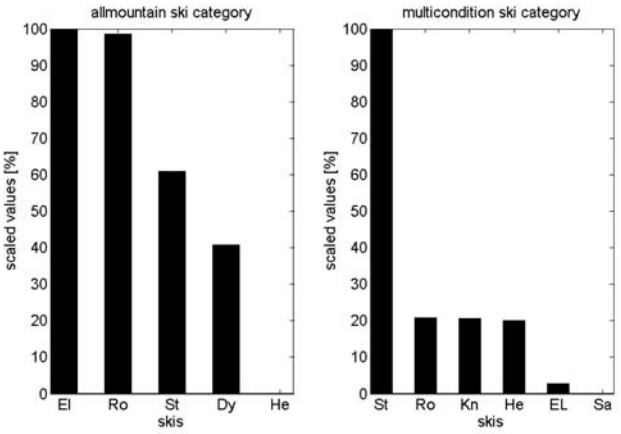

Figure 5 - Pairwise comparison results of two ski categories on 5 and 6 skies and 19 and 20 testers per category.

4- Discussion

4.1 Inconsistency test of decision matrices

In the discussion of the results the inconsistency test of the decision matrices among testers (Cochran's Q-test) helps in a first place to find reliable information about the tester group. In case of the snowboard the preferences of all testers grouped together showed significant inconsistent opinions, so that the results of all testers were not convincing. Consistent preferences were for the most parts observed when different groups of skill levels were evaluated separately. The inconsistent results among experts might be, besides different opinions, also intensified by the small number of experts participating in the study. The consistency among the beginners and advanced riders demonstrated that it makes sense to evaluate and discuss the snowboarders with different skill levels separately. Because of their consistency the preferences of the beginners and advanced groups were most relevant. A similar consideration might be applied to the design test. The testers of the Allmountain category showed consistent results whereas the testers of the Multicondition skis were inconsistent and therefore not that meaningful.

4.2 Scaled preference values

For the design test of the Allmontain ski category the ski types El and Ro are very close together on the first and second place in the preferences of the testers. In a simple order of a ranking scale (1...5), EL would be the winner of the test. However the additional information of the distance to the second ski Ro would lead to another conclusion that both skis were equal in design. This additional information besides the ranking is one advantage of the PCT method presented here. Applied to the test of the anti slip pads, the pad without rim was preferred last in the advanced group for the backside as well as for the frontside turn. The distance to the anti slip pads with rim was 80% in the backside turn so that the rim was extremely useful for enhancing the steering abilities during the backside turn.

4.3 Summary

The mathematical calculation of the PCT matrices was presented and demonstrated in detail so that it can be replicated and applied to another similar problem. The strength of the PCT method in decisional effectiveness was existent which was shown in the consistent results of the testers. Especially the additional information of tester consistency as well as the distance between different abilities is another advantage of this method compared to simple ranking procedures. Since the data are based on standard normal distribution different test can also be compared with each other. The drawback of this method is that with a high number of abilities (n) the number of tests (n*(n-1)/2) increases and it required high effort to evaluate all possible combinations. Further the dichotomic source data does not allow for inferential statistics testing.

5- References

[CW1] Choo E.U., Wedley W.C. A common framework for deriving preference values from pairwise comparison matrices, Computers & Operations Research 31 893–908, 2004

[D1] Dym C. Rank Ordering Engineering Designs: Pairwise Comparison Charts and Borda Counts Research in Engineering Design, 13, 236–242, 2002.

[H1] Hull, C. L., "The Computation of Pearson's r from Ranked Data," Journal of Applied Psychology, 1922, Vol. 6 (4), pp. 385-390.

[MD1] Martin D, Dodd S. Techniques for Obtaining Rank Orderings, Sociological Methods & Research, Vol. 1, No. 3, 317-327 (1973)

[S1] Sheskin D.J. Handbook of Parametric and Nonparametric Statistical Procedures, CRC Press, February 2007, pp 867

[T1] Thurstone, L.L. A law of comparative judgement. Psychological Review, 34, 273-286, 1927

Hot Glide Wax Treatment and the Hardness of the Ski Running Surface (P163)

Leonid Kuzmin[1], Mats Tinnsten

Topics: Ski & other Winter Sports; Materials; Performance Sports.

Abstract: In the cross country skiing community, hot wax treatment of the ski running surface (SRS) is used in order to influence the surface hardness of the skis in relation to the hardness of the snow crystals. This is discussed in a number of scientific papers and recommended in almost every ski waxing manual. The general idea is to decrease (soften) the surface hardness by the use of a soft glide wax treatment for wet snow conditions and to increase (harden) the hardness of the surface by a hard (synthetic) glide wax treatment for cold, dry snow conditions. The question is; does the hot glide wax treatment of the ski running surface influence the surface hardness? And if so, in what way?

In our experiment, ski base specimens of UHMWPE (transparent and "graphite") were treated with ski glide wax. Half of the specimens were treated with soft yellow glide wax, and half with hard green glide wax. After the wax treatment, the surface hardness (Shore D) was measured with a durometer. The study revealed that: both soft glide wax and hard glide wax treatment make the SRS softer; after a long immersion (12 hours) in the bath of melted glide wax, both the hardness of the specimens treated with soft glide wax and of those treated with hard glide wax decreased significant. Conclusion: The hot wax treatment of the SRS with available glide waxes cannot make the SRS harder than it was initially (unwaxed).

Keywords: ski base, glide wax, hardness.

1- Introduction

The application of glide wax is still an art. Skiers and technicians have enormous collections of glide waxes. Through years of experience, skiers and technicians have tried to learn which products work best for specific snow conditions. However, very often (too often) there is only a weak correlation between the effort expended and the result.

In our opinion, the huge number of unproved theories regarding ski glide preparation is a primary obstacle to achieving the optimum ski glide. In (Karlöf *et al.*, 2005) we can read that: "The purpose of ski wax is to reduce adhesion forces, to reduce surface

1. Dept. of Engineering, Physics and Mathematics, Mid Sweden University, Teknikhuset (Q), Plan 3, SE-831 25 Östersund - E-mail : leonid.kuzmin@miun.se

tension, and to prevent ploughing by adjusting the slider base hardness to the hardness of the snow. For example, by applying harder waxes the slider surface hardness is increased…", but this paper does not include any comparative data regarding the hardness of the ski base and the glide waxes. Another work that examines the effects of the hardness of glide wax is (Rogowski *et al.*, 2005). However, this paper does not either present the comparative hardness of waxed and unwaxed ski bases.

The general opinion, which we agree with, is that the hardness of the ski running surface (SRS) appreciably influences the ski glide properties on the snow surface. However, our literature review discovered no studies that had investigated the effects of hot wax treatment on SRS hardness. Moreover, in our literature review of another winter sport event, speed skating, we did not find similar arguments regarding "various running surface hardnesses for various ice hardnesses". The development of skate blade material consists in achieving a steady increase in hardness, regardless of the hardness of the ice, see for instance (Yang, 1988) and (Kuehmann *et al.*, 2002).

2- Methods

2.1 General approach

The choice of tools, wax, ski base material and the procedure for SRS preparation was based on direct application to cross-country (XC) skiing. Our primary aim with the study was to monitor the changes in the hardness of the SRS in relation to different periods of test specimens treating (dipping) in molten glide wax.

2.2 Materials

The ski base material we used is made by Gurit (Ittigen) AG (former IMS Kunststoff AG). For our samples we used both transparent base (TB) and "graphite base" (GB). The transparent base samples were made from P-Tex® 2000; a pure ultra-high molecular weight polyethylene (UHMWPE). The "graphite base" samples were made from P-Tex® 2000 Electra®. The "graphite base" is a mixture of UHMWPE and amorphous graphite (black). The specimens were machined as shown in Figure 1.

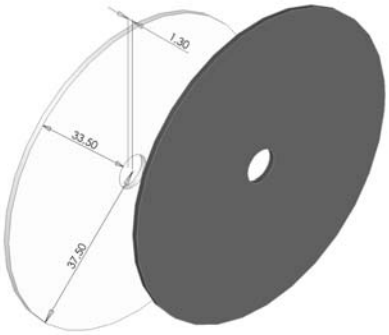

Figure 1 - ski base specimens.

The glide waxes used in our experiment were made by STAR SKI WAX (Italy). We employed only two waxes: NA2 (0°/-4°C), which is the softest, and NA8 (-8°/-20°C), which is the hardest in the NA range.

2.3 Apparatus

To melt the glide waxes and to keep them at a temperature of 119° ± 2°C during the treatment we used a Serenit® Electric burner. To control and record the temperature we employed a CENTER 306 Data Logger Thermometer, which has 0,1°C resolution ± 0,3% accuracy. To measure the hardness we employed a Shore® S1 Portable Digital Durometer (Instron) with 0,1 resolution.

2.4 Experimental setup and carrying out

1) The initial hardness of the transparent base and the "graphite base" were measured; 2) We melted two glide waxes (NA2 and NA8) in two separate stainless steel vessels on two electric burners. Both burners were adjusted to sustain a temperature of 119°C; 3) The specimens were immersed (soaked) in the molten glide waxes for the p_n period [min], where $p_n = 3^n$, n ε[1, 6] except for $p_0 = 0$ which is a starting point; 4) Directly, after the molten glide wax bath, the specimens were placed between two PTFE plates under a 40 kg weight to press out the excess wax and flatten the specimens; 5) After the specimens had cooled, we scraped away any remaining excess wax with a plastic scraper; 4) We waited for five days before measuring the hardness, to allow time for the wax to solidify. We consider this ample time for solidification, as nobody would normally wax their skis five days before a race; 5) Hardness measurements were performed, recorded and treated statistically.

3- Results

3.1 Visual observations

Even with the naked eye, it was possible to see how the specimens changed after treatment (dipping) in the molten glide wax baths. Figure 2 shows the specimens after three minutes (p_1) of treatment, and Figure 3 after four hours and three minutes (p_6) of hot wax treatment. The difference between these two pictures can be clearly observed.

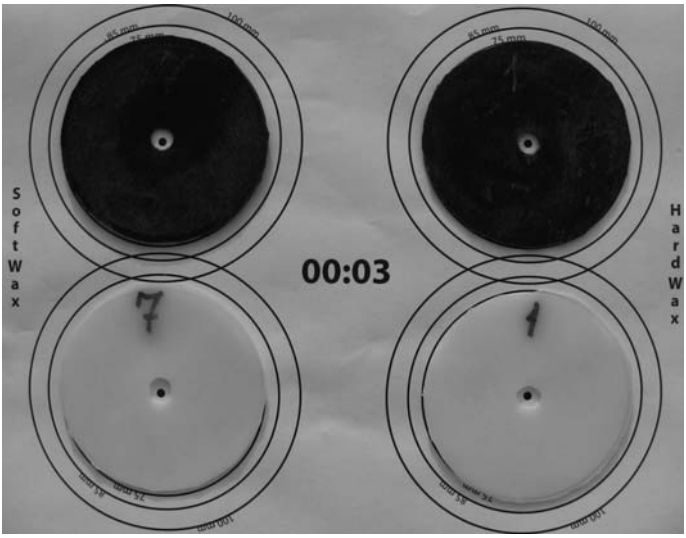

Figure 2 - specimens after three minutes in the molten glide wax bath.

The specimens in Figure 3 are significantly swollen in comparison with the specimens in Figure 2.

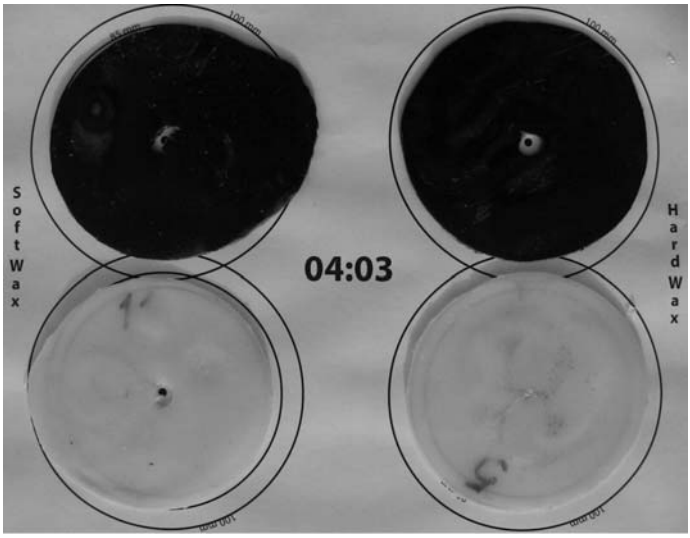

Figure 3 - specimens after four hours and three minutes in the molten glide wax bath.

3.2 Hardness measurements

Five hardness tests (Shore D) was performed on each specimen. In Figure 4 the results of the measurements are presented as an arithmetical mean of the five hardness tests. The sample standard deviation $s = \sqrt{\frac{1}{4}\sum_{i=1}^{5}(H_i - \overline{H})^2}$ is presented as error bars on the chart in Figure 4.

From the chart in Figure 4 it is clear that all the specimens, regardless of the ski base material and glide wax, become softer and softer after treatment. It is especially interesting that even the specimens treated with hard glide wax (NA8) also become softer. This observation is in strong contrast to the universally recognised purpose of hard glide wax application. Table 1, which shows our measurements, confirms this observation:

Table 1 - hardness of utilised materials.

Material	Hardness (Shore D)
P-Tex® 2000 Electra®	65,7 ± 0,7
P-Tex® 2000	64,8 ± 0,6
Glide wax NA2 (0°/-4°C)	12,9 ± 0,8
Glide wax NA8 (-8°/-20°C)	50,4 ± 3,3

To avoid speculation that our result validation only applies to STAR glide waxes, we made hardness tests using a number of other major glide wax brands. The measurement values of tests with similar glide waxes were comparable, which agrees very well with conclusions from (Rogowski *et al.*, 2005).

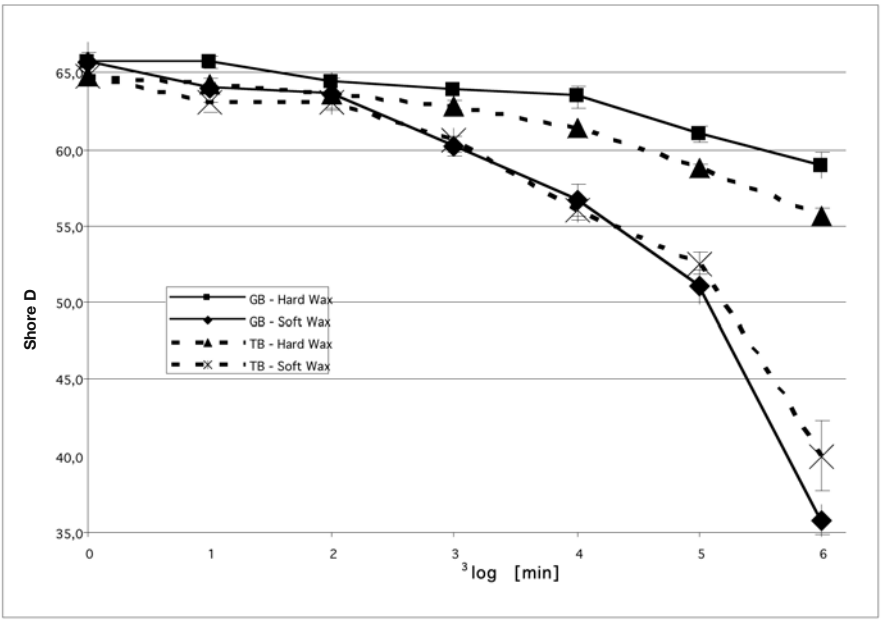

Figure 4 - SRS hardness in relation to period of dipping in the molten glide wax bath.

4- Discussion

Obviously hot wax treatment influences the SRS hardness and the observed results are due to a dilution process. We would not describe this process as "impregnation", "penetration", "absorption" or "saturation". All such terms imply some kind of ski base poro-

sity, in which we don't believe. To quote from e-mail correspondence with Urs Geissbühler (Research & Development Manager, Gurit (Ittigen) AG): "There are no "pores" in press sintered UHMWPE as some wax manufacturers have been telling people over the last 40 years."

In ours believe, it is a pure dilution process, as we observed in this experiment, as in the old alchemist maxim: "similia similibus solvuntur". The behaviour of this process could be described in (Oral *et al.*, 2007) by Fick's second law of diffusion, where the concentration of the solute as a function of depth and time is

$$C(x,t) = C_0 \operatorname{erfc}\left(\frac{x}{2\sqrt{Dt}}\right) \quad (1)$$

where C_0 is the saturation concentration of the material, x is the depth, D is the diffusion coefficient, and t is the time. The complementary error function, erfc(z), is simply [1-erf(z)]. The variables D and C_0 are very dependent on the melting temperature. Since the diffusion of molten glide wax is believed to be limited to the amorphous regions of the polymer, soaking with molten glide wax should have no effect on the crystallinity of the UHMWPE (ski base) below the melting point (Oral *et al.*, 2007). On this assumption, it is easy to understand why the softer material (hard glide wax NA8, see Table 1) is not able to make the harder material (ski base, see Table 1) even harder.

From our results we can draw the conclusion that the hot wax treatment of the SRS with available glide waxes cannot make the SRS harder than it was initially (unwaxed). Our results and conclusion are in agreement with the summary regarding microcrystalline wax from (Mathia *et al.*, 1989).

In the light of our results, it seems to be more effective to use a completely unwaxed ski base for cold dry snow conditions (aggressive snow). At the same time, in practice it will be necessary to treat the ski base with hard glide wax if the ski base has previously been treated with a soft glide wax. In this case treatment with a hard ski wax will succeed in making the SRS harder than before.

5- Acknowledgements

The authors are grateful to Urs Geissbühler from Gurit (Ittigen) AG for the ski base material and for the fruitful discussions regarding optimal SRS treatment

6- References

KARLÖF, L., TORGERSEN, L. & SLOTFELDT-ELLINGSEN, D. (2005) Why is ice and snow slippery? The Tribo physics of skiing. Oslo, Swix Sport AS.

KUEHMANN, C. J., BERNIKOWICZ, P. A., OLSON, G. B., WISE, J. P. & CAMPBELL, C. E. (2002) Case hardened steel blades for sports equipment and method of manufacture. Northwestern University.

MATHIA, T., MIDOL, A., LANTÉRI, P. & LONGERAY, R. (1989) Topography physicochemistry and wear in sliding of ski soles in regard to rheology of snow. 5th International Congress on Tribology, EUROTRIB 89. Helsinki, Finland, Elsevier.

ORAL, E., WANNOMAE, K. K., ROWELL, S. L. & MURATOGLU, O. K. (2007) Diffusion of vitamin E in ultra-high molecular weight polyethylene. Biomaterials, 28, 5225-5237.
ROGOWSKI, I., GAUVRIT, J.-Y., LEONARD, D. & LANTERI, P. (2005) Typology of the gliding waxes in cross-country skiing: Comparison between classifications based on the chemical composition and those based on the physical and physicochemical properties. Cold Regions Science and Technology, 43, 140-149.
YANG, J. (1988) Heat-Treatment of 65 Mn Steel Racing Skates. Heat Treatment of Metals (China), 54-59.

Creating 3D muscle lengths and moment arms from the Visible Human Dataset (P166)

Krämer C., Böhm H., Senner V.[1]

Topics: Biomechanics, Modelling.

Abstract: In musculoskeletal models knowledge of changing muscle lengths and moment arms during motion is crucial to calculate accurately joint load, muscle's force and muscle's energy consumption. Especially in complex 3D joint motions, moment arms are not available in the literature. In this study a framework is presented for calculating the athlete's individual muscle lengths during sports by means of motion analysis. Bones were simulated by use of anatomical data and presented as triangulated surface meshes. Muscle length was calculated as the shortest path from origin to insertion by means of the dijkstra algorithm. The validity of the calculated muscle lengths was tested for a simple elbow flexion motion on existing data in the literature. Therefore this approach might be confident to calculate valid individual muscle length in complex joint positions. The algorithm worked well for muscles running directly beyond the bones, but no underlying muscles or tissues can be considered. Therefore in the next step, muscles should be modelled as volumetric tetrahedral meshes to simulate muscles' deformations during motion.

Keywords: muscle length, simulation, dijkstra algorithm.

1- Introduction

Simulation of the musculoskeletal system has important applications in sport equipment research and development. The accuracy of the muscle, bone and tendon geometry is of paramount importance in all simulation models. Knowledge of changing muscle lengths and moment arms during motion is requried to calculate joint load, muscle's force and muscle's energy consumption [BC1, BK1]. Especially in complex 3D joint motions, moment arms are not available in the literature. Moment arms can be described by functions of joint angles, derived from fitting polynomials to anatomical data [PY1]. In general, moment arms and muscle lengths are calculated based on muscle paths running beyond complex geometries, such as cylinders and hyperboloids [CJ1, GP1]. The reliability of this approach is limited, because as joints move, the muscle

1. Technische Universität München, Department Sport Equipment and Materials - E-mail: kraemer,boehm,senner@sp.tum.de

changes shape and interacts with underlying muscles, bones and other tissues. A recent trend is to use anatomically based approaches to simulate muscle data by use of the Visible Human Dataset (VHD) to model realistic, for example to create virtual characters [DC1, FM1, TS1].

The aim of this study is to present a framework for simulating high resolution musculoskeletal geometry from the VHD to calculate the athlete's individual muscle lengths during sports by means of motion analysis, exemplified for the elbow joint.

2- Method

The VHD consists of high-resolution images of millimetre-spaced cross sections of an adult male and female [US1] (Figure 1).

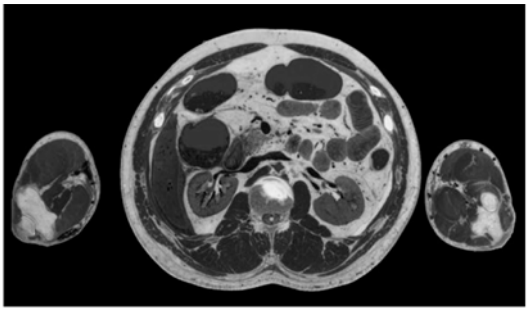

Figure 1 - Anatomical slice through the torso and the upper limb from VHD.

The bones of the upper limb of one male human arm were segmented from the VHD and presented as triangulated surface meshes (Figure 2). The number and size of the triangulated faces define the resolution of the bone's representation: the higher the number of faces, the more accurate but the more time consuming is the calculation of muscle's length.

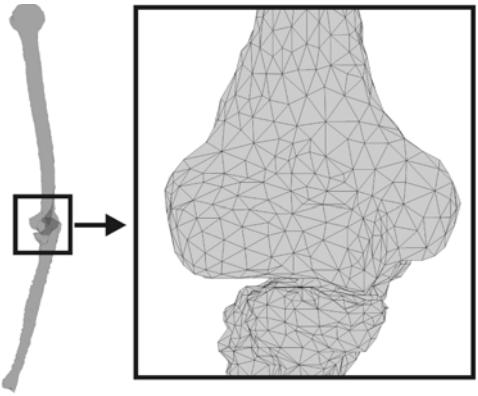

Figure 2 - Segmented ulna and humerus from VHD data, presented as triangulated surface meshes.

Muscle lengths of one flexor (m. brachialis) and extensor (m. triceps brachii caput laterale) during elbow flexion were determined by calculating the shortest path, from origin to insertion, over the bone surface along the edges of triangulated faces by means of the dijkstra algorithm (Figure 3) [D1]. Calculations and graphic presentation were performed with MatLab (Matworks, USA).

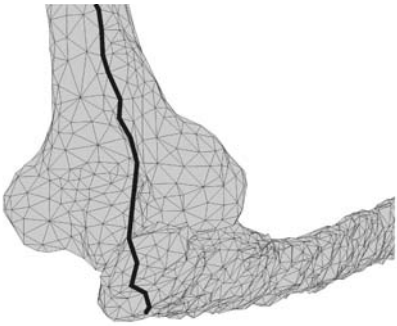

Figure 3 - Calculation of muscle length (black line) by means of dijkstra algorithm.

Markerbased motion analysis (Vicon MX-460, Oxford Metrics, Oxford, England) of the elbow flexion was executed. Markers were placed on well defined anatomical landmarks according to recommendations of the International Society of Biomechanics [WH1]. The recorded data of markers' trajectories and the bones' surface meshes were loaded in a graphical user interface (gui) within the MatLab virtual reality toolbox (Figure 4). Additionally a joint sphere was implemented: inside the joint sphere the bones were connected with additional faces to allow the muscle to find its path from one bone to the other. Origin and insertion of the muscles were from literature [W1].

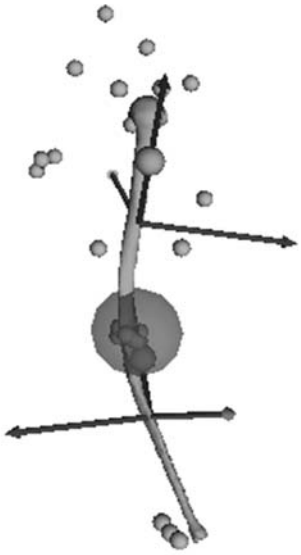

Figure 4 - Gui with bones, marker positions and joint sphere.

The bones were placed and scaled in the gui to fit the markers' positions. Thereby the bones' sizes were adjusted to the athlete's anthropometry. The bones were fixed to the markers and therefore moved along the markers trajectories, when the recorded elbow flexion was changed. Frame by frame the configuration of the bones and joint sphere for the particular joint angle during elbow flexion was saved as surface meshes and the length of muscle path was calculated (Figure 5).

Figure 5 - Bone position and muscle path for various joint angles during elbow flexion.

Moment arms then can be easily calculated, because the moment arm is the derivative of the muscle length with respect to joint angle.

3- Result and Discussion

In Figure 6 the muscle length against the elbow flexion angle is shown for the m. triceps brachii caput laterale and m. brachialis respectively. The results are compared with results from polynomials fitted to anatomical data [PY1]. Muscle lengths calculated with dijkstra algorithm and from anatomical data show the same trend. Differences might be caused by different bone lengths, because of different origin and insertion points or because of the choice of the joint sphere that connects the bones.

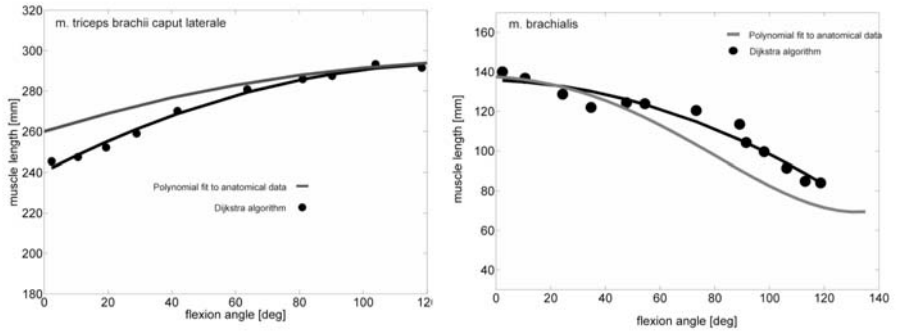

Figure 6 - Length of (a) m. triceps brachii caput laterale and (b) m. brachialis against joint angle.

With the presented approach it is possible to calculate individual muscle lengths during sports recorded via motion analysis. The model shown here represents the muscle length changes of a simple elbow flexion joint motion, but can be transferred easily to complex joint movements. Calculation of muscle lengths is semi-automatic. The bones are fixed to the markers and therefore change their positions during the motion automatically, manual repositioning is rarely necessary. Definition of origin and insertion can be done within the local coordinate systems of the bones. The positioning of the joint sphere to define the connection of the bones is most difficult and done manually. For muscles that wrap around a joint (here m. triceps brachii caput laterale) the positioning of the joint sphere works well, but muscle length is underestimated about maximal 2 cm, because no muscle volume is considered and the muscle path follows directly the surface of the bone. During elbow flexion the muscle is stretched, becomes thinner and therefore the centroid line of the muscle path lies closer to the bone's surface. This is the reason why data calculated with dijkstra algorithm and data from fitted polynomials lies closer together when the elbow is flexed. For muscles that lift from bone's surface and "jump" from one bone to the other (here m. brachialis) (Figure 5) it is difficult to scale the size of the joint sphere because it is not known where the muscle leaves the bone and therefore the calculated muscle length differs from real values (about maximal 2 cm). The problem of positioning the joint sphere for muscles that lift from the bone's surface is seen in Figure 6: calculated muscle lengths of m. brachialis scatter much more then for m. triceps brachii caput laterale.

The method of calculation muscle length with dijkstra algorithm works well as long as the muscle path runs over the bone's surface. To simulate underlying structures (muscle or tissue) it is necessary to model volumetric muscle properties. Furthermore no muscle deformation was considered. Therefore the next step will be segmenting muscles from the VHD and present them as volumetric deformable tetrahedral meshes.

4- References

[BC1] Böhm H., Cole G.K., Brüggemann G.P., Ruder H. Contribution of muscle series elasticity to maximum performance in drop jumping. Journal of Applied Biomechanics 22: 3-13, 2006.

[BK1] Böhm H., Krämer C. Optimization of Human Motion exemplified with Handbiking by means of Motion Analysis and Musculoskeletal Models. In: Human Motion Understanding, Modelling, Capture and Animation. Springer Series: Computational Imaging and Vision (36), Rosenhahn, B.; Klette, R.; Metaxas, D. (Eds.). 409-427, 2007.

[CJ1] Charlton I.W., Johnson G.R. Application of spherical and cylindrical wrapping algorithms in a musculoskeletal model of the upper limb. Journal of Biomechanics, 34: 1209–1216, 2001.

[D1] Dijkstra E.W. A note on two problems in connection with graphs. Numerische Mathematik 1: 83–89, 1959.

[DC1] Dong F., Clapworthy G., Krokos M., Yao J. An Anatomy-Based Approach to Human Muscle Modeling and Deformation. IEEE Transactions on Visualization and Computer Graphics, 8(2), 2002.

[FM1] Fernandez J., Mithraratne F., Thrupp S., Tawhai M., Hunter P. Anatomically Based Geometric Modeling of the Musculo-Skeletal System and Other Organs. Biomechanics and Modeling in Mechanobiology, 3, 2003.

[GP1] Garner B.A, Pandy M.G. The Obstacle-Set Method for Representing Muscle Paths in Musculoskeletal Models. Computer Methods in Biomechanics and Biomedical Engineering, 3: 1-30, 2000.
[PY1] Pigeon P, Yahia H, Feldman A.G, .Moment Arms and Lenghts of Human Upper Limb Muscles as Functions of Joint Angles. Journal of Biomechanics, 29(10): 1365-1370, 1996.
[TS1] Teran J., Sifakis E., Blemker S.S., Ng-Thow-Hing V., Lau c., Fedkiw R. Creating and Simualating Skeletal Muscle from the Visible Human Data Set. IEEE Transactions on Visualization and Computer Graphics. 11(3): 317-328, 2005.
[US1] US National Library of Medicine, The Visible Human Project. 1994, http://www.nln.nih.gov/research/visible/.
[W1] Winters J.M., Woo S.L-Y. Multiple Muscle Systems. Biomechanics and Movement Organization. Springer-Verlag, New York Inc., 1990.
[WH1] Wua G., van der Helm F.C.T., Veeger H.E.J., Makhsous M., van Roy P., Anglin C., Nagels J., Karduna A.R., McQuade K., Wang X., Werner F.W., Buchholz B. ISB: Recommondation on Definiions of Joint Coordinate System of Various Joints for the Reporting of Human Joint Motion - Part II: Shoulder, Elbow, Hand and Wrist. Journal of Biomechanics, 38: 981-992, 2005.

Development of a New Technique to Evaluate Abrasivieness Artificial Turf (P168)

Mercedes Sanchis, David Rosa, Javier Gámez, Enrique Alcántara, Carmen Gimeno, Maria José Such, Jaime Prat, Ricardo Dejoz[1]

Abstract: Several studies can be found that compare the risk of injury on artificial turf and natural grass, mainly regarding the risk of injury in ankle and knee. A main problem of artificial turf is, however, related to the injuries due to sliding and it has not been studied in depth.

These skin injuries (called turf-burns) are caused by a combination of two effects: abrasion, which damages the upper layer of human skin (possibly related to coefficient of static friction) and a rise of temperature that leads to skin burning (possibly related to dynamic coefficient of friction).

The test device currently used to measure abrasiveness on artificial turf does not reproduce the real sliding of a sportsman; it allows the comparison between different artificial turf surfaces but it is very difficult to know the effect of this surface in players' skin. On the other hand, only dynamic coefficient of friction is obtained.

For this reason, the Institute of Biomechanics of Valencia (IBV) has developed a test device simulating the same vertical force and velocity than the sliding trackle. A tool cover with a film of silicone slides over the artificial turf and the static and dynamic coefficient of friction are obtained.

The aim of this study is to obtain a good correlation between mechanical properties of artificial turf and human perception; then, it will be possible to know (from mechanical properties) the effect of different artificial turfs in human skin when players slide over them.

To obtain this objective, six prototypes of artificial turf were tested using IBV test device and the damage of the silicones were evaluated by means of analysis of roughness and image analysis (Scanning Electron Microscopy); the results were related to the coefficient of friction and the subjects' opinion (by means of a subjective study consisting of a survey about abrasiveness). A good correlation between damage on silicone after test and subjective study results were obtained. However, the correlation between coefficient of friction and subjective study was not good since artificial turf surfaces with similar coefficient of friction were considered different by subjects.

Keywords: artificial turf, skin injury, abrasiveness.

1. Instituto de Biomecánica de Valencia, Universidad Politécnica de Valencia- Edificio 9C, Camino de Vera s/n, E-46022 Valencia, Spain - E-mail: mercedes.sanchis, david.rosa, javier.gamez, enrique.alcantara, carme.gimeno, mjose.such, jaime.prat, ricardo.dejoz@ibv.upv.es

1. Introduction

During the last years, artificial turf pitches have become commonly used for sports like hockey, tennis, rugby and football. The acceptance of this sport surface has found objections in sports like football because first generations of artificial turf showed many problems and differences respect to the natural grass. These differences have been reduced but a serious problem exists yet: skin injuries due to sliding. This problem has been called "turf-burns". The risk of this turf burn curbs the players when playing on artificial turf (Lees and Nolan, 1998).

Gaulrapp *et al.* found that the number of injuries on artificial turf was higher than on natural grass and these skin injuries frequently occur during a sliding trackle (Gaulrapp *et al.*, 1999). These injuries are caused by two mechanisms: burn and scrape. It is possible that burn is due to an increase of temperature and it occurs when the player is sliding on the surfaces; it is possible that the scrape occurs when this slide starts because the friction is higher in this moment.

This problem is being studied and some testing devices have been developed. Verhelst *et al.* have developed a new testing device to evaluate the increase of temperature and coefficient of friction of artificial turf pitches. It consists of a ramp from which a sledge is launched onto the field and the temperature at the contact surface between the sledge and the field is measured. The sliding distance is also measured and the calculation of the coefficient of friction is carried out (Verhelst *s*, 2007).

The test device currently used to evaluate abrasiveness of artificial turf is the FIFA experimental set-up, which consists of an apparatus that applies a load of 100 N over artificial turf and makes a circular movement. The contact surface is made of silicone and the test device measures the coefficient of friction between this silicone surface and the artificial turf. After this, changes in frictional properties on silicone are measured to check the damage in this surface (FIFA Quality Concept, 2006).

However, this method does not measure the coefficient of friction when the slide starts, that is, the static coefficient of friction (which is possibly related to scrapes in skin), and no information regarding the increase of temperature is provided. This test device only measures the dynamic coefficient of friction (possibly related to skin burns). For this reason, IBV has developed a new test device to evaluate the coefficient of friction (both static and dynamic) on artificial turf pitches and a methodology to evaluate the damage on silicone, validating the results by means of a subjective study (Saaty, 1988).

2. Methodology

The test device (Figure 1) reproduces the sliding trackle. A surface is coated with an artificial skin (silicone used by FIFA for the determination of skin/surface friction) and it is slid on the artificial turf surface. The machine provides a constant vertical force (150 N) and a constant velocity (0.4 m/s); the horizontal force required to produce the displacement is acquired by the software developed by IBV.

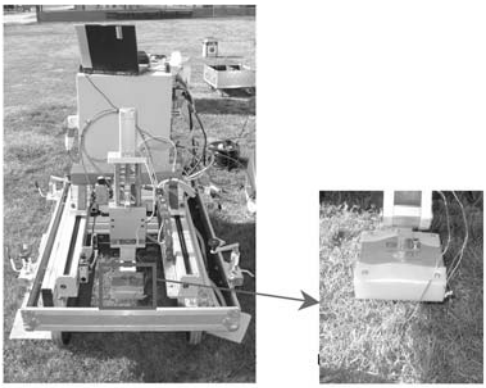

Figure 1 - Test device and the surface coated with artificial skin (silicone).

The variables obtained from this test (Figure 2) are COFpeak and COF. The former (COFpeak) is the coefficient of static friction and it is possibly related to scrape (which damages the upper layer of the human skin) while the latter (COF) is the coefficient of dynamic friction, related to a rise of temperature (that possibly leads to skin burning).

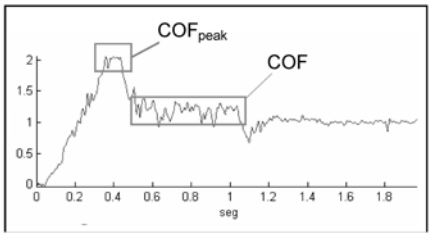

Figure 2 - Mechanical test results.

Six artificial turf carpets were tested (without infill). A description of the samples is given in Table 1.

Table 1 - Description of samples.

	Stitches (per 10cm)	Dtex	Fibre material	Type of fibre	Pile height (mm)
A	17	11000	poliethylene1	fibrillated	60
B	17	11000	poliethylene2	fibrillated	60
C	15	12500	poliethylene1	fibrillated	60
D	17	11000	poliethylene1	monobench	60
E	17	11000	poliethylene3	monobench	60
F	17	11000	poliethylene3	monobench	60

COFpeak and COF were obtained from nine repetitions of the test in each sample (the silicone was changed after each three repetitions).

After that, the damage of the silicone was evaluated by an analysis of roughness and also by means of image analysis (Scanning Electron Microscopy). The variables obtained from roughness analysis are Rp (the maximum value of the profile from the mean line, that is, the height of the highest point of the profile from the mean line) and Rv (the absolute value of the minimum value of the profile deviations from the mean line, that is, the depth of the lowest point of the profile from the mean line). The roughness was measured in two directions: the direction of advance of the machine and the opposite one.

The variables obtained from image analysis were the equivalent diameter of the observed particles. It is possible that a different size of particles shows a different damage in skin.

In adition, a subjective study was carried out. Five people (three men and two women) took part in this study, consisting of a survey in which participants rubbed their forearm against artificial turf carpets and answered several questions regarding the abrasion perception. They evaluated the abrasiveness of different samples in a scale from 1 (no abrasiveness) to 9 (very abrasiveness). After that an Analytic Hierarchy Process (AHP) (two-way comparison of artificial turf samples by means of forearm rubbing) was carried out.

Finally, a statistical treatment was carried out and the correlation between all variables (subjective and objective) was obtained.

3. Results

Experiments were carried out in the laboratory (nine sliding tests on each one of the six carpets). The results obtained from the sliding test device (COFpeak and COF) are showed in Figure 3.

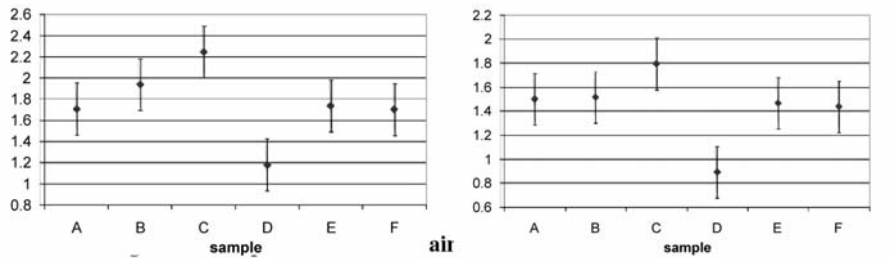

Figure 3 - COFpeak and COF obtained for each of the six samples.

The sample D shows the lowest COF (static and dynamic), with significant differences ($p<0.05$) in comparison with the rest of the samples. There are not significant differences between the rest of the samples.

Three silicones were obtained for each carpet to analyse the damage after the sliding test. The roughness was measured in two directions (the direction of advance of the sliding test and the perpendicular one) since it was possible to expect a different damage in these two directions. Significant differences between them were not found and

Scanning Electron Microscopy was used to understand these results. Figure 4 shows a silicone surface after sliding test:

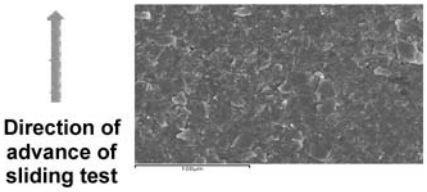

Figure 4 - SEM images (500x); silicone after sliding test.

It is clear that the damage on the silicone is different of the expected damage, similar to cuts in the direction of advance of the test device. However, the sliding test moved particles of the silicone and for this reason, the roughness in two directions (the direction of advance of test device and perpendicular direction) does not show significant differences.

Then, all roughness measurements (in two directions) were used to obtain mean values of Rp and Rv. The roughness values for the six samples are shown in Figure 5:

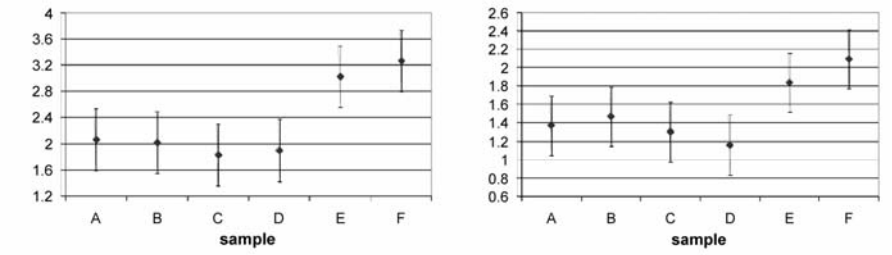

Figure 5 - Roughness test (Rp and Rv) results.

From the SEM images, the equivalent diameter of particles was measured. The percentage of images with an equivalent diameter bigger than 20 μm was obtained. The results showed that samples with a higher roughness values provided a higher equivalent diameter of particles.

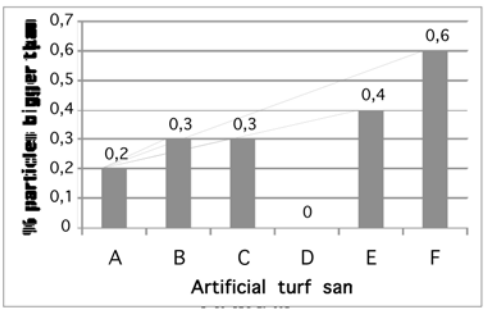

Figure 6 -

The silicones tested over different artificial turf samples are shown in the following pictues. It is possible to observe bigger particles in samples with a higher equivalent diameter and roughness values.

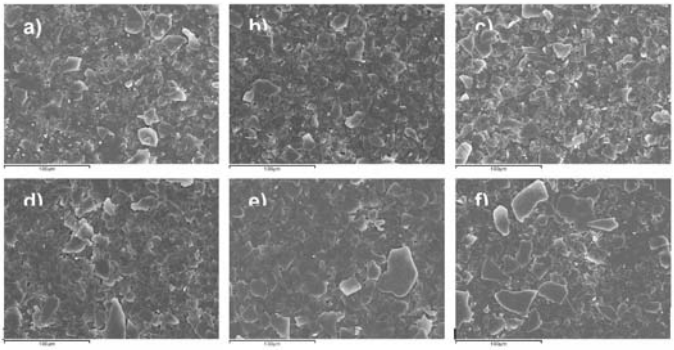

Figure 7 - SEM images (500x); silicone tested over artificial turf sample: a) A; b) B; c) C; d) D; e) E; f) F.

Next graphs show that there is no relation between COF or COFpeak and roughness (Rp and Rv). As can be seen in the graphs, it is possible to obtain large differences of roughness values for a similar coefficient of friction. Then, it is possible that the damage in silicone was associated with a different cause (not related to the coefficient of friction).

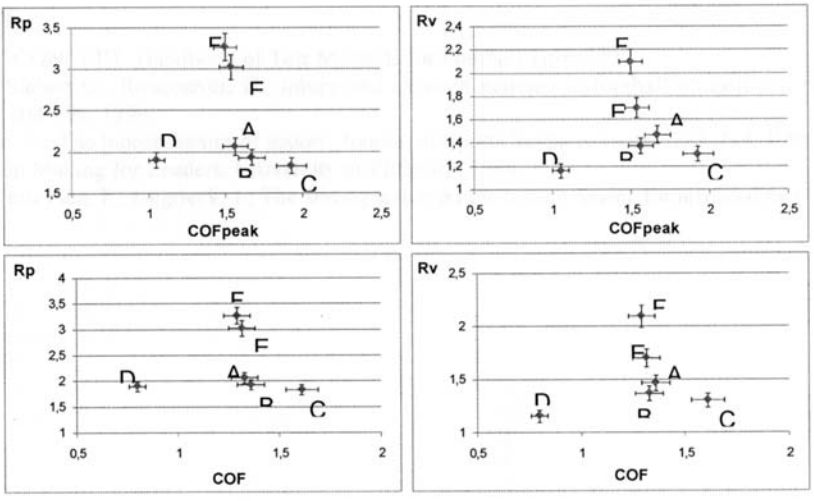

Figure 8 - Coefficient of friction and roughness relation.

The results of subjective study show a good correlation with roughness or damage in the silicone. Figure 9 shows the classification of the samples from minimum to maximum abrasiveness:

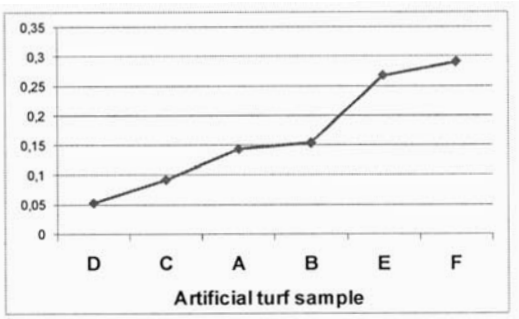

Figure 9 - Subjective study results (classification of the samples from minimum to maximum abrasiveness).

Participants in the study considered that the most abrasive sample was F. As can be observed from the study of roughness, the silicone tested in this sample shows the highest damage, that is, the highest values of Rp and Rv. The order of samples from lesser to larger abrasiveness in the subjective study exhibits an excellent agreement with the roughness analysis results.There is a good correlation between human perception and the study of roughness results.

4. Discussion and Conclusions

The evaluation of abrasion in skin is a very difficult task since a silicone is being used as a substitute of the skin. The subjective study showed, however, that there is a good correlation between human perception and the damage in the silicone after the mechanical test.

The first hypothesis was that a relation exists between the coefficient of friction and the abrasiveness of artificial turf (or injury in skin). It is also possible that there is a relation between this coefficient of friction and injury, although additional reasons of burns in players' skin can be expected. The correlation between the coefficient of friction (static or dynamic) and the damage in silicone (roughness values) is not a good, and therefore it seems plausible that another mechanism of damage occurs.

The use of image analysis (Scanning Electron Microscopy) allows the observation of bigger particles in silicones with higher values of roughness. Therefore, image analysis presents a good correlation with human perception: the samples evaluated as more abrasive have produced a higher damage in silicone.

The study of roughness in silicone after the sliding test can be a good prediction of the abrasiveness of artificial turf.

5. References

[F1] FIFA QUALITY CONCEPT. Handbook of Test Methods for Football Turf. 2006.

[GS1] Gaulrapp, H., Siebert C., Rosemeyer, B., Injury and exertion patterns in football on artificial turf. Sportverletzung – Sportschaden. 13, pp. 102-106, 1999.

[LN1] Lees, A., Nolan, L., The biomechanics of soccer. Journal of Sports Science. 16, pp. 211-234, 1998.
[S1] Saaty, T., Decision Making for Leaders. University of Pittsburg. 1998.
[VV1] Verhelst, R., Verleysen, P., Degrieck, J., The sliding tester: a new testing device for artificial turf.

Aerodynamic Study of Ski Jumping Flight Based on Inertia Sensors (171)

Yuji Ohgi[1], Nobuyuki Hirai[2], Masahide Murakami[2], Kazuya Seo[3]

Topics: Ski & other Winter Sports.

Abstract: Aerodynamic forces, drag and lift were estimated by the body attached inertia sensors and high speed videography in ski jumping. Last ISEA conference, the authors presented our new method for the aerodynamic study on ski jumping. In this paper, we propose more robust and reliable measurement system by using wireless technology. Wireless 6DOF inertia sensor platform, which has a built-in tri-axial accelerometer and three single axial gyroscopes, was attached on the jumper's low back. The authors adopted IEEE802.15.4 for the start trigger and real time monitoring during long training session. Sensor also has a flush memory inside for one hour data storage at 250Hz. The primary target of the present study is to extract the aerodynamic force data during real jumping flight. Angular velocity on the sagittal plane was directly measured from the gyroscope. Then we could obtain the jumper's body pitch angle by its time integration. The accelerations with respect to the body local coordinate system which was determined by the body pitch angle, indicated the drag and lift forces. The assessment of the aerodynamic forces of ski jumping was examined by both of the sensor data and the kinematical data in this study.

Key words: Ski Jumping; Accelerometer; Gyroscope; Drag and Lift; Wireless

1- Introduction

Ski jumping has been attracted fluid dynamics scientists because of its highly complex phenomenon. As for the biomechanical aspect, kinematical and kinetical methods were applied in the field studies (Babiel, Hartmann, Spitzenpfeil and Mester 1997; Kaps, Schwameder and Engstler 1997; Komi and Virmavirta 1997; Yamanobe and Watanabe 1999). Traditional and popular method for kinematical study was an image analysis method. On the other hand, as for the kinetical study, force platform data analysis method during the last few seconds on the inrun slope has been examined. For the flight phase, experimental wind tunnel tests were conducted (Seo, Watanabe and Murakami

1. Graduate School of Media and Governance, Keio University, Fujisawa Japan - E-mail: ohgi@sfc.keio.ac.jp
2. Graduate School of Systems and Information Engineering, Univ. of Tsukuba, Tsukuba Japan
E-mail: murakami@kz.tsukuba.ac.jp
3. Faculty of Education, Art and Science, Yamagata University, Yamagata Japan - E-mail: seo@e.yamagata-u.ac.jp

2004a ; Seo, Murakami and Yoshida 2004b). Then ski jumper's optimum flight trajectories by the numerical simulation were reported. Most of these studies were conducted for the motion either on the slope or in the air. No scientific approach could achieve the total kinematical and kinetical data analysis from the start, inrun, take-off, and steady flight to landing. The wide range with extreme high speed of their performance follows that we have a difficulty for our videographical observation. Therefore, in order to solve these methodological problems, the authors have been applied inertia sensors for ski jumping. Ohgi, *et al.* estimated the fluid dynamic forces, drag and lift, which acted on the jumper's body by using body attached inertia sensors (Ohgi, *et al.*, 2006, Ohgi, *et al.* 2007). In these studies, the authors adopted a tri-axial accelerometer and single axial gyroscope with data acquisition card on PDA. Since a ski jumper is the sentient athlete and his performance is always influenced by the small difference on his environmental conditions. For this reason and his safety, our PDA based data acquisition was too heavy for the jumpers and not a reliable system. Miniaturisation and weight saving contributes for the continuous and safe experiment. The purpose of this study was to quantify the ski jumper's motion and their aerodynamics forces in the flight phase by using a wireless inertia sensor and videographical method.

2- Methods

2.1 Inertia Sensor Measurement

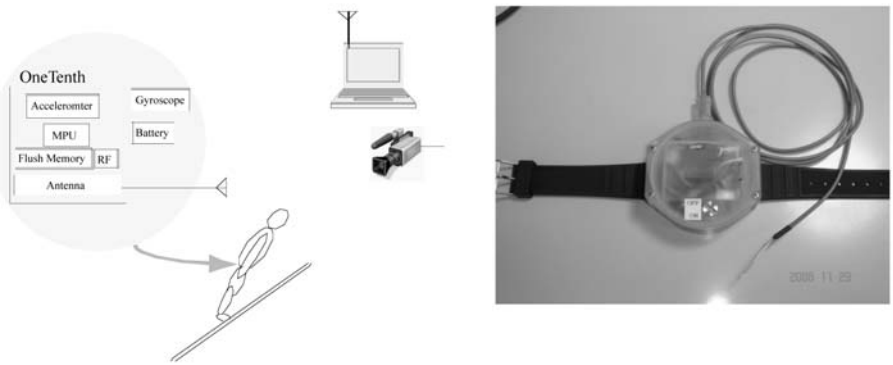

Figure 1 - Schematic illustration of our experimental setting and 6DOF wireless data logger.

Figure 1 shows the schematic illustration of our experimental setting and our wireless inertia sensor logger. The authors applied a wireless 6DOF inertia sensor platform for the ski jumping monitoring. It has a built-in tri-axial accelerometer and three single axial gyroscopes and was attached on the jumper's low back beneath the jumping suit. The core technology of our sensor platform is OneTenth (AR'S Co. Ltd.) chip which was originally developed for human movement analysis by AR'S and Keio University research group. MPU and peripherals including accelerometer, flush memory and RF are four layered all-in-one packaging by SiP (System In Package) process. The measurement

range of accelerometer and gyroscope were suitable for our human movement. IEEE802.15.4 was adopted for the start trigger and real time monitoring during long experimental session. For the ideal condition with external antenna, the wireless range covers 100m. In the real field experiment, the wireless data transmission sometimes makes trouble by unexpected environmental conditions. For example, on the ski jumping sliding slope, it is usually built by steel skeleton structure. It causes an interference of the radio. Therefore, our sensor platform has flush memory inside for the complete data storage. Thus, RF monitoring is available for sensor's life and dead observation. Whilst the calibration for the acceleration is easily achieved by using the gravitation, it is difficult for us to calibrate the angular velocity in the field experiment. In addition, the temperature change makes drift for its linearity. For this reason, a transportable calibration tool was equipped for the wireless inertia sensor (Fig. 2). The angular velocity was controllable by the feedback loop circuit and the voluntary rotation up to 2000 deg/s was accomplished. This calibration table was also designed for the acceleration calibration beyond the gravitation by using its centrifugal acceleration.

Table 1 - The specifications of 6DOF wireless sensor platform.

dimensions	Φ 55 × 22 (mm)	Waterproofed
weight	77 (g)	with rechargeable battery
MCU	16bit MCU (16M Hz)	Renesas, M16C
Accelerometer	±10 (G)	Hitachi Metals, H48D
Gyroscope	±600 (deg/s)	Epson Toyocom, XV3500B
RF	IEEE802.15.4 (2.4GHz)	Ti/Chipcon, cc2420
Storage	128 (Mbit)	NOR type Flush
A/D	10 bit	250 Hz

2.2 Videographical Measurement

In the field measurement at Hakuba Ski Jumping Stadium, two high speed video cameras were equipped for the velocitimetry. From the jumper's left side, a compact high speed camera (Photron Inc., Fastcam-R2, 250Hz) was configured for the jumper's close-up image at a distance of 15m to take both pre and post take-off phases. From the opposite right side, at a distance of 40m, a more higher resolution camera (Photron Inc., Fastcam-1024PCI, 500Hz) was set up for the wide range of the flight phase. For the video analysis, the authors defined two-dimensional coordinate system and the ski jump is

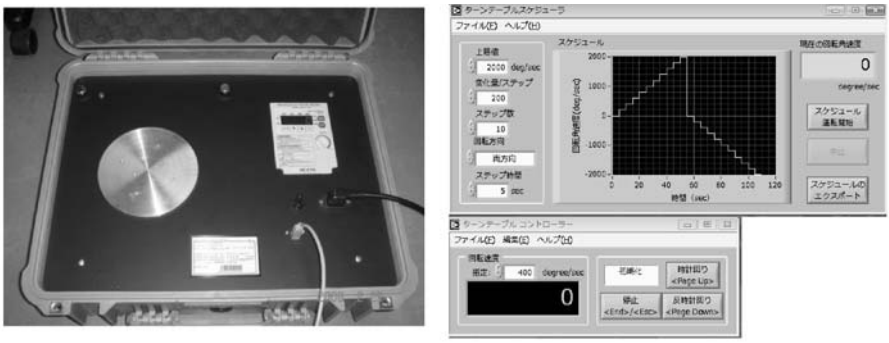

Figure 2 - Calibration tool for the angular velocity and its control software.

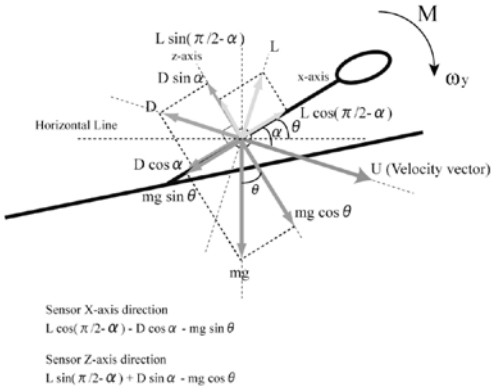

Figure 3 - Ski jumper_ski model and its coordinate system

assumed to be performed on the sagittal XZ plane on the global coordinate system, which was located on the edge of the slope. Subject was a high school ski jumper (171.0cm, 55Kg, six years career). Jumper's head (helmet), hip, knee, ankle, toe, top and tail of the ski were digitized for the analysis. Also, a local coordinate system was defined on the jumper's hip (Fig. 3). The x–axis of the acceleration is along with the jumper's spine and directing to the neck and the z-axis is defined from the jumper's front to back. Thus, the y-axis is pointing from jumper's right to left. As for the gyroscope sensor, it rotated around y–axis of the local coordinate system (Fig. 3). Positive sign of the angular velocity means that the jumper takes forward tilting motion and negative corresponds to the backward tilting, vice versa. In Fig. 3, U indicates a velocity vector of the centre of gravity of the jumper'ski model. For our convenience, we assumed the hip joint to be a centre of gravity. And our sensor unit was also assumed to be attached on the same location. The jumper's trunk and lower extremities were combined as a single segment and its angle θ, α represented his flight motion in the air. θ is the trunk angle β to the hori-

zontal plane, α is angle between trunkand the velocity vector U. Then, flight angle , is defined by (α–θ).

3- Results and discussion

3.1 Sensor data analysis

Figure 4 shows an example of the inertia sensor data. Each event such as start (ST), take off (TO) and landing (LA) are indicating as its abbreviation in the figure. During the inrun phase (ST – TO), the acceleration Ax along with the jumper's spine and A_z pointing from jumper's front to back indicating stable before the curvature radius. In Fig. 4, from 6.5 sec to take off, we can recognize vibrating fluctuations on the A_z acceleration. This can be also seen our last experiments. After the inrun sliding, the skier is exposed to the large centrifugal force during the curvature radius. He must stand and keep his crouching style. Therefore, his attempts to keep his crouching style appeared on the A_z signal. This evidence quite matches to the skiers' and coaches' knowledge. Right after his take off, both the accelerations A_x and A_z had several sinusoidal peaks, then it attenuated in 0.5 second. At this moment, its vibrating frequency was nearly 50Hz which is very similar to the second ordered natural flexural frequency of the alpine ski and snowboard (Fischer, C., *et al.*, 2006). According to the visual observation in our experiment, the second ordered vibration is obvious right after the take off. It means the ski is vibrating with its node at the boot center. After 0.5 second, the acceleration A_x and A_z were very stable except his landing instant. The acceleration A_x, which is along with jumper's spine was almost zero. On the other hand, the acceleration A_z which is along with the jumper's front to back was kept 7 to 8 m/s^2 during his flight phase. As for the angular velocity ω_y, the jumper performed to raise his body during the curvature radius. Negative angular velocity with respected to the y-axis means that he made his trunk arise. Predictably, the angular velocity ω_y changed negative, then it changed positive at the take off moment. There was a similar attenuating vibrating pattern on the angular velocity after the take off. Then, it kept small positive value during the flight phase around 20 to 30 deg/s. Before the landing, it changed rapidly positive to negative for the preparation to the telemark position.

3.2 Image data analysis

Based on the two–dimensional image analysis method, the authors obtained the digitized coordinates of skier-ski model. From the left side close image, we obtained the initial trunk angle with respected to the global coordinate system. This initial trunk lean angle, θ_0 would be used as the initial value for the time integration of the angular velocity. For the velocity vector U, with respected to the global coordinate system, right side camera image was used (Murakami, *et al.*, 2008). Almost one third of jumper's flight phase was captured and we obtained the trajectories of the skier–ski model. Basically, in this paper, the authors used this image analysis result for the flight angle β.

3.3 – Aerodynamic force

Aerodynamic forces acting on the ski jumper are drag and lift. These forces can be described on both the global or local coordinate systems. We can express them on the global coordinate system as follows,

$$D = -m\,(-\ddot{x}\cos\beta + \ddot{z}\sin\beta + g\sin\beta) \quad (1)$$

$$L = m\,(\ddot{x}\sin\beta + \ddot{z}\cos\beta + g\cos\beta) \quad (2)$$

Now the authors would like to express these equations on the sensor coordinate system, which is equivalent to the jumper's trunk oriented coordinate system. Before this procedure, we have to make sure the theoretical feature of the accelerometry. Originally, obtained acceleration from the body attached accelerometer has four components as follows:

$$\mathbf{A}_b = \ddot{\mathbf{p}} + \mathbf{g} + \ddot{\boldsymbol{\omega}} \times \mathbf{r} + \boldsymbol{\omega} \times (\boldsymbol{\omega} \times \mathbf{r}) \quad (3)$$

In eq. (3), p is the displacement vector of the origin of the local coordinate system with respect to the global coordinate system, g is the gravity, ω is the angular velocity of the specified point p and r is the radius of the rotation (Ohta, *et al.*, 2005). Here, we have some assumptions for the obtained accelerations A_x and A_z. We supposed that the center of gravity was almost equivalent to the hip joint and our sensor device was fixed on there. Therefore, the radius of the rotation on the local coordinate system might be zero (r = 0). In addition, as we mentioned above, the ski jumping is assumed to be symmetrical. That means the jumper has no rotational motion around both the x and z axes. Thus, the accelerometer outputs could be supposed that it had no rotational acceleration components, both the centrifugal acceleration and the tangential acceleration on these axes. Therefore, we hypothesized that obtained acceleration had translational and gravitational accelerations as its components. The forward tilting angle, θ could be obtained by the time integration of the gyroscope data. Then the angle α could be obtained by the sum of the forward tilting angle and the flight angle β which was already calculated by our cooperative research work (Murakami, *et al.*, 2008). Therefore, obtained acceleration must be as follows,

$$A_x = \ddot{x}\cos\theta + \ddot{z}\sin\theta - g\sin\theta \quad (4)$$

$$A_z = -\ddot{x}\sin\theta + \ddot{z}\cos\theta - g\cos\theta \quad (5)$$

Once we obtained jumper's forward tilting angle θ by the time integration of the angular velocity ω_y and the flight angle β by the video image analysis, we could estimate horizontal and vertical accelerations with respect to the global coordinate system. Then, we could estimate the aerodynamic forces, drag and lift by using eq.(1) and eq.(2).

Figure 5 shows an example of estimated drag and lift forces by the inertia sensor and the video image analysis methods. The magnitudes of both the drag and lift were similar. However, while the result by the video image analysis method was very smooth, our

sensor based estimation has large fluctuations on its signal. At the present stage, the authors cannot conclude reliable evidences on the reason of these fluctuations. Off course, the sensor signals data themselves had typical vibrating noises which were influenced by the jumper's motion, the friction between the body and the jumper suit and wind induced effect. In the analytical procedure, there were several differences on the data manipulation between the sensor based and the video based analysis methods. On one hand, the video analysis method, the obtained coordinates were smoothed by using second ordered numerical differentiation (Murakami, *et al.*, 2008). This strong smoothing function obviously brings the noisy coordinates data to the smoothed and flat resultant aerodynamic forces. On the other hand, in this paper, the authors adopted the IIR digital low pass filter at the 10 Hz cut-off frequency for the inertia sensor data. It means that the obtained signal has relatively high frequency components in the calculated results. Moreover, at present, we could not measure the flight angle β and the initial body lean angle θ without the video analysis method. That means the estimated aerodynamic forces were based on both the sensor data and the image data.

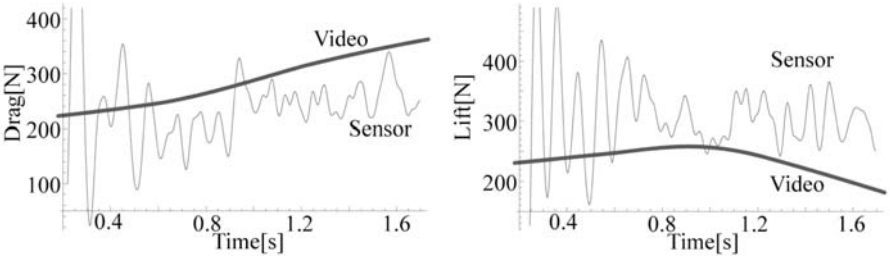

Figure 5 - Estimated aerodynamic forces by the inertia sensor method and the video analysis method.

4- Conclusions

The authors applied a 6DOF wireless inertia sensor platform to the ski jumping monitoring. Simultaneously, the video image analysis method was adopted for the jumper's forward tilting angle and his trajectory in the air. Sensor platform was available for the jumper's training session up to one hour. And miniaturisation provided some sense of security to the jumpers. Using the sensor and the video analysis data, the authors estimated the aerodynamic forces, drag and lift during ski jumping flight phase. Although, the results of the estimated aerodynamic forces, drag and lift indicated similar amplitude comparing our cooperative research project based on the video analytical method, these had fluctuated noise on the force time histories. For our further study, elucidation of the evidence of these fluctuations on the force data should be remained.

5- Acknowledgement

This research was partially supported by the Ministry of Education, Science, Sports and Culture, Grant-in-Aid for Exploratory Research, 19650167, 2007.

6- References

[BH1] Babiel, S., Hartmann, U., Spitzenpfeil, P. and Mester, J. Ground reaction forces in alpine skiing, cross-country skiing and ski jumping., Science and Skiing, Müller E. *et al.* (Eds) 200-207, 1997.
[F1] Fischer, C., *et al.*, Dynamic properties of materials for alpine skis, Sports Engineering, 6, 263-268, 2006.
[KS1] Kaps, P., Schwameder, H. and Engstler, G. Inverse dynamic analysis of take-off in ski jumping, Science and Skiing, Science and Skiing, Müller E. *et al.* (Eds) 72-83, 1997.
[KV1] Komi, P.V. and Virmavirta, M., Ski-jumping take-off performance : Determining factors and methodological advances. Science and Skiing, Müller E. *et al.* (Eds) , 3-26, 1997.
[M1] Murakami, M., Hirai, N., Seo, K. and Ohgi, Y., Aerodynamic study of ski jumping flight based on high-speed video image, presented at this conference, 2008.
[OS1] Ohgi, Y., Seo, K., Hirai, N., Murakami, M., Measurement of jumper's body motion in Ski Jumping, The Engineering of Sports 6, Eckehard, Fozzy Morriz, and Steve Haake, eds., pp.275-280, 2006.
[OS2] Ohgi, Y., Seo, K., Hirai, N. and Murakami, M., Aerodynamic forces acting in ski jumping, Journal of Biomechanics, Vol. 40, Supplement 2, S402, 2007.
[OO1] Ohta, K., Ohgi, Y., Kimura, H., Hirotsu, N., Sports Data, Kyoritsu Pub., 2005. (in Japanese)
[SW1] Seo, K., Watanabe, I. and Murakami, M., Sports Engineering, 7, 31-39, 2004.
[SW2] Seo, K., Murakami, M. and Yoshida, K., Sports Engineering, 7, 97-104, 2004.
[YW1] Yamanobe, K. and Watanabe, K., Measurement of take-off forces in ski jumping competition, Japanese Journal of Biomechanics in Sports and Exercise, 3, (4), 277-286, 1999.

The spin decay of sports balls in flight (P172)

David James[1], Steve Haake

Abstract: The ability to understand and predict the flight trajectory of a sports ball is important in many fields of sports engineering. The aerodynamic coefficients of sports balls have been studied in detail and yet aerodynamic models generally assume that spin rates are constant during flight. This study examines the spin decay of sports balls in flight in order to improve the accuracy of aerodynamic models. Several types of sports ball (tennis ball, worn tennis ball, football, oversize tennis ball) were launched in a sports hall using artificial bowlers at various speeds and spin rates. The start and end of the trajectories were filmed using two high speed video cameras and the resulting measurements were used to assess the spin decay of each ball as well as the factors affecting spin decay. The data shows a strong linear relationship between spin decay and the product of initial spin and speed for all the different sports balls tested. However, the constant in this linear relationship was found to be different for each of the different balls and was assumed to be dependent on the physical attributes of the different balls. Dimensionless parameters were derived such that the differences between the sports ball spin characteristics could be more easily identified. It was found that the rate of spin decay is largely dependent on the balls moment of inertia; however, its surface roughness and its boundary layer flow regime are also of importance.

Keywords: Aerodynamics, spin decay, football, tennis, trajectory

1- Introduction

The aerodynamic behaviour of sports balls has been studied by many authors. The majority of studies have used wind tunnel experiments to ascertain the effects of Reynolds number (Re) and spin parameter (α) on the ball's lift and drag coefficients. Other studies have measured the trajectories of sports balls to determine their aerodynamic behaviour, and more recently computational fluid dynamics has been used. However, relatively few studies have published data on the behaviour of a ball's spin rate decay, an attribute of the ball's dynamics that affects its trajectory and the accuracy of aerodynamic models.

The first quoted rates of spin decay were recorded by Lieberman (1990). Leiberman conducted experiments on golf balls and found that their spin decayed between a

1. Sports Engineering Research Group, Sheffield Hallam University, UK - Email: d.james@shu.ac.uk

quarter and two thirds for trajectories lasting between six and eight seconds. Smits and Smith (1994) developed this knowledge by suggesting that at a constant velocity, a golf ball's spin rate decreases exponentially with time. They suggested that the spin rate decay for a golf ball could be described by the following equation.

$$\frac{d\omega}{dt} = cU_{\infty}\omega \tag{1}$$

Where c is a constant, U_{∞} is the initial velocity and ω is the initial spin rate. In another study on golf balls, Tavares *et al.* (1998) used radar measurements to determine the spin rate decay with balls of different moments of inertia and different dimple patterns. They showed that spin rate decay increased with deeper dimples and with lower moments of inertia, but only at relatively high spin rates.

Tarnowski (2004) investigated the spin decay of tennis balls by using high speed video to capture the start and end of the trajectory inside a sports hall. Tarnowski found that the final spin rate was linearly proportional to the initial spin rate regardless of the initial spin rate or velocity, however the time duration of the trajectory was not recorded and the relationship in equation 1 could not be confirmed.

In their sports ball aerodynamics review paper, Haake *et al.* (2007) reinterpret the data from Tarnowski by using an aerodynamic model to ascertain the trajectory time duration. They concluded that that a tennis ball's spin rate decay can be described by using equation 1, but also comment that experiments on different types of sports ball would be very interesting and may lead to a better understanding of the effects of inertia, flow regime and surface roughness.

This study will take a closer look at the spin decay relationship proposed by Smits and Smith (equation 1) in regard to a number of different sports balls and will explore some of the physical attributes that leads to this behaviour.

2- Experimental Arrangements

The testing procedure used bowling machines to project the balls and high speed video cameras to record images of the balls' spin rate, velocity and launch angle at the start and end of trajectory. The tests were conducted in a sports hall to reduce effects of wind and other uncertainties found with outdoor testing. As the experiments were carried out indoors no hard balls were tested that could cause damage or breakages. The experimental arrangement is shown in figure 1.

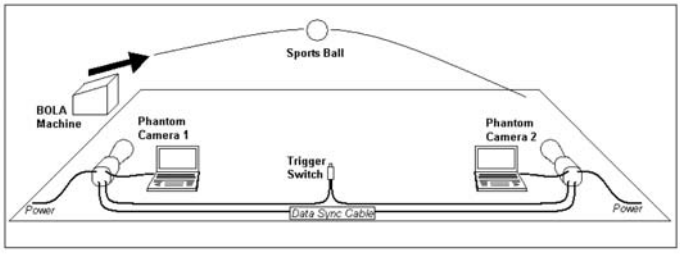

Figure 1 - Experimental arrangement used to capture ball dynamics at the start and end of the trajectory.

High speed video cameras were positioned at a set distance apart and the bowling machines were adjusted to provide a relatively constant launch velocity. Spin rates were changed from between -360 $rads^{-1}$ and 380 $rads^{-1}$. In order for the ball to pass through the view of both cameras, the angle of launch was changed for each different spin rate condition.

A number of different sports balls were used in the experiments; these balls are described below:

A new, pressurised ITF approved tennis ball. The balls had not been used for any purpose prior to testing and were still inside their sealed containers. The balls were marked with a fibre tipped pen to aid in the processing of the video footage. The balls' radius measured 0.33 metres.

A worn tennis ball. These tennis balls were not old, and were actually identical to the new tennis balls; however their surface was abraded with Velcro to simulate a worn surface. Their surface was marked with a fibre tipped pen to aid image processing and their radius was considered to be 0.33 metres.

An extremely large tennis ball (similar in size to a football). This ball was selected to investigate the effects of moment of inertia; the ball had the same design and surface covering as a standard tennis ball its radius measured 0.115 metres. A comparison of the standard tennis ball and the large tennis ball is shown in figure 2.

A football. The ball was inflated to its recommended pressure and had a radius of 0.11 metres.

In order to project the different sports balls, two different types of bowling machine were used. Both machines used rotating disks to project the balls thereby allowing varying amounts of spin to be applied. A standard tennis BOLA machine was used to project the standard size tennis balls. The machine was fitted with a barrel to improve launch angle consistency. A football BOLA machine was used to project the football and the large tennis ball. This machine was developed as a prototype and is not commercially available. Figure 3 shows pictures of the two bowling machines.

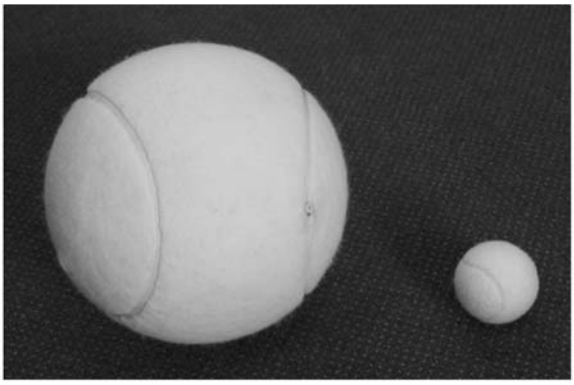

Figure 2 - A comparison of the large tennis ball and a standard tennis ball.

Figure 3 - The tennis BOLA machine and the football BOLA machine.

The two high speed video systems used in the testing were Vision Research, Inc Phantom V4. The cameras were connected to each other and synchronized so that accurate timings of the trajectory duration could be measured. The cameras were set to run at 500 frames per second; this speed provided ample resolution for accurate image processing.

Measurements of the ball centres and rotation were taken manually from the video footage by using a bespoke software package (Richimas V3.2). This data was then processed to calculate speed, angle and spin rate. More than 100 video sequences were analysed using this method.

The authors have a great deal of experience of measuring the dynamics of sports balls using high speed video techniques and every attempt was made to minimise the effect of experimental uncertainties. However, relatively large errors are inevitable when measuring spin rates and these become more evident when comparing the dynamics at the start and end point of a trajectory. The trajectory duration was therefore set to be as long as possible to minimise the effect of spin measurement errors, but the resulting data is subject to significant uncertainty. A full error analysis was conducted and it was concluded that spin measurements were subject to an uncertainty of 10 $rads^{-1}$, and speed measurements to an uncertainty of 0.3 ms^{-1}.

Following the trajectory experiments, the moments of inertia for the different sports balls were measured. This was achieved by using the Bifilar suspension technique.

3- Results and Discussion

Within this paper there is not sufficient space to present the full experimental results; nonetheless, by using dimensional analysis, the trajectory data can be organised into a compact form. A common dimensionless parameter can be used to describe the spin rate

of the ball; the spin rate parameter (a) is defined as the ratio of peripheral velocity to translational velocity and is shown in equation 2.

$$\alpha = \frac{\omega r}{U_\infty} \tag{2}$$

Another dimensionless parameter that useful to describe the data is spin rate decay (*SRD*). Smits and Smith (1994) derived *SRD* from the spin rate parameter. Starting with equation 2, if the spin rate (ω) is replaced by the change in spin rate ($d\omega/dt$), the balls radius (r) is replaced by r^2 and the initial velocity (U_∞)is replaced by U_∞^2 there exists a new dimensionless parameter that describes spin rate decay.

$$SRD = \frac{d\omega/dt\, r^2}{U_\infty^{\,2}} \tag{3}$$

Figure 4 shows the relationship between the spin parameter (α) and spin rate decay for all the sports balls tested. Allthough there is significant scatter in the data, it can be seen that there are clear differences in the spin decay behaviour between the different balls and that they adhere to the linear spin decay relationship proposed by Smits and Smith (1994).

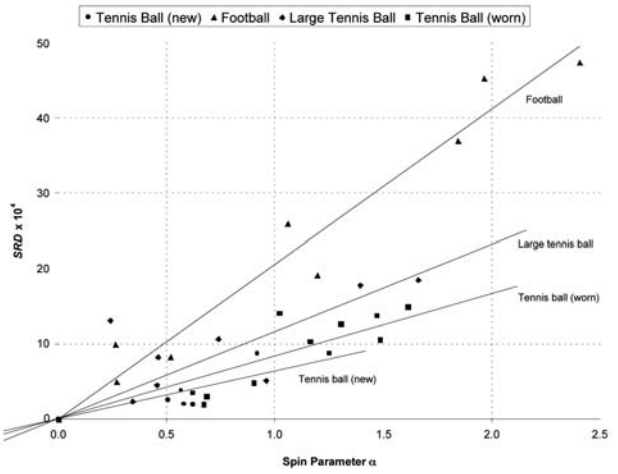

Figure 4 - A comparison of the spin rate parameter against spin rate decay for all sports balls tested.

The new tennis ball and the old tennis ball exhibit generally similar spin decay behaviour, but as expected, the spin rate of the worn tennis ball slows to a greater extent. This is presumably due to the increased roughness of the nap creating higher skin friction. The spin rate decay of the football can be seen to be the highest out of all the balls tested; whilst this may be suprising due to the ball's relatively smooth surface and presumably low skin drag, it can be explained by the flow conditions around the ball. Due to the spacial restraints of indoor testing and the need to have as long a trajectory duration as possible, the launch speeds of all balls were relatively slow (typically 7 ms^{-1}). In the case

of the football, the Reynolds Number was always subcritical and hence the flow around the ball was laminar. It is assumed that this laminar flow regime contributes significantly to the spin decay of the football, whilst the spin decay of the tennis ball is caused by individual fibres of the felt penetrating through its forced turbulent boundry layer and into the flow of the free stream. Haake *et al.* (2007) suggest that the spin decay of a tennis ball is approximately 6.5 times greater than that of a golf ball. The authors also postulate that a football is likely to exhibit behaviour more similar to a golf ball due to their relatively similar surfaces; whilst this may be the case for a football travelling at speeds of greater than 10.3 ms^{-1} ($Re > 153{,}000$) where the flow is turbulent, it is clearly not the case at low speeds where the flow around the football is laminar.

4- Conclusions

The spin decay of various sports balls was studied by analysing their trajectories using high speed video in an indoor environment. As has been suggested by previous authors, it was found that the spin decay of all balls was linearly proportional to initial spin and velocity. Although the study provides valuable data to allow the complete modelling of sport ball trajectories, it is far from clear as to what is the most influential factor in causing spin decay. The study showed that moment of inertia, surface roughness and flow regieme all affect the spin rate decay of sports ball in flight.

5- References

[HG1] Haake, S. J; Goodwill, S. R; Carre, M. J. A new measure of roughness for defining the aerodynamic performance of sports balls. Journal of Mechanical Engineering Science Part C: 221, 789-806.

[L1] Lieberman, B. Estimating lift and drag coefficients from golf ball trajectories. Science and Golf: In Proceedings of the World scientific congress of golf (Ed. A. J. Cochran), 1990, pp. 187–192 (E&FN Spon, London, UK).

[SS1] Smits, A. J. and Smith, D. R. A new aerodynamical model of a golf ball in flight. Science and Golf II: In Proceedings of the World scientific congress of golf (Ed. A. J. Cochran and M. R. Farrally), 1994, pp. 340–346 (E&FN Spon, London).

[T1] Tarnowksi, K. Analysis of tennis impacts on a realistically supported racket. M.Eng Dissertation, University of Sheffield, 2004.

[TS1] Tavares, G.; Shannon, K. and Melvin, T. Golf ball spin decay model based upon radar measurements. Science and Golf III: In Proceedings of the World scientific congress of golf (Eds M. R. Farrally and A. J. Cochran), 1998, pp. 464–473 (E&FN Spon, London, UK).

Optimised preliminary design of a kayak-ergometer using a sliding footrest-seat complex (P174)

Mickaël Begon[1], Floren Colloud[2]

Topics: Sailing/Water Sports, Biomechanics, Innovation & Design, Modelling
Abstract: In sport sciences, ergometers are frequently used to provide a sheltered experimental environment. In situ, the measurement difficulties ranged from to the 3D kinematics to the contact forces. However, an ergometer has to reproduce the dynamics of the in situ movement for an accurate mechanical analysis. During a kayaking task, an ergometer with a sliding footrest-seat complex (trolley) reproduces better the acceleration of the *Kayak-Athlete-Paddle* system over the whole kayaking cycle. The purpose of this study was to improve the design of this ergometer using optimization of the mechanism of the footrest-seat complex translation. The whole body kinematics and the paddle tip forces were recorded for twelve flatwater athletes. Firstly, the acceleration of the *Athlete-Paddle* system was estimated using the propulsive force and a drag model Secondly, the *Ergometer-Athlete-Paddle* model was developed within HuManS toolbox to perform simulations. These simulations were driven by the kinematics tasks of the athlete. The output of the simulation was the antero-posterior absolute acceleration. The elastic cord linking the frame to the sliding complex was modelled as a polynomial function of order 3: $F=a_3x^3+a_2x^2+a_1x$, with x the position of the trolley on the frame. The parameters of this model were optimised by matching the accelerations of the *Athlete-Paddle* system over a whole cycle of the two cases. The fitness function was defined as the root mean square difference between the two cases and was minimized using an evolutionary algorithm. The optimization was carried out with two elastic cord models: a simple spring ($a_3=a_2=0$) and the full model which fits well a bungee.
Keywords: Experimentation, Simulation, Optimisation, Equipment, Human

1- Introduction

In sport sciences, ergometers are frequently used to provide a sheltered environement for (*i*) training athletes during semi-specific conditions, (*ii*) evaluating athlete's physical abilities and (*iii*) performing scientific researches. The instrumented ergometers (*e.g.*

1. School of Sport and Exercise Sciences, Loughborough University, Ashby Road, Loughborough, Leicestershire LE11 3TU UK - E-mail: M.Begon@lboro.ac.uk
2. Laboratoire de Mécanique des Solides UMR6610 CNRS Université de Poitiers, Bd Marie et Pierre Curie, BP 30179, 86962 Futuroscope France - E-mail: floren.colloud@univ-poitiers.fr

[BC1], [CB1], [H1]) are useful in facilitating the analysis of numerous cycles in order to better understand, for example, the relationship between segment coordination and performance. The popular success of using ergometers is mainly the consequence of (i) the validity of the physiological variables collected compared to the in situ condition, (ii) the high correlation between the both performance (on ergometer and in situ, respectively) and (iii) the good reproduction of the athlete's kinematic with respect to a frame embedded to the ergometer.

An ergometer has to reproduce the kinematics but also the dynamics of the in situ condition in order to perform a precise analysis. In rowing, Colloud *et al.* [BC11] have compared two rowing ergometers fitted with a fixed versus a free-floating stretcher. They showed that, for similar kinematics, athletes generated significant different force patterns when the two conditions were compared. The fixed condition showed higher contact forces in general and particularly at the beginning of the rowing cycle. As a result, the joint torque values were higher for the fixed condition. Thus, Dickson [D1] showed that the fixed condition produced consistently larger compressive and shear forces at the catch when compared to the fixed and the free-floating stretcher mechanisms, because of larger body accelerations. This maximum compression force may place the vertebral body at disk while the large compressive force produced during repetitive flexion at the catch may lead to injury of the inter-vertebral ligaments and discs. These changes between the two conditions may have implications for the recruitment timing and/or order of the major muscular groups involved in ergometer rowing.

During a kayaking task, Begon and Colloud [BC1] showed that an ergometer with a sliding footrest-seat complex (trolley) reproduced significantly better the kayak acceleration than an ergometer with a fixed trolley. A simple mechanism was used to reproduce the dynamics of the *Athlete-Paddle-Trolley* system. The trolley can move back and forth on a static frame. A bungee linked the back of the frame with the trolley. The forces applied to the paddle tips accelerate the system. The bungee decelerates the system between two kayaking strokes.

An experimental analysis, highlighting the dynamic differences between on-water and ergometer conditions in kayaking, involves kinematic and kinetic data of the whole body. The experimental difficulties range from the measurement of three-dimensional (3D) kinematics of the whole body to the measurement of the contact forces generated by the athlete. On-water, accurate 3D kinematics measurements remain a challenge for the future. This comparison will be helpful to improve ergometer designs but presents some limitations. Firstly, this experimental approach is time consuming; moreover elite athletes are not able to modify their well known patterns while testing new equipments or conditions. An alternative approach is to use computer simulation models.

The aim of this study is to present a method for optimizing ergometer conception. This paper is focused on an sliding kayak-ergometer (section 2) in order to reproduce the acceleration generated in flatwater kayak based on a hydrodynamic model [BC1]. The following sections (sections 3 to 4) describe the model of this hybrid system athlete-ergometer (see [BS1] for additional details). The forward dynamics introduced in section 5 aims to calculate the acceleration of athlete which is compared to the acceleration obtained using a hydrodynamic model (section 5). An evolutionary algorithm opti-

mizes the bungee cord characteristics by minimizing the difference between the two accelerations using two models: a spring model (only the stiffness is given) and a 3-order polynomial function.

2- Ergometer with a sliding footrest and seat complex

A kayak ergometer [B1] was designed using a static frame on which a trolley (i.e. footrest and seat complex) moved back and forth (Fig. 1). An air brake simulated the water drag on the blade. The characteristics (stiffness and damping) of the bungee cord linking the back of the frame with the trolley determined, partially the dynamics of the athlete.

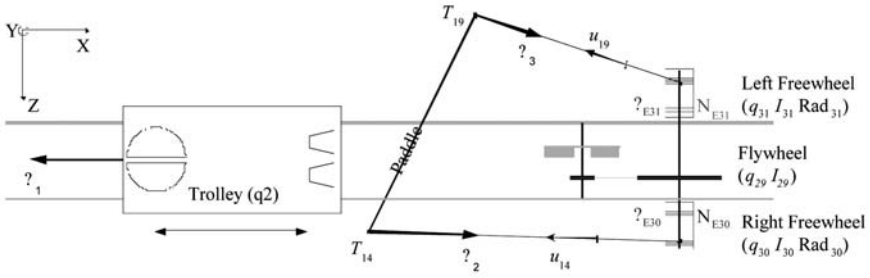

Figure 1 - Schematic diagram and notations of the ergometer with sliding trolley and the air brake (upper view).

3- Ergometer-kayaker model

The model "ergometer-kayak" was implemented under HuMAnS [WB1]. The dynamics was represented as Lagrangian dynamics with Lagrange multipliers for introducing the contacts forces:

$$\mathbf{M(q)\ddot{q} + N(q,\dot{q})\dot{q} + G(q) = \tau + C^T\lambda} \quad (1)$$

where the vector $\mathbf{q}$, $\dot{\mathbf{q}}$ and $\ddot{\mathbf{q}}$ represent the generalized coordinates, their speed and acceleration. $\mathbf{M(q)}$, $\mathbf{N(q,\dot{q})}$ and $\mathbf{G(q)}$ are the inertia matrix, the other inertial nonlinear effects (Coriolis and centrifugal forces) and the gravity effects respectively. The vector τ represents the joint torques and $C^T\lambda$ the contact forces.

The kayaker-paddle-trolley model was composed of 18 bodies (Fig. 2). 22 degrees of freedom (*DoF*) described the kayaker movement ($q_1=[q_1 \ldots q_{22}]^T$). Due to the numerous contacts with the trolley and the paddle, there were two closed-loops. Six additional *DoF* represented the position and orientation of the trolley ($q_2=[q_{23} \ldots q_{28}]^T= [0\ 0\ 0\ q_{26}\ 0\ 0]^T$). On the present ergometer, only the anteroposterior translation of the root could vary. The state of the air brake was given by three extra *DoF* $q_3=[q_{29,\ 30,\ 31}]^T$. Finally, the simulated displacement of the kayaker on water was defined by q_{32}.

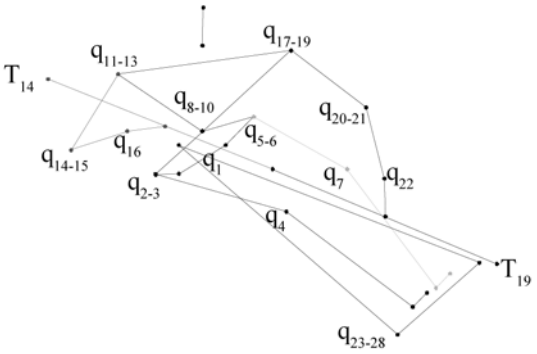

Figure 2 - Schematic diagram of the system "athlete-trolley": q_i represents the degrees of freedom et T_i the tags for describing the segments.

The kinematic tasks have to characterize the performance and the technique of the kayakers. The performance is associated with the paddle kinematics. According to a kinematics analysis of 12 elite kayakers, the main difference was the rotation of the pelvic and scapular girdles (q_1 and q_{10}). These tasks (x) were fitted by Fourier series with one harmonic.

The generalized coordinates of the lower limbs closed-loop were solved by an iterative procedure, based on the Newton-Raphson approach. By inversion of the Jacobian matrix ($J_{i,j}= \partial x_i/q_j$), q were adjusted until satisfying the task equation.

The problem of the upper limbs was solved by introducing a damped pseudo-inverse of J ($J^{+\lambda}$) and an optimization term. The null space of the Jacobian matrix was used to optimize a secondary task by projection of its gradient. The chosen function [F1] kept the joint angles as far as possible to the joint limits. The adjustment of q was expressed by:

$$\Delta q = J^{+\lambda}\Delta x + (1 - J^{+}J)\frac{2\alpha(q_i - \overline{q}_i)}{\Delta q_i^2} \quad (2)$$

where α is the weighting between the first and the second tasks; Δq_i is the range of motion of the joint i and $\overline{q}_i$ its average position.

4- Forward dynamic problem: calculation of q_{26} and q_{32}

The aim of the simulation was to calculate the state of the trolley (q2, q̇2) according to the kayaker movement. The inertia parameters (mass, position of the centre of mass and moment of inertia) of the segments were calculated using the table of de Leva [D1]. The segment length and the mass of the body were measured for each kayaker.

The contact forces of the system "athlete-paddle-trolley" are forces applied on the paddle tips (λ_2 and λ_3) and the tension of the bungee cord linking the trolley to the frame (λ_1). This last force was expressed as a function of the trolley position:

$$\lambda_1 = a_3 q_{26}^3 + a_2 q_{26}^2 + a_1 q_{26} \equiv O_1 \quad (3)$$

or $\lambda_1 = a_1 q_{26} \equiv O_1$

where a_1, a_2, a_3 are the parameters to be determined during the optimization procedure.

According to the mechanism of the air brake described in section 2 (Fig. 1), the paddle tip force comes from the tension of elastic cord, the air brake resistance, the pulley radius and the time derivative of the air brake angular momentum. The time derivatives of the angular momentum of the air brake (δ_{29}, δ_{30} and δ_{31}) were written according three different cases; for example if the shaft is driven by the right pulley the dynamics is:

$$\begin{cases} \delta_{29+30} = (I_{29} + I_{30})\ddot{q}_{30} = \tau_{E_{30}} + \tau_{29} + \dfrac{u^x_{14}}{\mathrm{Rad}_{30}}\lambda_2 \\ \delta_{31} = I_{31}\ddot{q}_{31} = \tau_{E_{31}} + \dfrac{u^x_{19}}{\mathrm{Rad}_{31}}\lambda_3 \end{cases} \quad (4)$$

where I is the inertia of each part (Fig. 1), τ_{29}, τ_{E30} and τ_{E31} are the air brake resistance torque and the torque due to the elastic tension for the right and left pulleys of radius Rad_{30} and Rad_{31} respectively. u^x_{14} and u^x_{19} represent the anteroposterior component of the unit vector of the right and left ropes.

Series of measurements with force and torque transducers and an angular velocity sensor were carried out in order to determine the models. Firstly, the moment generated by the elastic cord (τ_E) was defined as an exponential function of the number of turns around the pulley. The physics of the air brake resistance was defined using a 2-order polynomial function of the flywheel velocity.

The second step is to expressed the pulley acceleration with respect to the known parameters (*i.e.* $\mathbf{q}$, $\dot{\mathbf{q}}$, $\ddot{\mathbf{q}}\mathbf{1}$) and to the unknown parameter ($\ddot{\mathbf{q}}\mathbf{2}$). The acceleration of the right pulley simplified:

$$\ddot{q}_{30} = A_{14} + B_{14}\ddot{\mathbf{q}}\mathbf{2} \quad (5)$$

where A_{14} and B_{14} involved the Jacobian matrix and Hessian vector of the paddle tips.

Booleans (b_{30} and b_{31}) are introduced into Eq. [5] and equivalent equation for the two other cases. Hence the expression of the force applied to the right paddle tip yields:

$$\lambda_2 = \frac{u^x_{14}}{\mathrm{Rad}_{30}}\left((I_{30} + b_{30}I_{29})\ddot{q}_{30} - \tau_{E_{30}} - b_{30}\tau_{29}\right) \quad (6)$$

Substituting for $\ddot{q}_{30}$ the expression of λ_2 simplifies to:

$$\lambda_2 = O_2 + P_2\ddot{\mathbf{q}}\mathbf{2} \quad (7)$$

If we consider then the structure of the vector q: $q=[q_1\ q_2]^T$, we can split the dynamics (Eq. [1]) to exhibit the same structure:

$$\begin{bmatrix} \mathbf{M}_{1,1} & \mathbf{M}_{1,2} \\ \mathbf{M}_{2,1} & \mathbf{M}_{2,2} \end{bmatrix} \begin{pmatrix} \ddot{\mathbf{q}}\mathbf{1} \\ \ddot{\mathbf{q}}\mathbf{2} \end{pmatrix} + \begin{bmatrix} \mathbf{N}_1 \\ \mathbf{N}_2 \end{bmatrix} \begin{pmatrix} \dot{\mathbf{q}}\mathbf{1} \\ \dot{\mathbf{q}}\mathbf{2} \end{pmatrix} + \begin{bmatrix} \mathbf{G}_1 \\ \mathbf{G}_2 \end{bmatrix} = \begin{bmatrix} \boldsymbol{\tau} \\ \mathbf{0} \end{bmatrix} + \begin{bmatrix} \mathbf{C}_1^T \\ \mathbf{C}_2^T \end{bmatrix} \boldsymbol{\lambda} \quad (8)$$

where the joint torques do not appear in the lower part:

$$\begin{bmatrix} \mathbf{M}_{2,1} & \mathbf{M}_{2,2} \end{bmatrix} \begin{pmatrix} \ddot{\mathbf{q}}\mathbf{1} \\ \ddot{\mathbf{q}}\mathbf{2} \end{pmatrix} + \mathbf{N}_2\dot{\mathbf{q}} + \mathbf{G}_2 = \mathbf{C}_2^T\boldsymbol{\lambda} \quad (9)$$

By substituting the contact force by Eq. [4] and Eq. [14], the anteroposterior acceleration of the trolley yields:

$$\ddot{q}_{26} = \frac{O_1 + O_2 + O_3 - \mathbf{N}_2\dot{\mathbf{q}} - \mathbf{G}_2 - \mathbf{M}_{2,1}\ddot{\mathbf{q}}\mathbf{1}}{\mathbf{M}_{2,2} - P_2 - P_3} \quad (10)$$

The acceleration $\ddot{q}_{32}$ of the athlete-paddle-kayak system of mass M was determined using a simple model of drag force $D = 3.5\dot{q}_{32}$ [E1]. Combined with corrected paddle tip forces in the anteroposterior direction, λ_2^* and λ_3^* (the force was considered only if the paddle is in the water using the elevation of the rope), this model gave precise results [B1]. Hence $\ddot{q}_{32}$ is given by:

$$\ddot{q}_{32} = \frac{\lambda_2^* + \lambda_3^* - 3.5\dot{q}_{32}}{M} \quad (11)$$

These ordinary differential equations were solved with root finding (i.e. the three different air brake dynamics) under Scilab.

5. Acceleration comparison

The accelerations of the athlete mass centre on ergometer ($\ddot{c}_E$) and on water ($\ddot{c}_W$) were calculated using analytical Jacobian Matrix and Hessian vector and the expression of the athlete acceleration relative to the trolley ($\ddot{c}_{A/T}$):

$$\begin{aligned} \ddot{c}_{A/T} &= \mathbf{J}(\mathbf{q}^*)\ddot{\mathbf{q}}^* + \mathbf{h}(\mathbf{q}^*, \dot{\mathbf{q}}^*) \\ \ddot{c}_E &= \mathbf{J}(\mathbf{q})\ddot{\mathbf{q}} + \mathbf{h}(\mathbf{q}, \dot{\mathbf{q}}) \\ \ddot{c}_W &= \ddot{c}_{A/T} + \ddot{q}_{32} - \ddot{c}_{A/T} \times \frac{M_A}{M} \end{aligned} \quad (12)$$

where M_A is the subject mass.

where $\ddot{\mathbf{q}}^\star$ is the same kinematics as $\ddot{\mathbf{q}}$ except for the trolley $q_{26} = \dot{q}_{26} = \ddot{q}_{26} = 0$.

The score of the simulation was the root mean square (RMS) difference between the two accelerations for one cycle after the simulation of 30 cycles to obtain a stable dynamics. The parameters of the bungee cord were optimized by minimizing the RMS difference using an evolutionary algorithm.

5- Conclusions

6- Acknowledgments

Dr Mickaël Begon was supported by a grant Lavoisier from Égide – Ministère des Affaires Étrangères. This study was supported by a grant from the Ministère de la Santé, de la Jeunesse et des Sports and the Fédération Française de Canoë-Kayak. The authors wish to acknowledge the kayakers who participated in this study and the developer team of the HuManS toolbox.

7- References

[B1] Begon M. Analyse et simulation tridimensionnelle de mouvement cycliques sur un ergomètre spécifique au kayak. Thèse de doctorat, Université de Poitiers, 2006.
[BC1] Begon M. and Colloud F. A kayak ergometer using a sliding trolley to reproduce accurate on-water mechanical conditions. In Journal of Biomechanics, 40(supplement 2): S439, 2007.
[BS1] Begon M. Sardain P. Simulation of paddling an kayak ergometer. Mathematical modelling in sport (IMA2007 - Manchester 24-26 juin 2007).
[CB1] Colloud F., Bahuaud P., Doriot N., Champely S. and Chèze L. Fixed versus free-floating stretcher mechanism in rowing ergometers: Mechanical aspects. In Journal of Sports Sciences, 24(5): 479—493, 2006.
[D1] De Leva P. Adjustements to Zatsiorsky-Seluyanov's segment inertia parameters. In Journal of Biomechanics, 29(9) : 1223-1230, 1996.
[D2] Dickson M. Master (Honours) thesis, University of Sydney, 2004.
[E1] Eclache J.-P. Le suivi de l'aptitude sur le terrain: application au canoë-kayak. In Bulletin de l'Association Sport Biologie, 3 : 166-169, 1997.
[F1] Fournier A. Génération de mouvements en robotique, application des inverses généralisées et des pseudo-inverses. Thèse d'État, Université de Montpellier, 1980.
[H1] Hawkins D. A new instrumentation system for training rowers. In Journal of Biomechanics, 33: 241-245, 2000.
[WB1] Wieber P.-B., Billet F., Boissieux L. and Pissard-Gibollet R. The HuManS toolbox, a homogeneous framework for motion capture, analysis and simulation. 9th International Symposium on the 3D analysis of human movement. Proceedings of the conference, 2006.

Dynamics of a String-Bed Damper on Tennis Rackets (P175)

Stefan Mohr, Robert Cottey, Daniel Lau, Caroline Gillet, Johan Kotze, Marc Jolly, Ralf Schwenger[1]

Topics: Tennis & other Rackets Sports

Abstract: An analysis of the vibration characteristics of a tennis racket system; frame, string-bed plus damper has been conducted. The influence of how the frequency spectrum is altered by the application of string dampers was investigated. Several experimental setups were used to determine how the vibration profile changed by varying the positioning and weight of the string damper. The vibration characteristics of the string-bed were initially evaluated by comparing vibration responses between frame-excited to string-excited frequency responses. Results show the effect that different damper configurations have on the amplitude and frequency of the vibration modes. The results indicate that string dampers must be tuned to provide optimised damping conditions for individual tennis racket configurations. In conclusion, this work has demonstrated that the damper has effects on the frequency response that go beyond a simple noise reduction or as an aesthetically pleasing addition to the racket.

Keywords: String damper; string-bed; racket; vibration.

1- Introduction

Examination of the vibration modes of a tennis racket frame are common, previous work measuring and describing the modes includes [B1], [B4], [B5], [F1], [BC1] and [C2]. According to other reports the resulting frame vibration amplitudes are often reduced by using soft grip materials [H1] and more effectively by the addition of a hand [B3] and [BC1]. The analysis of string-bed vibration is less well documented, its frequency has been documented by [B3]. There are several references that refer to the function of a device applied to the string-bed with a variety of results; that it is purely psychological [B3], does not significantly reduce the amplitude of the frame [B3], [B2], [WD1] and [SN1], since it only reduces the sound emitted [LK1], [C2], and one study concluded that a material applied to the strings "appreciably reduced the amplitude of the string-bed vibrations, which had an apparent effect on the frame vibrations" [TS1]. Fewer articles were found which investigated the shifting of frequencies; [C1] described

1. Head Sport AG, Wuhrkopfweg 1, A-6921 Kennelbach, Austria - E-mail: s.mohr, r.cottey, d.lau, c.gillet. j.kotze, m.jolly, r.schwenger@head.com

a reduction from 110 to 100 Hz of the fundamental frequency by holding the racket compared to a freely suspended racket. [SD1] show how the fundamental frame frequency is reduced by 1.5 Hz with the addition of a 5 g damper. But to the authors knowledge no previous work has concentrated on how the string-bed frequencies change with the application of a damper. This paper is an introduction into the understanding of the complex mechanics of the string-bed frequencies with the application of dampers with varying mass and location.

2- Experimental Method

The racket used in the testing was a HEAD Microgel Radical Pro; the damper a HEAD Logo Damper; both are shown in Figure 1.

Figure 1 - HEAD Microgel Radical Pro and HEAD Logo Damper.

The racket has a 645 cm^2 head size, a constant beam height of 21 mm and total unstrung weight of 325 g. The racket was strung with a HEAD Ultra Tour (polyester monofilament, 1.2 mm diameter). The string-bed tension corresponded with a Dynamic Tension Value of 35, measured with an ERT300 device. The racket was suspended from a stable fixture with thin nylon threads to allow a free-free vibration analysis. A charge accelerometer was used to measure the vibration response of the frame and was located at the butt of the racket. Acceleration measurements were taken in the direction perpendicular to the surface of the string-bed. An instrumented hammer was used to apply a defined single impulse to the racket. The charge signal from the accelerometer was recorded and analysed in Diadem 9.1 software from National Instruments. Using a Fast Fourier Transformation (FFT) analysis the frequency spectrum of the frame and string-bed modal response were calculated. First an unstrung racket was investigated to identify the frame oscillation modes. The racket was then strung and the test repeated to discover the frequencies of the coupled frame-string-system.

Subsequently a string-bed damper was added and its effect on the spectrum investigated. Finally the optimised weight and location of the damper was determined by a series of experimental setups. To investigate the fundamental dynamics of the tennis racket and string-bed system, a detailed FEM model of a strung HEAD Microgel Radical Pro was constructed. The aim of this model was to calculate the different oscillation

modes shapes. The model contained the frame and string-bed, but did not include the grommet set or grip construction since there influence to the discussed effects are small.

3- Dynamics of the HEAD Radical Pro

3.1 – Frame Excitation Experiments

Figure 2 shows the perpendicular vibration spectra of the frame excitation for the rackets in three states - unstrung (blue curve), strung (violet) and strung with damper (yellow).

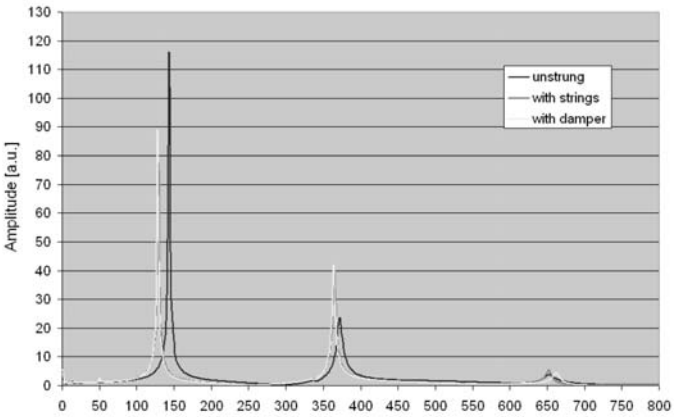

Figure 2 - Spectra HEAD Radical Pro: unstrung, strung and strung with damper.

For the strung and unstrung racket the three major peaks which can be identified as the first three bending modes of the frame. Torsion modes are not visible due to the experimental setup. However, with additional tests the first torsion mode was found to be at 345 Hz, close to the second bending mode. Table 1 summarises the frequencies of the bending modes shown in Figure 2.

Table 1 - Frequencies of the bending modes from the spectra shown in Figure 2. Subscripts b – bending mode, s – string-bed mode.

Racket	f_{b1} [Hz]	f_{b2} [Hz]	f_{b3} [Hz]	f_{s1} [Hz]	f_{s1} [Hz]
unstrung	143	372	665	--	--
strung	129	365	653	723	--
strung + damper	128	364	--	533	660

Stringing the racket has lowered the first and second bending modes by approximately 15 Hz but has little effect on the third mode. Adding the damper to the string-bed has little additional effect on the first and second bending modes, but dramatically changes the mode structure in the frequency domain above 500 Hz.

Applying the excitation impulse to the yoke predominantly excites the frame modes. In Figure 2 all modes except the last peak shown of the strung racket with damper

(yellow curve) are frame modes. The string-bed and other modes are discussed in the next section with the results from a string-bed excited impulse are given. Introducing the excitation impulse directly onto the string-bed the string-bed modes will be revealed, giving a more complete picture of the vibration during a normal ball impact. String excitation is closer to play conditions when the ball strikes the string-bed. The ball impact excites primarily string-bed vibrations which propagate across the string-bed to the frame causing it to be excited. The act of a good damper influences this energy transfer from strings to frame in such a way that no unpleasant sound waves are emitted.

3.2 String Excitation Experiments

Figure 3 shows the vibration mode spectras for the string-bed excitation of the racket in two states - strung and strung with damper.

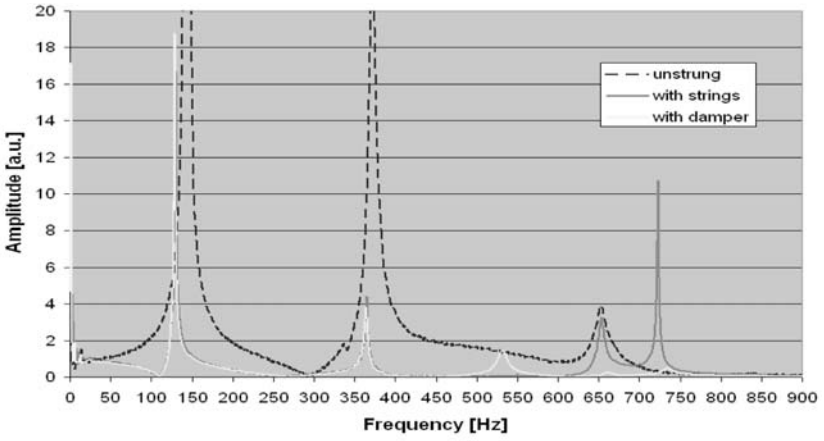

Figure 3 - Spectra with the excitation on the strings. The spectra of the unstrung racket is added for explanatory reasons.

Additionally the unstrung spectrum from Figure 2 has been added to act as reference. Compared to the unstrung racket (blue curve), the strung racket (violet curve) has one new vibration mode at 723 Hz, the first string-bed mode. The shape of this mode can be seen in Figure 5.

Adding the 2.3 g damper to the 15 g heavy string-bed produces a qualitatively different vibration spectrum (yellow curve, Figure 3). In the frequency range from 0 to 500 Hz the strung racket without damper has the same modes as the strung racket with damper, indicating that the damper has little effect on the first two bending modes. In particular there is neither a big change in amplitude nor in the width of the resonance peaks, which is normally associated with a dampening effect or energy dissipation. Figure 4 shows the frequency range above 500 Hz in greater detail.

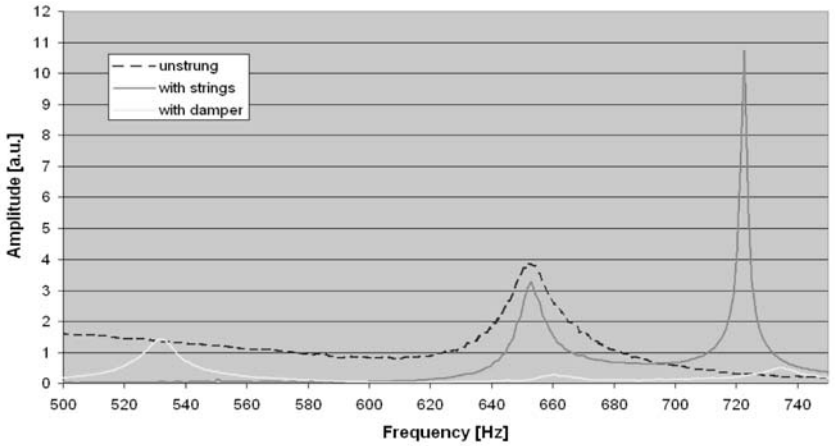

Figure 4 - Spectra with the excitation on the strings, above 500 Hz.

The damper shifts the first string-bed mode to 533 Hz (yellow curve). The frequency peaks at 660 and 736 Hz are the second and third string-bed modes.

It is important to note that the third frame bending mode at 653 Hz was not detectable for the setup with the damper. Overall we find that adding the damper shifts the first string-bed below the third bending mode. The third bending frame mode is nearly terminated, the second and third string-bed modes are shifted from above 900 to 660 respectively 736 Hz. The modes in the spectra of Figure 3 are summarized in Table 2.

Table 2 - Frequencies of the bending modes from the spectra shown in Figure 3. Subscripts b – bending mode, s – string-bed mode.

Racket	f_{b1} [Hz]	f_{b2} [Hz]	f_{b3} [Hz]	f_{s1} [Hz]	f_{s2} [Hz]	f_{s3} [Hz]
unstrung	143	372	653	--	--	--
strung	129	365	653	723	--	--
strung + damper	128	364	--	533	660	736

3.3 Modal Structure of the strung Radical Pro

To verify and visualise the results from the vibration analysis a FEM model of the Radical Pro was developed. All simulations were done with ANSYS. The numerical modal analysis was performed with and without the damper. The simulations reproduced all of the experimentally determined modes and are presented in Figures 5 (without damper) and 6 (with damper). The shapes of the modes and how they are modified when the damper is applied are discussed later. The modes for the strung racket without damper are shown in Figure 5 and presented in ascending frequencies.

Figure 6 shows the frequency spectra with the addition of the damper, indicating that the first string-bed mode has shifted to below the third frame bending mode. The second and third string-bed modes are now below 900, at 660 and 736 Hz respectively.

The FEM simulations show that there is little difference for the strung frame with and without damper for the first and second bending modes and the first torsion mode. These modes are not modified due to the small mass of the dampener; a 2.3g damper is less than 1% of the racket mass. However this is not the case for the first and second string-bed and the third frame bending mode which are modified significantly when a dampener is added. In particular the node line of the second string-bed is changed dramatically from the centre of the string-bed without the damper (Figure 5.f) to close to the yoke (Figure 6.f) with the damper.

The node of the third string-bed mode is unchanged as the damper is located right at the node line (see Figures 5.g and 6.g).

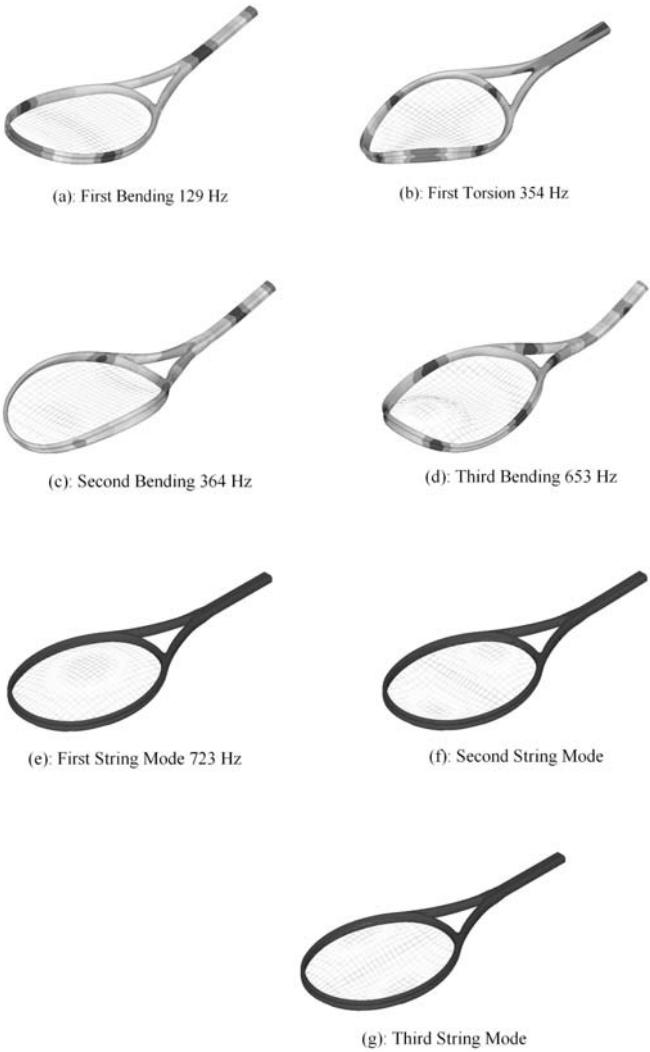

Figure 5 - Vibration Modes of the strung HEAD Microgel Radical Pro without damper below 900 Hz.

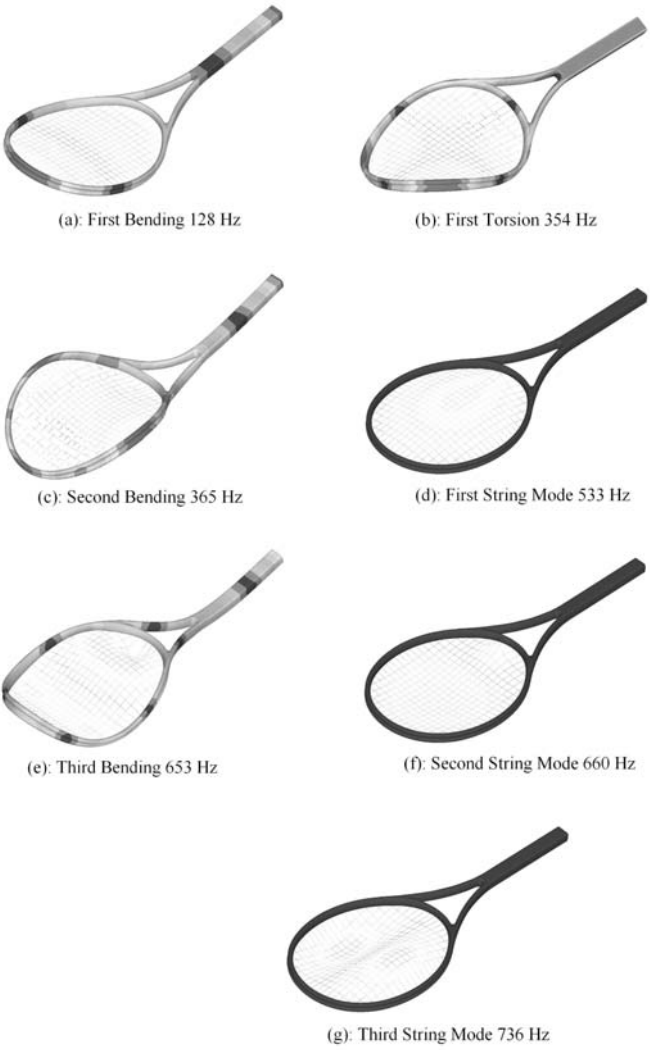

Figure 6 - Vibration Modes of the strung HEAD Microgel Radical Pro with damper below 900 Hz.

4- String damper optimisation

The previous results show the effect the string-bed and damper have on the racket vibration spectra. In this section we explore how the damper can be optimised. Since adding a damper adds mass at a certain position in the string-bed, we carried out two further experimental series investigating how to optimise the damping effect by varying these two parameter (mass and position).

4.1 – Position-Optimisation

The strung Radical Pro was equipped with a basic HEAD Logo Damper; its location was changed from 0 cm (touching the yoke) to 2.5 cm which is its normal positioning (touching the first cross string). From one measurement to the other the position of the damper was chanced by 0.5 cm.

The excitation impulse was applied to the string-bed as before. Figure 7 shows these results.

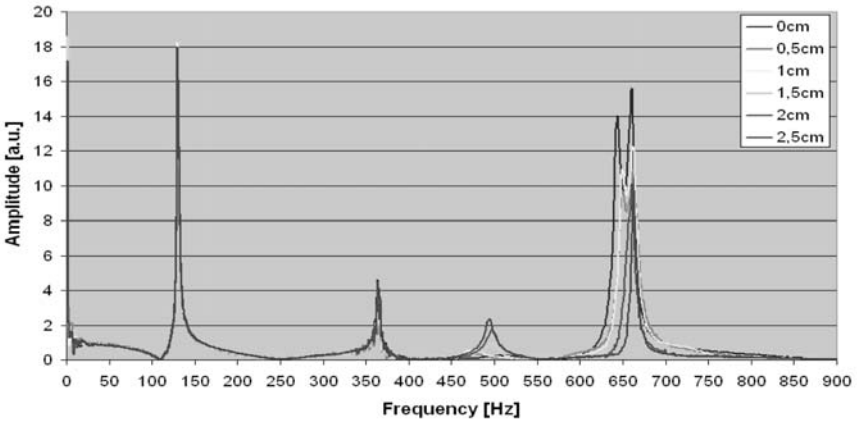

Figure 7 - FFT-Spectra of the strung HEAD Microgel Radical Pro with a HEAD Logo Damper applied at different positions from the yoke. Frequency range from 0 to 900 Hz.

The spectra presented in Figure 7 show that the damper and its position has almost no effect on the first and second bending modes. Figure 8 shows the results magnified over the frequency range 400 to 800 Hz.

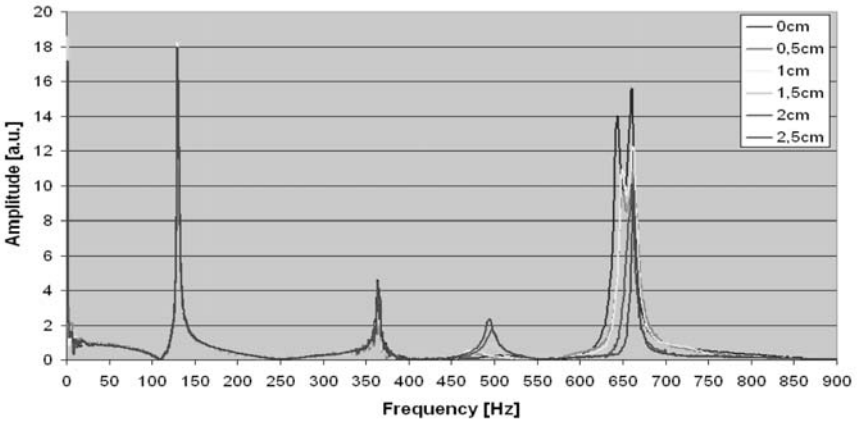

Figure 8 - FFT-Spectra of the strung HEAD Microgel Radical Pro with a full HEAD Logo dampers applied at different positions from the yoke. Frequency range from 400 to 800 Hz.

The audible "ping" can be heard with the damper positioned next to the yoke (0 cm) indicating that the "ping" is associated with the third racket bending mode (see blue curve). As the damper is positioned with greater distance from the yoke the "ping" is reduced and the sound changes to what could be described as more "solid". Figure 8 shows this change of sound with the reduction of the third frame bending peak. Moving the damper away from the yoke increases the amplitude of the first string-bed peak at approximately 500 Hz. The third peak visible in Figure 8 is identified as the second string-bed mode, its amplitude decreases to a minimum with the damper location at 1.5 cm. Acoustically there is little effect on the audible sound with the change of the damper from 1.5 to 2 cm. This indicates that the second string-bed bending frequency is not important acoustically, but once again that the main acoustic function of the damper is in the elimination of the third frame bending mode. These tests conclude that, for this setup, the 2.3 g HEAD Logo Damper should be located further than 1.5 cm away from the yoke.

4.2 Mass-Optimisation

In this final experimental section we vary the mass of the damper applied at a constant distance of 2.5 cm. The full HEAD Logo damper weighs 2.3 g. Lead was added to the damper to increase the weight up to 3.2 g, and for weights below 2.3 g, small pieces of the rubber material were removed with a knife. The results are shown in the Figures 9 and 10. Figure 9 shows once more that the frequency peaks below 400 Hz are not affected by adding the damper.

The main effect identified when the damper mass is increased is the frequency shift of the first string-bed mode from high to low on the scale (550 to 470 Hz). If the damper mass is greater than 1.7 g the third frame bending mode vanishes. This indicates that an efficient string damper at a position of 2.5 cm should have a minimum mass of 1.7 g. A greater mass still shifts the first string-bed mode to lower frequencies but has no additional sound effect, since the third bending mode has already disappeared.

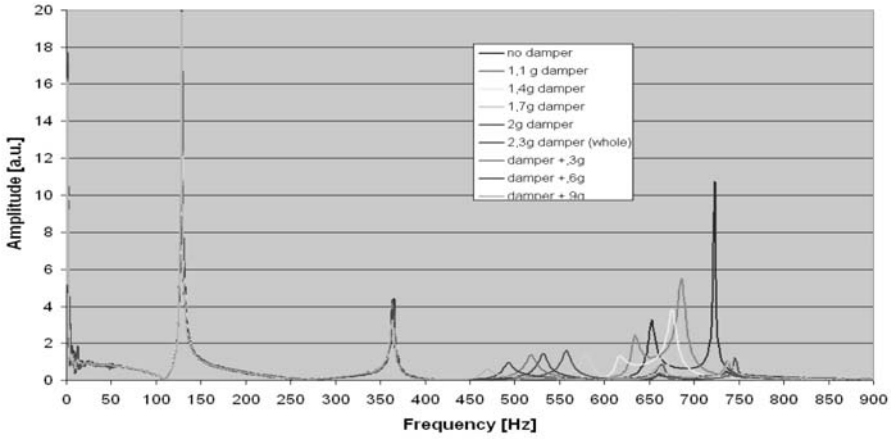

Figure 9 - FFT-Spectra of the strung HEAD Microgel Radical Pro with dampers of different mass. Frequency range from 0 to 900 Hz.

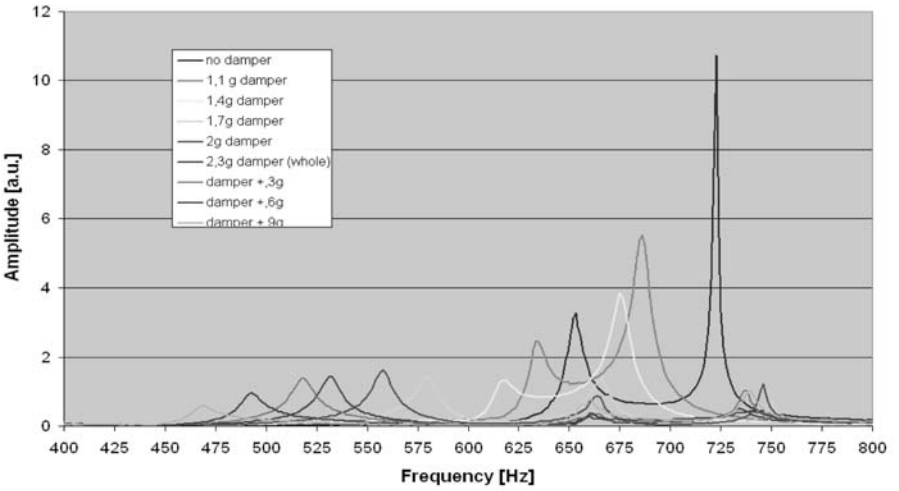

Figure 10 - FFT-Spectra of the strung HEAD Microgel Radical Pro with dampers of different mass. Frequency range from 400 to 800 Hz.

4- Summary, Conclusions

The terminology damper is misleading. A simple commercial string damper like the HEAD Logo damper is not damping any modes of a strung tennis racket in the sense of adding friction or energy dissipation. Dampers on tennis rackets due not modify the first three bending modes of frame significantly. Dampers act like string-bed mode shifters. It has been demonstrated that they have a huge effect on the shape and frequency of the string-bed modes.

In the work presented in this paper it was shown that the strung HEAD Microgel Radical Pro would emit an undesirable "ping" sound with the excitation of the third frame bending frequency. If the first string-bed, which is excited by the ball and string-bed contact, is close to the third frame bending mode this "ping" sound occurs. The damper shifts the first string-bed mode to a frequency below this mode, leaving the third bending mode barely visible in the vibration spectra. The first string-bed mode is shifted from 723 Hz into the region between 500 and 550 Hz, a move of more than 150 Hz to a frequency range where no sound active modes are present. This is the fundamental mechanism of the damper presented in this study. Since the mechanism has been shown to have little to do with energy dissipation, the fundamental design parameter for these dampers are mass and the intended position on the string-bed. The material of the damper has only a minor effect in the system.

In the case of the HEAD Microgel Radical Pro used in this study, the design of an optimum damper should be that it has a minimum mass of 1.7 g and must be positioned further than 1.5 cm away from the yoke. Generally there would be no ideal universal damper that would work perfectly for all racket, string and string tension combinations. A good damper must be engineered for the racket and string set-up it will be used in. The designer must be aware of the modal structure of the system as a whole, as the

damper primary function is mode shifting and not as previously thought providing energy dissipation.

5- References

[B1] Brody H. Physics of the tennis racket II: The "sweet spot". American Journal of Physics. 49(9), 816-819, 1981.
[B2] Brody H. Vibration Damping of Tennis Rackets. International Journal of Sport Biomechanics, 5, 451-456, 1989.
[B3] Brody H. How would a physicist design a tennis racket? Physics Today. March, 26-31, 1995.
[B4] Brody H. The modern tennis racket. Proceedings of the 1st International Conference on the Engineering of Sport, Sheffield UK. Edited by S.Haake. Published by A.Balkema, Rotterdam. pp.79-82, 1996.
[B5] Brody H. Physics of tennis. III. The ball-racket interaction. American Journal of Physics. 65(10), 981-987, 1997.
[BC1] Brody H., Cross R., & Lindsey C. The physics and technology of tennis. Published by USRSA, 2002.
[C1] Cross R. The dead spot of a tennis racket. Am. J. Phys. 65(8), 754-764, 1997.
[C2] Cross R. Properties of tennis equipment: balls that bite, rackets that don't vibrate and strings don't make any difference. Proceedings of the 2nd International Conference: Tennis Science and Technology. Edited by S.Miller. Published by International Tennis Federation, London, UK, 2003.
[H1] Hatze H. The effectiveness of grip bands in reducing racquet vibration transfer and slipping. Med. Sci. Sports Exerc,. 24(2), 226-230, 1992.
[LK1] Lammer H. & Kotze J. Materials and tennis rackets. Materials in sports equipment, Woodhead Publishing Limited, Cambridge, UK. Edited by M Jenkins, Chapter 9. pp. 222-248, 2003.
[SD1] Spurr J. & Downing M. Good vibrations: the effect of fundamental frequency on tennis racket power. Tennis Science and Technology 3. Pub. ITF, Roehampton, 2007
[SN1] Stroede C., Noble L. and Walker H. The effect of tennis racket string vibration dampers on racket handle vibrations and discomfort following impacts. Journal of Sports Science, 17, 379-385, 1999.
[TS1] Tomosue R., Sugiyama K., Yoshinari K., Yamamoto K. The effectiveness of damping material in reducing impact shock in the tennis forehand drive, Science and Racket Sports, Edited by T. Reilly, M. Hughes and A. Lees, 140-145, 1995.
[F1] Fairley T E. Some measurements of tennis racket vibration and its transmission to the hand. United Kingdom Informal Group Meeting on Human Response to Vibration, Derby, UK, 1985.
[WD1] Wilson J F., and Davis J.S. Tennis racket shock mitigation experiments. Journal of Biomechanical Engineering. 117, 479-484, 1995.

Second Lives for the Third Age: Using Virtual Worlds to Encourage Exercise Participation in Older People (P176)

Ben Heller[1], Jonathan S. Wheat[1], Sue Mawson[2], Peter Wright[3]

Topics: Reality & Computer application in Sports, Fitness.
Abstract: Falls are associated with considerable morbidity, mortality and cost to society and health services every year. Falling is most common in older people, with accident and emergency admissions in the UK ranging from 2.7% per year for ages 60-64 up to 9.5% for the over 75s. There is strong evidence that balance-retraining exercises can be of significant benefit. Recovery and long term maintenance of balance are strongly influenced by the regularity, task-specificity and volume of training. Resource constraints require the great majority of this training to take place outside the health-care system. In motivated patients treatment may be effective; however, in other cases, patients may lose interest in performing repetitive tasks and may not complete the therapy programme.

There is growing interest in the use of computer-games as a rewarding activity to motivate patients to practise rehabilitation skills, but most computer games are not designed, and may not be appropriate, for an over-75 age-group. We have interfaced low-cost balance-measurement platforms to a computer to allow older people to control "avatars"; (3D mannequins) dancing in a 3D simulated environment. We chose dance as it is an age-appropriate, single or multiple-participant activity. The movements required to control the avatars were based-on balance rehabilitation exercises.

We piloted the system with 6 older people (ages 80-91) undertaking exercise classes for balance rehabilitation. Although the cohort had no previous computer-experience and represented a wide-range of physical abilities, they were all able to control basic avatar movements, with some participants able to control a rich-set of dance movements after only a few minutes practice. All participants enjoyed the experience.

It appears that older people are able to enjoy interaction with virtual environments, and this, together with appropriate sensors, may be a useful mechanism to motivate exercise in this age group.
Keywords: Balance, computer games, virtual worlds.

1. Sports Engineering Research Group Sheffield Hallam University, Sheffield UK - E-mail : { b.heller, j.wheat}@shu.ac.uk
2. Centre for Health and Social Care Research Sheffield Hallam University, Sheffield UK.
3. Art and Design Research Centre Sheffield Hallam University, Sheffield UK TOPICS: Reality & Computer application in Sports, Fitness.

1- Introduction

1.1 Falls

There is an age-related decline in sensorimotor performance (Stelmach and Worringham, 1985), this contributes to an increased likelihood of falling with age (Rubenstein and Josephson 2002). Falls are the leading cause of injury-related hospitalisation in an older population (Baker and Harvey, 1985) with accident and emergency admissions ranging from 2.7% per year for ages 60-64 up to 9.5% for the over 75s (Scuffham *et al.*, 2003); this costs the UK government £981 million per year with most of the costs arising from over-75s. As well as the direct physical consequences of a fall, fear-of-falling leads to additional limitation of activity (Tinetti *et al.*, 1988). Falls cause significant loss of autonomy and independence, affecting not only the individuals concerned, but the health care system, carers and the broader community. Affected individuals include the independent-living, 'well-elderly', as well as the 'frail elderly' (Morley, 2002).

It has been demonstrated that targeted rehabilitation through active participation and engagement in contextually-appropriate repetitive and intensive movements as part of an exercise programme (e.g. the Otago programme) can promote recovery (Campbell *et al.*, 1997). However, these exercises are typically completed individually at home and can be tedious, which can lead to problems with motivation. There is evidence that programmes are only effective with good compliance (Campbell *et al.*, 2005).

1.2 Virtual Rehabilitation

It has been suggested that computer games and virtual reality (virtual rehabilitation) are a suitable way to make rehabilitation exercises more engaging. Betker *et al.* developed 3 simple video games for a balance-training system(Betker *et al.*, 2006); their results with three adult (one young and two middle-aged) subjects show that the video games were effective in increasing practice time, and hence improving balance. NeuroCom offer 3 games (Puzzle Master™, NeuroPong™ and Solitaire) as options for the commercial Balance-Master and Equitest Force plate systems (Neurocom 2008). Some additional applications of computer games for balance rehabilitation are reported by Sveistrup (2004). Advantages of virtual rehabilitation include the ability to simulate challenging but safe and ecologically valid environments, whist maintaining experimental control. Additionally, environments and scenarios can be customised for individual clients, and progressively altered as function is regained or lost (Weiss *et al.*, 2004).

Although these computer games may improve engagement for younger participants, they may not be suitable for the older people most at risk of falling who typically will not have been previously exposed to computers.

1.3 Virtual worlds

A **virtual world** (also sometimes known as a metaverse) is a computer-based simulated environment intended for its users to inhabit and interact via **avatars** (a user's representation of himself or herself, in the form of a three-dimensional model). Two of the best

known virtual worlds are *Second Life* (Linden Labs) and *World of Warcraft* (Blizard). Virtual worlds allow users to interact with each other and the world. Some, such as Second Life, allow significant customisation of the environment and avatar appearance and capabilities.

Because of their ability to model the real world in a very rich and expandable way, there is some inherent familiarity in the environments and scenarios presented; hence virtual worlds may provide suitable virtual environments and virtual activities for older people to explore. Additional benefits include the ability to interact and socialise with other avatars, both human and machine-controlled.

Control of avatars in virtual worlds is most commonly achieved by traditional computer input methods (mouse and keyboard). This may be non-intuitive for older users without significant computing experience, or may be impossible for those lacking fine motor control.

1.4 Motion sensors

As an alternative to traditional computer input methods, it may be advantageous to identify a user's physical movements and use them to control similar avatar movements in an intuitive manner; this may lead to a much deeper engagement in the virtual environment (Weiss *et al.*, 2004). Options for motion capture are traditional marker-based systems, or easier to use but less accurate, markerless systems. As an alternative to kinematic motion capture, we propose using force platform data with algorithms to detect the centre-of-pressure patterns corresponding to a limited set of user movements, and using these to control avatar movement. This provides a considerable advantage of ease-of-use, as no markers or cameras are required. Additionally it allows direct measurement of balance parameters. Rather than directly replicating user movements in the virtual space, using detection of user movements to trigger pre-programmed avatar movement sequences breaks the one-to-one link between user motion and avatar motion. This permits users with limited motor ability to activate complex avatar movements.

1.5 Dance as a Rehabilitation Paradigm

There is growing interest in training patients with tai-chi-style exercises for their positive effect on balance(Li *et al.*,2005). However, tai-chi may not be culturally appropriate for an older European population. Dance is a popular social and exercise activity for older people, and there is some evidence that it may improve balance in this population (Shigematsu *et al.*,2002). Hence we have chosen to explore the use of virtual dance as a rehabilitation activity. There have been some intriguing implementations of dance in virtual worlds (Gras 2007); typically, the dance movements are pre-programmed, motion captured sequences, triggered by mouse or keyboard. For more intuitive user control, we propose using motion sensing to detect user movements and use these to trigger pre-recorded dance sequences.

1.6 Second Lives for the Third Age

We propose a convergence of virtual worlds and sensor technology to control avatar movements (specifically dance movements) in a virtual world. We term this *Second Lives for the Third Age*. Potential benefits of this approach for rehabilitation include:

1.6.1 Engagement/motivation

Environments and activities in the virtual world may be chosen from a limitless range to suit the user's abilities and interests. These may be very task specific (e.g. walking in a complex visual environment such as a supermarket), or fantasy (such as walking on a tight-rope across Niagara Falls). No matter how challenging the activities, they will all be inherently safe.

1.6.2 Non-one-to-one mapping

As user movements trigger, rather than directly control avatar movements, the mapping can be changed, this allows

- **Progression**: as the user's abilities changes, the mapping between user and avatar movements can be adjusted to maintain the rehabilitation stimulus.
- **Universal access**: users with varying abilities (from severely disabled to fully able-bodied) can interact equally in the virtual space.

1.6.3 Virtual performance

A fixed period of rehabilitation (e.g. 12 weeks) can be used to develop a performance in the virtual world that, as culmination of the rehabilitation programme, can be enacted to friends and family, and potentially to millions of users within the virtual world. This may provide a strong structure and focus to the rehabilitation programme.

1.6.4 Socialisation

Limited mobility due to physical frailty and fear of falling can lead to social isolation. The use of virtual worlds allows these users to interact (and dance with) other users, friends and family.

1.6.5 Inherent monitoring of performance

The user's performance (e.g. balance parameters) is inherently measured and can be automatically transmitted to a therapist or stored for later download. It may also be analysed on-line to detect any changes which might require notification of health-care professionals, such as sudden deterioration of balance.

2 - Pilot study

We conducted a small pilot study as a demonstration of principle and to assess how users in the target age group (75+) interacted with a virtual environment.

2.1 Methods

2.1.1 System design

Several dance movements were captured using a Motion Analysis Corporation motion capture system with a full body marker set. The selected movements comprised walking forwards, backwards and to either side, jumping, spinning and kicking. The motion capture files were processed and converted to *.htr* (hierarchical translations and rotations) format.

Low-cost, bilateral force platforms were developed by modifying the 4 load-cell outputs from commercial weighing (bathroom) scales, mounted on a wooden platform to prevent toppling and to allow adjustment of separation (Fig. 1). The amplified outputs from up to 4 sets of 2 platforms were recorded using a 32 channel A/D converter (NI USB-6229, National Instruments).

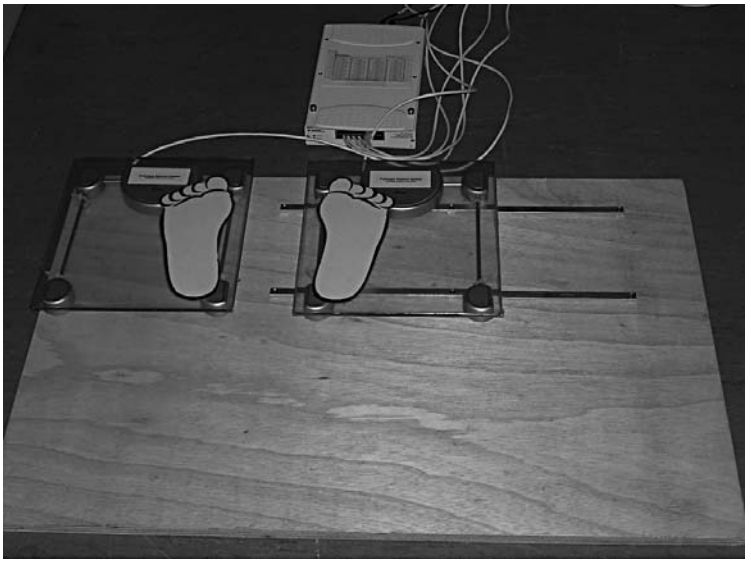

Figure 1 - One pair of modified weighing scales and data collection device.

A simple, proof-of-principle, self-contained virtual environment was developed in Microsoft Visual Studio 2005, using the DirectX graphics library. We based the avatar features on a 3D laser-scan of a human head. The environment is shown in figure 2. In use, the centre of pressure (COP) range-of-motion for each user was calibrated; after this, algorithms detected the characteristic COP pattern of various movements, and triggered the appropriate dance sequences. Leaning in a particular direction (a translation of the COP) caused the avatar to walk in the same direction. A bend of the knees (which was detected as a fall in total vertical load below and then a rise above bodyweight) triggered an avatar jump; a lateral tap of one foot caused the avatar to kick on the same side, rising on to the toe of one foot triggered a spin away from that side.

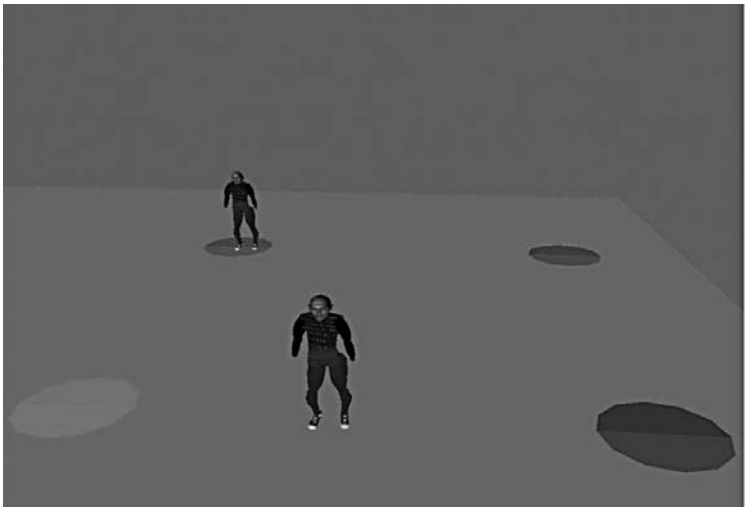

Figure 2 -The virtual environment with 2 avatars present (the users see the avatars from behind). The circles are targets for the tests (see text).

By combining these simple primitive movements, a crude 'Texas Line Dance' style dance could be performed.. This style of dance was chosen as it allowed the avatar to always face in the same direction (away from the user). We hypothesised that this would make control of direction more intuitive – i.e. a weight-shift to the right would cause the avatar to move to the right on the screen.

2.1.2 Participants

Following local ethical committee approval, the system was piloted with 6 women (ages 80-91, mean 86.2) who had a previous history of falling and were currently undertaking exercise classes for balance rehabilitation. No-one in this cohort had any previous computer experience.

2.1. 3 Testing

Each participant was allowed approximately 10 minutes of familiarisation with the system on day one and then tested on their ability to control avatar movements (following a short re-familiarisation) 7 days later. Testing consisted of:

1. Basic control – navigating the avatar between a series of 4 targets arranged in a square pattern (see Fig. 2).
2. Advanced control – as above, but performing a different action on each target (kick, spin, jump).

The time to completion for each test was measured for each participant. If a participant couldn't complete a particular task within 60s, they were asked to move-on to the subsequent task. Results are given in table 1.

Participant	Age	Time to complete simple task (s)	Time to complete complex task (s)	jump	spin	kick
1	80	205	318	2	0	1
2	91	85	117	2	2	2
3	88	66	225	2	1	1
4	82	143	328	2	0	1
5	85	52	163	2	2	2
6	91	55	170	2	1	2
mean	**86.2**	**101.0**	**220.2**	**2.0**	**1.0**	**1.5**

Table 1 - Times to complete tasks. For jump, spin and kick a score of 2 means task completed without assistance, 1 = assistance was required, 0 = task could not be completed.

2.2 Results and Discussion

The results in table 1 show that all participants were able to control basic avatar movements (left, right, forwards, backwards). There was a range of abilities present, as evidenced by the almost four-fold difference in timing to complete the task between the fastest and the slowest participants. It should be noted that as none of these participants had any previous computing experience, concepts of mapping physical movements to screen movements that might be second-nature to someone familiar with mice or joysticks presented some difficulties

The more complex tasks again highlighted a range of performances within the group. Of all these tasks, jumping was the most reliably performed, the kick was intermediate and the spin was the least reliably performed. It is interesting to speculate that the jump was the most natural mapping (a rapid bend of the knees as in a jump countermovement); the spin was the least intuitive, involving transferring weight onto the toes of just one foot. In future work we would like to include motion sensing to allow actual trunk rotation to trigger a spin, it is not possible to detect this purely from force-platform data. A longer period of familiarisation may well have helped the participants who were having difficulties in completing the tasks. Incorrectly placed feet often led to difficulty in performing an action; more advanced sensors, such as detection of cop relative to actual foot position or a camera view of their foot position might be helpful.

Although we didn't formally collect data on the user-experience, all the participants reported that they enjoyed using the system and that they would like to repeat the experience.

3- Conclusions and Further Work

The primary purpose of this work was to determine if older people were able to successfully interact with a dance simulation in a virtual environment. Our participants, representing a range of physical and cognitive abilities, were all able to do this, albeit to varying extents.

Further works will involve:

1. Introducing more sensors, to allow collection of a wider range of movements.
2. Using a richer virtual environment, possibly Second Life or an equivalent.

3. Exploration of the interaction between remote multiple participants (including able-bodied participants).
4. Conducting a larger-scale study to look at clinical impact.

4- References

[BH1] Baker SP, Harvey AH. Fall injuries in the elderly. Clin Geriatr Med.;1:501–512, 1985

[BS1] Betker AL, Szturm T, Moussavi, ZK, Nett C, "Video Game–Based Exercises for Balance Rehabilitation: A Single-Subject Design". Arch Phys Med Rehabil Vol 87, 2006

[CR1] Campbell AJ, Robertson MC, Gardner MM, Norton RN, Tilyard MW, Buchner DM.. Randomised controlled trial of a general practice programme of home based exercise to prevent falls in elderly women BMJ;315:1065-1069, 1997

[CR2] Campbell, A J., Robertson, M C., La Grow, S. J, Kerse, N. M, Sanderson, G. F, Jacobs, R. J, Sharp, D. M, Hale, L. A, Randomised controlled trial of prevention of falls in people aged 75 with severe visual impairment: the VIP trial BMJ 331: 817, 2005

[G1] Ricard Gras – Duel http://www.machinima.com/film/view&id=14779 2007

[LH1] Li F, Harmer P, Fisher KJ, McAuley E, Chaumeton N, Eckstrom E, Wilson NL. Tai Chi and fall reductions in older adults: a randomized controlled trial. Journal of Gerontology: MEDICAL SCIENCES, Vol. 60A(2), 187–194 2005

[M1] Morley JE. A fall is a major event in the life of an older person. J Gerontol A Biol Sci Med Sci.;57:M492–M495, 2002

[NC1] NeuroGames, NeuroCom International, Official website: www.onbalance.com/neurocom/products/NeuroGames.aspx

[RJ1] Rubenstein LZ, Josephson KR. The epidemiology of falls and syncope. Clin Geriatr Med., 18:141–158, 2002

[S1] Sveistrup H. Motor rehabilitation using virtual reality. Journal of NeuroEngineering and Rehabilitation 1:10 1-8, 2004

[SC1] Scuffham P, Chaplin S, Legood R Incidence and costs of unintentional falls in older people in the United Kingdom J. Epidemiol. Community Health, 57: 740-4. 2003

[SC2] Shigematsu R, Chang M, Yabushita N, Sakai T, Nakagaichi M, Nho H, Tanaka K. Dance-based aerobic exercise may improve indices of falling risk in older women. Age and Ageing, 31 (4) 261 -6, 2002

[SW1] Stelmach GE, Worringham CJ. Sensorimotor deficits related to postural stability: implications for falling in the elderly. Clin Geriatr Med.;1:679–694. 1985

[TS1] Tinetti ME, Speechley M, Ginter SF. Risk factors for falls among elderly persons living in the community. N Engl J Med. 319:1701–1707, 1988

[WR1] Weiss PL, Rand D, Katz N, Kizony R, Video capture virtual reality as a flexible and effective rehabilitation tool. Journal of NeuroEngineering and Rehabilitation, 1:12, 2004

Design of an Ice Hockey Stick Test Machine (P178)

Matthew McQueen[1], John McPhee[2]

Topics: Hockey stick testing machine, design, sports engineering.
Abstract: With the introduction of one-piece composite ice hockey sticks in the early 21st century, renewed attention has been drawn to hockey stick design, specifically with respect to durability. While one-piece composite ice hockey sticks have provided a performance upgrade over their wood and aluminum predecessors, at least anecdotally, these sticks break far more frequently — very frequently during the slapshot. The failure occurs either at the connection between the blade and shaft or along the shaft itself, due to the large bending loads during the shot. The objective of this work is to create a system that dynamically tests hockey sticks in a repeatable manner to reduce the experiment variability associated with human testing. A motion analysis of the slapshot by an experienced player reveals that the motion of the stick is mainly two-dimensional during the period when it is subjected to large bending loads by the ice surface. Based on this, we synthesize a four-bar mechanism with a coupler curve that matches the required stick trajectory. A literature and patent search confirms this machine as an original design.
Key words: Hockey, Stick, Slapshot, Testing, Machine Design.

1- Introduction

With the adoption of one-piece composite ice hockey sticks over the last decade, attention has been drawn to their design, specifically with respect to durability. While composite sticks have provided a performance upgrade over their wood and aluminum predecessors, at least anecdotally (Stefanyshyn and Worobets, 2006), these sticks are breaking far more frequently, either due to slashing or shooting. The slash occurs between the blade and the lower hand, causing the shaft to break (Villasenor *et al.*, 2006). The other failure mode is during a slapshot, when the stick breaks due to the large 3-point bending loads that arise.

In golf, robots are used to test clubs and balls in a highly controlled and repeatable manner. We have not found a similar machine for the hockey slapshot, probably because of the added complexity of having the hands separated by some distance on the shaft.

1. Mechanical Engineering, University of Waterloo, Ontario, Canada N2L 3G1 Phone: 1-403-680-6359 Fax: 1-403-485-6870 - E-mail: matthew.mcqueen@gmail.com
2. Systems Design Engineering, University of Waterloo, Ontario, Canada N2L 3G1 - Phone: 1-519-888-6491 - Fax: 1-519-746-4791 - E-mail: mcphee@real.uwaterloo.ca

This hand separation, combined with the blade hitting the ice well before contact with a puck, is what gives rise to the large 3-point bending loads.

To design a machine that will execute a slapshot, we first collected motion analysis data for a high-calibre hockey player. We tracked the 3-dimensional motion of the two hands on the shaft, which showed that the shaft trajectory is approximately planar from the time the stick hits the ice, to the time that the puck leaves the blade. With this result, and using kinematic analysis software, we synthesized a four-bar mechanism that generated an appropriate coupler curve for the shaft. We then simulated the full robot using multibody dynamics software, to determine the size of the motors required to drive a slapshot, and the resulting reaction forces in the robot joints. A tabletop prototype of the machine was built, and initial results meet our expectations.

The paper is structured as follows. The criteria for a successful design are given in the next section, along with the constraints on the final machine design. Section 3 provides the motion analysis results from actual slapshots, while the kinematic synthesis of a suitable machine is presented in Section 4. The final design and prototype are described in Section 5, followed by our conclusions.

2- Design Criteria and Constraints

As with any machine design problem, we begin with a statement of the design criteria and constraints.

2.1 Criteria

A successful solution to our machine design problem should satisfy the following criteria:

- Replicates human slapshot in a repeatable manner
- Portable within a single facility
- Cost not prohibitive for academia or amateur organizations
- Ability to be used indoors

Portability within single facility refers to the desire for the machine to move from one area to another area within a single facility. Limiting the cost of the machine will allow amateur organizations, whose budget is not as large as hockey stick manufacturers, to purchase the system to do their own equipment performance testing. Finally, it is important that the machine be able to be used indoors, in standard lab setting, with a 3.05 m ceiling.

2.2 Constraints

Hard constraints on our machine design include the following:

- Base footprint of 122 cm x 122 cm or less
- Mass less than 70 kg
- Safe high speed camera mounting position
- Strain gauges are easily mountable in testing areas of interest

Limiting the machine to a 122 cm × 122 cm base footprint will allow it to be easily moved on a pallet. Specifying a maximum mass of 70 kg allows the machine to be moved by two or three people onto a pallet, again making the system more portable. The mass of this system is also representative of a lightweight hockey player and, in combination with the 122 cm × 122 cm base footprint, will ensure the system will not roll over. Finally, since this machine does not conduct any specific testing itself, it is important that any data collection equipment the user may want to use, such as high speed cameras and strain gauges on the hockey stick, are mountable on or near the stick in easy and safe locations.

3- Motion Analysis of Hockey Slapshot

To determine the motion followed by the hands and stick during a slap shot, an OptoTrak motion capture system was used to collect experimental data. 19 slap-shots were taken by a highly-proficient amateur hockey player, the first 12 at 30 Hz, with the remaining 7 at 166 Hz. Refer to figure 1 for a photo of the test apparatus. The OptoTrak system outputted the x, y, z, and t coordinates for each sensor into a text file that was then read into Microsoft Excel and Matlab for further analysis.

Figure 1 - Test apparatus.

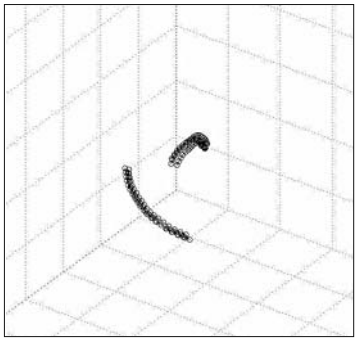

Figure 2 - Isometric view of hand. markers.

The first step in the analysis of the data was to determine the time phase of interest. Since the objective of this machine is to recreate the stick bending, the back swing and follow through zones are not as important. The contact time zone, from when the stick contacts the ice to the time the puck is released, is the phase of interest.

Using six markers on the hands (three on the top hand, three on the bottom hand), a three-dimensional plot of their positions versus time was generated. Refer to figure 2. This plot, in combination with high-speed video, was used to understand the movement of the hands that is to be reproduced by the designed mechanism.

4- Kinematic Synthesis of Hockey Slapshot Mechanism

From an examination of the experimental data, it seemed that the motion of the stick was two-dimensional during the contact time zone. To test out this hypothesis, we calculated the three Cartesian components (*a,b,c*) of the vector between the two hands at each time step, as shown in equation (1). We then calculated the vector from the lower hand at one time frame to its position at the next frame. The unit vector normal to these two vectors, computed in equations (3-4), defines the plane in which the stick is moving at a given time. This vector was nearly constant during the contact time zone, in confirmation of our hypothesis.

$$\vec{V}_1 = (a_1, b_1, c_1) = (x_{1,1}, y_{1,1}, z_{1,1}) - (x_{2,1}, y_{2,1}, z_{2,1}) \quad (1)$$

$$\vec{V}_2 = (a_2, b_2, c_2) = (x_{2,0}, y_{2,0}, z_{2,0}) - (x_{2,1}, y_{2,1}, z_{2,1}) \quad (2)$$

$$\vec{n} = \vec{V}_1 x \vec{V}_2 \quad (3)$$

$$\hat{n} = \frac{\vec{n}}{|\vec{n}|} \quad (4)$$

$$\theta = \cos^{-1}\left[\frac{\hat{n}_{avg} \cdot \hat{n}_k}{|\hat{n}_{avg}||\hat{n}_k|}\right] \quad (5)$$

The average $\hat{n}_{avg}$ value of the unit normal vector was calculated and used in equation (5) to compute an angle of 35º between the average plane of motion and the vertical axis ($\hat{n}_k$), which is consistent with the measured angle of 36º between the blade and the shaft. This constant angle will be used to incline a planar mechanism that will drive the hockey stick through the desired motion. We chose to create this trajectory using a coupler curve for a 4-bar mechanism, which is capable of generating complex trajectories from only 1 input.

To design this mechanism, we used the FOURBAR computer simulation package (Norton, 2008). The initial step in the FOURBAR analysis was to use a predefined mechanism with a desirable coupler curve as a starting point for the analysis. The next step was to scale-up the design to include a 152.4 cm coupler (length of a hockey stick), with the rocker and crank connecting at the top and 91.4 cm (space between the hands) from the top, respectively. Finally, numerous iterations were performed to achieve a 4-bar coupler curve that provided the closest match to the experimentally-measured hand motions. Refer to Figure 3. The final dimensions are summarized in Table 1.

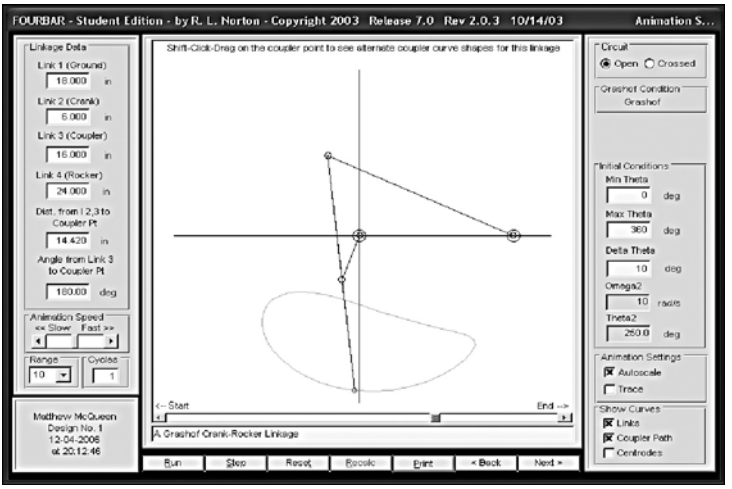

Figure 3 - FOURBAR mechanism design.

Link	*Dimension [cm]*	*Other Variables*	*Values [cm]*
L_1 (Ground Link)	82.68	O_4 (Location of 2nd pin on ground)	(82.55, -12.70)
L_2 (Crank)	30.48	Dt (Distance to coupler point)	60.96
L_3 (Coupler)	91.44		
L_4 (Rocker)	107.97		

Table 1 - 4-bar mechanism dimensions.

5- CAD Design and Prototype

The other main design considerations are the frame and the stick attachment. For a tabletop prototype of the proposed machine, the green wedges in Figure 4 were constructed out of a cold rolled steel sheet and bent to the required dimensions. They were bolted to a base of plywood, blue in Figure 4, and covered with synthetic practice ice (white) in the contact zone. Finally, although the weight and footprint of the

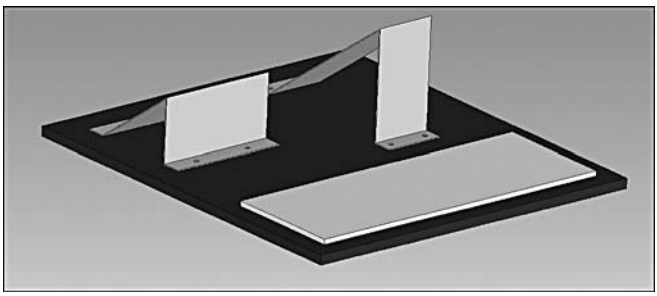

Figure 4 - Base assembly.

base are sufficient to keep the machine anchored to the surface during operation, there will be points on the base where the system can be further anchored using C-clamps.

As explained in Section 4.0, the stick lies along the coupler of the 4-bar machine. The top hand is located at the pin joint between the coupler and the rocker while the bottom hand is located at the pin joint between the crank and the coupler. The stick will physically attach using a modified C-clamp, as shown in Figures 5 and 6. The yellow component is a screw with a hemispherical end attachment meant to simulate the pressure of the thumb gripping the stick. This threaded connection will force the shaft against the pink face of the main clamp which will simulate the palm of the hand. As the exact grip force exerted on the stick is unknown, the screw will be sufficiently tightened to prevent any slipping during operation. Since the stick will undergo significant bending compared to the coupler of the mechanism itself, the clamping mechanism will have a bearing on the bottom, the red component in Figures 6 and 7, to allow for rotation about the pinned joints connecting the coupler to the crank and rocker. In other words, the two clamps are free to rotate on the coupler link, which is essential if the stick is to bend in order to store and release energy.

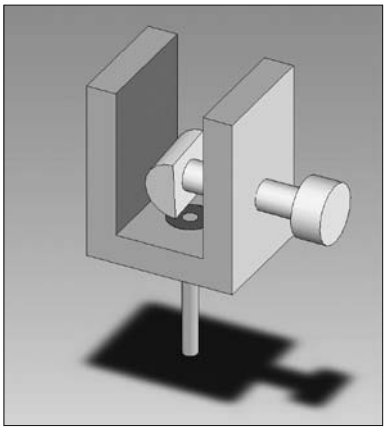

Figure 5 - Stick clamp assembly (a).

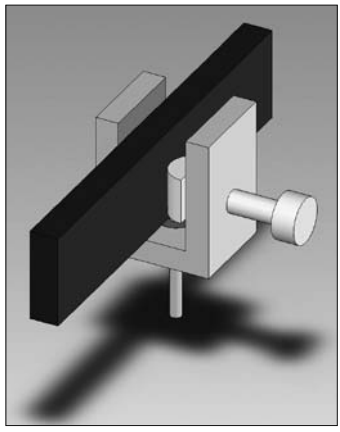

Figure 6 - Stick clamp assembly (b).

Using the dimensions from Table 1, a quarter-scale design was created using SolidWorks. This design was used as the basis for the construction of a tabletop prototype, shown in Figures 7 and 8.

Figures 9 and 10 show the machine at various stages of operation. Figure 10 shows the position of the machine at the contact point, which is when the stick is hitting the puck. In this scenario, the hockey stick would be bending ; however this SolidWorks CAD model does not have the capability to show bending. Figure 10 shows the machine in the follow through position. To reset the machine, the motion must continue forward

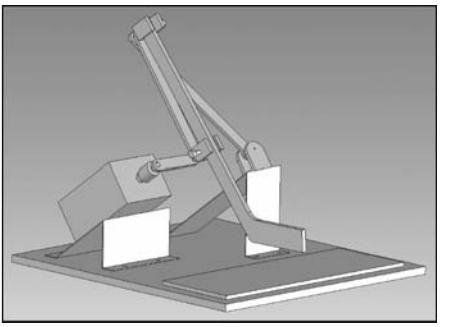

Figure 7 - CAD design.

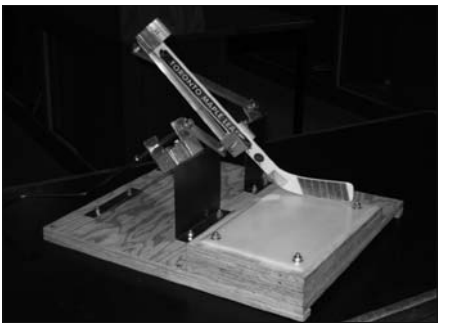

Figure 8 - Prototype design.

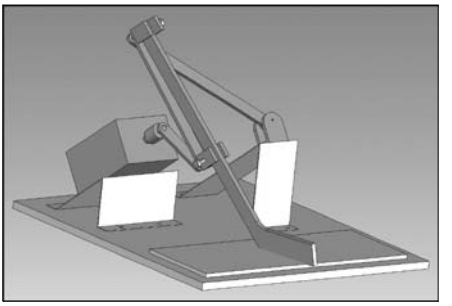

Figure 9 - Contact position.

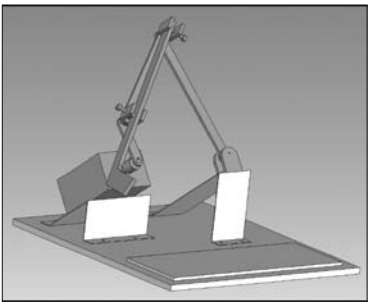

Figure 10 - Follow through position.

rather than in reverse. This is due to the interference between the stick and the ice in the contact zone.

As shown in Figure 8, the tabletop prototype is currently driven by a hand crank. To determine the amount of torque required from a motor, as well as the pin reaction forces, the computer program Working Model was used to generate a multibody

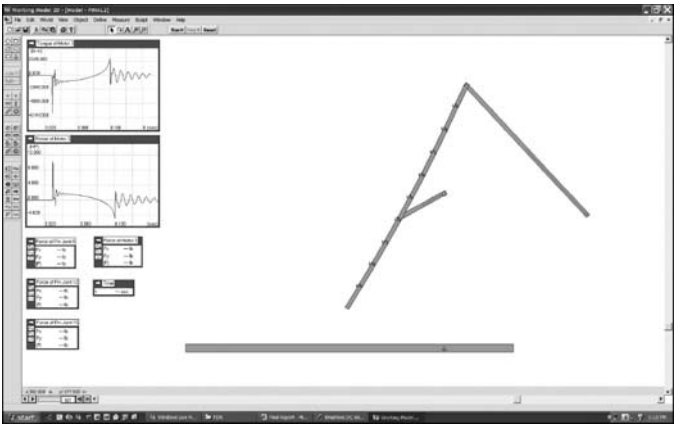

Figure 11 - Working model simulation.

dynamic model of a motor driving a slapshot. To represent the flexibility of the stick in a finite segment model, it was divided into 10 segments pin-connected by rotational springs whose stiffnesses are obtained from the Young's modulus (E) and cross-sectional moment of inertia (I) of the stick (Reckdahl, 1996). Figure 11 shows a snapshot of the Working Model simulation at one timestep. We are currently constructing a new prototype driven by a DC brushless electric motor, sized using the Working Model simulation results.

6- Conclusions

From our motion analysis results, the trajectory of a hockey stick is mainly two-dimensional from the time it strikes the ice in a slapshot, to the time the puck leaves the blade. Using this information, a planar 4-bar mechanism, inclined at an angle of 35º to the vertical, was designed to drive a hockey stick through a trajectory representative of a slapshot. This machine provides the basis for repeatable testing of hockey sticks under conditions corresponding to a slapshot. A provisional patent application has been filed with the United States Patent and Trademark Office (McPhee and McQueen, 2007), and we are currently working on the next generation of this test machine.

7- References

[N08] Norton, R.L, Linkage Design, http://www.designofmachinery.com/Linkage/ fourbar.html, 2008.

[MM07] McPhee, J. and McQueen, M., Hockey Stick Test Machine, USPTO Provisional Patent Application 60/996,039, filed 25 October 2007.

[VT06] Villasenor, A., Turcotte, R.A., and Pearsall, D.J., Recoil Effect of the Ice Hockey Stick During a Slap Shot, In Journal of Applied Biomechanics, vol.22, no.3, pp.202-211, 2006.

[SW06] Stefanyshyn, D.J., and Worobets, J.T., Energy Return and Puck Speed of Hockey Sticks, In Journal of Biomechanics, vol.39, p.S189, 2006.

[R96] Reckdahl, K., Modeling Uniform Flexible Bodies in Working Model, Working Model Technical Note WMTN13, 1996.

A Novel Approach to Personalising the Mechanical Properties of Sprint Footwear (P179)

Dan Toon[1], Candice Majewski[2], Hadi Zarringhalam[2],
Neil Hopkinson[2], Mike Caine[1]

Topics: Athletics; Performance Sports; Shoes; Innovation and design, Materials.
Abstract: A novel method for adapting the mechanical properties of sprint shoe sole units is explored. Five different ratios of glass to nylon were mixed and laser sintered to produce standard test samples and sprint shoe sole units. Samples were subjected to standard tensile test procedures and sole units were tested in a purpose built fixture. In-filling nylon-12 with higher ratios of glass increased longitudinal bending stiffness. The mean force in extension over the tested range was 8.9 and 16.0 N for the 0% and 50% glass filled sole units respectively. The mean force in flexion over the tested range was 11.6 and 17.7N for the 0% and 50% glass filled sole units. However, increased stiffness comes at the expense of ductility and mechanical evaluation over the shoes functional range resulted in mechanical failure for the sole units in-filled with 50% glass. Further work on alternative base and infill materials needs to be conducted before the technique is suitable for functional footwear.
Key words: Footwear personalisation; stiffness; sprinting; selective laser sintering; design.

1- Introduction

Performance enhancement through the application of footwear and associated technologies has been the subject of considerable study. There is a significant amount of evidence from recent publications demonstrating that an engineering approach to footwear design can improve performance. Specifically, for sprinting it has been determined that increasing shoe bending stiffness typically resulted in improved sprint performance. However, it was further asserted that tuning of an athlete's shoe stiffness to their individual characteristics is required if performance is to be maximised (Stefanyshyn and Fusco, 2004).

1. Sports Technology Institute, Loughborough Science & Enterprise Park, Loughborough, Oakwood Drive, Leicestershire, UK - E-mail: {D.Toon, M.P.Caine}@lboro.ac.uk
2. Rapid Manufacturing Research Group, Wolfson School of Mechanical and Manufacturing Engineering, Loughborough University, Leicestershire, UK - E-mail: {C.E.Majewski, N.Hopkinson}@lboro.ac.uk

To date, the common methodology for changing mechanical properties of footwear has been to manually adapt a standard shoe (Stefanyshyn and Nigg 2000, Roy and Stefanyshyn 2002, Stefanyshyn and Fusco 2004). Toon et al. (2007) established an alternative method to modify the mechanical properties of sprint shoes through the application of Selective Laser Sintering (SLS) to produce nylon-12 sprint shoe sole units which are then assembled to a standard upper. Using this approach longitudinal bending stiffness is adapted by varying the thickness of the sole unit. However, it is thought that some athletes may be able to perceive differences in thickness and furthermore, the requirement for a larger stiffness range has deemed it necessary to explore alternative techniques. Consequently, the current paper discusses a material science approach to customising the mechanical properties of SLS sprint shoe sole units.

2- Methodology

2.1 Selective Laser Sintering

Rapid Manufacturing (RM) is a family of technologies whereby three-dimensional parts are produced directly from computer-aided design (CAD) data, using a layer-by-layer approach. Major benefits include the elimination of the requirement for tooling and the ability to produce far more complex geometries than are possible using conventional manufacturing techniques. Selective Laser Sintering (SLS) is one such RM process, whereby a laser is used to selectively sinter layers of powdered material. Figure 1 shows a schematic of the process.

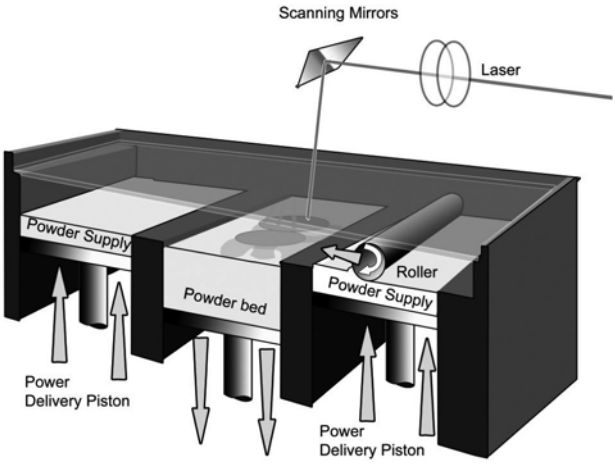

Figure 1 - SLS schematic (Hopkinson et. al., 2005).

SLS is capable of processing a wide range of materials (polymers, metals and ceramics) and can produce parts with good mechanical properties, that are chemically stable over time. For these reasons the SLS process was considered ideally.

Three-dimensional CAD data for the sprint shoe sole units were generated and then converted into STL file format for production using the SLS process. The STL file format provides a triangulated surface representation of the part, suitable for use on most RM machines. The file is split into discrete 2D layers ready for manufacture. The machine is then filled with powdered material and preheated to approximately 12°C below the melt temperature of the material. A laser then scans the cross-sectional area identified for the current slice, providing enough energy to melt the area, and thus sintering the powder into a solid layer. A fresh layer of powder is deposited across the bed and the process is repeated until the part is complete. Once the build has completed, the part is left to cool and then removed from the un-sintered powder.

2.2 Material selection and preparation

Nylon-12 was in-filled with 0, 12.5, 25, 37.5 and 50% glass and a range of standard tensile test specimens (BS EN ISO 527-2:1996) and sole units, 3 mm in depth, were produced using SLS. The use of glass-filled Nylon 12 powder (50% glass beads, 50% Nylon 12 by weight) nominally increases the Young's Modulus of a part from 1,586 MPa to 4,068 MPa (3D Systems Corporation), and it was therefore anticipated that the stiffness of parts produced could be controlled by the inclusion of different percentages of glass-filler.

Mechanical mixing of nylon-12 and glass-filled nylon-12 was carried out for 30 minutes using an industrial mixer, ensuring an even distribution of glass-beads. Powder was installed in batches and all specimens were produced on a 3D Systems SLS Vanguard machine with HiQ upgrade. Sole units were arranged within the build volume such that five pairs were nested with their mediolateral axis parallel to the z-axis of the build. Two rows of standard test parts were also included at the base of the build volume.

2.3 Mechanical Testing

All parts were conditioned at 20°C (+/- 1°C) and 50% (+/-5 %) relative humidity, according to the test standard specification. Tensile tests were performed using a Zwick Z030 tensile testing machine fitted with an extensometer. The Zwick software, TestXpert, was used to enable the calculation of Young's Modulus.

Mechanical testing of the sole units was carried out using a purpose built fixture (shown in Figure 2), designed in accordance with the ASTM standard for flexibility of running shoes (ASTM F-911 – 85). Force measurements were recorded in extension and flexion with each sole unit fixed at 70% shoe length from the rear. For extension the sole units were pulled vertically upwards using a stirrup system and for flexion the sole units were compressed vertically downwards. The speed of the test machine was fixed at 1,000 mm/min and five test cycles in extension and flexion were recorded. The data presented is a mean of the last 3 cycles for the left and right units.

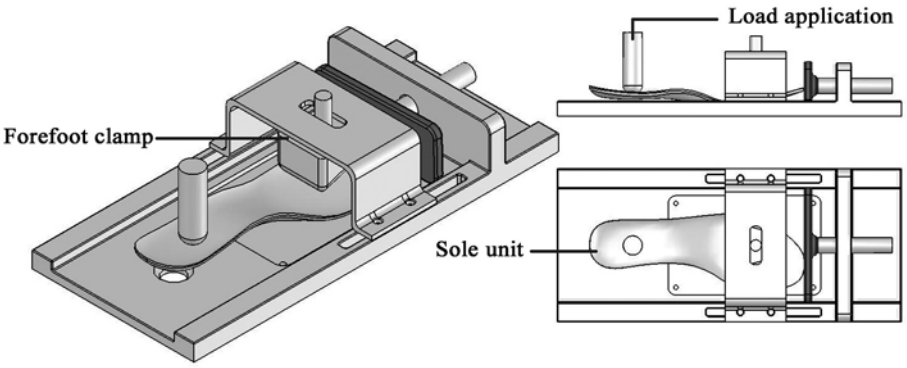

Figure 2 - Mechanical test fixture.

3- Results

The graphical data in Figure 3 shows that an increase from 0 % to 50 % glass filler led to a corresponding increase in the Young's Modulus. Young's modulus is calculated by dividing the tensile stress by the tensile strain and is considered a measure of stiffness. The increase over the range tested was from 2816 MPa to 7,227 MPa, or 157%. The average standard deviation of the data was 419 MPa.

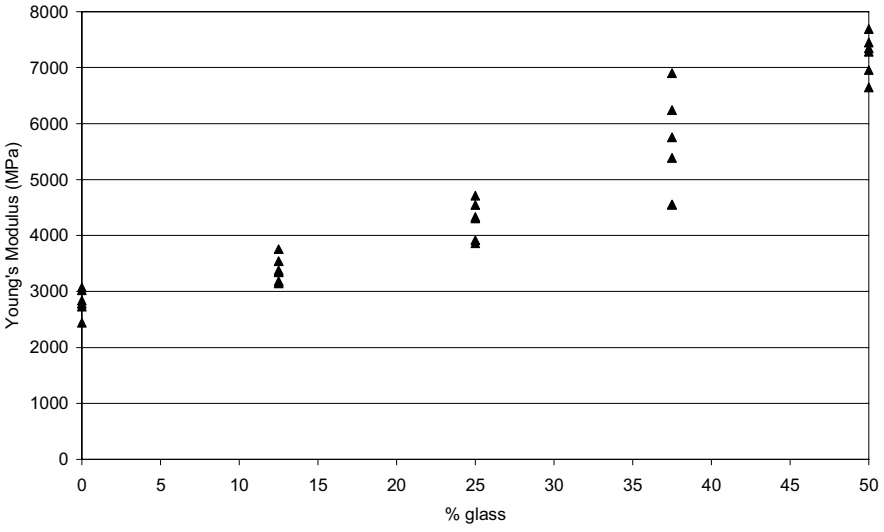

Figure 3 - SLS sample parts Young's Modulus.

Figures 4 and 5 present the results of the flexion and extension tests on the sole units.

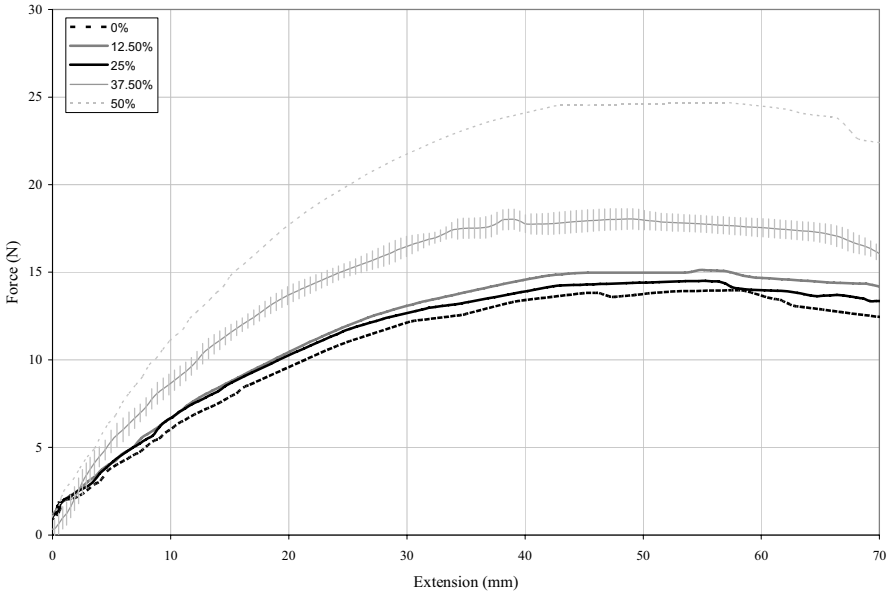

Figure 4 - Force vs. extension SLS sole units.

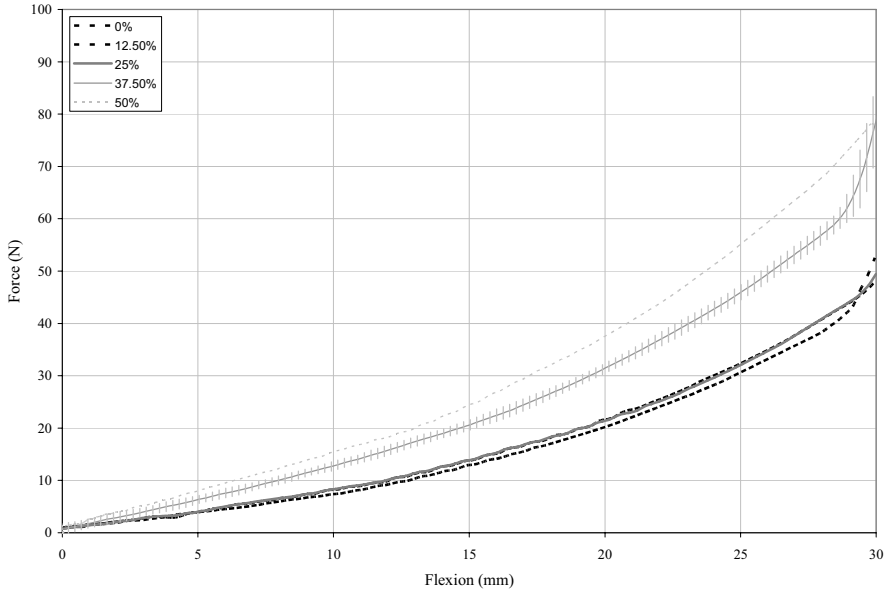

Figure 5 - Force vs. flexion SLS sole units.

The graphical data in Figure 4 and Figure 5 shows that an increase from 0 to 50% glass filler led to a corresponding increase in bending force for extension and flexion. The SLS sole units with 37.5% glass filler are shown with error bars of ± 1 standard deviation and this is typical for all tested sole units. The mean force in extension over the tested range was 8.9 and 16.0 N for the 0% and 50% glass filled sole units respectively. The mean force in flexion over the tested range was 11.6 and 17.7N for the 0% and 50% glass filled sole units.

4- Discussion

Personalisation of the mechanical properties of footwear is achievable using selective laser sintering. The tool-less process has several advantages over conventional manufacturing methods including the ability to produce complex geometries and internal structures. The current investigation has highlighted an additional advantage of the rapid manufacturing process with particular relevance to personalisation. It has been shown that mechanical properties can be quickly and easily modified by adapting the ratio of compatible infill materials.

Five different ratios of glass to nylon were mixed and successfully laser sintered to produce standard test samples and sprint shoe sole units. Tensile testing of standard parts showed that Young's modulus increased as the ratio of glass to nylon was increased. Flexion and extension mechanical tests data for the sole units concurred with this relationship. However, the variations in effective bending stiffness were only discernable between 25, 37.5 and 50% glass filler in extension and 25 and 37.5% glass filler in flexion.

With increasing stiffness elongation at break is often compromised, this is demonstrated in the case of the 50% glass filled example which suffered catastrophic failure. A crack was initiated on the medial aspect of the perimeter at the primary point of flexion and propagation rapidly occurred until failure on the fourth cycle. The failure type was consistent and not due to any alternative mechanisms such as surface defects or contamination. The results suggest that 37.5% glass-filler provides a substantial increase in longitudinal bending stiffness without compromising mechanical integrity. However, the behaviour of the sole units under mechanical fatigue has not yet been investigated.

5- Conclusion

The current investigation has shown that mechanical properties of materials can be adapted using the selective sintering process with different ratios of infill material. The use of glass as an infill material to adapt the bending stiffness of sprint shoe sole units resulted in an increase in bending stiffness, but this came at the expense of ductility. Further investigations could focus on the region between 25 and 50 % glass filler, to identify the maximum percentage before catastrophic failure, and whether the range of stiffnesses required can be produced within this range. Alternative base and filler materials may also provide a good range of stiffness whilst maintaining the required levels of ductility. Another approach to be investigated is the adaptation of design features and geometry in order to achieve the require range of longitudinal bending stiffnesses.

7- References

[3S1] 3D Systems Corporation datasheets, Duraform® PA and Duraform® GF, http://www.3dsystems.com, site accessed 20th February 2008

[HH1] Hopkinson, N., Hague, R.J.M. and Dickens, P.M., Rapid Manufacturing: an Industrial Revolution for the Digital Age, Chichester, West Sussex: John Wiley and Sons Ltd; 2005. ISBN 0470016132

[RS1] Roy, J.-P. and Stefanyshyn, D.J. Influence of Metatarsophalangeal Joint Bending and Shoe Sole Length on Jump Height Performance, Proceedings of the Fourth World Congress of Biomechanics, 2002

[SN1] Stefanyshyn, D. J. and B. M. Nigg. Influence of Midsole Bending Stiffness on Joint Energy and Jump Height Performance. Medicine and Science in Sports and Exercise 32(2): 471-476, 2000.

[SF1] Stefanyshyn, D. J. and C. Fusco. Increased Bending Stiffness Increases Sprint Performance. Sports Biomechanics 3: 55-66, 2004

[TH1] Toon, D., Hopkinson, N. and Caine, M. Design and construction of as sprint spike with a selective laser sintered nylon sole unit, 8th Footwear Biomechanics Symposium, Taipei., 2007

Testing Procedures for Baseball Chest Protection Equipment (P181)

Kim B. Blair, Ph.D.[1], Mike Vasquez[2], Paul Groudas[2]

Topics: baseball protective equipment.
Abstract: In this experiment we attempted to define and implement a series of repeatable tests to quantify the effects of impacts on various types of baseball catcher's equipment. After investigating several procedures, the bulk of the testing done was to determine the coefficient of restitution on different areas of the testing specimens. Four types of fully assembled catcher's gear were tested for this set of experiments along with individual padding samples from the gear. Typically catcher's gear is composed of variable thickness and density ethylene-vinyl acetate foam. However some of the newer models incorporate memory foams into their design. Because of the inherent design differences of the padding samples significant attention was paid to the distinct padding areas in each sample.
Each sample was impacted five times in 2-3 distinct padding areas. The incoming and outgoing velocity of the impactor was measured. From this, COR was computed. The COR was tested in two ways, first through direct baseball impacts and secondly through a specific localized impactor. Results showed that there were significant differences between padding samples, and even between different locations on the same sample.
Key words: baseball, padding, protection.

1- Introduction

Baseball is a game of inches and in many cases slight advantages in equipment such as a bat or padding can have a large effect on the outcome of the game. In the case of catcher's equipment its primary function is player protection from baseballs traveling at velocities near 40 m/s. However it is not uncommon during game situation for balls to deflect off the catcher's padding and remain in play. Ideally the equipment would both maximize protection and minimize rebound after a ball has struck the padding (Figure 1).

1. Xenith, LLC, 672 Suffolk Street, Lowell, MA USA - E-mail: kblair@xenith.com
2. Massachusetts Institute of Technology, Sports Innovation @ MIT - E-mail: {vasquezm, pgroudas}@mit.edu

Figure 1 - One of the co-authors (P. Groudas) «field testing» catcher's gear.

The goal of this project was to compare two different test methodologies and categorize the performance of various brands of catcher's gear using these different test methodologies. Limited work has been done on the dynamics of protective padding. Matsubayash and Lieu [ML1] evaluated chest protectors and headgear for competition taekwondo using an aluminum impactor striking a mounted chest protector housing an accelerometer. Avalle, Belingardi, and Montanini [AB1] have investigated the mechanical properties of EPP, PUR, and PS/PA foams under room temperature conditions using energy absorbtion diagrams. However, isolated foam tests may not be indicative of the perfamance of catcher's padding due to the foam being compressed between other material layers and the elasticity of those layers. To date there have been no published detailed studies of baseball chest protector padding.

2- Methods

Two unique test setups were examined. The first apparatus used a pitching machine to impact the catcher's padding with baseballs. The second apparatus used a steel impactor to deliver precisely located impacts to the padding. The specific methods are described below.

2.1 Direct Baseball Impacts

Using a modified version of ASTM standard F1887-02, a testing apparatus (Figure 2) was constructed incorporating a Jugs two-wheel pitching machine as the ball delivery system [A1]. The machine delivered baseballs at an average speed of 29.1 m/s. Opposite the pitching machine the padding samples were mounted on a wood sheet attached to a steel hardback via four C-clamps. The padding was then strapped flat against the wood surface using two one inch cords positioned at the top and bottom of the padding. Two light gates spaced 30.5 cm apart with the closest 20.3 cm from the impact surface were set up in front of the padding to record the inbound and outbound ball velocities. The ratio of the outgoing to incoming ball velocities is used to calculate the coefficient of restitution (COR) of the padding.

Each sample was impacted five times in the solarplex (center of the chest) region of the protective padding. Prior to each round of testing the baseball impact position was marked on the setup and the padding was aligned so that the middle of the pad was centered on that location.

The testing took place over period of two sessions using Rawlings R100 baseballs (Rawlings, Inc., St. Louis, MO, USA). The baseballs were kept at ambient room temperature conditions before the two sets of tests. The average mass of the baseballs used was 145 grams.

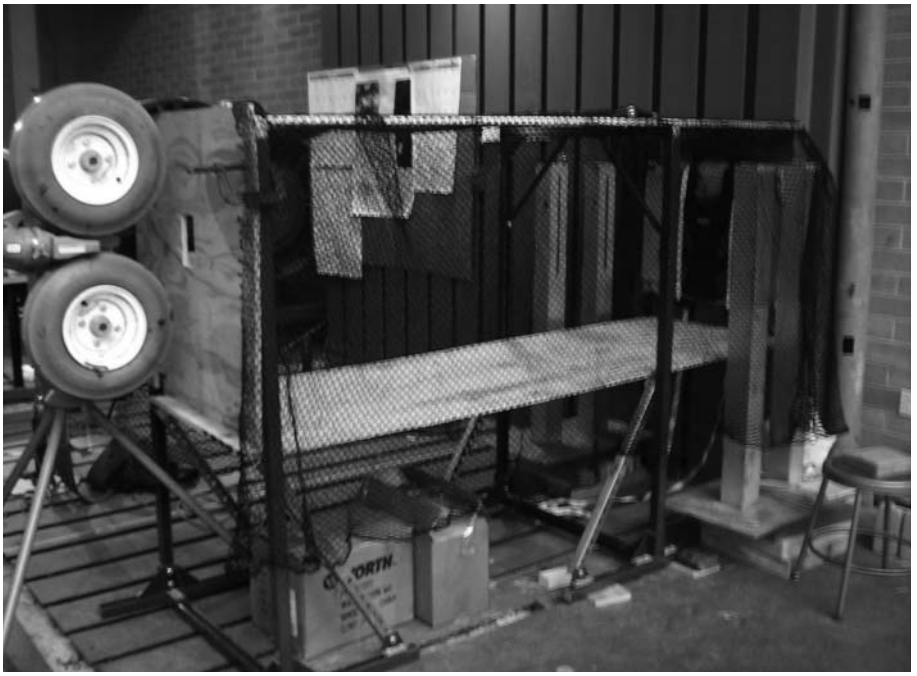

Figure 2 - Pitching machine COR setup.

2.2 Free Rolling Energy Device (FRED)

The second test setup incorporated the use of an apparatus called a 'free rolling energy device' or FRED. This device consists of three components: the impact device, the specimen holding assembly, and the data acquisition system. For this particular setup, the impact device and specimen holder have been chosen on the basis of availability. However, the method of data acquisition involved two sets of light gates spaced 7.62 cm apart that would record the speed of the impactor before and after impact.

Figure 3 provides an illustration of the system. A hand winch is used to compress the springs in the system, which is then locked in place. The spherical striker (3.18cm diameter) is then positioned against the main rod with the use of an electromagnet. When released, the springs propel the main rod and the striker rod forward. The elec-

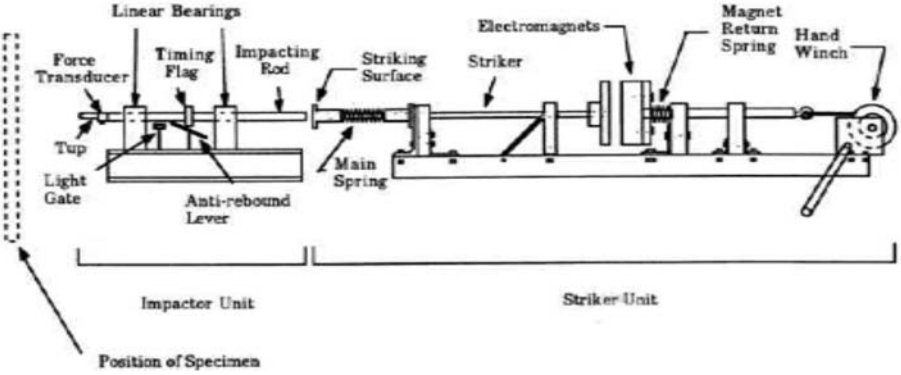

Figure 3 - Schematic of free rolling energy device.

tromagnet releases the striker rod to impact the impacting rod, which in turn impacts the test sample. While a complicated system, it minimizes the amount of mass actually striking the sample, relying on the speed of the impacting rod to generate the required energy at impact. The inbound and outbound velocity of the impacting rod is measured using light gates. The average speed of impact was 3.40 m/s. As above, the COR was calculated for each impact. The testing was completed over two testing sessions in ambient environmental conditions.

In order to more completely compare the various padding specimens each specimen was tested on the FRED machine in several places. Unlike the pitching machine test the impactor on FRED was very precise and allowed for testing of the different padding types on each sample. The primary impact was at the solarplex region where the padding samples had the thickest amount of padding. The second impact position was a spot on the side of the padding where softer more flexible materials are used (Figure 4).

Figure 4 - Padding impact regions, 1 – Solarplex, 2 – Side.

2.3 Samples Tested

Four different padding samples were provided by the research sponsor Rawlings. Each sample was commerically available at the standard adult size. Due to the variation in materials for each sample, a recovery period was given after each impact to allow for the

foam to return to its original shape. Special attention was paid to those samples containing memory foams to ensure complete recovery occured prior to the second impact.

3- Results

3.1 Direct Baseball Impacts

The baseball's initial and final velocity was calculated after each impact in this setup. These velocities were then used to calculate a COR value.

Figure 5 shows the average and standard deviation for a set of five 29.1 m/s baseball impacts on each pad. The data from Figure 5 clearly indicates that in this specific setup Sample 1 padding offers the least rebound. The average COR for Sample 1 was 0.57±0.08 while the other three padding samples performed at a COR value of 0.67.

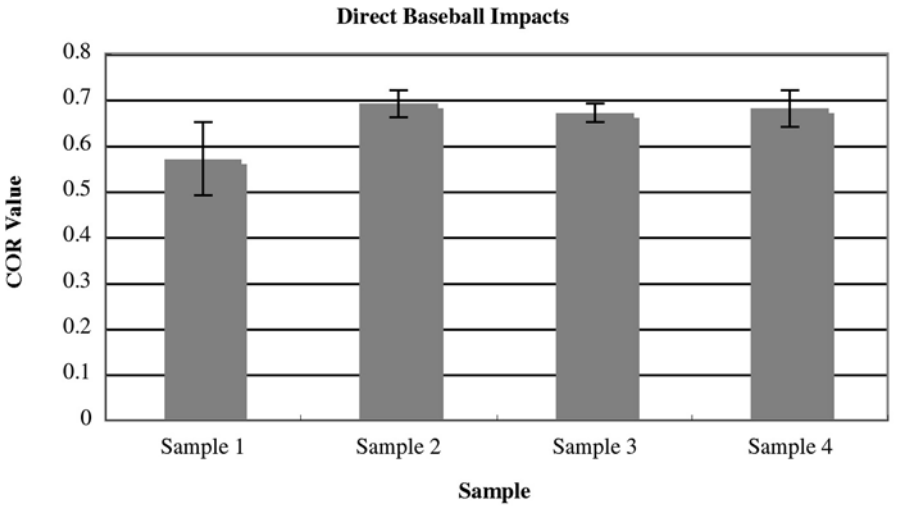

Figure 5 - COR results from pitching machine tests.

3.2 Free Rolling Energy Device

The data collection process for the FRED tests were very similar to those of the direct baseball impact tests. However instead of calculating the COR values of a baseball this set of experiments measured the COR of the impactor as it struck the padding.

Figure 6 shows the average and standard deviation for two impact sets on each pad. A similar pattern emerged compared to the pitching machine tests. Sample 1 had a lower average COR near the solarplex region (Location 1) of the padding. However there did exist some performance differences between the primary and secondary padding locations in samples 1, 2, and 3.

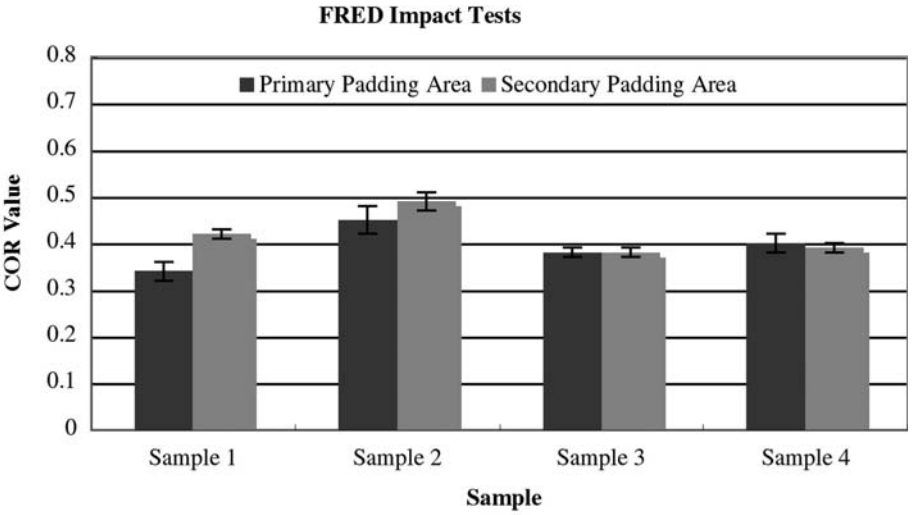

Figure 6 - COR results from FRED tests.

3.3 Statistical T-test

A statistical T-test was competed to compare the COR results within each test method with the results collected Table 1.

(A)

Sample Combination	T-Value
1 and 2	3.73
1 and 3	3.45
1 and 4	3.02
2 and 3	1.51
2 and 4	0.66
3 and 4	0.44

(B)

Sample Combination	T-Value
1 and 2	4.63
1 and 3	2.6
1 and 4	5.85
2 and 3	3.6
2 and 4	2.48
3 and 4	1.43

Table 1 - Statistical T-tests of direct baseball impacts (A) and FRED impacts (B).

The shaded T-values show which combinations of padding samples that were not statistically different. With the others, there is 95% confidence that the data is significantly different.

4- Discussion

4.1 FRED and Pitching Machine Tests

There was a similar trend that was observed when the data of each setup was compared. In both test setups, the data resulted in a performance gradient that was nearly identical. For the direct ball impacts Sample 1 (0.57) had the lowest COR followed by Sample 4 (0.68), Sample 3 (0.67), and Sample 2 (0.69). Comparatively, for the FRED tests the Sample 1 (0.34) also had the lowest COR followed this time by Sample 3 (0.38), Sample 4 (0.40), and Sample 2 (0.45).

Nevertheless the absolute values for the direct ball impacts were much higher than those of the FRED tests. The most reasonable explanation for this is the difference impactor speed and the impactor itself. The FRED apparatus delivered impacts at much lower velocities with an impactor that was smaller than a baseball. However the steel impactor absorbs very little energy during the impact while the softer baseball contributes to the total COR calculation in direct impacts. In addition there is a difference in energy distrubution for each setup. For the direct baseball impact tests an average of 61.4 joules of energy were delivered per impact over the baseball's area. On the other hand FRED impacts delivered 9.13 joules per impact.

4.2 Statistical T-test

One interesting point that is observed is how only one versus three combinations were statistically insignificant in the FRED tests. This is likel due to the inherent variability in the pitching machine setup (exact impact position and spin).

5- Conclusions

The goal of this project was to investigate different ways to test baseball protective chest padding. In the past there has not been significant testing in this area of equipment. As a first step in better comparing and characterizing this equipment we performed two tests. First impacting the padding with a pitching machine delivered baseball and a second set of tests using a precisely controled small impactor on specific areas of the pad.

The two tests resulted in a similar performance gradient for each set of pads. However we feel that future tests must incorporate direct ball impacts rather than using a smaller impactor. The baseball velocity can be tuned to more realistic speeds and will distribute the force similar to that seen in an actual game.

Future iterations on these tests may try to investigate the actual force and force distribution on the player's body. In addition, a better test must be developed to describe how the padding actually fits onto a player's body while they are in the correct position.

6- References

[A1] ASTM (2002) Standard Test Method for Measuring the Coefficient of Restitution (COR) of Baseballs and Softballs, F1887-02.

[A2] Adair, R.K. (2002) The Physics of Baseball, 3rd Edition, HarperCollins Publishers Inc. New York.
[AB1] Avalle, M., G. Belingardi, and R. Montanini. (2001) Characterization of polymeric structural foams under compressive impct loading by means of energy absorption diagram. International Journal of Impact Engineering, Vol 25, 450-572.
[ML1] Matsubayashi, K. and D.K. Lieu. (1993) Evaluation of Chest Protectors and Headgear for Competition Taekwondo. Advances in Bioengineering, BED-Vol 26.

7- Acknowledgements

Special thanks is given to Brian Hoying and the research and development team at Rawlings. They provided the scope of the project as well as the testing samples. The authors would also like to acknowledge the aid given by the technical staff at MIT's Department of Aeronautics and Astronautics: Dave Robertson, John Kane, Dick Perdichizzi, and Todd Billings.

Holistic Innovation in Sports (P183)

Eckehard Fozzy Moritz[1]

Topics: innovation management, holistic innovation.
Abstract: This paper introduces a new perspective on the fostering of innovation in sports. Point of departure is the concept of holistic innovation, a complement to existing innovation concepts especially useful for radical innovation in complex settings. On this basis, a methodology to support systematic work on such innovation ventures, the Innovatorics, is introduced. The paper concludes with discussing some more general considerations regarding the fostering of successful innovation.
Key words: innovation, innovation management, holistic innovation, vision.

1- Scope and purpose of this contribution

This article has been written for maximum use value and easy digestion of innovators. It is the bold attempt to comprise and adapt the practically relevant contents of the just-published book "Holistische Innovation" [M1] in a concise English summary; to condense a couple of hundred pages down to six. The downside: There are few literature references; the article gives a complex scenario rather than a couple of well-founded statements. For those ill-satisfied: I did this differently in the compilation of my book; you may want to read it if you like to know more about the academic backgrounds. Regarding the scientific basis, holistic innovation is clearly a showcase of Mode 2 knowledge production [NS1]. And the topic area of innovation, sports, is here understood on the basis of a very wide definition as "special form of human movement behaviour" [H1] with manifold interrelations with its psycho-social and economic environment. Subjective interpretation decides whether an activity is sports or not. Anyway, innovators have more relevant things to do than argue whether an activity is sports or not. They should help fulfil expectations and objectives of users and stakeholders; however the result may then be categorized.

This contribution will address three areas of possible support for innovation in sports: the concept of holistic innovation that forms the basis for the discussion that

1. SportKreativWerkstatt, München, Germany - E-mail: efm@sportkreativwerkstatt.de

follows, the process of innovation, focussing on the early stages of radical innovation in complex settings, and a summary of other activities important for successful innovation.

2- The concept of holistic innovation

Today most innovation activities in the sports industry are marketing-oriented. Companies are asking customers or assuming on the basis of their experience how existing products may be changed so that new sales incentives are generated. Innovation in academia is usually evaluation-driven: The focus of developments is to achieve goals and validate this achievement on the basis of paradigms established in the scientific community. Innovations in sports user communities are directly geared to satisfying the sports needs and wants inside these communities.

Of course, there is nothing wrong with either approach. All are satisfying the more or less imminent needs of the respective innovators. However, important potentials of innovation are hardly realized with these strategies:

- Innovations in areas where neither activities nor products exist yet (example: products that motivate senior citizens to move (for primary prevention) and that are integrated into their living environments and daily routines)
- Innovations beyond development and evaluation corridors (example: virtual skiing systems as fun sports devices)
- Innovations as a result of environmental changes (example: non motorized all weather shopping vehicles affordable by all as environment-friendly and healthy alternative to existing traffic in mega cities)
- Innovations to shape the future into a desired direction (example: cool fun and health equipment for computer kids)

The concept of holistic innovation has been developed as a basis to derive activities and strategies to tackle this sort of innovation ventures. Fig. 1 summarizes core perspectives of holistic innovation – opposing them to common more segregated approaches to innovation here termed reductionistic innovation.

A few implications of this concept must suffice here:

- Visions play a core role in holistic innovation. They constitute the point of departure for innovation, not the status quo. This is especially important in complex areas like sports: "L´innovation sportive… impose une vision heuristique et anthropologie de énvironment social, sportif, economic e technologique." [H2]. Innovation is then generated using the so-called backcasting, "beginning with an imagined end goal, which is then worked back to derive the investments and activities that must take place in order to enact that future." [CF1]
- Value added is important, but with a comprehensive understanding of "value". In the early stages of radical innovation it is counter-productive to quantify potential value added; however, it is possible to improve value added.
- Innovation must be embedded. This sociological term describes the interrelation of innovation with its environment [G1]. This must be acknowledged in all stages of the innovation process, starting with the embedded creation of system visions, up to the generation of system solutions rather than products alone.

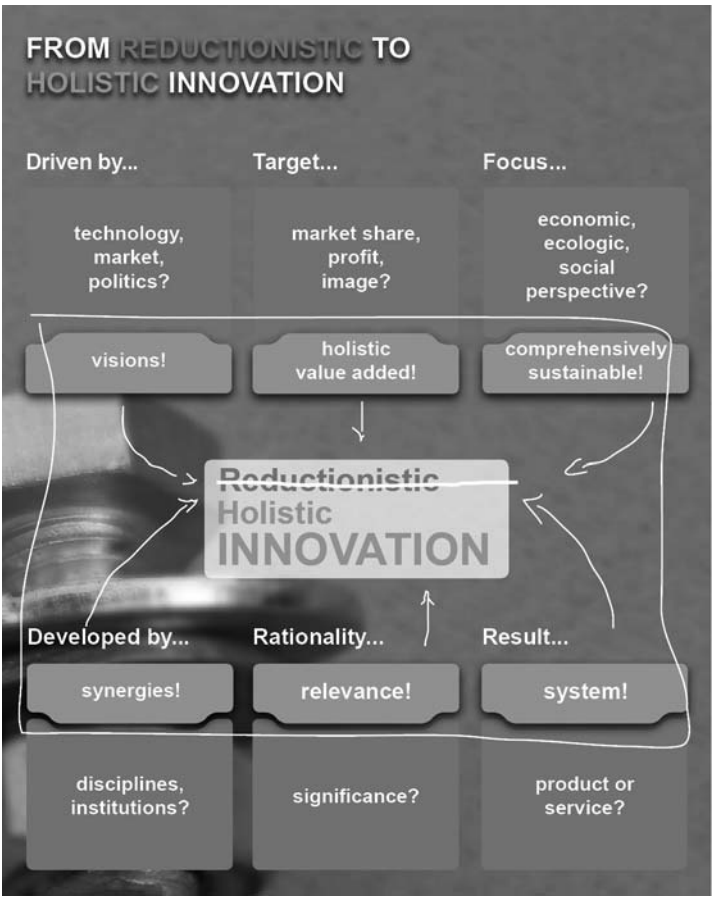

Figure 1 - Perspectives on Holistic Innovation.

- Relevance is more important than significance. Zadeh has pointed out the existence of an uncertainty principle between significance and relevance in complex problem solving [F1]: You can either have one or another. Radical innovation in sports, especially in popular sports, needs relevance!

3- The process of holistic innovation

The concept of holistic innovation and the focus on the early stages of radical innovation taken here demand a new process for the generation of innovation. Veryzer [V1] is even convinced that for radically new products conventional approaches may be inappropriate of even detrimental. And aside from pure experimentation (e.g. "probe and learn", [VB1]) there are hardly any process models for the so-called fuzzy front end of innovation.

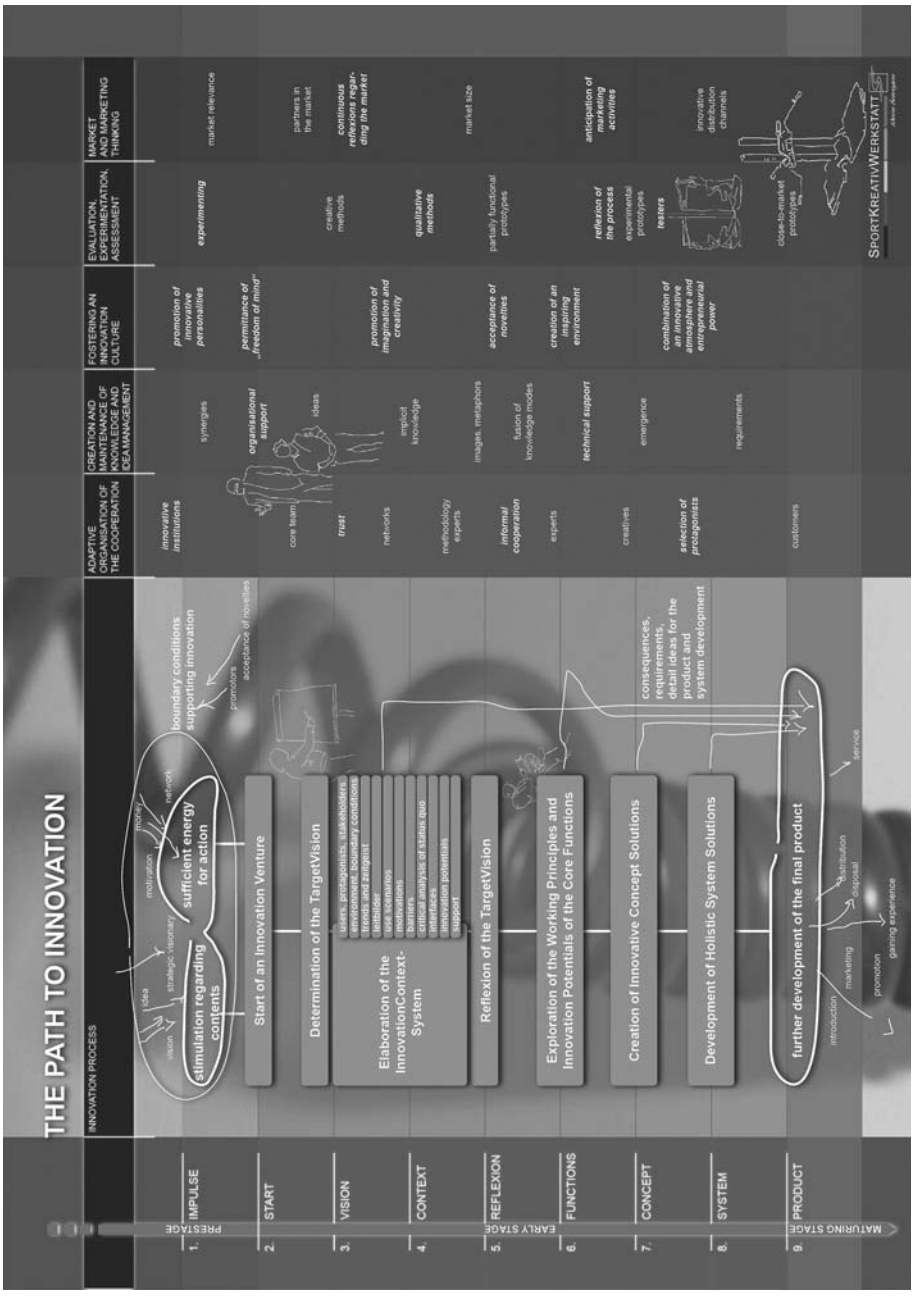

Figure 2 - The Innovatorics.

Fig. 2 shows the master plan that we have developed, in a mix of adaptations of novel problem solving approaches, amalgamation of existing methods, transfer of conceptions of scientific self-innovation, and constant empirical optimization, to support systematic work on holistic innovation. We have called it Innovatorics. To give a first orientation, it consists of a process model (left), and of a summary of activities that cannot directly be linked to individual stages of the process. The process model constitutes a macro-strategy for innovation, work on the individual stages is supported by particular methods introduced comprehensively in [M1].

The main storyline of the process model works as follows:

- In the **pre-stage**, it is important for innovators to make sure that the innovation has best possible preconditions to be successful (however marvellous the process, there is no truly radical innovation without some risk remaining). Activities here include work on the quality of the stimulus regarding contents (vision, objective, idea), the accumulation of sufficient energy and resources for action, and the constant maintenance of an environment hospitable to innovation. Fig. 3 shows a holistic vision of the future of skiing, developed in cooperation with ispo, from which a number of innovation options for the skiing and tourism industry have been derived.

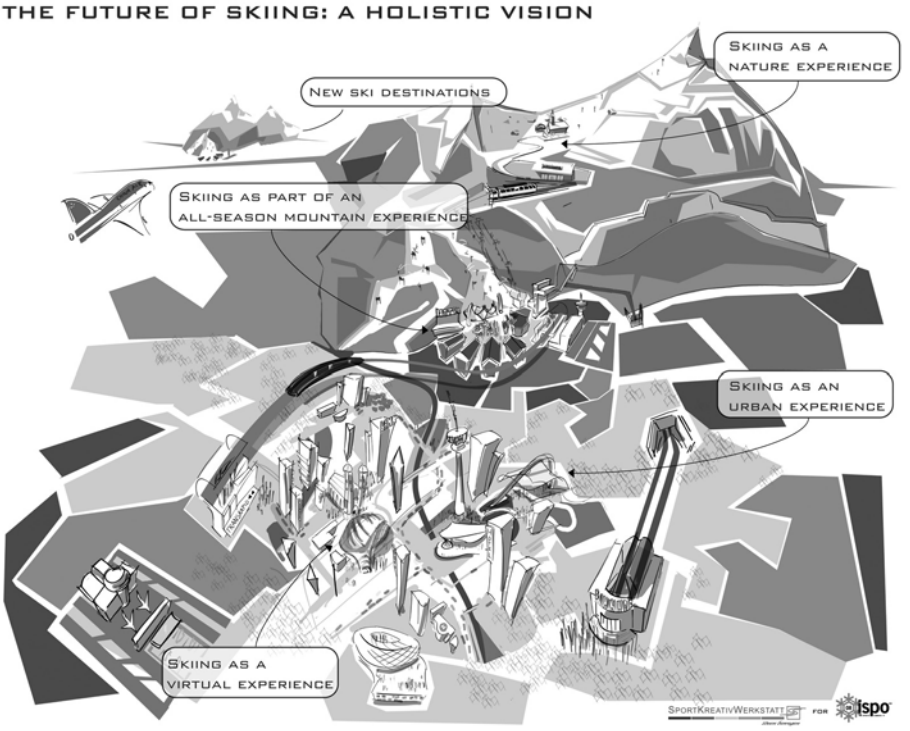

Figure 3 - System Vision "The Future of Skiing" (www.ispo.sportkreativwerkstatt.de).

- At the **defined start** of an innovation venture innovators must, among other things, clarify whether a radical innovation is possible and desirable at all, decide in which organizational setting they will work, and accumulate all resources possible (focussing especially on generative resources like competences and trust).
- The next activity is to summarize the imagination of the socio-technical essence of the desired innovation in what we have called a **TargetVision.** It is important here to find a good level of abstraction with respect to the intended scope of innovativeness, and to focus on those objectives and aspects of the innovation that have to be decided at this point already. In an explorative project in the area of entertainment fitness we have formulated the TargetVision "to develop an effective device for fitness training that uses the fascination of information and animation technologies to increase the attractiveness of training, and to enable distributed collaborative use through interlinking the devices."
- To ensure a best-possible **embedding** of the innovation, in the next step the TargetVision is contextualized; that means, the context system into which the innovation will be realized is explored. To facilitate this work and yet ensure that the relevant perspectives are taken into account, we have defined a set of dimensions that encompass the most important aspects of the environment. It is important to note here that the dimensions given in Fig. 2 have been optimized for innovation ventures in popular sports; in other fields a different set of dimensions might be necessary.
- The results of the exploration of the InnovationContextSystem often suggest some adaptations in the formulation of the TargetVision, in order to improve likelihood and extent of success.
- Next comes the exploration of the **core functions**. The rationale is that users do not care for products, they care for functions. Unfortunately this is often forgotten by technology-oriented developers. To give an example, for them a skateboard is typically interpreted as a technical artefact consisting of two axles with a certain type of kinematics, four wheels with good grip and little abrasion, and a deck with little weight and enough stiffness. For typical users, however, a skateboard is a tool allowing the performance of tricks, comfortable-enough transportation, re-appropriation of city landscapes and integration into "scenes". Innovators targeting novel rolling equipment must therefore understand the principles and innovation potentials of core functions like "performing tricks", "appropriation of city-landscape" and "integration into communities", and not perform kinematics calculations yet.
- Only then, on the basis of quite a lot of preparatory work, are **concept solutions** developed. This ensures a best-possible focussing of creativity: The scope for innovativeness has been opened up at exactly the most important issues, the core functions, and narrowed down through the concentration on core functions at the same time. In this stage, first possible constituents of the concept solution must be identified: Functions like "motivation to move" can be realized by a product, a course, an event; or everything at the same time. Concept generation itself is best performed in heterogeneous teams; however, with individual working periods as well: Ingenuity of a concept is not democratic; quality and balance is.

- As told earlier, holistic innovation also means the creation of **system solutions**. Consequently, the concept ideas must now be developed into a comprehensive system innovation. In sports, this includes the consideration of functions like production, maintenance, transport, and orientation, taking into account aspects like safety, community integration, competitions, events, and attractiveness to media, and envisioning style language, accessories, clothing and learning systems. At times, system considerations even help to find the right focus: Fig. 4 shows different designs of a fitness equipment allowing for cooperation and creative play, where the most promising concept, the MultiFlex, has been found only when discussing introduction and learning approaches.

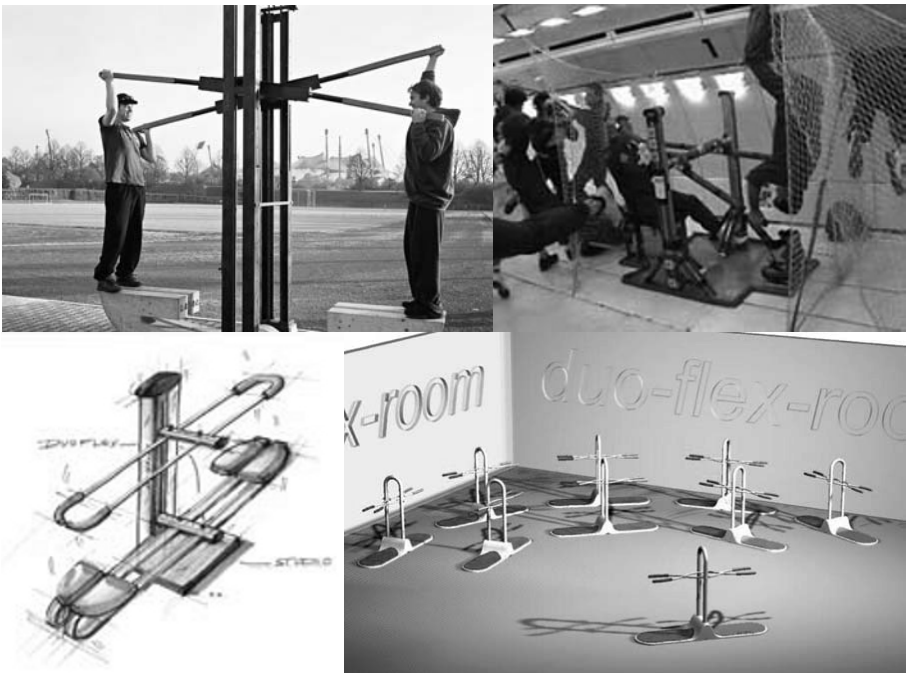

Figure 4 - DuoFlex Concepts. From top left to bottom right: Outdoor, Zero-Gravity, Studio, MultiFlex.

- Having a concept idea and a system solution, at this stage more conventional approaches to **product development** may be applied [E1]. Important from the perspective of holistic innovation is the focussing on the ConceptCore, and the translation of functions from the perspective of users into (technical or system-related) functions from a solution perspective. A respective process is being introduced in [M1].

A few words regarding the practical application of the innovatorics: It must be clear that the complete model presented in Fig. 1 is only applicable for radical innovation in sports. For incremental innovation, it may make sense to apply a reduced process, especially focussing on product development. For other innovation areas characterized by a

complex setting and multifaceted and not clearly technologically described objectives the innovatorics may be applied as well, however, with an adapted approach regarding contextualization. Finally, the innovators themselves are more important for the success than the best of process: They must be able to be imaginative, creative (also regarding methods), experimental, and contribute to the generation of synergies.

4- Further means and measures to support holistic innovation

There are of course many more means to support successful innovation than orientation at a process model. These are summarized on the right side of the Innovatorics. As examples of the most relevant ones, in the following I will briefly discuss innovation culture, innovation management, idea and knowledge management and the organisational home of innovation:

- To arrive at and maintain an effective **innovation culture** must be a continuous activity for innovators. Constituents are mental and physical creative spaces, fostering of imagination, openness towards new approaches and solutions, and, especially in sports, empathy towards human needs.
- **Innovation management** is including but also transcending project management. Especially, innovation management must be quite flexible with resource planning, focus more on generative resources, and on activities like network maintenance, build-up of trust and social cohesion, and an adaptive organization of cooperation.
- **Idea and knowledge management** is at the same time difficult and vital. Lots of knowledge is tacit, von Hippel [H3] calls it "sticky", and thus difficult to formalize and store in whatever media. Furthermore, knowledge is often generated in innovation ventures and is only meaningful in the relevant context. Existing knowledge may be made use of in the creation of synergies, which demands a fusion of knowledge modes. Helpful approaches can be the use of innovative WIKI-based systems, the use of pictures and metaphors, and the build-up of supportive social structures.
- The best **organizational homes** for radical innovation are often neither big companies nor academic institutions – both of which suffer from strong institutional fragmentation and disciplinary rationalities. Better are open innovation systems, similar to learning organizations, with a stable core team that can manage work on the brink of structure and chaos, embedded into a network of external stimulators, experts, rationalizers, and evaluators.

5- References

[CF1] Connor G.C., Veryzer R. The nature of market visioning for technology-based radical innovation. In Di Benedetto C.A. (Ed.). The Journal of Product Innovation Management, 18: 231-246, Blackwell Publishing, Elsevier, 2001

[E1] Ehrlenspiel K. Integrierte Produktentwicklung (3rd Edition). Karl-Hanser Verlag, München, 2007

[F1] Fischer E.P. Die andere Bildung. Ullstein, München, 2003

[G1] Giddens A. The Consequenses of Modernity. Stanford University Press, 1991
[H1] Haag H. (Ed.). Sportphilosophie. Verlag Karl Hofmann, Schorndorf, 1996
[H2] Hillairet D. L´innovation sportive. L´Harmattan, Paris, 1999
[H3] Hippel E. v. Sticky information and the locus of problem solving. Implications for Innovation. In Management Science, 40: 429-439, 1994
[M1] Moritz E.F. Holistische Innovation. Konzept, Methodik, Beispiele. Springer, Heidelberg, 2008
[NS1] Nowotny H., Scott P. and Gibbons M. Rethinking science: knowledge in an age of uncertainty. Polity, Cambridge, 2001
[VB1] Verworn B., Herstatt C. Prozessgestaltung der frühen Phasen. In Herstatt C., Verworn B. (Eds.). Management der frühen Innovationsphasen: 195-214, Gabler-Verlag, Wiesbaden, 2003
[V1] Veryzer R.W. Discontinuous Innovation and the New Product Development Process. In Journal of Product Innovation Management, 15: 304-321, Elsevier, 1998

Detecting Location using Sensors Based on the 802:15:4 Wireless Standard (P184)

Jose Luis Gomez, Ben Heller

Topics: Measurement Systems; Virtual Reality & Computer application in Sports.
Abstract: The 802:15:4 wireless standard is designed to provide low data-rate but very long battery life and very low complexity wireless networking. It operates in the industrial, scientific and medical radio bands; 868 MHz in Europe, 915 MHz in the USA and Australia, and 2.4 GHz worldwide. It is designed to be simpler and cheaper than other wireless standards such as Bluetooth and WiFi. It achieves greater range and noise immunity compared to Bluetooth at the expense of lower data rates by using a spread-spectrum modulation technique. As such it appears to be an attractive standard to use for wireless sensing.
We have used the Jennic 5139, a single chip implementation of the 802:15.4 standard to develop a family of 'smart' sensors for data-collection in sports applications, including accelerometers, rate-gyroscopes and pressure sensors. One feature of the standard is the ability to read the received-signal-strength-indicator (RSSI). This gives an indicator of separation between a transmitter and a receiver and has been suggested as a means of triangulating location.
The ability to cheaply and accurately detect location of an athlete in a realistic environment would be of great benefit in many sporting applications. Using our sensors we measured RSSI vs. separation, both in a free-field situation and when the transducer was worn by an athlete. We show that in real-life situations RSSI is able to locate an athlete to the nearest node, but not sufficient to pin-point their position between nodes. It is noted that the newly ratified 802.15.4a standard claims to deliver sub 1m accuracy ranging and may well provide a suitable low-cost wireless location technology
Keywords: wireless sensors, 802.15.4, location detection.

1- Introduction

1.1 Measurement of Location

The ability to accurately and easily measure location of a sports-man or sports-equipment has many potential uses. As well as providing basic quantification of performance, it plays an important role in coaching using Notational Analysis, a technique for opti-

Sports Engineering Research Group, Sheffield Hallam University, UK - Email: {j.gomez, b.heller}@shu.ac.uk

mising sporting performance based on analysis of successful and unsuccessful patterns of play (Hughes and Franks, 2004)

There are several tracking technologies, each with different characteristics, appropriate for different sports.

1.1.1 Video Tracking

One of the most widely used techniques is video-tracking; by using multiple, calibrated cameras, several objects may be tracked simultaneously, with an inaccuracy that varies linearly with the field of view. An example of the use of this technology is the ProZone system, used by several Premiership football clubs. Eight cameras are mounted around a pitch to record player and ball movement, then following the game, player position is marked-up by a combination of manual and automatic tracking. Outputs include statistics on distances, speeds, passes, tackles, etc. Video systems have the advantage that they are non-intrusive, players are not required to wear or carry any equipment. However, tracking is often labour intensive, even automated systems require much manual intervention. Also, players can often obscure each-other, requiring multiple cameras to ensure uninterrupted views. An example of a completely-automated tracking system is the Hawkeye system (Hawkeye-Innovations Ltd, UK), which uses several high-speed video cameras to accurately track the location of a rapidly moving ball with applications in tennis, cricket and snooker amongst other sports.

1.1.2 Global Positioning System

This is a navigation system based on the reception of signals from a constellation of satellites managed by the US military. The system gives a 90% confidence error of approximately 10m, reducing to 1m if a satellite-based augmentation system such as WAAS or EGNOS is used. More accuracy can be achieved if differential GPS is used. The error in determining speed is approximately 0.2m/s (Witte and Wilson, 2004). GPS is typically used outdoors, but modern, high-sensitivity receivers may allow indoor use if signal attenuation is not too great. GPS hardware has significantly reduced in size, power consumption and price over the past few years, and is an attractive tracking technology for sports use. Examples of commercially available sports tracking devices include the *SPI Elite* (GPSport, 2008) and the *SportsDo system,* which logs GPS information to a smartphone, and optionally transmits to a central portal for real-time tracking (SportsDo, 2008).

GPS-based tracking systems have the advantage that they do not require additional infrastructure, and so can be used over very wide areas, anywhere in the world. Disadvantages are update rates limited to approximately one per second, the requirement for a receiver to maintain satellite visibility and the relatively large size of the devices (approximately the size of mobile phones).

1.1.3 Radio-Frequency Time-of-Flight

As the speed of light is accurately known, the time-of-flight between transmission and reception of a wireless signal can be used to calculate positional separation between transmitter and receiver. Use of two receivers allows 2D location information to be deter-

mined, 3 or more (non co-linear) transmitters allow 3D location information. Accurate measurement of position requires very accurate timing, for example, a timing-error of one nano-second gives a distance error of 0.33m. Despite these severe timing constraints, some commercial sports systems have been developed. The *Trakus* (TKS Inc, USA) system is being trialled as a way of tracking horses during races in US racetracks. The Cairos soccer ball tracking system (Cairos Technologies AG, Germany) originally used time-of-flight transmitters located in the ball and player's shin-pads to locate ball and players to high accuracy throughout the firld-of-play, more recent versions use a magnetic location system to track the ball near the goalmouth only.

Radio-frequency time-of-flight systems can provide high-accuracy, high update-rate, automated tracking, but require fixed infrastructure that can be expensive and difficult to move.

1.1.4 Other Approaches

Various other approaches have been adopted, including ultrasound (Smith *et al.*,2004S, Addlesee, 2001), magnetic tracking systems e.g. Flock-of-Birds, (Ascension Technology Corp.), measuring the extension of a thin line tethered to the athlete (SpeedProbe 5000, Applied Motion Research Australia, 2008) and even 'smart floors'(Orrand and Aboud, 2000). Whereas these systems may be very suitable for specific applications, they have various restrictions that prevent them being generally-useful tracking systems.

1.2 Wireless sensors

We are developing sensors-networks for ambulatory monitoring in sports and health (Heller and Haake, 2005). There are several enabling wireless technologies to be considered for this application: Ultra-Wideband, Wireless Ethernet (WiFi or 802.11.x standards), Bluetooth, IEEE 802.15.4 (Zigbee[1]). The choice of appropriate wireless standard must be determined from the characteristics of the application, particularly power-consumption, range, bandwidth and networking ability. For our application critical parameters were the ability to network multiple sensors and the minimum size of each sensor. As size is governed by battery-size for realistic applications, minimal power-consumption was a critical parameter. Ultra-wideband and Wireless Ethernet are both high-power, high data-rate protocols and were therefore rejected. Bluetooth and 802.15.4 are both suitable for small battery-powered devices, but because of its greater range and lower-power consumption (at the expense of a lower data rate) (Baker, 2005) we chose to use the 802.15.4 standard. The particular implementation we use is the JN5139 single chip module from Jennic Ltd, UK. This provides an integrated solution combining RF circuitry, antenna and microcontroller (figure 1).

1. The 802.15.4 standard is often referred-to as Zigbee; in fact, Zigbee is an additional networking protocol that uses the 802.15.4 protocol.

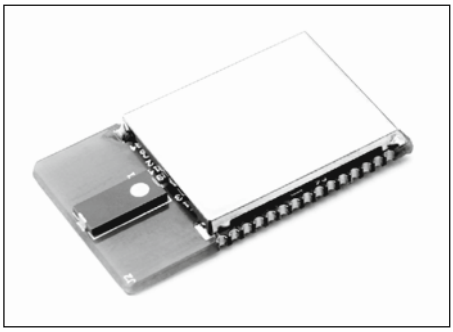

Figure 1 - JN5139 wireless module with integrated ceramic chip antenna.

1.3 Detecting Location using Received Signal Strength

Hightower *et al.* (Hightower *et al.*, 2000) describe a method for location detection based on estimating distance from signal strength, and then triangulating multiple readings to determine 3D position. They were only able to obtain approximately 3m accuracy, but this was, at least in part, due to only 2 bits of signal strength information being available. Lowton *et al.* (2006) determined the ability of 802.15.4 wireless nodes to measure separation using received signal strength; they concluded that separation measurement was unreliable for distances > 1m, but could be determined to an accuracy of approximately 0.1m in the range 0 to 1m. However, their measurements were made in free-space, and did not take-into account the effect that proximity to the body would have on the received signal strength. As 2.4GHz radio waves are highly absorbed by the body, this is likely to have a significant effect.

In order to assess the ability of 802.15.4 wireless nodes to determine location in realistic conditions, we conducted the following experiment.

2- Methods

Two 802.15.4 wireless sensor boards (JN5139, Jennic Ltd, UK) were used for the evaluation. Custom software was written to continuously transmit data from one of the boards, and receive the data and output signal strength on an LCD display on the other board.

Both boards were mounted on a non-metallic support at a height of 50cm above a concrete floor in a large laboratory, with the receiver separated by 3m from the end wall and 5m from each side-wall. The transmitter was moved at regular increments along the laboratory centre-line, and received signal strength was measured at each position. The parameter returned was an 8 bit value termed the 'link-quality indicator' (LQI), 0 is the worst transmission and 255 the best. The measurements were repeated with a hand placed directly in front of the transmitter, at a separation of 5cm from the antenna. This was to simulate realistic, body-worn environments in which the orientation of transmitter relative to the body is unknown.

3- Results

Signal-strength data were collected and are plotted in figure 2.

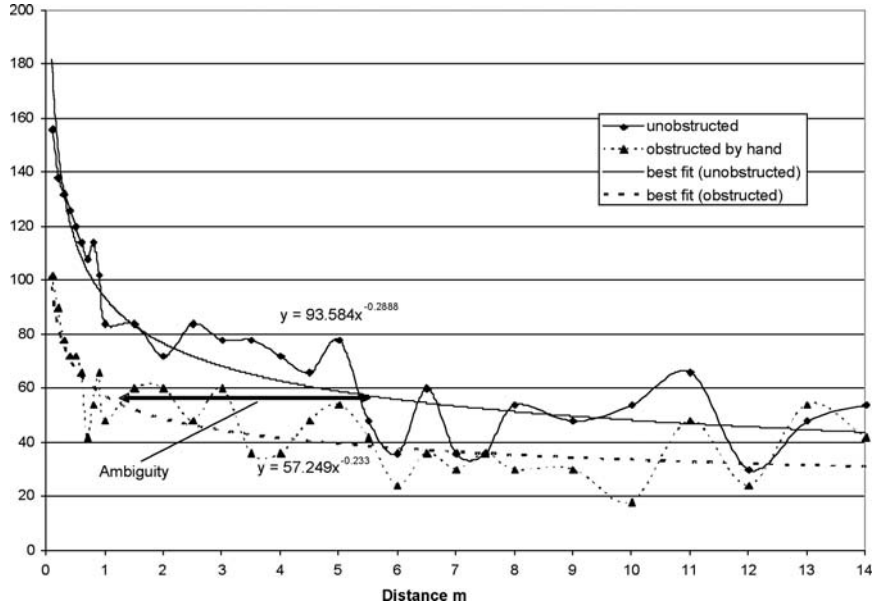

Figure 2 - received signal strength vs. separation.

4- Discussion

It can be seen that there is a fall-off of signal strength with separation. However, even in the un-obstructed data, there is much scatter. The most likely reason for this is the presence of local standing waves arising from reflections from the ground. There might also be an effect caused by antenna orientation, although the antenna was arranged to have isotropic propagation in the horizontal plane, so small misalignment should not have had much effect. The unobstructed data support the finding of Lowton et al. (2006), that the signal strength can be used to track location within 1m of the receiver, to an accuracy of 0.1m. Beyond 1m the graph is non-monotonic and there is considerable ambiguity in location corresponding to each signal strength measurement, an ambiguity which increases with distance. One use for a system like this would be to place receiver nodes at known locations around a known route (e.g. a running track), and determine approximate location when the transmitter came close (within 1m) of each receiver node.

It can be seen that the data with obstruction approximately tracks the unobstructed data, but at a reduced power level. Unfortunately there is unlikely to be a-priori information about whether the antenna is obstructed or not, so the range between obstructed and unobstructed curves for a given signal strength determines the ambiguity of position measurement. The maximum receive power in the obstructed case (10cm) is similar to the unobstructed power at 0.9m, and by 1m in the obstructed case, power is at a level which is ambiguous to a radius of over 5m for the unobstructed case. The arrow on the diagram shows the ambiguous region between the best fit lines. The ripples in the line mean that actual ambiguity is considerably greater that this, and additional uncertainty about antenna orientation would increase errors even further.

It should be noted that a new physical layer for the 802.15.4 standard has recently been published. Termed 802.15.4a it allows a choice of two frequency ranges – 'chirped' signals at 2.4 GHz, or ultra-wideband pulses at various frequencies up to 10 GHz. The 2.4GHz approach has the advantage of being almost universally usable, has a bit rate of 1Mb/s, but does not provide a ranging function. The UWB approach can provide bit-rates from 0.1 to 26 Mb/s, and a ranging accuracy of 1m (or better for some channels) using bi-directional time-of-flight (De Nardis, Di Benedetto, 2007). Once silicon meeting this standard is released, it seems likely that it will become a very attractive protocol for wireless sensors requiring a location detection function.

5- Conclusions

If it can be arranged that the antenna will never be obstructed by the body, then wireless sensors using the 802.15.4 standard are suitable for detecting position within approximately 1m of a receiver node. If obstruction is a possibility, then location detection is so poor that it is comparable to, or worse than GPS accuracy, and there is little merit in using this technique and it will be preferable to wait for 802.15.4a UWB silicon.

6- References

[AC1] Addlesee M, Curwen R, Hodges S, Newman J, Steggles P, Ward A, Hopper A. Implementing a Sentient Computing System. IEEE Computer Magazine, Vol. 34, No. 8, August 2001, pp. 50-56

[AM1] Applied Motion research http://www.appliedmotionresearch.com/products.html 2008

[B1] Baker N. Zigbee and Bluetooth. Strengths and weaknesses for industrial applications. IEEE Computing and Control Engineering 2005;16:20–5.

[DD1] De Nardis, L. Di Benedetto, MG. Overview of the IEEE 802.15.4/4a standards for low data rate Wireless Personal Data Networks. 4th Workshop on Positioning, Navigation and Communication, 2007. WPNC '07., Hanover, 2007, 285-9

[GP1] GPSport GPS tracking system http://www.gpsports.com/ 2008

[HB1] Hightower, J., Boriello, G., Want, R., SpotON: An Indoor 3D Location Sensing Technology Based on RF Signal Strength, UW CSE 2000-02-02, University of Washington, February 2000

[HF1]Notational Analysis of Sport: Systems for Better Coaching and Performance in Sport, Mike Hughes, Ian Franks eds Routledge 2004

[HH1] Heller B, Haake SJ. The SMART sensor project: empowering the user. In proceedings of Asia Pacific Conference on Sports Technology (APCST). Tokyo 2005

[LB1] Lowton M, Brown J, Finney J. Finding NEMO: On the Accuracy of Inferring Location in IEEE 802.15.4 Networks. 2nd International ACM Workshop on Real-World Wireless Sensor Networks (REALWSN '06) 2006.

[OA1] Orr R, Abowd G. The smart floor: a mechanism for natural user identification and tracking, CHI '00 extended abstracts on Human factors in computing systems The Hague, 2000, 275-6

[SB1] Smith A, Balakrishnan H, Goraczko M, Priyantha N, Tracking Moving Devices with the Cricket Location System, Proc. 2nd USENIX/ACM MOBISYS Conf., Boston, MA, June 2004

[SD1] SportsDo mobile-phone tracking system http://www.sportsdo.net/

[WW1] Witte TH, Wilson AM Accuracy of non-differential GPS for the determination of speed over ground. Journal of Biomechanics 37 (2004) 1891–1898

Use of Static Stiffness Behaviour to Characterise Field Hockey Sticks (P185)

Derek Covill[1], Joe Farr[2], Tim Katz[1], David White[2]

Abstract: The aim of this paper was to quantify the static stiffness behaviour of a variety of field hockey sticks, and to move towards a standard for their characterisation. A range of stick designs were tested at two different sections of the stick for bending stiffness. An Instron 8500 tensile and compressive testing apparatus was used to load the sticks in a simple 3-point bending regime and the results were independent of testing geometry. The mean flexural rigidity (EI product) of the samples ranged from 430-1069 Nm^2 towards the handle, and 310-636 Nm^2 towards the head and these were directly comparable to those measured in other studies of field hockey sticks. Small but acceptable variations (standard deviation of 2%) were associated with the simplified compression adjustment factor, and these could be reduced further by minimising the compression at the point of load. The flexural rigidity for sticks of the same design were shown to vary considerably (up to 15% standard deviation from the mean).
Key words: Hockey stick, characterisation, bending, stiffness, flexural rigidity.

1- Introduction

Field hockey sticks are used to both push and drive the ball when controlling, passing, stopping and shooting during training and match play. As a result, variables contributing to how a hockey stick feels and performs include the mass, centre of mass location, shaft stiffness, resistance to twist and breaking force (Marino, 98). Although players may not be able to perceive stick stiffness directly, they have been reported to perceive these effects indirectly through ratings of comfort and power (Carré and McHutchon, 2006).

1. School of Environment and Technology, University of Brighton, Cockcroft Building, Lewes Rd, Brighton, UK, BN2 4GJ - E-mail: {d.covill, j.farr, t.katz}@brighton.ac.uk
2. South East Knowledge Exchange, University of Brighton, Cockcroft Building, Lewes Rd, Brighton, UK, BN2 4GJ

At present the static stiffness behaviour and variation in static stiffness of field hockey sticks have not been studied at length. Moreover, a standard is required in order to characterise field hockey sticks and their performance. Sticks tested under rigorous and standardised procedures will provide consumers with valuable information on the stiffness rating, hysteresis and quality assurance of hockey stick designs and their manufacturers.

The stiffness behaviour of field hockey sticks has not been studied in terms of the variability associated with cost, manufacturing repeatability, location along the stick, span length and ambient temperature. This study aims to investigate the following research questions:

1) How do experimental factors influence the measurement of static stiffness behaviour in hockey sticks?
2) How does the stiffness in a variety of sticks of the same model vary?
3) How do sticks vary in stiffness according to the location along the stick?

2- Literature review

Of the little research that has been conducted on the properties of hockey sticks, most has been focused on analysing the dynamic properties of the blade (Baroud *et al.*, 1999; Moreno *et al.*, 2004) and the impact behaviour between the blade and the ball or puck (McHutchon *et al.*, 2004). Furthermore, research in this area has been dominated by analysis of ice hockey sticks, with only few publications giving mention to field hockey sticks.

Several of these studies have included measurements of stiffness in field hockey sticks ranging from 308-1041 Nm^2 (McHutchon *et al.*, 2004) and ice hockey sticks ranging from 13-19 kNm^{-1} (Pearsall *et al.*, 1999) and 7.45-7.95 kNm^{-1} (Marino, 1998) although only the field hockey stick results were independent of testing geometry. Unfortunately the above studies have not presented published experimental details such as span length, point load locations, or specimen temperature conditions which would be required to conduct a repeat stiffness test.

In an investigation into the influence of stick stiffness on the velocity of ice hockey pucks during a slap shot, Pearsall *et al.* (1999) reported that sticks with a lower stiffness generated higher puck velocities. Conversely, Carré and McHutchon (2006) demonstrated a contradicting trend for field hockey sticks, reporting a 10% increase in post-impact ball velocity for a 100% increase in stick stiffness when struck from stationary. This fundamental difference between ice hockey and field hockey sticks appears to be in the nature by which they were used. The ice hockey sticks were tested in a slap shot where bending was prevalent as the stick pushed the puck forward while the field hockey equivalent involved a more dynamic impact between the stick and the ball.

Links have started to become clearer between the perceived performance of sticks and those properties measured in the laboratory (Carré and McHutchon, 2006). The growing understanding of these links between measurable properties and emotional responses of users is providing manufacturers and product developers with an insight into how consumers rate and select their products. Therefore a quantified system of stiffness measurement could significantly aid sports consumers in their stick choice.

3- Methods

3.1 Theory

Flexural rigidity (*EI*) can be used to describe the stiffness of a beam independently of the testing geometry, and as a function of the beam's cross section and material properties. In a simply supported bending arrangement, the flexural rigidity (in Nm^2) can be determined by solving equation (1).

$$EI = \frac{FL^3}{48\delta} \tag{1}$$

Where F is the force (N) applied in the centre of the span, L is the span length (m) and δ is the deflection of the beam (m). This theory assumes a homogenous section and material, and large span lengths compared to stick height.

Although there are obvious perturbations from this idealised case in practice, the use of consistent span/position means that direct comparisons can be made between sticks.

3.2 Equipment

Data was recorded using an Instron 8500 tensile and compressive testing apparatus which provided load vs. deflection data for each test when loading and unloading the sticks. The sticks were fixed at a span of 228 mm and the load was applied at the midpoint of these supports, which were rollers with steel plates to provide protection. Sticks were placed face down to allowing the convex curvature of the stick to flatten when loaded. The span was positioned in two separate locations, A (173 mm from head to point of compression) and B (388 mm from head to point of compression), to give an indication of the change in stiffness along the minor axis of the shaft. Figure 1 shows the experimental setup for a typical 3-point bending test.

Nine stick models were tested ranging from a basic model in the low price bracket to a more advanced model in the higher price bracket. Table 1 shows the variety of sticks used. Six different sticks from each model (apart from models 1, 3, 5 and 6 where only one or two sticks were used) were tested for repeatability within the model types. This would give an indication of the differences attributed to the manufacturing process.

Four tests were conducted on one stick of model 8 to investigate the errors associated with the experimental setup and the repeatability of stick behaviour.

As the deflection was measured through the applied force head any compression apparent at the point of contact needed to be accounted for. To do this, sticks were loaded to similar values in a compression regime, and the displacement values under bending were adjusted accordingly. Over a range of sticks in model 1, the compression adjustment was tested for consistency.

Stick number	Mass (g)	Estimated composition		
		Carbon %	Aramid %	Fibreglass %
1	603±14	20	20	60
2	602±13	30	20	50
3	605±33	90	10	0
4	567±12	35	15	50
5	581	85	15	-
6	576	85	15	-
7	564±24	50	5	45
8	609±15	50	15	35
9	583±9	100	-	-

Table 1 - Variety of hockey sticks used.

3.3 Procedures

The loading/unloading was applied at a constant rate of 0.05 mm/second up until 4 mm deflection with concurrent load and deflection measurements taken every second. The loads applied were well within the elastic limit for the sticks and the room temperatures were between 15-20°C.

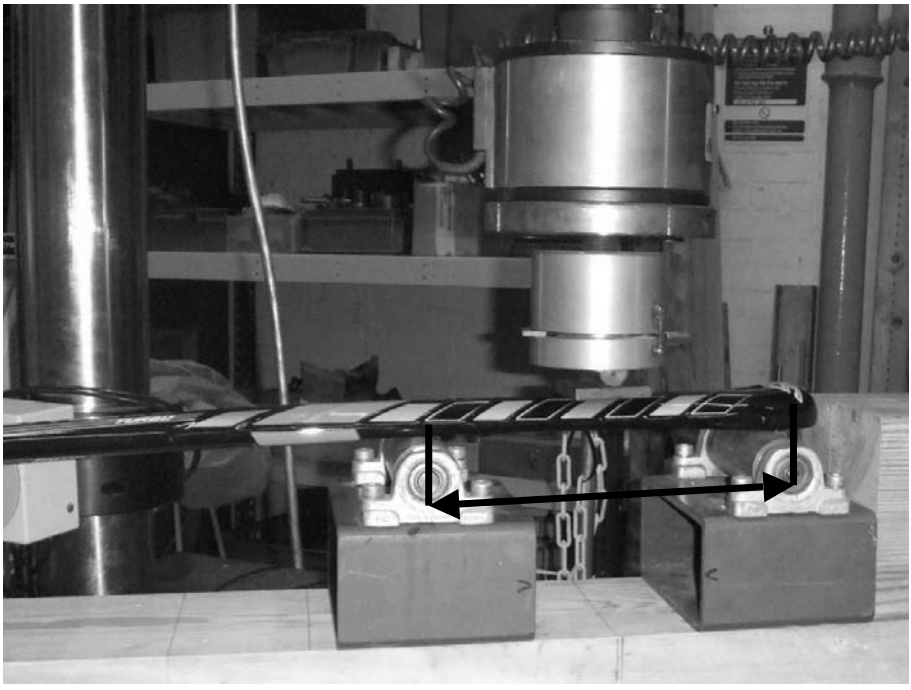

Figure 1 - The 3-point bending test setup.

4- Results

The repeatability of the experimental methods and the performance of a particular stick were tested 4 times for a stick in model 8. It was found that the range of stiffness values for the individual stick varied from 544-566 Nm^2 (mean 552 Nm^2, standard deviation 10 Nm^2).

The force vs displacement curves for sticks were relatively linear (r^2=0.99) over the 3.5 kN range as shown in Figure 2, which shows the force vs displacement curve for the loading and unloading cycles of stick 1.

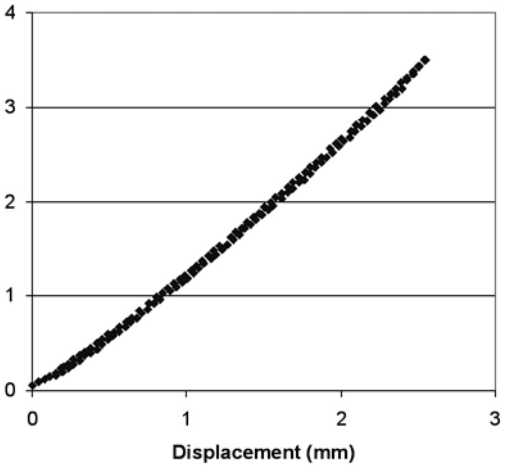

Figure 2 - Force displacement curves for model 1 during loading and unloading cycles.

The mean flexural rigidity values for a range of sticks (models 1-9) were between 310-636 Nm^2 when loaded in span A, and between 430-1069 Nm^2 when loaded in span B. These mean values with standard deviations can be seen in Table 2. In all cases the mean flexural rigidity was lower in span A than span B. In some cases the standard deviation approaches 15% of the mean value indicating significant variation between different sticks in the same model.

Stick model	*Number tested*	*Mean flexural rigidity ±sd in position A (Nm^2)*	*Mean flexural rigidity ±sd in position B (Nm^2)*
1	2	310±13	430±21
2	6	329±23	631±35
3	2	453±19	567±24
4	6	410±28	451±65
5	1	505	1069
6	1	387	607
7	6	471±28	730±75
8	6	552±23	646±29
9	6	636±30	742±38

Table 2 - Flexural rigidity values for sticks 1.9.

Figure 3 shows the ranges in flexural rigidity ranked in ascending order at span location B. It can be seen that as the stiffness values at location B increase, those at location A do not match this trend.

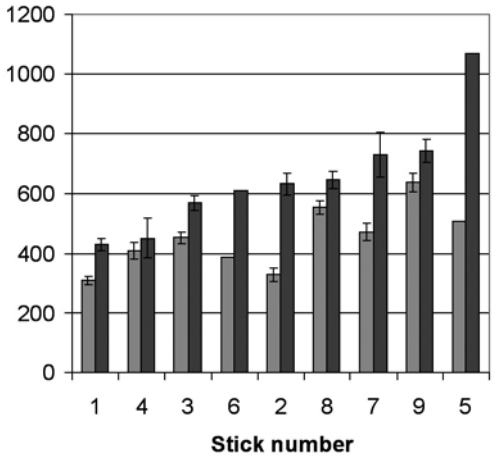

Figure 3 - Flexural rigidity values at span location A (left) and b (right) for various stick designs (±sd).

5- Discussion

The mean flexural rigidity values for the variety of sticks tested in this study ranged from 310-636 Nm^2 when loaded in span A, and between 430-1069 Nm^2 when loaded in span B. These values for span B are similar to those measured by McHutchon *et al.*, which ranged from 308-1041 Nm^2 (2004). The sticks tested by McHutchon *et al.* (2004) ranged from a low-end wooden stick to a high end carbon fibre stick. The sticks tested in this study ranged from a low-end predominantly fibreglass model to a high-end carbon fibre model. It is interesting to note that only the values measured at span B (measured further up the stick) are comparable to those measured by McHutchon *et al.* The values measured at span A are considerably lower than those from span B indicating that the stiffness of the stick shaft is variable along its length. How this change in stiffness along the length is related to the perception of stiffness or the performance of the stick is relatively unknown. However, it is suggested that stiffness changes in regions closest to the handle will be perceived more notably than those toward the head of the stick. This is because increased flexibility at the handle leads to greater displacement of the head.

The differences in stiffness at span locations A and B can be attributed to the changes in cross-section at these locations. At the midpoint of span location A the section is flatter and wider than the one at B as indicated in Figure 4 which shows typical sections at these points. The flatter and wider section of the section in A will have a lower second moment of area than B and this corresponds to a lower *EI* product since the elastic modulus (*E*) may not change significantly. The individual designs of the different stick models explains why the ratios of stiffness at A:B are not consistent.

Figure 4 - Typical sections at the point of load for span A (left) and B (right).

This study has provided a simple 3-point bending setup to measure the stiffness of field hockey sticks with adjustments made to account for compression of the sticks at the point of loading. Testing within one model showed that the compression adjustment was proportional to the bending deflection measured under equivalent loads. This meant that adjustments to the measured values of flexural rigidity could be applied by using compression measurements of a single stick representative of that model. Although this was a simplified method of adjusting the bending stiffness, it was not without its limitations. The repeatability of tests on a single stick could be represented by the standard deviation from the mean which was approximately 2% of the mean value for the flexural rigidity (552±10 Nm^2). This highlighted the variability in stiffness values as a result of the compression adjustment factor.

Variables that were considered but not varied or analysed in this study included the stick temperature during the tests and the loading rate. Since the energy absorption behaviour of composites is variable with temperature (Hamada *et al.*, 1996) it is anticipated that changes to a stick's temperature will have significant affects on its overall stiffness. Likewise the loading rate is expected to have a significant affect on the overall stiffness behaviour of the sticks, as the stiffness and strength of composites are highly dependent on loading rate (Suvorova *et al.*, 1991). In practice and match situations, the ambient and stick temperatures are expected to vary widely with global location, season and venue, while the loading rates are expected to vary widely with a player's age, ability and strength. Hence, further work is required to understand the effects of stick temperatures and loading rates on stick stiffness, and to identify a suitable rate for the consistent measurement of static loading.

Variations in stick stiffness within a model type can be attributed to the techniques used to manufacture them. Like other field sports, such as willow bats used in cricket, the composite hockey stick designs tested in this study were hand-laid before being processed. This technique introduced variations in the wall thicknesses and layer consistency which can affect the second moment of area and material homogeneity along the length of the shaft. In some cases the wall thickness, distribution of resin and location of the central beam may vary considerably between sticks of the same model. Although these inconsistencies in the manufacturing processes may at first appear to be a limiting factor for manufacturers, it can be argued that this variability allows for more variety and choice for consumers who may have particular preferences for balance, mass and stiffness. Regardless, a simple means to quantify and characterise sticks according to their physical properties would benefit consumers in making choices and provide feedback to manufacturers on issues of quality and consistency of their products. A simply supported bending regime has the greatest bending moment directly beneath the applied force. This may accentuate any inconsistencies within the flexural rigidity along the shaft, but it does make it easier to identify areas of major influence.

6- Conclusions

This study has outlined a simple means to determine the static stiffness behaviour of field hockey sticks in an attempt to move towards their characterisation. Small but acceptable variations (standard deviation of 2%) were associated with the simplified compression adjustment factor, and these could be reduced further by minimising the compression at the point of load. The stiffness values away from the head of the stick (at span B) were considerably higher than those closer to the head (at span A). This was attributed to the change in section along the shaft, from a wide flat profile near the head of the stick to a thin narrow profile further up the shaft. Stiffness values for the range of sticks tested in this study ranged from 430-1069 Nm^2 at span location B, and 310-636 Nm^2 at span location A. These were directly comparable to those measured in other studies of field hockey sticks. The moduli of rigidity for sticks of the same design were shown to vary considerably (up to 15% standard deviation from the mean) as a result of the hand-laying process by which they were made. Further work is required to minimise the compression of sticks in bending and to investigate the effects of stick temperature and loading rate on their stiffness behaviour. It may also be worthwhile to decouple the applied loads from the measured deflection completely. Using a compound bending arrangement, where the supports each supply a bending moment which is constant across the test region may provide a more integrated (and hence consistent) set of readings. How these would be perceived by users is unknown. By using simple supports, but iteratively shifting the test region incrementally along the shaft could provide a stiffness profile that would illuminate the variations within a stick and their effects.

7- References

[BS1] Baroud G., Stefanyshyn D. and Bellchamber T. Performance enhancement of hockey sticks using numerical analysis. In Proceedings of the XVth Congress on the International Society of Biomechanics (eds. Herzog and Jihna), 827, 1999.

[CM1] Carré M. and McHutchon M. Understanding human perception of field hockey stick performance. In The Engineering of Sport, 6(3), 237-242, 2006.

[HR1] Hamada H., Ramakrishna S. and Sato H. Effect of Testing Temperature on the Energy Absorption Behavior of Carbon Fiber/PEEK Composite Tubes. In Journal of Reinforced Plastics and Composites, 15 (1), 30-47, 1996.

[M1] Marino G. Biomechanical investigations of performance characteristics of various types of ice hockey sticks. In Proceedings of the International Society of Biomechanics of Sport (Riehle and Vieten), 184-187, 1998.

[MC1] McHutchon M., Curtis D. and Carré M. Parametric design of field hockey sticks. In The Engineering of Sport, 5(1), 284-290, 2004.

[MW1] Moreno D., Wood J. and Thompson B. Dynamic analysis techniques for the design of the ice hockey stick. In The Engineering of Sport, 5(1), 263-269, 2005.

[PM1] Pearsall D., Montgomery D., Rothsching D. and Turcotte R. The influence of stick stiffness on the performance of ice hockey slap shots. Sports Engineering, 2, 3-11, 1999.

[SS1] Suvorova Y., Sorina T. and Gunyaev G. Rate dependences of the strength of carbon-fiber-reinforced plastics. In Mechanics of Composite Materials, 26(4), 480-484, 1991.

Finite Element Analysis of the Heat Transfer in Footwear (P186)

Derek Covill[1], Zhongwei Guan[2], Martin Bailey[3], David Pope[1]

Topics:

Abstract: This paper outlines the use of finite element analysis to describe the heat transfer in footwear. Experiments were conducted to determine the temperature distribution in footwear with a variety of environmental temperature and footwear properties considered. Finite element models describing the heat transfer between the foot, sock and shoe are presented with the conductivity, specific heat and density properties of each material presented taken from literature. Based on foot geometry obtained from plaster casts, these models predicted temperatures within footwear with conduction, convection and radiation taken into account. Results from the models were compared with experimental findings with generally good agreement; however the models were limited by a simplified heat input value based on whole body values which did not account for the counter current heat exchange and also by the absence of evaporation as a mode of heat transfer which was significant in hotter conditions. A sensitivity analysis on the heat transfer models showed that the major contributors to the in-shoe conditions under dry heat transfer were the ambient temperature and the initial temperatures of the foot, while the heat flux and sock conductivity also had a minor affect. Further studies are required to include the effects of evaporation and to include the counter current heat exchange as a control for heat input to the foot.

Key words: Finite element analysis, heat transfer, footwear, temperature.

1- Introduction

In the same way that clothing provides insulation for the body to limit the amount of heat lost to the environment, footwear also has a role to insulate the feet to reduce the amount of heat transferred to or from the environment. This thermal protection can be particularly important in cold conditions or when the body is emitting large amounts of

1. School of Environment and Technology, University of Brighton, Cockcroft Building, Lewes Rd, Brighton, UK, BN2 4GJ - Phone: +44 (0) 1273 642214 - E-mail : d.covill, d.j.pope}@brighton.ac.uk

2. Department of Engineering, University of Liverpool, Brodie Tower, Brownlow Street, Liverpool, UK, L69 3GQ - Phone: +44 (0)1517 945210 - Email: zhongwei.guan@liverpool.ac.uk

3. Chelsea School, University of Brighton, Hillbrow, Gaudick Road, Eastbourne, UK - Phone: +44 (0)1273 643744 - E-mail : m.p.bailey@brighton.ac.uk

heat, as excessive or restricted heat loss can unbalance the body's homeostasis causing thermal discomfort. A balance needs to be achieved between the amount of heat generated by or supplied to the feet, and efficiency of heat loss to optimise foot temperatures and comfort experienced in footwear. This study aims to address the issues that are relevant for determining in-shoe conditions in an attempt to understand the mechanisms of heat transfer in footwear. A 2-D finite element model of the heat transfer in footwear is presented, taking into account material properties of the foot, sock and shoe, and the heat transfer mechanisms considered were conduction, convection and radiation over an 80 minute period. Simulated in-shoe temperatures were compared with experimental values in order to evaluate the model.

2- Background information

There have been many attempts to model human and animal thermoregulation systems, most of which are used to predict core temperature and other indicators of heat strain. Such models are a function of a wide variety of variables, including individual characteristics (sex, age, mass, fitness level, fat content, VO_2 max, metabolic output and surface area) clothing input (insulation, thickness, permeability and absorption) and environmental factors (ambient temperature, RH or vapour pressure, radiation conditions and air motion) (Havenith, 1997; Lotens, 1992). Overall, the models propose to define relationships (often empirically) between these variables and those which define the thermoregulatory state of a whole body (core temperature, skin temperature, skin blood flow, sweat rate, skin wetness). Some assume the body to take the form of basic shapes such as cylinders and spheres (Boregowda *et al.*, 1997), others simply apply theories in one-dimension (Ghaddar *et al.*, 2003).

Typically, thermal models involving the foot have stemmed from whole body and clothing models. Lotens (1989) and Lotens *et al.* (1989) used a similar approach in an attempt to scale down the body to represent the foot only. In this 1-dimensional model, the foot is considered to consist of two compartments, the skin (where the control of blood flow was assumed to occur) and the thermally passive core. There were also assumptions on how the heat was to be transferred from the blood to the skin. Perhaps the most significant inclusion of this model was the non-linear (exponential) blood control function. This model was developed to predict the average foot skin temperature in ambient temperatures well below the 15°C linear threshold. It produced a relatively good correlation between predicted and measured results from 2 experiments where the temperature difference was up to 3°C ($r=0.87$ and $r=0.95$), but this did not take into account activity or the transient nature of heat transfer (Kuklane *et al.*, 2000).

3- Experimental methods

Nine subjects were chosen to represent the general population and so no physiological, gender, age or ethnic factors were taken into consideration. Prior to each test, they were informed of the experimental procedures and agreed to abstain from eating or drinking for at least 2 hours prior to the experiment to maintain relatively consistent hydration levels. Shoes and socks were conditioned in the chamber for at least 2 hours. This was

limited due to the constant use of the chamber for other experiments. The socks and the left shoe were weighed. Subjects completed the informed consent forms, and then bathed their feet in a footbath regulated at 33°C for at least 5 minutes before drying them thoroughly. The footbath was introduced to ensure the superficial regions of the foot were at the same temperature consistently for each test, and 33°C was considered to be a comfortable temperature for the foot (Oakley, 1984). Subjects were required to sit upright with both feet flat on the floor, in order to minimise any effects related to posture that might affect the blood flow to the feet. This passive period lasted 35 minutes. Three Hygrometrix temperature and humidity sensors were placed inside the right shoe. They were located in the toe region (equidistant between digits 1 and 2, 1cm above the insole), in the arch region (1cm above the insole) and in the heel (in the middle of the heel, 1cm above the insole). These positions were chosen in order to map the climate in the anterior, middle and posterior regions of the shoe and since these locations are indicative of the variation across the entire length of the shoe. Temperatures were logged for 35 minutes in each location at 30 second intervals. Perceptions of comfort within the shoe were also recorded on a scale from 1 (Very comfortable) to 7 (Very uncomfortable) every 5 minutes.

4- Modelling methods

Conduction, convection and radiation are the main forms of body heat transfer (Cengel, 1998), with the evaporation of sweat also contributing significantly depending on the environmental conditions. Conductive heat transfer is characterised by the temperature difference across a solid or fluid body, the thermal conductivity of the material, the thickness of the material and the area of the surface from which the heat is transferred. This can be expressed as (Simonson, 1981):

$$Q = -kA\frac{dT}{dx} \tag{1}$$

Where Q is the heat lost (W), k is the thermal conductivity (W/m°C) A is the surface area (m^2), and $\frac{dT}{dx}$ is the temperature gradient (°C/m). Convective heat losses are those which take place from the surface of a solid body to the moving fluid surrounding it (Cengel, 1998). Like conduction, convection is characterised by a temperature gradient, however convection relies not on the 'thickness' of a material layer but on the properties and flow of the surrounding fluid. This is represented by the convection co-efficient such that convective heat transfer is calculated by (Holman, 2002):

$$Q = hA(T_s - T_a) \tag{2}$$

Where h is the convection coefficient (W/m^2°C), A is the surface area (m^2), T_s is the local skin temperature and T_a is the ambient temperature (°C). In the case of footwear, convection is considered to occur from the outer layer of the shoe to the environment at a rate of 8.3 W/m^2/°C W/m^2.°C according to convection coefficients presented by Cengel (1998) for still materials with an estimated air velocity of 1m/s. This form of heat loss is increased significantly when walking or running due to the increased circulation of air.

Thermal radiation, in the form of electromagnetic waves, is the energy emitted by objects because of their temperature. All bodies at a temperature above absolute zero (–273°C) emit thermal radiation (Cengel, 1998). For the purposes of this study, the radiation was considered between the foot and the surrounding environment. The heat transfer rate was calculated by:

$$Q = \varepsilon\sigma A[(T - T_z)^4 - (T_\infty - T_z)^4] \quad (3)$$

where ε is the emissivity of the skin surface, a dimensionless constant, taken to be 0.97 from (Cengel, 1998), σ is the Stefan-Boltzman constant (5.67 x 10^{-8} W/m^2K^4) (Cengel, 1998), T is the temperature at this point on the surface (°C), T_∞ is the ambient temperature (°C) and T_z is absolute zero (–273°C).

The amounts of heat lost from the whole body by each of these mechanisms vary depending on the environmental conditions. In cool conditions (10°C), conduction and convection are the major heat loss methods, while in hotter conditions (30°C) evaporation of sweat is the most prominent method as the temperature gradient between foot and environment diminishes (Givoni and Belding, 1962; Collins and Weiner, 1962).

The metabolic heat generated within the foot was represented by a simplified model of 58 W/m^2 which was based on the whole body metabolic rate. Finite element models were created using ABAQUS 6.3, and all components used 2-D 4-node quadrilateral heat transfer elements (DC2D4). A plaster cast of a subject's foot was taken to provide a 2-D geometrical outline for the foot in this model. The corresponding shoe was placed over a negative plaster casting of the mould and both were cut along the mid-sagital plane of the foot to give the 2-D representation shown in Figure 1, which shows the mesh of this 2-D section along with the location of the nodes used to compare with corresponding experimental measurements of temperature.

Rather than having a single shoe component, this model differentiated between the materials used for the upper and the sole. A sock layer between the shoe and foot was also included. Table 1 presents the material properties for this model based on values obtained from literature (Boregowda *et al.* 1998; Cengel, 1998).

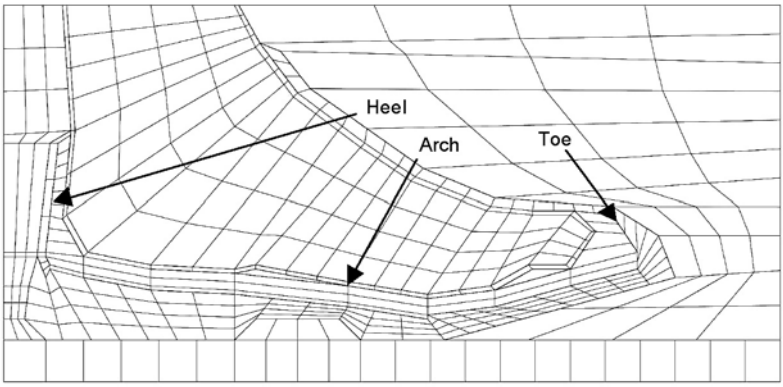

Figure 1 - Generated mesh representing the foot, sock, shoe and air in the environment model. Nodes corresponding with measurement locations also indicated.

Model Part	*Specific Heat, C_P (J/kg.°C)*	*Density, ρ (kg/m^3)*	*Thermal Conductivity (W/m^2K)*
Foot	1260	810	0.2
Sock (cotton)	1300	80	0.06
Shoe upper (leather)	2010	998	0.16
Shoe sole (soft rubber)	2010	1100	0.13
Air (inside shoe)	1005	1.2	0.026
Ambient Air (outside shoe)	1005	1.2	0
Floor (aluminium)	903	875	177

Table 1 - Material properties of model components.

5- Results and discussion

The temperatures (in °C), heat flux magnitudes (in W/m^2) and heat flux vector (in W/m^2) results from the model in 15°C are presented in Figure 2. Foot temperatures are shown in (a), foot heat flux vectors in (b), foot heat flux magnitudes in (c), shoe temperatures in (d), shoe heat flux vectors in (e) and shoe heat flux magnitudes in (f). The heat flux vectors were useful for showing the relative magnitude of the heat flux and more importantly the direction of flow. It can be seen in the figure below that the heat flux is largest in the dorsal surface of the foot, and also from the shoe upper. The sole provides the largest amount of insulation in the shoe and hence there is very little heat flow from the foot through this region.

Equilibrium temperatures after 35 minutes are presented in Table 2 below. This figure shows both the experimental temperatures with standard deviations and modelled temperatures.

	15°C			25°C			35°C		
	Toe	Arch	Heel	Toe	Arch	Heel	Toe	Arch	Heel
Experimental Temperatures ±sd (°C)	15.7±0.6	17.1±0.4	18.6±0.4	25.2±0.5	28.0±0.2	26.4±0.6	35.4±0.3	35.8±0.4	34.9±0.5
Modelled Temperatures (°C)	16.0	17.6	18.5	25.9	27.9	27.0	34.2	34.9	34.7

Table 2 - Experimental and modelled temperatures.

It can be seen that there is a reasonable correlation between the trends in the three shoe zones in each of the ambient temperatures. It is interesting to note that the modelled temperatures are considerably lower for the ambient condition of 35°C. This highlights a particular limitation of this model, by not including the effects of evaporation, which would liberate heat and increase the temperature inside the shoe. The simplified metabolic heat generated within the foot of 58 W/m^2 is also a limiting factor as it is based on the whole body metabolic rate, and would vary according to changes in envi-

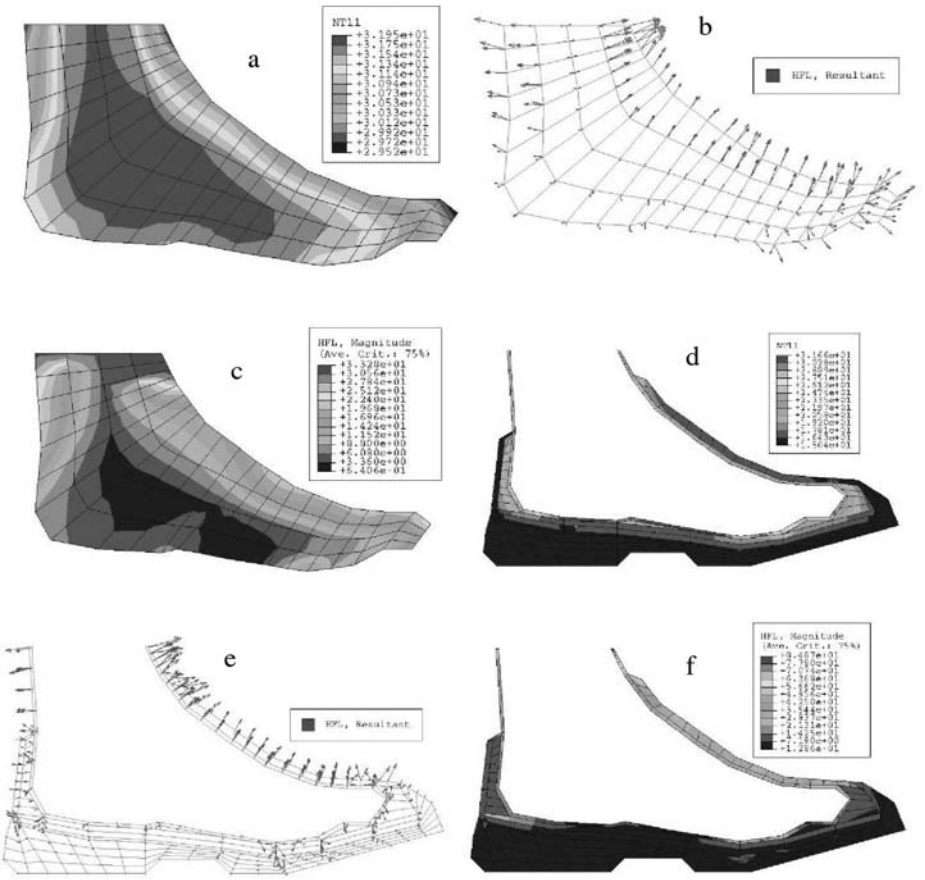

Figure 2 - Finite element model simulation of (a) foot temperatures (°C), (b) foot heat flux vectors (W/m^2), (c) foot heat flux magnitudes (W/m^2), (d) sock/shoe temperatures, (e) sock/shoe heat flux vectors, (f) and sock/shoe heat flux magnitudes in 15°C.

ronmental conditions and activity. The sensitivity of the 2-D heat transfer model for various parameters was investigated by changing these parameters separately, and their effect compared with a reference condition (25°C at rest with a heat flux of 60W/m^2 wearing a normal shoe) as shown in Table 3. It appeared that the ambient temperature and initial shoe temperature were the most influential parameters for in-shoe temperature with temperature changes greater than 2°C. Initial foot temperature, and the insulated shoe produced changes of up to 2°C, while the initial sock temperatures and sock insulation influenced the conditions by up to 0.5°C. The ground temperature was relatively unimportant; suggesting that the insulation provided by the sole was adequate and considerable air movement from wind or activity would be required to influence in-shoe temperatures. In terms of comfort, subjects on average felt that the 25°C condition was the most comfortable after 35 minutes; however there was only a marginal difference between this condition and that at 35°C. Figure 3 shows the mean comfort perceptions

	Toe	Arch	Heel
15°C heat flux=60W/m^2	---	*0*	-
25°C heat flux=0W/m^2	-	-	*0*
25°C heat flux=60W/m^2	*0*	*0*	*0*
25°C heat flux=120W/m^2	+	+	+
35°C heat flux=60W/m^2	+++	+	+++
Initial foot temperature 29°C	-	--	--
Initial foot temperature 37°C	++	++	++
Initial ground temperature 15°C	*0*	*0*	*0*
Initial shoe temperature 15°C	--	---	-
Initial shoe temperature 35°C	+++	+++	++
Initial sock temperature15°C	*0*	-	-
Initial sock temperature 35°C	*0*	+	+
Wet shoe (k=0.2)	-	*0*	-
Wet sock (k=0.08)	*0*	--	-
No convection (h=0)	-	*0*	*0*
Walking at 2m/s (h=12W/m^2/°C) (Cengel, 1998)	*0*	*0*	*0*
Insulative sock (double thickness)	*0*	+	+
Insulative shoe (double thickness)	++	++	++

Where 0=$|\Delta T| \leq 0.1$; +/–=$|\Delta T| \leq 0.5$; ++/——=$|\Delta T| \leq 2.0$; +++/———=$|\Delta T| > 2.0$).

Table 3 - Changes in calculated in-shoe temperatures after 35 minutes induced by modified parameters.

for these conditions. It is interesting to note that subjects initially felt that sitting in 15ºC was more comfortable than at 35ºC, but at a time approaching 10 minutes this was reversed with 35ºC becoming more comfortable (sloping down) while 15ºC and 25ºC became less comfortable (sloping up). This could be an interesting finding for stores trying to maximise the levels of comfort experienced by customers. Further studies are required to investigate the effects of a temperature transition to simulate moving into a cool store from the warm environment, or vice versa.

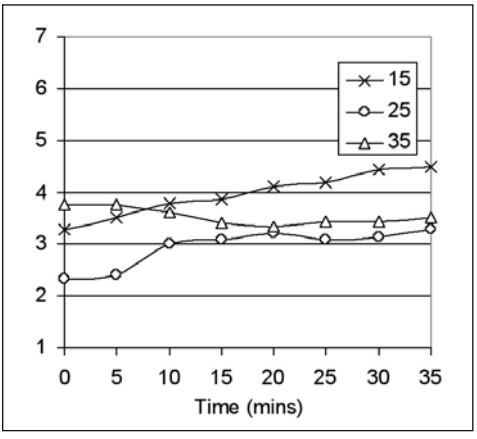

Figure 3 - Mean comfort perceptions of subjects in 15, 25 and 35°C.

6- Conclusions

The model presented in this study shows a reasonable agreement between the experimentally measured temperatures within the shoe and those established with a simplified thermal finite element model. This 2-D model was best suited to the mild conditions where the effect of sweating was less and the gradient between core and skin was not too high, however it was also suitable for any lower than 35°C, where the effects of sweating are not significant. The sensitivity analysis showed that the major contributors to the in-shoe conditions were the ambient temperature and the initial temperatures of the foot, while the heat flux and sock properties also had a minor affect. The limiting factors for these numerical models were the simplified metabolic heat generated within the foot and the lack of evaporation as a mode of heat loss. Further studies are required to include the effects of evaporation, to include the counter current heat exchange as a control for heat input to the foot and to include a dynamic heat loading to simulate activity.

7- Acknowledgements

The authors would like to thank Clarks for their support in kind, and the Chelsea School in the University of Brighton for the use of their environmental chamber.

8- References

[BT1] Boregowda S., Tiwari S., Chaturvedi S. Simulation of human thermoregulation using finite element method ASME Bioengineering Conference, 35, (1997), pages 83-84.

[C1] Cengel Y.A., Heat transfer: a practical approach. McGraw-Hill, New York, (1998).

[GG1] Ghaddar N., Ghali K., Jones E. Integrated human-clothing system model for estimating the effect of walking on clothing insulation. International Journal of Thermal Sciences, 42, (2003), pages 605-619.

[GB1] Givoni G., Belding H. The cooling efficiency of sweat evaporation. Biometeorology 20, (1962), pages 304-314.

[H1] Havenith G., Individual heat stress response. Ph.D thesis (1997).

[H2] Holman J.P., Heat transfer 9th Edition. McGraw Hill, London (2002).

[L1] Lotens W. A., Heat transfer from humans wearing clothing. Ph.D. thesis, TNO-Institute for Perception, (1992).

[L2] Lotens W. A., A simple model for foot temperature simulation. Soesterberg: TNO Institute for Perception IZF, (1989).

[LH1] Lotens W. A., Heus R., Van De Linde F., A 2-node thermoregulatory model for the foot. Thermal Physiology (1989), pages 769-775.

[KH1] Kuklane K.,Holmer I., Havenith G., Validation of a model for prediction of skin temperatures in footwear. Journal of Physiological Anthropology 19(1) (2000), pages 29-34.

[O1] Oakley E.H.N., The design and function of military footwear: a review following experiences in the South Atlantic. Ergonomics 27 (1984), pages 631-637.

[S1] Simonson J.R., Engineering heat transfer. Macmillan Press Ltd, London (1981).

[CW1] Collins K., Weiner J. The control and failure of sweating in man. Biometeorology, 18, (1962), pages 280-284.

Determination of the Optimal Saddle Height for Leisure Cycling (P188)

Javier Gámez[1], Manuel Zarzoso[2], Alex Raventós[1], Marta Valero[1], Enrique Alcántara[1], Amparo López[1], Jaime Prat[1], Pedro Vera[1]

Abstract: Several studies have been done on road racing cycling and triathlon to determine the optimal saddle height (LINF) in terms of efficiency. However, cycling is becoming nowadays not only a popular sport but also a mass mean of transport were comfort takes priority over efficiency. The aim of this study is to determine an optimal saddle height (LINF) to improve comfort in leisure cycling. Five male subjects (height mean=172.2 cm, std=1.34 cm; crotch height mean=81.25cm, std=0.88cm) tested 9 prototypes of the company ORBEA with 3 levels of LINF. The test consisted in one hour cycling in lab conditions and four different techniques were used to evaluate the LINF: 3-D movement analysis was used to parameterize the knee extension and medio-lateral deviation; surface EMG was used in 3 leg muscles (gastrocnemius, rectus femoralis and tibialis anterior) to measure muscular activity; 16 pressure sensors were placed in seat and hand-grip to obtain peak pressures on both locations; finally, subjects were interviewed following a questionnaire to obtain subjective perception. Parametric results were studied using ANOVA analysis ($p<0.05$) and post-hoc analysis (Tukey-B), while Kruskal-Wallis analysis was used for non-parametric data ($p<0.05$).According to the data analysis, LINF best level was the intermediate one, which reduced muscular activation and peak pressure. Besides, with this level no injury risk was found regarding knee extension and mediolateral desviation. In addition, opinion data analysis showed that subjects prefer the intermediate level of LINF ($p<0.05$).
Finally, a comfort coefficient was calculated using the mean value of the experimental sample crotch height and the optimal level of LINF proposed (LINF/ crotch height). The value obtained was 0.872 which is sensibly lower than the racing coefficient shown in literature (LINF coeficient= 0.883). In conclusion, this study proposes some biomechanical criteria in order to improve comfort in leisure cycling.

Key words: cycling, saddle height, biomechanics, comfort.

1. Instituto de Biomecánica de Valencia, Universidad Politécnica de Valencia, Edificio 9C, Camino de Vera s/n, E-46022 Valencia, Spain - E-mail: {javier.gamez,alex.raventos,marta.valero,enrique.alcantara,amparo.lopez,Jaime.prat,pedro.vera}@ibv.upv.es
2. Department of Physiology, University of Valencia - E-mail: manuel.zarzoso@uv.es

1- Introduction

Cycling is not only a popular sport but also a mass mean of transportation. The bicycle is an essential device for a lot of people´s everyday life, and a source of transport that has been recognized as beneficial for both, our health and our environment. As a sport, there have been many attempts in order to determine the optimal design parameters, which enhance the maximum efficiency of the bicycle, based on performance as well as physiological and biomechanical criteria. Design variables as seat height (Ericson *et al.* 1985, Jorge and Hull 1986, Price and Donne 1997), seat tube angle (Too 1991, Heil *et al.* 1995, Price and Donne 1997, Garise and Doran 2000, Ricard *et al.* 2006), crank length (Mc Daniel *et al.* 2002), pedal cadence (Takaishi *et al.* 1996, McIntosh *et al.* 2000) or longitudinal foot position on the pedal (Ericson *et al.* 1985) have been studied in triathlon and road bicycles. Nevertheless, there are few references focused in the analysis and improvements of leisure cycling desing, althought it is a very interesting niche market for bicycles manufactures.

In leisure cycling comfort takes priority over efficiency or motor performance, but the majority of the studies do not analyse the comfort and subjective varibles. A new aproach based in a user-centered design is deemed necessary, in order to link better with user needs and aims; so users' opinion and anthropometric measurements must lead the design requirements of this type of products.

Saddle height is one of the most importants variables in the bikes design; in the literature, we can find a coefficient recommendation for road bikes (0.885 X crotch height), but there is not any saddle height coeficient in leisure bikes. Thus, the aim of this study consist of determine an optimal saddle height (LINF) coeficient to achieve a good level of comfort in leisure cycling.

2- Methods

2.1 Experimental protocol

The experimental sample tested in a randomized order nine prototypes provided by ORBEA S. Coop. Ltda; with three levels of LINF calculated according to the road saddle height coeficient (0.885 * crotch height) (table 1). Each session consisted of a warm-up, a test of maximal effort and the cycling in lab conditions during one hour at 100W. Two different conditions were used: 1-flat terrain and 2-slope of 10%. Data were obtained measuring simultaneously the movement, pressure and EMG, two times in each condition. A detailed explanation of the protocol is presented in the figure 1.

LEVEL	RELATION WITH ROAD SADDLE HEIGHT COEFFICIENT	VALUE
LINF 1	(0.885 * crotch height) – 35 mm	684.1 mm
LINF 2	(0.885 * crotch height) – 10 mm	709.1 mm
LINF 3	(0.885 * crotch height) + 15 mm	734.1 mm

Table 1 - Saddle heights.

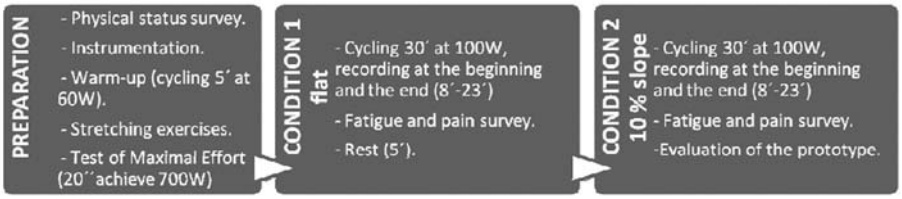

Figure 1 - Study procedure.

2.2 Subjects

Five male recreational cyclists took part in this study. Mean age was 26.60 years old (SD = 5.94), height 172.2 cm (SD = 1.34) and mean crotch height 81.25 cm (SD = 0.88); we want to highlight the low values of the COF (table 2). All of them were informed about all study details, aim ocedures; and written consent was collected.

SUBJECT	AGE (years)	HEIGHT (cm)	TRUNK (cm)	UPPER LIMB (cm)	CROTCH HEIGHT (cm)
1	25	171,17	63,70	60,47	80,03
2	24	174,50	64,80	62,00	80,63
3	22	172,17	65,13	64,30	81,67
4	25	171,77	65,40	61,07	81,80
5	37	171,40	66,20	64,80	82,13
Mean	**26,60**	**172,2**	**65,05**	**62,53**	**81,25**
SD	**5,94**	**1,34**	**0,91**	**1,93**	**0,88**
COF	**22.56 %**	**0,77 %**	**1,39%**	**3,08%**	**1,08%**

Table 2 - Anthropometric measures of the five subjects who took part in this study.

2.3 Instruments

2.3.1 Kinematic analysis

In order to evaluate the movement, 3D motion capture system, called KINESCAN/IBV, was used (4 cameras, 50 hz). The biomechanical model consist of eight markers affixed to skin (figure 2), and there were others three markers to define the plane of the bicycle. The variables analyse were knee lateral deviation and knee extension.

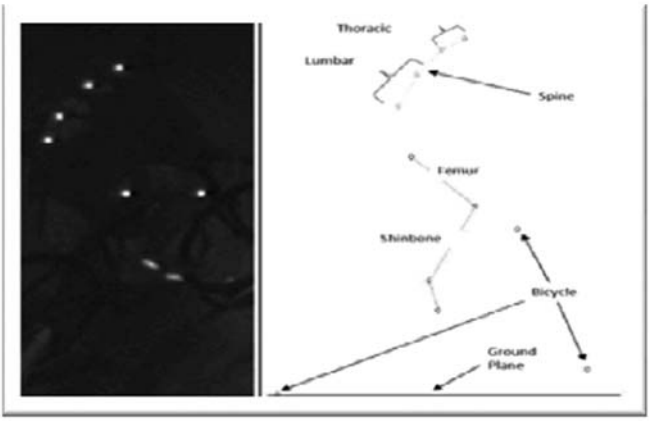

Figure 2 - Model used in the kinematic analysis.

2.3.2 EMG analysis

Wireless surface EMG was used to determine the activity of the three selected muscles: gastrocnemius, rectus femoralis and tibialis anterior. After clearing an area of the skin for electrode attachment, the electrodes were positioned on the midline of the muscles on the right leg.

The data collected was treated using a mathematical software (Matlab) which calculated the normalized Root Mean Square (RMS) and after the i-RMS per cycle. Then, the percentage of activation was determined dividing the iRMS measured during the cycling phase and the iRMS from the test of maximal effort.

$$activation\ percentage = 100 \cdot \frac{trial\ muscle\ activation}{maximal\ muscle\ activation}$$

2.3.3 Pressure analysis

Synchronous measures of hand and saddle pressure were recorded with a custom pressure measuremnt system (figure 3). Eight resistive pressure sensors were used in the handlebar and another eight in the saddle (4 to measure pressure in the pubis and 4 in the ischion), with a frequency of 100 Hz.

The signal of all 16 sensors was registered and the maximum pressure was obtained. Then, a mean maximum pressure of hand, perineum and ischion was calculated with the average of the sensors located in each zone.

Figure 3 - Pressure analysis system.

2.3.4 Subjective measures

To assess the subjective perception, 3 questionnaires were designed to evaluate: (1) the previous physical status of the subject, (2) the fatigue and slight pain in different corporal zones after each condition of the experiment and (3) the evaluation of the prototype.

2.4 Data treatment and analysis

Parametric results were studied using an ANOVA analysis test ($p<0.05$) and a post-hoc analysis test (Tukey-B), while Kruskal- Wallis analysis was used for non-parametric data ($p<0.05$).

The estimation of the comfort coefficient calculated as follows:

$$COMFORT\ COEFICIENT = \frac{Mean\ LINF}{Mean\ CROTCH\ HEIGHT}$$

3- Results

3.1 Biomechanical analysis

The table below shows the results obtained from the biomechanical analysis (table 3):

	KINEMATIC ANALYSIS		EMG ANALYSIS			PRESSURE ANALYSIS	
	Knee Lateral Deviation	Knee Extension	Gatrocnemius Activation	Rectus Femoralis Activation	Tibialis Anterior Activation	Hand	Perineum
LINF_1	- **^{a}	- **^{a}	- *^{a}	+ *^{a}	+ **^{a}	+ **^{a}	- **^{a}
LINF_2	+ **^{b}	½ **^{b}	- *^{a}	- *^{b}	- **^{b}	- **^{b}	½ **^{b}
LINF_3	+ **^{b}	+ **^{c}	+ *^{b}	- *^{b}	- **^{b}	- **^{b}	+ **^{c}

**p<0,01; *p<0,05

Table 3 - ANOVA results of the biomechanical variables. The groups established by post-hoc analysis appear as "a", "b" and "c".

From the movement analysis we can learn that knee lateral deviation and knee extension increased as LINF augmented. The pressure analysis showed that LINF increased, pressure decreased in hand and was bigger in perineum. Regarding muscular activation, the results showed that the level of design which elicited the lowest level of activation was the intermediate one.

3.2 Subjective analysis

The influence of LINF upon subjective perception was assessed using the Kruskal-Wallis test. Data analysis revealed that, concerning general pain feeling and fatigue, the only variables that reached statistical signification were pain feeling in knee and perineum. In knee, pain feeling was higher with LINF 1 and decreased in LINF 2 and LINF 3; in pubis, we can observe an opposite behavior, being higher with LINF 3 and decreasing with the other two levels.

In addition, the variables, which exerted an important effect in the evaluation, were opinion of saddle height, position, cycling and comfort, we can see that the best LINF is the second one (table 4).

	Pain and Fatigue				Evaluation			
	Pain feeling Condition 1 (flat)		Pain feeling Condition 2 (10% slope)		Saddle Height	Position	Cycling	Comfort
	Knee	Pubis	Knee	Pubis				
LINF_1	+ **	- **	- *	- *	- *	- *	- *	- *
LINF_2	½ **	½ **		- *	+ *	+ *	+ *	+ *
LINF_3	- **	+ **	+ *	+ *	- *		- *	- *

**p<0,01; *p<0,05

Table 4 - Results of the analysis of the subjective variables.

3.3 Comfort Coefficient

The **confort coefficient** estimated was **0.872.**

4- Discussion and conclusion

In this study, we aimed at determining the optimal saddle height (LINF) to improve comfort in leisure cycling. Several studies have evaluated biomechanical and physiological variables, based on a performance perspective. Hence, we have presented an alternative approach, considering other biomechanical and subjective variables to assess comfort, which takes priority over efficiency in leisure cycling. To evaluate comfort, we have considered both subjective and objective (biomechanical) variables.

According to data analysis, LINF 2 reduced muscular activation and peak pressure. Regarding to the movement analysis we can see that this level is the best one, because the range of movement of the knee has less injury risk. Overall, LINF 2, the intermediate saddle height of 709.1 mm, seems to be the best parameter which fits the optimal saddle height; objective and subjective data supports this assumption.

The coefficient propose in this study is slight lower than the road bikes coefficient. That could be possible because the mechanical demands are less important than the comfort demands.

This study propose a saddle height for achieve a good level of comfort in leisure cycling.

5- References

[EN1] Ericson M., Nisell R., Arborelius U. and Ekholm J. Muscular activity during ergometer cycling. In Scandinavian Journal of Rehabilitation Medicine, 17(2): 53-61, 1985.

[GD1] Garside I. and Doran D. Effects of bicycle frame ergonomics on triathlon 10-km running performance. In Journal of Sport Sciences, 18(10): 825-833, 2000.

[HW1] Heil D., Wilcox A. and Quinn C. Cardiorespiratory responses to seat-tube angle variation during steady state cycling. In Medicine and Science in Sports and Exercise, 27(5): 730-735, 1995.

[JH1] Jorge M. and Hull M. Analysis of EMG measurements during bicycle pedalling. In Journal of Biomechanics, 19(9): 693-694, 1986.

[MN1] McIntosh, B., Neptune R. and Horton J. Cadence, power and muscle activation in cycle ergometry. In Medicine and Science in Sports and Exercise, 32(7): 1281-1287, 2000.

[PD1] Price D. and Donne B. Effect of variation in seat tube angle at different seat heights on submaximal cycling performance in man. In Journal of Sport Sciences, 15(4): 395-402, 1997.

[[RH2] Ricard M., Hills-Meyer P., Miller M. and Michael T. The effects of bicycle frame geometry on muscle activation and power during a Wingate anaerobic test. In Journal of Sports Science and Medicine, 5: 25-32, 2006

[T1] Too D. The effect of hip position/configuration on anaerobic power and capacity in cycling. In Journal of Applied Biomechanics, 7(4): 359-370, 1991.

[TY1] Takaishi T., Yasuda Y., Ono T. and Moritani T. Optimal pedaling rate estimated from neuromuscular fatigue for cyclists. In Medicine and science in Sports and Exercise, 28(12): 1492-1497, 1996.

Relationship between Pelvic Motion, Torque, and Metabolic Energy in Running (P189)

Evie N. Burnet, Ross A. Arena, Peter E. Pidcoe

Abstract: PURPOSE: To investigate the relationship between frontal plane pelvic angle, gluteus medius muscle (GM) torque, and changes in metabolic energy demands while running. METHODS: Five healthy, female subjects (mean age 22.8 ± 2.2) were obtained from a sample of convenience. Subjects were recreational runners who ran ≥ 5 miles per week (mean 28.0 miles ± 15.2). Subjects were asked to run on a treadmill for 30 minutes at a self-selected speed (6.52 mph ± 0.2). *Torque* – GM isometric strength was determined prior to the run with the subject side lying using a hand-held dynamometer (Lafayette Instruments), and converted to torque. *Kinematics* – Three-dimensional data on pelvic position was sampled at a rate of 60 Hz using an electromagnetic kinematic tracking system (MotionMonitor™, Innovative Sports Training) with sensors (Polhemus Fastrak) secured over the posterior superior iliac spines. *Metabolic Energy* – Oxygen consumption (VO_2) was obtained through ventilatory expired gas analysis (SensorMedics, Inc., Yorba Linda, CA) during rest, exercise and five minutes into recovery. The change in VO_2 between 25-30 minutes (average value) was determined (ΔVO_2) as was the time constant of VO_2 recovery kinetics. MatLab v 7.1 was used for kinematics analyses. A Pearson's Correlation was calculated using SPSS v 14.0; statistical significance was defined as $p<0.05$. RESULTS: The rate of change in maximum pelvic drop was significantly correlated with GM torque ($R^2=0.942$) and VO_2 recovery kinetics ($R^2=0.939$). A positive trend between torque and recovery kinetics existed ($R^2=0.785$). However, ΔVO_2 was not correlated with pelvic motion, torque, or kinetics. CONCLUSION: It appears that subjects with an increased GM torque could tolerate a larger degree of pelvic drop. VO_2 recovery kinetics were not influenced by ΔVO_2, rather by biomechanical factors. These findings suggest that increased pelvic motion during running results in metabolic inefficiency, and could therefore adversely affect running performance.
Key Words: Running, pelvic kinematics, torque, and metabolic energy.

1- Introduction

Running continues to be an increasingly popular fitness activity. Meanwhile, the combination of running's repetitive loading and the increasing number of runners contributes to running-related injuries. The majority of musculoskeletal running injuries have been

P.O. Box 980224, Richmond, VA 23298 (804) 828-0234 - E-mail:enburnet, raarena, pepidcoe@vcu.edu

classified as overuse in nature, and can be traced to training errors, or anatomical or biomechanical factors (Macera *et al.* 1989, James et al. 1978, Hreljac *et al.* 2000).

The stance phase of running is a closed kinetic chain activity, during which proximal stability is needed to control the absorption of contact forces. If proximal instability exists, the body may become biomechanically disadvantaged in absorbing contact forces, which in turn could place the runner at an increased risk for lower extremity injury (Marti *et al.* 1988, Ferber *et al.* 2002). Ferber et al (2002) found that females who had a history of lower extremity stress fracture exhibited greater peak vertical impact ground reaction forces (vGRF), loading rates, and peak tibial acceleration. Similar results were reported by Hreljac *et al.* (2000) in a group of male and female runners who sustained at least one overuse injury attributed to running. Ferber *et al.* (2003) additionally studied gender differences between kinetic and kinematic data for twenty male and female recreational runners. In the frontal plane of stance phase, females had a significantly greater peak hip adduction angle, hip frontal plane negative work, and peak hip adduction velocity as compared to males.

Running is primarily a sagittal plane activity; therefore, muscles associated with the frontal or transverse planes could in theory become weakened without cross training or strengthening. Gluteus medius muscle (GM) weakness, specifically, has been linked to running-related injury (Fredericson *et al.* 2000, Leetun *et al.* 2004, Niemuth *et al.* 2005, Cichanowski *et al.* 2007). These findings may suggest that strength imbalances may be associated with or predispose an athlete to injury, or injuries may lead to strength imbalances.

One running gait deviation that may be present secondary to GM weakness is frontal plane pelvic drop. Pelvic drop occurs when the ipsilateral hip abductors are weak, leading to hip drop or a Trendelenburg sign, such that there is a resulting downward obliquity of the opposite hip during its swing phase. Weakness in the hip musculature, especially the abductors, may impair efficient transference of forces, increase thigh adduction, and lead to pelvic drop (Mann *et al.* 1986). Without compensation, an increased frontal plane pelvic drop could create a mechanically unstable system, which could result in an increased vGRF.

Previous research has demonstrated a vGRF of 2 to 5 times body weight during running (Cavanagh 1990, Hreljac 2004). Altered gait mechanics, however, can create a mechanically disadvantaged system, and lead to an increased vGRF. Ferber *et al.* (2002) found that female runners with a history of lower extremity stress fracture had a 36% greater vGRF (3.87 versus 2.48 times body weight) compared to controls. This scenario might not only increase the risk of injury, but also lead to a decreased running performance.

A relationship between the vGRF and metabolic cost during steady-state level running has been shown (Farley and McMahon 1992). Factors that increase the energy required while running will increase VO_2, hindering running performance. As described previously, an increased frontal plane pelvic drop might in theory contribute to these biomechanical variables. Therefore, research is needed to quantify this relationship. Do altered mechanics lead to increased energy demands, hindering running performance? If a direct relationship exists between frontal plane pelvic drop and metabolic energy,

then a runner with increased frontal plane pelvic drop will reach a point where he is metabolically unable to perform at the same level as a healthy runner. A better understanding of this relationship is therefore needed when working with athletes in order to optimize their running performance.

Therefore, the purpose of this investigation is to quantify the relationship between frontal plane pelvic angle, GM torque, and changes in metabolic energy demands while running.

2- Methods

Five healthy, female subjects (mean age 22.8±2.2) were obtained from a sample of convenience. In accordance with the Virginia Commonwealth University institutional review board, the subjects provided consent, and completed a self-report running questionnaire. Subjects were recreational runners who ran ≥ 5 miles per week (mean 28.0 miles ±15.2).

Subjects' body weight and leg length were first obtained. Subjects' gluteus medius isometric strength was tested in a manner that has been previously reported as reliable using a hand-held dynamometer (Lafayette Instruments, Lafayette, IN), then converted to torque (Bohannon 1997, Cahalan *et al.* 1989, Jaramillo *et al.* 1994).

With the subject standing on the treadmill (Cateye EC-T220), kinematic sensors (Polhemus Fastrak) were secured over bilateral posterior superior iliac spines using double-sided tape. Three-dimensional kinematic data on pelvic motion was sampled at a rate of 60 Hz using an electromagnetic kinematic tracking system (MotionMonitor™, Innovative Sports Training).

The rate of metabolic energy consumption (VO_2 consumption and VCO_2 production) was measured using ventilatory expired gas analysis (SensorMedics, Yorba Linda, CA) during rest, while running, and over a five-minute recovery. While, ventilatory expired gas analysis was obtained using a metabolic cart (Vmax Spectra29, SensorMedics, Inc., Yorba Linda, CA). VO_2 consumption and VCO_2 production were measured as a function of time. The volume was then normalized to the subject's BW for comparison. Ambient air with known oxygen concentration was inhaled through a mask that covered the subject's mouth and nose, and measurement of the volume and percentage of O_2 expired was used to calculate the amount of O_2 consumption.

Subjects were then asked to run on a treadmill for 30 minutes at a self-selected speed (6.52 mph ± 0.2). Kinematic data were collected every 2 minutes during the run from start to end, and used to calculate the angle of pelvic drop. The rate of change in the angle of pelvic drop was calculated over the 30 minute run. The change in VO_2 between 25-30 minutes (average value) was determined (ΔVO_2) as was the time constant of VO_2 recovery kinetics. MatLab v 7.1 was used for kinematics analyses. A Pearson's Correlation was calculated using SPSS v 14.0; statistical significance was defined as $p<0.05$.

3- Results

Averages and standard deviations for overall results are summarized in Table 1.

	Average ± Standard Deviation
Maximum pelvic drop (deg)	-4.83 ± 2.30
Rate of change in pelvic drop	-0.023 ± 0.054
Torque (Nm)	97.9 ± 22.4
Recovery kinetics (ml/kg/min)	67.19 ± 10.75
ΔVO_2 (ml/kg/min)	37.06 ± 3.94

Table 1 - Summary of Results.

The rate of change in maximum pelvic drop was significantly correlated with GM torque (R^2=0.942) and VO_2 recovery kinetics (R^2=0.939). A positive trend between GM torque and recovery kinetics existed (R^2=0.785). However, ΔVO_2 was not correlated with pelvic motion, torque, or kinetics.

4- Conclusions

It appears that subjects with an increased GM torque could tolerate a larger degree of pelvic drop. However, this led to a trade-off in metabolic efficiency.

VO_2 recovery kinetics were not influenced by ΔVO_2, rather by biomechanical factors. These findings suggest that increased pelvic motion during running results in metabolic inefficiency, and could therefore adversely affect running performance.

These results may be of significance in the rehabilitation and athletic training setting as they imply that a rehabilitation program solely focused on GM strengthening will not decrease frontal plane pelvic drop. In turn, the continued presence of an increased frontal plane pelvic drop would hinder running performance. Because of the small sample size, more subjects are planned to confirm these results.

5- References

[B1] Bohannon R. Reference values for extremity muscle strength obtained by hand-held dynamometry from adults aged 20 to 79 years. In Archives of Physical Medicine and Rehabilitation, 78(1): 26-32, 1997.

[CJ1] Cahalan T., Johnson M., Liu S., and Chao E. Quantitative measurements of hip strength in different age groups. In Clinical Orthopaedics and Related Research, 246: 136-145, 1989.

[C1] P. Cavanagh. In Biomechanics of Distance Running, 1990.

[CS1] Cichanowski H., Schmitt J., Johnson R., and Niemuth P. Hip strength in collegiate female athletes with patellofemoral pain. In Medicine and Science in Sports and Exercise, 39(8): 1227-1232, 2007.

[FM1] Farley C. and McMahon T. Energetics of walking and running: insights from simulated reduced-gravity experiments, 73(6): 2709-2712, 1992.

[FD1] Ferber R., Davis I., Hamill J., Pollard C., and McKeown K. Kinetic variables in subjects with previous lower extremity stress fractures. In Medicine and Science in Sports and Exercise, 34(5): S5, 2002.

[FD2] Ferber R., Davis I., and Williams D. Gender differences in lower extremity mechanics during running. In Clinical Biomechanics, 18(4): 350-357, 2003.

[FC1] Fredericson M., Cookingham C., Chaudhari A., Dowdell B., Oestreicher N., and Sahrmann S. Hip abductor weakness in distance runners with iliotibial band syndrome. In Clinical Journal of Sports Medicine, 10(3): 169-175, 2000.
[H1] Hreljac A. Impact and overuse injuries in runners. In Medicine and Science in Sports and Exercise, 36(5): 845-849, 2004.
[HM1] Hreljac A., Marshall R., and Hume P. Evaluation of lower extremity overuse injury potential in runners. In Medicine and Science in Sports and Exercise, 32(9): 1635-1641, 2000.
[JB1] James S., Bates B., Osternig L. Injuries to runners. In The American Journal of Sports Medicine, 6(2): 40-49, 1978.
[JW1] Jaramillo J., Worrell T., and Ingersoll C. Hip isometric strength following knee surgery. In Journal of Orthopaedic and Sports Physical Therapy, 20(3): 160-165, 1994.
[LI1] Leetun D., Ireland M., Willson J., Ballantyne B, and Davis I. Core stability measures as risk factors for lower extremity injury in athletes. In Medicine and Science in Sports and Exercise, 36(6): 926-934, 2004.
[MP1] Macera C., Pate R., Powell K., Jackson K., Kendrick J., and Craven T. Predicting lower-extremity injuries among habitual runners. In Archives of Internal Medicine, 149(11): 2565-2568, 1989.
[MM1] Mann R., Moran G., and Dougherty S. Comparative electromyography of the lower extremity in jogging, running, and sprinting. In The American Journal of Sports Medicine, 14(6): 501-509, 1986.
[MV1] Marti B., Vader J., Minder C., and Abelin T. On the epidemiology of running injuries: the 1984 Bern Grand-Prix study. In The American Journal of Sports Medicine, 16(3): 285-293, 1988.
[NJ1] Niemuth P., Johnson R., Myers M., and Thieman T. Hip muscle weakness and overuse injuries in recreational runners. In Clinical Journal of Sports Medicine, 15(1): 14-21, 2005.

Relationship Between Gluteus Medius Muscle Activity, Pelvic Motion, and Metabolic Energy in Running (P190)

Evie N. Burnet, Ross A. Arena, Peter E. Pidcoe

Abstract: PURPOSE: To investigate the relationship between gluteus medius muscle (GM) activity, pelvic motion, and changes in metabolic energy demands while running. METHODS: Five healthy, female subjects (mean age 22.8±2.2) were obtained from a sample of convenience. Subjects were recreational runners who ran ≥ 5 miles per week (mean 28.0 miles±15.2). Subjects were asked to run on a treadmill for 30 minutes at a self-selected speed (6.52 mph±0.2). *Muscle Activity* – Surface electromyography (sEMG) data was collected on the GM at a rate of 1000 Hz (MyoSystem 1200™, Noraxon). *Kinematics* – Three-dimensional data on pelvic position was sampled at a rate of 60 Hz using an electromagnetic kinematic tracking system (MotionMonitor™, Innovative Sports Training) with sensors (Polhemus Fastrak) secured over the posterior superior iliac spines. *Metabolic Energy* – Oxygen consumption (VO_2) was obtained through ventilatory expired gas analysis (SensorMedics, Inc., Yorba Linda, CA) during rest, exercise and five minutes into recovery. The change in VO_2 between 25-30 minutes (average value) was determined (ΔVO_2) as was the time constant of VO_2 recovery kinetics. MatLab v 7.1 was used for kinematics analyses. A Pearson's Correlation was calculated using SPSS v 14.0; statistical significance was defined as $p<0.05$. RESULTS: Peak GM amplitude exhibited a positive trend with VO_2 recovery kinetics ($R^2=0.807$) and the rate of change in pelvic drop ($R^2=0.647$). Pelvic drop and kinetics were significantly correlated ($R^2=0.942$). However, ΔVO_2 was not correlated with peak GM activity, pelvic drop, or kinetics. CONCLUSION: VO_2 recovery kinetics were not influenced by ΔVO_2, rather by biomechanical factors. Subjects with increased pelvic drop exhibited increased GM activity, and these two variables led to increased kinetics. These findings suggest that increased pelvic motion during running results in metabolic inefficiency, and could therefore adversely affect running performance.

Key Words: Running, pelvic kinematics, muscle activity, and metabolic energy.

P.O. Box 980224, Richmond, VA 23298 (804) 828-0234 - E-mail: enburnet, raarena, pepidcoe@vcu.edu

1- Introduction

Running is an increasingly popular sport, both at a recreational and competitive level. As the number of runners increase, so does the number of running-related injuries, and in turn an increase in medical expenses and a decreased fitness level can result. In the orthopaedic and sports medicine setting, physical therapists frequently treat individuals with running related injuries. Therefore, prevention, accurate assessment, and treatment are essential to the process of decreasing injury and reinjury rates, as well as returning the runner to sport as quickly as possible.

As therapists and researchers expand their focus in injury prevention and treatment to proximal joint mechanics, the lumbo-pelvic hip complex and its role in closed kinetic chain activities has become a focus. More specifically, frontal plane pelvic drop is a component of core stability that could be identified as a weak link in the running kinetic chain that could explain some running deviations and injuries. Pelvic drop occurs when the ipsilateral hip abductors are weak, leading to hip drop or a Trendelenburg sign, such that there is a resulting downward obliquity of the opposite hip during its swing phase. Electromyography has shown that a hip abduction moment is created by the gluteus medius muscle (GM), and to some extent the tensor fascia, during the stance phase of running. At FS, these muscles eccentrically contract to control hip adduction, and then concentrically contract from the support phase into propulsion to create hip abduction (Mann *et al.* 1986).

Therapists often employ strengthening as a means to correct gait deviations such as pelvic drop. If, however, factors exist other than GM strength that impact frontal plane pelvic drop, and the treatment plan focuses solely on strengthening, the clinician may not reduce pelvic drop or decrease the risk of injury. Unfortunately, there is a research void assessing the underlying causes of frontal plane pelvic drop in runners. Factors such as GM activation pattern and changes in frontal plane pelvic drop have not been addressed in the running population.

Previous research has identified changes in GM amplitude in subjects with chronic conditions (Beckman and Buchanan 1995, Sims *et al.* 2002, Long 1993). These findings indicate GM muscle dysfunction related to amplitude, not necessarily strength. Is there a change in the muscle's activation pattern in an injured runner? If so, then addressing GM strength alone may not be sufficient to return the runner to premorbid status.

Steady-state oxygen consumption (VO_2) at a given running velocity has been strongly correlated with distance running performance (Conley and Krahenbuhl 1980, Costill 1967, Costill *et al.* 1973, Paavolainen *et al.* 1999). Factors that increase the energy required while running will increase VO_2 and hinder running performance. Inefficient running gait mechanics, to include increased vertical ground reaction force and vertical oscillation of the body's center of mass, have been associated with an increased VO_2, secondary to increased energy costs conditions (Heise and Martin 2001, Kyrolainen *et al.* 2001, Williams and Cavanagh 1987). Increased frontal plane pelvic drop could contribute to an increase in these biomechanical variables or muscle activity requirements, thereby adversely affecting running performance.

There is a research void quantifying the link between GM muscle activity, pelvic drop, and metabolic energy demands. Yet, an understanding of this relationship would

be important when working with runners. Therefore, the purpose of this study was to investigate the relationship between GM activity, pelvic motion, and changes in metabolic energy demands while running.

2- Methods

Five healthy, female subjects (mean age 22.8±2.2) were obtained from a sample of convenience. The subjects provided consent in accordance with the Virginia Commonwealth University institutional review board, and then completed a self-report running questionnaire. Subjects were recreational runners who ran ≥ 5 miles per week (mean 28.0 miles±15.2).

With the subject positioned prone on a plinth table, rubbing alcohol was used to abrade the skin and reduce skin impedance. The surface electromyography (sEMG) system (MyoSystem 1200™, Noraxon) electrodes were attached parallel to the GM muscle fibre approximately one-inch below the midpoint of the iliac crest bilaterally to collect GM muscle activity (Delagi and Platt 1980). The sEMG ground electrode was placed over the left fibular head. sEMG data was sampled at 1000 Hz.

With the subject standing on the treadmill (Cateye EC-T220), kinematic sensors (Polhemus Fastrak) were secured over bilateral posterior superior iliac spines using double-sided tape. Three-dimensional kinematic data on pelvic motion was sampled at a rate of 60 Hz using an electromagnetic kinematic tracking system (MotionMonitor™, Innovative Sports Training).

The rate of metabolic energy consumption (VO_2 consumption and VCO_2 production) was measured using ventilatory expired gas analysis (SensorMedics, Yorba Linda, CA) during rest, while running, and over a five-minute recovery. While, ventilatory expired gas analysis was obtained using a metabolic cart (Vmax Spectra29, SensorMedics, Inc., Yorba Linda, CA). VO_2 consumption and VCO_2 production were measured as a function of time. The volume was then normalized to the subject's BW for comparison. Ambient air with known oxygen concentration was inhaled through a mask that covered the subject's mouth and nose, and measurement of the volume and percentage of O_2 expired was used to calculate the amount of O_2 consumption.

Subjects were then asked to run on a treadmill for 30 minutes at a self-selected speed (6.52 mph±0.2). Ten seconds of kinematic and sEMG data were collected every 2 minutes during the run, and used to calculate an average peak GM amplitude and angle of pelvic drop for each trial. The change in VO_2 between 25-30 minutes (average value) was determined (ΔVO_2) as was the time constant of VO_2 recovery kinetics. MatLab v 7.1 was used for sEMG and kinematics analyses. A Pearson's Correlation was calculated using SPSS v 14.0; statistical significance was defined as $p<0.05$.

3- Results

Averages and standard deviations for overall results are summarized in Table 1.

Peak GM amplitude exhibited a positive trend with VO_2 recovery kinetics ($R^2=0.807$) and the rate of change in pelvic drop ($R^2=0.647$). Pelvic drop and kinetics were signifi-

	Average ± Standard Deviation
Maximum pelvic drop (deg)	–4.83 ± 2.30
Rate of change in pelvic drop	–0.023 ± 0.054
GM peak amplitude (v)	0.17 ± 0.049
Recovery kinetics (ml/kg/min)	67.19 ± 10.75
ΔVO_2 (ml/kg/min)	37.06 ± 3.94

Table 1 - Summary of Results.

cantly correlated (R^2=0.942). However, ΔVO_2 was not correlated with peak GM activity, pelvic drop, or kinetics.

4- Conclusions

Subjects with increased pelvic drop exhibited increased GM activity, and these two variables contributed to increased recovery kinetics. However, VO_2 recovery kinetics were not influenced by ΔVO_2. Recovery kinetics were therefore affected by biomechanical factors. The results indicate a link between frontal plane pelvic drop, GM activity, and metabolic inefficiency. These findings suggest that increased pelvic motion during running results in metabolic inefficiency, and could therefore adversely affect running performance.

What is still uncertain is whether frontal plane pelvic drop is caused in part by GM activity changes, or if runners with pelvic drop develop changes in GM activity. Future research is planned to investigate the link between GM peak amplitude timing and onset to pelvic drop in a larger sample size to address these questions. Based on these initial findings, the presence of an increased frontal plane motion might indicate possible GM activation changes and detriments to performance. This relationship should be taken into consideration when treating runners with increased frontal plane pelvic motion.

5- References

[BB1] Beckman S. and Buchanan T. Ankle inversion injury and hypermobility: effect on hip and ankle muscle electromyography onset latency. In Archives of Physical Medicine and Rehabilitation, 76(12): 1138-1143, 1995.

[CK1] Conley D. and Krahenbuhl G. Running economy and distance running performance of highly trained athletes. In Medicine and Science in Sports and Exercise, 12(5): 357-360, 1980.

[C1] D. Costill. The relationship between selected physiological variables and distance running performance. In The Journal of Sports Medicine and Physical Fitness, 7(2): 60-66, 1967.

[CT1] Costill D., Thomason H., and Roberts E. Fractional utilization of the aerobic capacity during distance running. In Medicine and Science in Sports and Exercise, 5(4): 248-252, 1973.

[DP1] Delagi E. and Platt D. Anatomic Guide for the Electromyographer, 1980.

[HM1] Heise G. and Martin P. Are variations in running economy associated with ground reaction force characteristics? In The European Journal of Applied Physiology, 84(5): 438-442, 2001.

[KB1] Kyrolainen H., Belli A., and Komi P. Biomechanical factors affecting running economy. In Medicine and Science in Sports and Exercise, 33(8): 1330-1337, 2001.

[LD1] Long W., Dorr L., Healy B., and Perry J. Functional recovery of noncemented total hip arthroplasty. In Clinical Orthopaedics and Related Research, 288: 73-77, 1993.
[MM1] Mann M., Moran G., and Dougherty S. Comparative electromyography of the lower extremity in jogging, running, and sprinting. In The American Journal of Sports Medicine, 14(6): 501-509, 1986.
[PN1] Paavolainen L., Nummela A., and Rusko H. Neuromuscular characteristics and muscle power determinants of 5-km running performance. In Medicine and Science in Sports and Exercise, 31(1): 124-130, 1999.
[SR1] Sims K., Richardson C., and Bauer S. Investigation of hip abductor activation in subjects with clinical unilateral hip osteoarthritis. In Annals of the Rheumatic Diseases, 61(8): 687-692, 2002.
[WC1] Williams K. and Cavanagh P. Relationship between distance running mechanics, running economy, and performance. In The Journal of Applied Physiology, 63(3): 1236-1245.

A New Technological Tool to Measure and Manage Strenght. AthletJump/IBV (P191)

Javier Gámez, Alberto Encarnación, David Garrido, Enrique Alcántara, José Montero, Carlos Soler, Pedro Vera, Ana Cruz García

Abstract: Coaches use different tools in order to measure the strenght such dynamometers, contact platforms or force plates. Because of that, the control of the training process became a difficult task, commonly the treatment of this information is difficult and the software is not usable enough. This situation became a barrier in the technology application in sport. The coaches need more than measure, they need easy and useful technological tools and scientific updated knowledge, which help and assess them in the training program. The objective of this paper is presenting a technological tool that is able to carry out two tasks: (1) measure explosive; (2) compare the test results of an athlete with his specific sport performance profile; Tool utilities are presented contextualized in soccer.
The explosive force is measure by the sport jumps with and without load, such SJ, CMJ, ABK, DJ and RJ. Kinetic variables are measured and analysed. The dymanic maximal force is measured by the most widespread weightlifting exercises, squat and bench press. The maximal power, the power curve and symmetry in force generation of lower and upper limbs are the most important variables presented by this technological application. All those variables are measured by a 3D force plate and kinematic movement analysis system. A data base is included to compare the physical sport state of the athlete analysed with the performance profile of his sport. There is not a similar product in the market, so this tool will help and assess coaches to control several strength manifestation and the training program, in a objective way; using a unique technological tool, integrating tests and variables of analysis, protocols and sport performance profiles database.
Key words: biomechanics, assess, strength, jump.

1- Introduction

Strenght is a fundamental physical capacity in the preparation of almost all sports, as in some sports is crucial to obtaining optimum performance. Every sport needs a specific orientation of the strenght. The main motor skills of the sports, both collective and indi-

Instituto de Biomecánica de Valencia, Universidad Politécnica de Valencia, Edificio 9C, Camino de Vera s/n, E-46022 Valencia, Spain - Phone/Fax +34 963 879 160/+34 963 879 169 - E-mail: {javier.gamez,alberto.encarnacion, david.garrido,enrique.alcantara,jose.montero,carlos.soler,pedro.vera,ana.cruz}@ibv.upv.es

vidual, are usually defined as actions taken in a very short time, powerful and accurate. Explosive strength and its variants are considered the main manifestation in sports, since it is associated with rapid movements (jumps, sprints, strikes, kicks, etc.), which occur frequently in most sports.

There are plenty of tools to analyze the strength. One of the most used and disseminated to analyze the jumps is the contact platform. Among the most important authors in the study of strength, Bosco develop a trading system based on this technology called "ergo jump" (Bosco *et al.* 1983, Bosco 1992, Araya *et al.* 1998, Cianciabella 1996). The contact platforms measure flight time in the jump and indirectly calculated the height equivalent of jumping through the study of kinematic variables.

Contact platform are easy to transport, its price and ease of use, turned over many years in a very tool used by both coaches as by scientific groups (Cianciabella 1996). However, this type of instruments or other similar used to analyze flight and contact time, provide non accurate and insufficient information according to the needs of coaches, as they are not able to offer the main parameters such as power. That instrument has errors in the data collection due to the protocol of the test (Gonzalez 1997).

By the other hand there are another kind of tool like force platforms that provides information about the force that sportman exerted on the three axes space (x, y, z), also called ground reaction forces (GRF). That platform it is an excellent tool for assessing many sport skills in a real context. On the other hand also can be used to measure different manifestations of the strength, accurate and reliable, such as the maximum isometric force (Paasuke *et al.* 2003, Komí *et al.* 1984), the explosive force through the squat jump (Driss *et al.* 2001, Rahmani *et al.* 2001), the elastic through the explosive jump with countermovement (Meital 2002, Busko 2005, Hunter and Marshall 2002) or elastic explosive reactive by drop jump (Bosco 1982).

Currently there are certain protocols for jump test extracted from the published literature (Bosco 1992, Driss *et al.* 2001, Rahmani *et al.* 2001, Meital 2002, Busko 2005, Hunter and Marshall 2002). These protocols presented some problems that make difficult to create performance profiles in order to be a useful tool to coaches. By the other hand on many occasions due to the complexity of the tools of measurement, and the difficult and long process of data analysis, the coaches do not use those tools for the valuation of performance. In other cases there is a mistrust on the part of professional sport in the potential of technological advances. In many cases the parameters that offer the forces platforms, are difficult to interpret and analyze. Besides computer applications of commercial equipment are difficult to use and often do not provide data useful and easy for coaches. All this makes it an instrument used only by staff researcher highly specialized and often remote from the actual context of sports. This situation causes a gap between scientific knowledge and sports training, authors such as Bartlett (2003) express their deep concern over this distance and suggested that investigators should be closer to the needs of professional sport. This context creates a significant need for professionals in the sport that must be remedied. The objective of this paper is presenting a technological tool that is able to carry out two tasks: (1) measure explosive strength; (2) compare the test results of a football player with his specific sport performance profile in soccer.

2- Methods

A force platform was used to measure the GRF (Dinascan/IBV, 800×800 cm, sampling frequency of 1000Hz). By the other hand specific software was design in order to manage and present data to the coach. The software proposes (C++) a measuring protocol. Each football player performed 3 repetitions, except RJ30" test, which took place a single repetition. The subjects were familiar with the test jump. Jump analyzed were squat jump (SJ), the countermovement jump (CMJ), abalakov jump (ABK), the horizontal jump (HJ), the drop jump (DJ) and repeated jump (RJ). The order used in the test jumps was as follows: CMJ, SJ, ABK, HJ, DJ and RJ. Between jumps there was a rest period of not less than 30 seconds and no more than 3 minutes.

The parameters that are calculated by AthletJump/IBV were: The **strength in the antero-posterior axis** was calculated as the greater amount of force, standardized to the weight of athlete that applies in this direction in the test HJ. The vertical **strength** was calculated as the summation of the top forces achieved in each of the test jump. The **coordination** was calculated by estimating the ABK jump height and its difference with the CMJ. The **reactivity** was calculated by analyzing the differences between the CMJ and the DJ 40cm. The **resistance** was calculated as the slope calculated used the heights of RJ test for 30 seconds. The **elasticity** was calculated as the difference between the values obtained SJ and CMJ. The **power** were calculated as the summation of the highest powers reached in all jumps, standardized mass of the subject, and **jump time** (speed related parameter) was calculates as execution times of the test jump (SJ, CMJ, DJ). The **symmetry** of the gesture was calculated as the displacement experienced by the center forces in the medio-lateral axis during the take-off. We used standard statistical methods, and were calculated averages and standard deviations (SD) of the sample (Table 1). The figure below shows an example of a histogram of the maximum power analyzed (figure 1).

A total of 40 players (men), belonging to the first division Spanish team were studied. All of them were evaluated in a rest period, in which they had no competition. The

	Mean	SD
Vertical Strengh (N/Kg)	49.34	11.97
Strenght axis x (N/Kg)	9.03	2.19
Simetry (%)	79.04	20.12
Simetry axis x (%)	66.55	21.66
Coordination	13.89	8.49
Reactivity	4.37	3.62
Resistence (%)	82.61	82.67
Elasticity	21	10.76
Power (W/Kg)	44.53	17.4
Jump time (s)	0.56	0.146

Table 1 - Parameters results of the biomechanical variables.

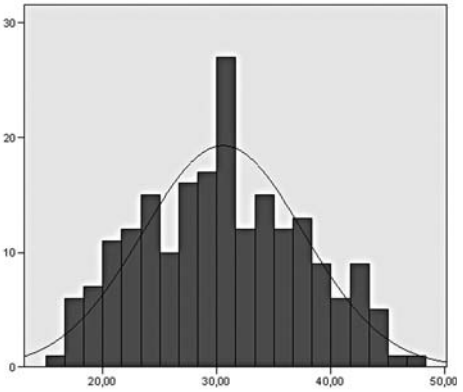

Figure 1 - Maximum power histogram.

N= 30	*MEAN*	*SD*
Age	19.79	3.78
Weight	75.17	9.03
Height	177.11	5.9

Table 2 - Subjects data.

anthropometric data of the experimental sample are presented in Table 1. None of the subjects suffered any injury that prevented him from carrying out the assessment test.

3- Results

Once the battery of tests is finished, the software provides an assessment by a large report that present the main variables of all the jump performed and two performance diagrams, technical and physical capacity. In the figure below the results of one soccer player are presented, the coach can realize with a quick view what are the performance parameters that must be improved, as for example, the elasticity or the coordination arms-legs.

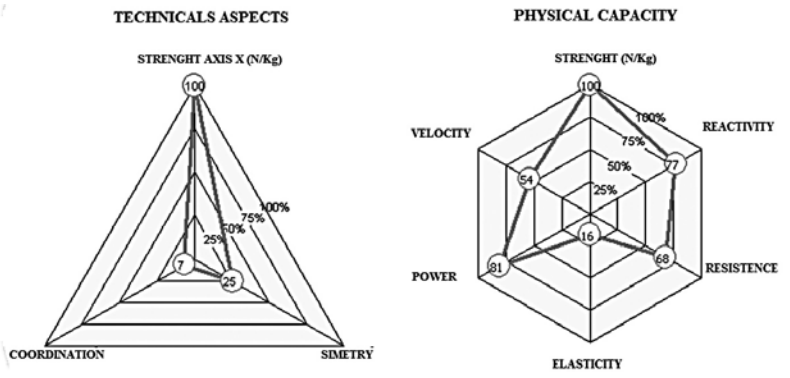

Figure 2 - Performance profile of one of the player of the team analyzed.

4- Discussion and conclusion

AthletJump/IBV allows a simple and useful assessment of the main variables in the performance with a real-time feedback. We presents a new technological tool, that mixed technology and scientific knowledge, able to offer an assessment of the strength parameters in football. This tool is capable to reduce the gap between trainers, coaches and biomechanical scientific knowledge.

5- References

[AR1] Araya, F., Rivera-Brown, A., Micheo, W., Torres, M., Del Rio, L., George, R., Reliability of the bosco ergojump anaerobic power test in trained adolescents. Medicine & Science in Sports & Exercise, 30, 5, pp.153, 1998.

[B1] Bosco, C., La valutazione della forza con il test di Bosco. Ed. Roma. Societa Stampa Sportiva, 1992.

[BA1] Baca, A., A comparison of methods for analyzing drop jump performance. Medicine and science in sports and exercise, 31, 3, pp: 437-442, 1999.

[BT1] Bartlett,R., The science and medicine of cricket: an overview and update. Journal of Sport Science, 21, 9, pp: 733-752, 2003.

[BL1] Bosco, C., Luhtanen, P., Komi, P.V. A simple method for measurement of mechanical power in jumping. European journal of applied physiology. 50, pp. 273-283, 1983.

[BU1] Busko, K., Power output and mechanical efficiency of human muscle in maximal cycle ergometer efforts at different pedalling rates. Biology of sport, 22, 1, pp: 35-51, 2005.

[C1] Cianciabella, J., What´s the ergo jump bosco system?, Lecturas: Educación Física y Deportes, Revista Digital. 1(3), 1996.

[DV1] Driss, T., Vandewalle, H., Quievre, J., Miller, C., Monod, H., Effects of external loading on power output in a squat jump on a force platform: a comparison between strength and power athletes and sedentary individuals. Journal of sports sciences, 19, 2, pp: 99-105, 2001.

[FL1] Fowler, N., Lees, A., A comparison of the kinetic and kinematic characteristic of plyometric drop – jump and pendulum exercises. Journal of Applied Biomechanics, 13, 3, pp: 260-275, 1998.

[GG1] Gónzalez Badillo, J.J., Gorostiaga, E., Fundamentos del entrenamiento de la fuerza. Aplicación al alto rendimiento deportivo. Inde, Barcelona, 1997.

[GP1] Garcia, J., Peleteiro, J., Rodgriguez J., Morante, J., Herrero, J., Villa, J., The Validation of a New Method that Measures Contact and Flight Times During Vertical Jump. International-journal-of-sports-medicine, 26, 4, pp: 294-302, 2005.

[HM1] Hunter, J., Marshall, R., Effects of power and flexibility training on vertical jump technique. Medicine and science in sports and exercise, 34, 3, pp: 478-486, 2002.

[K1] Komi, P.V., Physiological and biomechanical correlates of muscle function: Effects of muscle structure and strength-shortening cycle on force and speed. In R.L. Terjung (ed.), Exercise and sport sciences rewiews, 12, pp:81-121, 1984.

[M1] Meital, N., Physiological and biomechanical characteristics of subjects utilizing different strategies in the vertical jump performance. Eugene, OR, Microform Publications, University of Oregon, 2002.

[PE1] Paasuke, M., Ereline, J., Gapeyeva, H., Age-related differences in knee extension rate of isometric force development and vertical jumping performance in women. Journal of sports medicine and physical fitness, 43, 4, pp: 453-458, 2003.

[RV] Rahmani, A., Viale, F., Dalleau, G., Lacour, J.R., Force/velocity and power/velocity relationships in squat exercise. European Journal of Applied Physiology, 84, 3, pp: 227-232, 2001.

Experimental Measurement of Selected Snowboard Mechanical Properties (P194)

Devinder Grewal, Eric Rossetter, Chris Lund, Benjamin J. Ewers, III

Abstract: Snowboard manufacturers attempt to design boards with mechanical properties that provide desirable ride and handling characteristics, adequate strength, and low manufacturing costs. Snowboards are typically a sandwich composite of several individual layers that vary significantly in geometry and composition. To better understand the influence of core materials and construction on a board's stiffness, ultimate failure load, and stored energy, several commercially available snowboards were tested to failure in three point bending. A series of representative boards were tested with three different core materials: foam, wood, and honeycomb. The results show that stiffness and ultimate failure load are strongly influenced by the core wrap thickness, while the energy storage is strongly influenced by the core material and construction method used.

1- Introduction

Snowboarding is an increasingly popular winter sport with over five million snowboarders hitting the slopes in the United States during 2002 [1]. As with other snow sports, snowboarders need equipment that is safe and satisfies the varied abilities of the participants. To this end, snowboard manufacturers produce boards with different materials and geometries to vary the board's flexibility, damping, weight, and cost to meet the demands of the consumer.

Currently, most snowboard manufacturers build a board and then test its mechanical properties, such as bending and torsional stiffness, as well as doing qualitative testing on the slopes. Based on the results of these tests the designers can alter the material composition, thickness, or shape to achieve the desired snowboard properties. In an effort to improve this design process Sutton [2] collected data from strain gauges and accelerometers during on-snow testing. This data provided information on the snowboard stiffness and damping, but does not show how the snowboard materials influence these factors. Brennan [3] modeled the torsional and bending stiffness of a snowboard based on the material properties, board geometry, and lay-up. Brennan's results show reasonable correlation with two snowboards manufactured by K2. A similar modeling

Principia Engineering, Inc., 220 Sansome Street, Suite 500, San Francisco, CA 94104.

approach has also been performed by Nordt [4] to understand the mechanical properties of alpine skis.

Although Brennan's snowboard model is a useful tool to predict the resulting stiffness given all the snowboard materials and dimensions, it does not give insight into the influence that construction type and individual material layers have on the overall stiffness, strength, and energy to failure.

The work presented in this paper looks at the stiffness, strength, and energy to failure for a variety of snowboards composed of three different core materials: foam, wood, and composite cores. The strength is taken to be the ultimate failure load. The resulting stiffness, strength, and stored energy is experimentally determined for each board and then correlated with the core material and outer layer dimensions. The results show that stiffness and strength are strong functions of the core wrap thickness. Normalizing the stiffness and strength for each snowboard by the core wrap thickness yields values that are comparable between all core types. However, the energy to failure of the board shows a stronger correlation with the core material and the construction methods of the board.

The energy to failure is similar between foam and wood core boards, while the honeycomb core board stored the least amount of energy.

1.1 Snowboard Construction

Basic snowboard construction consists of five layers as shown in Figure 1 [3].

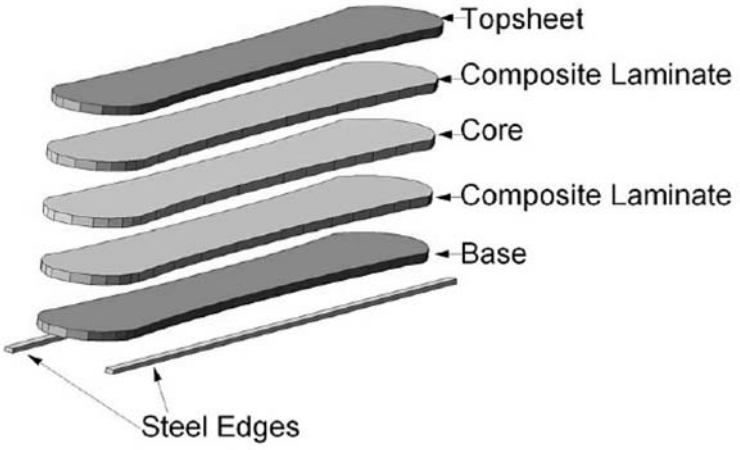

Figure 1 - Snowboard Construction.

The top layer is usually made of a polymeric material and contains the snowboard's graphics. This layer is not a significant structural element in the snowboard. As the name suggests, the core wrap surrounds the core of the snowboard and is usually made of glass fiber and very rarely made of carbon fiber or aramid fiber (comprises layers 2 and 4). The core wrap may consist of multiple layers of a material and some designs use sections of additional core wrapped material near the edge of the snowboard. In general, the core of the snowboard (layer 3) is considered to be one of the most important materials in

determining the board's overall weight, flexibility, and strength. Most snowboards manufactured today use wood cores while some high-end boards use honeycomb cores.

Lower-end boards sometimes use foam cores, which are generally thought to be too flexible and weak for typical adult users. The base (layer 5) is the portion of the board in contact with the snow. It is typically constructed of either extruded, sintered, or graphite infused polyethylene. This is a porous material that absorbs wax to provide a smooth low friction surface. Steel inserts are attached along both edges of the snowboard to provide a strong sharp edge to protect the board and aid in turning and stopping. This edge is made of high-strength and high-toughness steel alloy.

2- Test Procedure

Seven snowboards were tested to failure in three point bending. Of the boards tested, one had a honeycomb core, three had wood cores, and the remaining three had foam cores.

Table 1 summarizes the boards used for the tests. Snowboard Wood C was not available for cross sections after the bending tests and as a result certain information (such as construction type) is not available for this board.

Snowboard ID	Core Type	Construction Type	Board Length (cm)
Foam A	Foam	Reinforced Side Cap	140
Foam B	Foam	Side Cap	142
Foam C	Foam	Standard Sandwich	140
Wood A	Wood	Standard Sandwich	156
Wood B	Wood	Standard Sandwich	155
Wood C	Wood	Not Available	154
Honeycomb	Honeycomb	Side Cap	155

Table 1 - Snowboards Tested.

The bending tests followed the general protocol outlined for alpine skis in ASTM F780-93a [5] with slight modifications to accommodate snowboard dimensions. The test fixture was installed in an Instron Model 4204 load frame. Each board was tested at three locations, the front, center, and rear end of the board between the binding and the edge of the board. Figure 2 shows the basic setup for the three point bending tests. The supporting rollers were placed 350 mm apart with the load applied between the rollers.

The outboard roller was placed at the contact point of the board. The board contact points are defined as the two points (one at the front of the board and one at the rear) that will contact a flat surface due to the curvature (also known as camber) of the board. The end effector of the Instron device was 12.7 mm thick steel with a 6.4 mm radius at the end.

The end effector contacted a 25 mm wide, thin steel plate, followed by a 25 mm wide section of rubber as in the ASTM standard. The steel plate and rubber sections spanned the entire width of the board. This setup allowed the force to be evenly distributed, avoiding a force concentration at the board surface.

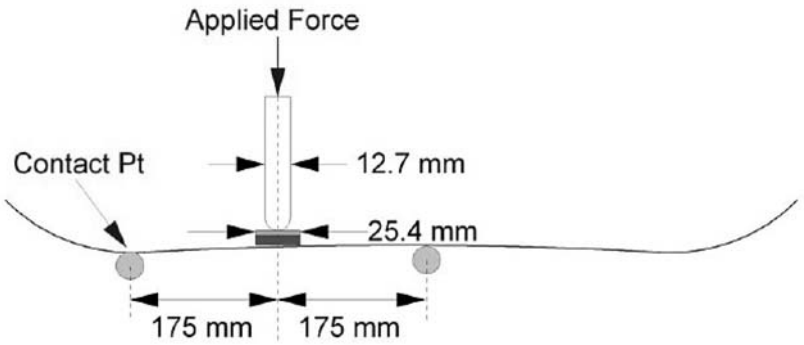

Figure 2 - Test Setup.

Each test was performed in displacement control at a loading rate of 25 mm/min until the load-displacement curve indicated failure. Figure 3 shows a typical force vs. displacement curve. The curve shows a roughly linear relationship between force and displacement at the beginning of the test. For each board a load range was chosen over which the slope was approximately constant. The stiffness was taken to be the slope between loads of 400 N and 2000 N. The strength of the boards was also determined from the peak load observed in testing. Finally, the energy to failure was determined by integrating the area under the load-displacement curve.

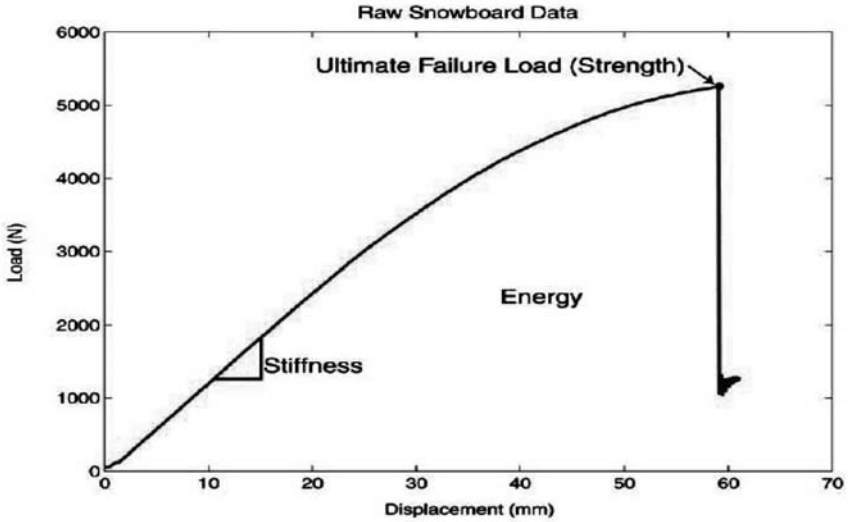

Figure 3 - Force vs. Displacement Data.

A non-paired, two-tail Student t-test was performed on the stiffness, strength, and energy results to determine if there is a statistical difference between the foam and wood cores. This was not done for the honeycomb core because only one board of this core type was available for testing.

3- Results

3.1 Snowboard Stiffness, Strength, and Energy to Failure

The average stiffness, strength, and energy to failure for the tip and tail tests are shown in Figures 4, 5, and 6. Note that for the honeycomb core board, only the tip test was performed. The trends for the stiffness and strength are extremely similar for the boards

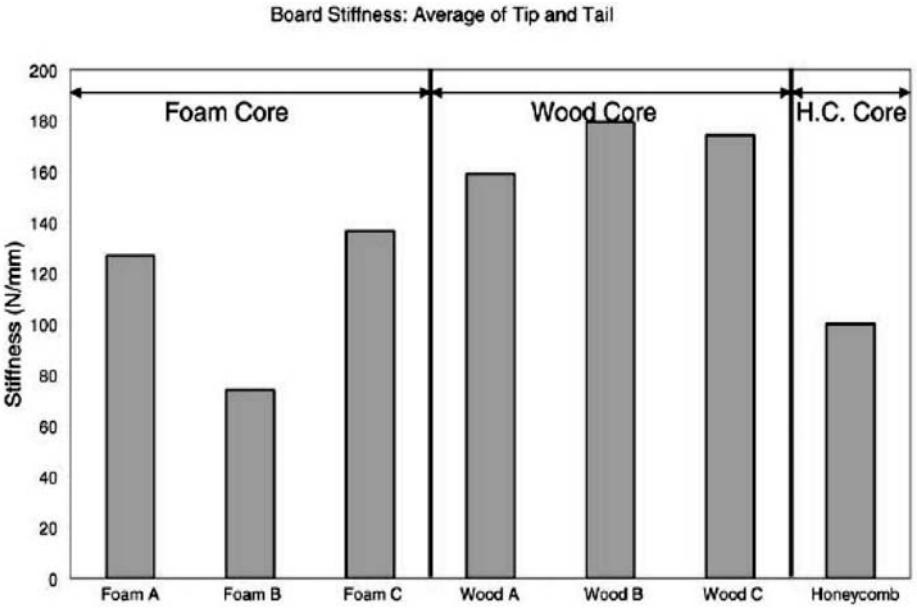

Figure 4 - Snowboard Stiffness.

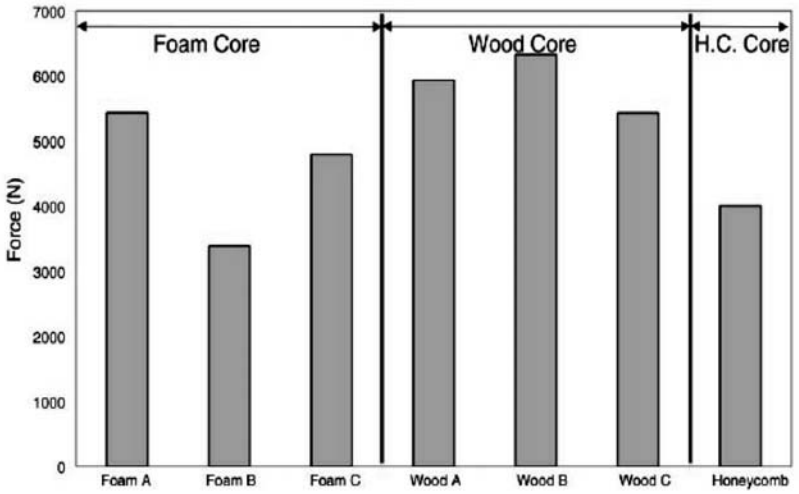

Figure 5 - Snowboard Strength.

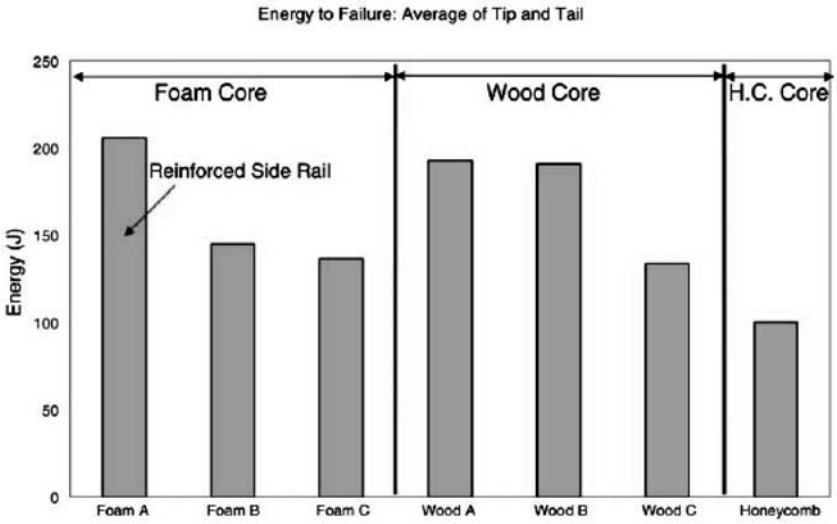

Figure 6 - Snowboard Stored Energy.

tested. The stiffness and strength are slightly lower for foam and honeycomb cores and slightly higher for wood core boards. However, with the exception of board Foam B, the other two foam boards have stiffness and breaking load values that are comparable to the wood core boards. One interesting result is the differences in stiffness and strength between the foam core boards. The Foam B board is roughly half the stiffness of the other foam core boards. This result suggests that other factors such as core wrap thickness, core thickness, and/or construction methods have a significant impact on the resulting board stiffness. This issue is explored in the following section. The t-test showed that there was a statistical difference between the stiffness of the foam and wood cores ($p=0.04$). The strength results for the foam and wood cores do not show a statistically significant difference ($p=0.1$). However, this result is expected and likely due to a lack of power in the data (more samples are needed to show a statistical difference).

The stored energy for the boards (Figure 6) shows a very different trend as compared with the stiffness and strength. The results show very little difference between core types. The energy storage of the foam core boards is roughly equivalent to boards composed of wood. The Foam B board with the lowest stiffness has an energy storage value comparable to board Foam C. The board with the maximum stored energy was a foam core board while the board with the minimum stored energy is the high-end honeycomb core board. Unlike the stiffness and strength results, there is not a huge variation between the different core types. The results of the t-test also confirm that there is no statistical difference between the foam and wood cores ($p=0.7$). The variation that exists in the foam core boards can be attributed to the construction method. Cross sections of the boards revealed that the Foam A board contained an extra core wrapped section near the board edges that did not exist in the other two foam core boards. These results suggest that the energy storage is influenced by the core type and the construction method.

3.2 Normalized Stiffness and Strength

The results from the three point bending tests showed significant variations in stiffness and strength for the foam core boards. This indicates that these parameters are not strong functions of the core material. In order to understand these fluctuations, cross sections were taken from each board to compare the thickness of the core wrap material.

The core wrap was chosen because it is the only significant structural component in the face skin. An example of two board cross sections is shown in Figure 7. The core wrap thickness used in the analysis was an average of the top and bottom core wrap thickness.

Table 2 summarizes the results of the core wrap properties

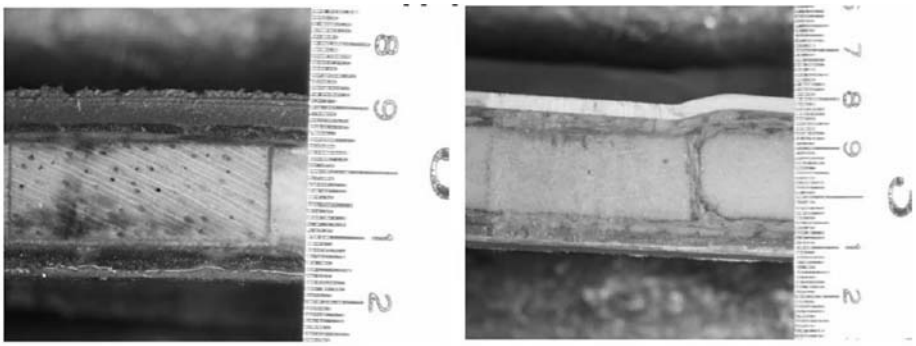

Figure 7 - Snowboard Cross Sections.

Snowboard ID	Core Type	Wrap Thickness (mm)	Fiber Orientation	Wrap Layers
Foam A	Foam	1.0	45° & 90°	2
Foam B	Foam	0.5	90°	1
Foam C	Foam	0.8	Both 90°	2
Wood A	Wood	0.8	90°	1
Wood B	Wood	1.0	45° & 90°	2
Wood C	Wood	Not Available	Not Available	Not Available
Honeycomb	Honeycomb	0.8	Both 90°	2

Table 2 - Core Wrap Thickness.

Interestingly, the trend of the overall core wrap thickness correlates well with the trends observed in the original stiffness and strength data. To see the correlation the stiffness and strength were divided by the core wrap thickness to obtain a "normalized stiffness" and "normalized strength". The results are shown in Figures 8 and 9. The general trend shows that the core wrap thickness has a pronounced effect on the stiffness and strength properties of the board. The normalized stiffness values for the foam cores vary by less than 28% as compared with the 46% variation in the raw stiffness. This normalized stiffness also reduces variation between core types. Averaging the stiffness values

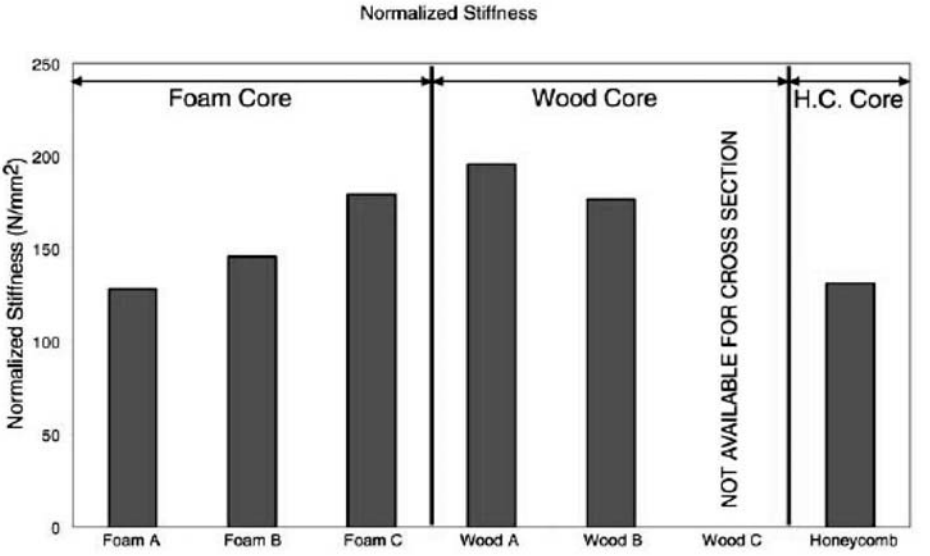

Figure 8 - Normalized Snowboard Stiffness.

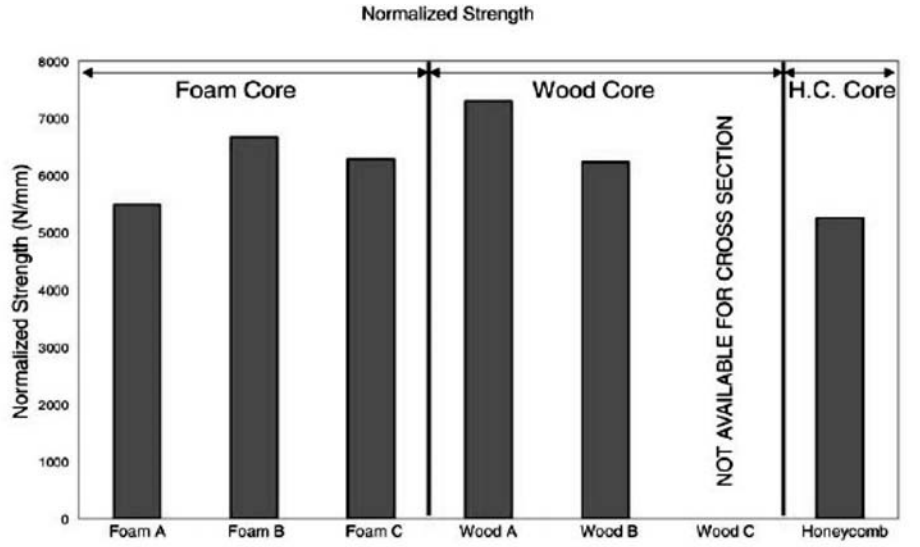

Figure 9 - Normalized Snowboard Strength.

(Figure 4) for each core type gives differences between the wood and foam cores of 35%, while the stiffness difference between the wood and honeycomb cores is 41%.

After normalizing the stiffness values (Figure 8), the differences between wood, foam, and honeycomb cores are 19% and 30%, respectively. The t-test results after the normalization show no significant difference between the foam and wood cores ($p=0.19$).

The normalized strength reduces the variation within the foam core boards and between the different core types even more significantly than it did for the stiffness

values. For foam core boards the largest variation in normalized strength is only 18% while the non-normalized strength shows a peak variation of 38%. The average nonnormalized strength (Figure 5) variation between wood and foam cores is 26%, and between wood and honeycomb cores the variation is 35%. After normalizing strength data (Figure 9) the difference between wood and foam cores is only 9% while the difference between wood and honeycomb drops to 22%. The t-test results after the normalization also show no significant difference between the foam and wood cores strengths ($p=0.38$).

The normalized data shows the significance of core wrap thickness to the stiffness and strength of a snowboard. The normalized data indicates that, in general, wood core boards may be marginally stiffer than foam or honeycomb cores. However, by varying the core wrap thickness, designers can achieve adequate stiffness values with foam and honeycomb cores.

4- Conclusions

The results of the three point bending tests show how stiffness, strength, and energy to failure correlate with snowboard materials and construction. The seven boards tested show that the stiffness and strength are more strongly influenced by the core wrap thickness and not the core material. The normalized stiffness values show comparable stiffness and strength results for foam core boards as compared to more costly boards containing wood or honeycomb cores. Of course, there is still some variation in the normalized stiffness and strength values. There are other attributes that contribute to these values that were not analyzed in this study, such as variations within a core type (i.e. not all foam cores are identical) or construction methods used for the snowboard.

Further work and analysis could look at the influence of these attributes on the stiffness, strength, and energy storage of a snowboard.

The energy stored at failure, however, is more closely related to core material and construction methods rather than the thickness of the core wrap. The results show that the energy storage of foam core boards can be comparable to wood cores, especially with construction methods that add additional reinforcement near the board edge. Surprisingly, the high-end honeycomb board stored the least amount of energy before failure. These tests illustrate that it is possible to construct foam core boards with stiffness and energy storage properties close to more expensive boards constructed with wood or honeycomb cores.

5- References

[1] SnowSports Industries America, 2003 SIA Snow Sports Fact Sheet, 2003, http://www.thesnowtrade.org.

[2] E.B. Sutton, Better Snowboards by Design, In Proceedings of the International Mechanical Engineering Congress and Exposition, November 2000.

[3] S. Brennan, Modeling the Mechanical Characteristics and On-Snow Performance of Snowboards, Ph.D. Thesis, Stanford University, March 2003.

[4] A. Nordt, G. Springer, and L. Kollar, Computing the Mechanical Properties of Alpine Skis, Sports Engineering, 2:65-84, 1999.

[5] ASTM, Annual Book of ASTM Standards, Volume 15: End User Products. ASTM, 2003.

Runalyser: Real Time Analysis of Running Technique in Practice (P196)

M. Wijnen[1], M.B. Hoppenbrouwers[1], J.W.M. Willems[1]

Topics: Athletics.
Abstract: Measurement systems are becoming more and more common in the training practice of athletes. In the lab, many parameters can be measured. On the track or on the road however, the technology is currently limited to measurement of heart rate, GPS position, and speed and distance based on acceleration measurement. These systems all focus on performance rather than technique. Running economy – the efficiency of the runner's movements – is largely determined by technique. So measurement of technique related parameters in the runner's natural environment would be a huge step forward, enabling athletes and coaches to work towards better running economy and thus also performance.
In this paper a working prototype of a system is shown that has been developed to measure both technique and performance related parameters for runners during actual field training and races. The system measures various parameters: feet roll off using a foot pressure sensor, GPS speed and distance, core temperature and heart rate. The feet pressure data is used to determine ground contact time, heel off time, pace frequency, gait line, and pressure distribution during roll-off.
The sensors transmit their data to a central computing unit, worn at the runner's back. This unit combines the data streams and sends them on to a host computer via a wireless internet link. The host computer runs data analysis software and presents the results on the internet. The system has been tested successfully during the Eindhoven half marathon on October 14th 2007. Analysis of data shows an early and gradual increase of contact times and heel-off times which is probably related to early fatigue in (biarticular) leg muscles due to a too fast start of the runner.
Future versions of the system will aim to decrease the size of the system, refine the data interpretation and incorporate new sensors such as EMG measurement.
Keywords: running technique, monitoring, wireless, contact time, core temperature.

1- Introduction

Athletes and coaches want to have insight into their performance development and performance determining factors. Therefore, measurement systems which can deliver objective and quantitative information are becoming more and more common in trai-

1. TNO Science & Industry, P.O. Box 6235, 5600MB Eindhoven, The Netherlands - Phone/fax: +31402650539, +31402650299. E-mail: {merijn.wijnen, marc.hoppenbrouwers, john.willems}@tno.nl

ning practice of athletes. Measuring in laboratory conditions is already common practice, especially for elite athletes, but there are some limitations. Firstly, continuous monitoring is not possible as tests are usually planned periodically. Secondly, the limited room in the lab complicates measuring for a longer time or at very high velocities in over ground running.

In daily training practice, on the track or on the road, technology is currently limited to measurement of heart rate, GPS position, and speed and distance based on accelerometer data. These systems all focus on performance rather than performance determining factors like running technique. Running economy refers to the amount of energy required at a given speed and is largely determined by technique (Foster & Lucia, 2007, Nummela *et al.*, 2007).

To highlight the relevance of feedback on running technique: when Haile Gebrselassi ran his world record in Berlin 2007 he was told by his coach, after having run about 30 kilometers, to change his stride length in order to avoid early fatigue.

2- Measuring system

Several theories about running technique are being applied to common training practice of runners. One of them is the *Bosch & Klomp method* (Bosch and Klomp, 2004) which is based on state of the art knowledge in biomechanics and exercise physiology. From this theory of running, reactivity is one of the key factors determining running economy and thereby running performance. In reactive running the muscle-tendon complex is used like a spring (stretch shortening cycle) which is able to return energy in an efficient way and reuse energy for vertical displacement of the body. Two possible parameters which give insight in reactivity are used are ground contact time and heel off time. It has already been shown that elite runners have brief contact with the ground (Nummela *et al.*, 2007). It is hypothesized that in effective running the heel should leave the surface rapidly. In other words short heel off times are to be kept short. This indicates efficient use of biarticular muscles (Bosch and Klomp, 2004).

To be able to measure all the parameters mentioned above, sensors were chosen and a system was designed that enables us to monitor the running technique of an athlete in real time on an outdoor track or field race. The system was coined: *The Runalyser*. Figure 1 shows the architecture of the system.

The system consists of three basic components that are all linked through a wireless serial interface: the footpod and the central acquisition unit (CAU) are both local to the athlete and the data processing and presentation server (DPPS) that is based at a remote location.

We chose to derive the above mentioned timing parameters that characterize a running technique by continuously measuring and analysing foot pressure data. To achieve this an insole was used that is capable of measuring the spatial distribution of applied foot pressure by means of capacitive sensing elements. For its high durability and ease of interfacing, Zephyr insoles were chosen. These insoles comprise eight predefined pressure sensitive area's. To interface with the insole an electronic circuit, the foot pod, was designed. This unit was built around a small Atmel atmega168 microprocessor. Capacitance is derived from the timing of pulses produced by a multichannel one-shot

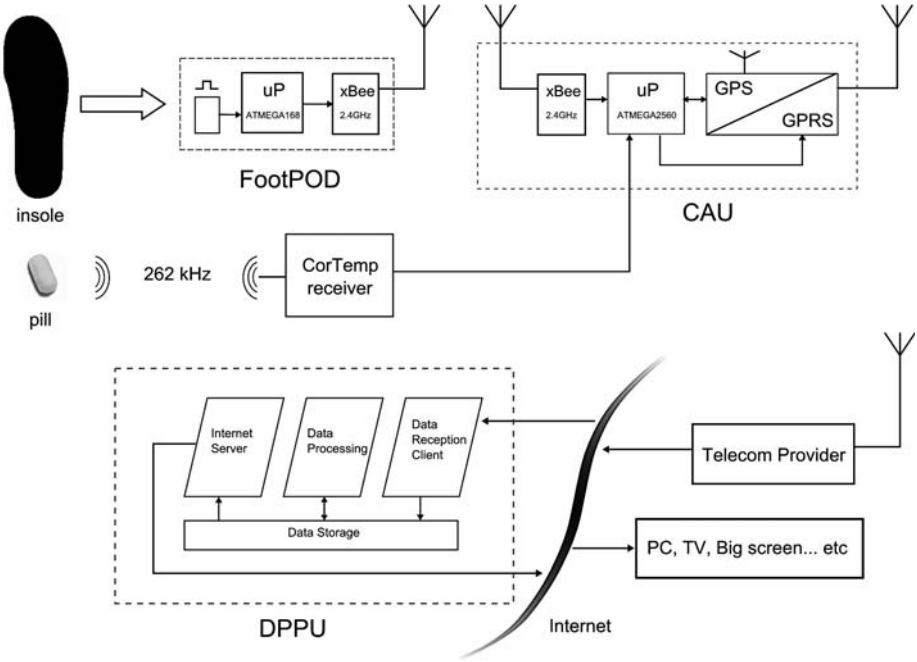

Figure 1 - Layout of the Runalyser: a real time system for monitoring running technique.

that is repeatedly triggered by the microprocessor. Thus we are able to measure the complete pressure distribution at a rate of 1,000 measurements per second.

The sensor data is processed locally in the foot pod to produce contact time, heel off time and flight time with a resolution of 1 ms. For remote gait line analysis, the values of the eight pressure sensors are also kept in memory at 14 fixed time intervals of 20ms starting at first contact. The combined timing and pressure distribution data of the most recent step is transmitted to the CAU every 5 seconds through a wireless Xbee serial interface at 2.4GHz from Maxstream. Thus the data flow in the complete Runalyser system is strictly paced by the foot pod. As shown in figure 2a, the foot pod and small lithium polymer battery are placed in a pouch that is strapped to the ankle of the athlete.

Figure 2b depicts the CAU that is worn in a pouch integrated in a belt around the waist of the athlete. This belt also contains the receiver of a Cortemp system by HQ Inc. that measures the athlete's core temperature by means of a pill swallowed by the athlete prior to the race. The CAU is built around an atmega2560 microprocessor which was chosen for its large number of predefined serial channels. The CAU interfaces with: the Cortemp receiver, an Xbee unit for reception of the foot pod data and a combined GPRS/GPS unit from Telit. Paced by the data received from the foot pod, the CAU subsequently interrogates the Cortemp receiver for the athletes core temperature and the GPS unit for the current geolocation, running speed and time. All data is combined into two data sentences of fixed length, to which a preamble and a CRC value are added. This data is then base-64 encoded and sent to the Telit unit which transmits the data over a GPRS connection. This connection constitutes a virtual serial data link between the CAU and the remote DPPS.

(**a**) (**b**)

Figure 2 - (a): Foot pod placed in a pouch worn at the athlete's ankle. **(b):** CAU worn in a belt.

Because of the high latency in a GPRS connection which can at times be larger that the five second interval at which new data is presented, no handshaking between DPPS and CAU is performed. This means that the DPPS is solely responsible for synchronizing with the data stream from the CAU and testing for data integrity. For smooth data handling a dual core PC was chosen as DPPS. On this PC three processes run in parallel. The first process is a client connected to the internet that receives and parses the data sent from the CAU over GPRS. The data is output and written to disk in time stamped files and a Google maps based html file for geolocation. This client was written in Visual Basic.

The second process is a data analysis routine developed in Matlab. Asynchronously, at a rate of once every 7 seconds it takes the data that was most recently stored. With each cycle graphs of heel off time, contact time, pace, speed and core temperature versus time are updated and stored. Additionally, the pressure data captured during the latest step are interpolated in space and sequenced in time into an animation to provide an insightful visual representation of the evolution of the pressure distribution during that step. A evolving gait line is also calculated and superimposed on the pressure distribution. All graphs are stored as jpg images and animated gifs, some frames of which as shown in figure 3.

The third and final process that runs on the DPPS is an internet server (Apache) that presents a web page with all processed data to the outside world.

3- Case study results

During the marathon in Eindhoven on October 14th 2007, one runner was equipped with the Runalyser. He ran 20 kilometers with the system and data was collected during the

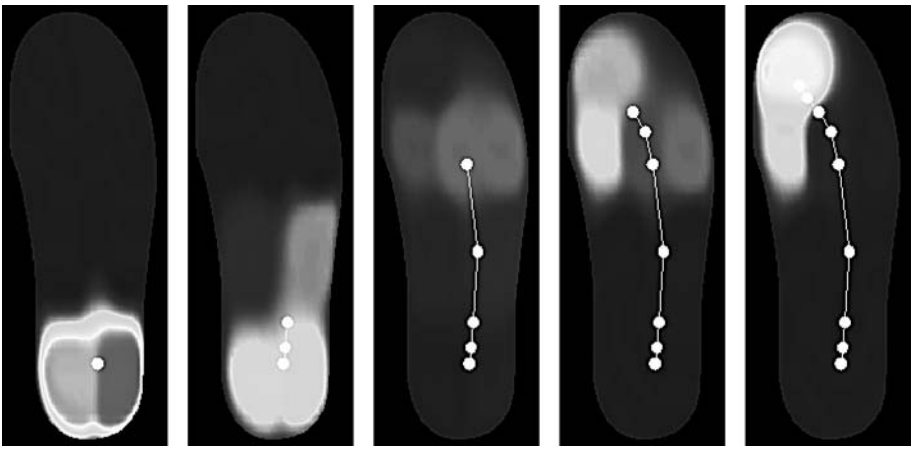

Figure 3 - Selection of a sequence of 14 time slices that display the pressure distribution during a step.

whole race. The web page was shown on a big TV screen in the VIP room. In this way the evolution of the athlete's performance could be monitored in real time. At several moments during the race, current results with commentary of an expert were also presented to the general public through a regional television station (Omroep Brabant) that covered the Marathon in a program that was transmitted live.

Figures 4a through 4d show the final graphs of all parameters that were measured as they looked at the end of the race. For this event, an extra interface was added to the DPPS client process that enabled monitoring the athlete's current heart rate. This real time data was provided over an internet connection by the company ChampionChip.

The contact time percentage is defined as percentage of the stride where the foot is in contact with the surface. Heel off time percentage is the percentage of the stance phase where the heel lifts are taking place. In figure 4 it can be seen that velocity and heart rate (4d) are decreasing after approximately one hour of racing. Also, core temperature increases above 39°C within approximately 40 minutes. Furthermore, it can be seen that contact times (%) and heel off times (%) increase slowly during the race accompanied by an increase in pace. This probably indicates a decreasing ability for fast force production by the leg muscles and this may limit the possible use of elastic energy within the muscle tendon complex. The decrease in heel off time percentage may be due to a progressive fatigue in especially biarticular muscles. We hypothesize elite runners show almost no marked differences in these running parameters during the race and thereby are able to maintain high running economy during endurance performance.

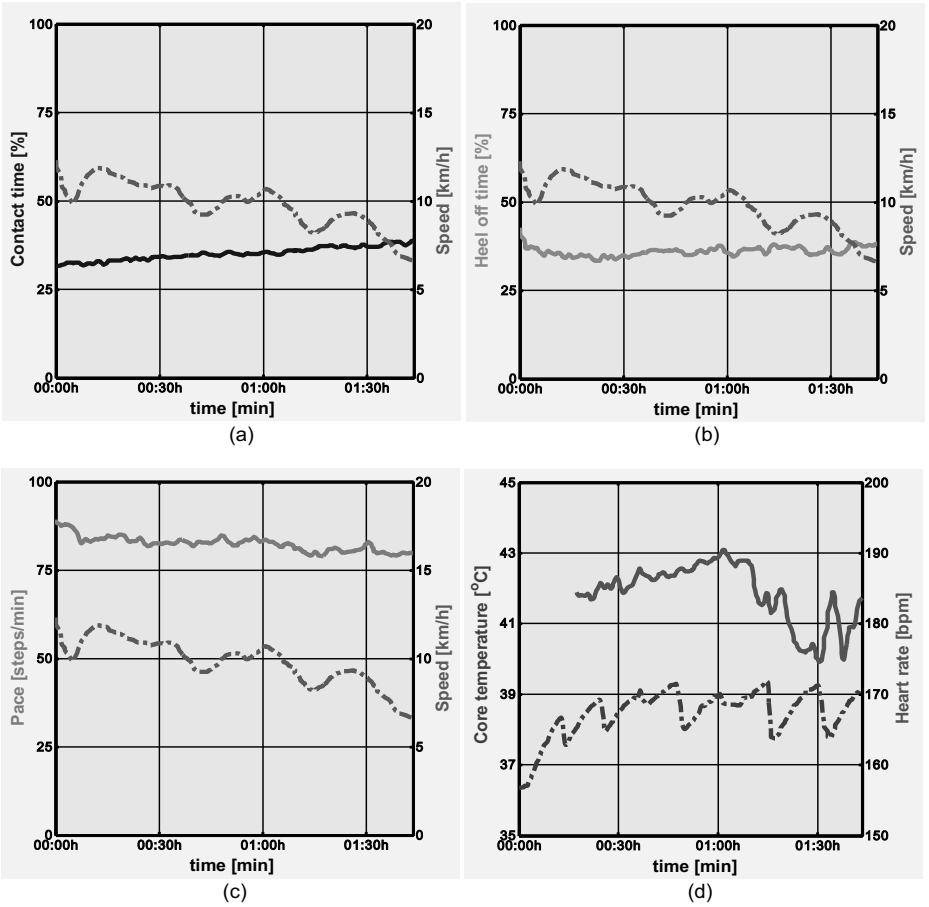

Figure 4 - For comparison, graphs 4a through 4c all show the runner's speed as the dash-dotted line. The drawn lines represent contact time, heel off time and pace respectively. Contact time (4a) and heal off time (4b) are expressed as a percentage of the time between two heal strikes. Pace or step frequency (4c) is defined as the reciprocal of the time between two consecutive heal strikes. Graph 4d shows the runner's core temperature as the dash-dotted line and his heart rate as the drawn line.

4- Future enhancements and improvements

Running speed was obtained as the value for the speed parameter from the GPS unit. The speed is internally inferred from the Doppler shift of the satellite signals that are used to calculate geoposition. Apparently, at least in our setup with the GPS receiving antenna placed within an enclosure at the back of our runner, this speed data is very noise and on average underestimates the actual speed of the runner. To suppress the noise, the speed data in figure 4 was low pass filtered by a moving average filter.

Also reception of the signal from the Cortemp measuring pill is not always optimal. Obvious misreadings were discarded. The oscillatory behaviour of the core temperature is a direct result of the intake of cold water by the runner. For publicity reasons the pill

was taken rather shortly before the start of the race, leaving the pill in the runner stomach during the race, rather than his intestines.

GPRS reception over the whole course was very good. Only four times during the whole two hour course was communication briefly lost, but was automatically restored within one minute.

In the current version of the Runalyser only a continuous auto-zeroing of the capacitive insole sensors is performed. In future versions, a full continuous auto-recalibration will be implemented to keep a well defined measure of the gait line.

Apart from improving the Runalyser hardware, studies are being executed to correlate the various parameters with running economy since easily identifiable and universally applicable patterns of efficient movement have not been found yet (Williams, 2007). Hereafter, we will try to correlate running technique with local load on the body to get more insight into the potential risk of injuries.

From a technical point of view, we foresee several routes along which the Runalyser can be further developed. First and foremost it can be seen as a tool that can help elite athletes understand their running economy and improve their training program and performance. In such a scenario, real time data processing and feed back as well as post data and trend analysis are valuable.

In a more 'light' version, the Runalyser could be a tool for the serious amateur runner to analyse and improve his running technique over time. Real time feedback would not be essential in this version, so the ability of logging all data during the race and post processing and long term trend analysis at home on a PC would suffice. Another possible application of the Runalyser is to evaluate the recovery from an injury. For example, by looking at the symmetry of running it can be evaluated if a former injury has still consequences for running technique.

Yet another embodiment of the Runalyser could be of interest to parties organizing and covering racing events. Presenting information on the actual performance and progress of their favourite runner could enhance spectator viewing experience. Also presenting live performance data to radio and television stations covering racing events can add to involvement of the spectator with the race. For such a version of the Runalyser real time data processing and transmission is of the essence, whereas long term trend analysis is not quite relevant.

Depending on the results of various trials that have been planned and market interest, other sensors might also be added to the Runalyser. Currently for example EMG measurements are considered.

5- References

[BK1] Bosch F. and Klomp R. Running Biomechanics and Exercise Physiology in Practice. Churchill Livingstone, 2004

[FL1] Foster C., Lucia A. Running economy: The forgotten factor in elite performance. Sports Med. 37(4-5):316-9, 2007

[NK1] Nummela A., Keränen T., Mikkelsson LO, Factors related to top running speed and economy. Int. J. Sports Med. 28(8):655-61, 2007

[W1] Williams KR. Biomechanical factors contributing to marathon race success. Sports Med. 37(4-5):420-3, 2007

Effects of Poles Stiffness, Slope and Type of Ground on Poling Forces in Hiking (P198)

Damien Fournet[1], Matthieu Foissac[1,2], Laurent Baly[2], Guillaume Millet[1]

Topic: Outdoor Sports

Abstract: Effects of poles stiffness, slope and type of ground on poling forces in hiking.

Introduction

Most manufacturers have developed damped or elastic poles but their efficiency has never been established. The main objective of the present study was to investigate the influence of hiking poles stiffness on poling forces. A secondary purpose was to examine the influence of slope, type of ground and the number of poles used on these forces.

Methods

Twelve healthy elderly experienced walkers (mean age 60.1 ± 8.5 yrs) were recruited for the study. The subjects tested hiking poles without damping (W0), and five damped poles, ranking from very rigid (W1) to very soft (W5), during uphill and downhill walking. They were asked to use the poles with the alternate stride technique, *i.e.* with an anti-phase movement of the arms relative to the legs, at a self-selected speed. The force exerted along the axis of the pole was obtained thanks to a mono-axis force sensor. Pole's inclination was also measured.

Results

The force patterns were significantly influenced by poles stiffness. Although no difference was found regarding any parameter between W0 and W1 to W4, W5 exhibited a lower impact peak force (~ 20%; $P < 0.05$) but a higher peak pushing force (+11%; $P < 0.05$) than the other poles. In uphill, regardless the pole stiffness, the maximal pushing peak force, the total impulse and the poling time were significantly higher ($P < 0.01$) and the impact peak force and angles significantly reduced (*i.e.* pole more vertical, $P < 0.01$) compared to downhill walking.

Discussion

The present results show that (i) most of the damped poles of the French market do not provide an efficient damping, (ii) a highly compliant pole is needed to significantly reduce the impact force and (iii) force patterns are strongly influenced by the slope.

Keywords: hiking; pole; biomechanics; stiffness; slope.

*1. PPEH Laboratory, Pavillon Médecine du Sport, Myologie, Hôpital Bellevue, 42 055 Saint-Etienne Cedex 2, guillaume.millet@univ-st-etienne.fr, * damienfournet@hotmail.fr*

2. Decathlon Biomechanics Laboratory, 4 boulevard de Mons. BP 299, 59 665 Villeneuve d'Ascq, France, {matthieu.foissac,laurent.baly}@decathlon.com

1- Introduction

Walking poles are now very popular in hiking. They were shown to reduce forces at the knee joint both during level (Brunelle and Miller 1998, Willson *et al.,* 2001) and downhill walking (Schwameder et al. 1999, Bohne and Abendroth-Smith, 2007). They also lead to an increased balance, especially while carrying a load on the back (Jacobson *et al.,* 2000). For these reasons, they are often used by elderly people. It has also been observed that the lower limbs muscles activation is reduced when using poles (Foissac *et al.,* 2008).

Despite these advantages, the physiological benefit of hiking poles is still controversial. The first studies related to the use of poles (Porcari *et al.,* 1997; Rodgers *et al.,* 1995) showed that the oxygen uptake was increased during level walking with poles compared to the no-pole condition. It is worth to note that the subjects were asked to have exaggerated arm movements in these two experiments. In uphill walking, the use of poles was shown to have no direct influence on energy cost (Knight and Caldwell, 2000, Foissac *et al.,* 2008). Also, no increase in oxygen consumption was found for different poles weights, from 200 g to 350 g (Foissac *et al.,* 2008).

For the last 10 years, manufacturers have incorporated damping systems to increase poles comfort. These systems are supposed to absorb shocks caused by the impact of the pole and therefore to provide a lower vibration transmitted to the subjects' arms. Yet, the efficiency of the damping systems has never been evaluated.

The aim of the present study was therefore to investigate the effect of damped poles on the poling forces. The effects of the slope, type of ground and number of poles used by the hiker were also studied.

2- Methods

2.1 Subjects

Twelve healthy volunteers (7 men and 5 women; (mean ± SD) age: 60.1 ± 8.5 yrs; height: 166.9 ± 9.1 cm; weight: 65.7 ± 8.1 kg) were recruited for the study. They were all regular hikers, accustomed to the use of poles, and performed a mean 17 km walk per week. A brief description of the experimentation was given to the subjects and their oral consent was obtained.

2. Procedure

The study was conducted on typical walking paths. The session lasted ~ 2 h for each subject. The first part of the experiment consisted in 12 different 30 s conditions. Five pairs of damped poles and 1 of rigid poles (W0) were compared. The five damped poles were chosen in order to have different stiffness, ranking for very soft (pole W5) to very rigid (pole W1). The 6 poles were randomly tested in uphill and downhill walking. In a second part of the experiment, the rigid (W0) and one damped pole (W4) were randomly compared both on a level stony and asphalt ground. These two conditions were tested with the subjects randomly using 1 or 2 poles.

For all conditions, the subjects were asked to walk at a self-selected speed (4.8 ± 0.4 km.h^{-1}) along a 30 m path. The average slope of the path was 16.3%. Their mean speed for each condition was obtained by dividing the total distance by the time, measured with a stopwatch. They were instructed to use the poles with an alternate stride technique, *i.e.* with an anti-phase movement of the arms relative to the legs. The poles were adjusted to 70% of their body height (Schwameder et al. 1999).

A strain gauge (Model LCMFD-500N, Omega Engineering Ltd, Manchester, UK; sampling frequency: 1000 Hz) located 5 cm below the handgrip was used to measure the forces exerted in the pole. The dynamic parameters considered are illustrated in figure 1: Poling Time (PT); Total Impulse (TI); Impact Peak (IP); Time to Impact Peak (TIP); Pushing Peak (PP); Time to Pushing Peak (TPP).

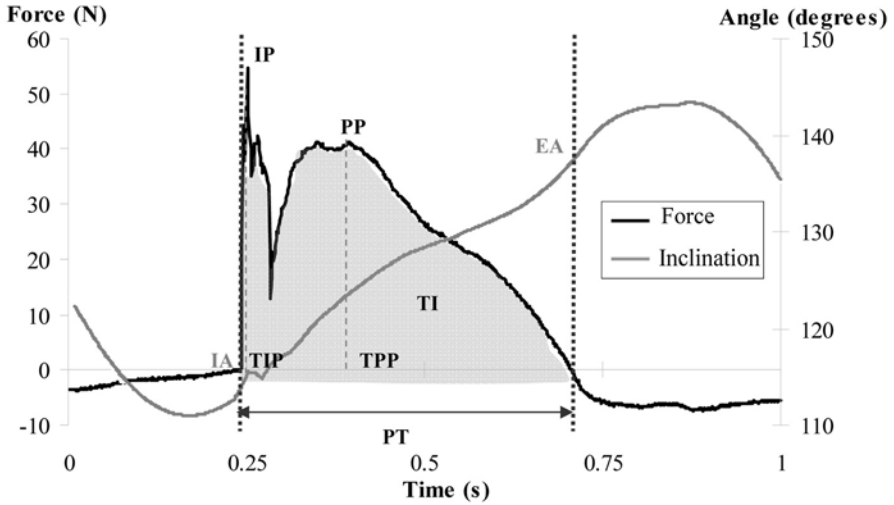

Figure 1 - Dynamics and angular parameters observed for one damped pole plant during a walking condition on asphalt. **IP**: Impact Peak; **TIP**: Time to Impact Peak; **PP**: Pushing Peak; **TPP**: Time to Pushing Peak; **PT**: Poling Time; **TI**: Total Impulse; **IA**: Impact Angle; **EA**: Angle at the End of the pushing phase .

A 3DOF orientation tracker (MTx, Xsens MT, Enschede, NL; sampling frequency: 100 Hz) was also connected to the pole to determine its angle during the step. All the data were synchronized and analyzed with Imago® software developed under Labview® (National Instruments, Austin, TX).

2.3 Statistical analysis

A two-ways (stiffness x slope) repeated measures ANOVA was used to test the effects of the different damping systems and the interaction with the slope. When a significant effect was found, significant pair-wise differences between conditions were determined using a Tukey *post hoc* test. To compare the 1 and 2 poles conditions, a two-ways (type of ground x 1 vs. 2 poles) repeated measures ANOVA was performed. An alpha level of $P < 0.05$ was required for statistical significance.

3- Results

3.1 Influence of pole stiffness

The pole stiffness significantly influenced IP (Figure 2), TIP ($P < 0.001$) and PP ($P < 0.01$). IP was not different between W0 and W1 to W4. Only the most compliant pole (W5) showed a significantly lower IP than W0 and W1 to W4. W5 also exhibited a significantly later TIP and higher pushing peak than all other poles, especially during downhill walking.

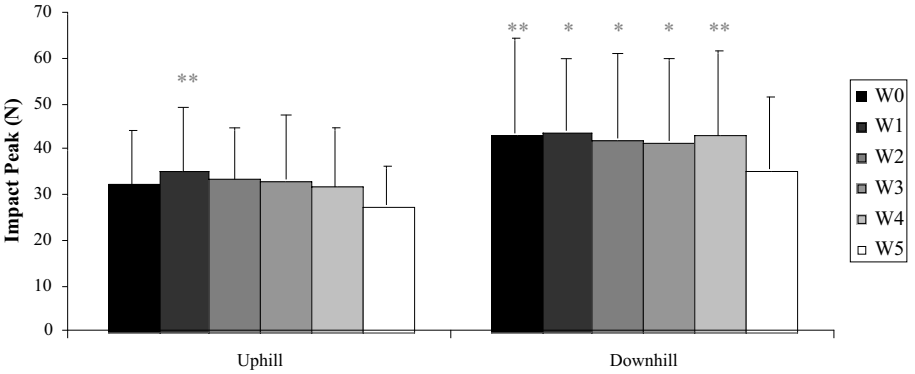

Figure 2 - Impact peak force for the two slope conditions. Significant differences with W5 (*: P < 0.05; **: P < 0.01).

3.2 - Influence of slope, type of ground and number of poles

Compared to uphill, downhill walking significantly reduced PT (-29%; $P < 0.01$), TPP (-26%; $P < 0.01$), PP (-28%; $P < 0.001$) and TI ($P < 0.01$) as shown in figure 3. On the contrary, significantly higher IP (+29%; $P < 0.01$), IA (+4%; $P < 0.01$) and EA (+4%; $P < 0.05$) were found in downhill. The self-selected speed adopted by the subject was 9% higher ($P < 0.05$) in downhill to compare with uphill walking.

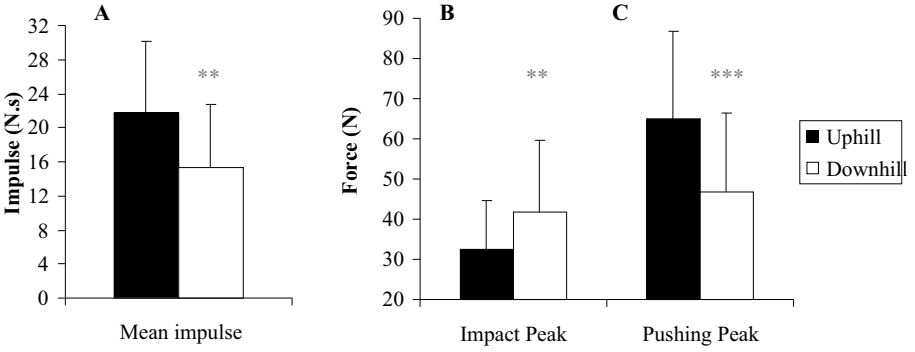

Figure 3 - Total Impulse (panel A), Impact Peak (panel B) and Pushing Peak (panel C) during uphill and downhill walking. Data represents the mean values of the 6 poles. Significant differences with uphill (**: $P < 0.01$; ***: $P < 0.001$).

IP arose significantly later ($P < 0.05$) on the stony path compared to the asphalt. No significant difference was found for IP or PP value between these two types of ground. Using 2 poles induced a higher IP (+17%; $P < 0.01$) and a reduced PT (-7%; $P < 0.05$), but did not influence PP for a given pole plant. However, when considering a stride, *i.e.* the sum of 2 consecutive pole plants, TI was significantly higher with 2 poles compared to 1 pole (+86%; $P < 0.01$).

4- Discussion

4.1 Influence of pole stiffness

The impact peak force was significantly lower for the less stiff pole (W5) than the other poles. It can therefore be assumed that this pole decreases the vibrations transmitted to the hand of the walker and then improves the comfort during a prolonged walk. Yet, perceived comfort as well as handle accelerations remain to be studied. In addition, it must be highlighted that W5 was at least twice as more compliant as most other existing damped poles which did not reduce the impact peak force to compare with a rigid pole.

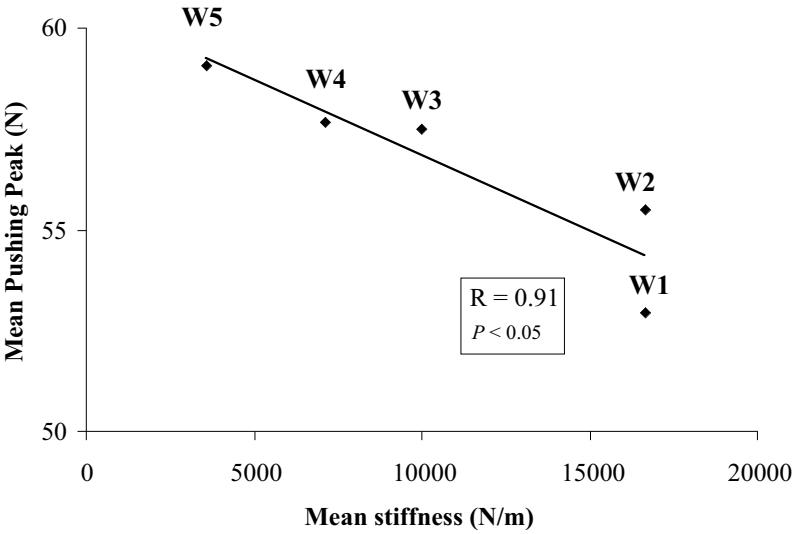

Figure 4 - Correlation between mean pushing peak (N) and the mean stiffness (N/m).

As shown in figure 4, when decreasing poles stiffness, the pushing peak amplitude increases. This phenomenon may be explained by the recoil of energy stored in the spring during the impact. It can then be speculated that the user would spend less energy to push on the pole with this type of pole. The level of activation of muscles used during poling has nevertheless to be performed to confirm this hypothesis.

4.2 Influence of slope, type of ground and number of poles

The shorter poling time during downhill walking could be explained by an increased walking speed and associated step frequency. In addition, the eccentric work performed

during downhill walking to slow the body centre of mass may lead to a higher braking using the poles, which was translated into an increased impact peak force. During uphill walking, the walker pushed more (+28 % for PP) to face gravity. In both cases, the poles helped to reduce the effects of gravitational forces and facilitated the vertical displacement of the body.

Using one pole allowed the walker to reduce IP and produce a higher impulse for a given pole plant. This could partly be explained by the fact that poling time was higher and that the subjects controlled the impact more carefully when using one pole. However, when considering a complete stride, TI was 46% lower for one pole than for 2 poles. It could then be assumed that the reductions of lower limb muscles activation and ground reaction forces previously reported with 2 poles to compare with no-poles (Schwameder et al. 1999, Knight and Caldwell, 2000, Foissac et al. 2008) would be almost twice lower with only one pole.

5- Conclusion

The main conclusions of the present study are that a compliant pole (i) significantly reduces the impact force transmitted to the hand and (ii) induces a higher pushing force. This could result in an increased comfort and possibly a better efficiency. Yet, this latter hypothesis remains to be tested. In addition, using two poles compared to one pole increases the passive shock but also the total force exerted by the walker on the poles during a stride. Finally, the slope influences poling forces whereas the type of ground seems to have limited effects.

6- References

[BA1] Bohne, M. and J. Abendroth-Smith. Effects of hiking downhill using trekking poles while carrying external loads. Med Sci Sports Exerc. 39:177-183, 2007.

[BM1] Brunelle, E. A., M.K. Miller. The effect of walking poles on ground reaction forces. Res Q Exerc Sport 69, 1998.

[FS1] Foissac M., B. R., Seux J., Belli A., Millet GY. Effects of hiking pole inertia on energy and muscular costs during uphill walking. Med Sci Sports Exerc, 2008.

[JW1] Jacobson, B. H., T. Wright, and B. Dugan. Load carriage energy expenditure with and without hiking poles during inclined walking. Int J Sports Med. 21:356-359, 2000.

[KC1] Knight, C. A. and G. E. Caldwell. Muscular and metabolic costs of uphill backpacking: are hiking poles beneficial? Med Sci Sports Exerc. 32:2093-2101, 2000.

[PH1] Porcari, J. P., T. L. Hendrickson, P. R. Walter, L. Terry, and G. Walsko. The physiological responses to walking with and without Power Poles on treadmill exercise. Res Q Exerc Sport. 68:161-166, 1997.

[RV1] Rodgers, C. D., J. L. VanHeest, and C. L. Schachter. Energy expenditure during submaximal walking with Exerstriders. Med Sci Sports Exerc. 27:607-611, 1995.

[SR1] Schwameder, H., R. Roithner, E. Muller, W. Niessen, and C. Raschner. Knee joint forces during downhill walking with hiking poles. J Sports Sci. 17:969-978, 1999.

[WT1] Willson, J., M. R. Torry, M. J. Decker, T. Kernozek, and J. R. Steadman. Effects of walking poles on lower extremity gait mechanics. Med Sci Sports Exerc. 33:142-147, 2001.

Development of Small-Sized Swimming Humanoids (P203)

Motomu Nakashima[1], Hideo Kobayashi[2]

Topics: Swimming humanoid.
Abstract: The primary objective of this study is to develop robots for research of the human swimming. In order to address this objective, two small-sized prototype models of the swimming humanoids were developed and evaluated. Both of the two developed humanoids have ten RC servo motors for the upper limbs, a plastic bottle for abdominal part, and floats for the head and lower limbs. In addition, the humanoids are remotely controlled from the ground via Bluetooth, and can perform the crawl stroke. The stature of the first model was 0.53m. From the swimming experiment of the first model in a pool, it was found that the buoyancy of the humanoid was not in balance. Solving the problem for the buoyancy balance, the improved second model was constructed. It has the structure basically the same as the first model although its stature becomes 0.79m. In the swimming experiment of the second model, two swimming forms and several stroke cycles are tested, and the swimming movement was measured by a three-dimensional motion analysis system. From the experiment, the swimming speed and the nondimensional stroke length were found to be 0.20~0.35 m/s and 1.02~1.31, respectively. Since the stroke length over 1.0 is equivalent with the competitive swimming of human, it indicates the possibility of the swimming humanoid.
Key words: Swimming, Humanoid, Crawl stroke.

1- Introduction

In most studies related to the biomechanics of human swimming, real swimmers have been used in the experiments. For example, Takagi and Sanders [TS2] attached pressure sensors on the hands of swimmers, and measured the surface pressure to estimate the thrust by the hand. Yamada *et al.* [YM1] visualized the flow filed around the hand of a swimmer. Takagi *et al.* [TS1] and Toussaint *et al.* [TG1] measured the 'Active Drag' during swimming. In these experiments, the swimming motions of the swimmers were assumed to be reproductive. However, it is generally difficult to obtain results with repro-

1. Tokyo Institute of Technology, 2-12-1-W8-2 Ookayama, Meguro-ku, Tokyo, 152-8552, Japan - E-mail : motomu@mei.titech.ac.jp
2. Graduate School of Tokyo Institute of Technology - E-mail : hkobayashi@hei.mei.titech.ac.jp

ductivity in the experiment using human. An alternative way is to use robots instead of real swimmers, since the robot motion can be sufficiently reproductive. Therefore, the primary objective of this study is to develop robots for research of the human swimming. In order to address this objective, two small-sized prototype models of the swimming humanoids were developed and evaluated.

2- Basic specifications of small-sized swimming humanoid

Joint motion of the swimming humanoid in this study was the crawl stroke, which is most common in the four strokes. Since upper limbs in the crawl stroke mainly produces thrust and lower limbs mainly produces the buoyant force [N1], only the upper limbs of the humanoid in this study were driven by actuators, while the lower limbs were simply floats made of buoyant material. In order to represent the swimming motion of the crawl, the mechanism of the upper limbs were designed to perform 5 DOF motion, that is, rotation, horizontal flexion/extension, adduction/abduction at the shoulder, and flexion/extension, pronation/supination at the elbow. All the mechanisms were waterproofed. The humanoid did not have any cable from the ground, that is, it had battery inside and was radio controlled.

3- Test model

3.1 Development

In order to confirm the validity of the basic structure, a test model was developed based on the basic specifications in the previous chapter. The test model consists of ten RC servo motors (KRS-2350ICS Red version, Kondo Kagaku Co.) for the upper limbs, a plastic vessel for the abdomen, head and lower limbs made of styrene foam. Figure 1

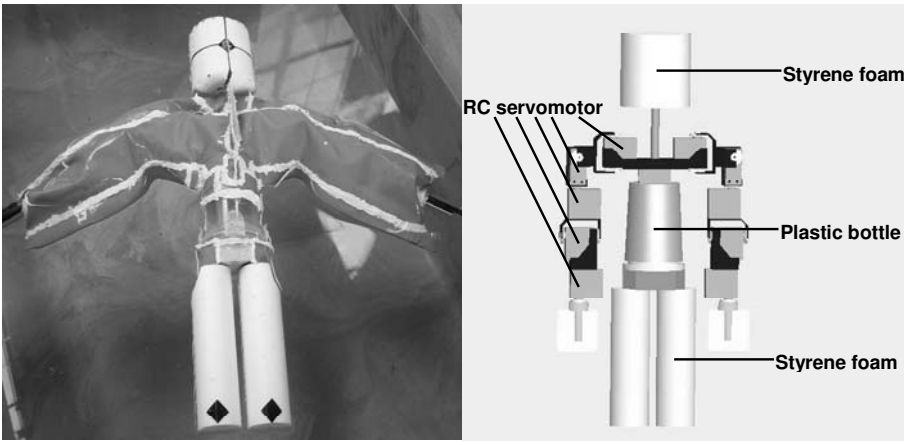

Figure 1 - Photograph and schematic view of test model.

shows a photograph and schematic view of the test model. In the plastic vessel for the abdomen, devices for motor control were installed. The installed devices were a servo motor controller (AGB-SC-01, Asakusa-Giken Co.), a Bluetooth serial adaptor for wireless control (Socket Communications Co.), and a battery. With respect to the lower limbs, two styrene-foamed cylinders were utilized for the buoyancy. The head was also made of styrene foam to prevent the unbalance of the buoyancy due to heavy upper limbs. With respect to the control method, the joint motion of the crawl stroke for one cycle was firstly divided into 18 steps. Then, the information of the joint angle was sent to the controller via Bluetooth in real time. The joint angle between each two steps was linearly interpolated by the controller. For the waterproofing, the whole upper limb parts were covered by rubber sheets glued by sealing bond. In order to prevent the rubber breaking by friction between the RC servo motors, pieces of soft sheet made of wet suit material were attached onto the appropriate spots of the upper limbs. A valve in the rubber part on the back of the humanoid was installed in order to deflate the inside air which might interfere the humanoid behaviour during swimming. The stature and weight of the test model were 0.53m and 2.0kg, respectively.

3.2 Experiment to measure swimming movement

An experiment to measure the swimming movement of the test model was conducted. Figure 2 shows the schematic diagram of the experimental setup. In the experiment, a marker was attached to the back of the head, and it was filmed using two cameras. By using three-dimensional motion analysis software (Pc-MAG, OKK inc.), the three-dimensional coordinates were computed. The joint motion given to the test model was based on a standard motion of the crawl stroke which was already created when developing the author's swimming human simulation model SWUM [NS1]. In addition, the standard motion was so modified that the humanoid could perform the 'recovery' motion. That is, the horizontal extension for 40 degrees all through the cycle was addi-

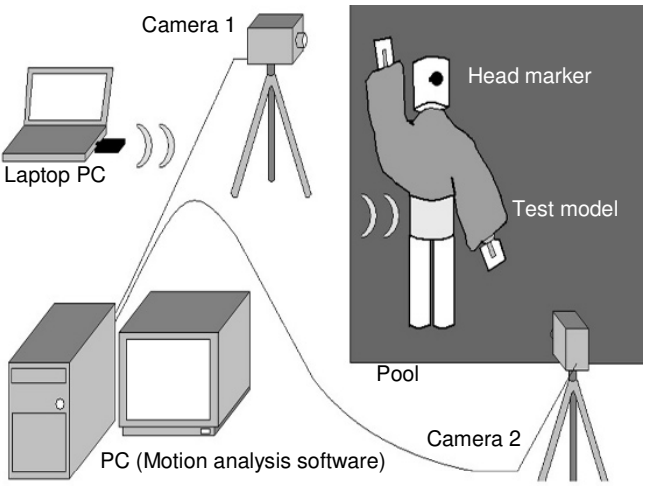

Figure 2 - Schematic diagram of the experimental setup.

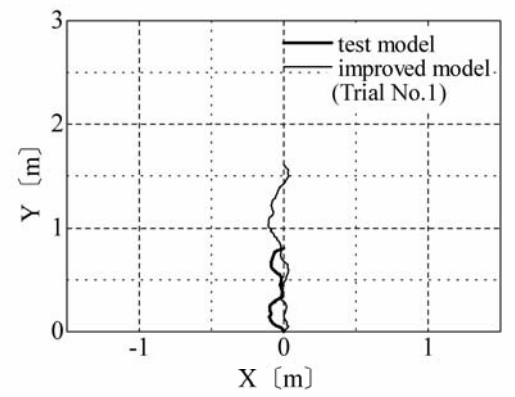

Figure 3 - Locus of head marker (Swimming motion A, cycle=4.4 s).

tionally given to the shoulder joint. This swimming motion was called 'Swimming motion A'. The cycle was 4.4s. The measurement was started after 4 or 5 cycles, when the swimming motion becomes stable. Figure 3 shows the locus of the head marker during the measurement. The results of the test model were depicted as a thick line. The measurement duration was 7.7s. In this figure, the origin is set to the position of the start time of the measurement, and the line going along the origin and end point is set as Y axis. The swimming speed and the non-dimensional stroke length, which is defined as the propelling length divided by the stature, were 0.12m/s and 1.00, respectively.

3.3 Problems of the test model

By the experiment, the following problems of the test model were found: First, the forearms were completely above the water surface in the 'entry and stretch' phase, in which the arm normally should be stretched forward in the water. This was because the model rolled in the direction where the opposite shoulder in the recovery phase sank due to the heaviness of the upper limbs. The second problem was that the lower limbs floated too higher. This was because the buoyancy of the lower limbs was excessive.

4- Improved model

4.1 Development

Referring to the problems of the test model revealed by its experiment, the second improved model was later constructed. Figure 4 shows the schematic of the second improved model. For the problem of the arm above the water surface in the stretch phase, a wedge-shaped plate was installed between the upper limb part and abdomen parts so that whole the upper limb part inclined to the front at 7 degrees. For the problem of the excessive buoyancy of the lower limb, brass weights were installed into the lower limb cylinders so that the specific gravity of the lower limbs became nearly 1.0. In addition, the body proportion became close to the actual human in the improved model. For the head part, the shape was changed from a cylinder into an ellipsoid. The shape of the hands was also changed. Both the thickness and length of the waist were

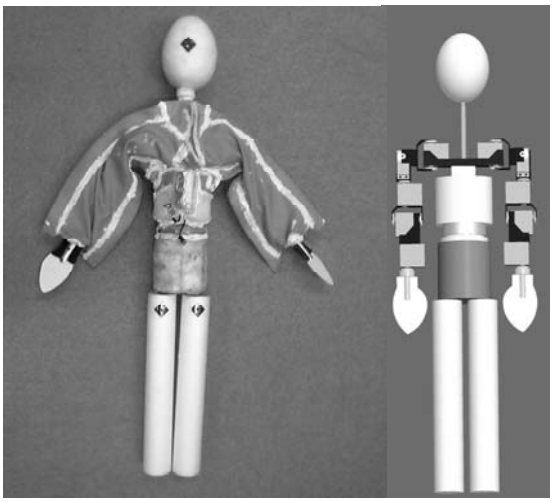

Figure 4 - Photograph and schematic view of improved model.

increased. The length of the lower limbs was increased. By these changes in dimensions, the size of the improved model became almost half of the human for all parts of the body. The resultant stature and the total weight became 0.79m and 3.2kg, respectively.

4.2 Experiment to measure swimming movement

An experiment to measure the swimming movement of the improved model was also conducted. In this experiment, two swimming motions were prepared, and the cycle was also changed. Table 1 shows the types of the swimming motion and the values of the cycle. The swimming motion A is the same as that for the test model described in Section 3.2. In the swimming motion B, the velocity of the push motion for both arms was increased by skipping one time step during each push motion from the 18 original time steps. Figures 3 and 5 show the loci of the head marker. In each figure, the origin is set to the position of the start time of the measurement, and the line going along the origin and end point is set as Y axis. The results of the swimming speed and the non-dimensional stroke length were also shown in Table 1. In Figure 5(a), the origins of the trials 1 and 3 were respectively shifted at 0.5m left and right for easiness to see. Trials 1, 2 and 3

Trial No.	Swimming Motion	Cycle [s]	Swimming Speed [m/s]	Nondimensional Stroke Length
Test Model	A	4.4	0.119	1.00
1	A	4.4	0.204	1.12
2	A	3.4	0.258	1.11
3	A	2.6	0.325	1.07
4	B	3.9	0.264	1.31
5	B	2.3	0.350	1.02

Table 1 - Experimental results.

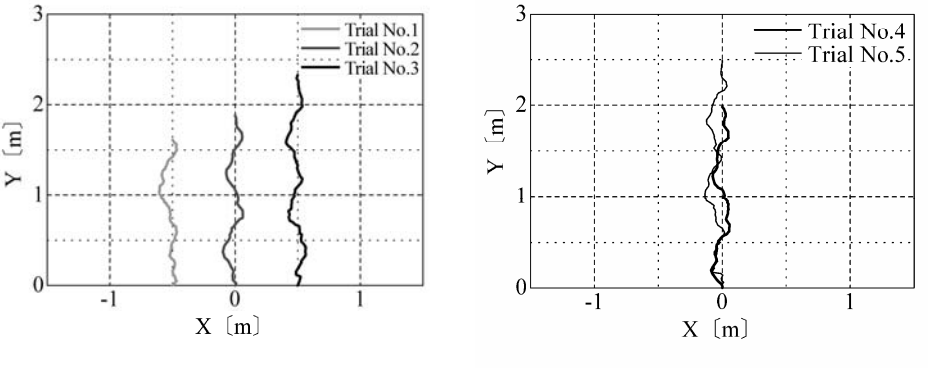

(a) Trial No. 1-3 (b) Trial No. 4-5

Figure 5 - Locus of head marker (Trial No.1-3).

had the same swimming motion but the different cycles. The swimming speed is found to increase for the shorter cycle, although the nondimensional stroke length decreases. Since Trials 4 and 5 had faster push motion, the swimming speed became larger than the trials of the swimming motion A. With respect to the nondimensional stroke length, Trial 4 seems the best. However, its swimming movement was found to be relatively unnatural from the video. In Figure 3, the results of the same swimming motion and the cycle for the test and improved model were shown. From this figure, it is found that the swimming speed of the improved model became 1.7 times larger than that of the test model. And the nondimensional stroke length of Trial 1 was 1.12, which value was almost the same as that of the competitive swimmer for short distance. These results would indicate the validity of the improvement in this study.

5- Conclusions

Two models of the small-sized swimming humanoid were constructed in this study. In the experiment to measure the swimming movement, the swimming speed 0.350m/s and the nondimensional stroke length 1.31 were attained as their best values. As one of the problems to be solved in near future, the method of waterproofing should be improved. In this study, whole the upper limbs were covered by rubber sheets. These sheets were found to hinder the motion of the motors, and to be easy to deteriorate. Therefore, other method would have to be examined, such as, waterproofing each motor component without any sheet covering whole the mechanism. Another problem to be solved is the improvement of the lower limbs. In this study, the lower limbs were not actuated. However, they would have to be actuated by motors in order to perform the lower limb motion, such as, flutter kick in the crawl. By these improvements, swimming in the four strokes (crawl, breast, back and butterfly) by the swimming humanoid would be realized.

6- References

[N1] Nakashima M. Mechanical Mechanical study of standard six beat front crawl swimming by using swimming human simulation model. In Journal of Fluid Science and Technology, 2(1): 290-301, 2007

[NS1] Nakashima M., Satou K. and Miura Y. Development of swimming human simulation model considering rigid body dynamics and unsteady fluid force for whole body. In Journal of Fluid Science and Technology, 2(1): 56-67, 2007

[TG1] Toussaint H. M., Groot G. de., Savelberg H. H. C. M., Vervoorn K., Hollander A. P. and Ingen Shenau G. J. Van. Active drag related to velocity in male and female swimmers. In Journal of Biomechanics 21: 433-438, 1988

[TS1] Takagi H., Shimizu Y. and Kodan N. A Hydrodynamic study of active drag in swimming. In JSME International Journal Series B, 42(2): 171-177, 1999

[TS2] Takagi H. and Sanders R. Measurement of propulsion by the hand during competitive swimming, In The Engineering of Sport 4 (Eds. Ujihashi, S and Haake, S.J.), 631-637, Blackwell Publishing, 2002

[YM1] Yamada K., Matsuuchi K., Nomura T., Sakakibara J., Shintani H. and Miwa T. Motion analysis of front crawl swimmer's hands and the visualization of flow fields using PIV. In Biomechanics and Medicine in Swimming X (Eds. Vilas-Boas J.P., Alves F. and Marques A.), 111-113, Portuguese Journal of Sport Sciences, Porto, 2006

Parametric Study of Bicycle Stability (P207)

Jason Moore[1], Mont Hubbard[2]

Topics: Bicycle, Modelling.
Abstract: Bicycles are inherently dynamically stable and this stability can be beneficial to handling qualities. A dynamical model can predict the self-stability. Previous models determined the sensitivity of stability to changes in parameters, but have often used idealized parameters occurring in the equations of motion that were not possible to realistically change independently. A mathematical model of a bicycle is developed and verified. The model is used together with a physical parameter generation algorithm to evaluate the dependence of four important actual design parameters on the self-stability of a bicycle.
Keywords: bicycle, stability, parametric, dynamics, linear.

1- Introduction

Bicycles are an important mode of transportation for many people. Handling is an issue for bicycles, as it is for all vehicles. Poor handling can result in accidents and make it difficult for people to learn to ride a bicycle. Different bicycle designs have different handling qualities and these are a function of the physical parameters of the bicycle and rider. Vehicle handling qualities have typically been quantified by relating vehicle dynamic properties to subjective rider opinion, but some information about handling qualities can be extracted from the vehicle dynamics alone.

Many dynamicists have explored the dynamics of a bicycle with a rigid rider over the past 150 years and the bicycle has long been known to demonstrate self-stability (Meijaard *et al.*, 2007). This stability has been proven through both experimentation (Kooijman 2006) and the development of a reasonably robust dynamical model of the vehicle. A typical bicycle is stable over a range of speeds. This range can be determined by examining the eigenvalues for negative real parts when the dynamics are linearized about a constant speed upright configuration. The stable speed range is dependent on various physical parameters such as the geometry, mass location and mass distribution.

Stability may not be the means to good handling qualities, but stability can be very important when the controller (the rider) is not skilled enough to stabilize the bicycle, such as when learning to ride or under other uncontrollable circumstances. A novice can benefit from stability at very low speeds and a typical rider could benefit from a broader

1, 2. Department of Mechanical and Aeronautical Engineering Sports Biomechanics Lab University of California, Davis 1 Shields Ave. Davis, CA 95616 USA - E-mail : {jkmoor,mhubbard}@ucdavis.edu

range of stable speeds (i.e. one that would cover the typical usable speed range of a bicycle).

Previous studies have shown how independently changing the idealized parameters can change the stable speed range of an uncontrolled bicycle (Åström *et al.,* 2005, Franke *et al.,* 1990, Limebeer and Sharp 2006). As an example, it has been shown that an increase in moment of inertia of the front wheel can lower the speed at which the bicycle becomes stable. But if one were to actually change the moment of inertia of a bicycle wheel there would likely also be a corresponding change in the mass of the front wheel. When designing and constructing a bicycle each physical parameter cannot be changed independently as in an idealized model. It would be beneficial to be able to estimate the change in stable speed range when adjusting the bicycle parameters dependently as one would have to do when actually constructing the vehicle.

We present a method of estimating the physical properties of a hands-free uncontrolled rigid-rider bicycle model, derive a linearized dynamical model of the bicycle, and calculate the changes in stable speed range for various parameter changes.

2- Methods

A dynamical model of the bicycle complex enough to demonstrate self-stability is needed in order to calculate the critical velocities that bound the stable speed range. The nonlinear equations of motion and the linearized system dynamics of the uncontrolled model were developed analytically with the symbolic manipulator Autolev® which is based on Kane's method (Kane and Levinson 1985). This model was then verified against the benchmark (Meijaard *et al.,* 2007) for accuracy. Also, a complementary method to estimate the physical parameters of the bicycle and rider was developed to allow for an infinite combination of realistic parameters. Using each of these, we developed algorithms that varied parameters of interest to show their effects on the stability of the bicycle model.

2.1 Bicycle Model

The Whipple bicycle model (Whipple 1899) was selected as an appropriate model. This model is made up of four rigid bodies (frame/rider, fork/handlebar and wheels) connected to each other by frictionless revolute joints. The wheels contact the ground under pure rolling and no sideslip conditions. This idealized model has been verified and benchmarked by Meijaard *et al.,* (2007) and has been shown to be representative of a realistic bicycle with high-pressure tires up to 6 m/s (Kooijman 2006).

The Whipple model was formulated using Kane's method. Four rigid bodies (C: rear wheel, D: frame/rider, F: fork/handlebar, G: front wheel), three intermediate reference frames (A: yaw, B: lean, E: steer axis) and eight generalized coordinates (q_i where i = 1,…,8) were used to characterize the bicycle configuration (Figure 1) within the Newtonian reference frame, N. The generalized coordinates are defined as follows: q_1 and q_2 locate the rear wheel contact point in the ground plane, q_3 is the yaw angle, q_4 the lean angle, q_5 the rotation angle of the rear wheel, q_6 the frame pitch angle, q_7 the steer angle and q_8 the rotation of the front wheel. The wheel contact points for the front

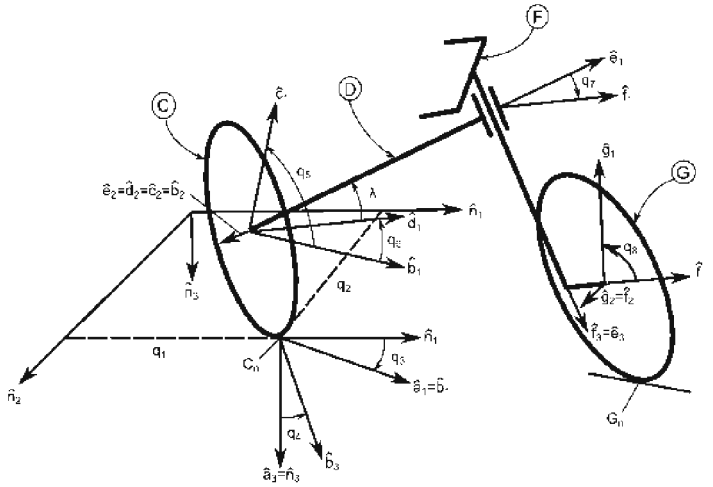

Figure 1 - Dynamical model of the bicycle.

and rear wheel are C_n and G_n, respectively. The Whipple model is further characterized by a minimum set of physical parameters. The geometrical parameters are depicted in Figure 2 and each body (C, D, F and G) has mass and moment of inertia.

A closed loop holonomic configuration constraint, arising from the fact that both wheels must touch the ground, complicates the model derivation. The constraint (Equation 1) is equivalent to a nonlinear relationship between the lean angle, steer angle and pitch angle. Pitch, q_6, is typically taken as the dependent coordinate and the constraint equation can be formulated into a quartic in the sine of the pitch (Psiaki 1979, Peterson and Hubbard 2008). To avoid having to solve the quartic algebraically, the derivative of the constraint equation is taken. This produces a velocity constraint equation that is linear in the derivatives of the pitch angle, steer angle and lean angle (Equation 2). This allows an explicit solution for the pitch angular velocity u_6, making it a dependent generalized speed.

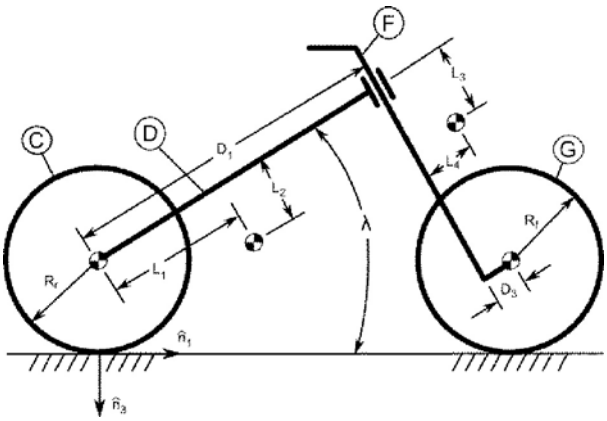

Figure 2 - Bicycle geometric parameters.

$$\bar{r}^{G_n/C_n} \cdot \hat{n}_3 = f(q_4, q_6, q_7) = 0 \tag{1}$$

$$\frac{d}{dt}\left(\bar{r}^{G_n/C_n} \cdot \hat{n}_3\right) = a \cdot u_4 + b \cdot u_6 + c \cdot u_7 = 0 \tag{2}$$

Four nonholomic constraints (Equation 3) further reduce the locally achievable configuration space to three degrees of freedom. The pure rolling, no side-slip, contact of the knife-edge wheels with the ground plane requires that there are no components of velocity of the wheel contact points in the $\hat{n}_1$ and $\hat{n}_2$ directions.

$${}^N\bar{v}^{C_n} \cdot \hat{n}_1 = {}^N\bar{v}^{C_n} \cdot \hat{n}_2 = {}^N\bar{v}^{G_n} \cdot \hat{n}_1 = {}^N\bar{v}^{G_n} \cdot \hat{n}_2 = 0 \tag{3}$$

Eight generalized coordinates, one of which is dependent, and three independent generalized speeds ($u_i = \dot{q}_i$ where i = 4,5,7) describe the system. The five generalized coordinates, q_i where i = 1,2,3,5,8, are ignorable, that is they do not occur in the dynamical equations of motion.

The nonminimal set of dynamic equations of motion (Equations 4 and 5) were formed with Kane's method. They are nonminimal because pitch angle, q_6, was not solved for explicitly. With this set of equations one must solve for the pitch angle numerically for its initial condition when simulating and for the fixed point when linearizing.

$$u_i = f(u_4, u_5, u_7, q_4, q_6, q_7) \text{ where } i = 4,5,7 \tag{4}$$

$$q_i = u_i \text{ where } i = 4,5,6,7 \tag{5}$$

The equations of motion are then linearized symbolically using Autolev® by calculating the Jacobian of the system of equations. The partial derivatives were evaluated at the following fixed point: $q_i=0$ where i=4,6,7, $u_i=0$ where i=4,7, and $u_5=-v/R_r$ where v is the constant forward speed of the bicycle.

The real parts of the eigenvalues of the state matrix characterize the stability of the system and can be calculated for various forward speeds. Figure 3 shows the real parts of the eigenvalues for the model using the benchmark parameter set given in Meijaard *et al.* (2007). The eigenvalues match those of the benchmark to the thirteenth decimal place for all eigenvalues and to the fourteenth decimal place for most eigenvalues. Furthermore, the linearized system was put in the benchmark canonical form and the associated matrices (M, C_1, K_0, and K_2) matched to the same precision as the eigenvalues. The high precision verifies that the correct Whipple model has been implemented.

2.2 Parameter Generation

The components of the state matrix are functions of 25 physical parameters of the Whipple model. Varying these parameters affects the stable speed range of the bicycle.

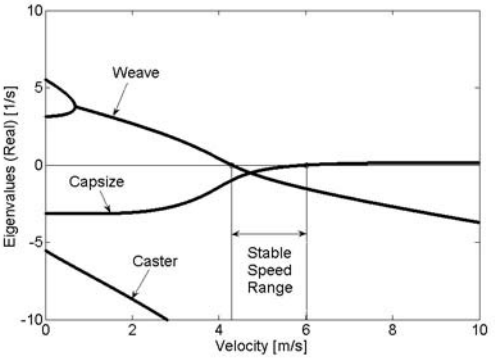

Figure 3 - Stable speed range of the benchmark bicycle showing the weave and capsize critical velocities.

We developed a method of estimating the mass, centres of mass, and inertial properties of the bicycle and rider from various typical geometric measurements such as wheelbase, trail, wheel diameter, limb length, body weight, etc. This allowed us to vary the parameter and always have a realistic bicycle and rider configuration. Unlike in previous studies, the physical parameters are interdependent (i.e. adjusting the front wheel diameter changes the wheel's mass and moment of inertia together with the bicycle's frame geometry). The bicycle frame and fork were modelled as a collection of uniform steel tubes and the wheels as tori. The rider was modelled as a collection of uniform rectangular prisms, cylinders and a sphere (Figure 4).

The nominal geometry, mass, and moments of inertia of the bicycle and rider were measured from a 58 cm 1982 Schwinn LeTour steel road bike and from a 72 kg, 182 cm tall adult male. The mass of each frame tube was determined from the volume and density of the tubes. The masses of the rider segments were calculated as percentages of the total body weight (Dempster 1955). Centres of mass and moments of inertia were

Figure 4 - Representative physical model of the bicycle and rider.

calculated based on the geometry and mass of the segments. The local parameters for each segment were summed for each rigid body and the geometry parameters were converted to the parameter set required by the Autolev® model. An algorithm was constructed to vary any input parameter and calculate the weave and capsize critical velocities.

3- Results

The stable speed range for the nominal bicycle configuration was between 3.59 m/s and 4.88 m/s. We chose four physical parameters to show the usefulness of the model: front wheel diameter, head tube angle, trail and wheelbase (Figure 5). Changes in the stable speed range were calculated by varying each parameter over a realistic range. Each figure (6-9) shows a depiction of the maximal and minimal geometry configurations and the nominal stable speed range is shown with a vertical line. The weave critical speed decreases as front wheel diameter increases but the higher capsize critical speed decreases

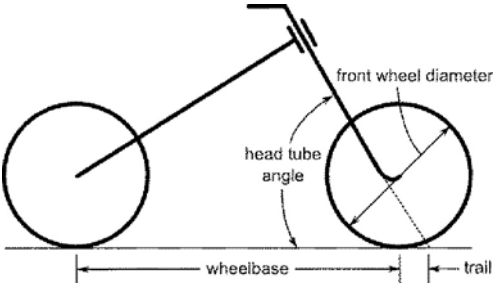

Figure 5 - Geometric parameters of interest.

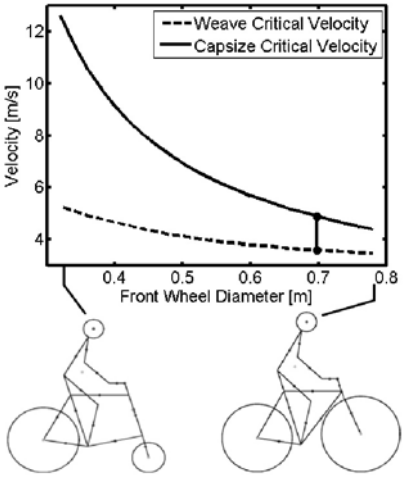

Figure 6 - Critical speed range vs. front wheel diameter.

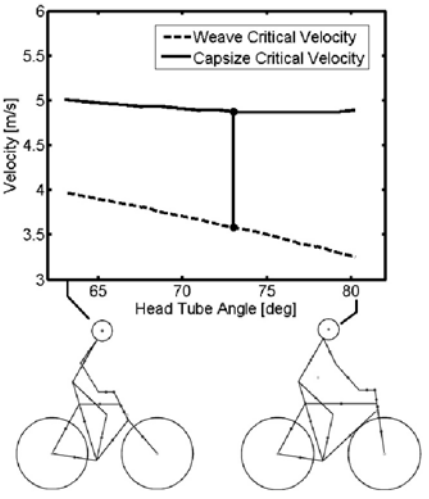

Figure 7 - Critical speed range vs. head tube angle.

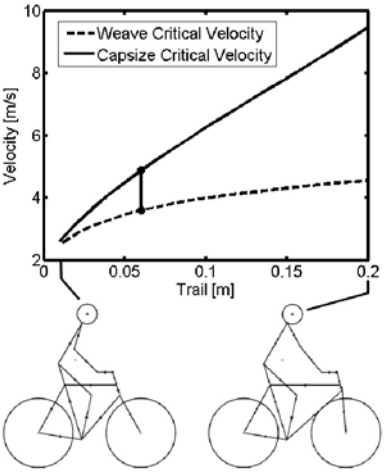

Figure 8 - Critical speed range vs. trail.

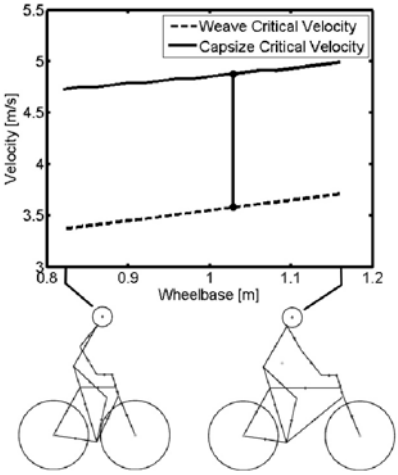

Figure 9 - Critical speed range vs. wheelbase.

even faster so the size of the stable speed envelope also decreases (Figure 6). A slack head tube angle (< 72 degrees) has a higher weave critical speed than a larger head tube angle but the capsize critical speed varies very little with changing head tube angle (Figure 7). As trail increases (Figure 8), the stable speed range broadens and the weave critical velocity increases. As wheelbase increases the stable speed range stays constant as both weave and capsize critical speeds increase at about the same rate (Figure 9).

4- Discussion

The results of these parameter studies are in agreement with previous studies and some anecdotal knowledge of bicycle handling. It has been shown that an increased idealized moment of inertia of the front wheel adds stability at low speeds (Åström *et al.,* 2005). The results (Figure 6) show that the weave critical speed does decrease with a larger front wheel thus providing inherent stability at low speeds. Slack head tube angles are found on many utility bicycles. These bicycles subjectively feel very unresponsive at low speeds and typically do not feel stable until moderate speeds are reached. The head tube angle results are in agreement with this anecdotal evidence in so far as the weave critical speed increases with decreasing head tube angle (Figure 7). The head tube angle results are interesting because the weave speed can be decreased with a steep head tube angle without adversely affecting the capsize critical speed, thus simultaneously increasing the stable speed range and decreasing the weave speed. This is ideal if it is assumed that a low weave critical speed is beneficial for take off and a broad stable speed range is beneficial for cruising with little control input. Trail is typically of particular interest, with many bicycle designers claiming that it is the most important parameter affecting handling qualities. Tim Paterek, an expert frame builder, claims that the comfort zone for trail falls between 5 cm and 6.5 cm for most bicycles (Paterek 2004). No correlation can be drawn from Figure 8 and Paterek's claims. Thus a more robust assessment of handling qualities is needed. As trail approaches zero the stable speed range diminishes and this

follows the observed instability of a caster with negative trail (the caster will always flip around to the stable configuration). Long bicycles such as tandems and some recumbents are typically hard to start, but handle better at higher speeds. The weave critical speed increases as wheelbase increases (Figure 9) which correlates with the difficulty in starting long wheelbase bicycles.

The Whipple model and the parameter generation algorithms discussed here can be particularly useful in the design of bicycles used to teach people how to ride. The idea would be to design for a very low weave critical velocity so that novices would not have to travel at higher speeds to benefit from the self stability inherent in the bicycle. Bicycles such as the ones used in the "Lose the Training Wheels" program (Klein 2008) and the Gyrobike (Ward 2006) are excellent examples. Bicycles can also be designed with a broader stable speed range that could potentially be used for situations in which a bicycle rider moving at higher speeds could benefit from self-stability. The tools developed here may be of value to bicycle designers. A turnkey software package could allow a layman to select the physical parameters when designing a bicycle to meet a desired stable speed range.

5- References

[ÅK1] Åström K., Klein R. and Lennartsson A. Bicycle dynamics and control. In IEEE Control Systems Magazine, 25(4): 26-47, 2005.

[D1] Dempster W. Space requirements of the seated operator. In Aerospace Medical Research Laboratory WADC technical report 55: 159, 1955.

[FS1] Franke G., Suhr P., and Rieb F. An advanced model of bicycle dynamics. In European Journal of Physics 11:116-121, 1990.

[KL1] Kane T. and Levinson D. Dynamics: Theory and Applications. McGraw-Hill , New York, 1985.

[K1] Klein R. Lose the Traing Wheels. www.losethetrainingwheels.org, 2008.

[K2] Kooijman, J. Experimental validation of a model for the motion of an uncontrolled bicycle. M.Sc. thesis, Delft University of Technology, 2006.

[LS1] Limebeer D. and Sharp R. Bicycles, Motorcycles and Models. In IEEE Control Systems Magazine, 26(5): 34-61, 2006.

[MP1] Meijaard J., Papadopoulos J., Ruina A. and Schwab A. Linearized dynamics equations for the balance and steer of a bicycle: a benchmark and review. Proc. Roy. Soc. A., 463(2084): 1955-1982, 2007.

[P1] Paterek T. The Paterek Manual for Bicycle Framebuilders, Henry James Bicycles, Inc., Redondo Beach, CA, 2004.

[P2] Peterson D. and Hubbard M. Analysis of the holonomic constraint in the Whipple bicycle model. In preparation for ISEA 2008.

[P3] Psiaki M. Bicycle stability: A mathematical and numerical analysis. Undergraduate thesis, Princeton University, 1979.

[W1] Ward L. Gyrobike: Preventing Scraped Knees. In Popular Mechanics, November 2006.

[W2] Whipple F. The stability of the motion of a bicycle. In The Quarterly Journal of Pure and Applied Mathematics, 30: 312-348, 1899.

Compression Garments: Evidence for their Physiological Effects (P208)

Stéphane Perrey[1]

Topics: Exercise physiology, muscular performance, textile, engineering processes.
Abstract: In fitness and leisure sports, compression clothing (e.g. tights, garments, stockings) has become popular with the need to minimise the stress of activity by improving physiological factors. The area of contact between textile material and human skin represents a complex parameter in which factors such as the deformational behaviour of fibrous material under pressure, surface hardness, and surface roughness play interactive and dependent roles. The nature of human skin surface morphology and bulk properties add further complexity. Early researches on compressive garments focused on increased venous blood flow due to the compression and its positive effects on venous thrombosis in post-operative patients. In healthy subjects, the compression stockings have been shown to increase cardiac output and stroke volume, suggesting that the venous return with the stockings was larger than without it. To date, improving venous return without causing physiological disorders is a major objective for product designers in the leisure sport sector. The favourable effects of compression clothing on the muscle pumping action of the cardiovascular system have led scientists to speculate whether increases in venous return could assist in the removal of blood lactate from exercising muscles. Actually, most of the studies suggest a distinct performance advantage to wearing compression tights during local and global dynamic exercise. Besides, the increased microcirculation provided by compressive garments may prevent post-exercise damage and pain by reducing oedema and helping promote recovery post training and competition. Future garment construction and/or areas of the body targeted may need to reflect the specific biological mechanisms and demands of the sport for which it's intended.
Keywords: stockings, athletic performance, muscle oxygenation, muscle fatigue, textile.

1- Introduction

Mechanical interventions, such as bandages and compression stockings, have found wide application in the treatment of venous insufficiency of the lower extremities (Agu *et al.*, 2004). Prolonged standing (e.g. at work) may accelerate the development of varicosities.

1. Faculty of Sports Science (UFR STAPS), EA 2991 Motor Efficiency and Deficiency Lab, 700 avenue du pic Saint Loup, 34090 Montpellier. E-mail : stephane.perrey@univ-montp1.fr.

Lack of movement when standing leads to prolonged, unvaried pressure exerted by the leg muscles on the deep veins. This increases the resistance to the return of blood through the venous system and exerts increased pressure on the valves of the perforating and superficial veins. Varicose veins may be associated with aching, fatigue, and a feeling of warmth in the affected veins. The use of physical compression is a conservative measure which in no way cures varicose veins but aims to prevent their deterioration. Compression is beneficial to a patient with reduced venous function for a variety of reasons. Distension of the superficial veins caused by the presence of high internal pressure may be reduced and the accompanying aching and pain may be alleviated. The application of external pressure may also lead to an improvement in venous valve function. Prevention of the development of oedema and improvements in the action of the calf muscle pump may also be possible, even with garments that produce only limited raised pressure at the ankle. Compression may be achieved with bandages or with graduated compression garment. Graduated compression is actually more used to provide compression and support in conditions related to moderate venous insufficiency or oedema (Agu *et al.,* 2004). Graduated compression garments exert classically the greatest degree of compression at the ankle, and the level of compression gradually decreases up the garment.

In healthy subjects, aerobic training is known to increase lower limb venous compliance and would predispose to varicose veins, venous insufficiency and orthostatic intolerance. Garments (elastic bandages or compression stockings), as massages post-exercise represent a mechanical manipulation of body tissues increasing deep venous flow, decreasing superficial venous flow and preventing cutaneous venous stasis (Bringard *et al.,* 2006, Mayrovitz and Larsen, 1997, Lawrence and Kakkar, 1980). This paper discusses some of the possible reasons for the expected benefits of compression garments use in healthy people during and after physical work. The effects of external compression on intramuscular pressure at rest and during exercise is discussed, as well as the effects on blood flow, venous return, tissue oxygenation and muscle fatigue. Actual technology of graduated compression is finally presented.

2- Mechano-physiological effects of external compression on lower and upper extremities

2.1 Haemodynamics

Numerous advertisements on clothing aided with special functions have been seen on magazines and popular press. Compression clothing is one of them. The advertisement publicises functions such as effective in improving the blood circulation and inhibiting the swelling. The applied compression may help, in part, by augmenting the calf muscle pump. The increase in venous return noted while wearing elastic compression stockings has been ascribed to the shunting of a greater blood volume through the deep veins as a result of compression of superficial veins and an improved capillary filtration (O'Donnell *et al.,* 1979). This shunting of blood through the deep veins while wearing elastic compression stockings is similar to the haemodynamic of exercise. That is to say

that with rhythmic exercise there is a decrease in the pressure within the superficial venous system as a result of a shunting of blood from these vessels to the deep perforating veins. Compression stockings may work by increasing femoral vein blood flow velocity, but the surface pressure gradient is not necessarily strictly graduated as stated in the study by Wildin *et al.,* (1998). Also, the increase in skin surface temperature associated with application of compression stockings may suggest a temperature related effect on skin blood flow, which may affect leg haemodynamics (Wertheim *et al.,* 1999). A few previous studies addressed the effects of moderate leg compression on arterial inflow (Lawrence and Kakkar, 1980, Mayrowitz 1997, Mayrovitz *et al.,* 1998, Thorsson *et al.,* 1987). In one of these studies, application of a maximally graded compression pressure of 30 mmHg did not change calf muscle blood flow (Lawrence and Kakkar, 1980) determined by measuring xenon-133 clearance. In another study (Thorsson *et al.,* 1987) conducted on male distance runners, moderate compression (40 mmHg) reduced the muscle blood flow in the thigh by ~50%. The reason for the discrepancy between these two previous studies is not readily apparent, because the method used to assess changes in leg blood flow was identical. However, the study in which a decrease of leg flow was reported in response to external pressure was performed in athletes. Whether there are systematic differences of flow control between athletes and nonathletes that may explain differences of flow adjustment in response to external compression remains to be clarified. Another previous study comprising 14 healthy subjects reported the effects of leg compression by bandaging on leg pulsatile blood flow using a nuclear MR flowmeter (Liu *et al.,* 1999). A flow increase of 29% was reported for a pressure increase of ~40 mmHg. Leg compression was produced by wrapping one leg from forefoot to knee with a four-layer bandaging system. The effect of lower compression pressures on the lower extremity was not studied however. Interestingly using a forearm model and individually fitted set of several compression sleeves, Bochmann *et al.* (2005) showed a clear relation between the increase of external pressure and the increase of muscle blood flow with a maximal flow effect at a forearm surface pressure increase of 20 mmHg. It is unknown whether systematic differences exist between the upper and lower extremities with respect to the pressure range that enhances blood flow or to the mechanisms that might be involved. The elastic sleeve covered the forearm from elbow to wrist, and it is generally assumed that the pressure exerted at the surface of the forearm is transmitted into the depth of the tissue to the arterial vessels, as under every pneumatic cuff. Furthermore, the human forearm is not subject to hydrostatic pressure differences to the same degree as the human leg. Most aforementioned reports (the majority) conducted on the leg and on the forearm suggest that external compression may not only augment venous return but also affect arterial flow regulation separately (Figure 1).

2.2 Physiological functioning and intramuscular pressure

When applied, garments compress the soft tissues of the limb at a right angle. This is a prerequisite for the compression garment to mechanically increase blood flow. These forces applied correspond to vectors with magnitude and direction, act on a defined area and create an elevated hydrostatic pressure in the tissues. Intramuscular pressure (IMP) is of major importance in blood flow and is often taken as a good estimate of muscular

tension. Pronounced increase in IMP is an important factor that may impair muscle blood flow and thereby oxygen availability to the muscle, which can consequently contribute to muscle fatigue (Styf 1999). IMP is the hydrostatic pressure that can be measured inside the muscles (catheter) and is primarily thought to reflect interstitial fluid pressure. During contraction IMP rises, however, the absolute level is highly variable between muscles and is depending among other things on the anatomy of the muscle itself and its surroundings (Styf 1999). A bulky muscle attains higher pressures than a thin muscle and a muscle with bony surroundings or a tight fascia shows relatively large increases because of the low compliance of these surroundings. Besides, the pressurisation of the skin at high degree may cause some physiological disorders. If not too high, the pressure applied to the skin by the garments may increase the interstitial fluid pressure around the capillaries and consequently assists in the transport of excess fluid back into the circulation (veins).

Whether the garments may have affected physiological functioning has been measured. From a local point of view, the main effect of elastic compressive stockings is to shift the linear relationship between IMP and muscular activity (EMG) amplitudes towards higher IMP values, because of the increase in rest IMP. In this condition, if the subjects dynamically contract their muscles, as in their daily activities, elastic compres-

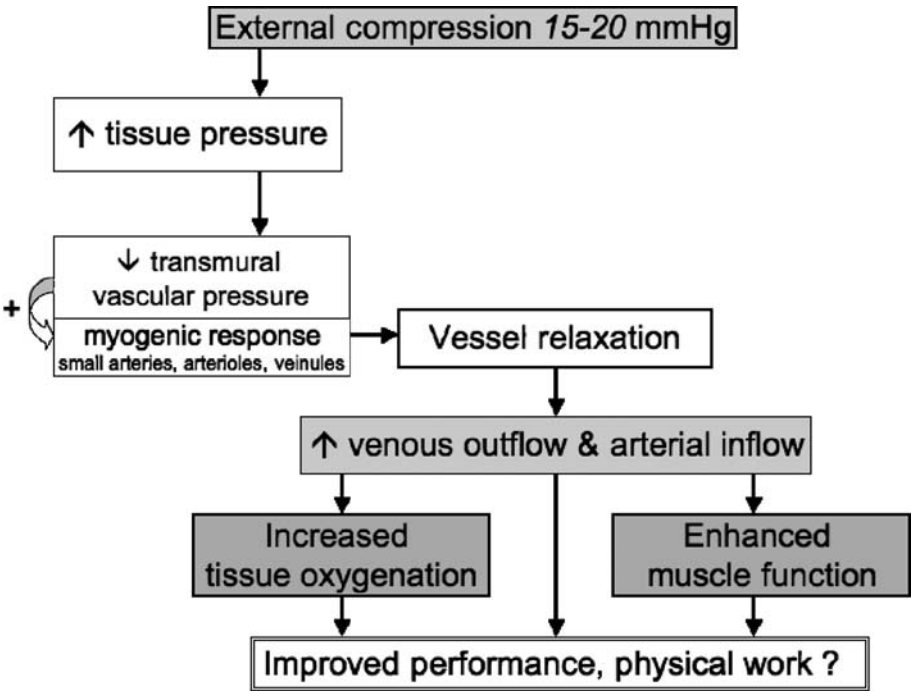

Figure 1 - External compression (range of 15-20 mmHg) elevates tissue pressure. Local muscle blood flow following causal chain is improved, which leads to increased tissue oxygenation and enhanced muscle function. Whether external compression improves physical work capacity is still unclear.

sive stockings may improve venous blood return. Indeed, if we compare the leg venous network to a collapsible tube, rest-IMP being higher when compressive stockings is worn, the diameter and the transmural pressure of the tube are reduced and the compliance of the tube is increased. As a result, a similar rise in IMP, induced by a dynamic contraction will induce a greater change in the mobilized volume, i.e. it will improve the efficacy of the "muscle pump". Near-infrared (NIR) spectroscopy technique relies on the relative transparency of tissues to near-infrared light and the presence in the 700-1100 nm wavelength region of two natural chromophores exhibiting oxygen-dependent absorption spectra namely, haemoglobin and cytochrome oxidase. These properties, coupled with the penetrative capability of NIR spectroscopy, provide a helpful research tool for studying tissue oxygenation and blood volume in deeper tissues at rest and during exercise. Using this technique, Agu *et al.* (2004) reported an increase in limb oxygenation in patients with venous insufficiency as observed also by Bringard *et al.* (2006a) in healthy sportsmen in different postures. With a more systemic approach, Berry and McMurray (1987) observed reduced lactate concentration during the recovery from a treadmill VO_2 max test, also supported by Chatard *et al.* (2004) following 5-min maximal effort and an 80-min recovery Conversely, Duffield and Portus (2007) reported no significant effect of garment in reducing lactate following high-intensity exercise. Compression garments were recently observed to significantly enhance running economy during submaximal exercise in trained runners but not at maximal intensity (Bringard *et al.*, 2006b). We may wonder if any above physiological benefits translate into performance.

2.3 Exercise performance and recovery

The use of compression clothing, such as elastic undergarments and tights, is showing more popularity among athletes and fitness enthusiasts. Since a few years, compression and their use in sport and exercise have increased exponentially. As with most new products, injury prevention and improved performance is purported to be a benefit from using such garments. While a significant body of research evidence exists describing the role of compression garments on vascular function in diseased patients (see above), less evidence exists for athletic sport performance. Compression garments are a relatively simple mechanical modality, which may have the potential to enhance sport performance and recovery from exercise or training. Sports scientists are constantly discovering new ways to take human athletic performance to the next level. Compression garments represent a way of safely and legally manipulating human physiology to produce an internal environment that is more conducive to high performance and faster recovery. However it has not been until more recently that the positive effects in athletic populations have been discovered. Exciting new research is emerging from numerous sports science laboratories around the world as to the multitude of beneficial effects that compression garments can provide the athlete. The underlying mechanism is attributed to enhanced blood flow to muscle, which is similar to the effect of active recovery. Improvements in microcirculation may prevail whilst wearing compression garments. The tights increase circulation (making it easier for your muscles to get oxygen) and decrease muscle vibration, which can make the legs tire out. Improvements in maximal

aerobic performance with compression garments have been reported in repeated 5-min maximal cycle efforts separated by an 80-min recovery (Chatard *et al.,* 2004). It has been suggested that excess oscillatory displacement of a muscle during a dynamic movement may contribute to fatigue and interfere with neurotransmission and optimal muscle recruitment patterns. Recent research reported that compression garments were able to significantly reduce longitudinal and anterior-posterior muscle oscillation by 0.32 and 0.40 cm respectively upon landing from a maximal vertical jump. Explosive muscular power is highly correlated with success in most sports. Research in track and field athletes has reported a significant increase in maximal vertical jump height when vertical jumps are measured wearing compression garments but without significant improvement in 10-, 20- or 60-min sprint time (Duffield and Portus, 2007, Bernhardt and Anderson, 2005). High intensity exercise produces lactic acid, which presents a challenge to the body's ability to maintain pH within the narrow physiological range. This in turn can negatively impact the force generating capacity of the muscle, which results in muscle fatigue and impaired athletic performance. Evidence supporting the increase in blood flow (see above) led to the assumption that compression garments may result in lower blood lactate levels during exercise (Berry and McMurray, 1987). Data published by Berry and McMurray showed a 14% decrease in blood lactate concentrations 15 minutes following high intensity exercise when compression garments were worn during and after exercise. Recent research (Maton *et al.,* 2006) on fatigue recovery reported compression garments did not increase fatigability during ankle dorsi-flexion and did not improve force recovery between repeated fatiguing static efforts. In contrast, Kraemer *et al.* (2001) reported a faster recovery of force production in single arm bicep curls following heavy eccentric exercise when wearing compression sleeves. Muscle damage is an inevitable consequence of high intensity exercise and any technique that can facilitate muscle repair and faster recovery is of large benefit to the athlete. Overall, the previous findings tend to suggest that compression garments may be benefits for their use as a recovery intervention tool rather than for improving physical performance.

3- Technology of graduated compression

While they may look very similar to the lycra® tights that were popular in the 80's there is far more physiology behind compression garments than meets the eye. Graded compression means that the compression exerted by the garments differs over a given distance. If long lower body garments are used as an example, compression at the ankle and calf is higher than at the thigh. This facilitates the flow of blood through the deep veins back towards the heart. This increase in blood flow and venous return to the heart is one of the reasons why compression garments are used in clinical applications such as prevention of deep vein thrombosis post surgery. Although graded compression garments have been used clinically for many years, it is only more recently that the potential beneficial physiological effects of graded compression have been acknowledged in the athletic environment. The basis on which graduated compression stockings were developed originated from the work of Sigel *et al.* (1975) (ultrasound technique) and later Lawrence and Kakkar (1980) (inert gas xenon-133 technique). To achieve maximal

increase in deep venous velocity with a decrease in pooling of blood in the calf veins, external static compression should exert a gradient pressure, highest in the ankle region and lowest in the upper thigh, therefore avoiding the relative tourniquet effect produced by applying equal pressure throughout the lower limb (Sigel *et al.*, 1975). Lawrence and Kakkar (1980) concluded that an optimal pressure gradient of 18 mmHg at the ankle, 14 mm Hg at the calf, 8 mmHg at the knee, 10 mmHg at the lower thigh and 8 mmHg at the upper thigh would generate the fastest venous flow. Previous studies suggest also that compression of the limb below the knee (i.e. stockings) contributes most to the increase of velocity of blood in the femoral side. Recent commercial graduated compression garments (stockings and tights) have since been manufactured to produce such a pressure profile. In all cases, the usefulness of the product is entirely dependent on the accuracy of the limb measurements and the correct selection of garments based on those measurements. The comfort given by support garment, and any possible effect on superficial and deep veins is directly related to the pressure exerted on the legs. A variety of garments is available, ranging from heavyweight elastic stockings to cosmetically acceptable nylon and elastane hosiery. Few studies of compression have been undertaken either by manufacturers concerned with establishing the correct design and strength of hosiery or in the course of clinical studies where it was necessary to describe a particular garment. According to the interface pressure, pressure is often drastically raised as the joint is flexed. Another factor that causes difficulty in this type of measurement is that the human leg does not conform to any uniform geometrical shape. The tension and pressure generated by the garments are therefore not uniformly distributed. Some companies quote the pressure exerted by their garments, but is this correct? The truth is that there is no globally accepted methodology to measure the compression that commercially available compression garments provide. This is why many manufacturers will quote compression data without indicating the methodology they used to measure it. Compression data means nothing if the method used cannot be proven to be reliable and valid. Furthermore the compression exerted will depend on the individual wearing the garment. Anthropometric measurements differ greatly between individuals and even two individuals with the same height and weight can vary greatly in limb girths. So when companies give a single reading for the compression provided at the ankle, calf and thigh, these readings likely only apply to a single person and if anyone else tried on the same compression garment the pressures would not be identical. The pressure that a garment exerts on the leg depends on both its tension and the radius of the limb at a given level. The tension depends on the elasticity of the material and the way it is made. The Laplace relationship states that compression (P) is inversely proportional to radius (R) for a constant rension (T) ($P = T/R$). Thus, a decrease in the radius over which the tension of the garment is acting will give an increase in compression. It follows that the compression exerted by hosiery on a distended vein, with a radius of curvature much smaller than that of the whole limb, will be proportionately greater than the compression exerted on the limb at that level. Gradations of compression garments increase from thigh towards the ankle, a principle which is physiologically sound. The hydrostatic component distending a varicose vein at any level will be greater towards the ankle for a standing person, and thus the support needed lower in the leg will be greater. The

garments are tailored to the leg contours so that the circumference increases towards the thigh and tension in the fibres is relatively constant along the length of the leg, but since the leg radius decreases towards the ankle the pressure will increase (Laplace relationship). Incorrectly fitted nylon and elastane hosiery did not exert significantly different pressures on the leg when compared with values obtained for the correct size. Compression values on the leg are unchanged so long as the garment is stretched within its elastic limits, and since elastane fibres are highly extensible there is a large working range. The final extensibility of the garment is determined by its construction and the proportion of elastane fibres contained in it. Hosiery constructed entirely from nylon is less able to stretch freely over different leg sizes since nylon has a high Young's modulus of extensibility. Movements of the leg while walking, however, will result in pressure fluctuations as the tension changes, and thus slight variations in measurements recorded from the resting leg are considered to be negligible. Although the compression exerted by some garments appears slight the control of distension achieved can be worth while. These are important considerations in the current debate regarding the relative merits of support garments of different constructions, and they seem to justify extension of the assessment procedure beyond measurement of compression to studies of the control of the distension of veins themselves. Finally, compression clothing is designed to provide some firmness to underlying tissue without restricting movement. Lycra or spandex is the majority material used in compression garments. Some manufacturers construct certain portions or panels of the garment with high Lycra content to overlay certain muscle groups or include rubber elastic re-enforcements. Usually the panels within garments are assembled in a way to provide targeted compression to the relevant muscle groups. Each targeted compression panel is designed to specific muscle groups allowing each muscle group to be independently supported by compression. The effect of this technological advance is enhanced comfort and user satisfaction in relation to the movement of the muscles.

4- Conclusion

Classically, compression garments are elastic, body-moulded suits with an engineering compression gradient that can be worn as upper-, or lower-body piece. Research studies have suggested a positive mechanical interaction between external compression and soft tissue, however the mechano-physiological processes may not be investigated using pressure-recording systems alone. This short current opinion suggests that with available technology the physiological responses (haemodynamic and metabolic components) to mechanical pressure brought by compressive garments should be investigated in more detail, both during static and dynamic loading to judge its real benefits in healthy people during physical work.

5- References

[AB1] Agu O., Baker D. and Seifalian A.M. Effect of graduated compression stockings on limb oxygenation and venous function during exercise in patients with venous insufficiency. In Vascular, 12(1): 69-76, 2004.

[BA1] Bernhardt T. and Anderson G.S. Influence of moderate prophylactic compression on sport performance. In Journal of Strength and Conditioning Research, 19(2): 292-297, 2005.
[BM1] Berry M.J. and McMurray R.G. Effects of graduated compression stockings on blood lactate following an exhaustive bout of exercise. In American Journal of Physiology and Medicine, 66: 121-132, 1987.
[BS1] Bochmann R.P., Seibel W., Haase E., Hietschold V., Rödel H. and Deussen A. External compression increases forearm perfusion. In Journal of Applied Physiology 99(6): 2337-2344, 2005.
[BD1] Bringard A., Denis R., Belluye N. and Perrey S. Effects of compression tights on calf muscle oxygenation and venous pooling during quiet resting in supine and standing positions. In Journal of Sports in Medicine Physical and Fitness, 46(4): 548-54, 2006.
[BP1] Bringard A., Perrey S. and Belluye N. Aerobic energy cost and sensation responses during submaximal running exercise—positive effects of wearing compression tights. In International Journal of Sports Medicine, 27(5): 373-378, 2006.
[CA1] Chatard J.C., Atlaoui D., Farjanel J., Louisy F., Rastel D. and Guézennec C.Y. Elastic stockings, performance and leg pain recovery in 63-year-old sportsmen. In European Journal of Applied Physiology 93(3): 347-352, 2004.
[DK1] Doan B.K., Kwon Y.H., Newton R.U., Shim J., Popper E.M., Rogers R.A., Bolt L.R., Robertson M. and Kraemer W.J. Evaluation of a lower-body compression garment. In Journal of Sports Science, 21(8): 601-610, 2003.
[DP1] Duffield R. and Portus M. Comparison of three types of full-body compression garments on throwing and repeat-sprint performance in cricket players. In British Journal of Sports Medicine, 41(7): 409-414, 2007.
[KB1] Kraemer W.J., Bush J.A., Wickham R.B., Denegar C.R., Gómez A.L., Gotshalk L.A., Duncan N.D., Volek J.S., Putukian M. and Sebastianelli W.J. Influence of compression therapy on symptoms following soft tissue injury from maximal eccentric exercise. In Journal of Orthopaedic and Sports Physical Therapy, 31(6): 282-290, 2001.
[LK1] Lawrence D. and Kakkar VV. Graduated, static, external compression of the lower limb: a physiological assessment. In British Journal of Surgery, 67(2): 119–121, 1980.
[LC1] Liu K., Chen L.E., Seaber A.V., Johnson G.W. and Urbaniak J.R. Intermittent pneumatic compression of legs increases microcirculation in distant skeletal muscle. In Journal Orthopedic Research, 17(1): 88–95, 1999.
[M1] Mayrovitz H.N. Compression-induced pulsatile blood flow changes in human legs. In Clinical Physiology 18(2): 117–124, 1998.
[ML1] Mayrovitz H.N. and Larsen P.B. Effects of compression bandaging on leg pulsatile blood flow. In Clinical Physiology, 17(1): 107–117, 1997.
[MT1] Maton B., Thiney G., Dang S., Tra S., Bassez S., Wicart P. and Ouchene A. Human muscle fatigue and elastic compressive stockings. In European Journal of Applied Physiology 97(4): 432-442, 2006.
[OR1] O'Donnell T.F. Jr, Rosenthal D.A., Callow A.D. and Ledig BL. Effect of elastic compression on venous hemodynamics in postphlebitic limbs. In the Journal of the American Medical Association, 242(25): 2766-2768, 1979.
[S1]Styf J. The effects of functional knee bracing on muscle function and performance. In Sports Medicine, 28(2): 77-81, 1999.
[SE1] Sigel B., Edelstein A.L., Savitch L., Hasty J.H. and Felix W.R. Jr. Type of compression for reducing venous stasis. A study of lower extremities during inactive recumbency. In Archives of Surgery, 110(2): 171-175, 1975.

[TH1] Thorsson O., Hemdal B., Lilja B. and Westlin N. The effect of external pressure on intramuscular blood flow at rest and after running. In Medicine Sciences in Sports and Exercise, 19(5): 469-473, 1987.
[WH1] Wertheim D, Harinath G, Melhuish JM, Williams RJ, Harding KG, Whiston RJ. In vivo pressure profiles of thigh-length graduated compression stockings. In British Journal of Surgery 86(4): 572, 1999.
[WH1] Wildin C.J., Hui A.C., Esler C.N. and Gregg P.J. In vivo pressure profiles of thigh-length graduated compression stocking. In British Journal of Surgery 85(9):1228-1231, 1998.

Improving the Performance of a Bobsleigh by Aerodynamic Optimization (P212)

A. Winkler[1], A. Pernpeintner[1]

Topics: Aerodynamic Optimization Process, Computational Fluid Dynamics and Wind Tunnel Testing.

Abstract: The performance of a bobsleigh is significantly affected by its aerodynamic properties. As it is typical for bluff bodies, the aerodynamic drag of a bobsleigh consists primarily of pressure drag and is dominated by its shape. The shape design of a bobsleigh is commonly based on intuitive shape modifications resulting from individual experiences of the athletes. This paper aims to present the process of optimizing the aerodynamic drag with tools used in road vehicle and race car aerodynamics. The starting point in the process has been the development of a parametric three-dimensional CAD-model including a simplified shape of the crew. Therewith varying bobsleigh versions have been created taking into account the geometric restrictions given by the regulations of the international bobsleigh federation (FIBT). Extensive CFD simulations have been performed to examine the flow and the aerodynamic forces acting on the respective shapes under racing conditions. This method has been applied in the preliminary design process whereas for the sake of the detail optimization additional wind tunnel tests on a 1:3 model scale have been performed. This was due to the fact that the examination of minor changes to the bob shape is more time consuming in CFD than using a proper wind tunnel model. The wind tunnel tests were also used for validating the CFD results. The findings of the wind tunnel experiments have been incorporated into the CAD model and a final optimized bob shape has been created. Further wind tunnel tests on a full scale prototype are planned to find out the ideal seat position and posture of the crew and to validate the previous computational and experimental results.

Key words: Bobsleigh, Aerodynamics, Computational Fluid Dynamics, Wind Tunnel Tests, Sports Engineering.

1. Lehrstuhl für Aerodynamik, Technische Universität München, Germany - E-mail: {andreas.winkler,albert.pernpeintner}@aer.mw.tum.de

1- Introduction

Bobsleighing is one of the fastest winter sports and the competitions are often decided by the narrowest time margins. The driving resistance is composed of the frictional forces between the runners and the ice track as well as of the aerodynamic drag. During the run a maximum velocity of about 130 km/h to 140 km/h is achieved. The aerodynamic drag accounts for roughly 25% of the total drag.

The open-topped cowling and the continuously changing boundary conditions given by the track result in a rather complex flow around the bobsleigh. However the aerodynamic shape design of a bobsleigh is commonly based on empirical methods. This might be due to the fact that the design and manufacture of bobsleighs is dominated by small and mid-size companies with limited personal and financial resources. A more fundamental aerodynamic optimization necessitates high performance computational and experimental tools that are successfully used in automotive and aircraft industry. Previous investigations using these tools have been either restricted to computational tools (Dabnichki *et al.* 2002, Togneri 2006, Reimann 2008) or to an experimental approach (Heckelmann 2001). Studies that combined both tools either focused on details of the flow (Dabnichki and Avital, 2006) or partly had to neglect the important influence of the runners (Lewis 2006). All of the mentioned studies have in common that they either concentrate on the investigation of the flow field around a given bobsleigh shape and/or deal with detail optimizations.

This paper aims to present the process of optimizing the aerodynamic drag of a two-man-bobsleigh by methods used in road vehicle and race car aerodynamics. The appropriate combination and application of these tools during the different design phases lead to an innovative bobsleigh design. The tools that are used typically during the preliminary design phase and the detail optimization phase are explained and an outlook is given what steps are required for the quality assurance of the aerodynamic development tools.

2- Parametric CAD-Model of the Bobsleigh

The major components producing an aerodynamic drag and the used coordinate system are depicted in Figure 1a. The coordinate system's origin is placed in the nose of the bobsleigh and the x_1-axis corresponds to the free stream

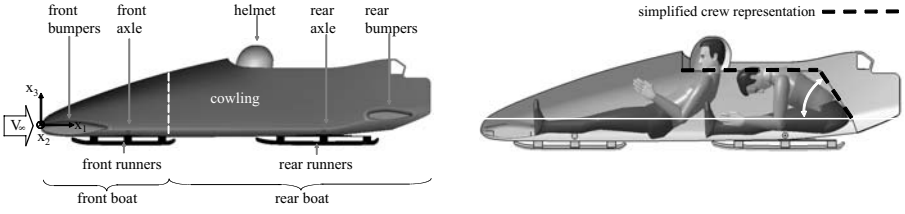

a) Components of a bobsleigh.

b) Side view of the crew representation.

Figure 1 - Bobsleigh components and representation of the crew.

direction V_∞. The components are the front bumpers (FB), the front axle (FA), the front runners (FR), the cowling, the pilot's helmet, the rear bumpers (RB), the rear axle (RA) and the rear runners (RR). From driving dynamic aspects the cowling is split into a front boat and a rear boat which are allowed to twist against each other. The resulting gap is sealed by a rubber joint. Depending on the ongoing bobsleigh trim a misalignment of the cowling may occur which leads to a further aerodynamic drag.

The drag of all components is dominated by pressure drag. It arises from boundary layer separation from the contour and from any sharp edges. The separated flow forms a wake behind the body and a negative pressure on the rear side. A second source of drag results from the shear stresses acting on the surface. With blunt shapes the typical percentage of pressure drag is 60 % up to almost 100 % so that the drag optimization focuses on the reduction of the pressure drag (Hucho 2002 & 2005). The drag reduction is primarily achieved by modifying the shape of the bobsleigh components. Since all components affect the whole flow field it must be kept in mind that modifications on isolated components only might yield non-reliable optimization results.

In order to systematically develop an optimal aerodynamic shape of the bobsleigh a three-dimensional parametric CAD-model was created using CATIA V5 © (Braß 2005). The first step was to identify the governing shape parameters and to implement them into a wire frame model. From the wire frame a surface model was created.

In order to limit the complexity of the CFD simulations the shape was simplified while keeping in mind the requests stated earlier. It was decided to neglect shape details like screws and nuts as well as the brake cavity on the bobsleigh bottom and the rubber joint between the front and the rear boat.

Considerable shape simplifications were made for the bob crew. The pilot's head was modelled by a generic helmet that was partially exposed to the flow. The bodies of the pilot and the brakeman were simplified by a horizontal and an oblique plane surface. These two surfaces were treated as being part of the cowling. Figure 1b shows a human crew and their simplified shape representation. While the helmet was kept on a fixed position which was derived from the pilot's position, the brakeman's back angle θ was varied.

Over 100 different shape versions were created whereby the rules of the international bobsleigh federation (FIBT 2005) have been respected. Each version was converted into the IGES data format in order to be compatible to the software used for the mesh generation. A preliminary optimized shape resulted from the CFD simulations and was chosen for being built as a wind tunnel model.

3 - CFD Simulations

In the preliminary design phase CFD simulations were performed using ANSYS CFX © (ANSYS CFX 2007). The flow was assumed to be incompressible, viscous and turbulent. In the current study the Reynolds averaged Navier-Stokes (RANS) approach was applied. The turbulence was modelled using the high Reynolds number SST model developed by Menter (Menter 1992). This

approach is based on the assumption that the turbulence structure can be described by a length scale and a time or a velocity scale which are determined by the turbulent kinetic energy and the turbulence dissipation rate. The SST model combines the advantages of both the well-known k-ε- and k-ω-model and it is recommended for flows with boundary layer separation.

The flow domain was discretised by an unstructured mesh with tetrahedral and triangular elements yielding both good mesh quality and adequate body shape resolution. Two different domains were defined representing a curve section and a straight section of the ice track. During the cornering there are no confining walls in the lateral direction close to the bobsleigh, whereas during the run through a straight section the confining walls of the track are close to the bobsleigh. The first domain D1 represents a curve section and is shown in Figure 2a including the nomenclature of the confining boundaries. In Figure 2b the domain D2 for representing a typical straight section of an ice track is shown.

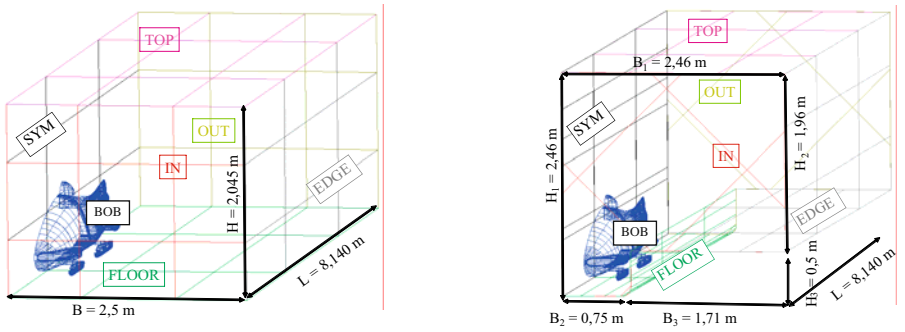

a) Domain D1 representing a curve section.

b) Domain D2 representing a straight section.

Figure 2 - Flow domains and their confining boundaries.

Figure 3a shows mesh M1 that was used for analyzing overall shape modifications. It consists of about 3,1 million elements and about 550 thousand nodes and resolves the boundary layer with 10 nodes. The wake region downstream of the bobsleigh is locally refined. Figure 3b shows mesh M2 which is similar to mesh M1 however has a even higher resolution within the gap between the bob and the floor. Therefore it consists of about 12 million elements and about 2 million nodes.

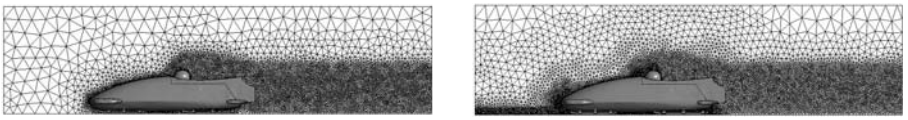

a) Mesh M1.

b) Mesh M2.

Figure 3 - Side view on the symmetry plane of the meshes generated with ICEM CFD ©.

The boundary conditions (BC) for the CFD simulations are shown in Table 1. BC1 is representing the conditions of a wind tunnel test with fixed floor whereas BC2 stands for moving floor in order to simulate the relative movement of the bobsleigh and the ice track.

Boundary	Boundary Condition
IN	flow velocity at the inlet V_{Δ} = 36,11 m/s
OUT	pressure difference at the outlet $\Delta p = p_{OUT} - p_{\Delta} = 0$
FLOOR	**BC1**: no-slip wall, resting floor ; **BC2**: no-slip wall, moving floor V_{FLOOR} = 36,11 m/s
TOP	free-slip wall
EDGE	free-slip wall
SYM	symmetry
BOB	no-slip wall

Table 1 - Boundary conditions on the flow domains.

An existing bobsleigh (RefBob) was used as reference shape. The effects of the different boundary conditions and domains on the aerodynamic drag are shown in Figure 4a. It is getting obvious that the total aerodynamic drag is dominated by the pressure drag that causes about 80% of the total drag. It is apparent that during a straight section (domain D2) the walls of the ice track cause an increase in drag of about 4% for BC1 and about 5% for BC2. Finally, the effect of the moving floor on the aerodynamic drag both for the cornering and the run through a straight section is shown. BC2 leads to a decrease in drag of about 1% which means that the wind tunnel results are slightly overestimated compared to a bobsleigh in racing conditions.

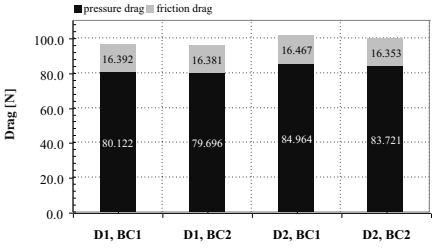

a) Friction drag and pressure drag of the RefBob for M2.

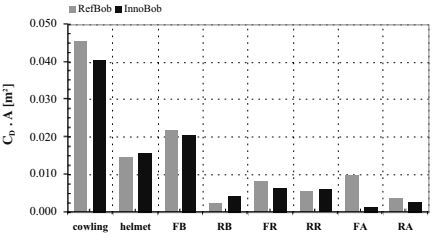

b) Partial drag areas using D1, M1 and BC1.

Figure 4 - Drags of the RefBob and the InnoBob.

The aerodynamic drag D is calculated by equation (1) and depends on the dimensionless drag coefficient C_D, the frontal area A of the bobsleigh and the dynamic pressure of the free stream:

$$D = C_D \cdot A \cdot (\rho_{\infty} / 2) V_{\infty}^2 \tag{1}$$

The drag is reduced by decreasing the drag coefficient and the frontal area. However both measures contradict each other occasionally. Thus optimization of the aerodynamic drag essentially means to balance the drag coefficient and the frontal area so that a minimum of drag is achieved. Concerning the bobsleigh, this balancing led to a shape version that showed a decrease in drag of about 13%. In Figure 4b the drag of the RefBob and the optimized shape (InnoBob) is assigned to the components using the drag area $C_D \cdot A$. The two most striking improvements are getting obvious for the cowling and the front axle. While the decrease in drag of the cowling is assigned to the overall shape modifications the sharp decrease at the cylindrical front axle was achieved by a larger covering by the cowling. These two examples confirm that the optimization of a bluff body must consider both the optimization of single elements but also the optimization of the system as a whole.

The open-topped cowling enforces the flow to separate at its leading edge and to form a kind of a delta wing vortex shown in Figure 5a. This type of vortex is known to possess high rotational velocities and consequently low local pressures. The pressure coefficient is defined by equation (2)

$$C_p = \frac{p_{local} - p_\infty}{(\rho_\infty / 2) V_\infty^2} \tag{2}$$

and is visualized in the x_2-x_3-cut-plane at position x_1 = 1.65 m in Figure 5b. It can be seen that the twisting streamlines correspond to a negative pressure coefficient and hence are a considerable source of drag. Simulations with two different back angles of the brakeman have shown that the negative pressure can be reduced by increasing the brakeman's back angle. Thus the position and posture of the brakeman has a considerable influence on the aerodynamic drag and was analysed further in the wind tunnel tests.

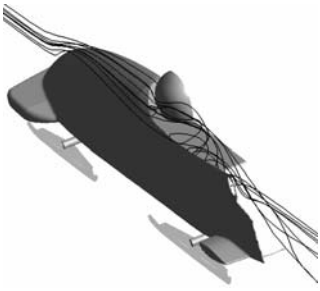

a) Vortex evolving from the leading edge.

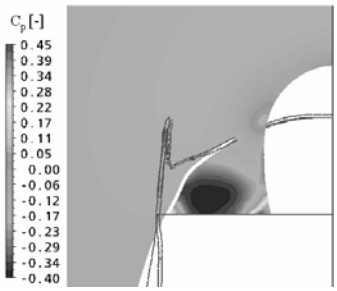

b) Back view on the pressure coefficient at x_1 = 1,65 m.

Figure 5 - Vortex evolving from the leading edge of the open-topped cowling for D1, M2 and BC1.

4- Wind Tunnel Tests

Wind tunnel tests on a 1:3 model scale were carried out in order to optimize shape details and to validate the CFD simulations. The model corresponded to the shape version with minimum drag developed in the preliminary design phase. The model was mounted on a flat plate in order to simulate a cornering and to resemble the flow domain D1. Optionally side panels could be mounted in the test section (Figure 6) in order to simulate a straight section of the ice track which is equivalent to the situation of domain D2.

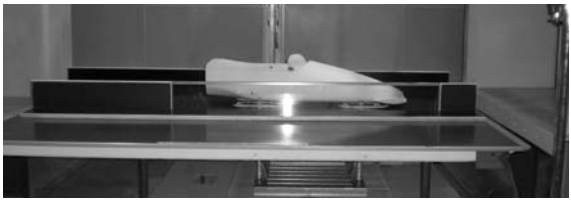

Figure 6 - Wind tunnel model and side panels mounted in the wind tunnel test section.

The drag coefficients obtained by CFD simulations and wind tunnel tests are compared in Table 2. From the drag coefficients two facts can be derived. First, the CFD simulations undervalue the experimental results by about 4%. Second, the increase in drag in the straight section shown by the CFD simulations is verified.

	Domain	Boundary Conditions	Mesh	C_D [-]
CFD	D1	BC1	M1	0.229
wind tunnel	without panels	-	-	0.239
CFD	D2	BC1	M1	0.247
wind tunnel	with panels	-	-	0.256

Table 2 - Comparison of the drag coefficients between CFD simulations and wind tunnel tests at $Re_\infty = 6{,}62 \cdot 10^5$.

The dependency of the drag on the brakeman posture gets quite obvious from the results depicted in Figure 7a. With increasing back angle the drag is

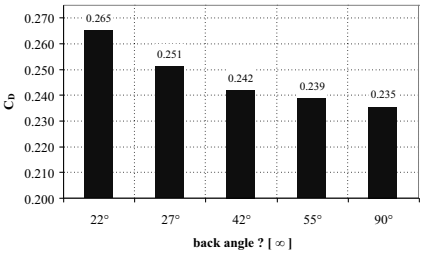

a) Influence of the brakeman's back angle on the drag.

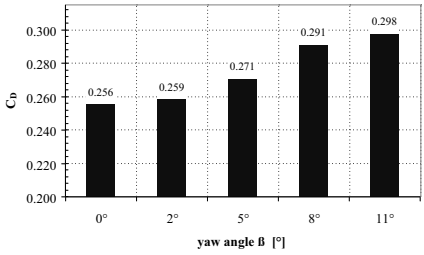

b) Influence of the yaw angle in the straight section.

Figure 7 - Influence of the brakeman's back angle and of the yaw angle on the drag at $Re_\infty = 6{,}62 \cdot 10^5$.

decreasing. However, it must be taken into consideration that there are some limits due to anatomical reasons. Therefore further wind tunnel tests with a full scale bobsleigh and a real crew are desirable.

Another aspect that was investigated was the influence of a yaw angle β on the aerodynamic drag. During a perfect run the bobsleigh's central axis always points in the direction of motion and hence the yaw angle is $\beta = 0$. However it may happen that the bobsleigh is yawing because of any pilot's failure. In order to simulate this case the bobsleigh was oriented at various yaw angles during wind tunnel tests in the straight section. Figure 7b shows the increase in drag with increasing yaw angle. This is caused by the increasing blockage of the ice track with a higher yaw angle.

There is a further potential for drag reduction at the rear part. Together with the floor this part forms a diffuser which leads to a decelerated flow in this region. Lower flow velocities yield higher pressures and result in a lower aerodynamic drag. The decisive variables are thereby the apex angle γ as defined in Figure 8a and the contour of the diffuser.

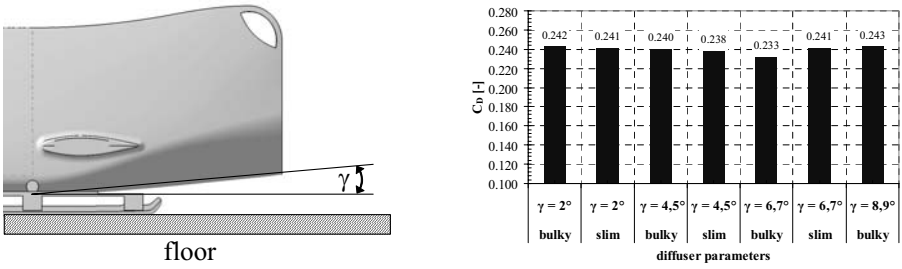

a) Side view and apex angle of the diffuser.

b) Diffuser optimization at $Re_\infty = 8{,}07 \cdot 10^5$.

Figure 8 - Diffuser geometry and optimization results.

The results of the diffuser optimization are shown in Figure 8b where bulky and slim stands for the different contours of the respective diffuser. It is apparent that minimum drag is obtained only for the proper combination of both parameters. While the slim diffusers yield a lower drag for $\gamma = 2°$ and $\gamma = 4{,}5°$ the bulky diffuser leads to a lower drag for $\gamma = 6{,}7°$.

The dependence of the drag on the bumpers' angle of attack was investigated resulting in an insignificant decrease with angles different from zero.

In order to provide a good push-start capability some shape corrections of the rear part were necessary. They were found to result in an unavoidable increase in drag. Several shape modifications were tested in order to minimize the negative pressure on the rear side.

The findings of the wind tunnel experiments have been incorporated into the CAD-model. Thus the final optimized shape version depicted in Figure 9

has been generated that is the basis for the production of a full scale prototype. Based on the results of the CFD simulations and the wind tunnel tests this aerodynamic optimized bobsleigh is expected to yield a drag reduction compared to the RefBob of about 13%.

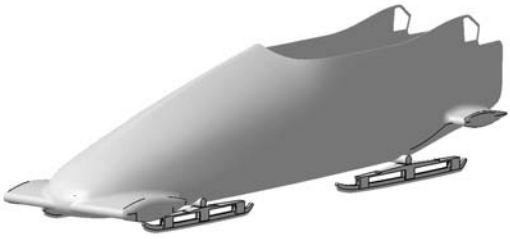

Figure 9 - Aerodynamically optimized InnoBob.

5 - Conclusions and Outlook

The process of improving the performance of a bobsleigh by reducing its aerodynamic drag was presented. For this purpose tools and methods have been applied that are successfully used in road vehicle and race car aerodynamics. Starting from a parametric three-dimensional CAD-model, many different shape versions were created. In the preliminary design phase CFD simulations were made to find a basic shape of minimum drag. Wind tunnel tests on a 1:3 scale model were performed for detail optimization and for validating the CFD results. In this manner an optimized shape version that shows a drag decrease of about 13% compared to an existing bobsleigh shape was found. A significant dependence of the aerodynamic drag on the brakeman's posture became evident. A bobsleigh prototype will be built and used for full scale wind tunnel tests and for tests under racing conditions, in order to perform a final evaluation and quality assurance of the aerodynamic development tools.

6 - References

[A1] ANSYS CFX-11.0. Online-Manual. 2007.

[B1] Braß E. Konstruieren mit CATIA V5 - Methodik der parametrisch-assoziativen Flächenmodellierung. Hanser Verlag, 3.Auflage, 2005.

[DA1] Dabnichki P., Avital E. Influence of the position of crew members on aerodynamics performance of two-man bobsleigh. Journal of Biomechanics 39, 2733-2742, 2006.

[DM1] Dabnichki P., Motallebi F., Avital. Protection versus performance in bobsleigh ergonomic design. Foruth International Conference on Engineering of Sport, Proceedings of ISEA, Blackwell Sciences, Oxford, pp. 346 - 352, 2002.

[F1] Federation Internationale de Bobsleigh et de Tobogganing (FIBT). Internationales Reglement. Ausgabe 2005.

[H1] Heckelmann I. Windkanaluntersuchungen zur Optimierung des Luftwiderstands eines Sportbobs. Term Paper, Lehrstuhl für Fluidmechanik, TU München, 2001.

[H2] Hucho W. Aerodynamik stumpfer Körper. Vieweg, 1. Auflage, 2002.

[H3] Hucho W. Aerodynamik des Automobils. Vieweg, 5.Auflage, 2005.
[L1] Lewis O. Aerodynamic analysis of a 2-man bobsleigh. Master of Science Thesis, Faculty of Aerospace Engineering, TU Delft, October 2006.
[M1] Menter F. Improved Two-Equation k-_ Turbulence Models for Aerodynamic Flows. NASA Technical Memorandum 103975, October 1992.
[R1] Reimann M. Verminderung des aerodynamischen Widerstands eines Rennbobs durch Formänderung und Nachlaufbeeinflussung. Term Paper, Lehrstuhl für Aerodynamik, TU München, 2008.
[T1] Togneri M. Computational fluid dynamic (CFD) modelling of the flow around a bobsled. Diploma Thesis, Lehrstuhl für Aerodynamik, TU München, 2006.

Determining Friction Coefficients for Round Balls: Comparing Basketballs (P213)

LeRoy W. Alaways[1], Zachary S. Szczerbinski[2], Nicolas Krumenacker[3]

Topics: Basketball; Testing.
Abstract: A new method to determine the coefficient of static friction for a round inflated ball is presented. Comparison of the coefficient of static friction between the National Basketball Association (NBA) original leather, "short-lived" synthetic, collegiate and playground basketballs on glass, wood, acrylic and powder-coated metal are presented. Results show that the original leather ball has a more robust coefficient-of-friction (COF) while the synthetic game-ball behaves poorly, especially when wet.
Keywords: Basketball; Friction Coefficients; Testing.

1- Introduction

In 1891, James Naismith invented the game of basketball; it included thirteen rules and was to be played with peach baskets and a soccer ball (Hubbard, 2000). In 1894, A.G. Spalding developed the first official basketball, this ball had four panels that were laced together and by 1970, the number of panels increased to eight and the lacing had disappeared. In 1983, Spalding's leather ball became the official game-ball of the NBA and remained untouched until the introduction of a composite ball in 2006. In January 2007, the new synthetic game-ball was retired and the classic all-leather game-ball regained its official status.

According to the NBA and Spalding, the introduction of the new game-ball on June 28, 2006 was a "significant development" in the design of sporting equipment (NBA, 2008). The new ball was constructed with CrossTraxxion™ technology using two interlocking panels. This design has one third less channel area allowing for an improved grip and the cover is a patented micro-fibre composite material providing moisture management throughout the game. The new design utilises two panels, as opposed to eight decreasing surface undulation allowing for a truer, "more consistent bounce". Spalding claims the new hydrophilic moisture management system spreads moisture evenly across

1. Department of Mechanical Engineering, Villanova University, 800 Lancaster Ave., Villanova, Pennsylvania, USA 19085 - leroy.alaways@villanova.edu
2. Engineer, Orthovita, Inc., 77 Great Valley Parkway, Malvern, Pennsylvania, USA 19355 - zacharyszczer@msn.com
3. Undergraduate Student, Department of Mechanical Engineering, Villanova University, 800 Lancaster Ave., Villanova, Pennsylvania, USA 19085 - nicolas.krumenacker@villanova.edu

the surface for rapid evaporation, and that the new ball performs like a "broken-in" basketball; ready for use upon first bounce. According to the equipment manager of the Philadelphia 76ers, traditional leather basketballs have to be broken-in for approximately 1-2 months before game use in order for the ball to perform consistently during the game (Rego, 2007).

Few studies have been presented reporting results on basketball COF, Okubo and Hubbard (2006) measured the COF between a basketball and an acrylic board. Weiss (2006) reported that Horwitz and De at the University of Texas, Arlington did tests in which they showed that NBA synthetic balls resisted sliding more strongly when dry on sheets of silicon, and that leather balls were easier to grip when wet.

The new synthetic game-ball's less-than-stellar NBA's experience lasted less than six months before it was retired. The investigation into the claims made above and the rapid retirement of the ball lead to the development of a new method to determine the coefficient-of-friction (COF) and a very interesting result.

2- Methodology

Four off-the-shelf basketballs (an NBA synthetic and NBA classic, a National Collegiate Athletic Association[1] (NCAA), and a playground ball) were acquired as listed in Table 1. All balls were NBA regulation size but varied in cost from US$35 to US$100. Note that for the remainder of the paper "synthetic" will refer to the new *retired* game-ball, "leather" will refer to the original leather game-ball, "NCAA" will refer to the collegiate game-ball, and "playground" will refer to the playground ball.

To initially determine the COF a tilt-platform as shown in Fig. 1 was used. In this test, to stop the ball from rolling down the ramp, three balls were taped together and placed on a sheet of glass. The sheet, of known length, L, was free to rotate about one end and a screw jack was placed under the other end of the sheet and slowly elongated. The coefficient of static friction is calculated from the tangent of the angle, q, formed between the glass and table at impending slip. To determine the angle, a plumb was hung from the rising edge to a meter-stick measuring the distance, D, from the rotation point and since L was predetermined the angle can quickly be found using trigonometry.

This method has an advantage in that it is very simple. However, as shown in Fig. 1 three balls are required or a ball must be cut into small pieces and at a cost of up to US$100 each, either option is not desirable. Additional problems occurred when the angle of impending slip formed was large enough for the three balls to tumble (solved

	Manufacturer	Model #	Size - cm (inch)	Cost (US$)	Court Use	Age
Synthetic Game-ball	Spalding	071339279	74.93 (29.5)	99.99	Indoor	12+
Leather Game-ball	Spalding	64-530E	74.93 (29.5)	79.50	Indoor	12+
NCAA Game-ball	Wilson	2189029	74.93 (29.5)	49.99	Indoor	12+
Playground	Spalding	N/A	74.93 (29.5)	34.99	Indoor/Outdoor	12+

Table 1 - General Basketball Information.

1.While most rules of basketball are standard, the NCAA is conference driven and what may be an official game-ball in one conference is not necessarily a game-ball in another conference.

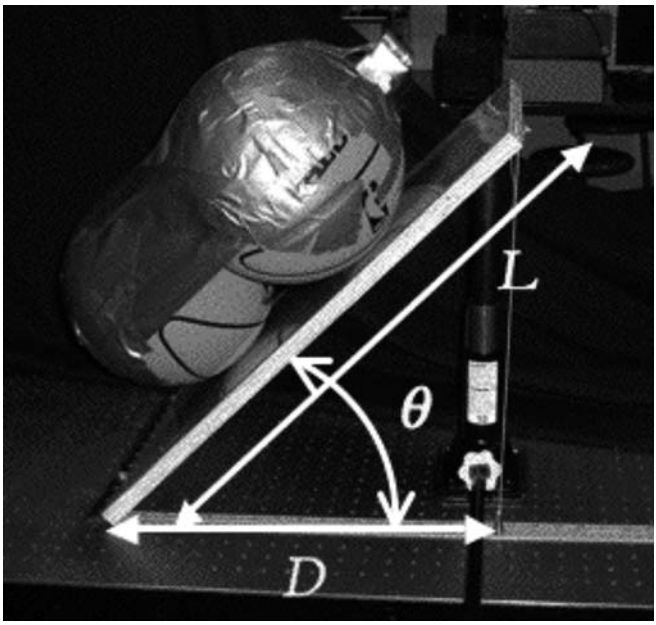

Figure 1 - Tilt test apparatus, note that an additional mass is added to the top of the balls to help reduce tipping. Note that L was 0.915 m for our testing.

with supplementary weighting). Also great care must be taken to insure that the balls and glass remained clean throughout testing. A positive feature with glass is that a stationary mark could be placed on the bottom surface of the glass that could be used as a visible indicator to help determine when the balls started to move.

To eliminate the need of using three balls a new friction test apparatus was designed for testing as shown in Fig. 2. This apparatus is adjustable to allow for testing of a single

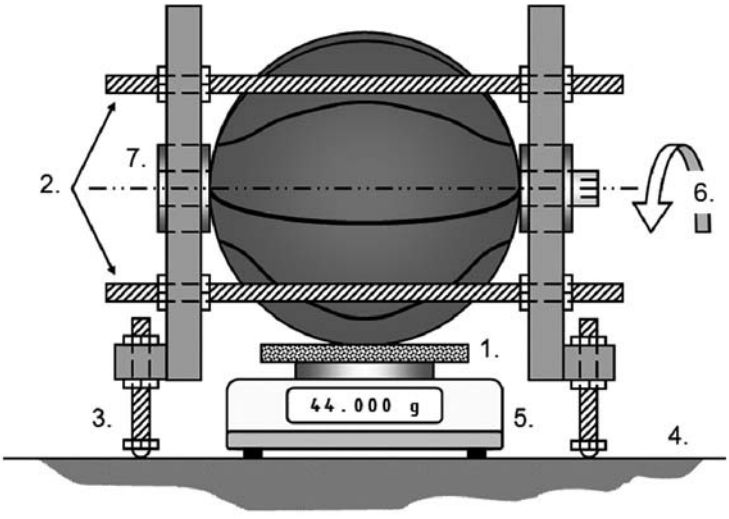

Figure 2 - New friction test apparatus.

ball of nearly any diameter on any surface. The key features include low-friction bearings to support the ball, a digital scale to determine the normal force, adjustable legs to allow for different thickness and to set the initial normal force, and a lever arm to apply a torque. The operator slowly increases the torque on the lever arm while watching the normal force values on the scale. In our set-up, a small pan was hung from a lever arm and small lead weights were added to the pan until the ball started to slip. It is of interest to note that the normal force would decrease just before any movement was noticeable and this observation helped determine the precise values of interest. To aid the operator determine if movement was occurring small bubble levels were placed on top of the ball and on the lever arm.

Figure 3 show a free-body-diagram of the forces of interest that act on the ball during testing. Note the weight of the ball is not included since the bearings take-up the weight and those forces pass through the ball's centre of rotation. The moment due to the friction force is equal to the moment from the applied force until slip and therefore the coefficient of friction can be determined from equation 1:

$$\mu = \frac{Lmg - B}{RN} \tag{1}$$

Where, L is the length of the moment arm from the centre of the bearing to the line of action of the weight, mg is the total applied force, R is the radius of the ball, N is the

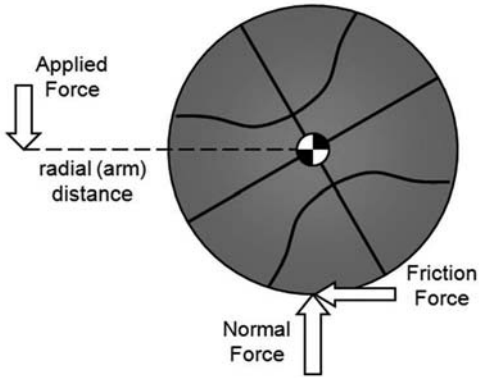

Figure 3 - Free-body-diagram of forces acting on ball.

normal force, and B is the bearing torque required to rotate the ball when it is not in contact with a test sample. The adjustable legs not only allows for testing of different sample thicknesses and ball diameters but allowed the operator to adjust the normal force acting on the ball. Typical normal forces found at impending slip were in the three Newton range and as a result, no measurable change in ball radius was observed. Note that a long moment arm was used and was mounted at its mid-point, this allowed for rotation of the ball in either direction and since the weight of the moment of arm was balanced about the axis of rotation, it did not have any effect on the system.

Small samples of glass, acrylic, wood flooring, and powder-coated steel (rim material) were acquired for testing. Clay was used to stop the test sample from slipping off

the scale when the force was applied to the moment arm. Additional tests where saline solution was applied to the surface were conducted.

3- Results & Discussion

To reduce costs tilt tests were conducted with only the playground ball and a 5 x 10 cm test specimen from a sacrificial ball. Table 2 shows the results from testing on a sheet of glass with fixed length of 0.915 m. A mean COF of approximately 1.0 was determined using both intact and a small sample of the ball. While performing the tests, it was noticed that the new off-the-shelf ball has a sticky feel to it that cleaning would not alleviate and that the test sample had a tendency to slowly creep down the glass and not suddenly move making it very difficult to determine the exact angle of slip.

	Distance *D* (mm)	Angle of slip (degrees)	COF on Glass	
			Mean	SD
3 Balls	651	44.6	0.99	0.119
Cut Slab of Ball	617	47.6	1.09	0.032

Table 2 - Tilt Test Results for new Playground ball (n=5 trials).

Tables 3 and 4 show the results obtained using the new COF test apparatus for all four balls on all four surfaces. Table 3 shows the results obtained for the dry surface and Table 4 gives the results when a saline solution was applied to the surface tested. These tests all show small standard deviations and consistent trends. It is noteworthy that when the saline solution was added during the leather ball tests on glass and hardwood that the COF changed by less than 10 percent, whereas the synthetic balls COF dropped by nearly two thirds. The tests results show poor performance by the NCAA ball with changing conditions; the NCAA ball tested was not leather but similar to the synthetic ball with a water-repelling outer surface. While these two balls and the playground ball repelled the saline solution, the leather ball absorbed it.

The playground ball was and still is a mystery, while the cover is a more plastic-like compound that does not absorb water, it retained a "sticky" and glossy shine that diminished during the new apparatus testing but still out performed the costly synthetic and NCAA game balls.

	Glass		Acrylic		Hardwood		Powder Coated Metal	
	Ave	SD	Ave	SD	Ave	SD	Ave	SD
Synthetic	1.22	0.060	0.96	0.062	1.54	0.084	0.81	0.068
Leather	0.50	0.085	0.62	0.020	0.42	0.087	0.62	0.094
NCAA	1.10	0.158	0.64	0.090	0.93	0.019	0.62	0.028
Playground	0.65	0.077	1.02	0.022	1.01	0.036	0.93	0.036

Table 3 - Average Values for Apparatus Test with Dry Conditions (n=5 trials).

	Glass		Acrylic		Hardwood		Powder Coated Metal	
	Ave	SD	Ave	SD	Ave	SD	Ave	SD
Synthetic	0.47	0.036	0.55	0.042	0.57	0.064	0.63	0.044
Leather	0.47	0.086	0.40	0.023	0.42	0.095	0.46	0.005
NCAA	0.48	0.062	0.43	0.029	0.70	0.020	0.52	0.037
Playground	0.27	0.083	0.95	0.115	0.72	0.060	0.47	0.057

Table 4 - Average Values for Apparatus Test with added Saline Solution (n=5 trials).

4- Conclusion

A new method to determine the coefficient-of-friction (COF) for round balls was discussed. The method was used to determine the COF of four basketballs on various surfaces in wet and dry conditions. The results show that the current NBA leather game-ball is more robust on wet and dry surfaces. In some cases the average COF for the leather ball did not change when saline solution was added, while the now retired synthetic ball's performance was dismal and was out-performed by a standard playground ball costing 60% less.

While the new method looks promising the values obtained were less than those obtained by a standard tilt-test, however that may be explained by the newness of the playground balls tested or glass samples used.

5- Recommendations/Future Work

A new version of the single ball test apparatus is currently being designed that will vary the applied torque by slowly increasing the moment arm length and will use an electronic tilt sensor to determine the moment of ball movement. Additional research using "broken-in leather" balls is also planned.

6- Acknowledgements

The initial work on this project partially fulfilled the master's degree requirements for Zachary Szczerbinski at Temple University in biomedical engineering. Special recognition goes to those in the Temple University Kinesiology Department for all their help with use in the Biokinetics Lab, especially Ryan Teirney, Sarah Shultz, and Jeff Driban and to Pioneer Powder Coating for services donated.

7- References

[H1] Hubbard, J. The Official NBA Encyclopedia. 3rd Edition. Double-Day. New York. 2000.

[N1] NBA.com Spalding New Game Ball Brochure, http://www.nba.com/media/newball_brochure_060628.pdf. Viewed February 29, 2008.

[OH1] Okubo H. and Hubbard M. Dynamics of basketball-rim interactions. In Sports Engineering, 7(1) : 15-29, 2004.

[R1] Rego, S. Personal conversation, May 7, 2007.

[W1] Weiss P. Dribble Quibble: Experiments find that new basketball gets slick. In Science News Online, http://www.sciencenews.org/articles/20061104/fob4.asp, 170(19), 2006. Viewed March 30, 2008.

Comparison Between Observed and Simulated Baseball Trajectories (P214)

LeRoy W. Alaways[1]

Topics: Baseball.
Abstract: The manually observed strike zone exit-plane locations of machined-pitched baseballs are compared to the simulated exit-plane locations. Using a five degree-of-freedom pitching machine located 16.764-m (55-ft) from home plate, multiple pitch trajectories were observed and recorded. Exit-plane locations were manually observed by impacting a foam-pad marked with a 7.62-cm (3-inch) grid located at the strike plane. The transient indentation in the foam-pad allowed the observer to record the impact location to within 2.54-cm (1-inch) in the horizontal and vertical. At the exit of the pitching machine, a 500 frame-per-second video camera recorded the first meter of flight for each observed pitch. Two retro-reflective markers were placed on the ball and using author developed software, the ball and marker centroids were determined automatically. Accurate measurements of ball-spin rate, velocity, and pitching machine exit-plane location were found from the centroid data. Using aerodynamic lift and drag data (Alaways & Hubbard, 2001) and baseball trajectory equation-of-motions (Alaways, 1998) simulated trajectories for each pitch and strike zone exit-plane locations were determined. Comparisons between the observed and simulated exit-plane locations show good correlation and validate existing aerodynamics models. Impact locations and visual inspection of the ball show that the surface roughness of the ball and thus the lift coefficient changes with increased ball usage.
Key words: Baseball; Aerodynamics; Data Acquisition.

1- Motivation

In the successful design of any machine the causality of each process must be accounted for. This is even more important when the machine involves human interaction such as in a pitching machine. Besides throwing a ball, a pitching machine has two major requirements; first it must be safe and second it must be predictable and it is the predictability that makes it safe.

1. Department of Mechanical Engineering, Villanova University, 800 Lancaster Ave., Villanova, Pennsylvania, USA 19085 - leroy.alaways@villanova.edu

The predictability comes from an in-depth knowledge of the workings of the machine and, in a pitching machine, the in-depth knowledge of the aerodynamics of the ball. As ridiculous as it may sound, the aerodynamics of the ball is the easy part in the research and development of a new pitching machine. The interaction of the ball and the throwing mechanism, in this case two spinning wheels, is a non-linear multi-degree-of-freedom problem that includes the age, initial orientation, and insertion speed of the ball, as well as the speed, separation distance, and inertia of the wheels. An even more important design property is the elasticity and durability of the wheel coating. Simply put there are too many parameters to control and therefore constraining the problem and observing the pitch outcomes due to varying a limited parameter set is the key to success in machine development.

If all the constraints are well defined then the main question for the designer is: what is the deviation due to only the aerodynamics of a pitched four-seam baseball at a particular delta in wheel speeds? This question can be restated as: what are the initial conditions put on the baseball and using these initial conditions can the trajectory of the pitch be predicted? Alaways (1998) presented the complete set of baseball trajectory equations-of-motion and showed that precise trajectories could be determined given accurate initial conditions and aerodynamic data. However, in the previous work the baseballs tested were usually identified as official American Major League Baseball (MLB) (Alaways, 1998; Alaways & Hubbard 2001; Alaways, 2008) or were not defined (see Alaways 2008). In the research and development of the pitching machine used for this study the tested baseballs were manufactured and selected with higher quality controls than MLB baseballs, however this resulted in a seam-height that was less prominent.

The objective of this work initially was to determine the initial conditions of a machine-pitched baseball using only one video camera and the characterised the wheel parameters. However, the outcome of the work resulted in comparing the final observed strike-zone exit-plane location to the predicted location using previously published lift data.

2- Methodology

Data on machined-pitched baseball using a state-of-the-art five degree-of-freedom pitching machine, that was still in the development phase, was collected and recorded via a high-speed video camera and human observations at the research and development centre for Fastball, Inc. in Seattle Washington.

The pitching machine, code-named Abner, used two spinning wheels, an automatic ball feeder, and was computer controlled yet highly adjustable. Wheel speed was controllable to the nearest RPM (revolution per minute) for each wheel, and the pitch, yaw, and roll angles of the launch tube were adjustable to the nearest 0.1 degree. Different wheel sets coated with various types of rubber and rubber-like materials were available for use and the "crush", radial distance between the wheel centres, was adjustable to the millimetre. Radar and light-tripped timing gates were located at the exit-plane to indicate a quick estimate of the pitch speed for later comparison.

A high-speed video camera was used to collect spin and velocity information of the ball was set up 5 meters from the perpendicular path of the ball at Abner's exit plane.

The camera was set to record at 500 frames per second and the field-of-view was zoomed to allowed capture of the first meter of flight. Though the camera's aperture was wide open and extra spotlights were located directly behind the camera, the video captured only the ball and reflective markers thus resulting with the elimination of all background noise even when the house lights were on.

Abner's exit-plane was located 16.764-m (55-ft) from the strike-zone impact-plane where a 45.72-by-152.40 cm (18-by-60 inch) foam-pad was set up perpendicular to the ball's trajectory. The foam-pad, marked in a 7.62-by-7.62 cm (3-by-3 inch) grid, was picked for its ability to leave a transient circular indentation when impacted. This indentation allowed an observer to estimate to within 2.54-cm (1-inch) the vertical and horizontal location of impact. The horizontal datum of the foam pad was 78.7 cm (31-inches) above the floor.

Before testing, the ball's mass properties (mass, diameter, seam height) were recorded and the ball was marked with a permanent marker so that it could be placed in an Fig. 1. Two reflective markers were applied approximately 2.5 cm apart on the side of the ball that will be facing the camera.automatic ball feeder in the same orientation for every pitch as indicated in.

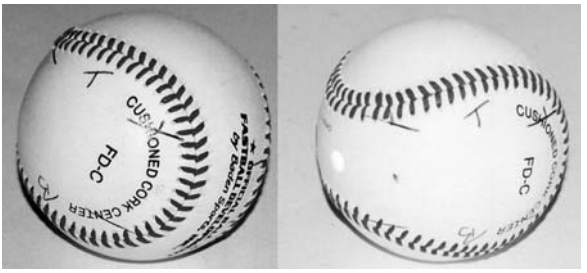

Figure 1 - Pre-test ball mark-up.

The goal of each test was to exam the effects of different wheel-materials, crush, and wheel speeds on the life, angular velocity and speed of the ball and therefore the accuracy of the pitching machines. Each individual test 25 different parameters were recorded from initial ball location first visible as the ball exits the machine to the observed impact location of the ball. For each pitch, the ball was automatically fed in the machine in a four-seam orientation and this was the only constant for the entire study. Figure 2 shows the typical spread of impacts as visually observed by the experimenter.

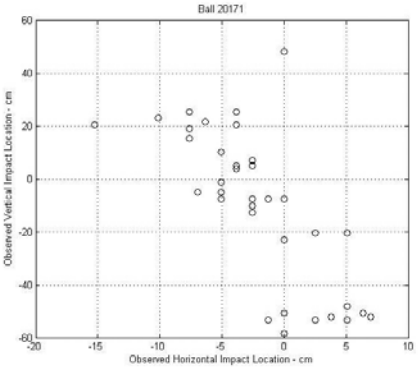

Figure 2 - Observed Impact Location for Test Ball 20171.

After all the data was collected, the initially conditions were determined from the video recorded and the impact plane location was estimated by way of simulation using MATLAB's ode45 routine and the equations-of-motion developed by Alaways (1998). The lift coefficient for the simulation was estimated using a straight-line approximation of the Sikorsky/Lightfoot four-seam data (Alaways, 2008) as shown in Fig. 3. Additionally the average lift coefficient that would be required was later determined using the non-linear squares method described in Hubbard & Alaways (1989).

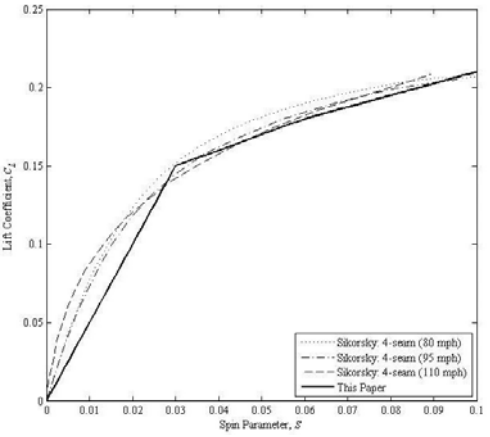

Figure 3 - Lift Coefficient versus Spin Parameter model used for this study.

3- Results & Discussion

Thousands of different tests were run over a three-week period and 718 tests were recorded using the high-speed video system. Figure 4 shows a typical test result and compares the observed vertical impact location and the simulated for ball 20171. The test protocol for ball 20171 is presented below in Table 1; this protocol was used to evaluate the effect of speed on the wheel's rubber material and crush height. Though it is not indicated in Table 1, the elevation angle on Abner was dropped by 1 degree after the 30th pitch and this is evident in Fig. 4. This test was stopped after 40 throws due to speed saturation; an indication that the spin rate was decreasing and that Abner would soon be throwing knuckleballs if higher pitch speeds were commanded.

Pitch #	Commanded Speed m/s (mph)	Average Actual Speed m/s (mph)
1-10	29.1 (65)	28.0 (62.7)
11-15	31.3 (70)	31.9 (71.3)
16-20	33.5 (75)	34.9 (78.2)
21-25	35.8 (80)	37.0 (82.7)
26-30	38.0 (85)	38.1 (85.3)
31-35	40.2 (90)	38.4 (86.0)
36-40	42.5 (95)	38.8 (86.7)

Table 1 - Test Protocol for Ball 20171.

Figure 4 shows a recurring theme in the test results; that as the ball ages the observed and estimated vertical impact location converged. This indicates that the aerodynamic model, i.e. lift coefficient model, was not precise for the ball used and that during the test the aerodynamics of the ball changed. This convergence can also be seen in the observed and estimated impact locations for ball 20166. The test protocol for ball 20166 is presented in Table 2, note again that after the 40th pitch the elevation angle on Abner was lowered 1-degree to insure that the foam-pad was impacted at the higher speeds and this is not indicated in Table 2 but is clearly seen in Fig. 4.

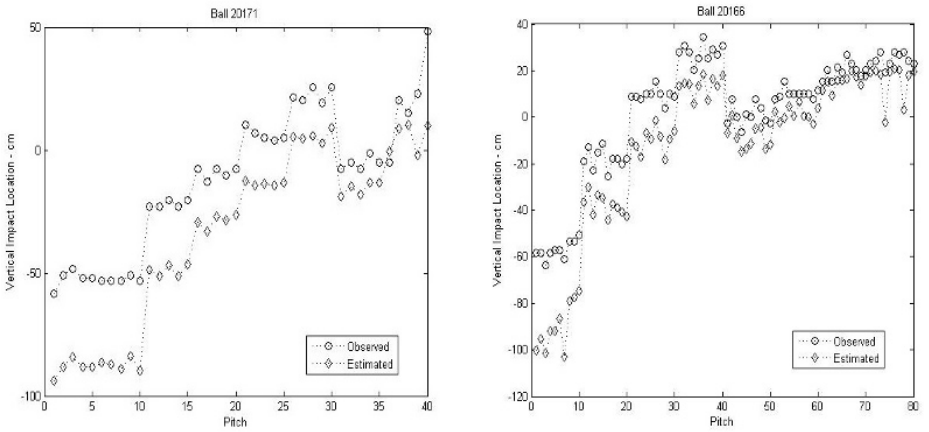

Figure 4 - Observed versus estimated vertical impact locations for ball 20171 and 20166.

Pitch #	Commanded Speed m/s (mph)	Average Actual Speed m/s (mph)
1-10	29.1 (65)	28.2 (63.2)
11-20	31.3 (70)	32.0 (71.6)
21-30	33.5 (75)	34.9 (78.2)
31-40	35.8 (80)	37.4 (83.7)
41-50	38.0 (85)	39.7 (88.8)
51-60	40.2 (90)	41.0 (91.7)
61-70	42.5 (95)	42.9 (95.9)
71-80	44.7 (100)	43.5 (97.3)

Table 2 - Test Protocol for Ball 20166.

In all tests, it was observed that ball-wheel interaction increased the ball's roughness and therefore increased the lift coefficient. The increase in roughness comes from both wear on the leather and from rubber deposits transferred to the ball from the wheels as shown in Fig. 4. In some cases, rubber build-up would dislodge from the ball at higher speeds and decrease the effective roughness.

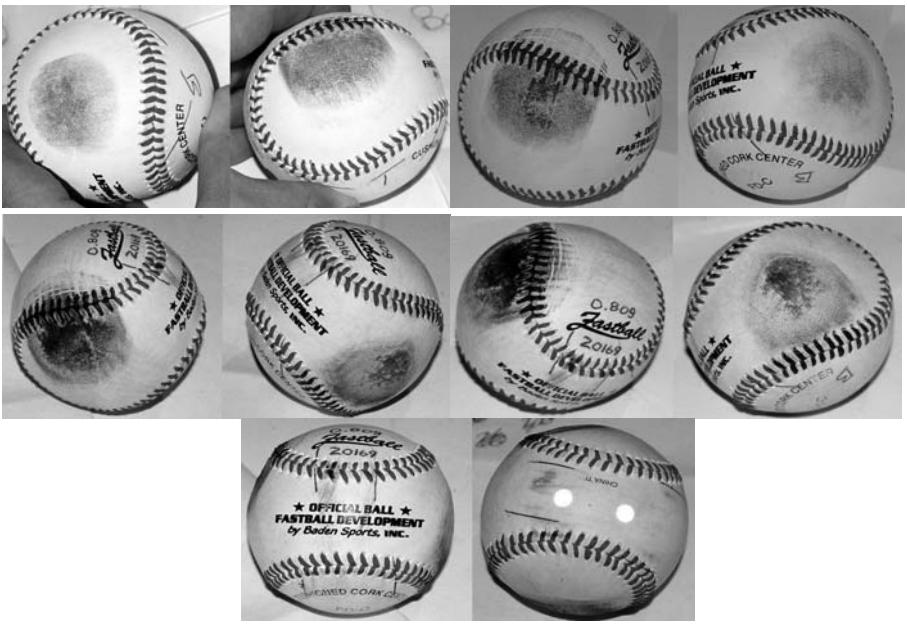

Figure 5 - Wear patterns on the top and bottom of ball 20169 after one, ten, forty, and fifty pitches. The bottom photo is a side-view taken, after the 40th pitch, in the direction of the spin axis. The black wear mark is rubber transferred from the throwing wheels.

Figure 6 shows the average lift coefficient for ball 20166 required to hit the observed impact location given the initial conditions determined for each pitch. Average coefficient is the value found if a constant lift coefficient was used throughout the entire trajectory. This figure shows the coefficient increasing with ball usage until the 30th pitch where it remains nearly constantly for the next 25 pitches before it starts to decrease. Since the coefficient was found after testing was completed no notes on the roughness

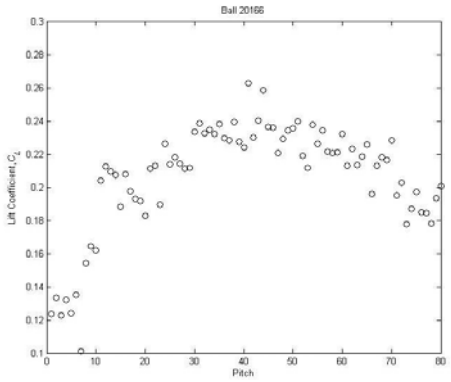

Figure 6 - Average lift coefficients for ball 20166.

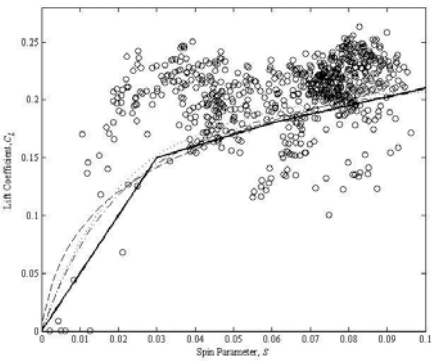

Figure 7 - Average lift coefficients for all pitches.

of the ball were taken. It is noteworthy the extremely low lift coefficient in the first ten pitches, due mainly to the glossy smooth surface of the new ball, and that while the lift coefficient was decreasing at the higher pitch numbers, the observed and estimated impact locations are converging in Fig. 4.

Overall, 718 pitches were filmed, digitised, and analysed. Though it was not the initial intent of this study, it is of great interest to compare the average lift coefficients found for each pitch to the lift model presented in Fig. 3. Figure 7 shows that in general, the average lift coefficient found is greater than the Sikorsky four-seam data but surface roughness effects are also clearly present in this data. These effects are seen in the coefficient values between 0.1 and 0.15 that come from the first five to ten pitches of each ball tested mentioned and shown in Fig. 6. However, the Sikorsky four-seam curve shows the general trend but under-values the lift coefficient at lower values of spin parameter.

4- Conclusion

A method of obtaining visually observed impact plane locations while simultaneously using high speed video to estimate, by means of simulation, the impact plane location for machine pitched baseballs was presented. The results show that the obtained values compare with very good correlation however the results also show that surface roughness plays a major yet unknown role in the lift coefficient. Average lift coefficient values for 718 pitches were compared with the Sikorsky four-seam lift coefficient curve and shows that generally, for the ball used in this study, the Sikorsky curve under-estimates the magnitude of lift at lower values of spin parameter.

5- Acknowledgements

The author would like to acknowledge and thank Richard Richings and the folks at Fastball, Inc. for allowing a baseball researcher to "play with" the world's greatest pitching machine and be paid while doing it.

6- References

[A1] Alaways, L.W Aerodynamics of the Curve-ball, Doctoral Dissertation, University of California, Davis, 1998

[A2] Alaways, L.W. Aerodynamics of a Curve-ball: The Sikorsky/Lightfoot Lift Data, Proceedings of the 7th ISEA Conference, Biarritz, France, 2008

[AH1] Alaways, L.W. & Hubbard, M. Experimental Determination of Baseball Spin and Lift, Journal of Sports Sciences, 19 (5), pp. 349-358, May 2001

[HA1] Hubbard, M. & Alaways, L.W. Rapid and Accurate Estimation of Release Conditions in the Javelin Throw, Journal of Biomechanics, 22 (6-7), pp. 583-595, 1989

Testing the Unconventional; The Ergonomic Paddle Shaft (P215)

Paul Ewart[1]

Topics: Water sports, Innovation & Design, Prevention & Health, Testing, Benchmarking.
Abstract: The use of composite materials in sports equipment has enabled design engineers to revolutionise their products. This is seen in all sports from cycling to skiing, climbing to kayaking. Along with performance enhancement products are also being designed with ergonomic considerations that reduce athlete stresses and support injury prevention. One aspect of product innovation seen to lag behind some radical new designs are the techniques to test or measure the equipment performance. A product that falls into this category is the 'Crank'. The 'Crank' is an adaptation of the kayak paddle shaft which has been designed to relieve stress in the wrists and forearms of the paddler. This work investigates standard mechanical methods used to test flexural properties of the paddle shaft and then looks at adapting this standard to the 'Crank'. This investigation shows that use of a symmetrical loading test is not suitable given the geometry of the 'Crank'. The unsymmetrical test method proposed here in conjunction with the improved testing apparatus is proven to be suitable for use as a standard testing regime. The test methods used here can provide mechanical data for custom shafts such as the crank and could be further developed as a tool for both performance and product benchmarking.
Key words: Crank, innovation, kayak paddle shaft, mechanical properties, testing method.

1- Introduction

Paddle shafts are traditionally tested using a three point bend setup, either with or without the blades attached. This provides an indicative measure of the mechanical properties of each paddle and/or shaft. As the flexural test creates both tensile and compressive stress within the shaft it is the ideal method to be used for destructive or non-destructive testing and will also approximate in use loading. Current quality control and performance assessment methods utilise the expertise of the manufacturer and were often developed in-house over a number of years. These in-house methods may not be conducive to innovation and product development, especially where unconventional shaft designs and composite materials are used.

1. Engcons c/o The University of Waikato, Private Bag 3105, Hamilton, New Zealand - E-mail : p.ewart@waikato.ac.nz

2- Background

Kayak paddles were conventionally made from wood using lamination and/or solid fabrication techniques that allow the grain to run longitudinally along the shafts axis. Wooden paddles are still being manufactured today and while some paddlers consider them outdated others still prefer the look and feel, especially for canoeing and rafting where there is only one blade attached to the shaft. Aluminium is widely used in shaft production and was once the material of choice but has since been relegated to entry level paddle construction only. Glass fibre reinforced thermoset composite; the material of choice in the 1980s was quickly superseded by the superior specific properties offered by carbon fibre. Glass fibre is still the main shaft material and is widely utilised, in combination with advanced reinforcement materials such as carbon and aramid fibre, due to its impact resistance when used in thermoset resins. Elite sports people will generally specify full carbon for its lightweight and stiffness regardless of reduced durability and the extra costs.

3- Technical problem

Conventional paddle shafts are straight thin walled tubes with a round cross section uniform through the entire length. They may also be ergonomically formed to have an elliptical section with the ends feathered to aid the natural paddling action. A more recent adaptation of the paddle shaft (Figure 1) improves the ergonomic factor by cranking the shaft, at the hand grip position, relative to the main axis of the shaft. It is said that by cranking the shaft the wrist is kept straighter which reduces the strain on the forearm, improves performance and reduces fatigue [D1]. One other important factor is the tension in the tendons that run from the fingers, across the wrist, and connect to muscles in the forearm (Figure 2).

Figure 1 - 'Crank' paddle shaft.

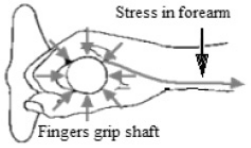

Figure 2 - Clamping pressure on the paddle shaft creating stress in the forearm tendons [D1].

Following the design and implementation of the 'crank' paddle shaft it has been found that conventional testing methods are not suited to the new design. One solution to this is to send shafts to external agencies for proving and performance verification after manufacture. Employing an external testing agency can be extremely expensive for the manufacturer and may not address all required parameters due to restrictions of conventional test protocols developed for monolithic materials.

4- Proposed solution

The performance of the 'crank' paddle shaft needs to be equal or better than the conventional shaft in order to provide a high performance alternative worth any increased cost. Although it has been shown that improved performance is not merely a mechanical property, even an improvement perceived by the athlete can provide the advantage needed for competition [RJ1] [RJ2]. Regardless of the subjective aspects of equipment assessment performance based on mechanical properties should still be considered essential in product design and mechanical testing is the only objective means of measurement. Where the 'crank' shaft geometry departs from the conventional shaft it is essential a rigorous test method is chosen that is a close comparison to end use. This will ensure that any weakness that may not be evident in design are quickly identified and eliminated prior to production and/or further iterations.

During the paddling action the power stroke, where the normal force on the blade is equal to the horizontal force (Figure 3), produces the greatest loading on the shaft [Nd1]. For the conventional shaft loading will produce quasi-linear stress distribution throughout the shaft length. However, the stress distributions through the crank will not be regular due to the geometry at the hand grip area. To imitate the paddling action a shaft kit (Figure 4) was made that could be used to mimic the loading of the paddle shaft during use.

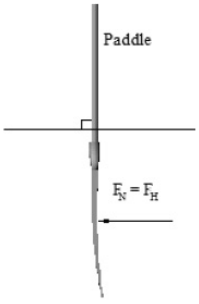

Figure 3 - Angle of greatest resistance during paddle action.

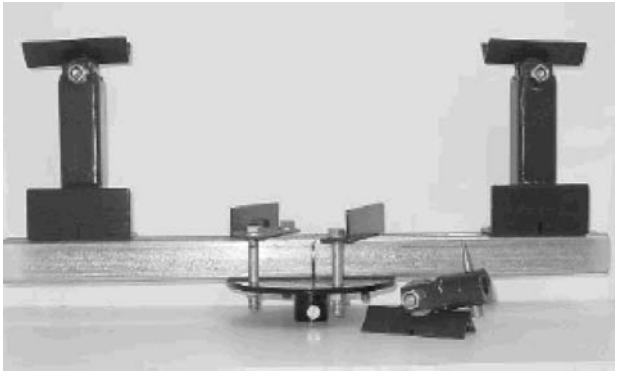

Figure 4 - Shaft test kit.

5- Method

A simple three point-bend test with a span of 450 mm and loads that produced initial deflection of 1mm and final load to break was used for the conventional paddle shafts. The same conditions (initial deflection of 2mm) were also used on the crank shafts, see Appendix I for data. Tested using Lloyd LR30C Universal testing machine, Calibration cert. No. ERN8905.

6- Discussion and results

While the three-point bend test is ideal for the conventional paddle shaft it is not suitable for the crank shaft. The cranked hand grip could not be loaded with the rigid load adaptor. When the loading adaptor was allowed to swivel the crank could be tested with the central load. It was further considered that although the crank could be tested with a central load this did not represent the in-use situation. During use the paddle shaft is loaded at both hand grip positions and the inner surface the submerged paddle blade. While the blades are not being considered here the crank test would be more valid with supports at one end of the shaft and perhaps at the centre of the shaft with loading at one hand grip. This will present the unsymmetrical loading seen during use, but will ensure the modified crank end of the shaft is fully tested. When the unsymmetrical loading was tested it was found that misalignment of the central shaft and shaft ends also require the load supports to swivel. From this test the method shown in Appendix II was produced. The initial testing was done within the elastic region of the shaft so that the shaft is not damaged during the test. This could be a suitable method of quality control post manufacturing with loads of less than 700N. The destructive testing followed the same process as above but the loads needed for breaking of the shafts was between 2000N and 5000N.

From the load and bend data (Appendix III) for the supplied carbon and carbon/kevlar shafts it can be seen that the cranks break at higher loads than the conventional shafts. The non-destructive tests show considerably higher loading for the crank at the deflection of 1.5 mm.

7- Conclusion

While there is currently no testing standard specific to the testing of the crank shaft the method investigated here can be considered suitable as an in-house standard. The application of the test method (Appendix II) using non-destructive loads and deflections not exceeding 1.5mm give easily comparable results that could be used as a quality control method to monitor both the manufacturing process and material supply. The test methods used here can provide mechanical data for custom shafts such as the crank and could be further developed as a tool for both performance and product benchmarking.

8- Acknowledgments

Kilwell Fibretube, Rotorua, New Zealand Sunspots Kayaks, Rotorua, New Zealand Technology New Zealand

9- References

[D1] Dawson, S. Feathers Blades, Cranks and Shafts. In Canoeist Magazine, September 1995.

[Nd1] Neives, A. F., de las Nieves, F. J. About the propulsion system of a kayak and of Basiliscus Basiliscus. In European Journal of Physics, 425-429. 1998

[RJ1] Roberts, J., Jones, R., Harwood, C., Mitchell, S., Rothberg, S. Human perceptions of sports equipment under playing conditions. In Journal of Sport Sciences, 19/7, 2001.
[RJ2] Roberts, J., Jones, R., Mansfield, S., Rothberg, S. Evaluation of vibrotactile sensations in the 'feel' of a golf club. In Journal of Sound and Vibration, (Article in press), 2004.

Appendix I. Crank 1ABCDSpan450mmLoad [N]568.2842.2685.3950.2Deflection2mmMod bending43.164.461.255.5Crank 1ABCDSpan450mmLoad [N]535.2702.0656.5713.8Deflection 2mmMod bending41.554.555.543.2Crank 2ShaftABCDSpan450mmLoad [N]650.0633. 25733.5901.5Deflection2mmModbending52.646.758.451.6ConventionalSymmetricalPCTWTexa lPCKTWPCGWWPCTWSpan450mmLoad [N]133.1133.3136.4248.2182.1Deflection1mmMod bending32.338.934.844.853.3To breakLoad [N]2920277028304080264 0Mod bending 3031.135.151.453.7Deflection17.2mm16.7mm16.0mm11.8mm10.0mmConventionalSymmetric alFC1FC2FC3FC4Span450mmLoad [N]443.3438.0428.8413.0Deflection1mmMod bending 61.864.665.662.6To breakLoad [N]2300251024402730Mod bending66.466.468.468.6Deflection 8.78mm9.56mm9.41mm10.5mmConventionalSymmetricalFG1FG2FG3FG4Span450mmLoad [N]260.7233.8262.0250.8Deflection1mmMod bending34.431.233.730.8BreakLoad [N] 2660264027502610Mod bending33.232.632.231.6Deflection18.7mm18.8mm19.7mm18.7mm Preliminary paddle shaft flexural testing results.Plane of bladePlane of crank

Appendix II. Proposed method for shaft only testing:

1. Test conventional carbon fibre and glass fibre shafts within their elastic limit to determine load and elastic modulus. Span 500mm, load point at 170mm from end.
Each shaft tested to deflection of 1.5mm at up to six positions around main axis. The position with the lowest load value was then reset and the shaft was tested until failure.
2. Test carbon and carbon kevlar crank shafts within their elastic limit to determine load and elastic modulus. Span 500mm with load point at 170mm to coincide with hand grip.
Each shaft tested to deflection of 1.5mm at four positions around main axis for each end. Start in line with plane of crank then turn 90 degree. The position with the lowest load value was then reset and the shaft was tested until failure. One end was used to measure the crank plan the other measured the flat plane.

Appendix III. ShaftTestSpan [mm]CrankPlane of crankBCDOD [mm]27.527.331.6ID [mm]22.522.727.8Mass [g]NDT 1.5mmLoad [N]568.21502.3453.3555.5Mod bending43.1178. 660.761.5DestructiveLoad [N]17552379340515320Mod bending104.8286.173.176Deflection [mm]17.829.911.210.0Plane of bladeBCDNDT 1.5mmLoad [N]535.21433.8423.0446.3Mod bending41.5160.458.344.1DestructiveLoad [N]438233044971Mod bending77.462.059.2Deflection [mm]12.820.012.6ConventionalSymmetricalC2CK1CK2G13G2OD [mm]28.529.629.629.029.0ID [mm]26.527.027.026.526.5Mass [g]188.0251.0248.0250.0245.0 NDT 1.5mmLoad [N]280.5311.9308.0272.4250.6Mod bending59.346.245.941.942.9 DestructiveLoad [N]3082373739862318 3082Mod bending40.4532.533.427.832.6Deflection [mm]23.123.125.217.024.723.0500 with 170 offsetA188.058.7305940.41Span 450 CL deflect. 1.5mmProposed paddle shaft test method results2Span 850 offset 170mm C128.526.5274.4A27.523.03No rubber support.

Development and Validation of an Automated Method to Detect Gait Events Using Acceleration and Angular Rate (P216)

Yoshihisa Sakurai[1], Yuji Ohgi[2], Takeo Maruyama[1]

Topics: Measurement Systems.
Abstract: The purpose of this study was to develop and validate an automatic procedure using accelerometers and angular rate sensors for detecting exact gait events: heel contact (HC), toe contact (TC), heel off (HO) and toe off (TO). For this purpose, two miniature-sized light sensors were attached to the right shoe which measured triaxial acceleration and biaxial angular velocity of various positions of the shoe while ground reaction force and marker data were recorded at the same time as reference measurements. Healthy men walked on a walkpath at self-selected normal speed with the instrumented shoes on. An automated algorithm was developed to detect HC, TC, HO and TO from the acceleration and angular velocity signals, which were compared with reference data from force plates and markers. The results showed that our method demonstrated similar HC and TO to those with force plates and markers. Moreover, this method well detected stance phase duration. However, TC and HO differed among the three methods (force plates vs. markers vs. sensors). We concluded that the system using inertia sensors can identify TC and HO accurately and be used in gait analysis.
Key words: Gait events; acceleration; angular rate; sensor.

1- Introduction

Gait events have been used to define walking phase. Force plates have been used to determine the timing of each gait event and this method is very precise and reliable. This conventional method, however, is restricted to laboratory environment, and determines only the heel contact (HC) and toe off (TO) although the timing of heel off (HO) and toe contact (TC) are also important in some situations (Ghoussayni *et al.*, 2004). For

1. Graduate School of Decision Science and Technology, Tokyo Institute of Technology, Tokyo, Japan - E-mail: sakurai.y.ac@m.titech.ac.jp
2. Graduate School of Media and Governance, Keio University, Kanagawa, Japan - E-mail: ohgi@sfc.keio.ac.jp

example, HO timing was indeed used to divide mid stance and terminal stance in gait analysis. To overcome these issues, footswitches and force sensitive resistors have been used to determine such gait events. These methods, however, may hinder normal walking. Another gait analysis method is ambulatory gait monitoring using the body fixed sensors to record quantitative gate data (Selles *et al.*, 2005), which removed the need for gyroscopes and accelerometers being placed under the foot and, therefore, did not disturb normal gait patterns. However, only HC and TO have previously been detected and TC and HO have not been investigated using the ambulatory gait monitoring (Jasiewicz *et al.*, 2006; Selles *et al.*, 2005).

The purpose of this study was to develop a completely automated identification system for gait events: HC, TC, HO and TO using both accelerometers and angular rate sensors. The validity of detected gait events from the sensors was compared to the data from force plates and marker data.

2- Method

2.1 Experiment

2.1.1 Subjects

Nine healthy males (age: 22.3 ± 2.4 yrs; height: 1.73 ± 0.08 m; weight: 62.3 ± 9.2 kg) participated in this study. Subjects had no known disorders that would influence their walking patterns, and provided informed consent prior to the experiments. All subjects wore walking shoes of the same kind (Mizuno, Inc.) during the test. Before measurement, subjects were familiarized with the experimental environment and protocol.

2.1.2 Sensor systems

Two inertia sensors (IMU 5 Degrees of Freedom, Spark Fun Electronics, Inc., USA) were used in this study (Fig. 1). Each sensor comprised one triaxial accelerometer (±3G, ADXL330, Analog Devices, Inc., USA) and one dual axis gyroscope (±500 deg/s, IDG-300, InvenSense, Inc., USA). Two types of sensor orientation were used with the first one handling the heel and toe of the right foot and the second one for the heel and dorsum of the right foot. These sensors measured angular velocities of transverse and longitudinal axes at the heel, and transverse and anteroposterior axes at the toe and dorsum.

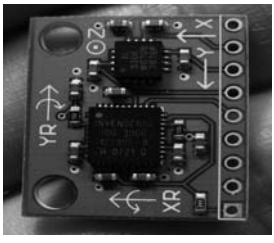

Figure 1 - Inertia sensor (IMU 5 Degree of Freedom).

2.1.3 Force plates

Vertical ground reaction force (GRF) was used as the comparison standard for the gait events (1 kHz). Two force plates (0.6m x 0.4m, Kistler, Inc.) were fixed one after the other along the pathway. Subjects walked with the right heel striking the first plate, and the ball of the same foot on the second plate with the left foot making no contact with the force plates (Ghoussayni *et al.*, 2004). First plate was used to determine the initial HC and HO and second plate was used for TC and TO. The GRF from only one particular force sensor out of four that were positioned nearest to the foot contact were used for analysis. We defined contact phase using a 0 digital value threshold from the vertical component of the sensor.

2.1.4 Motion data

The 3D coordinates of the markers were detected using MAC 3D System (Motion Analysis, Inc.). Motion data was measured at 250 Hz. The sacral marker was used to calculate walking speed, which was determined at HC. Markers on the heel and the first and fifth metatarsals were used to identify gait events, which were compared to the sensor technique in the later analysis.

2.1.5 Protocol

Subjects walked a 7.2 m pathway at their self-selected normal speed, and contacted with force plates with their third or fourth step from the start. Subjects were asked to repeat the walk for the two sets of sensor orientation until five successful trials were measured. Each trial was considered to be successful when the borderline of the two plates sit within two lines that were drawn across the shoe (approximately 10 cm apart) during the foot contact. GRF was also checked to see whether only the right foot landed on the force plates.

2.2 Data analysis

The obtained data were processed offline using Matlab (The MathWorks, Inc.). Sensor signals from the toe and dorsum showed similar characteristics, so we only used the data set of the heel and dorsum. Motion data were converted to 1 kHz using spline interpolation.

2.2.1 Extraction of one cycle

First, we extracted one gait cycle including HC from raw time series data. Swing phase was identified by cross correlation (Li & Caldwell, 1999) using the search window located 200 ms before and 200 ms after the maximal value of forward-direction acceleration at the dorsum (Fig. 2, A). This search window width was chosen empirically. We cut time series of coefficient of cross correlation by the moment of cross 0.7 (Fig. 2, B). We also neglected the point that was too close the previous point.

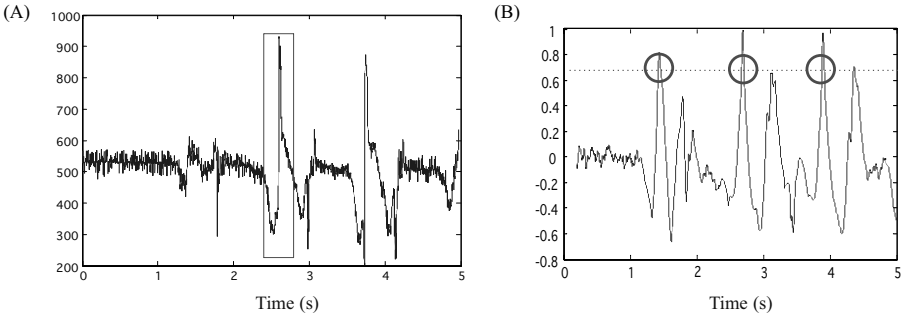

Figure 2 - (A) Time series of forward-directed acceleration at dorsum and search window. (B) Coefficient of cross correlation.

2.2.2 Detection of heel contact (HC)

To identify HC, first we extracted short time domain including HC using forward-directed acceleration from the heel sensor. When the heel hit the ground, impact acceleration is generated (Fig. 3, A). HC was, therefore, determined from the impact acceleration using derivation of vertical-directed acceleration and angular velocity of transverse axis.

2.2.3 Detection of heel off (TO)

We extracted short time domain including TO from the stance phase using vertical acceleration from the heel sensor. Then, TO was identified by a peak forward-directed acceleration (Jasiewicz *et al.*, 2006) from the dorsum sensor (Fig. 3, B). Vertical acceleration of from the toe sensor was also used to avoid false detection.

2.2.4 Detection of toe contact (TC)

Stance phase was determined using HC and TO. TC was detected using forward-directed acceleration at the dorsum. In detail, sensor data were firstly smoothed by a fourth-order Butterworth low-pass filter at the cut-off frequency of 100 Hz. Then, we subtracted the mean value of the foot flat phase from acceleration. Next, we found the smallest local minimum value, and the adjoining local maximum was thought to be the timing of TC (Fig. 3, C).

2.2.5 –Detection of heel off (HO)

After TC, the heel should not move until the beginning of HO. HO was determined in a similar way to the detection of TC. For HO detection, normalized angular velocity of transverse axis at the heel sensor which was subtracted by the mean value of the flat phase was used. We defined HO as the timing that angular velocity started to fall below zero for a continuous duration (Fig. 3, D). Angular acceleration of transverse axis from the heel sensor was also used to avoid false detection.

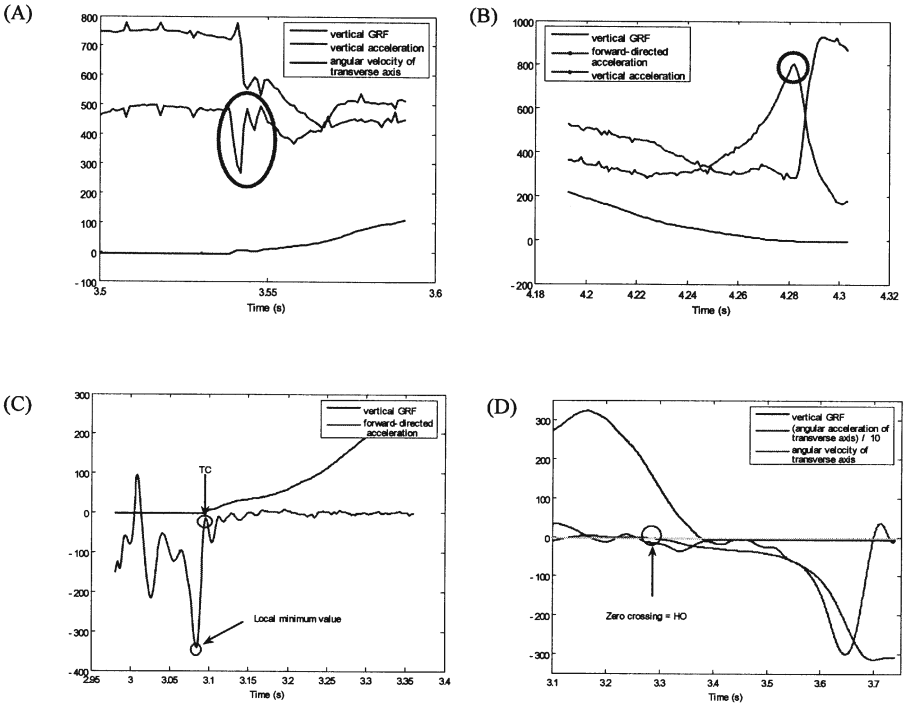

Figure 3 - (A) Time series of vertical GRF, vertical acceleration, and angular velocity of transverse axis of heel sensor around HC. (B) Time series of vertical GRF, forward-directed acceleration, and vertical acceleration of toe sensor around TO. (C) Time series of vertical GRF and forward-directed acceleration of toe sensor around TC. (D) Time series of vertical GRF and angular velocity and angular acceleration of transverse axis of heel sensor around TO.

3- Results and Discussion

Total of 45 steps were analyzed from nine subjects. The average walking speed was 1.07 m/s (SD = 0.19). This speed was slightly slower than previous study for normal walking (Ghoussayni *et al.*, 2004).

3.1 Gait events

To evaluate the accuracy of detection, gait events (HC, TC, HO, and TO) identified from the sensor data was compared with those from force plates and markers. Bland-Altman plots (Bland and Altman, 1986) were created to indicate mean errors, 95% confidence intervals for the bias, and 95% confidence intervals of the errors. From these results (Fig. 4 and Table 1), only the detection of HO did not have systematic error (95% confidence interval for the bias). Random error (95% confidence interval of error), however, showed a wide range (from –0.077 to 0.087). On the other hand, HC and TO had systematic errors and small random errors (maximally 20ms). We concluded that only detec-

	FP			Marker		
	Mean error (SD)	95% confidence interval for the bias	95% confidence interval of error	Mean error (SD)	95% confidence interval for the bias	95% confidence interval of error
HC	0.002 (0.005)	[0.001, 0.004]	[-0.008, 0.012]	-0.003 (0.001)	[-0.003, -0.002]	[-0.006, 0.000]
TC	-0.029 (0.016)	[-0.024, -0.034]	[-0.060, -0.002]	-0.025 (0.010)	[-0.029, -0.022]	[-0.046, -0.005]
HO	0.114 (0.053)	[0.098, 0.130]	[0.010, 0.218]	0.005 (0.042)	[-0.008, 0.018]	[-0.077, 0.087]
TO	-0.008 (0.004)	[-0.009, -0.006]	[-0.016, 0.000]	0.002 (0.003)	[0.001, 0.003]	[-0.004, -0.009]

Table 1 - Mean, SD, 95% confidence intervals for the bias, and 95% confidence intervals of error of the detection of HC, TC, HO, and TO (n = 45).

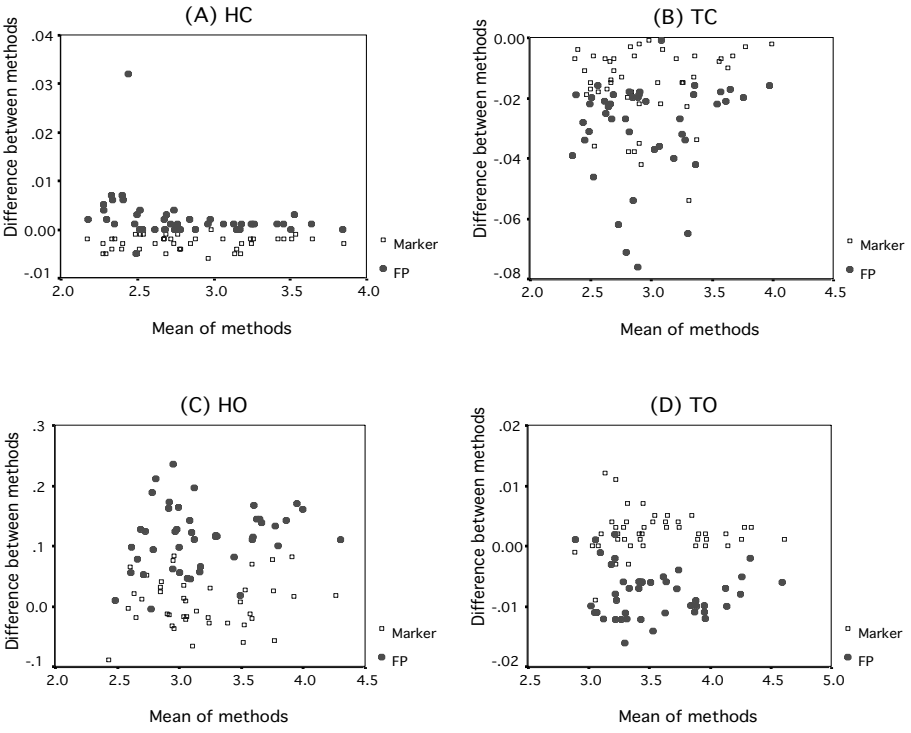

Figure 4 - Bland-Altman plot for the force plates and sensors method difference and marker and sensors in the estimation of the (A) HC timing, (B) TC timing, (C) HO timing, and (D) TO timing.

tion of HC and TO using inertia sensors demonstrated a good accuracy. We opined that the discrepancies between sensor method and force plate for TC and HO existed because of unconvincing ability of the current force plates setting to detect true TC and HO (relatively large areas were considered to be the heel and toe). This resulted in much earlier TC and later HO timing for force plates than the sensor method.

3.2 Intervals

We compared only HC-TO interval (stance phase duration) using Bland-Altman plots (Fig. 5 and Table 2) because of their accuracy as discussed above. The result showed that the stance phase duration from sensor was about 10ms longer than that from force plates and 5ms longer than that form markers. However, we believe that these differences were small, and thus sensor method produced similar stance duration to the other two techniques.

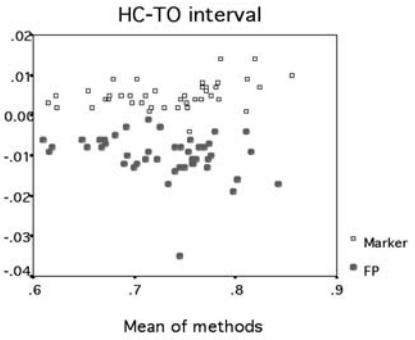

Figure 5 - Bland-Altman plot for the force plates and sensors method difference and marker and sensors in the estimation of the stance phase duration.

	FP			Marker		
	Mean error (SD)	95% confidence interval for the bias	95% confidence interval of error	Mean error (SD)	95% confidence interval for the bias	95% confidence interval of error
Stance phase duration	0.010 (0.005)	[-0.008, 0.012]	[-0.021, 0.000]	0.005 (0.003)	[0.004, 0.006]	[-0.001, 0.012]

Table 2 - Mean, SD, 95% confidence intervals for the bias, and 95% confidence intervals of error of the HC-TO interval (n = 45).

4- Conclusion

We have used inertia sensors and automated algorism to detect four gait events (HC, TC, HO, and TO) and compared them with the reference data from force plates and markers. We concluded that the timing of HC and TO, and stance phase duration were similar between the current sensor method and the reference methods providing sufficiently reliable data in gait analysis. This method may allow walking analyses in various situations such as outdoor or treadmill conditions.

5- References

[BA1] Bland JM. and Altman DG. Statistical methods for assessing agreements between two methods of clinical measurement. In Lancet, 307-310, 1986

[GS1] Ghoussayni S., Stevens C., Durham S. and Ewins D. Assessment and validation of a simple automated method for the detection of gait events and intervals. In Gait and Posture, 20(3): 266-272, 2004

[JA1] Jasiewicz JM., Allum JH., Middleton JW., Barriskill A., Condie P., Purcell B. and Li RC. Gait event detection using linear accelerometers or angular velocity transducers in able-bodied and spinal-cord injured individuals. In Gait and Posture, 24(4): 411-417, 2006

[LC1] Li L. and Caldwell GE. Coefficient of cross correlation and the time domain correspondence. In Journal of Electromyography and Kinesiology, 9(6): 385-389, 1999

[SF1] Selles RW., Formanoy MA., Bussmann JB., Janssens PJ. and Stam HJ. Automated estimation of initial and terminal contact timing using accelerometers; development and validation in transtibial amputees and controls. In IEEE transactions on neural systems and rehabilitation engineering, 13(1): 81-88, 2005

Evaluation of the Estimation Method on the Hip Joint Centre Location During Instep Kicking Motion (P217)

Koshi Yamada[1], Takeo Maruyama[1]

Topics: Biomechanics.
Abstract: The purpose of this research was to evaluate the estimation methods of the hip joint centre (HJC) location for calculating kinematic parameters of knee and hip joints during dynamic movement, in this reserch, instep kicking motion. Twelve skilled soccer players participated in the experiment. To estimate the HJC location, they were instructed to do ad hoc movements including hip flexion/extension and abduction/adduction movements performed on several planes of different orientations, followed by a circumduction movement. Then, subjects performed their maximal instep kick, which were recorded using motion capture system at 250Hz. The coordinates of the HJC were estimated using three methods and compared. The first used marker coordinates on left and right greater trochanters, the second empirical relations between the HJC location and the length between anterior superior illiac spines, which had been called predictive method, and third bias compensated least squares method, which had been called functional method. Then, maximal hip extention and knee flexion angles during instep kicking motion were calculated based on three methods, and compared statistically. As a result, the hip joint centre location estimated by first method changed so much in the pelvic anatomical frame during dynamic exercise, and maximal hip extension and knee flexion angles were different from results by other two methods significantly. However, predictive methods gave almost the same results as functional method which had been said to be most accurate method in a previous study. Consequently, method using markers on the greater trochanters could not be appropriate for kinematic analysis during dynamic exercise, and predictive method was recommended for use because of its accuracy and easiness for application.
Key words: hip joint centre; functional method; predictive method; instep kicking motion.

1. Department of Human System Science, Tokyo Institute of Technology, Tokyo, Japan - E-mail: yamada.k.am@m.titech.ac.jp

1- Introduction

When we evaluate human movement, we often calculate kinematic and kinetic parameters, such as joint angle, joint force, and joint moment. Various factors have influence on kinematic and kinetic analysis, and through gait analysis estimation error of the joint center have been known for its critical influence on the result. Especially, the hip joint centre (HJC) have been known for its difficulty for estimating the location, because it is difficult to identify using palpable bony landmarks. Therefore, many researchers have argued on methods for accurate estimation of the HJC location in the field of clinical biomechanics. Estimation methods suggested so far can be classified into two categories. One is predictive method, and the other is called functional method. The former method uses empirical relations between palpable bony landmarks and the HJC, the latter regards the HJC as a fixed point in a pelvic anatomical frame, and estimates the coordinates of the HJC by fitting a sphere to the trajectory of the marker placed on the thigh during ad hoc movement for estimation. Validation of the functional methods have been conducted by some researchers through comparing the estimated value with the 'true' location measured using MRI or ultrasound wave (Kirkwood *et al.*, 1999; Hicks and Richards, 2005). As a result, it has been reported that functional method gives the better estimate than other estimation methods. A recent study proposed an optimized protocol for the functional method (Camomilla *et al.*, 2006).

From the clinical demand, some researchers investigated how the estimation error of the HJC location influences on kinematic or kinetic parameters in gait (Holden and Stanhope, 1998; Stagni *et al.*, 2000), but few studies applied these methods in other movements, especially more dynamic exercise observed in sports activities. Therefore, we were interested in how the difference of the estimation methods influenced on kinematic analytical results during dynamic movement, and determining which method we should use and we should not use for analyzing dynamic exercise from a motion analysts' perspective. In this paper, we estimated the HJC location using three different methods and investigated the influence of the estimation error on the kinematic parameters during instep kicking motion.

2- Methods

2.1 Experiment

Twelve healthy male skilled soccer players (age 21.75±1.96yr; body weight 64.67±8.05 kg; height 1.74±0.06m) participated in the experiment. Before the experiment, informed consent was obtained. We conducted the experiment in a labolatory. We placed twenty reflective markers which were used to identify anatomical landmarks, and four markers were placed on the thigh (two markers on each thigh) to estimate the HJC location. The motion was recorded using MAC 3D system with 10 Eagle cameras (Motion analysis Co., California) at 250 Hz. To estimate the HJC location, we instructed subjects to do ad hoc movements which included hip flexion/extension and abduction/adduction movements performed on several planes of different orientations, followed by a circumduction movement (Camomilla *et al.*, 2006). Then, subjects performed their maximal instep kick

by two steps, aiming at a target. All motion data were smoothed by the bidirectional fourth-order butterworth low-pass filter at the cutoff frequency of 10Hz. The X-axis of ground coordinate system and local coodinate system of each segment was set to the anterior/posterior direction with its positive direction forwards, Y-axis was set to medial/lateral direction with its positive axis from right to left, and Z-axis was set to vertical direction with its positive direction upward.

2.2 Estimation of the HJC location

We estimated the HJC location by three different methods. In the latter two methods, we regarded the HJC as a fixed point in the pelvic anatomical frame (PAF, Fig. 1), which were defined as follows. The origin is the midpoint between the anterior superior illiac spines (ASISs), the z-axis is defined as the line passing through the ASISs with its positive direction from left to right; the x-axis lies in the quasi transverse plane defined by the ASISs and the midpoint between the posterior superior iliac spines (PSISs) with its positive direction forwards; the y-axis is orthogonal to the xz plane with its positive direction proximal.

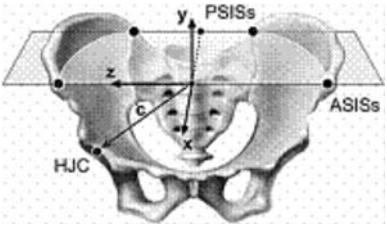

Figure 1 - Pelvic anatomical frame (Camomilla *et al.*, 2006).

2.2.1 Method 1

We assumed the HJC is on the line between right and left greater trochanters, and divides the line 0.18 to 0.82. We calculated the HJC location by Method1 in global coordinate system. Then, for comparing the estimate by Method1 with the estimates by Method2 and 3, we transformed the estimated value from Method1 into the coordinate in pelvic anatomical frame.

2.2.2 Method 2

We estimated subject-specific coordinates using predictive method suggested in a previous study (Bell *et al.*, 1990). We assumed the right HJC located (x, y, z) in the PAF, and then we estimated the coordinates as follows,

$$x = -0.19L, \quad y = -0.30L, \quad z = 0.36L$$

where L represents the distance between right and left ASISs which was calculated from motion capture data.

2.2.3 Method 3

We regarded the HJC as a fixed point in the PAF (Fig. 1), and estimated subject-specific coordinates using functional method suggested in a previous study (Camomilla *et al.*,2006). We used the coordinates of five markers, two of which were placed on the thigh for this estimation, and others were placed on greater trochanters, medial and lateral femoral epicondyles. Estimation method was divided into two steps, because the estimate calculated through first step is biased. The calculation through second step is for bias compensation (Gamage and Lasenby, 2002; Halvorsen, 2003).

2.3 Comparison of methods

We calculated the HJC location by Method 2 and 3 in the PAF. To compare estimation results between Method 2 and 3, we calculated average and standard deviation of the estimated coordinates in twelve subjects. Then, we calculated knee and hip joint angles of kicking leg during instep kicking motion for each estimated value of the HJC location. Joint angle calculation was conducted using YZX–Euler angle. To compare the results from kinematic analysis, we analyzed knee flexion/extension and hip flexion/extension angles during the interval from right toe-off to just before ball impact. Then, we calculated the maximam hip extension angles (MHE) and the maximam knee flexion angles (MKF). Average and standard deviation of MHE and MKF angles were calculated and compared.

2.4 Statistics

We used paired t-test and one-way ANOVA with the Bonferroni method for multiple comparisons with SPSS (SPSS, Inc.). The criterion for statistical significance was $p < 0.05$ for all statistical analyses.

3- Results and Discussion

3.1 Estimation of the HJC location

The results of comparison of the HJC location estimation were shown in Table1, and we showed the result of estimated value by Method 1 in the PAF in Fig. 2. In Fig. 2, we can see the results from Method 1 changes a lot in the PAF during kicking motion. We considerd that was because the marker on the greater trochanter moves much relative to the PAF during dynamical exercise than more static exercise such as gait. In addition, Method 1 used only two markers to estimate the HJC location, so the estimate from Method 1 would be sensitive to mesurement noise and artifact.The HJC coordinates in PAF estimated by Method 2 and 3 is constant, because we regarded the HJC as a fixed point in the PAF. However, only the Y coodinates estimated by Method 2 and 3 are different significantly (Table 1).

	Method2	Method3
X component	-48.67±3.19(mm)	-50.12±9.16(mm)
Y component	-76.85±5.06(mm)	-103.09±9.59(mm)
Z component	92.22±6.05(mm)	95.73±5.20(mm)

Table 1 - The average distance from the origin of PAF in x, y, and z directions of all subjects (mean±SD).

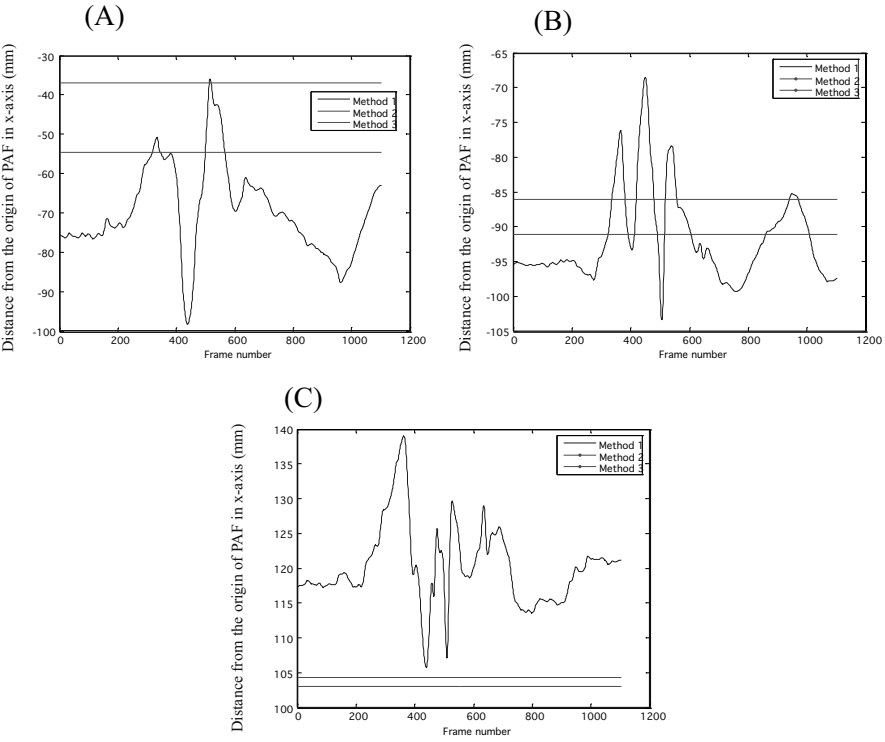

Figure 2 - The distance from the origin of PAF of a subject (A) X-axis component, (B) Y-axis component, and (C) Z-axis component.

3.2 Comparisons of the knee and hip joint angle

The results of average angles of MKF and MHE in three methods were shown in Table 2. In Fig. 3, we showed a time series of knee and hip flexion/extension angle in all methods for a representative subject. The MKF and MHE angles calculated using Method 1 were different from those of Method 2 and 3 significantly. However, both angles had no difference between Method 2 and 3, so we could say Method 1 is not appropriate for kinematic analysis for dynamic exercise, but Method 2 gave almost the same results to that by Method 3 which had been said to be most accurate method (Hicks and Richard, 2005).

	MKF angle	MHE angle
Method 1	101.98±9.69	17.74±5.07
Method 2	97.42±9.62	19.73±5.61
Method 3	96.47±9.05	20.25±5.86

Table 2 - Comparisons of MKF and MHE angles.

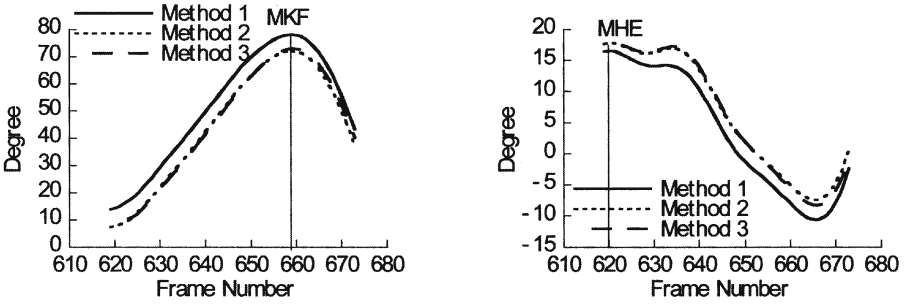

Figure 3 - Time series of knee and hip flexion/extension angles knee (flexion(+)/ extension(–)), hip(extension(+)/flexion(–)).

3.3 Limitations and future works

Although Method 3 have been said to be most accurate estimation method of the HJC location, we can not propose that Method 3 gives the 'true' HJC location. When we estimated the HJC location by Method 2 and 3, we assumed the HJC was a fixed point in the PAF, but actual femoral head might move a little especially in dynamic exercise. However, it can be said that estimated value by Method 1 moves too much in the PAF, because it was influenced by dynamic exercise itself and noise during dynamic exercise. Therefore, we consider Method 2 and 3 were more appropriate estimation method during dynamic exercise. In this research, the estimated value of the HJC location by Method 2 and 3 were different in medial-lateral direction, but that difference did not give much influence on kinematic parameter. However, it was reported a little difference in the HJC location gave much influence on hipjoint moment(Stagni *et al.*, 2000). We will argue on how the difference in the hip joiny centre location influence on kinetic parameters during dynamic exercise in a future work.

4- Conclusions

For kinematic analysis of instep kicking motion, Method 2 gave almost the same results with Method 3 which had been said to be most accurate method. Method 1 gave signi-

ficantly different results from Method 2 and 3, so Method 1was not recommended for use when we analyse dynamic exercise. Although Method 2 gave significantly different estimation results of the HJC location in the medial-lateral direction, it can be said that we should use Method 2 for kinematic analysis of dynamic exercise, such as instep icking motion because of its accuracy and easiness of application.

5- Acknowledgements

The authors would like to thank K.Miura and H.Furukawa, NTT DoCoMo R&D Centre for providing the experimental circumstance in this study.

6- References

[CC1] Camomilla V., Cereatti A., Vannozzi G., and Cappozzo A. An optimized protocol for hip joint centre determination using the functional method, In Journal of Biomechanics 39, 1096-1106, 2006

[HR1] Hicks JL. and Richards JG. Clinical applicability of using spherical fitting to find hip joint centers, In Gait and Posture 22, 138-145, 2005

[GL1] Gamage SSHU. and Lasenby J. New least squares solutions for estimating the average centre of rotation and axis of rotation, In Journal of Biomechanics 35, 87-93, 2002

[H1] Halvorsen K. Bias compensated least square estimate of the centre of rotation, In Journal of Biomechanics 36, 999-1008, 2003

[SL1] Stagni R., Leardini A., Cappozzo A., Benedetti MG., Cappello A. Effects of hip joint centre mislocation on gait analysis results, In Journal Biomechanics 33, 1479-1487, 2000

Kinematics and EMG Analysis of Expert Pole Vaulter's Lower Limb During Take off Phase (P218)

Maud Bassement[1]*, Cyril Garnier[1], François-Xavier Lepoutre[1], Mark Goss Sampson[2]

Topics: Motor control, biomechanics.

Abstract: Introduction: The critical phase, in jumping events in track and field, appears to be between touchdown and take-off. Since obvious similarities exist between the take off phase in both long jump and pole vault, numerous 3D kinematics and electromyographic studies have only looked at long jump. Currently there are few detailed kinematics electromyographic data on the pole vault take-off phase. The aim of this study was therefore to characterise kinematics and electromyographic variables during the take-off phase to provide a better understanding of this phase in pole vaulting and its role in performance outcome.

Material and methods: Six pole-vaulters took part in the study. Kinematics data were captured with retro reflective markers fixed on the body. Hip, knee and ankle angle were calculated.

Differential bipolar surface electrodes were placed on the following muscles of the take-off leg: tibialis anterior, lateral gastrocnemius , vastus lateralis , rectus femoris , bicep femoris and gluteus maximus. EMG activity was synchronously acquired with the kinematic data. EMG data were rectified and smoothed using a second order low pass Butterworth Bidirectional filter (resulting in a 4th order filter) with a cut-off frequency of 14 Hz.

Results: Evolution of hip, knee and ankle angle show no significant differences during the last step before touchdown, the take-off phase and the beginning of fly phase.

Meanwhile, strong differences in EMG signal are noted inter and intra pole vaulter.

However for a same subject the EMG activities seem to converge to some phase locked point.

Discussion: All pole vaulters have approximately the same visible coordination

This coordination reflects a different muscular control among pole vaulters but also for a considered pole vaulter. These phase locked point could be considered as invariant of motor control i.e. a prerequisite for a normal sequence of the movement and performance realization.

Key words: EMG, motion analysis, Take-off, Pole-vaulting, Performance.

1. Université de Valenciennes, LAMIH – UMR CNRS 8530, Le mont Houy, 59313 Valenciennes Cedex 09, France - E-mail : (maud.bassement, cyril.garnier, Francois-xavier.lepoutre)@univ-valenciennes.fr

2. Centre for Sport and Exercise Science, School of Science, University of Greenwich, Chatham Maritime, Kent ME4 4TB - E-mail : M.A.Goss-Sampson@greenwich.ac.uk

1- Introduction

The pole vault is one of four jumping events in track and field. Many factors come into play in the event; physical, psychological, and even environmental factors. All have an influence. Successful competitors must have a variety of qualities, including height, speed, strength, confidence, jumping ability, correct technique, and mental preparedness. The choice of pole can also affect a vaulter's jump considerably: too elastic, and it will cause the vaulter to enter too far into the pit, resulting in vaulting under the bar; too stiff, and it can throw the vaulter backwards, to land back on the runway or in the metal box into which the pole was planted. The athletes' principal difficulty lies in using their horizontal velocity to obtain the best vertical velocity so that their choice of pole bends as it should to lift them over the bar.

The pole vault in itself is usually broken down into six phases. The first, *the approach*, involves sprinting down the runway. Phase two, *the plant and take-off*, generally begins three steps before the final step of the sprint. During this phase, the athletes work to translate the kinetic energy gathered during the approach into potential energy stored in the pole. During the *swing and row* phase (phase 3), the vaulter swings the take-off leg forward and rows downward with the arms. The hips are extended upward with legs outspread and shoulders down during the *rockback* (phase 4), resulting in the vaulter turning upside down. The *turn* (phase 5) is, as it name implies, is when the vaulter turns 180º, trying to move toward the bar without touching it. During the sixth phase, the *fly-away*, if the previous phases have been executed correctly, energy will be released and will propel the vaulter over the bar.

As a closed skill, pole-vaulting may call upon a specific motor pattern inscribed in long-tem memory, in which the different propositions and relational structures [B1] [SM1] amassed by the expert have been stored. Movements can also be stored in memory as perceptible events, through which anticipated characteristic effects can be represented[MK]. However, muscular patterns can also be considered as an indicator of how the central nervous system produces the movement [C1]. To the best of our knowledge, no experimentation has been done to examine how the pole vaulter's muscles manage the energy transfer needed to execute a jump, though this has been studied for the long jump [KS1]. In that long jump study, an analysis of the take-off phase highlighted the elements needed for success, while also stressing the differences in the muscular and joint coordination of novices and experts. In an effort to explain how the movement is controlled [IC1], electromyographic activity, kinematic data, and ground reaction force have all been used to identify the patterns of intermuscular coordination during both the long jump [KS1] and sprinting [JV1]

The break down of the vault analyzed in this study deals specifically with the *plant and take-off* phase, which we divided into approach, touch-down (TD) and take-off (TO), thus defining a three-step technique. We then analyzed this technique to identify the specific muscular activity and kinematics involved in the jump of a pole vaulter. We postulate that the motor pattern stored by experts is composed of muscular sequences, which are thus segmental, particularly during the touch-down and take-off phases mentioned above. This motor pattern helps to optimize the take-off movement to insure the best energy transfer between the approach and the jump.

Identifying the specific pattern of coordination that is used by experts should increase our understanding of how the central nervous system produces such movement.

2- Methods

Six country-level pole-vaulters (age: 19.8 ± 3.7 years, height 1.7 ± 0.08 m, body mass 62 ±9.5kg) took part in the study, which was conducted according to the Helsinki guidelines. The study was reviewed and approved by the local ethics committee.

For this study an indoor pole vault was installed in the laboratory with a 15m tartan track covered run-up. Prior to capture a $36m^3$ volume centred on the plant box was calibrated (average residual of 1.8 mm) allowing for capture of the two strides prior to take-off through to the first 3m of the vault height. A Z-vertical, X-horizontal and Y-medio-lateral coordinate system was used for the volume capture.

Thirty seven 19 mm soft retro reflective markers were fixed to anatomical landmarks for segment identification and 3D motion tracking. Kinematics data were captured at 200 Hz using a 10 camera (MCU240 Proreflex) retro reflective motion capture system (QTM, Qualisys, Sweden). Following a warm-up period, all participants, wearing their personal spikes and using their preferred poles, carried out at least 8 vaults off a 6 step run-up. The five best technical vaults were then used for subsequent analysis. The marker coordinates used in this study allowed a 12 segment link model to be defined for each participant, the segments being; head-torso, pelvis, left and right foot, shank, thigh, top arm and forearm.

Differential bipolar (10mm centre to centre) surface electrodes (Delsys DE-2.3) were placed along the longitudinal axis of the following muscles of the takeoff leg (left one): tibialis anterior (LAT), lateral gastrocnemius (LGL), vastus lateralis (LVL), rectus femoris (LRF), bicep femoris (LBF) and gluteus maximus (LGlut). A single reference electrode was placed on the 7^{th} cervical vertebral process and all leads connected to the electrodes were secured with tape to avoid artefacts from limb movements. EMG activity was synchronously acquired with the kinematic data at 2000Hz via QTM exported within a C3D file format and subsequently analysed in Visual 3D. EMG data were rectified and smoothed using a second order low pass Butterworth Bidirectional filter (resulting in a 4^{th} order filter) with a cut-off frequency of 14 Hz.

Every trial of each subject was broken down into three phases

The first phase of the technique is the final stride of the *approach*. This step ends just before the touchdown (TD). The second phase begins when the takeoff foot lands on the floor (touchdown: TD) and ends when this foot is lifted off the floor (takeoff: TO). The third phase begins just after the foot leaves the floor and ends when the vaulter gathers the body for the jump. Each phase is normalized and expressed in percentages to make it easier to situate the different elements.

Statistical Analysis

Due to the small group size correlations between the vault height and analysed variables were carried out using the non-parametric Spearman's Rank correlation with significances set at $p<0.05$. T Test was used to determine significant differences ($p<0.05$) between couple variables.

The coefficient of multiple correlation (CMC) used by [KR1] was used in this study to evaluate reproducibility of kinematics and electromyographic waveform data. The coefficient of variance (CV) was also calculated.[MA1].

3- Results

3.1 Kinematics data

The hip angle shows a small standard deviation during the three phases. The hip angle is in constant increase from the first phase until 30% of the third phase. The hip extension continues throughout the two first phases and so after the take-off. After, the hip angle decrease until the end of the movement. The knee angle has a standard deviation smaller in phase 1 and 2 than phase 3. The knee angle increase until 75% of the first phase, then it decrease until the middle of second phase. This decrease occurs during the touchdown. After 50% of the second phase, the knee angle increase until 10% in phase 3. It seems the end of the increase occurs just after the take-off. After this event, the knee angle decrease progressively, corresponding to the phase where the subject brings his body in the posture called the tuck: this is accomplished by tucking both legs in toward the chest. The ankle angle has a standard deviation very large even if the waveform seems to be same during the first and second phases. The third phase show, as the knee angle, a standard deviation more important. As the knee angle, the ankle angle begins by increasing until 75% of the first phase. After what, the ankle angle decrease until the middle of phase 2 and then increase until 10% of the phase 3. As the knee angle that occurs just after the take-off, but the ankle angle not decrease after this peak. It seems to stay stable until 75% of phase 3.

The phase 3 is different by subject technique that could explain the variability of both angle and time. This phase depend also of the realization of this type of jump, not really an entire jump.

The CMC representing inter subject repeatability between waveforms for joint kinematics are shown in Table 1. The repeatability is the best for the movements of the hip. Considering phase by phase the repeatability are better during the second phase than other phases for the knee angle and for the ankle angle. The ankle angle had lower reproducibility than the other angle.

	HIP	KNEE	ANKLE
CMC all phase	0 .94	0 .64	0.52
CMC phase 1	0.8	0.58	0.00
CMC phase 2	0.8	0.90	0.25
CMC phase 3	0.89	0.59	0.00

Table 1 - CMC of waveforms for hip, knee and ankle joint kinematics.

Determinations coefficients (r2) are calculated for each subject for each phase to establish the correlation between each jump for the same subject. A r2 above 0.77 are considered to correspond to acceptable correlation. The phase where it's found a r2 above 0.77 are noticed in table 2. These results (table 2) show invariants intra subject. For each expert, the hip angle is the same for each jump during all phases. Only the

second subject shows variability in his pattern for this angle in phase 3. For the knee angle, each expert shows repeatability in their jump for phase 1, 2 and 3 except for the two first subjects, there is variability in phase 3. For ankle angle, each expert shows invariants in their jump during phase 2, and for 4 subjects out of six in phase 1 and for 2 subjects out of six in phase 3.

This whole kinematics results reveal that it exist invariant both each subject and the expert group. Actually, if experts have invariant intra subject and inter subject in phase 1 for the hip angle, we can say the group of expert have the same pattern for hip angle in phase 1. That's certain for hip angle in phase 1 and 2, and for knee angle in phase 2.

	HIP	KNEE	ANKLE
Subject 1	Phase 1, 2, 3	Phase 1, 2	Phase 1, 2, 3
Subject 2	Phase 1, 2	Phase 1, 2	Phase 1, 2
Subject 3	Phase 1, 2, 3	Phase 1, 2, 3	Phase 2
Subject 4	Phase 1, 2, 3	Phase 1, 2, 3	Phase 1, 2, 3
Subject 5	Phase 1, 2, 3	Phase 1, 2, 3	Phase 2
Subject 6	Phase 1, 2, 3	Phase 1, 2, 3	Phase 1, 2

Table 2 - Phases for which correlations among waveforms for hip, knee and ankle joint kinematics are found for each subject.

3.2 Electromyographic data

The muscular activity permits the movement of segment, so have to be the origin of these kinematics invariants.

The CMC and CV of each muscle, among the pole-vaulters, are transcript in the table3 and permit to show a high CMC even if the CV is high too. For the LBF, the CMC are lower than the other muscle correlation. The highest correlation is LGL value of CMC.

	LGL	LAT	LBF	LGlut	LRF	LVL
CMC	0.89	0.87	0.68	0.80	0.82	0.85
CV	40.7 %	21.7 %	40.6%	66.3	40%	53%

Table 3 - CMC and CV for the averaged electromyographic activity of the six subjects.

The CV values of LGlut are higher than the values of other muscle. The value for LAT is only 21.7%, is the lowest. There is lots of variation between subjects, but the waveform seem be repeatability between all subjects.

Table4 shows the muscle for which there are correlation for each phase and each subject. The instant of TD and TO are also tested 2% before and after the moment.

For all subject the waveform of LRf during phase 1 and at TD show repeatability intra subject. That is also the case for LGL at TO.

Phases 1, 2, 3 are cut every 25% to locate more precisely the phase locked point.

In phase 1, LVL show locked point for the first 3/4 of the phase 1, except for subject 4 and 5 between 50 and 75%, for LAT is between 0 and 25% for all subjects except second subject, for the LRF between 50 and 100% for all subjects and also 25 and 50% for all subject except the subject 4 and for LGL is between 0 and 25% for subject 1, 3, 4 and 5.

	PHASE 1	TD	PHASE 2	TO	PHASE 3
Subject1	LVL, LRF	LAT, LGL, LRF	LGL, LVL, LRF	LGL, LRF	
Subject 2	LVL, LRF	LAT, LGL, LVL LRF, LGlut	LGL, LRF, LVL	LAT, LGL, LRF	
Subject 3	LVL, LRF	LVL, LRF	LGL, LVL	LAT, LGL, LVL LGlut	LRF
Subject 4	LRF, LBF, LGlut	LBF, LRF	LGL, LAT, LRF	LGL, LRF	LAT, LVL
Subject 5	LVL, LRF	LVL, LBF, LRF	LVL	LGL	
Subject 6	LGL, LAT, LVL LRF, LGlut	LRF	LGL, LAT, LRF	LGL, LVL, LRF	LRF

Table 4 - Correlated muscles during each phase and at TD and TO for each subject.

In phase 2, LVL show locked point between 50 and 75% for all subjects, for LGL is between 50 and 75% for all subjects and 75 and100% for all subjects except the second one.

In phase 3 there isn't phase locked point

These results show, as for kinematics' data, there are invariants in expert muscular activity. LRF, LAT, LGL and LVL in phase 1, LGL and LVL in phase 2. The difference of muscle activated during the movement seem show a difference about the control way. For the subject 1, 2, 4 and 6 for example, during all the movement the LRF have the same activity during all of their jumps. And for the subject 3 and 5 there are correlation in all jumps for the LVL. As these muscles are antagonist we can ask the question of the preferred muscle for guide the movement.

4- Discussion

The results of the present study indicate that, first, expert in pole-vaulting exhibit a similar movement to realize their performance. That kinematic is the result of learning and of an optimization of what have to be done to realize the jump. Second, the results emphasize, also, the motor pattern used by the athletes to produce that movement. If there is phase locked-point among the athletes, each one is using particular motor pattern to produce the same movement at some instant. That similarity among the take-off is showing the presence of individual motor program that is used by the athletes to produce a similar gesture. But, the differences among athletes are the reflection of personal experience, that is to say the way brain is using to create a movement.

The pole vaulting is a motor realization which seems to be optimized according to the required goal, i.e. to transform horizontal velocity in vertical velocity to bend the pole and realize the performance. To the best of our knowledge, no study has been realized on the muscular activity during pole vaulting. This experiment shows such activity and tries to make the connections between such activity and the angular evolution of the athletes showing the lower limb muscular coordination used by the experts to optimize energetic transfer.

The energetic transfer in pole vaulting has, to our knowledge, been studied relatively little; the articles published have been primarily in the field of biomechanics [AS1]; [MC1];[SA1][SA2]. The research that has been done has sought to improve the pole vaulter's technique by identifying performance criteria and by describing the forces exerted by the vaulters on the pole as well as those engendered by the pole itself. [MC1]

attempted to study the "take-off phase more precisely". In fact, this phase has been identified by several researchers as the principle parameter for success in pole vaulting [H1]. The take-off appears to be a key part of a successful jump, in that it is during this phase that the kinetic energy created during the approach and stored in the pole is transmitted to allow the vaulter to cross over the bar. It is the potential internal energy of the pole, combined with muscular efforts of the lower limbs, that propels pole vaulter to the highest possible point. Thus, this essential take-off phase must be better controlled to permit a more efficient exchange of energy [L1].

According to gesture, there is strong correlation among the athletes. To realize the energetic transfer, they use the same movement coordination in accordance with what the coach is expected. To succeed the switch, the experts need to increase the rigidity of his leg to decrease absorption and to allow an optimal transmission of energy forwards for the success of the jump. Our results on the jump with the pole are in agreement with the studies of Farley [FH1] or Jacobs [JV1] concerning the race, or like Laffaye [LT1] on the jump. These studies show that an angle of the knee more closed reduced rigidity of the leg while decreasing the shock by absorption. The experts of this study seem to have optimized this part of phase 1 by having a strong rigidity of the leg. Then on top of the angle of the knee, the angle of ankle must allow the success of the switch. An angle of ankle more closed must allow a better restitution of energy for the success of the jump. The evolution of these angles requires training for the technical realization. This training will allow a better motor control of the articulations by the intermediary of muscular activities.

According to muscular activities, all the subjects exhibit the same activity of LRf during phase 1 and at TD. That is also the case for LGL at TO. Such activities could be considered as phase locked point i.e. invariant of motor control among the athletes. To realize a correct take-off, convenient with the coach attempt, pole-vaulters need to acquire a prerequisite for a normal sequence of the movement and performance realization. That prerequisite is hitting by the LRf and LGL at key moment. Such activities have to be performed at correct moment. To realize that, each athlete is using different muscular strategies. But, for one athlete, it is always the same strategy that is used. For example, at TD, subject 3 is using the LVL while subject 4 is using the LBF.

The results of that study show that to realize a same movement, in the kinematic level, experts in pole-vaulting have learn a specific motor control with concordance in muscular activities for specific instant. But, to rise that moment, athletes are using different motor strategies which are to be correlated with their own experience. To produce a complex movement, the central nervous system is making use of specific individual motor program.

More studies are needed to better understand how the central nervous system manages a known movement but also, to produce a new one. In that case, the central nervous system might make use of parts of a motor program. If there is a motor program for pole-vaulting take-off, it might have some similarities with the one used to perform take-off in long-jump or hurdles for example which are similar activities in demand of using horizontal velocity to obtain the best vertical velocity.

5- References

[AS1] Arampatzis A. Shade F. and Bruggeman G.P. Effect of the pole-human body interaction on pole vaulting performance. Journal of biomechanics 2004; 37: 1353-1360

[B1] Bernstein N. The coordination and regulation of movement. In Pergamon Press: London 1967

[C1] Cassim F. Le contrôle moteur: quels outils neurophysiologiques pour l'explorer? Abstracts/ Neurophysiologie clinique 2002; 32: 275-283

[FH1] Farley, Houdjik, Van Strien, Louies. Mechanism of leg stiffness adjustement for hopping on surface of different stiffnesses. Journal applied Physiology 1998; 85: 1044-1055

[H1] Hay J. The take-off in the long jump and other running jump. Scientific Proceeding ISBS 1999

[IC1] Ivanenko Y., Capellini G., Dominici N., Poppele R.E. and Lacquaniti F. Coordination of locomotion with voluntary movements in humans. Journal of neuroscience, 2005; 25(31):7238-7253

[JV1] Jacobs R. and Van Ingen Schenau G.J Intermuscular coordination in a sprint push-off. Journal of biomechanics, 25(9): 953-965, 1992

[KR1] Kadaba M.P., Ramakrishnan H.K., Wootten M.E., Gainey J., Gorton G. and Cochran G.V.B., Repeatability of Kinematic, Kinetic, and Electromyographic Data in Normal Adult Gait, Journal of Orthopaedic Research, 7 (6): 849-860, 1989.

[KS1] Kakihana W., Suzuki S. The EMG activity and mechanics of the running jump as a function of take-off angle. Journal of Electromyographie and Kinesiology; 11: 365-372, 2001

[L1] Linthorne N.P. Energy loss in the pole vault take-off and the advantage of the flexible pole. Sports Engineering; 3: 205-218, 2000

[LT1] Laffaye G., Taiar R., Bardy B.G. Effet de l'instruction sur la regulation de la raideur des members inférieurs lors de saut en contre haut. Sciences et sport, 20 (3) :136-143, 2005

[MA1] Morey-Klapsing G., Arampatzis A. and Brüggemann G. P. Choosing EMG parameters: comparison of different onset determination algorithms and EMG integrals in a joint stability study, Clinical Biomechanics, 19: 196–201, 2004

[MC1] Morlier J, Cid M. Three-dimensional analysis of the angular momentum of a pole vaulter. J. Biomechanics; 29(8): 1085-1090, 1996

[MK1] Mechsner F, Knoblich G. Do muscles matter for coordinated action? Journal of Experimental Psychology: human perception and performance; 30 (3): 490-503, 2004

[SA1] Schade F, Arampatzis A, Bruggemann G.P. Reproductibility of energy parameters in the pole vault. Journal of biomechanics; 39: 1464-1471, 2006

[SA2] Schade F. Arampatzis A, Bruggeman G.P. Influence of different approaches for calculating athlete's mechanical energy on energetic parameters in the pole vault. Journal of Biomechanics; 33: 1263-1268, 2000

[SM1] Schack T. and Mechsner F. Representation of motor skills in human long-term memory. Neuroscience Letters; 391: 77-81, 2006

Ventilation: a Reliable Indicator of Oxygen Consumption During Physical Activities of Various Intensities? (P222)

Gastinger, S.[1], Nicolas, G.[1], Sorel, A.[1], Gratas-Delamarche, A.[1], Zouhal, H.[1], Delamarche, P.[1], Prioux, J.[2]

Abstract : Several methods have tried to quantify physical activity using the relation between heart rate (HR) and oxygen consumption ($\dot{V}O_2$). Considering the limits of this relation, we focus our work on another physiological index: ventilation ($\dot{V}_E$). The aim of this study is to show that $\dot{V}_E$ is more strongly correlated with $\dot{V}O_2$ than HR. Eight male subjects carried out four physical activities of various intensities: walking at 4 km.h^{-1}, walking at 4 km.h^{-1} with load, running at 8 km.h^{-1} and cycling at 60 W. The ventilatory parameters ($\dot{V}O_2$ and $\dot{V}_E$) were measured by a portable indirect calorimetry system (VO2000 MedGraphics) and HR was measured with a cardiofrequencemeter. Coefficients of determination (r^2 linear) of the relations $\dot{V}O_2$= f ($\dot{V}_E$) and $\dot{V}O_2$= f (HR) were calculated for each subject (on each activity [r^2_{Ttot}: 64 regressions], on all the four activities [$r^2_{4activities}$: 16 regressions]) and then for the eight subjects joined together on all the four activities (r^2_{global}: 2 regressions). Results showed that the r^2_{Ttot} of the relation $\dot{V}O_2$= f ($\dot{V}_E$) were significantly higher than those of the relation $\dot{V}O_2$= f (HR) for the tasks: walking at 4 km.h^{-1} ($p<0.001$), walking at 4 km.h^{-1} with load ($p<0.001$), running at 8 km.h^{-1} ($p<0.05$). The mean values of $r^2_{4activity}$ of the relation $\dot{V}O_2$= f ($\dot{V}_E$) were significantly higher than those of the relation $\dot{V}O_2$= f (HR) ($p\leq0.001$). Finally, the r^2_{global} of the relation $\dot{V}O_2$= f ($\dot{V}_E$) were higher than those of the relation $\dot{V}O_2$ = f (HR). In view of these results, it seems that $\dot{V}_E$ is more strongly correlated with $\dot{V}O_2$ than HR. This approach seems very promising in order to develop a new method for the quantification of physical activity. Nevertheless, other experiments with a more significant number of subjects and activities have to be carried out to validate this first study.

Key words: Physical activity, ventilation, heart rate, oxygen consumption.

1. Laboratoire Mouvement, Sport, Santé (M2S) : Physiologie et Biomécanique. UFR APS, Université Rennes 2. Avenue Charles Tillon – CS 24414 – 35044 Rennes Cedex. - Gastinger Steven: gastingersteven@yahoo.fr, steven.gastinger@univ-rennes2.fr - Gratas-Delamarche Arlette : arlette.delamarche@univ-rennes2.fr - Zouhal Hassane: hassane.zouhal@univ-rennes2.fr - Nicolas Guillaume: guillaume.nicolas@univ-rennes2.fr - Sorel Anthony: anthony.sorel@univ-rennes2.fr - Delamarche Paul: paul.delamarche@univ-rennes2.fr

2. ENS – Cachan. Antenne de Bretagne, Campus de Ker-Lann. 35170 Bruz Cedex - Prioux Jacques: jacques.prioux@bretagne.ens-cachan.fr

1- Introduction

Physical activity represents the most variable part of the human energy expenditure (Ravussin and Gautier 2002). This activity is mainly composed of NEAT (Not Exercise Activity Thermogenesis) which can be divided into body postures (sitting and standing), activities of ambulation and fidgeting (Levine, 1999). To consider total daily energy expenditure (TDEE) under free living conditions, one of the most current approaches consists in using the relation between heart rate (HR) and oxygen uptake ($\dot{V}O_2$) ($\dot{V}O_2 = (HR \times V_{es}) \times (CaO_2 - C\dot{V}O_2)$), where V_{es} represents the volume of systolic ejection ($ml.min^{-1}$), CaO_2 is the amount of oxygen carried by arterial blood ($ml.100ml^{-1}$) and $C\dot{V}O_2$ is the amount of oxygen carried by venous blood ($ml.100ml^{-1}$)). This method was very largely studied (Garet *et al.*, 2005, Kurpad *et al.*, 2005, Hiilloskorpi *et al.*, 2003, Livingstone *et al.*, 2000, Rayson *et al.*, 1995) and proves to be adapted to estimate TDEE: the cardiofrequencemeter is an easily portable device which does not present any invasive character. Nevertheless, the use of HR to consider energy expenditure (EE) can be criticized, because of the variability of this parameter during activities of low and very high intensities (Achten and Jeukendrup. 2003, Haskell *et al.*, 1993). The same way, many other studies (Davidson *et al.*, 1997, Montoye *et al.*, 1996, Melanson and Freedson 1996) showed that emotional stress, high ambient temperature, high water content, dehydration, body posture or diseases may imply HR variations without any $\dot{V}O_2$ variation. All these limits account for the difficulties of measuring a precise EE from HR measurements. Thus, we propose to explore another physiological parameter, complementary of HR, which is also in strong relation with $\dot{V}O_2$.

Ventilatory output or ventilation ($\dot{V}_E$) also varies during physical activity (Wasserman *et al.*, 1986, Saltin and Astrand 1967). To the best of our knowledge, the use of $\dot{V}_E$ to estimate EE, from its relation with $\dot{V}O_2$ ($\dot{V}O_2 = \dot{V}_E \times (FiO_2 - FeO_2)$), where FiO_2 represents the fractional concentration of O_2 in inspired air and FeO_2 is the fractional concentration of O_2 in expired air was never carried out, contrary to HR. However, $\dot{V}_E$ does not necessarily require the use of a facial mask to be measured. McCool *and al.*, (2002) indeed proposed a light and portable system to measure $\dot{V}_E$ based on 4 coupled magnetometers. This system, compared with the measurement carried out by spirometry, enables a precise measurement of tidal volume (V_T), inspiratory (T_I) and expiratory time (T_E), in sitting and standing position and condition of exercise. Considering this new technology, it may now be possible to use $\dot{V}_E$ in order to estimate TDEE. Such an approach may therefore provide new prospects to TDEE estimation, compared to the limitations of HR measurements. The use of $\dot{V}_E$ seems justified since, in the field of psychophysiology, Rousselle *and al.* (1995) showed that a mental stress induced a sharp increase in cardiac performance (HR and cardiac flow: $\dot{Q}$) before its fast reduction, whereas the respiratory answer ($\dot{V}_E$ and $\dot{V}O_2$) remained stable. Furthermore, this study showed that a physical exercise involved a concomitant increase in the cardiovascular and respiratory performances. Nevertheless, it may be questioned which of the two parameters $\dot{V}_E$ or HR is better correlated with $\dot{V}O_2$. The purpose of this methodological study is to answer this question during daily life activities. In order to examine this problem, we postulate the following hypothesis: when the intensity of exercise is light to moderate, $\dot{V}_E$ is more strongly correlated with $\dot{V}O_2$ than HR. Thus $\dot{V}_E$ would be a para-

meter more reliable than HR, but also complementary of HR, to appreciate $\dot{V}O_2$ and estimate ultimately EE. This second point will not be investigated in this study and will be the subject of later experiments. To validate our assumption we compared the relations $\dot{V}O_2 = f(HR)$ and $\dot{V}O_2 = f(\dot{V}_E)$ during four physical activities of various intensities.

2- Materiel and methods

2. 1 Subjects

Eight healthy males, aged 25.5 ± 0.96 years, voluntarily took part in this study. The mean size and weight (± their standard error (SE)) were 182 ± 1.78 cm and 74.5 ± 2.00 kg respectively. A written assent has been signed by each subject who had been informed about the development of the study. The protocol had been approved by the local ethics committee. The subjects did not present any pathological disorder and had a healthy diet.

2.2 General organization

Each subject carried out four different physical activities on a treadmill (Gymrol, Super 2500) and on a cycle ergometer (Ergomeca). Each activity was maintained for a 6 minutes period. The protocol began with a walk at 4 $km.h^{-1}$, interrupted by a 2 minutes rest period, then followed with a walk at 4 $km.h^{-1}$ with load. The load applied to the subject was a backpack stuffed with 5 kg. After 2 minutes of rest, each subject carried out a running exercise at 8 $km.h^{-1}$, followed by a 4 minutes rest period, and realized a cycling exercise at 60 W. Each subject had the instruction to remain silent during exercises or rests periods. Each subject was verbally encouraged to continue its effort.

2.3 Gas exchange and heart rate measurements

During each physical activity, gas exchange was measured using a portable system (VO2000 MedGraphics) in order to determine $\dot{V}O_2$ ($l.min^{-1}$) and $\dot{V}_E$ ($l.min^{-1}$). These parameters were recorded breath-by-breath and all the seven cycles, the two extreme values (maximum and minimal) were removed. Before each series of test, the gas analyser was calibrated in an automatic way. A pump enabled to take samples of room air, a valve generated the microsamples, and the sensors measured the content of oxygen (O_2) and carbon dioxide (CO_2). The ambient temperature and the barometric pressure were also measured by the device. A cardiofrequencemeter (Polar T31) placed on the thorax, monitored continuously the heart rate (HR), and was synchronized with the gas exchange measurements.

2.4 Estimate of maximal theoretical oxygen consumption ($\dot{V}O_2max$) of the subjects

The theoretical $\dot{V}O_2max$ of the subjects was calculated using the formula below (Wasserman *et al.*, 1987). It corresponds to the theoretical $\dot{V}O_2max$ which would be obtained during a treadmill test. It applies to a non-obese male population and takes into account the age (in years) and the weight (in kg) of the subjects:

$$\dot{V}O_2max \text{ (theoretical)} = \text{weight} \times (56.36 - [0.413 \times \text{years}])$$

2.5 Statistical analyses and results expression

The calculation of the coefficients of determination (r^2) (see Table 1) was carried out from the following methodology. For each subject (n=8) and each activity (n=4), a linear regression was established between $\dot{V}O_2$ and $\dot{V}_E$ on the one hand and between $\dot{V}O_2$ and HR on the other hand (*i.e.*, 64 regressions). From each regression, $\dot{V}O_2 = f(HR)$ and $\dot{V}O_2 = f(\dot{V}_E)$, r^2 was calculated over the total time (Ttot) of each activity. At the end, two r^2_{Ttot} were thus determined by activity for each subject. For each activity, all the individual values of r^2_{Ttot} were averaged and are reported in Table 1.

	$\dot{V}O_2 = f(\dot{V}_E)$	$\dot{V}O_2 = f(HR)$
Subjects (n = 8)	r^2_{Ttot}	r^2_{Ttot}
Walking without load at 4 km.h^{-1}	0.82 (***)	0.32
Walking with load at 4 km.h^{-1}	0.85 (***)	0.28
Running at 8 km.h^{-1}	0.95 (*)	0.79
Cycling at 60 W	0.79^{NS}	0.55

: Significant difference between the r^2_{Ttot} (: $p<0.05$, ***: $p<0.001$)

^{NS}: No significant difference

Table 1 - Coefficient of determinations (r^2_{Ttot}) from the relations $\dot{V}O_2 = f(\dot{V}_E)$ and $\dot{V}O_2 = f$ (HR.) over the total duration of each activities.

In the second step of our analysis, the data set of $\dot{V}O_2$, $\dot{V}_E$ and HR of the four activities were gathered for each subject. From the data collection of each subject, a linear regression was established between $\dot{V}O_2$ and $\dot{V}_E$ on the one hand and between $\dot{V}O_2$ and HR on the other hand (*i.e.*, 16 regressions). The $r^2_{4activities}$ of each regression as well as the respective averages were calculated (Table 2).

Finally, the data set of $\dot{V}O_2$, $\dot{V}_E$ and HR of the four activities was gathered. From this representation (see Graph 1), a linear regression was established between $\dot{V}O_2$ and $\dot{V}_E$ on the one hand and $\dot{V}O_2$ and HR on the other hand (*i.e.*, 2 regressions).

The use of the Mann Whitney test enabled us to calculate the level of signification of the correlations and to specify if there exist a significant difference or not between the r^2_{Ttot} from the relations $\dot{V}O_2 = f(HR)$ and $\dot{V}O_2 = f(\dot{V}_E)$ during the same activity. The same test was applied to calculate the level of signification for the mean values of $r^2_{4activities}$.

	$\dot{V}O_2 = f(\dot{V}_E)$	$\dot{V}O_2 = f(HR)$
Subjects (n = 8)	$r^2_{4activities}$	$r^2_{4activities}$
Subject 1	0.977	0.841
Subject 2	0.985	0.839
Subject 3	0.970	0.922
Subject 4	0.985	0.752
Subject 5	0.984	0.840
Subject 6	0.986	0.948
Subject 7	0.906	0.731
Subject 8	0.955	0.847
Mean	0.969 ($^{£££}$)	0.84
SE	0.0097	0.0261

$^{£}$: Significant difference between the $r^2_{4activités}$ ($^{£££}$: $p<0.001$)

Table 2 - Coefficient of determination ($r^2_{4activities}$) from the relations $\dot{V}O_2 = f(\dot{V}E)$ and $\dot{V}O_2 = f(HR)$, for each subject, over the total duration of all four physical activities.

The mean values of $\dot{V}O_2$ of the subjects during the four activities were calculated in the following way. For each subject, the mean value of $\dot{V}O_2$ of the four activities was calculated over the total time of exercise. These individual values of $\dot{V}O_2$ were then averaged to obtain the four $\dot{V}O_{2mean}$ of the studied activities. These values made it possible to determine the intensity level of the various activities. A one way repeated measures ANOVA test (followed by Tukey test) was carried out to compare the mean values of $\dot{V}O_2$ of the subjects. Values of $p<0.05$ were considered significant.

3- Results

3.1 Coefficient of determination over the total duration of the four physical activities:

The mean values of the r^2_{Ttot} from the relations $\dot{V}O_2 = f(HR)$ and $\dot{V}O_2 = f(\dot{V}_E)$ for the four studied activities are represented in Table 1. The r^2_{Ttot} of the linear regressions from the relation $\dot{V}O_2 = f(\dot{V}_E)$ are significantly higher than those obtained from the relation $\dot{V}O_2 = f(HR)$ for the walk at 4 $km.h^{-1}$ without ($p<0.001$) and with load ($p<0.001$), and for the running at 8 $km.h^{-1}$ ($p<0.05$). No significant difference is observed between the r^2_{Ttot} of the linear regression, during cycling exercise at 60 W.

3.2 Coefficient of determination, by subject, over the total duration of all four physical activities

The individual values of the $r^2_{4activities}$ from the relations $\dot{V}O_2 = f(HR)$ and $\dot{V}O_2 = f(\dot{V}_E)$ for all four studied activities are represented in Table 2. The $r^2_{4activities}$ of the linear regressions from the relation $\dot{V}O_2 = f(\dot{V}_E)$ are always higher than those obtained from the relation $\dot{V}O_2 = f(HR)$. The mean value of $r^2_{4activities}$ of the linear regression calculated for the relation $\dot{V}O_2 = f(\dot{V}_E)$ is significantly higher than that obtained from the relation $\dot{V}O_2 = f(HR)$ ($p<0.001$).

3.3 Coefficient of determination of the eight joined together subjects, over the total duration of all four physical activities

The r^2_{global} from the relations $\dot{V}O_2 = f(HR)$ and $\dot{V}O_2 = f(\dot{V}_E)$ for the four studied activities are respectively $r^2_{global} = 0.583$ and $r^2_{global} = 0.949$. Graph 1 represents the linear regressions from the relations $\dot{V}O_2 = f(\dot{V}_E)$ and $\dot{V}O_2 = f(HR)$ for the eight joined together subjects.

3.4 Estimated mean values of $\dot{V}O_2$max of the subjects and mean values of $\dot{V}O_2$ of all subjects during the four activities

The mean value of the theoretical $\dot{V}O_2$max of the subjects is 3.4 ± 0.10 l.min^{-1}. Our results show that the mean value of the highest $\dot{V}O_2$ is observed during running at 8 km.h^{-1} ($\dot{V}O_{2mean} = 1.97 \pm 0.09$ l.min^{-1}). The mean values of $\dot{V}O_2$ during cycling, and walking at 4 km.h^{-1} with and without load are respectively 1.15 ± 0.07 l.min^{-1}, 0.83 ± 0.06 l.min^{-1} and 0.81 ± 0.06 l.min^{-1}. The mean values of $\dot{V}O_2$ of the walking activities at 4 km.h^{-1} with and without load are not significantly different from each other ($p=0.998$). On the other hand, all the other mean values of $\dot{V}O_2$ are significantly different the ones from the others ($p<0.05$).

4- Discussion

The aim of this study was to compare the relations $\dot{V}O_2 = f(\dot{V}_E)$ and $\dot{V}O_2 = f(HR)$ during four physical activities of various intensities: walking with and without load, running at 8 km.h^{-1} and cycling at 60 W. All these activities were studied because they correspond to intensities of physical activities found under free living conditions (Ainsworth *et al.*, 2000). Our hypothesis was the following : when the intensity of exercise is light to moderate, $\dot{V}_E$ is more strongly correlated with $\dot{V}O_2$ than HR. Usually, a light intensity exercise is considered at a level lower or equal to 45 % of $\dot{V}O_2$max, and a moderate intensity exercise is between 45 and 65% of $\dot{V}O_2$max (Friedlander *et al.*, 2007). The mean values of $\dot{V}O_2$ observed during the activities of walking with and without load, running at 8 km.h^{-1} and cycling at 60 W vouch for the light to moderate intensity level of these activities.

Our results show significant differences (Table 1) of r^2_{Ttot} in favour of the relation $\dot{V}O_2 = f(\dot{V}_E)$ compared to the relation $\dot{V}O_2 = f(HR)$ for walking with and without load and running at 8 km.h^{-1}. Moreover, a significant difference (Table 2) in $r^2_{4activities}$ in favour of the relation $\dot{V}O_2 = f(\dot{V}_E)$ compared to the relation $\dot{V}O_2 = f(HR)$ is established. At last, the r^2_{global} from the relation $\dot{V}O_2 = f(\dot{V}_E)$ is higher than that from the relation $\dot{V}O_2 = f(HR)$. Thus, our results seem to show that $\dot{V}_E$ is more strongly correlated with $\dot{V}O_2$ than HR. $\dot{V}_E$ would be thereby a more reliable indicator of the level of $\dot{V}O_2$ reached during physical activities of light to moderate intensities. Our hypothesis seems to be confirmed.

To check our hypothesis, we choose to use a linear regression and to compare the two relations $\dot{V}O_2 = f(\dot{V}_E)$ and $\dot{V}O_2 = f(HR)$.

The study of the relation $\dot{V}O_2 = f(\dot{V}_E)$ provides the following equation: $\dot{V}O_2 = \dot{V}_E \times (FiO_2 - FeO_2)$ where FiO_2 represents the fraction of oxygen in inspired air and FeO_2 is the fraction of oxygen in expired air. FiO_2 is a constant parameter (FiO_2 = 20.95% on the sea level). In 1967, Saltin and Astrand showed that the increase of $\dot{V}_E$ in relation with $\dot{V}O_2$ is semi-linear, the progression of $\dot{V}_E$ becoming relatively more important than $\dot{V}O_2$ when the intensities of exercises become high. An exponential increase is observed for high intensities of exercises (> to 65 % of $\dot{V}O_2$max). The intensities of the activities studied being light to moderate, the values of $\dot{V}_E$ and $\dot{V}O_2$ remain located in the linear part of the curve. For this reason, we chose to characterize the relation $\dot{V}O_2 = f(\dot{V}_E)$ by a linear relation.

The relation $\dot{V}O_2 = f(HR)$ is also characterized by a linear relation. This relation is widely accepted for a physical exercise which is progressive, involves important muscular masses and long enough to allow the adaptation of the cardiovascular and ventilatory systems (Astrand and Ryhming 1954). Thus, a linear relation exists for a broad range of intensity of exercise, such as those presented in this study. Nevertheless, during light and very high intensities of activity this relation becomes non-linear (Achten and Jeukendrup 2003).

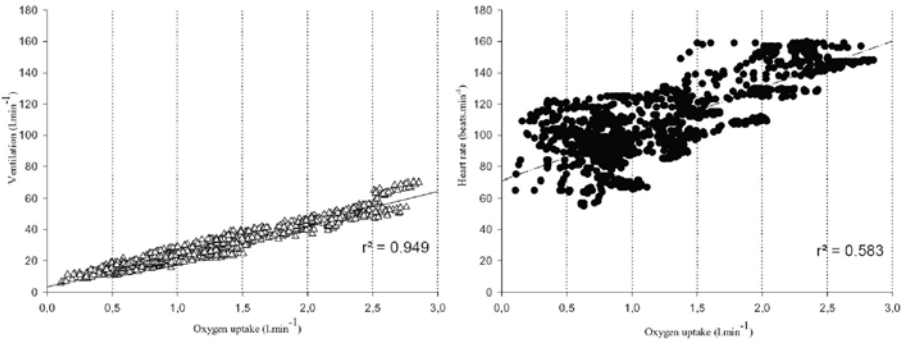

Graph 1 - Linear regressions from the relations $\dot{V}O_2 = f(\dot{V}_E)$ and $\dot{V}O_2 = f(HR)$ on all four physical activities of the eight joined together subjects.

The most interesting result of this study is that $\dot{V}_E$ seems to be a parameter much better correlated with $\dot{V}O_2$ than HR. This is characterized by significant differences of r^2_{Ttot} and $r^2_{4activities}$ in favour of the relation $\dot{V}O_2 = f(\dot{V}_E)$ compared to the relation $\dot{V}O_2 = f(HR)$, during the four physical activities of various intensities. This result is observed by the calculation of the linear regressions carried out on activities studied separately (Table 1), but also by the calculations realized by gathering the activities for each subject (Table 2). Thus, by calibrating the regression for a given individual, it might be possible in the long term to predict $\dot{V}O_2$ from the measurement of $\dot{V}_E$. Moreover, this result is also observed on the eight subjects joined together during the four studied activities (Graph 1).

The differences of r^2_{Ttot}, $r^2_{4activities}$ and r^2_{global} from the relations $\dot{V}O_2 = f(\dot{V}_E)$ and $\dot{V}O_2 = f(HR)$ may be explained by the different mechanisms of control of $\dot{V}_E$ and HR (Strange *et al.*, 1993, Whipp and Ward 1982). To date, no study was able to prejudge, on a strictly physiological level, of the preferentially interest to use HR compared to $\dot{V}_E$ for estimating $\dot{V}O_2$. HR was so far the only usable cardiorespiratory parameter under free living conditions, because HR is easy to measure by mean of a noninvasive device. The easy mode of measurement of HR, in free living condition, is always used in current studies (Kurpad et al. 2005). Nevertheless, it is currently possible to precisely measure V_T, fr, T_I, T_E and to calculate $\dot{V}_E$ thanks to a noninvasive device using magnetometry (Mc Cool *et al.*, 2002). We currently develop a portable magnetometer system, which could permit to measure V_T, fr, T_I, T_E and to calculate $\dot{V}_E$ without any use of a facial mask. Moreover, ventilatory parameters seem less sensitive than HR to variable conditions of temperature and stress, which reinforces the interest to estimate EE in free living condition. It is probable that the use of $\dot{V}_E$ and HR, at the same time, would increase the degree of accuracy in the estimation of EE. Additional work is still to realize to demonstrate this statement.

5- Conclusion

This study shows the innovative and fundamental result that $\dot{V}_E$ is more strongly correlated with $\dot{V}O_2$ than HR during exercises of light to moderate intensities. This hypothesis was checked by comparing the relations $\dot{V}O_2 = f(\dot{V}_E)$ and $\dot{V}O_2 = f(HR)$ established by linear regression during four physical activities of various intensities. This study shows the interest of using at the same time $\dot{V}_E$ and HR to characterize the physical activity of a subject. Nevertheless, other studies with a more significant number of subjects placed in various experimental situations must be realised to confirm our ventilatory hypothesis. Such studies could aim to test the relations $\dot{V}O_2 = f(\dot{V}_E)$ and $\dot{V}O_2 = f(HR)$ on varied intensities exercises (walking without and with load) and on intermittent exercises (walking / running transition).

6- References

[AJ1] Achten, J., Jeukendrup, AE. Heart rate monitoring: applications and limitations. Sports Med. 33(7): 517-38. Review, 2003

[AH1] Ainsworth, BE., Haskell, WL., Whitt, MC., Irwin, ML., Swartz, AM., Strath, SJ., O'Brien, WL., Bassett, DR. Jr., Schmitz, KH., Emplaincourt, PO., Jacobs, DR. Jr., Leon, AS. Compendium of physical activities : an update of activity codes and MET intensities. Med. Sci. Sports Exerc. 32(9): S498-504, 2000

[AR1] Astrand, PO., Ryhming, I. A nomogram for calculation of aerobic capacity (physical fitness) from pulse rate during sub-maximal work. J. Appl. Physiol. 7 (2): 218-21, 1954

[DM1]Davidson, L., McNeill, G., Haggarty, P., Smith, JS., Franklin, MF. Free-living energy expenditure of adult men assessed by continuous heart-rate monitoring and doubly-labelled water. Br. J. Nutr. 78: 695–708, 1997

[FJ1] Friedlander, AL., Jacobs, KA., Fattor, JA., Horning, MA., Hagobian, TA., Bauer, TA., Wolfel, EE., Brooks, GA. Contributions of working muscle to whole body lipid metabolism are altered by exercise intensity and training. Am J Physiol Endocrinol Metab. 292 (1): E107-16, 2007

[GB1] Garet, M., Boudet, G., Montaurier, C., Vermorel, M., Coudert, J., Chamoux, A. Estimating relative physical workload using heart rate monitoring: a validation by whole-body indirect calorimetry. Eur. J. Appl. Physiol. 94(1-2): 46-53, 2005

[HY1] Haskell, WL., Yee, MC., Evans, A., Irby, PJ. Simultaneous measurement of heart rate and body motion to quantitate physical activity. Med. Sci. Sports Exerc. 25: 109–115, 1993

[HP1] Hiilloskorpi, HK., Pasanen, ME., Fogelholm, MG., Laukkanen, RM., Manttari, AT. Use of heart rate to predict energy expenditure from low to high activity levels. Int. J. Sports Med. 24(5): 332-6, 2003

[KR 1] Kurpad, AV., Raj, R., Maruthy, KN., Vaz, M. A simple method of measuring total daily energy expenditure and physical activity level from the heart rate in adult men. Eur. J. Clin. Nutr. 60(1): 32-40, 2005

[L1] Levine, JA., Eberhardt, NL., Jensen, MD. Role of nonexercise activity thermogenesis in resistance to fat gain in humans. Science 283: 212–214, 1999

[LR1] Livingstone, MB., Robson, PJ., Totton, M. Energy expenditure by heart rate in children: an evaluation of calibration techniques. Med. Sci. Sports Exerc. 32(8): 1513-9, 2000

McCool, FD., Wang, J., Ebi, KL. Tidal volume and respiratory timing derived from a portable ventilation monitor. Chest 122(2): 684-91, 2002

[MF1] Melanson, EL., Freedson, PS. Physical activity assessment: a review of the methods. Crit. Rev. Food. Sci. Nutr. 36: 385-96, 1996

[MK1] Montoye, HJ., Kemper, HCG., Saris, WHM. Measuring physical activity and energy expenditure. Champaign (IL): Human Kinetics: 72-9, 1996

[RG1] Ravussin, E., Gautier, JF. Determinants and control of energy expenditure. Ann. Endocrinol. 63: 96-105, 2002

[RD1] Rayson, MP., Davies, A., Bell, DG., Rhodes-James, ES. Heart rate and oxygen uptake relationship: a comparison of loaded marching and running in women. Eur. J. Appl. Physiol. Occup. Physiol. 71(5): 405-8, 1995

[RB1] Rousselle, JG., Blascovich, J., Kelsey, RM. Cardiorespiratory response under combined psychological and exercise stress. Int. J. Psychophysiol. 20(1): 49-58, 1995

[SA1] Saltin, B., Astrand, PO. Maximal oxygen uptake in athletes. J. Appl. Physiol. 23(3): 353-8, 1967

[SS1] Strange, S., Secher, NH., Pawelczyk, JA., Karpakka, J., Christensen, NJ., Mitchell, JH., Saltin, B. Neural control of cardiovascular responses and of ventilation during dynamic exercise in man. J. Physiol. 470: 693-704, 1993

[WW 1] Wasserman, K., Whipp, BJ., Casaburi, R. Respiratory control during exercise. In: Handbook of Physiology: The Respiratory System, a Control of breathing, sect. 3, Vol 2. Fishman, AP., Cherniak, NS., and Widdicombe, JG., (Eds). Bethesda MD: Am. Physiol. Soc., p. 595-620, 1986
[WH1] Wasserman, K., Hansen, JE., Sue, DY., Whipp, BJ. Principes of exercise testing and interpretations. In Lea and Febiger, Philedelphia (Eds), p. 50-80, 1987
[W1] Whipp, BJ., Ward, SA. Cardiopulmonary coupling during exercise. J. Exp. Biol. 100: 175-9, 1982

Roller Ski Rolling Resistance and its Effects on Elite Athletes' Performance (P225)

Mats Ainegren[1], Peter Carlsson[2], Mats Tinnsten[3]

Abstract: Modern ski-treadmills allow cross-country skiers, biathletes and ski-orienteers to test their physical fitness in a laboratory environment whilst performing classical and free-style (skating) techniques on roller skis. For elite athletes the differences in performance between test occasions are quite small, thus emphasising the importance of knowing the roller skis' rolling resistance in order to allow the correct comparison between the results from different test occasions. In this study the roller skis' rolling resistance has been measured with a fixture on the ski-treadmill. The results show that the rolling resistance is significantly influenced by temperature and weight. The study also investigates the influence of significant changes in rolling resistance on biological variables. The results show that during sub maximal exercise, heart rate, blood lactate concentration, and oxygen uptake are significantly influenced by different rolling resistances.
Keywords: Rolling resistance, roller skis, power, oxygen uptake.

1- Introduction

Modern ski-treadmills allow cross-country skiers, biathletes and ski-orienteers to test their physical fitness in a laboratory environment whilst performing classical and free-style (skating) techniques on roller skis (Rundell 1995, Calbet *et al.* 2005, Holmberg *et al.* 2005). For elite athletes the differences in performance between test occasions are quite small, thus emphasising the importance of knowing the roller skis' rolling resistance (μ_R) in order to allow the correct comparison between the test results.

Only a few authors have studied the μ_R of roller skis. The method described in earlier work is based on force measurements carried out using a skier wearing a backpack filled with varying mass. The skier then tries to distribute his weight evenly on both roller skis, whilst rolling on the treadmill. However, the data presented when using this method shows varying results and no reliability for the method has been presented (Hoffman *et al.* 1990, Hoffman *et al.* 1995, Millet *et al.* 1998). In 1990 Hoffman *et al.* noticed the

1. Swedish Winter Sports Research Centre, Dept. of Health Sciences, Dept. of Engineering, Physics & Mathematics, Mid Sweden University - Email : Mats.Ainegren@miun.se
2. Dept. of Engineering, Physics & Mathematics, Mid Sweden University - Email : Peter.Carlsson@miun.se
3. Dept. of Engineering, Physics & Mathematics, Mid Sweden University - Email : Mats.Tinnsten@miun.se

importance of allowing the roller skis to become warm prior to making force measurements. However, the time needed for the warm-up process was not reported and nor was the difference in μ_R (in Hoffman *et al.* 1990 called the dynamic friction coefficient μ) when comparing warm and cold roller skis. If μ_R is temperature dependent, it could be of great importance to know the temperature when comparing biological results from different test occasions, since the roller skis may have different initial temperatures due to different test histories.

In Ainegren *et al.* (2007) results from a study are presented using a specific method, without human influence, which shows very good repeatability in measuring the μ_R for roller skis. The results from a warm-up study show a significant change in μ_R during the first 30 minutes of rolling on the treadmill, where μ_R decreased to about 60-65% and 70-75% of its initial value for freestyle and classical roller skis respectively. For the following 30 minutes no significant change was observed. A comparison between temperature and μ_R shows that μ_R decreases as long as temperature increases and that a stabilized value of μ_R corresponds to a stabilized temperature in the roller bearings. In contrast to Hoffman *et al.* (1990, 1995), this study shows a significant negative correlation between normal force and μ_R, while only insignificant or small differences in B_R were observed for different velocities and treadmill inclinations.

Earlier studies have investigated the physiological responses to different μ_R. However, the μ_R measurements were made on a ski treadmill while the biological measurements were made outdoors, in other environments and on other surfaces, i.e. on an asphalt oval (Millet *et al.* 1998) and on an asphalt roadway (Hoffman *et al.* 1998). It would thus be of great value to study the biological responses to different rolling resistances as a case where all measurements are made with stationary and comparable conditions. Our questions are whether a significantly different μ_R causes significant changes to heart rate, oxygen uptake, blood lactate, ratings of perceived exertion, cycle rate and cycle length during sub maximal exercise, as well as time to exhaustion on incremental maximal tests? Further, is maximal oxygen uptake dependent on μ_R?

2- Methods

2.1 Subjects and Equipment

A total of twenty (20) elite athletes who compete in cross country skiing, biathlon and ski-orienteering at a national level, volunteered to make physiological tests by roller skiing on a motorized treadmill (RL 3500, 300 · 250 [*cm*], Rodby Innovation AB, Vänge, Sweden). The inclination and velocity was checked using a digital water slope and a tachometer respectively. Five women and five men (age 25.9 SD 5.86, height 174.9 *cm* SD 7.59, weight 66.9 *kg* SD 6.6, *B-Hb* 138.7 $gr \cdot L^{-1}$ SD13.2, pole length 157.6 *cm* SD 6.0 90.2%/body height SD 1.0) performed tests using freestyle technique (gear 3,V2), and four women and six men (age 26.0 SD 5.14, height 176.5 *cm* SD 11.7, weight 72.8 *kg* SD 11.5, *B-Hb* 146.9 $gr \cdot L^{-1}$ SD 9.6, pole length 149.3*cm* SD 9.4 84.6 %/body height SD 0.7) performed tests using classical technique (diagonal stride).

The rolling resistances of the roller skis (Pro-Ski, Sterners, Nyhammar, Sweden) were measured on the treadmill surface in a fixture specially produced for this purpose

(RRMS, Side System AB, Oviken, Sweden) and with the method described in Ainegren et al. (2007). With the coefficient of rolling resistance, B_R, defined as the ratio of the total resisting force to the total normal force, the following relationship was established:

$$\mu_R(N_{Total}, \alpha) = \frac{F_r + F_f}{N_r + N_f} = \frac{S - mg\sin\alpha}{mg\cos\alpha} \quad (1)$$

Angle α is the inclination of the treadmill, S is the force registered in the load cell, m is the total mass on the wheel, g is the acceleration of gravity, N is normal force, F is the force due to rolling resistance, index r and f indicate the rear and forward positions of the forces (on the rear and forward wheel), and N_{Total} is the sum of the normal force on the rear and forward wheels. The power from work loads (P_w) were calculated in units of watts by the power from elevating the transported mass against gravity (P) and overcoming the rolling resistance ($P\mu_R$) with the following equation:

$$P_w = P + P_{\mu_R} = mg\sin\alpha \cdot v + mg\cos\alpha \cdot \mu_R \cdot v \quad (2)$$

where v is the velocity of the treadmill expressed in $m \cdot s^{-1}$. Maximal power output ($P_{W\max}$) performed at incremental maximal tests was calculated with a method used in bicycle research and described in Padilla *et al.* (2000, in Padilla; Wmax = Wf + [(t/240) x 35), with the following equation:

$$P_{W\max} = P_w + P_R \cdot (t/60) \quad (3)$$

t is the time the last P_w was maintained (s), 60 is the time on each P_w, and P_R is the relative power output difference between the last two P_w.

The metabolic measurements for oxygen uptake (VO_2) and heart rate (HR) were made using the AMIS 2001 (Innovision A/S, Odense, Denmark) and a Polar heart rate monitor (Polar Electro OY, Tampere, Finland). Venous blood samples for analyses of blood lactate (*B-Hla*) were made with a 2 *ml* syringe from a 200 *cm* (1.5*ml*) extension set (ALARIS medical UK ltd, Hampshire UK) connected to a venflon (Becton Dickinson, Helsingborg, Sweden) in vena cephalic and analysed with Biosen 5140 (EKF-Diagnostic, Magdeburg, Germany). Samples of hemoglobin (*B-Hb*) were analysed in a Hemocue B-Hemoglobin (Helsingborg, Sweden). Measurements of weight and height were made with SECA equipment (Ergonordic, Bromma, Sweden). The subjects used their own ski poles with a special tip for the treadmill's rubber surface (Jakobsen V., Oslo). The study was approved by the Ethics Committee of Umeå University, Umeå, Sweden.

2.2 Procedure and protocol

The test subjects performed the same type of test on three different test occasions, and there was a time of 6.4 days between each occasion (4-12). Two of the test occasions (T1, T2) were carried out on the same pair of roller skis with a non-significant difference in B_R and a third occasion (T3) was using a pair of roller skis with a significantly different μ_R . On T3 the B_R was 47% lower for the freestyle roller skis and 50% higher for the classical roller skis (Freestyle roller skis; T1; B_R = 0.01772, T2; B_R = 0.01707, T3; B_R = 0.00941. Statistics between T1/T2; t = 1.388 p = 0.199, T1/T3; t = 16.837 p = 0.000.

Classical roller skis; T1; B_R = 0.01969, T2; B_R = 0.01974, T3; B_R = 0.02949, T1/T2; t = -0.274 p = 0.790, T1/T3; t = -30.534 p = 0.000). The order for when to use which roller skis was randomized, and the test subjects had no knowledge of the actual B_R of the roller skis. During the test period the subjects had been given instructions on standardised behaviour to follow, such as avoiding unfamiliar strenuous exercise, taking the same kind, intensity and amount of exercise throughout the whole period, and not to exercise the day before and the same day of the test occasions. Food intake should be normal for the subject and a meal should be eaten 2-3 hours before each test occasion. Tests were also carried out at the same time of day on every test occasion for each subject.

Before each test occasion the roller skis were warmed-up to achieve a stable B_R (Ainegren et.al. 2007). In connection with the tests using freestyle technique (which took place before the classical) the freestyle roller skis were warmed up by a non-test person roller skiing on the treadmill for 30 minutes. Before the classical tests the classical roller skis were warmed-up in a low-temperature oven, for at least half an hour, to a running temperature (T) corresponding to a certain normal force on the roller skis ($T = 24.43 + 0.0234 \cdot N_{Total}$). Before each test occasion the subjects filled out a standard health form to declare their physical condition. Following this there was a 10-minute rest lying on a bench, whereupon the equipment for blood sampling was applied and the samples of *B-Hb* were taken and immediately analysed. Thereafter weight and height were measured.

The test procedure started with the subjects warming up on the roller skis for 10 *min* below the upcoming protocol's initial P_w. After this the B_R for one of the roller skis (a) was measured for 30*s* (mean 10-30*s*) at 0º, 2.78 $m \cdot s^{-1}$. Thereafter the subjects continued to warm-up for another 5 *min* with the specific test technique for the protocol's initial P_w followed by a one-minute break to put on a nose clip and a mouthpiece for the VO_2 measurements.

The test protocols contained two sub maximal P_w of 10 *min* each. For the first sub maximal P_w ($P_{w\,sub1}$) in the freestyle technique the treadmill had an inclination of 2º (women) and 3º (men) with a velocity of 2.78 $m \cdot s^{-1}$ for both men and women. At the second sub maximal P_w ($P_{w\,sub2}$) the inclination was the same but the speed was increased to 3.89 $m \cdot s^{-1}$. In the classical technique the treadmill had an inclination and velocity of 2º and 2.22 $m \cdot s^{-1}$ (women) and 3º and 2.36 $m \cdot s^{-1}$ (men) at $P_{w\,sub1}$, and 4º and 2.50 $m \cdot s^{-1}$ (women) and 5º and 2.64 $m \cdot s^{-1}$ (men) at $P_{w\,sub2}$. After $P_{w\,sub2}$ there was a 5 *min* cool down period at the P_w corresponding to $P_{w\,sub1}$ and a 1 *min* break with an option of drinking some water before an incremental maximal test ($P_{w\,max}$) was started. The freestyle $P_{w\,max}$ had a constant inclination of 3º (women) and 4º (men) and a starting velocity of 2.78 $m \cdot s^{-1}$. The treadmill velocity was then increased every minute by 0.278 $m \cdot s^{-1}$ until the point of exhaustion. The classical $P_{w\,max}$ had a constant velocity of 2.78 $m \cdot s^{-1}$ (women) and 3.058 $m \cdot s^{-1}$ (men) throughout the entire test. The inclination was then increased by 1º per minute during the test, starting at 4º, until exhaustion. The $P_{w\,max}$ was terminated when the subjects signalled by taking out their mouthpiece. At this signal the time to exhaustion (*TTE*) was observed.

Ratings of perceived exertion (Borg 1998, RPE 6-20) were carried out for breathing, arms, and legs during the last minute on each $P_{w\,sub}$ and directly after exhaustion. Lactate samples were taken during the last 30s of each $P_{w\,sub}$ and 1 minute after exhaustion.

Between the samples the system was flushed with isotonic *NaCl* to avoid coagulation. Thus, each sampling started with discharging a volume of >3 *ml* before the actual sample was taken, and a capillary was filled with blood and put in a cuvette which was carefully mixed and analysed within 10 *min*. During the last minute of the $P_{w\,sub}$ the subjects were filmed with a 2-d video camera for analyses of cycle rates (*CR*). Cycle length (*CL*) was also analysed by dividing the velocity by *CR*. Results for VO_2 and *HR* were calculated as mean values from the 10th *min* of the $P_{w\,sub}$, and from 30*s* of the adjacent highest values of the $P_{w\,max}$ in order to determine $VO_{2\,max}$ and HR_{max}. Within 2 *min* after exhaustion a measurement of B_R for the second roller ski (*b*) was performed using the same weight as for roller ski *a* on all three test occasions. The B_R from each test occasion was then estimated as the mean value of roller skis *a* and *b*. A complementary study to determine B_R as a function of different normal forces was completed using weights at 5 *kg* intervals. Thus within the range of normal forces, N_{Total}, 222.7-615.1 corresponding to weights 22.7-62.7 *kg* , the following relationship was established for the freestyle roller skis: (T1 and T2) $B_R = -0.000023 \cdot N_{Total} + 0.030438$, ($r = -0.970$, $p = 0.000$) (T3) $B_R = -0.000012 \cdot N_{Total} + 0.015830$, ($r = -0.990$ $p = 0.000$), and for the classical roller skis: (T1 and T2) $B_R = -0.000026 \cdot N_{Total} + 0.034790$, ($r = -0.987$, $p = 0.000$) (T3) $B_R = -0.000016 \cdot N_{Total} + 0.0352635$, ($r = -0.996$ $p = 0.000$).

2.3 Statistical analyses

The statistical analyses were done in SPSS for Windows statistical software release 12.0.1 (SPSS Inc., Chicago, Illinois) with paired student *t* test and the Pearson product-moment correlation coefficient *r*. The significant level was set to $p < 0.05$.

3- Results

The results are presented in two tables, for the freestyle (Table 1) and the classical study (Table 2). Tests were also made regarding the influence of different test occasions on cycle length (*CL*) and ratings of perceived exertion (*RPE*). However the results showed only insignificant or small influences on *CL* and *RPE* (not presented here).

4- Discussion and conclusions

A 47% decrease in the rolling resistance (μ_R) of the freestyle roller skis resulted in a 12% decrease in power (P_w) in both sub maximal workloads ($P_{w\,sub1}$, $P_{w\,sub2}$), see Table 1. Increasing the μ_R by 50% for the classical roller skis resulted in a 12% and 8% increase in P_w on $P_{w\,sub1}$ and $P_{w\,sub2}$ respectively, see Table 2. The incremental maximal tests resulted in a ~10% increase and a ~7% decrease in maximal power ($P_{w\,max}$) for the freestyle and classical tests respectively. The change in $P_{w\,max}$ is due to the significantly changed time to exhaustion (*TTE*), due to the significant change in μ_R , by ~22% and ~13% for the freestyle and classical tests respectively. This change in $P_{w\,max}$ occurred without any significant change in maximal heart rate (HR_{max}) and maximal oxygen uptake ($VO_{2\,max}$).

The results of cycle rate (*CR*), in the freestyle part of the study, show a significant difference between test occasions with significantly different μ_R (T1/T3) as well as

	$P_{w\ sub\ 1}$ ~59%/$VO_{2\ max}$			$P_{w\ sub\ 2}$ ~77%/$VO_{2\ max}$			$P_{w\ max}$		
P_w	108.8	108.5	95.4	152.3	151.8	133.6	213.9	215.5	236.0
mean, SD	T1	T2	T3	T1	T2	T3	T1	T2	T3
d, d[%], t, *p*	T1/T2	T2/T3	T1/T3	T1/T2	T2/T3	T1/T3	T1/T2	T2/T3	T1/T3
	CR [*l · min*$^{-1}$]			*CR* [*l · min*$^{-1}$]			*TTE* [*m.ss*]		
mean	25.3	23.8	24.1	27.1	26.0	25.6	7.42	7.56	9.33
SD	2.4	2.1	2.6	2.4	2.2	2.5	1.14	1.02	1.07
d	-1.5	0.3	-1.2	-1.1	-0.4	-1.5	0.14	1.37	1.51
d [%]	-5.9	1.3	-4.7	-4.1	-1.5	-5.5	3.0	20.4	24.0
t	3.051	-0.732	2.677	2.535	1.300	3.223	-1.111	-10.168	-6.841
p	0.014*	0.483	0.025*	0.032*	0.226	0.010*	0.295	0.000***	0.000***
	B-Hla [*mmol · L*$^{-1}$]			*B-Hla* [*mmol · L*$^{-1}$]			*B-Hla* [*mmol · L*$^{-1}$]		
mean	1.51	1.33	1.06	3.45	3.26	2.11	9.88	9.75	10.33
SD	0.48	0.22	0.3	1.39	0.92	0.91	2.01	1.7	1.61
d	-0.18	-0.27	-0.45	-0.19	-1.15	-1.34	-0.13	0.58	0.45
d [%]	-11.9	-20.3	-29.8	-5.5	-35.3	-38.8	-1.3	5.9	4.6
t	1.146	2.831	3.466	0.549	4.647	3.880	0.267	-1.360	-0.772
p	0.281	0.020*	0.008**	0.596	0.001**	0.004**	0.795	0.207	0.460
	HR [*l · min*$^{-1}$]			*HR* [*l · min*$^{-1}$]			HR_{max} [*l · min*$^{-1}$]		
mean	152.5	150.0	139.9	177.8	177.9	167.3	195.2	195.4	195.4
SD	15.4	11.9	11.1	11.3	9.3	9.9	8.5	8.1	6.6
d	-2.5	-10.1	-12.6	0.1	-10.6	-10.5	0.2	0.0	0.2
d [%]	-1.6	-6.7	-8.3	0.1	-6.0	-5.9	0.1	0.0	0.1
t	1.268	3.014	2.875	-0.077	3.241	3.051	-0.305	0.092	-0.184
p	0.237	0.015*	0.018*	0.941	0.010*	0.014*	0.767	0.929	0.858
	VO_2 [*L · min*$^{-1}$]			VO_2 [*L · min*$^{-1}$]			$VO_{2\ max}$ [*L · min*$^{-1}$]		
mean	2.34	2.29	2.12	3.06	3.03	2.78	3.96	3.93	4.05
SD	0.43	0.37	0.41	0.55	0.54	0.55	0.74	0.65	0.68
d	-0.05	-0.17	-0.22	-0.03	-0.25	-0.28	-0.03	0.12	0.09
d [%]	-2.1	-7.4	-9.4	-1,0	-8.3	-9.2	-0.8	3.1	2.3
t	1.298	5.692	5.860	0.812	10.369	4.125	0.581	-2.101	-1.244
p	0.227	0.000***	0.000***	0.438	0.000***	0.000***	0.576	0.065	0.245

* $p < 0.05$, ** $p < 0.01$, *** $p < 0.001$

Table 1- Data (n=10) from tests with freestyle technique in two sub maximal exercises and an incremental maximal test. T1 and T2 represent the mean and SD from test occasions one and two with the same pair of roller skis. T3 is data from tests with a pair of roller skis with a significantly lower rolling resistance of 47%. d is differences, t and *p* statistics, between the three test occasions (T1/T2, T2/T3, T1/T3).

between test occasions with insignificant differences in μ_R (T1/T2), as shown in Table 1. In the classical part of the study a significant difference was found only in $P_{w\ sub2}$ and between one of the two test occasions with insignificant μ_R and the test occasions with significantly different μ_R (T2/T3, Table 2). Comparisons of the *CR* and VO_2 between $P_{w\ sub1}$ and $P_{w\ sub2}$ show that an increase in VO_2 by ~32% and ~42% for the freestyle and classical study respectively, only increases *CR* by ~9%. Cycle length, and ratings of perceived exertion, also resulted in small differences between the test occasions (not presented here) Thus, these results indicate that *CR* and *CL* is only slightly influenced by changes in μB_R and P_w when roller skiing on a treadmill.

The results of *B-Hla* show significant differences between the test occasions with significantly different μ_R except for $P_{w\ sub1}$ in the classical part of the study which had a lower P_w than $P_{w\ sub1}$ in the freestyle study (~51%/$VO_{2\ max}$ and ~59%/ $VO_{2\ max}$ respectively). The *B-Hla* was lower in the classical than in the freestyle part of the study, as shown in Table 2 and Table 1. The lactate response curve doesn't have a linear increase to a linear increase in exercise (Gore C.J., 2000). For elite athletes, performing incremental light to moderate exercise, there can be a baseline where lactate doesn't increase

	$P_{w\ sub\ 1}$ ~51%/$VO_{2\ max}$			$P_{w\ sub\ 2}$ ~72%/$VO_{2\ max}$			$P_{w\ max}$		
P_w	103.5	103.5	116.5	180.4	180.5	194.9	394.0	394.0	366.3
mean, SD	T1	T2	T3	T1	T2	T3	T1	T2	T3
d, d[%], t, *p*	T1/T2	T2/T3	T1/T3	T1/T2	T2/T3	T1/T3	T1/T2	T2/T3	T1/T3
	CR [*l* · *min*$^{-1}$]			*CR* [*l* · *min*$^{-1}$]			*TTE* [*m.ss*]		
mean	37.6	37.0	37.7	40.7	40.2	41.4	6.20	6.26	5.34
SD	3.9	4.4	3.8	3.3	3.6	3.6	1.10	1.12	0.58
d	-0.6	0.7	0.1	-0.5	1.2	0.7	0.06	-0.52	-0.46
d [%]	-1.6	1.9	0.3	-1.2	3.0	1.7	1.6	-13.5	-12.2
t	2.112	-1.231	-0.081	1.445	-2.606	-1.397	-1.089	5.327	7.020
p	0.064	0.250	0.937	0.182	0.028*	0.196	0.305	0.000***	0.000***
	B-Hla [*mmol* · *L*$^{-1}$]			*B-Hla* [*mmol* · *L*$^{-1}$]			*B-Hla* [*mmol* · *L*$^{-1}$]		
mean	0.96	0.92	1.10	2.06	2.20	3.02	9.95	9.54	9.19
SD	0.35	0.33	0.44	1.02	0.92	1.46	1.77	1.49	1.93
d	-0.04	0.18	0.14	0.14	0.82	0.96	-0.41	-0.35	-0.76
d [%]	-4.2	19.6	14.6	6.8	37.3	46.6	-4.1	-3.7	-7.6
t	0.510	-1.451	-0.999	-1.104	-3.719	-3.384	1.625	1.059	2.575
p	0.622	0.181	0.344	0.298	0.005**	0.008**	0.139	0.317	0.030*
	HR [*l* · *min*$^{-1}$]			*HR* [*l* · *min*$^{-1}$]			HR_{max} [*l* · *min*$^{-1}$]		
mean	129.9	131.2	138.2	161.8	164.3	169.5	186.5	188,0	187.9
SD	17.6	14.3	14.8	14.8	12.6	12.5	5.2	4.6	4.5
d	1.3	7.0	8.3	2.5	5.2	7.7	1.5	-0.1	1.4
d [%]	1.0	5.3	6.4	1.5	3.2	4.8	0.8	-0.1	0.8
t	-0.615	-2.617	-2.669	-1.552	-2.743	-4.250	-1.941	0.426	-1.316
p	0.554	0.028*	0.026*	0.155	0.023*	0.002**	0.084	0.681	0.224
	VO_2 [*L* · *min*$^{-1}$]			VO_2 [*L* · *min*$^{-1}$]			$VO_{2\ max}$ [*L* · *min*$^{-1}$]		
mean	2.36	2.36	2.52	3.33	3.36	3.54	4.63	4.61	4.55
SD	0.50	0.55	0.59	0.71	0.69	0.75	0.89	0.92	0.91
d	0.00	0.16	0.16	0.03	0.18	0.21	-0.02	-0.06	-0.08
d [%]	0.0	6.8	6.8	0.9	5.4	6.3	-0.4	-1.3	-1.7
t	0.170	-4.193	-3.474	-1.047	-5.027	-5.020	0.579	1.487	1.378
p	0.869	0.002**	0.007**	0.322	0.001**	0.001**	0.577	0.174	0.202

* $p < 0.05$, ** $p < 0.01$, *** $p < 0.001$

Table 2 - Data (n=10) from tests with classical technique in two sub maximal exercises and an incremental maximal test. T1 and T2 represent the mean and SD from test occasions one and two with the same pair of roller skis. T3 is data from tests with a pair of roller skis with a significantly higher rolling resistance of 50%. d is differences, t and *p* statistics, between the three test-occasions (T1/T2, T2/T3, T1/T3).

significantly with an increase in P_w. During harder exercise the ratio of increased lactate to increased P_w is quickly changed due to oxygen deficiency. Thus *B-Hla* is more sensitive to a change in P_w (a significant change in rolling resistance) during harder exercise.

The results from $P_{w\ sub1}$ and $P_{w\ sub2}$ for heart rate (*HR*) and oxygen uptake (VO_2) show, for both the freestyle and classical tests, that a significant change of ~50 % in rolling resistance (increasing or decreasing) significantly changes *HR* and VO_2 by ~6% and ~7% respectively, while measurements between test occasions with insignificant differences in B_R show no significant differences for *HR* and VO_2 , as shown in Table 1 and Table 2.

The present study investigated the biological responses to a significant change in rolling resistance of roller skis, similar to results reported in a warm-up study (Ainegren *et al.* 2007). The results show that most of the investigated variables are significantly changed and influenced by differences in rolling resistance and that measurements in other environments than stationary and comparable conditions, such as in a laboratory, provide unreliable and misleading results.

Thus, roller skiing on sub maximal steady state exercise with significant changes in rolling resistance, ~50%, results in significant changes in oxygen uptake, heart rate and blood lactate, while the effects on cycle rate, cycle length and ratings of perceived exertion are insignificant or relatively small. Incremental maximal tests show that time to exhaustion is significantly changed, while there are insignificant changes in $VO_{2\,max}$ and HR_{max}, and that changes to *B-Hla* and ratings of perceived exertion are insignificant or small.

5- Acknowledgements

We would like to thank Professor Bengt Saltin (Copenhagen Muscle Research Centre and Mid Sweden University) for his support during the development of testing methods. Many thanks also goe to the athletes who participated in the study. Finally we would also like to thank Glenn Björklund (Mid Sweden University) and Robin Johansson (Swedish X-country Ski association) for their good will in warming up the roller skis in the free-style part of the study.

6- References

Ainegren M., Carlsson P. and Tinnsten M. (on review, submitted the journal of International Sports Engineering 2007-10)

Borg G (1998). Borg's Perceived exertion and pain scales. Champaign, Ill.: Human Kinetics.

Calbet J.A., Holmberg H-C., Rosdahl H., van Hall G., Jensen-Urstad M. and Saltin B. (2005). Why do arms extract less oxygen than legs during exercise?. American Journal of Physiology, Regulatory, Integrative and Comparative Physiology, 289, 1448-1458.

Gore C.J. (2000) Physiological Tests for Elite Athletes. Australian Sports Commission. Human Kinetics. 50-65.

Hoffman D.M., Clifford S.P., Bota B., Mandli M. and Jones M.G. (1990). Influence of body mass on energy cost of roller skiing. International Journal of Sport Biomechanics, 6, 374-385.

Hoffman D.M., Clifford S. P., Watts B.P., O´Hagan P.K. and Mittelstadt W.S. (1995). Delta efficiency of uphill roller skiing with the double pole and diagonal stride techniques. Canadian Journal of Applied Physiology, 20, 465-479.

Hoffman D.M., Clifford S.P., Snyder S.P., O´Hagan P.K., Mittelstadt W.S., Roberts M.M., Drummond A.H. and Gaskill E.S.(1998). Physiological effects of technique and rolling resistance in uphill roller skiing. Medicine and Science in Sports and Exercise, 30, 311-317.

Holmberg H.C., Lindinger S., Stoggl T., Eitzlmair E. and Muller E. (2005) Biomechanical analysis of double poling in elite cross-country skiers. Medicine and Science in Sports and Exercise, 37, 807-818.

Millet Y.G., Hoffman D.M., Candau B.R., Buckwalter B.J. and Clifford S.P. (1998) Effect of rolling resistance on poling forces and metabolic demands of roller skiing. Medicine and Science in Sports and Exercise, 30, 755-762.

Padilla S., Mujika I., Orbananos J. and Angulo F. (2000) Exercise intensity during competition time trials in professional road cycling. Medicine and Science in Sports and Exercise, 32, 850-856.

Rundell K.W. (1995) Treadmill roller ski test predicts biathlon roller ski race results of elite U.S. biathlon women. Medicine and Science in Sports and Exercise, 27, 1677-1685.

Aerodynamics of Time Trial Bicycle Helmets (P226)

Vincent Chabroux[1], Caroline Barelle[2], Daniel Favier[3]

Topics: Bicycle.

Abstract: During a time-trial (TT) stage on flat track at 50 $Km.h^{-1}$, aerodynamic drag force represents 90% of the power developed by the runner (Belluye and Cid, 2001). Given the drag resistance impact on TT performances, aerodynamics optimization of posture and equipment is thus an essential point (McLean and al. 1994, Martin 1996). The purpose of this study concerns the aerodynamic comparison of six TT helmets which the aim is to minimize the aerodynamic drag. The aerodynamics drag resistances (R_D) of nine professional cyclists using these different TT helmets allow to quantify their aerodynamic performances, the visor and the frontal vents influences according to head and trunk tilts assumed during stages. Experiments were carried out in a wind tunnel at a free-stream velocity of 13.9 $m.s^{-1}$. A 3D motion analysis system SIMI MOTION measured cyclists postural angles (three head and two trunk tilts). Statistical analysis shows that drag resistance and frontal area of a TT posture is significantly lower than the classical road posture (-14.9%). Coefficients of drag in road and TT posture are not significantly different ($p>0.05$). Besides, interaction between the global posture and the helmet inclination is significant ($p<0.05$). In TT posture, drag resistance connected with the natural inclination of the helmet is significantly lower ($p<0.05$) than high (-3.4%) and low inclination (-1.5%). Usual inclination of the helmet provides a drag coefficient reduction of 2.2% compared with the other inclinations (not significantly different together). In high inclination, frontal area is significantly higher (2.4%).Without changing the frontal area, the visor allows a significant reduction of the drag coefficient for low and high inclination (-1.5%), and thus of the drag resistance. This reduction is not significant for the natural inclination. Whatever the helmet orientation, frontal vents have no significant influence on drag coefficient and on frontal area.

Key words: Aerodynamic, drag, helmets, time trial, cycling.

1, 2, 3. Institute of Movement Sciences (ISM), UMR6233 of CNRS / University of Mediterranee.ISM Wind Tunnel Platform, 163 avenue de luminy, case 918, 13288 Marseille cedex 9, France -E-mail: (1) chabroux@crans.org; (2) barelle@free.fr; (3) daniel.favier@univmed.fr

1- Introduction

During cycling, three external forces are applied to the couple bicycle/cyclist: weight, aerodynamic drag force and contact force between road and wheels. Weigth influence depends mainly on the road slope. If the road is horizontal, weight doesn't reduce the speed. However, contact force and aerodynamic drag force act like speed-reducing factors. Contact force is depending on weight and friction factor between road and wheels. During a TT stage on flat track, at an average speed close to 50 $Km.h^{-1}$, aerodynamic drag force represents 90% of the total power developed by the runner (Belluye *and al.*, 2001). This aerodynamic drag resistance (R_D) is given by the equation below (1).

$$R_D = \frac{1}{2} \cdot \rho \cdot A_P \cdot C_D \cdot V^2 \quad (1)$$

Where R_D is the aerodynamic drag resistance (N), ρ is the air density ($Kg.m^{-3}$), A_p is the projected frontal area of the couple bicycle/cyclist (m^2), C_D is the aerodynamic drag coefficient and V is the air velocity ($m.s^{-1}$). Measurements of drag resistance, projected frontal area and air velocity are discussed in the next section.

Given the drag resistance impact on TT performances, aerodynamics optimization of posture and equipment is thus an essential point. Previous studies (McLean *and al.*, 1994, Martin 1996) defined four postural criteria reducing cyclists drag resistance: back parallel to the ground, elbows closed up, forearms tilted between 5° and 20° with respect to the horizontal, knees closed up to the frame. In order to reduce the drag resistance (R_D) and thus to improve the TT cyclists performances, the purpose of this study concerns the aerodynamic comparison of six TT helmets having different shapes. Indeed, the main aim of the helmets is to protect the head from impacts. Moreover, shape design of TT helmets avoids flow separation occurrences in order to minimize the global cyclist aerodynamic drag. To perform this aerodynamic comparison, a series of tests was carried out in a wind tunnel, on different helmets depending on the postural angles.

The aerodynamics drag resistances (R_D) measured with these different helmet shapes allowed to quantify the external geometry influence, the visor influence and the frontal ventilation influence according to head tilt and global posture (trunk inclination). In addition, measurements of the projected frontal area (A_p) of the couple bicycle/cyclist allowed to work out the aerodynamic drag coefficient (C_D) relative to the use of each helmet.

2- Methods

2.1 Subjects

Nine professional male cyclists (age: 25.0±3.4 years; height: 1.79±0.06 m; weight: 69.3±5.5 kg; mean±σ) volunteered as subjects for this study. Each subject and a sport director of this professional cycling team gave informed consent prior to the tests campaign.

2.2 Equipment

Six different helmets were compared in this study. Three of them were *Louis Garneau Rocket* helmets (1, 4, 5) with the same external geometry (size M) as shown in Figure 1. One of these helmets was equipped with a large visor (4) and another had two large frontal vents (5) as shown in Figure 7. The other helmets were a *Giro Rev 6* helmet (2, Figure 2) and a *LAS Cronometro* helmet (3, Figure 3). In order to assess the performances of these TT helmets, the aerodynamic characteristics of a road cycling helmet (*Louis Garneau Titan Carbon* helmet) (6, Figure 4) were also studied. The bicycles used in these experiments were TT bicycles equipped with rear disc racing wheels and adapted to the cyclists anthropometric characteristics.

Figure 1 - Louis Garneau Rocket (1, 4, 5).

Figure 2 - Giro Rev 6 (2).

Figure 3 - LAS Cronometro (3).

Figure 4 - Louis Garneau Titan Carbon (6).

2.3 Wind tunnel

Experiments were carried out in the test-section of the S1L subsonic wind tunnel (Marseille, France). Characteristics of this wind tunnel are a free-stream velocity up to V_∞ = 100 m.s^{-1}, a turbulence intensity lower than 0.3% and a constant temperature within the test-section ($\Delta T<1°C$). During these experiments, the free-stream velocity was fixed at the average speed in TT stages: i.e. 13.9 m.s^{-1}. The velocity in the wind tunnel was mesured and monitored by a Pitot-static tube installed at the upstream entrance to

the test-section. Considering the test-section dimensions (octagonal section with inside circle of 3 m in diameter; length: 6 m), no walls boundary layer effects were interfering during measurements.

2.4 Instrumentation

2.4.1 Drag force measurement

In order to determine the drag force of the couple bicycle/cyclist, a cycletrainer was fastened on a drag-mesurement platform mounted in the middle of the test-section. This platform was equipped with ball-bearing slides in the direction of the wind tunnel and with a dynamometer measuring the drag force. The dynamometer voltage was amplified and recorded at 1000 Hz by a computer over a period of five seconds. Data were median filtering (rank: 4; length: 1000 samples) by a LabView program. The accuracy of the drag force measurement is 0.1 Newton. A preliminary measurement allowed to obtain the drag force of the platform equipped with the cycletrainer and therefore to measure the drag force of the couple bicycle/cyclist.

2.4.2 Frontal area measurement

In order to work out the drag coefficient (C_D), the projected frontal area of the couple bicycle/cyclist was measured by a digital camera (frame rate: 250 Hz, resolution: 640 × 480 pixels). Image processing was carried out by computerized planimetry (ImageJ 1.36b) measuring the couple bicycle/cyclist aera in pixels. The camera positioning relative to the reference dimension and the cyclist may be critical for the frontal area measurement (Olds and Olive, 1999). In order to not disturb the upstream flow, the camera was fixed downstream the cyclist, at a distance of 3.5 m from the crankset axis at the height of the saddle. A square reference board (area = 0.42 m^2), placed next to the crankset and perpendicular to the wind tunnel axis, has allowed to calculate a pixel/m^2 conversion ratio. The camera focal length corresponded to the reference board position. A frontal area model, in TT posture, according to the cyclists anthropometric characteristics (Heil 2001), the head tilt and the helmet length will be provided from these measurements.

2.4.3 Postural angles measurement

In order to measure the cyclists postural angles, the 3D motion analysis system SIMI MOTION (SIMI Reality Motion Systems GmbH, Germany) was installed in the test-section of the wind tunnel so as to not disturb flow upstream the couple bicycle/cyclist. This system is composed of three digital cameras (frame rate: 250 Hz, resolution: 640 × 480 pixels) synchronized by the motion analysis software. Head and trunk tilts were measured using two markers on each helmet (positioned horizontally) and two markers on the cyclist (posterior superior iliac spine and acromion).

For each helmet, the cyclists have assumed two trunk inclinations with respect to horizontal (α_1= 34.8°±2.8; α_2= 17.4°±3.4; mean±σ) corresponding to a road posture (hands on handlebar and arms straight) and to a TT posture (hands on aerobars,

forearms on armrests and arms bent). For both orientations of the trunk, the cyclists have assumed three head inclinations with respect to horizontal (β_1= -66.4°±4.3; β_2= -36.2°±9.2; β_3= -9.5°±9.1 (for α_1) and β_3= -16.8°±8.7 (for α_2); mean±σ) corresponding to a low, an usual and a high tilt. These six postures allowed to determine the aerodynamical efficiency of the different helmets according to the positions assumed by the cyclists during a TT stage.

2.4.4 Statistical analysis

Standard parametric statistics were used throughout. Repeated-measures analysis of variance was used to test for significant differences between the drag resistance(R_D), the frontal area (A_p) and the drag coefficient (C_D) using each helmet and for each of the six postures (n=9). In the event of a significant *F*-ratio, *post-hoc* analysis was performed using Newman-Keuls *t*-test. An alpha level of 0.05 was adopted for all analyses. All results are reported as mean±σ.

3- Results

3.1 Global posture influence

In order to quantify the drag reduction corresponding to a TT posture (α_2) compared with a road posture (α_1), a first statistical analysis was carried out on the whole configurations. This study shows that the drag reduction of a TT posture is significant (R_D: 37.8±0.5 N vs. 44.5±0.7 N; $p<0.05$) and provides an average gain of 14.95%. This reduction is only due to the significantly lower frontal area in TT posture (A_p: 0.342±0.007 m^2 vs. 0.398±0.006 m^2; $p<0.05$). Indeed, coefficients of drag in road and TT posture are not significantly different ($p>0.05$). One can be note that the interaction between the global posture and the helmet inclination is significant ($p<0.05$) and this is studied in the following section.

3.2 Helmet slope influence

In order to study the influence of the helmet inclination on the aerodynamic performances, a statistical analysis was carried out on the whole TT helmets, for each inclination and according to both global postures (Figure 5).

For the TT posture (α_2), helmet inclination has a significant influence ($p<0.05$) on drag resistance, on drag coefficient and on frontal area. The *post-hoc* comparison shows that drag resistance connected with usual inclination of the head is significantly lower (R_D: 37.2±0.6 N) than the low slope (R_D: 37.8±0.5 N), which is itself significantly lower than the high slope (R_D: 38.5±0.6 N). On one hand, drag coefficient related to the usual tilt of the head is also significantly lower (C_D: 0.91±0.01) than the high (C_D: 0.93±0.01) and the low inclination (C_D: 0.93±0.02). On the other hand, low inclination of the head (β_1) is shown to be the orientation minimizing the frontal area (A_p: 0.339±0.007 m^2), not significantly when compared with usual orientation (A_p: 0.340±0.007 m^2) but significantly in comparison with high inclination (A_p: 0.347±0.007 m^2).

For the road posture (α_1), the orientation of the helmet is also shown to have a significant influence ($p<0.05$) on the drag resistance, on the drag coefficient and on the frontal area. However, unlike for the TT posture, influence between low and usual inclinations of the helmet is not significant ($p>0.05$) on drag resistance, on drag coefficient and on frontal area. However, there is a significant difference of drag resistance ($p<0.05$) between these two orientations (R_D: 43.6±0.7 N; 43.67±0.8 N) and high inclination (R_D: 46.2±0.7 N). Moreover, drag coefficient (C_D: 0.926±0.008; 0.919±0.013) ($p>0.05$) likewise the frontal area (A_p: 0.392±0.007 m^2; 0.395±0.006 m^2) ($p>0.05$) of low and usual inclinations are significantly different in comparison with drag coefficient (C_D: 0.947±0.013) ($p<0.05$) and frontal area (A_p: 0.407±0.006 m^2) ($p<0.05$) of high inclination.

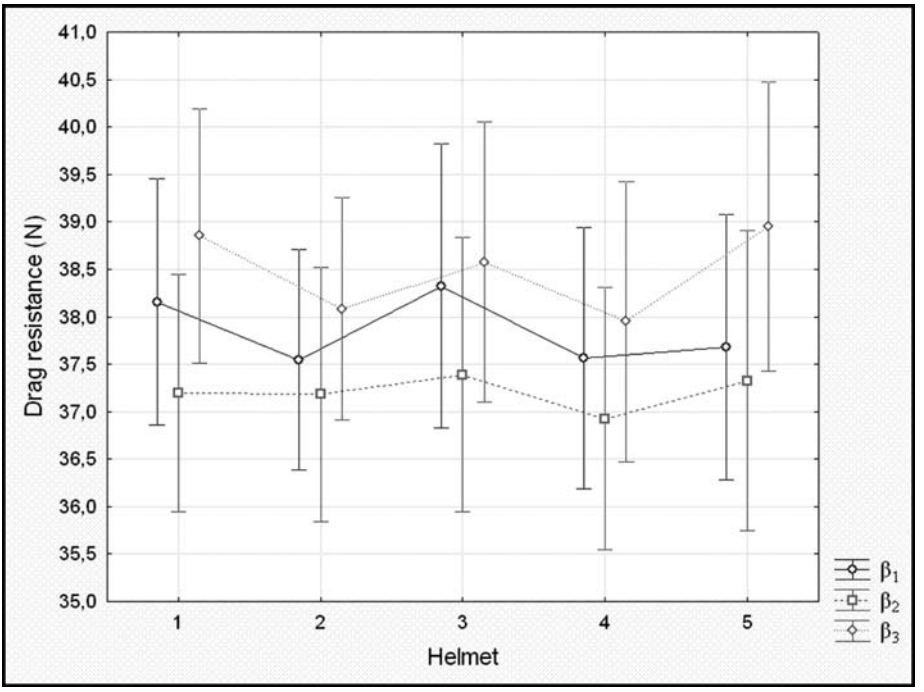

Figure 5 - Helmet orientation influence on drag resistance in TT posture.

3.3 Helmets comparison

In TT posture and for the whole head slopes, helmets drag resistance and drag coefficient are significantly different ($p<0.05$). The most aerodynamic helmet (4) is equipped with a large visor (R_D: 37.5N ±0.6; C_D: 0.92 ±0.01) but it is shown to be not significantly different than helmet 2 (R_D: 37.6N ±0.5; C_D: 0.92 ±0.02). This helmet (2) has great aerodynamic performances due to its frontal surface lower than those of the other helmets (A_p: 0.340m^2 ±0.006). The aerodynamics performances of these two helmets (2, 4) are significantly better than the others tested and allow a mean drag resistance gain of 0.62N (- 1.62%).

TT helmets allow a significantly decrease of drag resistance (mean: -2.4%; max: - 3.5%) when compared to the road helmet (6) (R_D: 38.8N ±0.8). Although it has a frontal surface significantly different only with respect to helmet 2, its drag coefficient is higher than all tested TT helmets (C_D: 0.95 ±0.02).

For only the usual slope of head (β_2), the statistical analysis shows that TT helmets drag resistance and drag coefficient are not significantly different ($p>0.05$). In this posture, helmet 3 has a significantly higher frontal surface (A_p: 0.343m^2 ±0.014) than the other helmets. For this heads slope (β_2), the road helmet (6) has a drag resistance significantly higher (R_D: 38.7N ±0.8) than other TT helmets (mean: +4%; max: +4.8%). Despite the fact that its frontal surface is not significantly different with TT helmets, this drag resistance rise is due to a significantly higher drag coefficient than TT helmets (C_D: 0.95 ±0.02).

3.4 Visor influence

Comparison of helmets 1 and 4 allows to analyze the visor influence on the aerodynamic performances. Indeed, these helmets have the same external geometry but one (4) is equipped with a large visor (height: 80mm). The visor does not change the frontal area. In road posture, statistical analysis shows that the visor has not a significant influence, neither on drag resistance, nor on the drag coefficient. However, in TT posture and for the whole heads slopes, the visor allows a significant decrease of drag coefficient (C_D: 0.93 ±0.02 vs. 0.92 ±0.01) and thus of drag resistance (R_D: 38N ±0.5 vs. 37.5N ±0.6) corresponding to a gain of 1.54%. In addition, the interaction of the visor with the slope of the head is also significant ($p<0.05$) on drag resistance and the drag coefficient (Figure 6). For a high slope of the head (β_3), statistical analysis shows a significant

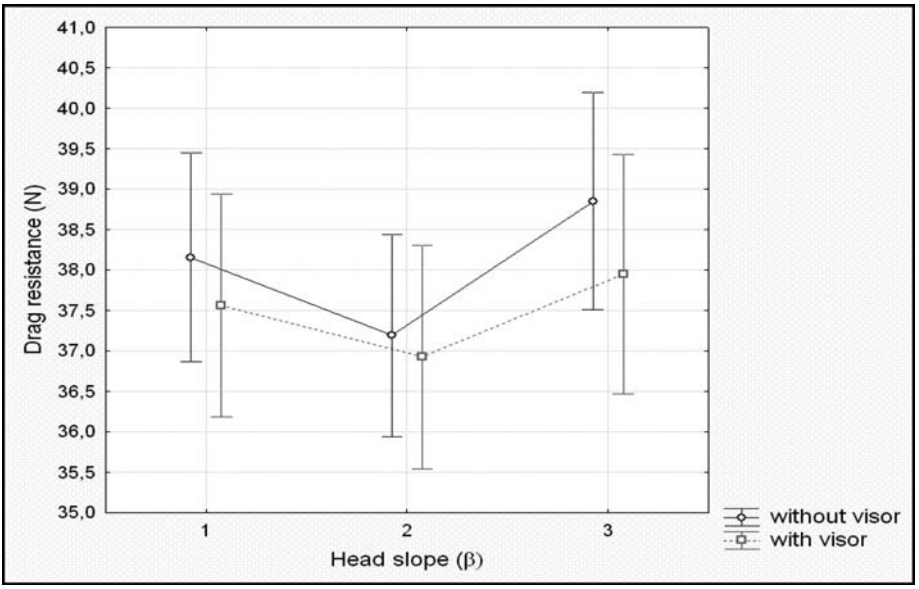

Figure 6 -Visor influence on drag resistance in TT posture.

decrease of drag coefficient (C_D: 0.93 ±0.01 vs. 0.92 ±0.01) and thus of drag resistance (R_D: 38.8N ±0.6 vs. 37.9N ±0.6) corresponding to a gain of 2.32%. For a low slope of the head (β_1), statistical analysis indicates a significant decrease of drag coefficient (C_D: 0.94 ±0.02 vs. 0.93 ±0.01) and thus of drag resistance (R_D: 38.2N ±0.6 vs. 37.6N ±0.6) corresponding to a gain of 1.56%. For a usual slope of the head (β_2), there is no significant reduction of drag resistance and drag coefficient ($p>0.05$).

3.5 Vents influence

Comparison of helmets 1 and 5 allows to study the vents influence on the aerodynamic performances. Indeed, these helmets have the same external geometry but one (1) has four frontal slits shaped vents (two of 5*39mm and two of 5*59mm) and the other presents five vents: two frontal rhombus shaped vents (85*29mm) and three slits shaped vents (5*54mm) on the top of the helmet (Figure 7). These vents do not change the frontal area. Statistical analysis shows that, for the whole slopes of the head, these different vents have not significant influence ($p>0.05$) on frontal area, as well as on drag resistance and drag coefficient.

Figure 7 - Vents on TT helmet.

4- Discussion

Comparison of two global postures conducts to quantify the gain generated by a TT posture with respect to a road posture. The important drag resistance decrease between these postures (-14.9%) is only due to the reduction of cyclists frontal area in the TT posture. Indeed, statistical analysis shows no significant difference on drag coefficient for these postures. Consequently, during a TT stage, cyclists have to keep their TT posture even if they believe to be most powerful when road slope increases.

Comparison between the whole TT helmets and the road helmet (6) shows a drag resistance improvement of 2.4% for the whole heads slopes, and 4% for the usual slope (β_2). Yet, the frontal area of road helmet is not significantly different from TT helmets. Consequently, its drag coefficient is worse than those of TT helmets and decreases its aerodynamic performances. Although classic events speeds are lower than TT speeds, it could be interesting to improve this kind of road helmet drag coefficient.

For the TT posture, statistical analysis shows that helmet inclination has a significant influence on drag resistance. Indeed, usual helmet slope (β_2) provides a drag resistance reduction of 1.72% with respect to a low slope (β_1) and of 3.3% with respect to a high slope (β_3). Actually, the low frontal area increase in usual slope with respect to the low slope (+0.25%) is in agreement with a drag coefficient decreasing of -1.92%. As a result, making frontal area and drag coefficient dot product, a usual helmet slope allows a drag resistance reduction of 0.65N (-1.72%) as shown in Table 1. Consequently, during a TT stage, cyclists have to keep their usual head slope even if they want to relax their cervical muscles.

		Low slope	**High slope**
	R_D	-1.72%	-3.33%
Usual helmet slope	C_D	**-1.92%**	**-1.43%**
	A_P	**+ 0.2 % (p>0.05)**	**-1.79%**

Table 1 - Helmet slope influence in TT posture.

On one hand, the comparison of TT helmets, for the whole head slopes, shows significant differences on drag resistance and drag coefficient. Aerodynamics performances of helmets 2 and 4 are significantly better than the others tested and allow a mean drag resistance profit of 0.62N (- 1.62%). On the other hand, for usual head slope (β_2), statistical analysis indicates no significant differences on drag resistance and drag coefficient for the whole tested helmets. Moreover, this analysis shows a frontal area significantly larger for helmet 3 with comparison to the other TT helmets. Such a frontal area increase is due to its higher length with respect to the whole TT helmet and does not improve its drag coefficient. Consequently, a higher TT helmet length induces a drag resistance rise. Helmet length could therefore acts like speed-reducing factor.

Comparison of helmets 1 and 4 shows the visor influence in TT posture. For the whole heads slopes, the visor presence produces a significant decrease of drag coefficient and thus of drag resistance corresponding to a gain of 1.54%. This improvement reaches 2.32% for a high head slope (β_3) and 1.56% for a low slope (β_1). However, these aerodynamic performances improvement are no significant for a usual head slope (β_2). As a result, given that cyclists do not preserve their usual head slope along a TT stage, it remains interesting that they use a helmet equipped with a visor.

5- Conclusions

During a TT stage, it has been shown that cyclists have to keep their TT posture, even if they believe to be most powerful when road slope increases. Moreover, they also need to keep their usual head slope, even if they want to relax their cervical muscles. In order to improve their aerodynamic performances, helmets used need to have a large visor in spite of the fact of this one has less impact for a usual head slope. In addition, it seems necessary to limit the TT helmets length and width in order to not increase the frontal area and thus the drag resistance.

6- Outline

In future works and in order to better understand parameters influence on TT helmets aerodynamic performances, it is planned to carry out a PIV analysis (Particle Image Velocimetry) of the downstream flow of the helmet. This detailed flow analysis will provide the characterization of a suited helmet geometry that will improve aerodynamic performances. It is also planned to develop an evolution modelling of the frontal area according to the cyclists posture, their head slope and helmets external geometry.

7- References

[BC1] N. Belluye, M. Cid Approche biomécanique du cyclisme moderne. In Science & Sports, 16: 71-87, 2001.

[H1] DP. Heil Body mass scaling of projected frontal area in competitive cyclists. In European Journal of Applied Physiology, 85(3-4): 358-366, 2001.

[ML1] BD. McLean, R. Danaher, L. Thompson, A. Forges, G. Coco Aerodynamic characteristics of cycle wheels and racing cyclists. In Journal of Biomechanics, 27: 675, 1994.

[M1] JC. Martin Aerodynamics and cycling. Master Athlete Physiology and Performance, 1996.

[OO1] T. Olds, S. Olive Methodological considerations in the determination of projected frontal area in cyclist. In Science & Sports, 17: 335-345, 1999.

Acquisition and Analysis of EMG Data During Special Slalom for Comparative Equipment Evaluation (P228)

Giuseppe Marcolin[1], Nicola Petrone[2]

Topics: Ski & other Winter Sports; Biomechanics; Measurement Systems; Performance Sports.
Abstract: The aim of this work was to develop a method for acquisition and analysis of EMG data during special slalom in the snow field. In particular the purpose was to find a reliable method for the acquisition of EMG signals on the slopes that could be synchronously correlated to the pole passing instants, the skier body posture and the ski angle of attack. This method allowed to evaluate the biomechanics of skiing technique and to study the effect of racing slalom skis equipment with different tuning conditions. A PDA PocketEMG (BTS-Italy) was employed for data acquisition: its dimensions and weight were optimal for not influencing skiers' behaviour. This compact system allowed to collect eight EMG channels from the right leg and back of the skier, two Biometrics goniometers fixed at the right knee and at the right hip and 2 accelerometers placed on the tibial shin protections to have the timing with respect to the pole passing. All data were recorded at 1kHz. Two inertial platforms X-Sens Mti were applied to the skis and synchronously recorded at 1000 Hz. A professional skier performed several slalom courses with different tuning conditions between 10 poles; in addition after passing the 10^{th} pole, a 60 m free slalom course was performed. For a given ski tuning, the tester technique was compared in terms of timing pattern at the poles, intensity of EMG activation at the different muscles and ski angle of attack in order to underline possible differences due to skiing equipment.
Key words: Special Slalom; ski tuning; EMG, ski technique, muscle action.

1. Department of Anatomy and Physiology University of Padova, Italy. Via Marzolo 3 - E-mail: giuseppe.marcolin@unipd.it
2. Department of Mechanical Engineering University of Padova, Italy. Via Venezia 1 - E-mail: nicola.petrone@unipd.it

1- Introduction

In alpine skiing, man and equipment are the elements of a complex bio-mechanical system where several factors are involved: ski geometrical and mechanical properties; plates, binding and boot configurations, skier's anthropometry and technical skills must be considered for the increase not only of skiing performance but also of safety and injury prevention. Recent researches focused on two specific topics: muscle properties and use during different courses (super G, giant slalom, special slalom and also freestyle mogul) and study of mechanical properties of skis, plates and boots. Tesch [T1] described the physiological demands in competitive alpine skiing and the physiological profile of elite skiers. Berg *et al.* [BE1] studied concentric and eccentric muscle use in relation to positions and angular movement velocities of the hip and knee joints. Hintermeister *et al.* [HO1] investigated muscle activity in slalom and giant slalom finding a similarity in muscle activation between the two disciplines with ample evidence of co-contraction suggesting a quasistatic component to skiing. Considering these previous investigations and the variables analyzed we decided to develop a method suitable first for evaluating different ski equipments and second for quantifying eccentric and concentric muscle actions. This analysis was applied at the two typologies of courses, slalom between short poles and free slalom, making a comparison to underline possible effects of the same equipment in the two different courses.

2- Material and Methods

2.1 Instrumentation

Data of each course were recorded by means of a 16 channels PDA PocketEMG (BTS-Italy) placed on the chest of the skier under the windbreaker: its dimensions were 145x95x20mm and the weight was 0.3kg. Eight channels were used to collect EMG data of the right leg and the back of the subject with bipolar surface electrodes placed on the muscle bellies along the direction of the fibers: the distance between each couple of electrodes was 25mm. The reference electrode was applied on C7. Two Biometrics goniometers were placed on the lateral part of the right knee and on the right hip. The last four channels of the PDA were employed for the signal collection of two strain gauged accelerometers (maximum range ±50g) stuck on the shin guards. Finally two inertial platforms XSens Mti-28A13G25D with maximum range of ±10g (linear acceleration) and ±1200deg/s (angular velocity) were fixed behind the posterior binding of each ski (Figure 1a). All data were synchronously recorded at 1Khz. Each course was also filmed via two commercial digital cameras at 25Hz: one from the front side an the other one from the left side of the skier.

2.2 Test Protocol

A professional ski tester with long experience in special slalom was involved in the study. Before starting the experimentation he was asked to read and sign an informed consent.

The first step of the test protocol consisted in the placement of the two goniometers with medical tape and of the bipolar electrodes for surface EMG (Figure 1b). Muscles analyzed were: Erector Spinae, Gluteus Maximum, Vastus Lateralis, Vastus Medialis, Biceps Femoris, Semimembranosus, Tibialis Anterior and Gastrocnemius Medialis. These muscles were all referred to the right side of the skier. The skin was shaved, scratched with abrasive paper and finally cleaned with alcohol before the placement of the electrodes to reduce impedance values. In the second step of the test protocol the skier was asked to perform Maximal Voluntary Contractions (MVCs) for each muscle in order to normalize EMG data collected on the slope (Figure 1c).

After a standardized warm up consisting on some stretching exercises for thigh, shank and trunk the tester performed 3 warm up courses to familiarize with the track. Ten short poles were placed in the snow (span 4 m, pace 12 m, named S0-S9 with odd numbers external turns for right leg) along a medium slope. Two additional poles at a span of 60 m were employed to mark the free slalom area.

Three boots, named A, B, C, were chosen for comparative evaluation and the skier was asked to perform at least two courses for each type of boot starting with the slalom between the short poles and concluding with the 60 m free slalom.

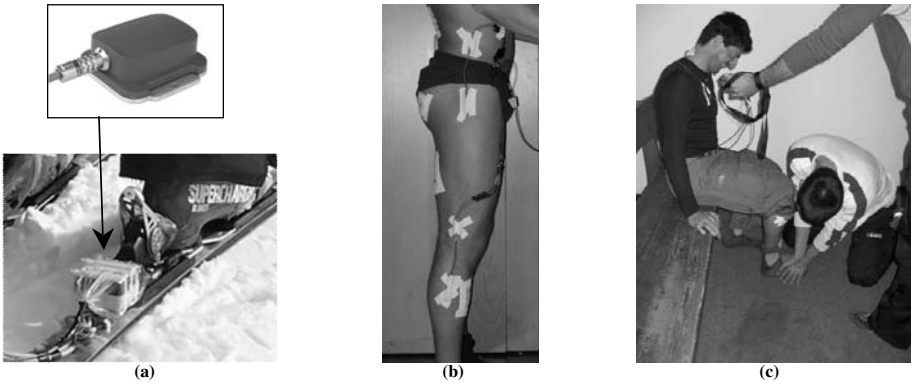

Figure 1 - (a) XSens Mti applied to the ski. (b) Electrodes and goniometer placement. (c) Tibialis anterior Maximal Voluntary Contraction.

2.3 Data Analysis

Analysis of courses between short poles started with the identification of two different types of cycle referred to the right leg of the skier: the internal turn cycle and the external turn cycle. Each cycle consisted of three consecutive poles for a total of 4 external turn cycles and 4 internal turn cycles in each run. The accelerometers signal on the shin guards provided the identification of the impact instant of the leg with the pole in such a way that cycles could be easily identified. Two additional poles were fixed on the snow to delimit the beginning and the end of the free slalom area. EMG raw signals of the

eight muscles were first rectified, then integrated with a mobile window of 200ms, filtered with a 5Hz low pass Butterworth filter and finally normalized with respect to the Maximal Voluntary Contractions (MVCs) and to the cycle length. The final step after the time normalization was to average 4 external turns of the same run to obtain the mean external curve of the run; the same procedure was applied to the internal turns. Three types of boot were tested. One way ANOVA for each muscle was used to analyze differences in the peak EMG of the mean external curve of each run with distinct equipments. Differences in levels of muscular activity were assessed for statistical significance ($p \leq 0.05$) and then, if appropriate, a Tukey post hoc test was calculated. In the 60 m free slalom movement cycles were identified by XSens Mti maxima roll values and than averaged in order to have a mean curve for each muscle and for each course.

To quantify knee flexor and extensor muscle activity and to relate them to angular displacement and velocity, data were analyzed as follows. The angle between thigh and shank (θ) was set at 180° with knee fully extended and the angular velocity (ω) of the knee was positive during extension and negative during flexion. Then the angular velocity, after low pass filtering at 5Hz, was multiplied by the integrated EMG signal (iEMG) of muscle flexors (Biceps Femoris and Semimembranosus) and extensors (Vastus Medialis and Vastus Lateralis) to obtain a set of curves that were defined as *pseudo Muscular Power* curves (pMP). The muscle Activation signal (iEMG) is in fact correlated to the Force at the muscle tendon, that is in turn correlated via the tendon lever arm to the muscle Torque applied to the joint. Given the complexity of the Activation-Force relationship and the Lever arm-Joint angle relationship, the product between Activation (iEMG) and joint angular velocity (ω) was named *pseudo Muscular Power* (pMP) and it was adopted as a meaningful parameter to discriminate eccentric and concentric muscle action from a mechanical point of view. In coherence with the angular convention, the muscle Torque contribution was set positive if acting in extension, both for extensor and flexor muscles: therefore the pMP resulting curves showed positive parts corresponding to concentric contractions and negative parts for eccentric contractions. Subsequently, the area enclosed between the positive part of the pMP curve and the time axis, calculated after integration versus time on a pre-defined time period, was associated with a *concentric pseudo Muscular Work* (pMW_C); conversely the area enclosed between the negative part of the pMP curve and the time axis was associated with an *eccentric pseudo Muscular Work* (pMW_E). Finally the ratio R_{MWEC} between pMW_E and pMW_C was introduced as an immediate index useful to estimate in a certain time period the relative amount of eccentric and concentric muscular work. A different method for evaluating the eccentric/concentric contraction amount, based on the simple analysis of the angular velocity sign, was applied to find how much time the muscle spent in a concentric or eccentric phase during a given time period. Looking at the angular velocity sign (positive for concentric, negative for eccentric contraction), the ratio R_{TEC} of eccentric and concentric contraction times was calculated. Both the two indexes R_{MWEC} and R_{TEC} were calculated over the interval between S2 and S7 poles as well as over the whole 60 m free slalom duration for each course.

3- Results

The mean curve (black solid line) and the Standard Deviation of external turns on the course with boot B are presented in Figure 2. EMG analysis of internal and external turn cycles showed a greater muscle activation in external turns for all muscles (Figure 3 and Figure 4) excluding Tibialis Anterior and Erector Spinae. Statistical analysis of EMG peak with the three boots showed for external turns significant differences for Tibialis Anterior (boot A versus boot C; $p \leq 0.05$), Gluteus Maximus (boot A versus boot B; $p \leq 0.05$) as showed in Figure 5 and Erector Spinae (boot B versus boot C; $p \leq 0.01$). Angular displacement (θ), angular velocity (ω), pseudo muscular concentric and eccentric power (pMP_C and pMP_E) of each muscle were calculated for each course in the interval between S2 and S7 poles and then for the whole 60 m free slalom and finally plotted as shown in Figure 6 and Figure 7. In each of the four graphs, θ is represented with a thick black line and ω with a thin black line. Their respective Y axis scale is on the right. The thin black line with circles represents iEMG muscle curve and refers to the Y scale on the left; pMP_C and pMP_E are plotted with a thick solid black line and with a grey solid black line respectively, referring to the Y axis scale on the right of the graphs. Short pole numbers from S2 to S7 are reported on the top of the graphs of Figure 6. In Table 1 R_{MWEC} and R_{TEC} indexes calculated for each boot over the interval between S2 and the S7 poles as well as over the whole 60 m free slalom duration are presented with the corresponding ski time.

S2-S7 POLES SLALOM	BOOT A t=5.12 sec		BOOT B t=5.03 sec		BOOT C t=5.60 sec	
	R_{MWEC}	R_{TEC}	R_{MWEC}	R_{TEC}	R_{MWEC}	R_{TEC}
Vastus Medialis	0.66	0.78	0.95	0.91	1.04	0.88
Vastus Lateralis	0.57		0.89		1.10	
Biceps Femoris	1.85	1.28	1.12	1.10	1.25	1.14
Semimembranosus	1.03		0.79		0.94	
60 m FREE SLALOM	**BOOT A t=7.52 sec**		**BOOT B t=7.43 sec**		**BOOT C t=7.58 sec**	
	R_{MWEC}	R_{TEC}	R_{MWEC}	R_{TEC}	R_{MWEC}	R_{TEC}
Vastus Medialis	1.07	1.08	1.14	1.38	0.70	1.02
Vastus Lateralis	1.06		1.21		0.74	
Biceps Femoris	0.93	0.93	0.97	0.72	1.46	0.98
Semimembranosus	0.57		0.43		0.52	

Table 1 - R_{TEC} versus R_{MWEC} for eccentric and concentric muscle evaluation in short poles and 60 m free slalom.

4- Discussion

In the present study results indicated that there was a big difference in EMG activity between internal and external turn cycles with the greatest activation in external turns as reported in Figure 3 and Figure 4 excluding Tibialis Anterior and Erector Spinae. During external turns, phenomena of co-contraction for knee flexors and extensors were observed in accord with Hintermeister *et al.* [HO1].

Statistical analysis showed significant differences in EMG peak activation for 3 muscles (Tibialis Anterior, Gluteus Maximum and Erector Spinae) out of eight while testing different boots during external turns, but no statistical differences were found in internal turns analysis.

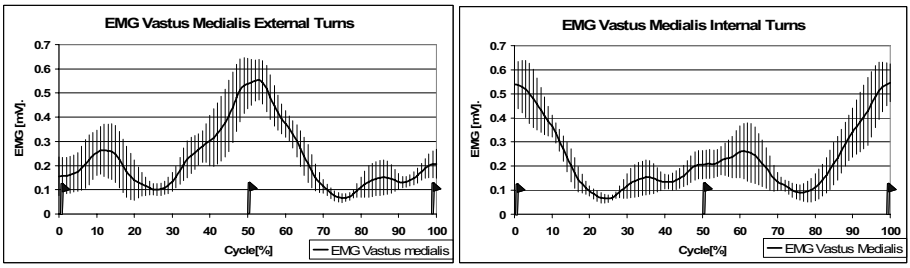

Figure 2 - Vastus Medialis EMG mean and Standard Deviation in External Turns with boot B (values expressed in millivolts).

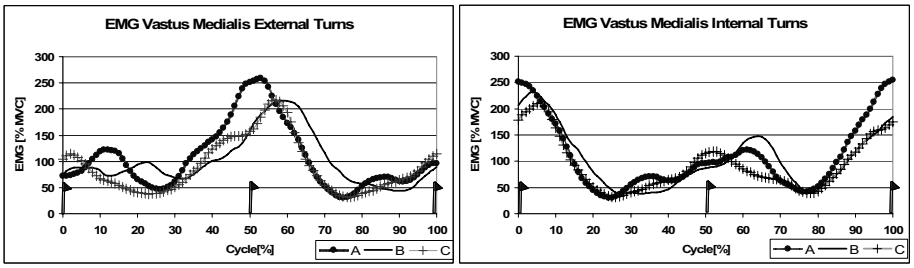

Figure 3 - Differences between external and internal turns in EMG mean activation of Vastus Medialis.

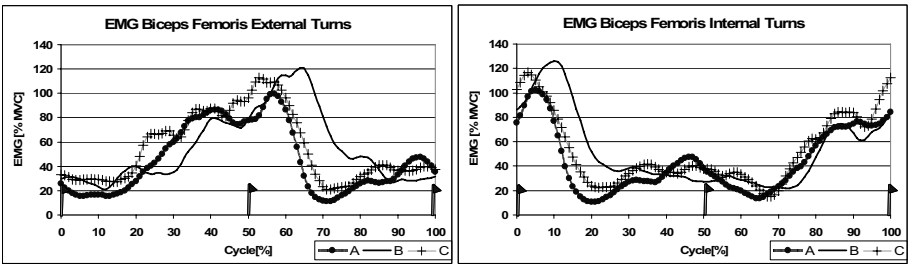

Figure 4 - Differences between external and internal turns in EMG mean activation of Biceps Femoris with the three boots (A, B, C).

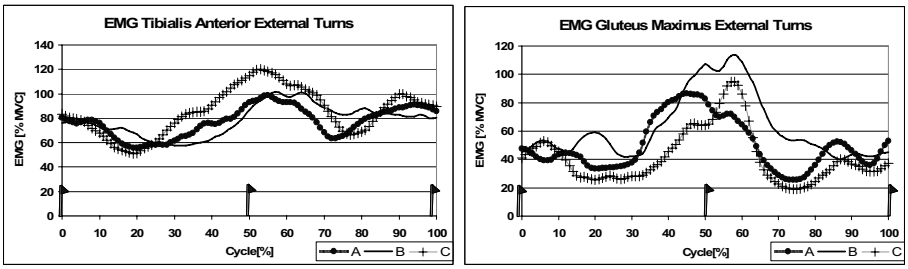

Figure 5 - EMG mean activation of Tibialis Anterior and Gluteus Maximum with the three boots (A, B, C) during external turns.

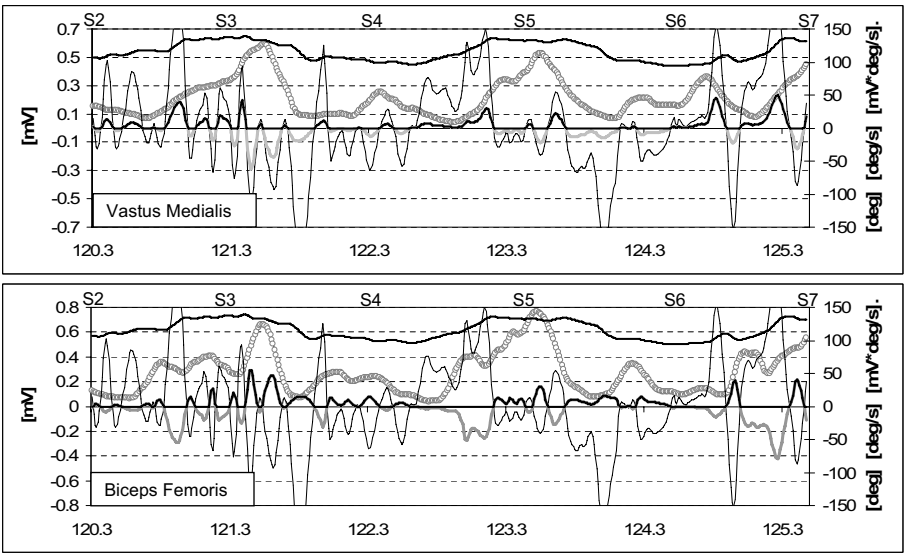

Figure 6 - Results of the analysis of Vastus Medialis and Biceps Femoris between poles S2 and S7.

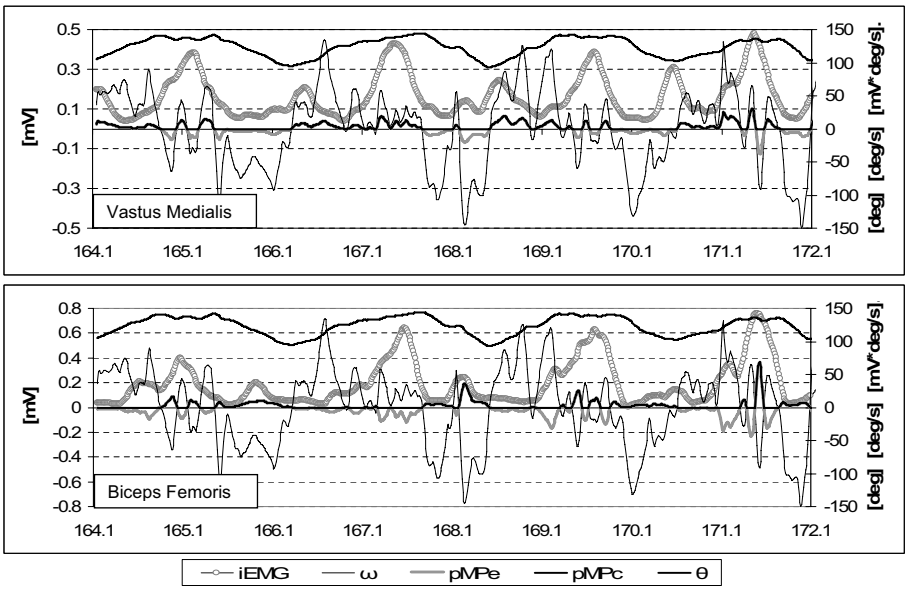

Figure 7 - Results of the analysis of Vastus Medialis and Biceps Femoris in free slalom.

The ratio between eccentric and concentric knee muscles action elaborated with the two methods showed appreciable differences. In slalom between short poles, the ratio between eccentric and concentric contraction calculated in terms of time duration using angular velocity (R_{TEC}) showed, relative to knee extensors, the highest value with boot B, then C and finally A. But analyzing the level of eccentric and concentric activation using R_{MWEC}, the highest value was obtained with boot C, then B and A. For knee flexors the ranking was A, C, B. R_{MWEC} allowed to appreciate a greater eccentric action of the Biceps Femoris rather than the Semimembranosus. In the 60mt free slalom there was an increase of eccentric action of the knee extensors for both the indexes calculated; the higher eccentric activity of Biceps Femoris was confirmed.

The introduction of concentric and eccentric pseudo Muscular Work (pMW_C and pMW_E) was useful to better understand the intensity of the eccentric and concentric activation. In fact, eccentric and concentric contraction calculated in terms of time duration using only the sign of angular velocity missed important functional information: how hard muscle fibres were working in that condition. The consequence is that a muscle which spent short times in eccentric action with a high activation shouldn't be trained as a muscle which spent for example short times eccentrically but with a low level of activation.

5- Conclusions

An integrated measurement system for EMG, for skier body posture and for ski angle of attack was developed. Electromyographical analysis allowed comparison of different equipment in terms of different levels of muscle activation even if small differences could be hardly detected. More research is needed to correlate the tester's subjective evaluation with engineering, biomechanical and physiological quantities.

A marked predominance of eccentric over concentric muscle actions was not observed. The evaluation of concentric and eccentric muscle action during special slalom between short poles and during the 60 m free slalom gave important information for the development of specific training programs in term of intensity of the stimulus, time duration and knee angular velocity. Further investigations with a higher number of professional skiers and with a higher number of courses could help to better understand knee flexors and extensors eccentric and concentric actions with respect to time and intensity of activation.

6- References

[BE1] Berg HE, Eiken O. Muscle control in elite alpine skiing. Med Sci Sports Exerc. 31(7): 1065-7, 1999.

[HO1] Hintermeister RA, O'Connor DD, Dillman CJ, Suplizio CL, Lange GW, Steadman JR. Muscle activity in slalom and giant slalom skiing. Med Sci Sports Exerc. 27(3): 315.22, 1995.

[T1] Tesch PA. Aspects on muscle properties and use in competitive Alpine skiing. Med Sci Sports Exerc. 27(3): 310-4, 1995.

7- Acknowledgements

The authors desire to thank the company Nordica SpA (TV –Italy) for supporting this research.

A New Evaluation System for Dynamic Muscular Strength Characteristics using Isoviscous Loading (P231)

Kenji Shigetoshi[1], Tadao Isaka[2], Sadao Kawamura[2]

Topics: Measurement Systems
Abstract: Measurement of human muscular strength is one of basic requirements in human motion science. In many previous researches, human torque patterns are measured as a function of joint angle position or a function of joint angle velocity, not both of them. However, the human torque characteristics should be represented by joint angle position and joint angle velocity for measurement of dynamic muscular strength characteristics. For this purpose, isokinetic loading systems have been used so far. In this paper, we point out that isoviscous loading systems are more effective than isokinetic loading systems in order to obtain the torque/joint angle velocity/joint angle position data. To realize the isoviscous loading systems, we utilize a direct drive motor and impedance control. The impedance control generates isoviscosity by reducing inertia effect and elastic effect. The performance of the loading system with isoviscosity is demonstrated through experimental results at first. Next, in the obtained torque/joint angle velocity/joint angle position data, repeatability on the same subject is confirmed and similarity on the shape of the surface in the three dimensional data space (torque/velocity/position) is investigated.
Key words: Isoviscous Load, Dynamic Muscle Strength Characteristics, Measurement, Mechanical Impedance Control, Isokinetic Load.

1- Introduction

Measurement of the maximum joint torque is important as basic data in human sport science. The maximum joint torque had been measured at some fixed joint angle positions in the sense of static measurement. Since the static measurement can not represent dynamic characteristics, it is necessary to measure maximum joint torque with motion. It is natural to use an isokinetic machine for measurement of maximum torque with fixed joint angle velocity. Marshall *et al.* expressed the maximum torque surface in joint

1. Seta Tsukinowa-cho, Otsu, Shiga, 520-2192, Japan - E-mail : sigetosi@belle.shiga-med.ac.jp
2. 1-1-1 Noji Higashi, Kusatsu, Shiga, 525-8577, Japan - E-mail : {isaka, kawamura}@se.ritsumei.ac.jp

angle velocity and joint angle position space using a commercial isokinetic machine (Marshall et al. 1990). However the torque oscillation appeared clearly at high speeds, which showed low reliability of the data. In general, the torque oscillation problems at high speeds have been pointed out in the measurement using the isokinetic machine (Lander *et al.* 1985, Seger *et al.* 1988, Kannus and Beynnon 1993).

In recent years, the importance of isoviscous load concept was pointed out by Itoh *et al.* Since this load increases in proportion to motion speed (joint angle velocity), the torque increases and decreases smoothly (Itoh *et al.* 1997). Therefore it seems that isoviscous loading systems are suitable for dynamic measurement of torque data. However, it is not clear whether repeatable torque data can be obtained by isoviscous loading systems because motion patterns with non-zero acceleration are freely generated by subjects.

In this paper, we developed an isoviscous loading system by using a direct drive motor and impedance control. The performance of the developed system to realize isoviscosity is experimentally investigated at first. Next, the data of torque-joint angle velocity-joint angle position with four subjects are measured. As the result, it is confirmed that repeatable data can be obtained by isoviscous loading systems. Moreover, similarity on the shape of the surface in the three dimensional data space (torque/velocity/position) is explained.

2- Comparison of isoviscous load with conventional load

In this section, it is shown that isoviscous load is superior to inertia load, elastic load and isokinetic load. Human joint motion needs an acceleration period and deceleration period due to the limitation of the range of motion. Thus the joint angle velocity must be zero at the end of motion.

Inertia load: If gravitational force is ignored, the area in joint angle velocity $\dot{q}$ and joint angle position q data-space becomes small because a deceleration period must be set in order to stop the motion within joint angle limitation. To increase the data points, it is possible to add other motions with different initial positions as seen in Figure 1 (thin solid line). However, it is drawback to increase the number of motions.

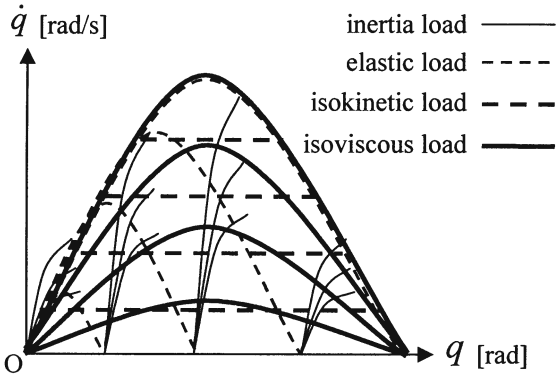

Figure 1- Characteristics of inertia, viscosity, elasticity and isokinetic loads.

Elastic load: Elastic load increases in proportion to the joint angle position and makes maximum resistance at the end of motion. Therefore, if we set large elastic coefficients, joint angle position changes must be small as seen in Figure 1 (thin dashed line). To increase the data points, we need other motions which start from other initial positions in the same manner as inertia load case.

Isokinetic load: In isokinetic load, maximum torque with fixed joint angle velocity is measured. As seen in Figure 1 (thick dashed line), motions can cover data points in $\dot{q}$-q space effectively in comparison with inertia or elastic cases. However, there are two problems in isokinetic loading systems. The first one is that the data before reaching the fixed speed are not used. The other one is that impacts of torque data appear after reached at the fixed speed. It makes oscillations in the torque data.

Isoviscous load: Comparing of isoviscous load with conventional other loads (inertia, elastic and isokinetic loads) in Figure 1 (thick solid line), isoviscous load can cover the data space efficiently. Moreover, torque data can be obtained without oscillations. On the other hand, it is not clear whether repeatable torque data can be obtained by isoviscous loading systems because humans can freely generate motion patterns with non-zero acceleration.

3- Measurement system

3.1 Overview of the measurement system

The developed measurement system is shown in figure 2. This system consists of an actuator to give load to a subject and a computer to calculate control input from the signals of the strain gauges and the rotary encoder. A direct drive motor with the rated output 30[Nm] is utilized and torque signals are obtained through the strain gauges. The angle of the lever arm is obtained from the rotary encoder (resolution: 0.51×10^{-6} [rad]) in the direct drive motor. The initial angle of the lever arm sets at 0.785[rad] (45[deg]) from downward vertical direction. A stand to rest the upper arm is fixed on the base table. There is a Velcro tape on this stand to fasten the upper arm on the stand. For safety, a stopper is implemented in order to limit the lever arm rotation from 0 to 2.6 [rad].

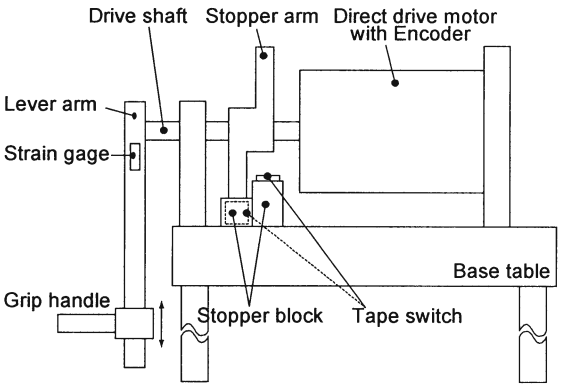

Figure 2 - Developed measurement system for the mechanical impedance control.

3.2 Control law of the measurement system

To develop an isoviscous loading system, we use impedance control, which can realize desired inertia, viscosity and elasticity coefficients. The mechanical part of the measurement system has the inherent inertia. Since impedance control can set smaller inertia than that of the original one, it is possible to realize more precise value of isoviscosity.

The ideal impedance model that should be realized is given by

$$m\ddot{\theta}_d + b\dot{\theta}_d + k\theta_d = \tau_h \tag{1}$$

where m, b, k, τ_h denote ideal inertia, ideal viscosity, ideal stiffness, and human generated torque, respectively. The desired trajectory of the actual system is θ_t (t) that stands for the ideal trajectory expressed by Eq. (1). If ideal impedance can be realized, motion should be θ_d (t). Hereafter, $\ddot{\theta}_d$, $\dot{\theta}_d$, θ_d become desired joint angle acceleration, the desired joint angle velocity and the desired joint angle position for the actual system. The dynamics of the actual system is expressed as

$$M\ddot{\theta} + B\dot{\theta} + g = u + \tau_h \tag{2}$$

where M, B denotes inertia coefficient, viscosity coefficient, respectively. $\ddot{\theta}$, $\dot{\theta}$, θ denote the actual joint angle acceleration, the actual joint angle velocity and the actual joint angle position. u denotes the control input.

To realize the ideal impedance, we set u

$$u = k_p(\theta_d - \theta) + k_v(\dot{\theta}_d - \dot{\theta}) + (\tilde{M} - m)\ddot{\theta}_d + (\tilde{B} - b)\dot{\theta}_d - k\theta_d + g \tag{3}$$

where k_p, k_v denote the feed back gains. $\tilde{M}$ and $\tilde{B}$ stand for an estimated inertia coefficient and an estimated viscosity coefficient, respectively. The desired angle, velocity and acceleration are calculated by the Runge-Kutta method from Eq. (1).

Now by substituting Eq. (3) into Eq. (2), we obtain

$$m\ddot{\theta}_d + b\dot{\theta}_d + k\theta_d + \eta = \tau_h \tag{4}$$

where η is given by

$$\eta = M(\ddot{\theta} - \ddot{\theta}_d) + (B + k_v)(\dot{\theta} - \dot{\theta}_d) + k_p(\theta - \theta_d) + (M - \tilde{M})\ddot{\theta}_d + (B - \tilde{B})\dot{\theta}_d . \tag{5}$$

If the system parameters are estimated with high accuracy and the feedback gains are set sufficiently large, η of Eq. (5) is nearly equal to zero and the desired impedance parameters are realized in actual system.

3.3 Accuracy of the mechanical impedance display

There are cases that ideal impedance values can not be realized due to limitation of the hardware such as the feedback delay. We then made clear the accuracy of the realized mechanical impedance and investigated the influence on the measurement. The accuracy of the mechanical impedance values on this study is shown form figure 3 to figure 5.

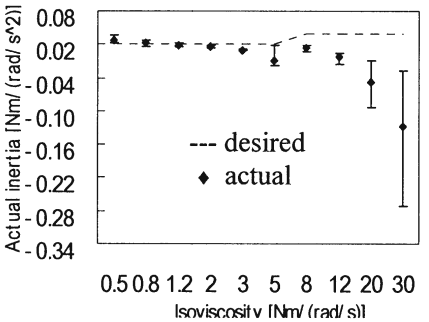

Figure 3- Ideal inertia and practical inertia.

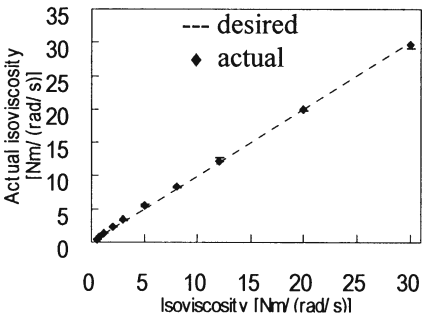

Figure 4 - Ideal viscosity and practical viscosity.

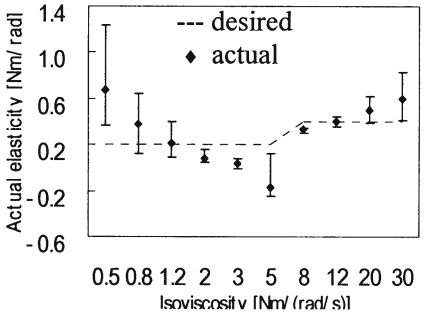

Figure 5 - Ideal elasticity and practical elasticity.

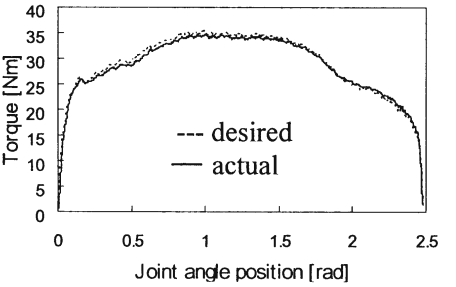

Figure 6 - Relation of torque and angle at 30.0[Nm/(rad/s)].

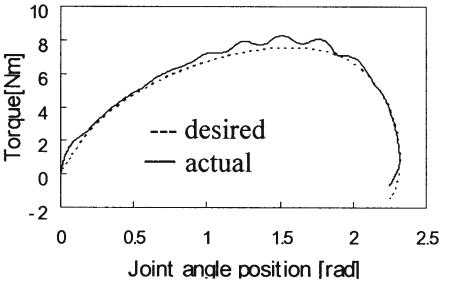

Figure 7 - Relation of torque and angle at 0.5[Nm/(rad/s)].

As seen in figure 4, the viscosity value could be almost equal to the ideal one. The inertia values and the elastic values had errors from the ideal values. Moreover, in some cases those values became negative as seen in figure 3 and figure 5. Even though the inertia and the elasticity values could not be equal to the ideal values, the errors were sufficiently small. Therefore, the actual torque curve is almost equal to the desired torque curve produced by the ideal impedance values as seen in figure 6 and figure 7. The figures show the worst cases with a maximum inertia error and a maximum elasticity error. From these results, it is confirmed that the influence on the measurement can be neglected.

4- Measurement experiment using isoviscous loading

4.1 Subjects

Four university students (mean age, stature and body mass: 21.3±0.5 (SD) years, 170.1±7.3 cm and 61.5±12.9) were participated in this study. Informed consent to participate in this study was obtained from all subjects.

4.2 Experimental condition

The movement measured was maximal voluntary elbow flexion from full extension to full flexion. The upper arm, forehead, hip and shoulders were fixed on the stand (see section 3.1) and the experimental chair with Velcro tapes. The centre of the elbow joint axis was aligned to the axis of the lever arm.

The maximum elbow joint torques of the subjects were measured with ten viscous coefficients: 0.5, 0.8, 1.2, 2.0, 3.0, 5.0, 8.0, 12.0, 20.0, 30.0 [Nm/(rad/s)]. The measurement was carried out from 0.5 to 30.0 [Nm/(rad/s)] continuously. A set of measurement from 0.5 to 30.0 [Nm/(rad/s)] was performed two times in a day and about five minutes rest time was set between two sets of measurements. This measurement continued in three days. The measurement data of the first day was ignored as the training for the developed system.

5- Results and Discussion

5.1 Comparison of an isoviscous loading system with an isokinetic loading system

We carried out the following two experiments to compare an isoviscous loading system with an isokinetic loading system.

Experiment 1. The isokinetic torque patterns of the right elbow were measured by Cybex 6000 where eleven different speeds were utilized.

Experiment 2. The isoviscous torque patterns of the right elbow were measured by the developed isoviscous loading system where 10 patterns of isoviscous values similar to isokinetic results are utilized.

These experiments were executed by a same person in different days. We instructed the subject to generate the maximum muscle strength. The results are shown in figure 8(A) and 8(B). The figures 8(A)-1 and 8(B)-1 represent three-dimensional lines of each motion in the cases of the isokinetic load and the isoviscous load. The figures 8(A)-2 and 8(B)-2 represent the surfaces in the three-dimension. To make the surface, a linear interpolation as seen in Figure (B)-1 was used to estimate the data values where there was no value of the data. To obtain the result shown in Figures 8(A), the data directly obtained from Cybex6000 were used in (A) cases and a low-pass filtered with 20 [Hz] cut-off-frequency was utilized in (B) case. As seen in the both figures, the isokinetic torque surface has lack of data in the high speed area because it is difficult to obtain the data in the high speed area.

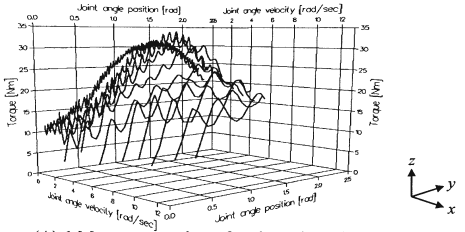

(A)-1 Measurement data of each motion with Isokinetic load

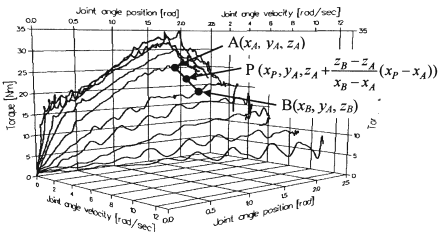

(B)-1 Measurement data of each motion with Isoviscous load

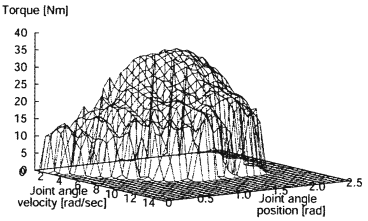

(A)-2 Surface of Isokinetic load data

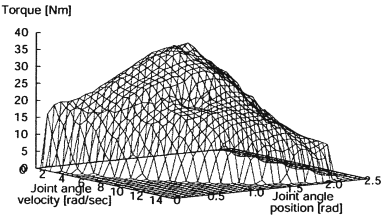

(B) -2 Surface of Isoviscous load data

Figure 8 - Experimental results to compare isoviscosity with isokinetic.

5.2 Measurement Results of Four subjects

Figures from 9 to 12 show the isoviscous torque surfaces about four subjects (subject A - D). The 2nd day and the 3rd day measurement results are shown by the solid line and the dashed line, respectively in each figure.

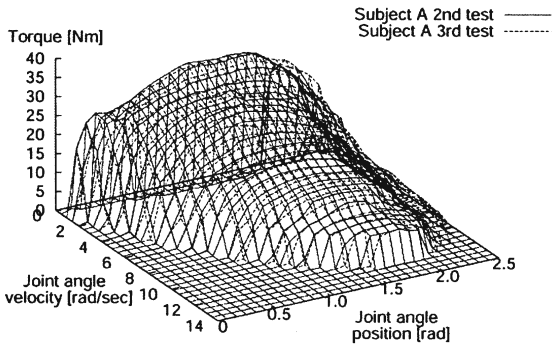

Figure 9 - Experimental results: Subject A.

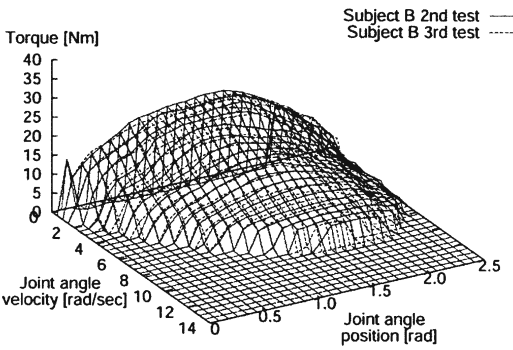

Figure 10 - Experimental results: Subject B.

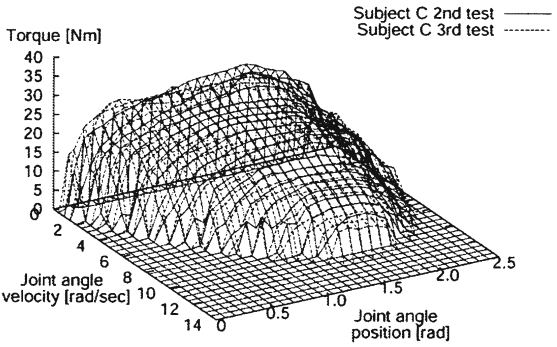

Figure 11 - Experimental results: Subject C.

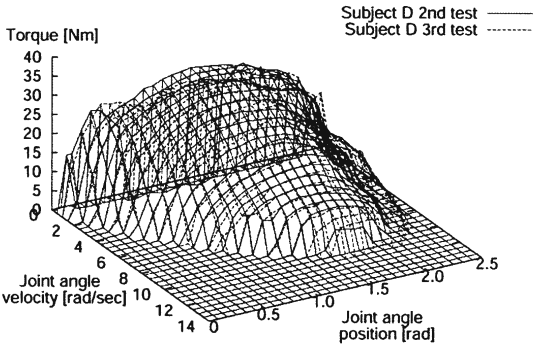

Figure 12 - Experimental results: Subject D.

5.3 Repeatability of Measurement Data

To investigate the repeatability of the measurement data, the average difference between the 2nd and 3rd day measurement is calculated by Eq. (6).

$$EN_X = \frac{1}{m \times n} \sqrt{\sum_{i=0}^{n} \sum_{j=0}^{m} (\tau_2(i,j) - \tau_3(i,j))^2} \tag{6}$$

where EN_X : average difference, X : subject name, i: joint angle position data point j: joint angle velocity data point, $\tau(i, j)$:the torque, m=141, n=51: the data point number and subscript (2, 3) : measurement day. If there is measurement value on one day and no measurement value on the other day, we did not count the data in Eq.(6). As the results, the intra-subject average difference was calculated using 94.5±5.1% of the original data. The results are shown by table 1. From this results, the maximum difference of the same subject is smaller than 2.0 [Nm].

Subject	Average difference [Nm]
A	1.960
B	0.953
C	1.971
D	1.981

Table 1 - Intra-subject average difference.

5.4 Comparison between subjects

To show the difference of the measurement data among the subjects, the average defe-rence between the subjects was calculated by Eq. (7).

$$EN_{XY} = \frac{1}{m \times n} \sqrt{\sum_{i=0}^{n} \sum_{j=0}^{m} (\tau_{kX}(i,j) - \tau_{kY}(i,j))^2} \quad (7)$$

where EN_{XY}: average difference between subjects, *k*:2nd / 3rd day, *X* , *Y* : subject name. The results showed the difference from 2.440 to 9.207 [Nm] as described in table 2. In this case also if there is measurement value on one subject and no measurement value on the other subject, we did not count the data in Eq.(7). As the results, the inter-subject average difference was calculated using 90.6±7.3% of the original data.

5.5 Comparison between subjects by normalizing with Subject A

To make clear characteristics of the data surface, we normalized the torque data of the subject B, C, D by the torque, the joint angle velocity and the joint angle data of the subject A. In the normalization, we multiply each data of subject B, C, and D by the ratios (maximum torque of A/maximum torque of others, maximum joint angle velo-city of A/maximum joint angle velocity of others, and maximum joint angle of A/maximum joint angle of others). The normalized results are shown in table 3. The differences between subjects are considerably small because the average difference of the intra-subject was obtained as about 2 [Nm]. The inter-subject average difference was calculated using 94.6Í3.8% of the original data.

Subject	Average difference [Nm]	
	2nd day	3rd day
A-B	9.207	8.974
A-C	4.229	2.440
A-D	2.986	2.612
B-C	5.984	7.167
B-D	7.434	7.221
C-D	2.672	2.469

Table 2 - Inter-subject average difference.

Subject	Average difference [Nm]	
	2nd day	3rd day
A-B	2.310	2.208
A-C	3.061	3.280
A-D	2.547	2.229

Table 3 - Inter-subject average difference after normalizing by Subject A.

6- Conclusion

We developed an isoviscous loading system to measure dynamic characteristics of human elbow torque. It was shown that the developed system in this paper could measure torque-joint angle velocity-joint angle position data effectively. In the data of ordinary students, there was no individual difference on the normalized data. However, it is still not clear whether various types of muscle strength characteristics or various shapes of the surface can be observed by isoviscous loading. To make clear this point, we

need to measure and analyze the data of many subjects that might have different muscle strength characteristics. It is one of the future works to investigate whether sports athletes have different shapes of the surface.

References

[IA1] Itoh, K., Mita, K., Akataki, K., Watakabe, M., Soeda, T., Nonaka, H. and Katoh, A. Mechanical properties of dynamic muscle contraction against viscosity resistance (isoviscous contraction) its comparison with isotonic and isokinetic contraction. In Japanese Journal of Physical Fitness and Sports Medicine, 46(2): 211-219, 1997

[KB1] Kannus, P. and Beynnon, B. Peak Torque Occurrence in the Range of Motion During Isokinetic Extension and Flexion of the Knee. In International Journal of Sports Medicine, 14(8): 422-426, 1993

[LB1] Lander, J. E., Bates, B. T., Sawhill, J. A. and Hamill, J. A Comparison between Free-Weight and Isokinetic Bench Pressing. In Medicine and Science in Sports and Exercise, 17(3): 344-353, 1985

[MM1] Marshall, R. N., Mazur, S. M. and Taylor, N. A. S. Three-dimensional surfaces for human muscle kinetics. In European Journal of Applied Physiology, 61: 263-270, 1990

[SW1] Seger, J. Y., Westing, S. H., Hanson, M., Karlson, E. and Ekblom, B. A New Dynamometer Measuring Concentric and Eccentric Muscle Strength in Accelerated, Decelerated, or Isokinetic Movements - Validity and Reproducibility. In European Journal of Applied Physiology and Occupational Physiology, 57(5): 526-530, 1988

Aerodynamics of a Curve-ball: The Sikorsky/Lightfoot Lift Data (P234)

LeRoy W. Alaways*

Topics: Baseball, Aerodynamics.
Abstract: In the 1940s and 50s, the United States was engaged in a national debate on whether the curve in baseball was an optical illusion. During this debate, Igor I. Sikorsky and Ralph B. Lightfoot investigated the lift force produced by a baseball spinning from zero to 1200 rpm (revolutions-per-minute) in a wind tunnel at free-stream velocities between 80 and 110 miles per hour[1] (35.8 and 49.2 m/s). A brief note about the findings were later published by Joseph Drury (1953) reporting Sikorsky had determined that a four-seam pitch could curve three time more than a two-seam pitch. However, the substantive supporting experimental data was never published and over the years appeared to have been lost. The Sikorsky/Lightfoot data set was rediscovered; it is compared to more recent aerodynamic lift data for golf and baseballs with excellent correlation. The data also shows that seam orientation (i.e. surface roughness) has a large influence on lateral deviation in a high velocity pitch.
Key words: Baseball; Aerodynamics; Lift Coefficients.

1- Introduction

Currently, the fact that a spinning spherical projectile deviates from a simple parabolic trajectory is now well accepted in the scientific community. In fact, the curve of a tennis ball was noted by Newton (1671) and a little over two hundred years later, Lord Rayleigh (1877), in his paper on the irregular flight of the tennis ball, credited Magnus with the "first" explanation of the lateral deviation. At roughly the same time, Tait (1896) was including this effect in his differential equations describing the non-parabolic trajectories of golf balls.

* *Department of Mechanical Engineering, Villanova University, 800 Lancaster Ave., Villanova, Pennsylvania, USA 19085 - leroy.alaways@villanova.edu*

1. While the author fully acknowledges the SI units, the historical units of baseball are feet, inches, pounds, and miles-per-hour. The data presented in this paper was measured in 1949 in pounds and miles-per-hour and converting this data to SI units distracts from its historical importance.

Portions of the public, on the other hand, were not convinced that the curve in baseball was real. This was reflected by a 1941 letter to the editor of the *New Yorker* (Madden, 1941) magazine that started a national debate on this subject. Two sources of the more interesting contributions to the debate, *Look* (Cohane, 1949) and *Life* (Baseball's Curve Balls: Are They Optical Illusions, 1941; Camera and Science Settle the Old Rhubarb About Baseball's Curve Ball, 1953) magazines both printed photographic essays for and against the curve. It was because of this issue and scientific curiosity that aerodynamicist Sikorsky enlisted the aid of Lightfoot, then Chief of Flight Research at Sikorsky Aircraft, to undertake a wind-tunnel investigation measuring the lateral force on spinning baseballs. This paper presents the original 1949 findings along with a comparison to the more recent aerodynamic lift data determined for spinning baseballs.

1.1 Non-dimensional comparison of lift coefficients

The first published findings of lift coefficient versus the non-dimensional spin parameter, $S = R\omega / V$, where: R is the radius of the ball, ω is the angular velocity, and V is the free-stream velocity of the ball with respect to the wind was presented by Maccoll (1928). Maccoll determined the lift and drag coefficients for 6-inch (0.152 m) diameter smooth spheres rotating at speeds up to 1800 rpm in free-stream velocities up to 23 miles per hour (10.3 m/s). Davies (1949) determined the aerodynamic forces on golf balls by measuring the final lateral deviation from a vertical line produced from spinning balls, rotating at speeds up to 8000 rpm, and dropped through the horizontal wind steam of a wind-tunnel operating at a velocity of 71.6 miles per hour (32 m/s). Davies tested both standard dimpled golf balls and smooth spheres. Briggs (1959) conducted a similar experiment to Davies but using baseballs along with smooth spheres. Briggs dropped balls spinning about a vertical axis at speeds up to 1800 rpm across the horizontal wind stream of a 6-ft (1.83 m) tunnel operating at speeds up to 102.3 miles per hour (45.7 m/s). Briggs then extrapolated that the maximum expected deviation for a pitched ball in play would range from 10 to 17 inches (0.254 to 0.432 m).

Bearman and Harvey (1976) examined, in a wind-tunnel, the aerodynamics of the golf ball. In their study, three models of a golf ball (conventionally-dimpled, hexagonally-dimpled and smooth) 2.5 times full-scale were used with a spinning apparatus mounted inside each model. Each model was carefully mounted in a wind-tunnel operating at a free-stream velocity of 82.8 miles per hour (37 m/s) that simulates flow over a golf ball at a velocity of 206.9 miles per hour (92.5 m/s). Bearman and Harvey then measured the lift force using a strain gage and the drag force with the wind-tunnel's balance. Lift and drag coefficients were then calculated for the conventionally- and hexagonally-dimpled balls.

Watts and Ferrer (1987) published their results on the lateral force for baseballs. In their study, Watts and Ferrer measured the lift force on spinning balls at free-stream velocities up to 40 miles per hour (17.9 m/s). Three balls were impaled, in different orientations, on rotating shafts and mounted on a Plexiglas test device. The lift and drag forces were determined through bending stresses in the Plexiglas supports. From their data, Watts and Ferrer claim that no noticeable difference occurs in lift force when comparing

four- and two-seam curve balls. Watts and Bahill, however, question the validity of their conclusion due to the low wind speed in a later publication (Watts and Bahill, 1990).

Smits and Smith (1994) measured and the lift, drag, and spin decay rate of golf balls using a wind-tunnel by mounting actual golf balls on thin metal spindles. Data was collected for the *S*-range of 0.08 to 1.3 at various values of Reynolds number and equates well with the previous published ball data.

Alaways and Hubbard (2001) used video to track baseballs in flight and then estimated the aerodynamic constants using nonlinear least squares. The velocities of the pitches were in the 65 to 75 mph (29.1 to 33.5 m/s) range and showed a convergence at the higher spin parameter values.

1.2 A Quick Theoretical Look at the Curve

The origins of and the equations describing the aerodynamic forces acting on a ball in flight are well defined. Alaways (1998) give a comprehensive discussion concerning these forces and the effect they have on the trajectory of spinning baseballs. However, a brief discussion of the lift force and resulting lateral deviation is presented here to show the motivation for the Sikorsky experiments.

The lift force, F_L, on the ball is given by the lift equation[2]:

$$F_L = \tfrac{1}{2} C_L \rho A V^2 \tag{1}$$

where: C_L is the lift coefficient, r is the density of air, and A is the cross-sectional area of the ball.

If only the lift force acts in the lateral direction and that the initial lateral velocity is zero, the lateral acceleration, a_L, of the ball is given by

$$a_L = \frac{F_L}{m}, \tag{2}$$

where m is the mass of the ball. The amount that the ball deviates laterally, d, in front of the plate is then determined by (assuming zero initial lateral deflection and zero initial lateral velocity)

$$d = \tfrac{1}{2} a_L t^2, \tag{3}$$

where t is the time for delivery. Combining Equations (1), (2) and (3) results in

$$d = \frac{C_L \rho V^2 t^2 A}{4m}. \tag{4}$$

2. In a letter to Joseph Drury (Lightfoot, circa 1950), Lightfoot calls the lift coefficient, "circulation" and states that the lift force is proportional to the circulation. Lightfoot gives credits to Kutta and Joukowsky for their mathematical treatment on this subject, however, if one is not careful with the changing language of engineering and replaces in the following calculations the lift coefficient with an angular velocity or circulation you will violate the Kutta-Joukowsky theorem.

The product V^2t^2 can be treated as a constant distance if one assumes that the ball is released from the same location. Assuming this distance to be 60.5 feet (18.44 m), the distance from pitcher's mound to home-plate, and setting r = 0.0763 lbm/ft^3 (1.20 kg/m^3), m = 0.311 lbm (0.141 kg) and A = 0.0448 ft^2 (0.0042 m^2); Equation (4) reduces to

$$d = 10C_L \text{ feet (or } d = 3.04C_L \text{ meters).} \quad (5)$$

Noting that d is directly proportional to C_L, which could be determined, was the motivating factors for undertaking the wind-tunnel analysis. In addition, from knowing the magnitude of C_L it would be possible to calculate the limits on the deviation one could expect. From the *Life* (Cohane, 1949) magazine article, an approximate 1 to 2 feet (0.305 to 0.610 m) of lateral deviation was determined, and therefore, experimentally determined lift coefficients as high as 0.2 were expected.

2- Methodology

The lift force was acquired, using a force balance, by measuring the lateral force generated on a spinning regulation Major League Baseball (MLB) impaled on a thin metal rotating shaft. A small variable-speed electric sewing-machine motor spun the shaft and this entire assembly (force balance, baseball, motor and shaft) was placed in a wind-tunnel at the Sikorsky Aircraft facilities. Rotation rates, measured with a stroboscope, varied from 0 to 1200 rpm in both clockwise and counter-clockwise directions perpendicular to the wind stream. This range of angular velocities was chosen to bracket the 600-rpm rotational speed found by visually examining the high-speed flash photographs presented in *Life* (Cohane, 1949). Free-stream velocities of 80, 95 and 110 miles per hour (35.8, 42.5, and 49.2 m/s) were used for four-seam curve balls to obtain the maximum amount of side force. For purposes of comparison, the ball was mounted in the two-seam configuration, producing a minimum amount of lift.[3] However, the two-seam tests were only conducted at 95 miles per hour (42.5 m/s). Though no longer available, hundreds of force and spin rate readings were recorded for each free stream velocity with uncertainties for both in the one-percent range (Lightfoot, 1997). The data was then faired resulting in the lift versus spin rate curves presented in Fig. 1.

The symmetry of the curves in Fig. 1 indicates a high repeatability in the data. An interesting feature is that the lift force for the four-seam curve is nearly triple that of the two-seam curve in the 95 miles per hour (42.5 m/s) data at rotation rates near 400 rpm.

3. Four- and two- seam curve ball are defined by the number of seams on the ball that trip the boundary layer of air at the ball's surface during rotation. This type of pitch is made possible due to the "hour-glass" design of the two pieces of leather that are stitched together forming the baseball's cover.

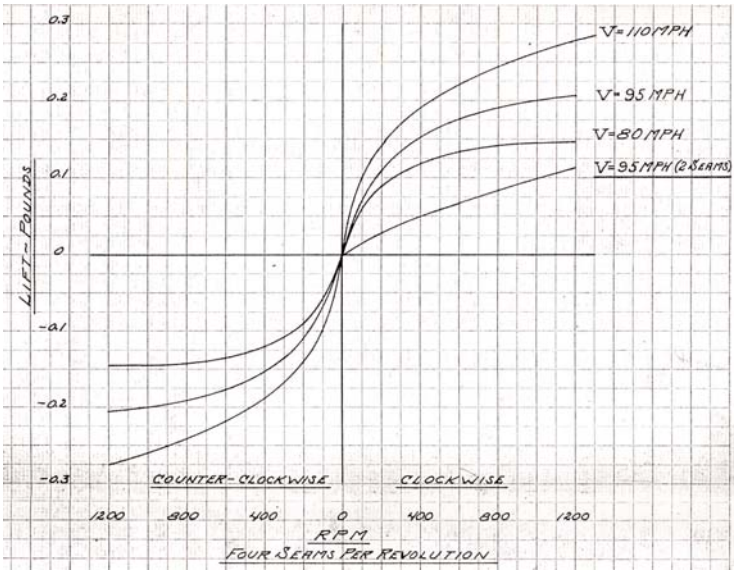

Figure 1 - Sikorsky lift force versus spin rate data for four- and two-seam curve balls[4].

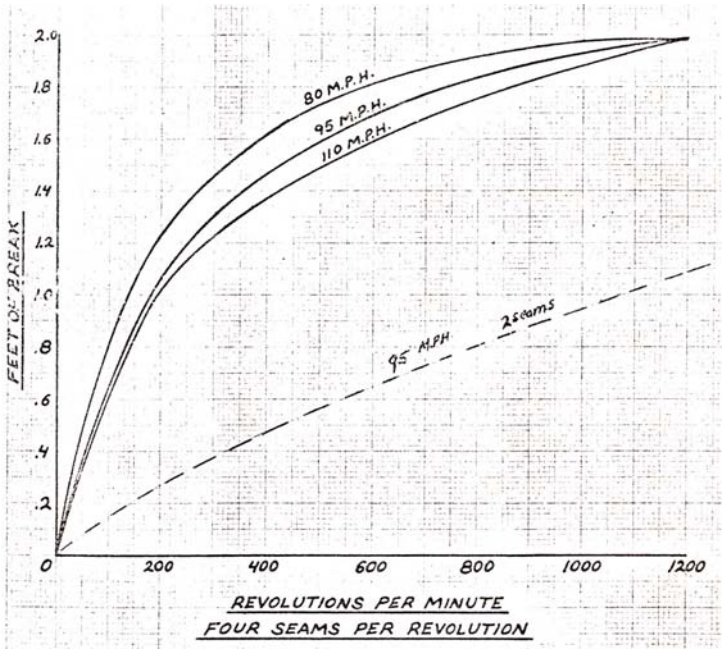

Figure 2 - Calculated lateral deviations ($d = 10.0C_L$) for four- and two-seam curve balls.

4. This figure and Fig. 2 are the original figures produced by Lightfoot in 1949 and are included in their original form to maintain the accuracy of the data.

3- Discussion

Determining C_L from the data in Fig. 1 using equation 1, and then applying equation 5, the lateral deviation versus spin rate was then determined. Figure 2 indicates that the amount of break is only slightly affected by forward velocity, but is strongly dependent on the rotational speed and axis of rotation. It is probable that the ball does not spin exactly about either the maximum or the minimum deviation axes during an actual pitch. If so, the amount of break obtained may be a value somewhere between the curves shown in Fig. 2. The values in Fig. 2 are also consistent with the estimated lateral deviation determined from the *Life* (Cohane, 1949) article.

An interesting and currently unexplainable feature illustrated in both Fig. 1 and Fig. 2 is the nearly constant values exhibited in the 80 miles per hour (35.8 m/s) data at the higher rotation rates. It would be of interest to investigate higher values of spin and other wind stream velocities to understand this more clearly.

Figure 3 is a compilation of the determined C_L versus S plots from the data of Sikorsky/Lightfoot, Davies (1949), Bearman & Harvey (1976), Watts & Ferrer (1987), Smits & Smith (1994), and of Alaways & Hubbard (1997). Figure 3 clearly shows a correlation amongst the ball data and that the data is bounded by roughness effects, either dimple size and shape or seam orientation.

The items of interest in the Sikorsky data of Fig. 3 are: the three four-seam plots are nearly identical, the large difference in the four-seam and two-seam data, and the correlation between the four-seam data with the Alaways & Hubbard data. The facts that the four-seam plots overlap and that a large difference exists in the four-seam and two-seam data shows that the location of the spin axis on the ball — not the rotation rate or release velocity — is the primary factor in lift coefficient magnitude. The correlation between the Sikorsky four-seam data and the Alaways & Hubbard data is more clearly seen in

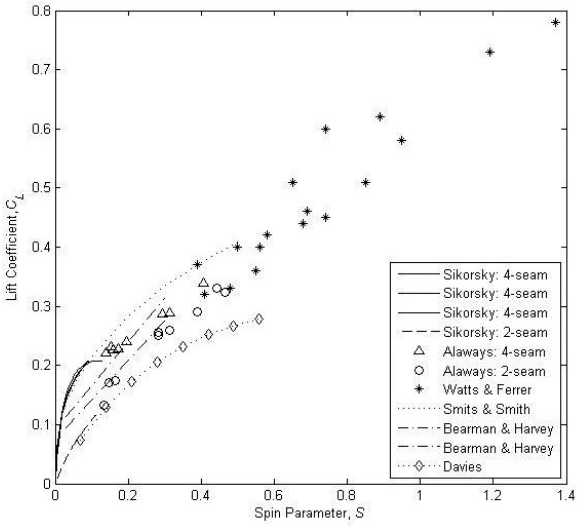

Figure 3 - Experimentally measured lift coefficient, CL, versus spin parameter, S.

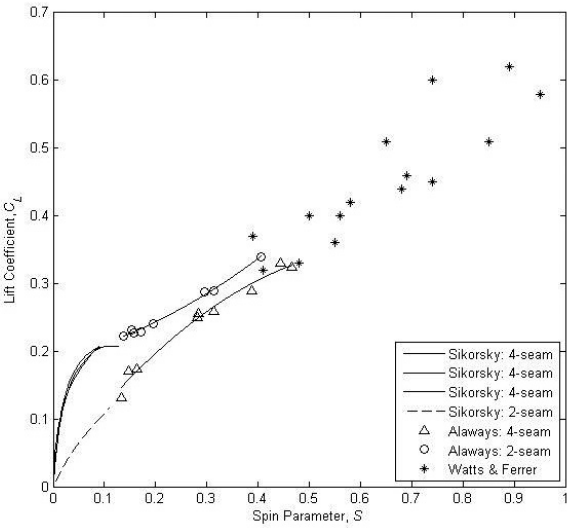

Figure 4 - Detailed portion of the lift coefficient versus spin parameter data for baseballs only.

Fig. 4 where the non-baseball data of Fig. 3 is removed and the axes are reduced to provide more detail in the S less than 1.0 range. Here, except for the nearly constant values of C_L exhibited by the 80 miles per hour (35.8 m/s) case, the values of C_L determined by Alaways & Hubbard appear to be a natural extension of Sikorsky's four-seam data.

4- Conclusion

The historical Sikorsky/Lightfoot lift data for baseballs is presented and shows that seam orientation with respect to the rotation axis has a large effect on the lift coefficient and hence lift force and lateral deviation for S values less than 0.2. The aerodynamic lift data for golf and baseballs appear to lie in a region defined by the roughness or seam orientation of the ball. It was also shown that for a given initial orientation the release velocity and rotation rates slightly affect the amount of break in the curve over a fixed distance.

5- Acknowledgments

The author would like to thank the late Ralph B. Lightfoot who collected the data in the early 1950s, meticulous maintained the results and personally asked me to publish them. The author also thanks and acknowledges the Sikorsky Aircraft Corporation/United Technologies for their co-operation in allowing these results to be published.

6- References

[A1] Alaways, L.W. Aerodynamics of the Curve-Ball: An Investigation of the Effects of Angular Velocity on Baseball Trajectories, Doctoral Dissertation, University of California, Davis, 1998.

[AH1] Alaways, L.W. & Hubbard, M. Experimental Determination of Baseball Spin and Lift, Journal of Sports Sciences, 19 (5), pp. 349 – 358, May 2001.

[B1] Baseball's Curve Balls: Are They Optical Illusions. In Life, 11, 83-89, 1941.

[BH1] Bearman, P.W. & Harvey, J.K. Golf Ball Aerodynamics. Aeronautical Quarterly 27, 112-122, 1976.

[B1] Briggs, L.J. Effect of Spin and Speed on the Lateral Deflection (Curve) of a Baseball; and the Magnus Effect for Smooth Spheres. American Journal of Physics 27, 589-596, 1959.

[C1] Camera and Science Settle the Old Rhubarb About Baseball's Curve Ball. In Life, 35, 104-107, 1953.

[C1] Cohane, T. Visual Proof that a Baseball Curves. Look, July 19, 74-77, 1949.

[D1] Davies, J.M. The Aerodynamics of Golf Balls. Journal of Applied Physics 20, 821-828, 1949.

[D1] Drury Jr., J.F. The Hell It Don't Curve! The American Mercury, May, 101-106, 1953.

[L1] Lightfoot, R.B. Personal letter to Joseph Drury, circa 1950.

[L2] Lightfoot, R.B. Personal conversation, 1997.

[M1] Maccoll, J.W. Aerodynamics of a Spinning Sphere. The Journal of the Royal Aeronautical Society 28, 777-798, 1928.

[M1] Madden, R.W. Our Skeptical Correspondents: Letter to the Editor. The New Yorker, May 24, 61-67, 1941.

[N1] Newton, I. New Theory about Light and Colours. Philosophical Transactions of the Royal Society 6, 3078, 1671.

[R1] Lord Rayleigh. On the Irregular Flight of a Tennis Ball. Messenger of Mathematics 7, 14-16, 1877.

[T1] Tait, P.G. On the Path of a Rotating Spherical Projectile. Transactions of the Royal Society of Edinburgh 39 Part 2 (16), 491-506, 1896.

[SS1] Smits A.J. & Smith, D.R. A New Aerodynamic Model of a Golf Ball in Flight, In The 1994 World Scientific Congress of Golf, ed. A J Cochran and M R Farrally, 340-347, St. Andrews, UK: E & FN Spon, 1994.

[WB1] Watts, R.G. & Bahill, A.T. Keep Your Eye On The Ball. New York: W.H. Freeman and Company, 1990.

[WF1] Watts, R.G. & Ferrer, R. The Lateral Force on a Spinning Sphere: Aerodynamics of a Curveball. American Journal of Physics 55 (1), 40-44, 1987.

Forelimb Kinematics of Galloping Thoroughbred Racehorses Measured on Dirt, Synthetic, and Turf Track Surfaces (P235)

Jacob Setterbo[1]*, Tanya Garcia[1], Ian Campbell[2],
Sun Kim[1], Mont Hubbard[1], Susan Stover[1]

Topics: Outdoor Sports; Biomechanics; Performance Sports.
Abstract: Forelimb kinematics of four three-year-old galloping Thoroughbred racehorses were compared between dirt, synthetic, and turf racetrack surfaces. Joint angles and angular velocities of the fetlock (metacarpophalangeal), carpal, elbow, and shoulder joints of the lead forelimb were extracted from high-speed video data. Linear mixed effect ANOVA models were used to assess the effect of track surface on the maxima, minima, and temporal components of the joint angles and angular velocities during the stance phase of stride. Joint angles at heel strike and the speed of the distal end of the proximal phalanx (P1) at heel strike were also analysed. Least square mean differences were used for pairwise comparisons between surfaces. Significant differences in the forelimb kinematics of Thoroughbred racehorses on dirt, synthetic, and turf track surfaces were found, but most differences were timing-related. For all joints, the joint angle maxima occurred later in stance for the dirt and synthetic surfaces than for the turf surface, and the joint angles at heel strike were significantly larger for the turf surface than for the synthetic surface. The time of the fetlock maximum extension angle was smaller ($P<0.05$) for the turf surface (mean ± SE, 41.9 ± 2.1% of stance) than for the dirt (49.9 ± 2.3%) and synthetic surfaces (48.2 ± 1.9%). The time of fetlock maximum flexion velocity was smaller ($P<0.10$) for the turf surface (76.8 ± 3.0%) than for the dirt surface (85.8 ± 3.1%). Results indicate differences in the timing of joint angle and angular velocity maximums are more prevalent than differences in the maximum magnitudes, and timing differences may result from differences in the deformability of the surfaces. Differences in kinematics may affect propensity for soft tissue injury.
Key words: horse; kinematics; race; surface; track.

1. University of California, Davis, USA - E-mail : {jjsetterbo, tcgarcia, sykim, mhubbard, smstover}@ucdavis.edu
2. Equine Veterinary Associates, Santa Ynez, CA, USA - E-mail : {campbellianp}@hotmail.com

1- Introduction

It has long been suggested that racetrack surfaces are a contributing factor to the injury of Thoroughbred racehorses. However, injuries are the result of numerous simultaneous factors, and epidemiologic studies have not isolated the exact role of race surface from other confounding factors such as horse age, exercise history, etc. (Wilson and Robinson, 1996). Racetrack surface is an attractive candidate for further investigation because it is a controllable risk factor; racetrack surface is intensively managed and is practical to change by the modification of surface material properties. The racehorse industry has recognised the potential for injury reduction through racetrack surface changes, as demonstrated by the replacement of dirt surfaces with synthetic materials at several race courses in the US over the last 3 years. However, the manufacture and selection of synthetic surface materials have been largely based on empirical evidence and marketing factors.

Kinematic analysis has been used in equine studies to show that horse dynamics vary with age (Butcher and Ashley-Ross, 2002), breed (Galisteo *et al.*, 1997), hoof morphology (van Heel *et al.*, 2006), and horseshoes (Wilson, 1992). Kinematics has also been used to compare different surfaces. A kinematic analysis of trotting horses on surfaces approximating road, firm ground, and soft ground found that a more deformable surface results in a significantly greater leg landing angle and hoof landing velocity (Burn and Usmar, 2005). However, it is not known how the kinematics of galloping horses are affected by the different track surfaces commonly used for horse racing: dirt, synthetic, and turf. A kinematic comparison of these track surfaces may help to better characterise the varying effects of the surfaces on the dynamics of the horse. Differences in kinematics result from different muscle activation patterns and forces, which result in different strains and forces on joints and tendons; thus, kinematic analysis may give insight into potential for injury.

Therefore, our purpose was to compare forelimb kinematics obtained from Thoroughbred racehorses during gallop on the three primary racetrack surfaces in the United States: dirt, synthetic, and turf. A secondary goal was to help move forward the scientific evaluation of new track surfaces to help prevent musculoskeletal injuries in racehorses.

2- Materials and Methods

2.1 Study Design

Forelimb kinematics were measured for four Thoroughbred racehorses during gallop on synthetic, dirt, and turf track surfaces at Keeneland Race Course in Kentucky. For each trial, hoof accelerations and ground reaction forces were also recorded (Setterbo *et al.*, 2008) using a triaxial accelerometer and an 860 g force-measuring horseshoe (force shoe). Horses were made accustomed to the weight and geometries of this additional equipment by application of dummy horseshoes and instrumentation cables during daily treadmill exercise for two weeks. Data were collected for travel on a straight corridor between timing gates on all three race track surfaces at one race course on each day for each horse. Horses were ridden by exercise riders. Because of track management

practices, track availability, and transport of equipment among surfaces, data were collected first from the synthetic surface training track, then from the dirt surface racetrack, and lastly from the turf surface racetrack. Speed was limited to slow gallop to minimise horse fatigue within one daily exercise session. Forelimb kinematics were compared between track surfaces.

2.2 Animals

Four three-year-old female Thoroughbred racehorses (age, 3 years; mean ± SD weight, 486 ± 6.7 kg) were studied. All horses were clinically sound and they had no subjectively observed gait abnormalities. The procedures used were approved by the Institutional Animal Care and Use Committee at the University of California, Davis.

2.3 Data Collection and Data Processing

Kinematic markers were painted on the skin at approximate centres of joint rotations and topographical bone landmarks to determine bone segment displacements and joint motion. Markers were placed over the spine of the scapula (at the junction of the proximal and middle thirds of the spine), caudal part of the greater tuberosity of the humerus, deltoid tuberosity, humeral origin of the lateral collateral ligament of the elbow joint, lateral tuberosity of the radius at the insertion of the lateral collateral ligament of the elbow joint, lateral styloid process of the radius, proximolateral aspect of the third metacarpal bone, third metacarpal fossa for the origin of the lateral metacarpophalangeal collateral ligament, distal end of the proximal phalanx (P1) at the origin of the lateral collateral ligament of the proximal interphalangeal joint, middle phalanx at the origin of the lateral collateral ligament of the coffin joint, and on two locations on a metal rod affixed to the hoof wall. Additional markers were placed on the neck and hind limb of the horse, but only forelimb kinematics were analysed in this study. At each position, a four by four inch area was painted using black non-toxic liquid latex paint. Then, at each specific anatomic location, a 1.5 inch diameter circle was superimposed over the black paint using white latex paint. One spherical kinematic marker was also adhered to the skin over the dorsal spine of the 6th lumbar vertebra and used to calculate horse speed.

Kinematic data were collected with a high-speed 500 Hz video camera (Fastcam PCI, Photron USA) for two seconds during gallop through a straight corridor on the training track or racetrack. A calibration cube was imaged within the corridor at the beginning of each data collection session on each surface. The horses, ridden by exercise riders, were warmed up at slower speeds before being galloped (left lead) through the data collection corridor; the horses were limited to 3-4 trials of slow gallop (mean ± SD, 7.03 ± 1.38 m/s) on each surface to prevent fatigue. Trials were omitted if the horse bucked or if a lead or gait change was observed during the trial. Kinematic data collection was triggered by horse interference with an infrared beam on the first timing gate crossed.

Using motion analysis software (Peak Motus 9.0, Vicon Motion Systems), the high-speed video position data were digitised and filtered using a digital low-pass Butterworth filter with a cut-off frequency of 10 Hz, chosen such that noise was removed without significantly affecting the data at the stride frequencies analysed in this study. Joint angles

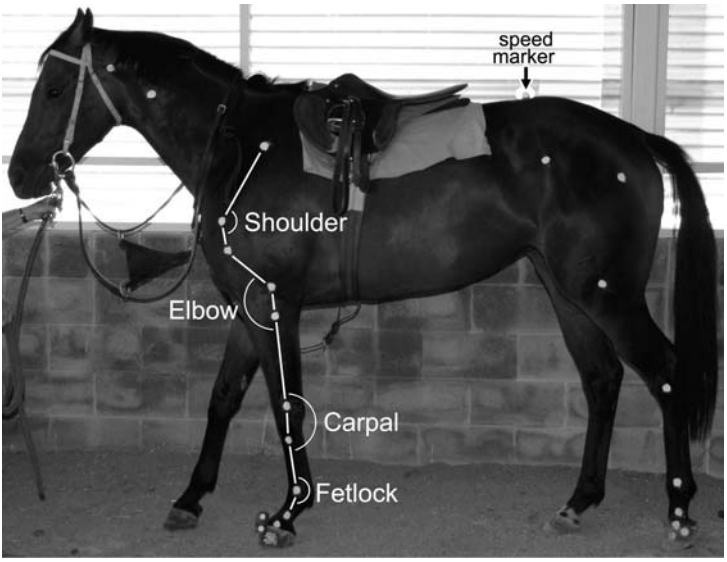

Figure 1 - Kinematic markers and joint angles of the forelimb for one horse. An increase in each angle is extension, while a decrease in each angle is flexion.

and angular velocities of the fetlock (metacarpophalangeal), carpal, elbow, and shoulder joints of the lead forelimb were extracted from the video data. Joint angles were measured on the caudal side of the fetlock, carpal, and shoulder joints, and on the cranial side of the elbow joint, such that an increase in joint angle corresponds to extension, and a decrease corresponds to flexion (Figure 1). The frames at which heel strike and toe off occurred were identified from video data. Using custom software (MATLAB, MathWorks Inc), all trials were normalised to their stance phase (time between heel strike and toe off). Trials which produced infeasible values or that had missing markers during stance phase were omitted. Maxima and minima of joint angles and angular velocities during stance, and the time at which they occurred as a percentage of stance, were then found (Excel, Microsoft Corp). The joint angle at heel strike, taken as the value at zero percent of stance, was also recorded. Markers below the distal end of P1 often were impeded by grass, dirt, or equipment cables during stance. Because of the lack of data from these markers attached or directly adjacent to the hoof, the speed of the distal end of P1 at heel strike (V_{P1}) was recorded to obtain a speed of the distal forelimb at contact. Horse speed was calculated as the average speed of the 6th lumbar vertebra marker.

Least squares means adjusted for date, horse, trial, and horse speed in linear mixed effect ANOVA statistical models that accounted for repeated measures were used to assess the effect of track surface on forelimb kinematics. The horse was included as a repeated effect, and all models included horse speed as a covariate to account for the effect of speed on dependent variables. The Akaike information criterion aided in variable selection for each model and in finding the best overall fit of each model (Ngo and Brand, 1997). Least squares means differences were used for pairwise comparisons

between surfaces. A commercially available software package (SAS, SAS Institute Inc) was used to analyse the data statistically. The level of statistical significance was considered to be $P = 0.05$ and of statistical trends $0.05 < P < 0.10$.

3- Results

A total of 49 trials from 6 different days were analysed. Horse speed ranged from 4.16 to 10.86 m/s (mean ± SD, 7.03 ± 1.38 m/s). The mean ± SD speeds on the different track surfaces were 7.67 ± 1.72 m/s, 6.74 ± 1.42 m/s, and 6.82 ± 0.85 m/s for the dirt, synthetic, and turf surfaces, respectively.

The fetlock, carpal, and elbow joint angles extended maximally during stance, while the shoulder joint flexed maximally (Figure 2). Maximum joint angles during stance were not significantly different between surfaces, but differences were found for the timing of maximum joint angles and for the joint angles at heel strike (Table 1). Maximum joint angles occurred at a smaller percentage of stance for the turf surface than for the dirt and synthetic surfaces for all joints considered, but only reached statistical significance for the fetlock joint. All joint angles at heel strike were significantly larger for the turf surface than for the synthetic surface, and the values differed by up to 10 degrees for the fetlock joint.

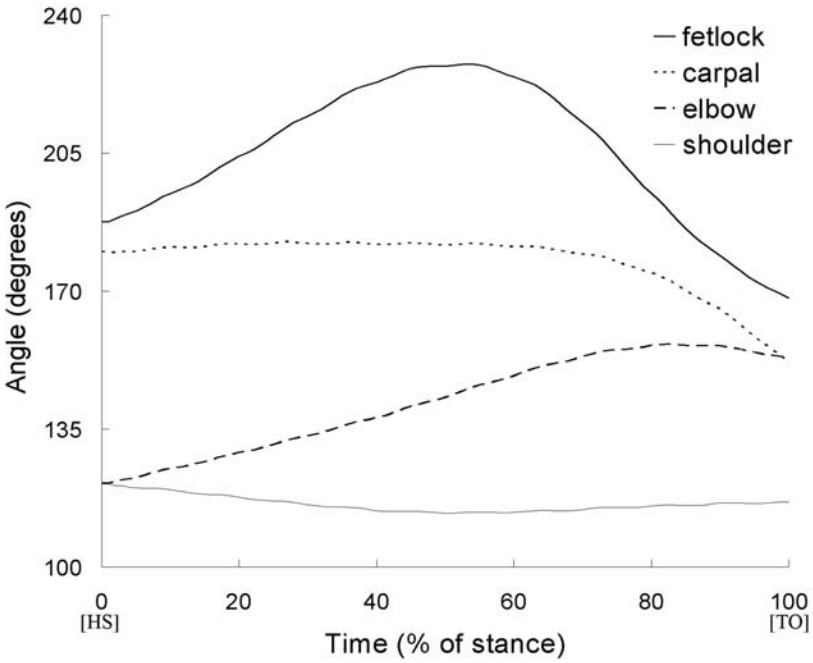

Figure 2 - Joint angles during stance of one horse galloping at 7.82 m/s on turf. Maximums=extension; minimums=flexion. HS=heel strike; TO=toe off.

Variable	Track			P-Value
	Dirt	Synthetic	Turf	
Fetlock joint angle				
at heel strike (degrees)	196.7 ± 5.6[1,2]	194.7 ± 5.4[1]	204.8 ± 6.3[2]	0.105
at max extension (degrees)	237.6 ± 4.8	238.1 ± 4.7	234.4 ± 5.4	0.443
time at max extension (% of stance)	49.9 ± 2.3[1]	48.2 ± 1.9[1]	41.9 ± 2.1[2]	0.054
Carpal joint angle				
at heel strike (degrees)	172.9 ± 2.6[1,2]	168.3 ± 2.4[1]	174.3 ± 2.9[2]	0.098
at max extension (degrees)	181.1 ± 1.0	179.9 ± 0.8	181.7 ± 0.9	0.297
time at max extension (% of stance)	45.0 ± 6.3	45.8 ± 5.6	37.5 ± 6.6	0.459
Elbow joint angle				
at heel strike (degrees)	118.0 ± 2.8[a,b]	116.4 ± 2.5[a]	123.5 ± 2.8[b]	0.143
at max extension (degrees)	152.7 ± 2.4	150.9 ± 2.2	152.7 ± 2.7	0.691
time at max extension (% of stance)	84.6 ± 1.8	84.5 ± 1.6	80.6 ± 1.9	0.179
Shoulder joint angle				
at heel strike (degrees)	119.8 ± 2.1[a,b]	117.8 ± 1.8[a]	121.3 ± 2.3[b]	0.223
at max flexion (degrees)	114.4 ± 1.8	112.7 ± 1.5	112.6 ± 1.9	0.583
time at max flexion (% of stance)	66.3 ± 4.9	65.2 ± 3.9	59.6 ± 4.8	0.415

[1,2] Surface values within a variable row that have different numeric superscripts are statistically different at P<0.05.
[a,b] Surface values within a variable row that have different alphabetic superscripts are statistically different at P<0.10.

Table 1 - Joint angle kinematic variables (mean ± SE) of galloping horses on dirt, synthetic, and turf track surfaces.

The fetlock and shoulder joints had maximum extension and flexion velocities during stance, while the elbow joint only had a maximum extension velocity (Figure 3). The carpal joint angular velocities were excluded from analysis because there was not a clear maximum during stance. Angular velocity kinematic variables related to maximum extension were not significantly different between surfaces, but differences were found for maximum flexion kinematic variables (Table 2). The time at which maximum flexion velocity of the fetlock occurred was significantly smaller for the turf surface than for the dirt surface. Maximum flexion velocity of the shoulder was significantly smaller for the synthetic surface than for the dirt and turf surfaces; the time at which this maximum flexion velocity occurred was significantly smaller for the turf surface than for the dirt and synthetic surfaces. Of all the joints analysed, the fetlock joint had the largest angular velocities during stance on all surfaces.

The V_{P1} value was significantly smaller ($P<0.05$) for the turf surface (mean ± SE, 2.13 ± 0.31 m/s) than for the dirt surface (3.26 ± 0.33 m/s), but neither were significantly different from that of the synthetic surface (2.67 ± 0.29 m/s).

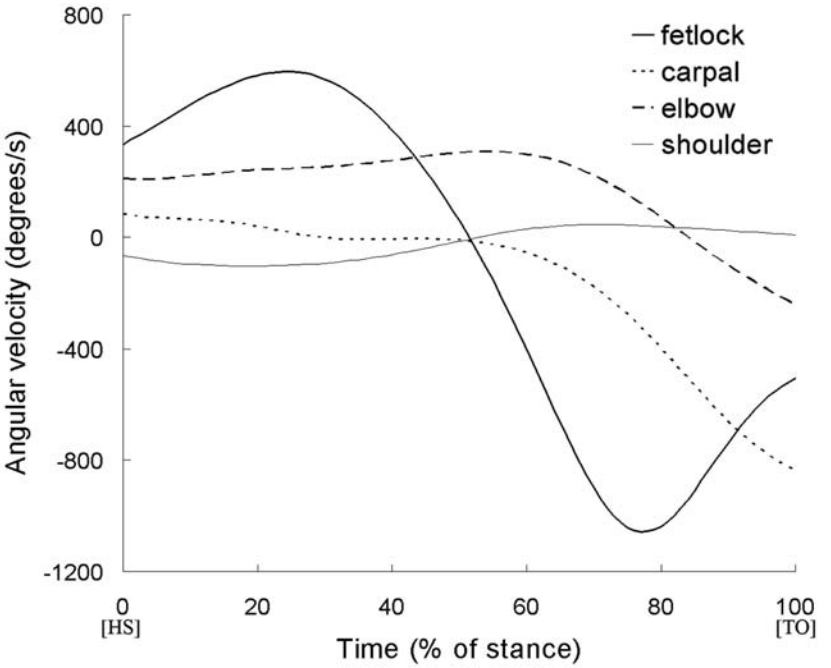

Figure 3 - Angular velocities during stance of one horse galloping at 7.82 m/s on turf. .Maximums=extension; minimums=flexion. HS=heel strike; TO=toe off.

	Track			
Variable	Dirt	Synthetic	Turf	P-Value
Fetlock angular velocity				
at max extension (deg/s)	632 ± 105	770 ± 101	769 ± 119	0.222
time at max extension (% of stance)	14.2 ± 2.8	11 ± 2.2	10.8 ± 2.5	0.609
at max flexion (deg/s)	-1058 ± 136	-1066 ± 109	-983 ± 123	0.831
time at max flexion (% of stance)	85.8 ± 3.1[a]	81.1 ± 2.6[a,b]	76.8 ± 3.0[b]	0.147
Elbow angular velocity				
at max extension (deg/s)	415 ± 42	363 ± 37	375 ± 42	0.592
time at max extension (% of stance)	33.4 ± 7.8	32.9 ± 6.9	35.9 ± 7.6	0.936
Shoulder angular velocity				
at max extension (deg/s)	38 ± 17	47 ± 13	59 ± 15	0.534
time at max extension (% of stance)	88.3 ± 3.8	85 ± 2.9	85.9 ± 3.2	0.753
at max flexion (deg/s)	-156 ± 15[1]	-109 ± 12[2]	-150 ± 12[1]	0.031
time at max flexion (% of stance)	23.6 ± 4.3[a]	21.1 ± 3.3[a]	12.9 ± 3.3[b]	0.082

[1,2] Surface values within a variable row that have different numeric superscripts are statistically different at P<0.05.
[a,b] Surface values within a variable row that have different alphabetic superscripts are statistically different at P<0.10

Table 2 - Angular velocity kinematic variables (mean ± SE) of galloping horses on dirt, synthetic, and turf track surfaces.

4- Discussion

Significant differences in forelimb kinematics were found between dirt, synthetic, and turf track surfaces. Differences in the timing of joint angle and angular velocity maximums were more prevalent than differences in the maximum magnitudes. The joint angles at heel strike and V_{P1} also differed between surfaces. The general joint angle versus time profiles were similar to previous studies (Back *et al.*, 1995b; Galisteo *et al.*, 1997).

Kinematic variables from joint angles showed that the timing during stance differed between track surfaces. The time of the fetlock extension maximum was significantly smaller for the turf surface (mean ± SE, 41.9 ± 2.1%) than for the dirt (49.9 ± 2.3%) and synthetic surfaces (48.2 ± 1.9%). The time at which maximum joint angles occurred was a smaller percentage of stance for the turf surface for all joints considered, as the times were 4% to 8% of stance earlier than those for the dirt and synthetic surfaces. The significantly larger joint angles at heel strike (for joints with extension maximums during stance) for the turf surface corroborate differences in the timing of the kinematics between surfaces; the maximum joint angles of the turf surface were similar to those of the dirt and synthetic surfaces but all kinematic events occurred earlier. This result is consistent with a previous suggestion that, for surfaces with different properties, the horse may be contacting the ground at different points in the swing phase without a large change in dynamics (Burn and Usmar, 2005). The top layer of the surfaces could also cause this timing difference, as the top layer of the turf surface may not be as deformable as the top layer of the synthetic surface and the hoof may not compact the top layer to the same degree. Less compaction means less time deforming the surface, so this may result in the kinematic events occurring earlier for the turf surface.

Kinematic variables from angular velocities also exhibited more timing differences than magnitude differences. For angular velocities, only the shoulder maximum flexion velocity was significantly different between surfaces. The shoulder maximum flexion velocity for the synthetic surface was only 55% and 61% of the dirt and turf surface values, respectively. This result is in contrast to the synthetic surface having the largest maximum fetlock extension and flexion velocities. There is likely a trade-off between different joint angular velocities – an increase in one joint angular velocity may result in a decrease in another. The times of maximum fetlock and shoulder flexion velocity were significantly smaller for the turf surface than for the dirt and/or the synthetic surfaces. Again it seems that kinematic events on the turf surface occur earlier in stance than on the other surfaces.

Of all the joints analysed, the fetlock joint had the largest angular velocities during stance on all surfaces. For example, the dirt surface maximum fetlock extension and flexion velocities were 632 deg/s and -1058 deg/s, respectively, while the next highest magnitude was 415 deg/s for elbow joint extension. Larger magnitude angular velocities can be considered as more rapid loading of the fetlock joint (Back *et al.*, 1995a) and will result in high tendon strain rates. This high rate of angular change helps explain why the fetlock joint area is the most often injured area in the horse (Cohen *et al.*, 1997). Although not significant, the maximum fetlock extension and flexion velocities were largest for the synthetic surface. Previous recorded vertical ground reaction forces, hoof

accelerations, and vibrations were lower for the synthetic surface compared to the dirt and turf surfaces (Setterbo *et al.*, 2008). The higher fetlock angular velocities on the synthetic surface may affect the propensity for soft tissue injury, which is not apparent from ground reaction force and acceleration studies.

Values of V_{P1} were compared between surfaces as a measure of the speed of the distal forelimb at contact. V_{P1} for the turf surface was 65% and 80% of the values for the dirt and synthetic surfaces, respectively. This lower speed for the turf surface may relate to the lack of a soft top layer, as a softer layer acts as a shock absorber and allows more deformation than a harder layer. The horse likely adjusts its stride dynamics in response to harder surfaces to reduce the distal forelimb speed at contact and thus reduce the shock and/or pain experienced. This speed difference could also relate to the horse contacting the ground at different points in the swing phase, which would result in different velocities at impact. These differences in distal forelimb speed agree with a previous study that found that a more deformable surface resulted in greater hoof landing velocity (Burn and Usmar, 2005).

Several aspects of this work make the results unique. The results apply to the specific track surfaces at Keeneland at the time of the study, and should be extended with caution to apply to other surfaces of the same type. For example, maintenance procedures and moisture content are known to affect measurements taken from track surfaces, and there are several different types of synthetic surface, each with its own unique surface properties. The additional equipment on the horse, specifically the force shoe and contralateral dummy shoe, likely affects the kinematics of the horse. However, the same equipment was used throughout the experiment so it is valid to compare between tracks in this study.

Limitations of the study include the identification of stance via video data and the range of speeds analysed in the study. Stance can be more accurately identified from ground reaction force data than from video data, but technical difficulties prevented the use of force shoe data for this purpose. Ideally, the range of speeds used when comparing kinematics should be small. Because of the time constraints of the experiment and in order to prevent fatigue, horses were slow galloped through the straight corridor at their comfortable speed determined by the exercise rider. Although this procedure resulted in a large range of speeds, differences in speed were accounted for in the statistical analysis by including speed as a covariate. In terms of digitisation error, when looking at the distance between markers during stance, the standard deviation was consistently at or below 5% of the mean but occasionally increased to more than 10%. This deviation is partially from skin displacement during movement, and an error of 5% is generally expected for kinematic analysis. However, it must be noted that derivatives taken from kinematic position data compound the error in the original position data; therefore, variables associated with velocities calculated from position data are generally less precise than variables associated with positions.

We conclude that there are significant differences in the forelimb kinematics of Thoroughbred racehorses on dirt, synthetic, and turf track surfaces. The differences in the timing of the kinematics are more prominent than differences in maximum magnitudes, and timing differences may result from differences in the deformability of the surfaces. It is possible that differences in kinematics may affect propensity for soft tissue injury.

5- Acknowledgements

Supported by a grant from the Grayson-Jockey Club Research Foundation, Inc. The authors thank Tara Johnson for racehorse and personnel management, and Ellen Jackson for donating racehorses to the study.

6- References

[BS1] Back W., Schamhardt H., Hartman W., and Barneveld A. Kinematic differences between the distal portions of the forelimbs and hind limbs of horses at the trot. In Am J Vet Res, 56(11): 1522-1528, 1995a.

[BS2] Back W., Schamhardt H., Savelberg H., van den Bogert A., Bruin G., Hartman W., and Barneveld A. How the horse moves: 1. Significance of graphical representations of equine forelimb kinematics. In Equine Vet J, 27(1): 31-38, 1995b.

[BU1] Burn J. and Usmar S. Hoof landing velocity is related to track surface properties in trotting horses. In Equine Comp Exerc Physiol, 2(1): 37-41, 2005.

[BA1] Butcher M. and Ashley-Ross M. Fetlock joint kinematics differ with age in Thoroughbred racehorses. In J Biomech, 35(5): 563-571, 2002.

[CP1] Cohen N., Peloso J., Mundy G., Fisher M., Holland R., Little T., Misheff M., Watkins J., Honnas C., and Moyer W. Racing-related factors and results of prerace physical inspection and their association with musculoskeletal injuries incurred in Thoroughbreds during races. In J Am Vet Med Assoc, 211(4): 454-463, 1997.

[GV1] Galisteo A., Vivo J., Cano M., Morales J., Miró F., and Agüera E. Differences between breeds (Dutch Warmblood vs Andalusian Purebred) in forelimb kinematics. In J Equine Sci, 8(2): 43-47, 1997.

[NB1] Ngo L. and Brand R. Model selection in linear mixed effects models using SAS® PROC MIXED. In SAS Technical Users Group International, Cary - NC, 1997.

[SG1] Setterbo J., Garcia T., Campbell I., Reese J., Wade J., Kim S., Hubbard M., and Stover S. Hoof accelerations and ground reaction forces of Thoroughbred racehorses measured on dirt, synthetic, and turf track surfaces. In Am J Vet Res, submitted, 2008.

[VV1] van Heel M., van Weeren P., and Back W. Compensation for changes in hoof conformation between shoeing sessions through the adaptation of angular kinematics of the distal segments of the limbs of horses. In Am J Vet Res, 67(7): 1199-1203, 2006.

[WR1] Wilson J. and Robinson R. Risk factors for equine racing injuries. In Compend Contin Educ Pract Vet, 18: 682-690, 1996.

[W1] P. Wilson. The effects of a compressible plastic shoe, the Seattle Shoe, on the kinematics of the strides of galloping Thoroughbred horses. In J Equine Vet Sci, 12(6): 374-381, 1992.

Classification of Aerial Acrobatics in Elite Half-Pipe Snowboarding Using Body Mounted Inertial Sensors (P237)

Jason W. Harding[1,4,5], Colin G. Mackintosh[3],
Allan G. Hahn[2], Daniel A. James[5,6]

Topics: Half-Pipe, Aerial Acrobatics, Technology, Rate Gyroscopes, Performance, Competition Judging.

Abstract: We have previously presented data indicating that the two most important objective performance variables in elite half-pipe snowboarding competition are air-time and degree of rotation. Furthermore, we have documented that air-time can be accurately quantified by signal processing of tri-axial accelerometer data obtained from body mounted inertial sensors. This paper adds to our initial findings by describing how body mounted inertial sensors (specifically tri-axial rate gyroscopes) and basic signal processing can be used to automatically classify aerial acrobatic manoeuvres into four rotational groups (180, 360, 540 or 720 degree rotations). Classification of aerial acrobatics is achieved using integration by summation. Angular velocity ($\omega_{i,j,k}$) quantified by tri-axial rate gyroscopes was integrated over time (t = 0.01s) to provide discrete angular displacements ($\theta_{i,j,k}$). Absolute angular displacements for each orthogonal axes (i, j, k) were then accumulated over the duration of an aerial acrobatic manoeuvre to provide the total angular displacement achieved in each axis over that time period. The total angular displacements associated with each orthogonal axes were then summed to calculate a composite rotational parameter called Air Angle (AA). We observed a statistically significant difference between AA across four half-pipe snowboarding acrobatic groups which involved increasing levels of rotational complexity ($P < 0.001$, $n = 216$). The signal processing technique documented in this paper provides sensitive automatic classification of aerial acrobatics into terminology used by the snowboarding community and subsequently has the potential to allow coaches and judges to focus on the more subjective and stylistic aspects of half-pipe snowboarding during either training or elite-level competition.

Key words: Automated Scoring, Technology, Gyroscopes, Acrobatics.

1. Department of Physiology, Australian Institute of Sport, AUSTRALIA, PO BOX 176 Belconnen ACT 2616 - E-mail: Jason.Harding@ausport.gov.au
2. Applied Research Centre, Australian Institute of Sport, AUSTRALIA. PO BOX 176 Belconnen ACT 2616 - E-mail: allan.hahn@ausport.gov.au
3. Applied Sensors Unit, Australian Institute of Sport, AUSTRALIA, PO BOX 176 Belconnen ACT 2616 - E-mail: colin.mackintosh@ausport.gov.au
4. Olympic Winter Institute of Australia, AUSTRALIA, 1/1Cobden Street South Melbourne VIC 3205 - E-mail: Jason.Harding@ausport.gov.au
5. Centre for Wireless Monitoring and Applications, Griffith University, AUSTRALIA, 170 Kessels Road Nathan QLD 4111 - E-mail: d.james@griffith.edu.au
6. Centre of Excellence for Applied Sport Science Research, Queensland Academy of Sport, AUSTRALIA, 170 Kessels Road Nathan QLD 4111 - E-mail: d.james@griffith.edu.au

1- Introduction

A current and relatively recent shift in performance assessment and athlete monitoring ideology is to move data collection and analysis from the sport science laboratory into the field. This shift can introduce objectivity into sporting environments normally reliant upon subjective perceptions to evaluate technique and performance. There are a number of examples of this shifting ideology becoming more prevalent in elite-level winter sport. Researchers for example have documented the use of an electromagnetic tracking system to quantify angular displacement and joint moment torques related to snowboard turns [DY1]. The same system has been used to calculate the degree of dorsiflexion, eversion and external rotation of the ankle joint complex during on-snow trials of snowboard boots [DT1] and a dynamometric platform focussed on field based load data acquisition has been developed and used to measure load components transmitted between boots and snowboard bindings [BP1]. Additionally, combinations of accelerometers and rate gyroscopes have been recently utilised to objectively describe the motion characteristics of ski jumping [OS1] and additionally, to collect measurements under skier's feet to gain objective insight into ground reaction force and an athlete's weight balance in the field [MS1]. At present elite-level half-pipe snowboarding seems well positioned to integrate technology and allow for some of the important technical aspects of the sport to be quantified. Interestingly, half-pipe snowboarding is a sporting discipline long exuding an anarchistic, non-conformist ideology with a focus on the aesthetic. Thus, successful integration of field-based monitoring afforded by micro-technology must be focussed upon relevant, practical information related strongly to training and competition performance.

We have recently documented the importance of air-time (AT) and degree of rotation (DR) on elite-level half-pipe snowboarding competition performance [HT1, HS1] and the capacity of signal processing using data obtained from accelerometers to automatically calculate aerial acrobatic AT [HS1]. Air-time, however, comprises only one objective aspect of an athlete's training and competition performance and capacity to automatically calculate this variable in the field can only ever provide part of the objective performance puzzle. It is therefore imperative to investigate the potential to objectively assess the DR component (Figure 1A) of aerial acrobatics. Although previously documented work [HT1, HS1] has highlighted the importance of DR on competition performance occurring during two World Cup competition finals, it is theorised the most likely benefit of automatic classification of aerial acrobatics will be in monitoring acute training load and long term training performance with elite-level athletes. The capacity to classify rotations automatically and to regularly log how often each manoeuvre is performed throughout routine training is theorised to provide a form of objective performance monitoring not currently used within half-pipe snowboarding. Theoretically tri-axial rate gyroscopes should allow objective assessment of DR and potentially contain information necessary to report on exact degree of rotation, direction of travel, direction of rotation, presence of inversion and ultimately provide unparalleled instantaneous acrobatic identification.

(A) (B)

Figure 1 - (A) Australian snowboard athlete mid-rotation during front-side 720 degree rotation and (B) displaying take-off angle typical of acrobatics performed in half-pipe snowboarding. Perisher Blue Australia 2007. Images: Heidi Barbay.

Rotation terminology used by half-pipe snowboarding practice communities is not based upon assessment of exact degree of rotation achieved. It is based upon a sport specific approximation. The take-off (Figure 1B) and more specifically the landing angles (similar but opposite to the take-off angle) associated with half-pipe snowboarding aerial acrobatics generate a situation where exact degree of rotation achieved will always be less than the terminology used to describe it. Theoretically, the degree of rotation achieved during rotations performed predominantly around a single axis is at least, 90 degrees less than the rotation the athlete is credited with based on conventional terminology. Rotational terminology can be based upon the following rules; an athlete will land aerial acrobatics travelling in the same direction they were initiated with in 180, 540, 900 and 1260 degree rotations. In contrast an athlete will land travelling in the opposite direction of the initiation during 360, 720 and 1080 degree rotations. These rules apply only in half-pipe and quarter-pipe snowboarding (resultant of the take-off and landing occurring on the same lip). Although snowboarders can ride forwards or backwards, these rules apply regardless of the direction of travel when aerials are initiated. Although the experienced snowboard community are trained to recognise aerial acrobatics, there is potential for automated classification to provide continual performance assessment (albeit a purely objective assessment) without constant human attention. Coaches, judges and support staff may thereby focus their attention on the more subjective aspects of performance whilst relying on automated inertial sensor feedback for continual recording of objective information.

This paper focuses on the capacity of tri-axial rate gyroscopes to automatically classify aerial acrobatics into four rotational groups of increasing complexity (180, 360, 540 and 720 degrees of rotation). These aerial acrobatics are regularly utilised by the competitive half-pipe snowboard community in training and competition environments. Basic signal processing techniques and the associated classification results will be presented promoting the use of body mounted inertial sensor data to provide objective information with relevance to a specific sporting practice community.

2- Methods

2.1 Subjects, Equipment, Experimental Procedure And Data Collection

Ten athletes were recruited to participate in this study. Data collection was performed during southern hemisphere winter seasons (2005 – 2007) at Perisher Blue Ski Resort (altitude 1720 m) on the resort's custom snowboard half-pipe (length 80 m, width 18 m, transition height 5 m, gradient ≈ 15 degrees). Data collection was performed during routine training sessions and competitions between 2005 and 2006. Experimental procedures were approved by the Ethics Committee of the Australian Institute of Sport on 18th August 2005 (ref: 20050808) and in accordance with Griffith University requirements, cleared under special review in January 2008 (ref : PES/01/08/HREC). Implementation of previously developed sensors [CI1, JD1] comprising of one tri-axial accelerometer (100Hz, ± 6g) and one tri-axial rate gyroscope (100Hz ± 1200d.s^{-1}) were used throughout data collection process. This paper focused on tri-axial rate gyroscope data as DR associated with aerial acrobatics relies on angular velocity for calculation. Data were processed in combination with a previously documented method of air-time calculation [HS1] in order to assess degree of rotation achieved during aerial acrobatics. Raw data was stored on board the sensor unit (256MB Trans Flash) for the duration of data collection process and sampled post collection by a computer software suite developed in house [M1]. Accelerometer components underwent 2-point static calibration in three orthogonal axes (up/down, forward/back and left/right) aligning each axes of sensitivity with and against the direction of gravity. Rate gyroscope components underwent a 2-point calibration integrating angular velocity over time throughout 0 and 90 degrees in three orthogonal axes (yaw, pitch, roll) prior to each data collection session [M1, GK1]. Panning video footage of each half-pipe run was collected using a Sony 3CCD 50Hz digital video camera from the bottom and centre of the half-pipe. Video footage was analysed by video analysis software (DARTFISH 2.5 Basic). A sensor was attached to the lower back of each athlete, situated ≈ 5cm to the left of the spine. Data were collected from one athlete at a time during routine national team training sessions and from all athletes concurrently during a half-pipe snowboard competition (AIS Micro-Tech Pipe Challenge 2007). Data collection allowed athletes to train and compete in routine fashion and eliminated constriction or alteration of performance. Panning digital video camera filmed complete half-pipe runs and tri-axial accelerometer / rate gyroscope data was collected for the duration of each data collection session. Data on 216 aerial acrobatic manoeuvres was collected.

2.2 Signal Processing

This study focused upon aerial acrobatics performed predominantly around a single axis (yaw) resulting in what are termed by the snowboard community as 'flat spins or rotations'. These rotations are essentially void of inversion (rotation in the pitch axis) and as such simplify classification. Classification of aerial acrobatics is achieved using integra-

tion by summation. Angular velocity ($\omega_{i,j,k}$) quantified by tri-axial rate gyroscopes was integrated over time (t = 0.01s) to provide discrete angular displacements ($\theta_{i,j,k}$). Absolute angular displacements for each orthogonal axes (i, j, k) were then accumulated over aerial acrobatic duration to provide total angular displacement achieved in each axis. The total angular displacements associated with each orthogonal axes were then summed to calculate a composite rotational parameter called Air Angle (AA).

2.3 Mathematical Representation of Signal Processing Technique

1. Rate gyroscope data (providing angular velocity) was sampled at 100Hz such that t= 0.01s and additionally in 3 orthogonal axes (***i, k, j***); of which one single axis of rotation is denoted by *j* in the following mathematical integration.
2. **N** = number of sample points associated with the air-time of one aerial acrobatic manoeuvre.
3. **AT** = air-time measured in seconds (calculated using a previously documented signal processing technique using acceleration [HS1].
4. **AA** = Air Angle; a measure of cumulative displacement achieved in all three orthogonal axes for the duration of aerial acrobatics.

$$\theta_{jn} = \int_{o}^{t} \omega_j dt$$

$$\text{At } t = t_n = n\Delta t, \quad \approx \sum_{i=1}^{n} \omega_{ji} \Delta t \ , \tag{1}$$

$$= \Delta t \sum_{i=1}^{n} \omega_{ji}$$

And

$$\omega_i = \frac{\partial \theta_i}{\partial t} \tag{2}$$

$$N = \frac{AT}{\Delta t} \tag{3}$$

Let

$$\Theta_{Nj} = \sum_{i=1}^{N} \left| \theta_{ji} \right| \tag{4}$$

$$AA = \sum_{j=1}^{3} \Theta_{Nj}$$

$$= \Delta t. \sum_{j=1}^{3} \sum_{i=1}^{N} \left| \omega_{ij} \right| \tag{5}$$

3- Results

3.1 Graphical Representation of Inertial Sensor Data and Air Angle Measurement

Figure 2 shows the distinct raw accelerometer data pattern exhibited throughout a half-pipe snowboard run. Previously described aspects of this rhythmical pattern is utilised to calculate air-time associated with aerial acrobatics [HS1]. Figure 2 additionally displays the mathematically derived Air Angle measurement (derived using raw rate gyroscope data) associated with each aerial acrobatic manoeuvre. The Air Angle measurement subsequently allows for reliable classification of these aerial acrobatics into discrete rotational groups (180, 360, 540, 720 or 900 degrees of rotation).

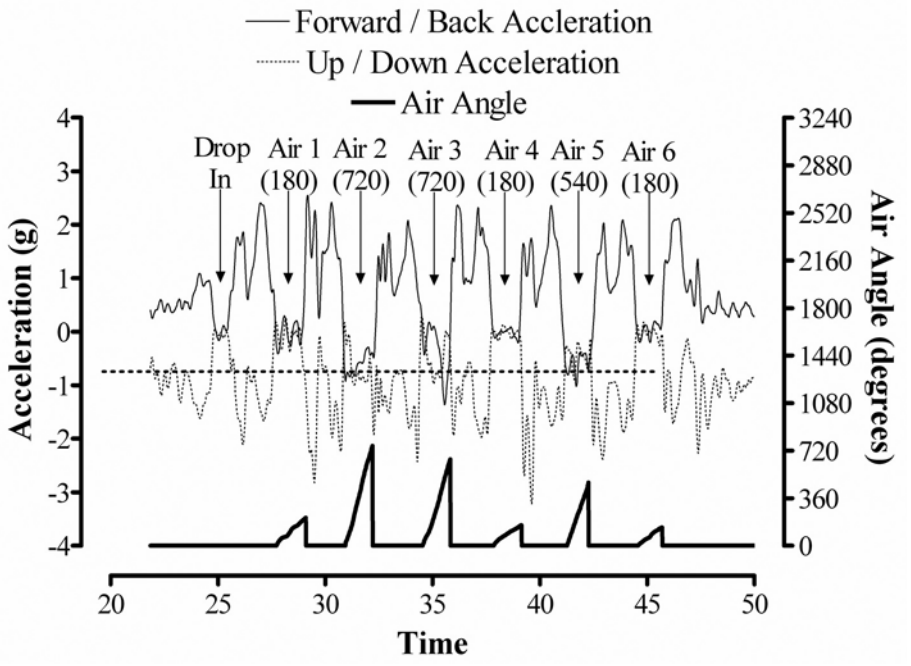

Figure 2 - Raw acceleration data used to calculate air-time, Air Angle measurement and subsequent classification of aerial acrobatics. Australian snowboarder routine during AIS Micro-Tech Pipe Challenge 2007. Perisher Blue Australia.

3.2 Statistical Assessment

Difference between average Air Angles measured for each rotational group (180, 360, 540, 720) was evaluated using a One-way ANOVA. All groups were normally distributed (Shapiro-Wilk statistic for 180, 360, 540 and 720 = .0987, 878, 942, 966, P = 0.141, 0.301,

0.086, 0.664 respectively) however, equal variances were not assumed (Levene statistic = 3.619, P = 0.013) and as such, a Dunnett T3 post-hoc test was used to determine significant differences between groups. Precision of estimation was described using 95% confidence limits. Significance was accepted at the level $p<0.05$. All statistical analysis was performed using SPSS 13.0 for Windows, SPSS Inc, Chicago Illinois USA, www.spss.com

3.3 Graphical and Tabular Representation of Air Angle Range

Figure 3 presents Air Angle (mean ± range) for aerial acrobatics and their relationship to one of four rotational groups routinely used by the practice community (based upon an approximation of angular displacement). Average Air Angle for each of the rotational groups became significantly greater for each of the rotational groups ($F = 2075.80$, $P < 0.001$). The clinical significance however is of the utmost importance. Absence of overlapping Air Angle measurements between four rotational groups ensures the measurement provides reliable classification of aerial acrobatics performed predominantly around a single axis during half-pipe snowboarding. Table 1 provides numerical information on Air Angle measurements and recommended ranges for reliable acrobatic classification. Mean differences relate to AA measurement of rotational group immediately below.

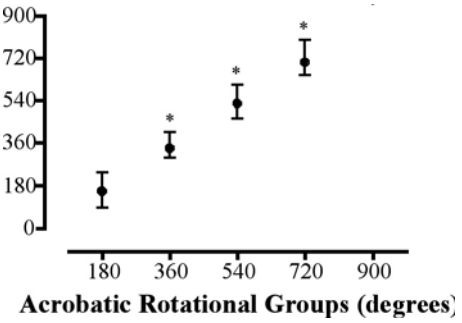

Figure 3 - Air Angle measurement (mean ± range) and relationship to four specific rotational groups (n = 216 acrobatic manoeuvres. * = statistical significance from the preceding rotational group (a group with a lower degree of rotation).

Rotational Group Degrees	n	Mean Degrees	SD Degrees	95% CL Degrees	Mean difference ± SEM Degrees	P value	Recommended Range Degrees
180	159	152.13	33.00	146.96 - 157.30	NA	NA	80 – 240
360	5	332.80	47.41	273.93 – 391.67	180.67 ± 21.36	P = 0.004	285 – 410
540	32	522.66	44.52	506.61 – 538.71	189.86 ± 22.62	P = 0.002	450 – 610
720	20	699.40	40.04	681.44 – 717.36	176.74 ± 11.64	P < 0.001	640 – 810

Table 1 - AA measurement information. Mean differences between rotational group and the preceding lower rotational group. Recommended AA ranges for successful classification of acrobatics using the method documented in this paper.

4- Discussion

This paper investigated the effectiveness of processing rate gyroscope data using integration by summation to classify half-pipe snowboarding aerial acrobatics into sport specific rotational groups. The signal processing of gyroscope data was used in combination with a previously documented method of quantifying acrobatic air-time using acceleration [HS1]. The calculation of air-time associated with aerial acrobatics provided the duration over which to assess angular velocity. The terminology used by the practice community to describe acrobatic rotation is based upon an approximation of angular displacement and the relationship between direction of travel at take-off and landing. Provided rotations are performed predominantly around a single axis, the signal processing method presented in this paper provides reliable classification of aerial acrobatics.

Mean differences in AA measurement between preceding rotational groups (for example between 360 and 180, 540 and 360, 720 and 540) were statistically significant (mean difference ± SEM = 180.67 ± 21.36, 189.86 ± 22.62, 176.74 ± 11.64; $P = 0.004$, 0.002, < 0.001 respectively). Of the utmost importance however, was the absence overlapping AA measurement limits between the different rotational groups (Figure 3, Table 1). Whilst 95% confidence limits provide tight upper and lower ranges of AA measurement for each rotational group, such statistically derived limits generate incorrect acrobatic classification as a number of AA measurements fall outside those ranges. The absence of overlapping AA measurement limits between groups therefore affords some flexibility outside statistically derived likelihoods whilst still ensuring reliable classification of aerial acrobatics. The recommended ranges the authors suggest for successful aerial acrobatic classification are provided in Table 1.

Developing the capacity to automatically classify aerial acrobatics was initiated based on the practical relevance of this information [HT1, HS1] and a focus on integrating objectivity into a sport that has relied on subjective performance assessment since inception. Alongside the previously documented ability to calculate air-time [HS1] the automation of aerial acrobatic classification is theorised to provide enhanced performance assessment during training and competition; freeing coaching and judging staff to focus intently on the subjective execution and overall composition of acrobatics incorporated into half-pipe snowboarding routines. The signal processing method documented however can not assess exact degree of rotation, direction of travel, direction of rotation or the presence of inversion and is focused upon acrobatics that are performed predominantly around a single axis. Subsequently, the impact on current performance assessment protocols is theorised to be limited. Coaches and judges are trained to recognise aerial acrobatics and whilst the classification system documented can automate that process, it does not provide any additional information to what can already be determined with the naked eye.

One of the problems with this method was an inability to reliably classify acrobatics performed in more than one axis, such as those that incorporate inversion. This was revealed in acrobatics above 540 degrees of rotation. Acrobatics up to 540 degrees (apart from a few specific inverted manoeuvres) are predominantly performed in one axis (yaw) as they are undemanding of most elite athletes. As the degree of rotation increases

however, athletes begin to employ inversion (and hence another axis of rotation) in order to successfully complete required rotation. It is upon processing these inverted manoeuvres that the method documented in this paper fails to reliably classify aerial acrobatics. Signal processing of inverted aerial acrobatic manoeuvres (all of which were 720 degree rotations) generated AA measurements that often fell below recommended ranges and were subsequently classified incorrectly (into a lower rotational group). This is the primary reason (in addition to limited samples of inverted 720 degree rotations) this paper focussed upon acrobatics performed predominantly in one axis. All acrobatics comprise a small component of rotation in all axes (unproblematic for classification via AA measurement) however aerial acrobatics incorporating inversion as a major component will require different signal processing.

Although the method is intuitively appealing (providing a measurement with the same units as rotational group terminology), it is unnecessary for acrobatic classification. Proportionality of angular velocity to angular displacement should theoretically allow classification of acrobatics in the same manner, albeit with a different unit of measurement, by accumulating and summating discrete, absolute angular velocity measurements over air-time. Furthermore, summation of angular displacements over three axes is void of physical reference, is essentially an arbitrary measurement and is the reason for the method's failure to classify acrobatics incorporating inversion. It does however provide an indication of acrobatic complexity and is a platform for future refinement of the concept. Considering the community perceive some inverted manoeuvres an easier method of achieving higher degree of rotation, AA measurements could potentially gauge acrobatic complexity. Future work however will focus on the calculation of exact degree of rotation, direction of travel, direction of rotation and presence of inversion. This work may enhance current training and competition performance assessment in snowboarding, skateboarding and surfing.

5- Acknowledgments

First and foremost, thank you to the snowboard coaches (Ben Wordsworth and Ben Alexander) and the athletes of the Australian national half-pipe snowboard team for their willingness to participate in these trials. We also thank Perisher Blue Ski Resort, NSW National Parks and Wildlife Service and Catapult Innovations for all funding and in-kind support. A special thanks to the Head of the Department of Physiology at the Australian Institute of Sport, Professor Chris Gore and all his staff for creating an environment focussed on innovative thinking and passionate debate in the name of rigorous scientific enquiry. Thank you to Dr. David Martin of the Department of Physiology at the Australian Institute of Sport for providing inspiration, guidance and emphasising attention to detail. Also thank you to Heidi Barbay for assistance during southern hemisphere winters and to the staff who helped conduct the AIS Micro-Tech Pipe Challenge; generating the data utilised in this paper. Results and media related to this competition can be can be viewed at www.AnarchistAthlete.com

6- References

[BP1] Bianchi L., Petrone N., Marchiori M. A dynamometric platform for load data acquisition in snowboarding: design and field analysis. In The Engineering of Sport 5, Hubbard, M., Mehta, R. D., Pallis, J.M. ISEA, 2, 187 –193, 2004.

[CI1] Catapult Innovations. Mini Max. http://www.catapultinnovations.com, Catapult Innovations Melbourne Australia, 2007.

[DT1] Delorme S., Tavoularis S. Kinematics of the Ankle Joint Complex in Snowboarding. In Journal of Applied Biomechanics, 21, 394 – 403, 2005.

[DY1] Doki H., Yamada T., Nagai C. Horaki, M. Development of a measurement system for snowboarding turn analysis. In The Impact of Technology in Sport, Subic, A., and Ujihashi, S. Taylor & Francis London., ASTA, 324 – 325, 2005.

[GK1] Green J., Krakauer, D. New iMEMS® Angular-Rate-Sensing Gyroscope. In Analog Dialogue 37(03), 2003.

[HS1] Harding J. W., Small J. W., James D. A. Feature Extraction of Performance Variables in Elite Half-Pipe Snowboarding Using Body Mounted Inertial Sensors, In BioMEMS and Nanotechnology III, edited by Dan V. Nicolau, Derek Abbott, Kourosh Kalantar-Zadeh, Tiziana Di Matteo, Sergey M. Bezrukov, Proceedings of SPIE Vol. 6799 (SPIE, Bellingham, WA, 2007) 679917, 2007.

[HT1] Harding J. W., Toohey K., Martin D. T., Mackintosh C., Lindh A. M., James D. A. Automated Inertial Feedback For Half-Pipe Snowboard Competition And The Community Perception. In The Impact of Technology on Sport II, Fuss F. K., Subic A., Ujihashi S. Taylor & Francis London., 20, 845 – 850, 2007.

[JD1] James D. A., Davey N., Rice T. An Accelerometer Based Sensor Platform for Insitu Elite Athlete Performance Analysis. In IEEE Sensors, Vienna., 2004.

[M1] Mackintosh C., G. LOGAN V21.0 Copyright ©. Australian Institute of Sport, CRC for Micro-Technology, 2004 – 2008.

[MS1] Michahelles F., Schiele B. Sensing and Monitoring Professional Skiers. IEEE Pervasive Computing, 4, 40 – 46, 2005.

[OS1] Ohgi Y., Seo K., Hirai N., Murakam M. Measurement of Jumper's Body Motion in Ski Jumping. In The Engineering of Sport 6, Moritz, E. F., Haake, S. Springer Science + Business Media, LLC., 1, 275 – 280, 2006.

A Modified Lift Mechanics Theory for Downhill Skiing and Snowboarding (P239)

Qianhong Wu[1]*, Qingjie Sun[2]

Topics: Skiing & Other Winter Sports.
Abstract: In a recent study, Wu, *et al.* (Med. Sci. Sports Exerc., Vol. 38, No. 6, pp. 1132-1146, 2006) have developed a new mathematical model to describe the lift mechanics of downhill skiing and snowboarding, where the lift contributions due to both the transiently trapped air inside a snow layer and the solid phase (snow crystals) were determined for the first time, and a model for the stability and control of skiing/snowboarding was developed. The lift generation highly depends on the permeability of snow, speed, friction, as well as the geometry of the ski/snowboard. In the current study, we shall extend Wu *et al.*'s theory to more complex planar shapes. A modified mathematical model is developed where a width factor, f(x), which characterizes the variation of width from the leading to the trailing edge of a snowboard, is introduced. We shall thoroughly investigate the force and moment balance on the planing surface due to the trapped air and the snow crystals, and examine their effects on the stability and control of a ski and snowboard. The performance of different commercial snowboards will be examined based on our revised model. This study and the previous lift mechanics theory for downhill skiing and snowboarding developed by Wu *et al.* have laid the foundation for the optimization of a ski/snowboard from a lift generation point of view.
Key words: snowboard, lift generation, porous media, optimization.

1- Introduction

The phenomenon of downhill skiing or snowboarding, in its simplest form, refers to the motion of a human being sliding down an inclined plane on a porous medium (snow layer), as shown in Figure 1. The lift mechanics of skiing is intended to answer a

1. Department of Mechanical Engineering, Villanova University, 800 Lancaster Avenue, Villanova, PA, 19085, USA - E-mail: qianhong.wu@villanova.edu
2. Animation School, Communication University of China, No.1 East Ding Fuzhuang Street, Chao Yang District, Beijing 100024, China - E-mail: qjsun@cuc.edu.cnn
** : Author to whom correspondence should be addressed*

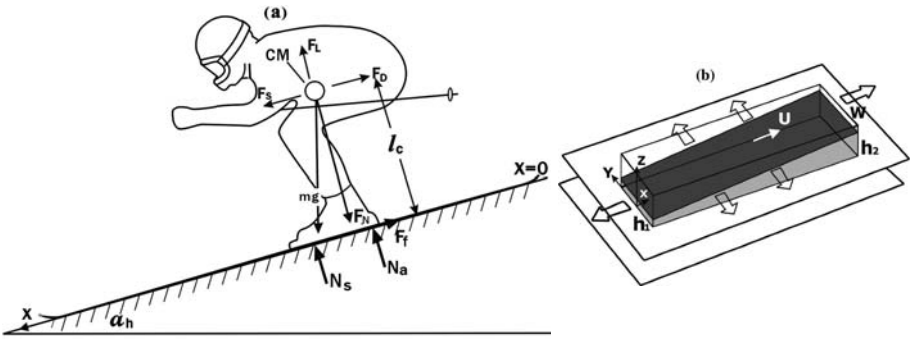

Figure 1 - (a): Forces upon a skier as he/she descends down the fall line. (b): Schematic illustration of a snowboard or ski compressing a layer of snow powder.

fundamental question, that is, why a 70 kg human can glide through a soft snow layer without sinking into the base as would occur if the motion is arrested. To answer this question, Feng and Weinbaum (2000) developed a new lubrication theory for highly compressible porous media, which demonstrated that the excess pore pressure generated by a planing surface (ski/snowboard) moving on a compressible porous layer (snow) scales as $\alpha^2 = h^2/K$, where h is the layer thickness and K is the Darcy permeability; and that α is of order 10^2 or larger for humans skiing, thus, the lift forces generated can be four or more orders of magnitude greater than classical lubrication theory. The huge enhancement in the lift arises from the fact that as the porous medium (snow) compresses, there is a dramatic increase in the lubrication pressure because of the marked increase in the hydraulic resistance that the fluid (air) encounters as it tries to escape from the confining boundaries through the compressed porous layer (snow).

The initial application of Feng & Weinbaum's theory was to the interaction of our red blood cells with the endothelial lining of our blood vessels, which is a half μm thick hydrated fibrous layer of glycoproteins and proteoglycans. One of the fundamental mysteries of microcirculation is how an 8 μm red cell is able to survive 10^5 passages through microcirculation during a typical lifetime of 120 days without undergoing hemolysis. This longevity is quite remarkable in that the red cell can travel at velocities that approach 100 times its diameter a second and can also pass, at much lower velocities, through muscular sphincters of a few μm diameters at the entrance to arterioles. The theoretical model in Feng and Weinbaum (2000) predicts that adhesive proteins in the opposing membranes of the red cell and endothelial cell would be in constant contact were it not for the large pressure (lift) forces generated within the matrix layer that prevent opposing membranes from touching. The same mechanism is applied to human skiing and snowboarding, and there is a remarkable hydrodynamic similarity between the motion of a red blood cell gliding over the compressed endothelial glycocalyx that lines our capillaries and a human skier or snowboarder skiing on fresh powder even though their difference in mass is of order 10^{15}, a is of order 10^2 or larger for both cases.

The concept of lift generation in porous media proposed by Feng and Weinbaum (2000) was recently qualitatively verified by Wu *et al.* (2004a, 2004b, 2005b), in which a specially designed porous-walled cylinder-piston apparatus as shown in Figure 2a was constructed to examine the build up and decay of the excess pore pressure inside a snow layer under sudden compaction. A theoretical model for the pore pressure relaxation in the porous cylinder was developed using consolidation theory and shows excellent agreement with the experiment data if the Darcy permeability of snow is chosen in the right range. The choice of the Darcy permeability is not arbitrary, it is based on Jordan *et al.* (1999) published data. In Figure 2b, one observes a rapid rise in pore pressure in response to the dropping of the piston and then a decay that occurs on a time scale of roughly 0.5 s. In contrast, the length of time that a 1.5 m snowboard would be in contact with a given patch of snow if it was travelling at 15 m/s would be 0.1 s. It is clear from the figure that after 0.1 s the excess pore pressure has only started to relax and much of the weight of the snowboarder would be supported by the air that is still trapped in the partially compressed snow layer.

The fundamental insights gained from these studies on the lift generation in porous media provide a new perspective for understanding the phenomenon of skiing and have further led to the first realistic model for the lift mechanics of downhill skiing and snowboarding developed by Wu *et al.* (2006a, 2006b). This new skiing mechanics theory incorporates lift contributions from both the transiently trapped air and the compressed ice crystals. It predicts that for fine-grained, wind-packed snow when the velocity of the skier is 20 m/s, approximately 50% of the total lift force is generated by the trapped air for snowboarding and 40% for skiing. For highly permeable fresh powder snow, the lift contribution from the pore air pressure drops to less than 20%. This theory captures the key physics of stability and control during skiing or snowboarding and realistically predicts the performance of skiing or snowboarding as a function of the skier's velocity, the sliding friction between the planing surface and snow, various snow types, as well as the geometry of a ski or snowboard. In recent studies by Tatsuno *et al.* (2007), Hiroyuki *et al.* (2007) and Scott *et al.* (2007), the ski-snow contacting pressure is measured, which showed consistant behaviour as that predicted by Wu *et al.*'s lift mechanics theory.

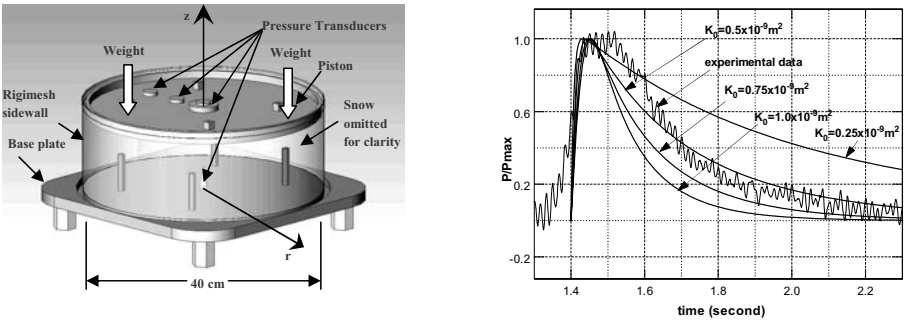

Figure 2 - (a): Schematic of snow compaction experiment apparatus. (b): Comparison between the theoretical predictions of the time-dependent pressure and the experimental data for various values of the initial Darcy permeability of snow. The test sample was wind-packed snow with initial thickness, h_0 = 11.43 cm, and applied mass m = 5.9 kg,

Wu *et al.*'s skiing mechanics theory is the first realistic model for the prediction of relative contributions of the trapped air and the ice crystals to the total lift. However, it has two major limitations. First, this theory is applicable to the simple case where the planing surface is of constant width in the axial direction, while commercially available skis/snowboards have complex geometries and variable width in order to reduce weight and improve performance while maintaining the strength and rigidity of the planing surface. Secondly, for a certain gliding condition such as the board geometry, the speed of the skier or snowboarder, the frictional coefficient between the board surface and the snow layer, the position of the skier's centre of gravity and the properties of snow, Wu *et al.*'s theory predicts a single neutral stability position. However, an experienced skier or snowboarder would tell you that there are several equilibrium positions instead of one. In the current study, we shall perform a systematic study to treat these limitations. We shall extend Wu *et al.*'s theory to more complex shapes where the width of the planing surface changes with the axial location. A modified mathematical model will be developed where a width factor, f(x), which characterizes the variation of width from the leading to the trailing edge, is introduced. We shall examine the performance of a commercial snowboard of certain geometric characteristics based on our new model. We shall thoroughly discuss the force and moment balance on a skier and re-examine their effects on the stability and control of skiing or snowboarding.

2- Methods

For a skier/snowboarder gliding with velocity U (U_x, U_y, U_z) over a snow layer as shown in Figure 1, the sudden compaction of the snow leads to the generation of pore air pressure inside the compressed layer, $\mathbf{N_a}$, as well as the solid phase lifting force from the ice crystals, $\mathbf{N_s}$. The normal component of the weight $\mathbf{mg}$, $\mathbf{F_N}$, is to be balanced by the summation of $\mathbf{N_a}$ and $\mathbf{N_s}$, $\mathbf{F_N} = \mathbf{mg}\cos\alpha_h = \mathbf{N_a}+\mathbf{N_s}$ where α_h is the angle of the inclined slope. Similarly, the sum of all torques about the centre of mass (CM) must be zero too, that is, $\mathbf{N_a}\cdot(x_{ccr}-x_a)+F_f\cdot l_c = \mathbf{N_s}\cdot(x_s-x_{ccr})$, where F_f is the snow friction force, $F_f = \eta\cdot\mathrm{N_s}$ where η is the coefficient of friction, l_c is the normal distance of the CM from the ski surface, x_{ccr}, x_a and x_s are the x coordinates of CM, centre of $\mathbf{N_a}$ and centre of $\mathbf{N_s}$, respectively. The lift force from the transiently trapped air is obtained by integrating the pore air pressure generated under the ski or snowboard. In Wu *et al.* (2006a, 2006b), a general equation for the pore pressure distribution beneath the planing surface was developed,

$$\nabla^2 P = -\mu A / K - (1/K)\nabla P \cdot \nabla K, \tag{1}$$

where μ is the viscosity of the air, and A is the vertical velocity gradient, $A = -U_z(x, y, h)/h$. For the case where there is no lateral tilt, $h = h(x)$, $K = K(x)$, $A = (U/h)dh/dx$ where $U = U_x$, the pressure distribution in the y direction is parabolic (Wu *et al.* 2005a) one obtained the centreline pressure distribution beneath a ski or snowboard,

$$\frac{d^2P_c(x)}{dx^2} + \frac{1}{K(x)}\frac{dK(x)}{dx}\frac{dP_c(x)}{dx} - \frac{8}{w(x)^2}\left[P_c(x) - P_0\right] + \frac{\mu A(x)}{K(x)} = 0, \tag{2}$$

where $w(x)$ is the local width of the planing surface, $P_c(x)$ is the centreline pressure corresponding to the cross section at the location x, P_0 is the pore pressure at the edge of the planing surface which is very close to the atmospheric pressure, and the local Darcy permeability is expressed as $K(x) = 0.077\exp[(1-(1-1/k)f(1-x/L)^{-1})\ln(K_2/0.077d^2)]$ d^2, where L is the length of the ski/snowboard; d is the mean diameter of the ice crystals; $k = h_2/h_1$, h_2 and h_1 are the local thicknesses of the snow layer at the leading ($x = L$) and trailing ($x = 0$) edges, respectively; and K_2 is the permeability beneath the leading edge, $K_2 = 0.077\exp[(h_0/h_2)\ln(K_0/0.077d^2)]d^2$, where h_0 and K_0 are the undeformed thickness and permeability of the snow layer, respectively. Wu *et al.* (2006a, 2006b) have examined the case when the width of the planing surface is a constant along the axial direction. However, commercially available skis/snowboards have complex geometries and variable width, as shown in Figure 3. If the nose width is W, one defines the width factor of a snowboard as $f(x) = w(x)/W$. Introducing dimensionless variables, $p' = (P-P_0)/P_0$, $p_c' = (P_c-P_0)/P_0$, $x' = x/L$, $y' = y/(W/2)$, $h' = h/h_2$ and $K' = K/K_2$, we obtain a dimensionless equation for $p_c'(x')$:

$$\frac{d^2 p'_c(x')}{dx'^2} + \frac{1}{K'(x')}\frac{dK'(x')}{dx'}\frac{dp'_c(x')}{dx'} - \frac{8}{\varepsilon f(x')^2}p'_c(x') + \frac{\theta_L}{K'(x')h'(x')} = 0, \tag{3}$$

where $\varepsilon = (W/L)^2$, $\theta_L = (\mu/P_0)(U/h_2)(dh/dx)(L^2/K_2)$. Eq. (3), subject to the boundary conditions $p_c'(0) = p_c'(1) = 0$, can be solved numerically. The transverse pressure distribution is determined based on its parabolic nature, $p'(x', y') = [1-(y'/f(x'))^2]p_c(x')$. The average dimensionless pressure generated by the trapped air inside the compressed snow layer is obtained by integrating the pore pressure over the entire surface,

$$P_{ava}' = \frac{2}{3}\left[\int_0^1 p_c'(x')f(x')dx' / \int_0^1 f(x')dx'\right]. \tag{4}$$

The solid phase (ice crystals) lift force is obtained from the quasi-static experiments performed by Wu *et al.* (2005b). This force in its dimensionless form is given by

$$p_s'(x') = P_{solid}(x')/P_0 = \left(P_{mg}/P_0\right)\cdot g\left(0.94\left[1-\lambda/k-\left(\lambda-\lambda/k\right)x'\right]/\left(\phi_0-0.06\right)\right), \tag{5}$$

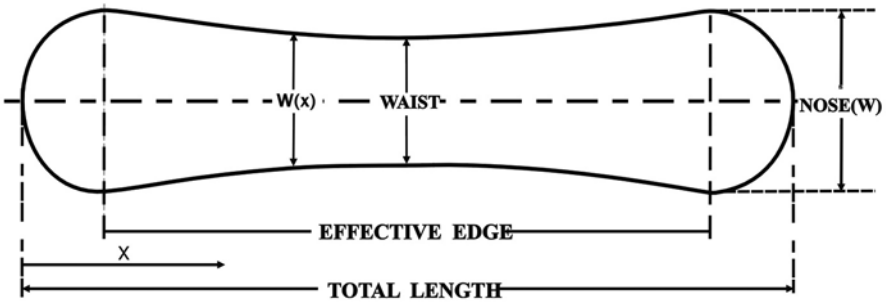

Figure 3 - Geometric snowboard dimensions described using common nomenclature (top view).

where P_{solid} (x') is the local solid phase pressure, $P_{mg} = (mg\cos\alpha_h)/A_s$ where A_s is the area of the snowboard, $g(x')$ is the empirical relation obtained in (Wu *et al.* 2005b), ϕ_0 is the undeformed porosity of the snow layer, and $\lambda = h_2/h_0$ is the compression ratio at the leading edge. The average pressure generated by the solid phase is then given by:

$$P_{avs}' = \left(\int_0^L P_{solid}(x)w(x)dx / \int_0^L w(x)dx\right) / P_0 = \int_0^1 p_s'(x')f(x')dx' / \int_0^1 f(x')dx'. \quad (6)$$

If one defines $P_{avload}' = P_{mg}/ P_0$, the normal force balance on the skier is equivalent to $f_{air} + f_{solid} = 1$ where $f_{air} = P_{ava}'/ P_{avload}'$ and $f_{solid} = P_{avs}'/ P_{avload}'$. Similarly, the moment balance equation can be written as $f_{solid}{\cdot}x_s' + f_{air}{\cdot}x_a' - F_f{\cdot}l_c' = x_{ccr}'$, where $x_{ccr}' = x_{ccr}/L$, $x_a' = x_a/L$, $x_s' = x_s/L$, $l_c' = l_c/L$ and $F_f' = F_f/\text{mgcos}\alpha_h$. When a skier glides down a slope at velocity U over an undeformed snow layer of thickness h_0 and Darcy permeability K_0 without changing his or her location of CM, one has to adjust the tilt angle γ (or the compression ratio from the leading to trailing edge, $k = h_2/h_1$) as well as the compression ratio at the leading edge, $\lambda = h_2/h_0$, to satisfy the force and moment balance equations.

3- Results and discussion

The lift distribution between the trapped air and the ice crystals strongly depends on the geometry of the planing surface, W/L; the speed of the skier or snowboarder, U; the frictional coefficient η; the location of CM (x_{ccr}', l_c'); and the properties of snow (K_0, ϕ_0, d), which have been extensively studied in Wu *et al.* (2006a, 2006b). In the current study, we shall focus on two major aspects of downhill skiing and snowboarding. First, we shall re-examine the force and moment balance equations and discuss their possible solutions; secondly, we shall investigate the effect of width variation in the axial direction on the performance of a skiing or snowboarding. The parameters chosen are as follows: m = 80 kg, α_h = 15°, η = 0.04, U= 20 m/s, $K_0 = 5.010^{-10}$ m^2, ϕ_0 = 0.6, d = 0.42 mm, h_0 = 10 cm, $x_{ccr}'= x_{ccr}/L$ = 0.45, l_c= 1.0 m.

For a given compression ratio, λ, at the leading edge, increase in the tilt angle (increasing k) will lead to the increase in both the lift force from the transiently trapped air and the ice crystals. Since the applied load is fixed, the compression ratio k from the leading to the trailing edge is uniquely determined based on the force balance equation. One can adjust the compression ratio, λ, at the leading edge and obtain a series of (λ, k) that satisfy the force balance. Each (λ, k) combination generates a value of $x_c' = f_{solid}{\cdot}x_s' + f_{air}{\cdot}x_a' - F_f{\cdot}l_c'$. When, and only when ($x_c' - x_{ccr}'$) vanishes, the moment balance is achieved. We choose a commercially available snowboard, A, as our studying case. The characteristic dimensions of the snowboard are as follows: total length = 1.38 m, effective edge length = 1.175 m, nose length = 0.308 m and waist length = 0.264 m. Figure 4a shows the change of ($x_c' - x_{ccr}'$) as a function of λ. It is clear from this figure that multi-solutions exist for this problem. In other words, there are several equilibrium positions for a given CM location. This observation reveals the non-linear nature of the stability and control of skiing and snowboarding. It is a revision of the lift mechanics theory developed by Wu *et al.* (2006a, 2006b)

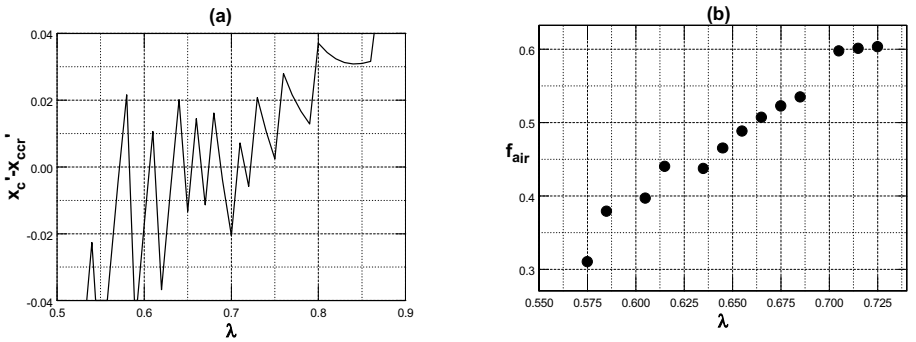

Figure 4 - (a): (x_c' - x_{ccr}') as a function of the pre-compression ratio of snow at the leading edge, λ, for snowboard A. Note x_c' - x_{ccr}'=0 corresponds to the neutral equilibrium position. (b): the contribution of trapped air to the total lift, f_{air}, at different equilibrium positions predicted in Figure 4(a).

where a unique (λ, k) was predicted. As a skier glides on a snow layer with an initial penetration depth at the leading edge, in order to achieve force and moment balance, he or she has to adjust the snow compression ratios both at the leading and at the trailing edges to the closest equilibrium location (λ, k) predicted in Figure 4a. One can shift from one equilibrium position to another by varying λ. This change is accompanied by a transfer of lift forces from the air to the solid phase or vice versa£¨and a change in angle of attack of the snowboard. Figure 4b shows the contribution of trapped air to the total lift, f_{air}, at different equilibrium positions. One notices from this figure that less compression at the leading edge (larger λ) leads to higher air lifting force, f_{air}.

It is evident from Figure 4b that the lift contribution from the trapped air, f_{air}, ranges from 30% to 60% for the different possible neutral equilibrium positions predicted in Figure 4a. The centreline pore pressure distributions beneath the surface of snowboard A for typical neutral equilibrium positions, (λ, k) = (0.575, 1.015), (0.645, 1.04) and (0.725, 1.085), are plotted in Figure 5. One finds from this figure that there are two pressure peaks along the length of the snowboard occurring near the nose section where the width of the snowboard is the maximum. This is in sharp contrast with the results predicted in Wu *et al.* (2006a, 2006b) for rectangular snowboards where single pressure peak was observed. One attributes this behaviour to the fact that the increased width of the snowboard at the nose prolongs the outflow of the trapped air in the lateral direction; hence on the time scale that the snowboard is in contact with the snow, higher pore pressure is generated at these two sections. Based on similar reasoning, a narrower section of the snowboard in the vicinity of the waist section that is near the centre of the snowboard entails a rapid pressure relaxation and hence a drop in the pore air pressure built-up. Evidently, the pore pressure reaches maximum near the trailing edge where maximum snow compression occurs. One also notices that as the compression ratio at the leading edge decreases, the compression ratio from the leading to the trailing edge, k decreases. In other words, if one compresses the snow at leading edge enough, he or she does not need much tilt angle to generate the required lifting forces.

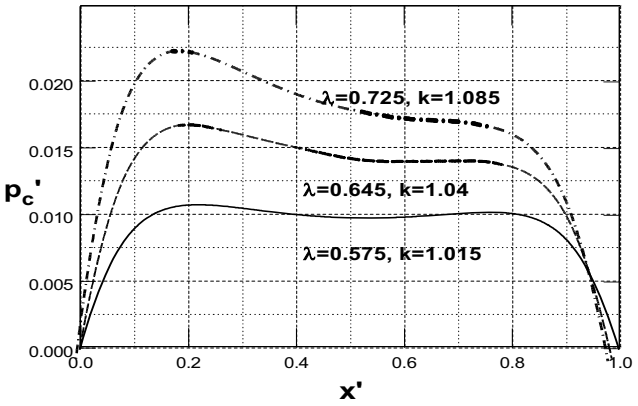

Figure 5 - Centreline pore pressure distribution beneath a commercially available snowboard, A, at three typical neutral equilibrium positions.

For a smooth, air-cushioned glide, one wants to have more lift from the pore air pressure; meanwhile, with more air trapped inside the snow layer, the frictional force that is proportional to the solid phase lifting force decreases. Thus, the lift contribution from the air to the total lift, f_{air}, provides us a criterion for evaluating the performance of a snowboard. One could optimize the shape of a snowboard by increasing its value of f_{air} (Wu *et al.* 2007).

4- Concluding remarks

In summary, we have developed a new realistic model for lift mechanics of downhill snowboarding, which incorporates the shape variation effect in the lift force generation. We have performed a thorough discussion of the neutral stability of the skier or snowboarder and made signification modifications to the skiing mechanics theory developed by Wu *et al.* (2006a; 2006b). This paper and the previous series of papers on the lift generation in a porous medium and mechanics of skiing and snowboarding (Feng and Weinbaum 2000, Wu *et al.* 2004a, 2004b, 2005a, 2005b, 2006a, 2006b, 2007) provide valuable guidance for future snowboard design from lift generation point of view.

5- References

[CW1] Colbeck, S. C. & Warren, G. C. The thermal response of downhill skis. Journal of Glaciology 37(126), 228-235, 1991.

[C1] Colbeck, S. C., Review of the processes that control snow friction. U. S. Army Cold Regions Research and Engineering Laboratory, Monograph April, 40p, 1992.

[C2] Colbeck, S. C., A review of the friction of snow skis. In Journal of Sports Sciences 12, 285-295, 1994a.

[C3] Colbeck, S. C., Bottom temperatures of skating ski on snow. In Med. Sci. Sports Exerc. 26(2), 258-262, 1994b.

[C4] Colbeck, S. C., Electrical charging of skis gliding on snow. In Med. Sci. Sports Exerc. 27(1), 136-141, 1995.

[FW1] Feng J. and Weinbaum S. Lubrication theory in highly compressible porous media: the mechanics of skiing, from red cells to humans. In Journal of Fluid Mechanics, 422: 282-317, 2000.
[JR1] Jordan, Rachel E., Hardy, Janet P., Perron, Frank E., Jr and Fisk, David J. Air permeability and capillary rise as measures of the pore structure of snow: an experimental and theoretical study. In Hydrol. Process, 13: 1733-1753, 1999.
[KY1] Kagawa, H., Yoneyama, T., Tatsuno D., Scott, N. and Osada, K. Development of a measuring system on the ski deflection and the contacting snow pressure in the actual ski turn. Proceedings of the 4th International Congress on Science and Skiing, 2007.
[SY1] Scott, N., Yoneyama, T., Kagawa, H. and Osada, K. Measurement of ski snow-pressure profiles. In Sport Engineering, 10 (3): 145-156, 2007.
[TY1] Tatsuno, D., Yoneyama, T., Kagawa, H., Kagawa, H., Scott, N. and Osada, K. Measurement of the ski deflection and ski-snow contacting pressure in the actual ski turn on the snow surface. Proceedings of the 4th International Congress on Science and Skiing, 2007.
[WA1] Wu Q., Andreopoulos, Y. and Weinbaum S. From red cells to snow-boarding: A new concept for a train track. In Physical Review letters, 93(19): 194501-194504, 2004a.
[WA2] Wu Q., Andreopoulos, Y. and Weinbaum, S. Lessons learned from the exquisite design of the endothelial surface glycocalyx and their amazing application. Design and Nature II, WIT press, UK, 2004b.
[WA3] Wu Q., Andreopoulos Y., Xanthos S. and Weinbaum, S. Dynamic compression of highly compressible porous media with application to snow compaction. In Journal of Fluid Mechanics, 542: 281-304, 2005b.
[WA4] Wu Q., Andreopoulos Y. and Weinbaum S. Riding on Air; A new theory for lift mechanics of downhill skiing and snowboarding. The Engineering of Sport 6, pp281-286, Springer, 2006b.
[WG1] Wu Q. and Ganguly, S. Study on the Optimization of a Snowboard. The Impact of Technology on Sport, pp833-838, Taylor & Francis, 2007.
[WI1] Wu Q., Igci Y., Andreopoulos Y. and Weinbaum S. Lift mechanics of downhill skiing and snowboarding. In Med. Sci. Sports Exerc, 38(6): 1132-1146, 2006a.
[WW1] Wu Q., Weinbaum S., and Andreopoulos, Y. Stagnation point flow in a porous medium. In Chemical Engineering Sciences, 60: 123-134, 2005a.

Technology And Half-Pipe Snowboard Competition - Insight From Elite-Level Judges (P240)

Jason W. Harding[1, 3, 4], Kristine Toohey[5], David T. Martin[1], Allan G. Hahn[2], Daniel A. James[4, 6]

Topics: Snowboarding, Half-Pipe, Technology, Inertial Sensors, Competition, Automated Judging, Community Perception

Abstract: Automated and objective information specific to half-pipe snowboarding has now been made available with micro-technology and signal processing techniques. In consultation with the practice community this has been introduced into training and competition in Australia. It is understood that any integration of technology into elite sport can effect change beyond the original purpose and can often generate unintended consequences. We have therefore evaluated the perceptions of key members of the elite half-pipe snowboard community in regards to how emerging technology could interface with the sport. Data were collected via semi-structured, open ended interviews with 16 international, elite-level half-pipe snowboard competition judges. This study revealed 8 dimensions and 42 sub-dimensions related to the community's perceptions to 5 major themes that emerged during interviews. The major themes included: 1. Snowboarding's Underlying Cultural Ethos 2. Snowboarding's Underlying Self-Annihilating Teleology 3. Technological Objectivity 4. Concept Management 5. Coveted Future Directions. There was dominant perception that an underlying self-annihilating teleology could exist within competitive half-pipe snowboarding. This was believed however to pose a distant threat on judging protocols to reliably assess performance. Judges sampled in this study were largely in favour of using automated objectivity to enhance the judging process however, with a number of caveats. Most importantly that objective information is to be used as a judging aid and not for automatic generation of scores. This would address the most

1. Department of Physiology, Australian Institute of Sport, AUSTRALIA, PO BOX 176 Belconnen ACT 2616 - E-mail: Jason.Harding,@ausport.gov.au

2. Applied Research Centre, Australian Institute of Sport, AUSTRALIA, PO BOX 176 Belconnen ACT 2616 - E-mail: allan.hahn@ausport.gov.au

3. Olympic Winter Institute of Australia, AUSTRALIA, 1/1Cobden Street South Melbourne VIC 3205 - E-mail: Jason.Harding,@ausport.gov.au

4. Centre for Wireless Monitoring and Applications, Griffith University, AUSTRALIA, 170 Kessels Road Nathan QLD 4111 - E-mail: d.james@griffith.edu.au

5. Department of Tourism, Leisure, Hotel & Sport Management, Griffith University, AUSTRALIA, 170 Kessels Road Nathan QLD 4111 - E-mail: k.toohey@griffith.edu.au

6. Centre of Excellence for Applied Sport Science Research, Queensland Academy of Sport, AUSTRALIA, 170 Kessels Road Nathan QLD 4111 - E-mail: d.james@griffith.edu.au

prevalent concern that integrating any automated objectivity into snowboarding could potentially remove freedom of expression and the opportunity to showcase athletic individuality - traits valued by the practice community. Our data highlight that successful implementation of emerging technologies in sport will be not be based on the type of technology developed but instead by the integration process which must feature a large element of control imparted to the key players within the sport.
Key words: Snowboarding, Objectivity, Judging, Community, Technological Integration.

1- Introduction

Half-pipe snowboarding is not a traditional Olympic sporting discipline. Snowboard competitors are required to perform an aerial acrobatic routine on a half-pipe made of snow (Figure 1) and performances are assessed with a subjective measure termed 'overall impression'. The sport is focussed upon the aesthetic [B1] where the method by which athletes achieve the competitive purpose is of utmost importance [W1]. Theoretically snowboarding like other boardriding sports exists indistinguishably between the vague boundaries of lifestyle, art and sport. It is believed half-pipe snowboarding's underlying anarchist, non-conformist, punk rock ideology, alongside the community's somewhat paradoxical view that a focus on style, execution and overall run composition is both a positive and negative aspect of its performance assessment method [HT1], will ensure ongoing partition from more traditional Olympic sports and their conventions. Perhaps as a result, the sport has until very recently received little attention from sport science and has had little to do with scientific enquiry into elite performance.

Although half-pipe snowboarding is judged by subjective measures, it has been documented that a strong relationship exists between a number of objective key performance variables (KPVs) such as air-time (AT), degree of rotation (DR) and an athlete's competition score [HT1, HS1]. Total air-time (TAT) and average degree of rotation (ADR), combined by multiple regression exhibit a very large [H1] correlation with an athlete's subjectively judged score and account for approximately 50 percent of the shared variance associated with that score. This correlation was based upon video

Figure 1 - Australian snowboard athlete in training. Breckenridge Colorado USA 2008. Image: Ben Alexander.

analysis of two Federation Internationalé de Ski (FIS) World Cup half-pipe snowboarding finals (Bardonecchia Italy 2005). There is potential for automatic calculation of this information to benefit training and competition judging protocols currently reliant on subjective measures. The integration of automated objectivity could allow coaches to assess athlete progression and training load in sport specific measures and as previously proposed could provide judges with an electronic 'memory board' (a record of an athlete's run characteristics currently written by hand) enabling their focus to shift toward execution and run composition when judging.

Until recently the only method available to objectively calculate information on performance variables in half-pipe snowboarding was by using video analysis software. The capture and post run processing of video data however, is not automatic and is labour intensive preventing rapid information feedback. We have therefore promoted the use of micro-technology and signal processing techniques to provide automatic calculation of sport specific objective information. The capability of tri-axial accelerometers (100Hz) to accurately and reliably calculate information on air-time during elite-level half-pipe snowboarding has recently been documented [HS1]. Additionally, the potential of raw tri-axial rate gyroscope data to classify half-pipe snowboarding aerial acrobatics will enable automatic classification of aerial acrobatics. Such automated assessment is theorised to introduce a measure of objectivity into the environment in which half-pipe snowboarding takes place which has been void of objectivity since its inception. Successful integration of this concept however, is reliant on positive practice community's positive perception of its utility and a willingness from researchers to consider the sporting discipline's underlying cultural ethos and coveted future directions.

Subjective perception of style and run execution has been previously identified by a small sample of the practice community as the main weakness of current subjective judging protocols. Interestingly and paradoxically, in this study subjective perception of style and run execution was also been indentified as the main strength of current subjective judging protocols [HT1]. The fact the same component of current competition judging criteria can be perceived as both strength and weakness offers some insight into snowboarding's underlying cultural ethos and reveals that both attributes are valued by the practice community. The perception the current competition judging criteria that rewards freedom of expression and potential to display athletic individuality is of the utmost importance to the practice community. Competition judging criteria has therefore taken into account what athletes value. Whether this focus can be maintained indefinitely in an era when there are calls for more objectivity in judging Olympic sports, is largely unknown. In addition to these external influences, internal forces also need to be considered. Previous research [HT1] has uncovered an awareness of what has been termed sport's overall self annihilating teleology [M1]. In elite half-pipe snowboarding, this is most likely to occur when increased numbers of athletes achieve optimal performance and outgrow the existing structure of the competition. It is theorised the integration of objectivity into judging protocols could in some ways address this issue. There are limits to its acceptability. For example, the practice community sampled unanimously opposed judging using objective information alone as it would remove what it considered to be prevailing judging strengths; that there is subjective perception of style

and run execution which allows athletic freedom of expression. Amalgamation of objectivity with current subjective measures was however positively perceived by the practice community as it was believed to improve judging reliability and still retain what the practice community values [HT1].

This paper extends on our previous findings and has sought assessment from a wider international community of elite-level half-pipe snowboard competition judges. The perception that an underlying self-annihilating teleology could exist within the discipline's competitive arena is further examined from a judging standpoint and the objective information judges perceive as potentially important elements of competition outcomes are revealed. This research focuses on initiating and maintaining a progressive partnership ideology with the practice community. In doing so it preserves a balanced approach sympathetic to the sporting discipline's underlying cultural ethos. This paper also affords elite-level competition judges a forum to communicate their perceptions on the potential impact and future management of proposed technological change within their sport.

2- Methods

The population for this study was selected by theoretical sampling and included 16 elite-level (professional level, FIS World Cup and Winter Olympic Games) half-pipe snowboarding judges. In light of FIS attempts to construct judging panels comprised of English speaking judges from a variety of nations to minimise potential national bias, the population sample for this study included elite-level judges from the following nations; Australia (n = 2), Spain (n = 2), Czech Republic (n = 1), Sweden (n = 4), New Zealand (n = 1), Netherlands (n = 1), United States of America (n = 2), Canada (n = 1), Slovenia (n = 1), Poland (n = 1). Subjects' level of experience in judging elite-level half-pipe snowboard competition ranged from 4 – 16 years. The results of this study were obtained by interviewing subjects on the impact of technological change on the culture of their sport. In-depth interviews were selected as the most suitable data collection tool because of the rich data that they provide. As a result of the near impossibility of conducting interviews with each international subject in person, subjects were interviewed by email correspondence between 27th January 2007 and 25th February 2008. Interviews were structured, conducted via email correspondence, involved posed, open ended questions, and responses were written by each subject. Not all subjects approached for this interview accepted. 16 out of 30 subjects approached for this interview accepted and provided anonymous responses. Interview transcripts were first examined to gain general familiarity. Dominant themes were noted and these formed categories. These categories became the codes by which transcripts were further interpreted. Manual coding was undertaken with a hierarchical three stage process [SC1] beginning with identification of 'open' codes. Open codes provided a broad set of categories with which to conduct subsequent reduction. 'Axial' coding subsequently divided each open code into several axial codes which reflected cultural dimensions employed to measure the perception of the practice community to specific issues. Axial codes were then divided into 'selective' codes. Selective codes provided researchers with the capacity to highlight the content of specific cultural dimensions [SS1]. Labels were selected that best described

conceptual contents of each code however, it is worth noting that labels represent researcher interpretation of content [SS1]. The number of occasions selective codes were mentioned revealed the significance of each sub-dimension to major cultural themes. A reliability measure used by [SS1] was adopted by this study. Where Smith and Shilbury calculated an inter-researcher reliability score, this study used one researcher undertaking a test-retest analysis on each interview one week apart hence; an intra-researcher reliability score was calculated. This study generated a satisfactory intra-researcher reliability level greater than 90%, as recommended [MH1]. All subjects sampled were elite-level competition judges and this was accepted as a limitation in assessing a more generaleralised practice community perception. The intent however for this particular study, was to assess this cultural group specifically and results therefore provide insight from an elite judging standpoint and not from the general community. Future studies would benefit from increased sample size and evaluating other international practice community members including athletes and coaches in addition to competition judges. The subjects read the 'information to participant' forms and signed 'informed consent' forms prior to taking part. Experimental procedures were approved by the Ethics Committee of the Australian Institute of Sport on 17th August 2006 (ref: 20060807) and in accordance with Griffith University requirements, cleared under special review in January 2008 (ref: PES/01/08/HREC).

3- Results

This paper investigated the perception of a sample of elite-level half-pipe snowboard competition judges to the integration of automated objective information into performance assessment criteria. Table 1 shows the 8 axial codes (dimensions) and 42 selective codes (sub-dimensions) related to 5 major themes (open codes) that emerged during the interview process. The major themes were: 1. Snowboarding's Underlying Cultural Ethos 2. Snowboarding's Underlying Self-Annihilating Teleology 3. Technological Objectivity 4. Concept Management 5. Coveted Future Directions. Interview quotes are used within discussion (shown in italics) to highlight significant practice community opinion.

Athletic Freedom	
1.	Athletic freedom of expression
2.	Freedom to showcase athletic individuality
3.	Athlete driven progression
4.	Athlete in control of competition performance
5.	Minimal set criteria in competition
6.	Subjective perception of style and overall run execution
7.	Snowboarding's soul / spirit / style / artistic merit
8.	Non-conformist nature of snowboarding
The Existence of a Self-Annihilating Teleology	
9.	An imminent threat to judging reliability
10.	A distant threat to judging reliability
11.	A currently occurring phenomenon
12.	A negative aspect of the sport
13.	A positive aspect of the sport
14.	A theory without any relevance in snowboarding
Objective Performance Variables	
15.	The importance of air-time and amplitude
16.	The difference between air-time and amplitude
17.	The diminishing importance of degree of rotation
18.	The negative aspects of the 'spin to win' approach
19.	The benefit of objective information on each individual trick
20.	Subjective perception of style and run execution
Theoretical Objective Weighting	
21.	Theoretical KPV percentages in amalgamated judging system
22.	No objective information should constitute any part of score
23.	Opposition to solely objective assessment
24.	Minimisation of automated technology's role in generating scores
Technology's Potential Role in Snowboarding	
25.	Automating memory boards
26.	Simplification of judging process
27.	Beneficial in unfavourable environmental conditions
28.	Beneficial where snowboard half-pipes increase in length
29.	Beneficial in athlete score protest situations
30.	The importance of objective 'revert' classification
The Negative Impact of Technology on Snowboarding	
31.	Opposition to integration of technological objectivity
32.	Removal of snowboarding's underlying cultural ethos / spirit / soul
33.	Potential for removal of athletic freedom of expression
34.	Removal of what the practice community values within the sport
35.	Forced integration on a practice community not consulted
36.	Potential to push athletes away from competition
Progressive Partnership Ideology	
37.	Scepticism toward integration of technological objectivity
38.	The need to assess athlete perceptions and coveted direction
39.	The capacity of the judging system to direct competition riding
Snowboarding's Future Directions	
40.	Sport retains cultural ethos and athletic freedom of expression
41.	Sport remains partitioned from traditional sporting conventions
42.	Sport retains competitive criteria that athletes value

Table 1 - Cultural dimensions and sub-dimensions (Axial and Selective Codes) associated with the four major themes.

4- Discussion

We have previously documented a capacity for technology and signal processing to calculate objective information on air-time and degree of rotation during snowboarding [HT1, HS1]. Originally investigated to allow objective assessment in training, this concept may also have potential to assist judging protocols and as such has been introduced into training and competition (AIS Micro-Tech Pipe Challenge) in Australia. Focussed on correct management of technological innovation in sport this paper has sought assessment from a wider international community of elite competition judges. As noted by respondent number 9, the consequences of technological change may be irreversible and can potentially corrupt the sport's perceived ethos.

'We must be very careful as we continue down the road [of amalgamating] snowboard competition and technology. If misused, it has the potential to ruin the pureness we find [in the sport] today'

Hypothetically, half-pipe snowboard competition could potentially suffer from sport's overall self-annihilating teleology [M1]. The most likely scenario would be increasing numbers of athletes achieving optimal performance, thereby outgrowing the structure of current half-pipe snowboard competition and impinging on the capacity of subjective judging criteria to reliably assess performance. There was dominant perception as noted by respondent number 9, that an underlying self-annihilating teleology [M1] could exist within competitive half-pipe snowboard competition, revealed by ten out of sixteen judges.

'It would be naive to think that a sport such as snowboarding will never get to a point where very little separates elite level athletes. The separation between riders we have clearly seen in the past will one day no longer be discernable by the human eye alone and at which point we will require the continued assistance that technology provides'

Whilst a majority of the community sampled believed this theoretical phenomenon could exist within half-pipe snowboarding competition, most perceived it as a distant threat. The most prevalent sub-dimension, as noted by respondents numbered 11 and 16 respectively, related to snowboarding's self-annihilating teleology was labelled, "a distant threat to judging reliability".

'I do not think snowboarding is there yet'

'I believe that most [of the community] understand we are a long way from [suffering the effects of] a self annihilating teleology'

Interestingly however, two subjects revealed this teleology to be a "currently occurring phenomenon". As noted by respondent number 14, whilst the effects of increasing numbers of athletes achieving optimal or similarly high levels of performance are currently being experienced in elite-level competition, it is actually having a positive effect on judging reliability.

'This is happening to a degree, but in the case of snowboarding it is making the sport easier to judge by making the runs more comparable. We are still a long way away from the time where every rider will be performing the same run but as the runs get more and more similar it is possible for the judges to look more at execution and less at difficulty'

Three judges perceived the existence of an 'underlying self-annihilating teleology' and the subsequent hypothesised affect on current judging reliability a "theory without any relevance in snowboarding" (three did not respond to the question). As noted by respondents numbered 11 and 15 respectively, judging criteria focused on "subjective perception of style and overall run execution" retains what is valued by the practice community and will perpetually allow for reliable performance assessment.

'I am not sure how well the [self-annihilating teleology] theory will apply to snowboarding. Judging when all the top riders are doing the hardest tricks and executing them well is exactly what it means to judge elite-level competitions. In fact, there are usually only a handful that has both the hard tricks and good execution. It's not so much about what they're doing as how they're doing it'

'I do not agree [with the concept of a self-annihilating teleology]. In the case of snowboarding the same trick, even the exact same run can be executed in a different way. Unless snowboarding judges start to dictate a certain perfect execution (like gymnastics) there will still be plenty of room to ride differently and to judge those differences in execution'

Not withstanding these views and regardless of the existence of an underlying self-annihilating teleology within the sport, it is proposed that automated objectivity could assist judging protocols to assess performance. Previous work however has shown unanimous and vigorous opposition to judging with objective information alone as it would remove the two prevailing judging strengths; that judging is focussed on subjective perception of style and run execution and that it allows athletic freedom of expression. The dominant perception from a wider international community of judges was essentially no different. Where previous work documented support for amalgamating objective and subjective information into judging [HT1], elite judges were largely (albeit cautiously) in favour of trialling automated objectivity as a judging aid only and vigorously opposed its use in determining judging criteria or automatic generation of scores. Adherence to this demand would address concern that integration of automated objectivity could remove what is valued by the community and as noted by respondent number 9, opportunity for athletes to control the delivery of their performance and freely express their snowboarding ability.

'We must always keep one thing in mind, that is to never remove the snowboarder's ability to display their creativity when riding and we must always provide riders the opportunity to dynamically change and be in control of the delivery of their performance'

The respondents evidenced a very strong practice community perception of what it means to be a snowboarder and the value of retaining the freedom and individuality that the sport entails (all sixteen judges mentioned some aspect of the underlying ideology associated with the sport). Proposing the integration of automated objectivity into an area of the sport (elite-level judging criteria) with the capacity to alter future directions understandably seems in conflict with the sport's underlying cultural ethos. Unsurprisingly, automated objectivity was not a term used to highlight the sport's cultural ethos and as noted by respondent number 5, opposition to integration of automated objectivity into snowboarding could potentially be quite vigorous.

'*This would be the death of half-pipe snowboard competition*'

In spite of opposition to automated objectivity expressed by a small number of subjects there was dominant practice community perception on the importance of air-time (and relationship to amplitude) on competition outcomes. Thirteen out of sixteen judges perceived air-time an important criterion in competition performance assessment, even though it is assessed subjectively (as amplitude) and were largely in favour of using automated objective information on air-time in some form whilst judging. The most prevalent air-time variable (mentioned by eight out of these thirteen subjects) was average air-time (AAT) as it provides indication of consistency over a complete competition run. As noted by respondents numbered 3 and 10 respectively, the importance of air-time is recognised by both elite-level judging panels and the practice community in general.

'Air-time is considered for every trick from a judging perspective'

'Athletes, coaches, judges, even my own mother agree that the amplitude [associated] with a trick is important'

Although air-time and its relationship (however tenuous) with amplitude constituted strong community perception, the perception on the importance of degree of rotation toward competition outcomes was not positive. Nine subjects mentioned they would use automated objectivity related to degree of rotation (seven would use average degree of rotation, ADR) in some form whilst judging however, all stated this information is not required and could negatively impact the sport's future directions. Focusing on degree of rotation as noted by respondent number 13, was largely perceived to promote a 'spin to win' approach to competition; an approach strongly opposed by elite-level judges.

'As for rotation, it seems to have played an increasing role in separating rider's scores over the years but I feel this has sometimes been in error. Not everybody agrees with the "spin to win" approach. More [rotations] is not necessarily better. Of course having said that, a rider who does large degree rotations must be rewarded, provided they have been executed well'

Judges however expressed an interest in automated and objective information related to other parameters associated with acrobatic rotation including; 1. The smoothness (consistent rotational velocity) of each rotation and 2. The exact degree of rotation (the amount of rotation completed during the air-time phase with objective reference to the amount of rotation reverted or completed after the landing). Unsurprisingly and as noted by respondent number 15, the strongest practice community perception was to allow 'subjective perception of execution and run composition' the most impact on athletic performance assessment. All judges mentioned that any performance assessment method utilised should still contain subjective perception. Judges were largely in favour of allowing subjective perception to contribute at least 50 percent of total competition run score in the theoretical amalgamation of automated objectivity and traditional subjective measures posed by this paper.

'A trick with high airtime and difficult rotation that is well executed with great style will usually score high. But if a rider is unstable and showing poor execution, not even lots of air time and [degree of] rotation will get him or her a high score'

Six out of sixteen judges sampled (the dominant perception) would use a combination of average air-time, average degree of rotation and subjective perception (25, 20 and 55 percent respectively) to award performance in the posed hypothetical judging system. Judges however vigorously and unanimously stated they would rather use objective information only as a judging aid. This may therefore be the potential niche for automated objectivity; as a judging aid and as an automated memory board (a record of an athlete's run characteristics currently written by hand). There was dominant community perception that although judges are trained to identify aerial acrobatics and subjectively assess amplitude, a system of automated objectivity could potentially aid performance assessment. As noted by respondent number 9, using automated objectivity in this manner could assist judging without negatively impinging on practice community future directions or the sports underlying cultural ethos.

> *'I see great potential for continued advancement and implementation of technology into snowboard competition to produce more accurate outcomes [however]; only if the athlete's ability to perform in an independent and creative [manner] is not compromised'*

5- Conclusion

Elite-level judges are largely in favour of trialling automated objectivity as a judging aid and would like to see development of automated competition memory boards. There is however strong opposition of using automated objectivity to determine any component of competition scores or judging criteria. This may be related to the vested interest of the population sampled. As judges they may feel their future career will be compromised if they can be replaced by an automated system of assessment. This may also be related to vested interest in maintaining snowboarding's cultural ethos and what is valued within the sport by the practice community. Judges were not however totally opposed to the idea nor were they opposed to greater consultation within the snowboarding community. There was however strong perception that further development and integration of this concept be conducted in close association with core community members and be controlled from within the sport.

6- Acknowledgments

First and foremost, thank you to the Snowboard coaches (Ben Wordsworth and Ben Alexander) and the athletes of the Australian national half-pipe snowboard team for their willingness to trial innovative technology and challenge conventional training protocols and competition judging formats. We also thank Perisher Blue Ski Resort, NSW National Parks and Wildlife Service and Catapult Innovations for all funding and in-kind support. A special thanks to the Head of the Department of Physiology at the Australian Institute of Sport, Professor Chris Gore and all his staff for creating an environment focussed on innovative thinking and passionate debate in the name of rigorous scientific enquiry. Also thank you to Heidi Barbay for assistance during southern hemisphere winters and to the staff who helped conduct the AIS Micro-Tech Pipe Challenge 2007; a competition that integrated automated objectivity and traditional judging into elite-level half-pipe snowboarding. Results and media related to this competition can be can be viewed at www.AnarchistAthlete.com

7- References

[B1] Best D. Physical Education and the Aesthetic. In Bulletin of Physical Education. 14(3): 12-15 1978.

[HS1] Harding J. W., Small J. W., James D. A. Feature Extraction of Performance Variables in Elite Half-Pipe Snowboarding Using Body Mounted Inertial Sensors. In BioMEMS and Nanotechnology III, edited by Dan V. Nicolau, Derek Abbott, Kourosh Kalantar-Zadeh, Tiziana Di Matteo, Sergey M. Bezrukov, Proceedings of SPIE Vol. 6799 (SPIE, Bellingham, WA, 2007) 679917, 2007.

[HT1] Harding J. W., Toohey K., Martin D. T., Mackintosh C., Lindh A. M., James D. A. Automated Inertial Feedback For Half-Pipe Snowboard Competition And The Community Perception. In The Impact of Technology on Sport II, Fuss F. K., Subic A., Ujihashi S. Taylor & Francis London., 20, 845 – 850, 2007.

[H1] Hopkins W. G. Analysis of validity by linear regression (Excel spreadsheet). In A new view of statistics. sportsci.org: Internet Society for Sport Science, sportsci.org/resource/stats/xvalid.xls, 2007 viewed on 2 November 2007.

[M1] Miah M. New Balls Please: Tennis, Technology, and the Changing Game. In S. Haake and O. A. Coe 2000 Tennis, Science and Technology, Blackwell and Science, London, 285-292, 2000.

[MH1] Miles M. and Huberman M. Qualitative data analysis (2nd ed). Thousand Oaks, Sage, California. 1994.

[SS1] Smith A. C. T. and Shilbury D. Mapping Cultural Dimensions in Australian Sporting Organisations. In Sport Management Review, 7, 133-165, 2004.

[SC1] Strauss A. and Corbin J. Basics of qualitative research. In Grounded theory, procedures and techniques. Newbury Park, Sage, California, 1990.

[W1] Wertz S. K. Are Sports Art Forms ? In Journal of Aesthetic Education 13(1): 107-109, 1979.

Information Return Device Concept: Baropodometric Biofeedback Application (P241)

A. Descatoire[1], P. Moretto[1-2]

Topics: Biomechanics; Handicap; Materials; Measurement Systems.
Abstract: Numerous studies on new biofeedback devices conception development were undertaken. They are used for some compensation methods of the data lost on sensors set. The aim of the study was carried out for introducing several approaches of investigations and test of the biofeedback device that support a plantar pressure analysis, for foot unloading processes implementation. The healthy man is walking in normal conditions first; on a walkway. The recorded load on 6 sensors has to be reduced next in a specified area. The pressure was considered at the beginning on metatarsal head, in time of 100 steps. The visual and auditory signals were then adjusted to a specific plantar pressure threshold setting. Peak and pressure time integral were evaluated for each condition. The Results showed that the subject performed 65% of success unloading steps. In the present case, the biofeedback device enabled us to modify the plantar support to prevent possible foot complication. In general, Biofeedback systems could show their interests in many applications: rehabilitation process, sport or to assist active-assistive orthotic devices.
Key words: "Biofeedback", "plantar pressure", "sport", "rehabilitation", "assistive device".

1- Introduction

The term Biofeedback refers to the use of an external device to increase an individual's awareness of sensory events that accompany performance.

The biofeedback device can be considered as an interesting therapeutic method when a self-regulated system is disturbed (André *et al.* 1986). Electromyographic biofeedback has mostly been used to correct simple motor tasks involving not more than one segment (Ingersoll and Knigh, 1991). However biofeedback methods are applicable, to correct complex abilities mobilizing several segments, if the feedback is based on a mechanical resultant of the movement such as the external force (White and Lifeso 2005, Dozza *et al.*

1. Laboratoire d'Etude de la Motricité Humaine, Faculté des Sciences du sport de l'Université de Lille 2, France - @ : aurelien.descatoire@etu.univ-lille2.fr
2. Laboratoire d'Automatique, de Mécanique, et d'Informatique Industrielles et Humaines (UMR-CNRS 8530) de l'Université de Valenciennes, France - @ : pierre.moretto@univ-lille2.fr

2005). The recent progress was achieved for the development of the measuring device conception, using force and pressure recording sensors, providing the user with new biofeedback interfaces. Previous studies have demonstrated different methods to measure plantar pressure (Pataky *et al.* 2000, Femery *et al.* 2004). Such systems use different sensors, as well as different acquisition systems, from the portable plantar pressure measurement system we have developed. Our plantar biofeedback provides both visual and audio feedback in order to correct the plantar pressure distribution, when local pressure exceeds a maximum determined threshold. These devices use a signal-warning system that may be particularly appropriate to the patient's disease, when suffering from lost nociceptive perception subsequent to metabolic diseases, infectious disorders or traumatic lesions.

2- Methods

2.1-Population

A 23-yr-old healthy man, weighing 80kg, without foot or gait abnormalities, took part in this trial after providing written informed consent in accordance with a protocol approved by an institutional review board.

2.2 Instrumentation

The whole biofeedback system is called B.I.R.D for Baro-Paedometric Information Return Device.

Previous studies used FSR sensors which detect normal force acting on the surface revealed a very simplified action of the foot on the sensor area whereas plantar ulcer were linked to normal and sheer stress (Pataky *et al.* 2000, Femery *et al.* 2004). The hydrocells from Paromed (Gmbh, Germany) consists of an inbuilt Wheatstone bridge, inserted in a capsule filled with incompressible fluid, which results in a pressure from the different components of the ground reaction force. This implies that the cells are sensitive to mechanical stress which has three components, pressure acting normally on the surface, anterio-posterior and medio-lateral shear stress acting tangential to the surface. The cells revealed more realistic measures of pressure acting under the foot. The sensors are calibrated by the manufacturer and a calibration file is provided for each sensor. An individual calibration for each sensor was performed to ensure that statements of the absolute pressure at different regions of the foot could be substantiated. Our bench testing results of the sensors confirm previous data (Femery *et al.* 2004, Chesnin *et al.* 2000) (table 1).

Dimensions (mm)	
Diameter	22
Active sensing diameter	18
Thickness	3
Measurement range	0 to 625 kPa
Uncertainty	± 1%
Stability	± 2% (at 400 kPa, deviation ± 2,5 kPa)
Hysteresis	0,1 kPa

Table 1 - The Main characteristics of the Hydrocells Paromed (Gmbh, Germany).

2.3 Customized Insole development

The Footscan plate [b] was used to detect the peak locations and to determine the sensor distribution of a customized insole. Two insoles (right and left) were thus customized comprising 6 Paromed hydrocells in each, distributed under the lateral heel (LH) and medial heel (MH), metatarsal heads 5 (M5), 3 (M3), and 1 (M1), and the Hallux. The insoles were connected to an amplifier and linked with a personal computer via a telemetrically joined data recorder. The metrological process and its feedback were organised for the biofeedback customised software package.

2.4 Visual and Auditory Feedback

The feedback from this device is intended to cue the subjects to initiate a new walking gait strategy. The visual feedback, which was returned to the subject through two control screens by video projection, consists of plantar footprint visualisation scenes that correspond with localisation of the insole sensor setting (fig. 1). On the left of the plantar footprint there is a scale of colours, from blue, green to red; illustrating pressure intensity at each of the sensors localisation point. A "scorer" was placed on the left side of the foot print, informing the user about the performances considered. The peak plantar pressures were recorded during a diagnostic walking trail (PP_{dt}) performed at preferred walking speed. The peak pressures under each footprint location were then defined and serve as reference. A 5% reduction in peak pressure would be sufficient to prevent foot ulceration at its most affected area (Descatoire *et al.* 2007). This threshold level is considered as PP_{CR} max value. The 20% reduction in peak pressure, considered as PP_{CR} min, enabled us to limit excessive relief resulting in dangerous plantar pressure redistribution (Descatoire *et al.* 2007). For the case study, the peak plantar thresholds ($PP_{CR\ Max}$ and $PP_{CR\ Min}$) of the sensor located under the first metatarsal head (M1) were determined as a 5% and 20% reduction in plantar pressure recorded during "Diagnostic test (dt)", respectively (i.e. $PP_{CR\ Max} = 0.95\ PP_{dt}$ and $PP_{CR\ Min} = 0.80 PP_{dt}$). The auditory feedback was implemented as an alarm trigger, combined with the visual feedback. It indicated the local pressure overload, at the selected area where the $PP_{CR\ Max}$ was noticed. On the contrary, only the visual feedback informed the subject when excessive relief occurred. Thus step-by-step, the subject concerned was informed of dynamic events at the footground interface, and remained aware of the overall foot condition.

2.5 Walking test

The non-disabled subjects performed the walking tests on a 25 m walkway. The subject concerned was equipped with the customised insoles inserted in neoprene shoes to match the form of the insoles. After a brief explication of the device, the subject performed the diagnostic walking test at his self selected walking speed. The plantar pressures of more than 100 steps were recorded. Then the subject used the Baropodometric Information Return Device (BIRD) to relieve the first metatarsal region (M1) of the right fàot using the visual and acoustic biofeedback. The M1 area was chosen for the trial because it is a well-known at risk area for the development of plantar ulce-

Figure 1 - B.I.R.D software interface: 65 Success Steps, 25 Moderate Steps, 10 Faulty Steps.

ration in neuropathic diabetic subjects (Lavery *et al.* 1997). The test enabled us to record the peak plantar pressure in unloaded conditions over 100 (50 right and 50 left steps) consecutive steps.

3- Results

Table 2 contains the results recorded during the diagnostic walking and the unloading processes. One step under BIRD condition was considered successful when the peak pressure value remained between $PP_{CR\ Max}$ and $PP_{CR\ Min.}$ If the peak pressure, recorded under M1, was greater than PP_{CRmin}, the relief was excessive and the step was considered as moderate success. For M1peak pressure, above the PP_{CRmax}, the relief was insufficient and the step was also considered as faulty.

	diagnostic Condition	Unloaded Condition		
		Success steps 20%<PP<5%	Moderate Success steps PP>20%	Failure steps PP<5%
% of step	-	65	25	10
PP mean	116.7	103.2	75.5	124.8
SD	22	11.8	8.1	5.8
PP min	96.1	97.7	63	116.3
PP max	176.8	110.1	87	133.2

Table 2 - Peak Pressure values measured under M1 during the diagnostic and the unloaded condition. Values are in kilopascals. PP min: minimum peak pressure, PP max: maximum peak pressure.

5- Discussion

Recent technologies have allowed us to modify and optimise existing biofeedback systems, in order to develop some additional diagnostic devices and/or to develop new rehabilitation methods based on "on-line" detection of abnormal walking parameter values. In the present case, the subject has relieved the first metatarsal with facilities (90% of the steps). Moreover, he performed 65% of success steps that would avoid dangerous plantar pressure redistribution. Our visual and auditory biofeedback provides a warning system that may play a valuable role in preventing injuries or ulceration by changing the walking pattern

6- References

[AB 1] Andre JM, Brugerolle de Fraissinette B, Chellig L. 1986. Le biofeedback en rééducation motrice. Ann Readapt Med Phys. 1986;29:289-310.

[IK 1] Ingersoll CD, Knight KL. Patellar location changes following EMG biofeedback or progressive resistive exercises. Med Sci Sports Exerc. 1991;23:1122-7.

[WL 1] White SC, Lifeso RM. Altering asymmetric limb loading after hip arthroplasty using real-time dynamic feedback when walking. Arch Phys Med Rehabil. 2005;86:1958-63.

[DC 1] Dozza M, Chiari L, Chan B, Rocchi L, Horak FB, Cappello A. Influence of a portable audio-biofeedback device on structural properties of postural sway. J Neuroengineering Rehabil. 2005;2:13.

[PF 1] Pataky Z, Faravel L., Da Silva J, Assal J. A new ambulatory foot pressure device for patients with sensory impairment. A system for continuous measurement of plantar pressure and a feedback alarm. J Biomech. 2000;33:1135-8.

[FM 1] Femery VG, Moretto PG, Hespel JM, Thevenon A, Lensel G. A real-time plantar pressure feedback device for foot unloading. Arch Phys Med Rehabil. 2004;85:1724-8.

[CS 1] Chesnin, K.J., Selby-Silversteun, L., Besser, M.P., 2000. Comparison of an in-shoe pressure measurement device to a force plate: concurrent validity of center of pressure measurements. Gait and Posture 12, 128-33

[DF 1] Descatoire A, Femery V, Moretto P. Plantar pressure redistribution after a high and low unload. In proceeding of the International Society of Biomechanincs. 2007. Taiwan, Taipei. Journal of Biomechanics 40, S177.

[LV 1] Lavery LA, Vela SA, Lavery DC, Quebedeaux TL. Total contact casts: pressure reduction at ulcer sites and the effect on the contralateral foot. Arch Phys Med Rehabil. 1997;78:1268-71.

This investigation was supported by funds from the Conseil Régional Nord-Pas de Calais, the Délégation Régionale à la Recherche et à la Technologie du CHRU of Lille and the Institut Régional de Recherche sur le Handicap (IFRH-25)

The Bike Fit of the Road Professional Cyclist Related to Anthropometric Measurements and the Torque of de Crank (P242)

*Jon Iriberri[1], Xabier Muriel[2] and Iosu Larrazabal[3]

Topics: professional road cycling, bike fit

Abstract: It has been demonstrated that the modifications in the bike fit or the voluntary position changes affects in different parameters; cardiovascular, mechanic, pathologies, comfort. The objetive of this study was to obtain new methods to optimize the fit of the competition road bicycle, according to the anthropometric variables and torque. The study group consisted of 28 male cyclist of professional U.C.I. We measured all the anthropometric variables according with the ISAK protocol. Them we measured 20 different measures of the bike, and simulated the measurements in our ergometer (SRM ergometer). We optimized the position, changing the variable lengths of the bike and the position of the cycling shoes cleats, based on the optimal crank torque. After this, we measured again the new lengths and angles, and we correlate with the anthropometric data, to obtain relation and formulas. We realised that the 21,42 % of the subject aren't in comfort with the position obtained by our formulas. Because this, we decided to separate into tree groups; the ones who had the relation of tall/ trocanter height > 1,94 , between 1,88-194 and < 1,88. Then when we divided the cyclists into three groups and again we applied the new formulas for each groups, the discomfort disappear. The correlations and the obtained formulas consequently, are more precise for all groups, except group 3 with the differentiation of the groups. It has been demonstrated that exist a relation with some bicycle measures and anthropometric data. Also, we can see that just one formula for all the subjects is not very precise, the fit is better if we difference the cyclist by their anthropometric data. The success of our formulas has been demonstrated, by mechanics improvals, with always subjective comfort of the cyclist, and with no pathologic cases after our job.

Key words: Bicycle Measurement, Systems Performance Sports, Bike fit, Anthropometry, Crank torque.

1. PEC Basque Government, Getxo 48992, Spain - j-iriberri@ej-gv.es
2. Oreki Fundation, 20160 Lasarte, Spain
3. Euskadi Fundation, 48160 Derio, Spain

1- Introduction

Optimal bicycle rider position may be considered to be a position in which a number of variables such as exercise economy, mechanical and metabolic efficiency, and comfort interact in a complex manner to minimise resistive forces and maximum bicycle velocity. Furthermore, position should minimise the risk of injury and comply with UCI regulations. Based on these variables, a number of methodologies have been proposed to optimise position.(Hamley and Thomas,1967), (Lemond and Gordis,1987), (E R Burke, 1994 and 2002), (Holmes *et al.*, 1994), (Harrison, 1970), (Morris and Londeree, 1997).

Any changes such as height or fore-aft position of the saddle are likely to result in changes in the range of motion of hip, knee and ankle (Houtz and Fisher, 1959), (Nordeen and Cavanagh, 1975) and (Nordeen-Snyder, 1997). In addition, a postural change may result through voluntary flexion or extension of the hip or trunk; or by changing the measurements or geometry of the cycle Welbergenandy Clijsen) said (Welbergenandy Clijsen,1990) . Furthermore, changing bicycle geometry, such as the angle of the vertical tube, may result in physiological as well as kinematic changes. Indeed, Gonzalez and Hull (,Gonzalez and Hull, 1989) describe five variables that effect the kinematic analysis of cycling: Crank length, saddle height, vertical tube angle, the pedalling cadence and the longitudinal position of foot respect to pedal. Moreover, it is also important to account for differences in mono- and bi-articular muscles, as they affect kinematics these kinematics (because mono-articular muscles shown bigger changes in their kinematics that the bi-articular muscles before a position change) (Li Li y G E Caldwell, 1998), (Savelberg y Meijer ,1994)

1.1 Bike fit systems

There are a number of formulas and methods which are formulated or designed to fit the bike to individual's anthropometric measurements, for instance .However, there is no consensus in opinion of riders or trainers as to the optimal method to fit a rider with a bicycle. The main limitations around fit methods are that they lack standardisation in the measurement of the bicycle or that they are not described in a manner which allows for repeatability of the methods suggested. Thus, comparison between different methods is problematic.

Although kinematic analysis of position is useful, comfort of the rider must also be taken into account. Indeed using a prescribed formula for rider position, of H H C M Christiaans and A Bremen (H H C M Christiaans and A Bremen ,1998), found that 60% of their subjects were uncomfortable in the position and that woman found the position less comfortable than males. They concluded that comfort on a bicycle is a individual and subjective preference and that the height of the saddle in relation to leg length was the most important positioning variable that is less subjective.

2- Study

The aim of this study was, therefore, to develop new formulas, with the use of individual anthropometric variables, to optimise rider position on subjects own competition race cycles.

2.1 Methods and Subjects

Participants were 28 male U.C.I. professional licence holders (mean ± s: body mass 71.7 ± 6 Kg, height 1.79. ± 0.64 m and sum of 6 skinfold 41.12 ± 6.45 mm as measured in accordance with ISAK protocol. An SRM (Schroberer Rad Messtechnik, Welldorf, Germany) scentific (8 strain gauges) ergometer was used to measure crank torque.

Initially, this ergometer was adjusted to replicate the dimensions of the riders own race cycle. Ergometer dimensions and cycle shoe cleat position were then adjusted until optimal crank torque was identified.

To ensure that the effect of pedalling technique on analyses was minimal, the technique of all riders was force (torque) application analysis was conducted and those who did not display optimal or close to optimal technique were excluded from the study. Although there is no consensus in what constituted optimal pedalling technique, we consider torque application similar to that shown in Figure 1 to be optimal.

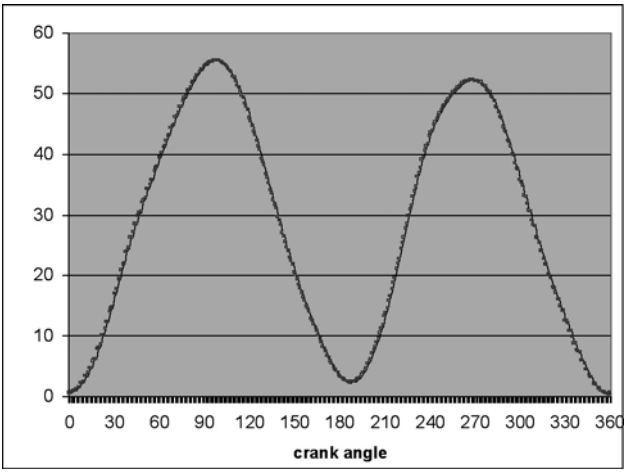

Figure 1 - Example of optimal torque application at 250 W and 90 rev·min.

The following objective criteria were used to select subjects (Broker, 2003)
- Less that 10% of difference between both legs in the 1/2 peak of torque.
- Less that 5% of difference between legs in the peak torque.
- Peak Torque between 85-100 degree of the pedal downstream.
- Minimum torque between 170-190 degree of the pedal downstorke.

Where riders did not initially meet these criteria, whilst riding at 250 W and 90 rev·min, position was adjusted and if on further analysis they still did not meet the criteria, they were excluded from the study.

2.2 Results and Discussion

Linear regression revealed that the relationship between rider position and anthropometric data could be described using the following equation:

$$\text{(Maximum length pedal-saddle= (Height} * 0.5138 + 0{,}5) \quad (1)$$

Pearson product moment correlations were used to measure the level of significance of highly significant relationship trocanter height and the maximum distance between the base of the pedal and the lowest point in the saddle.

($r = 0.92$ $p<0.05$) . Furthermore, the relationship between of the length, among the base of the pedal and the lowest point in the saddle and the height was greater ($r = 0.92$, $P<0.05$).

Although the results are good statistically, based on the subjective evaluation, 6 subjects were not comfortable in the position obtained using this formula. To optimize the formula, we proceeded differentiating the subjects, in function to the proportion of the longitude of the legs, trocanterear height, with the height of each one. Consequently, riders were then divided into 3 groups, according to height/trocanter relationship, as shown in table 1.

	Height/trocanter	r value	Formula
Group 1	>1.94	0.999 p<0.01	maximum length pedal-saddle = (height *0.8836) - 67.688
Group 2	1.94 - 1.88	0.963 p<0.05	maximum length pedal-saddle = (height *0.5319) - 2.8594
Group 3	<1.88	0.903 p>0.05	maximum length pedal-saddle = (height *0.4194) + 18.058

Table 1 - Relationship between rider position and anthropometric data (n = 28).

As demonstrated by the r values, the strength of the relationship between rider position and anthropometric variables was improved in group 1 and group 2, but not in group 3 by taking into account the height/trocanter relationship.

The formulas that we have obtained off the rest of variables of the bicycle aren't so significant statistically, surely because they are based on in the subjective perception, except the setback length. Even this way, we propose some formulas, that they can approach with a very small error to the ideal position above the bicycle. Since, there aren't published formulas in reference to the setback length of the saddle, the distance between the saddle and the handlebar, neither to the difference of height between the saddle and the handlebar. Table 2.

Bicycle variable	Formulas	
Longitude between crank set and saddle	=(0,56 x height)-24,64	r^2: 0,926
Saddle setback	=(height-157,06)/3,02	r^2: 0,474
Distance among saddle and handlebar	=(0,495 x height)-30,805	r^2: 0,882
Difference of height between saddle and handlebar	=(height-154,96)/2,30	r^2: 0,49

Table 2 - Formulas with lowers statistical relation.

2.3 Conclusions

There is not a standard methodology to optimize the cyclist's position, because, just as we have pointed out, several variables are more subject to perceptive factors than anthropometric factors . On the other hand, the longitudes among the base of the pedal, the crank set and the handlebar with the saddle, seem to have a high relationship with the anthropometric variables.

We want to point out according to our own experience, that these formulas, as many other, might take to error, if we doesn't keep in mind the pedaling technique. Because of the changes of the of the angle of the ankle kinetics, makes the kinetics of the angle of the knee and hip also change..

However, we have not been able to find relationship between the anthropometric data and the position of the shoe cleeps, except the anatomical angle of the foot. Neither in the literature we have been able to find, with enough scientific rigor, outside the own experience of some author, any methodology that determines the position of the shoe cleeps. On the other hand, our own experience has taught us that the variations in the shoe cleeps, vary the form of applying the force in the pedal, the torque.

In fact, we show another way to optimize the cyclist's position, but in this occasion, based on the optimized torque, this is, in an efficient bicycle position.

In conclusion, these data suggests that anthropometric measurement and proportions must be taken into account when trying to determine optimal position. These formulae might be an alternative method to improve cyclist torque, when a crank torque measurement system is not available.

3- References

[Br1] Broker Jeff, In "High-Tech Cycling-2nd Edition". Human Kinetics.2003

[Bu1] Burke E R. "Proper fit of the bicycle". Clinics in Sports Medicine. 1994.13;1:1-15

[Bu2] Burke Edmund R,PhD. "Serious Cycling-2nd Edition". Human Kinetics (2002).

[CB1] Christiaans Henri H. C. M y Bremen Angus. "Comfort on bicycles and the validity of a commercial bicycle fitting system". Applied Ergonomics(1998). 29;3.pp:201-211.

[FD1] Faria I, Dix C, and Frazer C. "Effect of body position during cycling on heart rate, pulmonary ventilation, oxygen uptake and work output". J. Sports Med., 1978. 18, p.p: 49-56.

[GH1] Gonzalez H y Hull M L. " Multivariable optimization of cycling biomechanics". J Biome.(1989). 22, 11/12:1151-1161

[HT1] Hamley E J y V Thomas. " Physiological and postural factors in the calibration of the bicycle ergometer".J. Physiol. (1967) 191:55

[H1] Harrison J Y. " Maximizing human power output by suitable selection of motion cycle and load". Hum. Factors (1970).12: 315-329.

[HP1] Holmes J C, Pruitt A L, Whalen N J. " Lower extremity overuse in Bicycling". Clin Sports Med.(1994);13,1:187-205.

[LG1] Lemond G y Gordis K. "Greg LeMond´s Complete Book of Bicycling". New York, NY, Perigee Books, 1987

[LC1] Li,Li and Graham E. Caldwell. "Muscle coordination in cycling: effect of surface incline and posture" .J Appl. Physiol(1998). 85 (3): 927-934

[ML1] Morris D M y Londeree B R. " The Effects of Bicycle Crank Arm Length on Oxygen Consumption". Can J. App. Physiol.(1997). 22 (5): 429-438.

[N1] Nordeen-Snyder K S. "The effect of bicycle seat height variation upon oxygen consumption and lower limb kinematics".Med and Sci. in Sports (1977). Vol 9, 2; 113-117

[SM1] Savelberg H.H.C.M. and. Meijer K "Contribution of mono- and biarticular muscles to extending knee joint moments in runners and cyclists".J App Phhysio(l994); 2241-2248
[WC1] Welbergen E y Clijsen L P V M. "The influence of body position on maximal performance in cycling". Eur J Appl Physi.(1990). 61:138-142.

Impact Behaviour of Ski-Boots against Different Obstacles (P243)

Nicola Petrone[1], Giuseppe Marcolin[2]

Topics: Ski & other Winter Sports; Biomechanics; Materials; Measurement Systems; Modelling; Safety;
Abstract: Impact events during skiing are frequents and can lead to damages on the equipment or injuries to the skiers. In particular, the ski-boot can be subjected to impacts either during skiing or during falling. Furthermore, kicking actions are frequent in the resorts after skiing and may involve high impacts energy. Aims of the work were: i) to evaluate impact loads acting on the boots worn by a skier during voluntary kicks against obstacles of different shapes; ii) to estimate the energies involved in the impacts for comparison with experimental impact tests on boots using a drop tower. Kinematic data were recorded by means of a stereophotogrammetric system (BTS-Italy) composed by 6 cameras working at 120 Hz. A 50 kN Futek load cell and 2 uni axial accelerometers fixed under the boot sole for vertical and horizontal acceleration were connected to an IMC Cronos data acquisition system to collect kinetic data at the obstacles with 50 kHz sampling rate. The tester was asked to perform 4 types of kick (toe kick, shell kick, heel kick and instep kick) against three types of obstacles (flat, round and prismatic) with the boot at room temperature. A session with the ski boot at -20° was also performed. A 2D lower limb rigid model was developed to estimate impact energy absorbed by the boot. The peak values of impact loads were measured with different types of obstacle or kicks directions and the highest speed value of 8.8 m/s during toe kicks was recorded. High value impact energies were estimated from the limb total energy loss during impact: the maximal value was of 128,3 J.
Finally comparison with experimental drop test values allowed engineering refinements of the drop tests procedures.
Key words: Ski boot, obstacle, kinematics, impact loads, impact energy.

1. Department of Mechanical Engineering University of Padova, Italy, Via Venezia 1 - E-mail: nicola.petrone@unipd.it
2. Department of Anatomy and Physiology University of Padova, Italy, Via Marzolo 3 - E-mail: giuseppe.marcolin@unipd.it

1- Introduction

Skiing is an ambient sport where high dynamic loads are involved. Impact events during skiing are frequents both coming from skiing manoeuvres and from accidents. These impacts can damage the equipment or lead to injuries to the skiers. Kicking actions against various obstacles are frequent in the resorts after skiing to shake off the snow from the boots. This kicking action may lead to high energy impacts with two consequences: i) high loads on ski boots can cause undesired boot damages and ii) corresponding high loads on the leg may also cause injuries to the skier [L1] [WL1]. For the first of this two statements, engineers need more data to define the proper boot tests and to calculate methodologies for loads estimation. For the second, biomechanical analysis and simulations are needed for injuries prevention.

Aims of the present work were two: first: to measure the impact forces between the boot and different types of obstacles; to compare the impact forces and velocities with different types of kicks and obstacles. Second to estimate the energies involved in the impacts for comparison with experimental impact tests on boots.

2- Material and Methods

2.1 Instrumentation

Kinematic data were recorded by means of a stereophotogrammetric system (BTS-Italy) composed by 6 infra–red cameras working at 120 Hz (Figure1a). Fourteen reflective markers were placed on pre selected landmarks of the right leg: 7 on the boot, 2 on the Posterior Superior Iliac Spines (PSIS), one on each Great Trochanter (GT), one on the Lateral Condilus of the femur (LC), one on the Tibial Tuberosity (TT) and one on the Fibula Head (FH). The correct application of this customized marker-set was essential for the kinematical analysis of the parameters under investigation. Infra-red cameras were placed at a height of 4mt in order to create an adequate calibrated volume. The support foot of the tester was on a Bertec force platform and ground reaction forces were synchronously recorded with the stereophotogrammetric system. Kinetic data at the obstacles were collected by means of a Futek load cell fixed on a concrete column and connected to an IMC Cronos acquisition system (Figure1b-1c). Two uni-axial accelero-

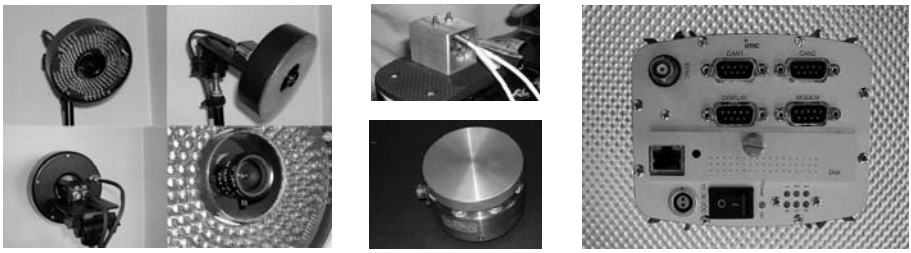

(a) (b) (c)

Figure 1 - Instrumentation. Infra-red cameras (a), accelerometers and load cell (b), IMC Cronos acquisition system (c).

meters placed under the boot sole (Figure 1b) were also connected to the acquisition device for the evaluation of the vertical and horizontal acceleration of the ski boot during each kick. All sensors were recorded at 50kHz.

2.2 Test Protocol

A professional tester from the boot company was involved in the study (height 177 cm, mass 70 kg) and he was asked to read and sign an informed consensus before starting the tests. After anthropometric measurements he wore the instrumented boot (with markers and accelerometers) and an operator placed the reflective markers on his pre-selected body landmarks. After a 10 minutes standardized warm up consisting of stretching and mobilization exercises for thighs and shanks, the subject was ready for the kicking session. In particular he was asked to perform 4 typologies of voluntary kicks (toe kick, shell kick, heel kick and instep kick) (Figure 2) against obstacles with different shapes (flat, round and prismatic) (Figure 3).

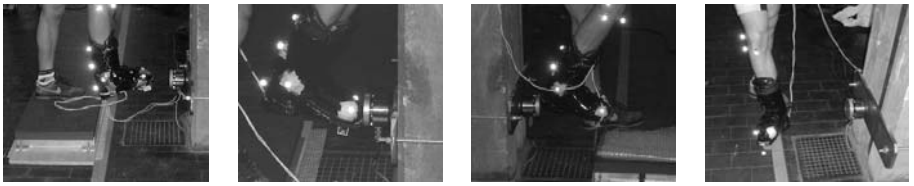

Figure 2 - Types of voluntary kicks from left to right: Toe kick, Shell kick, Heel kick and Instep kick.

Figure 3 - Types of obstacle: Flat, Round (20mm radius) and Prismatic (90° edge angle; 1 mm fillet radius).

The first session was performed with the boot at room temperature (20°) starting with the flat obstacle and the toe kick. After three series of three consecutive kicks, the kicking direction changed with the order: toe, shell, heel and then instep kick. This procedure was repeated for the three obstacles (flat, then round, then prismatic) with 2 minutes rest between series of kicks and 5 minutes after each changing of obstacle.

A second session of voluntary kicks was performed after three hours of boot conditioning at -20° with the same procedures described before for the session at with the boot at room temperature.

Two additional Motion Capture tests were performed on the boot alone for the calculation of its Center of Mass and Momentum of Inertia. In the first test the boot with markers was suspended in 3 positions with a cable having 3 markers placed on it; in the second, several boot oscillations in the sagittal and frontal planes were recorded.

2.3 Data Analysis

The first step for kinematics analysis was the 3D raw data reconstruction (Figure 4a-4b-4c). Then with a dedicated BTS software we developed a protocol for Centers of Mass calculation of thigh, shank and foot using Dempster body segments inertial parameters. The boot Center of Mass was calculated suspending it in the calibrated volume of the Capture System by means of a cable with 3 markers placed on it: the intersection of the 3 straight lines, each passing through the three cable markers, represented the coordinates of the boot Center of Mass with respect to the markers placed on the boot. In addiction a 2D X_jY_j reference system was defined for each body segment and for the boot to have their angular displacement (θ_j) and velocity (ω_j) with respect to the global XY Reference System. A 2D lower limb rigid model with fixed pelvis (Figure 4d) could be developed. Finally the definition of the kicking cycle was identified as starting at the highest value of the boot Center of Mass Y_b and ending 0.35 seconds after the impact with the obstacle.

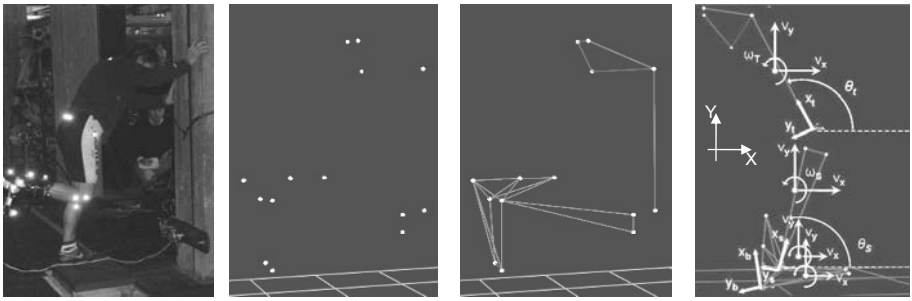

Figure 4 - 3D kinematics reconstruction data (BTS Software) and 2D lower limb rigid model with fixed pelvis hypothesis.

In the kinetic data analysis we considered the peak value (F_{peak}) of the recorded impact force (F_{imp}) for each kick, the impact duration (t_c) and the force impulse (Dp) as showed in Figure 5.

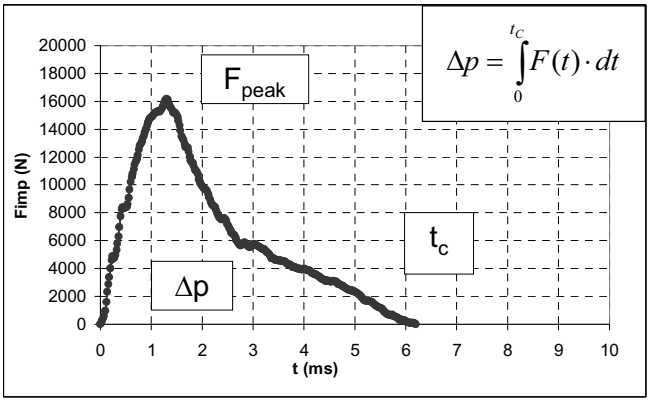

Figure 5 - Parameters considered for kinetic analysis.

Kinematics and kinetic data allowed to estimate the energy variation during the impact of the boot with the different obstacles using two methods of analysis. In the first one the Total Energy Loss (DE_T) was estimated as the lower limb Total Energy variation during the impact (Equation 1) with reference to the lower limb rigid model. Index *j* is referred to the four rigid bodies part considered in the model (thigh, shank, foot and boot).

$$\Delta E_T = E^i - E^f \quad \text{where} \quad E_T = \sum_j (m_j \cdot g h_j + \frac{1}{2} m_j v_j^2 + \frac{1}{2} I_{cmj} \omega_j^2)$$

$$\text{at} \quad t^i = 0 \text{ and } t^f = t_c \qquad (1)$$

The second method consisted in the estimation of the Linear Momentum Variation of an Equivalent Lumped Mass. From kinematics we had the variation of the boot velocity before and immediately after the impact ($\_v=v_i-v_f$).

$$\Delta p = \int_{ti}^{tf} F(t) \cdot dt \quad (2) \qquad m^* = \frac{\Delta p}{\Delta v} \quad (3)$$

$$\Delta E_{imp^*} = \frac{1}{2} \cdot m^* \cdot (v_i^2 - v_f^2) \qquad (4)$$

From Equation 3 we obtained the Equivalent Lumped Mass m^* and then the Lumped Mass Impact Energy DE_{imp^*}(Equation 4). Energy analysis with the two methods was limited only to toe kicks and shell kicks.

3- Results

The Impact force (F_{imp}) of the most representative kicks are presented in Figure 6. In each plot the thick black line corresponds to the flat obstacle; the grey line corresponds to the round obstacle and the thin black line corresponds to the prismatic obstacle.

Comparison of kinetic data of the maximal kicks showed impact speed almost homogeneous for the different obstacles. Considering the four typologies of kicks, the highest impact speed was recorded in toe kicking and its value was of 8.86 m/s. Peak forces showed the highest values with flat obstacle, than with round and finally the lowest values with the prismatic obstacle. Analyzing the different types of kick, the highest peak forces were recorded in toe kicks, than in shell kicks, than in heel kicks and last in instep kicks. These data are presented in Figure 7 together with the effect of the temperature on F_{imp} e t_c.

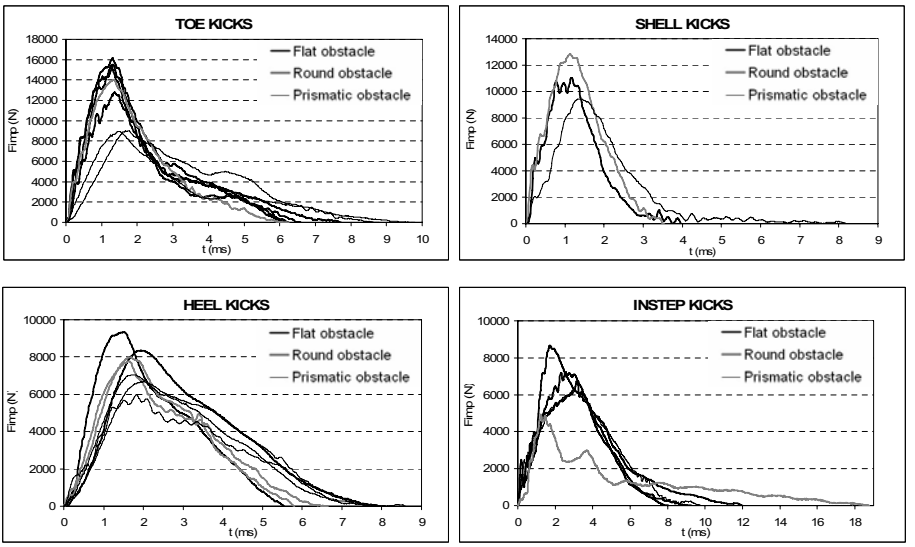

Figure 6 - Impact Force (Fimp) of the 4 types of kicks against the 3 typologies of obstacles (Flat, Round and Prismatic).

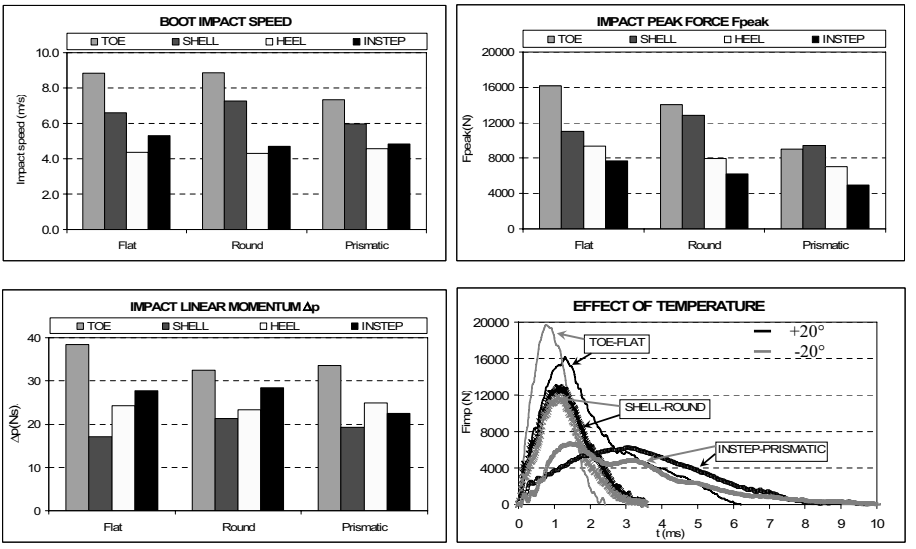

Figure 7 - Kinematic and kinetic results comparison.

Energy results presented in table 1 showed DE_T values calculated with the Limb Model and the lumped model in toe kicks and shell kicks. In toe kicks DE_T values from the limb model method were consistently lower than DE_{imp^*} values obtained with the Lumped Model method while no consistency was found for shell kicks.

TEST	POSITION	OBSTACLE	TEMPERATURE	DURATION (ms)	Fpeak (N)	Momentum (Ns)	BOOT TIP vxi (m/s)	LIMB ΔET (J)	LUMPED ΔEimp* (J)
TFA3	TOE	Flat	amb	6.3	16165	38	8.817	**128.3**	**164.4**
TRA1	TOE	Round	amb	6.3	14032	32	8.860	**117.1**	**132.2**
TPA2	TOE	Prismatic	amb	8.8	9023	34	7.336	**80.5**	**112.3**
SFA1	SHELL	Flat	amb	4	11019	17	6.584	**81.9**	**55.9**
SRA1	SHELL	Round	amb	3.7	12830	21	7.272	**60.8**	**70.4**
SPA1	SHELL	Prismatic	amb	8.5	9444	19	5.967	**76.7**	**55.7**

Table 1 - Kicking Energy comparison: Lower Limb total energy variation (DE_T) versus Lumped Mass Impact Energy variation (DE_{imp^*}).

Impact tests on boots were performed on a drop tower at DolomitiCert Laboratories (BL-Italy) equipped with calibrated photocells for speed measuring as shown in Figure 8. The boots were conditioned at –20°C for at least 2 hrs and were placed on a tilting support fixed to the instrumented anvil, properly oriented to obtain impacts on the front part of the shells within 50 seconds to avoid warming. The falling height was consistently kept in order to achieve speed impacts as close ad possible to the 8.8 m/s as recorded in the kicking tests and impacts were performed on a set of boots wearing a silicon dummy foot and realistic clamping as well as on a set of boots consisting in the shell only, without the dummy foot. Results of the tests are reported in Table 2. The impactor mass was progressively modified in order to obtain different impact energies: impacts were performed on several samples in a sequence of high and low energy values in order to converge as rapidly as possible to the minimum Failure Energy value (named $minE_{fail}$) from the boots failing the test, and to the maximum Sustained Energy value (named $maxE_{sust}$) from the boots passing the test. The impact energy values are presented in a decreasing order and the two values of $minE_{fail}$ and $maxE_{sust}$ for the two types of boots are highlighted.

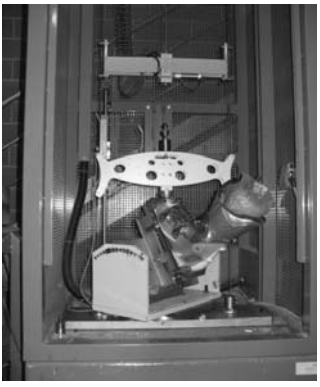

Figure 8 - Impact tests at the Drop Tower.

Test type	Sample	Mass [kg]	Speed [m/s]	Energy [J]	Impact Result	
With Dummy Foot	*DF5*	*8.5*	*8.6*	*315.8*	*Fail*	
	DF2	*7.0*	*8.4*	*248.7*	*Fail*	
	DF3	***6.5***	***8.3***	***223.9***	***Fail***	***minE$_{fail}$***
	DF6	**6.0**	**8.5**	**214.7**	**Pass**	**maxE$_{sust}$**
	DF4	5.0	8.6	185.8	Pass	
	DF1	3.0	8.5	107.6	Pass	
Shell Only	*SO1*	*2*	*8,6*	*73,1*	*Fail*	
	SO2	*1,9*	*8,6*	*68,4*	*Fail*	
	SO4	*1,4*	*8,3*	*48,5*	*Fail*	
	SO3	***1,4***	***8,2***	***47,5***	***Fail***	***minE$_{fail}$***
	SO5	**1,3**	**8,2**	**43,5**	**Pass**	**maxE$_{sust}$**

Table 2 - Results from Drop Tower tests, following decreasing values of impact Energy, from tests with the Dummy Foot and Shell Only.

4- Discussion

In this study results indicated that impact forces developed when kicking a ski boot against an obstacle, are very high. More specifically, the highest values of Impact Force (F_{imp}) were recorded in toe kicks and flat obstacle. Changing the kicking direction F_{imp} decreased as well as the boot impact speed. This can be related to the Lower Limb ability in performing maximal actions in different directions. The kicking session after conditioning the boot for three hours at -20° showed appreciable differences in terms of F_{peak} and t_c; this was particular evident for toe kicks and flat obstacle where we had an increase of the F_{peak} and a decrease of t_c . This phenomenon was certainly due to the effect of the cold temperature on the material of the boot shell and it has to be considered when defining the material due to the complex skier's biomechanics.

Energy results comparison reported in Table 1 showed lower values of Impact Energy with Lower Limb method than with the Lumped Mass method. DE_T was considered to be more representative of the lower leg biomechanics: in any case it has to be considered as an upper limit estimation of Impact Energy absorbed by the boot because it includes Energy dissipated by the soft tissues and wobbling masses [NH1].

The analysis of Table 2 show that the Impact Energies that can be sustained by the tested boots before failure were about five times higher with dummy foot and boot properly closed than on the boot shell. The dummy foot conditions is much closer to the real kicking action conditions, whereas the shell only testing condition is much more economical for manufacturers.

The comparison of drop tower test values of $minE_{fail}$ on dummy foot with the maximum recorded kicking Energy from motion capture tests show that a high safety margin is present, even when comparison is made with the highest value of kicking energy recorded on a toe-flat kicking combination. In this case, a safety margin of 1.75 is shown by the boot with the dummy foot. Boots tested in a shell only condition are failing at about the 37% of the maximum recorded kicking energy.

Based on these values, standard tests for impact resistance on boots can be defined.

5- Conclusions

The Peak values of impact loads were measured with different types of obstacles and kicks directions. The highest values of kicking velocity and F_{peak} were obtain with toe kicks. The effect of the temperature on the boot material was also investigated showing an increase of the F_{peak} and a decrease of t_c in toe kicks. Further investigations are needed to better analyze the effect of temperature in the other kicking conditions.

The total energy loss was measured with two different methods (DE_T and DE_{imp^*}) with values obtained from limb model consistently lower than values from lumped model, in toe kicking. Further investigations are necessary to refine the experimental procedure considering the role of soft tissues and wobbling masses effects.

Finally energy results from biomechanical tests comparing with drop tests values should be taken in account for drop test procedure refinement.

6- References

[L1]. Lindbeck L. Impulse and moment of impulse in the leg joints by impact from kicking. J Biomech Eng. 105 (2): 108-14, 1983.

[NH1]. Nigg B, Herzog W. Biomechanics of the musculo skeletal system. Wiley&Sons, 1995.

[WL1]. Warhemberg H, Lindbeck L, Ekholm J. Dynamic load in the human knee joint during voluntary active impact to the lower leg. Scand J Rehabil Med. 10(2): 93-8, 1978.

7- Acknowledgements

The authors desire to thank the company Nordica SpA (TV – Italy) for supporting the research and DolomitiCert Laboratories (BL – Italy) for hosting the drop tower tests.

Acquisition of Structural Loads Acting on the Mast of a 420 During Sailing (P244)

G. Pellicioli[1], N. Petrone[1]

Topics: Sailing/water sports; Innovation and Design; Measurement Systems.
Abstract: Aim of the work was the design, calibration and installation of an instrumented mast and standing rigging system on a 420 sailboat for the dynamic measurement of structural loads during sailing.
By means of several calibrated strain gauge bridges, the bending moments in the planes at seven significant sections along the mast, together with the axial load on the mast and the pulling of standing rigging were measured. The resulting bending moment diagrams were plotted along the mast and shall allow designers to improve the mast's cross section profile or material selection. Moreover, the accurate knowledge of loads acting on the standing rigging and on the mast-step will support the optimized design of the boat shell.
Keywords: 420 sailboat, mast, strain gauges, structural analysis, in field acquisition.

1- Introduction

The development of innovative mast sections and the appropriate selection of materials for masts are possible after the measurement of the load spectra acting on the system during sailing. Moreover, the accurate knowledge of loads acting on the standing rigging and on the mast-step will support the optimized design of the boat shell.

Due to the complexity and variability of sail loads and wind conditions an experimental approach was chosen. The mast and the standing rigging measurement systems were designed, calibrated and installed in order to measure the dynamic structural loads during navigation. A not-invasive measuring system was necessary to reproduce the real sailing conditions, so a light but strong, reliable and waterproof strain gauge system was conceived and applied. The mast was strain gauged with 16 channels applied at seven significant sections in Full, Half and Quarter bridges: the strain output was calibrated after application of known loads at known locations. Each shroud was directly strain

1. via Venezia 1, Padova, Italy, Department of Mechanical Engineering, University of Padova - giacomo.pellicioli@gmail.com - nicola.petrone@unipd.it

gauged in correspondence of the chain-plate and was calibrated during tensile testing on a servohydraulic machine. A two component load cell was designed to measure the vertical and longitudinal loads at the mast-step.

The mast was calibrated in a laboratory, installed on a 420 sailboat and used during training and regatta operations. Tests were performed both in the laboratory and on the sea, under expert coaching.

Results deriving from this experimental procedure may also be used in a second design step to validate a numerical model of the redundant system mast-hull [BM1]. Furthermore, the knowledge of the mast's deflection line in the longitudinal and lateral planes is fundamental for an effective sail design: displacement measurements are difficult to accomplish in a rough environment like a sail regatta, so an indirect structural approach can be adopted to reconstruct the deflection line of the mast.

2- Design of the measuring system

2.1 Mast description

The mast used for this research project is produced by Super Spars company (Fareham, New Hampshire, England). It is made of aluminium alloy by extrusion, cutting and welding. The surface is anodized to prevent corrosion; linear density given by the constructor is 0.94 kg per meter of lenght. The mast is 6200 mm long; the main section measures 57.5 x 70.5 mm, and it is uniform for about 4500 mm of the total length, while the remaining part of the extruded is tapered till the top section that is 32.5 x 34.5 mm. In correspondence of the mast head and of the mast step there are two steel components that respectively allow the movement of the mainsail halyard and of running rigging.

2.2 Reference frame

The boat reference frame adopted is a system of three axes x, y, z orthogonal each other. The origin of the coordinate system was placed in correspondence of the centroid of the mast cross section. Then, x axis was oriented in the direction of the axis of symmetry of the section, that is the direction of the longitudinal axis of the boat; z axis develops in the direction from the step to the head of the mast (see Figures 1 and 2).

Figure 1 - Reference frame adopted.

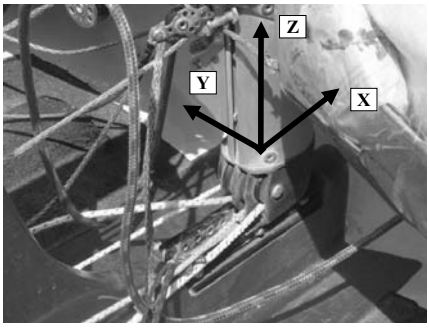

Figure 2 - Particular of the mast-step with reference frame.

2.3 Individuation of measuring points

After an accurate preliminary study of the different possible loading configurations and of the effects on the system mast-hull generated by the combined action of standing and running rigging, the points of measurement chosen are listed in Table 1.

Sect. n°	POINTS OF MEASUREMENT	MEASURED LOADS	MEASURING CHANNEL
7	Mast head	F_z	M7N
6	Above shrouds' junction	M_{fx}	M6Mx
5	Under shrouds' junction	F_z, M_{fx}, M_{fy}	M5My, M5eL, M5eR
4	Under cross-trees' junction	M_{fx}, M_{fy}	M4My, M4Mx
3	Under the parrel	F_z, M_{fx}, M_{fy}	M3My, M3eL, M3eR
2	Mast hole	F_z, M_{fx}, M_{fy}	M2My, M2eL, M2eR
1	Above vang's connection with the mast	F_z, M_{fx}, M_{fy}	M1My, M1eL, M1eR
S	Shrouds	T_L, T_R	S_SX, S_DX
F	Mast step	F_z, F_x	FFx*, FFz*
			* : laboratory measurements

Table 1 - List of measuring points, measured load components and agreed names of measuring channels.

Fundamental loads considered for the definition of measuring systems were bending moments in the lateral and longitudinal planes (M_{fx} and M_{fy}) and axial load (N), as shown in Figure 3. Against a structural analysis of the mast during the navigation, the boat with sails hoisted was taken as reference situation.

Figure 3 - (a) Lateral plane and Mfx measured. (b) Longitudinal plane and Mfy measured. (c) Global view of measuring points. Axial load F_z, not represented in the above pictures, was measured at mast sections 1, 2, 3, 5, 6, 7 and at mast step F.

2.4 Installation of measuring system

2.4.1 Configurations used

Wheatstone bridge were used for the measurement of resistance changes from strain gauges. The typologies of connection used are: Quarter bridge, Half bridge, Full bridge, depending on measured loads [DR1].

The bending moment in the longitudinal plane M_{fy} has been measured in sections number 1, 2, 3, 4 and 5 with four strain gauges for each section connected with a Full Wheatstone bridge. Strain gauges used have a 0.6 mm measuring grid to fulfill narrow dimensional bonds by the sides of the mainsail's head. The bending moment in the lateral plane M_{fx} has been measured in sections 4 and 6 with two strain gauges with Half bridge connection. At sections 1, 2, 3 and 5 also axial load N was measured, by means of lateral strain gauges connected with Quarter bridge. In linear elastic field, through the combination of the value of strains measured, it was possible to calculate lateral bending moment M_{fx} and normal stress N. In section 7 only axial load was measured with a Full bridge. Some examples of strain gauged sections are given in Figure 4.

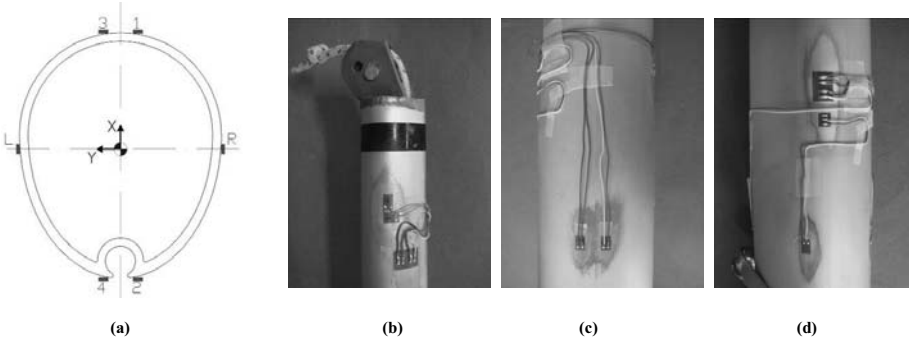

Figure 4 - (a) Scheme of strain gauging of the section. (b) Right side of section 7. (c) Front side of section 1. (d) Right side of section 1.

Loads acting on shrouds were measured with Full bridge strain gauges installed on the two chain-plates (see Figure 5), while for the measuring of forces F_x and F_z have been used a dynamometric platform during the tests made in the laboratory and a custom load cell during the navigation.

2.4.2 Calibration

The calibration of all measuring systems was carried out in the laboratory. Strain gauge bridges installed on the mast were calibrated with many static tests by applying different cantilever loads in the two planes. Measuring systems installed on the chain-plates and the load cell were calibrated on a servohydraulic machine. Cases of non-linearity have were not discovered.

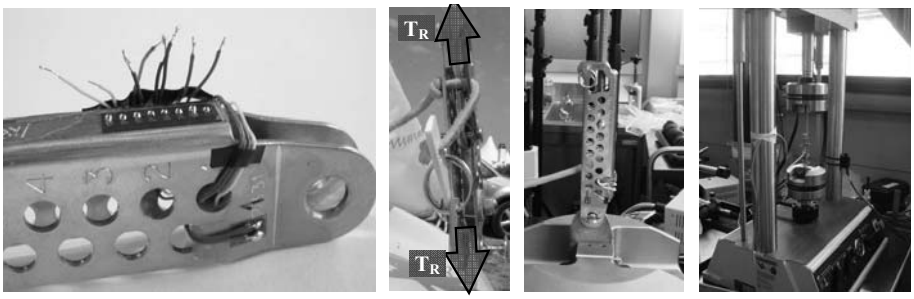

Figure 5 - (a) Chain-plate during strain gauging. (b) Forces acting on the chain-plate. (c) Calibration of the measuring system installed on the chain-plate. (d) Servohydraulic machine used for the calibration.

Through experimental procedures, the constants of calibration were obtained. These values correlate strain measurements to the force or the bending moment acting on a point and were used during data analysis [PP1].

For the verification of the good positioning of lateral strain gauges, a cantilever test was made with strain gauges connected at Quarter bridge. Moreover, the neutral axis was calculated experimentally; the average of strains measured by the two strain gauges in the same side (1-3, 2-4) under a known bending moment was calculated and the neutral axis of bending was located by the intersection between the axis of symmetry and the line representing the strain gradient.

3- Laboratory tests

The same system of constraints existing on the boat (i.e. mast hole, shrouds' connections, ...) was accurately reproduced in the laboratory to make possible some calibration procedures and the verification of the measuring systems reliability. During the laboratory tests a dynamometric platform was used to measure forces F_x and F_z acting at mast step, as shown in Figure 6.

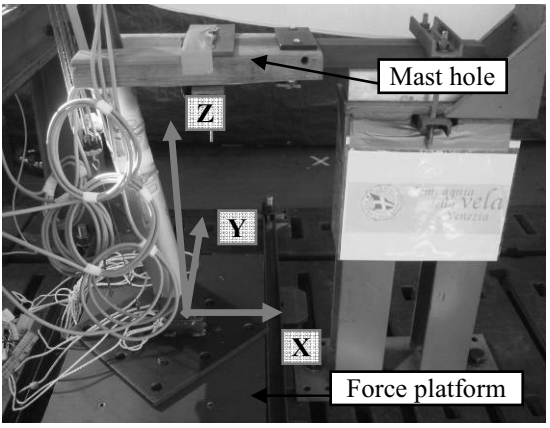

Figure 6 - Particular of the system of constrains reproduced in the laboratory: mast hole and force platform.

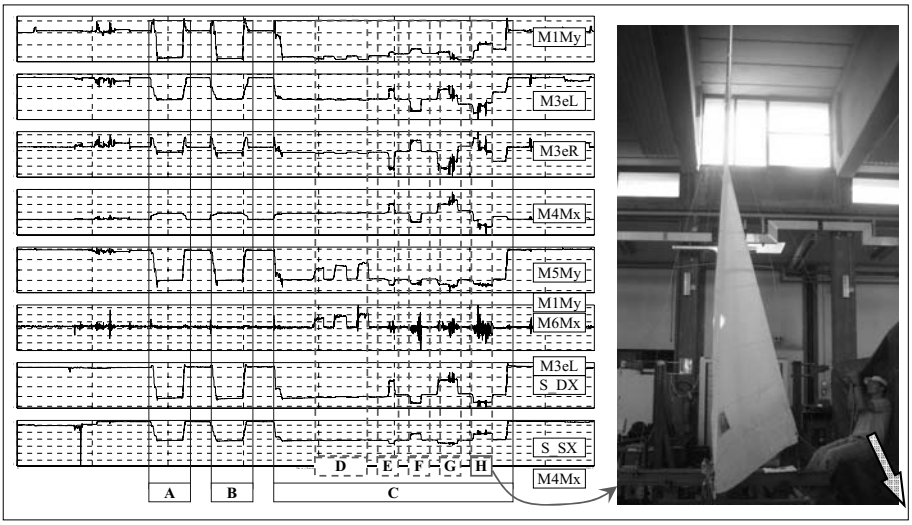

Figure 7 - Example of data acquisition in the laboratory (for space reason only eight of the 20 measuring channels are shown).

The laboratory tests aimed to reproduce the normal procedure of boat manning and to evaluate the pure effect of a man hanging on the trapeze. In particular, with reference to Figure 7:

- A and B: hoisting and lowering of the jib;
- C: with jib hoisted: D: applying loads at the mainsail halyard, E and G: man at the right trapeze, F and H: man at the left trapeze.

The maximum values measured at the mast step with the dynamometric platform were: F_z=-5090 N and F_x=370 N. In Figure 8, diagrams of average loads acting on the mast during some important stages of the tests are shown [PP1].

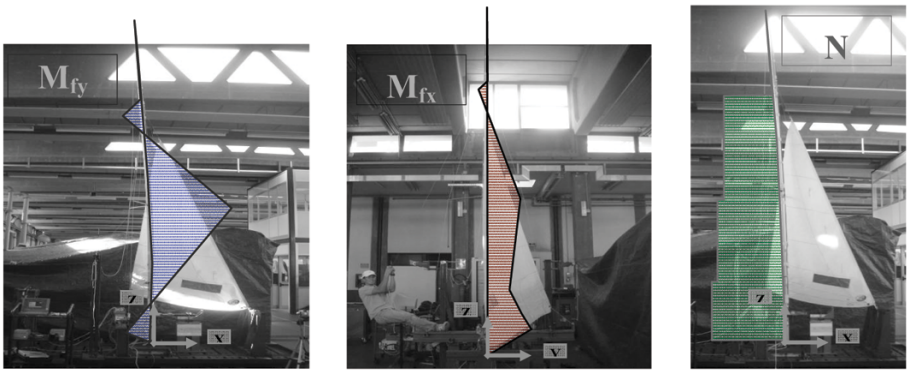

Figure 8 - (a) Bending moment Mfy when jib is hoisted. (b) Bending moment Mfx with man at the right trapeze. (c) Normal load N in the same conditions of (a).

4- Sailing tests

Navigation tests were performed in the Adriatic sea with different wind conditions (6-8 m/s). During sailing test the boat was also equipped with a miniature, gyro-enhanced Attitude and Heading Reference System (AHRS); this instrument was applied close to the mast hole (see Figure 10) to measure angles of roll, pitch and yaw of the sailboat and to evaluate their variation for different wind and sea conditions and different rigging adjustments.

The light and compact acquisition system adopted was positioned with its battery near the mast-step (see Figure 9) into a protective case. Because of the concrete possibility of damage and the impossibility to make repairing during navigation, the robustness and the reliability of measuring systems had to be granted. To prevent measuring system from damage and short circuit, all strain gauges and their connections were insulated with silicone. Then, the long cables for data acquisition were fixed to the mast with narrow bands and adhesive tape.

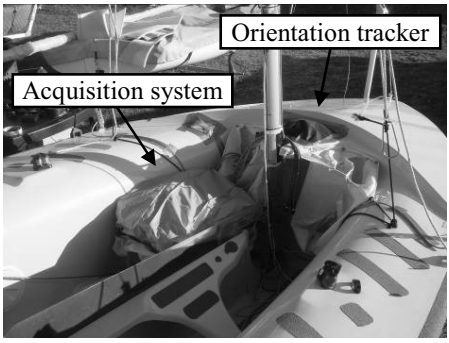

Figure 9 - Position of the acquisition system.

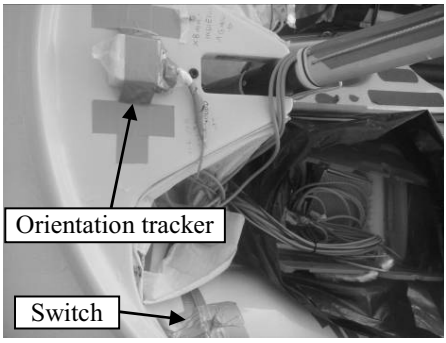

Figure 10 - Particular of the mast hole.

Under expert coaching several training and regatta operations were made. Figure 11 shows an over view of a navigation test made with medium-strong wind and lasted about 30 minutes. During this test the sailboat:

- sailed close to the wind on starboard tack (M and O) and on port tack (N and P) with bowman (80 kg) at the trapeze;
- sailed beam reach with the spinnaker on port tack (Q) and on starboard tack (R);
- made several tacking and jibing between different point of sailing.

As a result, diagrams of the bending moment acting on the mast during navigation are shown in Figures 12 and 13, whereas in Table 2 the values of the mean bending moment acting on the lateral plane are collected.

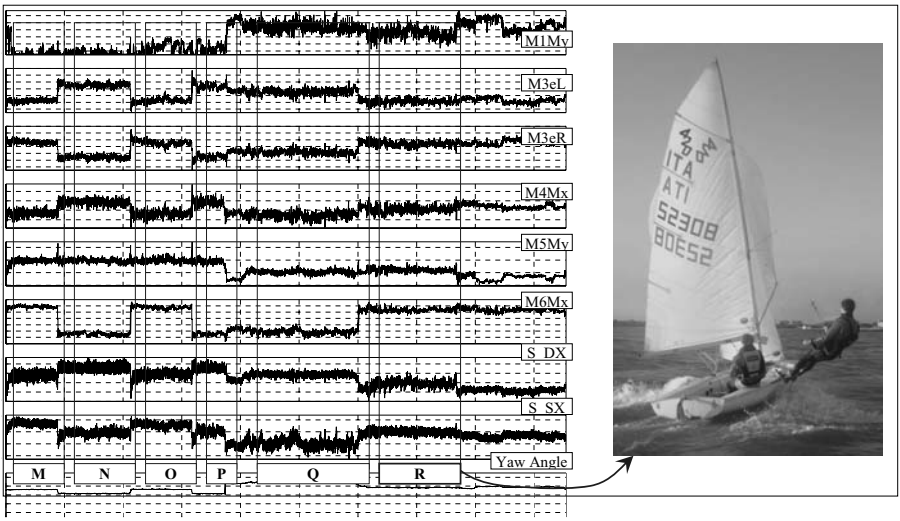

Figure 11 - Example of data acquisition during the navigation (for space reason only eight of the 19 measuring channels are shn).

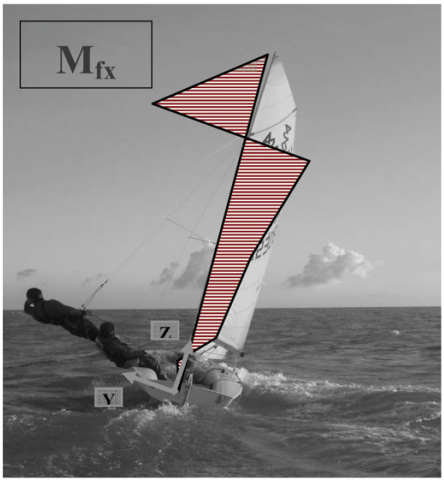

Figure 12 - Sailing close to the wind (P).

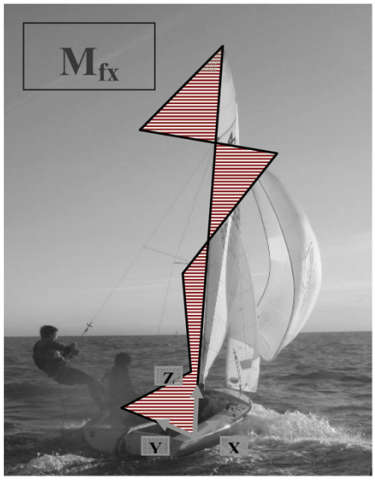

Figure 13 - Sailing beam reach with the spinnaker (Q).

Lateral bending moment M_{fx} (1) *Reference values*	Close to the wind				Beam reach (with spinnaker)	
	On starboard tack (M)	On port tack (N)	On starboard tack (O)	On port tack (P)	On starboard tack (Q)	On port tack (R)
M_{fx}_0 [Nm] (1)	0	0	0	0	0	0
M_{fx}_1 [Nm]	7.292757	-2.10908	-1.39593	0.81597	-57.5667	42.2464
M_{fx}_2 [Nm]	14.5	-4.19342	-2.7755	1.622373	-114.458	83.99742
M_{fx}_3 [Nm]	-92.0222	53.21949	-87.7752	43.76334	-3.8911	-86.7365
M_{fx}_4 [Nm]	-28.5101	50.1443	-34.2323	50.15393	-42.2075	9.376603
M_{fx}_5 [Nm]	-73.4861	99.77632	-69.4275	101.8089	104.7426	-70.4357
M_{fx}_6 [Nm]	131.4615	-145.881	122.4108	-145.126	-124.684	99.03314
M_{fx}_7 [Nm] (1)	0	0	0	0	0	0

Table 2 - Mean values of the bending moment Mfx acting during the different point of sailing with medium-strong wind condition. The asymmetry between the starboard and the port tack values are due to the hanger-on bending moment generated by hoisting.

5- Design of the load cell

A two components load cell was designed (see Figure 14) to measure the vertical and the longitudinal loads, F_z and F_y, at the mast step. Its shape was conceived to be mounted on the boat replacing the original mast step joint (as shown Figure 2). Two Full Bridge strain gauges are installed on both internal and external faces of the thin sides as shown in Figure 15. In Figure 16 are shown the results of a FEM analysis of the load cell: x normal stress after a load F_z = 1000 kg.

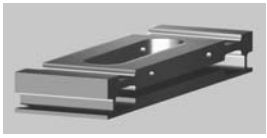

Figure 14 - 3D Model of the load cell.

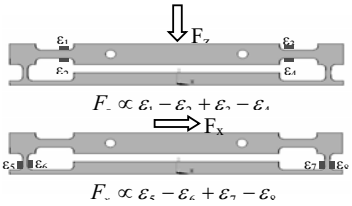

Figure 15 - Principle of working of the load cell.

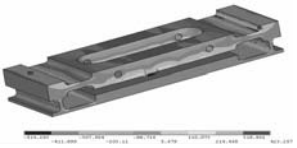

Figure 16 -Distribution of X-Component of Stress with F_z = 1000 kg.

6- Conclusions

A measurement system for both laboratory and sailing tests was developed. Data acquired during the navigation shall allow designers to improve the mast's cross section profile or material selection. Moreover, the accurate knowledge of loads acting on the standing rigging and on the mast-step will support the optimized design of the boat shell. Besides the analysis of the structural loads, data acquired may also be used to study the mast stiffness, after the estimation of the deflection lines, to improve sail design. The adopted methodology is generic and can be applied to other dinghies (as 470, 29er and 49er).

7- Acknowledgments

Compagnia della Vela Yacht Club (Venice, Italy); Super Spars (Fareham, New Hampshire, England); Dr. Renato Pellicioli.

8- References

[BM1] Bottacin G., Meneghetti G., Quaresimin M., Zordan A. Design, Analysis and Testing of a New Composite Sailing Mast. By Sea, 2004.
[DR1] Dalley, J.W., Riley, W.F. and Meconnel. K.G. Instrumentation for Engineering Measurement. John Wiley & S., 1999.
[PP1] Pellicioli G. and Petrone N. Analisi strutturale dell'albero di una deriva classe 420. Tesi di laurea, Università di Padova, 2007 (in Italian).

Structural Optimization of Classic and Skating Skirolls after Field Testing (P245)

N. Petrone[1], C. Pollazzon[1], T. Morandin[2], G. De Bettio[2]

Topics: mechanical engineering, measurement systems: application and design, construction theory

Abstract: Modern skirolls are made of composite materials or combinations of metal and plastic parts. Aims of the present work were: i) the acquisition of field load spectra on instrumented skirolls; ii) the fatigue life prediction of modern skirolls after constant amplitude fatigue testing; iii) the structural optimisation of the skirolls and the redesign for a target mission.

Two pairs of traditional aluminium skirolls were strain gauged in order to measure the bending actions in the vertical and horizontal planes: two full bridge measured the vertical plane bending at two different locations, whereas two half bridges applied at the two wheel supports measured the lateral loads. A rugged data acquisition system was used to record several sessions of classical and skating technique on four elite and amateur athletes. The system allowed to measure the instantaneous load values and positions during the push phases: typical load patterns were obtained and peak values were normalised to the testers body weight giving 125% B.W. in the classical technique and 137% B.W. in the skating technique. Field load spectra were collected during typical ski sessions and compared with fatigue test data from a fatigue test bench at DolomitiCert laboratory. The knowledge of in field load spectra and the skiroll fatigue curves allowed to perform the fatigue life prediction of the existing skirolls and to compare it with a target mission. A solid model of each skiroll was reconstructed with ProE® and FEM analysed with Ansys®. The finite elements model was validated comparing the results of the simulation with the laboratory tests. A new optimised profile of the skiroll was developed in order to get a uniform permissible bending stress. With this new profile the fatigue life increased of 20 times with a mass increment of only 6% per skiroll.

Keywords: skiroll, field load acquisition, fatigue optimization, FEM analysis.

1. via Venezia 1, Padova, Italy, Department of Mechanical Engineering, University of Padova - nicola.petrone@unipd.it
2. Z.I. Villanova, Longarone (BL), Italy, DolomitiCert Laboratories - tommaso.morandin@certottica.it

1- Introduction

The use of skirolls as training devices has become more and more popular not only between the nordic skiing athletes but also as a sport discipline itself. Technical requirements are proper rolling resistances for training and enhanced stiffness versus mass properties: this lead to the development of several composite material skirolls in the market that, despite the high performance, may show poor comfort properties in terms of ability of damping the road roughness induced vibrations. An innovative solution was explored after combining the high stiffness of aluminium alloy webs with the damping properties of a plastic compound.

Purpose of the investigation was the structural analysis of an innovative set of classic and skating skirolls made of two stiff aluminium beams embedded in a compact C-shaped plastic mould as shown in Figure 1.a for the skating skiroll. The use of two combined materials, after a proper structural analysis, can lead to an optimal combination of stiffness and damping properties as experienced during comparative testing of the Traditional extruded aluminium beam skiroll versus the Innovative metal-plastic skiroll.

During pilot tests, performed after suspending a 55 kg mass at the skiroll midpoints and exciting a free vibrating mode, the damping properties were recorded via a LVDT applied to the midpoint of a Traditional full metal (thin line) and an Innovative metal-plastic (thick line) skiroll. The damping coefficient of the Innovative skiroll is 39 % higher than the Traditional metal skiroll.

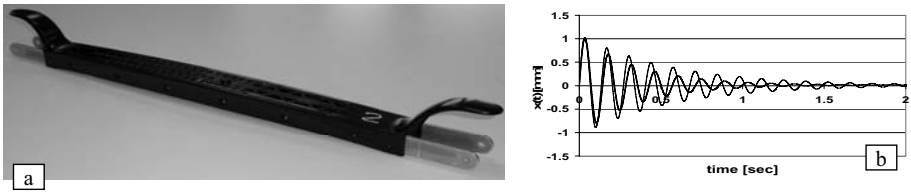

Figure 1 - (a) The innovative metal-plastic skating skiroll. (b) Comparison of damping properties between full metal (thin line) and metal-plastic (thick line) skirolls.

Given the encouraging positive properties of these innovative devices, aims of the present work were: i) the acquisition of field load spectra on instrumented skirolls; ii) the fatigue life prediction of innovative skirolls prototypes after constant amplitude fatigue testing and iii) the structural optimisation of the skirolls for the target mission.

The magnitude of loads Normal (FN) and Lateral (FL) to the skiroll upper surface, together with the point of application of forces are the data needed for an engineering design of the skirolls. The measure of loads at the foot and the poles [MH1] can describe the athlete's technique: a set of instrumented skirolls can therefore work either as engineering development tool or as training evaluation device that allows to correlate the foot loads with the metabolic and the EMG activity [MP1].

2- Field load data acquisition

2.1 Instrumented skirolls

Two pairs of traditional aluminum skirolls were strain gauged in order to measure the bending actions in the vertical and horizontal planes of their hollow rectangle cross section: two full bridge channels measured the vertical plane bending moments Mf_A and Mf_P at two different locations, whereas two half bridges applied at the two wheel supports measured the lateral loads FL_A and FL_P. The value of FN were estimated by equation (1), the point of application Xco by equation (2) where L is the span between wheels and other quantities are represented in Figure 2.b [PP1]. Accurate patterns of normal and lateral loads were obtained together with information about the instantaneous point of applications of forces.

$$FN = \frac{a \cdot Mf_P + b \cdot Mf_A}{a \cdot b} \qquad (1) \qquad X_{co} = \frac{Mf_A \cdot L \cdot a \cdot b}{a \cdot Mf_P + b \cdot Mf_A} \qquad (2)$$

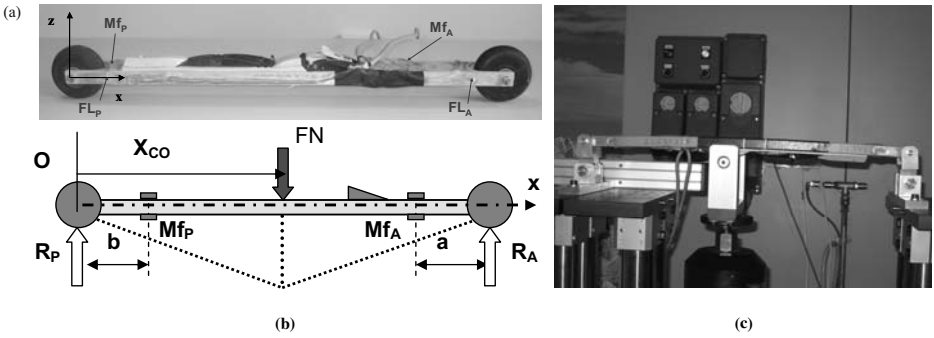

Figure 2 - (a) The traditional metal skiroll instrumented for skating tests. (b) Sketch of the relevant dimensions used for the load analysis. (c) Instrumented skiroll under calibration at the DolomitiCert test bench.

2.2 Field test results

A rugged data acquisition system was used to record several sessions of classical and skating technique on four athletes, two Elite (E1, E2) and two Amateur (A1, A2) athletes: tests were performed on 3.3 km tracks with low, medium and high slopes.

The system allowed to measure the instantaneous load values FN and point of application Xco during the push phases: typical load patterns were obtained and normalized to the testers body weight and to the ground contact cycle as shown in Figure 3.a for skating ad Figure 4.a for classic technique. Mean curves were defined and compared between the four testers, as reported in Figure 3.b and 4.b showing clear technical differences between the Elite and the Amateur athletes.

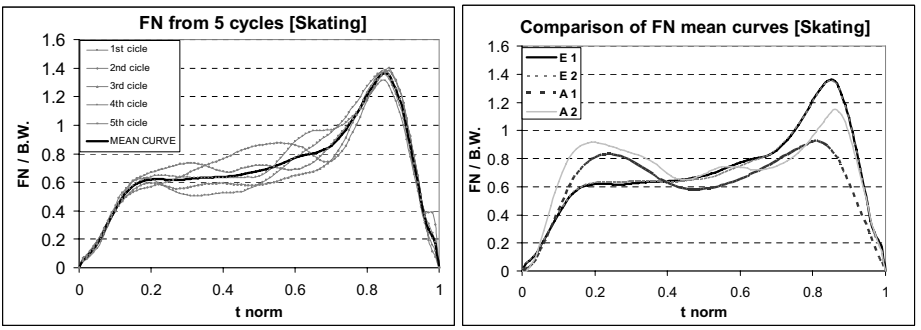

(a) (b)

Figure 3 - Skating technique. (a) Normalized load curves of 5 consecutive cycles for tester E1. (b) Comparison of mean curves of four testers.

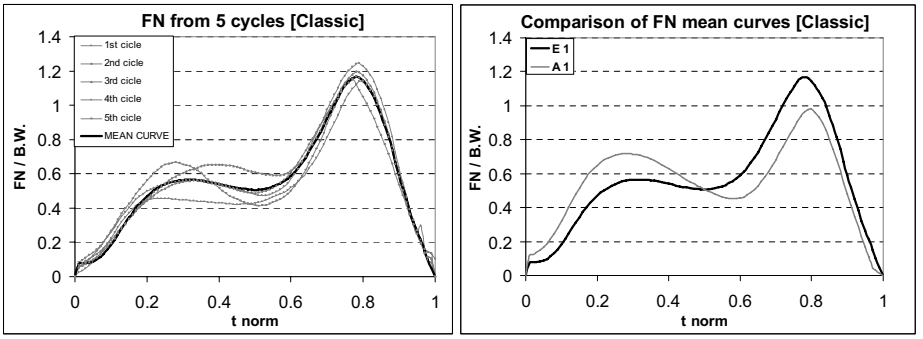

(a) (b)

Figure 4 - Classic technique. (a) Normalized load curves of 5 consecutive cycles for tester E1. (b) Comparison of mean curves testers A1 and E1.

Peak values reached 140 % B.W. in skating and 125% B.W. in classic technique. The resulting data from elite and amateur skating athletes show clear differences in the shape of normalized force signals. Elite athletes push pattern present a sharp final peak load, whereas amateur curves show twin peaked curves. Differences between Elite and Amateur are evident also for the Classic technique.

Cumulative load spectra from track tests of known length tests were obtained after cycle counting from the two classes of testers and are reported in Figure 5.

These plots are useful for the skiroll fatigue design as they express the cycle fatigue content of two different types of users on the same track length, showing higher damaging levels from the Elite athletes.

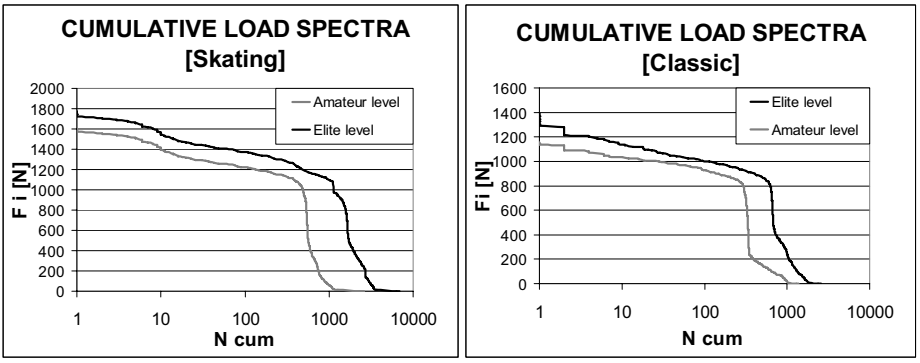

Figure 5 - Cumulative load spectra for skating (a) and classic (b) techniques.

3- Fatigue life prediction after laboratory testing

The fatigue behaviour of the metal-plastic skiroll prototypes was evaluated after constant amplitude fatigue testing on a servo hydraulic MTS test bench at the DolomitiCert Laboratories as shown in Figure 2.c. After application of Miner linear damage summation hypothesis, a fatigue life prediction procedure under variable amplitude loading was performed for the two types of skirolls and the two skill levels (Elite, Amateurs) to assess the ability of survival to the target life assumed for design.

The first results for the skating skirolls showed that only 15% of the Target Life with Elite athletes or 25% of the Target Life with Amateurs athletes could be achieved by the skating prototypes, whereas on the classic skiroll prototypes, given an increased span of 650 mm instead of 550 mm of skating skirolls, the predicted lives were below the 10% of the Target Life.

These results suggested to perform a structural optimisation procedure on the original skiroll design in order to reach the target life with the minimum mass increase.

4- Structural optimisation after FEM analysis

A Finite Element Model of the Metal-Plastic Innovative skirolls was developed in ProE® solid modelling code and analysed by Ansys® code so that several possible design changes could have been simulated in a virtual environment: brick mesh refinement procedures were performed in order to converge to the correct number of elements. Load conditions were simulated by applying a normal force FN at the midpoint of the skiroll like in the fatigue tests setup. Simulations with FN applied to the centre of pressure COP were also performed, as well as lateral force FL as recorded in the field tests. Restraints were placed at the two wheel axis simulating the isostatic overall behaviour of the skiroll beam.

The skiroll structure was split in several sub components, as illustrated in Figure 6. The two main webs in Figure 6.a, made of aluminium alloy, were considered the main load bearing components. Their lateral surface was completely embedded in a plastic

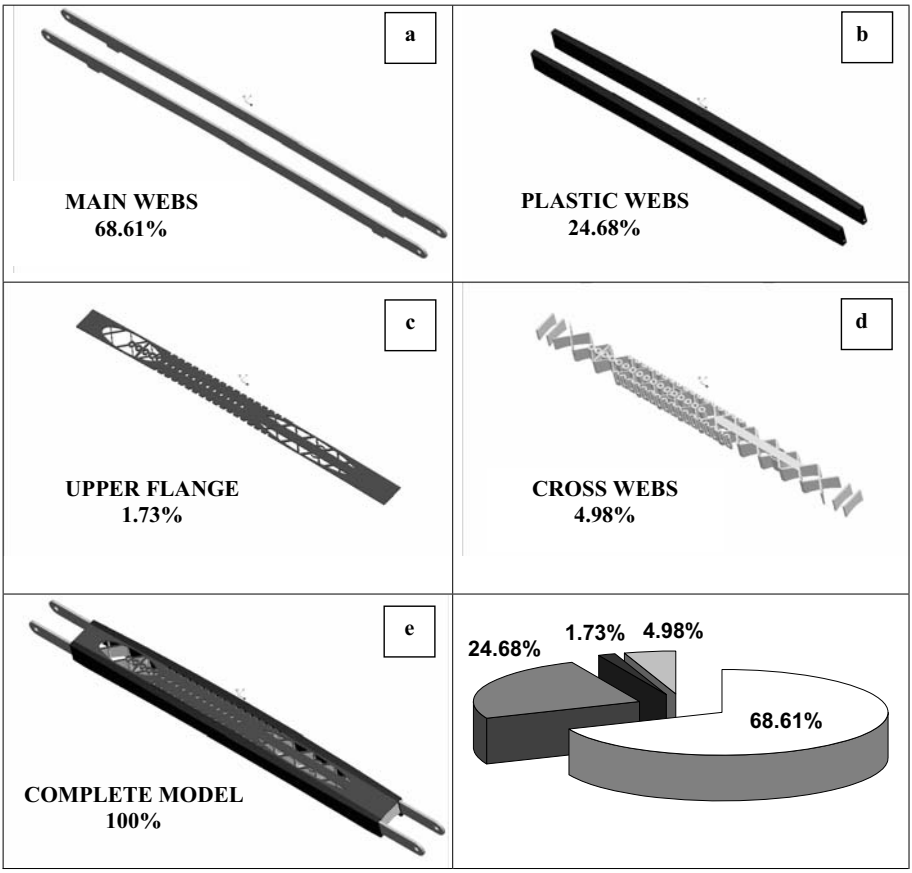

Figure 6 - Relative contribution of the different sub-components of the metal-plastic skiroll to the complete model stiffness.

mould, named "plastic webs" in Figure 6.b. The C-shape of the skiroll presented an upper plastic flange (Figure 6.c) with several holes for binding placement. The two wings of this C-shaped cross section were connected by a cross web system (Figure 6.d) lying underneath the upper flange. The complete model of the skiroll was obtained after addition of these components without neglecting any feature of the real component (Figure 1 & 6.e) apart from two curved lips at the wheels that had no structural function.

The skiroll optimisation stage was carried out with the aim of obtaining the desired target life of the skiroll with the minimum mass increase. The stiffness behaviour of the skiroll was also considered as a performance parameter to control: bending stiffness was defined as the ratio between bending load FN applied at the skiroll midpoint and deflection f. First prototypes of the innovative metal-plastic skiroll showed a bending stiffness of 115 N/mm after experimental testing: these value were comparable with the stiffness of 125 N/mm presented by the traditional aluminium skiroll used for the field load acquisition tests. The FEM analysis were used to evaluate the relative contribution of the different sub-components to the overall stiffness in order to identify the most advanta-

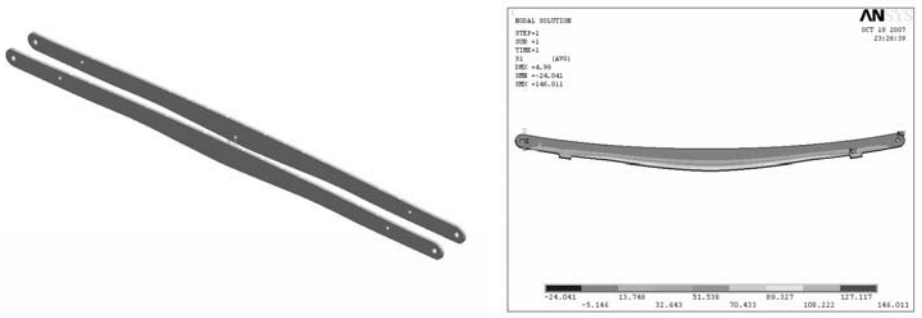

Figure 7 - Optimised main aluminium webs and results of the FEM bending simulation.

geous approach to a structural optimisation procedure. As shown in Figure 6, the main aluminium webs resulted to give the 68 % of the overall stiffness, followed by the plastic webs that contributed for the 24 % .

On the basis of these results, the fatigue optimisation procedure was applied to the aluminium main webs. Given the target life, the maximum permissible fatigue stress acting on the aluminium webs was calculated and adopted as the target stress level. Moreover, the profile of the aluminium webs was redefined in order to achieve a uniform stress state along the skiroll length under bending test conditions. This ended up with a parabolic beam profile of the main webs and a uniform stress state on the aluminium webs as shown in Figure 7. The addition of plastic parts to the main aluminium webs was assumed to add a safety margin to the complete skiroll that therefore was produced in the second optimised version and submitted to experimental stiffness and bending fatigue tests.

The stiffness results of the optimised skiroll were experimentally evaluated either on the aluminium webs alone and on the final complete moulded model: stiffness of the aluminium webs alone resulted of 103 N/mm, whereas stiffness of the optimised skiroll was 154 N/mm, corresponding to a 34 % stiffness increase of the optimised skiroll with respect to the first prototype. The mass increase of the optimised skiroll was restricted to 6%, so that a net significant specific stiffness increase was achieved. Fatigue tests were performed on several specimens of the optimised skiroll showing a life longer that 1.6 million cycles under a pulsated load FN of 1000 N , that was assumed as the target bench life of the devices.

5- Conclusions

The structural analysis of innovative metal-plastic skirolls was performed following the engineering approach based on three stages: the field load acquisition, the laboratory fatigue testing and the numerical analysis for design optimization. Field tests were performed on classic and skating skirolls involving four athletes and using two pairs of instrumented skirolls that allowed to record the load patterns, the peak values and the cumulative load spectra from different skill levels. Peak loads bending normal force FN

of 140 % B.W. during skating and 125 % B.W. in classic technique were recorded. Fatigue tests on the first prototypes highlighted the lack of durability with respect to the assumed target life. A FEM analysis of the skiroll allowed to find the relative contribution of different sub-components to the overall stiffness and to focus on the aluminum main webs for the subsequent optimization procedure, due to their 68 % contribution to overall stiffness. Optimization of stress distribution on the beams allowed to achieve the fatigue target life of the new prototypes that additionally presented a stiffness increase of 34 % despite a mass increase of only 6 %. The high stiffness, damping and durability properties of the final skiroll design ensure a successful application to elite and amateur athletes market.

6- References

[MH1] Millet G.Y., Hoffman M.D., Candau R.B., Clifford P.S., Poling forces during roller skiing: effects of grade, Med Sci Sports Exerc. 1998 Nov;30(11):1637-44.

[MP1] Millet G.Y., Perrey S., Candau R., Rouillon J.D., Relationships between aerobic energy costs, performance and kinematic parameters in roller ski skating, Int. J. Sports Med. 2002, Apr; 23(3): 191-5.

[PP1] N. Petrone, C. Pollazzon, T. Morandin, G. De Bettio, In-field acquisition of foot loads on skating and classic skirolls, 4th Int. Conf. On Science and Skiing, Dec. 2007, St. Cristoph am Arlberg – Austria.

Monitoring of Bioimpedance Data during Exercise in Cyclists (P247)

Marie-Valérie Moreno[1], Gilbert Moreno[2], Florent Hubert[1]

Topics: Bicycle, Innovation and design, Measurements system, Industrial design.
Abstract: the objective of this study was to observe if it's possible to measure reliable bioimpedance data with our prototype during exercise, despite the movement of the body in this sport. In a second time, we wanted to investigate the reliability of fat mass measurement after exercise. Finally, we wanted to study if it is possible to observe variations of metabolism by bioimpedance during effort.

12 cyclists of the cycling club of Tour de Salvagny (TAC) participated to the study. We used two devices, a foot-to-foot impedancemeter, Tanita® Innerscan® for fat mass, and our prototype of multifrequency impedancemeter, BioparHom® Z-Metrix®, to measure the resistance (R), the reactance (X), the phase,angle and the resistances of extracellular (Re) and total body (Rinf) compartment, obtained by our model derived from Cole-Cole model. A measure was made each 1min30s during exercise. We asked cyclists to stabilise their effort at 75% of their maximal heart rate reserve during 30 minutes and then attempt a maximal effort once or twice. We showed that measurement of fat mass after exercise is not relevant, with a foot-to-foot or wrist-ankle impedancemeter using these equations in standing position, which were originally developed for standing position. We saw that during a constant effort, the signal was stable. We observed the variations of metabolism of cells'membranes thanks to phase angle parameter during maximal effort. We noted a difference in metabolic behaviour between hard training and low training subjects.

To conclude, our prototype can be reliable for monitoring bioimpedance data despite the movements during exercise but we have to modify our equations to obtain a reliable fat mass after exercise.
Key words: bioimpedance, monitoring, resistance, reactance, phase angle, body composition.

1. BioparHom, La Base, Technolac, 73310 Le Bourget du Lac, France - (marie-valerie.moreno,florent.hubert)@bioparhom.com
2. TAC, 169 chemin le verger, 69380 Chasselay, France - gilbert.moreno@wanadoo.fr

1- Introduction

Body composition analysis by bioimpedance is a convenient tool as it is non invasive and can be repeated frequently. It can be used during exercise with an adapted device. In sport, bioimpedance is seen as a no reliable technique, that's why we wanted to investigate two devices: a foot-to-foot (FFI) and a wrist-ankle (WA) impedancemeters.

The aim of this study was, firstly, to observe if it's possible to measure reliable bioimpedance data with our prototype of Z-Metrix® during exercise, despite the movement of legs in cycling. In a second time, we want to see the effect of a loss of water on the results of body Fat Mass (FM). Finally, we wanted to investigate if we could observe changes in fluid or bioimpedance data during exercise.

2- Materials and methods

12 cyclists of the cycling club of Tour de Salvagny (TAC) participated to the study. Their physical characteristics are summarised in Table 1.

Cyclists Data	Mean	sd
Age (years)	45.0	8.8
Weight (kg)	73.4	5.2
Height (cm)	177.6	7.6

Table 1 - Principal physical characteristics of our 12 cyclists (men).

We did measurements before and after exercise in standing position and on the bicycle with our WA device, but it was impossible to do the same protocol with the FFI because of its design.

We asked cyclists to do an effort during 30 minutes and to try to stabilise their effort at 75% of their heart rate reserve, obtained by the difference between maximal heart rate and heart rate at rest. Then they attempt a maximal effort once or twice. A whole body measurement with Z-Metrix® was made each 1min30s during exercise. The aim was to be sure that athletes do not loose FM during this protocol.

Two impedancemeters were used in this study, a multifrequency BioparHom Z-Metrix® (WA) measuring whole body with two electrodes on right hand and two on right foot as described in (Jaffrin *et al.*, 2002), and a Tanita InerScan® (FFI) with 4 reusable electrodes under heels and toes which give essentially Fat Mass (FM). The first device uses patented equations to calculate: the resistance of extracellular compartment (Re), resistance of total body compartment (Rinf) using a new model derived from Cole-Cole model (Cole and Cole, 1941), FM, Lean Body Mass (LBM), Bone Mineral Content (BMC), total body water (Vt), extracellular water volume (Ve), intracellular water volume (Vi) and various estimation of sodium and potassium extra or intracellular concentration, (ECENa, ICK, ECK) plasmatic volume (Vp), red cell volume (Vred_cell), blood volume (Vblood), hydration rate of FFM (Vt/FFM), hydration rate of body (Vt/W). The second device gives FM in percentage. FFM is calculated as the difference

between Weight and FM. It requires entering manually in the software of both devices the subject height, age and sex, while his weight is measured by the FFI to within 0.1 kg and manually entered for the WA.

In addition, we have used Kotler's equations (Kotler *et al.*, 1996) to obtain total body potassium TBK (in mmol) estimated from the reactance X and resistance R at 50 kHz by

$$TBK_{\sigma} = 44.89\, H^{1.6} / Xcp^{-0.5} + 18.52\, W - 386.66 \quad (1a)$$

$$TBK_{\varphi} = 1.248\, H^{2.07} / Xcp^{-0.36} + 5.79\, W - 230.51 \quad (1b)$$

where Xcp in ohm is the equivalent reactance given by

$$Xcp = X + R^2 / X \quad (2)$$

Wang's muscle mass in kg was calculated using (Wang *et al.*, 2003)

$$Muscle\ Mass\ Wang = 0.0093\, TBK + 0.024\, A - 3.21 \quad (3)$$

Body cell Mass in kg was calculated using Leweling's equations (Leweling, 1995)

$$BCMl = FFM - 0.29 Ln(Phase\ Angle°) \quad (4)$$

Where Phase Angle in degree is calculated by

$$Phase\ Angle = Arctan\ (X/R) \quad (5)$$

We used paired Student t-tests as statistical method.

3- Results

3.1 Is there a difference between bioimpedance data in standing position and on bicycle position?

Table 2 shows some parameters measured by Z-Metrix®, firstly in standing position and secondly on bicycle. We can observe mean and standard deviation of the parameters, compared with paired Student t-test. We see that there is a significantly difference between Vt, Ve, Vi and BMC obtained in standing position and on bicycle if we express them in liter. That confirms the study of Fenech (Fenech *et al.*, 2002) who supposed that current lines change during modifications of position. But, if we express Ve and Vi in percentage of Vt, and BMC in percentage of weight, the difference between the two position is not significant. We can suppose that the variations of one balance the other. We can think that this is the same for Ve/Vi, Ve/Vt and Re/Rinf. However, this is not the case for LBM and Muscle Mass. Although there is a non-significant difference for these parameters (X, Phase Angle, FFM and $BCMl/H^2$), all the others data are significantly different, measured in standing position or on bicycle (R, Re, Rinf, TBK, Vp, Vred-cell, Vblood, ECENa, ECK and ICK).

	Standing Position			On bicycle Position	
Data	**Mean**	**sd**	**Student t-test**	**Mean**	**sd**
Phase Angle(°)	6.8	0.4	0.231	6.8	0.4
BCMl/H_	11.9	0.9	0.513	11.8	0.9
FFM (kg)	67.4	4.7	0.945	67.1	4.9
FFM (% W)	91.9	2.4	0.979	91.4	2.3
FM (kg)	6.0	1.9	0.945	6.3	1.8
FM (%W)	8.1	2.4	0.979	8.6	2.3
LBM (kg)*	62.0	3.2	0.016	61.6	3.2
LBM (% W)*	84.9	7.2	0.018	84.2	6.8
BMC (kg)*	3.4	0.2	0.010	3.3	0.2
% BMC (/FFM kg)	3.7	0.3	0.086	3.6	0.3
BCMl Leweling (kg)	37.6	2.8	0.544	37.2	3.2
BCMl Leweling (%)	51.2	1.7	0.505	50.6	1.9
Muscle Mass Wang (kg) *	34.0	2.1	0.034	33.6	2.3
Muscle Mass Wang (%) *	46.4	1.3	0.039	45.8	1.1
Vt (liter)**	47.9	2.8	0.003	47.2	2.8
Ve (liter)***	20.7	1.3	0.001	20.5	1.3
Ve (% Vt)	43.3	0.6	0.616	43.3	0.6
Vi (liter)*	27.2	1.6	0.014	26.7	1.6
Vi (% Vt)	56.7	0.6	0.616	56.7	0.6
Hydration of Fat Free Mass (%)*	71.1	15	0.039	70.4	1.5
Hydration of body (%)**	65.3	2.0	0.005	64.4	1.5
Ve/Vt	0.4	0.0	0.616	0.4	0.0
Ve/Vi	0.8	0.0	0.633	0.8	0.0
Re/Rinf	1.4	0.0	0.586	1.4	0.0
Estimation of Plasmatic Volume Vp (liter)**	3.7	0.2	0.004	3.6	0.2
Estimation of Vred_cell (liter)**	2.4	0.1	0.004	2.3	0.2
Estimation of Vblood (liter)**	6.0	0.3	0.004	5.9	0.3
Rinf (ohm)**	356.8	21.1	0.005	364.6	20.2
Re (ohm)***	487.2	24.5	0.001	497.5	28.3
Reactance 50 kHz (ohm)	48.0	2.5	0.459	48.6	3.8
Resistance 50 kHz (ohm)***	401.4	22.0	0.001	410.1	21.7
TBK Kotler (mmol)*	4030.9	230.9	0.034	3983.1	253.7
Estimation of ECENa (mmol/l)	169.7	2.8	0.938	169.7	2.6
Estimation of ECK (mmol/l)	9.7	0.3	0.966	9.7	0.3
Estimation of ICK (mmol/l)	141.0	1.4	0.124	141.4	1.8

Table 2 - comparison between body composition data measured in standing position and on bicycle position. *, P t-test<0.05; **, P t-test<0.01; ***, P t-test<0.001

We propose that in order for measures of bioimpedance for cyclists, it is more reliable to take the reference of monitoring in position on the bike. Of course, to make an assessment of body composition, the most relevant is to do it in standing position.

3.2 Is there a difference between Fat Mass measured by a foot-to-foot impedancemeter and a wrist-ankle impedancemeter?

Table 3 shows mean and standard deviation of FM obtained with our two impedancemeters FFI and WA. We observe that there is a non significant difference (P=0.183) between the two percentage of fat mass before the exercise.

Data	Mean	sd	Student t-test
% FM of FFI	9.4	3.1	0.183
% FM of WA	8.1	2.4	

Table 3 - comparison of percentage of FM obtained by the Foot-To-Foot (FFI) and the Wrist-Ankle (WA) impedancemeters.

3.3 Is there a difference between Fat Mass measured before and after exercise?

Table 4 summarises the measurements of FM made before and after exercise obtained by our two impedancemeters. Our protocol was made for not inducing loss of FM during exercise but for inducing a loss of water. We can observe that the two impedancemeters indicate a significant loss (P<0.001) of FM. This shows that we can assume that bioimpedance cannot be reliable to indicate FM after an effort, water lost affects FM, in kg or in percentage. However, we want to indicate that equations of Z-Metrix® were not yet developed to be used in standing position. They were developed to be used in lying position. Maybe with the future new equations for standing position, that type of problem will disappear. If not, we shall have to modify our equation to integrate that point.

Data	Mean	sd	Student t-test
FM of FFI (kg)	-1.1	0.6	0.00005
FM of WA (kg)	-1.4	0.5	7.10^{-6}
% FM of FFI	-1.5	0.8	0.00007
% FM of WA	-1.9	0.7	0.00001

Table 4 - Comparison between FM measured before and after exercise, obtained by two types of impedancemeter, a foot-to-foot (FFI) and a wrist-ankle (WA) impedancemeter.

3.4 Is it possible to obtain reliable bioimpedance data during monitoring exercise?

Figure 1 shows the monitoring of reactance (X) during an isometric contraction of leg at 50% of Maximal Voluntary Contraction (MVC). Despite the contraction of the muscle, we obtain a stable reactance with our WA impedancemeter. We verified that during an effort without movement, our bioimpedance data are stable.

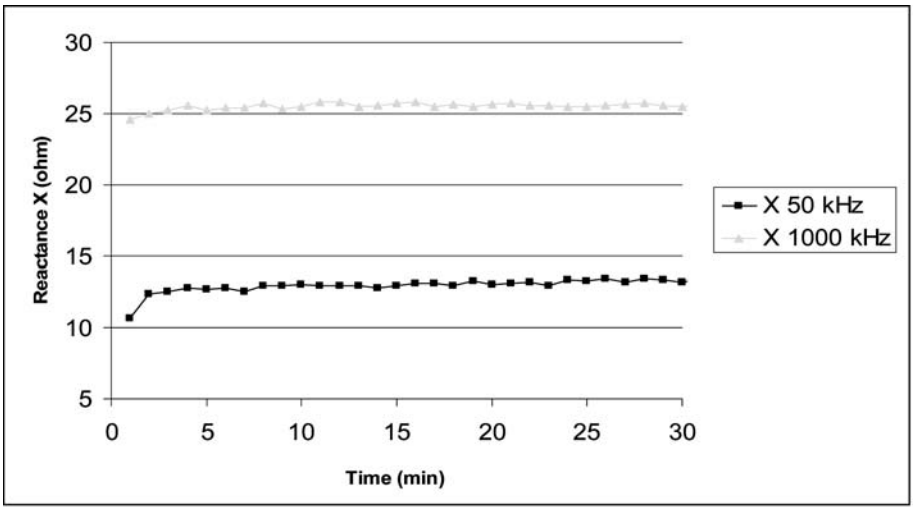

Figure 1 - Monitoring of reactance (ohm) during an isometric contraction (50% MVC).

Figure 2 shows the monitoring of phase angle, during our exercise, in two representative subjects of hard training cyclists HT (about 4 hours of training, 6 times per week) and low training cyclists LT (about 4 hours of training, 2 times per week). Peaks correspond to maximal effort (maximal heart rate). During the first part about 9 minutes of warm up, the phase angle is more o less stable, till the beginning of rising to the maximal heart rate. We observe that HT subject have a significant variation of phase angle during the peak but this is not the case in the LT subjects. That shows that HT have the capacity of increasing the activity of cells'membranes. We can suppose that permits them to avoid cramps for example. It may be noted that the second time of rising to maximal heart rate, the body seems to need less metabolic activity to achieve the same heart rate.

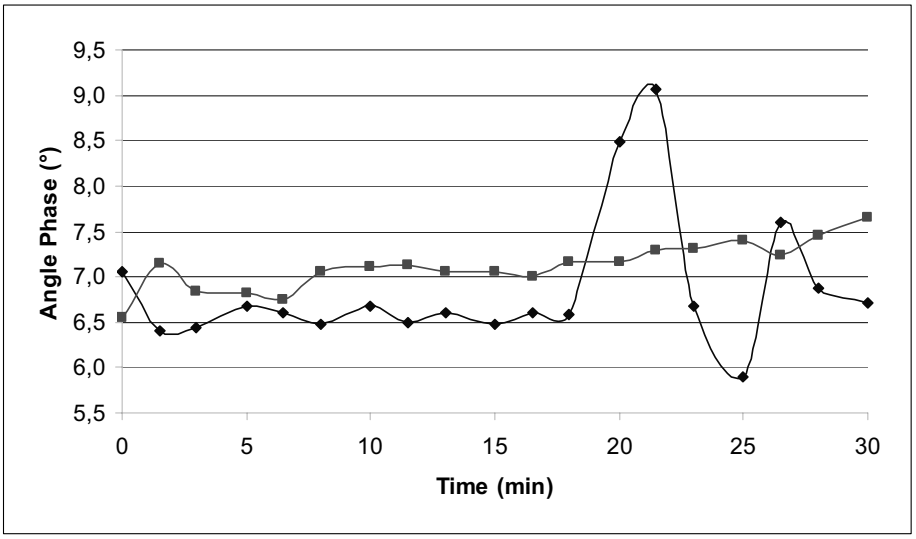

Figure 2 - Monitoring of phase angle (°) during exercise. In blue, data of hard training cyclist and in red, data of low training cyclist. Peaks correspond to maximal effort (maximal heart rate).

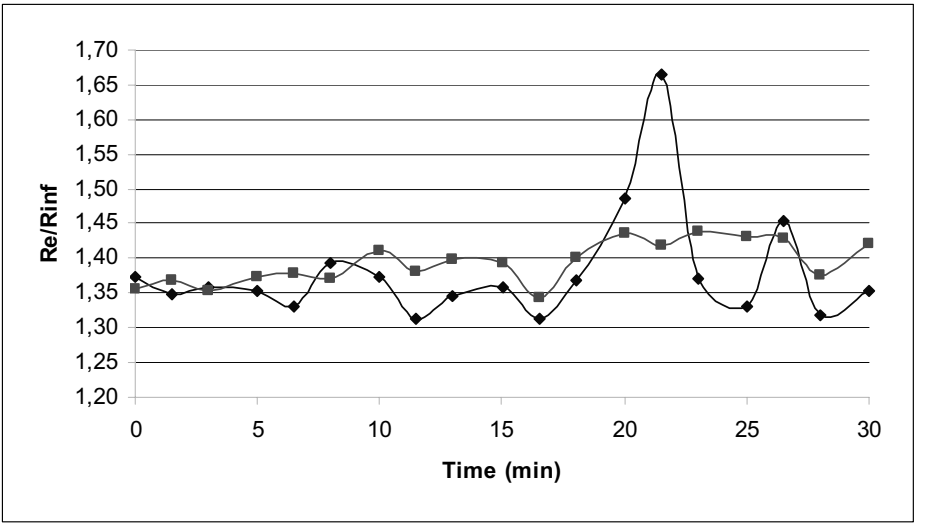

Figure 3 - Monitoring of phase angle (°) during exercise. In blue, data of hard training cyclist and in red, data of low training cyclist.

Figure 3 shows the variations of Re/Rinf ratio during exercise. We see the increase of the ratio during the peak, corresponding to maximal heart rate. We observed the same phenomenon for the two subjects but it's more significant for HT subject. We can deduct that during the peak of activity, fluids pass from extracellular compartment to intracellular compartment, that's why the reactivity of cells'membranes is very important.

4- Conclusion

We saw that positioning on bike change current lines and thus data of body composition. Then to have a reference during monitoring body composition of cyclists, it would be more relevant to take the reference data when the subject is on the bicycle.

We saw that equations to obtain FM after an exercise have to be modified to be reliable. Before these modifications, bioimpedance have to be used before an effort.

We observed that bioimpedance can be relevant to monitor cyclists even if they are in movement.

Bioimpedance permits to follow the cells'membranes activity during a peak of activity, showing the difference between a hard and low training subject. We showed the fluids'movement from extracellular to intracellular compartment during maximal activity.

5- References

[JF1] Jaffrin M.Y., Fenech M., de Fremont J-F., Tolani M.. Continuous monitoring of plasma, interstitial and intracellular fluid volumes in dialysed patients by bio-impedance and haematocrit measurements. In ASAIO J, 48:326, 2002.

[CC1] Cole KS., Cole RH. Dispersion and adsorption in dielectrics. In Journal of Chemical Review, 209-241, 1941.
[3] Kotler DP., Burastero S., Wang J., Pierson RN. Prediction of body cell mass, fat-free mass and total body water with bioelectrical impedance analysis: effects of race, sex and disease. In American Journal of Clinical Nutrition; 64, 489S-97S, 1996.
[WZ1] Wang Z., Zhu S., Wang J., Pierson R., Heymsfield SB. Whole-body skeletal muscle mass : development and validation of total-body potassium prediction models. In American Journal of Clinical Nutrition, 77, 76-82, 2003.
[L1] Leweling H. Zusammensetzung des körpers. Ernährungs-medizin (Biesalski,H. K.,ed.), In Georg Thieme Verlag, 3-12, Stuttgart, Germany, 1995.
[FJ1] Fenech M., Jaffrin MY., Malmen U. Reversibility of artefacts of fluid volume measurements by bioimpedance caused by position changes during dialysis. In the International Journal of Artificial Organ, 25(3):217-22, 2002.

Optimization of Torque in Pole Vaulting using Genetic Algorithm (P248)

Shigemichi Ohshima[1] and Atsumi Ohtsuki[1]

Topics: Modelling.
Abstract: Pole vaulting has progressed rapidly in terms of improved mechanical properties and better appearance by using poles made of flexible fiberglass material. Competitive pole vaulting requires specific characteristics that promote higher jumps. Analysis of the dynamics of pole vaulting basically requires a thorough consideration with the aim of having a high flexibility of the pole and all joint torque actions of the body. In this research, simulation analysis to optimize the joint torque was done by using Genetic Algorithm. The system consists of a combination of a flexible pole and several links (vaulter). In the present genetic algorithm, the joint torque of the vaulter was expressed in terms of trigonometric functions. The expression for the torque was given by the amplitude, angular frequency and phase of the model equation. The overall evaluation function was the height and the control parameters were the joint torque, vaulter's speed, and pole stiffness. The result of the optimum torque with respect to time readily obtained from our genetic algorithm show similar trend with published results obtained by inverse dynamic analysis.
Key words: Pole vaulting, Elastica, Simulation, Optimization, Genetic Algorithm.

1- Introduction

Pole vaulting is a game for clearing the highest jump height achieved in a competition. A vaulter takes off due to kinetic energy, and also generates joint torque as a time function during a pole vault, works on a pole, and, as a result, gets height.

Therefore, the height obtained changes greatly with combination of various parameters, such as takeoff speed, the pole characteristic, and torque of each joint produced by a vaulter. The purpose of this research is to determine the optimal solution of such a combination problem. However, since the joint torque actions change during pole vaulting, modelling the equations and use them as control parameters of an optimization

1. Department of Mechanical Engineering, Meijo University, Nagoya, Japan - E-mail: {ohshi , ohtsuki}@ccmfs.meijo-u.ac.jp

problem is a difficult task to handle. One of the approaches taken to tackle the problem is the inverse approach. The analysis of inverse dynamics presumes each joint torque which should be generated by a pole vaulter using the information which were obtained from recordings of camera images of a pole vaulting competition and vaulter model (McGinnis, 1986). These results were then used in order to identify the difference in the techniques used among pole vaulters. However, the torque histories obtained from inverse dynamics analysis is not necessarily the optimal torque, and it is not necessarily the optimal torque for all other vaulters as the physique and takeoff velocity differ appreciably.

In this paper, a genetic algorithm is used to solve the optimization problem of the joint torque of pole vaulting. A complete system model is used to study the effects of different initial conditions and the effect of time variations in the control torques during the vault. The optimal joint torque history that a vaulter should generate is taken as an optimization problem that aims at the height as the objective function using direct dynamics and a genetic algorithm.

2- Model

2.1 Model of Pole-Vaulter System

The schematic configuration of a model of pole-vaulter system model is given in Figure 1. The pole-vaulter model was represented by the large deflection pole and seven segments rigid links. In this paper, motion of a vaulter and the deformation plane of a pole are assumed to be two-dimensional motion perpendicular to a cross bar for simplification. Although in the actual pole vault a vaulting is three-dimensional motion, the pole must bend out of this plane, and vaulter performs a twisting motion during the flyaway phase, these motions were neglected here. In addition, complexity of in pole vaulting widens due to the loop formed by the vaulter's arms and the pole between his handgrips. Since the torque generated by the vaulter's spread arms must be acting on the pole, the pole model must include this effect. The reaction forces acting at the left hand were replaced by force-couple system acting at the upper end of the pole. Furthermore, since the mass of the pole is relatively small (2 - 4%) compared to that of the vaulter, the mass of a pole is neglected.

2.2 Pole Model

The pole model (shown in Figure 1) was analyzed using nonlinear large deflection theory for a thin rod. The moment *MB* and compressive force *P* generated by a vaulter are simultaneously applied to the pole (length *L*) at the upper end. In denoting the deflection angle by θ, the arc length by s, the radius of curvature by *R* and the bending moment by *M*, the relationship among these parameters are given by:

$$1/R = M/EI = -d\theta/ds\,,\ dx = ds \cdot \cos\theta\,,\ dy = ds \cdot \sin\theta \qquad (1)$$

where *E* is the Young's modulus and *I* is the second area moment of the cross section about the neutral axis. In order to facilitate the discussion of large deformation behaviour, the following non-dimensional variables are introduced/

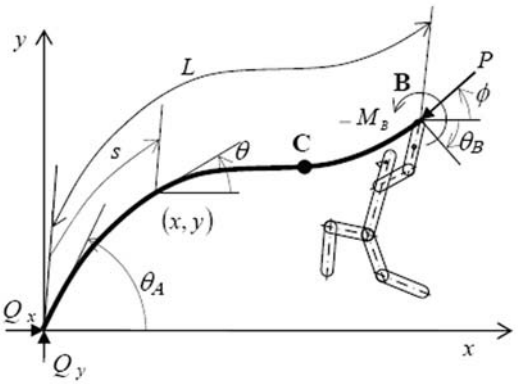

Figure 1 - Schematic configuration of pole–vaulter system.

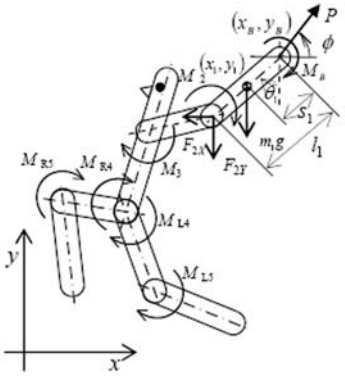

Figure 2 - Link segment model of vaulter.

$$\zeta = s / L\ ,\ \xi = x / L\ ,\ \eta = y / L\ ,\ \lambda = PL^2 / EI\ . \tag{2}$$

The basic nonlinear equation for large deformation is derived as follows.

$$d^2\theta\ d\zeta^2 = -\lambda \cdot \sin(\theta - \varphi). \tag{3}$$

Considering the boundary conditions at the upper end of the pole, *i.e.* the bending moment $M/\ \theta = \theta_B = M_B$ or $d\theta/\ d\zeta = M_B\ L\ EI = \beta$, , and setting the following relationships in equation (4), the nonlinear differential equation (3) can be reduced to equation (5) as a result of the variable change from θ to ϕ .

$$1 - \cos(\theta - \phi) = 2k^2 \cdot \sin^2 \Phi\ ,\ k = \sqrt{2[1 - \cos(\theta_B - \phi) + \beta^2 / \lambda]/2} \tag{4}$$

$$d\theta/d\zeta = \pm\sqrt{2\lambda[1 - 2k^2 \sin^2 \Phi - \cos(\theta_B - \phi)] - \beta^2} = \pm 2k\sqrt{\lambda} \cdot \cos\Phi \tag{5}$$

The non-dimensional arc length ζ at arbitrary position on the elastic curve is obtained by integrating equation (5).

$$\zeta = \{3K(k) + F(k, \Phi)\} / \sqrt{\lambda}\ . \tag{6}$$

Furthermore, the non-dimensional horizontal and vertical position ξ_B, η_B at the end of the pole is given by

$$\xi_B = \frac{2k \cdot \sin\phi \cdot \cos\Phi_B - \cos\phi \cdot \Psi(\Phi_B)}{3K(k) - F(k, \Phi_B)}\ ,$$

$$\eta_B = \frac{-2k \cdot \cos\phi \cdot \cos\Phi_B - \sin\phi \cdot \Psi(\Phi_B)}{3K(k) - F(k, \Phi_B)}\ , \tag{7}$$

where, $\Psi(\Phi) = -\{3K(k) + F(k,\Phi)\} + 2\{3E(k) + E(k,\Phi)\}$ and $F(k,\Phi)$, $E(k,\Phi)$ are the Legendre-Jacobi elliptic integrals of the first and second kinds, respectively.

2.3 Vaulter Model

The mathematical model of the vaulter shown in Figure 2 is represented by seven rigid link segments, namely, a forearm (l_1), an upper arm (l_2), torso (l_3), right thigh (l_{R4}), right shank (l_{R5}), left thigh (l_{L4}) and left shank (l_{L5}). The joint moments acted on each segment to either side of each joint, and horizontal and vertical reaction forces acted at each joint. The moment (M_B) and force (magnitude P, direction φ) act simultaneously on the forearm top (point B) becomes we have modeled both arms on one arm from the pole. The equations that described the motion of the model are derived using Newtonian mechanics.

$$\begin{aligned} m_i\ddot{x}_i &= F_{iX} - F_{i+1X} \quad , \\ m_i\ddot{y}_i &= F_{iY} - F_{i+1Y} - m_i g \, , \\ J_i\ddot{\theta}_i &= \{F_{iX} \cdot s_i + F_{i+1X} \cdot (l_i - s_i)\} \cdot \cos\theta_i - \{F_{iX} \cdot s_i + F_{i+1X} \cdot (l_i - s_i)\} \cdot l_i \sin\theta_i - M_{i+1} + M_i \, , \end{aligned} \tag{8}$$

where (x_i, y_i) is the location of the c.m. of the i-th segment. Further, ( ) &x&i , &y&i are expressed with ( ) &x&B, &y&B as follows:

$$\begin{aligned} \ddot{x}_i &= \ddot{x}_B + \sum_{n=1}^{i}\left(-s_{n-1}\cos\theta_{n-1}\cdot\ddot{\theta}_{n-1} + s_{n-1}\sin\theta_{n-1}\cdot\dot{\theta}_{n-1}^{\,2}\right) + \sum_{n=1}^{i}\left(-s_n\cos\theta_n\cdot\ddot{\theta}_n + s_n\sin\theta_n\cdot\dot{\theta}_n^{\,2}\right) \\ \ddot{y}_i &= \ddot{y}_B + \sum_{n=1}^{i}\left(l_{n-1}\sin\theta_{n-1}\cdot\ddot{\theta}_{n-1} + l_{n-1}\cos\theta_{n-1}\cdot\dot{\theta}_{n-1}^{\,2}\right) + \sum_{n=1}^{i}\left(s_n\sin\theta_n\cdot\ddot{\theta}_n + s_n\cos\theta_n\cdot\dot{\theta}_n^{\,2}\right) \end{aligned} \tag{9}$$

Considering boundary conditions at the forearm, hip joint and tip of the legs,

$$\begin{aligned} &F_{1X} = P\cos\phi \, , \quad F_{1Y} = P\sin\phi \, , \quad M_1 = M_B \, , \\ &F_{4X} = (F_{L4X} + F_{R4X}) \, , \; F_{4Y} = (F_{L4Y} + F_{R4Y}) \, , \; M_4 = (M_{L4} + M_{R4}) \, , \\ &F_{6RX} = F_{6LX} = 0 \, , \; F_{6RY} = F_{6LY} = 0 \, , \; M_{R6} = M_{L6} = 0 \, , \end{aligned} \tag{10}$$

and by eliminating constraint force F^* acting at the joints form these equations, we obtain the nine differential equations. These differential equations can be numerically integrated with a Runge-Kutta integration.

3- Genetic Algorithms

Genetic algorithms are search algorithms inspired by the mechanics of genetics and natural selection. These search algorithms combine survival of the fittest among chromosome-like string structures with a structured yet randomized information exchange. It evolves candidate solutions to problems that have large solution spaces and are not amenable to exhaustive search or traditional optimization techniques. Genetic algorithms have been applied to a broad range of optimization problems since their inception by Holland (1975). In this paper, a genetic algorithm is used to solve the optimization problem of the joint torque of pole vaulting.

3.1 Objective Function

The pole vault competes for height, so in this simulation, we have chosen the height of the center of mass to be the objective function of an optimization problem. According to the rules, the crossbar may be set anywhere in the range (-0.9m<x<-0.1m), so the height is the maximum height that can be attained for the trajectory within the crossbar setting range (Figure 3). In calculating of the maximum height, at first, we calculated the trajectory of vaulter for the case in which the vaulter's grip is sustained throughout. Then trajectories for different release times where calculated by assuming reaction force of the pole to be zero. This produces a parabolic trajectory for the center of the mass (Figure 4). Upon calculating be different trajectories one can easily determine the maximum height attained within the range. In other words, the position of the crossbar for maximum height can be readily determined by just setting the crossbar at the maximum height.

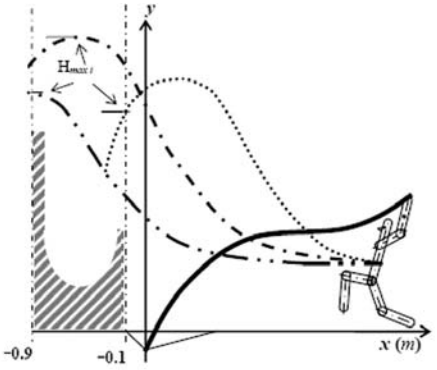

Figure 3 - Vault trajectories showing the maximum attainable vault height within the allowable range.

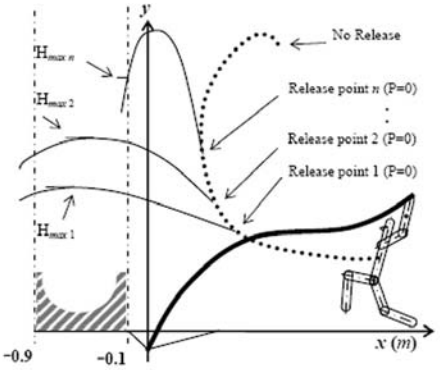

Figure 4 - Vault trajectories obtained from different release point.

3.2 Control Parameters

The height of the pole vault is influenced with various parameters, i.e., vaulter's physical constitution, takeoff velocity and direction, pole length and stiffness, joint torques and so on. Except the joint torques, these parameters are independent to time.

The parameter independent of time can be expressed as one control parameter for optimization. However, since it is dependent to time, the joint torque cannot be directly expressed as a control parameter for optimization. Then, in this study, we proposed expressing a joint torque with the sum of trigonometric functions. The expression for the torque was given by the amplitude (τ_{ij}), angular frequency (ω_{ij}), phase (ψ_{ij}) and factor of declination (γ).

$$M_i' = \tau_{i1}\sin(\omega_{i1}t+\psi_{i1}) + \tau_{i2}\sin(\omega_{i2}t+\psi_{i2}) + \tau_{i3}\cdot e^{-\gamma t}\sin(\omega_{i3}t+\psi_{i3}),$$

$$M_i' = M_i - M_{i+1} \quad (i : \text{link number}) \qquad (11)$$

Thus, one torque was expressed by ten control parameters as a function of time. Therefore, the control parameters expressing seven joint torque are 70 control parameters.

4- Simulation Results

In our simulation, pole length of L=5.2 m, vaulter's height of 1.8 m and weight of 77 kg where used as the primary input. The initial conditions, control parameters and range of joint angles were selected by considering realistic range that can be achieved.

Table 1 shows the range of the angles that can be achieved in flexing the joints. Table 2 shows the vaulter's parameter and corresponding initial conditions. The table 3 shows, the initial conditions of the grip (upper end of the pole) at takeoff. Table 4-1 shows the maximum values of the control parameter in expressing the joint torque. The table 4-2 shows the range of the parameters stiffness and initial velocity of the grip.

Table 1 : Range of joint angles.

θ_1	$\theta_1 > -60,\ 80 > \theta_1$
θ_2	$(\theta_3 - 190) < \theta_2,\ \theta_2 < (\theta_3 + 120)$
θ_3	$(\theta_2 - 30) < \theta_3,\ \theta_3 < (\theta_2 + 30)$
θ_{L4}, θ_{L5}	$\lvert\theta_{R4} - \theta_{L4}\rvert > 180$
	$(\theta_{R4} - 160) < \theta_3,\ \theta_3 < (\theta_{R4} + 60)$
	$(\theta_{L4} - 160) < \theta_3,\ \theta_3 < (\theta_{L4} + 60)$
θ_{R4}, θ_{R5}	$\theta_{R4} > \theta_{R5},\ \theta_{R4} < (\theta_{R5} + 170)$
	$\theta_{L4} > \theta_{L5},\ \theta_{L4} < (\theta_{L5} + 170)$

Table 2 : Vaulter parameters and corresponding initial conditions.

	m_i (kg)	l_i (m)	$\theta_{i\,t=0}$ (deg)	$\dot{\theta}_{i\,t=0}$ (deg/s)
Link 1	3.388	0.36	52.5	70
Link 2	4.158	0.36	37.5	550
Link 3	42.966	0.60	20.0	70
Link R4	8.47	0.42	70.0	60
Link R5	4.774	0.53	−55.0	−400
Link L4	8.47	0.42	−32.5	850
Link L5	4.774	0.53	−32.5	850

Table 3 : Initial conditions at taking off the ground.

$\dot{y}_{g\,t=0} = -1.00$ (m/sec)	
$x_{g\,t=0} = 4.52$ (m)	$y_{g\,t=0} = 1.87$ (m)

Table 4-1 : Maximum value of the control parameters.

	$M_{1\,t=0}$	M_2	M_3	M_{R4}	M_{R5}	M_{L4}	M_{L5}
τ_{i1}(Nm)	50	50	250	60	60	60	60
τ_{i2}(Nm)	25	25	125	30	30	30	30
τ_{i3}(Nm)	25	25	125	30	30	30	30
ω_{i1}(rad/sec)	10	10	10	10	10	10	10
ω_{i2}(rad/sec)	10	10	10	10	10	10	10
ω_{i3}(rad/sec)	10	10	10	10	10	10	10
ψ_{i1}(rad)	2π	2π	2π	2π	2π	2π	2π
ψ_{i2}(rad)	2π	2π	2π	2π	2π	2π	2π
ψ_{i3}(rad)	2π	2π	2π	2π	2π	2π	2π
γ	3	3	3	3	3	3	3

Table 4-2 : Range of control parameters.

EI(Nm²)	3100 ∼ 3500 (default 3200)
$\dot{x}_{g\,t=0}$ (m/sec)	−5.7 ∼ −6.2 (default −5.8)

The result of the optimise simulation, for joint torque, stiffness and horizontal speed are presented in three different cases. The first case, shown in Figure 5, is calculated based on the joint torque. The second case, shown in Figure 6, takes account of joint torque and stiffness. The third case, shown in Figure 7, adds the horizontal speed of the grip in addition to the joint torque and stiffness. The overall result of the simulation show that the maximum fitness increases with generation and appropriate combination of the control parameter produces higher fitness values. Furthermore, as can be seen in Figure 6, variation of the stiffness and joint torque with respect to generations show a rather steady stiffness values while the fitness increases appreciably. This means one can select the pole stiffness and increase the fitness. On the other hand, an optimal value for the horizontal speed was attained at 5.95 m/s upon simultaneously changing the stiffness and the joint torque.

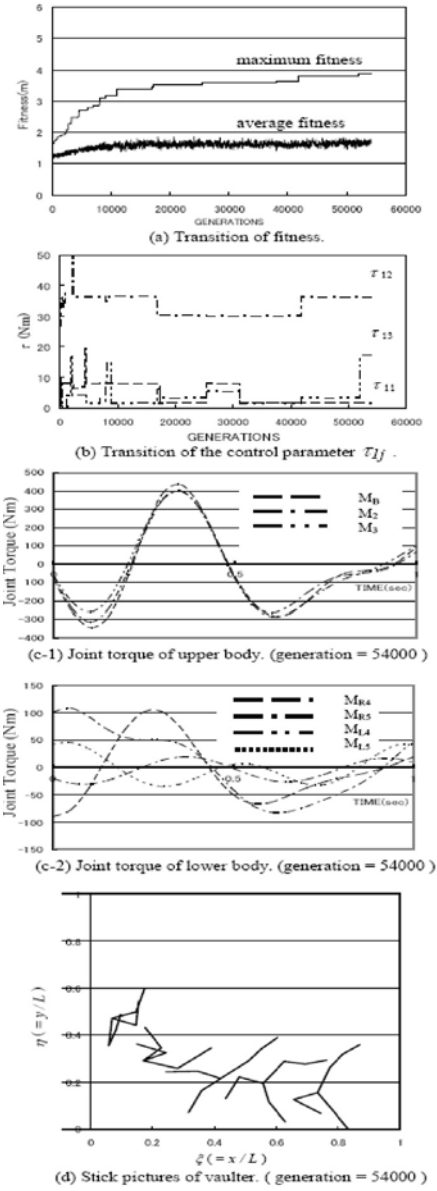

Figure 5 - Genetic algorithm of pole vaulting for optimum fitness values. (Control parameters : M').

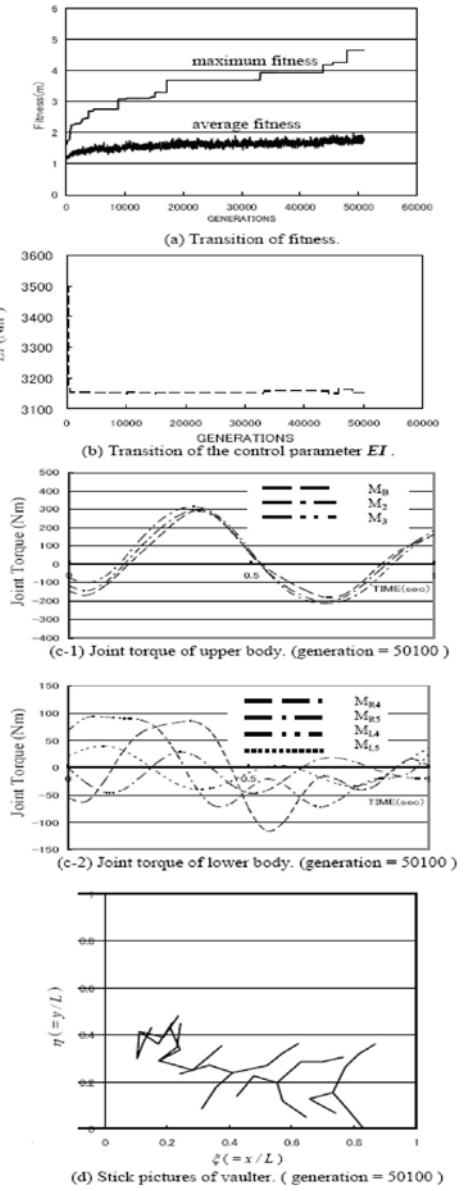

Figure 6 - Genetic algorithm of pole vaulting for optimum fitness values. (Control parameters : M' and EI).

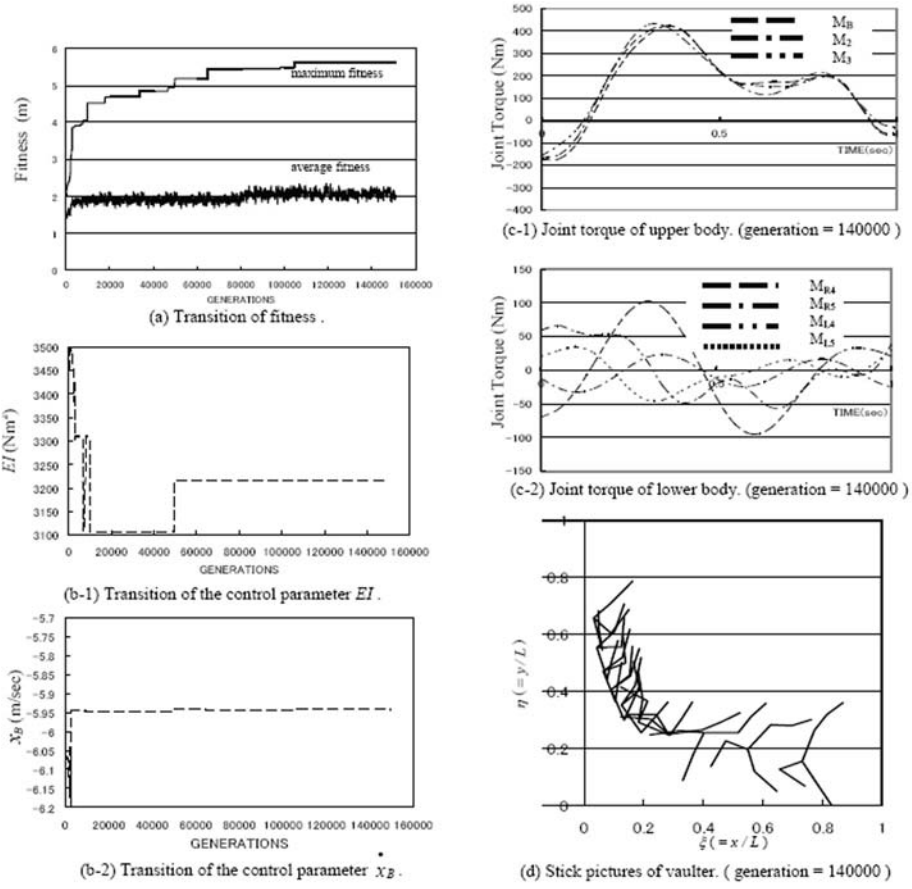

Figure 7 - Genetic algorithm of pole vaulting for optimum fitness values. (Control parameters: M' , EI and x).

5- Conclusions

We have shown in this paper that, a genetic algorithm is used to solve the optimization problem of the joint torque of pole vaulting. The model is used to study the effects of different initial conditions and the effect of time histories in the control torques during the vault. The optimal joint torque history that a vaulter should generate is taken as an optimization problem.

The results of our simulations show similar trends with published results obtained by inverse dynamic analysis (McGinnis, 1986).

Acknowledgements

The authors are grateful for the financial support of the Nitto Foundation.

6- References

[H1] Hubbard, M. Dynamics of the pole vault. Journal of Biomechanics, 13:965-976, 1980
[H2] Holland, J. Adaptation in Natural and Artificial Systems. The University of Michigan Press, 1975
[MB1] McGinnis, P. and Bergman, L. An inverse dynamics of the pole vault. International Journal of Sports Biomechanics, 2:186-201, 1986

A new Dimensionless Number for Dynamic Similarity during Running (P250)

Nicolas Delattre[1], Pierre Moretto[1,2]

Topics: Biomechanics.
Abstract: This abstract aims to present the assessment of a new dimensionless number for the study of dynamic similarity (DS) during running by using a computer simulation. Previous studies on walking (Bisiaux *et al.*, 2003, Moretto *et al.*, 2007) induced DS between subjects and reported a decrease of data variability by using the Froude number, a dimensionless number founded on mechanical energy transfers occurring during walking. Delattre *et al.* (2007) reported that the use of the Strouhal number (another dimensionless number based on the spring-mass model (SMM) for the mechanics of running) enabled to induce DS between running subjects. However it seems to us that this approach could be refined. As it has been made to highlight Nfr from the inverted pendulum model, we proposed to consider mechanical energy transfers occurring at the centre of gravity of a simulated SMM. We built two different-sized and proportional SMM, and computed E_P (potential energy), E_K (kinetic energy), E_E (elastic energy). Results showed that the ratio $R=(E_P+E_K)/E_E$ was constant and reached identical value for both SMM (4.1±0.72 and 4.1±0.71) from 30 to 70% of the simulation time. Taking the limits of the simulation into account, we conclude that the dimensionless number R could theoretically be used to induce DS during running. Future investigation has to assess R for DS *in vivo*.
Key words: running, spring-mass model, dimensionless, dynamic similarity, mechanical energy.

1- Background

Dynamic similarity is a widely used concept in physics and engineering to test a design with a scale model prior to building final design. The concept of dynamic similarity has the same role in studies of movement as geometric similarity has in the study of shape.

1. Laboratoire d'Etudes de la Motricité Humaine, FSSEP, 9 rue de l'Université, 59790 Ronchin, Université de Lille 2, France - E-mail: nicolas.delattre@univ-lille2.fr
2. Laboratoire d'Automatique, de Mécanique et d'Informatique industrielles et Humaines – UMR CNRS 8530, Université de Valenciennes et du Hainaut-Cambrésis, Le Mont Houy 59313 Valenciennes Cedex 9, France - E-mail: pierre.moretto@univ-lille2.fr

When two systems are dynamically similar, one could be made identical to the other by multiplying all lengths by a scale factor C_L, all masses by another scale factor C_M, and all times by a third scale factor C_T. Two subjects moving in a dynamically similar fashion thus can be considered as two scale models. This concept was applied to locomotion (Alexander et al., 1983), and appeared to be very useful because it allowed making quantitative comparison between individuals of a wide range of sizes.

Dynamic similarity between two systems is possible only in particular circumstances, which depend on the nature of forces involved. For example, because gravitational forces are important during walking, dynamic similarity between two individuals requires them to have equal values of the Froude number $Nfr=v^2/g.l$ (with v: forward speed, g: gravitational acceleration, l: leg length). Nfr represents the dimensionless expression of the speed and was highlighted from the pendulum-like mechanics of walking (Figure 1A). This model consists of a point mass (representing the body mass at the centre of gravity) oscillating at the end of a massless rigid segment length (l) representing the leg. According to the inverted pendulum model, the maximum speed of walking is imposed by the gravity and the leg length (Alexander, 1992). Indeed, during a step, Cg follows a curved trajectory and has an acceleration v/l (with v: forward speed, l: leg length) toward the ground contact point. When the leg is vertical, this acceleration is directed vertically downwards and can not be greater than g, the gravitational acceleration: $v^2/l \leq g \Leftrightarrow v^2/g.l \leq l$. This inequality set a speed limit for walking, and predicts the walk-to-run transition should theoretically appear when Nfr equals to 1. Experimental data showed that Humans naturally switch from a walk to a run when Nfr equalled about 0.5 (Alexander, 1989, Thorstensson *et al.*, 1987).

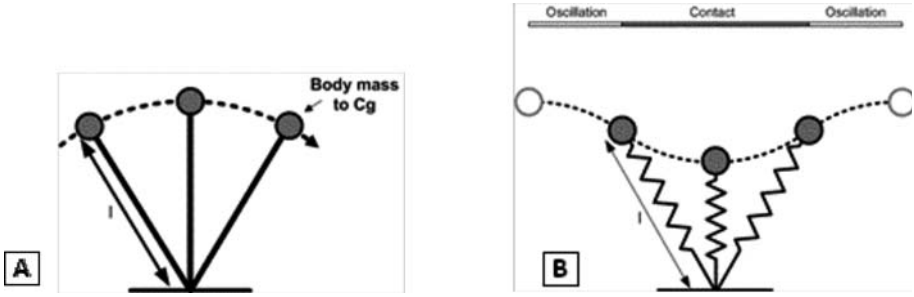

Figure 1 - A: the inverted pendulum model for the mechanics of walking. B: the spring-mass model for the mechanics of running.
l: initial leg length before touch down.

Fundamental of the pendulum-like mechanics of walking is the exchange of kinetic energy ($E_K=0.5mv^2$, with m: body mass, v: the forward speed) and the gravitational potential energy ($E_p=mgh$, with m: body mass, g: gravitational acceleration, h: height of Cg). Between touchdown and mid-stance, the forward speed of the centre of mass (Cg) decreases as this latter moves upwards. In this phase, kinetic energy is converted to gravitational potential energy. Between mid-stance and toe-off, the forward speed of Cg increases as this latter moves downwards. In this phase, gravitational potential energy is

converted back in kinetic energy. E_K and E_P evolutions have the same magnitude and are out of phase (Cavagna *et al.*, 1966, Farley *et al.*, 1998). The ratio of these two energies is thus constant, and reduces to Nfr. Equal values of Nfr were shown to ensure dynamic similarity between humans during walking (Bisiaux *et al.*, 2003, Moretto *et al.*, 2007), and between different animals species during running (Farley *et al.*, 1993). As a matter of principle, it is not expected that equal values of Nfr make possible dynamic similarity during running, because Nfr is founded on the pendulum-like mechanics of walking, and thus does not take any elastic phenomenon into account. Some studies (Bullimore *et al.*, 2008, Donelan *et al.*, 2000) showed that Nfr was necessary, but not a sufficient condition for dynamic similarity during running.

In addition to E_P and E_K, elastic energy ($E_E=0.5k.\Delta l^2$, with k: leg stiffness; Δl: variation in leg length) was shown to have an important role for mechanical energy conservation during running (Cavagna *et al.*, 1964). Tendons and other springs can be used to store elastic energy and then to return it by elastic recoil. The spring-mass model (Figure 1B) enables to take E_E into account, and has been widely used to describe the mechanics of running.

Considering that two runners behave each like such a vibrating system, Alexander (Alexander, 1989) suggested that dynamic similarity between them requires they have the same values of the Strouhal number Str=(Frequency.Length/Speed). Str represents a dimensionless frequency, and in its expression, while the leg length appears to be the only length that can be used, any frequency and any speed component of the center of gravity (Cg) can be used. Donelan and Kram (Donelan and Kram, 2000) showed that dynamic similarity in simulated sub-gravity was not met with the use of Str including the natural frequency of the spring-mass system and the vertical landing speed. Delattre *et al.* (Delattre *et al.*, 2007) used Str including stride frequency and forward speed and reported that Str made possible to meet inter-subject similarity only for some kinetic parameters. Another dimensionless number, the Groucho number $Gr = v_y \cdot f_0 / g$ (with v_y; vertical landing speed, f_0: natural frequency of the spring-mass system, and g: gravitational acceleration), was proposed (McMahon *et al.*, 1987). Gr represents a dimensionless vertical landing speed and was primarly used to distinguish between hard and soft running modes. However it has been shown that Gr did not predict dynamic similarity during human running (Donelan and Kram, 2000).

It appears that neither Nfr, nor Str, nor Gr can be used for perfect dynamic similarity during running. On the contrary, Nfr is suitable for dynamic similarity during walking, because it is founded on mechanical energy transfer occurring in the pendulum-like mechanics, to which walking has been likened. To the best of our knowledge, there are no available studies dealing with dynamic similarity which have focused on mechanical energy transfers occurring on a spring-mass model.

This study aimed to consider mechanical energy transfer occurring at the centre of gravity of simulated spring-mass models in order to highlight a new dimensionless number that could be applicable for dynamic similarity during running. During the stance phase of running, the E_P and E_K variations are in phase, whereas E_K and E_E are out of phase (Biewener, 2006, Cavagna *et al.*, 1964, Lee *et al.*, 1998). Therefore, the ratio $R=(E_P+E_K)/E_E$ is expected to be constant during the stance phase of running. Like for

Nfr during walking, this new dimensionless number will have (i) to be constant during the running cycle, and (ii) to equal the same value for two dynamically similar spring-mass models.

2- Methods

We created a computer simulation with Working Model 2D 7.0 (Design Simulation Technologies, Inc., USA). We built a first spring-mass model (SMM #1) based on data of Ferris *et al.* (Ferris *et al.*, 1999) (Table 1). We then built a second spring-mass model (SMM #2) dynamically similar to the first. As a starting point, we defined the inter-models scale factors for lengths (L), masses (M), and times (T) dimensions as C_L, C_M, and C_T respectively. L, M and T are fundamental dimensions, thus all other mechanical parameters can be defined from them. Therefore, the scale factor for all other mechanical parameters can be determined from C_L, C_M, and C_T. For example, according to Newton's second law, a force (F) is expressed in Newtons, and its dimension is $M.L.T^{-2}$. Accordingly, between two subjects moving in a dynamically similar fashion, the scale factor for forces (C_F) equal the product of concerned scale factors: $C_F=C_M.C_L.C_T^{-2}$.

We defined the initial spring length of SMM #2 as to be 0.985m, which implied that C_L equalled 1.13. Assuming that body densities of the two models were identical, the scale factor for masses was $C_M=C_L^3=1.45$, and the mass of SMM #2 was 76.9kg (Table 1). The scale factor for times was determined as follows: E_P and E_K have the same dimension $M.L^2.T^{-2}$, and thus the same inter-subject scale factors. On one hand, the ratio between E_{P1} and E_{P2} of two subjects S_1 and S_2 involves the simplification of constant g, and returns to the ratio of masses that multiplies ratio of lengths, i.e. $C_M.C_L$. On the other hand, E_K equals to $0.5.m.v^2$, has $M.L^2.T^{-2}$ as dimension that involves that scale factor for kinetic energies is $C_M.C_L^2.C_T^{-2}$. Scale factors between E_P and E_K are the same, thus:

$$C_M.C_L=C_M.C_L^2.C_T^{-2} \Leftrightarrow C_L.C_L^{-2}=C_T^{-2} \Leftrightarrow C_T^{-2}=C_L^{-1} \Leftrightarrow C_T=C_L^{0.5}$$

Scale factor for times (C_T) corresponds to the square root of the scale factor for lengths (C_L) and thus equals 1.06. Scale factors for the other parameters of the simulations (spring stiffness, initial Theta, horizontal and vertical speeds) were computed from C_L, C_M, and C_T.

Parameter	Unit	Dimension	SMM #1	Scale factor	SMM #2
Initial spring length	m	L	0.87	1.13	0.985
Mass	kg	M	53	1.45	76.9
Contact time	s	T	0.282	1.06	0.3
Spring stiffness	$kN.m^{-1}$	$M.T^{-2}$	6.9*	1.28	8.84
Initial Theta	deg	Dimensionless	26.6	1	26.6
Initial horizontal speed	$m.s^{-1}$	$L.T^{-1}$	3	1.06	3.19
Initial vertical speed	$m.s^{-1}$	$L.T^{-1}$	-1	1.06	-1.06

Table 1 - characteristics of the two simulated spring-mass models (SMM #1 and SMM #2). Initial Theta corresponds to the angle between the vertical and the spring. Parameters of SMM #1 were those of Ferris *et al.* (Ferris *et al.*, 1999) with *: hard surface with adjusted leg stiffness. In dynamically similar conditions, the scale factor for angles equals to 1, meaning that angles between systems are identical in the same phase of the movement (Moretto *et al.*, 2007).

Data from each simulation enabled us to compute the gravitational potential energy E_P=m.g.h, the kinetic energy E_K=0.5m.v^2, and the elastic energy E_E=0.5k.Δl^2 (with m: mass, g: gravitational acceleration, h: vertical Cg position, v: speed, k: spring stiffness, Δl: variation in spring length).

3- Results

For each of the two models, Theta and spring length had the same value at the initial (touchdown) and at the final (toe-off) instants of the simulation (Table 2).

Parameter (unit)	SMM #1		SMM #2	
	Initial	**Final**	**Initial**	**Final**
Theta (deg)	**26.6**	**26.6**	**26.6**	**26.6**
Spring length (m)	**0.87**	**0.87**	**0.985**	**0.985**

Table 2 - theta and spring length at initial and final instants of the simulation for SMM #1 and SMM #2.

The Table 3 shows that scale factors computed from measured parameters matched the scale factors predicted from C_L, C_M, and C_T. There is a single scale factor for lengths (l: spring length, fx: horizontal displacement of the centre of gravity during the stance phase, Δl_{max}: maximal spring compression), and a single scale factor for energies (E_P, E_K, E_E) between the two models.

Parameters	SMM #1	SMM #2	Scale factor	
			Measured	Predicted
Δx	**0.78**	**0.886**	**1.14**	**1.13**
Δl_{max}	**0.211**	**0.239**	**1.13**	**1.13**
E_P	**342.6**	**562.9**	**1.64**	**1.64**
E_K	**173.1**	**284.5**	**1.64**	**1.64**
E_E	**153.6**	**252.6**	**1.64**	**1.64**

Table 3 - Measured parameters and their scale factor between SMM #1 and SMM #2 compared to the predicted scale factor. Δx: horizontal displacement of the centre of gravity during the stance phase; Δl_{max}: maximal spring compression; E_P: gravitational potential energy; E_K: kinetic energy; E_E: elastic energy. Predicted scale factor for lengths (Δx, Δl_{max}) was C_L=1.13. Predicted scale factor for energies (E_P, E_K, and E_E) was $C_M.C_L^2.C_T^{-2}$=1.64.

The Figure 2 shows that, during the first half of stance phase, E_P and E_K decreased, while E_E increased. Conversely, during the second half of stance phase, E_P and E_K increased while E_E decreased. For both SMM #1 and SMM #2, the R=(E_P+E_K)/E_E ratio reached the same mean value and was constant (4.1±0.7) between 30 and 70% of contact time. When out of the 30-70% of time contact interval, the ratio was not constant anymore and reached much high values.

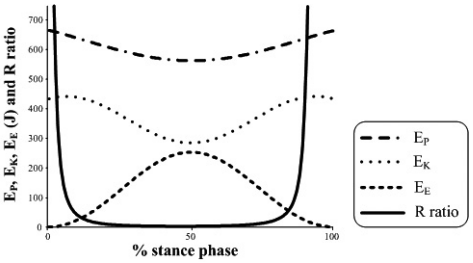

Figure 2 - Evolution to time of E_P, E_K, E_E, and R ratio for SMM #2.

4- Discussion

The two models SMM #1 and SMM #2 bounced symmetrically (Table 2), which proved that the scaling principle used to determine parameters of SMM #2 led to a consistent simulation with a mechanical energy exchange which is typical of running gait (Figure 2) (Biewener, 2006, Cavagna *et al.*, 1964). Moreover, our method enabled us to make SMM #2 dynamically similar to SMM #1, with a single scale factor for lengths (l, Δx, Δl_{max}), and a single scale factor for energies (E_P, E_K, E_E) between the two models (Table 3) as suggested by Alexander and Jayes (Alexander and Jayes, 1983).

Our results showed that the $R=(E_P+E_K)/E_E$ ratio i) was constant during the stance phase of running, and ii) reached the same value for two different-sized spring-mass models which are in similar dynamic conditions. The high ranked values obtained for R ratio before 30% and after 70% of stance phase were due to the absence of elastic energy (E_E, denominator of our R ratio) at the first and at the last instant of the simulation because the spring was not yet compressed ($\Delta l=0$). This phenomenon occurred because the spring-mass model did not allow any initial elastic energy to be considered prior to leg touch down. This was a limit of simulated spring-mass model, because in human running, a leg muscles pre-activation occurs before heelstrike (Komi, 2000, Wakeling *et al.*, 2001) and thus enables a potential elastic energy storage prior to ground contact.

By taking our approach in the opposite direction, our findings revealed that when two spring-mass models behaved in such a way that they had the same value of the $R=(E_P+E_K)/E_E$ ratio, there was between them a scale factor for lengths, another scale factor for masses, and a third scale factor for times, i.e. they moved in dynamically similar fashion. It thus appeared that our R ratio could be used as dimensionless number to induce dynamic similarity between different-sized runners, because it included mechanical energy transfers occurring during running (Biewener, 2006, Cavagna *et al.*, 1964, Lee and Farley, 1998). More generally, because it was based on the spring-mass model, the R ratio could be used for the study of dynamic similarity during bouncing gaits in both humans and animals. Previous studies on walking (Bisiaux *et al.*, 2003, Moretto *et al.*, 2007) showed that dynamic similarity led to a lower inter-subject variability when data were expressed in their dimensionless form. This lower data variability could be useful to enhance the ability of a statistical analysis to distinguish between groups. It could be very interesting to obtain these results during running gait.

We propose to call the R dimensionless ratio "Mo-De-La" in reference to its authors (Moretto, Delattre, Lafortune), and to evoke the idea of running modelling: Modela number = $\frac{E_P + E_K}{E_E}$. Because this dimensionless number was based on mechanical energy transfers occurring at the Cg of a simulated bouncing mass, future investigation should aimed to validate it during *in vivo* human running.

5- References

[A1] Alexander R.M. Optimization and gaits in the locomotion of vertebrates. In Physiol Rev, 69(4): 1199-227, 1989.

[A2] Alexander R.M. Simple models of walking and jumping. In Hum Movement Sci, 11: 3-9, 1992.

[AJ1] Alexander R.M., Jayes A.S. A dynamic similarity hypothesis for the gaits of quadrupedal mammals. In J. Zool., 201: 135–152, 1983.

[B1] Biewener A.A. Patterns of mechanical energy change in tetrapod gait: pendula, springs and work. In J Exp Zoolog A Comp Exp Biol, 305(11): 899-911, 2006.

[BM1] Bisiaux M., Moretto P., Lensel G., Thevenon A. Determination of an expected plantar pressure threshold: dimensionless approach use to reduce the variability of the plantar pressures. In Ann Readapt Med Phys, 46(8): 539-44, 2003.

[BD1] Bullimore S.R., Donelan J.M. Criteria for dynamic similarity in bouncing gaits. In J Theor Biol, 250(2): 339-48, 2008.

[CM1] Cavagna G.A., Margaria R. Mechanics of walking. In J Appl Physiol, 21(1): 271-8, 1966.

[CS1] Cavagna G.A., Saibene F.P., Margaria R. Mechanical Work in Running. In J Appl Physiol, 19: 249-56, 1964.

[DL1] Delattre N., Lafortune M.A., Moretto P. Dynamic similarities and dimensionless approach to running. In J Biomech, 40(Suppl 2): S316, 2007.

[DK1] Donelan J.M., Kram R. Exploring dynamic similarity in human running using simulated reduced gravity. In J Exp Biol, 203(Pt 16): 2405-15, 2000.

[FF1] Farley C.T., Ferris D.P. Biomechanics of walking and running: center of mass movements to muscle action. In Exerc Sport Sci Rev, 26: 253-85, 1998.

[FG1] Farley C.T., Glasheen J., McMahon T.A. Running springs: speed and animal size. In J Exp Biol, 185: 71-86, 1993.

[FL1] Ferris D.P., Liang K., Farley C.T. Runners adjust leg stiffness for their first step on a new running surface. In J Biomech, 32(8): 787-94, 1999.

[K1] Komi P.V. Stretch-shortening cycle: a powerful model to study normal and fatigued muscle. In J Biomech, 33(10): 1197-206, 2000.

[LF1] Lee C.R., Farley C.T. Determinants of the center of mass trajectory in human walking and running. In J Exp Biol, 201(Pt 21): 2935-44, 1998.

[MV1] McMahon T.A., Valiant G., Frederick E.C. Groucho running. In J Appl Physiol, 62(6): 2326-37, 1987.

[MB1] Moretto P., Bisiaux M., Lafortune M.A. Froude number fractions to increase walking pattern dynamic similarities: application to plantar pressure study in healthy subjects. In Gait Posture, 25(1): 40-8, 2007.

[TR1] Thorstensson A., Roberthson H. Adaptations to changing speed in human locomotion: speed of transition between walking and running. In Acta Physiol Scand, 131(2): 211-4, 1987.
[WV1] Wakeling J.M., Von Tscharner V., Nigg B.M., Stergiou P. Muscle activity in the leg is tuned in response to ground reaction forces. In J Appl Physiol, 91(3): 1307-17, 2001.

Essential Ski Characteristics for Cross-Country Skis Performance (P251)

Mikael Bäckström[1], Leon Dahlen[2], Mats Tinnsten[3]

Abstract: Winner or trail hog? Much depends on the ski characteristics. The manufacturing of skis is a complicated process involving several materials and different process steps. This gives as a result that every ski obtains unique characteristics such as span curve and bending stiffness etc. For high performance skiers as the member of the Swedish ski team the importance of equal characteristics of each ski in a pair is vital. The process of matching skis to a pair is the process of finding two individual skis with the most similar characteristics. This is traditionally done by hand with simpler equipment. Our measurement system is developed for faster and more accurate ski characteristics assessment. The characteristics do impose the overall performance of the ski. It produces the span curve with very high accuracy and gives a good representation of the pressure distribution over the full length of the ski. The measured characteristics could, in our opinion, also be used in selecting skis for different weather and track conditions. The ski measurement system has been used by the Swedish cross-country team during the last 2,5 years which have resulted in a faster and more accurate matching of skis. In collaboration with the Swedish ski team have also an investigation concerning correlation between ski characteristics and weather and track conditions has been initiated with some preliminary results already obtained.
Key words: Cross-country skis, ski characteristics, pressure distribution, matching of skis.

1- Introduction

No singular cause determines the overall performance of a race ski. First of all, we have of course the definition of performance to be established. Parameters in cross-country skiing are typically: glide, grip, weight, stability, and the performance is often rated through a combination of those parameters reflected on if the skis are for classical or skate races? (Ekström, 1981; Ekström, 1987).

1, 2, 3. Department of Engineering, Physics and Mathematics, Mid Sweden University, 831 25 Ostersund, Sweden - E-mail: Mikael.Backstrom@miun.se - Leon.Dahlen@miun.se - Mats.Tinnsten@miun.se

However, there are some structural ski factors that are more essential than others when considering glide and grip in general (Kuzmin and Tinnsten, 2006). The manufacturing process of skis consists of many steps influencing the final ski characteristic. As a result of the manufacturing strategy, with great parts of manual labor, do the products show variances in quality? This implies that each ski is an individual with its own features. In order to achieve a pair of skis that could satisfy a number of different demands, the first task is to actually pair skis with similar attributes. The next task is to transfer these attributes to ski pair characteristics.

It is almost impossible to obtain more explicit information from the manufacturers of skis about their construction methods and design to achieve certain ski characteristics. This is treated as business secrets and is used as a sales argument for high-end race skis. Hence, many of the manufacturers do have their own equipment/method to classify their skis.

One of the main features that are constructed into a ski is the rigidity and stiffness along the length of the ski. An example of this is the result of cooperation between Salmon and Subaru Factory Team. This is a very important feature influencing the span of the ski and hence also the pressure distribution under the ski in interaction with the snow (Antti *et al.*, 1993, Internet www1). Since the predominant factor for glide and grip depends on the pressure distribution of the skis, the means and method to measure this is of greatest importance (Erkkilä *et al.*, 1986).

Recently private companies have also presented machines that measure span curves and to some extent rigidness of the ski (Internet www2). This can of course be of guidance to know more about some of the important parameters but principles have to be developed further.

In order to have the ability to measure the pressure distribution and the ski span curve, a completely new measuring apparatus was designed and manufactured. This was done as a result of the lack on the market of a computerized logging device with accuracy and speed to fulfill our demands for research work.

2- Experimental setup and method

A measurement device designed to perform measurements of ski characteristics has been developed. One ski at a time can be measured for ski characteristics such as span curve and the ski ground-pressure distribution when loaded. The experimental setup consists of a frame made of aluminium, a load unit and a measurement system. A simplified overview of the experimental setup is presented in Figure 1.

The aluminium frame (4) and (5) is designed to withstand the forces generated from the loading unit without any significant deformations. The load unit is mounted on the beam (6) and the applied load, measured by a load cell, can be adjusted to the desired value by a power screw in contact with the ski. The load cell is connected to a digital display and the whole load unit can be adjusted along the ski depending on where the load should be applied. A detailed view of the load unit is shown in Figure 2. Accuracy of the load cell is ±0.05 kg.

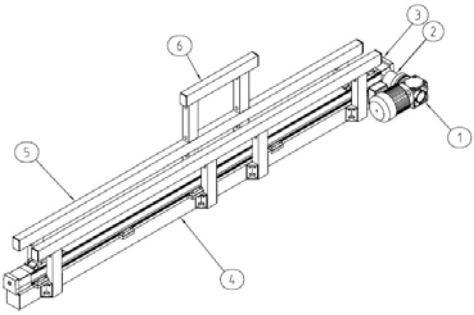

Figure 1 -View of the ski test rig.

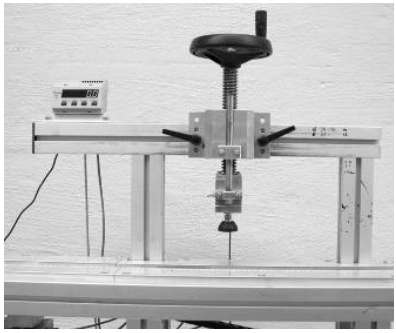

Figure 2 - The load unit.

To obtain the span curve two linear position sensors are used. One sensor is used to measure the position of the ski surface above the reference surface (5) and one to calibrate for differences of straightness of the reference surface. By the load cell the distribution of the contact force of the ski surface in contact with the reference surface (5) can be measured when the ski is loaded. The longitudinal pressure distribution, hereafter denoted PPD (the proportional pressure distribution), is directly proportional to the contact force. The load cell has a capacity of 1 kN. All the sensors are transported by a linear drive unit (3) continuous during measuring over the whole measuring range of a ski length. The linear drive unit is driven by a gear motor (1) connected together by a coupling (2). Signals from the sensors are sampled continuously at a frequency of 200 Hz and stored in a computer. When the sensors reach the end of the measuring length the linear drive unit will stop automatically. The position of sensors during measuring is measured by an incremental shaft encoder connected to the rotating part in the linear drive unit. The maximum length of a ski which can be measured is 2.1m. Computer software has been developed to sample signals and show the result of measured span curve and the pressure distribution which will be presented in tables and diagrams. One measuring cycle consist of measuring a pair of skis.

The first step in the measuring process is to open a new ski test and record data of the skier into the computer software. After this the type of ski (classic or skate) is specified. To measure a pair of skis the first ski is placed and fixed in the test rig, where after the load unit is positioned where the load should be applied.

The ski is loaded to the desired value with the power screw and the measuring process on the computer is initiated. The measuring process is started by activating the gear motor to the linear drive unit. First the span curve will be measured, then the pressure distribution. After this the ski is unloaded and replaced with the other ski in the pair and the measuring process is repeated. When the measuring process is ended the software produces the result of the data automatically and tables and diagrams for both skis are presented. In Figure 3 the ski is placed in the test rig and prepared to be measured.

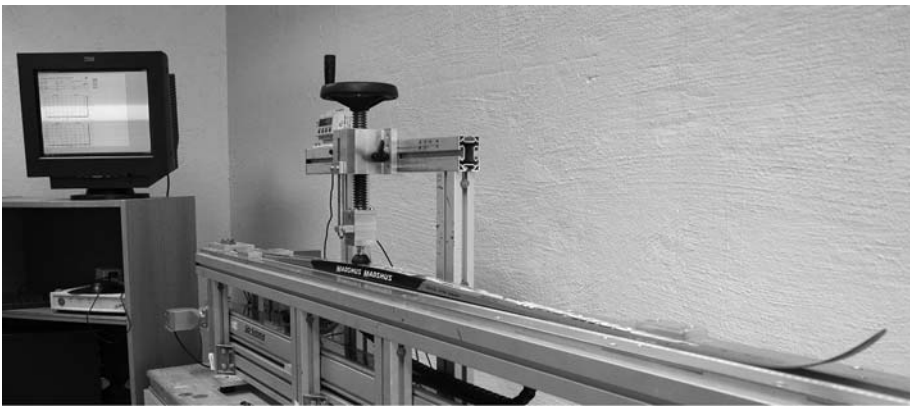

Figure 3 - The ski placed in the test rig.

3- Results

Measurements have been conducted to a load of 40.0 kg for both classic and skating skis for men. For women the load has been between 25 to 30 kg for classic skis and 35 kg for skate skis. The position where the load should act is for skate skis 70 mm behind the point of balance of the ski for both men and women. For classics skis the position of load is placed 140 mm for men and 100 mm for women behind the point of balance of the ski. More than 500 pair of skis have been studied by this method by the Swedish ski team for more than 2.5 years.

In Figure 4 the results from measuring a pair of skate skis is shown. Figure 4 a) shows that the PPD curve is similar for the same for both skis and the span curve in Figure 4 b) has a span maximum of 3.30 mm at a distance of 993 mm from the rear end of the ski. The PPD curve also shows that the maximum value at the front glide zone is lower than at the rear glide zone.

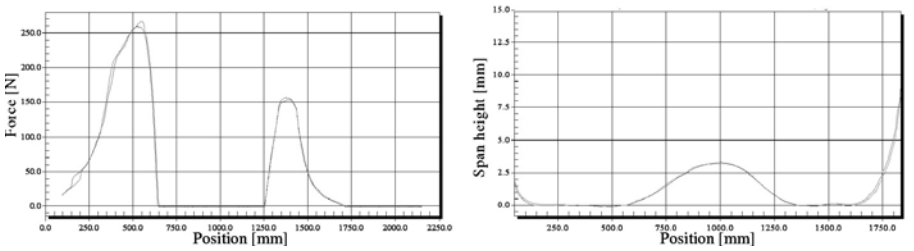

Figure 4 - The PPD curve (a) and the profile of the span curve (b).

Figure 5 shows how results from measurements of classic skis in the test rig can differ when comparing skis delivered from ski manufacturers. By this test, skis that differ too much can be sorted out in an early state of the selecting process of skis for the skiers.

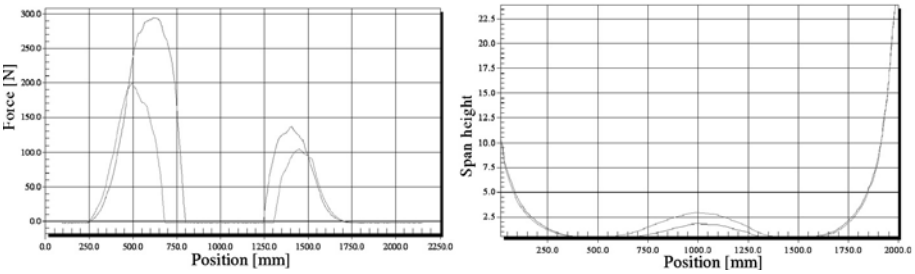

Figure 5 - PPD curve and span curve of a pair of classics skis.

Figure 6 shows the measured pressure distribution profile of two different pair of classic skis for the same skier. The curves for the front glide zone pressure distribution can differ between the skis and the profile in Figure 6 a) shows a smoother profile compared to the profile in Figure 6 b). This is also the case for the rear glide zone pressure distribution profile.

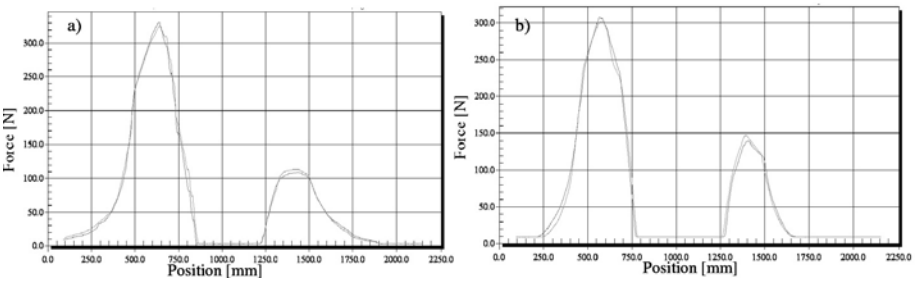

Figure 6 - PPD profiles of two different pair of skis.

In Figure 7, a typical relationship between the front and rear pressure distribution curve is shown for men (a) and women (b). The ration between the rear top and the front top of the force distribution curve is much higher for men compared to women.

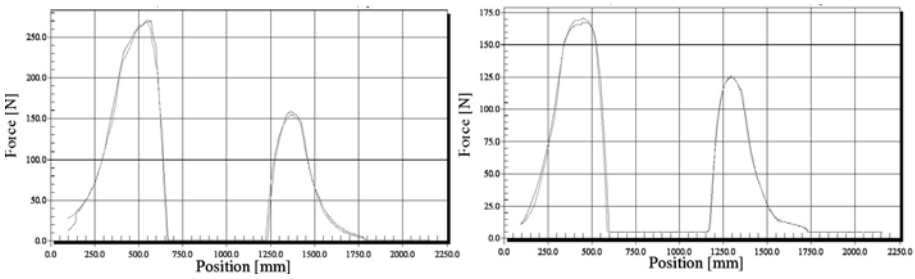

Figure 7 - View of a typical profile of the PPD curve for men (a) and women (b).

4- Discussion and conclusions

Although the Swedish national team in cross country skiing have used the ski measurement system intensely for nearly three years there is no clear correlation between the ski pressure distribution or the span curve and to the weather or track conditions. Initially the team used the system to determine the skis span curve with higher accuracy and less time consumption than with earlier methods. Later they also began to routinely determine the pressure distribution for the team members` skis. At present, nearly all skis in the national team have been measured and all of the data been saved. The measurements have been performed using a predefined method, i.e. the weight on the ski, the point of applying the weight etc. has been equal from measurement to measurement. According to Mikael Book, former member of the waxing team in the national team, the measurement system has provided the team with a much faster and more accurate measurements of the span curve. The system also has provided the team with new knowledge of the skis pressure distribution curve and facilitated the process of pairing two individual skis to a pair. According to Mikael Book, he and the team has gained experience and understanding of ski performance by using the system and it has also simplified the selection of skis for a particular race occasion. Although no comprehensive explanation exists for what makes the skis glide optimally related to weather conditions, some factors have been revealed. For skating skis used in cold conditions, the maximum span height should be lower than in warm/wet conditions. Also the arching of the span and the pressure zone in front of the binding should be longer in cold conditions compared to warm/wet conditions. For skis used in the classical techniques, the grip wax and consequently the maximum span height is of the most importance regardless of weather conditions. Here also the span length, especially in front of the binding, is of great importance.

5- Future consideration

The results from this study reveal the problem of understanding in which way different characteristics of a modern cross country racing ski influence its performance in a race situation. Here the span and the mean (perpendicular to the ski) pressure distribution curve have been investigated in order to find some correlations to weather and track conditions. There are of course several other characteristics that are of great interest when trying to understand what makes a ski perform well on the track. The mechanical construction together with the material and the assembly of the ski is of course of great importance – this gives together with the chosen materials the span curve and the pressure distribution for the track. If the pressure distribution and span characteristics are known then a method for attaining this could be developed. But also other characteristics that are believed to be of great importance must be investigated; torsional stiffness, vibration characteristics, material and structure of the running surface, etc.

6- References

Antti P. Leppävouri, Matti Karras, Heikki Rusko, and Jukka T. Viitasalo, "A new method of measuring 3-D ground reaction forces under the ski during skiing on snow", Journal of Applied Biomechanics, 9, 315-328, 1993

Ekström H., "The force interplay between the foot, binding, and ski in cross-country skiing", Skiing Trauma and Safety, Sixth International Symposium, ASTM STP 938, American Society for Testing and Materials, Philadelphia, pp. 100-109, 1987

Ekström H., "Force interplay in cross-country skiing", Scand. Journal of Sports Science, 3 (2), pp. 69-78, 1981

Erkkilä J., Pihkala P., Rahnikainen A. and Spring E., "Studies of the mechanical properties of cross-country skis", Acta Polytechnica Scandinavica, Appiel Physics series No. 154, Helsinki, 1986

Internet www1, http://biomekanikk.nih.no/xchandbook/ski4.html, 2008

Internet www2, http://www.ernordic.com/ski_data.htm, 2008

Kuzmin and Tinnsten, "Dirt absorption on the ski running surface - Quantification and influence on the gliding ability", Sports Engineering pp 137 - 146 International Sports Engineering Association - Sheffield, UK2006

Extreme Sports Perceived by Students of Faculties of the Physical Education, Tourisms and Recreation (P252)

Robert Bak[1], Roman M. Kalina[2]

Topics: Extreme sports.
Abstract: The aim of the research was to check two issues: (1) what elements, according to the students, are decisive with regarding one aspect of physical activity as extreme? (2) which sports in the surroundings are regarded as extreme? A number of 193 students (120 men students, 73 women students) of the physical education and the tourism and recreation were provided with the questionnaire surveys from the Rzeszów University (Poland).
The students have associated the extreme physical activity with the one which is conceived as a danger for health and life most commonly (73%). To identify this issue they were describing it as: „danger" (21%), „ threat of health" (20%), „risk" (20%), „ threat of life" (10%). Males more often (15%) than females (5%) have associated the extreme forms of physical activity with „risk" (15%) and with „threat of health" (6%).
A rock climbing is an extreme sport connected with „land" most frequently listed (28%), „diving" connected with „water" is listed by 30%, and parachuting connected with „air" – 60%.
Only 5% of respondents assume that „the cooperation difficulty" of the problems, connected with the physical activity, decides about its extremity. However, burdening the organism with the physical effort is a factor to recognise a given physical activity as extreme (e.g. ski expedition to the North Pole).
The findings show that there is a necessity of including the knowledge about the extreme forms of human activity in the educational system of the physical education and the tourism and recreation specialists. The results that have been presented are a part of research grant and the students choice and preferences about extreme sports. This research concerns the system of selection of candidates and training in military, police formations etc. and at rescue services among others.
Key words: extreme sports, students physical education, students tourisms and recreation.

1. Faculty of the Physical Education, University of Rzeszow, Towarnickiego 3, 35-959 Rzeszow - E-mail: robo@interia.pl
2. Faculty of the Physical Education, University of Rzeszow, Towarnickiego 3, 35-959 Rzeszow - E-mail: kom.kalina@op.pl

1- Introduction

The term "extreme sports" is one of the best recognized term since some years in the whole world. More and more people are prepared to undertake the risky physical activity which is commonly associated with sport. The Extreme Sports Channel was established in 1999. It is the first television channel dedicated to promoting the quickly developing extreme sports and new lifestyle. Nowadays it is available in 60 European, African and Middle East countries. The programmes are broadcasted twenty-four hours a day, seven days a week, for almost 20 millions of viewers in 12 languages. The examples of growing popularity of extreme sports might be multiplied. New clubs and associations, another magazines, television programmes, web pages are being developed. When one Google "extreme sports" 21,900,000 answers can be found.

On the one hand this phenomenon is diligently documented by reports of the participants who work in an extreme conditions (e.g. Ardito 200, Messner 2003). On the other hand this phenomenon is studied more and more precisely by scientific methods (e.g. Gikow 2005, Kalina and Bąk 2007). However, there is no generally accepted definition of extreme sports (the extreme form of physical activeness). Matuszyk (2002) claims *"the extreme sports are those in which the important element of sport's fight is the activity of its subject directed on the stability of extreme situation in which the fight goes"*. In these groups he lists "sports of the space" (e.g. climbing, alpinism) with its characteristic aspects: social, symbolic, personality. In ours researches we use Kalina's definition (2002)where is the division into "*extreme sports in the broad sense*" and „*extreme sports in a narrow sense*". To the first group we rate: „*(...) Olympic sports and all variations of professional sports, as well as certain forms of physical activities which go beyond the formula of Olympic sport, but because of the character of the performance of the risk undertaken they demand from the athlete not only specific physical and/or mental predisposition but also an adequate training*". Extreme sports in a narrow sense would include „*(…) only those Olympic disciplines and those domains of professional sport, as well as those forms of physical activities which go beyond the formula of Olympic sport and the practicing of which is associated with a high health or life hazard*".

One of the most important problem is identification of extreme form of physical activity including extreme sports by persons professionally involved in physical training (from reaction to a professional sport). The aim of researches was to decide about two issues: (1) Which elements according to students decide about recognizing a particular physical activity as extreme? (2) Which sports that are situated in a given environment (land, water, air) are considered as extreme?

2- Method and material

There were 193 students of physical education and tourism and recreation of Rzeszów University (Poland) that were put into questionnaire's researches – 120 of them were male students and 73 were female students. The students were examined with help of anonymous questionnaire. In this questionnaire were two main questions:

1. List the most important, according to you, element which authorize to recognize a particular sport or physical activity as extreme.

2. List extreme sports which are carry out in a particular environment - land, water, air.

We have recognised three areas as scientific criterion of identification of extreme forms of physical activity: (1) risk health's or lives, (2) difficulty coordinating, (3) burdening the organism with a physical effort (Kalina and Bąk 2007).

3- Results

The researches that were carry out have proven (fig. 1), that 73 % of students associate the extreme forms of physical activity (including extreme sports) with danger for heath and life. Only 5% show on the necessity of revealing the high level of physical coordination so that this physical activity could be accomplished. However, no one pointed out on completely high burden of organism with physical effort which constitutes extreme challenge for human organism.

The elements that are counted to the area 1, respondents expressed with the expressions "danger", "threat of health"(21% each), "risk" (20%) or "threat of life" (10%) (fig.2). When we take the gender of respondents into consideration: "danger" – women 9%, men 11%, "threat of health" – women 6%, men 15%, "risk" - women 5%, men 15%, "threat of life" – women 4%, men 6%.

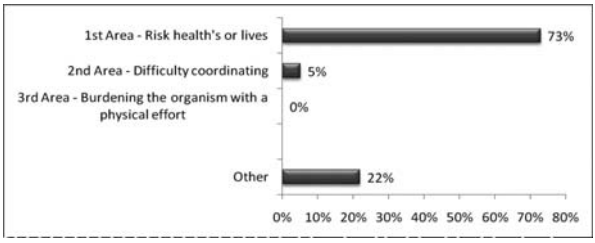

Figure 1 - Declared the students answers (n=193) with subordinating to the area of identification.

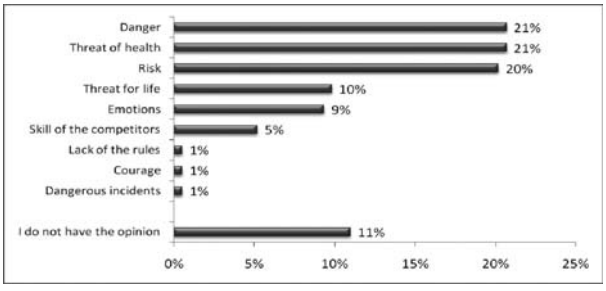

Figure 2 - The structure of declared by students (n = 193) the elements of the identification of the extreme forms of the physical activity.

Most of presented answers are qualified to the first area of identification of extreme forms of physical activity (73%), however, none respondent associated this activity with the third area (fig. 1).

While identifying the kinds of physical activity (extreme sports), students of studied group displayed with significant knowledge of the phenomenon. They qualified the forms of physical activity that they know in an accurate way depending on environment in which these forms are accomplished (fig. 3, 4, 5). Students identified accurately

33 kinds of sports (accurately – in a way of ascribing the correct kind of environment, in which they were accomplished).

From the forms of physical activity in water environment (fig. 3) the most frequently listed were diving (30%); windsurfing (16%); waterskiing and kitesurfing (10% each). Other forms of physical activity were listed by 1% to 9% of respondents. 14% of respondents were not decided.

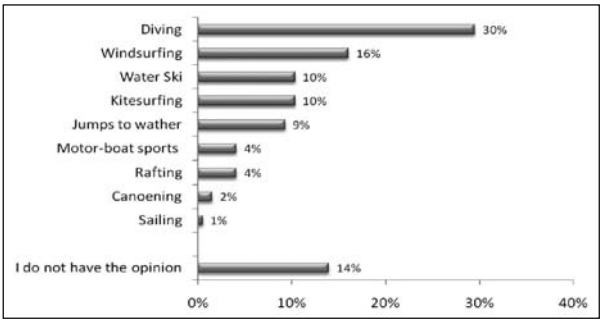

Figure 3 - The structure of declared by students (n=193) the kinds of extreme sports realized in the water environment.

Among declared answers that are related to sports done in air environment (fig. 4) most of the respondents pointed out on parachute jumps (60%), what seems to be obvious when because of the association of air sports mostly with parachuting that can be presented in different forms and variants. It was listed one after the other on B.A.S.E. jumping (17%), bungee jumping and paragliding (8% each). 1% of respondents showed on aerobatic manoeuvres. In the group 6% of respondents could not show any form of physical activity.

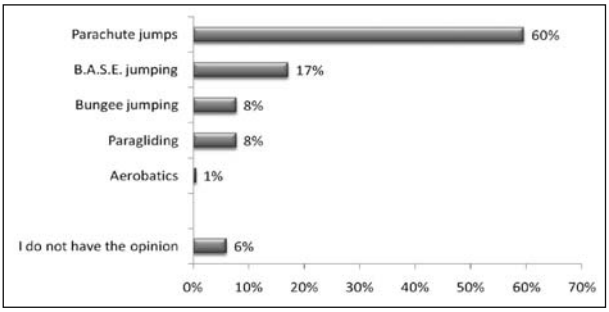

Figure 4 - The structure of declared by students (n=193) the kinds of extreme sports realized in the aerial environment.

The result of the research that considers the knowledge about the forms which are realized in air environment (fig. 5) showed that they are the most numerous group that is familiar for respondents. They are associated mostly with climbing (28%) and motocross (12%). The other forms were pointed out by 1 to 7 % of respondents. 17% of respondents could not show any form of physical activity that is realized in that kind of environment.

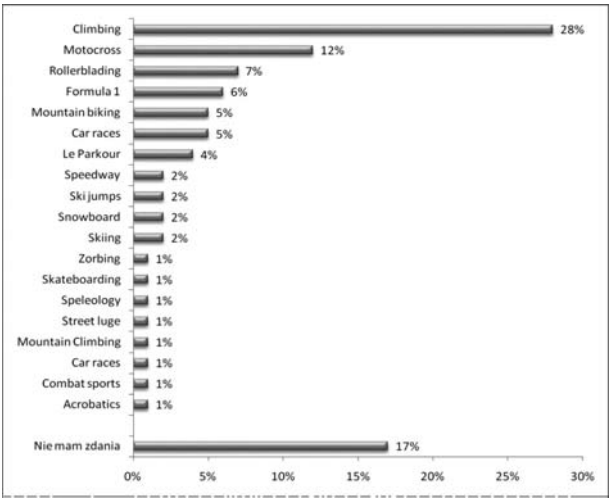

Figure 5 - The structure of declared by students (n=193) the kinds of extreme sports realized in the land environment

Two of the respondents had some difficulties in identifying the form of activity called bungee jumping. They had wrongly decided that it was a land sport, than they had change their decision and as a result decided correctly that this was air sport. This fact means that at the beginning they did not understand the essence of the experiences connected with the jump and with free falling of course in the limit of the freedom which is given by harness and special line.

4- Discussion

The results of the researches showed that in students' declarations which considers the most important criterion of identification of extreme forms of physical activity are common elements. The biggest group equate the extreme forms of physical activity with "threat of health" or "threat of life" and "risk" (that we connect with loosing health or life). It means that the main criterion of extreme is direct danger of loosing health or life. Only small number of people showed on significant difficulty that coordinates these forms of activity, by connecting it with necessary abilities of sportspersons. According to accepted models of criteria of identification of forms of physical activity (Kalina and Bak 2006), elements showed by the respondents were contained in two (from three possible) areas of identification. The lack of references to the *"burdening the organism with a physical effort"* criterion proves that students unfortunately do not associate irrational physical effort with the factor that can make essential threat for a human. The media ones for a while inform even about deadly descents during sport fight or individual physical activity (jogging, gym etc.). The biggest number of students declare that they do climbing, mountain cycling and combat sports. These are sports and forms of extreme physical activity that are popular in academic environment in many countries. Despite that students declared that they train more original forms like canoeing, le parkour, paragliding or diving. In Polish universities' education there is no subject which considers problems of extreme forms of physical activity or extreme sports. In studies

program of physical education and partly also in tourism and recreation the exercises that are consider as extreme are included, however when optional classes are taken into consideration there has to be noticed that students have the possibility to take part in classes devoted to rock climbing and diving.

The presented results are part of research grant which considers perception and students' preferences about extreme sports. The application of these researches are also about the system of candidates' selection and trainings in military, police and different units and also in rescue service (life-saving). In the nearest future there have to be taken into account that persons of motoricity abilities which are qualified as extreme forms of physical activity will be used in emergency (anti – terrorist) and rescuing operations. For universities there is a perspective of implementing the theory and the practice of the extreme forms of physical activity.

5- Results

1. The perception of the phenomenon of the extreme forms of physical activity (including extreme sports) among students of physical education faculties and students of tourism and recreation is low.
2. The results of the researches justify the necessity of including the knowledge about the extreme forms of physical activity in physical education, tourism and recreation specialists' educational system.
3. The knowledge of kinds of the extreme forms of physical activity that are classified according to the environment in which they are realized, in the studied group is comparatively high.

6- References

[A1] Apter M. (1992). Dangerous Edge: The Psychology of Excitement, Free Pr.

[A2] Ardito S. (2000) History of the Great Mountaineering Adventures, The Mountaineers Books, Seattle.

[G1] Gikow L. (2005). Extreme sports, Scholastic Library Pub.

[K1] Kalina R. M. (2002). Definition and criteria of the identification of extreme sports – research and educational perspectives, Wychowanie Fizyczne i Sport, tom XLVI, nr 1, część 1, Warszawa, AWF, 511-514.

[KB1] Kalina R.M., Bąk R. (2007) „Extremum of the motor recreation" [In:] Duricek M., Gallo P. (red.) Trendy Pohybovej Rekreacie a Sucasny Zivotny Styl , Univerzita Pavla Jozefa Safarika v Kosicach (Slovakia), s. 166-169

[M1] Matuszyk A., (2002). Sporty ekstremalne – kwalifikacja genologiczna i sugestie typologizacyjne, Wychowanie Fizyczne i Sport, tom XLVI, nr 1, część 1, Warszawa, AWF, 229-231.

[M2] Messner R. (2003) „Die Weisse Einsamkeit. Mein langer Weg zum Nanga Parbat", Pier Verlag GmbH, Munchen

The computer record and analysis of struggle dynamics of the judo fight (P253)

Jerzy Kulasa[1], Roman M. Kalina[2]

Topics: Innovation & Design.
Abstract: The purpose of every sport rivalry is the result (in general victory). In the judo like in every sport fights, rivalry consist on direct wiping off two competitors. The result of that kind of fight is correlated with the level of training and in the same time with health, psychomotor competence and the tactical preparation. However, it is difficult to decide by using some analytical methods whether the competitor is able to win in a given and next fights. The winner is the one who, according to the principal judo rule, will use in an optimal way his brain together with the body. That is why according to some judo experts assessment the data from the competitors fights' observations might be more prognostic. The simplest analyses are the observations done by registering events using video, or writing the results down on the paper sheets and processing this information e.g. by adding determined action. The modern approach provides necessity of analyzing some events during the fight (as well as record) in the function of time. The method of observation data registering together with using some symbols which are a set of codes of given catches and throws in judo is a very time consuming and troublesome method in the sense of processing information. Also laborious is method which the observation data are registered in a traditional way by using special sheets.

The modern computer technologies enable to register the data much faster and also they enable data's multifaceted processing. The pilot research shows that applying this innovative method is highly effective.

The main aim of this work is the presentation of the method. Using this method goes beyond the format of judo fights and might be applied in all kinds of sport fights and self-defense.
Key words: struggle dynamics; judo fighting; innovation; software tools; combat sports.

1. Faculty of the Physical Education, University of Rzeszow, Towarnickiego 3, 35-959 Rzeszów - jkulasa@wp.pl
2. Faculty of the Physical Education, University of Rzeszow, Towarnickiego 3, 35-959 Rzeszów - kom.kalina@op.pl

1- Introduction

The aim of each competition is the result (most often that is a victory). In judo, like in most martial arts, rivalry is all about direct clash between two competitors. The result of this fight is correlated with the level of training, which depends on health, psychomotor competence and the tactical preparation. By using analytical methods it is hard to decide whether the competitor is able to win in this and in the following fights. The reason for that is that during the fight all quantitative and non-quantitative features are revealed in a syntactic way. The winner is the one who, according to the main principle of judo, uses his brain and body in an optimal way (Kalina 2000, Kano 1974). That is why, according to some judo experts, more prognostic are the data from the competitors' fights observations.

The long-term practice of applying different registering and sports fight analysis methods by scientists and coaches shows the best how important is this issue. The simplest analysis' are about observation of events that are registered by audio technique, video, writing results on the paper sheets, and processing this information by e.g. summing given activities (the number of throws, the time of fight in ne – waza etc.).

The first global scale attempts in reference to judo were taken in 1964 during the 18th Olympics Games in Tokyo. The events during the fight were recorded by the tape recorder (Doi 1971). In the next few years researchers were using special observation sheets (Sikorski 1971). Together with the development of the technique they started using the video (Matsumoto *et al.* 1978, Sikorski 1971, Sterkowicz and Kęsek 1990). During the 1980s they tried to use computers for registering and fight analyses. They even tried to create a special programs for this, the forerunner of that were Polish scientists (Franecki *et al.* 1985, Naumienko and Franecki 1988, Baranowski 1989). Despite of registering in the traditional way or by using computer technologies, researchers were also using different languages – from the description according to the judo terminology (e.g. seoi-nage, kata-gatame) to he computer symbolism (Naumienko and Franecki 1988) or graphic symbols (Adam *et al.* 2005, Laskowski 2006). The method of recording the observation data by using symbols, which in fact are the set of particular judo holds and throws codes is especially difficult in a sense of processing information.

The most important in the modern analysis of events during the fight (as well as the record) is the assumption of the need to consider the function of time (Sterkowicz and Maślej 1999). The greater accuracy of this method (e.g. in comparison with the sheet of the observation) is a real possibility to full reproducing the course of the fight - following after oneself events (the attacks, defences, penalties etc.).

The attempts of that kind of record (processing the information) were taken while using all already mentioned languages. The empiric method of researching of fights dynamic is the closest one to the possibility of using the function of time in registering and judo analysis – in the same time it is the main empirical order of combat sports theory (Kalina 2000). The central advantages of this method is the possibility of not only analyzing events in the function of time but also relating the observation data to actual result of the fight (Kalina 2002, Boguszewski and Boguszewska 2006). This method is used in different kinds of combat sports as well.

All the mentioned methods are characterized by many inconveniences (labour intensity, need to archive the audio/video material and the observation sheets, limited comparison of fights of particular competitor and potential rivals in the short time etc). However, the most serious restriction is fights' analysis and comparisons during a particular championship. The organization and the data processing does not allow coaches and competitors to gain some useful information while steering their activity in a very short time.

2- The specific feedback systems in sport

Registering, description, analysis and vetting of competitors activities are impossible during the competitions and training (in which competitors are taken part) without using the high quality of testing procedures which meet objectivity's and accuracy's criterion. That is why in a number of disciplines and sport events fast working feedback systems, which are about modern computer technologies is used more and more frequently (Baca and Kornfeind 2006). These technologies enable much faster data registering, their transforming and also the presentation of collected results. Real time and rapid feedback systems provide innovative and effective support to coaches and athletes (Broker and Crawley 2001). The benefits which arise from the usage of these systems depends on how precisely they can register the particular competitor's activities or how precisely they can create analyses or characteristics and also they depends on how fast and clear these information might be made available to coaches and for competitors. It is possible also to apply feedback systems in the case of the registration and analysis of dynamics of the judo fight. The usage of the advantages of database and of programs that manage these bases may make the coach's work faster and more effective.

3- Human factor in the relation "computer technologies – sport"

A pilot study proves that the interest of Polish sports fight coaches (83%) about the possibility of using specialist programs of judo fight analysis in their training work is getting higher (Figure 1).However, it was settled that 94% of coaches who declare that they are using computer in their work, use in fact mainly the popular programs like the editor of the text, the spreadsheet etc. No one has confirmed that they use a specialists programs that are created for running the trainings and supporting the combat sports. The result of this questionnaire surveys might be connected with the difficulties of reaching to the appropriate programs by 67% of coaches (Figure 2). The analysis of this survey make it possible to notice that the educational factor will be essential. The lack of knowledge is declared by 37% of coaches, and the lack of abilities by 22%. During the programs developers' trainings the information that 70% of costs were given to train the users and to maintain the system were presented.

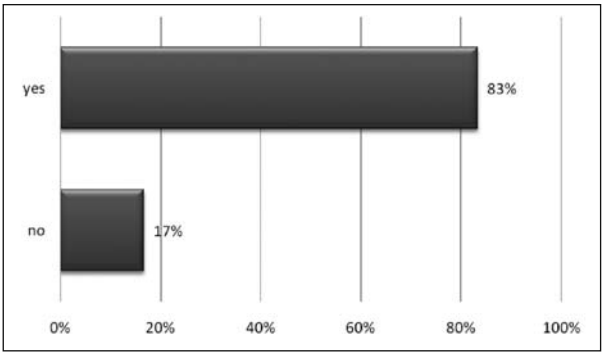

Figure 1 - The proportion of coaches who declared willingness to use specialists fight analysis programs in the training process.

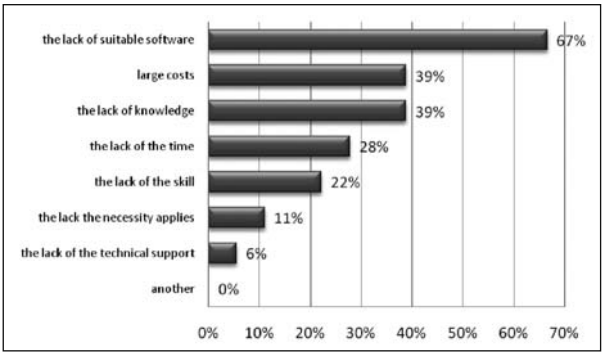

Figure 2 - The proportion of obstacles of using computer in the training work.

4- Relational database as an information management device

Due to the huge amount of generated data during the fight the coach has no possibility to embrace all variable and their numerous combinations. The only chance is the use of computer device that helps in organizing and managing a big amount of information which considers competitor itself and the event on the mat. The data might be managed with help of word processor however, it is difficult to find particular pieces of information in a huge amount. The usage of the spreadsheet is also problematic due to the fact that the attempt of finding information with using more than one criterion is impossible.

The database is the collection of data which are stored in files within the systematized structure (Elmasri and Navathe 200). The systematized structure enables to carry inquiries processing data via providing software that is ordering with relational databases managing system. That is a system based on relational model as the data in this system are organized into the structures which are built on sets and logical relations. The postulates that define relational model are called the rules of the standardization. These rules exist to limit the possibilities of storing the data that are repeated in few tables it means

to reduce the level of refund and to ensure the cohesion in database. In the registering of judo fight dynamic the data are insert with the usage of computer by the coach or the assistant in a systematic way. That makes it possible to gather all necessary information in one place. The appropriate registration and analyses should be made before preparatory activity. The coach inserts the general information about his competitors and their potential opponents (age, weight, country etc) in a form of a chart. Before the appropriate competitions he inserts the data concerning these competitions (name, place etc). The classification of techniques used in the offense and defense and also the combination of punishments for violating the rules should be the constant elements of the data. In special cases coach should have the opportunity to modify and add new techniques in which the main techniques, contracts, techniques which consists of few moves and time are put together. The general logical scheme of the system is showed in the Figure 3.

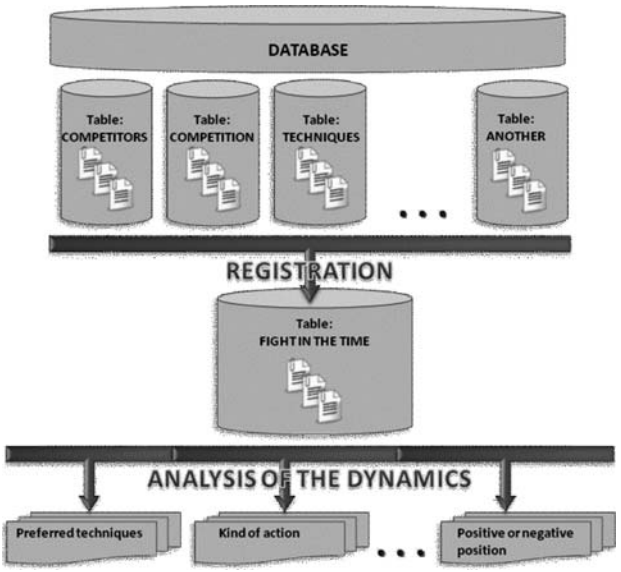

Figure 3 - The general logical scheme.

Thanks to increased number of fights the coach has the possibility to analyze and to generalize the information that concerns the competitor's behaviour during the single fights or during many fights that were carry out in competitions. The final effect might concerns the generating of detailed reports which inform the coach about:

- What kind of activities the competitor does in particular moments during the fight (are these active, passive, technical, not technical activities)
- Effectiveness of those activities
- What are his preferable methods of fights and defence
- When there is adjudication in the fight

5- Discussion and Conclusion

System of the computer registration and analysis of judo fight's dynamic can hand down some precious clues about the strong and weak points of competitor, the whole team or

the opponent. Searching new information throughout analyses of data helps in getting previously unknown but potentially effective knowledge. System of the reflexive information, based on the computer technology might be helpful in improving the training process and divulging factors which are decisive when taking athlete's success into consideration. The application of a given method are far beyond judo fight formula and might be used in all kinds of sports fights and also in self-defence.

6- References

[AS1] Adam M., Smaruj M., Laskowski R. Graficzna metoda rejestracji walki w judo. COS, Warszawa, Sport Wyczynowy, 5-6: 485-486 (in polish: abstract english), 2005.

[B1] Baranowski T. Systemy komputerowe na Igrzyskach Olimpijskich w Seulu. Sport Wyczynowy, nr 1, 1989.

[BB1] Boguszewski D, Boguszewska K. Dynamics of judo contests performed by finalists of European Championships (Rotterdam 2005), Arch Budo (http://www.archbudo.com/) 2(2):OA40-44, 2006.

[BC1] Broker J. P., Crawley J. D. Ad-vanced sport technologies: Enhancing Olympic performance. [in:] J. R. Blackwell (ed.) Proceedings of the XIXth ISBS Symposium, San Francisco 2001, 323-327.

[BK1] Baca A., Kornfeind P. Rapid Feedback Systems for Elite Sports Training, IEEE Pervasive Computing, vol. 5, no. 4, pp. 70-76, Oct-Dec, 2006.

[D1] Doi M. Analiza walk na Igrzyskach Olimpijskich w Tokio. Biuletyn Kodokanu 1967, 7 (W:) Judo, Biblioteka Trenera, PKOl, Warszawa, 1971.

[EN1] Elmasri R., Navathe S.B., Data Models, Database Languages and Database Management Systems, 3rd ed., Benjamin/Cummings, 2000.

[FS1] Franecki J., Sikorski W., Che_stowski P. Komputerowy system analizy walk judo, Instytut Sportu, Warszawa, 1985.

[K1] Kalina R.M. Teoria sportów walki. COS, Warszawa, 2000.

[K2] Kalina R.M. Metoda pomiaru dynamiki walki w sportach walki. In: T.Ulatowski (eds.) Zastosowanie metod naukowych na potrzeby sportu. Biblioteka PTNKF, Warszawa, pp. 245-256 (in polish), 2002.

[K3] Kano J. L`education par le judo. In: J.L. Jazarin: le judo ecole de vie. Paris, 1974.

[L1] Laskowski R. Skuteczność techniczna i taktyczna zawodniczek reprezentacji Polski w judo w wieloletnim procesie treningowym, Wydawnictwo Uczelniane AWFiS, Gdańsk, 2006.

[MT1] Matusmoto Y., Takeuchi Y., Nakamura R. Analytical Studies on the Contests performed at the All Japan Judo Championship Tournament . Bulletin of the Association for the Scientific Studies on Judo. Kodokan, Report 5, p. 83, 1978.

[NF1] Naumienko B.J., Franecki J. 1988. Komputerowa analiza walki judo. Sport Wyczynowy, nr 9, 20, 1983.

[S1] Sikorski W. Obserwacje walk judo. Wyniki badań judo. INKF, Warszawa, 1971.

[S2] Sikorski W. Obserwacje walk judo. Wyniki badań judo. INKF, Warszawa, 1971.

[SK1] Sterkowicz S., Kęsek M. Przygotowanie techniczno-taktyczne zawodników i zawodniczek judo. Rocznik Naukowy AWF w Krakowie, t. 24, p.239, 1990.

[SM1] Sterkowicz S., Maślej P. Analiza przebiegu walki judo na podstawie jej struktury czasowej – badania porównawcze. COS, Warszawa, Sport Wyczynowy, 7-8: 415-416, 1999.

Dynamic Model of a Badminton Stroke (P254)

Maxine Kwan[1], Michael Skipper Andersen[1], Mark de Zee[2], and John Rasmussen[1]

Topics: Tennis & other Racket Sports; Modelling.
Abstract: The purpose of this paper is to contribute to the understanding of dynamic racket behaviour in badminton. The paper describes the development of a dynamic model of a badminton stroke based on experimental data. Motion capture and strain gauge experiments are performed to clarify the movement and accelerations of a badminton smash stroke. Subsequent data processing reveals that due to the speed and acceleration of the movement, neither of the two methods provides the complete picture of the racket's dynamic behaviour, but computational processing of the combination of experimental data together with physical modelling of the racket mechanics allows for an understanding of the basic mechanisms underlying racket movement and deformation. The paper concludes that the elastic deflection of the racket creates a narrow window of opportunity during which the impact is enhanced by the racket's elastic behaviour, and this window must be closely synchronized with the timing of the stroke.
Key words: badminton; racket; dynamics.

1- Introduction

Although badminton racket technology has advanced considerably, the relationship between design and response is still rather poorly understood. A review of the literature turns up very little on badminton rackets, whereas design of tennis rackets has been studied quite extensively (Brody 1995, Cross 1999, Lees 2003). Some tennis studies could be applicable to badminton as well as other racket sports in general, but given the distinct styles of play, the design goals of a tennis racket and a badminton racket are probably quite different.

1. Dept. of Mechanical Engineering, Aalborg University, 9220 Aalborg East, Denmark - E-mail: {mak,msa,jr}@ime.aau.dk
2. Dept. of Health Science and Technology, Aalborg University, 9220 Aalborg East, Denmark - E-mail: mdz@hst.aau.dk

As the "world's fastest racket sport", the game of badminton is very much about speed. With smashes reaching up to 200 mph (322 km/h), the racket is subjected to significant dynamic effects (BBC 2000). A dynamic model is therefore necessary to properly analyze racket performance. During the stroke, the racket experiences transverse deflection due to the high rotational and translational accelerations. It is likely that this deflection plays an important role in the transfer of momentum to the shuttlecock. Skilled players perceive significant differences between different high-quality rackets that superficially appear similar in terms of stiffness and mass properties. This indicates that small differences in the racket design have a large influence on the dynamics properties. An understanding of racket dynamics is therefore essential for further improvement of racket design.

2- Motion Capture Experiment

Motion capture data were taken for ten trials of a smash stroke performed by an advanced player using a Qualisys ProReflex system of eight cameras at the maximum frame rate of 240 Hz. Six markers were placed on the racket, two on the handle and four on the head, illustrated in Figure 1. A 12 mm spherical marker was fixed at the base, and reflective tape was used for the other five markers. Position data of the markers were passed through a low-pass Butterworth filter with a cut-off frequency of 35 Hz and subsequently interpolated using a 6th order B-spline. An optimization-based method designed for over-determinate systems was then applied to determine the kinematics of the system (Andersen *et al.* 2006). The racket was modelled as a flexible multi-body system with 8 degrees of freedom (dof), where the handle was considered a rigid segment. A universal joint between the handle and shaft allowed for transverse and lateral movement, approximating transverse and lateral deflection. The results of the kinematic analysis are shown in Figures 2 and 3.

Due to the high accelerations involved and the limitations of the motion capture system used, the accuracy of the marker positions may have been compromised. As seen in Figure 2, the error between measured and calculated marker positions are below 4 mm during most of the stroke. However, the errors increase up to nearly 2 cm around

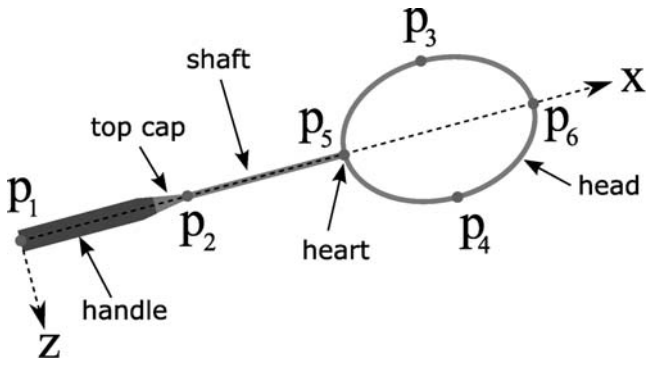

Figure 1 - Illustration of racket anatomy and racket marker placement for motion capture.

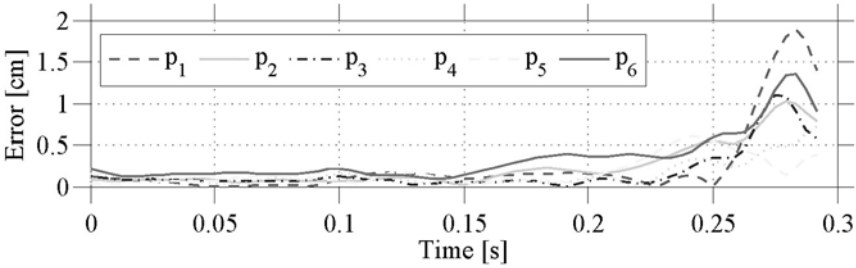

Figure 2 - Error between calculated and measured marker positions during pre-impact part of stroke. Impact occurs just before t=0.3 s.

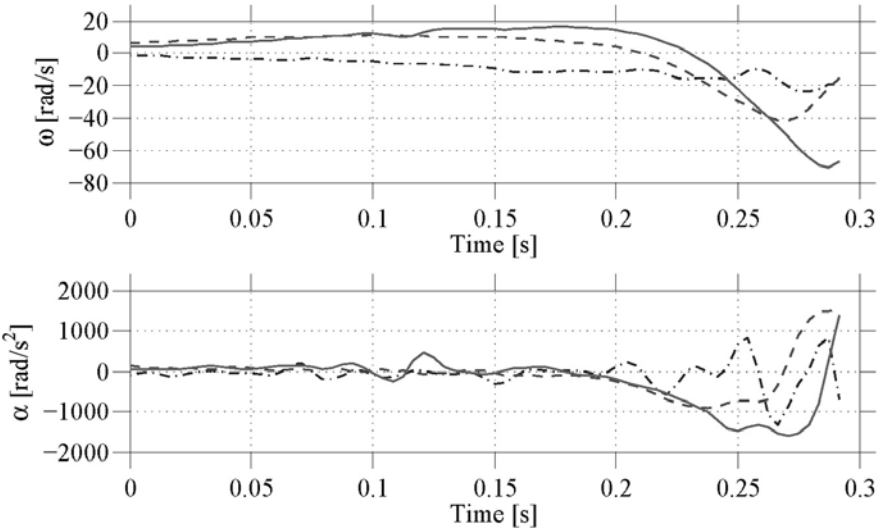

Figure 3 - Angular velocities [rad/s^2] and accelerations [rad/s^2] of the racket about its axial x-axis (solid), y-axis (dash-dot), and z-axis (dash) during pre-impact part of stroke. Impact occurs just before t=0.3 s.

the time just before impact where accelerations are presumably the highest. This suggests that measured marker positions near the moment of impact are less reliable, as a consequence of the increasingly high accelerations. The effects of the error can be seen in the calculated angular velocities and accelerations in Figure 3. Angular kinematics are given with respect to the local reference frame, defined in Figure 1. The angular accelerations are noisy and somewhat high, with peak accelerations around 1500 rad/s^2.

The resulting load on the racket was then computed, despite the inconsistencies described above. The load is proportional to the acceleration normal to the racket, containing contributions from both linear and angular accelerations. The normal acceleration generated at the tip of the racket is shown in Figure 4. At the tip of the racket, the normal acceleration is dominated by the rotational component, implying that the

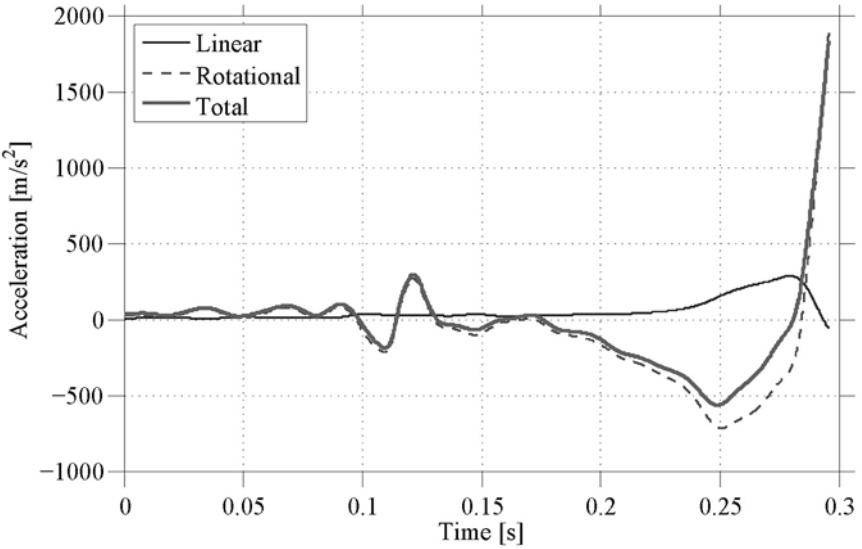

Figure 4 - Contributions to total normal acceleration of racket tip (thick solid) from translational accelerations (thin solid) and rotational effects (dash) during pre-impact part of stroke. Impact occurs just before t=0.3 s.

angular accelerations contribute much more to the speed of the racket tip than the linear accelerations. The acceleration is especially noisy during backswing, from t=0 to 0.2 s, followed by an increase (in the negative direction) as the racket accelerates forward. As the racket continues forward, unloading of the racket begins (t=0.25 s) as the normal acceleration decreases back to zero. The exceedingly high deceleration (in the positive direction) into the impact (t > 0.28 s) is unrealistic, perhaps an artifact of the noisy angular accelerations.

3- Strain Gauge Experiment

The motion capture experiment revealed that the high accelerations in the motion combined with the spatial and temporal resolution limitations of the system makes it difficult to obtain reliable values for the accelerations, and thus for the dynamic forces in the system. An alternative is to measure a more direct representation of the forces in the system, namely the strain in racket shaft.

Two strain gauges were placed on the end of the shaft 8 mm from the top cap in a half-bridge configuration. Ten trials of a smash stroke were performed by the same player and the same racket from the motion capture trials. Through a series of simple bending tests of the racket in a clamped condition with a concentrated end load, a linear relationship between the strains and the measured deflection at the tip of the racket was determined, shown in Figure 5. Using this relationship between strain and end deflection for a concentrated load, the end deflection assuming a triangular distributed load was calculated as a function of the strain.

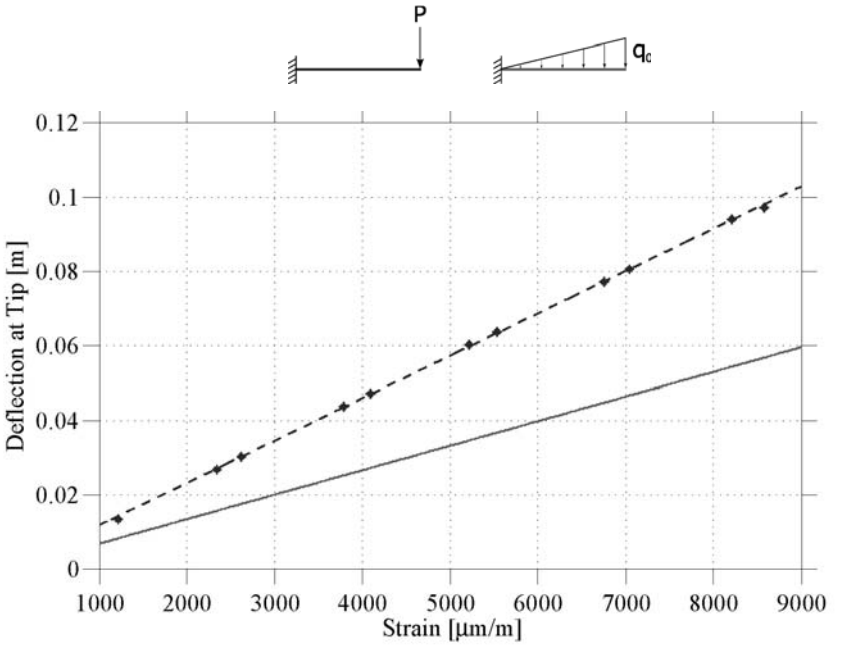

Figure 5 - Linear relationship (dash) between measured strain at shaft base and measured deflections at tip (stars) for concentrated load. Calculated tip deflection for an increasing triangular distributed load (solid).

Applying the linear relationship to the smash stroke data gives the tip deflection curves seen in Figure 6. Over a stroke, the maximum strain of around 8000 μm/m corresponds to a tip deflection of about 5 cm.

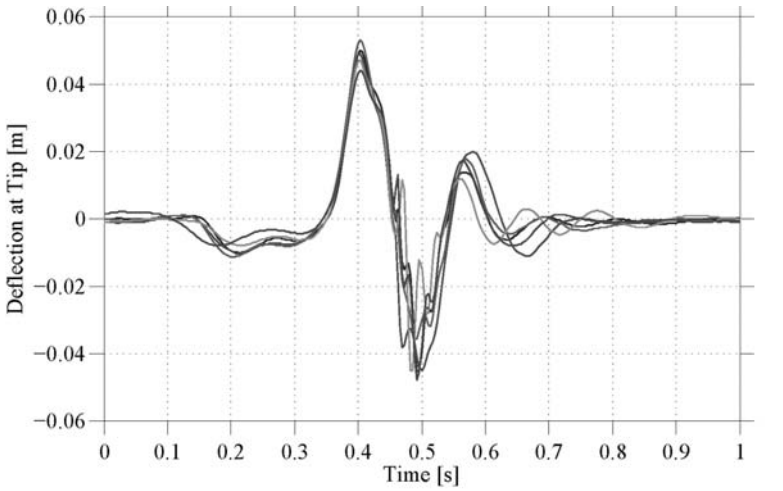

Figure 6 - Deflection at racket tip over one full stroke from five trials. Impact occurs around t=0.46 s.

The pre-impact part of the stroke consists of a backswing (~0.2 s) followed by the forward stroke (~0.1 s). In Figure 6, a negative deflection of the racket can be seen (t=0.14-0.34 s) during the backswing, followed by a much greater positive deflection during the forward stroke until impact around t=0.46s. For the maximum benefit from the elastic deformation of the racket, impact should occur when the slope of the deflection of the racket is steepest, where the tip velocity will be highest. However, the elastic deformation will still be advantageous as long as the racket tip is moving forward (towards the shuttle), indicated by a negative deflection slope in this case, so there is a narrow window of about 0.1 s where slight deviations in the timing of the impact can be tolerated.

As perhaps a more reliable source than the motion capture data, the strain gauge data was also used to derive racket kinematics. The racket was assumed to experience rotation only, due to an applied torque at the handle. The magnitude of the torque _ was computed from the strain ε, given by $\tau = EI\,\varepsilon / r$ where EI is the flexural rigidity of the shaft and r is the shaft radius. The angular acceleration of the racket due to the torque was determined from $\alpha = \tau / (I_{cm}+md^2)$ where I_{cm} is the racket moment of inertia, m is the total mass, and d is the distance from the strain gauge to the racket centre of mass. The resulting normal acceleration of the racket tip is given in Figure 7.

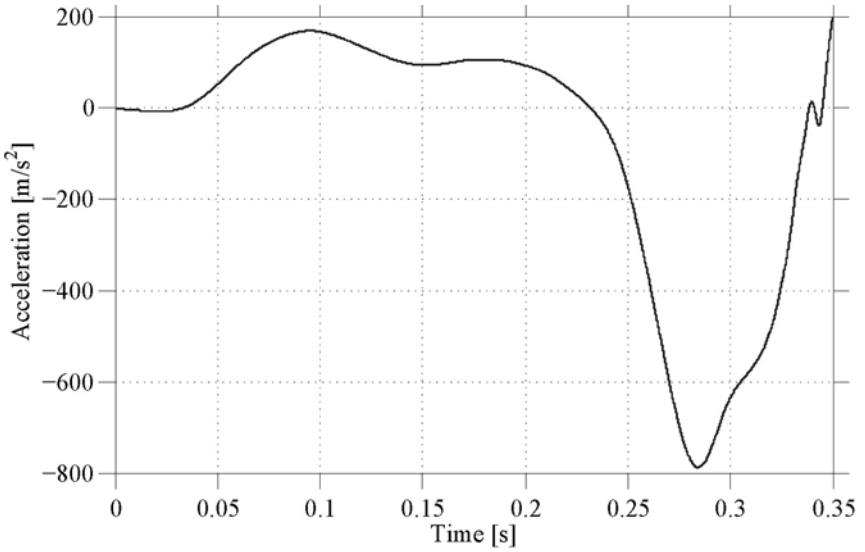

Figure 7 - Estimated normal acceleration of racket tip during pre-impact part of stroke, calculated from strain measurements. Impact occurs just before t=0.35 s.

Comparing with the normal acceleration derived from motion capture data in Figure 4, the shape of the curves during the forward swing phase are quite similar, with the peak acceleration near 800 m/s^2.

4- Computational model

The simplified racket model is composed of two uniform beam elements, representing the shaft and the head of the racket. Each element has uniform mass per unit length, ρA, and uniform flexural rigidity, EI. The handle is assumed to be completely rigid.

In addition to the six degrees of freedom from rigid body motion, the racket is allowed to bend in the transverse direction. The deflection of the beam w is then given by $w(x,t) = N(x)\, q(t)$ with shaping functions $N(x)$ and displacement vector $q(t)$ containing the linear and rotational displacements at each node.

Dynamic equations describing the flexible motion of the racket due to both inertial and centrifugal effects are derived using the extended Hamilton's principle, similar to methods described by Yang *et al.* (2004) and Montagny *et al.* (2003). Applying Lagrange's equations, the non-linear equations of motion take the form:

$$[m]\,\{\ddot{q}\} + ([k] - [k_1] + [k_2] + [k_3])\{q\} = [c]^T + [c_1]^T \qquad (1)$$

where m and k are the mass and stiffness matrices of the beam element. Dynamic stiffening, due to centripetal forces, centrifugal forces arising from rotation, and centrifugal forces arising from translation, is represented by the stiffness matrices k_1, k_2, and k_3, respectively. The forcing functions due to rotational and translational accelerations are given by the vectors c and c_1, respectively. The equations were solved using a fourth order Runge-Kutta integration.

Using kinematic inputs from the motion capture data, the beam model produces the deformation curve seen in Figure 8. In the clamped case, the predicted deflections are

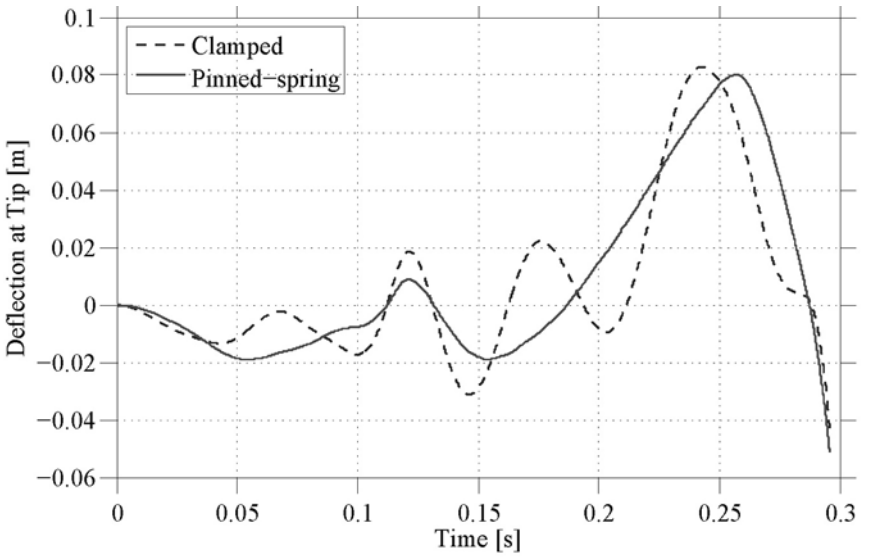

Figure 8 - Deflection at beam tip during pre-impact part of stroke for clamped condition (dash) and pinned with spring k_t=50 N-m/rad (solid), using motion capture data. Impact occurs just before t=0.3 s.

somewhat high, but the frequency of the dynamic response is also too high. One possible explanation is the clamped boundary condition, which may not be very representative of the handheld case (Cross 1999, Brody 1995). To "loosen up" the boundary conditions, the end of the racket was changed from clamped to pinned with a torsional spring of stiffness k_t. A very stiff spring (k_t > 1e6 N-m/rad) approaches the clamped condition, and lowering the stiffness leads to a reduction in the response frequency. Figure 8 shows the elastic deflection at the tip, over one stroke with k_t=50 N-m/rad.

Figure 9 shows the deflections of the racket tip using kinematic inputs from the strain gauge data, for the clamped condition and the pinned case with a torsional spring of stiffness k_t=50 N-m/rad. In both Figures 8 and 9, the deflections of the racket tip are still rather high, when compared to the values found from strain gauge measurements, shown in Figure 6. This could be caused by an overestimation of the accelerations from the experimental data and/or a lack of damping in the model.

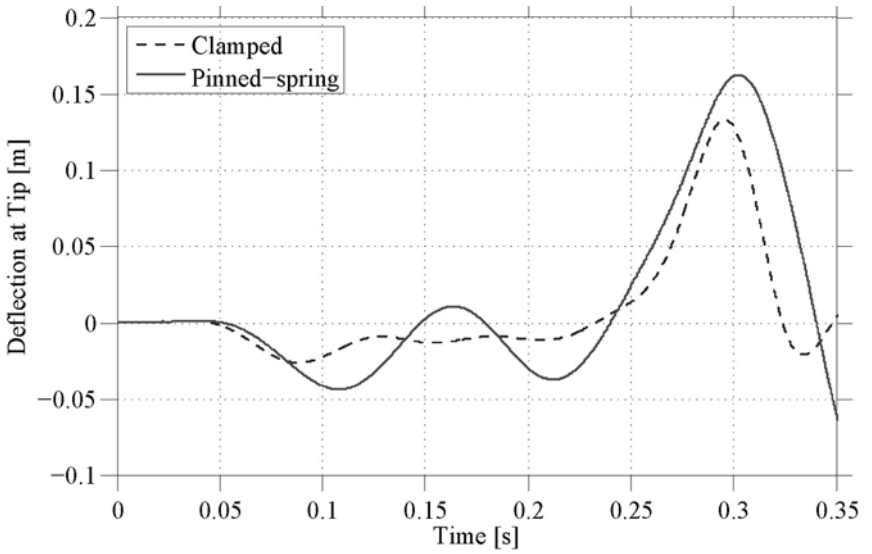

Figure 9 - Deflection at beam tip during pre-impact part of stroke for clamped condition (dash) and pinned with spring k_t=50 N-m/rad (solid), using strain gauge data. Impact occurs just before t=0.35 s.

5- Conclusions

Although none of the experimental and computational methods seem to completely capture the dynamics of the racket swing, the agreement between the methods is good enough to reveal that the racket exhibits an elastic deformation of about 5 cm during the acceleration of the stroke when used by a skilled player. The results also show that the elastic deformation swings back and may increase the impact velocity if the timing of the stroke is right. The ideal timing of the impact is when the racket has recovered from the backwards deflection and has attained its maximum forward velocity due to

the elastic deflection. The results indicate that the window of opportunity where the velocity is close to maximum is only 0.02 s. If this window is missed, the elastic deflection will lose its full advantage or even become disadvantageous. This is likely the reason why small differences in stiffness and weight distribution in the racket can influence the perceived quality of the racket so significantly.

6- Acknowledgments

This work was supported by Active Sportswear.

7- References

[A1] Andersen M.S., Damsgaard M., Christensen S.T., Rasmussen J. Kinematic Analysis of Overdeterminate Systems. In Proceedings of the 19th Nordic Seminar on Computational Mechanics, Lund - Sweden, 2006.

[B1] The fastest racquet sport. In BBC SPORT, 9 Aug. 2000. <http://news.bbc.co.uk/sport2/hi/olympics2000/racquet_sports/841333.stm>

[B2] Brody H. How would a physicist design a tennis racket? In Physics Today, 48(3):26-31, 1995.

[C1] Cross R. Impact of a ball with a bat or racket. In American Journal of Physics, 67:692-702, 1999.

[L1] Lees A. Science and the major racket sports: a review. In Journal of Sports Sciences, 21:707-732, 2003.

[M1] Montagny J., Berlioz A., Dufour R. Transient behaviour of flexible structures: application to badminton rackets. In Mecanique & Industries, 4:113-118, 2003.

[YJ1] Yang J.B., Jiang L.L., and Chen D.C.H. Dynamic modelling and control of a rotating Euler-Bernoulli beam. In Journal of Sound and Vibration, 274:863-875, 2004.

Maximal Energy Expenditure in Professional Road Cycling (P255)

Jon Iriberri[1], Josu Larrazabal[2], Xabier Muriel[3]

Topics: Bicycle; Measurement Systems; Modelling; Performance Sports.
Abstract: The workload demands in professional cycling races have previously been estimated indirectly through monitoring heart rate (Mujika and Padilla 2001, Jeukendrup and Van Diemen 1998). However, this method does not take different variations due to the influences on heart rate, for example: cardiovascular drift, rider position, or the "day to day" variation. On the other hand, the mechanical power output that is produced by the cyclist to propel the bicycle may be the most direct indicator of exercise intensity being considered as an absolute variable. In many studies, research has focused on timetrial protocols in order to determine the relationship between peak power output, lactate threshold and time trial performance, the power requirements in the 4000-m individual and team pursuits or seasonal changes in power of competitive cyclists (Broker *et al.* 1999, Paton and Hopkins 2005). However, just a few number of scientists have studied the measurement of maximal power output in mass start races (Vogt *et al.* 2006).
Key words: Energy expediture, professional cycling.

1- Introduction

Recently, we have had news about the first data about energy expenditure in high level proffesional road cycling (Vogt *et al.* 2006). We have see that there is a great relation betwen our obtained data and the data of those new studies. This is avery important point because is really difficult to get direct data from sport competition, when is a very important sport event. This can be the reason that explain the few quantity of information in the literatura about this interesting topic.

1. PEC Basque Country Government, 48992 Getxo, Spain -j-iriberri@ej-gv.es
2. Euskadi Fundation,48160 Derio, Spain
3. Oreki Fundation, 20160 Lasarte, Spain.

The first aim of this study has been to measure the maximum mean power output during different target durations that have been defined in professional road cycling and describe the relationship between these factors. According to this first objetive, we have developed a matematical stimation of energy metabolisms through the power output profile. In this way, we can easily identificate the metabolism related to the intensity. This relationship might be useful durind the training period and in competitive strategy

2- Method

The data of eight professional road cyclists have been studied. All cyclists were members of different UCI-Pro Tour category cycling teams (29,8 +/-2,5 years old, 177+/-8,0 cm, 67,1+/-1,9 kg). All athletes gave us their written approad in order to use their data. During three seasons, in many races, total and partial work, power output, heart rate, cadence, velocity, and distance were measured using SRM powercrank system (SRM, Trainingsystems, Schoberer Rad Messtechnik, Jülich, Germany). The SRM system is a crank-based device that measures the mechanical power output to the bike through the multiplication of the torque applied to the cranks, and the speed at which they turn. The crankset experiences tiny deformation when torque is applied. The SRM system measures this deformation using strain gauges attached to components inside the crank. The sample frequency was in intervalls of 1 to 5 seconds. Data registered during the competition by the SRM system were transmitted to a conventional PC and processed with the software provided with the SRM system. Raw data analysis was then conducted using a specially designed software program to determine overall averages for power in different durations.

Maximal mean power output and energy data was selected in each target duration.

3- Results

The data we obtained data was explained in a graph and it showns us that is exist a matematichal relation expresed by the following equation (figure 1):

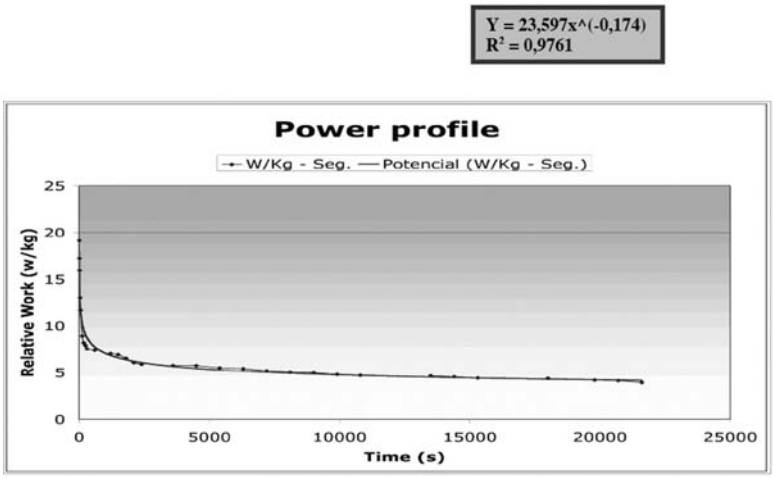

Figure 1 - Power profile from the obtained data.

Then, with the equation developed second to second, we have defined polinomial lines to join the data until the r2 of the equation of each polinomial line value was equal to the r2 of our equation (0,9761) or higher (Figure2). This figure shows the tipical relation in sports between energy expenditure and time of exposure. From our point of wiew, this form can be explained attending to human energy metabolism systems: aerobic, lactic-anaerobic and alactic-anaerobic. Those metabolism has particular caracteristics, durantions and power output capacity . But the interpretation of this is difficult because the three metabolisms are working at the same time in some kind of efforts. The diference of power output (expressed as a relative work) can be a good method to clasification the presence of the metabolisms.

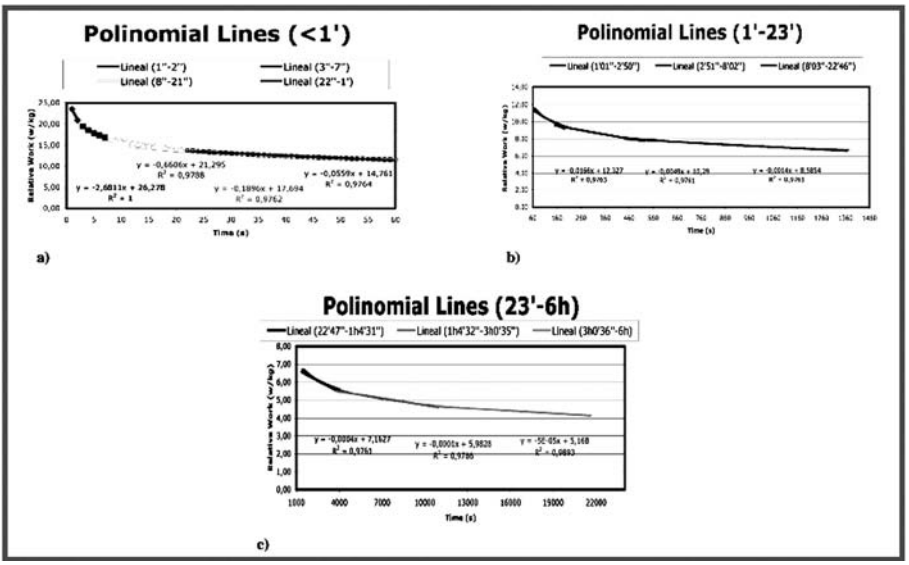

Figure 2 - Fractionated power profile. Where a) until 1 minute, b) from 1 minute to 23 minutes and c) from 23 minutes to 6 hours.

4- Discussion

As we can see in the figure 2, through the equation from the previously recorded durations (figure 1), we have found other target lenghts that relates to with the polinomial lines (figure 2). Each new target duration is expressed by an equation and we think that it might explain the power output coming from each energy metabolism. The equations might relates to the diferent metabolisms (table 1).

As a sumary, these parameters might be used as a reference to better understand the demands in professional cycling and as a prediction factor of cycling performance in order to choose the best training and racing strategy.

Duration	Equation	R^2	Predominant Metabolism
1"-2"	*y = -2,6811x + 26,278*	*1*	Alactic Glucolisis (ATP)
3"-10''	*y = -0,6606x + 21,295*	*0,9788*	Alactic Glucolisis (Pcr)
10''-20''	*y = -0,1896x + 17,694*	*0,9762*	Anaerobic Glucolisis
20''-1'	*y = -0,0559x + 14,761*	*0,9764*	Anaerobic Glucolisis
1'-3'	*y = -0,0166x + 12,327*	*0,9763*	Peak Aerobic Glucolisis (VO2max)
3'-8'	*y = -0,0049x + 10,29*	*0,9761*	Peak Aerobic Glucolisis (VO2max)
8'-23'	*y = -0,0014x + 8,5854*	*0,9761*	Muscle Aerobic Glucolisis
23'-1h	*y = -0,0004x + 7,1627*	*0,9761*	Blood Aerobic Glucolisis
1h-3h	*y = -0,0001x + 5,9828*	*0,9766*	Blood Aerobic Glucolisis
3h-6h	*y = -5E-05x + 5,168*	*0,9893*	Aerobic Lipolisis

Table 1 - The equations for the diferent durations and the predominant metabolisms suggested.

5 - References

[BK1] Broker J. P.,Kyle C.R., and Burke E.R. Racing cyclist power requirements in the 4000-m individual and team pursuits. In Med. Sci. Sports Exerc., Vol. 31, No. 11, pp. 1677-1685, 1999.

[JV1] Jeukendrup A., and Van Diemen A. Heart rate monitoring during training and competition in cyclists. In Journal of Sports Sciences, 16, S91-S99, 1998.

[MP1] Mujika I., and Padilla S. Physiological and Performance Characteristics of Male Professional Road Cyclists. In Sports Medicine; 31 (7): 479-487, 2001.

[PH1] Paton C.D., and Hopkins W.G. Seasonal changes in power of competitive cyclists: implications for monitoring performance. In J Sci Med Sport; 8: 4: 375-381, 2005.

[VH1] Vogt S., Heinrich L., Schumacher Y.O., Blum A., Roecker K., Dickhuth H.H., and Schmid A. Power output during Stage Racing in Professional Road Cycling. In Med. Sci Sports Exerc., Vol.38, No. 1, pp. 147-151, 2006.

An Integrated Approach toward Testing Sports Equipment (P260)

Violaine Sevrez[1], Guillaume Rao[1], Laurent Vigouroux[1], Reinoud, J. Bootsma[1], Eric Berton[1]

Topics: Biomechanics, Sports Equipment.
Abstract: Recent improvements in material technology, together with generalization of testing, prototyping, and benchmarking, have impacted on performance in many sports. However, sports equipment properties are often tested through mechanically based standardized protocols. Such protocols would ignore the effects on equipment resulting from mechanically unpredicted manoeuvres performed by athletes aiming for performance, injury protection or comfort. Their use may thus turn out to be of limited use in the evolution of sports equipments towards perfection, as a first-rate equipment is not only the one including high-tech materials but also the one interacting in the best way with the athlete using it.

This study aimed at determining, through the example of the backward giant circle on the high bar, whether or not the effects of standardized tests on sports equipment are comparable with the effects caused by real athletic practice. A comparison between the characteristics of the kinematics predicted from a pure mechanical analysis of the giant circle and those observed in real situations during performance of giant circles by seven elite gymnasts' pointed out differences. According to the mechanical analysis, the gymnasts should be maximally extended at vertical handstand and maximally flexed at the moment of passing through the lower point upwards. Maximal extension in fact occurred when their body center of mass had rotated approximately 120° from the handstand and maximal flexion occurred approximately 100° after having passed through the lower point.

This result suggests that manufacturers should realize that standardized test only provide limited information, as differences in kinematics between the predicted and observed solution are associated with differences in the force exerted. Integration of the effect of intentional actions of the athlete using the equipment as a constraint in test procedures would render these more comprehensive thus allowing development of more efficient equipment.
Key words: Biomechanics, Testing, Mechanical analysis, On site analysis, Sports equipment.

1. UMR 6233 Institut des Sciences du Mouvement « E.J. Marey », Marseille, France -
E-mail: {violaine.sevrez,guillaume.rao,laurent.vigouroux,reinoud.bootsma,eric.berton}@univmed.fr

1- Introduction

Recent improvements in materials technology resulting from an increased understanding of biomechanics and the engineering aspects of sports equipment performance, together with generalization of testing, prototyping, and benchmarking prior to introducing new equipment have impacted performance in a range of sports. There is no doubt that the endless aspiration for increased performance in all sports will continue to drive composite manufacturers to develop lighter and more specialist materials. Such efforts might however not be efficient without a concurrent evolution of testing protocols since first-rate sport equipment is not only the one incorporating high-tech materials but also the one interacting in the best way with the athlete using it. Sports equipment properties are currently often tested by means of standardized tests based on purely mechanical/physical analyses. The results of such tests may turn out to be limited in their contribution towards the evolution of sport equipment as they do not take into account the effects on equipment resulting from manoeuvres dictated by performance, injury protection or comfort constraints bearing upon the athlete. When the kinematics observed in real situations are similar to those predicted from a mechanical analysis of the task, standardized tests for sport equipment would be well suited for athletes, and manufacturers could carry on relying on them. Any differences between the observed and predicted kinematics would however imply that (part of) the manoeuvres decisive to the athletes' performance, injury protection or comfort are ignored by the mechanical analysis. In this latter case, standardized tests would be likely to have an effect on equipment that is removed from what it undergoes during real sport activity, and manufacturers should be careful in the interpretation of their results. In order to make valuable the biomechanical and engineering efforts toward improvement of sport equipment a deeper understanding of the control mechanisms of human sport movement would thus be essential.

This study aimed at investigating whether or not the effect of standardized tests on equipment is consistent with the effect of real practice. We focused on the giant swing on the high bar in gymnastics as it is a task highly constrained from a mechanical point of view, requiring the production of actions at specific moments in time and space. The giant swing consists in departing from the handstand on the high bar and returning to it after having passed by suspension, without releasing the bar at any time. In order to determine whether the effect of real practice on equipment could be estimated using a mechanical analysis of the task we proceeded in two successive steps. We first performed a mechanical analysis of the task in order to predict the theoretical kinematics that should be adopted if the gymnast would be driven solely by the laws of mechanics. We then analysed the real kinematics from recordings of seven elite women gymnasts performing giant circles on the high bar with either no added load or with 2 or 4 kg loads placed at three different locations (shoulder, hip, and ankle).

2- Mechanical analysis

This first part of the study aimed at determining the characteristics of the kinematics pattern that should be adopted if the gymnast would be driven solely by the laws of

mechanics. Just as a pendulum, the gymnast is subject to various external forces such as gravity, Coriolis forces, inertia and centrifugal forces and can thus be regarded as a suspended point mass located at the body center of mass. Such a pendulum is described by the following equation:

$$\ddot{\theta} + \frac{g}{r}\sin\theta = 0 \tag{1}$$

In accordance with the well known behaviour of a pendulum, the longer the pendulum length, the longer oscillation period and reciprocally the shorter the length, the shorter the oscillation period. As perpetual motion does not exist because of friction forces, a gymnast performing a giant circle needs to compensate for energy lost in order to keep the oscillations going. As the mass is constant through the exercise, equation 1 reveals that the unique means or mechanism for oscillations control is through length variation (i.e.: changes of the distance *r* between the bar and the body center of mass, figure 1). In agreement with this finding, Bauer (1983) demonstrated that the solution of the equation of a pendulum of variable length can be used for constructing congruent trajectories for the giant circle when considering the displacement of the center of mass. As a simplified model of the motion, he proposed that the gymnast instantaneously raises or lower the body center of mass at particular instants during the cycle. Starting an oscillation at a point away from the vertical, the center of mass is assumed to remain in the low (extended) position until the mass is directly beneath the bar before being raised instantaneously in order to insert energy into the system by decreasing the moment of inertia about the bar and thus increasing the potential and kinetic energy. A limitation of Bauer's model is that he considered instantaneous changes in length, leading to trajectories which consist of sectors with piecewise constant radii, while the position of the center of mass should be expected to change smoothly as the gymnast regulates it's «length». Stilling and Szyszkowski (2002) addressed the oscillations of such a pendulum of smoothly variable length (equation 2)

$$\ddot{\theta} + 2\frac{\dot{r}\dot{\theta}}{r} + \frac{g}{r}\sin\theta = 0 \tag{2}$$

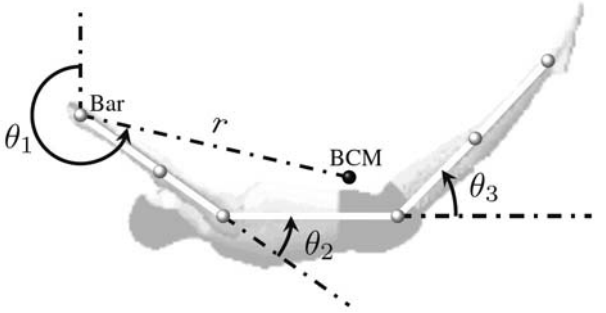

Figure 1 - Body segments model of a gymnast performing a backward giant circle. From the bar, white dots respectively represent the wrist, elbow, shoulder, hip, knee and ankle markers. The black dot represents the location of the body center of mass (BCM). *r* is the distance between the bar and the BCM.

They demonstrated that by having the pendulum length increase or decrease a Coriolis force that opposes or aids the motion is generated, thus respectively decreasing or increasing the rotational motion of the system. Equivalent conclusions with respect to the effects of length variation on rotational motion have been drawn by considering the principle of conservation of angular momentum law [W1]. To obtain a net amplification effect, the gymnast should gradually move the BCM further to or away from the bar so that the distance *r* between the bar and the BCM is maximal when the angular velocity and the Coriolis force are minimum (near handstand) and minimal when the angular velocity and the Coriolis force are maximum (near vertical suspension).

3- On site analysis

The second part of the study aimed at determining the characteristics of the kinematics of elite gymnasts performing giant circles under different task constraints in order to obtain a benchmark against which the realismof the solution predicted by the mechanical analysis of the task can be evaluated.

3.1 Materials and Methods

3.1.1 Participants

Seven elite junior female gymnasts volunteered for participation in the experiment. Their ages ranged from 12 to 13 years (mean 12.43 ± 0.54 years), their standing height ranged from 1.35 to 1.54 m (mean 1.45 ± 0.06 m), and their body mass ranged from 28.0 to 47.5 kg (mean 38.14 ± 6.85 kg). Participants gave their informed consent prior the inclusion in the study, which was approved by the local ethics committee.

3.1.2 Task

Gymnasts were instructed to performed backward giant circles on the high bar under different loading conditions. They were asked to respect the code of points of the International Gymnastics Federation, namely to execute the giant circles with the legs together and without motion at the elbows or knees joints. After a few trials performed to allow for adaptation to the experimental situation, participants were requested to perform seven subsequent giant circles in each experimental condition. No temporal constraints were imposed during the session. Each condition was spontaneously initiated, after a verbal signal from the experimenter. Data acquisition began at the signal.

3.1.3 - Apparatus

Joints locations in two dimensions were recorded using a Basler video camera operating at a sampling frequency of 100 Hz. The camera was placed perpendicularly to the plane of motion 8.50 m away from the right side of the participant at a height of 2.75 m, such that the x-axis was aligned with the anterior-posterior direction, and the y-axis was

aligned with the vertical direction. Six markers were attached to the participants' skin on anatomical landmarks (Zatsiorsky, 2002) over the following right body side joints: wrist, elbow, shoulder, hip, knee and ankle.

3.1.4 Design

Combining a control condition (unloaded) with three different load locations (with loads symmetrically placed on the upper arms near the shoulder joints, on the waist, or on the lower legs near the ankles) and two different magnitudes of load (2 or 4 kg total) gave rise to seven different experimental conditions. Participants performed all experimental conditions in a single experimental session lasting about 30 min. The order of presentation of the conditions was randomized.

3.1.5 Data analysis

In order to examine stable performance, of the seven giant circles recorded only giant circles two to six were analysed. Marker locations were digitized and transformed to 2D positions in the plane of motion using SIMI motion software. The position data were filtered using a fourth-order Butterworth low-pass filter with a zero phase shift and a 6 Hz net cut-off frequency [W2]. Masses and moment of inertia of the segments of individual participants were estimated using the anthropometric tables of Zatsiorsky and Seluyanov [ZS1]. Body orientation was defined as the angle between the vertical and a line from the bar through the body centre of mass [YH1]. The body orientation angle, shoulder angle and hip angle were estimated on the basis of displacement data. After segmentation of the five giant circles per condition based on body centre of mass position with respect to the bar, movement time was calculated for each participant and each condition as the average time between two passes of the centre of mass through the vertical above the bar.

3.2 Results

Despite the fact that 4-kg added load amounted to 10.5% of the total body weight on the average, all seven gymnasts were able to perform the task as requested in all loading conditions indicating that gymnasts adapt their gesture to the mechanical constraints of the task.

3.2.1 Swing duration

A repeated measures analysis of variance (ANOVA) on swing duration with factors load location and load magnitude revealed a significant main effect of location ($F_{2,12}$ = 341.23, $p < .001$) as well as a significant interaction between location and magnitude ($F_{2,12}$ = 42.83, $p < .001$). As can be seen from Figure 2, the magnitude and location of the loads systematically affected the duration of the swing. Post-hoc analysis (Tukey HSD) of the interaction revealed that swing duration varied ($ps < .001$) over load locations and magnitudes, except when the loads were placed at the level of the waist.

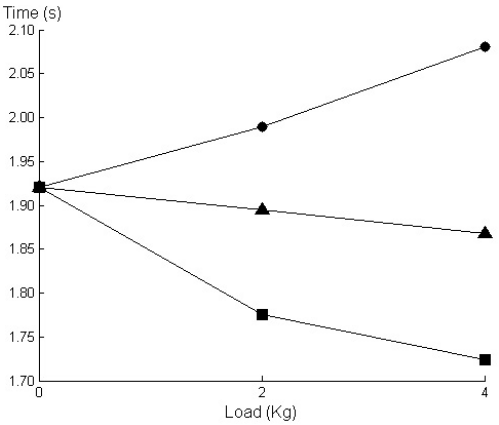

Figure 2 - Effect of adding 2 or 4 kg loads at the ankle (circles), waist (triangles) or shoulder (squares) level on total swing duration. Note the influence of load at the ankle and shoulder levels, while no effect is seen when the load is located at the waist.

In the unloaded condition, swing duration was 1.92 ± 0.16 s. With the loads placed at the level of the ankles, thereby increasing the average distance between the rotation axis and the BCM relative to the unloaded condition, swing duration increased (1.99 ± 0.14 s for the 2-kg and 2.08 ± 0.09 s for the 4-kg loads). With the loads placed at the level of the shoulders, the average pendulum length (r) and swing duration decreased (1.78 ± 0.17 s for the 2-kg and 1.72 ± 0.19 s for the 4-kg loads). Placing the loads at waist level did not displace the location of the body center of mass to a significant degree and revealed swing durations close to that of the unloaded condition (1.90 ± 0.08 s for the 2-kg and 1.87 ± 0.12 s for the 4-kg loads).

3.2.2 Angular kinematics

Repeated measures ANOVAs (two load magnitudes and three load locations) performed on the magnitude of peak shoulder extension revealed a significant main effect of load location ($F_{2,12} = 5.62$, $p < .01$) as well as a significant interaction between load location and magnitude ($F_{2,12} = 18.64$, $p < .001$). The variations were however quite small (less than 2°) and not systematic with both minimal and maximal shoulder extension occurring when the loads were placed at the waist level (-4.2° and -6.0° for the 2 and 4-kg load respectively). Same types of ANOVAs performed on peak hip extension revealed no significant effect (ps > .08).

ANOVAs performed on the magnitude of peak joint flexion revealed main effects of load location ($F_{2,12} = 15.16$, $p < .001$ for the shoulder and $F_{2,12} = 25.00$, $p < .001$ for the hip) as well as a significant interaction between load location and magnitude ($F_{2,12} = 14.12$, $p < .001$ for the shoulder and $F_{2,12} = 8.7$, $p < .01$ for the hip). Peak shoulder flexion ranged from 37.8° for the 4-kg load at the ankles to 41.7° for the 4-kg load placed at the level of the shoulders. Peak hip flexion ranged from 42.46° for the 2-kg load placed at the level of the ankles to 45.8° for the 4-kg load placed at the level of the waist.

ANOVAs performed on the percentage of swing time at which peak joints extension were reached revealed main effects of load location ($F_{2,12}$ = 5.1, p < .01 for the shoulder and $F_{2,12}$ = 10.00, p < .001 for the hip) as well as significant interactions between load location and magnitude ($F_{2,12}$ = 6.6, p < .001 for the shoulder and $F_{2,12}$ = 5.2, p < .01 for the hip). Time to peak shoulder extension ranged from 50.6% for the 2-kg load at the waist to 52.8% for the 4-kg load at the shoulders. Time to peak hip extension ranged from 45.5% for the 4-kg load at the ankles to 47.1% for the 4-kg load at the shoulder.

ANOVAs performed on the percentage of swing time at which peak joints flexion were reached revealed main effects of load location ($F_{2,12}$ = 123.4, p < .001 for the shoulder and $F_{2,12}$ = 75.5, p < .001 for the hip) as well as significant interactions between load location and magnitude ($F_{2,12}$ = 12.1, p < .01 for the shoulder and $F_{2,12}$ = 6.1, p < .05 for the hip) Time to peak shoulder flexion ranged from 67.9% for the 4-kg load placed at the level of the ankles to 74.3% for the 4-kg load placed at the level of the shoulders. Time to peak hip flexion ranged from 60.3% for the 4-kg load placed at the level of the ankles to 65.0% for the 4-kg load placed at the level of the shoulder.

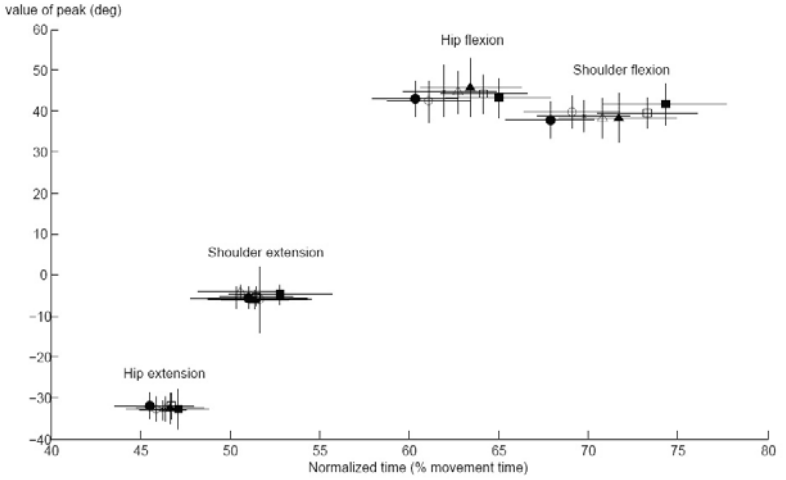

Figure 3 - Means and standard deviations (indicated by error bars) of the magnitudes of peak extension and flexion of the shoulder and hip joints as a function of their moment of occurrence expressed as the percentage of swing duration for the unloaded (*), 2-kg (open symbols) and 4-kg (filled symbols) loads placed at the level of the ankles (circles), waist (triangles) and shoulders (squares).Horizontal error bars stand for peaks' moment of occurrence while the vertical ones stand for peaks' value.

Taken together, as revealed by a global view of Figure 3, these analyses demonstrated that load location and magnitude subtly but systematically influenced the timing and, to a lesser degree, the magnitude of peak joint extension and flexion. These effects were generally more pronounced for the shoulder joint than for the hip joint. Peak joint extension and flexion were reached earlier when the loading increased the distance between the rotation axis and the BCM (i.e. for loads fixed at the ankle). They were reached later when the loading decreased *r* namely when the loads were attached at the shoulder.

3.2.3 Pendulum length

The variations observed over different loading conditions in the magnitude and timing of shoulder and hip joint extension and flexion gave rise to variations in the pattern of change in pendulum length. In line with the results reported in the foregoing section with respect to peak joint extension and flexion, loading the gymnasts affected the variation of pendulum length (r) in its timing rather than in its magnitude. Indeed, the magnitude of pendulum length variation (calculated as the maximal minus minimal length observed during a swing) revealed no significant effects of load location or magnitude (ps > .15), for an average variation of 9.25 ± 0.19 cm. The moment of occurrence of the maximal pendulum length also did not vary over loading conditions (Fs < 3.0), occurring at an average of 39.5 ± 0.4% of swing duration (118.8 ± 2.1° BCM rotation angle). However, the ANOVA on the moment of occurrence of minimal pendulum length revealed a significant main effect of load location ($F_{2,12}$ = 82.7, p < .001) and a significant interaction between load location and magnitude ($F_{2,12}$ = 13.1, p < .01). Minimal pendulum length was reached earliest (65.0% equivalent to 282.4° BCM rotation angle) for the 4-kg load placed at the ankles and latest (71.7% equivalent to 294.0° BCM rotation angle) for the 4-kg load placed at the shoulders (ps < .05).

4- Discussion and Conclusion

This study was aimed at determining through the example of the giant swing on the high bar whether or not the effect of standardized test procedure on equipment may be consistent with the effect of real practice. This problem was addressed by comparing the features of the kinematics predicted through the mechanical analysis and those observed during performance of the task in a real situation under different mechanical constraints.

The mechanical analysis of the giant circle predicted that, just as for a pendulum of variable length, the total movement time should be a function of the distance between the bar and the BCM and that the gymnast should be maximally extended when the BCM passes through the highest point of its trajectory and maximally flexed when the BCM passes through the lowest point. The pattern of result obtained with respect to swing duration in real situations corroborated the mechanical interpretation of the gymnast circling on the high bar as a pendulum system. On site analysis of gymnasts performing giant circles in the control condition however revealed that gymnasts' center of mass is further from the bar for θ_1 = 120.2 ± 2.1° and closer to the bar 103.58 ± 1.6° after having passed by the vertical suspension (θ_1 = 283.58 ± 1.6°). The observed kinematics differed from the kinematics predicted by the mechanical analysis described in section two, thereby suggesting that the mechanical analysis provided only restricted knowledge of the activity thus possibly leading to test protocols with an effect on equipment that is quite different from what it undergoes during real sport activity. A close look at the kinematics adopted in presence of additional loads further revealed that gymnasts adopt different kinematics in presence of additional constraints. Such regulation of the gesture in the presence of additional load was not predicted through the mechanical analysis of the task but seems decisive to fulfil task requirements. As (part

of) the manoeuvres that are decisive to the athletes' performance, injury protection or comfort seem ignored by the mechanical analysis, a deeper understanding of the way athletes regulate their gesture is necessary for the design of more comprehensive test protocols.

There is no doubt that optimizing the performance of sports equipment calls for the best possible materials and the best possible engineering of these. However, a deep understanding of the control mechanisms of sporting actions is necessary for improvement of sport materials as standardized test may have effects on equipment that are removed what it undergoes during real sport activity. Manufacturers should thus be careful in the interpretation of results from standardized tests protocols and should explore the use of an integrated approach for the testing of sports equipment. In order to make validate the biomechanical and engineering efforts toward improvement of sport equipment a deeper understanding of the control mechanisms of human sporting actions is thus essential. The design of appropriate test protocols necessitates both the comprehension of the task from a mechanical point of view and awareness of how athlete regulate their movement patterns to prevent manufacturers from engaging in potentially less important technological developments. Such an integrated method leads to more comprehensive test protocols that mimic the solicitations the apparatus faces in real situation while taking into account the mechanisms critical for task regulation for performance, injury protection or comfort.

5- References

[B1] Bauer W.L. Swinging as a way of increasing the mechanical energy in gymnastic maneuvers. In Matsui H, Kobayashi K, Biomechanics VIII-B, Illinois USA; 801-806, 1983.

[SS1] Stilling D.S.D. and Szyszkowski W. Controlling angular oscillations through mass reconfiguration: a variable length pendulum case. In International Journal of non-linear mechanics, 37,89-99, 2002.

[W1] J. Walker. How to get the playground swing going: a first lesson in the mechanics of rotation. In The amateur Scientist, 106-109, 1968.

[W2] Winter DA. Biomechanics & motor control of human movement, 2nd ed., New York: John Wiley & Sons, 1990.

[YH1] Yeadon, M.R. and Hiley, M.J. The mechanics of the backward giant circle on the high bar. In Human Movement Science, 19, 153-173, 2000.

[ZS1] Zatsiorsky, V. and Seluyanov, V. The mass and inertia characteristics of main segments of the human body. In Matsui H, Kobayashi K, Biomechanics VIII-B, Illinois USA; 1152-1159, 1983.

Management of New Ideas during Early Design Phases of Innovative Products in the Surf Industry (P261)

Olivier Pialot[1,2], Jérémy Legardeur[1,3]

Topics: Surf industry.
Abstract: This paper focuses on the early design phases of innovative projects in the surf and sliding industry. More precisely, the questions of the innovation opportunities development and new ideas management are addressed here from a theoretical model and methodology perspectives and a software tool proposition for the information management during the early design phases. Our model is based on three dimensions (Potential Technology and Concept) and highlights the need of interactions between them regarding strategic and operational levels. Starting from the analysis of the three dimensions of our PTC model, different opportunities for the innovation are identified. Based on a case study of the design of a surf wetsuit, the paper presents the ID^2 software tool (Innovation Development and Diffusion) dedicated to structure the preliminary exchanges among all stakeholders involved in the innovation process. This tool is mainly oriented towards the consolidation and the diffusion of new ideas in the early phases of innovative development.
Key words: Early design phases, Innovation process, PTC model, C-K theory.

1- Needs and challenges for innovation in the board-sport industry

This paper focuses on the early design phases of innovative products that are one of the important challenges for large companies of the surf industry. Indeed, the board-sports industry is a fantastic opportunity for innovation based on the good health of these companies, the youth and dynamism of their employees and their ability to innovate and launch new projects. Having been considered for a long time as the playground for

1. ESTIA Research, Bidart, France - E-mail : {o.pialot,j.legardeur}@estia.fr
2. INPG Grenoble University - G-SCOP, Grenoble, France
3. IMS - Bordeaux 1 University, Bordeaux, France

surfers who only thought about doing the turnover necessary to let them live their passion, the board-sports industry has changed into a real economic market with continuous growth for over 10 years, where the leaders are quoted on the stock exchange and are at the head of a world market of more than 10 billion Euros. The board-sports industries activities are now transversal and multidisciplinary and are developed through industrial alliances with strong partners across the continents of North America, Australia and Asia and in other industrial sectors (information technology, automobile, electronics, textiles). The products of this industry are increasingly technical. As an example composite materials are increasingly used to manufacture surf boards and fins, snowboards, skate boards, accessories and clothing are developed with new materials (neoprene with a high level of elasticity, waterproof and breathable textiles), or with new functions (communicating products, video and portable music etc.). This sector has a particular distribution network where knowledge of the sector and the brand's authenticity are necessary in the eyes of the end consumer … even those who do not play the sports. The board-sports companies are becoming serious competitors for the biggest outdoor sports companies, for example Nike or Adidas. More over the international leaders in the fashion market are another form of competition because they target the prêt-a-porter market with a strong network of stores and high-level marketing. So this means that marketing campaigns are not sufficient to win market share. These companies need to develop more and more products and services innovations. However innovations contain complex socio-technical phenomena and processes especially when new ideas of innovative concepts (such as products or services) are proposed. These innovation processes are complex because the first operations of innovative product developments are not well-defined phases of the design activity. Indeed, they are not well-known and combine different aspects such as creativity aspects but also socio-technical negotiation among different stakeholders (i.e. design, marketing, supplier, R&D, and others). In this paper, we propose a model to support innovation in early design phases combined with a methodological approach. The aim is to manage elements that contribute to the definition of the future innovation.

2- Existing innovation models and approaches

The early design phase's context has a high impact on the innovation process efficiency. The difficulties and weaknesses of the involved cooperation processes have been extensively studied (Merlo and Legardeur, 2004), especially when a new concept or a new idea is taken into consideration. During these early phases, exploring new alternatives, such as new technical concepts or technologies, is very difficult and off-putting as the actors find themselves devoid of knowledge in certain areas and tend to remain faithful to traditional solutions that are already proven to be stable and reliable. In the economical field, there are a variety of different innovation theories that have been proposed in the literature. In general, one can distinguish between two principal innovation models: the "science push" model (innovation pushed by the science), and the "demand pull" model (innovation pulled by the demand). These two models are mainly based on the two classical concepts in economy: the offer and the demand. However, they cannot be regarded

separately since the offer and the demand have to be taken into account in order to understand and manage the innovation process (Mowery and Rosenberg 1979, Rothwell *et al.* 1988). In the hierarchy model (Gomory 1999) (sometimes also called "step by step" model), the innovation process is considered as a linear progression towards increasingly practical solutions. The Roozenburg and Eckels model (Roozenburg and Eckels, 1995) follows the same idea, but integrates many parallel components (production, product, and marketing). Kline and Rosenberg consider the innovation as a central chain of design with iterative feedback loops that is interconnected with the knowledge sphere (Kline and Rosenberg, 1986). According to the Weelwright and Clark model (Weelwright and Clark, 1992), a new concept development process caused and taken around a selective funnel by taking account of two dimensions: the offer (Technology) and the demand (Market). Concerning process point of view, Perrin shows that design is « the heart of innovation process » (Perrin 2001). So Innovation is a process to transform an abstract thing into concrete thing (Rodenacker 1970). Hatchuel distinguish Innovative Design and Rule based Design (Hatchuel 1996, LeMasson and Magnusson, 2001). In Innovative Design, product identity is mobile and is progressively established. The performance of Design type process is based on innovation spaces exploration mechanisms. This progressively innovation concepts development is agree with the "actor-network" theory proposed by sociologists Callon and Latour (Callon and Latour, 1986). Innovation is the result of confrontations and compromises between various actors. During Innovation process, both product and actor representation are always changing. It's the "translation model": to adopt an innovation, it's necessary to adapt it and transform it. In the following paragraphs, we provide a detailed background on the PTC multi-input and the C-K theory since they are the key elements of our approach.

2.1 The PTC multi-input model that supports innovation in early design phases

In 2006, we proposed the PTC multi-input model (potential technology concept multi-input model) for the early phases of innovation processes (Pialot *et al.* 2006). Our model integrates both the technological dimension and the market opportunities via the potential dimension. The PTC model is illustrated in Figure 1. The particular characteristic of the PTC model is the association of a concept to a potential of added value of one or more technologies. Its main objective is the synthesis and confrontation of the data coming from the technological survey, the market survey, and the different concepts of

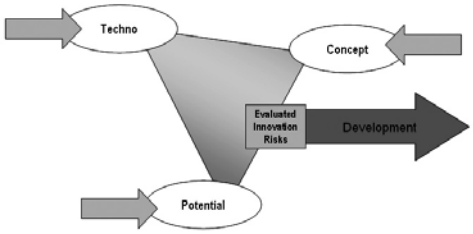

Figure 1 - "Potential-Technology-Concept" model.

solution coming from the idea's portfolio of the company. Furthermore, the PTC model claims (i) to provide a framework in the very early phases for an evaluation of the innovative opportunities and their associated risks, and (ii) to propose a flexible methodology for the exploration of innovation opportunities based on multiple inputs: the potential of added value identification, the technological opportunities emergence, and the innovative concept generation or collection.

We propose to build "PTC Trihedron" as an association of "potential", "techno", and "concept" dimensions relating to a product or a system. The potential of added value dimension models the existing gap between the product and the current or future customer expectation. The potential should take into account not only the approaches concerning the analysis of the customer's need, but also its change dimension. Therefore, the clear identification of the product added value induced by the potential is not only integrated in the analysis of the current need, but also in the analysis of the changes (e.g. usage, way of life). This dimension is relating to the following questions: "Why?", "For who?", "When?" and "Where?". The technology dimension encompasses the technologies (e.g. material, physical principle) and the production techniques for the new product development. The aim is to identify the opportunities offered by the technology (e.g. mechanical, electronic, magnetic) that can open the domain of "the possible". This Dimension is relating to the Question "How?". The concept dimension is related to the different ideas of the new concept of solution issued from any creativity method, from a tools or ideas box, and from the portfolio of the company. This Dimension is relating to the Question "What ?".

It is very difficult to characterize and structure the innovation process phases in order to present the complex dynamics of informal exchanges that the different actors' encounter. Moreover, it is quite hard to structure the richness (but randomness) of the existing creativity methods. The contribution of the PTC model is to highlight the complex character and the need of combinations and confrontations of "multi-input" opportunities for innovation. The multi-input aspect for the innovation regroups the potential, technology and concept dimensions. Their exploration provides many innovation opportunities to the company, and the PTC model's architecture corresponds to the different opportunity origins that exist in reality. For example, every stakeholder in the company can identify relating to a system a problem or a change (potential dimension), identify the use of another material or a different process (technology dimension) or have a new idea of solution (concept dimension). This new intention is manifested in a proposition of a system with one or more new elements on one or more PTC dimension. We obtain a new PTC Trihedron that we then develop regarding the three dimensions. In fact, in the PTC model, the three dimensions are linked and aim to foster the networking between them. In fact, every new input proposition is analysed regarding the three dimensions of the model to add elements from Potential, Techno or Concept dimension to complete the definition of PTC Trihedron. This approach on the three PTC dimensions provides a framework for a first evaluation of innovative opportunities and allows the limitation of the risks related to a future innovation (in order to understand the risks related to innovation, see (Halman *et al.* 2001).

During early design phases, every dimension is not stabilized and changes occur at any time. These changes must be quickly propagated to the other dimensions during the early development to foster decision-making with the most appropriate information and knowledge. The main goal is to propose a multi-dimensional analysis in order to foster point of view confrontations in the very early design phases, according to Callon and Latour theory. This model can also be used as a mapping tool in order to manage the innovation strategy of the company.

2.2 The C-K theory for a conceptual exploration and development of the solution space

The C-K theory, initially proposed by Hatchuel in 1996 (Hatchuel 1996), is named "C-K theory" because its central proposition is a formal distinction between concepts (C) and knowledge (K). The starting point is an interpretable concept without any logical status, or, in other words, a comprehensible idea that cannot be directly materialized. Attention! This starting Concept noted C0 is different to the Concept of Concept Dimension. In fact, C0 encompasses two previously seen notions: "the system" and "the new intention". For a better understanding, consider "Keys that cannot get lost" as an example. "Keys" is the system and "that cannot get lost" the new intention. The principle of the C-K theory is to progressively add properties to the concept by switching between the concept space and the knowledge space. Adding the properties supplies an interpretable "object" that can be finally materialized by a stakeholder. On the one hand, if the property we add to a concept is already known in the knowledge space, we have a restricting partition. On the other hand, if the property we add is unknown in the knowledge space involved in the concept definition, we have an expansive partition. Creativity and innovation are due to expansive partitions of concepts. The tree diagram resulting of the development of the initial concept highlights the exploratory character of the C-K theory. Some branches of the tree are cancelled, others further developed. This formalism supports the exploration by a conscious and progressive development of the different solution concepts starting from the initial concept. The stakeholders have control over innovation concepts development. In this point, the C-K theory differs from the "classical" creativity methods where first several concepts are generated arbitrarily before evaluating them. Moreover, the C-K theory keeps in memory not only the paths that have been followed, but also the mobilized knowledge and the concept expansions. For further details on the C-K theory, we refer the reader to (Le Masson et al. 2006).

3- From the PTC Model to a methodological approach to innovate

Starting from the analysis of the three dimensions of the PTC model (potential, technology, concept), different opportunities for the innovation are identified. In order to develop every identified opportunity, each dimension has to be explored in order to confront the point of views, and thus to innovate. To realize the exploration in the concept, potential and technology dimensions, we propose to open workshops relating to

the questions asked by each dimension: "Why?", "For who?", "When?", "Where?", "How?" and "What?". During the C-K reasoning, Hatchuel et al. propose to use design spaces. A design space is a limited working context that allows learning within the design process. This restriction of the reasoning, or, in other words, localized workshop, is realized for a particular issue and the conclusions are then reintegrated in the principal reasoning. The workshops that we propose are close to Design spaces in "Zoom" spirit but are on the face of it proposed and relating to the three dimensions. So, by starting from the initial proposition and exploring these different workshops, we obtain a lot of properties or elements on the three dimensions relating to the innovation opportunity. In C-K theory, the added properties to initial concept C0 have no specific origin. In the PTC model, the elements from the three dimensions P, T and C you must to combine are not defined. C0 encompasses the two notions "the system" and "the new intention". The progressively added properties are relative to the questions of the different workshops: "Why?", "For who?", "When?", "Where?", "How?" and "What?". So they are relative to the three dimensions: Potential, Techno and Concept. The workshops related to the three dimensions are used throughout the entire design process and "feed" a C-K reasoning continuously. We remind that the formalism C-K supports exploration reasoning by a conscious and progressive addition of properties to develop different solution concepts starting from the initial concept C0: the identity of the future innovation is progressively established. Figure 2 illustrates how the properties issued from the three dimensions refer to a C-K reasoning. The "tree diagram" form of properties is not obligatory.

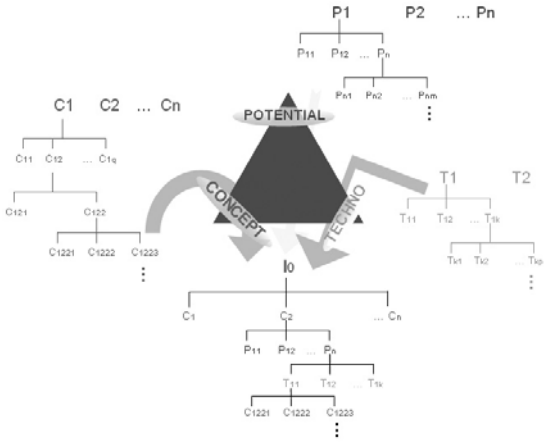

Figure 2 - C-K reasoning resulted from the exploration in the three dimensions.

The limitation of the C-K theory is double: the origin of the initial concept C0 is not specified and the exploration of properties that feed the reasoning is not guided. The PTC model precisely completes these two lacks. In fact our model give a framework for the exploration of innovation opportunities based on multiple inputs: the potential of added value identification, the technological opportunities emergence, and the innovative concept generation or collection. Moreover, PTC model induces to open different workshops based on multiple inputs: the potential of added value identification, the technological opportunities emergence, and the innovative concept generation or collection to obtain various properties from the three dimensions. So the result of this process

is to have best leverage on the elements that contribute to the future innovation identity. Each of the workshops allows all the stakeholders to work in the way they are used to, while being the most inspired. The existence of the three workshops throughout the entire process enforces the continuous exploitation of all the three dimensions. We are convinced that this is a prerequisite for innovation. Consequently, the obtained knowledge and information is rich and accurate in order to better orientate the choices in the early design phases of the innovation process.

4- Towards a tool for innovative concepts management

Until now, the presented process proposes to progressively establish the future innovation identity. Adding the properties supplies an interpretable "object" that can be finally materialized by a stakeholder. To refine the stabilized identity and to develop and to evaluate each innovation opportunity, we propose to use the ID^2 software tool proposed by Legardeur (Legardeur *et al.* 2005). ID^2 is mainly oriented towards the synthesis and the sharing of information about different concepts of solution. The principle is to compare the new proposition with others existing products or projects to emphasize and develop the add value and to define specifications of the future innovation. For this, ID^2 tool provides a collaborative platform for negotiation around a concept-criteria table: the different concepts that should be compared are spread along the columns, and the criteria along the lines of the table. The multidisciplinary team enriches each concept with its knowledge and criteria (Garro *et al.* 1998). The previous explorations supply several criteria for the choice of the innovation. The idea is to exploit these identified criteria in ID^2 tool. The stakeholders progressively supply criteria and have an influence on the C-K reasoning refinement and the development of the innovative solution. By this way, they control innovation development. We can imagine certain interactivity between the mobilized criteria in ID^2 and the C-K reasoning phases. The aim would be finally to track back the mobilized criteria that lead to the definition and development of the chosen concept. For every criterion, we propose to define a results objective in order to have (i) a related concept development or performance indicator and (ii) an estimation of its reliability and maturity. Consequently, the indicator tells us by its value whether the result comes from a formal test or a vague estimation of a stakeholder. Indeed, the reliability consideration takes a non-negligible importance in the early phases of innovation processes where the information is less mature and the input is often unofficial, private, or fuzzy. As a consequence, when the concept-criteria table in the ID^2 software tool is filled, it becomes an interactive tool for managing the innovative definition and development concepts and provides a solid basis for choosing innovation specifications and the right strategies.

5- The "Heated surfing wetsuit" case study

So far, we have presented a new exploration method that integrates the three necessary dimensions that have to be considered for innovation. The theoretical results have been

tested on different examples, and we present here a student's case study of the imagination of a "heated surfing wetsuit". Three workshops are opened. In the added value potential workshop, the questions "Why?", "For who?", "When?" and "Where?" are studied. We started by the identification of various categories of clients that could be potentially interested in the heated surfing wetsuit. For each potential client, the usage value has been analyzed by exploring the different situations that are involved in the given sport. The case study has been restricted to the design space on diving wetsuits that have been studied extensively in order to understand the thermal behaviour. This study supplied conception criteria of the wetsuits. For the technology dimension, a flowchart of the potential technologies has been first created. The aim was to analyze if an existing technology could be used, and to discuss the advantages and drawbacks of every technology. Then, an expert group familiar with the textile industry has been consulted in order to gain the most precise insight about the future of these materials. Finally, more locally, a design space on the physical contradiction between the thickness of a material and its thermal isolation has been studied by using some principles of the TRIZ method (Altshuller 1999). In the concept dimension, Figure 3, some different elements have been modelled: the surfing, the role of a wetsuit, and the heat notion. This information have brought up several questions and various problems, and several design spaces have been created. As a consequence, we acquired a lot of knowledge and many criteria have been identified.

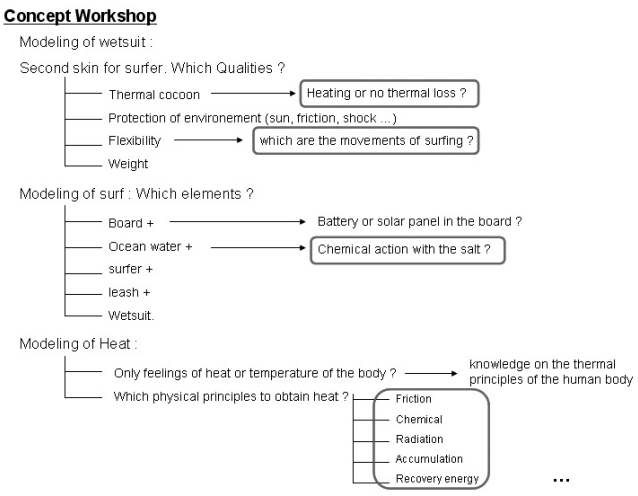

Figure 3 - An extract of the design space of the concept dimension.

All theses different and rich explorations on the three dimensions supply a lot of different properties. Theses properties are combined to advance the reasoning about an innovative conception, and a synthesis in the form of a C-K tree structure can be seen in Figure 3. We see that the stakeholders have control over elements that contribute to the definition of the future innovation.

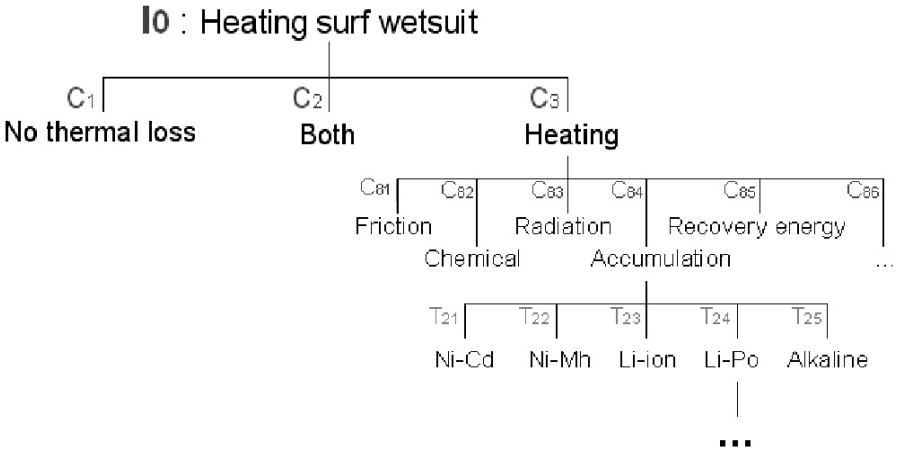

Figure 4 - Reasoning in the form of a C-K structure.

We have now seen how to practically apply our proposition to manage the exploration of the three dimensions on the example of a heated surfing wetsuit. Students work stop at the C-K reasoning tree. The continuation would be ID^2 platform use in order to manage the innovation concept development via criteria.

6- Conclusion

New product/process ideas are thus developed during periods of negotiation and research of solution, which are often informal and unpredictable. At this level the goal of these phases is first of all to be able to bring together a certain amount of data and information in order to justify and consolidate the idea while creating a configuration in which it is possible to launch an innovative project. The PTC (Potential –Technology – Concept) approach is one way to structure this complex process of emergence of a new innovative solution. To have more control over innovations development during this process, the efficiency of the method and tools implies a clear strategic vision of the product, the internal company politics, i.e. a "guide". The results issued from the field (Lauche 2003) reveal the importance of such internal politics during the early phases.

7- References

Altshuller G. (1999) TRIZ The innovation algorithm ; systematic innovation and technical creativity translated by Lev Shulyak and Steven Rodman, Technical Innovation Center Inc., Worcester, MA.

Callon M., Latour B. (1986) « Les paradoxes de la modernité. Comment concevoir les innovations? », Prospective et santé, 36.

Garro O., Brissaud D., Blanco E. (1998) Design Criteria. In the proceedings of 9th Symposium on information control in manufacturing INCOM'98, Advanced in Industrial Engineering, Nancy – Metz, 24-26 june.

Gomory R. (1989) From the Ladder of Science to the Product Development Cycle. Harvard Business Review, Nov.-Dec.
Halman J., Keizer J., Song M. (2001) Risk Factors in Product Innovation Projects. In Conference The Future of Innovation Studies, Eindhoven University of Technology, the Netherlands, 20-23 September.
Hatchuel A. (1996) Les théories de la conception, Paris.
Hatchuel A., Le Masson P., Weil B. (2004) C-K Theory in Practice : Lessons from Industrial Applications. In the proceedings of the 8th International Design Conference, Design 2004, Editor D. Marjanovic, Dubrovnik, 18-21 May, pp. 245-257.
Kline S., Rosenberg N. (1986) An Overview of Innovation. In Landau, R., Rosenberg, N. The Positive Sum, National Academy Press, Washington.
Lauche K. (2003) Sketching a Strategy: Early Design in Different Industrial Sectors. In International Conference on Engineering Design, ICED 03 Stockholm, Folkeson Gralen Norell Sellgren (Ed.), Design Society, pp. 125-126.
Legardeur J. Fischer X., Vernat Y., Pialot O. (2005) Supporting Early Design Phases by structuring innovative ideas: an integrated approach proposal. In the CD-Rom proceedings of the 15th International Conference on Engineering Design, Melbourne, 15-18 august.
Le Masson P., Magnusson P. (2002) Towards an Understanding of User Involvement Contribution to the Design of Mobile Telecommunications Services, 9th International Product Development Management Conference, European Institute for Advanced Studies in Management and Ecole des Mines de Paris, (Ed.), Sophia Antipolis, France: 497-511.
Le Masson P., Weil B., Hatchuel A. (2006) Les processus d'innovation : conception innovante et croissance des entreprises, Lavoisier Paris, ISBN 2-7462-1366-4.
Merlo C., Legardeur J. (2004) Collaborative tools for innovation support in product design. In the proceedings of the 8th International Design Conference, Design 2004, Editor D. Marjanovic, Dubrovnik, 18-21 May, pp. 787-792.
Mowery D., Rosenberg N. (1979) The Influence of Market Demand Upon Innovation: A Critical Review of Some Recent Empirical Studies, Research Policy, vol.8, pp. 102-153.
Perrin J. (2001) «Concevoir l'innovation industrielle, méthodologie de conception de l'innovation», CNRS éditions, Paris, ISBN : 2-271-05822-8.
Pialot O., Legardeur J., Boujut J.F., Serna L. (2006) Proposition of a new model for early phases of innovation processes. In the proceedings of the 9th International Design Conference, Design 2006, pp. 603-610, Editor D. Marjanovic, Dubrovnik, 15-18 May.
Rodenacker W.G. (1970) Methodishes Konstruieren, Heidelberg, Berlin 1970 (seconde édition, Springer, New York, 1976), in Engineering design, Springer verlag, London, 1988.
Roozenburg N.F., Eckels J. (1995) Product Design: Fundamentals and Methods, John Wiley & Sons.
Rothwell R., Schott K., Gardinier J.P. (1988) Design and the Economy: The Role of Design and Innovation in the Prosperity of Industrial Companies, Design Council, London.
Weelwright S.C., Clark K. (1992) "Revolutionizing Product Development", The Free Press.

The management of sporting innovation at Decathlon. Between rationality and chaos (P262)

Guillaume Richard*, Yann Abdourazakou*

Abstract: The point under study is the first of such a nature. We investigated the management of innovation in the company called Decathlon. In recent years, vertical integration has rarely been so much developed as in the leading company of sporting goods' distribution in France. Based on the group's "sporting universe" concept, it now challenges some bigger firms' on their main segment. We interviewed the head of innovation for Decathlon's brands in France and Europe. Since the 1990's, Decathlon's strategies have not taken a unique and rational way towards success. Sometimes unexpected, they do not fit the traditional and rational management model of this aspect of competition between firms. Finally, some non technological aspects of innovation play a key role in the group's success.

Now a major force in the domain of sports equipment, the company Decathlon represents today almost half the French market in the distribution of sporting articles[1]. From bikes to rucksacks, from hiking boots to tennis rackets, this brand has acquired a great deal of savoir-faire in the conception, the realization and the production of its "universe" brand. By way of an example, Decathlon is the biggest producer of bikes (Btwin) in the whole of France, the number 1 in the country for rucksacks and the fourth largest producer in the world of sporting goods. The producer of sporting equipment has thus made the choice of a differentiation through innovation[2]. The model of innovation used by the company has allowed it to obtain a durable advantage in relation to other distribution brands such as Intersport and Go Sport. Its originality is based on a culture of innovation associated with certain values such as pleasure, accessibility and a "practical" character regarding the use of the products. How has the company developed two of its leading products? The "2 second" tent and the wet suit "Inergy" illustrate the production logic of the "sporting" innovation at Decathlon. Based on a resources approach, the objective of this research project was to study the organizational capacities developed by the group in terms of "sporting" innovation.

* *Équipe de recherche en sciences sociales du sport - ER3S, Laboratoire Sport Identité Culture - SIC, Faculté des Sciences du Sport et de l'Éducation Physique, Université Lille 2, 9, rue de l'Université, 59 790 Ronchin.*

2. The sports market in France (articles and services destined for the practice of sport and leisure activities) can be estimated at approximately 8.9 bn € in 2006. This figure is made up in the following way: 6.7 bn € turnover realized by 4 000 shops specializing in sports and leisure articles. The specialized commerce is dominated by national and international companies, of which the first five (Decathlon, Intersport, Go Sport, Sport 2000 and SED / Twinner) alone represent more than 80% of the specialized turnover. Approximately, 2.2 bn € realized by the other companies in non specialized distribution (department stores, prêt à porter, footwear, mail order catalogs, etc). Source: www.filieresport.com, consulted 07.09.07.

2. Unlike other leading companies such as Salomon, 70% of innovations come from R&D (Decathlon Creation). "The policies of innovation in the sporting industry: the case of the equipment producer Adidas", Revue européenne de management du sport, nº 14, December 2005, p. 10. Moreover the companies efforts are mainly concentrated on innovation and the quality of products.

1. Positioning of the research

Innovation management within a company varies according to the sectors in which they are positioned. These characteristics can go as far as being specific to the company itself (Smallbone, Leigh and North, 1995). An important part of the variations observed depend especially on the personality of the "director-owner" (Smallbone, Leigh and North, 1995; Autio and Lume, 1998). The usual classification is between two types of innovation: product innovation and process innovation (Abernathy and Utterback, 1978). The notion of life cycle makes it possible to highlight the two main orientations of companies involved in an innovation process: to accentuate the continuity in the innovative activity or to look for a break with the past by developing new skills (Autio and Lume, 1998). The firm thus manages its innovation process between the exploitation of existing sources and the exploration of unknown horizons. Two traps however, lie in wait for the company going through the innovation process: that of failure and that of success. The result is not simply the consequence of the activities of research and development (R&D) but a process which will engender uncertainty and instability (requirement of new skills, modification of the distribution of resources, re-evaluation of the strategic universe…). In this case, two types of interaction exist. It is thus possible to distinguish an initial interaction between the different functions involved in the innovation process (integrated model), and a second one acting between the company going through the innovation process and its sector environment.

The research carried out is of an exploratory nature and the collection of data combines documentary analysis and the maintenance technique. The documentary data are used as the basis for comparison and interpretation to the primary data. As regards the method of collecting the primary data, we chose the interview because of its absence of formalism. Firstly, this method which is only slightly directive, seemed more adapted to one of the leading company directors, unfamiliar with more sophisticated techniques. Secondly, allowing the interviewee to structure his own answers, the interview made it possible to capture the subject's logic before rationalization *a posteriori* inherent to any form of longer reflection. Breaking down by topics[3] allowing one to understand the process of innovation at Decathlon and the acquisition of distinctive skills. Based on the interviews, the resources approach makes it possible to highlight the specific assets of a hyperfirm[4] (Marchesnay, 1997) in its strategic development. The main objective of this approach is to understand why, within a single environment, companies are different. Above all it allows us to identify the factors which maintain these differences and which are the source of different levels of performance between them. Therefore, we opted for a prolonged interview[5] because this form of inquiry is, according to the authors, the only one capable of putting the person interviewed at ease so that he or she speaks freely of the innovations developed within Decathlon.

---

3. See recapitulation table, p 9-12.

4. Large company (LC) with more than 250 salaried workers.

5. Prolonged interviews do not aim at producing quantified data and so do not need to be numerous. They are not supposed to be 'representative'. Beaud S. and Weber F., 1998, Guide de l'enquête de terrain, p. 117. In an interview, more than constituting a cross-secation, the aim above all is to carefully chose one's interviewee, in our study, the innovation director for the Passion brand of Decathlon.

2. The resources approach

Our work is based on the postulate that certain non technological determinants of innovation[6], in particular the organizational capacities developed for innovation play a significant role in Decathlon success model. Which factors make it possible to explain the obtaining and the development of durable competitive advantages in a single sector? What are the characteristics of the skills which appear initially? With what and how historically do they combine with one another? In order to answer such questions, it is necessary to operationalize the resources approach and the concept of "core competencie" (Hamel, Prahalad, 1996). The concepts of "resource" or of "strategic assets" spring from the will to describe with precision the company's potential as a whole. Here they constitute elementary entities making it possible to define this potential (Barney, 1991, Dierickx and Cool, 1989; Peteraf, 1990; Wernerfelt, 1984). A resource is also a potential which must be used in the goal of creating value for the client (Barney, 1991 in Rindova and Fombrun, 1999). The aim is to appreciate the characteristics of certain firms capable of identifying and imposing certain of their strong points as rules of the competitive game. Wernerfelt (1984) defined a resource as a tangible or intangible asset belonging to the company. For Grant, (1991): "*resources are more or less complex to construct or acquire, which determines their power of differentiation*". A skill is defined as a capacity to realize a task or an activity by way of resources. Makadoc (2001) makes an even clearer distinction between resource and capacity. From his point of view, a resource is an observable asset (but not necessarily tangible) which can be evaluated and exchanged just like a brand, a plot of land or a licence. A capacity, on the other hand, is not observable (thus necessarily intangible) and can neither be evaluated or exchanged in part but as a whole. The notion of resource, in its proper sense, is rarely questioned: it designates the two elements necessary for a company to function: the resources and the capacities. Indeed, the resources specified in this way do not suffice to express the internal potential: one is not concerned with the exploitation thereof (Penrose, 1959). The notion of skill is more complex. It was tackled very early (Selznick, 1957) under the topic of distinctive skills (domains in which companies excel). Hofer and Schendel (1978) were the first to establish the link with resources. Since then, even though certain authors (Hitt and Ireland, 1985; Peteraf, 1993) continue to see the link with distinctive skills as paramount, most approach skills from the resources point of view. Thus skills are an opportune combination of resources. According to the approach based on resources, organizations are made up of a set of organizational resources and capacities. When these different organizational resources and capacities are heterogeneous, rare and difficult to imitate or acquire, they are considered as strategic assets. The presence or absence of these strategic

6. For the authors, innovation can be defined as a complex and cooperative collective process. It is the use of a savoir-faire and a technical culture which has been created over time thanks to an internal dynamic, particular to the company. Each company presents itself as a configuration of agents and of economic, social, cultural elements with specific modes of organization and regulation. According to us, only those which are introduced on to the market are worthy of the title 'innovation' or those in the production process. However, as Cross, (2001) pointed out, the word 'innovation' is one which, to maintain its efficacity, cannot be blocked in to the frame of a definition which would take away all the word's magic, all the ambiguity of its attraction. It is a term which is defined by itself through social usages. It has an imaginary element which cannot be cut into clearly circumscribed parts.

assets thus explains the differences in performance between the organizations which are in competition at a given time on a given market (Amit and Shoemaker, 1993; Arrègle, 1996; Barney, 1991; Eisenhardt and Martin, 2000; Grant, 1991; Hamel and Prahalad, 1995, Peteraff, 1993; Teece and *al.*, 1997, Wernerfelt, 1994). According to St-Amant and Renard (2004), organizational capacity concerns the *"deployment, the combination and the coordination of resources, skills and knowledge through different value systems to put into practice strategic objectives*[7]*"*. The principle of the approach based on resources (Penrose, 1959; Barney, 1991) therefore consists in modelling the company on a set of resources which, respected and combined lead to a certain number of specific organizational aptitudes (Métais, 1997). Developing a durable competitive advantage supposes having resources difficult for competitors to imitate and appreciated by clients within a complex process. Can rationality and chaos constitute distinctive skills in sporting innovation?

Rationality and chaos: two organizational possibilities for sporting innovation?

In 1995, Microsoft presented its "Internet" strategy. The latter was based on technologies brought together from within the Microsoft Network which launched itself into a frontal attack against AOL. Two years later, at a meeting for former employees, an executive in the company, blocked by a snow storm, visited the campus to pass the time. There, flabbergasted, he discovered how the students were surfing the "web" and realized Microsoft's monumental mistake which consisted in setting up an ownership type technology in a world that had become free and open. The email he sent to his company president, Bill Gates, had monumental consequences. The latter decided to completely reconsider the strategy that the company had adopted up until that time, to risk $300m and to affect 2 000 engineers to a new division working exclusively on the Internet. This example illustrates a brutal strategy turn around on behalf of one of the biggest companies in the world. Above all, it shows that one of the contemporary characteristics linked to the ever more rapid changes of the corporate environment is the flexibility and the permeability of the environment. Today, more often than not, the key to the strategy is a question of movement, change, adaptation, going back, hesitations, seizing opportunities, and accompanying emergence (Thiétart, 2000). In complex systems, several opposing forces are in play at any one time. Certain push towards instability and disorder. For example, in the company called "3 M", individual initiative and experiment are encouraged. The employees have fifteen minutes per day to do activities that they want to without constraint. This sufficient liberty is given to the researchers, to innovate, by giving them access to sufficient resources in order to explore without constraint new domains. On the contrary, other forces lead to stability and order. For example, in companies, planning, monitoring, and structuring are forces which encourage stability. Planning, by favouring information and communication, is a means to deal with

7. St-Amant G and Renard L. (2004), Aspects théoriques d'un cadre de développement des capacités organisationnelles.

complex decisions. **Through the breaking down of the general objective into elementary tasks, executives in a hyperfirm can organize innovation** and set up a system of planning which improves the visibility of the medium and long term actions within the organization. This breaking down also improves the quality of the numerous links to the environment. Finally it helps to close a system which is too complex to be apprehended in a general way. The main aim of monitoring is to control what the company does. As a formal tool, it contributes towards better surveillance and coordination of the different tasks undertaken in the framework of a particular mission. Structures are there to create formal links between actors, to delegate responsibilities, and to clarify the allocation of tasks and actions, and therefore to reinforce stability. Other forces can create instability and disorder, like, for example, rupture style innovations coming from competitors or a modification of the rules governing competition.k

Most research has highlighted the limits of the classic model of the company which has to evolve in a turbulent environment. Being conditioned by rational thought and a very present formalism in the strategies of directors, numerous hyperfirms often miss opportunities which appear within their organization or environment. It is, in effect, reassuring for the strategist, to have recourse to a directive and planned style of management rather than a more supple and chaotic perspective. Procedures have been put into place in each one of them aimed at reassuring department heads notably in order to enable them to avoid all forms of disorder.

Sports companies come up against ever more complex problematics in terms of the management of "sporting" innovation[8]. Over the last thirty years, the development of technological innovation has been the subject of thorough theoretical analysis. Certain researchers have concentrated on the strategic vision (Hamel, Prahalad, 1995), others on the management of R&D (Tarondeau, 1991), on the management of innovative projects (Giard, 1991) and finally on the marketing of innovation (Gaillard, 1997). These research findings have often been applied outside of the sporting sector (the food, the pharmaceutical, the chemical or the electric industry) and have therefore often excluded from debate the specificities of the sports sector in terms of marketing notably (Desbordes, Ohl, and Tribou, 1999). Sport encourages the consumption of goods with a strong technological added value (AV) but it is often linked to symbolic values which can at times extract its only practical use. Oriented towards technological marketing to attract new clients, the capacity for innovation constitutes the main resource of sporting companies engaged in the sectors with a strong technical and technological AV. The Decathlon model thus illustrates the development of a strategic resource in the sector: an original "sporting" model of innovation. Our problematic consisted in examining, based on the model of Decathlon, whether a firm allows chaos to develop in its management style. The case of the organization of innovation at Decathlon seems to suggest that it is at the frontier of chaos that "sporting" innovation is created.

8. For Hillairet (1991), sporting innovation is an abstract phenomenom resulting from the succession, the combination and the accumulation of innumeurous changes. L'innovation sportive - Entreprendre pour gagner, Paris, L'Harmattan, p. 9. We have left in inverted comas the term "sporting" to underline our theoretical position towards the author.

3. Decathlon's innovation model

Innovative companies have often rethought their management model through introducing a certain form of liberty. This capacity to create a certain form of flexibility constitutes a strategic resource which makes it possible to develop a culture of innovation at all levels. The latter is an important factor regarding creativity within the organization which then becomes a capacity to innovate. A certain liberty, even a certain disorder, often seems necessary for creativity and innovation to emerge; innovation, which today in the face of competition from Asian countries is the only means of survival. However, this disorder implies that the hyperfirm take certain risks the consequences of which it will not necessarily be able to control. Furthermore the company will continually be at the limit of no longer controlling anything; a frontier which belongs to implicit knowledge and which it is difficult to appreciate in a rational way. But it is the capacity to know this limit and to go as close as possible to it which will make or break the company and the experts which make it up. More than the sum of their knowledge or their degree of specialization, it is their capacity to grasp and solve complex situations which is paramount today. Based on two examples of sporting products from the main Decathlon brand, we now present an analysis of the innovation strategies in the industry of sports articles (ISA) in order to put two hypotheses to the test:

H1: innovation can be opportunistic (a complex and unpredictable process) but which necessitates, basically, a form of company organization known as "creative and innovative";

H2: innovation fulfils a need to solve a technical problem to attract new consumers and to free up market shares in sectors with a strong technical and technological AV. Here it would rather be part of a rational approach.

From its creation in 1976 onwards, Decathlon has relied on innovation to propose quality sporting articles thanks to its Decathlon research centre, situated in Villeneuve d'Ascq. However, this **innovation culture** is not solely focussed on the technological aspect. Indeed, the hyperfirm only rarely innovates on the latter rather it concentrates mainly on its commercial approach or on the conception of new sporting products. It would be reductive to, even destructive for a company, whatever its size (hypofirm[9] - Marchesnay, 1997), to only focus on one aspect of innovation[10]. Since 1997, the R&D centre Decathlon Creation has studied the human body in movement. Its objective is to improve the safety, the health, the comfort and the pleasure of sportsmen and women. With the research department and the design teams[11] within the brands, innovation is really at the heart of the company. Indeed, almost 300 engineers work on R&D, concep-

9. Small company (SM) when firms have between 10 and 20 salaried workers and Very small company (VSC) for between 1 and 9.

10. Innovation is a large, ambivalent concept, which has many faces according to the type of approach in which one is based (economy, sociology…). The vision and the interpretation of innovation will differ. Indeed, for too many people, innovation is still limited to technological innovation. It cannot be reduced to only to research. In truth, it covers very varied domains: technological innovations, social ones, schooling ones, financial ones, organizational ones… For example, innovation can be defined as the successful production and assimilation of what is new in economic and social spheres. It is important to consider innovation, above all, as a social phenomenon.

11. The Decathlon design centre is the second most important after that of Renault. There are approximately 80 designers. For the authors design is one of the motors of innovation.

tion and tests. The director of innovation[12] describes the innovation process at Decathlon as very macro, the latter can be broken down into three stages. **The initial stage is called "vision"**, its objective is to identify new targets and new approaches. In keeping with the brand's philosophy, this strategic phase makes it possible to "*define relevant targets (…) and with a strong potential for innovation*". Indeed, the definition of need in relation to a use is paramount for a brand. Based on comments from customers, feedback from shops and remarks from athletes, the project director thus defines the specifications of utilization. The next step is the technical specifications, in which engineers process the components collectively[13]. The technical specifications define the components and the assembly procedures according to the specifications of utilization.

The second phase, more classic in style, is **the project phase** in which one projects on the "sporting" innovation, the creative part to find ideas. The following stage is R&D, initial study and creation of the project as such. From then on, the head of industrial prototypes realizes a first prototype in the prototypes and industrialization workshops[14] in Villeneuve d'Ascq. Once the prototype has been created, it is not only tested in laboratories using torture tests but also in realistic conditions, on the field, by "the testers club", a panel of clients and Decathlonians, in order to test the quality and the safety of the product. It is necessary to produce several prototypes before deciding on the final

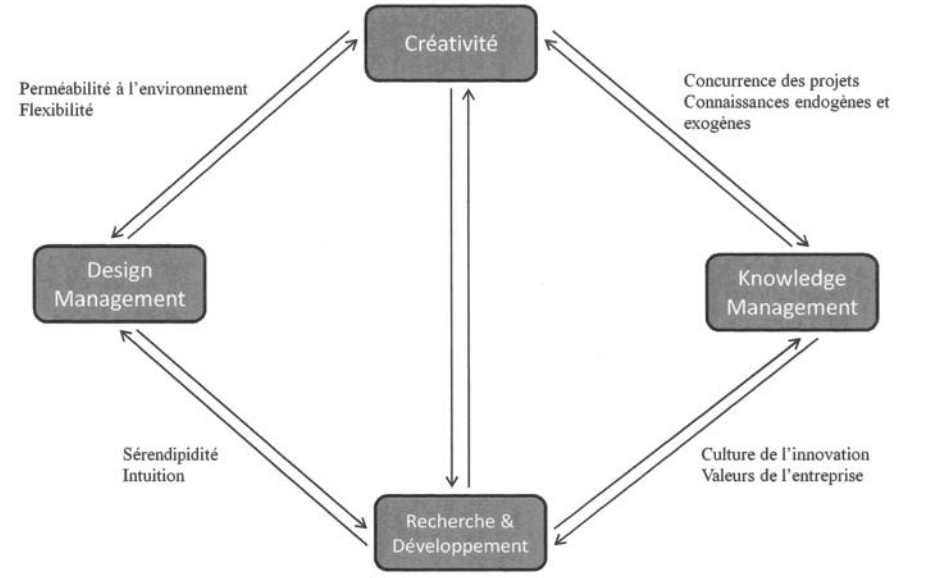

Source: personal elaboration.

Figure 1 -The 4 principles to manage and organize innovation at Decathlon Creation.

12. Information gathered on the 22.08.07, at Decathlon Campus, from the director of innovation since 2005 for the Passion brands at Decathlon.

13. It is paramount to add that Decathlon also collaborates with 60 laboratories and engineering schools in France and abroad.

14. 100% of Decathlon products are prototyped.

one. Once the product has been perfected, a final list of technical specifications is then sent to the different countries where the Decathlon production offices are found. The fabrication will then be undertaken by a sub-contractor, paid by Decathlon, based permanently in the country in question. It is their responsibility to supervise the sub-contracting; the supplying of components by chosen sub-contractors, the quality of the end product and the delivery dates in the Decathlon production warehouses. All the fabrication stages are thus monitored by the company, from the choice of components, the fabrication process, to the finished product delivered to the warehouses.

The last phase which is in no way negligible is **commercialization and communication**. This stage of implanting the product consists in presenting it to possible customers, in the shops, in the specialized press and via advertisements. The weight of these three phases can vary from one project to another. "*There are products which will be perfectly inspired from Vision (Decathlon), others which will be great opportunities and which will upset the first part but bring a revolution to the market*" said the director of innovation. However, according to the nature of the project, it is not always advisable to systematically reproduce the same process for a new sporting product. This is why Decathlon tries to follow this general procedure: "*you need quantity, you need a lot of ideas (…), the process consists in trying in some way to enrich the reflection, to always be creative (…)*". Concerning its organization, Decathlon has "*a slightly chaotic, organic logic*": "*it's not very structured, we try to think outside the box, we put everything behind it and whatever it costs we come up with something*". This original process gives a certain liberty, freedom of spirit and creativity to each one of the Passion brands: "*it is in the interest of each brand to concentrate on a certain number of priorities but we try to define an optimal level to constitute the means and then, have a chance for the product to emerge successfully*". However, this heterogeneity has the same objective; the commercial success of the sporting product. This is why Decathlon stands out from its competitors such as Adidas and Nike. In terms of innovation, the latter have a much more marketing style approach with much wider targets. The main objective for Decathlon is to highlight the technicity of its products to attract consumers who are sportsmen and women.

3.1 The case of the Quechua "2 seconds" tent

Decathlon has created instant tents called "2 seconds", this being the time it takes to set up the tent. This tent, which unfolds and sets up itself, is as spacious as it is compact, once it is folded into its carry bag. This new generation of tents was conceived in answer to customer demands; rapid setting up ("*Throw it into the air, it comes back down already in place!*") and as compact as possible for transport. Its waterproofing was tested in a laboratory (under 450 liters/h/m^2) and during mission tests[15]. An international copyright was applied for. On the practical level all one has to do is throw the tent into the air or place it on the ground and it unfolds itself and sets itself up into position. Jean-François Ratel was the creator of this unique concept. An inventor for Decathlon, he solved the problem

15. Made up of engineers, product leaders and sportsmen and women of all levels, their objective is to collect "on the spur of the moment", information allowing the brand Passion to reach towards maximum quality.

for numerous hikers and campers. Indeed, after many hours hiking setting up a tent can be an arduous task. It was by creating a game tent in the way of a prototype that he managed to perfect the "2 seconds" tent. With a double roof, the model which is sold integrated, in its system, synthetic breathable arches and canvas, to avoid condensation. Lighter and more fun, the Quechua "2 seconds tent" hangs on to the outside of rucksack using a special strap. It only takes 10 seconds to fold it back up again after use.

The "2 seconds" tent is categorized as a level 4 innovation at Decathlon[16], this means that it is a major innovation, not only regarding the nature of the product but also that of the process. For users and for the tents market, this product introduces an exceptional usage benefit. Indeed, this tent has restructured the market of tents in so far as the company created a new need, a new market, that of self-setting up tents with a double roof. By launching this product, Decathlon asked itself a double question: replace or create a new market? For approximately ten years, the project leader was aware of what the customers wanted: a tent which could be set up rapidly, compact and light, and which could be carried easily using a rucksack. The test people (the testers club) were dreaming of a tent which could be set up like that and would throw their arms into the air to show what they meant! However, no technical solution was available to answer the criteria; weight, size, setting up. A priority of functions choice was made, rapid setting up, the weak point of tents.

	Quotes
Project origin	The origin of the project goes back to approximately 1995*: "Assembly tents, instant assembly systems like that have existed for years on the market but mono roof types, shelters"*. The starting point goes back to 2003-2004, said the director of innovation: *"in fact, there was an opportunity, a bit of a risky move, unforeseen, rather an opportunity which got people interested in this type of setting up which created, provoked, the project! (…) It was really a latent need which was identified and an opportunity, a really random thing that happened and wow what have we got here*?" Indeed, 4 elements were at the origin of the project: *"there was another alternative project which was sort of in the same style or spirit, which was already being worked on here at Decathlon. The market research really underlined the importance of the setting up and there was an outside element which proposed something to us which was about the same thing"*.
Structure	Decathlon has a human and equipment structure which is conducive to innovation and to creativity where human capital has its importance: "*in terms of internal organization, we had someone who was taking care of innovation for Quetcha and whose job it was to develop innovation and who had the time and the motivation and therefore it was their job which made it possible to liaise and make it all happen (…). And if there had been nobody to take charge of it with a slightly different approach, their was a project leader, who didn't have this rupture style approach or risk taking style so it was a combination of opportunities; project/product ideas. But at the same time there was something else, a human and organizational context which meant that it could all come together! It was an internal / external mixture if you look at all the parameters, (…), if you take away any of these elements it just might not have happened"*.
Launching	The launch was very complicated and laborious*: "there was risk taking and a need to reassure ourselves, to say "yes" it can work!"* Indeed, the "2 seconds" tent was in competition with other projects and the innovation strategy at Decathlon is rather particular. *"The project leader was working on the umbrella system, other systems existed, more complicated, heavier so he had his mind on that, he had been working on it for some time (…)"*. It was as part of a logic of diversity that Decathlon launched a multitude of projects at the same time, they were not focused on specific research axes or constrained in any way. For the innovation director *"you could say that it was a stroke of luck but at the same time, it is also a question of creating lots of opportunities to have more chances so that one or two exceptional projects emerge"*.

16. This is the highest category of innovation at Decathlon. The categories range from 1 to 4 according to two main criteria concerning, on the one hand, the use and, on the other hand, the technical aspect. Based on these two axes and the level of rupture four classes of innovation have been set up. Level 1 is the lowest in terms of modification of the use and the technical aspect. In this case we are in the domain of improvement, of progress rather than rupture style innovation. The highest categories are those which mange to modify the usage, based on new technology or by slightly changing the techniques or the procedures, at diverse degrees (category 4).

3.2 The case of the wet suit Tribord Inergy

Developed with the technical partners[17] of Tribord such as Nicholas Capdeville (Three times winner of the World Body board Championship), Emmanuelle Joly (Five times winner of the European Surfing Championship and the French school of surfing excellence[18]), the Inergy wet suit allows total freedom of movement[19]. For its creation, numerous studies of the human body in movement were carried out as well as a study of the skin using a scanner. Conceived for use in body board and surfing, the Inergy wet suit is made out of Duramesh Neoprene[20], giving it maximum elasticity; this also has the advantage of limiting the freezing effect at the level of the trunk, that is to say a brutal interruption of movement by the person wearing it. Ultraspan / Xtend anatomically designed suit parts create perfect adjustment for joints and the back and thus limits stiffness in the arms. These different parts of the suit are both sewn and glued together (S-Seal) which limits the amount of water that gets inside. Another technical characteristic is the pre-forming of the chest part which was thought out taking into consideration women's expectations. Thus, this product was conceived to offer as many sensations as possible when in contact with the water and to guarantee, at the same time, optimal thermal comfort with a total freedom of movement. The benefits for users are significant; more ease, less fatigue and more pleasure. The brand Tribord applied for an exclusive patent for the Inergy wet suit.

---

17. For the Quechua brand, numerous technical partners participate in the elaboration of new products such as Karine Ruby (World Champion in snowboard and boardercross) who spends five weeks per year conceiving and testing new equipment developed by the brand. Richard Gay (gold medallist in bump skiing at the last Olympic Games) also participates in the conception of the new line of clothes in skiing technique. The team which won the Gauloise Raid, contributes to the development of the Raid type equipment. Recently, high mountain guides and ski instructors have started to use Quechua equipment and specialized shops in the resorts have applied for permission to stock the brand products. Moreover, this association with famous sportsmen and women in these sports is an opportunity for the brand to submit its range of products to intensive use and thus to improve, its products gradually through experience under these very testing conditions.

18. The French School of Surfing Excellence is a sports study section of a high level, based at the Rene Cassin High school in Bayonne and which is made up of the best young national surfers.

19. For the director of innovation, "the taking into account of the freedom of movement was minimal, almost inexistant on the market". The Inergy wet suit is considered at Decathlon to be a technological innovation.

20. After negotiation, Decathlon was able to benefit from savoir-faire from Yamamoto, world leader in neoprene (Japan). The technical advance of the Inergy wet suit was decisive for its production. The preparatory work by the R&D team, directed by Philippe Freychat, made it possible to obtain greater production volumes. Indeed, "the VA that we brought into the project also served as a way to re-establish our place on the market, show our ambitions and then obtain some means from this industrialist (…)".

	Excepts of the interview
Origin of the project	Even though the project developed by Tribord in 2003-2004, the procedure was different to that of the "2 seconds" tent. At the origin, this wet suit was destined to be used for surfing in which technical skills and the fluidity of movement are essential. Decathlon went to great lengths to respond to several technical constraints: *"the aim of the wet suit was to bring much greater freedom of movement with a product which protects from the cold"*. Indeed the first main objective of a wet suit is to protect a surfer from the cold. However, the thicker the neoprene, the greater the loss of freedom of movement; this will necessarily affect technical gestures. In order to solve this problem, Decathlon "*set out from a much more scientific, R&D, point of view on the understanding of the elasticity of the skin in order to base the construction of the wet suit on this"*. After research work *"we made tests with filament on the skin to imagine all the surfer's movements etc. and after, based on all this knowledge we added a development of knowledge about materials to identify all the different natures of neoprene, in terms of stretch, tonicity etc. because elasticity is not the only way to allow movement but there is also perhaps the accompaniment to the tonicity, the nervous return, I mean neoprene which will make it easier for surfers to ride the wave"*.
Nature of product	The result obtained by Decathlon is "*a completely exclusive combination which unites in the best way possible, the demands regarding protection from the cold of the human body and the problematics of ease, freedom of movement, elasticity of the human skin*". For the Tribord Inergy wet suit, *"the approach is much more directed, driven, and voluntary*". Defined as an innovation of the second level, this is a much more technical product and the benefit regarding its usage is much more subtle for the user. Compared to the "2 second" tent, this strategic product[1] "*is designed for high level surfers, there is another approach concerning price. Evidently we are going to reach people, regular surfers, and even more occasional ones who want to have a good quality product from the start. But, it is, in effect, a product designed for the specialized market"*. Contrary to the Inergy wet suit, the "2 seconds" tent is, both an endogenous and exogenous innovation regarding the company
Structure	The organization of Decathlon makes possible a certain permeability, it is open to the outside world: *"we often meet inventers, we are open to propositions, we often receive the latter and that guy arrived just at the right time[2]"*. The resources people allow the company to improve its knowledge or to conceive a new sporting product. *"It's strange but there is nevertheless an effect when someone comes from the outside, often people pay attention. They give more credit to an idea that comes from the outside than to one that's internal, I don't think it would have had the same impact (…). Therefore we worked especially hard to find a solution, we positioned ourselves much more clearly. In that respect, it got things off to a good start (…)"*.
Objective	With this "sporting" innovation, the company's goal was to *"position ourselves very clearly on an existing market and to gain a greater share of the market without upsetting everything"*. The fortuitous meeting enabled the Decathlon Creation teams to create an innovative sporting product: *"our problematic, to make it a real innovation, coherent with our offer and what we want to do, was to give it a double roof, it was to have a double roof so to find a technical principle which makes it possible, with the double roof, to have a tent, a real one!"*. Single roof tents which were self setting up had already existed for a few years, which is why Decathlon, aware of this technical problem (condensation), took up a clear position "*if we used this principle and if we added our constraints, our requirements concerning the double roof, the size (…). And there, it was a real technical problematic which was in front of us which we didn't have the solution to. So, afterwards, there was some serious internal work, teams of engineers, model specialists, project leader, designers to find solutions to the technical problematic"*.

1. The director of innovation points out that this innovation "is much more oriented on becoming the leader in or very good at neoprene wet suits". This is why, Decathlon found a slightly different approach angle; total freedom of movement.
2. "He arrived at just the right moment, in the right context because we were working on that point, because we were looking for that, you see".

4. Decathlon's model of "sporting" innovation

As we have seen, the two "sporting" innovations mentioned took different paths within Decathlon. The latter generated its two products under total independence, at the very

heart of the company using its research centre[21]. The "sporting" innovations are endogenous, on the one hand, because they are the result of a real innovation culture. On the other hand, they are exogenous since Decathlon encourages a certain permeability and flexibility in relation to the environment. As its leader points out, innovation is entirely internal (Decathlon Creation): "*created, led from top to bottom (…). We maintain several forms of creativity during the project, therefore some options, ideas emerge along the way*". He gives the example of the Inergy wet suit which was in competition with another wet suit project: "*it was the other project that had the upper hand and in fact there was a test phase and the results were deplorable so that we had to go to the original project and accelerate it. You see it wasn't a simple straight road, so to speak, there were instituted phases that meant that this project came to fruition rather than another* (…)". However, this emergence of innovating projects is due to an organization based on chaos, uncertainty. "*The difficulty in the company is that there is inertia, everyone's busy, I can't say hey I've got a great idea, stop everything! (…). There was a moment of latency in the company, the time necessary for us to decide that the idea was good and what's difficult is to get people's time,*

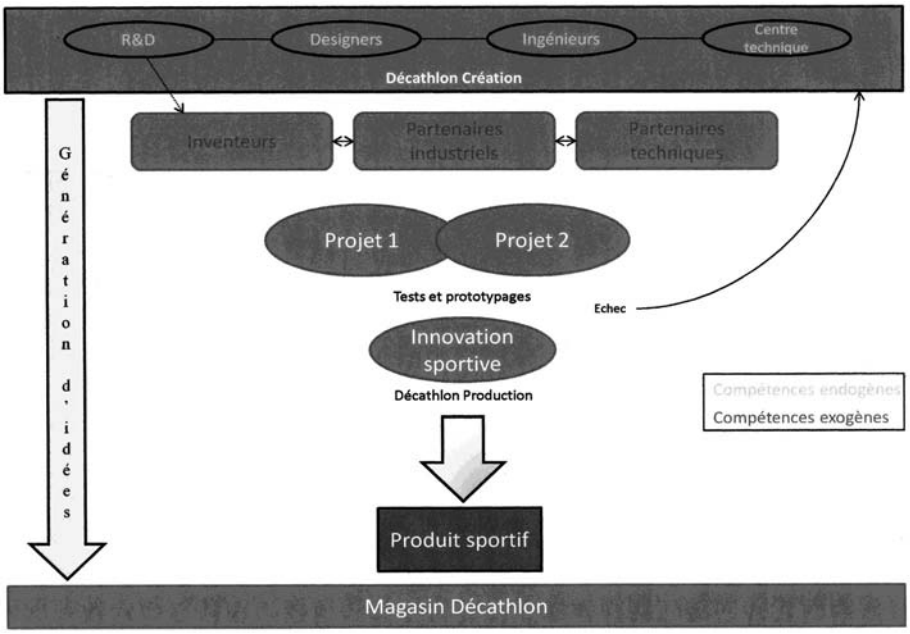

Source: personal elaboration.

Figure 2 - Innovation and creativity management at Decathlon Creation

21. However, an industrial partnership was set up for the "2 seconds" tent with a tent maker situated in Asia. Already a subcontractor, this company corresponded to the requirements of Decathlon: "it was necessary to find a capable industrialist, who would dare to produce this kind of product, who was ready to question their own means of production (…). We had to find someone who had the savoir-faire in tents, someone capable, audacious, who wanted to innovate, so there was also the state of mind, inventive, knowing the volumes we wanted, we were serious, it was a fairly big risk (…). It was the only form of partnership that there was. After that, we've got the engineers, designers, model specialists, a really internal team which worked, which did a lot here for Quechua Sallanches in fact to move the project forward".

their attention, the finances (…). So there you've got real risk taking, real organization within the company (…)". From then on, the innovation process (from the product's development cycle to its being on the shop shelf) took between 18 and 20 months.

At Decathlon, innovation management is thus centred around a very mobile dynamic and based on the free will of the company members. Everything is set up so that innovation and creativity are developed as much as possible without hierarchical or technical constraints. The director of innovation underlines that "*(…) It's very organic at Decathlon, it's not over structured, we really go for it, and whatever happens, we produce something, it's a bit like brainstorming*". This original vision of innovation management is specific to the company which does everything possible so that the projects come to fruition. Each of the Passion brands concentrates its means on a certain number of priorities and constitutes, in the best way possible, the necessary means, in terms of people and equipment, for the development of "sporting" development. However, this organization can be considered as an opportunity and as a weakness. Indeed conceiving a sporting product on a chaotic model is risky and can pose problems for the company but it can also be a great way forward for the latter and thus help to win market shares.

Seen from the outside, this "creative and innovative" organization can be observed as a weak point and be subject to criticism. However, within the company, they defend themselves saying; *"it's both an opportunity and a weakness… it can be perceived as a weakness since in effect sometimes, things can get a little confusing but at the same time, this chaos means that we sometimes come up with something exceptional (…) For myself, I feel that we create the chaos and try to control it (…) I think that the chaos can be used as a great force".* It is true that going from an idea to innovation is often considered to be risky, mysterious and impossible to master. Kanter (1998) said that "*the conditions within the organisation - structure and social set up - can actively stimulate and produce innovation, as long as these conditions take into account the "organic", "natural" and even "wild" side of innovation".* At Decathlon, this "generating of ideas" takes place in a disordered way whilst following a directive axis, a creative logic. Therefore, the company has a complex approach towards innovation since numerous projects are being led at the same time.

5- Conclusion

The interest of this article has been to highlight the performance factors of a producer-retailer of sporting articles in the management of its innovation. They are part of the culture of innovation developed at Decathlon. The state of balance between order and chaos in the company depends on the combination and the relative weight of the different aspects of knowledge present within or outside the company. However, the different resources of the organization must be coordinated effectively to transform something into a commercial success. The hyperfirm has developed its organizational capacities between the rational management of innovative projects and a "creative chaos". The presence of certain skills within the group makes it possible to solve certain technical problems and orient the company towards a certain type of approach. It can adopt a classic approach when it has the skills linked to the development of a new sporting product. Inversely, certain products do not correspond to the state of the knowledge and

the skills available within the firm. In this way the system can turn itself towards "chaos" so as to encourage the permeability towards the environment around the company and in so doing inspire its executives. This polyvalence is a distinctive quality (Hamel & Prahalad, 1996) since it provides a greater reactivity than in its sector (clients, investors…) in relation to the competitors of the brand. The two "sporting" innovations studied here reflect this distinctive quality by producing two different pathways in the development of two innovative products. The brand's organizational capacities are mainly to be found in the rational and chaotic management of innovation. The balance between these two basically opposing dimensions, constitutes one of the company's distinctive qualities.

6- Bibliography

ABERNATHY W.J. et UTTERBACK J.M., 1978, "Patterns of industrial innovation", *Technology Review*, June-july, n° 80, pp. 16-30.

AMIT R. et SHOEMAKER P.J., 1993, "Strategic assets and organizational rent", *Strategic Management Journal*, vol. 14, n° 1, pp. 33-46.

ARRÈGLE J.L., 1996, « Analyse Resource Based et identification des actifs stratégiques », *Revue Française de Gestion,* n° 108, pp. 25-36.

AUTIO E. et LUME A., 1998, "Does the Innovator Role Affect the perceived Potential for Growth? Analysis of Four Types of New, Technology-Based Firms", *Technology Analysis & Strategic Management*, vol. 10, n° 1, pp. 41-54.

BARDIN L., 2001, *L'analyse de contenu*, Paris, Presses Universitaires de France.

BARNEY J., 1991, "Firm Resources and Sustained Competitive Advantage", *Journal of Management*, vol. 17, n° 1, pp. 99-120.

BEAUD S. et WEBER F., 1998, *Guide de l'enquête de terrain*, Paris, La Découverte.

CONNER K.R. et PRAHALAD C.K., 1996, "A Resource-Based Theory of the Firm: Knowledge Versus Opportunism", *Organization Science*, vol. 7, n° 5, pp. 477-501.

CROS F., 2001, *L'innovation scolaire*, Paris, Institut National de Recherche Pédagogique.

DESBORDES M., OHL F. et TRIBOU G., 1999, *Marketing du sport*, Paris, Économica.

DIERICKX I. et COOL K.O., 1989, "Asset stock accumulation and sustainability of competitive management", *Management Science*, vol. 35, n° 12, pp. 1504-1511.

GAILLARD J.M., 1997, *Marketing et gestion de la Recherche et Développement*, Paris, Économica.

GIARD V., 1991, *Gestion de projet*, Paris, Économica.

GRANT R.M., 1991, "The resource-based theory of competitive advantage: implications for strategy formulation", *California Management Review*, vol. 33, n° 3, pp. 114-135.

HAMEL G. et PRAHALAD C.K., 1995, *La conquête du futur*, Paris, InterÉditions.

HILLAIRET D., 1999, *L'innovation sportive - Entreprendre pour gagner*, Paris, L'Harmattan.

HITT M. et IRELAND D., 1985, "Corporate distinctive competence, strategy, industry and performance", *Strategic Management Journal*, vol. 6, n° 3, pp. 273-293.

HOFER C.W. et SCHENDEL D.E., 1978, *Strategy formulation: analytical concepts*, St Paul Minn west.

KANTER R.M., 1988, "When a thousand flowers bloom: structural, collective, and social conditions for innovation in organization", *Research in organizational behaviour*, vol.10, pp. 169-211.

KATHLEEN M., EINSENHARDT K. et MARTIN J.A., 2000, "Dynamic Capabilities: What are they?", *Strategic Management Journal*, vol. 21, n° 10-11, pp. 1105-1121.

MAKADOC R., 2001, "Towards a synthetis of resource- based and dynamic capacity views of rent creation", *Strategic Management Journal*, vol. 22, n° 5, pp. 387-402.
MARCHESNAY M., 1997, « Petite entreprise et entrepreneur », *Encyclopédie de gestion*, Économica, tome 2, article 119, pp. 2 209-2 219.
MÉTAIS E., 1997, Intention *stratégique et transformation de l'environnement concurrentiel - Enjeux d'une conception de la stratégie centrée sur les ressources de l'entreprise*, Thèse de Doctorat en Sciences de Gestion, IAE d'Aix-en-Provence, Université d'Aix-Marseille III.
PENROSE E., 1959, *The theory of the growth of the firm*, New York, Oxford University Press.
PETERAF M.A., 1993, "The cornerstones of competitive advantage: a resource-based view", *Strategic Management Journal*, vol. 14, n° 3, pp. 179-191.
RINDOVA A. et FOMBRUN C. J., 1999, "Constructing Competitive Advantage: The Role of Firm–Constituent Interactions", *Strategic Management Journal*, vol. 20, n° 8, pp.691-710.
ST-AMANT G. et RENARD L., 2004, *Aspects théoriques d'un cadre de développement des capacités organisationnelles*, Cahier de la recherche de l'ESG-UQAM, document 03-04.
SELZNICK P., 1957, *Leadership in Administration*, New York, Harper and Row.
SMALLBONE D., LEIGH R. et NORTH D., 1995, "The characteristics and strategies of high growth SMEs", *International Journal of Entrepreneurial Behaviour & Research*, vol. 1, n° 3, pp. 44-62.
TARONDEAU J.C., 1991, *Recherche et Développement*, Paris, Vuibert.
TEECE D.J., PISANO G. et SHUEN A., 1997, "Dynamic capabilities and strategic management", *Strategic Management Journal*, vol. 18, n° 7, pp. 509-533.
THIÉTART R.A., 2000, « Gérer entre l'ordre et le chaos », *Cahier de Recherche DMSP*, n° 283, mai 2000, pp. 1-11.
TRIBOU G. et MADEC I., 2005, « Les politiques d'innovation dans l'industrie du sport : le cas de l'équipementier Adidas », *Revue européenne du management du sport* (REMS), n° 14, décembre, pp. 1-18.
WERNERFELT B., 1984, "A resource-based view of the firm", *Strategic Management Journal*, vol. 5, n° 2, pp. 171-180.
WERNERFELT B., 1995, "The resource-based view of the firm: Ten years after", *Strategic Management Journal*, vol. 16, n° 3, pp. 171-174.

Exercise History and Remodelling Stress Fracture are Related to Cortical Bone Ultimate Strength (P264)

Rachel Entwistle[1]*, Sara Sammons[1], Scott Hazelwood[2], David Fyhrie[3], Susan Stover[1]

Abstract: Mechanical load deforms bone tissue first elastically then plastically. The tissue adapts to the load through internal remodelling and external modelling. Large or repetitive loads can induce significant damage and cause large changes in bone shape and density. Remodelling initially causes transient osteoporosis during damage removal. Intense exercise can damage bone material, we hypothesised that exercise history reduces bone ultimate strength and that ultimate strength is reduced in bones with evidence of stress fracture syndrome. Equine humeri from 18 Thoroughbred racehorses were categorised on the basis of periosteal callus (none, mild, moderate, severe). The location of the callus was consistent with stress related modelling at the proximocaudal stress fracture site. Cortical cores from the humeral diaphysis distal to the callus site were monotonically compressed to failure (strain rate: $0.01s^{-1}$). The effect of stress fracture callus severity on ultimate strength was assessed using non-parametric tests. The relationships between ultimate strength and exercise history variables were examined with univariate and stepwise linear regression ($p<0.05$). Cores with mild and moderate callus had 5.0% and 6.6% lower ultimate strength than cores without callus. High speed exercise distances (race, work, and total event distances in the 2-4 months before death) had positive, linear, univariate relationships with ultimate strength ($r^2>0.23$). Average total high speed distance was the only parameter retained in the stepwise model ($r^2=0.42$). Degradation of material properties occurred in cortical diaphyseal bone material of bones with early evidence of stress fracture syndrome at a distant site, and was related to intense exercise. Thus, remodelling events likely associated with stress fracture syndrome are not isolated to the site of stress fracture.

Keywords: Biomechanics, Ultimate Strength, Stress Fracture, Bone Callus.

1. J.D. Wheat Veterinary Orthopaedic Research Laboratory, School of Veterinary Medicine, University of California at Davis, Davis, CA USA.

2. Biomedical and General Engineering Department, California Polytechnic State University, San Luis Obispo, CA USA.

3 Lawrence J. Ellison Musculoskeletal Research Centre, School of Medicine, University of California at Davis, Sacramento, CA USA.

**rentwistle@ucdavis.edu, +1 (530) 754-6979.*

1- Introduction

Mechanical load deforms bone tissue first elastically then plastically. The tissue reacts to the load through internal remodelling and external modelling. Reaction time is dependent on the changes in loading conditions and animal age (Huang, Lin e*t al.* 2003; Firth and Rogers 2005). Bone modifications include changes in bone mineral density (Kohrt, Ehsani *et al.* 1997; Huang, Lin *et al.* 2003; Joo, Sone *et al.* 2003; Firth and Rogers 2005), moment of inertia (Hsieh and Silva 2002; Joo, Sone *et al.* 2003), and cross-sectional area (Hsieh and Silva 2002; Joo, Sone *et al.* 2003). The skeleton can withstand higher loads as a result of successful adaptation (Hsieh and Silva 2002; Huang, Lin *et al.* 2003).

Large, repetitive loads can induce damage and stimulate geometric bone changes (Raab, Smith *et al.* 1990; Hsieh and Silva 2002; Warden, Hurst *et al.* 2005). The magnitude and direction of loading will effect how (i.e. geometric or density changes) and where a response is seen in the bone tissue (Kohrt, Ehsani *et al.* 1997; Huang, Lin *et al.* 2003; Warden, Hurst *et al.* 2005). Thoroughbred racehorses adapt to racing and training by laying down new bone in characteristic locations. After initially achieving race speeds in training, dorsal-medial expansion occurs in the third metacarpal bone in young Thoroughbreds (Nunamaker, Butterweck *et al.* 1989). The Thoroughbred humerus also lays down a bony callus in characteristic stress fracture locations as a response to racing and training (Stover, Johnson *et al.* 1992). High speed training induces greater stresses in the bone. The bone reacts by quickly laying down new bone in areas of highest stresses or strains (Nunamaker, Butterweck *et al.* 1990; Davies 2006). This additional material (endosteal and periosteal callus) maintains physiologic stresses and strains in and around the affected area of bone.

The remodelling process is capable of substantially affecting the structural integrity of bone and its ability to resist fatigue loading (Martin, Burr *et al.* 1998). Increased microdamage density in bone tissue leads to elevated remodelling rates (Mori and Burr 1993). The remodelling process removes damage by replacing damaged bone tissue with new bone tissue. Under normal loading circumstances, balance is maintained between damage accumulation and new bone replacement. With high intensity loading, microdamage accumulates quickly and stimulates elevated remodelling. Elevated remodelling can induce a transient period of osteoporosis when damaged tissue resorption exceeds new bone formation. Bone adaptation to intensive loads can be overwhelmed by excessive damage accumulation and subsequent bone material loss. Successful adaptation requires a balance between the resorption and formation processes.

Because intense exercise can damage bone material and inhibit successful adaptation, we hypothesised that exercise history affects bone ultimate strength. We also hypothesised that the ultimate strength of bone material from bones with evidence of stress fracture syndrome is reduced consequent to intense remodelling. Our objectives were to determine the relationships for ultimate strength with exercise history parameters, with stress fracture status, and with callus maturity for humeri collected from Thoroughbred racehorses.

2- Methods

2.1 Specimen Collection and Categorisation

Eighteen humeri, from 18 necropsied Thoroughbred racehorses (6 [F]emale, 7 [G]elding, 5 [M]ale; 2-4 yrs), were collected and classified into stages based on the presence of periosteal stress fracture callus (affected/control). Affected specimens were further classified into stages of callus maturity at the proximocaudal aspect of the humeral neck (Stages 1, 2, or 3). Control bones (Stage 0) had no evidence of periosteal callus or disruption/discolouration of the periosteal surface (10 specimens) (Figure 1). Stage 1 specimens had no or minimal periosteal elevation; red-brown discolouration compatible with haemorrhage or hyperaemia; and smooth, firm texture (3 specimens). Stage 2 callus had raised elevation less than 2 mm thick; discolouration; and soft, rough texture characteristic of woven bone (3 specimens). Stage 3 callus had raised elevation greater than or equal to 2 mm thick; discolouration; and smooth, firm texture characteristic of consolidating bone tissue (2 specimens).

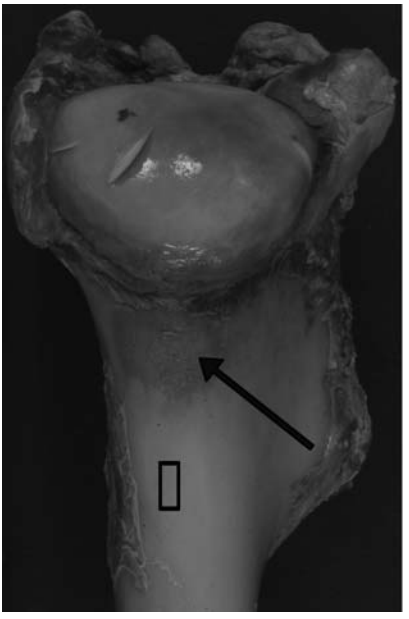

Figure 1 -Caudal view of proximal equine humerus with stress fracture callus. Black arrow shows Stage 2 periosteal callus at affected region. Black rectangle illustrates location (to scale) and orientation of cortical core relative to the callus site.

Cortical core specimens were harvested from a site, approximately 35mm distal to the callus location (Figure 1). Right cylindrical cores (6mm diameter, 15 mm long) were drilled (Craftsman 15 _ inch drill press, Sears, Roebuck & Co., Hoffman Estates, IL) from the caudal cortex of the diaphysis, such that they were parallel to the long axis of the bone. Specimens were irrigated with cooled saline while a hollow, diamond-tipped drill bit (Starlite Industries, Inc., Rosemont, PA) was used to core the specimens (720 RPM) Cores were stored in calcium buffered, saline soaked paper towels and stored at -20°C until the day of testing (Gustafson, Martin *et al.* 1996).

2.2 Mechanical Testing

On the day of testing, specimens were allowed to thaw to room temperature (≈25°C). Cores were placed between two parallel steel platens and a small pre-load was applied before testing. Specimens were monotonically compressed to failure at an apparent strain rate of 0.01 sec^{-1} (ASTM E 9-89a (Reapproved 2000)). Mechanical testing was done using an axial-torsional, servohydraulic materials testing system (Model 809; MTS Systems Corp., Minneapolis, MN) running Testware SX software. During testing, load (MTS Systems Corp. load cell; 15000 N) and displacement data were collected at a rate of 20Hz. Stress vs. strain curves were generated from load and displacement data and known specimen geometries. Using a custom software program (Matlab®), the ultimate strength was defined as the point of maximum stress on the stress vs. strain curve.

2.3 Exercise Histories

Exercise histories for each horse were obtained from an existing database (Bloodstock Research Information Services, Inc., Lexington, KY, USA). Data obtained included accumulated distances at racing speeds for training and racing events where events were described as a timed, high speed work or race. A custom program was used to analyse the data and break it down further into specific exercise history parameters used for analysis (Hill, Gardner *et al.* 2004). Included in these variables were accumulated distances and distance rates during the horse's career. Distances are reported in furlongs, where 1 furlong = 1/8 mile.

2.4 Statistical Analyses

2.4.1 Categorical Analyses

Non-parametric statistical analyses were used to examine the effects of the presence of stress fracture (affected, control), callus maturity (0, 1, 2, 3), age (2-4) and sex (F, G, M) on ultimate strength (SAS Institute Inc., Cary, NC). A one-sided Wilcoxon test was used to examine the effect of the presence of stress fracture on ultimate strength with the expectation that affected specimens would have lower ultimate strength than controls. Significance was set at $p<0.05$. A Kruskal-Wallis test was used to examine the effect of callus maturity, age and sex on ultimate strength. Pairwise comparisons were examined between individual groups using post-hoc one-sided Wilcoxon tests. Because samples sizes were small within callus stages, significance was set at $p<0.10$. Otherwise, $p<0.05$ was used, with a statistical trend defined as $0.10>p>0.05$.

2.4.1 Regression Analysis

The relationships between ultimate strength and age, callus severity (0, 1, 2, 3), and all exercise history parameters were examined using univariate linear regression. For callus maturity, control bones were treated two ways for the regression analysis; assuming deviations from normal (Stages 0, 1, 2, 3), and assuming that stages of disease preceded successful adaptation (Stages 1, 2, 3, 0). Statistical significance was set at $p<0.05$ and

statistical trends were defined by 0.10>p>0.05. For those exercise history parameters that did not have a complete set, a 13 horse sample size was used for analysis. Variables initially included in the multivariate regression analysis had univariate regression p-values less than 0.20.

Because only 13 of the 18 horses had complete exercise history data and the multivariate analysis required observations to have a complete data set, multivariate analyses used the 13 horse sample size. Forward stepwise regression was used to enter parameters into the model. Parameters were entered if p<0.50 and retained in the model if they increased the correlation coefficient (R^2) by at least 10% from the previous step.

3- Results

3.1 Categorical Results

Median ultimate strength was 6.5% lower for affected horses when compared to control horses (p = 0.003) (Table 1). Ultimate strength for horses with Stage 1 callus was 8.3% lower and for horses with Stage 2 callus was 6.6% lower than the ultimate strength of the control horses (p=0.007). Ultimate strength for Stage 3 was 9.8% higher than Stage 1 and 7.8% higher than Stage 2 (p=0.075).

	Control	Affected	Callus Stage		
Material Property	**Stage 0**	**Stages 1-3**	**Stage 1**	**Stage 2**	**Stage 3**
	(n=10)	**(n=8)**	**(n=3)**	**(n=3)**	**(n=2)**
Ultimate Strength (MPa)	248.3 (267.2-236.0)	**232.1** (254.0-221.5)	**227.8**[a] (221.5-232.1)	**232**[a] (235.0-226.2)	250.2[b] (254.0-246.4)

Bold values indicate a statistically significant difference from control horses (p<0.05 for affected horses, p<0.10 for Stages 1, 2, 3)

[ab] Values that share a superscript within a row are not statistically different at the p<0.10 level.

Table 1 - Cortical core ultimate strength (median, (range)) for control and affected specimens

No statistically significant differences were observed between groups for age or sex (Table 2). Trends were evident between ages 2 and 4; Age 4 had 22.8% greater ultimate strength than Age 2 (p=0.056). Also, females had higher (5.3%) ultimate strength than geldings (p=0.050).

	Age			Sex		
Material Property	**2 (n=4)**	**3 (n=11)**	**4 (n=3)**	**F (n=6)**	**G (n=7)**	**M (n=5)**
Ultimate Strength (MPa)	232.1[1] (248.4-226.2)	246.8[1,2] (260.8-221.5)	258.0[2] (267.2-236.0)	247.5[1] (260.8-232.0)	235.0[2] (258.0-221.5)	248.4[1,2] (267.2-227.8)

[12] Values that share a superscript within a row are not statistically different at p<0.10

Table 2 - Ultimate strength distribution (median, (range)) by age and sex.

3.2 Regression Results

The univariate analysis produced six significant relationships. Age, average race distance, average work distance and distance accumulated in the second month, and third and fourth month, prior to death had a positive relationship with ultimate strength (0.048>p>0.021, R^2>0.22) (Table 3). When controls were classified as Stage 4, a highly significant relationship with callus stage was found (p<0.001).

Material Property	Regression Parameter	Age (years)	*Average Race Distance (fur)*	*Average Work Distance (fur)*	Distance 2nd Month (fur)	Distance 3rd & 4th Months (fur)	Callus Maturity (Controls=Stage4)
		(n=18)	*(n=13)*	*(n=13)*	(n=18)	(n=18)	(n=18)
Ultimate Strength (MPa)	Slope	9.5	*8.3*	*12.0*	0.6	0.4	8.1
	Intercept	215.3	*198.4*	*195.9*	237.3	237.2	218.3
	R^2	0.22	*0.4*	*0.38*	0.23	0.23	0.59
	p-value	0.048	*0.021*	*0.024*	0.043	0.046	< 0.001

Table 3 - Significant results from univariate regression analyses for cortical cores. Italics indicate a 13 horse analysis, otherwise 18 horses were used. (Note: fur=furlong).

Statistical trends were also observed for three exercise history parameters. Average event distance, distance accumulated in the last four months prior to death and the number of active days had a positive relationship with ultimate strength ($0.089>p>0.058$, $R^2>0.17$) (Table 4).

Material Property	Regression Parameter	Average Event Distance (fur)	Number of Active Days	Distance Last 4 Months (fur)
		(n=18)	(n=18)	(n=18)
Ultimate Strength (MPa)	Slope	5.2	0.02	0.2
	Intercept	219.2	237.34	236.1
	R^2	0.17	0.17	0.21
	P value	0.089	0.085	0.058

Table 4 - Statistical trends from univariate regression analyses for cortical cores between ultimate strength and exercise history parameters. Italics indicate a 13 horse analysis, otherwise 18 horses were used. (Note: fur=furlong).

From the multivariate regression analysis, only one parameter was entered and was retained in the model as significant (Table 5). Other added variables failed to increase the correlation coefficient by 10% or more.

Material Property	Parameter	Coefficient	p-value	R^2
Ultimate Strength (MPa)	Intercept	196.9	< 0.001	0.42
	Average Event Distance (fur)	10.8	0.017	

Table 5 - Sequential regression model selection results from ultimate strength vs. exercise history parameters. For the stepwise model selection, the 13 horse sample size was used.

4- Discussion

Ultimate strength may correlate with bone remodelling activity. Ultimate strength is lowest in cortical bone material from humeri when there are early stages of stress fracture callus at a proximal humeral site. Horses with catastrophic humeral fracture usually have periosteal callus bridging the fracture line, evidence of pre-existing stress fracture (Stover, Johnson *et al.* 1992). Stress fractures occur when the rate of microdamage accumulation exceeds the rate of damage repair, or bone remodelling. One possible explanation for weak bone material is transient osteoporosis related to elevated bone remodelling. In the early phase of remodelling (resorption), osteoclasts quickly remove

damaged bone material, resulting in temporary osteoporosis. In subsequent months, refilling occurs; osteoblasts lay down new bone material, alleviating the focal osteoporosis. Although stress fractures occur as focal lesions in characteristic skeletal locations related to athletic activity, it is possible that remodelling is accelerated more generally throughout affected bone organs. Because specimens from humeri with late stage callus had ultimate strengths similar to specimens from humeri without callus, late stages of callus maturity may indicate completion of bone remodelling, resolution of osteoporosis, and successful adaptation of the diaphysis to altered loading conditions. Histologic verification would be required to substantiate this theory.

Responses to training intensity and duration may affect ultimate strength. Increasing skeletal loads induce musculoskeletal adaptation. High speed racing and training induce large principal compressive strains in the third metacarpal bone of naïve Thoroughbred racehorses (Nunamaker, Butterweck *et al.* 1990). Presumably, large strains cause microdamage in affected bones, and stimulate skeletal adaptation through the modelling and remodelling processes. Because repair is rate limited, and likely optimal in young, healthy athletes, and microdamage generation is variable with training intensity, an imbalance can develop when training intensity exceeds the repair rate (Stover 2003). Horses training and racing for long distances may have a greater propensity to develop an unmanageable amount of microdamage in the bone tissue. A sudden accumulation of microdamage would cause an increase in remodelling, leading to the transient period of osteoporosis.

Training regimen plays an important role in healthy maintenance of cortical bone tissue. Studies have shown that rapid accumulation of high-speed exercise distances can have protective effects or increase risk of catastrophic fracture in racehorses (Estberg, Gardner *et al.* 1998; Verheyen, Newton *et al.* 2006). In general, intense racing or training within a two-month period or less increases the risk of catastrophic injury (Estberg, Gardner *et al.* 1998; Verheyen, Price *et al.* 2006; Verheyen, Newton *et al.* 2006). For exercise histories greater than one to two months, the accumulation of high speed gallop exercise has a protective effect, (Verheyen, Price *et al.* 2006). Our results confirm the long term accumulation aspect of this study; training distances have a positive relationship with ultimate strength. The exercise history parameters we analysed were from the 12 months prior to death. Although reported differently, the various thresholds in these studies could be related and representative of the point at which microdamage accumulation transitions from manageable to unmanageable.

Exercise history variables that captured recent high speed exercise events were related to ultimate strength. Distances within four months of horse death were related to ultimate strength, with the most recent distances having the greatest influence on ultimate strength (i.e., greatest regression coefficient). The time period for these exercise variables corresponds to key time periods in the bone remodelling process. The remodelling process begins by the recruitment of cells, followed by the resorption and reversal phases taking approximately 30 days to complete (in humans) (Martin, Burr *et al.* 1998). The refilling phase takes three months to complete (in humans) and involves the deposition of new bone by osteoblasts (Martin, Burr *et al.* 1998). Together, the resorption and formation phases take approximately four months to finish. If the concentration of

microdamage is high as a result of a particular event or number of events in a short period of time, it would make sense that the bone would be most fragile in the following four months. Less material would be present due to resorption with greater porosity due to the slow refilling process.

Sample size affected the results of the regression analyses. Five horses were removed for the stepwise regression analysis because of the requirement for a complete data set. The horses removed from the univariate analysis for the stepwise analysis were mostly affected specimens (1-Stage 0, 2-Stage 1, 1-Stage 2, and 1-Stage 3). These horses either had no recorded races (4 horses) or works (1 horse). The stepwise analysis showed that average event distance best predicted ultimate strength. In the univariate analysis however, average total distance yielded a statistical trend instead of statistical significance. The smaller sample size may better represent the true adaptation behaviour from the greater percentage of control bones (69%) within the dataset. The control bones could represent the true nature of humeral adaptation while the affected specimens represent deviations from the normal. With less affected specimens, it may be easier to isolate the factors that are most influential in the true nature of adaptation of this bone.

5- Conclusion

This study looked at associations for exercise history and for periosteal stress fracture callus with ultimate strength of cortical bone material from a site distal to the site of stress fracture. We found that the ultimate strength of distal bone tissue is lower for specimens from humeri with stress fracture callus than for specimens from humeri without callus. More specifically, specimens from humeri with early callus (Stage 1 or 2) have lower ultimate strength than specimens from humeri without callus (Stage 0) or humeri with late callus (Stage 3). In general, ultimate strength increased with age, but when considered as individual groups, no differences were seen. Ultimate strength was not different among genders. Exercise event distances and rates also had a positive relationship with ultimate strength. In the multivariate model, average event distance, alone, best explained the variability in ultimate strength. Together, these results contribute to a general understanding of how ultimate strength is affected by stress fracture, periosteal callus maturity and training regimens.

6- References

[D1] Davies, H. M. S. (2006). Estimating peak strains associated with fast exercise in Thoroughbred racehorses. International Conference on Equine Exercise Physiology. Fontainebleau, France, Equine Veterinary Journal. 36: 383-386.

[EG1] Estberg, L., I. A. Gardner, et al. (1998). «A case-crossover study of intensive racing and training schedules and risk of catastrophic musculoskeletal injury and lay-up in California thoroughbred racehorses.» Prev Vet Med 33(1-4): 159-70.

[FR1] Firth, E. C. and C. W. Rogers (2005). «Musculoskeletal responses of 2-year-old Thoroughbred horses to early training. Conclusions.» N Z Vet J 53(6): 377-83.

[GM1] Gustafson, M. B., R. B. Martin, et al. (1996). «Calcium buffering is required to maintain bone stiffness in saline solution.» J Biomech 29(9): 1191-4.

[HG1] Hill, A. E., I. A. Gardner, et al. (2004). «Effects of injury to the suspensory apparatus, exercise, and horseshoe characteristics on the risk of lateral condylar fracture and suspensory apparatus failure in forelimbs of thoroughbred racehorses.» Am J Vet Res 65(11): 1508-17.
[HS1] Hsieh, Y. F. and M. J. Silva (2002). «In vivo fatigue loading of the rat ulna induces both bone formation and resorption and leads to time-related changes in bone mechanical properties and density.» J Orthop Res 20(4): 764-71.
[HL1] Huang, T. H., S. C. Lin, et al. (2003). «Effects of different exercise modes on mineralization, structure, and biomechanical properties of growing bone.» J Appl Physiol 95(1): 300-7.
[JS1] Joo, Y. I., T. Sone, et al. (2003). «Effects of endurance exercise on three-dimensional trabecular bone microarchitecture in young growing rats.» Bone 33(4): 485-493.
[KE1] Kohrt, W. M., A. A. Ehsani, et al. (1997). Effects of Exercise Involving Predominantly Either Joint-Reaction or Ground-Reaction Forces on Bone Mineral Density in Older Women. 12: 1253-1261.
[MB1] Martin, R. B., D. B. Burr, et al. (1998). Skeletal Tissue Mechanics. New York, Springer-Verlag New York.
[MB2] Mori, S. and D. B. Burr (1993). «Increased intracortical remodeling following fatigue damage.» Bone 14(2): 103-9.
[NB1] Nunamaker, D. M., D. M. Butterweck, et al. (1989). «Some geometric properties of the third metacarpal bone: a comparison between the thoroughbred and standardbred racehorse.» J Biomech 22(2): 129-34.
[NB2] Nunamaker, D. M., D. M. Butterweck, et al. (1990). «Fatigue fractures in thoroughbred racehorses: relationships with age, peak bone strain, and training.» J Orthop Res 8(4): 604-11.
[RS1] Raab, D. M., E. L. Smith, et al. (1990). «Bone mechanical properties after exercise training in young and old rats.» J Appl Physiol 68(1): 130-4.
[S1] Stover, S. M. (2003). «The epidemiology of Thoroughbred racehorse injuries.» Clinical Techniques in Equine Practice 2(4): 312-322.
[SJ1] Stover, S. M., B. J. Johnson, et al. (1992). «An association between complete and incomplete stress fractures of the humerus in racehorses.» Equine Vet J 24(4): 260-3.
[VP1] Verheyen, K., J. Price, et al. (2006). «Exercise distance and speed affect the risk of fracture in racehorses.» Bone 39(6): 1322-1330.
[VN1] Verheyen, K. L., J. R. Newton, et al. (2006). «A case-control study of factors associated with pelvic and tibial stress fractures in Thoroughbred racehorses in training in the UK.» Prev Vet Med 74(1): 21-35.
[WH1] Warden, S. J., J. A. Hurst, et al. (2005). «Bone adaptation to a mechanical loading program significantly increases skeletal fatigue resistance.» J Bone Miner Res 20(5): 809-16.

Analysis of the Holonomic Constraint in the Whipple Bicycle Model (P267)

Dale Peterson[1], Mont Hubbard[2]

Topics: Bicycle, Modelling.
Abstract: In this work, we examine the holonomic constraint of the Whipple bicycle model on a level surface. In the Whipple model, one must enforce a constraint which ensures that the front and rear wheels touch the ground. We first derive the constraint in an intuitive geometric fashion and then verify that the constraint can be expressed as quartic polynomial in the sine of the frame pitch. We present three methods for enforcing the constraint in a dynamic model and comment on the differences and practical issues involved in each method.
Key words: Whipple model, bicycle, quartic polynomial, holonomic constraint.

1- Introduction

The modelling of a bicycle is a task which presents many challenges: a multi-body system with a complex holonomic constraint, four nonholonomic constraints, complex geometry, and a nontrivial number of degrees of freedom. The hands free bicycle has been researched extensively: a review paper Meijaard *et al.* (2007), chronicled much of the bicycle research to date, and presented a benchmark model that was verified by several other authors both by hand and by commercial simulation software. This benchmark model is based upon what is commonly referred to as the Whipple bicycle model (Whipple 1899). The key features of the model are four rigid bodies (two wheels, the bicycle frame, and the bicycle fork) connected by three frictionless revolute joints, and knife edge or toroidal wheels rolling with no slip.

1, 2. Mechanical Engineering Department, Sports Biomechanics Laboratory, University of California, Davis, One Shields Ave. Davis, CA 95616 - E-mail: {dlpeterson,mhubbard}@ucdavis.edu

The holonomic constraint of the Whipple bicycle model enforces that both wheels touch the ground. The formulation of this constraint can be done in several ways. However, only one author (Psiaki 1979) presents the full nonlinear derivation and states that an analytic solution exists. Unfortunately, his approach is from an analytic geometry point of view and is rather nonintuitive and hard to follow. There is little discussion in the literature of the specifics of how to handle this holonomic constraint once it is obtained.

We derive the holonomic constraint equation for the Whipple bicycle model in a physically intuitive manner and show in a similarly intuitive fashion that this constraint can be represented as a quartic polynomial in the sine of the frame pitch. For generality, we include in our model the case of toroidal tires, which doesn't complicate the analysis much. We present three methods to implement the constraint into a bicycle model, and compare the differences between each method. The methods for dealing with this complex holonomic constraint are applicable to many other systems that have holonomic constraints that are not easily solved explicitly.

2- Methods

2.1 Formulation of the constraint

Figure 1 shows schematic representation of a bicycle. The bicycle consists of a rear wheel R, a frame B, a fork and handlebar assembly H, and a front wheel F. Intermediate frames L and S will be used to simplify the analysis. The points of the rear and front tires in contact with the ground are denoted by *NR* and *NF*, respectively. The four rigid bodies are connected by revolute joints whose axes pass through the points R^*, S^* and F^*. Dextral sets of orthonormal vectors $\mathbf{r}_i$, $\mathbf{b}_i$, $\mathbf{h}_i$, $\mathbf{f}_i$, $\mathbf{l}_i$, $\mathbf{s}_i$, and $\mathbf{n}_i$ (i = 1, 2, 3) are fixed in R, B, H, F, L, S, and a Newtonian reference frame N, respectively. The ground plane is defined to be the plane spanned by $\mathbf{n}_1$ and $\mathbf{n}_2$, with $\mathbf{n}_3$ taken to be positive downwards into the ground.

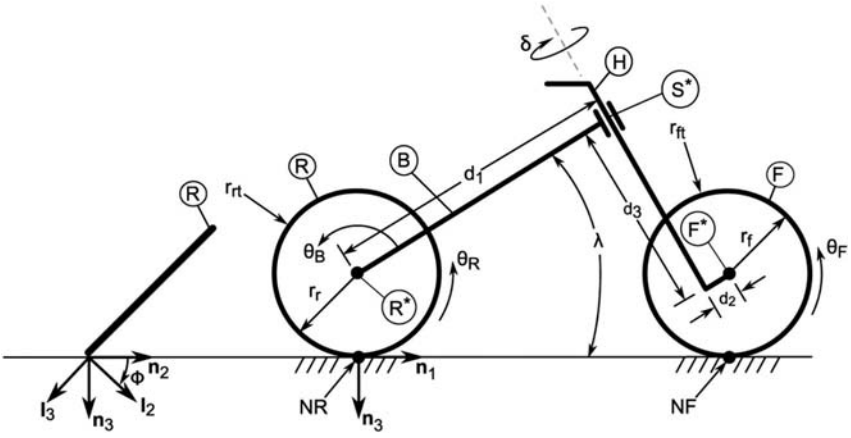

Figure 1 - On the left, the rear wheel in a leaned configuration. On the right, the bicycle in the upright configuration.

Five generalized coordinates are used to configure the four rigid bodies: ϕ, the frame lean angle; θ_R, the rear wheel angle; θ_B, the frame pitch angle; δ, the steer angle; and θ_F, the front wheel angle. Seven geometric parameters are used: r_r, the rear wheel radius; r_{rt}, the rear tire casing radius; d_1, the distance between the points $R^\star$ and $S^\star$ in the $\mathbf{s}_1$ direction; d_2, the fork offset; λ, the head angle complement; r_f, the front wheel radius; and r_{ft}, the front tire casing radius. The distance d_3 is a convenient parameter to use in order to locate the front wheel, but it is dependent upon the choice of the other seven parameters. It is assumed that $\phi \in (-\pi/2, \pi/2)$ and $\lambda \in (-\pi/2, \pi/2)$, and that r_r, r_{rt}, r_f, r_{ft} are all non negative.

The first step to formulating the constraint equation is to write the vector from the rear contact point *NR* to the front contact point *NF*. This requires that orientations, locations and geometry of each of the four rigid bodies be defined. We begin at the rear of the bicycle and work forward. To orient the lean frame, L, in N, $\mathbf{l}_i$ is initially aligned with $\mathbf{n}_i$ (i = 1, 2, 3) and L is subjected to a right hand rotation ϕ about $\mathbf{n}_1 = \mathbf{l}_1$.

The rear wheel R is modelled as a torus with $\mathbf{r}_1$ and $\mathbf{r}_3$ in the plane of symmetry and $\mathbf{r}_2$ along the axis of symmetry. To orient R in L, $\mathbf{r}_i$ is initially aligned with $\mathbf{l}_i$ (i = 1, 2, 3) and R is subjected to a right hand rotation θ_R about $\mathbf{r}_2 = \mathbf{l}_2$. $R^\star$ denotes the geometric center of R. The distance from the rear wheel contact point, *NR*, to $R^\star$ is $-r_{rt}\mathbf{n}_3 - r_r\mathbf{l}_3$. The bicycle frame, B, has $\mathbf{b}_1$ and $\mathbf{b}_3$ in the plane of symmetry. B is is connected to R at $R^\star$, by a revolute joint to permit rotation of B relative to R about an axis parallel to $\mathbf{r}_2$ (equivalently $\mathbf{b}_2$). To orient B in L, $\mathbf{b}_i$ is initially aligned with $\mathbf{l}_i$ (i = 1, 2, 3) and B is subjected to a right hand rotation θ_B about $\mathbf{b}_2 = \mathbf{l}_2$. To orient S, the steer axis frame, $\mathbf{s}_i$ is initially aligned with $\mathbf{b}_i$ (i = 1, 2, 3) and S is subjected to a right hand rotation λ (fixed) about $\mathbf{s}_2 = \mathbf{b}_2$. The point $S^\star$ lies along the steer axis, a distance $d_1\mathbf{s}_1$ from the rear wheel center, $R^\star$.

The fork and handlebar assembly, H, has $\mathbf{h}_3$ aligned with what is commonly known as the the steer tube of the fork. H is connected to B by a revolute joint to permit rotation of H relative to B about an axis parallel to $\mathbf{s}_3$. To orient H in S, $\mathbf{h}_i$ is initially aligned with $\mathbf{s}_i$ (i = 1, 2, 3) and H is subjected to a right hand rotation δ about $\mathbf{h}_3 = \mathbf{s}_3$. The front wheel, F, is modelled as a torus in the same fashion as the rear wheel, with $\mathbf{f}_1$ and $\mathbf{f}_3$ in the plane of symmetry, $\mathbf{f}_2$ along the axis of symmetry, and $F^\star$ being the geometric center of F. F is connected to H at $F^\star$ by a revolute joint to permit rotation of F relative to H about an axis parallel to $\mathbf{h}_2$. To orient F in H, $\mathbf{f}_i$ is initially aligned with $\mathbf{h}_i$ (i = 1, 2, 3) and F is subjected to a right hand rotation θ_F about $\mathbf{h}_2 = \mathbf{f}_2$. $F^\star$ is located a distance $d_2\mathbf{h}_1 + d_3\mathbf{h}_3$ from $S^\star$. Finally, in order to locate the front contact point, one first forms the vector $\tilde{\mathbf{f}} = \mathbf{n}_3 - (\mathbf{h}_2 \cdot \mathbf{n}_3)\mathbf{h}_2$, which lies in the plane of the wheel and points toward the ground contact point. *NF* is then located a distance $r_f\tilde{\mathbf{f}}/\|\tilde{\mathbf{f}}\| + r_{ft}\mathbf{n}_3$ from $F^\star$.

The vector from the rear contact point to the front contact point is then

$$\begin{aligned} {}^{NR}\mathbf{p}^{NF} &= {}^{NR}\mathbf{p}^{R^*} + {}^{R^*}\mathbf{p}^{P^*} + {}^{P^*}\mathbf{p}^{F^*} + {}^{F^*}\mathbf{p}^{NF} \\ &= -r_{rt}\mathbf{n}_3 - r_r\mathbf{l}_3 + d_1\mathbf{s}_1 + d_2\mathbf{h}_1 + d_3\mathbf{h}_3 + r_f\tilde{\mathbf{f}}/||\tilde{\mathbf{f}}|| + r_{ft}\mathbf{n}_3 \end{aligned} \tag{1}$$

Due to the symmetry of the wheels, ${}^{NR}\mathbf{p}^{NF}$ is independent of the angles of rotation

of each of the wheels. Thus ϕ, θ_B, and δ are the only generalized coordinates present in ${}^{NR}\mathbf{p}^{NF}$. If knife edged wheels are assumed ($r_{rt} = r_{ft} = 0$), five geometric parameters are needed in order to describe the bicycle, one choice being w, c, λ, r_r, r_f, where w and c are the wheelbase and trail respectively, as in Meijaard e*t al.* (2007). In modelling the bicycle using Kane's method, d_1 and d_2 are a more natural choice because these distances are constants having to do with the frame and the fork, whereas w and c vary with the configuration of the bicycle. Since much of the other literature uses w and c, it is useful to be able to convert these quantities to those used in this model. A simple sketch of the bicycle in the upright configuration will confirm that

$$d_1 = (w + c)\cos\lambda - (r_r + r_{rt})\sin\lambda \tag{2}$$

$$d_2 = (r_f + r_{ft})\sin\lambda - c\cos\lambda \tag{3}$$

$$d_3 = \left(r_r + r_{rt} - r_f - r_{ft} + (d_1 + d_2)\sin\lambda\right)/\cos\lambda \tag{4}$$

Again, d_1 and d_2 are independent parameters used instead of w and c, and d_3 is dependent upon the choice of (r_r, r_{rt}, r_f, $r_f t$, λ, d_1, d_2). It is used as a way of simplifying the following analysis.

2.2 Exhibition of the quartic

The constraint is formed by requiring that ${}^{NR}\mathbf{p}^{NF}$ have no vertical component:

$$\begin{aligned} 0 &= {}^{NR}\mathbf{p}^{NF} \cdot \mathbf{n}_3 \\ &= -r_{rt} - r_r c_\phi + r_{ft} + r_f\left(1 - (s_\phi c_\delta + s_{\lambda\theta_B} s_\delta c_\phi)^2\right)^{\frac{1}{2}} - d_1 s_{\lambda\theta_B} c_\phi + d_2(s_\phi s_\delta - s_{\lambda\theta_B} c_\phi c_\delta) + d_3 c_{\lambda\theta_B} c_\phi \\ &= f(\phi, \theta_B, \delta) \end{aligned} \tag{5}$$

where symbols s_x, E_x, s_{xy}, c_{xy}, stand for $\sin x$, $\cos x$, $\sin(x + y)$ and $\cos(x + y)$ respectively, and x and y may be any of the angles λ, ϕ, θ_B, or δ. While it is not immediately clear that this is a quartic polynomial in the sine of pitch, the introduction of some intermediate coefficients will help in manipulating the equation. From the double angle formula, we can replace $s_{\lambda\theta_B}$ with $s_\lambda c_{\theta_B} + c_\lambda s_{\theta_B}$, and $c_{\lambda\theta_B}$ with $c_\lambda c_{\theta_B} - s_\lambda s_{\theta_B}$. Collecting terms of c_{θ_B} and s_{θ_B}, and introducing the following coefficients,

$$\alpha_0 = -(r_{rt} + r_r c_\phi - r_{ft} - d_2 s_\phi s_\delta)/r_f \tag{6}$$

$$\alpha_1 = -c_\phi((d_1 + d_2 c_\delta)s_\lambda - d_3 c_\lambda)/r_f \tag{7}$$

$$\alpha_2 = -c_\phi((d_1 + d_2 c_\delta)c_\lambda + d_3 s_\lambda)/r_f \tag{8}$$

$$\alpha_3 = s_\phi c_\delta \tag{9}$$

$$\alpha_4 = c_\phi s_\delta s_\lambda \tag{10}$$

$$\alpha_5 = c_\phi s_\delta c_\lambda \tag{11}$$

we can then write the constraint equation as

$$0 = \alpha_0 + \alpha_1 c_{\theta_R} + \alpha_2 s_{\theta_R} + (1 - (\alpha_3 + \alpha_4 c_{\theta_R} + \alpha_5 s_{\theta_R})^2)^{\frac{1}{2}} \tag{12}$$

At this point the constraint is formulated as an equation with c_{θ_B} and s_{θ_B} terms, and coefficients, independent of θ_B, involving λ, ϕ, d_1, d_2, λ, r_r, r_{rE}, r_f, and r_{ft}. Moving the first three terms to the left hand side of the equality, squaring both sides, expanding, replacing $c^2_{\theta_B}$ with $1 - s^2_{\theta_B}$ and collecting terms of c_{θ_B} and s_{θ_B} results in

$$\alpha_0^2 + \alpha_1^2 + \alpha_3^2 + \alpha_4^2 - 1 + 2(\alpha_0\alpha_2 + \alpha_3\alpha_5)s_{\theta_R} + (-\alpha_1^2 + \alpha_2^2 - \alpha_4^2 + \alpha_5^2)s_{\theta_R}^2$$
$$= -2(\alpha_0\alpha_1 + \alpha_3\alpha_4)c_{\theta_R} - 2(\alpha_1\alpha_2 + \alpha_4\alpha_5)c_{\theta_R}s_{\theta_R} \tag{13}$$

Now, we define another set of coefficients,

$$\beta_0 = \alpha_0^2 + \alpha_1^2 + \alpha_3^2 + \alpha_4^2 - 1 \tag{14}$$

$$\beta_1 = 2(\alpha_0\alpha_2 + \alpha_3\alpha_5) \tag{15}$$

$$\beta_2 = -\alpha_1^2 + \alpha_2^2 - \alpha_4^2 + \alpha_5^2 \tag{16}$$

$$\beta_3 = -2(\alpha_0\alpha_1 + \alpha_3\alpha_4) \tag{17}$$

$$\beta_4 = -2(\alpha_1\alpha_2 + \alpha_4\alpha_5) \tag{18}$$

which allows the constraint to be written as

$$\beta_0 + \beta_1 s_{\theta_R} + \beta_2 s_{\theta_R}^2 = \beta_3 c_{\theta_R} + \beta_4 c_{\theta_R} s_{\theta_R} \tag{19}$$

Squaring both sides and again replacing $c^2_{\theta_B}$ with $1 - s^2_{\theta_B}$, we obtain

$$\beta_0^2 + 2\beta_0\beta_1 s_{\theta_R} + (2\beta_0\beta_2 + \beta_1^2)s_{\theta_R}^2 + 2\beta_1\beta_2 s_{\theta_R}^3 + \beta_2^2 s_{\theta_R}^4$$
$$= \beta_3^2 + 2\beta_3\beta_4 s_{\theta_R} - (\beta_3^2 - \beta_4^2)s_{\theta_R}^2 - 2\beta_3\beta_4 s_{\theta_R}^3 - \beta_4^2 s_{\theta_R}^4 \tag{20}$$

Matching terms and introducing the set of coefficients

$$\gamma_0 = \beta_0^2 - \beta_3^2 \tag{21}$$

$$\gamma_1 = 2(\beta_0\beta_1 - \beta_3\beta_4) \tag{22}$$

$$\gamma_2 = 2\beta_0\beta_2 + \beta_1^2 + \beta_3^2 - \beta_4^2 \tag{23}$$

$$\gamma_3 = 2(\beta_1\beta_2 + \beta_3\beta_4) \tag{24}$$

$$\gamma_4 = \beta_2^2 + \beta_4^2 \tag{25}$$

finally allows the constraint to be written in a form easily recognizable as a quartic in the sine of pitch:

$$0 = \gamma_0 + \gamma_1 s_{\theta_R} + \gamma_2 s_{\theta_R}^2 + \gamma_3 s_{\theta_R}^3 + \gamma_4 s_{\theta_R}^4 \tag{26}$$

2.3 Enforcing the constraint in a dynamic model

The bicycle is most commonly described with eight generalized coordinates: two coordinates for the rear wheel contact point in the ground plane, one coordinate for the yaw angle of the rear wheel in the ground plane, and the remaining five as described in the previous section. In forming the expressions for the center of mass locations of the bicycle frame, fork, and front wheel, it is convenient to introduce the frame pitch θ_B as a generalized coordinate. As has been shown, however, the frame pitch is not an independent generalized coordinate — the constraint equation above, $f(\phi, \theta_B, \delta)$ provides a relationship between ϕ, δ, and θ_B. The pitch of the frame is not intrinsically interesting for several reasons, the main one being that in a first order linearization about $\phi = \delta = 0$, θ_B is zero. In studying the linearized dynamics of the bicycle about the upright configuration, frame pitch plays no role and all of the preceding analysis is for naught. However, if one is interested in studying the linearized dynamics of the Whipple model about a configuration other than the upright one (e.g. in a steady turn) the pitch constraint does come into play and must be accounted for. If the nonlinear dynamics are to be explored, one needs to have an accurate way to implement the constraint. From a more physical point of view, the lean and steer coordinates are also more interesting to study because they are directly affected by a human when riding a bicycle, whereas the pitch of the frame is not a coordinate over which a human rider has direct control.

Associated with the seven independent generalized coordinates are seven generalized speeds.The four nonholonomic constraints arising from the no slip conditions of the wheels imply that only three of these speeds are independent. Most commonly, these independent speeds are chosen to be the lean rate, $u_\phi = \dot{\phi}$, the rear wheel angular velocity, $u_{\theta_R} = \dot{\theta}_R$, and the steer rate, $u_\delta = \dot{\delta}$. There are other choices of independent generalized speeds, but these suffice and for the purpose of the following discussion we assume their use.

There are at least three methods to implement the constraint into a dynamic model.

1. Analytic Elimination. The first method is to solve the quartic analytically for pitch and eliminate it completely from any calculations that require pitch. This method results in seven kinematic and three dynamic differential equations:

$$\dot{q} = u_q \qquad (q = x, y, \psi, \phi, \theta_R, \delta, \theta_F) \tag{27}$$

$$\dot{u}_q = f_q(\phi, \delta, u_\phi, u_{\theta_R}, u_\delta) \qquad (q = \phi, \theta_R, \delta) \tag{28}$$

Quartic polynomials are the highest order polynomials for which a general analytic solution exists, therefore it may seem natural to attempt to solve the constraint analytically. The expression for the solution to the quartic is not a simple one and is not shown here, but essentially, once the coefficients of the quartic are known (described in the previous section), the roots can be computed analytically. In order to take this 'direct

solution' approach, one must identify the correct root of the quartic, equation (26). Having obtained the correct root to the quartic, the arcsin is computed, and it is substituted algebraically as a function of ϕ and δ so that θ_B no longer appears in the equations of motion.

2. Dynamic Inclusion. The second method is to include the pitch as a dynamic variable in the formulation of the equations of motion and introduce another generalized speed associated with it (e.g. $u_{\theta_B} = \dot{\theta}_B$). To enforce the holonomic constraint, the time derivative of it is calculated and treated as a fifth nonholonomic constraint that replaces the holonomic constraint. The time derivative of the holonomic constraint is linear in the generalized speeds associated with pitch, lean, and steer, and so one obtains the relationship

$$u_{\theta_B} = -\left(\frac{\partial f}{\partial \phi}\dot{\phi} + \frac{\partial f}{\partial \delta}\dot{\delta}\right) / \frac{\partial f}{\partial \theta_R}$$

$$= -\left(\frac{\partial f}{\partial \phi}u_{\phi} + \frac{\partial f}{\partial \delta}u_{\delta}\right) / \frac{\partial f}{\partial \theta_R} \tag{29}$$

This shows that the extra generalized speed u_{θ_B} introduced is in fact a dependent generalized speed. This method results in eight kinematic and three dynamic differential equations:

$$\dot{q} = u_q \qquad (q = x, y, \psi, \phi, \theta_R, \theta_B, \delta, \theta_F) \tag{30}$$

$$\dot{u}_q = f_q(\phi, \theta_B, \delta, u_{\phi}, u_{\theta_R}, u_{\delta}) \qquad (q = \phi,\ D_R, \delta) \tag{31}$$

The difference between this method and the first one is that it trades the analytic solution for the pitch in exchange for integrating an extra kinematic equation for pitch that satisfies the constraint equation (5). It is important to note that in this formulation, θ_B will appear explicitly in the differential equations for the independent generalized speeds. When implementing the constraint this way, one must ensure that the initial conditions for ϕ, θ_B, and δ satisfy the constraint equation. This is most easily done by choosing an initial ϕ and δ and solving the constraint numerically for θ_B.

3. Numerical Replacement. This method is identical to the previous one, except that the kinematical differential equation for pitch is removed, and the pitch is calculated numerically at each time step (i.e., given ϕ and δ, solve equation (5) for θ_B). In this method, seven kinematic and three dynamic differential equations must be integrated, and implicit in this method is that the pitch is being determined numerically (e.g. Newton-Raphson) at every time step.

3- Results

All of the described methods were implemented on a benchmark bicycle with the following geometric parameters: $r_r = 0.3$m, $r_{rt} = r_{ft} = 0.0$m, $r_f = 0.35$m, $w = 1.02$m, $c = 0.08$m, $\lambda = \pi/10$ *rad*. The inertial parameters of the four rigid bodies were identical to those presented in Meijaard *et al.* (2007). The equations of motion were derived using Autolev, a symbolic manipulator specialized for modelling of mechanical systems. A A 5.0 second

numerical integration was done with ode45() in Matlab, with the following initial conditions and integration settings: AbsTol = 1e-7, RelTol = 1e-8,
$\phi(0) = \delta(0) = 0.0$ rad, $\phi(0) = 0.5$ rad/s; $\dot{\delta}(0) = 0.0$ rad/s, $\dot{\theta}_R(0) = 15.\bar{3}$ rad/s. A step size of 0.001 seconds was used.

Because of the way equation (5) is formulated, given ϕ and δ, there is only one physically meaningful solution for θ_B. However, in the process of formulating the quartic polynomial, three meaningless solutions are introduced when the constraint is squared twice. The difficulty in implementing the algebraic elimination method is that there is no single analytic expression for the correct root (i.e. the one that is real valued and physically relevant). In practice, this means that for a given ϕ and δ, it is not obvious which analytic expression for the solution to the quartic to use in order to calculate the correct θ_B. This renders this method effectively useless.

Implementing the constraint by integrating a second kinematic diferential equation turns out to work very well, and furthermore, was the simplest to implement. A key requirement of this method is that the intial condition for lean, steer, and pitch must satisfy the constraint equation (5). When the equations were integrated in this fashion, the constraint was satisfied to machine precision, $|f| \leq 2_e - 16$. The integration took approximately 33.2 seconds to complete.

The final method of implementation, in which the kinematic differential equation for pitch is removed and pitch is obtained by numerically solving the constraint at each time step, resulted in the identical simulation results as in the second method, but simulation times were slightly longer, about 43.3 seconds. A Newton-Raphson algorithm was implemented to solve the constraint equation at each time step, and an initial guess of $\theta_B = 0$ was used.

4- Conclusion

An intuitive geometric approach was used to formulate the constraint equation for the Whipple bicycle model. It was shown through a sequence of straightforward manipulations that this constraint equation is in fact a quartic polynomial in the sine of frame pitch. Three methods for enforcing this constraint equation were suggested. Algebraic elimination of pitch is not practical to implement, but two methods that are practical were presented. The first requires one extra one extra kinematic differential equation to be integrated. The other requires that the constrainst be solved numerically at every time step in order to evaluate the right hand sides of the differential equations. Both of these methods produce identical simulation results, but the former results in equations that are numerically integrated in approximately 75% of the time of the latter method. Additionally, less work is required to derive the equations in this manner, and there is no need to implement and tune a numerical solver. Thus it is recommended that researchers interested in exploring bicycle dynamics (or any other dynamic system with symbollically differentiable holonomic constraints) simply integrate an extra equation rather than attempt either of the other two methods.

In practice, explict analytic expressions for solutions to a constraint equation are often difficult to determine or may not exist at all (e.g. polynomial equations of order

five or higher, transcendental equations, or inequality constraints). It is therefore useful to have other approaches to satisfying the constraint. If the constraint is such that a numerical algorithm can solve it quickly, it makes sense to use this method and implement this numerical algorithm into the integration routine. If the constraint equation can be differentiated symbolically, however, it may make sense to use this approach and integrate one extra equation. It is important, though, to verify that the constraint is indeed satisfied throughout the integration period.

5- References

[MP1] Meijaard J., Papadopoulos J., Ruina A. and Schwab A. Linearized dynamics equations for the balance and steer of a bicycle: a benchmark and review. Proc. Roy. Soc. A., 463(2084): 1955-1982, 2007.

[P2] Psiaki, M. Bicycle Stability: A mathematical and numerical analysis. B.A. Thesis, Department of Physics, Princeton University, 1979.

[W1] Whipple F. The stability of the motion of a bicycle. In The Quarterly Journal of Pure and Applied Mathematics, 30: 312-348, 1899.

Structural Behaviour of Ski Safety Barriers during Impacts of an Instrumented Dummy (P268)

N. Petrone[1], C. Pollazzon[2], T. Morandin[2]

Topics: Ski & other Winter Sports; Biomechanics; Materials; Measurement Systems; Modelling; Safety

Abstract: Aim of the work was the development of a full scale test method for performing impact tests under controlled conditions on the safety barriers usually adopted during the ski world cup events at the arrival arena. A tower pendulum was designed in order to accelerate a wooden dummy of the total mass of 70 kg up to a maximum speed of about 60 km/h. The dummy was instrumented at the centre of mass with three accelerometers in the X,Y,Z directions, connected to a IMC Cronos data acquisition system and sampled at 50 kHz each. From the measure of AccX (parallel to the suspension cable), AccY (lateral) and AccZ (parallel to the impact direction), a resultant acceleration AccR was defined for the analysis. The impacts were filmed from three different locations via commercial video cameras and subsequently analysed with Dartfish® SW to measure each impact speed. Tests were performed on the ground at a suitable location next to Cortina-Italy with soil properties similar to the snow properties: the tower can be used also in winter.
Different safety barriers underwent the tests: types A (air), B and C (foam). Type B were parts of a modular system composed of foam mattresses stitched together. Tests were performed both with the barriers placed against a wooden wall fixed to the ground and with the typical poles and cables used in the snow. The peak values recorded for the decelerations were greater than 20 g with the fixed wall and around 14 g with the poles, showing in some cases a tendency of the dummy to jump over the pole barriers.
The method successfully allowed to compare the absorbed kinetic energy of the foam mattresses with some air mattress as those used in competitions.
Key words: impact, ski slopes, safety barriers, tower pendulum, instrumented dummy, deceleration.

1- Introduction

Safety of skiing is a crucial issue for the development of this sport activity and consequently for the related economy of sport equipments and ski resorts development. The increasing number of skiers in the ski areas, even if seasonally related to the pre-

1. via Venezia 1, Padova, Italy, Department of Mechanical Engineering, University of Padova - E-mail: nicola.petrone@unipd.it
2. Z.I. Villanova, Longarone (BL), Italy, DolomitiCert Laboratories - E-mail: tommaso.morandin@certottica.it

sence/absence of snow, is bringing to attention the problem of active and passive safety of skiers . Despite statistics show that most of the injuries are related to individual falls or to accidents between skiers, a minor percentage is correlated to impacts with fixed obstacles in the slopes: unfortunately, these accidents can be highly dangerous due to the high speed and deceleration involved [C1].

Ski competitions are well known events having a high influence in the development of alpine areas due to the attraction and the worldwide resonance of the happening: in these occasions, very high speed and sharp turns are common and the safety of athletes is the most important requirement to be fulfilled [F1]. Safety barriers and protective nets are widely used in international competitions and not rarely accidents during competitions are unfortunately showing athletes impacting at high speed with the barriers or the nets. The arrival arena is the most crowded area of the racing slope and barriers have to be prepared to stop a possible falling athlete without obstructing the view over the finish line or the parterre. It is usual to see long installation of safety barriers that have to be easily placed and removed by the organizers, but have also to be light, efficient in the crash events and cost effective.

The present work dealt with the development of a standard full scale test method to be applied to safety barriers in order to evaluate their efficiency in decelerating an anthropometrical dummy, under different fixation conditions.

2- Materials and methods

2.1 Tested specimens

The work was performed using different types of barriers, ranging from air based systems to foam based systems. Air barriers were named type A, foam barriers were named type B and type C. Air based systems are recent developments consisting of a set of inflatable tubes, usually made of PVC plastic sealed sheets and are becoming more and more popular due to their lightweight construction and economical transportation costs. Major disadvantages of these barriers can be found in their sensitivity to atmospherical conditions and to the risk of permanent damage after an impact requiring their complete substitution.

Foam based barriers used in this work were an innovative modular system based on a foam mattress of 2.5×1.3×0.40 m dimensions, covered with PVC sheets and stitched by cables. The structures can be composed by two opposed halves based on a square-wave profile that can be faced and piled up to give greater energy absorption thickness or can be shifted and compacted for easy storage or transportation, as shown in Figure 1. The different combination of half-mattresses that can be stacked as combination of 1 half-Mattress, 1 Mattress (Fig. 1a), 1& Half Mattress (Fig. 1b), 2 Mattresses (Fig. 1c): B_1 is a 1 Mattress barrier, B_1.5 is 1& Half Mattress barrier and so on.

Type C was defined as a reversed version of barrier B with unusual orientation of the square-wave profile.

The barriers were tested under two very different restraint conditions: the first was a rear wooden wall fixed to the ground as shown in Figure 1a-c, the second was a typical

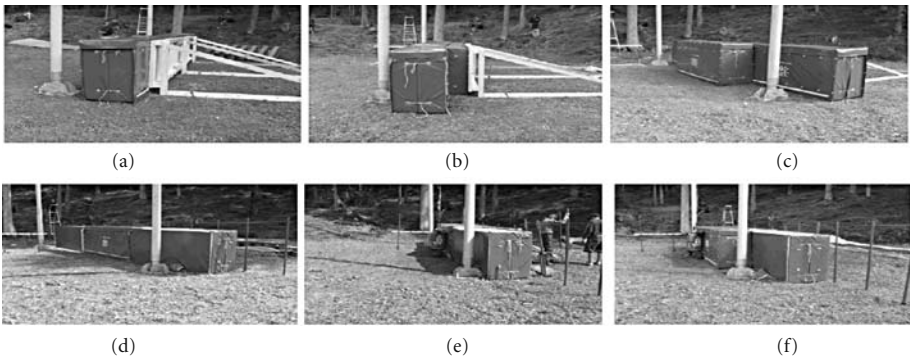

Figure 1 - The innovative foam barrier under the testing tower. (a-b-c) Fixed wall restraint on barriers type B-1, B_1.5 and B_2 respectively. (d-e-f). Spaced PVC poles acting as a restraint on barriers type B-1, B_1.5 and B_2 respectively.

rear distribution of PVC poles and connecting cables plunged in the ground at a span of 0.64 m as shown in Figure 1d-f. The latter condition is more representative of the real snow conditions, the former is corresponding to an extreme condition of barrier against a rock or a bridge wall.

2.2 Instrumentation

An instrumented dummy was used during the tests in order to measure the deceleration of the dummy during the impact. The dummy was a wooden cylindrical dummy with a total mass of 70 kg including four lateral appendices simulating the limbs as presented in Figure 2. Three accelerometers were placed at the dummy Centre of Mass as shown in Figure 2b-c. The PCB accelerometers had a full scale of 50 g and were connected to a IMC Cronos data acquisition system, controlled by a Laptop, that enabled a sampling rate of 50 kHz per channel. The reference system of the accelerometers was defined as follows: X axis parallel to the suspension cable, positive upwards, Z axis parallel to the Impact Direction, Positive backwards, Y axis in the lateral direc-

Figure 2 - (a) The wooden dummy used in the test with description of the XYZ acceleration reference system (b-c) Details of the three accelerometers installed into the dummy.

(a) (b) (c)

Figure 3 - The tower pendulum (a) Side view of the main tower with barriers ready for tests and the dummy hanging freely. (b) Overall view of the testing set-up ready for an impact tests (c) Detail of the dummy ready at the tip of lifting column.

tion. From the measure of AccX, AccY and AccZ, a resultant acceleration AccR was also defined for the analysis.

The tower pendulum shown in Figure 3 was installed and used to perform the impact tests: the suspension cable length resulted of 11.42 m, the dummy Center of Mass is placed at 0.45 m from the suspension ring so that the overall pendulum length at the

Centre of Mass is LCM=11.87 m. An additional column placed in front of the pendulum was prepared with a pulley at the tip to lift the dummy at its maximum height before impacts.

The impacts were filmed from three different viewpoints (right side, left side front, left side back) with commercial video cameras and subsequently analysed with Dartfish® sw in the right side view to measure each impact speed. Tests were performed on the ground at a suitable location next to Cortina-Italy with soil properties similar to the snow properties: the tower can be used also in winter.

2.3 Test method

The test impacts were performed on brand new barriers, after proper placement and fixation under the tower, moving the barriers to avoid successive impacts on the same point and replacing the rear fixation poles in the case of failure. To perform an impact, the dummy was lifted via a nylon traction cable running on a low friction pulley placed at the tip of the lifting column. At the given signal, the traction cable was quickly released and the dummy was free to fall, guided only by the pendulum suspension cable and consistently oriented with the Z axis perpendicular to the barrier surface.

The theoretical impact speed, vT can be estimated from the drop height of 11.87 m giving a theoretical impact speed of 15.26 m/s, equivalent to 55 km/h. Due to small variations in the lifting height and to some air and traction cable friction effects, the actual impact speeds were measured by the right side video camera images, mostly confirming the theoretical predictions.

2.4 Data Analysis

From the measure of AccX, AccY and AccZ, a resultant acceleration AccR was defined as the vector summation of AccX, AccY and AccZ.

(a) (b) (c)

Figure 4 - Test Nr. 18 on type B_1.5 barrier with poles, null speed instant. (a) Right side view. (b) Left-front view. (c) Left-rear view.

Due to the presence of the Suspension Cable, some vibrations were measured as coming from the cable vibrating in the longitudinal direction. The measured signals were Low Pass filtered at 900 Hz in the AccX- AccY direction and 1500 Hz in the AccZ direction.

Video data recorded by the cameras from the three different viewpoints were analysed frame-by-frame and rearranged to obtain the simultaneous view of the same phenomenon from three points. As an example, the right side, left-front and left-rear views of test Nr 18 at the instant of null longitudinal speed are reported in Figure 4.

3- Results

A total number of 24 impact tests was performed: during tests Nr. 15 and 16 some accelerometer signals were lost so those tests were not analyzed. The remaining 22 test results are reported in Table 1, with description of the type of barrier (A, B or C), the type of

Test Nr.	Barrier type	Rear support	Angle of impact	Impact speed [m/s]	Max AccZ [g]	AccZ at 2nd peak [g]	Max AccR [g]
1	A	Fixed Wall	0°	15,50	12.54	12.54	12.81
2	A	Fixed Wall	0°	15,30	11.99	11.99	12.16
3	A	Fixed Wall	0°	15,10	11.53	11.53	11.65
4	B_1.5	Fixed Wall	0°	15,00	15.24	12.74	15.30
5	B_1.5	Fixed Wall	0°	15,60	16.61	12.66	16.75
6	B_1.5	Fixed Wall	0°	14,90	13.31	12.80	14.63
7	B_1.5	Fixed Wall	0°	15,50	16.54	10.20	17.18
8	B_1	Fixed Wall	0°	15,30	20.57	14.43	21.56
9	B_1	Fixed Wall	0°	15,10	19.47	19.47	19.53
10	B_2	Fixed Wall	0°	15,70	14.99	9.15	16.46
11	B_2	Fixed Wall	0°	14,90	12.52	11.64	12.56
12	C_1.5	Fixed Wall	0°	15,30	13.86	13.86	13.86
13	C_1.5	Fixed Wall	0°	14,30	14.76	14.76	14.92
14	A	Fixed Wall	0°	14,50	14.44	14.44	14.45
17	B_1.5	Poles	0°	14.90	13.13	----------	14.24
18	B_1.5	Poles	0°	14.50	12.51	----------	12.56
19	B_1	Poles	0°	14.60	13.01	----------	13.12
20	B_1	Poles	0°	14.80	12.36	----------	12.42
21	A	Poles	0°	14.50	9.04	7.95	9.42
22	A	Poles	0°	15.00	9.38	8.71	9.45
23	A	Fixed Wall	45°	14.00	7.61	----------	8.03
24	B_1.5	Fixed Wall	45°	14.00	10.13	----------	10.16

Table 1 - Results of impacts on safety barriers.

rear support to the barrier (fixed wall or poles), the angle between the dummy speed and the normal to the barrier surface (0° or 45°) and the impact speed as measured from the side camera view after processing with Dartfish® software.

The acceleration values in Z direction are reported in terms of Maximum peak value (6th column) and AccZ value at the second peak (7th column) when present. In fact, as it can be seen from Figure 5a and 5c, in the case of tests with the rear fixed wall, a second peak usually occurred corresponding to the bottoming out of the barrier material and to the dummy getting almost in direct contact with the wall. When the two values of column 6th and 7th are the same, it means that the maximal absolute peak was recorded at the second peak, that is at the bottoming out of the barrier. In the case of absence of a second peak, the column is empty. The last column reports the Maximum value of the Resultant acceleration AccR. As it can be appreciated, the AccR maximum values are usually very close to the maximum values of the AccZ, as the dummy was impacting consistently in the Z direction.

The plots of the three acceleration components can be seen in Figures 5, 6 and 7. In Figure 5, the behavior of type A and B barriers is compared in the case of fixed wall or rear poles, within an interval of 1 second. Figures 6 and 7 report the acceleration graphs of type B with a higher resolution and in junction with the video frames recorded by the left front camera.

From the knowledge of impact and rebound speed when the rear fixed wall was used, the energy absorbed by the barrier Eabs was calculated as the difference between the kinetic energies before and after the impact. This parameter was considered an indicator of the ability of absorbing the kinetic energy of the skier during the impact: this infor-

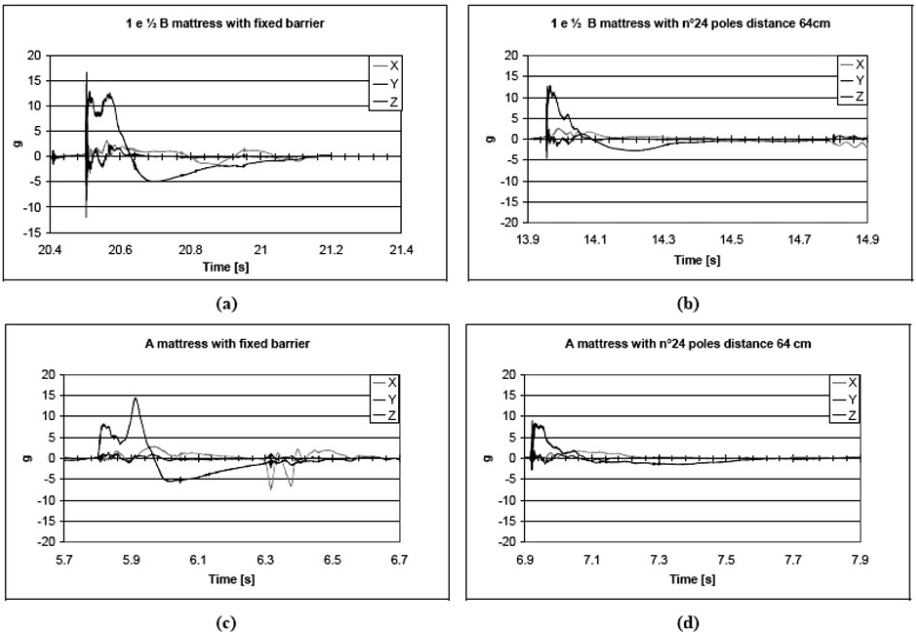

Figure 5 - (a) Test Nr. 5. (b) Test Nr. 17. (c) Test Nr. 14. (d) Test Nr. 21.

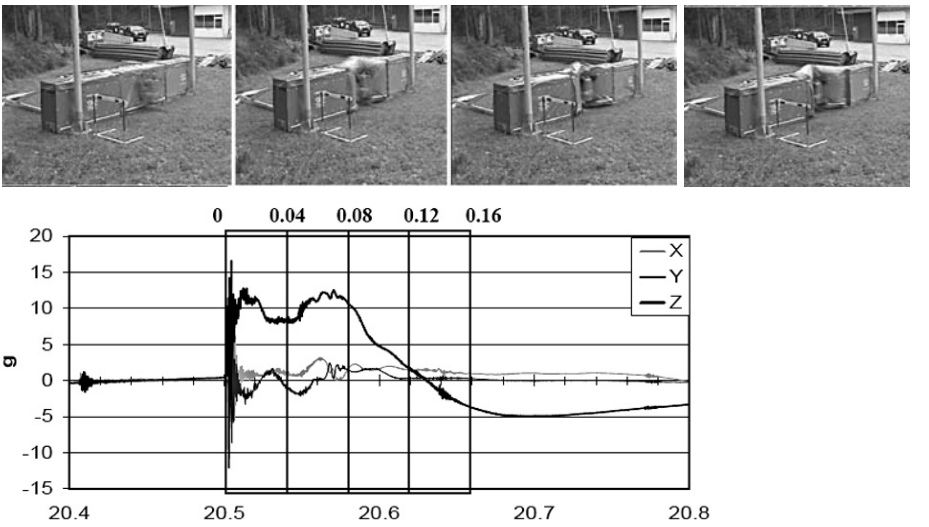

Figure 6 - Test Nr. 5. Type B_1.5 MATTRESS with fixed barrier

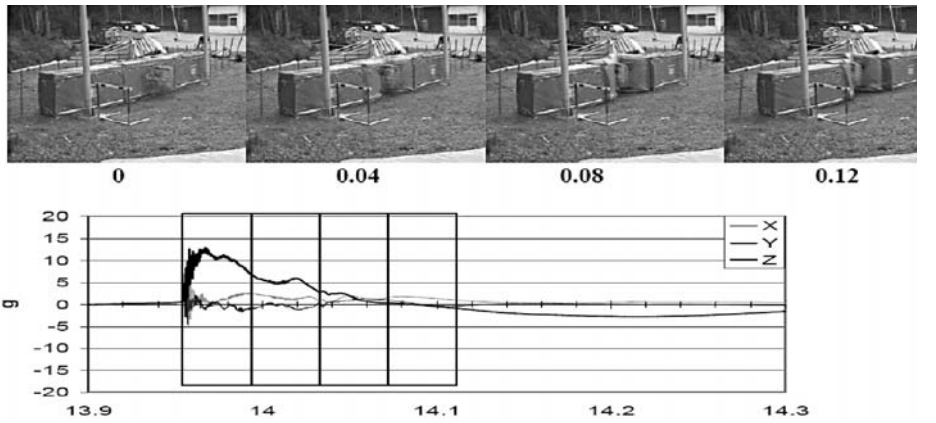

Figure 7 - Test Nr. 17. Type B_1.5 MATTRESS with 24 poles at a span of 64 cm.

mation, matched with the peak deceleration value can help in comparing different materials or defining the most suitable solutions for different applications in the snow field.

The impact and rebound speeds from each test with fixed rear wall are reported in Table 2. Based on the impact speed, the initial kinetic energy Eki was calculated as well as the absorbed energy Ekabs by difference with the final kinetic energy: in the last column, the absorbed energy is expressed as a percentage of the initial kinetic energy.

Finally, from the integration of acceleration AccZ signal and the knowledge of the impact speed, the instantaneous speed curve $v_z(t)$ was estimated: at the v_z=0 m/s instant, the mass was supposed to be fully decelerated and the dummy to have reached its deepest penetration distance in the barrier. This information was not easily retrieved from the

Test Nr.	Type of barrier	Impact Speed [m/s]	Rebound Speed [m/s]	Ek_i [J]	E_{abs} [J]	E_{abs}/Ek_i [%]
1	A	15,50	7,10	8408	6644	79,0
2	A	15,30	6,90	8193	6526	79,7
3	A	15,10	6,70	7980	6409	80,3
4	B_1.5	15,00	3,60	7875	7421	94,2
5	B_1.5	15,60	3,90	8517	7985	93,8
6	B_1.5	14,90	4,00	7770	7210	92,8
7	B_1.5	15,50	4,20	8408	7791	92,7
8	B_1	15,30	3,70	8193	7714	94,2
9	B_1	15,10	3,70	7980	7501	94,0
10	B_2	15,70	3,80	8627	8121	94,1
11	B_2	14,90	3,50	7770	7341	94,5
12	C_1.5	15,30	3,30	8193	7812	95,3
13	C_1.5	14,30	4,70	7157	6384	89,2
14	A	14,50	6,20	7358	6013	81,7

Table 2 - Energy absorption results from impacts with fixed rear wall.

video analysis. Furthermore, the integration of speed signal gave the instantaneous displacement z(t) of the dummy into the barrier material: this curve shall be compatible with the known thickness of the barrier and its supposed minimal compaction thickness. The Force/Displacement curves, estimated during these full scale high speed tests, are the equivalent of a compression tests on a material specimen: in particular the barrier Force/Deflection curves were obtained at a realistic strain rate and with an anthropometrical dummy as indenter.

4- Discussion

The impact speed from the 22 analysed tests resulted to vary between 50 km/h and 56.2 km/h: these values have to be considered meaningful for typical resort activities, but need to be raised to reproduce the possible higher speeds recorded during the competitions.

Fixed wall tests, despite their harshness with respect to real parterre configurations, were considered very important tests for the material giving a clear mechanical behaviour evaluation: they seem to be the most repeatable tests and also the most conservative, where all barriers showed the highest deceleration peaks.

On a fixed wall, all barriers showed a double peaked deceleration curve (Fig. 5), but the behaviour of type A and type C barriers resulted different from the type B barrier in terms of coincidence of the maximum peak of AccZ with the second peak.

This can be interpreted as a better triggering behaviour of A and C. Anyway, given the lower energy absorption values showed in Table 2 by type A compared to type B or type C, type A bottoming out should be correlated to a relatively high amount of kinetic energy still present in A at the impact with the fixed wall.

The highest overall value of AccZ equal to 20.57 g was obtained on B_1 tests with fixed walls: these confirmed the manufacturer's recommendations of using always at least the B_1.5 configuration.

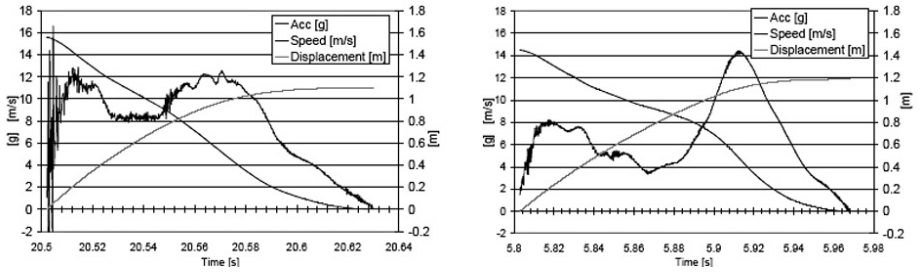

Figure 8 - Integration of AccZ signal to obtain speed and displacement signals with Fixed Wall. (Left) Test Nr. 5 on type B_1.5 (Right) Test Nr. 14 on type A.

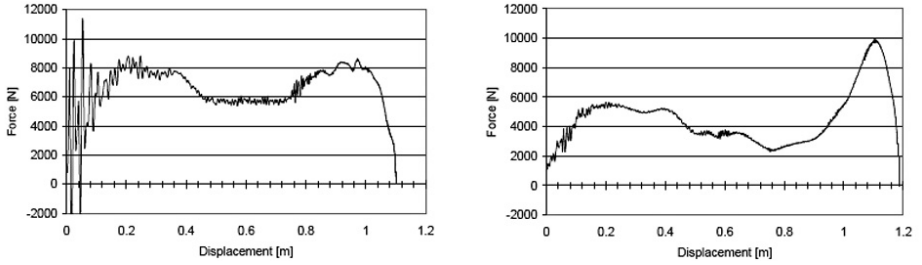

Figure 9 - Force-displacement crashing curves of the two barriers with Fixed Wall. (Left) Test Nr. 5 on type B_1.5 (Right) Test Nr. 14 on type A.

Tests performed with poles acting at the rear showed consistently lower values and no double peaked curved for the types B barriers, whereas double peaks were obtained again with type A. Despite the lower values of peak deceleration AccZ showed by type A barriers with poles, another criterion also was introduced for the barrier qualification after observing the video frame sequence: type B barrier were able to absorb the mass energy along a stroke mostly parallel to the ground, whereas type A barriers were producing a clear tendency to a vertical positive motion, in other words to "jump over" the barrier. This parameter also has to be considered in the overall qualification of the barriers.

Finally, the type B and C were showing an absorption ability of about 93% with fixed wall against a value of about 80% of type A barriers: anyway the overall qualification of the barrier will be based on a combination of the performance indices presented.

The proposed test method resulted to be significantly able to reproduce the energy levels involved in real field impacts under standard and repeatable conditions: some limitations were identified in the impact maximum speed, in the absence of snow, in the presence of the support cable and in the absence of realistic limbs and ski equipments on the dummy. The impact speed can be improved with higher pendulum tower and tests performed during winter will ensure the snow-poles behaviour. The presence of the cable can be solved by a disconnecting device that could be activated few milliseconds before the impact so that the dummy is free of impacting unrestrained onto the barriers. The evolution of the dummy limbs, not included at this stage of the research to avoid

the limb orientation variability in the tests, will be carried out in the future in order to better simulate the possible body postures assumed by athletes during real impacts.

5- Conclusions

A method for performing full scale impact tests under controlled conditions on safety barriers used in ski resorts and competitions was developed. The tower pendulum allowed to impact a 70 kg wooden dummy on different types of barriers at speed slightly lower than 60 km/h. Three accelerometers placed at the dummy centre of mass were sampled at 50 kHz each and the impacts were filmed from three different locations to measure the impact speed and to follow frame by frame the kinematics of the impact. Three types of safety barriers named A (air), B (foam) and C (foam) were studied. Tests were performed both with the barriers placed against a wall fixed to the ground and with the typical poles and cables used in the snow. The peak values recorded on barrier type B for the decelerations were greater than 20 g with the fixed wall and around 14 g with the poles; type A showed lower ability of energy absorption and higher tendency of the dummy to jump over the barrier. Type C showed the highest energy absorption with peak acceleration lower than B.

The proposed method enabled to successfully compare the absorbed kinetic energy of the foam mattresses with some air mattress as those used in competitions and can be proposed as a standard approach for the full scale evaluation of such safety devices.

6- Acknowledgements

The authors desire to thank the Vidori Silvano company of S. Vito (BL-Italy) for supporting the research.

7- References

[F1] FIS: Specifications for Competition Equipment and Commercial Markings, in: Alpine Ski Rules - Edition Northern Hemisphere (2006) - www.fis-ski.com

[C1] Centro Studi Sicurezza e Cultura della Montagna, Treviso, Italy, Annual Report 2007.

[M1] M. A. Macaulay, Introduction to Impact Engineering, Chapman and Hall, 1987.

Structural Behaviour of Slalom Skis in Bending and Torsion (P269)

Matteo De Gobbi[1], Nicola Petrone[2]

Topics: Ski & other Winter Sports, Measurement Systems.
Abstract: In the present work, an integrated approach to the ski structural evaluation problem is presented involving several activities and based on data of different nature. The research stages were Laboratory tests, Field tests and Analysis Software developments; these activities were synchronously carried out in order to give to engineers the information needed for a correct ski design, involving also information from the other disciplines like biomechanics and material sciences.
The ski stiffness properties in bending and torsion are two fundamental design parameters and a Contact Method and an Optical Method were compared in this work, leading to equivalent results. After application of proper sensors on a pair of racing skis, the calculated deflection curves and the measured deflection curves were compared to confirm the possibility of applying the method during field tests.
To achieve the in field bending and torsion diagram on the ski, two slalom racing skis were used and strain sensors were applied to the top foil of the skis at sections regularly distributed along the ski. The ski were calibrated during laboratory tests under different bending and torsion test conditions. In the field tests, three professional testers were involved, different for skill levels and anthropometrics, and special slalom courses with short poles were performed. As a results, the instantaneous bending and torsion moment curves on the ski were evaluated: the deflected shape of the ski was evaluated, projected onto the snow surface and visualized at each frame in the snow field after developing a specific LabVIEW application. Quantitative index were introduced to compare the inner and outer ski during the courses.
The results of these analysis can be of interest not only to the ski-binding-boot manufacturers, but also to the whole ski community as the proper scientific knowledge of the skiing phenomena allow for virtual analysis of performance, comfort and safety improvements.
Keywords: ski; bending, torsion, in-field acquisition, deflection.

1. Department of Mechanical Engineering University of Padova, Italy, Via Venezia 1 - E-mail: matteo.degobbi@unipd.it
2. Department of Mechanical Engineering University of Padova, Italy, Via Venezia 1 - E-mail: nicola.petrone@unipd.it

1- Introduction

Ski science has been continuously developing since the early '70s when the first technical analysis of this complex man-ski-snow interacting system were developed [S1]. The presence of well known ISO standards for the evaluation of stiffness and strength properties of ski is due to the industrial interests into the ski business but also to the need of precise safety regulations to prevent failures or injuries for the users [I1]. The recent success of carving skis has improved the easiness of skiing and the diffusion of this sport activity also to a major number of persons. Despite these facts, the scientific knowledge of the structural behaviour of the different part of the system is still object of research and several efforts are posed in the different directions of study needed for a complete design process like the ski mechanical characteristics, the skier's biomechanics, the snow-ski contact mechanics [F1], [BP1], [CL1].

One of the major reasons of complexity in the problem is the difficult experimental evaluation of the man-ski-snow behaviour in the field, if a minimum disturb from the measurement system is required. For instance, loads at the binding-ski interface are measured but usually after interposition of thick and stiff aluminium load cells that are adding masses difficult to neglect and that are stiffening the real ski and its deflection in the snow [F1]. Some recent measurement systems were able to integrate several physical information in a single data logger, addressing either the pressure or the deflection behaviour of the ski [S2].

When addressing the development of racing skis, the weight and performance requirements are usually so strict that only systems that result to be not invasive for the ski or the tester are allowed and can be considered.

In the present work, an integrated approach to the problem is presented as several activities were performed and data of different natures were synchronously collected in order to give to engineers the information needed for a correct ski design procedure, involving also information from the other disciplines like biomechanics and material sciences.

The results of these analysis can be of interest not only to the ski-binding-boot manufacturers, but also to the whole ski community as the proper scientific knowledge of the skiing phenomena allow for virtual analysis of performance, comfort and safety improvements. Moreover, the possibility of measuring the skiing technique on skilled champions allow to functionally evaluate the athletes and to develop proper training methods and techniques.

The work was developed over a relatively long period and will be split in Laboratory tests, Field tests and Analysis Software developments.

2- Laboratory tests: ski structural behaviour in bending and torsion

The ski stiffness properties in bending and torsion are two fundamental design parameters and need to be accurately known along the ski length: the ISO standard prescribe the test methods for defining an overall bending and torsional stiffness parameter [I1], but special methods need to be developed to obtain the EJ bending stiffness or the GJ

torsional stiffness at any location along the longitudinal x-axis of the ski. Several methods were developed by manufactures and researchers: in the present work, a Contact Method and an Optical Method are compared.

The real design variable of a racing ski is its deflection under carving conditions and the ability of obtaining a curvature radius projected on the snow corresponding to the target curvature radius described by the skier. After application of proper sensors on a pair of racing skis, the calculated deflection curve and the measured deflection curves were compared to confirm the possibility of applying the method during field tests.

2.1 Stiffness tests by contact method

A pair of Nordica® SLR-WC special slalom racing skis were adopted as benchmark skis: these 1,650 mm long skis presents a sandwich construction and are used in combination with special racing plates.

At the manufacturer plant an integrated flexible test bench is available to perform bending and torsion characterization tests by Contact Method: a sensing device based on LVDT transducers can be repeatedly applied to the ski lower sole during a three point bending (Fig. 1a) or a torsion loading (Fig. 1b). The result of the test is the EJ or GJ stiffnes profile along the x-axis with a 50 mm resolution as shown in Figure 1 where the curves are normalized to the maximum recorded value.

Tests were performed on the ski alone (Flat), the ski-plate assembly (Plate) and the ski-plate-binding-boot assembly (Boot) in bending: torsion tests can be performed only with plates due to the clamping and loading devices configuration. Results of comparative tests on the ski in the different assembly configurations and from bending and torsion are reported in Figure 2.

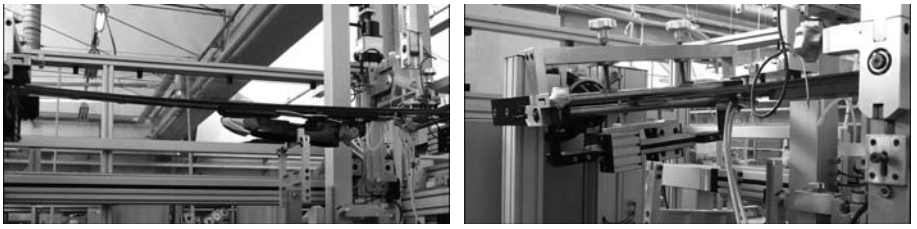

Figure 1 - Bending (left) and Torsional (right) stiffness tests by contact method setup.

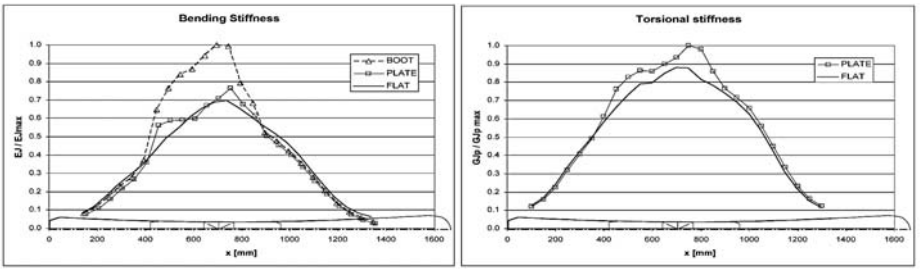

Figure 2 - Bending and torsional normalized stiffness tests results on ski only, ski-plate and ski-plate-binding-boot assembly.

Contact method stiffness tests are static tests and require a long procedure due to repeated measurements: moreover, no information can be obtained about the dynamic and vibrational properties of the ski. Due to these limitations, an Optical Method was developed at the Department of Mechanical Engineering, University of Padova.

2.2 Stiffness tests by optical method

Motion capture systems are fundamental tools for the biomechanical analysis in orthopaedics an sport science. The system is usually based on a set of reflective markers of 15 mm diameter placed at significant landmarks on a subject whose position is measured on a calibrated 3D volume by means of calibrated infrared cameras.

In this work, a mechanical application of the motion capture system Smart BTS® was evaluated and a set of miniaturized markers of 5 mm diameter was customized: camera lens were changed in order to obtain a smaller volume calibration and a resolution of 0.5 mm within a measuring volume of about 2.5×2.5×2 m covered by 6 infrared camera sampling at 60 or 120 Hz.

The markers were placed along the two ski edges at a span of 50 mm and the ski was supported between rollers and loaded at a midpoint as in the ISO bending set-up specifications: the setup and a corresponding motion capture image are shown in Figure 3.

The two states of the ski, unloaded and loaded, were captured and the deflection in bending or torsion was evaluated as a difference of y-coordinates at each couple of markers along the ski x-axis: from the knowledge of the applied bending moment curve and the estimation of the radius of curvature in the deformed state, the local EJ values can be rapidly estimated at all ski sections in one shot. The two curves of EJ obtained by Contact or Optical method on the same ski are compared in Figure 4 after normalization to the maximum EJ value obtained with the boot: the two curves are very close except from the central part where the effect of the plate is concentrated.

The greater advantage of Optical Method is the synchronous acquisition of all sections and a reduced testing time: furthermore, the sampling frequency of 120 Hz allow to perform on the ski basic modal analysis after exciting different shapes up to frequencies of 40-50 Hz, that are anyway significantly affecting the ski performances and dynamics.

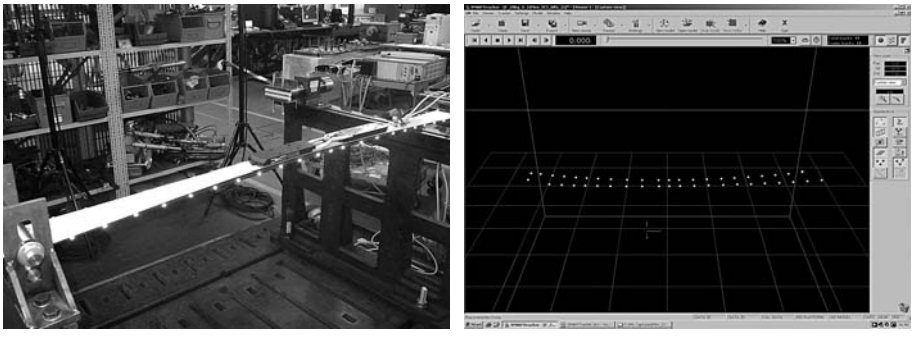

Figure 3 - Optical method tests setup. Ski under testing with 5 mm reflective markers placed on the ski edges (left) and resulting image in the motion capture system (right).

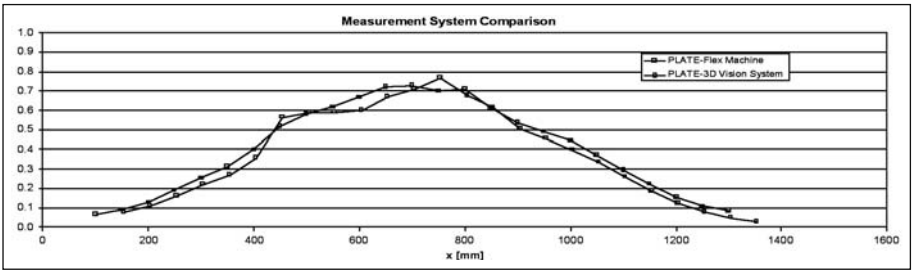

Figure 4 - Comparison of contact and optical stiffness measurement methods after bending tests.

2.3 Structural deflection analysis

The original part of the work was the development of a pair of strain gauged skis suitable for strain measurement during real courses in a snow field: this would enable to measure the distribution of bending and twisting moments acting along the ski during real events. Two racing skis were used and strain gauges were applied to the top foil of the skis at 11 sections regularly distributed along the ski. This approach was adopted in order to apply a very small additional mass to the ski shovel and tail (180 gr per ski) and to ensure the realistic structural and dynamic behaviour of the ski.

The ski were calibrated during laboratory tests under different bending and torsion test conditions with a HBM UPM 100 strain unit, in order to evaluate the calibration constants correlating the bending and twisting applied moments and the strain signals. From the knowledge of ski stiffness properties at each section, the local ski curvature along the ski x-axis can be estimated and, after double integration, the deflection curve of the ski can be calculated from the strain measurements, both in bending and torsion.

The validation of the method was obtained after measuring the ski deflection curve by Optical Method on a bending test with a load of 319 N applied to a complete system composed by a dummy foot, a racing boot, the racing bindings, the racing plate and the ski placed freely on two rollers as shown in Figure 5a. The vertical displacement along the x-axis, calculated from the integration of bending moment curves resulted very accurately matching the displacement measured with the Optical Method, as reported in Figure 5b.

(a)

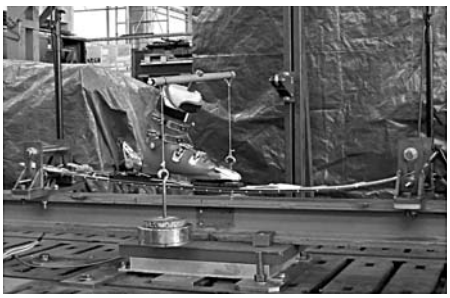

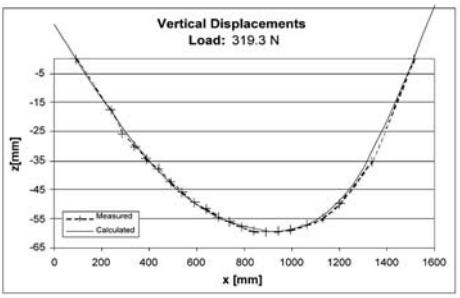

(b)

Figure 5 - Validation of the structural deflection method by comparison between measured and calculated displacements.

These encouraging results suggested to adopt the instrumented skis during test sessions in the field to collect synchronously the strain signal at the ski sections during real slalom manoeuvres.

3- Field tests: structural behaviour of skis during slalom

Field tests were performed after developing a complete portable data acquisition system. Mechanical structural information were collected together with biomechanical information such as the knee flexion angles and the muscle activation levels. A set of accelerometers was placed on the leg composite protections and recorded together with 10 EMG signals in order to have the timing with respect to the pole passing. Portable data acquisition units PocketEMG® from BTS-Italy were used for data collection in the field. The unit is based on a PDA system and allows to measure 16 EMG channels at 10 kHz sampling rate; the unit can support 4 Biometrics® goniometers and was customized to collect also bridge sensors like strain channels and accelerometers. The dimensions (145×95×20 mm) and weight (0.3 kg) of the PocketEMG® allow to place it easily in a pocket of the ski suite without influencing the skier behaviour in the slope.

Two inertial platforms X-sense Mti were applied to the skis and synchronously recorded at 100 Hz (Fig. 6). Pilot tests performed on a slalom course with giant and special slalom short poles confirmed the reliability of the developed system and allowed to obtain the bending and torsion diagrams at each sections during the courses.

Three elite skiers were subsequently involved in the study, wearing the instrumented racing slalom skis: their data are reported in Table 1. Several courses of Special Slalom

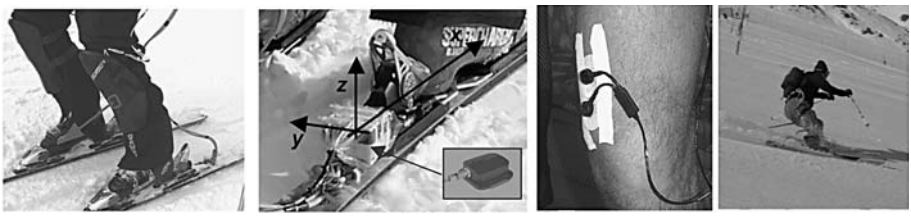

Figure 6 - Field tests instrumentation.

ID tester	Tester 1	Tester 2	Tester 3
Age	34	43	33
Mass [kg]	90	74	85
Height [cm]	183	175	185
Skill Level	National racing ski trainer	National racing ski trainer	Former WC atlete
Ski discipline	Special and Giant slalom	Extreme Freeride	Special and Giant slalom

Table 1 - Description of the three testers involved in the study.

followed by Giant Slalom were performed on a slope of known shape and orientation: some courses were performed with all the available recording channels on the left ski, using at the right ski an equivalent dummy ski. Other courses were performed with both instrumented skis.

The results of courses performed recording the left ski only, are reported in Figure 7 for comparison between the three testers at two different instants: the pole passing instant, as revealed by the accelerometer signal at the shank protections, and the instant of maximum recorded bending moment. The delay between these two instants is named t_{max} and the position of maximum estimated bending moment is defined x_{max} and is reported as a fraction of the ski length l. Maximum Bending moments are normalized to the absolute maximum moment recorded in the session Mf_{max}.

The three curves of each plot are the bending moment curve (higher smoothed curve), the torsion moment curve (lower linear curve) and the estimated deflection curve (hinged at the plate extremities, with two tips pointing upwards). The latter curve in particular has to be seen as the important result of the field data collection session to be compared with the skiers boot trajectories in the snow: comparison of these two geometrical curves can help in evaluating the correct ski design and the amount of carving versus skidding ski motion.

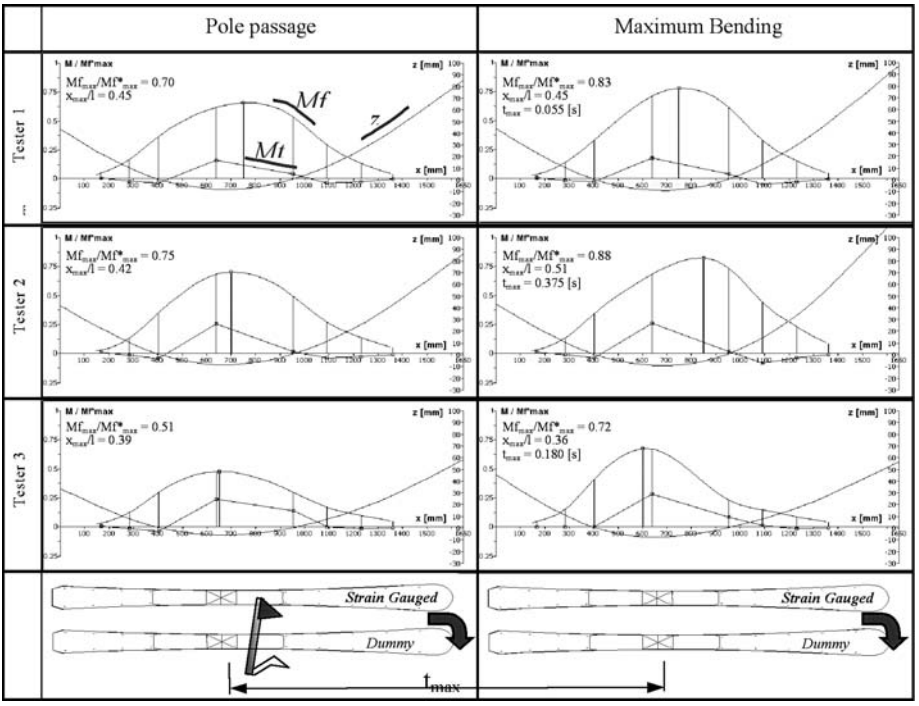

Figure 7 - Results of field tests for a special slalom right turn on the left ski acting as outer ski: comparison between the three tester behaviour and the two successive instants of pole passing and maximum bending.

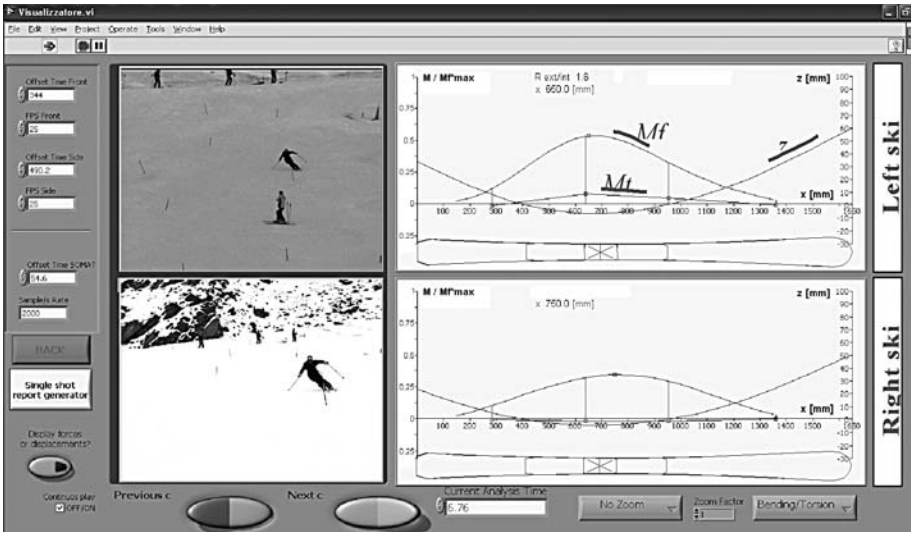

Figure 8 - Results of field tests for a special slalom right turn on both skis.

The results of courses performed recording the two skis are reported in Figure 7 for tester 1 at a generic instant before the pole in a right turn. The x coordinate of the section presenting the maximum estimated bending moment x_{max} is reported for the inner and outer skis. The three curves in Figure 8 are the same of Figure 7 but the differences between inner and outer ski can be synchronously appreciated. To estimate this difference, the ratio $R_{ext/int}$ between external ski and internal ski bending moment was introduced and is equal to 1.6.

In the picture, the two frames obtained from two commercial video cameras can be synchronously played back to help the comprehension of the ski structural behaviour compared to the skier's body posture and position along the course.

4- Integrated analysis software development

The great amount of collected data required the development of an analysis tool enabling their integrated analysis. Therefore, an Integrated Analysis Software was implemented based on a modular architecture in Labview and able to process data of different nature ranging from the ski structural data, the accelerometers data, the Mti orientation data, the EMG and knee flexion data and the digital video files.

The structural analysis applications inbuilt in the SW are shown in Figure 8 whereas Figure 9 shows as the combination of ski orientation and deflection data can be presented with respect to the snow surface. Snow surface along the slope and at each pole was reconstructed after applying statically the skis to the snow surface without edging at each pole.

All geometrical, mechanical, structural information of skis are inserted and combined in the SW for the estimation of the deflected geometry of the ski.

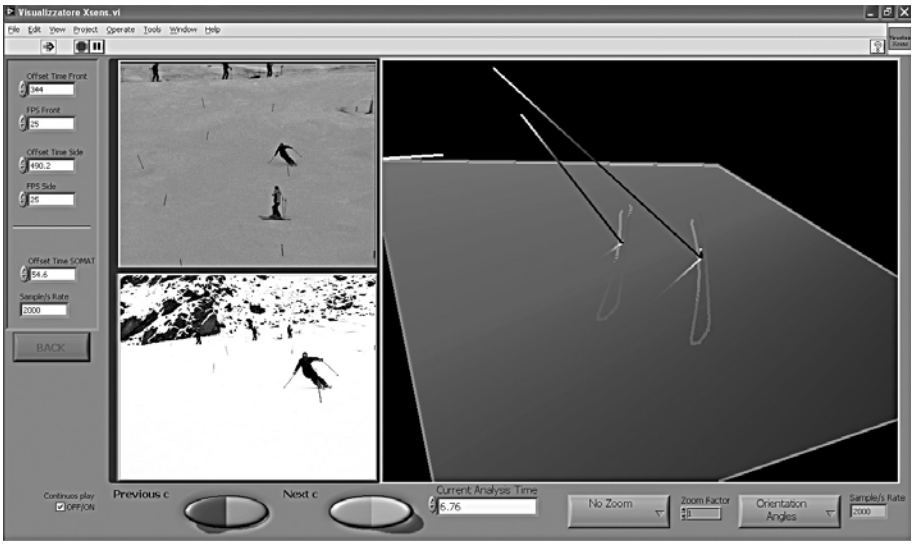

Figure 9 - Integrated analysis software application showing the instantaneous deformed shape of the ski and its instantaneous orientation with respect to the snow surface.

5- Discussion of results

Field tests results as presented in Figures 7 and 8 can be discussed from several points of view. The single tester can be analysed in terms of his symmetric loading pattern behaviour: as in Figure 8, the bending curves M_f of the left (outer) and the right (inner) ski are clearly different in terms of shape and peak values, depending on the loading actions at the bindings but also on the ski absolute orientation to the snow surface and the leg posture. The value of this analysis is that the deflection line indicated as z in Figure 7 has to be considered the deformed shape of the ski during the ski turn, without any influence of additional stiffening load cell plates.

The field tests also allowed to evaluate the tester's technique in passing the poles, with respect to the timing interval between the pole and the maximum bending moment instant, defined as t_{max}: as it can be appreciated form Figure 7, Tester 1 seems to be anticipating the turn and its maximum bending instant is very close to the pole (t_{max}= 0.055s) whereas Tester 3 has a 0.180 delay and Tester 2 has a 0.375 s delay. The latter results was due to the lower skill ability of Tester 2 in slalom events: on the contrary, the best time trial performance were given by Tester 3.

The bending curves are quite different between the three testers and can be easily correlated with the position of the Centre of Pressure on the boot sole, indicating a forward or backward leaning on the ski under examination.

As a conclusion, the consistent application of the proposed approach enables to develop a sound experience from field testing and a clearer knowledge of the structural behaviour of the ski that are important for the ski design but can be also useful for high level athletes training.

6- Conclusions

Laboratory tests performed on a special slalom ski by a contact method and an optical method gave equivalent results of bending and torsion stiffness curves along the ski. A set of strain gauged ski was used for predicting the ski deflection under complex conditions and was validated by the optical method. Field tests were performed with an integrated data collection system on special and giant slalom courses involving three testers that were compared in terms of maximal bending actions and timing when passing the poles. An integrated Labview SW was developed to support structural data processing and ski design procedures.

7- Acknowledgements

The Authors desire to thank the company Nordica S.p.A (TV-Italy) for supporting the research.

8- References

[S1] V. Senner: Synopsis of Current Developments: Modelling and Measurement Equipment in Skiing, in: ISEA conference, Munich (2006).
[I1] ISO: Alpine skis: Determination of the elastic properties in: ISO 5902 (1980).
[CL1] F. Casolo, V. Lorenzi, M. Giorla: Relevance of Ski Mechanical and Geometrical Properties in Carving Technique in: II ICSS, St. Christoph am Arlberg (1999).
[BP1] F. Bruck, Lugner P., H. Schretter: A Dynamic Model for the Performance of Carving Skis, Skiing Trauma and Safety in: 14° Volume, ASTM STP 1440 (2003).
[F1] P. A. Federolf, Finite Element simulation of a carving snow ski, PhD Thesis, ETH 16065, Zurich 2005.
[S2] N. Scott, T. Yoneyama, H. Kagawa and K. Osada, Measurement of Ski snow-pressure profile, Sports Engineering (2007), 10, 145-156.

Finite-Element Analysis of the Collision and Bounce between a Golf Ball and Simplified Clubs (P271)

Katsumasa Tanaka[1], Hiroshi Oodaira[1], Yukihiro Teranishi[2], Fuminobu Sato[2], Sadayuki Ujihashi[1]

Topics: Golf.
Abstract: The objective of this study was to develop a finite-element (FE) model which could accurately simulate the behaviour of golf impacts, and to investigate the effect of a shaft on the clubhead upon the rebound of a ball, by conducting FE analysis on a ball colliding with a simplified club. The clubs were constructed by holding simplified clubheads by a locking ring fitted onto a steel shaft. The clubheads were designed based on the mass, volume and position of the centre of gravity (CoG) of commercial clubheads, so as to enable a typical golf impact. Three circular, hollow, titanium alloy bodies of constant mass, with increasing loft angles, were manufactured. FE models with linear elasticity of the clubs, which consisted of the clubheads, a locking ring and a shaft, were constructed. The FE model of the ball consisted of 8-node solid elements, and the material model was expressed as a hyper-elastic/viscoelastic model. Impact experiments were also conducted for comparison to confirm the accuracy of the FE models. The results of the impact simulations closely matched the experimental results. Impact behaviour was analysed by varying the impact point of the ball colliding with the full clubs and the lone clubheads and then comparing the ball/club and ball/clubhead collision results. The differences between the two most extreme values for the rebound angle and spin rate tended to be smaller in the club impact cases than in the clubhead impact cases. This tendency was estimated to depend on the relationship between the shaft position and the loft angle/CoG of the clubhead.
Key words: Finite-element analysis, Impact experiment, Golf ball, Clubhead, Shaft.

1- Introduction

Flexing the large, thin face of a golf driver head provides kinetic energy to the golf ball after impact by reducing its deformation and the associated viscoelastic energy loss during clubhead/ball impact. The driver head with a high coefficient of restitution

1. Tokyo Institute of Technology, 2-12-1-W8-14, Ookayama, Meguro-ku, Tokyo, Japan - E-mail: ktanaka@mei.titech.ac.jp
2. Mizuno Corporation, 1-12-35, Nanko-Kita, Suminoe-ku, Osaka, Japan - E-mail: yteranis@mizuno.co.jp

(CoR) has contributed to the increase in ball driving distance. Concerned that this high-performance equipment is outdating golf courses and ruining the game, the Royal and Ancient Golf Club of St Andrews, together with the United States Golf Association, has committed to new rules, setting an upper limit for driver CoR, and thereby does not permit the use of products with high CoRs.

The initiation of CoR regulation was a turning point in club development. Methods of numerical analysis, including the finite-element (FE) method, are among the most effective ways to solve this golf impact problem. FE models that allow the precise estimation of CoR *via* computer simulations are in demand among developers wishing to create high-performance clubs that meet the current rules. In addition, the design and development of clubs has so far focused mainly on the launch conditions of a ball after impact, most notably the launch angle and spin rate of the ball, as well as its launch velocity. The initial launch conditions need to be improved not only by way of a clubhead with a high CoR but by altering the characteristics of the club, including the shaft. Therefore, it is important to understand precisely which club characteristics affect the behaviour of the ball during and after impact. Previous research (Tanaka *et al.* [TO1]) has investigated the interactions between the mechanical properties of a clubhead and the rebound of a ball by conducting FE analyses (FEAs) of balls' collisions with simplified clubheads. It is possible to effectively understand the influence of the shaft at impact by comparing the results of club simulations with these previous results.

The objective of this study is to construct an FE model which can accurately simulate the behaviour of golf impacts, and to investigate the effect of the presence of a shaft on the rebound of a ball, by conducting an FEA of a ball colliding with a simplified club.

2- Construction of FE models of simplified clubs and a golf ball

2.1 Specifications of the simplified clubs

The clubs were constructed by holding simplified clubheads in a locking ring fitted onto a steel shaft. The clubheads, which were simplified in shape, were designed and manufactured with clearly defined mechanical properties, as shown in Figure 1 and Table 1. The simplified clubheads were designed with reference to the mass, volume and position of the centre of gravity (CoG) of commercial clubheads, so as to allow the creation of

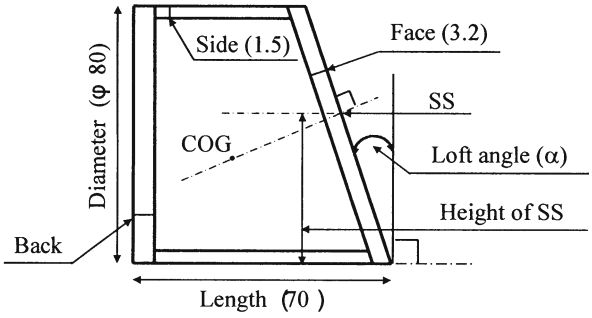

Figure 1 - Cross-section of a simplified clubhead.

Model ID	Head 0	Head 10	Head 20	1W
Loft angle [°]	0	10	20	-
Mass [g]	213.6	217.1	214.1	180-210
Volume [cm^3]	351.9	316.4	278.7	380-440
Thickness of backside [mm]	1.5	2.0	2.5	-
Sweet Spot ratio [-]	0.50	0.55	0.58	0.51-0.63

1W: Commercial number 1 wood (driver)

Table 1 - Mechanical properties od simplified clubheads.

typical golf impacts. Three circular, hollow, titanium alloy bodies of constant mass, with increasing loft angles, were manufactured. This constant mass with changing loft angle was made possible by altering the thickness of the back face, as shown in Table 1. The thickness of the impact face and cylindrical portion were 3.2 and 1.5 mm, respectively, for all clubheads. The sweet spot (SS) ratio was defined as the ratio of the height of the SS to the diameter of the clubhead. This ratio was used to represent the positions of the CoGs of the clubheads. A steel shaft was used, as its mechanical properties could be measured experimentally and determined precisely using FEA. The length and weight of the shaft were 1000 mm and 93.4 g, respectively. A locking ring, to which the hosel was mounted by welding, was manufactured to hold the clubheads, as shown in Figure 2. The ring was made of the same titanium alloy as that of the clubheads. The shaft and the hosel were joined together with glue. The clubhead and ring were fixed by a bolt and a nut, so that the shaft position could be altered. In this study, the distance between the face and the shaft was 9 mm in the case of Head 0 and 0 mm in the case of Heads 10 and 20, as shown in Figure 2a, and the lie angle was 90 degrees.

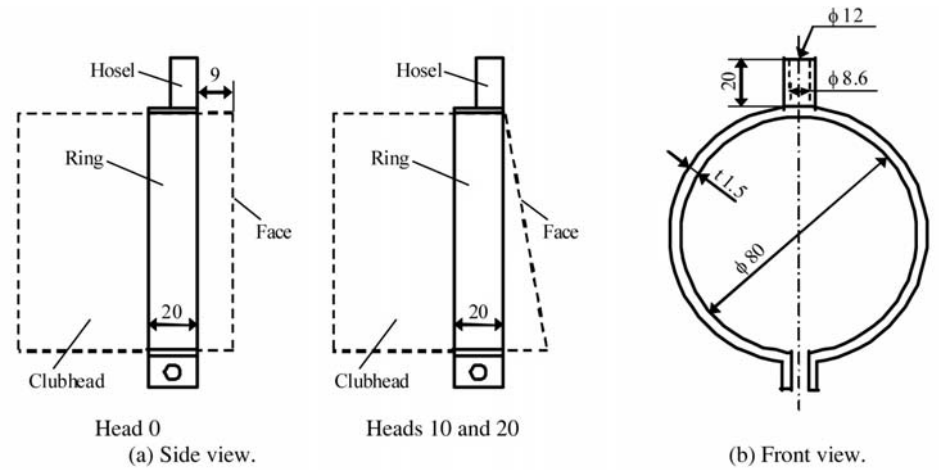

Figure 2 - Locking ring.

2.2 Construction of FE models

2.2.1 Club models

FE models of 3 clubs, which each consisted of 3 clubheads, a locking ring and a shaft, were constructed as shown in Figure 3 and expressed as linear elastic models. These models were used as half models in the FEAs of this study, with plane symmetry applied. Table 2 shows the mass and the numbers of the nodes and elements for each club model. The clubhead models were composed of 8-node solid and 4-node shell elements, and their material properties, Young's modulus, Poisson's ratio and density, were 115 GPa, 0.30 and 4,500 kg/m^3, respectively. The shaft model was composed of 4-node shell elements, and the same material properties for the shaft model were 210 GPa, 0.30 and 7,900 kg/m^3, respectively. The ring model was composed of 8-node solid elements and the material properties of the ring model were the same as those of the clubhead models.

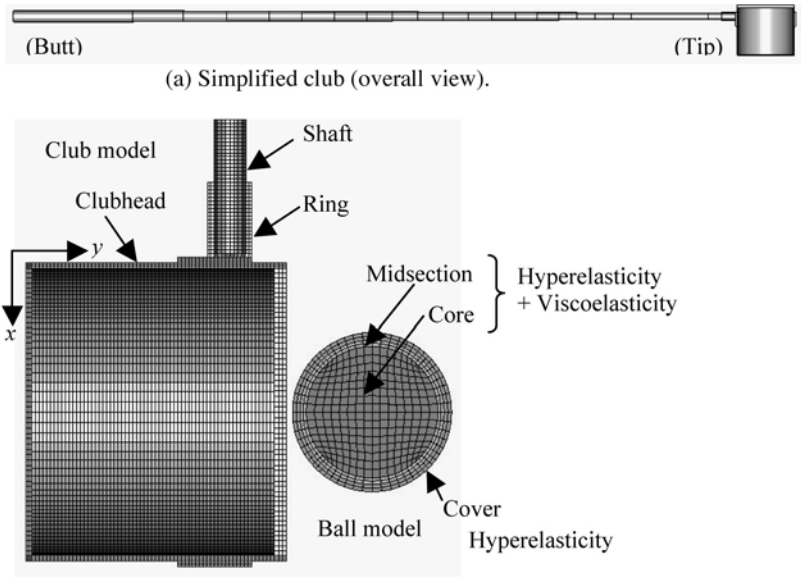

(a) Simplified club (overall view).

(b) Simplified clubhead (Head 0) and ball with ring and shaft tip.

Figure 3 - Constructed FE models.

Model ID	Mass [g]	No. of nodes	No. of elements
Club 0	175.9	36013	30962
Club 10	175.9	37466	32372
Club 20	176.6	41190	36045

Table 2 - Data on simplified club half models.

2.2.2 Ball model

An FE model of a 3-piece ball, which consisted of an outer cover, midsection and core, was constructed from 8-node solid elements, as shown in Figure 3b. This model was also used as a half model in the same way as were the club models. The outer diameters of the individual layers of the ball model were determined by measuring those of a real ball. Table 3 shows the outer diameters of the individual sections and the numbers of nodes and elements for the ball model. The material model of the cover was expressed as a hyperelastic model, whereas the material models of the midsection and core were expressed as viscoelastic models with hyperelasticity (Tanaka *et al.* [TS1]). In this study, the Mooney-Rivlin model was used as the hyperelastic model, and the three-element model was used as the viscoelastic model (The Japan Research Institute [T1]).

	Diameter [mm]	No. of nodes	No. of elements
Core	35.4	2601	2048
Midsection	38.8	2403	1536
Cover	42.8	2403	1536
Ball model	42.8	5805	5120

Table 3 - Data on the ball half model.

3.1 Impact experiments between the ball and the simplified clubs

Experiments were conducted in order to produce a typical impact between the ball and the club, and the constructed FE models of the clubs and ball were validated by comparing their results to those from the experiments. A 3-piece ball was fired from an air gun, in a strain-free and non-rotational condition, colliding with the face of a club whose shaft's butt side was immobilised, as shown in Figure 4. The behaviour of the ball and

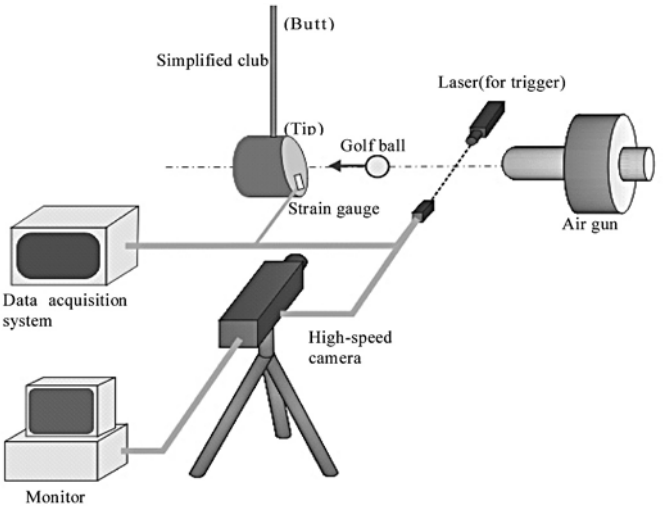

Figure 4 - Experimental apparatus.

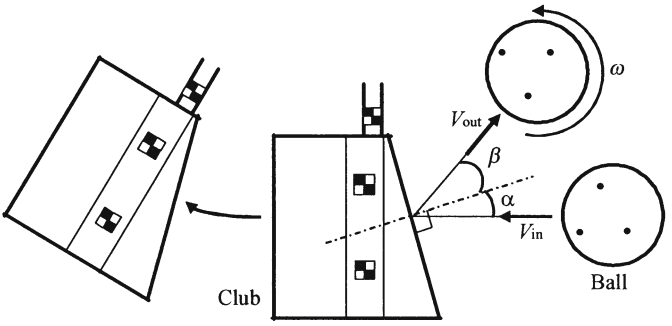

Figure 5 - Impact behaviour of ball as ascertained from a high-speed camera.

club during and after impact was recorded using a high-speed camera (20,000 fps, shutter speed 1/100,000 s). The velocities of incidence (V_{in}) and rebound (V_{out}), rebound angle (β) and spin rate (ω) of the ball were ascertained from photographs taken by the high-speed camera, as shown in Figure 5. In addition, the strain responses of the clubhead (on the impact and back faces) and shaft were measured using strain gauges affixed to them. The impact velocity of the ball was varied between 30, 40, and 50 m/s. The impact position was initially at the SS of the clubhead, and it was then varied within the range of 20 mm from the SS at ±5 and ±10 mm intervals.

3.2 FE analyses of the collisions between the balls and clubs and validation of the accuracy of the FE models

The impact behaviour of the ball and clubheads was obtained from the simulations conducted with the FE models under the same conditions as those of the experiments, and the results of the FEAs were compared with those from the experiments to confirm the accuracy of the FE models. The commercial FE code LS-DYNA (Ver. 970) was used for the simulations. Friction between the ball and the impact face of the clubhead was expressed as Coulomb friction, and the friction coefficient was found to be 0.3, based on work conducted by Nakasuga and Hashimoto (Nakasuga and Hashimoto [NH1]).

Figure 6 shows the results for V_{out}, β and strain response (at the face and shaft of Club 10, at a velocity of 50 m/s), for both the experiment and the FEAs, from an impact at the SS of the clubhead. The simulation results for the V_{out} and β (Figure 6a and b) closely match the experimental results for a range of impact velocities (30-50 m/s) and loft angles (0-20 degrees). The simulation results for the strain response of the clubhead and shaft (Figure 6c) also agree with the experimental results.

Figure 7 shows the results for V_{out} (Clubs 0 and 20) and ω (Club 20) at a velocity of 40 m/s, for both the experiment and the FEAs, with changes in the impact point of the ball. The x-axis represents the distance between the SS and the impact point. "0" represents an impact point agreeing with the SS, while a negative x-axis value means that the impact point is situated on the sole rather than the SS. A positive x-axis value means that the impact point is situated on the crown of the clubhead. The simulation results gene-

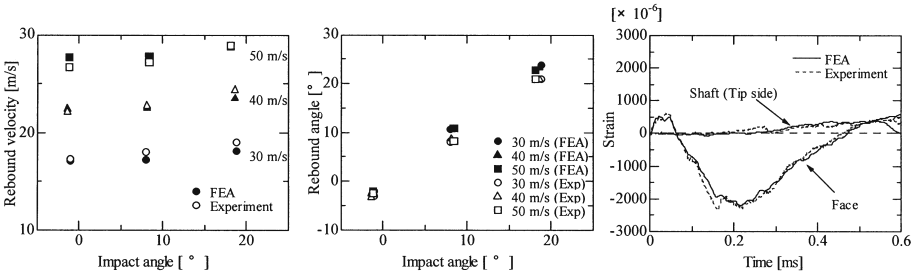

(a) Rebound velocity V_{out}. (b) Rebound angle β. (c) Strain response (Club 10, V_{in}=50 m/s).

Figure 6 - Experimental and FEA simulation results.

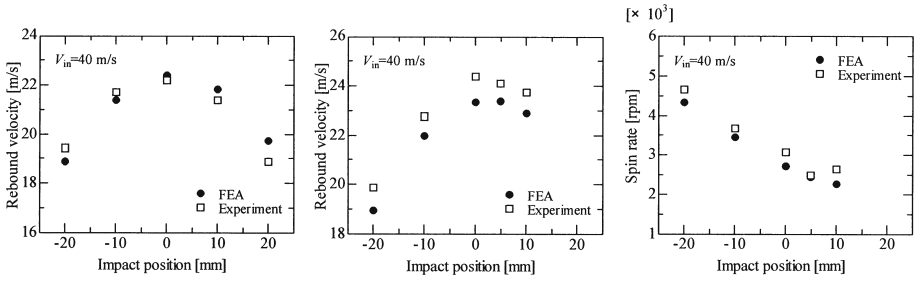

(a) Rebound velocity V_{out} (Club 0). (b) Rebound velocity V_{out} (Club 20). (c) Spin rate ω (Club 20).

Figure 7 - Experiment and FEA simulation results for the collision between the ball and Club 0/20 at different ball impact points.

rally match the experimental results. Although the simulated and experimental V_{out} results for Club 20 do not match as closely as do those for Club 0, the simulation results for V_{out} tend qualitatively to agree well with the experimental results regarding the impact point of the ball. These results indicate that the constructed models are able to accurately express the impact behaviour of a ball and club within the typical range of golf impacts.

4- Effects of the shaft on the clubhead upon ball rebound

Impact behaviour was analysed using the constructed models by varying the impact point of the ball's collision with the full clubs and the lone clubheads and comparing the results from the ball/club and ball/clubhead collisions. In these simulations, the impact velocity of the ball was 40 m/s, and the impact point of the ball was varied (vertically) from the sole through the SS to the crown of the impact face. Figure 8 shows the resulting ball launch conditions from the FEAs of the collision between the ball and both the clubheads and the clubs with different ball impact points. In these figures, η (x-axis) was defined as equation (1), and was used as the dimensionless parameter representing the distance between the SS and the impact point. "0" represents an impact point agreeing with the SS, a negative h indicates an impact point situated on the sole rather than the

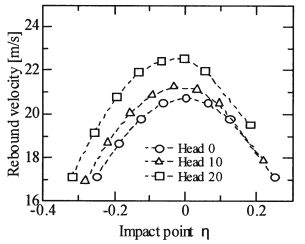

(a) Rebound velocity V_{out} of a ball colliding with clubheads.

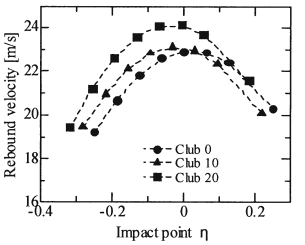

(b) Rebound velocity V_{out} of a ball colliding with clubs.

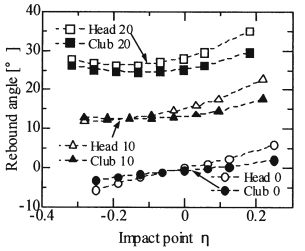

(c) Rebound angle β.

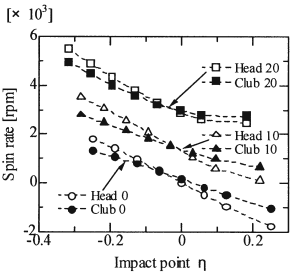

(d) Spin rate ω.

Figure 8 - FEA results for the ball/club and ball/clubhead collisions with different ball impact points.

SS, and a positive η means that the impact point is situated on the crown of the clubhead.

$$\eta = \frac{\left(\text{Height of impact point}\right) - \left(\text{Height of SS}\right)}{\left(\text{Height of clubhead}\right)} \tag{1}$$

4.1 Effect on rebound velocity

V_{out} in club collisions is greater than that in lone clubhead impacts, for a given impact point (Figure 8a and b). This tendency is caused by differences between the club and clubhead impact cases in the impact loads obtained from the FEAs. The shaft restrains the movement of the clubhead during and after impact, and the load in the case of the club impact tend to be greater than that of the clubhead impact as a result.

Additionally, the differences between the two most extreme values of V_{out} tend to be lower in the cases of club impacts than in those of clubhead impacts, for given ball impact points (Figure 8a and b). This tendency is especially apparent in the case of the loft angle of 20 degrees as compared to the loft angles of 0 and 10 degrees. Head 20 has a greater tendency to rotate than Heads 0 and 10, as its impact point is far from the SS of the clubhead, because the inertia moment of Head 20 is the smallest among the clubheads used in this study. The rotational energy of the clubhead negatively correlates with the translational energy of the ball, and a decrease in the rotational energy of the clubhead leads to an increase in the rebound velocity of the ball. Furthermore, the rotation of Head 20, which has the smallest inertia moment, tends to decrease as a result of the shaft more easily than that of Heads 0 and 10, when the impact point is located far from

the SS of the clubhead. Thus, the movement of Head 20 is more greatly affected by the shaft than Heads 0 or 10, and the difference between the variation range of V_{out} of Head 20 and that of Club 20 with changes in the impact point of the ball tends to be greater than those of Head 0/Club 0 and Head 10/Club 10 as a result.

4.2 Effect on rebound angle

The range of β variation for the club impacts with changes in the impact point of the ball tends to be narrower than that for the clubhead impacts (Figure 8c). The shaft on the clubhead causes a decrease in clubhead rotation, especially when the impact point of the ball is located far from the SS, and the decrease in clubhead rotation mainly affects the tendencies of β upon the club impact. In the case of a collision with the crown of the clubhead, a significant difference is observed between β for the club and that for the lone clubhead, regardless of the loft angle. In the case of a collision with the sole, the tendencies of β for the club and clubhead vary with the loft angle; β for Club 20 tends to be smaller than that for Head 20, whereas β for Club 0/10 tends to be greater than that for Head 0/10 as the impact point of the ball moves towards the sole of the clubhead. This tendency indicates that the shaft has a stronger effect on variations in β in case of a collision with the crown than in case of a collision with the sole, and that variations in β in the cases of sole collision depend on the loft angle as well as the shaft.

In addition, the effect of the shaft is estimated to depend on the relationship between the shaft position and the position of the CoG of the clubhead, as well as the loft angle. For Club 20, the CoG of the clubhead tends to be located near the axis line of the shaft, whereas it tends to be located posterior to this axis line for Clubs 0 and 10. This positional relationship between the shaft and the CoG is also assumed to change the degree of clubhead rotation during impact, and to lead to the difference in the tendencies of β between the loft angles of 0 and 10 on one hand, and 20 on the other.

4.3 Effect on spin rate

ω, in the cases of collision with both the club and clubhead generally tends to decrease as the impact point moves from the sole towards the crown (Figure 8d). This tendency seems to be mainly caused by a gear effect at impact. In the case of a collision with the sole of the clubhead, the club's ω tends to be smaller than that of the clubhead, whereas in the case of a collision with the crown, the club's ω tends to be greater than that of the clubhead. The shaft on the clubhead contributes to the decrease in clubhead rotation, especially when the impact point of the ball is located far from the SS, and the decrease in clubhead rotation suppresses the gear effect. As a result, the range of ω variation tends to be narrower for club impacts than for clubhead impacts, with changes in the impact point of the ball. In addition, this tendency is similarly observed regardless of the loft angle. This indicates that the tendency of ω is assumed to be dependent on the mechanical properties of the clubhead, such as loft angle, as well as the shaft, under the golf impact conditions used in this study.

However, ball sliding and rolling is estimated to occur on the face during impact. Deflection of the impact face, in addition to ball deformation, also occurs and this

complex interaction, as well as the gear effect, is believed to be dependent on the spin rate. Therefore, it is necessary to quantify this complex behaviour during impact in order to investigate the effect of the mechanical properties of the clubhead and shaft in more detail.

5- Conclusions

FE models of a golf ball and simplified club, simulating typical golf impacts, were constructed. The results of the impact simulations closely matched the experimental results in the typical range of ball/club impacts.

Impact simulations were conducted using the constructed FE models by varying the impact point of the ball's collision with full clubs and lone clubheads, and the effects of the shaft on the clubhead upon the rebound of the ball were investigated. The differences between the two most extreme values of rebound velocity, angle and spin rate in the case of the club impacts tended to be smaller than those in the case of the clubhead impacts. The decrease in the variation of the rebound velocity was attributed to the effect of the shaft, and the effect of the shaft was likely to depend mainly on the inertia moment of the clubhead. The variation in the rebound angle in the crown impact cases tended to be heavily influenced by the shaft and in the sole impact cases, it tended to be affected by the loft angle, as well as the shaft. The effect of the shaft on the rebound angle was also estimated to depend on the relationship between the shaft position and the position of the CoG of the clubhead. The shaft contributed to the suppression of the gear effect, which was one of the causes of the generation of ball spin.

6- References

[NH1] Nakasuga M. and Hashimoto R. Measurement of tangential force of golf ball impact (in Japanese). Proceedings of the Japan Society of Mechanical Engineers, 97-10-2: 42-45, 1997.

[T1] The Japan Research Institute, Limited. LS-DYNA ver.970 USER'S MANUAL Volume II, 2003 (in Japanese).

[TO1] Tanaka K., Oodaira H., Teranishi Y., Sato F., Ujihashi S. Experimental and finite-element analyses of a golf ball colliding with simplified clubheads. The Impact of Technology on Sport II: 235-240, 2007.

[TS1] Tanaka K., Sato F., Oodaira H., Teranishi Y., Sato F., Ujihashi S. Construction of the finite-element models of golf balls and simulations of their collisions. Proceedings of the Institution of Mechanical Engineers, Part L: Journal of Materials: Design and Applications, 220/1: 13-22, 2006.

Experimental Investigation of Youth Baseball Bat Performance (P273)

Joshua W. Jones[1], James A. Sherwood[2] and Patrick J. Drane[3]

Topics: Baseball, bats.
Abstract: The batted-ball performances of youth wood and nonwood bats are examined through experimental methods. The goals of the study are to build a database of performance data on youth bats using a hitting machine in a controlled laboratory environment and to examine how the lab data compare using three performance metrics including the current BPF certification metric. The performance metric that best correlates the lab data with field performance is found to be the BBS metric.
Key words: Youth, Baseball, Batted Ball Speed, Ball Exit Speed Ratio, Bat Performance Factor.

1- Introduction

The use of aluminium and composite bats (also known as nonwood bats) in youth baseball is a controversial topic. Initially, aluminium bats were used to reduce team operating costs associated with replacing wooden bats, which are more prone to breaking than aluminium bats. The nonwood bats typically have a lower moment of inertia (MOI, commonly referred to as "swing weight") which allows making contact with the ball easier than with the "heavier" swing-weight wood bats. With the advent of high-performance aerospace grade aluminiums, manufacturers were able to make relatively thin-walled barrels, thereby developing the trampoline effect during the bat-ball collision, which in turn results in batted-ball speeds that can be greater than those off wood bats. For players who have trouble making contact with a wood bat, the nonwood bats provide encouragement to keep playing baseball. Composite bats introduce the potential for even greater batted-ball speeds than those off aluminium bats.

1. One University Ave. Lowell, MA 01854, USA - E-mail: Josh@baseballrc.eng.uml.edu
2. E-mail : James_Sherwood@uml.edu
3. E-mail : Patrick_Drane@uml.edu

The controversy arises in the allegation that the nonwood bats exhibit batted-ball speeds which are significantly greater than wood batted-ball speeds. As a result, many towns and state legislatures have introduced bills banning the use of nonwood bats. These new laws are being considered despite the lack of scientific data to support such bans. Some laws banning nonwood bats have been rejected due to the lack of scientific data, but others have passed despite the lack of credible data. These bans could potentially lead to many youth players becoming discouraged from playing baseball if the light swing-weight nonwood bats are removed from the game. The aim of this research is to construct a database of youth baseball bat performance, which will be a credible scientific database documenting the performance of the wood and nonwood youth bats, and to use this database to investigate a potential revision of the current performance metric and the associated bat testing protocol. Such data could lead to a performance standard that can assure the nonwood bats hit the same as their wood counterparts without eliminating the light swing-weight nonwood bats from the game.

2- Background

The current test for youth bat performance is called BPF (Bat Performance Factor) per ASTM F1881 (2005) Standard Test Method for Measuring Baseball Bat Performance Factor. The BPF consists of a baseball being fired at a stationary bat, which is supported on a "low-mass" freely spinning turntable, impacting at the COP (Center of Percussion), and the inbound and rebound speeds of the baseball are measured. The COR (Coefficient of Restitution) of each baseball used in the test is characterized using the ASTM Standard F1887 (2002), which is performed at 26.8 m/s (60 mph). The *BBCOR* (Batted Ball Coefficient of Restitution) is calculated using the inbound and rebound speeds of the ball, the moment of inertia (MOI) and the ball mass,

$$BBCOR = (BESR - 0.5)(1 + k) + k \tag{1}$$

where,

$$k = \frac{m_{ball}(x^2)}{MOI} \tag{2}$$

where x is the distance from the pivot (15.24 cm (6 in.) from the knob) to the impact location and m_{ball} is the mass of the baseball used in the test.

The BPF test is performed at 26.8 m/s (60 mph). The *BPF* is calculated as,

$$BPF = \frac{BBCOR}{COR} \tag{3}$$

Another bat-performance test commonly used is the BESR (Ball Exit Speed Ratio) test. The BESR test is performed by firing a baseball at a stationary bat, which is supported on a "low-mass" freely spinning turntable. The bat is impacted at multiple locations along the barrel of the bat until a "sweet spot" has been isolated. The "sweet spot" is the location on the bat that results in the highest BESR value. The calculation of the *BESR* is,

$$BESR = \frac{V_{reb}}{V_{inb}} + 0.5 \tag{4}$$

where V_{reb} is the speed of the ball after impacting the bat and V_{inb} is the initial velocity of the ball.

The NCAA developed a variation of the BESR test to certify bats that are to be used at the high school and college levels in the United States. The *NCAA BESR* is given by,

$$NCAA\ BESR = \frac{V_{out} - \delta v}{V_{in} + \delta v} + 0.5 \tag{5}$$

where V_{in} is the initial ball speed coming into the collision, V_{out} is the rebound speed of the baseball and,

$$\delta v = V_{in} - V_{contact} \tag{6}$$

with,

$$V_{contact} = V_{swing}\left(\frac{L - 15.24 - z}{L - 30.48}\right) + V_{pitch} \tag{7}$$

where V_{swing} is the bat swing speed as measured 15.24 cm (6 in.) from the tip of the barrel and V_{pitch} is the pitch speed. The sum of V_{swing} and V_{pitch} is the value of V_{in} used in Equation (6). The lengths L and z are measured in cm for Equation (7).

It is often useful to calculate the projected field speed of the ball after impacting a moving bat. This parameter is called *BBS*, and can be calculated as,

$$BBS = v\,(BESR - 0.5) + V\,(BESR + 0.5) \tag{8}$$

where, *BBS* is the batted-ball speed, *n* is the speed of the pitched ball and *V* is the speed of the bat at the impact location. For this calculation, the speed of the bat is based on a swing-speed model.

The swing-speed model used in this research is based on a batting-cage study (Greenwald *et al.* 2001) of high school, college and semi-pro baseball players. The swing-speed data were analyzed to provide a swing-speed model that adjusts swing speed according to MOI (Nathan 2003). The Nathan model is based on a standard swing for a given MOI and length, and the swing speed adjusts according to changes in these two parameters. This flexibility allows the model to be adapted to younger players, but the standard swing speed, which will need to be derived from a youth swing-speed study, is not precisely known at this time in the youth-bat research. The swing-speed model used in the current research is based on a standard bat which is 86.36-cm (34-in.) long and has an MOI of 2749 kg-cm^2 (15000 oz-in^2) (about the knob) with a swing speed of 18 m/s (40 mph) as measured 15.24 cm (6 in.) from the tip of the barrel. Swing speed is scaled up or down according to MOI and then scaled depending on length of the bat and impact location. The nominal pitch speed assumed for a youth pitcher is 22.5 m/s (50 mph) for the current research. Thus, the speeds used in Equation (7) for the youth-bat study are $V_{swing} = 18$ *m/s* and $V_{pitch} = 22.5$ *m/s*.

3- Results

As the relative speed between the bat and the ball increases, the probability for denting and cracking increases. To minimize the level of denting and/or cracking of the bats in the laboratory testing, the 26.8-m/s (60-mph) BPF test was performed first, and then the NCAA-type BESR test was completed at 40.2 m/s (90 mph). The 40.2-m/s (90-mph) test conditions assumed a pitch speed of 22.5 m/s (50 mph) and a nominal swing speed of 18 m/s (40 mph). BBS calculations were obtained using the data from the BESR test. Each of the investigated bat performance metrics were then plotted as a function of MOI.

The COP used in the BPF test was found from the data obtained during the MOI test. The MOI was found by placing a clamped bat on a pivot and timing the period of oscillation with light gate sensors. Some of the lightest bats were not able to be performance tested in the moving-ball stationary-bat method used in this research because of their relatively low MOIs (less than 550 kg-cm^2 (3000 oz-in^2) as measured 15.24 cm (6 in.) in front of the knob). The ball rebound speeds from these lighter bats were too slow to pass through both sets of sensors, thus the rebound speed could not be measured. A very low MOI would usually correspond to a relatively thin barrel wall, so durability at 40.2-m/s (90-mph) test speeds was typically compromised. Thus, the NCAA-type tests at 40.2 m/s (90 mph) could yield measurable rebound speeds, but the bat was dented and/or cracked in the process.

3.1 BESR

For the BESR tests, an impact speed of 40.2 m/s (90 mph) was used. The 40.2-m/s (90-mph) speed was the most appropriate impact velocity with respect to average youth batters that did not compromise the durability of the bat during the test, i.e. that did not dent or crack the barrels of the bats. The results for the *NCAA BESR* were calculated according to Equation (5) and plotted against MOI. The *NCAA BESR* as a function of MOI gives a good qualitative correlation of lab test data to field performance for high school and college bats. The calculated *NCAA BESR* results for the youth wood and nonwood bats are shown in Figure 1. The testing was conducted using baseballs randomly selected from a lot (typically 144 baseballs) with a known nominal BESR value using a standard bat of known *NCAA BESR* performance.

Wood youth bats typically have a barrel diameter of 5.72 cm (2.25 in.), and the nonwood youth bats are made in two barrel sizes. One nonwood size is comparable to the wood bats with a 5.72-cm (2.25-in.) diameter barrel, and the other size, known as big-barrel bats, has a barrel diameter of 6.99 cm (2.75 in.). It can be seen in Figure 1 that the big barrel bats generally have a higher BESR value than the wood bats of the same MOI, while the 5.72-cm (2.25-in.) barrel-diameter nonwood bats are shown to have a lower BESR value than the wood bats of the same MOI. Youth baseball players are known to prefer nonwood bats over wood bats as the players hit further using nonwood bats than with wood bats. The data shown in Figure 1 do not support what is observed in the field. Thus, Figure 1 implies the *NCAA BESR* is not a good metric for relating lab measurements to field performance for these youth bats.

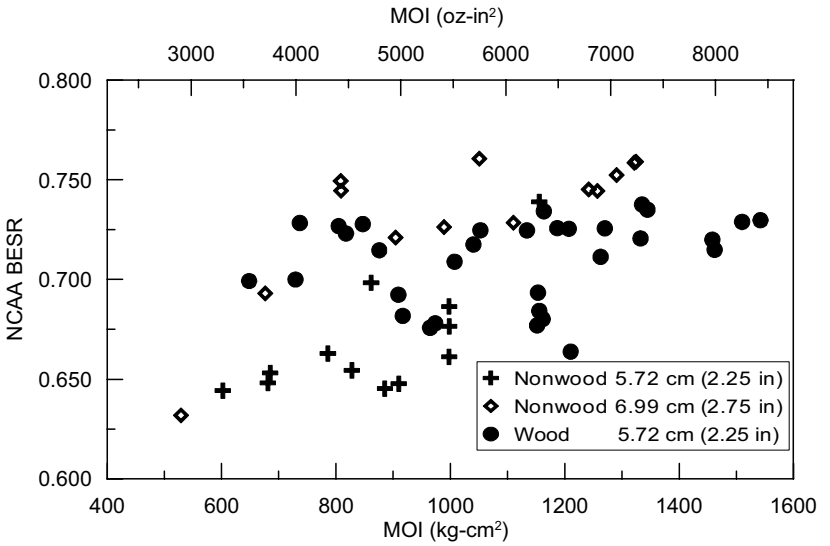

Figure 1 - NCAA Ball Exit Speed Ratio vs. Moment of Inertia.

College and high school bats are required to fall within limited ranges for length, weight and MOI. The minimum difference between the weight measured in ounces and the length measured in inches has to be greater than or equal to -3. For example, a 34-in. (86.36 cm) long bat cannot weigh any less than 31 oz. (880.7 g). These limited ranges of length, weight and MOI allow the possible *NCAA BESR* values for college and high school bats to correlate well with projected field batted-ball speeds. The same good correlation is not true for the youth bats.

Youth bats can exhibit a length (in inches) to weight (in ounces) difference as much as 14.5 units and can span a wider range of allowable MOIs and lengths than do the college and high school bats. As a result, there are many combinations of lengths and weights for youth bats that can exhibit the same MOI. Because of the multiple combinations of weight and length, the *NCAA BESR* value is not a good metric for comparing the relative performance of youth bats. A 5.72-cm (2.25-in.) barrel nonwood bat and a 5.72-cm (2.25-in.) barrel wood bat can have the same MOI but can differ in length by up to 10.16 cm (4 in.). Even if the two bats have the exact same *NCAA BESR* in addition to identical MOI, they can differ in batted-ball speed by several kilometers per hour. The reason for the disparity in batted-ball speed is the difference between the lengths of the bats. The longer nonwood bat shares a similar sweet spot (in this case defined by the location of the maximum BBS measured from the tip of the barrel), but ends up several cm further away from the hands due to the extra length of the bat, yielding a higher bat speed at the point of impact. This behavior can be observed in the data which are summarized in Table 1.

In Table 1, the three bats have nearly equal BESR values. The only variations among the bats are the MOIs, lengths and locations of the sweet spots. These differences are large enough to cause significant differences among the swing speeds at the sweet spots and therefore a noticeable difference in the respective batted-ball speeds. The difference in BBS would not be obvious if looking at a plot of *NCAA BESR* vs. MOI where Bat IDs JJ022 and JJ044 would essentially overlap.

Bat ID	Length cm (in.)	Weight g (oz.)	MOI kg-cm² (oz-in²)	Sweet Spot Location cm (in.)	Calculated Swing Speed km/h (mph)	BESR	BBS km/h (mph)	Type	Barrel Diameter cm (in.)
JJ044	80.963 (31.875)	513.3 (18.105)	910 (4975)	17.8 (7.0)	67.6 (42.0)	0.678	93.2 (57.9)	nonwood	5.72 (2.25)
JJ022	73.500 (28.938)	606.7 (21.400)	917 (5013)	15.2 (6.0)	61.0 (37.9)	0.679	86.4 (53.7)	wood	5.72 (2.25)
JJ054	78.740 (31.000)	633.5 (22.345)	1152 (6297)	16.5 (6.5)	63.1 (39.2)	0.677	90.3 (56.1)	wood	5.72 (2.25)

Table 1 - Comparison of wood and nonwood bats having similar Moments of Inertia and Ball Exit Speed Ratios.

3.2 BPF

The BPF test was performed on the youth bats according to ASTM Standard F1881 (2005). This test is performed at 26.8 m/s (60 mph). The *COR*, as measured per ASTM Standard F1887 (2002), is found for a single ball. This one baseball is impacted onto the bat at the center of percussion for six valid hits. The BPF test measures the *BBCOR* and normalizes the *BBCOR* by dividing the *BBCOR* by the ball *COR*.

The current BPF limit for 5.72-cm (2.25-in.) barrel youth bats is 1.15, and there is no BPF limit for the 6.99-cm (2.75-in.) barrel youth bats. The BPF values for the youth bats tested in this research were plotted against MOI and are shown in Figure 2. According to these BPF data, four of the 5.72-cm (2.25-in.) nonwood bats that were tested in the current study performed at or below the 1.15 BPF limit, and two of the bats had BPF values just above the 1.15 limit. Figure 2 shows no correlation between BPF and MOI. The wood bats have a relatively uniform BPF values between 1.05 and 1.10 regard-

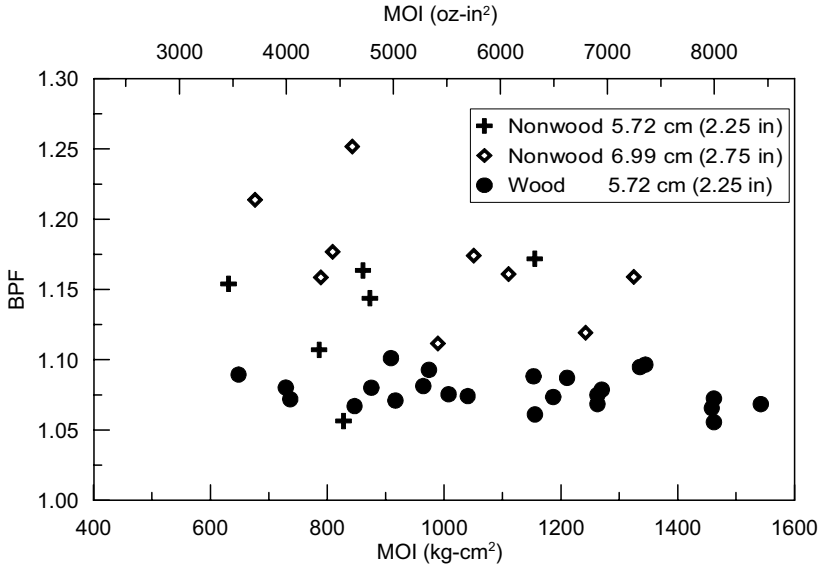

Figure 2 - Bat Performance Factor vs. Moment of Inertia.

less of the MOI of the bat. This relatively uniform BPF value is because the barrel of a wood bat is relatively rigid in comparison to the hollow-barrel nonwood bats. As a result of the "rigid" barrel, the wood bats do not exhibit any trampoline effect, and the *BBCOR* is essentially the same for all wood bats. The BPF data given in Table 2 show no correlation to field projected BBS. All of the bats have essentially the same BPF value, but the bats exhibit a wide range of field projected BBS values. This lack of correlation is also true when comparing BPF to other physical properties of the bat such as length and weight.

Bat ID	Length cm (in.)	Weight g (oz.)	MOI kg-cm² (oz-in²)	Location cm (in.)	BESR	BBS km/h (mph)	BPF	Type	Diameter cm (in.)
JJ063	73.820 (29.063)	465.9 (16.4)	631 (3449)	12.40 (4.88)	0.605	88.2 (54.8)	1.15	nonwood	5.72 (2.25)
JJ010	71.120 (28.000)	618.0 (21.8)	789 (4314)	12.37 (4.87)	0.701	92.9 (57.7)	1.16	nonwood	6.99 (2.75)
JJ025	78.740 (31.000)	612.3 (21.6)	1111 (6072)	14.48 (5.70)	0.729	97.7 (60.7)	1.16	nonwood	6.67 (2.63)
JJ007	81.280 (32.063)	686.1 (24.2)	1325 (7243)	15.29 (6.02)	0.764	101.2 (62.9)	1.16	nonwood	6.99 (2.75)
JJ005	81.123 (31.938)	683.2 (24.1)	1242 (6791)	15.75 (6.20)	0.756	100.4 (62.4)	1.12	nonwood	6.67 (2.63)

Table 2 - Comparison of Bat Performance Factor results.

In Table 2 the first four bats have nearly identical BPF values. The projected BBS shows no correlation to the BPF measured for these bats. Because the first four bats are ~1.16, it would be expected that a bat having a lower BPF should produce a slower batted-ball speed. However, Bat ID JJ005 has a lower BPF than the rest of the bats in Table 2 but has a projected BBS greater than all but one bat. Because it is possible for a bat to meet the BPF criterion of 1.15 or less but have a higher BBS than a bat that fails to meet the 1.15-BPF criterion, BPF is a poor metric for measuring bat performance. As mentioned previously, the big barrel nonwood bats are not required to perform at or below a BPF of 1.15.

3.3 BBS

The batted-ball speeds were calculated using Equation (8) and used the swing-speed model by Nathan. The BBS calculation requires the use of a swing-speed model to account for variations in bat swing speed as function of MOI.

A relatively slow swing-speed input must be used because of durability issues. The test was conducted at 40.2 m/s (90 mph). The assumed pitch speed was 22.5 m/s (50 mph), so the resulting swing-speed used in Equation (8) had to be 18 m/s (40 mph). Typical impact speeds may be higher or lower, so future research should be completed to support or to correct the pitch and swing speeds used to evaluate youth bats in this study. Because it is most accurate to match the relative bat/ball speed used in the BBS calculation to the relative bat/ball speed used during testing, and the standard youth swing model has yet to be established, the magnitude of the predicted BBS for the current study may only be approximate. The BBS method is very useful at a minimum for qualitatively ordering the relative performance of the bats to each other.

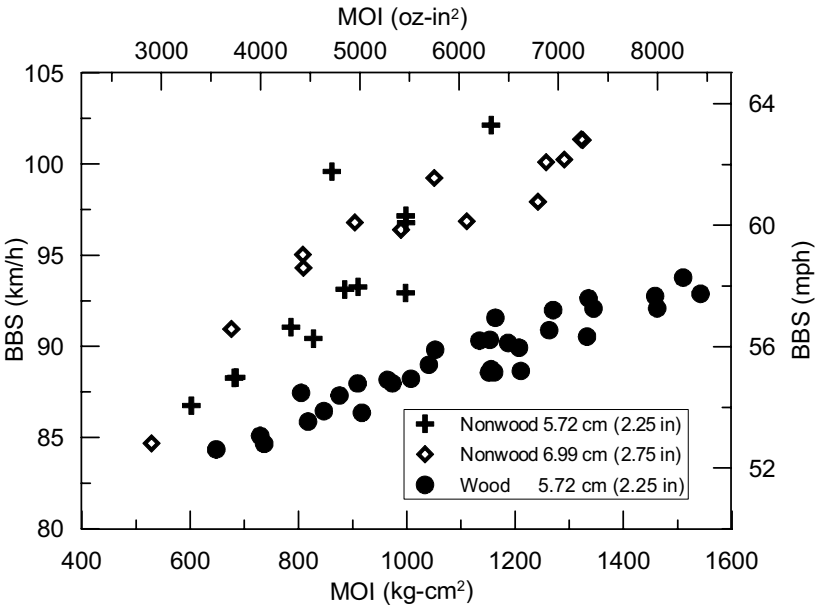

Figure 3 - Batted-Ball Speed vs. Moment of Inertia.

The BBS values calculated from the youth bat data are plotted as a function MOI in Figure 3. The BBS data for each class of bats (wood, 5.72-cm (2.25-in.) nonwood and 6.99-cm (2.75-in.) nonwood) exhibit an essentially linear correlation with MOI. The 6.99-cm (2.75-in.) diameter bats are typically hitting 1.8 to 2.6 m/s (4 to 6 mph) faster than the wood bats, and the 5.72-cm (2.25-in.) diameter bats are outperforming the wood bats by approximately 0.9 to 2.6 m/s (2 to 6 mph). The BBS values plotted in Figure 3 are a consequence of the swing-speed model, so these values should not necessarily be taken as representative of batted-ball speeds in the field. However, the data do imply a measurable difference among the classes of bats. The BBS data explain why youth players can hit further with the nonwood bats than the wood bats. Such a conclusion could not be made using the BPF and NCAA BESR metrics.

The BBS metric looks to be the best measure for relating lab measurements of bat performance to projected field performance for youth bats. The BBS vs. MOI data for the wood bats could be used as a benchmark for the conclusion of an upper bound on youth bat BBS values as a function of MOI. To improve the accuracy and credibility of the method, a swing-speed model developed from youth batters should be used in the BBS calculations. Further research and sample size will be needed to determine to what extent the nonwood bats outperform the wood bats.

4- Conclusion

The performance of youth bats can be characterized a number of ways, but some metrics yield misleading results and may not be a good measure for governing performance. BBS has been shown to be a practical metric for projecting field performance provided a credible swing-speed model is available. Using the BBS metric to relate lab measure-

ments to projected field performance supports qualitative field observations and shows that youth nonwood bats typically outperform wood bats. Further research and sample size will be needed to determine to what extent the nonwood bats outperform the wood bats, including a swing-speed study.

5- References

[A1] ASTM F1881, Standard Test Method for Measuring Baseball Bat Performance Factor, 2005.
[A2] ASTM F1887, Test Method for Measuring the Coefficient of Restitution (COR) of Baseballs and Softballs, 2002.
[CG1] Greenwald R.M., Penna L.H., and Crisco J.J., Differences in Batted Ball Speed with Wood and Aluminium Baseball Bats: A Batting Cage Study, J. Appl. Biomech., 17, 241-252 (2001).
[N1] Nathan, A., Characterizing the performance of baseball bats, Am. J. Phys., Vol. 71, No. 2, February 2003.

An Experimental Investigation of the Effect of Use on the Performance of Composite Baseball Bats (P274)

James A. Sherwood[1] and Patrick J. Drane[2]

Topics: Composites, baseball, bats.
Abstract: The choice of materials used to make baseball bats has evolved over the years from traditional solid wood to aluminium and now to composites. To determine whether or not a bat's design is in compliance with the batted-ball performance standard for a given league, a new bat is tested in a hitting machine where the bat is subjected to a limited number of hits. Considering the material behaviour that occurs within a composite material subjected to numerous impacts, the batted-ball performance of composite bats can theoretically improve with use as the polymer-matrix develops microcracks. These microcracks can soften the barrel of the bat which may allow the trampoline effect to increase. As the trampoline effect increases, there is potential for the batted-ball speed to increase. This paper will discuss the observed evolution of the performance for six currently popular composite baseball bats that were subjected to cycles of performance testing followed by repeated use in a controlled laboratory setting. None of the six composite baseball bats exhibited a significant change in performance. Some of the composite bats did exhibit poor durability.
Key words: Composites, baseball, bats, performance, durability.

1- Introduction

The construction of baseball bats used at the amateur level of play has evolved over the past 40 years from traditional solid wood to aluminium and to combinations of materials, i.e. composites. As the choice of materials has evolved so has the potential hitting power of the bats. To allow these bats to be used without compromising the balance between offense and defence, governing bodies have come to depend on comprehensive laboratory test methods to measure the batted-ball performance of these nonwood bats and to use these same test methods to help in the setting of performance limits.

1. One University Ave. Lowell, MA 01854, USA - E-mail: James_Sherwood@uml.edu
2. E-mail : Patrick_Drane@uml.edu

It is commonly accepted from a material-science perspective that with each bat/ball impact the microstructure of the bat material can be altered. Wood bats can flake, i.e. delamination of the wood rings, and crack. In aluminium bats, the material changes can be in the form of microcracking and denting. The microcracking can lead to a softening of the barrel, which in turn can lead to a change in the trampoline effect and a resulting change in batted-ball speed. The denting is a result of plastic deformation, which in turn can work harden the material and increase the strain energy that can be stored in the bat and subsequently returned to the ball.

In the last five years, bat manufacturers have been implementing fabric-reinforced composite materials into their designs. Composite materials admit the option for a variety of matrix and reinforcement materials and allow the designer to tailor the material properties along the barrel and handle of the bat, thereby being able to tune the bat designs to span a range of barrel and handle stiffnesses that could never be achieved with aluminium. An additional design parameter is how the material behaviour can change with use. This last design parameter is one that is cause for concern and the motivation for the current study to investigate how the performance of a composite baseball bat can change with use.

2- Background

The test methodologies used by the various governing bodies for amateur baseball all quantify bat performance using new bats tested in a hitting machine. The number of hits in these tests can range from as few as six at one location on the barrel of the bat to as many as 60 over a 5.08-cm (2-in.) span along the barrel. At the conclusion of the test, the bat design is determined either to comply or not comply with the respective governing body's performance limit. The procedure for certifying whether or not a new bat model is compliant with the performance standards of the respective governing body is to simulate a bat/ball collision in a controlled lab environment. The testing is conducted on a new bat, i.e. a virgin specimen. Depending on the chosen performance metric and its associated limit, the bat is concluded to be either compliant or noncompliant with the performance standard. For example, the NCAA uses a BESR (Ball Exit Speed Ratio) as its metric for performance, and Little League uses BPF (Bat Performance Factor) as its metric for performance.

Drane and Sherwood (2002) found that the performance of aluminium bats can change with use. They subjected bats to hundreds of hits using a hitting machine in the lab and players in the field and took batted-ball performance measurements periodically throughout the study. The data concluded that one bat showed an increase in performance while another bat showed a decrease in performance with use. While the data did not support a trend for a change in performance up or down, the data did support that aluminium-baseball-bat performance can change with use.

In the last decade, many composite bat designs have been introduced in amateur baseball and softball. Because these bats are relatively new to the game, there are limited quantitative lab data and qualitative field performance observations for this class of bats in comparison to wood and aluminium bats. However, one outstanding data point is a

qualitative observation of a composite softball bat. It was discovered by softball players that this bat design exhibited batted-ball performance that increased with use. As a result, players would subject the bat to an accelerated "break in" by subjecting the bats to extreme impact conditions, e.g. hitting the bat against a tree, before using the bat in a game. This bat design tilted the balance of the game to the advantage of the offense. The Amateur Softball Association (ASA) was concerned that such bat performance could compromise the integrity of the game. In response to this concern, the ASA changed its certification test methodology from BPF (Bat Performance Factor) as described in ASTM Standard F1881 (2004) to using BBS (Batted-Ball Speed) similar to the test as described in ASTM F2219 (2007). The current ASA bat performance standard requires a softball bat to perform at or below the ASA BBS limit for the useful life of the bat. Thus, the laboratory certification test subjects the bats to virtually hundreds of hits by using a barrel rolling process and then subsequent performance testing in a hitting machine to quantify if and how the BBS changes with use.

To date, there are no known qualitative or quantitative data showing that any of the composite baseball bats currently being used at the high school and college levels are showing increasing or decreasing batted-ball speeds with use. The objective of the current study was to test a sample of current composite baseball bats and subject them to repeated baseball impacts using laboratory hitting machines to simulate the "life" of a composite baseball bat and examine if and how the batted-ball performance evolves with use.

3- Methodology

A total of six high-performance composite bats and one aluminium bat were tested in the current study. The aluminium bat was included as a reference point. All of the bats were 86.4-cm (34-in.) long and weighed approximately 879 g (31 oz.). The bats selected for the study had previously been certified to be in compliance with the NCAA BESR bat performance standard and were found to perform very close to the upper bound for the NCAA BESR. The bat performance was measured using a hitting machine, and the bats were subjected to accelerated hitting using a durability machine that can be programmed to scatter hits along the length of the barrel for a range of prescribed hit locations and speeds. The durability machine can shoot baseballs at the rate of one ball every 5 s at relative bat/ball speeds between 26.8 and 80.5 m/s (60 and 180 mph). These speeds correspond to the bunting of a knuckle ball (essentially zero bat swing at a slow pitch) and to the tip of a fast swinging bat hitting a fastball (relatively fast swing at a very fast moving baseball), respectively. Thus, the durability machine can span the range of bat/ball collisions that can occur on the field.

The batted-ball potentials of the bats were measured using the test protocol described in the NCAA Standard for Testing Baseball Bat Performance (2006). In the current study, there were two deviations from the NCAA protocol. The test was not stopped if a bat was found to exceed the upper limit for performance, and the performance test examined five locations along the length of the barrel regardless whether or not the sweet spot could or could not be isolated within the five hit locations. The five

locations were 12.7, 14.0, 15.2, 16.5, and 17.8 cm (5.0, 5.5, 6.0, 6.5 and 7.0 in.) from the tip of the barrel. All valid and invalid hits were counted in the total hits on a bat. After the initial performance measurement of N hits, each bat was then subjected to 100-N additional hits in the durability machine to get a total of 100 hits on each bat. The hits in the durability machine were scattered over the same 12.7 to 17.8 cm (5.0 to 7.0 in.) locations from the tip of the barrel. The relative bat/ball speeds in the durability machine were between 58.1 and 62.6 m/s (130 and 140 mph). Each bat was then retested in the hitting machine to measure its performance followed by another 100-N hits in the durability machine, and so on.

The cycle of performance testing followed by hits in the durability machine were continued until the bat cracked enough such that the cracks would be obvious to a player or umpire and the bat would be deemed unacceptable for use in a game. Conditions for the stopping the test included:

– Crack that could be seen without the need of close inspection;
– Protruding composite fibers;
– Separation of barrel from the handle.

4- Results

All of the bats cracked in the barrel with the exception of one of the composite bats, C1, which broke in the handle after being subjected to over 1000 total hits. Two of the six composite bats (C3 and C4) broke before the second performance cycle was completed, and thus, there are no performance data on those bats beyond that measured on the "new" bat. One composite bat (C2) broke during the initial performance test, so there are no data for that bat. Figure 1 is a photograph of Bat ID C2, which had the barrel completely separate from the handle during the performance testing. With 50% of these "high-performance" composite bats failing due to cracking with less than 100 hits, there appears to be a serious durability problem for some of the composite baseball bat designs.

Figure 1 - Complete separation of handle and barrel for Bat ID C2.

Of the three composite bats that have multiple complete-performance tests (C1, C5 and C6), the largest change in performance for a bat from one test to another was the drop of 0.012 in BESR at the sweet spot for Bat ID C6. This drop of 0.012 in the BESR value is equivalent to about a 2% drop in batted-ball speed in the field. The largest increase in performance for any of the composite bats after the initial test was only 0.001 in BESR at the sweet spot. This difference is within the variability of the test which is ±0.003. The aluminium bat (Bat ID M1) exhibited performance values of BESR at the sweet spot within 0.004 of the initial measured performance for each of the subsequent five performance tests.

Figure 2 shows how the change in maximum BESR value evolved with each set of 100 hits on the seven bats. For viewing convenience, the BESR axis has divisions of 0.007, which corresponds to a change of 0.45 m/s (1 mph) in batted-ball speed. The change in the maximum-BESR data are summarized in Table 1. Bat ID C6 showed the biggest change in performance with usage—a drop of 0.012 in the maximum BESR value. This drop of 0.012 was followed by an increase of +0.005. The bat then failed during the next 100-hit sequence. This up and down change in the BESR performance may be an indication of material degradation that eventually resulted with the bat developing a serious crack. Bat ID M1 is the aluminium bat, and its maximum BESR performance oscillated up and down within the resolution of the test—implying essentially no change in performance. The aluminium bat failed due to cracking in the barrel. Bat ID C1 exhibited the best durability by lasting 1000 hits. Its barrel showed little sign of material degradation. Bat ID C1 eventually failed in the handle—most likely as a consequence of low-cycle fatigue due to the alternating stresses developed in the handle during testing. After 100 hits and 400 hits, there were measurable changes in the performance of Bat ID C1. However, each of these measurable changes was a decrease in BESR relative the value measured on the new bat.

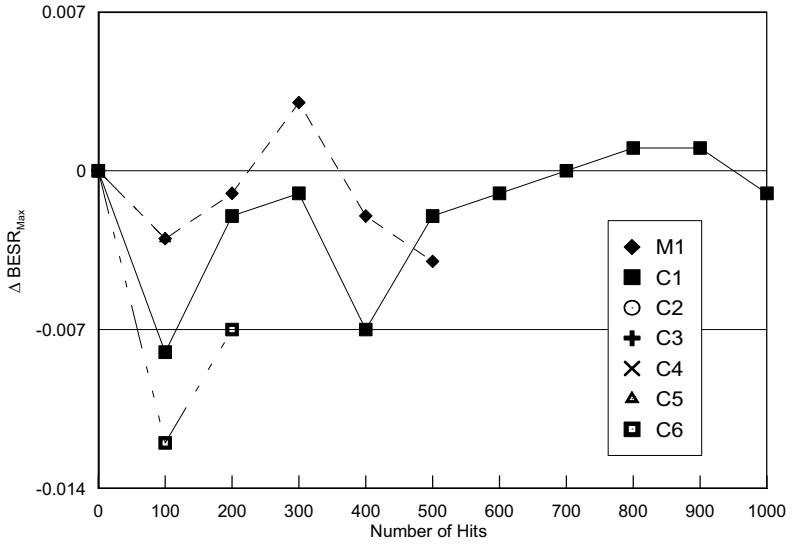

Figure 2 - Change in Max BESR.

Bat ID	Number of Hits										
	0	100	200	300	400	500	600	700	800	900	1000
M1	0.000	-0.003	-0.001	+0.003	-0.002	-0.004	--	--	--	--	--
C1	0.000	-0.008	-0.002	-0.001	-0.007	-0.002	-0.001	0.000	0.001	0.001	-0.001
C2	--	--	--	--	--	--	--	--	--	--	--
C3	0.000	--	--	--	--	--	--	--	--	--	--
C4	0.000	--	--	--	--	--	--	--	--	--	--
C5	0.000	-0.003	--	--	--	--	--	--	--	--	--
C6	0.000	-0.012	-0.007	--	--	--	--	--	--	--	--

Table 1 - Change in Maximum BESR.

An alternate method for analyzing the performance data is to look at the average BESR across the barrel of the bat. The average BESR is the average of the BESR values for the five axial locations tested. Figure 3 shows how the change in average BESR value evolved with each set of 100 hits. The average-BESR data are summarized in Table 2. Bat ID C6 shows the largest change with a drop of -0.007 in its average-BESR. None of the bats show a significant change in BESR performance relative to that of the new bat.

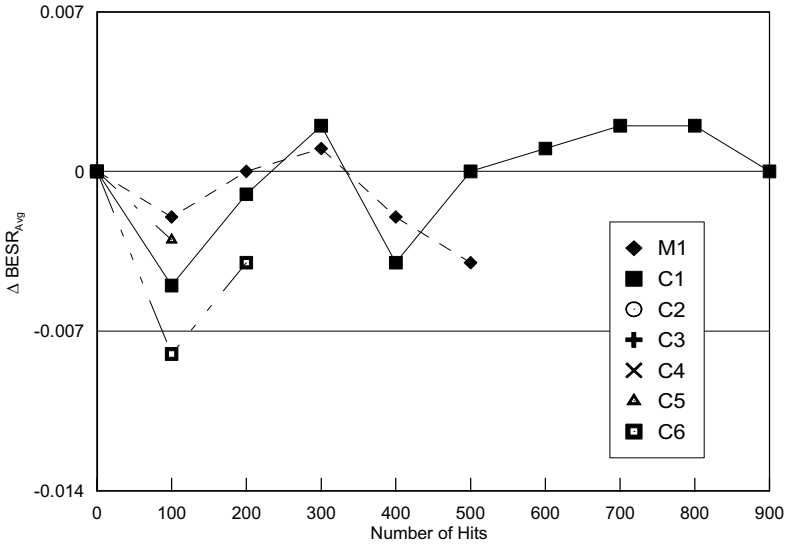

Figure 3 - Change in Average BESR.

Bat ID	Number of Hits										
	0	100	200	300	400	500	600	700	800	900	1000
M1	0.000	-0.002	0.000	0.001	-0.002	-0.004	--	--	--	--	--
C1	0.000	-0.005	-0.001	0.002	-0.004	0.000	+0.001	+0.002	+0.002	0.000	0.000
C2	--	--	--	--	--	--	--	--	--	--	--
C3	0.000	--	--	--	--	--	--	--	--	--	--
C4	0.000	--	--	--	--	--	--	--	--	--	--
C5	0.000	-0.003	--	--	--	--	--	--	--	--	--
C6	0.000	-0.008	-0.004	--	--	--	--	--	--	--	--

Table 2 - Change in Average BESR.

5- Conclusion

A set of six "high-performance" composite baseball bats and one aluminium baseball bat were tested to see how their respective batted-ball performances would evolve with use. None of the bats showed a significant change in the resulting batted-ball-speed performance using the NCAA BESR performance testing protocol. Three of the six baseball bats failed with less than 100 hits—implying that some of the composite bat designs are not durable.

6- References

[A1] ASTM F1881, Standard Test Method for Measuring Baseball Bat Performance Factor, 2004.
[A2] ASTM F2219, Standard Test Methods for Measuring High-Speed Bat Performance, 2007.
[DS1] Drane P.J., and Sherwood J.A., «The Effects of Moisture Content and Workhardening on Baseball Bat Performance,» Proceedings of the 4th International Conference on the Engineering of Sport, Kyoto, Japan, 2002.
[N1] NCAA Standard for Testing Baseball Bat Performance, 2006. http://www.ncaa.org/champadmin/baseball/bat_standards/2006_certification_protocol.pdf
(last checked 27-March-2008).

The Effect of Baseball Construction on the Game of Baseball (P275)

Patrick J. Drane[1], James A. Sherwood[2], Joshua W. Jones[3], Timothy P. Connelly[4]

Topics: baseballs.
Abstract: Many leagues have introduced or tightened performance regulations of baseball bats over the past decade as the technology to quantify their performance has improved. However, little to no emphasis has been spent on understanding the range of baseballs that are used across the different levels of play, and as a result, baseball regulations are typically limited to size, weight and coefficient of restitution at 26.8 m/s (60 mph). This paper will explore many of the different baseballs that are used and highlight the similarities and the differences with respect to the construction, overall size and weight, and performance among these baseballs. Coefficient of restitution, both the standard using a flat wood block and cylindrical using a solid-steel half cylinder, and compression tests are used to evaluate the performance in a controlled lab environment..
Key words: Baseball, Coefficient of Restitution, COR, CCOR, Compression.

1- Introduction

Generally, baseballs are recognized by a specific size, weight and seam pattern. Other than these properties, the general public may have little idea of what is inside the ball. Most official game baseballs have wool-winding layers that surround a cork-and-rubbe7r center, called the pill (Reach 1925), and a finished exterior of cowhide or synthetic leather. The baseball has experienced little change over the past century, but some manufactures have recently introduced thin layers within the ball that are intended to increase durability or reduce the effects of moisture without changing the overall performance, size and weight (Subic 2007). Some leagues at the early youth levels have introduced relatively soft baseballs in an effort to reduce injuries from being hit by a baseball and to make youth players comfortable with playing the game by reducing the fear of injury from a batted or thrown ball.

1. One University Ave. Lowell, MA 01854, USA - E-mail: Patrick_Drane@uml.edu
2. E-mail: James_Sherwood@uml.edu
3. E-mail: jjones@baseballrc.eng.uml.edu
4. E-mail: tconnelly@baseballrc.eng.uml.edu

The University of Massachusetts Lowell Baseball Research Center (UMLBRC) has the equipment and expertise to investigate many different aspects of the baseball. Since 2000, the UMLBRC has directed most of its efforts in baseball testing to compliance testing for Major League Baseball, which has very tight specifications for each component of the baseball. The objectives of these compliance tests has been to establish a database of year-by-year performance of the major league baseball and to ensure there are no changes in the construction and performance of the baseballs. This experience of testing baseballs for each specific component's properties for compliance and consistency and seeing essentially no difference from test to test led to the interest to explore the differences in construction and performance among baseballs for other levels of play. The typical Major League game uses around ten dozen baseballs per game. In contrast, the operating costs for amateur baseball teams may be limited to using three to ten baseballs per game. Thus, the construction of amateur baseballs may need to account for a durability factor that is not critical to a major league ball. This paper will present a comparison of a variety of different baseballs from different manufacturers and for different leagues in an effort to quantify the performance, hardness and construction of the different baseballs.

2- Methodology

The test procedure for this study included two traditional metrics and a new metric for evaluating performance. The traditional measures were COR (Coefficient of Restitution) and static compression. The new metric was CCOR (Cylindrical Coefficient of Restitution), which was recently developed as part of measuring dynamic stiffness. The dynamic-stiffness measure is not presented as part of this study, because there are several aspects of the test that are still being developed at this time. The CCOR tests were performed at 26.8 m/s (60 mph) and 40.2 m/s (90 mph) to replicate a range of impact conditions that these baseballs experience in the field.

This study does not include all of the different constructions or manufacturers of baseballs. Rather the goal of this study was to survey some of the popular contemporary baseballs used by the various leagues. Therefore, the initial task was to obtain many different baseballs. A sample of two baseballs for each of 20 different constructions was evaluated for performance through the standard COR test and cut in half to reveal the construction. From these 20 types of baseballs, nine baseball models were chosen to investigate the ranges of COR values and variety of constructions. The final selection included models from different manufacturers.

With the diverse assortment of baseball models, the work began to evaluate the respective performances with the tools available. The UMLBRC has the capabilities to perform tests on baseballs ranging from the standard static compression using a universal material testing load frame to CCOR and COR performance testing using a high-speed air cannon and two-wheel pitching machine, respectively. Sections 2.1 through 2.4 will discuss each of the procedures used for the testing of the baseballs.

2.1 Size and Weight

The size of a baseball is defined by its circumference. A steel rule PI tape was used to make these measurements. This type of measurement allows the circumference to be measured to within 0.254 mm (0.01 inches). The circumference was measured in two directions, across two seams and across four seams. The average of these two circumference measurements is reported as the circumference of the ball. The weight of each baseball was measured using a digital scale with an accuracy of 0.14 g (0.005 ounces).

2.2 Standard Static Compression

The static compression of each baseball was measured similarly to the process described in ASTM standard F1888 (2002). This test compresses the baseball between two flat steel plates at a rate of 0.42 mm/s (1 in./min). The test is stopped at a displacement of 6.35 mm (0.25 inches) and is repeated on two additional orthogonal axes of the baseball. The compression value of the baseball is reported as the average of these three measurements.

2.3 COR (Coefficient of Restitution)

The dynamic performance of a baseball is typically measured using a setup to measure the coefficient of restitution (COR) of the ball. This setup at the UMLBRC utilizes a combination (two-wheel) pitching machine, a ballistic speed gate capable of measuring speed in both directions and a rigid wall with a wood hitting surface. This test is performed in accordance with the ASTM standard F1887 (2002). The pitching machine was set to fire the ball with little to no spin at a speed of 26.8 m/s (60 mph, 88±1 ft/s). The ballistic speed gates are set 30.48 cm (12 in.) apart with a gate located 30.48 cm (12 in.) from the solid ash hitting surface. The ball speeds $V_{Inbound}$ and $V_{Rebound}$ were measured, and the COR was calculated as,

$$COR = \frac{V_{\mathrm{Re}bound}}{V_{Inbound}} \tag{1}$$

Each baseball was tested to obtain six valid COR measurements, and the reported COR is the average of these six values.

2.4 CCOR (Cylindrical Coefficient of Restitution)

The cylindrical coefficient of restitution (CCOR) is a measure of the dynamic performance of the baseball similar to the COR. However, the CCOR test uses a cylinder for the target rather than the flat-plate target used in the COR test. The use of the cylinder, which has a diameter similar to the barrel on a bat, is a better simulation of how the ball is used in the game than the flat plate. At the UMLBRC, the CCOR test setup utilizes a high-speed air cannon capable of firing a baseball with no spin at speeds from 26.8 m/s (60 mph) to over 51.4 m/s (115 mph). The CCOR tests used in this study were performed at the speeds of 26.8 and 40.2 m/s (60 and 90 mph). The CCOR was calculated as,

$$CCOR = \frac{V_{\text{Re}bound}}{V_{Inbound}} \tag{2}$$

Each baseball was tested to obtain six valid CCOR measurements, and the reported CCOR is the average of these six values.

3- Results

Nine different baseball models were investigated in the study. This section presents cross-section views of each baseball construction and summarizes the results of each model's coefficients of restitution (COR and CCOR) using different speeds and impact surfaces and compression testing. To make the data blind with respect to the manufacturer and model, each baseball is designated throughout the paper with a letter A through I. The letters were designated after the tests had been concluded and were ordered with A having the lowest COR value and I having the highest COR value. This labeling and ordering is intended to assist in the comparison of the results among the different figures and tables.

3.1 Construction

The baseballs selected for the study ranged in construction and included many different materials and designs. This study purposely included non-competition grade baseballs in order to explore the large range of ball constructions and performances that are currently available. Figure 1 shows the cross-section views of each of the nine ball models examined in this study. Table 1 briefly describes the construction and the level of play is denoted as [recreational], [youth], [high school] or [collegiate].

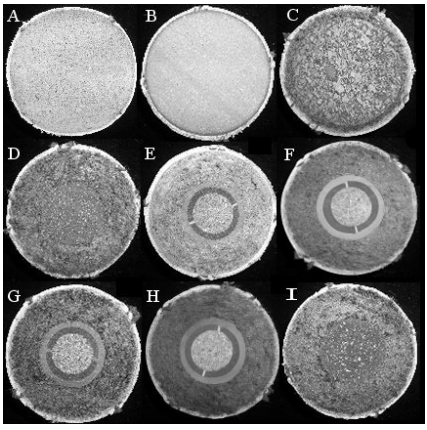

Figure 1 - Cross-sectional views of the baseballs investigated.

Model	Comments
A	Sponge core, synthetic cover (would rip at stitching after a few 40.2 m/s (90 mph) CCOR tests) [recreational]
B	Polymer core [youth]
C	Large cushioned cork core, thin wool winding layer [youth]
D	Small cushioned cork core, thick wool winding layer [youth]
E	Small cork center within two rubber layers as core, thick wool winding layer [collegiate]
F	Small cork center within two rubber layers as core, thick wool winding layer [youth]
G	Small cork center within two rubber layers as core, thick wool winding layer [youth]
H	Small cork center within two rubber layers as core, thick wool winding layer [high school]
I	Small cushioned cork core, thick wool winding layer [youth]

Table 1 - Ball Constructions.

The baseball constructions varied significantly, but the overall appearance and feel of most of the balls were the same. With the exception of Model A, which has a "spongy" feel, all of the balls feel relatively hard. The average weights and circumferences are listed in Table 2. Baseballs are generally identified as being 141.7 to 148.8 g (5.00 to 5.25 oz.) in weight and having a circumference of 22.9 to 24.1 cm (9.0 to 9.5 in.). Again, with the exception of Model A which was slightly lighter than the rest of the baseballs, all of the baseballs were essentially the same weight and circumference.

Ball Model	A	B	C	D	E	F	G	H	I
Weight, g (oz)	133.1 (4.69)	143.9 (5.07)	141.6 (4.99)	146.1 (5.15)	144.6 (5.10)	145.4 (5.13)	143.5 (5.06)	146.0 (5.15)	144.3 (5.09)
Circumference, cm (in.)	22.7 (8.94)	23.0 (9.04)	22.9 (9.00)	22.9 (9.02)	23.0 (9.07)	22.8 (8.99)	23.0 (9.05)	22.8 (8.99)	23.0 (9.05)

Table 2 - Summary of Average Ball Weights and Circumferences.

3.2 Performance and Hardness

The measures of dynamic performance are COR and CCOR. Hardness was measured using the compression test. Figure 2 identifies the average values for all of the dynamic performance and hardness tests for each model of baseball. With the exception of Model A, which has already been described to be very different than the other baseball models, the measured COR at 26.8 m/s (60 mph) was higher than the CCOR at the same speed. The CCOR at 40.2 m/s (90 mph) was lower than the both tests at 26.8 m/s (60 mph). There are several additional trends among the COR and CCOR data. Baseball models B, D, G, and H had only a slight difference between the two dynamic tests at 26.8 m/s (60 mph). Baseball models C, E, F, and I had CCOR values at 26.8 m/s (60 mph) that were almost halfway between the COR test at 26.8 m/s (60 mph) and the CCOR test at 40.2 m/s (90 mph). The baseball models with similar constructions did not have similar performance criteria and therefore the metrics of performance could not be predicted by any observation of the cross section of a baseball. Models of the bat/ball collision that use ball COR to predict batted-ball speeds should consider using ball CCOR at the appropriate collision speed instead of COR because the COR value and CCOR are different. The static compression values are also identified on the plot in Figure 2 to show the relative hardness of each baseball model. There does not appear to be any trend among the COR and CCOR values and the compression of the baseball.

The ball construction can result in differences of performance at different impact speeds and different impact surface contours, not only because of the nonlinear behaviors of the individual materials, but also because of the combination of materials that compressed during the significant deformation of the baseball during impact. The compression of the baseball models on the cylindrical surface during the CCOR tests at 26.8 m/s (60 mph) are shown in Figure 3. High-speed video was recorded during an impact of each model at a frame rate of 5000 frames per second. The frame of maximum deflection is displayed in Figure 3 for each model. All nine frames show that an impact

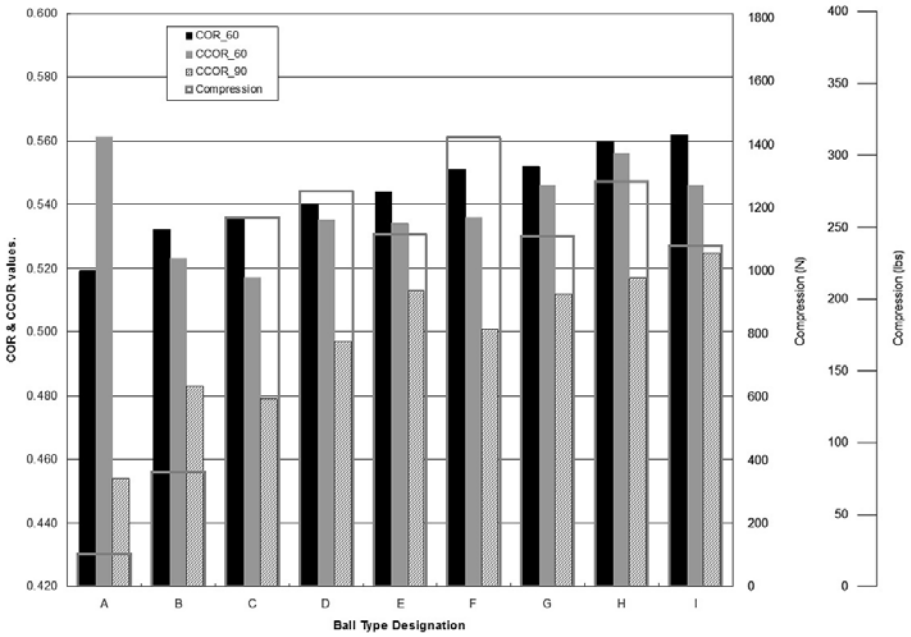

Figure 2 - Average COR, CCOR and Compression values for each ball model.

speed of only 26.8 m/s (60 mph) results in deformation of each ball model that can be significant. Model A, which has a very low static compression value, shows a dramatic compression with high-speed impacts. Frames B through I show the ball models with very similar deformation magnitudes relative to each other during the 26.8-m/s (60-mph) impact.

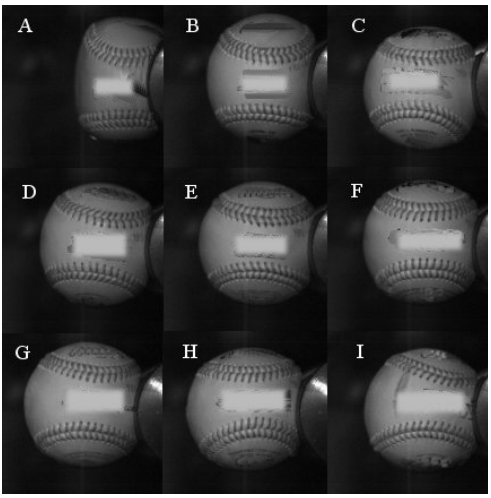

Figure 3 -CCOR tests of each ball model at 26.8 m/s (60 mph).

The deformations of the baseballs during impact were significant and varied with both the shape of the impact surface and the speed of the impact. The high-speed video frame of maximum impact during the three test configurations are shown for ball models A and C in Figures 4 and 5, respectively. Ball model A, which has a significantly lower static compression value than the other ball models, shows a very dramatic compression during all three test configurations. Ball model C, which is typical of the other baseball models examined in this study, shows a representative compression of the baseballs that are used at the different levels of play which include most competitive youth leagues, high school and college baseball.

Figure 4 - High-speed video frames of impact for Model A [Left: 26.8 m/s (60-mph) COR, Middle: 26.8 m/s (60-mph) CCOR, and Right: 40.2 m/s (90-mph) CCOR].

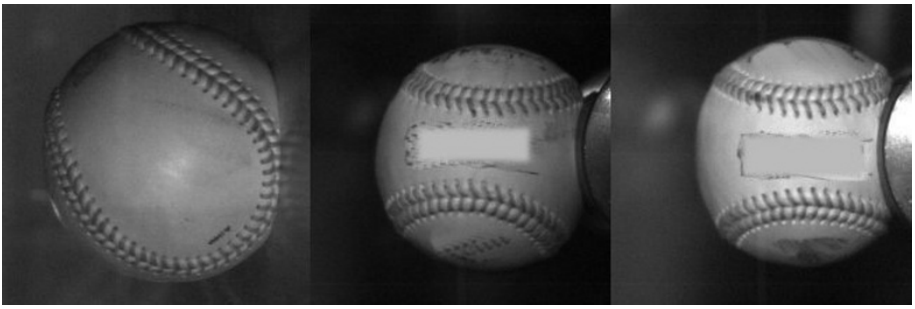

Figure 5 - High-speed video frames of impact for Model C [Left: 26.8 m/s (60-mph) COR, Middle: 26.8 m/s (60-mph) CCOR, and Right: 40.2 m/s (90-mph) CCOR].

4- Conclusion

Performance and construction results for nine different baseball models used throughout the different levels of amateur baseball were presented. The wool-wound baseball models performed essentially the same and exhibited similar trends for the different COR and CCOR tests. The ball construction can result in differences of performance at different impact speeds and different impact surface contours, not only because of the

nonlinear behaviors of the individual materials, but also because of the combination of materials that compressed during the significant deformation of the baseball during impact. Though the trends have similarities, the data show that it may be important to use CCOR at the proper impact speeds to obtain at true measure of the baseball's performance especially when using a COR value in a bat/ball collision model to predict batted-ball speed.

5- References

[A1] ASTM F1887, Standard Test Method for Measuring the Coefficient of Restitution (COR) of Baseballs and Softballs, 2002.

[A2] ASTM F1888, Test Method for Compression-Displacement of Baseballs and Softballs, 2002.

[R1] Reach M. Method of Manufacturing Baseball Centers. United States Patent Number 1530410, 1925.

[S1] Subic A. Materials in sports equipment: volume 2. Woodhead Publishing Limited, Cambridge, 164-165, 2007.

Does the Use of a Light Discus Modify the Throwing Pattern? A Study of Kinematical and Electromyographical Data of the Throwing Arm (P276)

Daniel Dinu[1], Françoise Natta[2], Pierre Portero[3], Henry Vandewalle[4]

Topics: Biomechanics of discus thrower
Abstract: Seven high-level discus throwers (best performance 57 ± 3 m) participated to the present study. During the same session, they performed 12 throws (6 with a 1.7 kg discus and 6 with a 2 kg discus) in a random order. The throwing distance was computed from the velocity vector (magnitude, direction, height) at ejection. Kinematical data were collected by means of 3 video-cameras and a 3-D modelling of the throwing movement was processed according to the DLT method. Surface electromyograms (sEMG) of 6 arm-and-shoulder muscles of the throwing arm [Biceps brachii ; Pectoralis major ; Deltoideus pars superior; Trapezius pars medialis; Deltoideus pars medialis; Latissimus dorsi] were recorded by means of a portable device. Thereafter, sEMG was integrated (iEMG) and related to the iEMG recorded during a maximal effort against an external resistance. Computed distance with a light discus was significantly longer and was the result of a faster discus speed at ejection. This was probably the result of an enhanced increase in discus velocity during the last throwing phase (Δt2da). There was no significant difference in the duration of the four preceding phases with 1.7 kg compared to 2 kg discus. The total duration of the throwing movement was not significantly different between 1.7 and 2 kg discus. The EMG patterns of the different muscles were similar with both discuses when the beginning and the end of the muscle activity were considered. There was no significant difference between discuses when iEMG was summated on the whole throwing movement and related to the iEMG previously recorded during a maximal effort. These results suggest that the lighter discus might be used for high level training without kinematical alteration of throwing.
Key words: Discus throwing, Kinematics, modelling, electromyography, throwing technique.

1. Laboratoire de Biomécanique et Physiologie, Institut National du Sport et de l'Education Physique, 11 Av. du Tremblay Paris, France - E-mail: daniel.dinu@insep.fr
2. Laboratoire Mouvement Action et Performance, Institut National du Sport et de l'Education Physique, 11 Av. du Tremblay Paris, France - E-mail: francoise.natta@insep.fr
3. Hôpital Avicenne, Bobigny, France - E-mail: henry.vandewalle@club-internet.fr
4. Université Paris XII, Créteil, France - E-mail: p.portero@rth.aphp.fr

1- Introduction

Discus throwing is a sport activity characterized by a complex technique (rotation and translation motion) which allowed to obtain the higher speed imparted to the discus at the release (Bartlett 1990). Athletes successful in this sport are able to rotate very fast in the throwing area (Bartlett 1990). To learn this complex technique, lots of coaches recommended doing the turn forward with an under mass discus. Nevertheless no data exists to know if the technique employed with an under mass discus (1.7 kg) is the same than with a competition discus (2 kg). Furthermore, in the discus literature, throwing technique is discussed mainly in relation with cinematographic data (Lindsay 1991, Stepanek and Susanka 1986). Simultaneously videographic and sEMG techniques can provide information about the pattern activity and the level activation of the involved muscles during throwing.

Detailed analysis of the discus throw is facilitated by subdividing the movement into phases, separated by "key moments" mostly related to foot contact. The generally agreed subdivision produces five phases of the throw, which are preceded by the preliminary swings and followed by recovery. These phases, which have various names in the literature, are for a right-handed thrower (Bartlett 1990b):

- *Preparation*, a double support phase starting from the change in discus direction at the end of its backward swing and ending when the right foot breaks contact (Δt_{1da}).
- *Entry,* a single support phase which finishes with the left foot breaking contact (Δt_{1sa}).
- *Airborne,* which finishes with the right foot re-contacting ($D\ t_s$).
- *Transition,* a single support phase which ends as the left foot lands (Δt_{2sa}).
- *Delivery,* which starts as a double support phase and which ends at release of discus (Δt_{2da}).

According to Barlett (1992), the doctoral thesis by Finanger (1964) is probably the only attempt to study electromyograhic activity during a real discus throw. Some electromyographic results of Finanger's study reported in Barlett review are difficult to explain:

- *deltoidus pars medialis* was only active during recovery, i.e. after discus release;
- *latissimus dorsi* was silent after a short burst of activity at the very beginning of the throw (during preparation phase and the beginning of entry) in contrast with the fact that hip lead over the shoulder and the arm is maintained back of the trunk.

However, as reported by Bartlett, there were many technical and methodological problems which limited the validity of some results in the pioneering study by Finanger.

We present the electromyographic data of six shoulder muscles, collected on high level throwers during a discus throw training session. In connection with surface electromyography (sEMG) of the shoulder muscles, we synchroneously collected 3D videographic data of the discus and the thrower's arm to relate muscle activity to the different phases of the discus throw.

The purpose of this study was to examine how mass of the discus influenced the kinematic characteristics and the activity of agonist muscles during throws using 3D videographic and surface electromyography (sEMG) techniques.

2- Methods and Procedures

Seven high-level discus throwers (23 ± 3 years, 108 ± 19 kg, 190 ± 6 cm, best performance : 57 ± 3 m) participated to the present study. During the same session in an indoor training hall, they performed 12 throws (6 with a 1.7 kg discus and 6 with a 2 kg discus) in a random order in the direction of a security web located 15 m in front of the throwing area. The throwing distance was computed from the velocity vector (magnitude, direction, height) at ejection (other factors were not taken into account). Kinematical data were collected by means of 3 video-cameras and a 3-D modelling of the throwing movement was processed according to the DLT method. Surface electromyograms (sEMG) of 6 arm-and-shoulder muscles of the throwing arm and shoulder [*Biceps Brach*ii (BB), *Deltoideus pars anterior*, (DA) and *pars medialis*, (DM) *Pectoralis Major* (PM), *Latissimus Dorsi* (LD), *Trapezius pars superior* (TS)]were collected and recorded by means of a portable device. Thereafter, sEMG was rectified and digitally integrated (iEMG) and, finally, related to the iEMG recorded during a maximal effort against an external resistance, performed before throwing.

A synchronisation signal was sent by a radio emitter to the EMG recorder and by small light emitting diodes (LED) to the three camcorders. The lights of these small LED were emitted a few millimetres in front of the lenses of the camcorders. The delay between LED signals and the EMG recorder signal was equal to 4 ms and taken into account in the synchronization process of the kinematic and EMG data.

2.1 Kinematic data processing

Coordinate transformation was performed so that the y-axis was horizontal and pointing towards the front and the x-axis was horizontal and pointing to the right of the throwing circle. The z-axis was pointing vertically upward. The z-y plane was parallel to a vertical plane that bisected the throwing sector. The horizontal velocity is the component of the resultants velocity in the x-y plane. The angle of release was determined from the horizontal and vertical velocities of release. Using the speed (v) and height (h) of release, the optimum angle of release (_) was computed using the following equation [1,2,3] (Lichtenberg and Wills, 1978):

$$\alpha = \sin^{-1}((2+2gh/v^2)^{-1/2})$$

where g is the acceleration of gravity. The kinematical parameters were computed using the equation for uniformly accelerated motion:

The vertical component or the release velocity $Vzf^2 = Vz_{te}^2 - 2gh$ [1]

Flight time: $t=(Vz_{te}-Vzf)/g$ [2]

Flight range: $dy=Vy_{te}\times t$ [3]

The effect of air forces friction, lift and drag were not taken into account in this model because we were unable to measure the attack and attitude angles from the videographic data. Only the calculated throws higher than 80 % of the individual annual best performance were taken into account for further analysis.

2.2 EMG data processing

Muscle activation onset and offset were detected according to the 3 S.D. procedure. First, the mean value of rectified sEMG and its standard deviation were calculated with a 500 ms running average. The lowest values of the mean rectified sEMG during a 500ms sample were considered as the baseline EMG and its standard deviation as baseline S.D. The onset of a sEMG burst corresponded to the time when EMG was 3 S.D. above baseline S.D. for 25 ms. Offset was detected as the point when EMG was under this 3 S.D. limit.

For each throw, sEMG activity was integrated (iEMG) for the different phases and for the entire throw. iEMG values were thereafter divided by the duration of each phase and normalized to $iEMG_{MVC}$ measured during isometric contraction (see Protocols).

2.3 Protocols

First the throwers warmed up during 15 minutes in the throwing area, under the control of their coach.

Then, the skin was cleaned with an alcohol-ether-acetone solution in order to reach electrode impedance under 5 kΩ. Thereafter, sEMG data were collected during maximal effort against an external resistance in order to express muscle activation in percents of activation during a maximal effort ($iEMG_{MVC}$). A physical therapist exerted a manual opposition to the action of the different muscle groups during specific manoeuvres with the help of an assistant fixing the lower body as previously proposed by Knudson and Blackwell (2000) in their study on trunk muscle action in tennis. Each contraction lasted for about 5 s. Finally, the subjects went back on the throwing area, and performed five throws at 5 minute intervals.

3- Results

The kinetics of discus velocity (1.7 *vs* 2 kg) during the different phases of the throw is presented on figure 1. After a slow acceleration during the preparation phase, there was a plateau in discus velocity during entry and airborne phases. Velocity began to increase again at the end of transition phase before a steep acceleration during delivery at the end of transition and its release speed. The delivery phase has been reported as responsible for 62 % of the release speed of the discus.

Computed distance with a light discus was significantly longer (47.8 ± 1.0 *vs* 42.7 ± 2.9 m), which was the result of a faster discus speed at ejection (21.1 ± 1.1 *vs* 19.6 ± 0.5 $m.s^{-1}$) which was probably the result of an enhanced increase in discus velocity (12.9 ± 1.4 *vs* 11.0 ± 1.0 $m.s^{-1}$) during the last throwing phase (Dt_{2da}). There was no significant difference in the duration of the four preceding phases with 1.7 kg compared to 2 kg discus (Fig. 1). The total duration of the throwing movement was not significantly different between 1.7 *vs* 2 kg discus (1.40 ± 0.3 *vs* 1.42 ± 0.2 s).

The typical EMG data of (DA), (DM) and (LD) during the different phases are presented on figure 2. The activity of (DA) was only observed during Δt_{2da}. In contrast, (LD) and (DM) were active during Δt_{1da} but were inactive during Δt_{2da}. This contrast between the activity of (DA) versus those of (DM) and (LD) were observed in all the subjects.

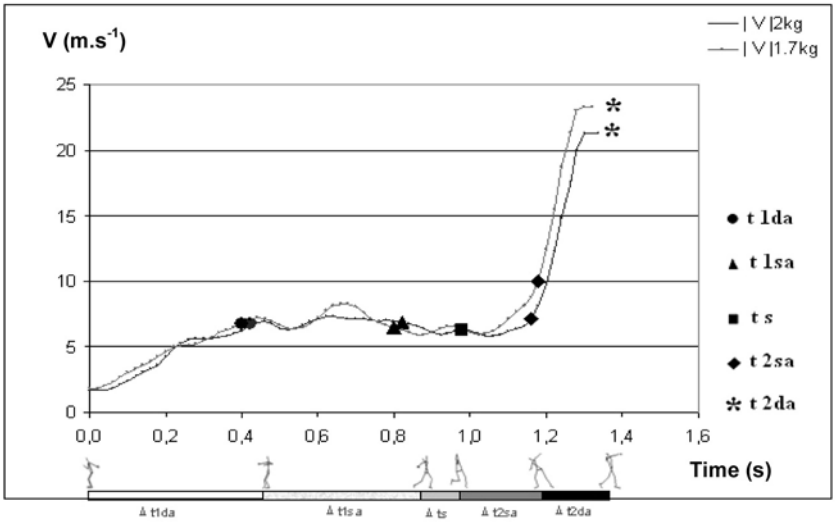

Figure 1 - Comparison of variation of discus speed for two mass of the discus 1.7 vs 2 kg.

Figure 2 presents the beginning and the end of the EMG bursts of the different shoulder muscles.

(TS) was the only muscle which was active at the beginning and the end of the throw. The other muscles which were activated during the last phase (PM, BB, and DA) were inactive during the first phases. There was no EMG burst during Δt_{2da} for DM which was mainly active during Δt_{1da} and the first half of Δt_{1sa}.

The EMG patterns of the different muscles were similar with both discuses when the beginning and the end of the muscle activity were considered. There was no significant difference between discuses when iEMG was summated on the whole throwing movement and related to the iEMG previously recorded during a maximal effort (Table 1).

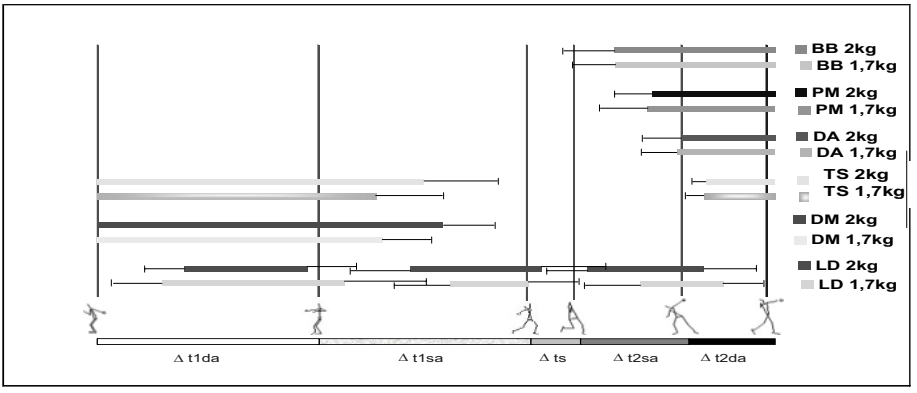

Figure 2 - Comparison of iEMG for different muscles of the arm and shoulder with 1.7 *vs* 2 kg discuses. iEMG data correspond to the whole throwing movement and are expressed as percent of iEMG during a maximal effort.

Muscles	Normalized total iEMG (%) (2 kg)	Normalized total iEMG (%) (1.7 kg)
Biceps brachii (BB)	26.24 ± 39.36	26,77 ± 11,12
Pectoralis major (PM)	22,36 ± 10,28	26,77 ± 11,12
Deltoïdus anterior (DA)	20,77 ± 10,88	23,71 ± 11,25
Trapezius superior (TS)	27,50 ± 10,34	27,70 ± 10,35
Deltoïdus medialis (DM)	29,39 ± 18,57	33,36 ± 29,23
Latissimus dorsi (LD)	41,87 ± 22,71	46,76 ± 13,60

Table 1 - Comparison of normalized iEMG for 6 muscles of the arm and shoulder with 1.7 *vs* 2 kg discuses. iEMG data correspond to the whole throwing movement and are expressed as percent of iEMG during a maximal effort.

4- Discussion/Conclusion

In contrast with the Finanger's data cited by Bartlett, an EMG activity of (DA) were observed during the throw and (LD) was activated not only at the beginning of the preparation phase but also during entry, airborne and transition in our elite throwers. The peak level of LD iEMG corresponded to 47.9 of $iEMG_{MVC}$.

For Deltoideus anterior, higher iEMG was always observed during [Dt_{2da}] phase whereas for Deltoideus medialis iEMG was always observed during [Dt_{1sa}] phase These results allow characterising muscle pattern activities in relation with throwing phases. (DA, PM and BB muscles). Moreover, during (Dt_{2da}) phase, the inter-thrower variability in the timing and the amount of EMG activity were more marked for some muscles. For example, one of the throwers showed a higher peak activity of the (DA) muscle. We hypothesize that the amount of iEMG activity is mainly related with the discus acceleration rather than the discus mass. These results allow characterising muscle pattern activities in relation with throwing phases.

The only significant difference between the 1.7 *vs* 2 kg discuses concerns the increase of velocity during the last phase (Dt_{2da}). All he other kinematical and electromyographical data were statistically identical when 1.7 *vs* 2 kg conditions were compared. Consequently, these results suggest that the lighter discus might be used for high level training without kinematic alteration of throwing. This should allow to decrease the risk of injuries in the beginners.

5- References

[**B1**] Bartlett, R.M. (1990) The biomechanics of the discus throw. In: Proceedings of the First International Conference on Techniques in Athletics, G.-P. Brüggemann and J.K. Rühl (Ed.); Köln; Deutsche Sporthochschule, 126-145.1990.

[**B2**] Bartlett, R.M. The biomechanics of the discus throw. J Sports Sci 10:467-510. 1992.

[**KB1**] Knudson D and Blackwell J. Trunk muscle actions in tennis. Int J Sports Med, 21. 320-322. 2000.

[**L1**] Lindsay, M. Biomechanical analysis of the discus. In: Report on the 1990 Championship in Athletics, vol. 1, (pp. 47-53): The throws (Ed), Bartlett, R.M. 1991.

[**LW1**] Lichtenberg, D.B. and Wills, J.C. Maximizing the range of the shot put. Am. J. Physics, 46: 546-549. 1978.

[**SS1**] Stepanek, J. and Susanka, P. Discus throw: Results of a biomechanics study. New Studies in Athletics, 1, (pp. 25-36). 1986.

Better Coaching the Paralympics Swimmers with the Computed Use of Stroke Rate-Velocity Relationship (P277)

Didier Seyfried[1]

Topics: Modelling Paralympics swimmers for boosting individual performance.
Abstract: A good number of mathematical relations found between the obtained speeds on clean swimming but equally on non-swim areas (starts, turns, underwater part) can be a source of potential help to the individual Paralympics swimmers if they can be computed. Looking to take the spontaneous frequency of swimming to take advantage of it in an applied way of better learning (for the swimmer) and better coaching has been a method we developed from 1993 in the national sport institute of Paris (INSEP) since it appeared to be the most effective in terms of swim economy. The stroke rate/velocity relationship is very interesting since its mastering has a lot of consequences on energy cost, delay of fatigue and better learning of the best stroke at any moment in training sessions or competitions. The stroke rate/velocity test is incremental and carried though the observation of 15 meters of clean swimming where 3 full cycles are measured considering the time and the spontaneous stroke rate of the swimmer, during 8 progressive steps. These starting points guided the development of several types of software beneficial to swimming training including NATAVIT (1995-2000) and AQUACYCLE (since 2000) but equally a concept of measurement automated in training (CHRONOCYCLE) particularly useful for French Paralympics swimming team.
Key words: Modelling, swimming, cadence, stroke length, Paralympics.

1- Introduction

Looking to take the spontaneous frequency of activity to take advantage of it in an applied way for better learning (for the swimmer) and better teaching (for the coach) has been an achievement since 1993. In swimming, the spontaneous stroke rate/velocity (Seyfried and Van Hoecke, 1993, Seyfried 1994) was at first an indicator then became a systemized test from 1995. It is used now in many countries, notably in swimming to determine if the rate and by result the distance per stroke, also called stroke length, used by a swimmer at a given moment -in training or competition- is the most effective in terms of swim economy (figure 1).

1. Laboratoire d'Informatique Appliquée au Sport, INSEP, 11 avenue du Tremblay, 75012 Paris, France - didier.seyfried@insep.fr

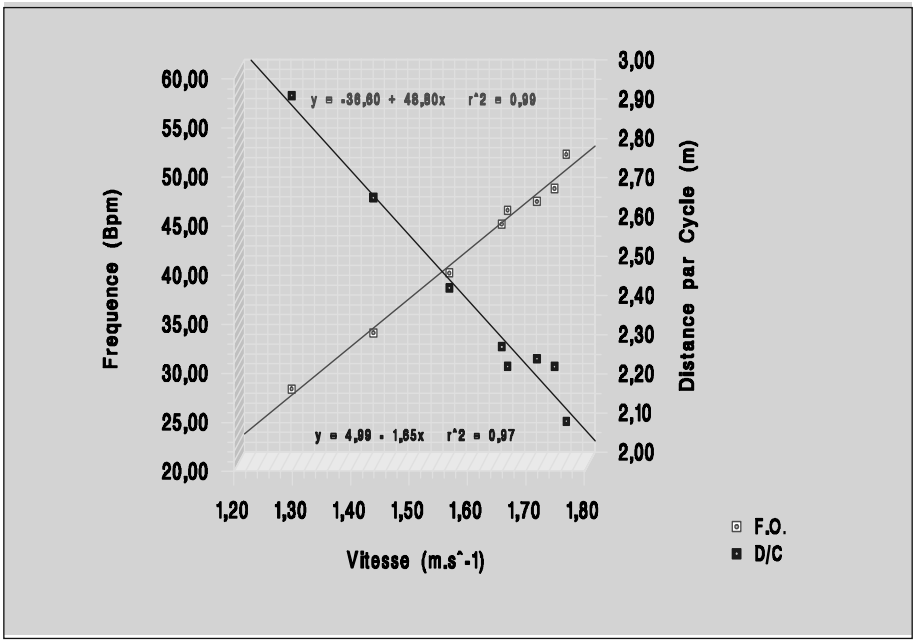

Figure 1 - Linear Relationships between Swim velocity, Frequency (F.O.) and Distance per stroke (D/C) in a swimmer.

Transforming the observations obtained from swimmers during previous evaluations to create more specifically their future training sessions as well as analysing them is the goal for most testing technicians. Mathematical relations found between the obtained speeds on clean swimming but equally on non-swim areas (starts, turns, underwater parts) can be a source of potential help to the individual swimmers if they can be calculated. Among them the stroke rate/velocity relationship is very interesting since its mastering has many consequences on energy cost, delay of fatigue (Swaine and Reilly,1983, Seyfried *et al.* 1994, Wakayoshi *et al.* 1993, Wakayoshi *et al.* 1995) and better learning of the best stroke at any moment in training sessions or competition (Chollet *et al.* 1997). This starting point guided the development of several types of software beneficial to swimming training including NATAVIT (1995-2000) (Seyfried and Trepagny, 1994) and AQUACYCLE (since 2000) but equally a concept of measurement automated in training or competitions -CHRONOCYCLE- specifically designed for Paralympics swimmers. In France and at INSEP in particular, the choice of a kinetic study of cyclic parameters evolving within useful swim velocities was at the origin of a hypothesis to test the relationship between stroke rate and velocity. This was confirmed through the development of standards for this test and through the use of various methodologies and tools. The applied usage in training of these tests for Paralympics was carried out through the use of individual test results established using tables (Microsoft Excel), then on the present Chronocycle software.

2- The system of evaluation and follow up in training

The stroke rate/velocity incremental test consists in observing 15 m of clean swimming during 6 to 8 progressive steps where 3 full strokes are measured considering the time and the spontaneous stroke rate of the swimmer (Figure 1).

It allows every swimmer to be given theoretical cyclic parameters vs. observed ones during future sessions. Theoretical Stroke Length (TSL) vs. Observed Stroke Length (OSL), Theoretical Stroke Rates vs. Observed Stroke Rates (OSR) and even Theoretical Stroke index (TSI) vs. Observed Stroke index (OSI), all of them being good reference factors in terms of swimming economy during the observations of training sessions and races i.e. between heats and finals (Figure 2).

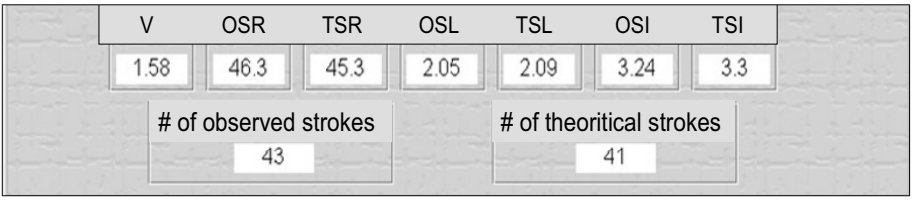

Figure 2 - Observed Stroke rates, Stroke lengths and stroke indexes compared with theoretical individual model.

3- Examples of applications in training

Different methods can help optimize the management of the cyclic fitting parameters to the velocity of the corresponding swims. The example of the relationship between stroke rate and the velocity of swims seems to be the most striking. After determining the equation rate velocity TSR, the software will compute the calculation of the ideal cyclic parameters for all the times for all distances and size of pool and of given send-offs. Software has been produced currently to record from a direct capture as well of a video file that one can see in one of the windows of the application. The capture was tested with a click of the mouse, keyboard, and an external remote control to the PC radio HF but it can potentially receive all types of triggers to the system (sensors, automatic recognition of pictures, light signals, sound cues).

This system provides a cyclic and technical resume with the swimmer immediately after each series (Figure 3). AQUACYCLE allows as well teaching possibilities. The swimmer can self-evaluate simply in terms of «arm hits» (Figure 4): checking the clock and counting the arm stokes is enough for better learning. These methods allow the swimmer to refine his or her mastery of spatial-mental skills, a critical step in the control of the cyclic parameters relating to velocity of swims. These situations - when objective information is given during or immediately after the stop of the exercise - are essential for the specific education of Paralympics swimmers. The mastery of the relationship between stroke rate and velocity allows one to work towards swimming at a constant speed and therefore to a stable rhythm, to adapt with better effectiveness to all likely velocities as necessarily tactical accelerations used by the swimmer.

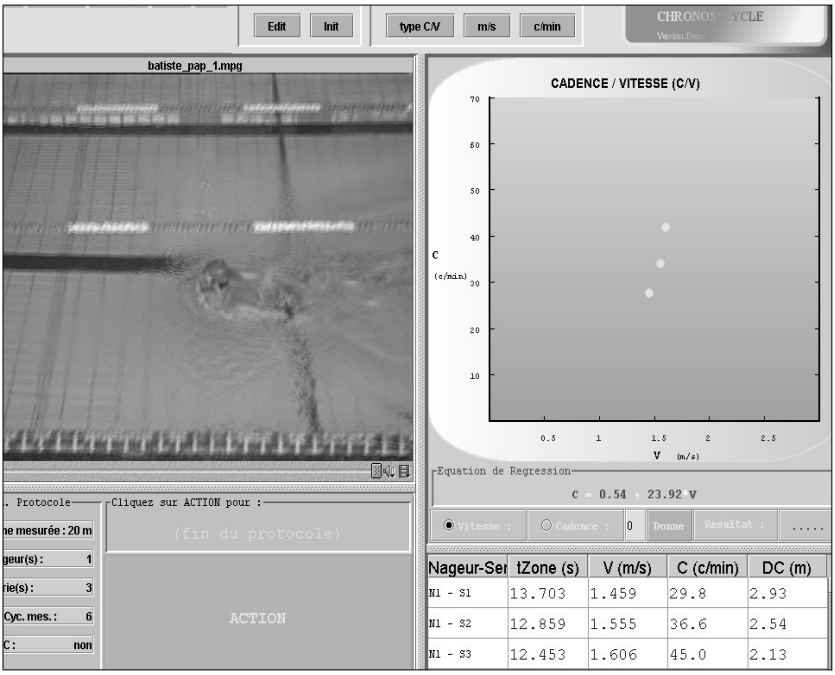

Figure 3 - Real-time cyclic and technical resume of the stroke rate/velocity test from the software screen.

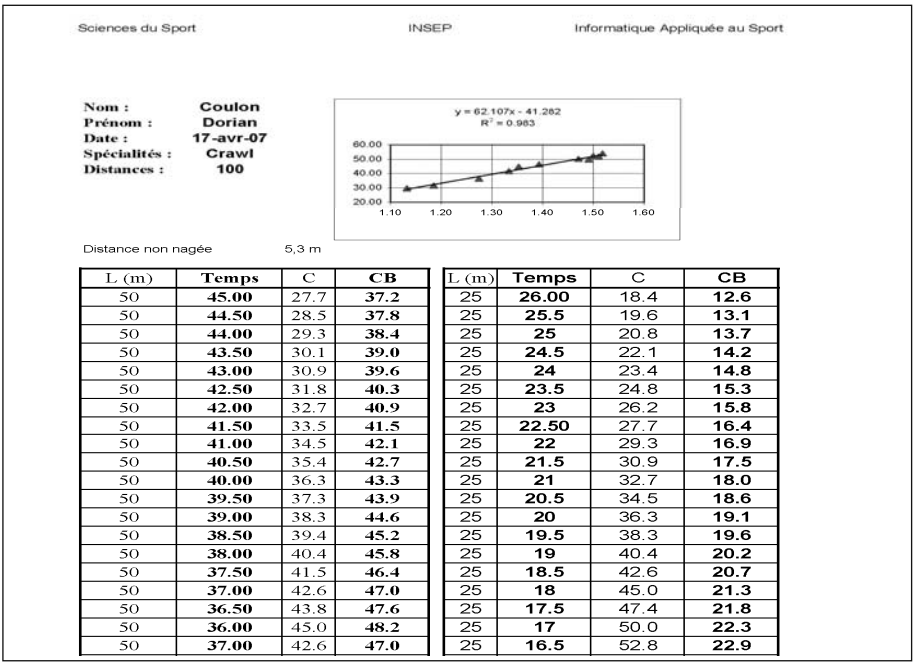

L (m)	Temps	C	CB
50	**45.00**	27.7	**37.2**
50	**44.50**	28.5	**37.8**
50	**44.00**	29.3	**38.4**
50	**43.50**	30.1	**39.0**
50	**43.00**	30.9	**39.6**
50	**42.50**	31.8	**40.3**
50	**42.00**	32.7	**40.9**
50	**41.50**	33.5	**41.5**
50	**41.00**	34.5	**42.1**
50	**40.50**	35.4	**42.7**
50	**40.00**	36.3	**43.3**
50	**39.50**	37.3	**43.9**
50	**39.00**	38.3	**44.6**
50	**38.50**	39.4	**45.2**
50	**38.00**	40.4	**45.8**
50	**37.50**	41.5	**46.4**
50	**37.00**	42.6	**47.0**
50	**36.50**	43.8	**47.6**
50	**36.00**	45.0	**48.2**
50	**37.00**	42.6	**47.0**

L (m)	Temps	C	CB
25	**26.00**	18.4	**12.6**
25	**25.5**	19.6	**13.1**
25	**25**	20.8	**13.7**
25	**24.5**	22.1	**14.2**
25	**24**	23.4	**14.8**
25	**23.5**	24.8	**15.3**
25	**23**	26.2	**15.8**
25	**22.50**	27.7	**16.4**
25	**22**	29.3	**16.9**
25	**21.5**	30.9	**17.5**
25	**21**	32.7	**18.0**
25	**20.5**	34.5	**18.6**
25	**20**	36.3	**19.1**
25	**19.5**	38.3	**19.6**
25	**19**	40.4	**20.2**
25	**18.5**	42.6	**20.7**
25	**18**	45.0	**21.3**
25	**17.5**	47.4	**21.8**
25	**17**	50.0	**22.3**
25	**16.5**	52.8	**22.9**

Figure 4 - Software Screen of stroke rates and stroke hits proposals at selected velocities on either 25 or 50m pool.

4- Discussion

The linear adjustments of the relationship of stroke rate/velocity and stroke length/velocity are more highly correlated as the level of expertise of the swimmers is increased. It is normal for the physical to be linked to drag as the distance per stroke diminishes in a manner inversely proportional to velocity according to a linear mathematic relationship (Figure 1). The Paralympics swimmers seem insufficiently educated in this approach when compared with Olympic swimmers. The observations of Paralympics swimmers in previous elite competitions indicate unnecessarily high stroke rates in comparison with their individual demonstrated ideal economy of swims for the given velocity. The confusion between « velocity and turn over » is all the more natural under the stress of competition. This is the reason it must be checked and practiced in training as well as specific competitions. We reinforce the fact that pace regularity and stroke rates, the technical management of race can be obtained by practice and is the fruit of very elaborate feed back (Seyfried 1997). In France, the number of repetitions at race velocity, while doing the report on the cyclic parameters is more and more used with the Paralympics swimmers for amazing efficiency. Work at sub-maximal speed deserves equally to be given to swimmers with a reference to cyclic objectives, for example a number of arms hits per pool length according to the speed of the swimmer.

Our evaluations show that for all the Paralympics swimmers that get faster over two years, the two values of stroke rate and stroke length still evolve in the direction of an increase in the distance per stroke and of a decrease in the rate. Nevertheless, only the improvement of performance in times must remain the objective. The increase of the distance per stroke for a velocity of given swims (and therefore the proportional decrease of the rate) is only interesting if the swimmer preserves the same « potential of rate » throughout his or her career to attain a race pace which always improves in competition.

5- Conclusion

This innovative computer software helps Paralympics coaches in their initial evaluation of elite athletes and in the analysis of their performances. It allows individual training plans to be printed for swimmers providing simple keys to success such as the number of strokes needed to swim a 50 m race in a certain time according to an individualised training model (Figure 4). This software employs a proven observation methodology and runs on a simple PC (Windows XP or Vista). It provides athletes with an opportunity to develop new strategies for training where an athlete can control his own preparation. The stroke rate-velocity relationship based on an incremental test of performance is calculated by the software according to a linear model validated in the scientific literature. A table of times and corresponding individual cyclical parameters is printable and relates the usual training and competition performance conducted over the length of the pool to optimal cyclical parameters. The acquisition of biomechanical indicators by trial and error across the spectrum of velocities allowing the movement in water, with « feedback » in the fastest possible manner on execution will probably be a learning curve for the Paralympics swimmer in the years to come.

6- References

[CP1] Chollet, D., Pelayo, P., Delaplace, C., Tourny, C. and Sydney M. (1997) Stroking characteristics variations in 100 m freestyle in different skill level swimmers. Perceptual and Motor Skills, 85, 167-177.

[S1] Seyfried, D. (1997) Evaluer et Analyser pour mieux entraîner : exemple du système développé à l'INSEP pour l'olympiade 1992-1996. In L'Entraînement, Analyse de l'activité. 2, 137-154, Atlantica.

[SV1] Seyfried, D. and Van Hoecke, J. (1993) Validation et intérêts du test Fréquence-Vitesse pour l'évaluation et l'entraînement du nageur de haut-niveau. In Actes du Congrès, 5° Journées de l'ACAPS, 339-340, Caen.

[SA1] Seyfried, D., Araar, N., Vallier, J.M. and Thomaidis, M. (1994) Analyse de paramètres biomécaniques et physiologiques au cours d'un protocole aérobie réalisé en crawl chez 18 nageurs de haut niveau. In Actes du Congrès, 1° Journées spécialisées de Natation, Lille.

[ST1] Seyfried, D. and Trepagny J.D. (1994) Conception et Développement du logiciel d'aide à l'entraînement NATAVIT pour les nageurs du CNE de l'INSEP. In Actes du Congrès, 1° Journées spécialisées de Natation, Lille.

[S2] Seyfried, D. (1994) Intérêts et Méthodologie du test Fréquence/Vitesse pour l'Evaluation et l'entraînement du nageur de 4 Nages. In Actes du Congrès, 1° Journées spécialisées de Natation, Lille.

[SR1] Swaine, I. and Reilly, T. (1983) The freely-chosen Swimming Stroke-rate at a maximal Swim on a Biokinetic Swim Bench. Medicine and Science in Sports and Exercise. 15, 371-375.

[WY1] Wakayoshi, K., Yoshida, T., Ikuta, Y., Mutoh, Y. and Myashita, M. (1993) Adaptations to Six months of Aerobic Swim Training: Changes in Velocity, Stroke Rate, Stroke Length and Blood Lactate. International Journal of Sports Medicine. 14, 368-372.

[WD1] Wakayoshi, K., D'Acquisto, L.J., Cappaert, J. and Troup, J.P. (1995) Relationship between Oxygen Uptake, Stroke Rate and swimming Velocity in Competitive Swimming. International Journal of Sports Medicine. 16, 19-23.

Subject Index

ORAL COMMUNICATION : gras
POSTER : maigre

SPORTS